APOPTOSIS AND SENESCENCE IN VERTEBRATE DEVELOPMENT

EDITED BY: Wolfgang Knabe, Marta Magarinos and Stefan Washausen
PUBLISHED IN: Frontiers in Cell and Developmental Biology

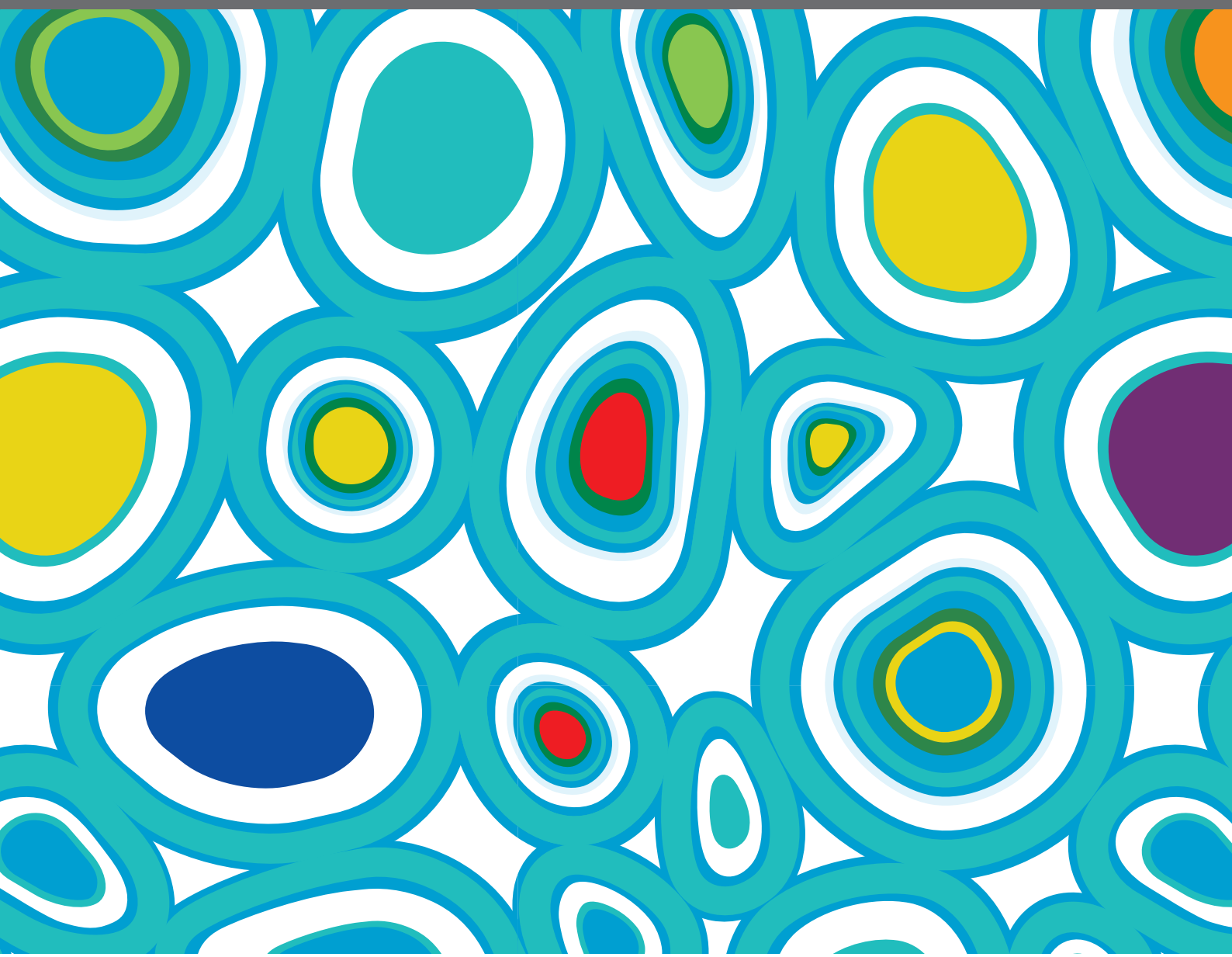

frontiers Research Topics

frontiers

ISSN 1664-8714
ISBN 978-2-88974-388-9
DOI 10.3389/978-2-88974-388-9

About Frontiers

Frontiers is more than just an open-access publisher of scholarly articles: it is a pioneering approach to the world of academia, radically improving the way scholarly research is managed. The grand vision of Frontiers is a world where all people have an equal opportunity to seek, share and generate knowledge. Frontiers provides immediate and permanent online open access to all its publications, but this alone is not enough to realize our grand goals.

Frontiers Journal Series

The Frontiers Journal Series is a multi-tier and interdisciplinary set of open-access, online journals, promising a paradigm shift from the current review, selection and dissemination processes in academic publishing. All Frontiers journals are driven by researchers for researchers; therefore, they constitute a service to the scholarly community. At the same time, the Frontiers Journal Series operates on a revolutionary invention, the tiered publishing system, initially addressing specific communities of scholars, and gradually climbing up to broader public understanding, thus serving the interests of the lay society, too.

Dedication to Quality

Each Frontiers article is a landmark of the highest quality, thanks to genuinely collaborative interactions between authors and review editors, who include some of the world's best academicians. Research must be certified by peers before entering a stream of knowledge that may eventually reach the public - and shape society; therefore, Frontiers only applies the most rigorous and unbiased reviews.
Frontiers revolutionizes research publishing by freely delivering the most outstanding research, evaluated with no bias from both the academic and social point of view. By applying the most advanced information technologies, Frontiers is catapulting scholarly publishing into a new generation.

What are Frontiers Research Topics?

Frontiers Research Topics are very popular trademarks of the Frontiers Journals Series: they are collections of at least ten articles, all centered on a particular subject. With their unique mix of varied contributions from Original Research to Review Articles, Frontiers Research Topics unify the most influential researchers, the latest key findings and historical advances in a hot research area! Find out more on how to host your own Frontiers Research Topic or contribute to one as an author by contacting the Frontiers Editorial Office: frontiersin.org/about/contact

APOPTOSIS AND SENESCENCE IN VERTEBRATE DEVELOPMENT

Topic Editors:
Wolfgang Knabe, Universität Münster, Germany
Marta Magarinos, Autonomous University of Madrid, Spain
Stefan Washausen, Westfälische Wilhelms-University, Germany

Citation: Knabe, W., Magarinos, M., Washausen, S., eds. (2022). Apoptosis and Senescence in Vertebrate Development. Lausanne: Frontiers Media SA.
doi: 10.3389/978-2-88974-388-9

Table of Contents

frontiers in Cell and Developmental Biology

EDITORIAL
published: 05 January 2022
doi: 10.3389/fcell.2021.834517

Editorial: Apoptosis and Senescence in Vertebrate Development

Wolfgang Knabe[*†] *and Stefan Washausen*[†]

Prosektur Anatomie, Westfälische Wilhelms-Universität Münster, Münster, Germany

Keywords: apoptosis, programmed cell death, cellular senescence, autophagy, macrophages, embryonic development, regeneration, vertebrates

Editorial on the Research Topic

Apoptosis and Senescence in Vertebrate Development

INTRODUCTION

In the history of developmental biology, apoptosis and senescence will foreseeably share at least four characteristics. Firstly, both have made their way into this field after detours. Thus, dead cells were admittedly discovered early within embryos of various vertebrate classes, well before the term apoptosis came into use (Kerr et al., 1972). Conceptually, however, ontogenetic cell death events were accepted and interpreted hesitantly, despite their meticulous temporal and spatial descriptions (Rabl, 1898-1899; Rabl, 1899-1900; Jokl, 1918, 1920; Ernst, 1926; Peter, 1936; Glücksmann, 1951). Correspondingly, the term senescence did not even originate from developmental biology at all, but rather from ageing research (Hayflick and Moorhead, 1961), and it was not until about 50 years later that contributions of permanent cell cycle arrests to embryonic development received adequate recognition (Muñoz-Espín et al., 2013; Storer et al., 2013). A second common feature of apoptosis and senescence is that both are part of their own wide spectrum of different forms. Thus, we are far from confident today that cell death events found during normal and/or disturbed development generally belong to the category "apoptosis". Rather, it could alternatively or additionally be necroptosis, parthanatos, entotic cell death, lysosome-dependent cell death, autophagy-dependent cell death, or linker cell-type death, to name just a few candidates (Yuan and Kroemer, 2010; Kutscher and Shaham, 2017; Galluzzi et al., 2018; Voss and Strasser, 2020). Likewise, differently mediated types of senescence are induced by aging, oncogenes, irradiation, chemotherapy, tissue damage, induced pluripotent stem cell reprogramming or developmental cues (Muñoz-Espín and Serrano, 2014; Herranz and Gil, 2018; da Silva-Álvarez et al., 2019; Rhinn et al., 2019; Varela-Nieto et al., 2019). Considering these diversities of forms, a third similarity between apoptosis and senescence can be compellingly deduced. Indeed, a whole arsenal of detection methods must be employed to identify apoptotic or senescent cells, respectively (Vanden Berghe et al., 2013; Majtnerová and Roušar, 2018; González-Gualda et al., 2021). Finally, a fourth common feature consists in the fact that we still know little about the functions of apoptosis and senescence in many developmental contexts. Especially, presumed regulatory and functional interrelationships between these two processes are still largely obscure. This Research Topic attempts to address the above described situation as follows. Our primary goal was to present new evidence for the occurrence and functions of programmed cell death/apoptosis and/or cellular senescence during normal vertebrate development. In order to promote interdisciplinary bridging, contributions to the fields "postnatal development", "*in-vitro* development", "aging", "disease", and "regeneration" were additionally included. Other papers critically investigate the significance of methods used to detect developmental senescence, or "canonical" and "non-canonical" roles of components of the apoptosis machinery.

OPEN ACCESS

Edited and reviewed by:
Inna N. Lavrik,
University Hospital Magdeburg, Germany

***Correspondence:**
Wolfgang Knabe
w.knabe@uni-muenster.de

†ORCID:
Wolfgang Knabe
orcid.org/0000-0003-1744-0734
Stefan Washausen
orcid.org/0000-0003-1482-2761

Specialty section:
This article was submitted to Cell Death and Survival, a section of the journal Frontiers in Cell and Developmental Biology

Received: *13 December 2021*
Accepted: *20 December 2021*
Published: *05 January 2022*

Citation:
Knabe W and Washausen S (2022) Editorial: Apoptosis and Senescence in Vertebrate Development. Front. Cell Dev. Biol. 9:834517. doi: 10.3389/fcell.2021.834517

SUMMARY OF THE ARTICLES

This Research Topic includes 20 articles written by 118 authors and reviewed by 41 referees, who in their entirety came from 25 different countries and six continents. The following section presents the focus and key findings of each article.

We open our Research Topic with a review on senescence and apoptosis as the architects of mammalian development (Wanner et al.). This overview starts by addressing zygotes and blastocysts, which are later revisited under *in vitro* conditions (Ramos-Ibeas et al.; Yu et al.). In the opposite direction, the chronological spectrum even covers transitions to ageing processes. Further main topics are epigenetic modifications and the ambivalence of several tumor suppressors [p53, Retinoblastoma (Rb), Inhibitor of Growth (ING)] which "play antagonistic roles by increasing fitness and decreasing mortality early in life but contribute to deleterious effects and pathologies later in life" or, in short, which reveal "antagonistic pleiotropy" (Wanner et al.).

Subsequently, de Mera-Rodríguez et al. examine to which extent senescence-associated ß-galactosidase and the cyclin-dependent kinase (CDK) inhibitor p21 are reliable *in vivo* markers of cellular senescence. The authors focus on retinal and limb development, but also outline other organ systems. Possible interrelationships between apoptosis and senescence are additionally considered. Given that ß-galactosidase activity overlaps with areas of cell death and, like p21, is also present in newly differentiated retinal neurons, both "senescence markers" may be less specific than previously thought. Ultimately, methodological concerns highlighted here underscore the recent postulate that proper detection of senescence must be based on experiments using at least three independent markers (González-Gualda et al., 2021).

We continue with a series of eight papers dealing with the nervous system, sense organs and craniofacial development. Firstly, Nie et al. revisit previously published work on the contributions of sumoylation processes to optic lens development (Yan et al., 2010; Gong et al., 2014). The question now is whether sumoylation is significant also during oxidative stress-induced cataractogenesis. In fact, the authors show that the E3 ligase PIAS1 (protein inhibitor of activated STAT-1) regulates p53 sumoylation to control stress-induced apoptosis of lens epithelial cells through the pro-apoptotic regulator Bax.

In the second place, Domínguez-Bautista et al. report on programmed cell senescence in the spinal cord and notochord of mouse embryos. They provide new evidence that senescent cells express different markers in different developmental contexts, in this case either the CDK inhibitors p16 (spinal motoneurons) or p21 (endothelial cells, notochord). Furthermore, it is demonstrated that senescent cells in the floor plate signaling centre (Muñoz-Espín et al., 2013) are joined by quiescent cells. Given that treatment with senolytics led to a reduction in the number of spinal motoneurons, Domínguez-Bautista et al. conclude that "programmed cell senescence cooperates with apoptosis to adjust the number of motoneurons".

The third paper in this series examines the anti-apoptotic role of the Bcl2 protein Mcl-1 (Myeloid cell leukemia-1) in the embryonic spinal cord, brainstem and forebrain (Flemmer et al.). Using the *Nestin-Cre Mcl-1* conditional knockout (*Mcl-1* CKO) mouse line, the authors detected apoptotic waves which, in the spinal cord, proceeded ventrodorsally and rostrocaudally from embryonic day 9 onwards. Consequently, Mcl-1 does not contribute to neural tube formation, but to the differentiation of neuronal precursor cells (NPC) into immature neurons. Breeding *Mcl-1* CKO mice with *Bax* null mice further demonstrated "that Mcl-1 promotes NPC survival primarily by inhibiting the activation of Bax, but that Bax is not the sole pro-apoptotic target of Mcl-1 during embryonic neurogenesis" (Flemmer et al.).

Following this, Nguyen et al. address the fact that caspases do not only perform "canonical" functions in the context of apoptosis, but also "non-canonical" functions in axon guidance, axon pruning, synapse maturation, and synaptic transmission. Furthermore, this review takes into account the signaling pathways that select between or execute apoptotic or non-apoptotic responses. Some of these signaling pathways are additionally explored in original papers belonging to this Research Topic (e.g.: Mcl-1: Flemmer et al.; Bax: Nie et al.; WNT, BMP, FGF: Díaz-Hernández et al.).

The fifth paper raises the question of how ethanol-induced apoptosis can be prevented in human neural crest cells (Li et al.). It thus continues earlier work documenting the occurrence of increased apoptosis in the nervous system, head and limbs of ethanol-exposed embryonic mice (Kotch et al., 1992, Kotch and Sulik, 1992a, Kotch and Sulik, 1992b; Kotch et al., 1995; Dunty et al., 2001, 2002). Here, an example is provided of how anti-apoptotic genes can be epigenetically suppressed (for a review, see Wanner et al.). Specifically, the vegetable-derived isothiocyanate sulforaphane "protects against ethanol-induced apoptosis (. . .) through diminishing ethanol-induced hypermethylation at the promoters of the genes encoding the inhibitor of apoptosis proteins" (Li et al.).

Next, Compagnucci et al. set out how apoptosis affects normal and abnormal craniofacial development. Continuity with previously featured teratological studies is obvious, as approximately one third of all human congenital malformations are manifested in the head and face (Twigg and Wilkie, 2015). The authors focus on epithelial-epithelial apposition, intraepithelial morphogenesis, epithelial compartmentalization and metameric organization of the cranial neural crest, exemplified by the jaw modules, the lambdoidal junction, the pharyngeal arch 1 hinge, and the upper jaw, respectively. Overall, developmental apoptosis appears to work less with the "sledgehammer" and much more as "subtle sculptor". Entirely in line with our rationale for launching this Research Topic, another conclusion is that "a comprehensive exposition of the normal, predictable spatiotemporal ontogeny of apoptosis explicitly in the craniofacial tissues of vertebrate embryos has yet to materialize" (Compagnucci et al.).

We proceed with early tooth development, which has emerged as an attractive model in mesenchymal stem cell research (Yu et al., 2015; Sharpe, 2016). Here, Kim et al. demonstrate that

hypoxia-responsive oxygen nanobubbles prevent hypoxia-induced pathological increases of apoptosis in the cap and bell stages of mouse tooth germs. It can therefore be assumed that hypoxia-responsive oxygen nanobubbles will be suitable for regenerative approaches in the dental field. Whether, in tooth germs, hypoxia-inducible factor-1 (HIF-1; Kietzmann et al., 2001) may also trigger senescence, possibly via p53, remains to be investigated.

The subsequent paper by Maeda starts by reviewing the hard tissues of adult teeth which all display unique structural, molecular and physiological senescence patterns. From here, Maeda builds bridges to cellular senescence of dental pulp (stem) cells including tooth germs, but also to the topic of regeneration. Undoubtedly, "dental pulp stem cells (. . .) have attracted considerable attention as promising cells for regenerative endodontics (. . .) and systemic regenerative medicine" (Maeda).

The following group of three articles is dedicated to trunk and limb development. We begin with a study on the teratogenic effects of caffeine in chicken embryos (Wu et al.). Caffeine exposure interferes with the expression of genes modulating apoptosis, proliferation, and differentiation of myogenic progenitors in differentiating somites as well as in the chest wall. Resembling the case of ethanol-treated human neural crest cells (Li et al.), increased apoptosis affected caffeine-treated myogenic progenitors. Unexpectedly, however, significantly increased proliferation rates were additionally recorded under the influence of caffeine. All pathological changes were suppressible by the administration of retinoic acid antagonists.

The second article illustrates that at least two different mechanisms are involved in the degradation of superfluous cells during digit formation (Montero et al.). Apoptosis seems to dominate the onset of interdigital tissue remodeling, but is later coincident with "destructive developmental cell senescence", which, however, is difficult to distinguish from other lysosomal pathway-mediated processes. A second type of (true?) senescence observed during digit formation shows no association with apoptosis, but is most likely related to tendon differentiation ("constructive developmental senescence"). Overall, the authors are certainly right to warn against overly rapid classification attempts in cases of cellular degradation pathway confluence.

The article closing the limb topic deals with the "anterior necrotic zone" (ANZ) which, in chicken embryos, promotes digit number reduction (Díaz-Hernández et al.). The authors show that cell death in the ANZ can be triggered either by inhibition of FGF or WNT signaling, or by activation of BMP signaling. Surprisingly, however, FGF signaling induces the expression of the pro-apoptotic genes *Dickkopf* (*Dkk*) and *Bmp4*. Furthermore, FGF8 in the apical ectodermal ridge and BMP4 in the anterior border of the limb are inhibited by BMP4. If, on the other hand, BMP4 is blocked by NOGGIN, *Dkk* expression in the ANZ gets reduced. Double treatment experiments support the hypothesis that during BMP4 activation, FGF signaling may represent the final step in the molecular cascade leading to early cell death in the ANZ (Díaz-Hernández et al.).

The following original paper highlights the importance of the ribosome biogenesis factor LTV1 for digestive organ development and hematopoiesis in zebrafish (Zhang et al.). In our thematic context, ribosomopathies are attractive, among other aspects, because they can trigger apoptosis or senescence via p53 (Fumagalli and Thomas, 2011; Turi et al., 2019; Da Costa et al., 2020). In *ltv1* knockouts, however, defects of exocrine pancreas as well as hematopoietic stem and progenitor cells were not associated with increased apoptosis, but with decreased growth rates. Also, a possible dependence on p53 could not be confirmed.

Three other papers explore senescence and/or apoptosis at particularly early developmental stages. At the outset, Palomino et al. take up the earlier observation, relevant not least to global fishing industry, that captive yellow-tail kingfish (*Seriola lalandi*) show lower survival rates due to the failure of their buoyancy system. Now, the authors report that animals living in captivity (stages 2/4C, morula, blastula, gastrula, and 24 hpf) exhibit massively increased apoptosis rates. In line with this, changes in the expression levels of cell death-associated genes are demonstrated (*bax*, *casp9*, *casp3*, *casp8*, Fas).

Next is a review on the occurrence of senescence and apoptosis during *in vitro* bovine embryo development (Ramos-Ibeas et al.). In pre-implantational embryos, protective senescence initially gains regulatory significance. Later during morula and blastula stages, apoptosis is in the foreground, whereby "embryonic quality is normally associated with lower apoptotic rates". Main parts of this work provide practical guidance on how to assess embryo quality using structural criteria and molecular markers for measuring senescence and apoptosis.

Correspondingly, Yu et al. address the question on how to predict bovine blastocyst quality. 42% of the blastocysts examined show cellular fragments in the perivitelline space before transfer, and 37% of these fragments are TUNEL-negative, i.e. non-apoptotic. Furthermore, neither correlative nor causal relationships were found between the occurrence of perivitelline fragments and blastocyst quality. The authors therefore conclude "that apoptosis and fragmentation are methods to remove abnormal cells from the embryo, and thereby protect the developmental competence of the embryo".

As with the retina (de Mera-Rodríguez et al.), we extend the scope of our Research Topic one last time to the postnatal developmental period, this time using the skin as an example. Specifically, Chou et al. intend to establish a mouse model that recapitulates key pathological features of human diseases associated with dysfunctions of the tumor suppressor gene *Wwox*. They show that *Wwox* deficiency leads to decreases in the proliferation and differentiation of keratinocytes as well as to increased apoptosis rates in $Wwox^{-/-}$ mouse epidermis, primary keratinocyte cultures and *Wwox* knockdown human HaCaT cells. Most probably, *Wwox* deficiency is mediated by the downregulation of prosurvival MEK/ERK signaling.

The two concluding articles of this Research Topic focus on possible links between apoptosis, senescence, development and regeneration. Firstly, Li et al. present a systematic summary of the different types of apoptotic extracellular vesicles (ApoEVs) which contain nucleic acids, protein lipids, mitochondria, and plasma

membrane, among others. Possible developmental and/or regenerative functions of ApoEVs include the apoptosis-induced activation of compensatory proliferation and/or differentiation processes as well as the elimination of senescent cells. Interestingly, senescent cells, owing to their senescence-associated secretory phenotype (SASP), display fascinating parallels to ApoEVs by releasing cytokines, growth factors or DNA fragments into their environment.

Molecular similarities between apoptosis-induced regenerative and developmental processes are also explored in the final review prepared by Guerin et al. Typical subjects of discussion are functions of BMPs in the limbs or those of Jun-N terminal kinase (JNK) in the brain. Furthermore, the importance of apoptosis for cell signaling and patterning mechanisms is being investigated. Overall, the authors conclude that, despite numerous commonalities, apoptosis-induced regeneration by no means simply recapitulates apoptosis-induced developmental mechanisms.

PERSPECTIVES

Taken together, the results of this Research Topic first of all show that numerous previously undescribed cases of ontogenetic cell death still await discovery. Furthermore, there is increasing evidence that developmental events may not be propelled by one type of cell death alone, but that several different types of cell death may be involved, either simultaneously or successively. We conclude from this that, even in developmental contexts where, for example, apoptosis safely fulfils specific functions, we should nevertheless explore the remaining spectrum of cell death forms. This need is all the more acute in cases where the functions of ontogenetic cell death are still unclear, or where experimental suppression of programmed cell death entails inconclusive results. Especially in the latter instance, switching between several types of cell death might be part of the embryo's "survival repertoire". Understanding such possible cell death transitions might also help to better appreciate similarities and differences between developmental and regenerative processes.

With the discovery of programmed senescence, the situation initially became even more complicated for developmental biologists interested in programmed cell death. That is why it is all the more imperative now to meticulously document examples of the complementary, simultaneous and/or successive occurrence of both processes in well-defined developmental contexts. We are convinced that without such systematic investigations it will hardly be possible to gain experimentally validated insights into the functional interactions of programmed cell death and senescence. To achieve these objectives, as in the case of programmed cell death, it will undoubtedly be necessary to solve numerous methodological problems that currently hamper the reliable diagnosis of senescent cells. Conversely, our ever-increasing knowledge about the regulatory potential of secretory active senescent cells will certainly inspire developmental biologists to take a fresh look at the developmentally relevant functions of ApoEvs as well as at the non-canonical functions of components of the apoptosis machinery.

Finally, we are left with the pleasant duty to express our sincere thanks to all those who helped to realize this Research Topic. We were particularly impressed by the constant willingness of both our authors and reviewers to contribute ambitiously to the optimization of submitted manuscripts through precise, critical and self-critical comments, questions and responses. Unwanted by all, the Corona pandemic has also left its marks on our project, as much through months of laboratory closures as through severe diseases affecting families and friends. It was therefore all the more encouraging to learn how much trust and tolerance still prevail in the scientific community. Especially the latter experience would never have become reality without the always excellent cooperation with the Frontiers Editorial Team.

AUTHOR CONTRIBUTIONS

All authors listed have made a substantial, direct, and intellectual contribution to the work and approved it for publication.

FUNDING

Our research on "apoptosis and senescence in vertebrate development", which also served as the basis for conducting the Research Topic documented here, was supported by a generous grant from the Rolf Dierichs Foundation (Münster) to WK.

REFERENCES

Da Costa, L., Leblanc, T., and Mohandas, N. (2020). Diamond-Blackfan Anemia. *Blood* 136, 1262–1273. doi:10.1182/blood.2019000947

Da Silva-Álvarez, S., Picallos-Rabina, P., Antelo-Iglesias, L., Triana-Martínez, F., Barreiro-Iglesias, A., Sánchez, L., et al. (2019). The Development of Cell Senescence. *Exp. Gerontol.* 128, 110742. doi:10.1016/j.exger.2019.110742

Dunty, W. C., Jr., Chen, S.-Y., Zucker, R. M., Dehart, D. B., and Sulik, K. K. (2001). Selective Vulnerability of Embryonic Cell Populations to Ethanol-Induced Apoptosis: Implications for Alcohol-Related Birth Defects and Neurodevelopmental Disorder. *Alcohol. Clin. Exp. Res.* 25, 1523–1535. doi:10.1111/j.1530-0277.2001.tb02156.x

Dunty, W. C., Jr., Zucker, R. M., and Sulik, K. K. (2002). Hindbrain and Cranial Nerve Dysmorphogenesis Result from Acute Maternal Ethanol Administration. *Dev. Neurosci.* 24, 328–342. doi:10.1159/000066748

Ernst, M. (1926). Über Untergang von Zellen während der normalen Entwicklung bei Wirbeltieren. *Z. Anat. Entwickl. Gesch.* 79, 228–262. doi:10.1007/BF02118264

Fumagalli, S., and Thomas, G. (2011). The Role of P53 in Ribosomopathies. *Semin. Hematol.* 48, 97–105. doi:10.1053/j.seminhematol.2011.02.004

Galluzzi, L., Vitale, I., Aaronson, S. A., Abrams, J. M., Adam, D., Agostinis, P., et al. (2018). Molecular Mechanisms of Cell Death: Recommendations of the Nomenclature Committee on Cell Death 2018. *Cell Death Differ.* 25, 486–541. doi:10.1038/s41418-017-0012-4

Glücksmann, A. (1951). Cell Deaths in Normal Vertebrate Ontogeny. *Biol. Rev. Camb. Philos. Soc.* 26, 59–86. doi:10.1111/j.1469-185x.1951.tb00774.x

Gong, L., Ji, W.-K., Hu, X.-H., Hu, W.-F., Tang, X.-C., Huang, Z.-X., et al. (2014). Sumoylation Differentially Regulates Sp1 to Control Cell Differentiation. *Proc. Natl. Acad. Sci. USA.* 111, 5574–5579. doi:10.1073/pnas.1315034111

González-Gualda, E., Baker, A. G., Fruk, L., and Muñoz-Espín, D. (2021). A Guide to Assessing Cellular Senescence *In Vitro* and *In Vivo*. *FEBS J.* 288, 56–80. doi:10.1111/febs.15570

Hayflick, L., and Moorhead, P. S. (1961). The Serial Cultivation of Human Diploid Cell Strains. *Exp. Cell Res.* 25, 585–621. doi:10.1016/0014-4827(61)90192-6

Herranz, N., and Gil, J. (2018). Mechanisms and Functions of Cellular Senescence. *J. Clin. Invest.* 128, 1238–1246. doi:10.1172/JCI95148

Jokl, A. (1918). Zur Entwickelungsgeschichte des Wirbeltierauges. *Anat. Anz.* 51, 209–239.

Jokl, A. (1920). Zur Entwickelung des Anurenauges. *Beiträge und Referate zur Anatomie und Entwickelungsgeschichte* 59, 211–256. doi:10.1007/BF02047518

Kerr, J. F. R., Wyllie, A. H., and Currie, A. R. (1972). Apoptosis: A Basic Biological Phenomenon with Wide-Ranging Implications in Tissue Kinetics. *Br. J. Cancer* 26, 239–257. doi:10.1038/bjc.1972.33

Kietzmann, T., Knabe, W., and Schmidt-Kastner, R. (2001). Hypoxia and Hypoxia-Inducible Factor Modulated Gene Expression in Brain: Involvement in Neuroprotection and Cell Death. *Eur. Arch. Psychiatry Clin. Neurosci.* 251, 170–178. doi:10.1007/s004060170037

Kotch, L. E., and Sulik, K. K. (1992a). Experimental Fetal Alcohol Syndrome: Proposed Pathogenic Basis for a Variety of Associated Facial and Brain Anomalies. *Am. J. Med. Genet.* 44, 168–176. doi:10.1002/ajmg.1320440210

Kotch, L. E., and Sulik, K. K. (1992b). Patterns of Ethanol-Induced Cell Death in the Developing Nervous System of Mice; Neural Fold States through the Time of Anterior Neural Tube Closure. *Int. J. Dev. Neurosci.* 10, 273–279. doi:10.1016/0736-5748(92)90016-s

Kotch, L. E., Dehart, D. B., Alles, A. J., Chernoff, N., and Sulik, K. K. (1992). Pathogenesis of Ethanol-Induced Limb Reduction Defects in Mice. *Teratology* 46, 323–332. doi:10.1002/tera.1420460403

Kotch, L. E., Chen, S.-Y., and Sulik, K. K. (1995). Ethanol-Induced Teratogenesis: Free Radical Damage as a Possible Mechanism. *Teratology* 52, 128–136. doi:10.1002/tera.1420520304

Kutscher, L. M., and Shaham, S. (2017). Non-Apoptotic Cell Death in Animal Development. *Cell Death Differ.* 24, 1326–1336. doi:10.1038/cdd.2017.20

Majtnerová, P., and Roušar, T. (2018). An Overview of Apoptosis Assays Detecting DNA Fragmentation. *Mol. Biol. Rep.* 45, 1469–1478. doi:10.1007/s11033-018-4258-9

Muñoz-Espín, D., and Serrano, M. (2014). Cellular Senescence: from Physiology to Pathology. *Nat. Rev. Mol. Cell Biol.* 15, 482–496. doi:10.1038/nrm3823

Muñoz-Espín, D., Cañamero, M., Maraver, A., Gómez-López, G., Contreras, J., Murillo-Cuesta, S., et al. (2013). Programmed Cell Senescence during Mammalian Embryonic Development. *Cell* 155, 1104–1118. doi:10.1016/j.cell.2013.10.019

Peter, K. (1936). Untersuchungen über Zelluntergang in der Embryogenese. *Z. Anat. Entwickl. Gesch.* 105, 409–428. doi:10.1007/BF02118396

Rabl, C. (1898-1899). Über den Bau und die Entwicklung der Linse. (II. Theil: Die Linse der Reptilien und Vögel.). *Zeitschr. F. Wiss. Zool.* 65, 257–368.

Rabl, C. (1899-1900). Über den Bau und die Entwicklung der Linse. (III. Theil: Die Linse der Säugethiere. Rückblick und Schluss.). *Zeitschr. F. Wiss. Zool.* 67, 1–138.

Rhinn, M., Ritschka, B., and Keyes, W. M. (2019). Cellular Senescence in Development, Regeneration and Disease. *Development* 146, dev151837. doi:10.1242/dev.151837

Sharpe, P. T. (2016). Dental Mesenchymal Stem Cells. *Development* 143, 2273–2280. doi:10.1242/dev.134189

Storer, M., Mas, A., Robert-Moreno, A., Pecoraro, M., Ortells, M. C., Di Giacomo, V., et al. (2013). Senescence Is a Developmental Mechanism that Contributes to Embryonic Growth and Patterning. *Cell* 155, 1119–1130. doi:10.1016/j.cell.2013.10.041

Turi, Z., Lacey, M., Mistrik, M., and Moudry, P. (2019). Impaired Ribosome Biogenesis: Mechanisms and Relevance to Cancer and Aging. *Aging* 11, 2512–2540. doi:10.18632/aging.101922

Twigg, S. R. F., and Wilkie, A. O. M. (2015). New Insights into Craniofacial Malformations. *Hum. Mol. Genet.* 24, R50–R59. doi:10.1093/hmg/ddv228

Vanden Berghe, T., Grootjans, S., Goossens, V., Dondelinger, Y., Krysko, D. V., Takahashi, N., et al. (2013). Determination of Apoptotic and Necrotic Cell Death *In Vitro* and *In Vivo*. *Methods* 61, 117–129. doi:10.1016/j.ymeth.2013.02.011

Varela-Nieto, I., Palmero, I., and Magariños, M. (2019). Complementary and Distinct Roles of Autophagy, Apoptosis and Senescence during Early Inner Ear Development. *Hear. Res.* 376, 86–96. doi:10.1016/j.heares.2019.01.014

Voss, A. K., and Strasser, A. (2020). The Essentials of Developmental Apoptosis. *F1000Res* 9, 148. doi:10.12688/f1000research.21571.1

Yan, Q., Gong, L., Deng, M., Zhang, L., Sun, S., Liu, J., et al. (2010). Sumoylation Activates the Transcriptional Activity of Pax-6, an Important Transcription Factor for Eye and Brain Development. *Proc. Natl. Acad. Sci. USA.* 107, 21034–21039. doi:10.1073/pnas.1007866107

Yu, T., Volponi, A. A., Babb, R., An, Z., and Sharpe, P. T. (2015). Stem Cells in Tooth Development, Growth, Repair, and Regeneration. *Curr. Top. Dev. Biol.* 115, 187–212. doi:10.1016/bs.ctdb.2015.07.010

Yuan, J., and Kroemer, G. (2010). Alternative Cell Death Mechanisms in Development and beyond. *Genes Dev.* 24, 2592–2602. doi:10.1101/gad.1984410

Conflict of Interest: The authors declare that the research was conducted in the absence of any commercial or financial relationships that could be construed as a potential conflict of interest.

Publisher's Note: All claims expressed in this article are solely those of the authors and do not necessarily represent those of their affiliated organizations, or those of the publisher, the editors and the reviewers. Any product that may be evaluated in this article, or claim that may be made by its manufacturer, is not guaranteed or endorsed by the publisher.

frontiers in Cell and Developmental Biology

REVIEW
published: 02 October 2020
doi: 10.3389/fcell.2020.573511

Extracellular Vesicles Derived From Apoptotic Cells: An Essential Link Between Death and Regeneration

Maojiao Li[1,2,3,4,5], *Li Liao*[1,2,3,4,5]* *and Weidong Tian*[1,2,3,4,5]*

[1] Engineering Research Center of Oral Translational Medicine, Ministry of Education, West China Hospital of Stomatology, Sichuan University, Chengdu, China, [2] National Engineering Laboratory for Oral Regenerative Medicine, West China Hospital of Stomatology, Sichuan University, Chengdu, China, [3] State Key Laboratory of Oral Diseases, West China Hospital of Stomatology, Sichuan University, Chengdu, China, [4] National Clinical Research Center for Oral Diseases, West China Hospital of Stomatology, Sichuan University, Chengdu, China, [5] Department of Oral and Maxillofacial Surgery, West China Hospital of Stomatology, Sichuan University, Chengdu, China

Apoptosis is a universal and continuous event during tissue development, restoration, repair, and regeneration. Mounting evidence has demonstrated that apoptosis is essential for the activation of tissue regeneration. However, the underlying mechanism remains elusive. A striking development in recent years comes from research on extracellular vesicles (EVs) derived from apoptotic cells. During apoptosis, cells secrete vesicles of various sizes containing various components. Apoptotic cell-derived EVs (ApoEVs) have been found to transit to neighboring cells or cells in distant tissues through the circulation. These vesicles could act as containers to transmit the nucleic acid, protein, and lipid signals to target cells. ApoEVs have been shown to promote regeneration in the cardiovascular system, skin, bone, muscle, kidney, etc. Moreover, several specific signaling pathways mediating the anabolic effects of ApoEVs have been classified. In this review, we comprehensively discussed the latest findings on the function of ApoEVs in tissue regeneration and disease prevention. These findings may reveal unexpected clues regarding the regulatory network between cell death and tissue regeneration and suggest novel targets for regenerative medicine. The findings discussed here also raise the question whether and to what extent ApoEVs contribute to embryonic development. This question is all the more urgent because the exact functions of apoptotic events during numerous developmental processes are still largely unclear.

Keywords: apoptosis, apoptotic cell derived extracellular vesicles, functional biomolecules, cell death, regeneration

OPEN ACCESS

Edited by:
Stefan Washausen,
Universität Münster, Germany

Reviewed by:
Ivan Poon,
La Trobe University, Australia
Christopher Gregory,
The University of Edinburgh, United Kingdom

***Correspondence:**
Li Liao
lliao@scu.edu.cn
Weidong Tian
drtwd@sina.com

Specialty section:
This article was submitted to Cell Death and Survival, a section of the journal Frontiers in Cell and Developmental Biology

Received: *17 June 2020*
Accepted: *14 September 2020*
Published: *02 October 2020*

Citation:
Li M, Liao L and Tian W (2020) Extracellular Vesicles Derived From Apoptotic Cells: An Essential Link Between Death and Regeneration. Front. Cell Dev. Biol. 8:573511. doi: 10.3389/fcell.2020.573511

INTRODUCTION

Apoptosis refers to the spontaneous and orderly cell death and is controlled by a cluster of genes to maintain homeostasis (Kroemer et al., 2005). It is estimated that over 50 billion cells undergo apoptosis in the human body every day to maintain homeostasis (Davidson and Steller, 1998; Pellettieri and Sanchez Alvarado, 2007; Bergmann and Steller, 2010; Fuchs and Steller, 2011; Hochreiter-Hufford et al., 2013; Arandjelovic and Ravichandran, 2015). Apoptosis is a common phenomenon in embryonic development, cell differentiation, tissue regeneration, and

other physiological processes, as well as in tumor, immune deficiency, organ atrophy, and other pathological processes. During organogenesis, the coordination of apoptosis and mitosis can maintain a constant number of cells in tissues and organs to shape the normal embryos, especially in the CNS and in the immune system (Penaloza et al., 2006; Zakeri et al., 2015). Apoptosis also plays an important role in the sculpting and reconstruction of tissue morphology (Kroemer et al., 2005; Elmore, 2007). Certain differentiated cells are regularly eliminated and replaced by the progeny of adult stem cells to maintain anatomical structure and function, which is usually called the balance between death and regeneration. As a part of normal embryonic development and tissue homeostasis, apoptosis has been shown to play a pivotal role in balancing death and regeneration. During apoptosis, apoptotic cells secrete vesicles of various sizes named apoptotic cell-derived extracellular vesicles (ApoEVs). Emerging evidence has revealed that extracellular vesicles could carry beneficial substances and be essential for cell communication. ApoEVs could be engulfed by target cells and promote regeneration in skin, bone, muscle, etc., by transporting bioactive molecules (e.g., proteins, lipids, and nucleic acids). Although several reviews have summarized the role of ApoEVs in immune regulation and cancer development (Caruso and Poon, 2018; Gregory and Dransfield, 2018; Gregory and Paterson, 2018; Laurenzana et al., 2018; Muhsin-Sharafaldine and McLellan, 2018a,b; Pavlyukov et al., 2018; Grant et al., 2019; Battistelli and Falcieri, 2020), the emerging findings of ApoEVs in tissue regeneration and embryonic development have not been systematically reviewed. Here, we introduce the function of ApoEVs in tissue regeneration, embryonic development, and disease prevention and discuss the therapeutic benefits of ApoEVs in regenerative medicine.

APOPTOSIS

The Process of Apoptosis

In most cases, apoptotic cells show very similar patterns of morphological changes. The noticeable morphological changes associated with apoptosis are the shrinkage of the cell, condensation of the nucleus and chromatin, breakage of the nucleus and cytoplasmic organelles, and cell membrane detachment and blebbing (Hacker, 2000; Saraste and Pulkki, 2000; Kroemer et al., 2005). During this process, a series of membrane-wrapped structures named ApoEVs are formed through cell membrane budding and blebbing (Merchant et al., 2017), and then are engulfed and digested by target cells (Tower, 2015). The clearance of cellular "corpses" commences at the earliest stages of apoptosis. Timely and effective phagocytosis of apoptotic cells and their contents can hardly recruit inflammatory cells and is conducive to avoid inflammation (Arandjelovic and Ravichandran, 2015; Medina et al., 2020).

The Mechanisms of Apoptosis

In 2012, the Nomenclature Committee on Cell Death (NCCD) initiated a new classification of cell death based on measurable biochemical characteristics, which divides the apoptotic pathway into intrinsic and extrinsic apoptosis.

The Intrinsic Apoptotic Pathway

The intrinsic apoptotic pathway is also known as the mitochondrial/cytochrome c pathway (Tower, 2015). Cytochrome c release from mitochondria is the key step. The decrease in mitochondrial transmembrane potential ($\Delta\psi$) is the first step of mitochondrial-mediated apoptosis. Cellular stresses, including DNA damage, oncogene activation, hypoxia, and oxidative stress, leads to the opening of or damage to the mitochondrial permeability transition pore (MPTP), a decrease in $\Delta\psi$, and an increase in mitochondrial permeability, which promote the release of cytochrome c and apoptosis-inducing factor (AIF) (Susin et al., 1999). Cytochrome c can recruit and activate Caspase-9. Thus, Caspase-9 activates caspase cascade reactions (Caspase-3, -6, and -7) to initiate irreversible caspase-dependent apoptosis (Slee et al., 1999; Joza et al., 2001; Elmore, 2007; Kuribayashi et al., 2014).

The Extrinsic Apoptotic Pathway

The extrinsic pathway is mediated by the death receptors of the tumor necrosis factor (TNF) receptor type 1 superfamily embedded on the cell membrane (Guicciardi and Gores, 2009; Tower, 2015). The binding of Fas ligand to Fas receptor recruits the adapter protein Fas-associated death domain protein (FADD), which recruits Caspase-8 zymogens to form the Caspase-8 activator named death-inducing signaling complex (DISC). Then the pro-Caspase-8/10 is activated through autocatalysis (Boatright and Salvesen, 2003), which initiates the apoptotic process (Elmore, 2007) and leads to the activation of the downstream effectors Caspases-3, -6, and -7 (Broker, 2005).

APOPTOSIS PROMOTES TISSUE DEVELOPMENT AND REGENERATION

Apoptosis has been regarded as a critical control point in development. Apoptosis is essential for successful embryonic development and the maintenance of normal tissue homeostasis (von Mühlen and Tan, 1995; Rieux-Laucat et al., 2003; Gaipl et al., 2005; Macchi et al., 2015). In tissue development, apoptosis can sculpt structures, drive morphogenesis, regulate cell number, eliminate useless, potentially dangerous and senescent cells, and participate in the regulation of regeneration and differentiation (Penaloza et al., 2006; Fuchs and Steller, 2011; Zakeri et al., 2015). In addition, some findings have shown the link between cell death and tissue regeneration. As proposed by Kondo in 1988 (Kondo, 1988), apoptosis promotes cell proliferation during tissue regeneration (Kondo, 1988; Hwang et al., 2004; Li et al., 2004, 2010; Ryoo et al., 2004; Vlaskalin et al., 2004; Kondo et al., 2006; Tseng et al., 2007; Chera et al., 2009; Pellettieri et al., 2010), which is named "apoptosis-induced compensatory proliferation (AIP)" (Huh et al., 2004; Pérez-Garijo et al., 2004; Kondo et al., 2006; Fan and Bergmann, 2008). For example, in the mid-gastric amputation model, effector caspases trigger the release of the mitogen Wnt3 to stimulate proliferation and regeneration

during apoptosis (Chera et al., 2009). Similarly, caspase activation promotes regeneration in the injured site in Xenopus tadpole tails after amputation (Tseng et al., 2007).

Apoptosis also subtly promotes cell differentiation. Caspase family activation in apoptosis is closely related to cell differentiation. For example, Caspases-3 and -9 promote monocyte differentiation to macrophages but not dendritic cells (Sordet et al., 2002). The absence of Caspase-8 leads to stagnation of macrophage differentiation. In stem cells (SCs), Caspase-3 can also mediate the differentiation of bone marrow stromal cells, neural SCs, embryonic SCs, and haematopoietic SCs (Feinstein-Rotkopf and Arama, 2009). The increased proliferation and regeneration can compensate for cell loss in the injured tissues (Brockes and Kumar, 2008).

Apoptosis can restore tissue regeneration by promoting the elimination of senescent cells (SnCs). SnCs accumulate in many vertebrate tissues with age and secret senescence-associated secretory phenotype (SASP) to inhibit regeneration (Downward et al., 2008; van Deursen, 2014). Jeon et al. (2017) found that selective elimination of SnCs attenuated the development of post-traumatic osteoarthritis (OA), reduced pain, and increased cartilage development. Intra-articular injection of a senolytic molecule that selectively killed SnCs promote repair and regeneration in aged mice. Thus, locally induced apoptosis of senescent cells is beneficial for tissue regeneration. In addition, apoptosis and cell senescence are complementary processes in the regression of embryonic tissues and share common regulatory signals. During the formation of free digits in the developing limbs, the Btg/Tob gene family is upregulated. Btg2 overexpression in mesodermal progenitors of the limbs increases oxidative stress and induces cell death and cell senescence, which inhibits limb outgrowth *in vivo* (Lorda-Diez et al., 2015).

APOPTOTIC CELL-DERIVED EXTRACELLULAR VESICLES

Apoptotic cell-derived extracellular vesicles (ApoEVs) are a group of subcellular membrane-bound extracellular vesicles generated during the decomposition of dying cells. ApoEVs can be generated by many types of cells, such as stem cells, immunocytes, precursor cells, osteoblasts, and endothelial cells (Jiang et al., 2017). At present, the classification of the ApoEVs is still controversial. Apoptotic bodies (ApoBDs) were the first identified ApoEVs (Ihara et al., 1998). However, with the development of detection technology, researchers have found smaller vesicles (Simpson and Mathivanan, 2012) produced by dying cells in addition to traditional apoptotic bodies. Although there is no well-defined criteria to distinguish ApoBDs from other ApoEVs, the vesicles can be classified by diameter: larger membrane-wrapped vesicles termed ApoBDs/ABs have diameters of 1000–5000 nm (Atkin-Smith et al., 2015), and the smaller vesicles termed apoptotic microvesicles (ApoMVs) or exosome-like ApoEVs (Park et al., 2018) have diameters of 50–1000 nm (Schiller et al., 2012; Ainola et al., 2018). Lacking standard classification makes it difficult to draw accurate conclusions on the functions of ApoEVs. In order to unify the classification, we re-summarize the subtypes of ApoEVs according to the size of the vesicles extracted by different isolation or characterization methods in **Tables 1**, **2**.

How to identify and isolate ApoEVs remains a critical issue. During apoptosis, the most typical feature is the transfer of phosphatidylserine (PS) to the surface of the lipid layer, which is also characteristic of ApoEVs (Hengartner, 2001). The translocated PS binds to Annexin V, a 36 kDa calcium phospholipid-binding protein (Kurihara et al., 2008). *In vitro*, Annexin V is widely used to identify and image cell death and ApoEVs because of its high binding affinity with PS (Subiros-Funosas et al., 2017). Another membrane change is the oxidation of surface molecules, which helps the binding of thrombospondin (Tsb) and the complement protein C3b to the membrane (Wu et al., 2019) and, in turn, is recognized by the recipient cells. Therefore, Annexin V, Tsb, and C3b are well-accepted ApoEVs markers (Akers et al., 2013). Fluorescence-activated cell sorting (FACS) and differential centrifugation are the most commonly used methods to purify ApoEVs. FACS achieves a purity of up to 99%, while differential centrifugation achieves up to 95% purity (Phan et al., 2018). The flow cytometry-based method can effectively detect the contents and cell origins of ApoBDs (Jiang et al., 2017). However, FACS can only detect the large ApoBDs since most flow cytometers only detect micron-sized cells or vesicles and cannot distinguish ApoBDs and ApoMVs. Differential centrifugation can isolate ApoEVs of different sizes, but the purity is lower than that of FACS. This method may not be suitable for isolating ApoEVs from complex samples compared with FACS. The protocol only compares the purity of ApoEVs extracted by these two methods, but there has been no functional comparison of ApoEVs extracted by different methods. The fluorescent labeling technique with Trp-BODIPY cyclic peptide (Subiros-Funosas et al., 2017) and the *in situ* ligation technique (Hauser et al., 2017) may be emerging technologies for distinguishing ApoEVs from other vesicles. To progress the field, it is critical to identify suitable criteria to distinguish different subtypes of ApoEVs and develop better experimental systems to track ApoEV formation.

The Formation of ApoEVs

The formation of ApoEVs can be divided into three key steps: (Step 1) membrane blebbing on the cell surface, which is now considered a prerequisite for the formation of ApoEVs (Lane et al., 2005); (Step 2) apoptotic membrane protrusions in the form of microtubule spikes, apoptopodia, and beaded apoptopodia, which secrete approximately 10–20 ApoEVs each time (Xu et al., 2019); and (Step 3) the formation of ApoEVs.

The production of ApoEVs is regulated in a dose- and time-dependent manner by different molecular factors, such as the Rho-associated protein kinase (ROCK1) (Coleman et al., 2001; Gregory and Dransfield, 2018; Aoki et al., 2020) and myosin-light chain kinase (MLCK) (Mills et al., 1998). Inhibitors of ROCK1, MLCK, and caspases can suppress this process. Functional microtubules help nuclear shrinkage, and MLCK contributes to the packaging of nuclear material into ApoEVs (Zirngibl et al., 2015). Actomyosin leads to an increase in cell contraction and hydrostatic pressure and the formation

TABLE 1 | The function of ApoEVs in regeneration.

Nomenclature used by the authors	ApoEVs types according to sizes	Original cell	Recipient cell	Diseases/ experimental effect	Mechanism	Role of vesicles	References
ApoBDs	Mix of ApoBDs and ApoMVs	Endothelial cells	Endothelial progenitor cells	Promote proliferation	Unclear	Unclear	Hristov et al., 2004
ApoBDs	Unclear	Cardiomyocytes	Cardiomyocyte precursors	Chronic post-infarction heart failure	Promote SC proliferation and differentiation	miRNA transfer?	Tyukavin et al., 2015
ApoBDs	ApoBDs	Macrophages	Epithelial cells	Promote proliferation	MiR-221 miR-222	miRNA transfer	Zhu et al., 2017
ApoBDs	Mix of ApoBDs and ApoMVs	Endothelial cells	Vascular cells	Atherosclerosis	Induced CXCL12-dependent vascular protection	miRNA transfer	Zernecke et al., 2009
ApoBDs	Mix of ApoBDs and ApoMVs	Epithelial stem cells	Epithelial stem cells	Promote proliferation and division	Activate Wnt8a	mRNA transfer	Brock et al., 2019
ApoBDs	ApoBDs	BMSCs	BMSCs	Osteopenia	Activate the Wnt/β-catenin pathway	miRNA transfer	Liu et al., 2018
ApoBDs	Mix of ApoBDs and ApoMVs	MSCs	Endothelial cells	Myocardial infarction	Regulate autophagy	Active lysosome function	Liu et al., 2020
CRK-MVs	ApoMVs	podocytes	Epithelial cells	Renal repair	Induce compensatory proliferation	Paracrine mediators?	Bussolati and Camussi, 2017
MOC- ApoBDs	ApoBDs	Osteoclasts	Pre-osteoblasts	Bone remodeling	Activate PI3K/AKT/mTOR/S6K signaling	RANK activator	Ma et al., 2019

ApoBDs, apoptotic bodies; SCs, stem cells; BMSCs, bone mesenchymal stem cells; MSCs, mesenchymal stem cells; PI3K, phosphoinositide 3-kinase; AKT, AKT Ser–Thr kinase; S6K, ribosomal protein S6 kinase; RANK, nuclear factor kappa B.

of blebs (Orlando et al., 2006). The plasma membrane channel pannexin 1 (PANX1) was recently described as a negative regulator of ApoBDs formation since trovafloxacin (a PANX1 inhibitor) promoted apoptotic cell disassembly (Poon et al., 2014a). However, the factors driving the formation of these individual ApoEVs is still unclear. The synergism of intracellular and extracellular factors is necessary for breaking apoptotic cells into individual vesicles, and some unknown elements separate membrane protrusions from the main cell body.

ApoEVs Are Biological Vectors Carrying Functional Biomolecules

Extracellular vesicles (e.g., Exos and MVs) mediate intercellular communication by carrying signaling molecules (Buzas et al., 2014). ApoEVs envelop the remaining components of dead cells (Crescitelli et al., 2013), which include proteins (e.g., from the nucleus, mitochondria, and plasma membrane), lipids and nucleic acids (e.g., mRNA, long non-coding RNA, rRNA, miRNA, or fragments of these intact RNA molecules). ApoEVs have been found to act as containers to carry the remnants of their original cells to promote regeneration (Halicka et al., 2000). Horizontal transfer of DNA can occur between adjacent cells through ApoEVs. For example, the DNA contained in endothelial cell-derived ApoBDs can induce the proliferation and differentiation of human endothelial progenitor cells *in vitro* (Hristov et al., 2004). DNA packaged into lymphoma-derived ApoBDs can be engulfed by fibroblasts, resulting in gene recombination (Holmgren et al., 1999). By shuttling microRNA-221/222, macrophage-derived ApoBDs promote the proliferation of lung epithelial cells (Zhu et al., 2017). MicroRNAs enclosed in ApoBDs from cardiomyocytes enhance the proliferation and differentiation of resident SCs *in vitro* (Tyukavin et al., 2015). Mesenchymal stem cells (MSCs) can engulf ApoBDs and reuse ApoBD-derived ubiquitin ligase RNF146 and miR-328-3p to promote bone regeneration (Liu et al., 2018). However, in Kogianni et al. (2008) showed that dying osteocytes release ApoBDs containing receptor activator of nuclear factor kappa-B ligand (RANKL) to recruit replacement osteoclasts, which can initiate osteoclastogenesis and localized bone destruction. Administration of ApoBDs carrying miR-126 inhibits atherosclerosis and induces CXCL12-dependent vascular protection (Zernecke et al., 2009). Besides, endothelial cell-derived miR-126 is transferred in ApoMVs to promote vascular regeneration and prevent atherogenesis (Nazari-Jahantigh et al., 2012). Interestingly, DNA and RNA cannot be simultaneously packaged into ApoBDs derived from HL-60 cells. Over 90% of ApoBDs containing RNA did not

TABLE 2 | The functions of ApoEVs in other diseases.

Nomenclature used by the authors	ApoEVs types according to sizes	Original cell	Recipient cell	Diseases/ experimental effect	Mechanism	Role of vesicles	References
ApoEVs	ApoBDs	Tumor cells	DCs	Antitumour immunity	Induce CD8+ and CD4+ T cell response	Activate (MHC)-I and MHC-II pathways	Horrevorts et al., 2019
ApoBDs	Unclear	Leukemic B cells	DCs	B-CLL	Antitumour immunity	Antigen presentation	Hus et al., 2005
ApoEVs	ApoBDs	Melanoma cells	Injected into mice	Melanoma	Antitumour immunity	Antigen presentation	Muhsin-Sharafaldine et al., 2016
ApoEVs	ApoMVs	Macrophages	DCs	Tuberculosis infection diseases	Antimicrobial immunity	Antigen presentation	Winau et al., 2006
ApoBDs	Unclear	Prion-infected apoptotic neurons	DCs	Prion disease	Promote clearance of prion via Mfge8	Prion transfer	Kranich et al., 2010
ApoPMN-MY	ApoMVs	Neutrophil	CD25+Th cells	Maintain immunological tolerance	Suppress the proliferation of CD25+Th cell	IL-2 suppressor	Shen et al., 2017
ApoBDs	Unclear	β cells	DCs	Type 1 Diabetes	Immune tolerance	Antigen presentation	Marin-Gallen et al., 2010

ApoEVs, apoptotic extracellular vesicles; DCs, dendritic cells; MHC, major histocompatibility complex; ApoBDs, apoptotic bodies; B-CLL, B-cell chronic lymphocytic leukemia; IL-2, Interleukin-2.

contain DNA, and vice versa, ApoBDs containing DNA did not contain RNA, which suggests that some biomolecules may selectively enter ApoEVs (Halicka et al., 2000). Human primary monocyte-derived macrophages can engulf ApoBDs containing autoantigens, suggesting that ApoEVs can play a role in antigen presentation in immunoregulation (Tran et al., 2002). Compared with the secretion of cytokines and growth factors, this mode of intercellular communication circumvents the "signal dilution effect" of soluble products released from apoptotic cells. Bioactive molecules entering the vesicles can act effectively on adjacent cells or distant tissues through circulation.

ApoEVs Can Be Recognized and Engulfed by Target Cells

Several signaling molecules expressed on ApoEVs can be recognized by target cells. Segundo et al. (1999) proposed that apoptotic blebs recruit macrophages to death sites. This study showed that many CD molecules (including CD11a, CD21, CD22, and CD54) were partly released from germinal center B cells in the form of ApoEVs, which stimulated the chemotaxis of human monocytes.

The inversion of PS and the change in oxidation of surface molecules also contribute to the recognition of ApoEVs. Besides, CX3CL1 and ICAM-3 are potential recognition proteins on ApoEVs. CX3CL1, an intercellular adhesion molecule known as a "find-me" signal, is expressed on ApoEVs and can be recognized by the CXCL1 receptor (CXCL1R) expressed on mononuclear phagocytes. The interaction between CX3CL1 and CX3CR1 induces the migration of macrophages to apoptotic Mutu-BL cells (Truman et al., 2008). ICAM-3, an intercellular adhesion molecule expressed on the ApoEVs derived from leukocytes, can attract macrophages to induce leukocyte death (Torr et al., 2012). In summary, signal molecules embedded on the surface of ApoEVs may act as signals for engulfing, transferring, and mediating intercellular communication.

THE FUNCTION OF APOPTOTIC EXTRACELLULAR VESICLES IN TISSUE REGENERATION

The transport of functional molecules through vesicles can be a new way to promote cell proliferation, tissue regeneration, and repair. Since ApoEVs can transmit bioactive molecules into neighboring cells or the cells in distant tissues through circulation, they play an active role in maintaining homeostasis after being phagocytized. ApoEVs produced by different cells have different effects on physiological and pathological processes. Here, we discuss the role of ApoEVs in tissue regeneration and disease treatment.

ApoEVs Trigger the Clearance of Damaged or Senescent Cells

Apoptotic cells are primarily engulfed and cleared by phagocytes, which is of considerable significance to the dynamic equilibrium and immune response of healthy tissues. The prompt removal of dead cells by phagocytes can prevent cytotoxic substances or antigens from leaking into surrounding tissues (Poon et al., 2014b), effectively leading to the maintenance of tissue homeostasis. This process can be divided into three stages: recruitment, identification, and phagocytosis (Gardai et al., 2006; D'mello et al., 2009; Ravichandran, 2011).

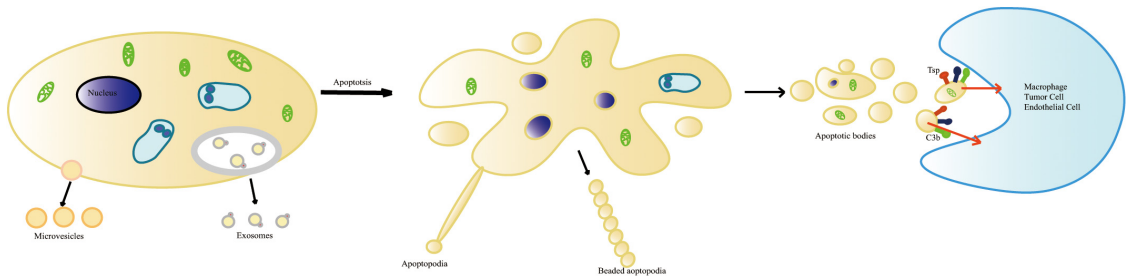

FIGURE 1 | The formation of apoptotic cell-derived extracellular vesicles during apoptosis. Healthy cells generate two types of vesicles: exosomes and microvesicles. Apoptotic progress includes several stages: shrinkage of the cell, the condensation of the nucleus and chromatin pyknosis or karyorrhexis, the breaking of the nucleus, and cytoplasmic organelles and cell membrane detaching and blebbing. The disintegration of the cellular content into distinct membrane-enclosed vesicles termed apoptotic cell-derived extracellular vesicles (ApoEVs). ApoEVs can be engulfed by different cells mediated by specific recognition between recognition receptors and ligands. During apoptosis, the surface of the ApoEVs reveals specific changes. These changes include phosphatidylserine ectropion to bind with Annexin V and oxidation of surface molecules to bind with Thrombospondin (Tsp) or the complement protein C3b.

Recipient cells recognize "eat-me" signals such as PS on ApoEVs and initiate the engulfment process (Peter et al., 2008; Battistelli and Falcieri, 2020; **Figure 1**). For example, dendritic cells (DCs) engulf glycan-modified melanoma-derived ApoEVs carrying dendritic cell-specific intercellular adhesion molecule-3-grabbing non-integrin (DC-SIGN) ligands (Horrevorts et al., 2019). Apoptosis induces the production of neuronal apolipoprotein-E (apoE), which helps to clear ApoBDs via apoE–receptor interactions (Elliott et al., 2007). Microglial cells phagocytose and degrade apoptotic material from ApoBDs via microglial lysosomal and proteasomal pathways mediated by the CD36 scavenger receptor (Stolzing and Grune, 2004). Suppression of the formation of ApoBDs impairs the clearance of apoptotic or damaged cells by monocytes and macrophages (Orlando et al., 2006; Witasp et al., 2007), suggesting that ApoEVs can effectively promote the clearance of apoptotic cells.

ApoEVs and Cell Survival, Proliferation, and Differentiation

Apoptotic cell-derived EVs are closely related to cell survival, proliferation, and differentiation. For example, ApoBD-rich medium (ApoBD-RM) from endothelial cells (ECs) promotes the proliferation of human endothelial progenitor cells (EPCs) *in vitro*, whereas ApoBD-depleted medium does not. ApoBDs engulfed by EPCs enhance EPC proliferation and differentiation (Hristov et al., 2004), which may contribute to the repair of damaged endothelial cells.

In addition, ApoBDs from cardiomyocytes enhance the proliferation and differentiation of resident stem cells (SCs) by transporting specific miRNAs (Tyukavin et al., 2015). Macrophage-derived ApoBDs promote the proliferation of recipient epithelial cells through ApoBD shuttling of miR-221 and miR-222 (Zhu et al., 2017). Endothelial cell-derived ApoBDs facilitate the survival of recipient vascular cells (human umbilical vein endothelial cells, mouse aortic endothelial cells, and smooth muscle cells) to survive. Selective enrichment of miR-126 in apoptotic endothelial cell-derived microvesicles stimulates the production of the chemokine CXCL12 in target cells, suppressing progenitor cell apoptosis (Zernecke et al., 2009).

The Wnt/β-catenin signaling pathway is a group of evolutionarily conserved signals that are essential in embryonic development and tissue regeneration. In a zebrafish model, ApoBDs containing Wnt-8a from dying SCs can promote the proliferation and regeneration of living epithelial cells and the communication with adjacent SCs. After phagocytizing ApoBDs, the Wnt signaling is activated to stimulate the division of basal SCs to maintain the total number of basal SCs in the tissue (Brock et al., 2019). ApoBDs activate the Wnt/β-catenin pathway to promote bone marrow mesenchymal stem cell (BMSC) proliferation and osteogenic, and lipogenic differentiation in Fas-deficient MRL/lpr and Caspase $3^{-/-}$ mice (Liu et al., 2018). Thus, activating the Wnt pathway via ApoEVs is essential for promoting cell proliferation and differentiation.

ApoEVs Promote Tissue Development and Regeneration

ApoEVs Promote the Regeneration of the Cardiovascular System

Mesenchymal stem cells-derived ApoBDs engulfed by recipient endothelial cells (ECs) promote angiogenesis and cardiac functional recovery in a rat myocardial infarction (MI) model by regulating autophagy (Liu et al., 2020). Cardiomyocyte-derived ApoBDs stimulate the proliferation and differentiation of cardiomyocyte precursors. In a Wistar rat heart failure model, cardiomyocyte-derived ApoBDs improve the heart's systolic function during the early apoptotic period (Tyukavin et al., 2015). In addition, human endothelial cell-derived ApoMVs carrying miR-126 upregulate CXCL12 in vascular cells, which recruits the incorporation of Sca-1+ progenitor cells to promote vascular protection and inhibit atherosclerosis (Zernecke et al., 2009). These findings underscore the functions of ApoEVs in cardiovascular regeneration.

ApoEVs Promote the Regeneration of the Kidney

CRK-containing microvesicles (CRK-MVs), a kind of ApoMV found in damaged glomeruli (Gupta et al., 2017), have been found to promote kidney regeneration. Apoptotic

podocyte-derived ApoMVs might induce compensatory proliferation of parietal epithelial cells and injured tubular epithelial cells. Notably, ApoMVs induce compensatory proliferation in most of the analyzed target epithelial cells (Gupta et al., 2017). Apoptotic MSC-derived EVs act as paracrine signals to promote the repair of nephrons after injury (Bussolati and Camussi, 2017).

ApoEVs Promote Bone Regeneration

Osteoporosis is a kind of systemic osteopathy caused by the imbalances in bone formation and bone resorption. Cerri (2005) showed that osteoblasts engulf bone cell-derived ApoBDs during the rat maxilla alveolar bone formation. Recently, (Liu et al., 2018) showed that systemic injection of exogenous BMSC-derived ApoBDs reversed MSC damage and improved the osteopenia in ovariectomized (OVX) mice. MSCs can engulf ApoBDs via integrin αvβ3 and inhibit Axin. The ApoBD-derived ubiquitin ligases RNF146 and miR-328-3p, thus activate the Wnt/β-catenin pathway. This finding confirms the role of ApoBDs in maintaining bone homeostasis and suggests the potential of ApoBDs in treating osteoporosis. ApoBDs also mediate intercellular communication between osteoclasts and osteoblasts. In bone remodeling, mature osteoclast-derived ApoBDs (mOC-ApoBDs) are taken up by pre-osteoblastic cells and prompt osteogenic differentiation by activating phosphoinositide 3-kinase (PI3K)/AKT Ser–Thr kinase (AKT) signaling (Ma et al., 2019; **Table 1** and **Figure 2**). Moreover, previous studies suggested that osteocyte-derived ApoBDs could recruit the osteoclasts and initiate local bone resorption (Yuan et al., 2018), suggesting that ApoBDs derived from different sources play distinct roles in bone remodeling.

ApoEVs During Embryonic Development

Apoptosis can be detected at many stages of mammalian early embryonic development. In the process of embryo formation and development, apoptosis can remove abnormal and redundant cells. Apoptosis in mammalian blastocysts is very important for the further development of normal embryos (Hardy, 1999; Fabian et al., 2005; Jezek and Kozina, 2009). During embryonic development, apoptosis can help systems matching, sculpt the body, remove the outlived sculpture, and protect the organism, especially in neurulation, eye or ear development/invagination, limb modeling, development of the immune system (Cohen, 1999; Buss et al., 2006; Lorda-Diez et al., 2015; Hosseini and Taber, 2018). Jurisicova et al. (1996) found that a large number of ApoBDs in fragmented human embryos during embryonic development has increased since the blastocyst stage (Fabian et al., 2005). In limb modeling, dying cells generate ApoBDs which are engulfed by macrophages (Penaloza et al., 2006).

Since ApoEVs could affect the proliferation and differentiation of stem cells in adult tissue, it is highly probable that a large number of ApoEVs also play irreplaceable roles in embryonic development. Until now, there has been little evidence on whether ApoEVs participate in the formation and development of embryos directly. Further investigations are necessary to uncover the possible roles of ApoEVs in embryonic development.

THE POTENTIAL OF ApoEVs IN DISEASE TREATMENT

Based on the importance of ApoEVs in tissue regeneration, ApoEVs have been applied in the treatment of several diseases including degenerative diseases, tumors, and inflammatory diseases.

ApoEVs in Degenerative Disease Treatment

In the cardiovascular system, ApoBDs from MSCs can promote angiogenesis and the heart's systolic function recovery to prevent myocardial infarction via the regulation of autophagy (Tyukavin et al., 2015; Liu et al., 2020). Cardiomyocyte-derived ApoBDs revive cardiomyocyte precursors, leading to the alleviation of heart failure in the early stage. Endothelial cell-derived ApoMVs can protect the vasculature and inhibit atherosclerosis by transferring miRNAs (Zernecke et al., 2009). In the urinary system, the ApoMVs can restore injured tubular epithelial cells and facilitate nephron repair via compensatory proliferation (Gupta et al., 2017). In bone diseases, BMSC-derived ApoBDs can maintain bone homeostasis and treat osteoporosis. Thus, ApoEVs may be a new tool for degenerative disease treatment. However, the above findings are limited to the experimental stage. Extensive study of the mechanism and effect of ApoEVs in the degenerative disease treatment are necessary before the clinical application.

ApoEVs in Tumor Treatment

Apoptotic cell-derived EVs from tumor cells have been shown to initiate antitumour immunity (Horrevorts et al., 2019). ApoEVs transfer pathogen carcinogens to antigen-presenting cells and protect the host from the tumor (Horrevorts et al., 2019). ApoEVs derived from tumor cells contain a high level of mannose glycans. These EVs can be engulfed by dendritic cells (DCs) more easily via dendritic cell-specific intercellular adhesion molecule-3-grabbing non-integrin (DC-SIGN). These DCs then act through both major histocompatibility complex (MHC)-I and MHC-II pathways to induce $CD8^+$ and $CD4^+$ T cell responses. It has been shown that allogeneic DCs engulfing ApoBDs from leukemic B cells stimulate antitumour immunity in B-cell chronic lymphocytic leukemia (B-CLL), suggesting that ApoBDs can serve as vaccines in tumor immunotherapy (Chang et al., 2000; Hus et al., 2005). ApoEVs derived from apoptotic melanoma cells (B16-OVA cells) initiate antitumour immunity and protect mice against subsequent tumor progression. The tumor antigen PMEL was found in ApoEVs and T cells, confirming that ApoEVs facilitate the transport of tumor antigens to antigen-presenting cells to promote antitumour immunity (Muhsin-Sharafaldine et al., 2016). Interestingly, although the PMEL in ApoEVs was lower than that in other vesicles, the antitumour protective effect of ApoEVs was more significant, suggesting that ApoEVs work through a different mechanism. Taken together, these findings indicate that ApoEVs can act as mediators of intercellular communication in the tumor. Specific ApoEVs may be useful biomarkers in monitoring disease progression. But

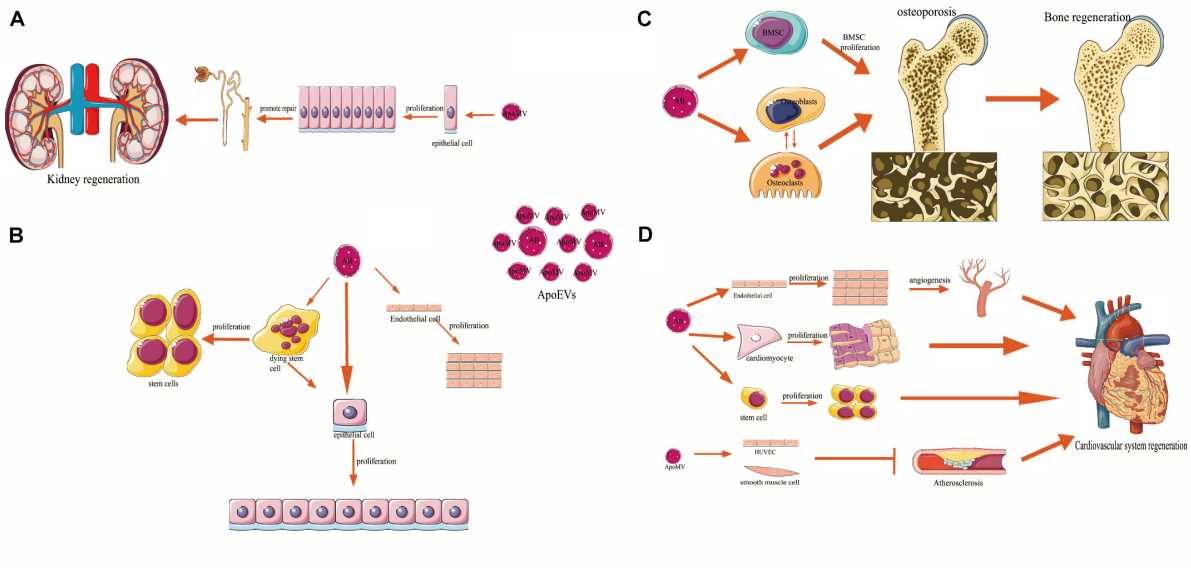

FIGURE 2 | The relation of apoptotic cell-derived extracellular vesicles (ApoEVs) to cell survival, proliferation, differentiation, and tissue regeneration. ApoEVs can be divided into two groups: the larger apoptotic bodies (ApoBDs, ABs) and the smaller apoptotic microvesicles (ApoMVs). **(A)** ApoMVs induce compensatory proliferation of parietal epithelial cells and injured tubular epithelial cells, thus helping nephron repair. **(B)** *In vitro* experiments, ApoBDs engulfed by human endothelial cells, and epithelial cells can promote the proliferation of their recipient cells, respectively. Besides, ApoBDs from dying stem cells can promote the proliferation and regeneration of living epithelial cells and the communication with adjacent stem cells. **(C)** Bone marrow mesenchymal stem cells and osteoblasts have been found to engulf ApoBDs. Exogenous ApoBDs reversed the MSCs damage and improved the osteopenia, which can promote bone regeneration. Besides, ApoBDs can mediate intercellular communication signal mechanisms in osteoclast–osteoblast, suggesting its function in bone regeneration. **(D)** Endothelial cells (ECs) can engulf ApoBDs and promote angiogenesis and cardiac functional recovery. ApoBDs stimulated proliferation and differentiation of cardiomyocyte precursors and resident stem cells (SCs). ApoMVs transfer signals to vascular cells, induce vascular protection and inhibit atherosclerosis, which underlines the functions of ApoEVs in regeneration of the cardiovascular system.

novel test methods to detect ApoEVs and their cargos efficiently and accurately are necessary.

ApoEVs in Immune and Inflammatory Disease Treatment

Apoptotic cell-derived EVs from apoptotic macrophages infected with *M. tuberculosis* can be engulfed by dendritic cells derived from peripheral blood mononuclear cells and splenic dendritic cells. Antigens on the ApoEVs are then presented to naïve $CD4^+$ or $CD8^+$ T cells to trigger antimicrobial immunity and eliminate *M. tuberculosis*, suggesting the potential use of ApoEVs as a vaccine (Winau et al., 2006). Whether ApoEVs can play a role in regulating the antimicrobial immunity against other pathogens remains to be explored. ApoBDs derived from prion-infected apoptotic neurons can be engulfed by microglia, which suppresses prion disease by promoting prion clearance via astrocyte-borne Mfge8 (milk fat globule epidermal growth factor 8) (Kranich et al., 2010; Tait and Green, 2010). Besides, apoptotic human polymorphonuclear neutrophil microvesicles (apoPMN-MVs, a kind of ApoMVs) selectively suppress the proliferation of $CD25^+$ T_h cells in a dose-dependent manner by downregulating IL-2 and IL-2R expression. This downregulation inhibits the activation of resting T cells, thereby maintaining immunological tolerance (Shen et al., 2017). Immature DCs derived from the bone marrow of non-obese diabetic mice engulf antigen-specific apoptotic bodies from β cells. These DCs reduce the secretion of proinflammatory cytokines, and prevent experimental type 1 diabetes, suggesting that antigen-specific ApoBDs engulfed by DCs play an essential role in immunosuppression (Marin-Gallen et al., 2010). However, whether apoptotic β cell-derived ApoBDs prevent diabetes by promoting islet cell regeneration needs further exploration (**Table 2**). Although ApoEVs can present antigen and facilitate immune defense response in some cases, ApoEVs can also act as an autoantigen to induce autoimmune diseases, such as systemic lupus erythematosus (Cocca et al., 2002), suggesting that ApoEVs may play a completely different role in different environments.

CONCLUDING REMARKS AND PERSPECTIVES

Regeneration and embryonic development are partly based on common regulatory gene networks which, in both cases, may drive similar or even identical apoptosis and/or senescence processes. Apoptosis is a critical process in embryogenesis and postnatal cell homeostasis by balancing proliferation and death. Apoptosis accompanies the generation of membranous vesicles termed apoptotic extracellular vesicles (ApoEVs). ApoEVs can transit to the target cells and exchange signaling molecules, including DNA, RNA, and proteins, to regulate cell proliferation and differentiation and tissue regeneration after phagocytosis.

Overall, there is compelling evidence to support the importance of ApoEVs in regulating tissue development and regeneration, such as in the cardiovascular system, urinary system, and bone. ApoEVs are potential components in the treatment of tumors, inflammatory diseases, and degenerative diseases. Therefore, the neglected ApoEVs could be considered as a key mechanism of intracellular communication. The ability of ApoEVs to proliferate and differentiate demonstrates a good balance between the beneficial effects of apoptosis and regeneration. Although there have been very few studies about the ApoEVs and their particular developmental processes, it is necessary to further explore the relationship between them. Compared with traditional drugs, ApoEVs have several advantages: (1) ApoEVs can be easily recognized by target cells through specific markers (PS, Tsb, and C3b); (2) the bioactive factors enveloped in ApoEVs provide essential signals to simultaneously promote the various functions of cells; (3) ApoEVs can affect adjacent tissues or distant tissue through the circulation. Emerging evidence has shown that ApoEVs are useful tools in tissue regeneration and disease treatment. Nevertheless, there remain several hurdles and challenges to be overcome before clinical applications of ApoEVs in disease treatment and tissue regeneration. Several critical questions need to be answered: How can ApoEVs play a decisive role in particular types of diseases? Do ApoEVs work by transferring specific contents directly or indirectly by recruiting cells or factors? How can the release, size, and specific cargo of ApoEVs be controlled? Is the formation of ApoEVs selective or cell-dependent? How can the transfer of bioactive molecules in ApoEVs be regulated? Is there a new way to distinguish different subtypes of ApoEVs? By addressing these questions, we will take a step closer to understanding ApoEVs in physiological and pathological conditions.

AUTHOR CONTRIBUTIONS

ML was responsible for collecting and collating documents and writing this review. LL and WT were responsible for writing and proofing the manuscript. All authors read and approved the final manuscript.

FUNDING

This work was supported by grants from the National Key Research and Development Program of China (2017YFA0104800), the Nature Science Foundation of China (81600912 and 31601113), the Fundamental Research Funds for the Central Universities (YJ201878), and Key Project of Sichuan Province (2019YFS0311 and 2019YFS0515).

REFERENCES

Ainola, M., Porola, P., Takakubo, Y., Przybyla, B., Kouri, V. P., Tolvanen, T. A., et al. (2018). Activation of plasmacytoid dendritic cells by apoptotic particles – mechanism for the loss of immunological tolerance in Sjogren's syndrome. *Clin. Exp. Immunol.* 191, 301–310. doi: 10.1111/cei.13077

Akers, J. C., Gonda, D., Kim, R., Carter, B. S., and Chen, C. C. (2013). Biogenesis of extracellular vesicles (EV): exosomes, microvesicles, retrovirus-like vesicles, and apoptotic bodies. *J. Neurooncol.* 113, 1–11. doi: 10.1007/s11060-013-1084-8

Aoki, K., Satoi, S., Harada, S., Uchida, S., Iwasa, Y., and Ikenouchi, J. (2020). Coordinated changes in cell membrane and cytoplasm during maturation of apoptotic bleb. *Mol. Biol. Cell* 31, 833–844. doi: 10.1091/mbc.E19-12-0691

Arandjelovic, S., and Ravichandran, K. S. (2015). Phagocytosis of apoptotic cells in homeostasis. *Nat. Immunol.* 16, 907–917. doi: 10.1038/ni.3253

Atkin-Smith, G. K., Tixeira, R., Paone, S., Mathivanan, S., Collins, C., Liem, M., et al. (2015). A novel mechanism of generating extracellular vesicles during apoptosis via a beads-on-a-string membrane structure. *Nat. Commun.* 6:7439. doi: 10.1038/ncomms8439

Battistelli, M., and Falcieri, E. (2020). Apoptotic bodies: particular extracellular vesicles involved in intercellular communication. *Biology (Basel)* 9:21. doi: 10.3390/biology9010021

Bergmann, A., and Steller, H. (2010). Apoptosis, stem cells, and tissue regeneration. *Sci. Signal.* 3:re8. doi: 10.1126/scisignal.3145re8

Boatright, K. M., and Salvesen, G. S. (2003). Mechanisms of caspase activation. *Curr. Opin. Cell Biol.* 15, 725–731. doi: 10.1016/j.ceb.2003.10.009

Brock, C. K., Wallin, S. T., Ruiz, O. E., Samms, K. M., Mandal, A., Sumner, E. A., et al. (2019). Stem cell proliferation is induced by apoptotic bodies from dying cells during epithelial tissue maintenance. *Nat. Commun.* 10:1044. doi: 10.1038/s41467-019-09010-6

Brockes, J. P., and Kumar, A. (2008). Comparative aspects of animal regeneration. *Annu. Rev. Cell Dev. Biol.* 24, 525–549. doi: 10.1146/annurev.cellbio.24.110707.175336

Broker, L. E. (2005). Cell death independent of caspases: a review. *Clin. Cancer Res.* 11, 3155–3162. doi: 10.1158/1078-0432.Ccr-04-2223

Buss, R. R., Sun, W., and Oppenheim, R. W. (2006). Adaptive roles of programmed cell death during nervous system. *Annu. Rev. Neurosci.* 29, 1–35.

Bussolati, B., and Camussi, G. (2017). Renal injury: early apoptotic extracellular vesicles in injury and repair. *Nat. Rev. Nephrol.* 13, 523–524. doi: 10.1038/nrneph.2017.117

Buzas, E. I., Gyorgy, B., Nagy, G., Falus, A., and Gay, S. (2014). Emerging role of extracellular vesicles in inflammatory diseases. *Nat. Rev. Rheumatol.* 10, 356–364. doi: 10.1038/nrrheum.2014.19

Caruso, S., and Poon, I. K. H. (2018). Apoptotic cell-derived extracellular vesicles: more than just debris. *Front. Immunol.* 9:1486. doi: 10.3389/fimmu.2018.01486

Cerri, P. S. (2005). Osteoblasts engulf apoptotic bodies during alveolar bone formation in the rat maxilla. *Anat. Rec. A Discov. Mol. Cell Evol. Biol.* 286, 833–840. doi: 10.1002/ar.a.20220

Chang, J., Peng, M., Vaquerano, J., Zhou, Y., Clinton, R., Hyun, W., et al. (2000). Induction of Th1 response by dendritic cells pulsed with autologous melanoma apoptotic bodies. *Anticancer Res.* 20, 1329–1336.

Chera, S., Ghila, L., Dobretz, K., Wenger, Y., Bauer, C., Buzgariu, W., et al. (2009). Apoptotic cells provide an unexpected source of Wnt3 signaling to drive hydra head regeneration. *Dev. Cell* 17, 279–289. doi: 10.1016/j.devcel.2009.07.014

Cocca, B. A., Cline, A. M., and Radic, M. Z. (2002). Blebs and apoptotic bodies are B cell autoantigens. *J. Immunol.* 169, 159–166.

Cohen, J. J. (1999). Apoptosis: mechanisms of life and death in the immune system. *J. Allergy Clin. Immunol.* 103, 548–554.

Coleman, M., Sahai, E., Yeo, M., Bosch, M., Dewar, A., and Olson, M. (2001). Membrane blebbing during apoptosis results from caspase-mediated activation of ROCK I. *Nat. Cell Biol.* 3, 339–345. doi: 10.1038/35070009

Crescitelli, R., Lasser, C., Szabo, T. G., Kittel, A., Eldh, M., Dianzani, I., et al. (2013). Distinct RNA profiles in subpopulations of extracellular vesicles: apoptotic bodies, microvesicles and exosomes. *J. Extracell Vesicles* 2:20677. doi: 10.3402/jev.v2i0.20677

Davidson, F., and Steller, H. (1998). Blocking apoptosis prevents blindness in Drosophila retinal degeneration mutants. *Nature* 391, 587–591. doi: 10.1038/35385

D'mello, V., Singh, S., Wu, Y., and Birge, R. (2009). The urokinase plasminogen activator receptor promotes efferocytosis of apoptotic cells. *J. Biol. Chem.* 284, 17030–17038. doi: 10.1074/jbc.M109.010066

Downward, J., Coppé, J.-P., Patil, C. K., Rodier, F., Sun, Y., Muñoz, D. P., et al. (2008). Senescence-associated secretory phenotypes reveal cell-nonautonomous functions of oncogenic RAS and the p53 tumor suppressor. *PLoS Biol.* 6:e60301. doi: 10.1371/journal.pbio.0060301

Elliott, D., Kim, W., Jans, D., and Garner, B. (2007). Apoptosis induces neuronal apolipoprotein-E synthesis and localization in apoptotic bodies. *Neurosci. Lett.* 416, 206–210. doi: 10.1016/j.neulet.2007.02.014

Elmore, S. (2007). Apoptosis: a review of programmed cell death. *Toxicol. Pathol.* 35, 495–516. doi: 10.1080/01926230701320337

Fabian, D., Koppel, J., and Maddox-Hyttel, P. (2005). Apoptotic processes during mammalian preimplantation development. *Theriogenology* 64, 221–231. doi: 10.1016/j.theriogenology.2004.11.022

Fan, Y., and Bergmann, A. (2008). Apoptosis-induced compensatory proliferation. The Cell is dead. Long live the Cell! *Trends Cell Biol.* 18, 467–473. doi: 10.1016/j.tcb.2008.08.001

Feinstein-Rotkopf, Y., and Arama, E. (2009). Can't live without them, can live with them: roles of caspases during vital cellular processes. *Apoptosis* 14, 980–995. doi: 10.1007/s10495-009-0346-6

Fuchs, Y., and Steller, H. (2011). Programmed cell death in animal development and disease. *Cell* 147, 742–758. doi: 10.1016/j.cell.2011.10.033

Gaipl, U. S., Voll, R. E., Sheriff, A., Franz, S., Kalden, J. R., and Herrmann, M. (2005). Impaired clearance of dying cells in systemic lupus erythematosus. *Autoimmun. Rev.* 4, 189–194. doi: 10.1016/j.autrev.2004.10.007

Gardai, S., Bratton, D., Ogden, C., and Henson, P. (2006). Recognition ligands on apoptotic cells: a perspective. *J. Leuk. Biol.* 79, 896–903. doi: 10.1189/jlb.1005550

Grant, L. R., Milic, I., and Devitt, A. (2019). Apoptotic cell-derived extracellular vesicles: structure-function relationships. *Biochem. Soc. Trans.* 47, 509–516. doi: 10.1042/BST20180080

Gregory, C. D., and Dransfield, I. (2018). Apoptotic tumor cell-derived extracellular vesicles as important regulators of the onco-regenerative niche. *Front. Immunol.* 9:1111. doi: 10.3389/fimmu.2018.01111

Gregory, C. D., and Paterson, M. (2018). An apoptosis-driven 'onco-regenerative niche': roles of tumour-associated macrophages and extracellular vesicles. *Philos. Trans. R Soc. Lond. B Biol. Sci.* 373:20170003. doi: 10.1098/rstb.2017.0003

Guicciardi, M. E., and Gores, G. J. (2009). Life and death by death receptors. *FASEB J.* 23, 1625–1637. doi: 10.1096/fj.08-111005

Gupta, K., Goldufsky, J., Wood, S., Tardi, N., Moorthy, G., Gilbert, D., et al. (2017). Apoptosis and compensatory proliferation signaling are coupled by CrkI-containing microvesicles. *Dev. Cell* 41, 674–684.e5. doi: 10.1016/j.devcel.2017.05.014

Hacker, G. (2000). The morphology of apoptosis. *Cell Tissue Res.* 301, 5–17. doi: 10.1007/s004410000193

Halicka, H. D., Bedner, E., and Darzynkiewicz, Z. (2000). Segregation of RNA and separate packaging of DNA and RNA in apoptotic bodies during apoptosis. *Exp. Cell Res.* 260, 248–256. doi: 10.1006/excr.2000.5027

Hardy, K. (1999). Apoptosis in the human embryo. *Rev. Reprod.* 4, 125–134.

Hauser, P., Wang, S., and Didenko, V. V. (2017). Apoptotic bodies: selective detection in extracellular vesicles. *Methods Mol. Biol.* 1554, 193–200.

Hengartner, M. (2001). Apoptosis: corralling the corpses. *Cell* 104, 325–328. doi: 10.1016/s0092-8674(01)00219-7

Hochreiter-Hufford, A. E., Lee, C. S., Kinchen, J. M., Sokolowski, J. D., Arandjelovic, S., Call, J. A., et al. (2013). Phosphatidylserine receptor BAI1 and apoptotic cells as new promoters of myoblast fusion. *Nature* 497, 263–267. doi: 10.1038/nature12135

Holmgren, L., Szeles, A., Rajnavölgyi, E., Folkman, G., Klein, G., Ernberg, I., et al. (1999). Horizontal transfer of DNA by the uptake of apoptotic bodies. *Blood* 93, 3956–3963.

Horrevorts, S. K., Stolk, D. A., van de Ven, R., Hulst, M., van Het Hof, B., Duinkerken, S., et al. (2019). Glycan-modified apoptotic melanoma-derived extracellular vesicles as antigen source for anti-tumor vaccination. *Cancers (Basel)* 11, 1266. doi: 10.3390/cancers11091266

Hosseini, H. S., and Taber, L. A. (2018). How mechanical forces shape the developing eye. *Prog. Biophys. Mol. Biol.* 137, 25–36.

Hristov, M., Erl, W., Linder, S., and Weber, P. C. (2004). Apoptotic bodies from endothelial cells enhance the number and initiate the differentiation of human endothelial progenitor cells in vitro. *Blood* 104, 2761–2766. doi: 10.1182/blood-2003-10-3614

Huh, J., Guo, M., and Hay, B. (2004). Compensatory proliferation induced by cell death in the *Drosophila* wing disc requires activity of the apical cell death caspase Dronc in a nonapoptotic role. *Curr. Biol.* 14, 1262–1266. doi: 10.1016/j.cub.2004.06.015

Hus, I., Rolinski, J., Tabarkiewicz, J., Wojas, K., Bojarska-Junak, A., Greiner, J., et al. (2005). Allogeneic dendritic cells pulsed with tumor lysates or apoptotic bodies as immunotherapy for patients with early-stage B-cell chronic lymphocytic leukemia. *Leukemia* 19, 1621–1627. doi: 10.1038/sj.leu.2403860

Hwang, J., Kobayashi, C., Agata, K., Ikeo, K., and Gojobori, T. (2004). Detection of apoptosis during planarian regeneration by the expression of apoptosis-related genes and TUNEL assay. *Gene* 333, 15–25. doi: 10.1016/j.gene.2004.02.034

Ihara, T., Yamamoto, T., Sugamata, M., Okumura, H., and Ueno, Y. (1998). The process of ultrastructural changes from nuclei to apoptotic body. *Virchows Arch.* 433, 443–447. doi: 10.1007/s004280050272

Jeon, O. H., Kim, C., Laberge, R. M., Demaria, M., Rathod, S., Vasserot, A. P., et al. (2017). Local clearance of senescent cells attenuates the development of post-traumatic osteoarthritis and creates a pro-regenerative environment. *Nat. Med.* 23, 775–781. doi: 10.1038/nm.4324

Jezek, D., and Kozina, V. (2009). [Apoptosis during embryo development]. *Acta Med. Croatica* 63(Suppl. 2):37.

Jiang, L., Paone, S., Caruso, S., Atkin-Smith, G. K., Phan, T. K., Hulett, M. D., et al. (2017). Determining the contents and cell origins of apoptotic bodies by flow cytometry. *Sci. Rep.* 7:14444. doi: 10.1038/s41598-017-14305-z

Joza, N., Susin, S., Daugas, E., Stanford, W., Cho, S., Li, C., et al. (2001). Essential role of the mitochondrial apoptosis-inducing factor in programmed cell death. *Nature* 410, 549–554. doi: 10.1038/35069004

Jurisicova, A., Varmuza, S., and Casper, R. F. (1996). Programmed cell death and human embryo fragmentation. *Mol. Hum. Reprod.* 2:93.

Kogianni, G., Mann, V., and Noble, B. (2008). Apoptotic bodies convey activity capable of initiating osteoclastogenesis and localized bone destruction. *J. Bone Mineral* 23, 915–927. doi: 10.1359/jbmr.080207

Kondo, S. (1988). Altruistic cell suicide in relation to radiation hormesis. *Int. J. Radiat. Biol. Relat. Stud. Phys. Chem. Med.* 53, 95–102. doi: 10.1080/09553008814550461

Kondo, S., Senoo-Matsuda, N., Hiromi, Y., and Miura, M. (2006). DRONC coordinates cell death and compensatory proliferation. *Mol. Cell Biol.* 26, 7258–7268. doi: 10.1128/MCB.00183-06

Kranich, J., Krautler, N., Falsig, J., Ballmer, B., Li, S., Hutter, G., et al. (2010). Engulfment of cerebral apoptotic bodies controls the course of prion disease in a mouse strain-dependent manner. *J. Exp. Med.* 207, 2271–2281. doi: 10.1084/jem.20092401

Kroemer, G., El-Deiry, W. S., Golstein, P., Peter, M. E., Vaux, D., Vandenabeele, P., et al. (2005). Classification of cell death: recommendations of the Nomenclature committee on cell death. *Cell Death Differ.* 12(Suppl. 2), 1463–1467. doi: 10.1038/sj.cdd.4401724

Kuribayashi, K., Mayes, P. A., and El-Deiry, W. S. (2014). What are caspases 3 and 7 doing upstream of the mitochondria? *Cancer Biol. Ther.* 5, 763–765. doi: 10.4161/cbt.5.7.3228

Kurihara, H., Yang, D. J., Cristofanilli, M., Erwin, W. D., Yu, D. F., Kohanim, S., et al. (2008). Imaging and dosimetry of 99mTc EC annexin V: preliminary clinical study targeting apoptosis in breast tumors. *Appl. Radiat. Isot.* 66, 1175–1182. doi: 10.1016/j.apradiso.2008.01.012

Lane, J. D., Allan, V. J., and Woodman, P. G. (2005). Active relocation of chromatin and endoplasmic reticulum into blebs in late apoptotic cells. *J. Cell Sci.* 118, 4059–4071. doi: 10.1242/jcs.02529

Laurenzana, I., Lamorte, D., Trino, S., De Luca, L., Ambrosino, C., Zoppoli, P., et al. (2018). Extracellular vesicles: a new prospective in crosstalk between microenvironment and stem cells in hematological malignancies. *Stem Cells Int.* 2018:9863194. doi: 10.1155/2018/9863194

Li, F., Huang, Q., Chen, J., Peng, Y., Roop, D., Bedford, J., et al. (2010). Apoptotic cells activate the "phoenix rising" pathway to promote wound healing and tissue regeneration. *Sci. Signal.* 3:ra13. doi: 10.1126/scisignal.2000634

Li, Z., Hu, D., Chu, Q., Wu, J., Gao, C., Zhang, Y., et al. (2004). Cell apoptosis and regeneration of hepatocellular carcinoma after transarterial

chemoembolization. *World J. Gastroenterol.* 10, 1876–1880. doi: 10.3748/wjg.v10.i13.1876

Liu, D., Kou, X., Chen, C., Liu, S., Liu, Y., Yu, W., et al. (2018). Circulating apoptotic bodies maintain mesenchymal stem cell homeostasis and ameliorate osteopenia via transferring multiple cellular factors. *Cell Res.* 28, 918–933. doi: 10.1038/s41422-018-0070-2

Liu, H., Liu, S., Qiu, X., Yang, X., Bao, L., Pu, F., et al. (2020). Donor MSCs release apoptotic bodies to improve myocardial infarction via autophagy regulation in recipient cells. *Autophagy* doi: 10.1080/15548627.2020.1717128 [Epub ahead of print].

Lorda-Diez, C. I., Garcia-Riart, B., Montero, J. A., Joaquín, R.-L., and Hurle, J. M. (2015). Apoptosis during embryonic tissue remodeling is accompanied by cell senescence. *Aging* 7, 974–985.

Ma, Q., Liang, M., Wu, Y., Ding, N., Duan, L., Yu, T., et al. (2019). Mature osteoclast-derived apoptotic bodies promote osteogenic differentiation via RANKL-mediated reverse signaling. *J. Biol. Chem.* 294, 11240–11247. doi: 10.1074/jbc.RA119.007625

Macchi, B., Marino-Merlo, F., Nocentini, U., Pisani, V., Cuzzocrea, S., Grelli, S., et al. (2015). Role of inflammation and apoptosis in multiple sclerosis: Comparative analysis between the periphery and the central nervous system. *J. Neuroimmunol.* 287, 80–87. doi: 10.1016/j.jneuroim.2015.08.016

Marin-Gallen, S., Clemente-Casares, X., Planas, R., Pujol-Autonell, I., Carrascal, J., Carrillo, J., et al. (2010). Dendritic cells pulsed with antigen-specific apoptotic bodies prevent experimental type 1 diabetes. *Clin. Exp. Immunol.* 160, 207–214. doi: 10.1111/j.1365-2249.2009.04082.x

Medina, C. B., Mehrotra, P., Arandjelovic, S., Perry, J. S. A., Guo, Y., Morioka, S., et al. (2020). Metabolites released from apoptotic cells act as tissue messengers. *Nature* 580, 130–135. doi: 10.1038/s41586-020-2121-3

Merchant, M. L., Rood, I. M., Deegens, J. K. J., and Klein, J. B. (2017). Isolation and characterization of urinary extracellular vesicles: implications for biomarker discovery. *Nat. Rev. Nephrol.* 13, 731–749. doi: 10.1038/nrneph.2017.148

Mills, J., Stone, N., Erhardt, J., and Pittman, R. (1998). Apoptotic membrane blebbing is regulated by myosin light chain phosphorylation. *J. Cell Biol.* 140, 627–636. doi: 10.1083/jcb.140.3.627

Muhsin-Sharafaldine, M. R., and McLellan, A. D. (2018a). Tumor-derived apoptotic vesicles: with death they do part. *Front. Immunol.* 9:957. doi: 10.3389/fimmu.2018.00957

Muhsin-Sharafaldine, M. R., and McLellan, A. D. (2018b). Apoptotic vesicles: deathly players in cancer-associated coagulation. *Immunol. Cell Biol.* 96, 723–732. doi: 10.1111/imcb.12162

Muhsin-Sharafaldine, M.-R., Saunderson, S. C., Dunn, A. C., Faed, J. M., Kleffmann, T., and McLellan, A. D. (2016). Procoagulant and immunogenic properties of melanoma exosomes, microvesicles and apoptotic vesicles. *Oncotarget* 7, 56279–56294. doi: 10.18632/oncotarget.10783

Nazari-Jahantigh, M., Wei, Y., and Schober, A. (2012). The role of microRNAs in arterial remodelling. *Thromb. Haemost.* 107, 611–618. doi: 10.1160/TH11-12-0826

Orlando, K. A., Stone, N. L., and Pittman, R. N. (2006). Rho kinase regulates fragmentation and phagocytosis of apoptotic cells. *Exp. Cell Res.* 312, 5–15. doi: 10.1016/j.yexcr.2005.09.012

Park, S. J., Kim, J. M., Kim, J., Hur, J., Park, S., Kim, K., et al. (2018). Molecular mechanisms of biogenesis of apoptotic exosome-like vesicles and their roles as damage-associated molecular patterns. *Proc. Natl. Acad. Sci. U.S.A.* 115, E11721–E11730. doi: 10.1073/pnas.1811432115

Pavlyukov, M. S., Yu, H., Bastola, S., Minata, M., Shender, V. O., Lee, Y., et al. (2018). Apoptotic cell-derived extracellular vesicles promote malignancy of glioblastoma via intercellular transfer of splicing factors. *Cancer Cell* 34, 119–135.e10. doi: 10.1016/j.ccell.2018.05.012

Pellettieri, J., Fitzgerald, P., Watanabe, S., Mancuso, J., Green, D., and Sánchez Alvarado, A. (2010). Cell death and tissue remodeling in planarian regeneration. *Dev. Biol.* 338, 76–85. doi: 10.1016/j.ydbio.2009.09.015

Pellettieri, J., and Sanchez Alvarado, A. (2007). Cell turnover and adult tissue homeostasis: from humans to planarians. *Annu. Rev. Genet.* 41, 83–105. doi: 10.1146/annurev.genet.41.110306.130244

Penaloza, C., Lin, L., Lockshin, R. A., and Zakeri, Z. (2006). Cell death in development: shaping the embryo. *Histochem. Cell Biol.* 126, 149–158. doi: 10.1007/s00418-006-0214-1

Pérez-Garijo, A., Martín, F., and Morata, G. (2004). Caspase inhibition during apoptosis causes abnormal signalling and developmental aberrations in *Drosophila*. *Development* 131, 5591–5598. doi: 10.1242/dev.01432

Peter, C., Waibel, M., Radu, C. G., Yang, L. V., Witte, O. N., Schulze-Osthoff, K., et al. (2008). Migration to apoptotic "find-me" signals is mediated via the phagocyte receptor G2A. *J. Biol. Chem.* 283, 5296–5305. doi: 10.1074/jbc.M706586200

Phan, T. K., Poon, I. K., and Atkin-Smith, G. K. (2018). Detection and isolation of apoptotic bodies to high purity. *J. Vis. Exp.* 138:58317. doi: 10.3791/58317

Poon, I. K. H., Chiu, Y. H., Armstrong, A. J., Kinchen, J. M., Juncadella, I. J., Bayliss, D. A., et al. (2014a). Unexpected link between an antibiotic, pannexin channels and apoptosis. *Nature* 507, 329–334.

Poon, I. K. H., Lucas, C. D., Rossi, A. G., and Ravichandran, K. S. (2014b). Apoptotic cell clearance: basic biology and therapeutic potential. *Nat. Rev. Immunol.* 14, 166–180. doi: 10.1038/nri3607

Ravichandran, K. S. (2011). Beginnings of a good apoptotic meal: the find-me and eat-me signaling pathways. *Immunity* 35, 445–455. doi: 10.1016/j.immuni.2011.09.004

Rieux-Laucat, F., Le Deist, F., and Fischer, A. (2003). Autoimmune lymphoproliferative syndromes: genetic defects of apoptosis pathways. *Cell Death Differ.* 10, 124–133. doi: 10.1038/sj.cdd.4401190

Ryoo, H., Gorenc, T., and Steller, H. (2004). Apoptotic cells can induce compensatory cell proliferation through the JNK and the Wingless signaling pathways. *Dev. Cell* 7, 491–501. doi: 10.1016/j.devcel.2004.08.019

Saraste, A., and Pulkki, K. (2000). Morphologic and biochemical hallmarks of apoptosis. *Cardiovasc. Res.* 45, 528–537. doi: 10.1016/s0008-6363(99)00384-3

Schiller, M., Parcina, M., Heyder, P., Foermer, S., Ostrop, J., Leo, A., et al. (2012). Induction of type I IFN is a physiological immune reaction to apoptotic cell-derived membrane microparticles. *J. Immunol.* 189, 1747–1756. doi: 10.4049/jimmunol.1100631

Segundo, C., Medina, F., Rodrıìguez, C., Martınez-Palencia, R. A., Leyva-Cobiaìn, F., and Brieva, J. A. (1999). Surface molecule loss and bleb formation by human germinal center B cells undergoing apoptosis: role of apoptotic blebs in monocyte chemotaxis. *Blood* 94, 1012–1020. doi: 10.1182/blood.V94.3.1012.415k05_1012_1020

Shen, G., Krienke, S., Schiller, P., Niessen, A., Neu, S., Eckstein, V., et al. (2017). Microvesicles released by apoptotic human neutrophils suppress proliferation and IL-2/IL-2 receptor expression of resting T helper cells. *Eur. J. Immunol.* 47, 900–910. doi: 10.1002/eji.201546203

Simpson, R. J., and Mathivanan, S. (2012). Extracellular microvesicles: the need for internationally recognised nomenclature and stringent purification criteria. *J. Proteom. Bioinform.* 5:2.

Slee, E., Adrain, C., and Martin, S. (1999). Serial killers: ordering caspase activation events in apoptosis. *Cell Death Differ.* 6, 1067–1074. doi: 10.1038/sj.cdd.4400601

Sordet, O., Rébé, C., Plenchette, S., Zermati, Y., Hermine, O., Vainchenker, W., et al. (2002). Specific involvement of caspases in the differentiation of monocytes into macrophages. *Blood* 100, 4446–4453. doi: 10.1182/blood-2002-06-1778

Stolzing, A., and Grune, T. (2004). Neuronal apoptotic bodies: phagocytosis and degradation by primary microglial cells. *FASEB J.* 18, 743–745. doi: 10.1096/fj.03-0374fje

Subiros-Funosas, R., Mendive-Tapia, L., Sot, J., Pound, J. D., Barth, N., Varela, Y., et al. (2017). A Trp-BODIPY cyclic peptide for fluorescence labelling of apoptotic bodies. *Chem. Commun.* 53, 945–948. doi: 10.1039/c6cc07879f

Susin, S., Lorenzo, H., Zamzami, N., Marzo, I., Snow, B., Brothers, G., et al. (1999). Molecular characterization of mitochondrial apoptosis-inducing factor. *Nature* 397, 441–446. doi: 10.1038/17135

Tait, S. W., and Green, D. R. (2010). Mitochondria and cell death: outer membrane permeabilization and beyond. *Nat. Rev. Mol. Cell Biol.* 11, 621–632. doi: 10.1038/nrm2952

Torr, E. E., Gardner, D. H., Thomas, L., Goodall, D. M., Bielemeier, A., Willetts, R., et al. (2012). Apoptotic cell-derived ICAM-3 promotes both macrophage chemoattraction to and tethering of apoptotic cells. *Cell Death Differ.* 19, 671–679. doi: 10.1038/cdd.2011.167

Tower, J. (2015). Programmed cell death in aging. *Ageing Res. Rev.* 23, 90–100. doi: 10.1016/j.arr.2015.04.002

Tran, H. B., Ohlsson, M., Beroukas, D., Hiscock, J., Bradley, J., Buyon, J. P., et al. (2002). Subcellular redistribution of la/SSB autoantigen during physiologic apoptosis in the fetal mouse heart and conduction system: a clue to the pathogenesis of congenital heart block. *Arthritis Rheum.* 46, 202–208. doi: 10.1002/1529-0131(200201)46

Truman, L. A., Ford, C. A., Pasikowska, M., Pound, J. D., Wilkinson, S. J., Dumitriu, I. E., et al. (2008). CX3CL1/fractalkine is released from apoptotic lymphocytes to stimulate macrophage chemotaxis. *Blood* 112, 5026–5036. doi: 10.1182/blood-2008-06-162404

Tseng, A., Adams, D., Qiu, D., Koustubhan, P., and Levin, M. (2007). Apoptosis is required during early stages of tail regeneration in Xenopus laevis. *Dev. Biol.* 301, 62–69. doi: 10.1016/j.ydbio.2006.10.048

Tyukavin, A. I., Belostotskaya, G. B., Golovanova, T. A., Galagudza, M. M., Zakharov, E. A., Burkova, N. V., et al. (2015). Stimulation of proliferation and differentiation of rat resident myocardial cells with apoptotic bodies of cardiomyocytes. *Bull. Exp. Biol. Med.* 159, 138–141. doi: 10.1007/s10517-015-2909-6

van Deursen, J. M. (2014). The role of senescent cells in ageing. *Nature* 509, 439–446. doi: 10.1038/nature13193

Vlaskalin, T., Wong, C., and Tsilfidis, C. (2004). Growth and apoptosis during larval forelimb development and adult forelimb regeneration in the newt (*Notophthalmus viridescens*). *Dev. Genes Evol.* 214, 423–431. doi: 10.1007/s00427-004-0417-1

von Mühlen, C., and Tan, E. (1995). Autoantibodies in the diagnosis of systemic rheumatic diseases. *Semin. Arthritis Rheum.* 24, 323–358. doi: 10.1016/s0049-0172(95)80004-2

Winau, F., Weber, S., Sad, S., de Diego, J., Hoops, S. L., Breiden, B., et al. (2006). Apoptotic vesicles crossprime CD8 T cells and protect against tuberculosis. *Immunity* 24, 105–117. doi: 10.1016/j.immuni.2005.12.001

Witasp, E., Uthaisang, W., Elenstrom-Magnusson, C., Hanayama, R., Tanaka, M., Nagata, S., et al. (2007). Bridge over troubled water: milk fat globule epidermal growth factor 8 promotes human monocyte-derived macrophage clearance of non-blebbing phosphatidylserine-positive target cells. *Cell Death Differ.* 14, 1063–1065. doi: 10.1038/sj.cdd.4402096

Wu, Z., Zhang, Z., Xia, W., Cai, J., Li, Y., and Wu, S. (2019). Extracellular vesicles in urologic malignancies-Implementations for future cancer care. *Cell Prolif.* 52:e12659. doi: 10.1111/cpr.12659

Xu, X., Lai, Y., and Hua, Z. C. (2019). Apoptosis and apoptotic body: disease message and therapeutic target potentials. *Biosci. Rep.* 39:BSR20180992. doi: 10.1042/BSR20180992

Yuan, F. L., Wu, Q. Y., Miao, Z. N., Xu, M. H., Xu, R. S., Jiang, D. L., et al. (2018). Osteoclast-derived extracellular vesicles: novel regulators of osteoclastogenesis and osteoclast-osteoblasts communication in bone remodeling. *Front. Physiol.* 9:628. doi: 10.3389/fphys.2018.00628

Zakeri, Z., Penaloza, C. G., Smith, K., Ye, Y., and Lockshin, R. A. (2015). What cell death does in development. *Int. J. Dev. Biol.* 59, 11–22. doi: 10.1387/ijdb.150220zz

Zernecke, A., Bidzhekov, K., Noels, H., Shagdarsuren, E., Gan, L., Denecke, B., et al. (2009). Delivery of microRNA-126 by apoptotic bodies induces CXCL12-dependent vascular protection. *Sci. Signal.* 2:ra81. doi: 10.1126/scisignal.2000610

Zhu, Z., Zhang, D., Lee, H., Menon, A. A., Wu, J., Hu, K., et al. (2017). Macrophage-derived apoptotic bodies promote the proliferation of the recipient cells via shuttling microRNA-221/222. *J. Leukoc Biol.* 101, 1349–1359. doi: 10.1189/jlb.3A1116-483R

Zirngibl, M., Furnrohr, B. G., Janko, C., Munoz, L. E., Voll, R. E., Gregory, C. D., et al. (2015). Loading of nuclear autoantigens prototypically recognized by systemic lupus erythematosus sera into late apoptotic vesicles requires intact microtubules and myosin light chain kinase activity. *Clin. Exp. Immunol.* 179, 39–49. doi: 10.1111/cei.12342

Conflict of Interest: The authors declare that the research was conducted in the absence of any commercial or financial relationships that could be construed as a potential conflict of interest.

frontiers in Cell and Developmental Biology

REVIEW
published: 23 October 2020
doi: 10.3389/fcell.2020.593761

Confluence of Cellular Degradation Pathways During Interdigital Tissue Remodeling in Embryonic Tetrapods

Juan A. Montero, Carlos I. Lorda-Diez and Juan M. Hurle**

Departamento de Anatomiia y Biologiia Celular and Instituto de Investigación Sanitaria Valdecilla (IDIVAL), Universidad de Cantabria, Santander, Spain

Digits develop in the distal part of the embryonic limb primordium as radial prechondrogenic condensations separated by undifferentiated mesoderm. In a short time interval the interdigital mesoderm undergoes massive degeneration to determine the formation of free digits. This fascinating process has often been considered as an altruistic cell suicide that is evolutionarily-regulated in species with different degrees of digit webbing. Initial descriptions of interdigit remodeling considered lysosomes as the primary cause of the degenerative process. However, the functional significance of lysosomes lost interest among researcher and was displaced to a secondary role because the introduction of the term apoptosis. Accumulating evidence in recent decades has revealed that, far from being a unique method of embryonic cell death, apoptosis is only one among several redundant dying mechanisms accounting for the elimination of tissues during embryonic development. Developmental cell senescence has emerged in the last decade as a primary factor implicated in interdigit remodeling. Our review proposes that cell senescence is the biological process identified by vital staining in embryonic models and implicates lysosomes in programmed cell death. We review major structural changes associated with interdigit remodeling that may be driven by cell senescence. Furthermore, the identification of cell senescence lacking tissue degeneration, associated with the maturation of the digit tendons at the same stages of interdigital remodeling, allowed us to distinguish between two functionally distinct types of embryonic cell senescence, "constructive" and "destructive."

Keywords: programmed cell death, apoptosis, extrinsic pathway, mitochondrial pathway, lysosomes, cell death genes, developmental senescence, tendon differentiation

OPEN ACCESS

Edited by:
Stefan Washausen, Universität Münster, Germany

Reviewed by:
Luis Covarrubias, National Autonomous University of Mexico, Mexico
Mirna Saraga-Babic, University of Split, Croatia

****Correspondence:***
Juan A. Montero
monteroja@unican.es
Juan M. Hurle
hurlej@unican.es

Specialty section:
This article was submitted to Cell Death and Survival, a section of the journal Frontiers in Cell and Developmental Biology

Received: *11 August 2020*
Accepted: *07 October 2020*
Published: *23 October 2020*

Citation:
Montero JA, Lorda-Diez CI and Hurle JM (2020) Confluence of Cellular Degradation Pathways During Interdigital Tissue Remodeling in Embryonic Tetrapods. Front. Cell Dev. Biol. 8:593761. doi: 10.3389/fcell.2020.593761

INTRODUCTION

Embryonic development, is a mostly plastic biological process that requires coordinate structural and architectural changes in cellular constituents. Among these changes are cell migration from one to other embryonic regions, differential proliferation of progenitors in specific embryonic regions, dissociation of epithelial tissues to form free mesenchymal progenitors, and aggregation and subsequent differentiation of cells to form organ primordia. It is believed that these cellular events are orchestrated at the local level by cell interactions mediated via secreted signals and/or changes in the composition and structure of the extracellular matrix that forms the substrate occupied by the cellular elements. Cell death is one additional embryonic process with a pivotal role in embryogenesis. As advanced by Glücksmann (1951) in the middle of the last century,

cell death is associated with most embryonic events. However, in a high number of cases, cell death is massive and accounts for the elimination of a large mass of tissue that sculpt the shape of an embryonic organ ("morphogenetic cell death"), or of the whole embryonic primordium corresponding to an organ that is lost in the course of evolution ("phylogenetic cell death"). The formation of free digits in tetrapods or the loss of the tail in the larvae of amphibian Anura during metamorphosis are illustrative examples of processes characterized by massive cell death. The direct impact of massive cell death in morphogenesis and its precise and reproducible temporospatial pattern were often considered evidence of a singular developmental mechanism programmed at their genetic level. According to this view the prospective dying cells will die even if they are previously isolated from the embryo to explant cultures (Saunders, 1966). This belief was reinforced by the direct association of changes in the pattern of cell death with the diversification of organ morphology as species become evolutionarily adapted to serve different functional requirements. A most illustrative example of this fact are the varieties in the pattern of interdigital cell death according to the pattern of digit webbing in species adapted to live in distinct habits. Thus, among the differences in humans, mice or chickens, interdigital cell death is absent or reduced in the developing bat wings (Weatherbee et al., 2006), in the developing flippers of aquatic mammalias (Cooper et al., 2018) and in the feet of swimming aquatic birds (Tokita et al., 2020). The discovery of "cell death genes" directly related to the physiological elimination of specific cells in the worm *C. elegans* (Ellis and Horvitz, 1986) and their evolutionary conservation in mammals (Peter et al., 1997) provided strong support for this idea.

The idea of a singular genetic regulation of embryonic cell death was reinforced by the proposal of a specific type of cell death, termed "apoptosis," (Kerr et al., 1972) accounting for cell elimination in most, if not all, physiological dying processes. However, research in the last decades have changed the view about the regulation of the embryonic cell death. Studies in a variety of models of embryonic tissue degeneration indicate that rather than being inherently programmed, cell death is locally regulated by extrinsic molecular interactions. The plasticity of the interdigital tissue in stages immediately prior to the onset of death provides solid support for the importance of extrinsic signals in the establishment of the degenerative process (see review by Montero et al., 2020). In addition, as will be discussed below, accumulating evidence has revealed that, far from being a unique way of embryonic cell death, apoptosis is only one among several redundant dying mechanisms accounting for the elimination of tissues in the course of embryonic development (Childs et al., 2014). Therefore, a detailed knowledge of the different dying cascades activated during each embryonic process would improve our understanding of the biological significance of cell death in developing systems.

AREAS OF INTERDIGITAL CELL DEATH

In developing vertebrates, digits are formed in the distal part of the limb primordium, termed the autopod, as radial prechondrogenic condensations (**Figure 1**). Between the differentiating digits rays, the mesodermal tissue remains undifferentiated, forming interdigital regions. The interdigital mesoderm undergoes degeneration once the digit primordia become established and progresses until the digits achieve their final morphology. This process lasts between 36 and 48 h in mouse and chick embryos and its sequence was traditionally mapped by vital staining with Neutral red or Nile blue (**Figure 2A**). Importantly, the intensity of the degenerating process in different species appears directly associated with the final morphology of the digits (Tokita et al., 2020). It is lower in species with webbed digits and very intense in species with free digits.

In this review we will survey the cell death effectors identified in the regressing interdigits of mammalian and avian species during the morphogenesis of the digits.

APOPTOSIS

The term of "apoptosis" was coined to define, a type of cell death, "active, and inherently programmed," that is distinct from "necrosis" (Kerr et al., 1972). In contrast to necrosis, cells undergoing apoptosis shrink and fragment without disintegrating their membranes and do not induce an inflammatory response (Kerr et al., 1972). The initial identification of regulatory genes, termed "cell death genes," that activate or inhibited physiological cell death in the worm *C. elegans* (Ellis and Horvitz, 1986) and the subsequent identification of homologous genes in vertebrates, sparked an enormous interest in apoptosis in developmental and cancer studies (Peter et al., 1997). A family of cysteine-aspartic proteases termed caspases was identified as central players of apoptosis in vertebrates, although their functions were found to be much wider than those of apoptosis (McArthur and Kile, 2018). Caspases are produced as inactive zymogens that are sequentially activated by proteolysis through complex molecular cascades. Several *initiator* caspases, Caspase 8 and Caspase 9, have the function of activate the *executioner* Capases 3, 6, and 7. The executioner caspases cleave many cytosolic and nuclear substrates, resulting in, among other effects, the activation of the Caspase-activated DNase (CAD; Nagata et al., 2003) and irreversible death of the cell. A biochemical hallmark of the degradation process is the fragmentation of DNA in the internucleosomal regions (Wyllie, 1980). This feature was widely employed to identify the apoptotic process by electrophoresis and by the TUNEL assay.

Two distinct apoptotic routes, extrinsic and intrinsic pathways, have been identified according to the signal that triggers the apoptotic molecular cascade (**Figure 3**). Regardless of the route, the apoptotic cells are TUNEL-positive and exhibit internucleosomal DNA fragmentation. These canonical features are observed at initial stages of interdigital tissue remodeling (Garcia-Martinez et al., 1993; Montero et al., 2016).

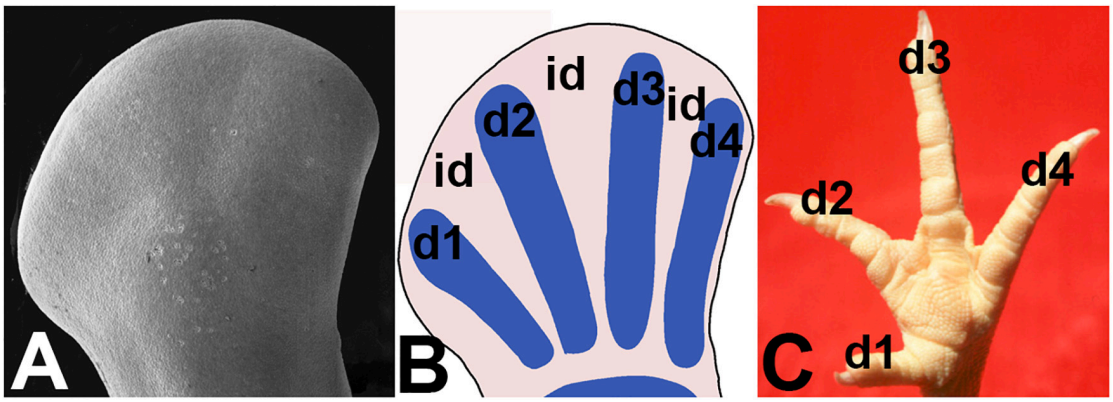

FIGURE 1 | Illustrations showing the changes associated with digit formation in the avian autopod. **(A)** SEM micrograph of the autopod at the most initial stages of digit formation. **(B)** drawing showing the formation of digit rays (d1-d2-d3-d4) and interdigits (id) in the mesodermal core of the autopod. **(C)** Final morphology of the digits (d1-d2-d3-d4) in the adult chicken.

Apoptosis Activated by the Intrinsic Pathway

The intrinsic route, also termed the *mitochondrial apoptotic pathway*, is characterized by permeabilization of the outer mitochondrial membrane. It is initiated following diverse stimuli affecting the cell or the cell environment. Many apoptotic-inducing stimuli recognized in different experimental settings to activate the intrinsic apoptotic pathway are associated with the remodeling of interdigits. These proapoptotic signals include the following: increased oxidative stress (Salas-Vidal et al., 1998; Eshkar-Oren et al., 2015), DNA damage (Montero et al., 2016), loss of cell-cell and/or cell-matrix adhesion (Zuzarte-Luis et al., 2006; Díaz-Mendoza et al., 2013), and growth factor withdrawal (Montero et al., 2001).

The initial stimuli activate a complex molecular machinery that involves the predominant participation of members of the BCL-2 protein family (gene homologous to *C. elegans* CED 9) characterized by sharing sequence and structural similarities. This gene/protein family comprises pro-apoptotic and pro-survival members (**Figure 3**). The two groups of factors have opposing effects that are translated to the outer mitochondrial membranes (Chen et al., 2015). The pro-apoptotic members can be grouped into two subgroups based on the number of BCL-2 homology domains (BH domains). Members of the first subgroup, termed BH3-only proteins, have only a BCL-2 homology domain (BH3), and include, BIM, PUMA, BID, BMF, NOXA, BIK, BAD, and HRK. The BH3-only factors become upregulated upon stimulation by the apoptotic signals mentioned above and block the pro-survival factors and/or activate directly the second subgroup of pro-apoptotic factors (multi-BH domain factors) constituted by BAX, BAK, and BOK (Ke et al., 2018) that cause permeabilization of the outer mitochondrial membrane and subsequent delivery of cytochrome C and mitochondrial genotoxic factors such as AIF (apoptotic inducing factor). Cytochrome C forms a complex with APAF-1 (apoptotic protease-activating factor-1) and pro-caspase 9, the "apoptosome," which activates initiator Caspase-9. This caspase activates the executioner caspases.

The pro-survival factors of the BCL-2 family include BCL-2, MCL-1, BCL-XL, BCL-W, and A1/BFL-1. These factors block the activation of BAX, BAK, and BOK, by the BH3-only pro-apoptotic factors, thus protecting cells from apoptosis (**Figure 3**).

Preferential expression domains of pro-survival factors in the developing digits and pro-apoptotic factors in remodeling interdigits have been reported. Thus, BCL-2, BCLXL (Novack and Korsmeyer, 1994; Bečić et al., 2016), and A1 (Carrió et al., 1996) show preferential expression domains in the developing digits, while BAK and BAX are preferentially expressed in the interdigital regions (Dupé et al., 1999; Bečić et al., 2016).

Despite the importance of cell death in embryonic development, mice subjected to individual deletion of the different components of this cascade (including A1, Bak, Bax, Bad, Bcl2, Bik, Bim, Bmf, Bok, Hrk, Puma, and Noxa) lack the digit phenotype and most of them develop normally (Ke et al., 2018; and reviews by Tuzlak et al., 2016; Voss and Strasser, 2020). Syndactyly was only observed in double (Bax/Bak; Bax/Bim; Bim/Bmf) or triple (Bax/Bak/Bok) knockout mice (see Voss and Strasser, 2020). These observations indicate a major role of multi-BH domain factors in the regulation of this route of apoptosis in the interdigits. However, BAX and, most likely also BAK, are regulators of the lysosomal membrane permeability (**Figure 3**), suggesting that its deletion may not only interfere with the apoptotic pathway but also interfere with the lysosomal role in cell death (review by Johansson et al., 2010). The penetrance of syndactyly in double KO of Bak and Bax is accentuated in triple KO that includes the autophagic regulator gene Atg5 (Arakawa et al., 2017). This finding is consistent with a cooperative role of distinct death pathways in interdigit remodeling. This interpretation is also consistent with the absence of the syndactyly (Chautan et al., 1999) after deletion of APAF-1, a component of the apoptosome that exerts a pivotal function in the activation

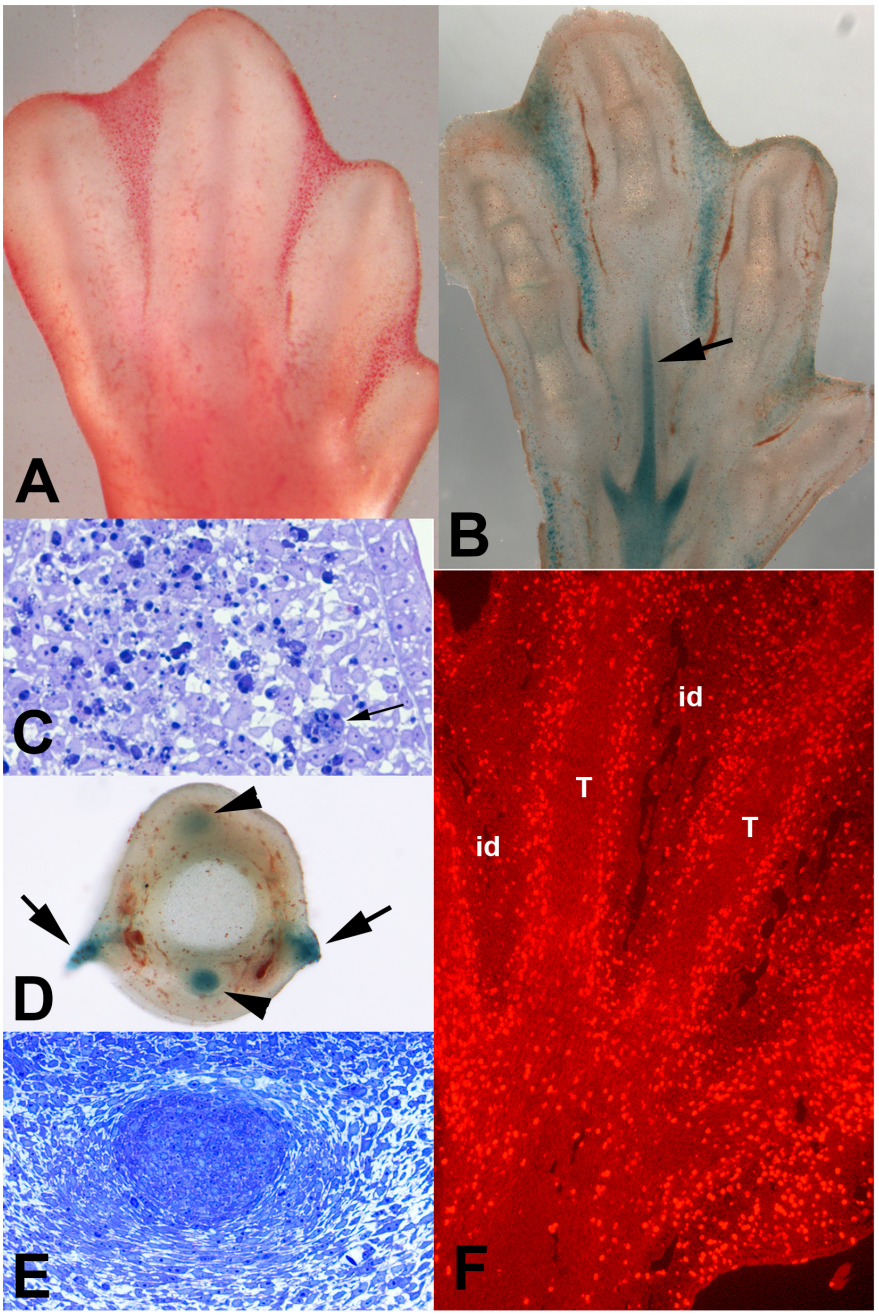

FIGURE 2 | Patterns of cell death and cell senescence in the developing autopod of chick embryos at incubation day 7.5. **(A)** areas of cell death (INZs) mapped by vital stained with neutral red. **(B)** Vibratome section of autopod at stage equivalent to that illustrate in **(A)** showing the pattern of SAβ-gal staining for cell senescence. Note the identical pattern of SAβ-gal and neutral red vital staining in **(A)**. Note also the positivity for SAβ-gal in the developing tendons (arrow). **(C)** Semithin section of the third interdigital space stained with toluidine blue to show the structure of the regressing interdigits. Note the abundance of dark dying cells. Arrow shows a large macrophage containing phagocytosed dead cells. **(D)** Transverse vibratome section of digit 3 at id 8, showing SAβ-gal staining in the interdigital margins of the digit (arrows) and in the extensor and flexor tendons (arrow heads) in course of differentiation. **(E)** Transverse section of digit 3 stained with toluidine blue showing a detailed view of the digit flexor tendon. The level of the section is indicated by black arrows in **(B)**. **(F)** longitudinal section of the autopod through the level of the flexor tendons after incubation for 30 min in bromodeoxyuridine (BrdU). Note the reduced proliferation in the interdigital regions (id) and in the core of the developing tendons (T) (originally published in Lorda-Diez et al., 2009).

of Caspase 9. This initiator caspase is responsible for the activation of the executioner caspases and occupies the last step in the mitochondrial apoptotic pathway (Yoshida et al., 1998). Microscopic analysis showed that non-apoptotic cell death accounts for the removal of the interdigital cells in APAF-1 mutant mice (Chautan et al., 1999).

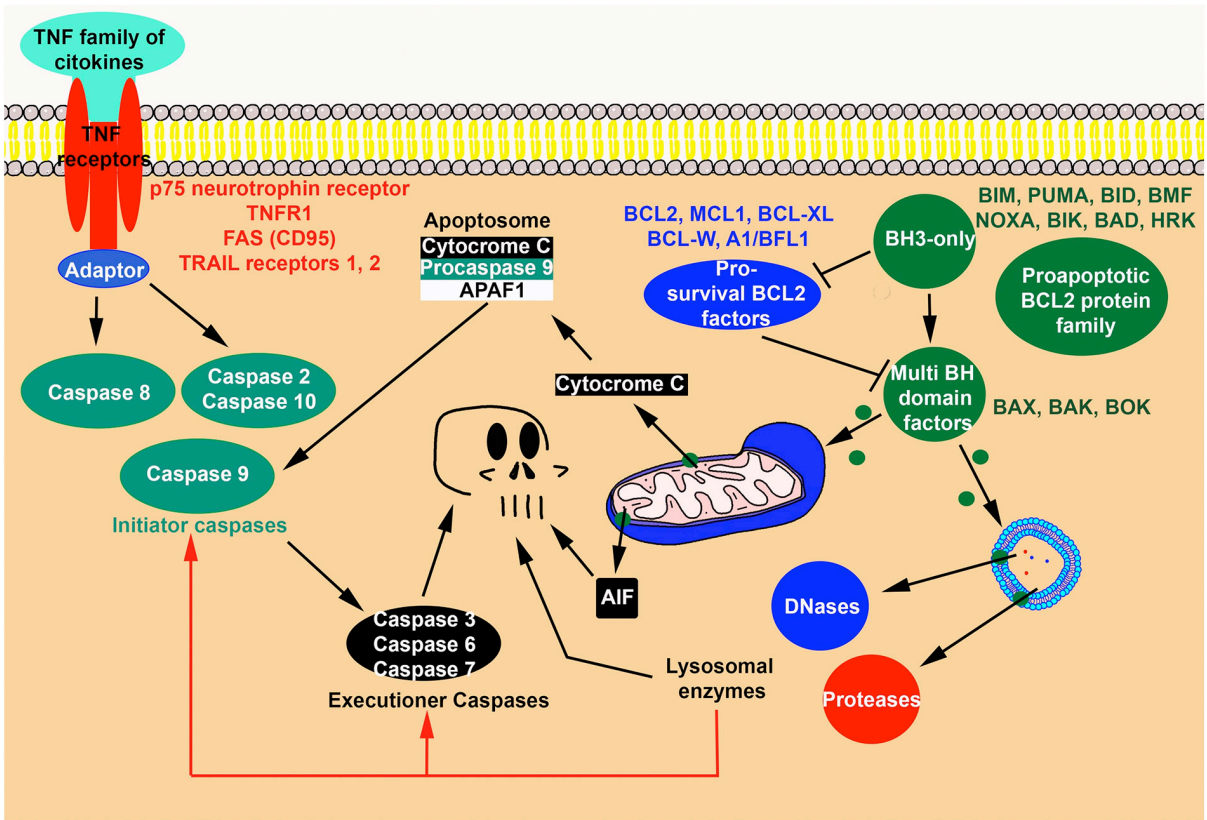

FIGURE 3 | Degenerative routes during physiological cell death. The scheme illustrates the confluence of degenerative signals originated via the apoptotic mitochondrial pathway, the extrinsic apoptotic pathway and the lysosomal pathway. Note also, that mitochondria may deliver non-caspase apoptotic signals, such as AIF.

Apoptosis Activated by the Extrinsic Pathway

Dying cells induced by this pathway are activated by signals external to the cell but are morphologically indistinguishable from apoptosis induced via the mitochondrial pathway (**Figure 3**). The receptors for the dying signal belong to a large superfamily of transmembrane receptors, termed the tumor necrosis receptor factor family (TNFR) comprising four major structurally homologous groups characterized by having an intracellular domain termed the death domain. The most representative members of these groups are $p75^{NTR}$ neurotrophin receptor, TNFR1, FAS (CD95), and TRAIL Receptors 1 and 2 (Sessler et al., 2013). The ligands of this pathway are diverse, and most belong to the TNF family of cytokines. In the canonical pathway, upon ligand binding, the death domain recruits adaptor proteins, also containing a death domain sequence, forming a signaling complex with pro-caspase 8, resulting in its activation or repression. This initiator caspase, in turn, activates the executioner caspases (see review by Mandal et al., 2020). However, the complexity of this route is much greater. On the one hand, many members of the signaling cascade perform developmental functions other than promoting cell death (Sessler et al., 2013). On the other hand, two other initiator caspases, Caspase 10 and Caspase 2 may also participate in the signaling pathway and, most importantly, the extrinsic pathway may switch to other routes of cell death, including necroptosis and apoptosis via the intrinsic pathway (Mandal et al., 2020).

The implication of the extrinsic pathway in interdigital cell death has been proposed based on the specific expression of members of this cascade in the regressing interdigits. Thus, during the formation of the digits in mice, FAS and FASLG together with active Caspase 8 were preferentially expressed in the regressing interdigit (Svandova et al., 2017). In chick embryos, the immunoreactivity for the ligand TNF alpha was reported in the areas of mesodermal cell death of the developing limb (Wride et al., 1994) and nuclear immunoreactivity for active Caspase 2 was intense in interdigital apoptotic cells (Zuzarte-Luis et al., 2006).

In contrast to the expression patterns reported above, genetic approaches have failed to demonstrate the implication of this pathway in interdigital tissue remodeling. Mouse deficient in Caspase 8 are lethal before the formation of digits (Varfolomeev et al., 1998), and humans deficient in Caspase 10 lack the digit phenotype (Wang et al., 1999). Aditionally, despite of the expression of Caspase 2 in the interdigital cells, mice deficient in *Caspase 2* gene lack the digit phenotype (Bergeron et al., 1998), and interdigital electroporation of siRNA for Caspase 2 in chick

embryos only delays, but does not inhibit, interdigit remodeling (Zuzarte-Luis et al., 2006). Together, these observations suggest that the above mentioned factors may be associated with other functions such as, remodeling of the extracellular matrix or as part of the engulfing and degradation of apopototic cells.

Executioner Caspases

The executioner caspases 3, 6, and 7 are activated by both the intrinsic and extrinsic pathways and their proteolytic activity accounts for apoptotic cell degradation. Positivity for the active form of these three proteases in the interdigital dying cells along with the presence in the remodeling interdigits of their targets in the process of degradation supports the implication of apoptosis in interdigital tissue remodeling (Zuzarte-Luis et al., 2006). Although no syndactyly is observed in mouse subjected to caspase gene silencing (Kuida et al., 1996; Zheng et al., 1999), interdigital treatments with pan-caspase inhibitors provided evidence for a major implication of the executioner caspases in the physiological elimination of interdigital cells (Jacobson et al., 1996; Zuzarte-Luis et al., 2006). However, whether inhibition of cell death by these chemical treatments is partial or total remains to be fully clarified.

DEVELOPMENTAL SENESCENCE AND THE LYSOSOMAL DEATH PATHWAY: SAME PROCESS WITH DISTINCT NOMENCLATURE?

The concept of cell senescence was originally formulated to describe the gradual loss of cell division capacity of cultured fibroblasts after several cell divisions (Hayflick, 1965). This finite mitotic capacity was explained as a protective mechanism secondary to the shortening of telomeres after several cell divisions (Harley et al., 1990) and was interpreted as a cell aging mechanism that avoid infinite proliferation of individual cells in multicellular organisms (replicative senescence). However, subsequent studies have shown that cell senescence is a common cell response that protects cells from physiological and/or pathological stresses including oncogene transformation (oncogene-induced senescence), hypoxia, oxidative stress, DNA damage or chemotherapeutic treatments. Consistent with this interpretation, senescence is a characteristic feature of benign and premalignant tumors and is induced in cancer tissues after cytotoxic treatments (Campisi and d'Adda di Fagagna, 2007). Cell senescence has been implicated in the pathogenesis of aging-related diseases (Baker et al., 2011) and is a common feature in degenerative diseases (Krizhanovsky et al., 2008; Muñoz-Espín and Serrano, 2014; Martínez-Cué and Rueda, 2020). The biological and biomedical interest in these observations promoted an enormous interest in the study and characterization of the cell senescence phenotype (reviewed by Gorgoulis et al., 2019). Cell cycle arrest is a major feature of cell senescence. This is associated with upregulation of tumor suppressor genes that block the progression of the cell cycle, such as p53, p16 (CDKN2A), and p21. Many morphological, structural, metabolic and molecular features are also common but are not fully specific characteristics of senescent cells. Two seminal markers additional to cell cycle arrest characterize senescence processes: (i) lysosomal hypertrophy; and (ii) activation of a secretory phenotype, termed SASP (senescence-associated-secretory-phenotype). The hypertrophy of lysosomes concerns the upregulation of most lysosomal enzymes (Kurz et al., 2000; Byun et al., 2009), but the detection of β-galactosidase at pH 6 (senescence-associated-β-galactosidase; SAβ-gal) is considered the most specific biomarker of cell senescence (Lee et al., 2006). The increased lysosomal activity is often associated with autophagy, which recycles cellular constituents providing energy and substrates required for the secretion of SASP components (Ivanov et al., 2013; see review by Shin and Zoncu, 2020). The SASP shows variations among senescent cells of different lineages, but common components of the SASP are proinflammatory cytokines and chemokines, growth factors, and matrix metalloproteinases. The SASP is thought to reinforce and spread senescence and activates immune responses that eliminate senescent cells (Acosta et al., 2013; Muñoz-Espín and Serrano, 2014).

In the last decade, in contrast to the protective role played by cell senescence in adult organisms, areas of massive cell senescence were observed during embryonic development in structures undergoing remodeling processes, such as the embryonic heart, otic vesicle, neural roof plate, limb primordia, or the mesonephros (Storer et al., 2013; Muñoz-Espín et al., 2013; Lorda-Diez et al., 2015, 2019; Varela-Nieto et al., 2019). It was proposed that cell senescence is primarily an embryonic process that is evolutionarily adapted to protect organisms from oncogenesis, premature aging and other cell stressors (Storer et al., 2013) via the elimination of unwanted or damaged cells (Muñoz-Espín and Serrano, 2014). In the embryonic models, the predominant view is that local remodeling signals promote cell senescence. However, the fate of senescent cells and their functional integration with other canonical embryonic degenerative processes, such as apoptosis, autophagy, extracellular matrix degeneration, or phagocytosis, await clarification (Childs et al., 2014; Li et al., 2018).

Cell Senescence Is a Feature of the INZs

Interdigital tissue remodeling (formerly described as, interdigital necrotic zones, INZ) during digit morphogenesis constitutes the most appropriate model to study the biological significance of cell senescence in developing systems (Lorda-Diez et al., 2015). Consistent with the senescence nature of this morphogenetic process cell cycle arrest and overexpression of p21, p63, p73, and the Btg/Tob tumor suppressor gene family are precocious features of interdigit remodeling (Tone and Tanaka, 1997; Vasey et al., 2011; Lorda-Diez et al., 2015; Svandova et al., 2017). Furthermore, SAβ-gal histochemical staining is a very precise marker of INZs (**Figure 2B**), and also identifies all other areas of embryonic cell death (Muñoz-Espín et al., 2013; Storer et al., 2013; Lorda-Diez et al., 2019). Remarkably, the pattern of SAβ-gal is indistinguishable from the pattern of staining with vital dyes (**Figures 2A,B**) or with specific lysosomal markers, such as LysoTracker (Zucker and Rogers, 2019). Classical descriptions of the embryonic areas of cell death have relied mainly on vital staining procedures. The staining similarity between SAβ-gal and

Neutral red or Nile blue is not surprising because vital dyes (Weijer et al., 1987), including LysoTracker (Zucker and Rogers, 2019), are markers of the lysosomal compartments (lysosomes, autophagosomes, or heterophagosomes).

Molecular compounds, such as tissue transglutaminase (tTG), which has been reported to be a marker of cell senescence (Kim et al., 2001), are specifically expressed in the developing interdigits (Dupé et al., 1999; Thomázy and Davies, 1999; Svandova et al., 2017). Importantly, immunohistochemistry and transcriptional analysis of INZ identified the prominent upregulation of characteristic SASP members (Dupé et al., 1999; Allan et al., 2000; Lorda-Diez et al., 2015; Svandova et al., 2017), including interleukin 8, Igf1, IgfBP5, HGF, Tgfβ2, AREGB (Amphiregulin B), matrix metalloproteinases (MMPs) (such as, MMP2, MMP9, MMP11, and ADAMTS9), and members of the TNF signaling pathway (such as TNF alpha, Fas (CD95), FasL, Tnfrsf1a, Tnfrsf21 (DR6), and Tnfrsf 23) (**Table 1**).

Cell Senescence and Tendon Formation During Digit Development

A central question about cell senescence in INZ (and also in other areas of embryonic cell death) is whether it is a degenerating event that precedes apoptosis or whether it is concurrent with apoptosis but plays a protective role against local stressors.

TABLE 1 | SASP components identified in the regressing interdigits.

Genes	6 id	7.5 id	8 id
		Expression fold changes	
Senescence-associated secretory phenotype (SASP; Lorda-Diez et al., 2015)			
IL8L1	1.00 ± 0.04	**11.10 ± 3.51***	**20.59 ± 5.18***
IL8L2	1.02 ± 0.08	**1.93 ± 0.22****	**3.12 ± 0.46***
AREGB	1.05 ± 0.19	**2.23 ± 0.43***	**2.46 ± 0.71***
HGF	1.01 ± 0.08	**1.98 ± 0.20****	**1.85 ± 0.37***
TGFβ2	1.03 ± 0.07	**1.85 ± 0.25***	**2.53 ± 0.53***
IGF1	1.00 ± 0.01	**5.72 ± 1.62***	**7.86 ± 2.20***
IGFBP5	1.00 ± 0.02	**7.70 ± 1.86****	**19.36 ± 4.44****
MMP2	1.01 ± 0.06	**2.79 ± 0.45****	**4.47 ± 0.78***
MMP9	1.00 ± 0.02	**2.49 ± 0.44****	**4.33 ± 0.91***
Adamts9	1.00 ± 0.04	**6.70 ± 1.11****	**22.66 ± 5.92***
FAS	1.02 ± 0.04	**1.88 ± 0.18*****	**1.81 ± 0.24***
TNFRSF21	1.00 ± 0.02	0.83 ± 0.12	**1.62 ± 0.25***
TNFRSF23	1.03 ± 0.14	**1.92 ± 0.31***	**3.28 ± 0.88***
Other SASP components upregulated in the interdigit			
TNFα		Wride et al., 1994	
MMP11		Dupé et al., 1999	
tTG		Dupé et al., 1999	
FASLG		Svandova et al., 2017	

*The upper part of the table shows components undergoing intense transcriptional upregulation in the third interdigits of the chick limb. Note the increased expression from the stage preceding interdigit remodeling (id 6) to the stage of peak degeneration (id 8). The lower part of the table corresponds to characteristic SASP components reported to be expressed at high levels in the regressing interdigits of mouse and human embryos. ***$p < 0.001$; **$p < 0.01$; *$p < 0.05$ statistical significance (bold) in differences of gene expression levels between 7.5id (middle column) and 8id (right column) vs 6 id (left column).*

The pattern of SAβ-gal staining in vibratome sections of the developing autopod reveals two extremely different domains: the interdigits and the core of the differentiating tendon blastemas (**Figures 2B,D**). As described above, the interdigital regions are very positive for SAβ-gal. Notably, these domains have a characteristic doted appearance consistent with a distribution of SAβ-gal in lysosomes and phagosomes of most interdigital cells. By contrast, the labeling of the tendon blastemas is very intense but uniform, consistent with the presence of a dense number of primary lysosomes per cell. The senescence nature of the tendon domains is supported by cell cycle arrest in the core cells of the tendons (**Figure 2F**; Lorda-Diez et al., 2009) and by the precise expression of Tgfbeta 2 and CCN matricellular proteins (Lorda-Diez et al., 2013) and IGFBP-5 (Allan et al., 2000), which are characteristic SASP members that promote senescence in adult tissues and other embryonic models (Jun and Lau, 2010; Muñoz-Espín et al., 2013; Gibaja et al., 2019). Considering the different structures of the tendon blastemas and interdigits (**Figures 2C,E**) and the disparate fate of both tissues, it is likely that senescence in the tendon blastemas reflects a distinct biological function. Tendon blastemas in the stages of interdigital remodeling, are in the course of differentiation characterized by the production and maturation of a hypocellular fibrous matrix associated with the expression of CCN matricellular proteins (Lorda-Diez et al., 2011). It is tempting to propose the similarity of this process to that during cutaneous wound healing in adult organisms where senescence, regulated via CCN matricellular proteins, functions as a modulator of fibrosis (Jun and Lau, 2010). The occurrence of cell senescence associated with cell differentiation but not with apoptosis is not an exclusive feature of the developing tendons. During eye development, cell senescence identified by specific SAβ-gal labeling, p21 gene expression and proliferation arrest, has been reported in differentiating neurons and photoreceptors of the developing retina (de Mera-Rodríguez et al., 2019). Similar findings were observed in the maturing ventricular myocardium of embryonic mice (Lorda-Diez et al., 2019). Whether these non-degenerative processes positive for SAβ-gal constitutes "true" cell senescence processes or reflects that distinct biological phenomena share mechanistic events remains to be clarified. It is tempting to suggest a double and opposite functional significance of senescence in developing systems. In most cases, cell senescence is coincident with zones of cell death identifiable by current techniques of vital staining, that we propose to term "destructive developmental cell senescence," to be distinguished from systems, such as the developing tendons or maturing retinal neurons, where senescence mechanisms appear associated with the establishment of low- or non-proliferative mature tissues. We propose the term "constructive developmental senescence" for these processes.

Lysosomal Implication in Interdigit Remodeling and Cell Senescence

The abundance of rounded dark dying cells in histological sections of interdigits during remodeling suggests that apoptosis is the predominant cell degenerative feature of this regressing tissue (**Figure 2C**). However, transmission electron microscopy

showed that, in addition to dark apoptotic cells, necrotic-like cell remnants with disintegrated cell membranes (**Figure 4A**), and healthy cells (deduced by their nuclear morphology) rich in lysosomal vacuoles are very abundant (**Figure 4B**). These vacuoles are of variable size. In some cases, the small size, structure, and content of these vacuoles allow their identification as autophagic. In other cases, vacuoles are large and their content suggests a heterophagic origin. Cell senescence is accompanied by an increased mass of lysosomes (Kurz et al., 2000) and intense autophagy (Young et al., 2009). Additionally, at least in some cancer models of senescence, cells are highly enriched for genes related to phagocytosis and actively engulf

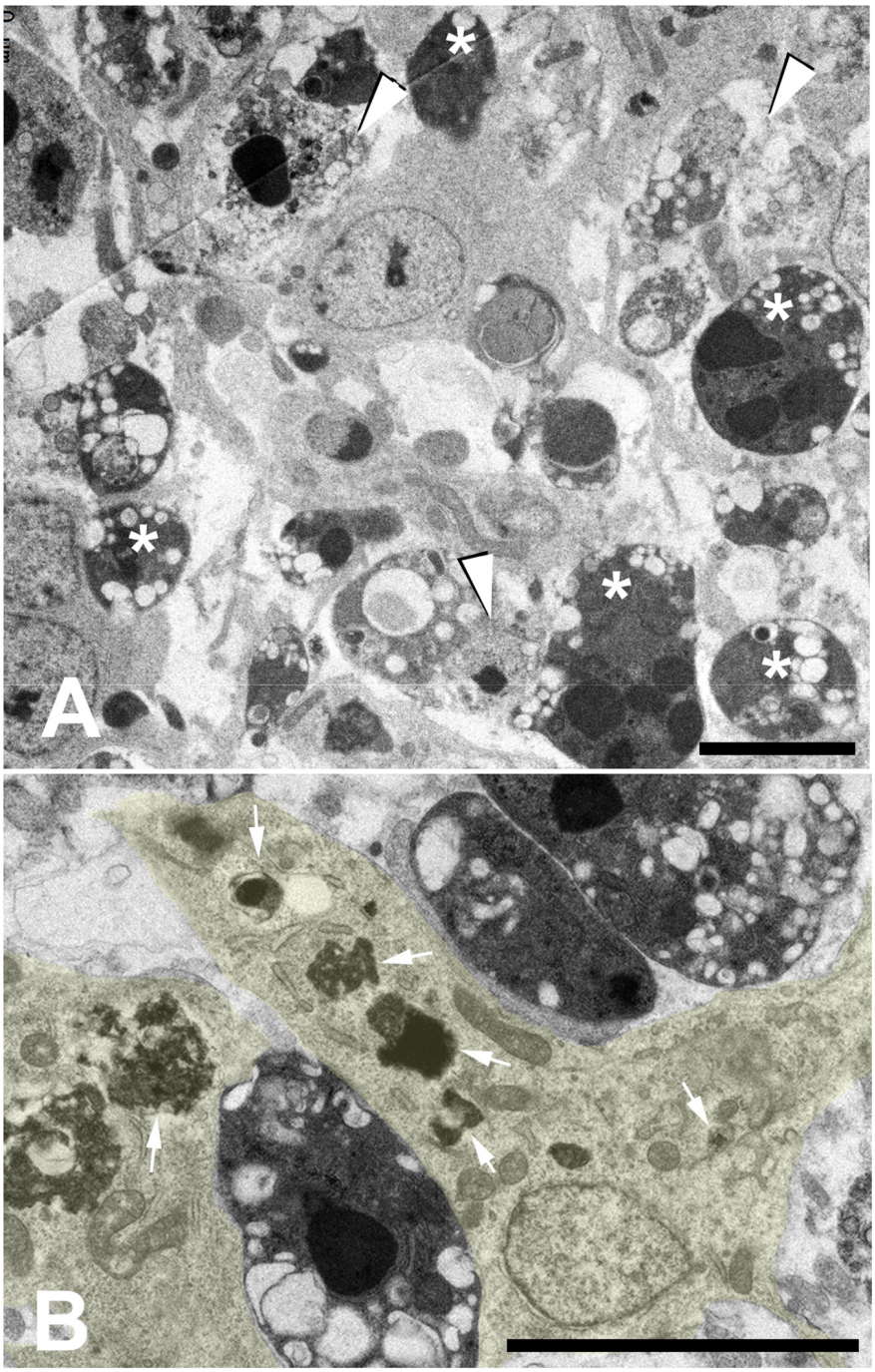

FIGURE 4 | Transmission electron microscopic images of the interdigital tissue during remodeling (incubation day 7.5). **(A)** low magnification view showing the presence of electron-dense apoptosis (*) and necrotic like cells with disintegration of cell membranes (arrow heads). **(B)** healthy interdigital cells (enhanced in yellow) located between dark apoptotic cells. Arrows show the abundance a phagosomes of different sizes within the cytoplasm. Magnification bar = 5 μm.

neighboring senescent cells (Tonnessen-Murray et al., 2019). These observations together with the absence of other identifiable cell populations in the regressing interdigits, except for large macrophages of hemopoietic origin (Cuadros et al., 1992) and blood vessels, indicate that cells rich in autophagic and heterophagic vacuoles are the ones labeled with SAβ-gal; and therefore, they are senescent cells.

Studies devoted to analyzing the involvement of lysosomes in the areas of embryonic cell death provided compelling evidence for active lysosomal participation in remodeling limb tissues (Hurle and Hinchcliffe, 1978), albeit the knockdown of lysosomal genes in mice do not cause syndactyly (Saftig et al., 1995; Deussing et al., 1998; Roth et al., 2000). The following observations support the active participation of lysosomes in interdigit tissue removal: (1) as mentioned above, lysosomes and digestive vacuoles containing the cell remnants of auto and/or heterophagic origin are very abundant in the interdigital mesoderm, including TUNEL-positive apoptotic cells (Zuzarte-Luis et al., 2006); (2) various lysosomal cathepsins and lysosomal DNases are intensely upregulated in the interdigits at both the mRNA and protein levels, even when interdigits are explanted to culture dishes, to eliminate the participation of exogenous professional phagocytes of hematopoietic origin (Zuzarte-Luis et al., 2007; Montero et al., 2010); (3) the microenvironmental pH value in the interdigits decreases during remodeling to levels only appropriate for acidic enzymes (Montero et al., 2010); (4) lysosomal enzymes are released into the cytoplasm of cells during degeneration (Hurle and Hinchcliffe, 1978; Zuzarte-Luis et al., 2007; Montero et al., 2010); (5) local treatments with the cathepsin D inhibitor pepstatin A significantly increased the inhibition of interdigital cell death by treatments with pan-caspase inhibitors (Zuzarte-Luis et al., 2007); (6) syndactyly observed in Bak/Bax double-knockout mice, is potentiated when combined with the silencing of the autophagic regulator gene Atg5 (Arakawa et al., 2017).

Although autophagy and even heterophagy are survival mechanisms that supply energy to support the secretory profile of senescent cells (Young et al., 2009; Tonnessen-Murray et al., 2019), the above-reviewed observations suggest that rather than protecting cells from local stressors, cell senescence, via lysosomal activation exerts an active and potent catabolic function in the elimination of interdigital tissue.

Lysosomal vs. Caspase-Dependent Dying Mechanisms: Sequential or Complementary Processes?

Whether the lysosomal- and caspase-dependent cell death are redundant and independent dying pathways, or if they constitute hierarchical mechanisms, are central questions to unravel the basis of interdigit remodeling. Studies of cell death during Drosophila metamorphosis provide examples of lysosomal cell death (autophagic) acting in parallel with caspases (salivary gland remodeling), independent of caspases (midgut cell death) and, upstream or downstream caspases in a context depend fashion (ovary maturation) (reviewed by Doherty and Baehrecke, 2018). In the case of the remodeling interdigits the identification of a common upstream regulation for both lysosomal cell death and apoptosis suggests a dual-parallel role of lysosomal and caspase-dependent cell death (Montero et al., 2016). DNA methyl transferases 1, 3A and 3B (DNMT1, 3A, and 3B) and the epigenetic regulators UHRF1 and 2 show high expression domains in the interdigital regions preceding the establishment of INZs. Gain- and loss-of-function experiments of DNMT3B and UHRF genes established a positive correlation between the expression level of these epigenetic regulators and cell death (Sanchez-Fernandez et al., 2019, 2020). Furthermore, interdigital progenitors are much more sensitive to genotoxic stimuli than cells of the growing digit tip that survive and account for digit outgrowth (Sanchez-Fernandez et al., 2020). Notably, local signals that are not harmful for differentiating progenitors cause DNA damage that interdigital cells try, but fail, to repair (Montero et al., 2016). According to these studies, failure to DNA repair triggers both apoptosis and lysosomal activation as a defensive response of cells against DNA damage. The sequence of lysosomal and caspase-dependent cell death that follows DNA damage after exposure to physiological (BMPs) or exogenous (H_2O_2) dying signals supports this interpretation (Montero et al., 2016). However, the complexity and promiscuity of the molecular machinery implicated in the different forms of cell death as well as the scarcity of interdigital phenotypes after gene silencing of the main players of each degenerative pathway, cannot rule out an alternative "hierarchical" function starting by caspase-dependent cell death and followed by lysosomal activation. Thus, mouse deficient in Apaf1, lacking caspase-dependent cell death, shows that apoptotic cells observed during physiological interdigit regression are substituted by cells with a rather necrotic appearance (Chautan et al., 1999). Whether this finding reflects that blocking caspases results in a context-dependent activation of lysosomes, as reported in fibroblast Bax/Bak$^{-/-}$ (Shimizu et al., 2004), or if physiological lysosomal cell death expands and replace caspases in the elimination of interdigital cells has not been fully ascertain. However, as we reported above, triple KO of Atg5/Bax/Bak$^{-/-}$ increases significantly the penetrance of syndactyly (i.e., the number of cells eliminated) observed in caspase-deficient mouse Bax/Bak$^{-/-}$ (Arakawa et al., 2017), thus supporting the dual role of both dying pathways. Considering that lysosomal activation represents a manifestation of cell senescence it is tempting to suggest, that this double activation of caspases and lysosomes is the basis of what we called "destructive developmental cell senescence."

ADDITIONAL POTENTIAL FUNCTIONS OF CELL SENESCENCE IN INTERDIGIT REMODELING: EXTRINSIC APOPTOTIC PATHWAY, RECRUITMENT OF MACROPHAGES AND EXTRACELLULAR MATRIX DEGRADATION

As described above, among the components of SASP identified in interdigit remodeling are members of the TNFR superfamily of transmembrane receptors, which participate in various models

of apoptosis activated by the extrinsic pathway. Because full characterization of the interdigital SASP has not been performed to date, additional members of the TNF signaling pathway produced by the senescent interdigital cells may be involved in the regulation of cell death. Similarly, cytokines and chemokines included in the SASP may contribute to recruit professional macrophages (Cuadros et al., 1992) to fully accomplish the elimination of dying cells and cell detritus. This is an important, but dispensable, aspect of the regression of the interdigital tissue (Wood et al., 2000).

A final important feature of interdigit remodeling is the degradation of the extracellular matrix, collapse of the blood vessels (Hurle et al., 1985) and the subsequent elimination of waste ectodermal tissue into the amniotic sac (Hurle and Fernandez-Teran, 1983; McCulloch et al., 2009; Kashgari et al., 2020). This aspect of tissue remodeling has been often neglected in developmental studies devoted to cell death-mediated morphogenesis. However, its dysregulation abrogates the formation of free digits (McCulloch et al., 2009; Kashgari et al., 2020). The abundance of secreted matrix metalloproteases in the SASP (described above) sustains without doubt this important aspect of interdigital tissue remodeling.

CONCLUDING REMARKS

The experimental data surveyed here support the occurrence of a unified process of embryonic tissue remodeling involving the activation of two main degenerative routes, namely, the lysosomal pathway-mediated and caspase-dependent cell death. From an historical point of view, the introduction of the term *apoptosis*, to define a type of cell death "active, and inherently programmed" distinct from "*necrosis*" (Kerr et al., 1972) led to a breakthrough in our knowledge of the control and biological significance of cell death in embryonic and non-embryonic processes. However, as a counterpart, the role of lysosomes was neglected, despite initial descriptions considering lysosomes as the primary cause of the embryonic remodeling processes (Salzgeber and Weber, 1966; Hurle and Hinchcliffe, 1978). The description of "*developmental senescence*" recovered lysosomes as major effectors of embryonic cell death, and the discovery of the SASP shed much light on our understanding of local signaling emanating from the degenerating cells that modulates the intensity and expansion of tissue remodeling. However, it is important to highlight the differences observed between two adjacent senescent processes occurring at the same stages in the developing autopod: interdigit remodeling and tendon tissue maturation. In contrast to reports in adult tissues where senescence is considered a protective process against stressors, interdigital senescence appears to be a destructive (Muñoz-Espín et al., 2013), but finely regulated process ("*destructive developmental cell senescence*"). By contrast, senescence in the developing tendons, is not associated with tissue degeneration and appears to be a constructive process that regulates tendon maturation ("*constructive developmental senescence*").

AUTHOR CONTRIBUTIONS

JM, CL-D, and JH discussed, reviewed, edited, and wrote the manuscript. All authors contributed to the article and approved the submitted version.

FUNDING

This work was supported by a grant (BFU2017-84046-P) from the Spanish Science and Innovation Ministry to JM.

REFERENCES

Acosta, J. C., Banito, A., Wuestefeld, T., Georgilis, A., Janich, P., Morton, J. P., et al. (2013). A complex secretory program orchestrated by the inflammasome controls paracrine senescence. *Nat. Cell Biol.* 15, 978–990. doi: 10.1038/ncb2784

Allan, G. J., Flint, D. J., Darling, S. M., Geh, J., and Patel, K. (2000). Altered expression of insulin-like growth factor-1 and insulin like growth factor binding proteins-2 and 5 in the mouse mutant Hypodactyly (Hd) correlates with sites of apoptotic activity. *Anat. Embryol.* 202, 1–11. doi: 10.1007/pl00008239

Arakawa, S., Tsujioka, M., Yoshida, T., Tajima-Sakurai, H., Nishida, Y., Matsuoka, Y., et al. (2017). Role of Atg5-dependent cell death in the embryonic development of Bax/Bak double-knockout mice. *Cell Death Differ.* 24, 1598–1608. doi: 10.1038/cdd.2017.84

Baker, D. J., Wijshake, T., Tchkonia, T., LeBrasseur, N. K., Childs, B. G., van de Sluis, B., et al. (2011). Clearance of p16Ink4a- positive senescent cells delays ageing-associated disorders. *Nature* 479, 232–236. doi: 10.1038/nature10600

Bečić, T., Bilan, K., Mardešić, S., Vukojević, K., and Saraga-Babić, M. (2016). Spatiotemporal distribution of proliferation, proapoptotic and antiapoptotic factors in the early human limb development. *Acta Histochem.* 118, 527–536. doi: 10.1016/j.acthis.2016.05.008

Bergeron, L., Perez, G. I., Macdonald, G., Shi, L., Sun, Y., Jurisicova, A., et al. (1998). Defects in regulation of apoptosis in caspase-2-deficient mice. *Genes Dev.* 12, 1304–1314. doi: 10.1101/gad.12.9.1304

Byun, H. O., Han, N. K., Lee, H. J., Kim, K. B., Ko, Y. G., Yoon, G., et al. (2009). Cathepsin D and eukaryotic translation elongation factor 1 as promising markers of cellular senescence. *Cancer Res.* 69, 4638–4647. doi: 10.1158/0008-5472.CAN-08-4042

Campisi, J., and d'Adda di Fagagna, F. (2007). Cellular senescence: when bad things happen to good cells. *Nat. Rev. Mol. Cell Biol.* 8, 729–740. doi: 10.1038/nrm2233

Carrió, R., López-Hoyos, M., Jimeno, J., Benedict, M. A., Merino, R., Benito, A., et al. (1996). A1 demonstrates restricted tissue distribution during embryonic development and functions to protect against cell death. *Am. J. Pathol.* 149, 2133–2142.

Chautan, M., Chazal, G., Cecconi, F., Gruss, P., and Golstein, P. (1999). Interdigital cell death can occur through a necrotic and caspase-independent pathway. *Curr. Biol.* 9, 967–970.

Chen, H. C., Kanai, M., Inoue-Yamauchi, A., Tu, H. C., Huang, Y., Ren, D., et al. (2015). An interconnected hierarchical model of cell death regulation by the BCL-2 family. *Nat. Cell Biol.* 17, 1270–1281. doi: 10.1038/ncb3236

Childs, B. G., Baker, D. J., Kirkland, J. L., Campisi, J., and van Deursen, J. M. (2014). Senescence and apoptosis: dueling or complementary cell fates? *EMBO Rep.* 15, 1139–1153. doi: 10.15252/embr.201439245

Cooper, L. N., Sears, K. E., Armfield, B. A., Kala, B., Hubler, M., and Thewissen, J. G. M. (2018). Review and experimental evaluation of the embryonic development and evolutionary history of flipper development and hyperphalangy in dolphins (Cetacea: Mammalia). *Genesis* 56:dvg.23076. doi: 10.1002/dvg.23076

Cuadros, M. A., Coltey, P., Nieto, C. M., and Martin, C. (1992). Demonstration of a phagocytic cell system belonging to the hemopoietic lineage and originating from the yolk sac in the early avian embryo. *Development* 115, 157–168.

de Mera-Rodríguez, J. A., Álvarez-Hernán, G., Gañán, Y., Martín-Partido, G., Rodríguez-León, J., and Francisco-Morcillo, J. (2019). Senescence-associated β-galactosidase activity in the developing avian retina. *Dev. Dyn.* 248, 850–865. doi: 10.1002/dvdy.74

Deussing, J., Roth, W., Saftig, P., Peters, C., Ploegh, H. L., and Villadangos, J. A. (1998). Cathepsins B and D are dispensable for major histocompatibility complex class II-mediated antigen presentation. *Proc. Natl. Acad. Sci. U.S.A.* 95, 4516–4521.

Díaz-Mendoza, M. J., Lorda-Diez, C. I., Montero, J. A., García-Porrero, J. A., and Hurlé, J. M. (2013). Interdigital cell death in the embryonic limb is associated with depletion of Reelin in the extracellular matrix. *Cell Death Dis.* 4:e800. doi: 10.1038/cddis.2013.322

Doherty, J., and Baehrecke, E. H. (2018). Life, death and autophagy. *Nat. Cell Biol.* 20, 1110–1117. doi: 10.1038/s41556-018-0201-205

Dupé, V., Ghyselinck, N. B., Thomazy, V., Nagy, L., Davies, P. J., Chambon, P., et al. (1999). Essential roles of retinoic acid signaling in interdigital apoptosis and control of BMP-7 expression in mouse autopods. *Dev. Biol.* 208, 30–43. doi: 10.1006/dbio.1998.9176

Ellis, H. M., and Horvitz, H. R. (1986). Genetic control of programmed cell death in the nematode *C. elegans*. *Cell* 44, 817–829.

Eshkar-Oren, I., Krief, S., Ferrara, N., Elliott, A. M., and Zelzer, E. (2015). Vascular patterning regulates interdigital cell death by a ROS-mediated mechanism. *Development* 142, 672–680. doi: 10.1242/dev.120279

Garcia-Martinez, V., Macias, D., Gañan, Y., Garcia-Lobo, J. M., Francia, M. V., Fernandez-Teran, M. A., et al. (1993). Internucleosomal DNA fragmentation and programmed cell death (apoptosis) in the interdigital tissue of the embryonic chick leg bud. *J. Cell Sci.* 106, 201–208.

Gibaja, A., Aburto, M. R., Pulido, S., Collado, M., Hurle, J. M., Varela-Nieto, I., et al. (2019). TGFβ2-induced senescence during early inner ear development. *Sci. Rep.* 9:5912. doi: 10.1038/s41598-019-42040-42040

Glücksmann, A. (1951). Cell deaths in normal vertebrate ontogeny. *Biol. Rev. Camb. Philos. Soc.* 26, 59–86.

Gorgoulis, V., Adams, P. D., Alimonti, A., Bennett, D. C., Bischof, O., Bishop, C., et al. (2019). Cellular senescence: defining a path forward. *Cell* 179, 813–827. doi: 10.1016/j.cell.2019.10.005

Harley, C. B., Futcher, A. B., and Greider, C. W. (1990). Telomeres shorten during ageing of human fibroblasts. *Nature* 345, 458–460. doi: 10.1038/345458a0

Hayflick, L. (1965). The limited in vitro lifetime of human diploid cell strains. *Exp. Cell Res.* 37, 614–636. doi: 10.1016/0014-4827(65)90211-90219

Hurle, J., and Hinchcliffe, J. R. (1978). Cell death in the posterior necrotic zone (PNZ) of the chick wing-bud: a stereoscan and ultrastructural survey of autolysis and cell fragmentation. *J. Embryol. Exp. Morphol.* 43, 123–136.

Hurle, J. M., Colvee, E., and Fernandez-Teran, M. A. (1985). Vascular regression during the formation of the free digits in the avian limb bud: a comparative study in chick and duck embryos. *J. Embryol. Exp. Morphol.* 85, 239–250.

Hurle, J. M., and Fernandez-Teran, M. A. (1983). Fine structure of the regressing interdigital membranes during the formation of the digits of the chick embryo leg bud. *J. Embryol. Exp. Morphol.* 78, 195–209.

Ivanov, A., Pawlikowski, J., Manoharan, I., van Tuyn, J., Nelson, D. M., Rai, T. S., et al. (2013). Lysosome-mediated processing of chromatin in senescence. *J. Cell Biol.* 202, 129–143. doi: 10.1083/jcb.201212110

Jacobson, M. D., Weil, M., and Raff, M. C. (1996). Role of Ced-3/ICE-family proteases in staurosporine-induced programmed cell death. *J. Cell Biol.* 133, 1041–1051. doi: 10.1083/jcb.133.5.1041

Johansson, A.-C., Appelqvist, H., Nilsson, C., Kågedal, K., Roberg, K., and Öllinger, K. (2010). Regulation of apoptosis-associated lysosomal membrane permeabilization. *Apoptosis* 15, 527–540. doi: 10.1007/s10495-009-0452-5

Jun, J.-I. I., and Lau, F. L. (2010). The matricellular protein CCN1 induces fibroblast senescence and restricts fibrosis in cutaneous wound healing. *Nat. Cell Biol.* 12, 676–685. doi: 10.1038/ncb2070

Kashgari, G., Meinecke, L., Gordon, W., Ruiz, B., Yang, J., Ma, A. L., et al. (2020). Epithelial migration and non-adhesive periderm are required for digit separation during mammalian development. *Dev. Cell* 52, 764–778.e4. doi: 10.1016/j.devcel.2020.01.032

Ke, F. F. S., Vanyai, H. K., Cowan, A. D., Delbridge, A. R. D., Whitehead, L., Grabow, S., et al. (2018). Embryogenesis and adult life in the absence of intrinsic apoptosis effectors BAX, BAK, and BOK. *Cell* 173, 1217–1230.e17. doi: 10.1016/j.cell.2018.04.036

Kerr, J. F., Wyllie, A. H., and Currie, A. R. (1972). Apoptosis: a basic biological phenomenon with wide-ranging implications in tissue kinetics. *Br. J. Cancer* 26, 239–257. doi: 10.1038/bjc.1972.33

Kim, J. H., Choy, H. E., Nam, K. H., and Park, S. C. (2001). Transglutaminase-mediated crosslinking of specific core histone subunits and cellular senescence. *Ann. N. Y. Acad. Sci.* 928, 65–70. doi: 10.1111/j.1749-6632.2001.tb05636.x

Krizhanovsky, V., Yon, M., Dickins, R. A., Hearn, S., Simon, J., Miething, C., et al. (2008). Senescence of activated stellate cells limits liver fibrosis. *Cell* 134, 657–667. doi: 10.1016/j.cell.2008.06.049

Kuida, K., Zheng, T. S., Na, S., Kuan, C., Yang, D., Karasuyama, H., et al. (1996). Decreased apoptosis in the brain and premature lethality in CPP32-deficient mice. *Nature* 384, 368–372. doi: 10.1038/384368a0

Kurz, D. J., Decary, S., Hong, Y., and Erusalimski, J. D. (2000). Senescence-associated β-galactosidase reflects an increase in lysosomal mass during replicative ageing of human endothelial cells. *J. Cell Sci.* 113, 3613–3622.

Lee, B. Y., Han, J. A., Im, J. S., Morrone, A., Johung, K., Goodwin, E. C., et al. (2006). Senescence-associated beta-galactosidase is lysosomal beta-galactosidase. *Aging Cell* 5, 187–195. doi: 10.1111/j.1474-9726.2006.00199.x

Li, Y., Zhao, H., Huang, X., Tang, J., Zhang, S., Li, Y., et al. (2018). Embryonic senescent cells re-enter cell cycle and contribute to tissues after birth. *Cell Res.* 28, 775–778. doi: 10.1038/s41422-018-0050-56

Lorda-Diez, C. I., Garcia-Riart, B., Montero, J. A., Rodriguez-León, J., Garcia-Porrero, J. A., and Hurle, J. M. (2015). Apoptosis during embryonic tissue remodeling is accompanied by cell senescence. *Aging* 7, 974–985. doi: 10.18632/aging.100844

Lorda-Diez, C. I., Montero, J. A., Diaz-Mendoza, M. J., Garcia-Porrero, J. A., and Hurle, J. M. (2011). Defining the earliest transcriptional steps of chondrogenic progenitor specification during the formation of the digits in the embryonic limb. *PLoS One* 6:e24546. doi: 10.1371/journal.pone.0024546

Lorda-Diez, C. I., Montero, J. A., Diaz-Mendoza, M. J., Garcia-Porrero, J. A., and Hurle, J. M. (2013). βig-h3 potentiates the profibrogenic effect of TGFβ signaling on connective tissue progenitor cells through the negative regulation of master chondrogenic genes. *Tissue Eng. Part A* 19, 448–457. doi: 10.1089/ten.TEA.2012.0188

Lorda-Diez, C. I., Solis-Mancilla, M. E., Sanchez-Fernandez, C., Garcia-Porrero, J. A., Hurle, J. M., and Montero, J. A. (2019). Cell senescence, apoptosis and DNA damage cooperate in the remodeling processes accounting for heart morphogenesis. *J. Anat.* 234, 815–829. doi: 10.1111/joa.12972

Lorda-Diez, C. I., Torre-Pérez, N., García-Porrero, J. A., Hurle, J. M., and Montero, J. A. (2009). Expression of Id2 in the developing limb is associated with zones of active BMP signaling and marks the regions of growth and differentiation of the developing digits. *Int. J. Dev. Biol.* 53, 1495–1502. doi: 10.1387/ijdb.072415cl

Mandal, R., Barrón, J. C., Kostova, I., Becker, S., and Strebhardt, K. (2020). Caspase-8: the double-edged sword. *Biochim. Biophys. Acta Rev. Cancer* 1873:188357. doi: 10.1016/j.bbcan.2020.188357

Martínez-Cué, C., and Rueda, N. (2020). Cellular senescence in neurodegenerative diseases. *Front. Cell Neurosci.* 14:16. doi: 10.3389/fncel.2020.00016

McArthur, K., and Kile, B. T. (2018). Apoptotic caspases: multiple or mistaken identities? *Trends Cell Biol.* 28, 475–493. doi: 10.1016/j.tcb.2018.02.003

McCulloch, D. R., Nelson, C. M., Dixon, L. J., Silver, D. L., Wylie, J. D., Lindner, V., et al. (2009). ADAMTS metalloproteases generate active versican fragments

that regulate interdigital web regression. *Dev. Cell* 17, 687–698. doi: 10.1016/j.devcel.2009.09.008

Montero, J. A., Gañan, Y., Macias, D., Rodriguez-Leon, J., Sanz-Ezquerro, J. J., Merino, R., et al. (2001). Role of FGFs in the control of programmed cell death during limb development. *Development* 128, 2075–2084.

Montero, J. A., Lorda-Diez, C. I., Certal, A. C., Moreno, N., Rodriguez-Leon, J., Torriglia, A., et al. (2010). Coordinated and sequential activation of neutral and acidic DNases during interdigital cell death in the embryonic limb. *Apoptosis* 15, 1197–1210. doi: 10.1007/s10495-010-0523-527

Montero, J. A., Lorda-Diez, C. I., Sanchez-Fernandez, C., and Hurle, J. M. (2020). Cell death in the developing vertebrate limb: a locally regulated mechanism contributing to musculoskeletal tissue morphogenesis and differentiation. *Dev. Dyn.* 14:dvdy.237. doi: 10.1002/dvdy.237

Montero, J. A., Sanchez-Fernandez, C., Lorda-Diez, C. I., Garcia-Porrero, J. A., and Hurle, J. M. (2016). DNA damage precedes apoptosis during the regression of the interdigital tissue in vertebrate embryos. *Sci. Rep.* 6:35478. doi: 10.1038/srep35478

Muñoz-Espín, D., Cañamero, M., Maraver, A., Gómez-López, G., Contreras, J., Murillo-Cuesta, S., et al. (2013). Programmed cell senescence during mammalian embryonic development. *Cell* 155, 1104–1118. doi: 10.1016/j.cell.2013.10.019

Muñoz-Espín, D., and Serrano, M. (2014). Cellular senescence: from physiology to pathology. *Nat. Rev. Mol. Cell Biol.* 15, 482–496. doi: 10.1038/nrm3823

Nagata, S., Nagase, H., Kawane, K., Mukae, N., and Fukuyama, H. (2003). Degradation of chromosomal DNA during apoptosis. *Cell Death. Differ.* 10, 108–116. doi: 10.1038/sj.cdd.4401161

Novack, D. V., and Korsmeyer, S. J. (1994). Bcl-2 protein expression during murine development. *Am. J. Pathol.* 145, 61–73.

Peter, M. E., Heufelder, A. E., and Hengartner, M. O. (1997). Advances in apoptosis research. *Proc. Natl. Acad. Sci. U.S.A.* 94, 12736–12737. doi: 10.1073/pnas.94.24.12736

Roth, W., Deussing, J., Botchkarev, V. A., Pauly-Evers, M., Saftig, P., Hafner, A., et al. (2000). Cathepsin L deficiency as molecular defect of furless: hyperproliferation of keratinocytes and pertubation of hair follicle cycling. *FASEB J.* 14, 2075–2086. doi: 10.1096/fj.99-0970com

Saftig, P., Hetman, M., Schmahl, W., Weber, K., Heine, L., Mossmann, H., et al. (1995). Mice deficient for the lysosomal proteinase cathepsin D exhibit progressive atrophy of the intestinal mucosa and profound destruction of lymphoid cells. *EMBO J.* 14, 3599–3608. doi: 10.1002/j.1460-2075.1995.tb00029.x

Salas-Vidal, E., Lomelí, H., Castro-Obregón, S., Cuervo, R., Escalante-Alcalde, D., and Covarrubias, L. (1998). Reactive oxygen species participate in the control of mouse embryonic cell death. *Exp. Cell Res.* 238, 136–147. doi: 10.1006/excr.1997.3828

Salzgeber, B., and Weber, R. (1966). The regression of the mesonephros in the chick embryo. A study of acid phosphatase and catepsin activity. Biochemical, histochemical, and electron microscopic observations. *J. Embryol. Exp. Morphol.* 15, 397–419.

Sanchez-Fernandez, C., Lorda-Diez, C. I., García-Porrero, J. A., Montero, J. A., and Hurlé, J. M. (2019). UHRF genes regulate programmed interdigital tissue regression and chondrogenesis in the embryonic limb. *Cell Death Dis.* 10:347. doi: 10.1038/s41419-019-1575-1574

Sanchez-Fernandez, C., Lorda-Diez, C. I., Hurle, J. M., and Montero, J. A. (2020). The methylation status of the embryonic limb skeletal progenitors determines their cell fate in chicken. *Commun. Biol.* 3:283. doi: 10.1038/s42003-020-1012-1013

Saunders, J. W. Jr. (1966). Death in embryonic systems. *Science* 154, 604–612. doi: 10.1126/science.154.3749.604

Sessler, T., Healy, S., Samali, A., and Szegezdi, E. (2013). Structural determinants of DISC function: new insights into death receptor-mediated apoptosis signalling. *Pharmacol. Ther.* 140, 186–199. doi: 10.1016/j.pharmthera.2013.06.009

Shimizu, S., Kanaseki, T., Mizushima, N., Mizuta, T., Arakawa-Kobayashi, S., Thompson, C. B., et al. (2004). Role of Bcl-2 family proteins in a non-apoptotic programmed cell death dependent on autophagy genes. *Nat. Cell Biol.* 6, 1221–1228. doi: 10.1038/ncb1192

Shin, H. R., and Zoncu, R. (2020). The lysosome at the intersection of cellular growth and destruction. *Dev. Cell* 54, 226–238. doi: 10.1016/j.devcel.2020.06.010

Storer, M., Mas, A., Robert-Moreno, A., Pecoraro, M., Ortells, M. C., Di Giacomo, V., et al. (2013). Senescence is a developmental mechanism that contributes to embryonic growth and patterning. *Cell* 155, 1119–1130. doi: 10.1016/j.cell.2013.10.041

Svandova, E. B., Vesela, B., Lesot, H., Poliard, A., and Matalova, E. (2017). Expression of Fas, FasL, caspase-8 and other factors of the extrinsic apoptotic pathway during the onset of interdigital tissue elimination. *Histochem. Cell Biol.* 147, 497–510. doi: 10.1007/s00418-016-1508-1506

Thomázy, V. A., and Davies, P. J. (1999). Expression of tissue transglutaminase in the developing chicken limb is associated both with apoptosis and endochondral ossification. *Cell Death Differ.* 6, 146–154. doi: 10.1038/sj.cdd.4400464

Tokita, M., Hiroya, I., Matsushita, H., and Asakura, Y. (2020). Developmental mechanisms underlying webbed foot morphological diversity in waterbirds. *Sci. Rep.* 10:8028. doi: 10.1038/s41598-020-64786-64788

Tone, S., and Tanaka, S. (1997). Analysis of relationship between programmed cell death and cell cycle in limb-bud. *Horm. Res.* 48(Suppl. 3), 5–10. doi: 10.1159/000191293

Tonnessen-Murray, C. A., Frey, W. D., Rao, S. G., Shahbandi, A., Ungerleider, N. A., Olayiwola, J. O., et al. (2019). Chemotherapy-induced senescent cancer cells engulf other cells to enhance their survival. *J. Cell Biol.* 218, 3827–3844. doi: 10.1083/jcb.201904051

Tuzlak, S., Kaufmann, T., and Villunger, A. (2016). Interrogating the relevance of mitochondrial apoptosis for vertebrate development and postnatal tissue homeostasis. *Genes Dev.* 30, 2133–2151. doi: 10.1101/gad.289298.116

Varela-Nieto, I., Palmero, I., and Magariños, M. (2019). Complementary and distinct roles of autophagy, apoptosis and senescence during early inner ear development. *Hear. Res.* 376, 86–96. doi: 10.1016/j.heares.2019.01.014

Varfolomeev, E. E., Schuchmann, M., Luria, V., Chiannilkulchai, N., Beckmann, J. S., Mett, I. L., et al. (1998). Targeted disruption of the mouse Caspase 8 gene ablates cell death induction by the TNF receptors, Fas/Apo1, and DR3 and is lethal prenatally. *Immunity* 9, 267–276. doi: 10.1016/s1074-7613(00)80609-80603

Vasey, D. B., Wolf, C. R., Brown, K., and Whitelaw, C. B. (2011). Spatial p21 expression profile in the mid-term mouse embryo. *Transgenic Res.* 20, 23–28. doi: 10.1007/s11248-010-9385-6

Voss, A. K., and Strasser, A. (2020). The essentials of developmental apoptosis. *F1000Research* 9:F1000FacultyRev-148. doi: 10.12688/f1000research.21571.1

Wang, J., Zheng, L., Lobito, A., Chan, F. K., Dale, J., Sneller, M., et al. (1999). Inherited human Caspase 10 mutations underlie defective lymphocyte and dendritic cell apoptosis in autoimmune lymphoproliferative syndrome type II. *Cell* 98, 47–58. doi: 10.1016/S0092-8674(00)80605-80604

Weatherbee, S. D., Behringer, R. R., Rasweiler, J. J. IV, and Niswander, L. A. (2006). Interdigital webbing retention in bat wings illustrates genetic changes underlying amniote limb diversification. *Proc. Natl. Acad. Sci. U.S.A.* 103, 15103–15107. doi: 10.1073/pnas.0604934103

Weijer, C. J., David, C. N., and Sternfeld, J. (1987). Vital staining methods used in the analysis of cell sorting in *Dictyostelium discoideum*. *Methods Cell Biol.* 28, 449–459. doi: 10.1016/S0091-679X(08)61662-3

Wood, W., Turmaine, M., Weber, R., Camp, V., Maki, R. A., McKercher, S. R., et al. (2000). Mesenchymal cells engulf and clear apoptotic footplate cells in macrophageless PU.1 *null mouse embryos*. *Development* 127, 5245–5252.

Wride, M. A., Lapchak, P. H., and Sanders, E. J. (1994). Distribution of TNF alpha-like proteins correlates with some regions of programmed cell death in the chick embryo. *Int. J. Dev. Biol.* 38, 673–682.

Wyllie, A. H. (1980). Glucocoticoid-induced thymocyte apoptosis is associated with endogenous endonuclease activation. *Nature* 284, 555–556. doi: 10.1038/284555a0

Yoshida, H., Kong, Y. Y., Yoshida, R., Elia, A. J., Hakem, A., Hakem, R., et al. (1998). Apaf1 is required for mitochondrial pathways of apoptosis and brain development. *Cell* 94, 739–750. doi: 10.1016/s0092-8674(00)81733-x

Young, A. R., Narita, M., Ferreira, M., Kirschner, K., Sadaie, M., Darot, J. F., et al. (2009). Autophagy mediates the mitotic

senescence transition. *Genes Dev.* 23, 798–803. doi: 10.1101/gad.519709

Zheng, T. S., Hunot, S., Kuida, K., and Flavell, R. A. (1999). Caspase knockouts: matters of life and death. *Cell Death Differ.* 6, 1043–1053. doi: 10.1038/sj.cdd

Zucker, R. M., and Rogers, J. M. (2019). Confocal laser scanning microscopy of morphology and apoptosis in organogenesis-stage mouse embryos. *Methods Mol. Biol.* 1965, 297–311.

Zuzarte-Luis, V., Berciano, M. T., Lafarga, M., and Hurlé, J. M. (2006). Caspase redundancy and release of mitochondrial apoptotic factors characterize interdigital apoptosis. *Apoptosis* 11, 701–715. doi: 10.1007/s10495-006-5481-5488

Zuzarte-Luis, V., Montero, J. A., Kawakami, Y., Izpisua-Belmonte, J. C., and Hurle, J. M. (2007). Lysosomal cathepsins in embryonic programmed cell death. *Dev. Biol.* 301, 205–217. doi: 10.1016/j.ydbio.2006.08.008

Conflict of Interest: The authors declare that the research was conducted in the absence of any commercial or financial relationships that could be construed as a potential conflict of interest.

frontiers in Cell and Developmental Biology

ORIGINAL RESEARCH
published: 27 October 2020
doi: 10.3389/fcell.2020.558432

Wwox Deficiency Causes Downregulation of Prosurvival ERK Signaling and Abnormal Homeostatic Responses in Mouse Skin

*Ying-Tsen Chou[1], Feng-Jie Lai[2,3], Nan-Shan Chang[4,5] and Li-Jin Hsu[1,6]**

[1] Institute of Basic Medical Sciences, College of Medicine, National Cheng Kung University, Tainan, Taiwan, [2] Department of Dermatology, Chimei Medical Center, Tainan, Taiwan, [3] Center for General Education, Southern Taiwan University of Science and Technology, Tainan, Taiwan, [4] Institute of Molecular Medicine, College of Medicine, National Cheng Kung University, Tainan, Taiwan, [5] Graduate Institute of Biomedical Sciences, College of Medicine, China Medical University, Taichung, Taiwan, [6] Department of Medical Laboratory Science and Biotechnology, College of Medicine, National Cheng Kung University, Tainan, Taiwan

Deficiency of tumor suppressor WW domain-containing oxidoreductase (WWOX) in humans and animals leads to growth retardation and premature death during postnatal developmental stages. Skin integrity is essential for organism survival due to its protection against dehydration and hypothermia. Our previous report demonstrated that human epidermal suprabasal cells express WWOX protein, and the expression is gradually increased toward the superficial differentiated cells prior to cornification. Here, we investigated whether abnormal skin development and homeostasis occur under *Wwox* deficiency that may correlate with early death. We determined that keratinocyte proliferation and differentiation were decreased, while apoptosis was increased in *Wwox*$^{-/-}$ mouse epidermis and primary keratinocyte cultures and *WWOX*-knockdown human HaCaT cells. Without WWOX, progenitor cells in hair follicle junctional zone underwent massive proliferation in early postnatal developmental stages and the stem/progenitor cell pools were depleted at postnatal day 21. These events lead to significantly decreased epidermal thickness, dehydration state, and delayed hair development in *Wwox*$^{-/-}$ mouse skin, which is associated with downregulation of prosurvival MEK/ERK signaling in *Wwox*$^{-/-}$ keratinocytes. Moreover, *Wwox* depletion results in substantial downregulation of dermal collagen contents in mice. Notably, *Wwox*$^{-/-}$ mice exhibit severe loss of subcutaneous adipose tissue and significant hypothermia. Collectively, our knockout mouse model supports the validity of WWOX in assisting epidermal and adipose homeostasis, and the involvement of prosurvival ERK pathway in the homeostatic responses regulated by WWOX.

Keywords: WWOX, tumor suppressor, keratinocyte proliferation, keratinocyte differentiation, stem cells, adipocytes

OPEN ACCESS

Edited by:
Wolfgang Knabe, Universität Münster, Germany

Reviewed by:
C. Marcelo Aldaz, The University of Texas MD Anderson Cancer Center, United States
Wen-Hui Lien, Catholic University of Louvain, Belgium

***Correspondence:**
Li-Jin Hsu
lijin.hsu@gmail.com;
ljhsu@mail.ncku.edu.tw

Specialty section:
This article was submitted to Cell Death and Survival, a section of the journal Frontiers in Cell and Developmental Biology

Received: *02 May 2020*
Accepted: *09 October 2020*
Published: *27 October 2020*

Citation:
Chou Y-T, Lai F-J, Chang N-S and Hsu L-J (2020) Wwox Deficiency Causes Downregulation of Prosurvival ERK Signaling and Abnormal Homeostatic Responses in Mouse Skin. Front. Cell Dev. Biol. 8:558432. doi: 10.3389/fcell.2020.558432

INTRODUCTION

WW domain-containing oxidoreductase (WWOX) has been initially known as a proapoptotic tumor suppressor (Chang et al., 2007; Lo et al., 2015; Schrock and Huebner, 2015). WWOX loss promotes tumor growth and cancer progression through allowing metastatic cancer cells to survive in WWOX-positive normal microenvironment (Chou et al., 2019a,b). Expression of WWOX

protein is essential for cell apoptosis induced by anti-cancer agents, UV irradiation, genotoxic stress, or ectopic p53 (Chang et al., 2003, 2005a; Abu-Remaileh et al., 2015; Chen et al., 2015; Janczar et al., 2017; Huang and Chang, 2018). Recently, *WWOX* gene has also been considered as a risk factor for human Alzheimer's disease (Kunkle et al., 2019). Ser14 phosphorylation and accumulation of WWOX protein in the brain contribute to the Alzheimer's memory loss in mice (Chang et al., 2015; Lee et al., 2017). WWOX also controls many biological functions, including bubbling cell death and genomic stability (Abu-Remaileh et al., 2015; Chen et al., 2015), suggesting that WWOX plays an important role in normal cellular/physiological homeostasis maintenance. Moreover, the first WW domain of WWOX participates in protein-protein interactions in multiple signaling pathways (Abu-Odeh et al., 2014; Liu et al., 2018; Saigo et al., 2018). Crosstalk of WWOX with many signal pathways also implies the involvement of WWOX in development and stemness maintenance (Chen et al., 2019).

Human newborns carrying homozygous mutations or deletions of *WWOX* gene exhibit growth retardation, severe neurological disorders, and early death (Abdel-Salam et al., 2014; Mallaret et al., 2014; Valduga et al., 2015). *Wwox* knockout ($Wwox^{-/-}$) mice display similar symptoms and die within 4 weeks after birth (Aqeilan et al., 2007; Ludes-Meyers et al., 2009). Previous studies have demonstrated that lipid metabolism, steroidogenesis, bone development and metabolism, and central nervous system are defective in $Wwox^{-/-}$ mice (Aqeilan et al., 2008; Aqeilan et al., 2009; Hussain et al., 2019; Cheng et al., 2020). The deficits in whole-body *Wwox* knockout mice may recapitulate the crucial clinical features of human pathological conditions (Cheng et al., 2020). However, the main cause leading to early death of WWOX-deficient newborns is still unclear. WWOX protein is abundant in many types of human epithelial tissues (Nunez et al., 2006). Mice carrying conditional depletion of *Wwox* in basal epithelial cells under the control of *keratin-5* (K5) promoter also die prematurely for unknown reasons (Ferguson et al., 2012), suggesting a vital role of WWOX in regulating proper epithelial functions and survival.

In normal human skin, WWOX protein is expressed in the innermost proliferative basal layer of epidermal keratinocytes and hair follicles (HFs), and its protein expression pattern displays an upregulation in a gradient toward outer differentiated suprabasal layers (Lai et al., 2005; Nunez et al., 2006). The maintenance of epidermal homeostasis depends on the coordination of basal cell proliferative capacity and basal-to-suprabasal differentiation processes. This phenomenon ensures epidermal barrier functions to protect the body from UV irradiation, pathogen infection and uncontrolled water loss for survival. The HFs, developed through the downward growth of epidermal basal keratinocytes into the dermis, contribute to thermoregulation. The maturation and regeneration of HFs largely rely on the self-renewal capacity of HF stem cells (HFSCs) and progenitors. Along with the epidermal stem cells, HFSCs are also crucial for epidermal self-renewal and homeostasis maintenance (Blanpain and Fuchs, 2009; Yi and Fuchs, 2010). Our previous study showed that WWOX is essential for UV-induced apoptosis in human HaCaT keratinocytes and squamous cell carcinoma cells (Lai et al., 2005). However, whether WWOX controls epidermal homeostasis and hair growth remains largely unclear. Moreover, the subcutaneous fat is involved in hair growth regulation and serves as a thermal insulator to prevent heat loss and maintain body temperature (Alexander et al., 2015). Body temperature reduction is a marker for imminent death in aging or microbial infection of mice (Ray et al., 2010; Gavin and Satchell, 2017). It has been shown that $Wwox^{-/-}$ mice exhibit lower serum lipid levels (Aqeilan et al., 2009). Notably, the influence of WWOX deficiency on the homeostasis of subcutaneous fat and body temperature remains to be investigated.

In this study, we showed that *Wwox* depletion in mice caused decreased proliferation and differentiation but increased apoptosis in keratinocytes. In addition, epidermal and HF stem cell numbers were reduced in $Wwox^{-/-}$ mice. The dysregulations were partly due to decreased prosurvival extracellular signal-regulated kinase (ERK) signaling in $Wwox^{-/-}$ keratinocytes. Strikingly, $Wwox^{-/-}$ mice lost more than 95% of the subcutaneous fat layer in dermal tissues. Collectively, $Wwox^{-/-}$ mice display aberrant epidermal functions, delayed hair morphogenesis and hypothermia, which may partly contribute to the life-threatening conditions in pre-weaning mice.

MATERIALS AND METHODS

Animals and Cell Culture

Whole-body *Wwox* gene knockout mice were generated as described previously (Tsai et al., 2013; Cheng et al., 2020). This study was carried out in accordance with the approved protocols for animal use from the Institutional Animal Care and Use Committee of National Cheng Kung University. Human HaCaT cell line was maintained in Dulbecco's Modified Eagle's Medium (GE-Hyclone, Logan, UT, United States) supplemented with 10% fetal bovine serum (FBS). HaCaT cells were cultured in keratinocyte serum-free medium or EpiLife medium containing 30 or 60 μM calcium ion, respectively, with the supplementation of human keratinocyte growth supplements (Life Technologies, Carlsbad, CA, United States) for reversion to a basal cell phenotype before differentiation induction. For differentiation and stratification induction, 1×10^6 cells were seeded in a 10-cm dish for 48 h and 2 mM calcium chloride was added to the cells. Primary keratinocytes were isolated and cultured according to a previous protocol (Jensen et al., 2010). Briefly, mouse skin was collected, and the connective tissue and subcutaneous fat were scraped-off. Skin tissues were then placed in 8 ml of dispase solution (BD biosciences) at 4°C for 6 h and/or 0.25% trypsin (Gibco) at 37°C for 2.5∼3 h with epithelium facing up. The disassociated skin epithelium was separated from the dermis, and the cells were further digested with 0.25% trypsin. After wash, the cells were then passed through a 40-μm cell strainer to remove debris or clumps. The isolated primary keratinocytes were cultured in keratinocyte growth medium (Cell Applications, Inc., San Diego, CA, United States) supplemented with 10% FBS overnight. The medium was replaced with serum-free keratinocyte growth medium fully supplemented with

keratinocyte growth factors and antibiotics (Cat. No. 131-500; Cell Applications, Inc.) on the next day. All cells were maintained at 37°C in 5% CO_2.

Histological, Collagen, and Nile Red Staining

Mouse skin tissues were fixed in 10% formalin/PBS and embedded in paraffin. Four-μm sections were deparaffinized in xylene, rehydrated in serial concentrations of ethanol (100, 95, 80, and 70%), and then stained with hematoxylin and eosin (H&E) solutions. For detecting collagen fibers, tissue sections were stained with hematoxylin, followed by a Sirius red solution (0.1% Sirius red in saturated aqueous solution of picric acid) for 1 h. For detecting intracellular lipid droplets, tissue sections were embedded using an OCT compound (Sakura, Tokyo, Japan). Nile red solution was prepared as described previously (Chou et al., 2005). Ten-μm frozen skin tissue sections were stained in Nile red solution for 10 min in dark, and then treated with 4% potassium hydroxide subsequently. Lipid droplets in skin tissues were examined under a fluorescence microscope (Olympus, Tokyo, Japan).

Immunohistochemical and Immunofluorescent Staining and Terminal Deoxynucleotidyl Transferase dUTP Nick End Labeling (TUNEL) Assay

Paraffin-embedded skin tissue sections were deparaffinized in xylene and rehydrated in serial concentrations of ethanol. Antigen retrieval was performed using microwave for 25 min in 10 mM citric buffer (pH = 6.0). For CD34 staining, skin tissues were embedded in an OCT compound (Sakura, Tokyo, Japan). The frozen tissue sections were air-dry, washed with distilled water and fixed in 10% formalin/PBS for 10 min at room temperature. For immunohistochemical staining, endogenous peroxidase was quenched using 3% H_2O_2. After blocking in a solution containing 1% bovine serum albumin and 0.1% saponin for 30 min at room temperature, the tissue sections were incubated in the primary antibody solution at 4°C overnight. For loricrin, fatty acid binding protein 4 (FABP4), CD34 and keratin 15 (K15) staining, the sections were incubated with horseradish peroxidase (HRP)-conjugated secondary antibody (Cell Signaling, Danvers, MA, United States) for 1 h at room temperature. For Ki67 staining, a polymeric HRP-conjugated secondary antibody (Novolink Polymer, Leica Biosystems, Newcastle upon Tyne, United Kingdom) and AEC substrate solution (DAKO, Carpinteria, CA, United States) were used. For ERK1/2, Thr202/Tyr204-phosphorylated ERK (pERK) and K15 staining, a polymer detection system (REAL EnVision, DAKO, Carpinteria, CA, United States) was used according to the manufacturer's instructions. The staining results were examined under a light microscope (Olympus BX51, Tokyo, Japan).

For immunofluorescence staining, tissue sections were incubated with primary antibody solution at 4°C overnight, and then with an Alexa 488- or Alexa 594-conjugated secondary antibody (Invitrogen) for 1 h at room temperature. TUNEL assay was performed according to the manufacturer's instructions (Millipore, Temecula, CA, United States). For staining the nuclei, tissue sections were incubated with a 4′,6-diamidino-2-phenylindole (DAPI) staining solution at room temperature for 5 min. The tissue samples were visualized under a fluorescence microscope (Olympus BX61, Tokyo, Japan) or a laser-scanning confocal microscope (Olympus FV1000, Tokyo, Japan).

Toluidine Blue Staining and Transmission Electron Microscopy

Mouse skin tissues were fixed in 4% glutaraldehyde/0.1M cacodylate buffer (pH 7.4) at 4°C overnight. After post-fixation using 1% OsO_4, samples were dehydrated and embedded in resin (Embed 812, EMS). Semithin sections (0.5 μm) were stained with 1% toluidine blue/2% sodium borate for 2 min, washed with distilled water and examine under a light microscope (Olympus BX51, Tokyo, Japan). Ultrathin sections (90 nm) were prepared, stained with 2% uranyl acetate for 20 min and 4% lead citrate for 3 min, and examined under a transmission electron microscope (JEOL JEM-1200EX, Tokyo, Japan) as described previously (Cheng et al., 2020).

Western Blot

Cellular protein extracts were prepared using a lysis buffer containing 1% Nonidet P-40, 0.5% Tween 20, 0.1% SDS, 10 mM $Na_4P_2O_7$, 10 mM Na_3VO_4, 10 mM NaF, and 1:20 dilution of protease inhibitor cocktail (Sigma, St. Louis, MO, United States) in PBS. To generate tissue protein extracts, a tissue homogenizer TissueLyser was used (Thermo Fisher Scientific). Proteins were quantified using a Bradford protein assay kit (Bio-Rad). Equal amounts of proteins were heated at 95°C in a sample buffer (250 mM Tris-HCl pH = 6.8, 500 mM dithiothreitol, 10% SDS, 0.1% bromophenol blue, 50% glycerol) for 10 min, and SDS-PAGE performed for protein separation (Tsai et al., 2013). The proteins were transferred to a piece of polyvinylidene difluoride membrane. After blocking with a skim milk-containing buffer, the membrane was hybridized with an indicated primary antibody in the blocking solution at 4°C overnight. After wash, HRP-conjugated secondary antibody was used (Cell signaling, Danvers, MA, United States) for probing. An enhanced chemiluminescence assay kit (Millipore) was used for protein detection.

Flow Cytometric Analysis

For propidium iodide (PI) staining, cells were fixed in a 70% ethanol/PBS solution, followed by staining in a PI staining solution (40 μg/ml PI and 100 μg/ml RNase in PBS) at room temperature for 30 min. For 5-bromo-2′-deoxyuridine (BrdU) staining, primary keratinocytes were fixed in a cytofix/cytoperm solution (BD) overnight and stained using a BrdU staining kit according to the manufacture's instructions (BD). The fluorescence intensity was determined using a FACScalibur (BD), and data analyzed using BD CellQuest Pro software.

Antibodies

The antibodies used in this study were as follows: K5 (1:1000, Covance #PRB-160P), keratin 10 (K10) for

immunohistochemistry (1:100, Covance #MS-159), K10 for western blot (1:10000, Abcam #ab76318), K15 (1:100, Thermo Fisher Scientific #MS-1068; 1:50, Santa Cruz #sc-47697), loricrin (1:1000, Covance #PRB-145P), Ki67 (1:150, DAKO #M7249), p63 (1:50, Santa Cruz #sc-8431), E-cadherin (1:40, Cell Signaling #3195), ERK1/2 (1:50, Santa Cruz #sc-514302), p-ERK (Thr202/Tyr204, 1:200, Cell Signaling #4370), CD34 (1:50, eBioscience #14-0341-82) and FABP4 (1:200, Abcam #ab13979). For detecting WWOX expression, an anti-WWOX antibody recognizing both human and mouse proteins was used (Chang et al., 2001, 2005b).

Skin Hydration State and Body Temperature Measurement

Skin hydration state was measured on shaved mouse dorsal skin using the MPA 5 system equipped with a Corneometer 825 probe (Courage + Khazaka electronic GmbH, Cologne, Germany). For measuring transepidermal water loss, mouse dorsal skin was shaved using hair removal cream, and the MPA 5 system equipped with a Tewameter TM300 probe was used (Courage + Khazaka electronic GmbH). Body temperature was determined on the shaved mouse dorsal skin surface using fiber-optic temperature sensors (Neoptix/Reflex signal conditioner, Quebec City, QC, Canada).

Statistical Analysis and Quantification Analysis

Statistical analysis was performed using Prism 6 software (GraphPad Software, San Diego, CA, United States). The measurements of epidermal thickness, dermal thickness, hair length, and hair width were performed using Image-Pro Plus 6 (Media Cybernetics, Rockville, MD, United States). Mean fluorescence and red color intensities on mouse skin surface were analyzed using ImageJ software (Wayne Rasband, National Institutes of Health). Quantitative analysis of immunohistochemical staining was performed using ImageJ plugin IHC Profiler (Varghese et al., 2014).

RESULTS

Wwox Loss Results in Reduced Epidermal Integrity

To investigate whether WWOX deficiency affects skin development, homeostasis and functions, whole-body knockout mouse models for *Wwox* gene were used in this study (Cheng et al., 2020). The absence of WWOX protein expression in $Wwox^{-/-}$ mouse skin was verified (**Figure 1A**). $Wwox^{-/-}$ mouse skin exhibited morphological abnormalities (**Figure 1B**). However, tumors or severe clinical cutaneous disorders, such as blisters, were not developed (**Figure 1B**). When assessing the skin barrier function, we did not find increased transepidermal water loss in $Wwox^{-/-}$ mice as the lipid layer was still maintained on the $Wwox^{-/-}$ epidermal surface (**Supplementary Figure S1**). However, the hydration levels of $Wwox^{-/-}$ epidermis were significantly reduced (**Figure 1C**). The $Wwox^{-/-}$ epidermal thickness was also significantly decreased at postnatal day (P) 21 (**Figures 1B,D**). These results suggest that WWOX is required for maintenance of normal epidermal function and homeostasis.

Wwox Is Associated With Keratinocyte Differentiation and Stratification

The multilayered structure of epidermis is established and maintained by the stepwise keratinocyte differentiation and stratification processes (Blanpain and Fuchs, 2009). Proper epidermal terminal differentiation is also required for skin hydration maintenance. Therefore, the consequences of WWOX deficiency on epidermal differentiation were investigated. By immunofluorescent staining, less $K10^+$ cells and $K5^+K10^+$ early differentiating progenitors were examined in $Wwox^{-/-}$ epidermis (**Figures 2A–C**). The numbers of loricrin-positive cells that represent late-differentiated keratinocytes were decreased in a majority of $Wwox^{-/-}$ mice (**Supplementary Figure S2A**). However, there were no statistical differences between wild-type and knockout mice due to $Wwox^{-/-}$ epidermal atrophy (**Supplementary Figure S2B**). As shown in **Supplementary Figure S2A**, loricrin was distributed loosely in $Wwox^{-/-}$ epidermal tissues. Moreover, the amount of keratohyalin granules and their fusion with the cell membrane were reduced in $Wwox^{-/-}$ epidermal keratinocytes, indicating defective keratinocyte terminal differentiation in $Wwox^{-/-}$ epidermis (**Figure 2D**).

To confirm whether WWOX is required for keratinocyte differentiation and stratification, *in vitro* culture of human HaCaT keratinocytes in serum-free keratinocyte medium was also tested (Deyrieux and Wilson, 2007). The addition of Ca^{2+} to subconfluent HaCaT cell culture has been shown to induce cell-cell association as well as keratinocyte differentiation and stratification (Hennings et al., 1980; Poumay and Pittelkow, 1995; Deyrieux and Wilson, 2007). WWOX protein expression was increased by Ca^{2+} treatment in HaCaT cells in a time-dependent manner (**Figure 2E**). Lentivirus-mediated knockdown of WWOX protein expression in HaCaT cells suppressed Ca^{2+}-induced expression of keratinocyte differentiation marker K10 (**Figure 2F**). Upon Ca^{2+}-induced differentiation and stratification, control cells became cuboidal and formed cell-cell junctions at day 1 (red arrow; **Figure 2G**). In contrast, the cell boundaries between adjacent WWOX-knockdown cells were less clear after *in vitro* culture for 1 day (black arrow; **Figure 2G**). Moreover, the control cells formed many stratification domes (piled-up cell clusters) after treatment of Ca^{2+} for 6 days, while much fewer stratification domes were observed in WWOX-knockdown cells (yellow arrows; **Figures 2G,H**). Together, these results suggest that WWOX is required for keratinocyte differentiation and stratification.

WWOX Loss Leads to Reduced Proliferation and Survival in Keratinocytes

The establishment and maintenance of epidermal multi-differentiated structure are highly dependent on the basal cell proliferative capacities (Blanpain and Fuchs, 2009). As

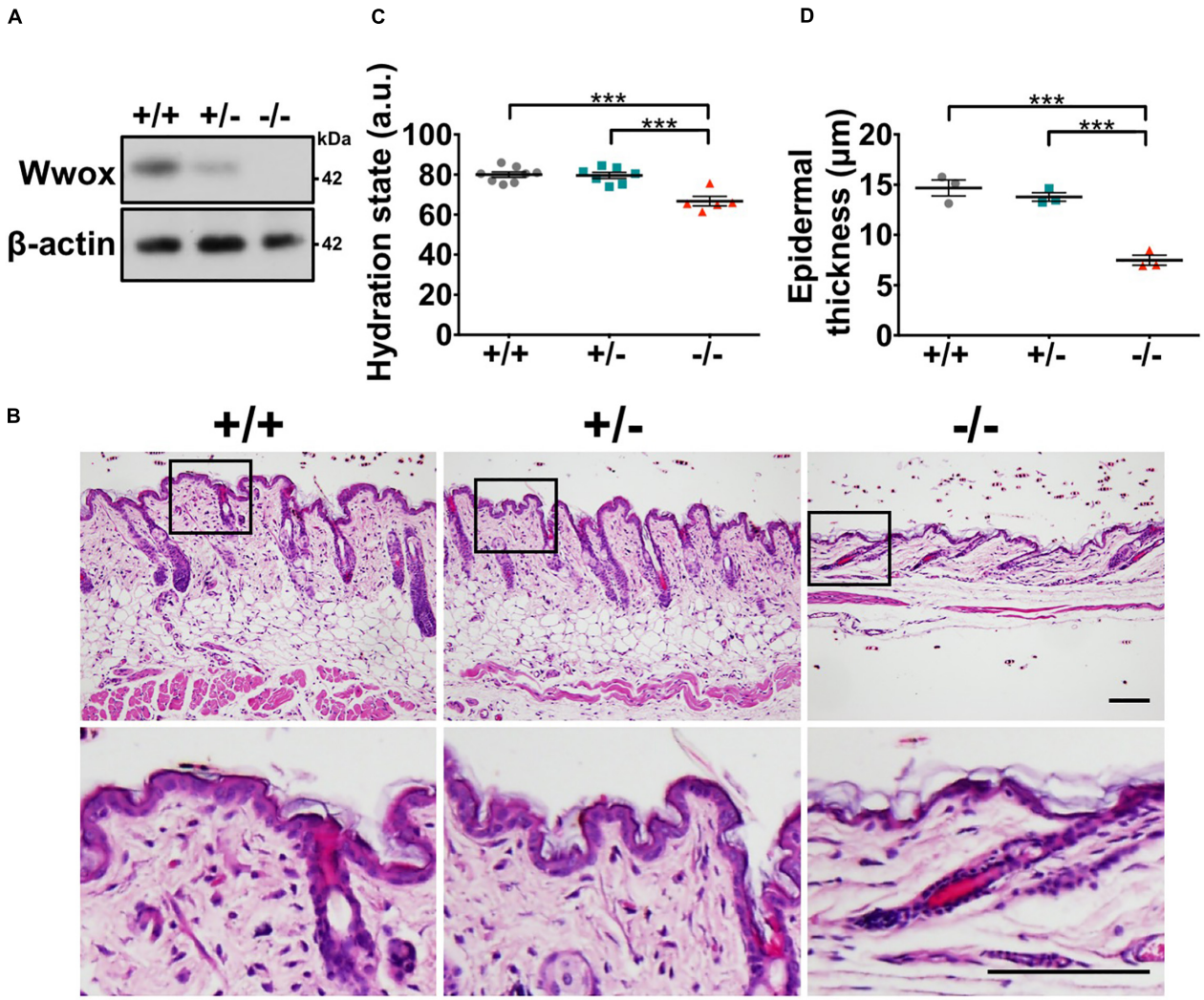

FIGURE 1 | *Wwox* knockout leads to reduced epidermal integrity. **(A)** Western blot analysis for WWOX protein expression in $Wwox^{+/+}$, $Wwox^{+/-}$, and $Wwox^{-/-}$ mouse skin at P21. β-Actin was used as a loading control. **(B)** H&E staining results of $Wwox^{+/+}$, $Wwox^{+/-}$, and $Wwox^{-/-}$ mouse skin tissue sections at P21. Scale bar = 100 μm. The lower panels are enlarged images from the boxed areas in the upper panels. **(C)** Mouse skin hydration status at ∼3-week-old ($Wwox^{+/+}$, n = 8; $Wwox^{+/-}$, n = 7; $Wwox^{-/-}$, n = 5). **(D)** Measurement of mouse epidermal thickness (n = 3). Data are presented as mean ± standard error of the mean (SEM). No animals were excluded from the analysis and no randomization was used in this study. One-way ANOVA and *post hoc* Tukey tests were performed for statistical analysis. ***$P < 0.001$.

basal keratinocytes express WWOX protein (Nunez et al., 2006), keratinocyte proliferation and cell growth under *Wwox* deficiency were examined. We determined that $Wwox^{-/-}$ mouse epidermis had significantly decreased Ki67-positive keratinocytes at P20 (**Figures 3A,B**). In primary $Wwox^{-/-}$ mouse epidermal keratinocyte cultures, the cell numbers were significantly reduced as compared with the control group after *in vitro* culture for 3 days (**Figure 3C**). A decreased incorporation of BrdU into $Wwox^{-/-}$ primary keratinocytes was also observed, indicating the reduction of proliferative activities in these cells (**Figures 3D,E**). PI staining for cell cycle analysis revealed that the percentages of $Wwox^{-/-}$ primary keratinocytes in S and G2/M phases at day 3 were also reduced (**Supplementary Figure S3**). The role of WWOX in regulating keratinocyte growth was also confirmed using HaCaT cells. In comparison with control cells, WWOX knockdown resulted in significant suppression of HaCaT cell growth (**Figure 3F**).

We assessed whether the decreased epidermal thickness in $Wwox^{-/-}$ mouse skin occurs as a result of increased cell death. Cell cycle analysis using flow cytometry revealed a higher percentage of $Wwox^{-/-}$ mouse primary keratinocytes in sub G0 phase than the control, suggesting that $Wwox^{-/-}$ keratinocytes tend to undergo apoptosis (**Supplementary Figure S3**). TUNEL assay further confirmed the higher percentage of apoptotic cells in $Wwox^{-/-}$ mouse epidermis than that of the wild-type control at P21 (1.77% in knock-out and 0.77% in wild-type) (**Supplementary Figures S4A,B**), suggesting that epidermal cell apoptosis is facilitated by WWOX loss.

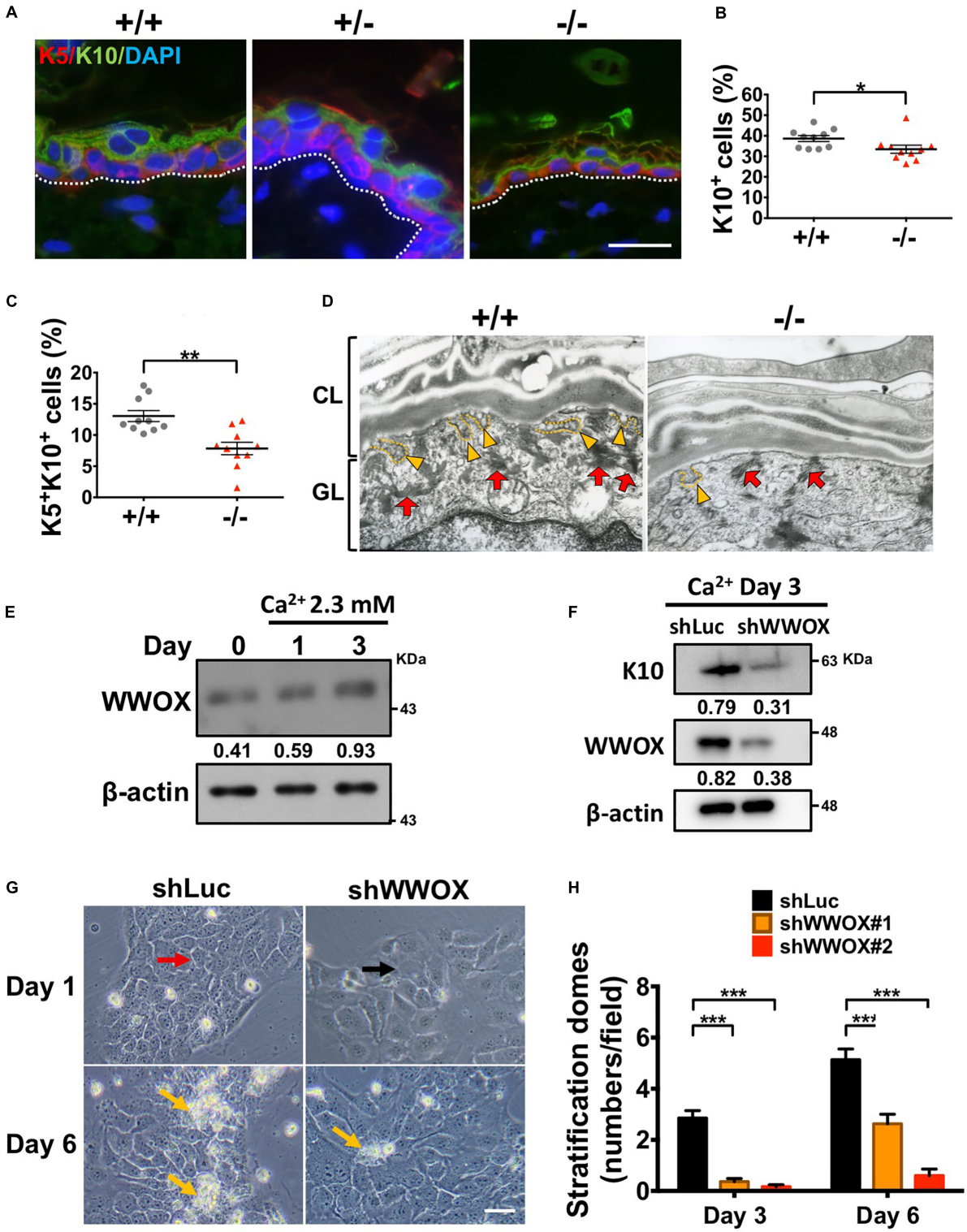

FIGURE 2 | WWOX loss leads to defective keratinocyte differentiation and stratification. **(A)** Immunofluorescence staining of *Wwox*$^{+/+}$, *Wwox*$^{+/-}$, and *Wwox*$^{-/-}$ mouse tissue sections for the expression of K5 (red) and K10 (green). DAPI was used for the staining of nuclei (blue). Dotted lines indicate the basement membrane. Scale bar = 20 μm. The percentages of epidermal K10^{+} **(B)** and K5^{+}/K10^{+} cells **(C)** were quantified (n = 10). Student's t-test was performed for statistical analysis. **(D)** Keratohyalin granules (red arrows) and fusion of granules with the cell membrane (yellow arrowheads) were examined by transmission electron microscopy. CL, cornified layer; GL, granular layer. Magnification: 30,000x. **(E)** WWOX protein expression in HaCaT cells was determined by western blot analysis after calcium

(Continued)

FIGURE 2 | Continued
chloride treatment for 1 and 3 days. β-Actin was used as a loading control. The numbers indicate the ratio of WWOX to β-actin protein levels in cells. **(F)** Western blot anslysis of WWOX and K10 protein expression in calcium chloride-treated control (shLuc) or WWOX-knockdown (shWWOX) HaCaT cells. β-actin was used as a loading control. **(G)** shLuc or shWWOX HaCaT cells were treated with 2 mM calcium chloride for 1 and 6 days. The cells with clear cell-cell junctions (red arrow) were observed in the control, but not shWWOX HaCaT cells (black arrow) at day 1. More stratification domes (yellow arrows) were observed in the control cells after treatment for 6 days. Scale bar = 50 μm. **(H)** HaCaT cells were treated with 2 mM calcium chloride for 3 or 6 days to induce differentiation. The stratification domes in the shLuc and shWWOX HaCaT cells were quantified. At least 15 fields were quantified from two and three independent experiments at day 3 and 6, respectively. Data are presented as mean ± SEM. One-way ANOVA and *post hoc* Tukey tests were performed for statistical analysis. $^{*}P < 0.05$, $^{**}P < 0.01$, $^{***}P < 0.001$.

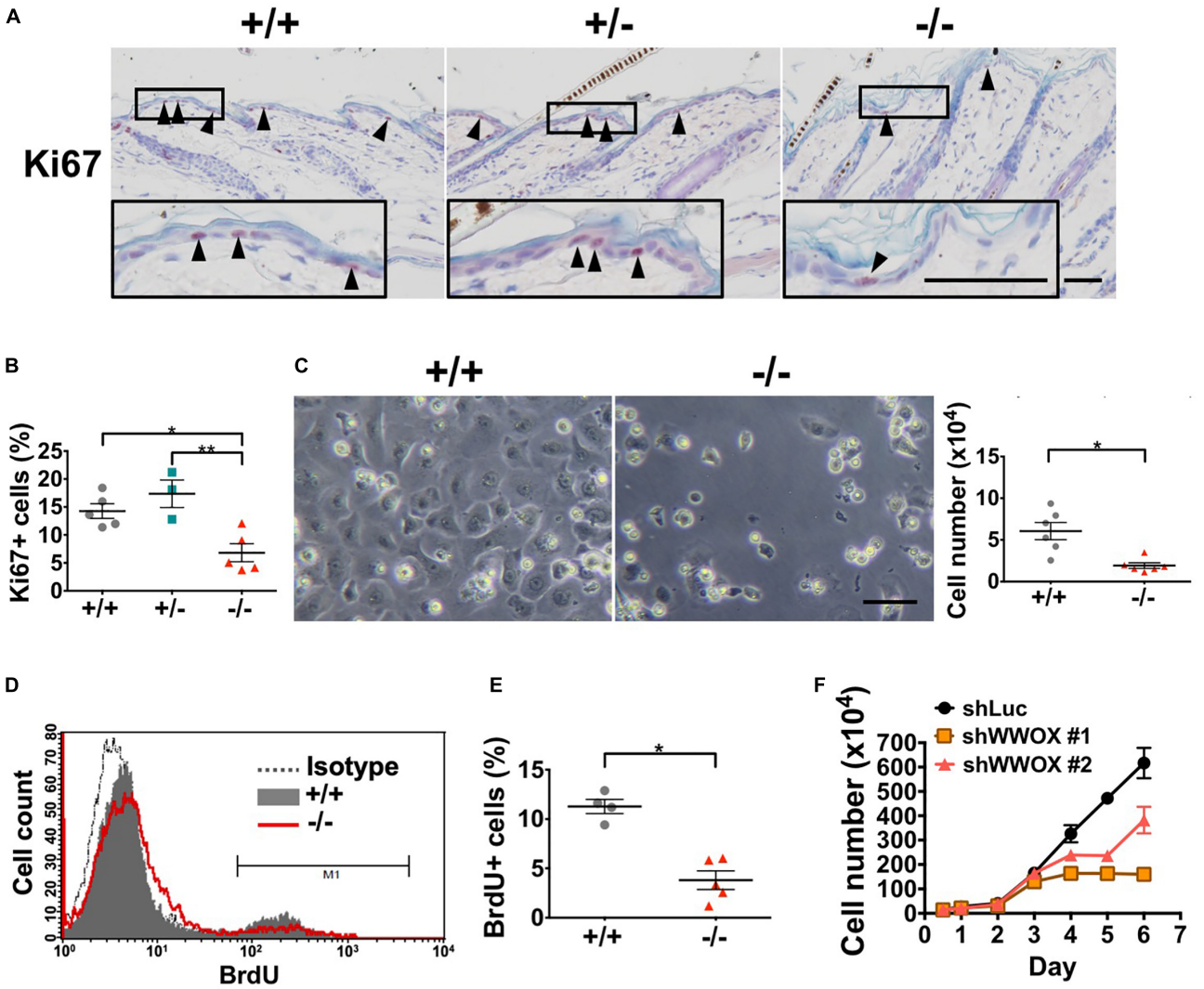

FIGURE 3 | WWOX loss suppresses keratinocyte proliferation at P20. **(A)** Immunohistochemical staining of *Wwox*$^{+/+}$, *Wwox*$^{+/-}$, and *Wwox*$^{-/-}$ mouse epidermal tissue sections for Ki67 (arrowheads). Nuclei were stained with hematoxylin. The lower panels are enlarged images from the boxed areas. Scale bar = 50 μm. **(B)** Quantification of epidermal Ki67-positive cells is shown (*Wwox*$^{+/+}$, $n = 5$; *Wwox*$^{+/-}$, $n = 3$; *Wwox*$^{-/-}$, $n = 5$). One-way ANOVA and *post hoc* Tukey tests were performed for statistical analysis. **(C)** Representative phase-contrast microphotographs of cultured primary keratinocytes isolated from *Wwox*$^{+/+}$ and *Wwox*$^{-/-}$ mice at ∼P20. The right panel indicates the cell numbers quantified using a hemacytometer after *in vitro* culture for 3 days. Scale bar = 10 μm. Paired *t*-test was performed for statistical analysis. **(D)** BrdU incorporation of the cultured primary *Wwox*$^{+/+}$ and *Wwox*$^{-/-}$ mouse keratinocytes was analyzed by flow cytometry. **(E)** Quantification of BrdU incorporation data is shown (*Wwox*$^{+/+}$, $n = 4$; *Wwox*$^{-/-}$, $n = 5$). Paired *t*-test was performed for statistical analysis. **(F)** Growth curves of control sh*Luc* and sh*WWOX* HaCaT cells. All data are presented as mean ± SEM. $^{*}P < 0.05$, $^{**}P < 0.01$.

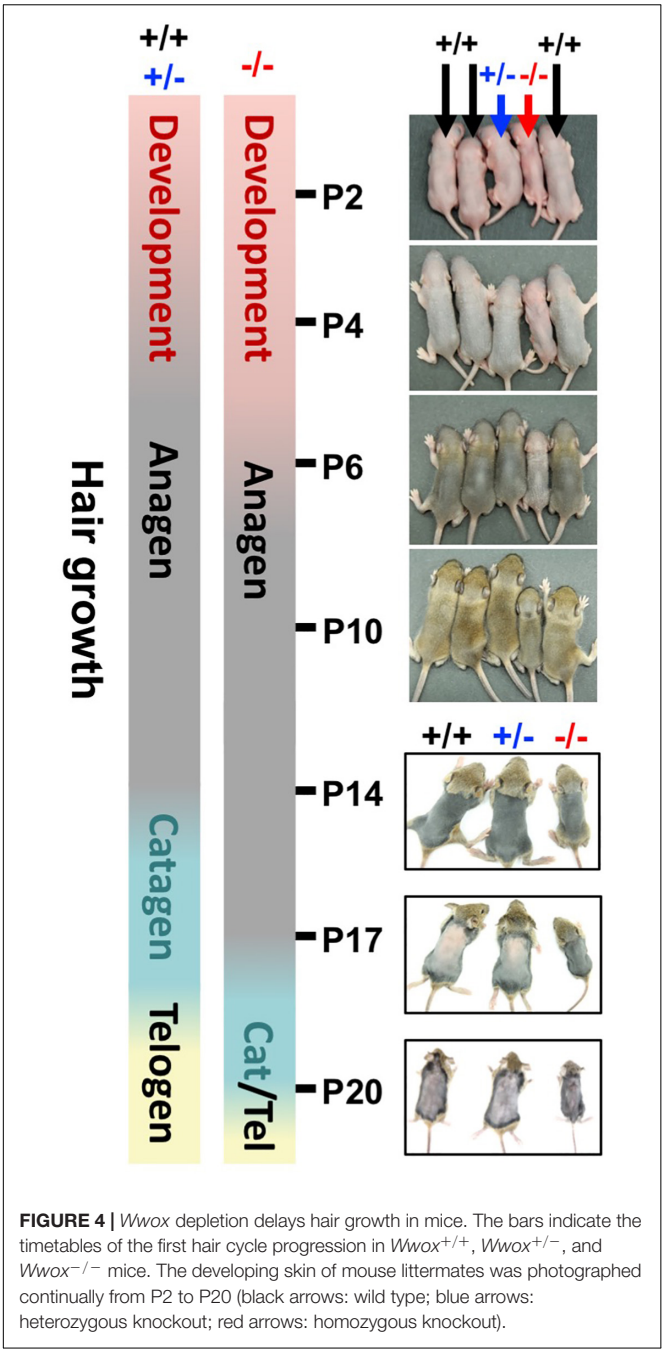

FIGURE 4 | *Wwox* depletion delays hair growth in mice. The bars indicate the timetables of the first hair cycle progression in $Wwox^{+/+}$, $Wwox^{+/-}$, and $Wwox^{-/-}$ mice. The developing skin of mouse littermates was photographed continually from P2 to P20 (black arrows: wild type; blue arrows: heterozygous knockout; red arrows: homozygous knockout).

Wwox Ablation Delays Postnatal HF Morphogenesis

HFs are formed by the downward growth of epidermal basal cells. HFSCs reside in HF bulges and are able to replenish the epidermal keratinocytes and maintain homeostasis (Blanpain and Fuchs, 2009). Since both epidermal basal cells and HF keratinocytes express WWOX protein (Nunez et al., 2006), the effect of WWOX loss on HF growth was investigated by examining a litter of mouse pups continuously after birth. $Wwox^{+/+}$ and $Wwox^{+/-}$ mice exhibited furs approximately at P4. However, $Wwox^{-/-}$ mice grew a first coat of hair after P6 (**Figure 4**). Compared with the $Wwox^{+/+}$ and $Wwox^{+/-}$ littermates, the relative fur length of $Wwox^{-/-}$ mice was shorter at P10 (**Supplementary Figure S5**). Histological analysis revealed shorter HF length in $Wwox^{-/-}$ mice from P3 to P21 (**Figures 5A,B**). Moreover, hair fibers were thinner and shorter in $Wwox^{-/-}$ mice at P21, as determined by the measurement of HF bulge and hair shaft widths and whisker length (**Figures 5B–D**). To study whether the deficiency of hair shaft production in $Wwox^{-/-}$ HFs is due to defective HF matrix, we detected an average smaller bulb width and a significantly reduced number of Ki67-positive proliferating cells in the hair bulbs of $Wwox^{-/-}$ mice at P7 (**Figures 5E–G**). However, the HF number and length showed no differences among $Wwox^{+/+}$, $Wwox^{+/-}$, and $Wwox^{-/-}$ mice at birth or the embryonic stages (**Figure 5A** and **Supplementary Figure S6**).

Starting from P4, mouse HFs undergo cyclic growth and degeneration with a phased series known as anagen, catagen, and telogen (Alonso and Fuchs, 2006). To assess the phase progression of the first hair cycle, mouse skin color and appearance were examined (Muller-Rover et al., 2001). After shaving, the skin color of $Wwox^{+/+}$ and $Wwox^{+/-}$ mice was brownish-black at P14 and turned pink at P17, indicating that their skin HFs were growing in anagen phase at P14 and entering into catagen phase at P17 (**Figure 4** and **Supplementary Figure S5**). In contrast, $Wwox^{-/-}$ HFs were still growing at P17 and entering into catagen around P20 (**Figure 4** and **Supplementary Figure S5**). To study the progression of first hair cycle in mice, histological analysis was performed. As most HFs entered catagen phase in wild-type mouse back skin at P18, few HFs reached the first telogen phase in these mice (**Figure 5H**). However, a large number of $Wwox^{-/-}$ HFs are still in anagen phase at P18 (**Figure 5H**). Compared with the wild-type control mice, $Wwox^{-/-}$ mice had more catagen HFs but less telogen HFs at P21, although no statistically significant differences were found (**Figure 5H**). Whether $Wwox^{-/-}$ mouse hair follicles have shorter catagen phase is unclear. In catagen phase, cells in the lower region of HFs undergo apoptosis (Alonso and Fuchs, 2006). At P18, TUNEL-positive cells were found in the catagen HFs of $Wwox^{+/+}$ and $Wwox^{+/-}$ mice but not in $Wwox^{-/-}$ anagen HFs (**Supplementary Figure S4C**). The TUNEL results revealed that wild-type HFs reached the first telogen at P18 and $Wwox^{-/-}$ HFs at P21 (**Supplementary Figure S4C**). Our data suggest that HF morphogenesis as well as the phase progression of the first hair growth cycle are delayed by *Wwox* ablation.

Wwox Sustains the Maintenance of Stem Cell Pool in Mouse Skin

The HFSCs give rise to all epidermal cell lineages (Senoo, 2013; Hsu et al., 2014). The completely specified HFSCs appear at birth in mouse skin. After undergoing initial expansion to accommodate HF development and hair growth, HFSCs become quiescent in early postnatal developmental stages (Nowak et al., 2008). Loss of HFSC proliferative activities disrupts postnatal HF development (Wang et al., 2013). In contrast, over-activation of HFSC proliferation results in depletion of stem cell pools as well as dysregulation of epidermal homeostasis (Niessen et al.,

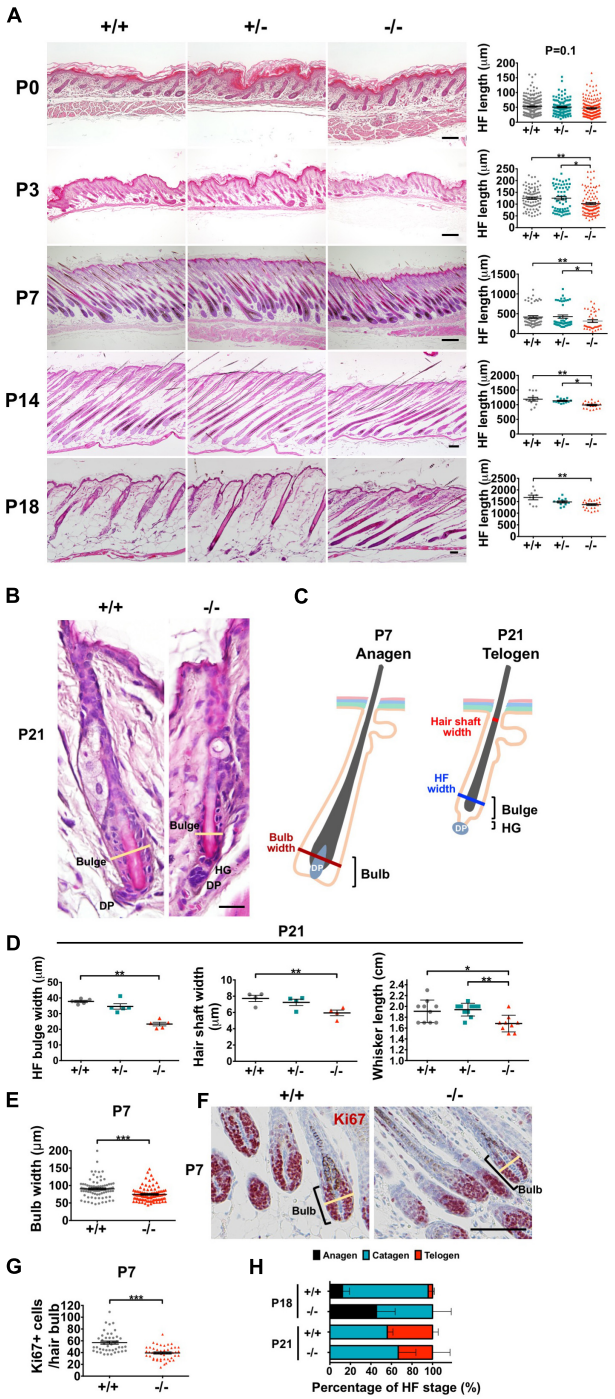

FIGURE 5 | *Wwox* deficiency leads to hair follicle atrophy in mice after birth. **(A)** Representative dorsal skin tissue sections of $Wwox^{+/+}$, $Wwox^{+/-}$, and $Wwox^{-/-}$ mice at birth (P0), P3, P7, P14, and P18 are shown (H&E stain). The quantification results of mouse anagen HF length are shown in the right panels. The numbers of HFs and mice analyzed (HFs/mice) were as the follows: at P0, $Wwox^{+/+}$ (224/5), $Wwox^{+/-}$ (108/3), and $Wwox^{-/-}$ (185/4); at P3, $Wwox^{+/+}$ (125/3), $Wwox^{+/-}$ (61/3), and $Wwox^{-/-}$ (107/3); at P7, $Wwox^{+/+}$ (52/4), $Wwox^{+/-}$ (42/4), and $Wwox^{-/-}$ (36/3); at P14, $Wwox^{+/+}$ (12/3), $Wwox^{+/-}$ (12/3), and $Wwox^{-/-}$ (20/4); at P18, $Wwox^{+/+}$ (9/4), $Wwox^{+/-}$ (12/4), and $Wwox^{-/-}$ (24/4). Scale bars: P0 = 50 μm; P3 = 100 μm; P7 = 200 μm; P14 = 100 μm; P18 = 50 μm.

(Continued)

FIGURE 5 | Continued

(B) Representative telogen HF images of dorsal skin tissue sections from $Wwox^{+/+}$ and $Wwox^{-/-}$ mice at P21 (H&E stain). The yellow lines indicate HF bulge width. HG, hair germ; DP, dermal papilla. Scale bar = 20 μm. **(C)** An illustration of anagen and telogen HFs. **(D)** The widths of telogen HF bulge (left, $n = 5$) and hair shaft (middle, $n = 4$) were analyzed using serial skin tissue sections from mice at P21. The hair fiber length of mouse whisker (right, $Wwox^{+/+}$, $n = 10$; $Wwox^{+/-}$, $n = 10$; $Wwox^{-/-}$, $n = 9$) was measured at P21. **(E)** HF bulb widths were analyzed using serial skin tissue sections from $Wwox^{+/+}$ and $Wwox^{-/-}$ mice at P7 (92 HFs/3 mice). Student's *t*-test was performed for statistical analysis. **(F)** Immunohistochemical staining of $Wwox^{+/+}$ and $Wwox^{-/-}$ mouse HF bulb sections for Ki67. Nuclei were stained with hematoxylin. The yellow lines indicate HF bulb width. Scale bar = 100 μm. **(G)** Quantification of hair bulb Ki67-positive cells at P7 is shown. Student's *t*-test was performed for statistical analysis. **(H)** The percentages of anagen, catagen and telogen HFs were examined in $Wwox^{+/+}$ and $Wwox^{-/-}$ mouse skin sections at P18 ($n = 4$) and P21 ($n = 4$). One-way ANOVA and *post hoc* Tukey tests were performed for statistical analysis. Data analyzed using properly sectioned tissue samples and whiskers are presented as mean ± SEM. One-way ANOVA and *post hoc* Tukey tests were performed for statistical analysis. $^{*}P < 0.05$, $^{**}P < 0.01$, $^{***}P < 0.001$.

2013; Ali et al., 2016). $Wwox^{-/-}$ mouse epidermis showed no increases in cell apoptosis during the delayed postnatal HF morphogenesis (**Supplementary Figure S4C**). However, increased cell proliferation (Ki67-positive) was detected in the HF junctional zone (JZ) in $Wwox^{-/-}$ mice between P3 and P8 as compared to that of the wild-type mice (**Figures 6A,B**). The JZ progenitors have been shown to commit to epidermal lineages (Kretzschmar and Watt, 2014). The enhanced cell proliferation in JZ also caused transient thickening of the epidermal tissues in $Wwox^{-/-}$ mice at P7 (**Figure 6C**). Next, we analyzed whether the increased cell proliferation in JZ at the early postnatal stage causes a change in HFSC populations. Staining of the bulge HFSC markers K15 and CD34 revealed a reduction in the number of bulge HFSCs in $Wwox^{-/-}$ mouse skin tissues at P21 as compared with the controls (**Figure 6D** and **Supplementary Figure S7**), suggesting that *Wwox* is involved in the maintenance of HFSC pool. Whether the enhanced proliferative activity of JZ progenitors in *Wwox*-deficient HFs at early postnatal days causes gradual loss of stem cell functionality and leads to HFSC exhaustion at a later stage remains further investigation.

Wwox Loss Reduces E-Cadherin, ERK, and p63 Expression in Keratinocytes

E-cadherin belongs to the family of cell adhesion molecules and is important for the formation of adherens junctions between the adjacent cells. The association of cytosolic β-catenin with E-cadherin at adherens junctions stabilizes E-cadherin expression in epithelial cells and the structure of intercellular junctions (Nelson and Nusse, 2004; Voronkov and Krauss, 2013), and play crucial roles in epidermal and HF development, stem cell renewal, and tissue homeostasis. Depletion of E-cadherin expression in the epidermis and HFs results in alteration of epidermal proliferation and differentiation, defects in HF development, and loss of stem cells. Herein, our data revealed that E-cadherin protein expression was decreased in the epidermis of $Wwox^{-/-}$ mice (**Supplementary Figure S8**).

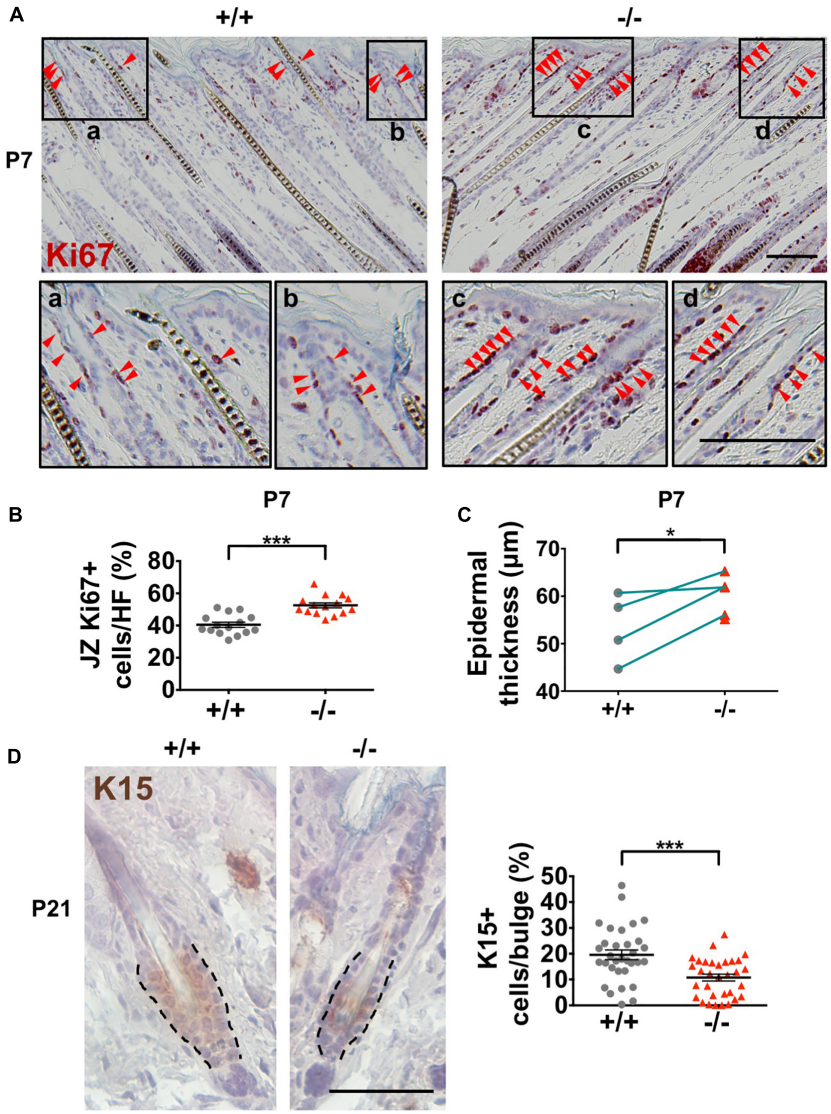

FIGURE 6 | Decreased HF stem cell numbers in *Wwox*$^{-/-}$ skin. **(A)** Immunohistochemical staining of *Wwox*$^{+/+}$ and *Wwox*$^{-/-}$ mouse skin tissue sections for Ki67 at P7. Red arrowheads indicate Ki67^{+} cells. The lower panels are enlarged images from the boxed areas. Scale bar = 100 μm. **(B)** Quantification of Ki67-positive cells in the JZ of *Wwox*$^{+/+}$ and *Wwox*$^{-/-}$ mouse HFs at P7 is shown. **(C)** Measurement of mouse epidermal thickness at P7 (n = 4). The green lines indicate paired *Wwox*$^{+/+}$ and *Wwox*$^{-/-}$ mice from the same litter. **(D)** Immunohistochemical staining of *Wwox*$^{+/+}$ and *Wwox*$^{-/-}$ mouse skin tissue sections for K15 at P21. Dotted lines depict the HF bulge regions. The quantification results of K15^{+} cells in the HF bulge region are shown in the right panel. The numbers of HFs and mice analyzed (HFs/mice) were *Wwox*$^{+/+}$ (32/3) and *Wwox*$^{-/-}$ (39/3). Scale bar = 50 μm. Data are presented as mean ± SEM. Student's t-test was performed for statistical analysis. *$P < 0.05$. ***$P < 0.001$.

Moreover, *Wwox*$^{-/-}$ epidermal keratinocytes expressed significantly reduced levels of pERK and total ERK1/2 protein (**Figure 7A** and **Supplementary Figure S9**, respectively). ERK protein phosphorylation in MAPK signaling is essential for cell proliferation. Therefore, the regulation of keratinocyte proliferation by WWOX may be partly through MAPK signaling. In agreement with a previous study (Salah et al., 2013), we determined reduced expression of epidermal progenitor marker p63 in *Wwox* knockout mouse epidermis (**Figure 7B**), suggesting that progenitor cell depletion occurs in the skin of *Wwox* knockout mice. Together, our results suggest that *Wwox* absence leads to compromised epidermal homeostasis, stem cell maintenance, and hair development that may be partly due to the loss of E-cadherin, ERK and p63 expression.

Wwox Knockout Mice Have Reduced Dermal Collagen Content, Lack Subcutaneous Fat, and Display Hypothermia

The stromal tissue beneath the epidermis is composed of dermis and subcutaneous fat layers (**Figure 8A**). Signaling

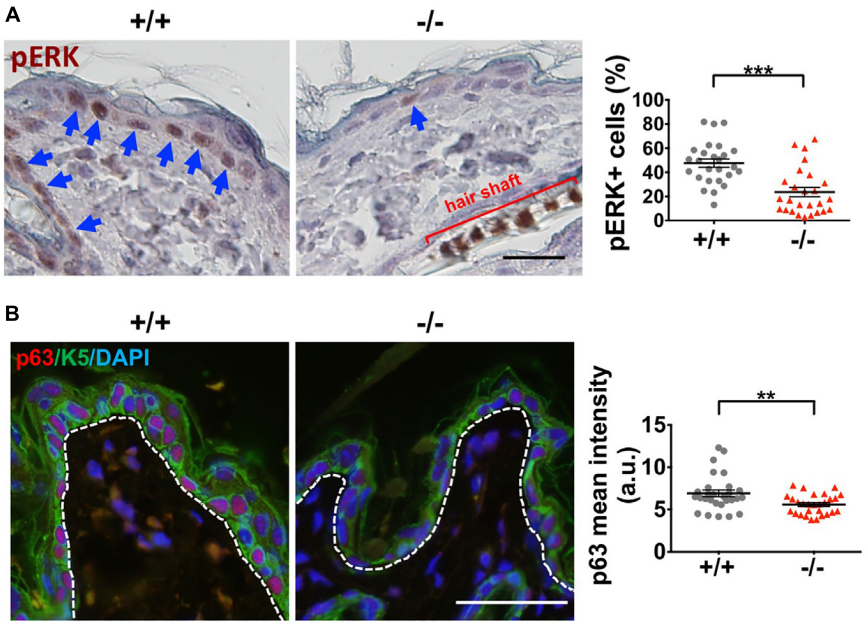

FIGURE 7 | *Wwox* knockout leads to decreased ERK and p63 expression in keratinocytes. **(A)** Immunohistochemical staining of $Wwox^{+/+}$ and $Wwox^{-/-}$ mouse epidermal tissue sections for pERK was examined under a light microscopy. The blue arrows indicate pERK-positive keratinocytes. Quantification results of pERK expression are shown in the right panel (25 regions/3 mice). All data are presented as mean ± SEM. Student's *t*-test was performed for statistical analysis. Scale bar = 20 μm. ***$P < 0.001$. **(B)** Immunofluorescence staining of $Wwox^{+/+}$ and $Wwox^{-/-}$ mouse skin tissue sections for p63 (red) and K5 (green) at P21 was examined under a confocal microscopy. DAPI was used for the staining of nuclei (blue). Dotted lines depict the location of basement membrane. The quantification results are shown in the right panel (28 regions/4 mice). All data are presented as mean ± SEM. Scale bar = 20 μm. **$P < 0.01$.

from the stromal cells is crucial for HF morphogenesis and epidermal homeostasis (Hsu et al., 2014; Fujiwara et al., 2018; Rognoni and Watt, 2018). Therefore, changes in stromal composition in mouse skin by *Wwox* gene ablation were examined. Histological analysis revealed that the stromal thickness of $Wwox^{-/-}$ mice was dramatically decreased (left panel in **Figure 8B**). The thickness of dermis was significantly reduced in $Wwox^{-/-}$ mice (**Supplementary Figure S10A**). By transmission electron microscopy, we found that the collagen content was reduced in the dermal layer of $Wwox^{-/-}$ mice (**Supplementary Figure S10B**). Sirius red staining results also revealed that the collagen fibers in $Wwox^{-/-}$ mouse dermis were thinner than those of the control littermates (**Supplementary Figure S10C**).

Decreased serum lipid level has been detected in $Wwox^{-/-}$ mice (Aqeilan et al., 2007). We found that $Wwox^{-/-}$ mouse subcutaneous fat layer lost at P21 by Nile red and toluidine blue staining (**Figure 8C**). Immunohistochemical staining for FABP4, a mature adipocyte marker, showed that only a few FABP4-positive cells have remained in $Wwox^{-/-}$ mouse dermal tissues (**Figure 8D**). These cells shrank and did not contain lipid droplets (black arrows; **Figure 8D**). Subcutaneous fat is vital for thermal regulation and maintaining body temperature (Alexander et al., 2015). Indeed, the average body temperature of $Wwox^{-/-}$ mice was significantly decreased (31.3°C in knockout and 35.8°C in wild-type mice; **Figure 8E**). Together, ablation of *Wwox* gene in mice leads to the change of stromal environment in the dermis that may compromise epidermal and HF development and tissue homeostasis. The loss of subcutaneous fat causes hypothermia in $Wwox^{-/-}$ mice.

DISCUSSION

In summary, our knockout mouse model provides the validity of WWOX in supporting epidermal homeostasis, HF development and stem cell maintenance. Lack of WWOX leads to reduced keratinocyte proliferation and differentiation, as reflected by significant reduction in epidermal thickness, dehydration state, and delayed hair development. Downregulation of E-cadherin expression and prosurvival MEK/ERK signaing pathway is implicated for the aberrant development under the WWOX-deficient setting *in vivo*. Human patients or mice carrying double allele mutation or deletion of *WWOX/Wwox* gene display growth retardation and early death (Aqeilan et al., 2008; Ferguson et al., 2012; Mallaret et al., 2014; Tabarki et al., 2015). Dramatic loss of adipose tissue in the subcutaneous area accounts for hypothermia and severe illness in newborns.

In addition, evidence was provided in this study that WWOX is involved in epidermal homeostasis and HF development through regulating keratinocyte proliferation, differentiation and stratification, and stem cell maintenance. It is likely as a result of orchestrating MEK/ERK signaling pathway. WWOX is an adaptor protein in MEK/ERK signaling pathway (Lin et al., 2011). MEK/ERK signaling has been reported to be regulated by WWOX (Lin et al., 2011; Chen et al., 2019). Activation

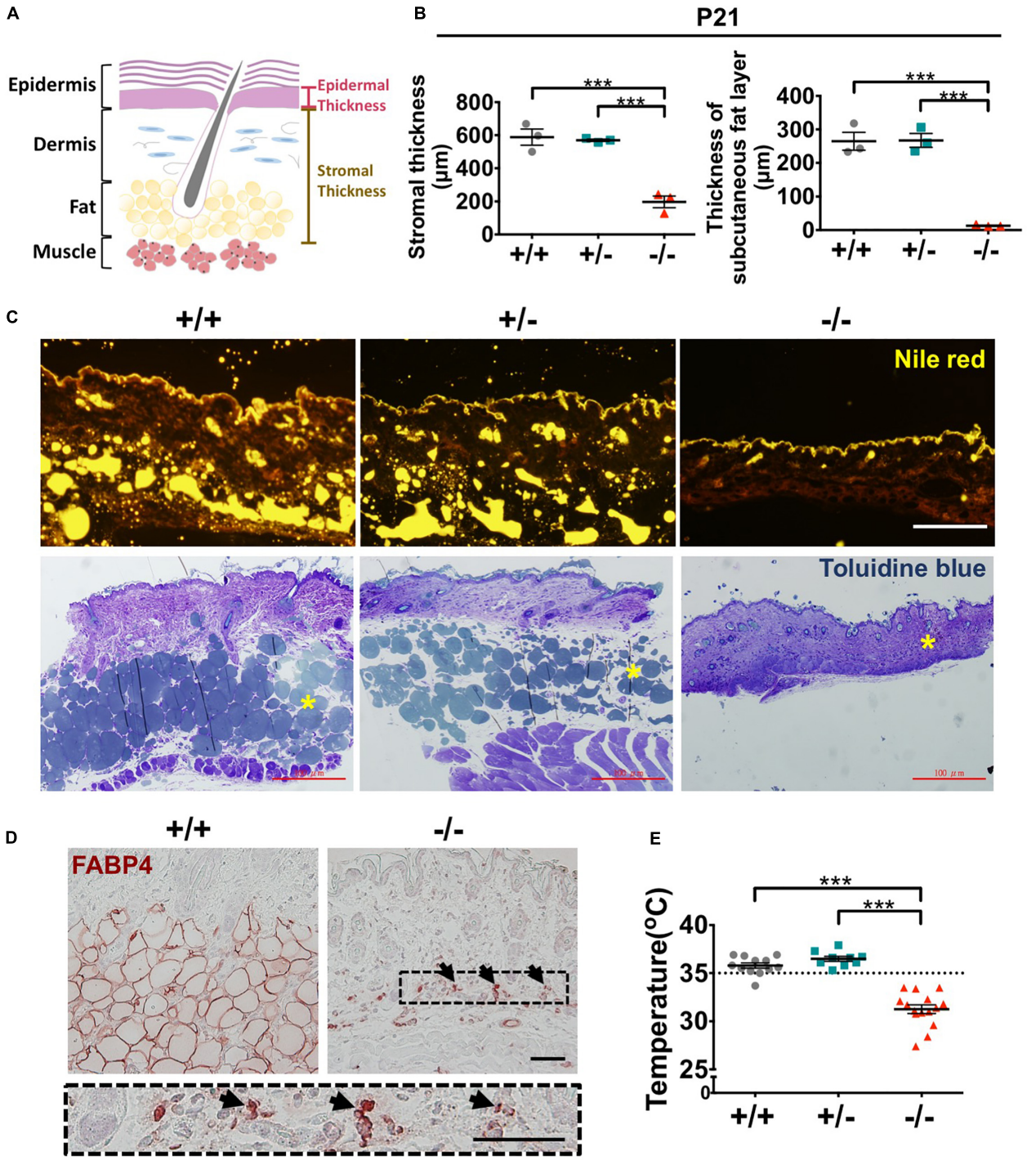

FIGURE 8 | *Wwox*$^{-/-}$ mice lack subcutaneous fat and display hypothermia. **(A)** A schematic diagram of epidermal and stromal thickness measurement. **(B)** Quantification of mouse stromal and subcutaneous fat layer thickness at P21 (n = 3). **(C)** Subcutaneous fat was detected by Nile red staining of frozen mouse skin tissue sections (upper panel) and toluidine blue staining of EMbed 812-embedded skin samples (lower panel). The yellow stars in the lower panel indicate subcutaneous fat layer. Scale bar = 100 μm. **(D)** Immunohistochemical staining of *Wwox*$^{+/+}$ and *Wwox*$^{-/-}$ mouse dermal tissue sections for FABP4. The lower panel is an enlarged image from the boxed area in *Wwox*$^{-/-}$ tissue section and the arrows indicate adipocytes. Scale bar = 50 μm. **(E)** Measurement of mouse skin surface temperature (*Wwox*$^{+/+}$, n = 12; *Wwox*$^{+/-}$, n = 9; *Wwox*$^{-/-}$, n = 15). All data are presented as mea ± SEM. Statistical analysis was performed using one-way ANOVA and *post hoc* Tukey tests. ***$P < 0.001$.

of MEK/ERK signaling is critical for keratinocyte growth and differentiation and stem cell functions. Conceivably, WWOX is required to control keratinocyte proliferation and differentiation.

Nunez et al. (2006) along with the data shown in Human Protein Atlas[1] have indicated that epidermal basal and suprabasal cells have weak to moderate WWOX expression. Lai et al. (2005) showed that the intensity of WWOX protein expression is increased toward superficial layers of human epidermis. Using an *in vitro* keratinocyte differentiation model, we determined that WWOX protein expression was increased after differentiation induction by treatment of Ca^{2+} in HaCaT cells. In addition, WWOX knockdown suppressed Ca^{2+}-induced differentiation marker K10 expression and stratification dome formation. Together, these findings suggest that WWOX plays an important role in the regulation of epidermal keratinocyte differentiation and stratification. In the case that subconfluent HaCaT cells are cultured with a low concentration of Ca^{2+}, the cells undergo proliferation but not differentiation (Bikle et al., 2012). Treatment with a high concentration of Ca^{2+} induces cell cycle exit, differentiation, and formation of desmosomes, tight junctions and adherens junctions in HaCaT cells (Bikle et al., 2012). In the absence of WWOX, reduced E-cadherin expression at the cell junctions and delayed cell-cell contact formation were observed. How WWOX regulates E-cadherin protein expression in epidermal keratinocytes is unknown. Whether the increased WWOX protein expression during keratinocyte differentiation is required for the assembly of adherens junctions for keratinocyte stratification remains to be investigated. Moreover, p63 is an essential molecule for initiating basal to spinous transition of epidermal keratinocytes (Blanpain and Fuchs, 2009; Wu et al., 2012). WWOX has been found to interact with ΔNp63α (Salah et al., 2013). Downregulation of p63 protein level was detected in $Wwox^{-/-}$ mouse epidermal keratinocytes in this study. However, it is unclear whether WWOX controls keratinocyte differentiation through p63.

Substantial evidences have suggested that the control of cell growth and apoptosis by WWOX may depend on cell types, such as their tissue origin, differentiation state or differences between normal, benign and malignant cells (Chang et al., 2007; Nowakowska et al., 2014). In coincidence with its tumor suppressor function, overexpression of WWOX protein in malignant lung, breast, pancreatic, cervical, and prostate cancer cells suppresses cell growth and increases cell apoptosis (Fabbri et al., 2005; Iliopoulos et al., 2007; Nakayama et al., 2008; Qu et al., 2013; Lin et al., 2015). In contrast, in low-grade invasive HT29 colon adenocarcinoma cells, increased WWOX expression promotes cell proliferation but inhibits apoptosis (Nowakowska et al., 2014). WWOX has been suggested to have pro-survival functions (Aqeilan et al., 2008; Abdel-Salam et al., 2014; Mallaret et al., 2014). Ludes-Meyers et al. (2009) showed that *Wwox* knockout mice exhibit severe metabolic acidosis and leukopenia and succumb to early death by 3 weeks of age. Targeted ablation of *Wwox* in mice leads to impaired steroidogenesis and reduced GABA-ergic inhibitory interneuron numbers (Aqeilan et al., 2009; Hussain et al., 2019). *Wwox* knockout causes a reduction in mouse bone osteoprogenitor cell growth but does not affect mammary gland cell proliferation (Aqeilan et al., 2008; Ferguson et al., 2012). Using a keratin 5-Cre-mediated knockout mouse model, Ferguson et al. (2012) showed that ablation of *Wwox* in mammary epithelium leads to impaired mammary branching morphogenesis. These findings suggest that WWOX is a protein with pleiotropic functions. A certain amount of WWOX expression may be necessary for maintaining normal physiological functions in cells. However, it remains largely unclear whether the phosphorylation status of WWOX protein in cells affects its functions. The distinct function of WWOX in various cell types may also be manipulated by the expression or mutation of WWOX-binding proteins, such as p53, BRCA, or Ras. How WWOX controls cell fates in coordination with these factors and their regulated signaling remains to be determined.

Both epidermis and HFs are squamous epithelium composed of multi-layered keratinocytes (Blanpain and Fuchs, 2009; Yi and Fuchs, 2010). The basal keratinocytes in the innermost layer are highly proliferative and undifferentiated cells. When these cells are committed to differentiation, they exit cell cycle and begin to differentiate (Fuchs and Raghavan, 2002). Downregulation of cell proliferation in basal keratinocytes has been shown to induce cell differentiation (Asare et al., 2017). A significant reduction in proliferative activity was determined in $Wwox^{-/-}$ mouse keratinocytes at ∼P20. However, we did not detect an increase of $K5^{+}K10^{+}$ double-positive differentiated progenitor cells in $Wwox^{-/-}$ mouse epidermis (**Figure 2A**). On the contrary, decreased keratinocyte differentiation was examined in $Wwox^{-/-}$ mouse epidermis and WWOX-knockdown HaCaT cells. One possibility to achieve it is that WWOX binds to particular proteins involved in both proliferation and differentiation in keratinocytes. However, the molecular mechanisms by which WWOX regulates both keratinocyte proliferation and differentiation remain to be investigated.

The integrity of HFSC niche is maintained by the balance between quiescence and activation status of cells. To produce rapidly cycling and highly proliferative transient amplifying cells, the quiescent stem cells in the epidermal basal layer may undergo asymmetric division (Hsu et al., 2014; Kretzschmar and Watt, 2014). Previous studies have shown that depletion of E-cadherin expression in cells disturbs spindle orientation and cellular polarity during cell division (Wang et al., 2018). In the present study, downregulation of E-cadherin expression was determined in $Wwox^{-/-}$ mouse epidermal keratinocytes. However, whether loss of WWOX expression in self-renewing epithelium causes aberrant cellular polarity in epidermal basal cells and disturbs asymmetric division is unknown. The regulation of cell fate, differentiation, and HFSC dynamics for maintaining tissue homeostasis by WWOX remains to be investigated.

Using a conditional knockout mouse model for *Wwox* gene in K5-positive basal cells, Ferguson et al. (2012) found that the mouse epidermis exhibits a normal two-layer structure. However, these conditional *Wwox* knockout mice die within 4 months after birth (Ferguson et al., 2012). Herein, an *in vitro* growth failure of isolated primary *Wwox* knockout mouse epidermal keratinocytes was examined, suggesting an intrinsic defect due to *Wwox* loss in these cells. Although the macro-morphology

[1] www.proteinatlas.org

of epidermis remains intact in these conditional knockout mice (Ferguson et al., 2012), loss of *Wwox* expression in the epidermal keratinocytes might affect cell proliferation, differentiation and adhesion, and impair skin barrier functions. Interestingly, the epidermal thickness was transiently increased at P7 (**Figure 6C**) but decreased at P21 in the whole-body *Wwox* knockout mice (**Figure 1D**). A temporary increase in proliferating progenitors observed in the JZ at P7 may lead to a gradual loss of quiescent HFSCs at the later stages. Whether stem cell exhaustion and aberrant keratinocyte proliferation and differentiation cause subsequent abnormality in skin barrier function and death in the keratinocyte-specific *Wwox* knockout mice is unclear. Both collagen and adipose tissues are important for epidermal tissue homeostasis and HF growth (Rognoni and Watt, 2018; Kruglikov et al., 2019). The significant reduction in dermal collagen and subcutaneous fat contents in whole-body *Wwox* knockout mice may result in decreased generation of signals for supporting keratinocyte growth and differentiation and cause more severe phenotypes in the skin.

Wwox knockout mice have been reported to exhibit epileptic seizure symptoms and hypoglycemia, which are highly related to mortality (Ludes-Meyers et al., 2009; Abdel-Salam et al., 2014; Cheng et al., 2020). In addition, hypothermia caused by the loss of subcutaneous fat may also lead to early death of *Wwox* knockout mice because low body temperature has been considered as a valid marker for imminent death (Ray et al., 2010; Mai et al., 2018). Downregulation of peroxisome-proliferator activated receptor-γ was examined in $Wwox^{-/-}$ mouse subcutaneous fat layer at P7 (data not shown). Whether WWOX regulates adipocyte maturation and function is unclear. Previous studies have revealed that *Wwox* ablation alters glucose and lipid metabolism and causes defective steroidogenesis in mice (Aqeilan et al., 2009; Abu-Remaileh and Aqeilan, 2014; Abu-Remaileh et al., 2019). Nevertheless, whether the fat loss in whole-body *Wwox* knockout mice is a consequence of metabolic dysregulation remains to be investigated.

CONCLUSION

Genetic ablation of *Wwox* causes severe dermal and epidermal disorders as well as hypothermia in mice. Most importantly, *Wwox* knockout mouse models may recapitulate the key pathological features of human diseases due to loss or dysfunction of WWOX. Using whole-body or conditional knockout mouse models, future studies will be needed to investigate the molecular mechanisms by which WWOX controls body temperature and regulates HFSC maintenance and keratinocyte proliferation and differentiation for maintaining tissue homeostasis in the skin.

DATA AVAILABILITY STATEMENT

The original contributions presented in the study are included in the article/**Supplementary Material**, further inquiries can be directed to the corresponding author.

ETHICS STATEMENT

The animal study was reviewed and approved by Institutional Animal Care and Use Committee of National Cheng Kung University.

AUTHOR CONTRIBUTIONS

Y-TC performed the experiments, analyzed the results, and prepared the manuscript. F-JL performed transmission electron microscopy and contributed to the discussion. N-SC contributed to the discussion and reviewed the manuscript. L-JH supervised the work and edited the manuscript. All authors contributed to the article and approved the submitted version.

FUNDING

This research was funded by the Ministry of Science and Technology, Taiwan, grant MOST 104-2320-B-006-016-MY3 (to L-JH), National Health Research Institute, Taiwan, grant NHRI-EX108-10734N1 (to N-SC), and Chi Mei Hospital and National Cheng Kung University Collaborative Research grants CMNCKU9902, 10008, 10204, 10302, 10406, 10502, 10603, 10701, and 10804 (to F-JL and L-JH).

ACKNOWLEDGMENTS

We thank Drs. Hamm-Ming Sheu and Jui-Chen Tsai, National Cheng Kung University, Taiwan, for helping with the measurement of skin hydration state and transepidermal water loss. We thank Dr. Dar-Bin Shieh, National Cheng Kung University, Taiwan, for the measurement of skin surface temperature.

SUPPLEMENTARY MATERIAL

The Supplementary Material for this article can be found online at: https://www.frontiersin.org/articles/10.3389/fcell.2020.558432/full#supplementary-material

REFERENCES

Abdel-Salam, G., Thoenes, M., Afifi, H. H., Korber, F., Swan, D., and Bolz, H. J. (2014). The supposed tumor suppressor gene *WWOX* is mutated in an early lethal microcephaly syndrome with epilepsy, growth retardation and retinal degeneration. *Orphanet J. Rare Dis.* 9:12. doi: 10.1186/1750-1172-9-12

Abu-Odeh, M., Bar-Mag, T., Huang, H., Kim, T., Salah, Z., Abdeen, S. K., et al. (2014). Characterizing WW domain interactions of tumor suppressor WWOX reveals its association with multiprotein networks. *J. Biol. Chem.* 289, 8865–8880. doi: 10.1074/jbc.M113.506790

Abu-Remaileh, M., Abu-Remaileh, M., Akkawi, R., Knani, I., Udi, S., Pacold, M. E., et al. (2019). WWOX somatic ablation in skeletal muscles alters glucose metabolism. *Mol. Metab.* 22, 132–140. doi: 10.1016/j.molmet.2019.01.010

Abu-Remaileh, M., and Aqeilan, R. I. (2014). Tumor suppressor WWOX regulates glucose metabolism via HIF1α modulation. *Cell Death Differ.* 21, 1805–1814. doi: 10.1038/cdd.2014.95

Abu-Remaileh, M., Joy-Dodson, E., Schueler-Furman, O., and Aqeilan, R. I. (2015). Pleiotropic functions of tumor suppressor WWOX in normal and cancer cells. *J. Biol. Chem.* 290, 30728–30735. doi: 10.1074/jbc.R115.676346

Alexander, C. M., Kasza, I., Yen, C. L., Reeder, S. B., Hernando, D., Gallo, R. L., et al. (2015). Dermal white adipose tissue: a new component of the thermogenic response. *J. Lipid Res.* 56, 2061–2069. doi: 10.1194/jlr.R062893

Ali, N. J. A., Dias Gomes, M., Bauer, R., Brodesser, S., Niemann, C., and Iden, S. (2016). Essential role of polarity protein Par3 for epidermal homeostasis through regulation of barrier function, keratinocyte differentiation, and stem cell maintenance. *J. Invest. Dermatol.* 136, 2406–2416. doi: 10.1016/j.jid.2016.07.011

Alonso, L., and Fuchs, E. (2006). The hair cycle. *J. Cell Sci.* 119, 391–393. doi: 10.1242/jcs02793

Aqeilan, R. I., Hagan, J. P., de Bruin, A., Rawahneh, M., Salah, Z., Gaudio, E., et al. (2009). Targeted ablation of the WW domain-containing oxidoreductase tumor suppressor leads to impaired steroidogenesis. *Endocrinology* 150, 1530–1535. doi: 10.1210/en.2008-1087

Aqeilan, R. I., Hassan, M. Q., de Bruin, A., Hagan, J. P., Volinia, S., Palumbo, T., et al. (2008). The WWOX tumor suppressor is essential for postnatal survival and normal bone metabolism. *J. Biol. Chem.* 283, 21629–21639. doi: 10.1074/jbc.M800855200

Aqeilan, R. I., Trapasso, F., Hussain, S., Costinean, S., Marshall, D., Pekarsky, Y., et al. (2007). Targeted deletion of Wwox reveals a tumor suppressor function. *Proc. Natl. Acad. Sci. U.S.A.* 104, 3949–3954. doi: 10.1073/pnas.0609783104

Asare, A., Levorse, J., and Fuchs, E. (2017). Coupling organelle inheritance with mitosis to balance growth and differentiation. *Science* 355:eaah4701. doi: 10.1126/science.aah4701

Bikle, D. D., Xie, Z., and Tu, C. L. (2012). Calcium regulation of keratinocyte differentiation. *Expert Rev. Endocrinol. Metab.* 7, 461–472. doi: 10.1586/eem.12.34

Blanpain, C., and Fuchs, E. (2009). Epidermal homeostasis: a balancing act of stem cells in the skin. *Nat. Rev. Mol. Cell Biol.* 10, 207–217. doi: 10.1038/nrm2636

Chang, J. Y., Lee, M. H., Lin, S. R., Yang, L. Y., Sun, H. S., Sze, C. I., et al. (2015). Trafficking protein particle complex 6A delta (TRAPPC6AΔ) is an extracellular plaque-forming protein in the brain. *Oncotarget* 6, 3578–3589. doi: 10.18632/oncotarget.2876

Chang, N. S., Doherty, J., Ensign, A., Lewis, J., Heath, J., Schultz, L., et al. (2003). Molecular mechanisms underlying WOX1 activation during apoptotic and stress responses. *Biochem. Pharmacol.* 66, 1347–1354. doi: 10.1016/s0006-2952(03)00484-2

Chang, N. S., Doherty, J., Ensign, A., Schultz, L., Hsu, L. J., and Hong, Q. (2005a). WOX1 is essential for tumor necrosis factor-, UV light-, staurosporine-, and p53-mediated cell death, and its tyrosine 33-phosphorylated form binds and stabilizes serine 46-phosphorylated p53. *J. Biol. Chem.* 280, 43100–43108. doi: 10.1074/jbc.M505590200

Chang, N. S., Schultz, L., Hsu, L. J., Lewis, J., Su, M., and Sze, C. I. (2005b). 17beta-Estradiol upregulates and activates WOX1/WWOXv1 and WOX2/WWOXv2 in vitro: potential role in cancerous progression of breast and prostate to a premetastatic state in vivo. *Oncogene* 24, 714–723. doi: 10.1038/sj.onc.1208124

Chang, N. S., Hsu, L. J., Lin, Y. S., Lai, F. J., and Sheu, H. M. (2007). WW domain-containing oxidoreductase: a candidate tumor suppressor. *Trends Mol. Med.* 13, 12–22. doi: 10.1016/j.molmed.2006.11.006

Chang, N. S., Pratt, N., Heath, J., Schultz, L., Sleve, D., Carey, G. B., et al. (2001). Hyaluronidase induction of a WW domain-containing oxidoreductase that enhances tumor necrosis factor cytotoxicity. *J. Biol. Chem.* 276, 3361–3370. doi: 10.1074/jbc.M007140200

Chen, S. J., Lin, P. W., Lin, H. P., Huang, S. S., Lai, F. J., Sheu, H. M., et al. (2015). UV irradiation/cold shock-mediated apoptosis is switched to bubbling cell death at low temperatures. *Oncotarget* 6, 8007–8018. doi: 10.18632/oncotarget.3153

Chen, Y. A., Lu, C. Y., Cheng, T. Y., Pan, S. H., Chen, H. F., and Chang, N. S. (2019). WW domain-containing proteins YAP and TAZ in the Hippo pathway as key regulators in stemness maintenance, tissue homeostasis, and tumorigenesis. *Front. Oncol.* 9:60. doi: 10.3389/fonc.2019.00060

Cheng, Y. Y., Chou, Y. T., Lai, F. J., Jan, M. S., Chang, T. H., Jou, I. M., et al. (2020). Wwox deficiency leads to neurodevelopmental and degenerative neuropathies and glycogen synthase kinase 3β-mediated epileptic seizure activity in mice. *Acta Neuropathol. Commun.* 8:6. doi: 10.1186/s40478-020-0883-3

Chou, P. Y., Lai, F. J., Chen, Y. A., Sie, Y. D., Kuo, H. L., Su, W. P., et al. (2019a). Strategies by which WWOX-deficient metastatic cancer cells utilize to survive via dodging, compromising, and causing damage to WWOX-positive normal microenvironment. *Cell Death Discov.* 5:97. doi: 10.1038/s41420-019-0176-4

Chou, P. Y., Lin, S. R., Lee, M. H., Schultz, L., Sze, C. I., and Chang, N. S. (2019b). A p53/TIAF1/WWOX triad exerts cancer suppression but may cause brain protein aggregation due to p53/WWOX functional antagonism. *Cell Commun. Signal.* 17:76. doi: 10.1186/s12964-019-0382-y

Chou, T. C., Tsai, J. C., Sheu, H. M., Jen, C. J., Shih, T. S., and Chang, H. Y. (2005). Topical exposure to carbon disulfide induces epidermal permeability alterations in physiological and pathological changes. *Toxicol. Lett.* 158, 225–236. doi: 10.1016/j.toxlet.2005.03.017

Deyrieux, A. F., and Wilson, V. G. (2007). In vitro culture conditions to study keratinocyte differentiation using the HaCaT cell line. *Cytotechnology* 54, 77–83. doi: 10.1007/s10616-007-9076-1

Fabbri, M., Iliopoulos, D., Trapasso, F., Aqeilan, R. I., Cimmino, A., Zanesi, N., et al. (2005). WWOX gene restoration prevents lung cancer growth in vitro and in vivo. *Proc. Natl. Acad. Sci. U.S.A.* 102, 15611–15616. doi: 10.1073/pnas.0505485102

Ferguson, B. W., Gao, X., Kil, H., Lee, J., Benavides, F., Abba, M. C., et al. (2012). Conditional Wwox deletion in mouse mammary gland by means of two Cre recombinase approaches. *PLoS One* 7:e36618. doi: 10.1371/journal.pone.0036618

Fuchs, E., and Raghavan, S. (2002). Getting under the skin of epidermal morphogenesis. *Nat. Rev. Genet.* 3, 199–209. doi: 10.1038/nrg758

Fujiwara, H., Tsutsui, K., and Morita, R. (2018). Multi-tasking epidermal stem cells: beyond epidermal maintenance. *Dev. Growth Differ.* 60, 531–541. doi: 10.1111/dgd.12577

Gavin, H. E., and Satchell, K. J. F. (2017). Surface hypothermia predicts murine mortality in the intragastric *Vibrio vulnificus* infection model. *BMC Microbiol.* 17:136. doi: 10.1186/s12866-017-1045-z

Hennings, H., Michael, D., Cheng, C., Steinert, P., Holbrook, K., and Yuspa, S. H. (1980). Calcium regulation of growth and differentiation of mouse epidermal cells in culture. *Cell* 19, 245–254. doi: 10.1016/0092-8674(80)90406-7

Hsu, Y. C., Li, L., and Fuchs, E. (2014). Emerging interactions between skin stem cells and their niches. *Nat. Med.* 20, 847–856. doi: 10.1038/nm.3643

Huang, S. S., and Chang, N. S. (2018). Phosphorylation/de-phosphorylation in specific sites of tumor suppressor WWOX and control of distinct biological events. *Exp. Biol. Med.* 243, 137–147. doi: 10.1177/1535370217752350

Hussain, T., Kil, H., Hattiangady, B., Lee, J., Kodali, M., Shuai, B., et al. (2019). Wwox deletion leads to reduced GABA-ergic inhibitory interneuron numbers and activation of microglia and astrocytes in mouse hippocampus. *Neurobiol. Dis.* 121, 163–176. doi: 10.1016/j.nbd.2018.09.026

Iliopoulos, D., Fabbri, M., Druck, T., Qin, H. R., Han, S. Y., and Huebner, K. (2007). Inhibition of breast cancer cell growth in vitro and in vivo: effect of restoration of Wwox expression. *Clin. Cancer Res.* 13, 268–274. doi: 10.1158/1078-0432.CCR-06-2038

Janczar, S., Nautiyal, J., Xiao, Y., Curry, E., Sun, M., Zanini, E., et al. (2017). WWOX sensitises ovarian cancer cells to paclitaxel via modulation of the ER stress response. *Cell Death Dis.* 8:e2955. doi: 10.1038/cddis.2017.346

Jensen, K. B., Driskell, R. R., and Watt, F. M. (2010). Assaying proliferation and differentiation capacity of stem cells using disaggregated adult mouse epidermis. *Nat. Protoc.* 5, 898–911. doi: 10.1038/nprot.2010.39

Kretzschmar, K., and Watt, F. M. (2014). Markers of epidermal stem cell subpopulations in adult mammalian skin. *Cold Spring Harb. Perspect. Med.* 4:a013631. doi: 10.1101/cshperspect.a013631

Kruglikov, I. L., Zhang, Z., and Scherer, P. E. (2019). The role of immature and mature adipocytes in hair cycling. *Trends Endocrinol. Metab.* 30, 93–105. doi: 10.1016/j.tem.2018.11.004

Kunkle, B. W., Grenier-Boley, B., Sims, R., Bis, J. C., Damotte, V., Naj, A. C., et al. (2019). Genetic meta-analysis of diagnosed Alzheimer's disease identifies new risk loci and implicates Aβ, tau, immunity and lipid processing. *Nat. Genet.* 51, 414–430. doi: 10.1038/s41588-019-0358-2

Lai, F. J., Cheng, C. L., Chen, S. T., Wu, C. H., Hsu, L. J., Lee, J. Y., et al. (2005). WOX1 is essential for UVB irradiation-induced apoptosis and down-regulated via translational blockade in UVB-induced cutaneous squamous cell carcinoma in vivo. *Clin. Cancer Res.* 11, 5769–5777. doi: 10.1158/1078-0432.CCR-04-2274

Lee, M. H., Shih, Y. H., Lin, S. R., Chang, J. Y., Lin, Y. H., Sze, C. I., et al. (2017). Zfra restores memory deficits in Alzheimer's disease triple-transgenic mice by blocking aggregation of TRAPPC6AΔ, SH3GLB2, tau, and amyloid β, and inflammatory NF-κB activation. *Alzheimers Dement.* 3, 189–204. doi: 10.1016/j.trci.2017.02.001

Lin, H. P., Chang, J. Y., Lin, S. R., Lee, M. H., Huang, S. S., Hsu, L. J., et al. (2011). Identification of an in vivo MEK/WOX1 complex as a master switch for apoptosis in T cell leukemia. *Genes Cancer* 2, 550–562. doi: 10.1177/1947601911418498

Lin, J. T., Li, H. Y., Chang, N. S., Lin, C. H., Chen, Y. C., and Lu, P. J. (2015). WWOX suppresses prostate cancer cell progression through cyclin D1-mediated cell cycle arrest in the G1 phase. *Cell Cycle* 14, 408–416. doi: 10.4161/15384101.2014.977103

Liu, C. C., Ho, P. C., Lee, I. T., Chen, Y. A., Chu, C. H., Teng, C. C., et al. (2018). WWOX phosphorylation, signaling, and role in neurodegeneration. *Front. Neurosci.* 12:563. doi: 10.3389/fnins.2018.00563

Lo, J. Y., Chou, Y. T., Lai, F. J., and Hsu, L. J. (2015). Regulation of cell signaling and apoptosis by tumor suppressor WWOX. *Exp. Biol. Med.* 240, 383–391. doi: 10.1177/1535370214566747

Ludes-Meyers, J. H., Kil, H., Parker-Thornburg, J., Kusewitt, D. F., Bedford, M. T., and Aldaz, C. M. (2009). Generation and characterization of mice carrying a conditional allele of the Wwox tumor suppressor gene. *PLoS One* 4:e7775. doi: 10.1371/journal.pone.0007775

Mai, S. H. C., Sharma, N., Kwong, A. C., Dwivedi, D. J., Khan, M., Grin, P. M., et al. (2018). Body temperature and mouse scoring systems as surrogate markers of death in cecal ligation and puncture sepsis. *Intensive Care Med. Exp.* 6:20. doi: 10.1186/s40635-018-0184-3

Mallaret, M., Synofzik, M., Lee, J., Sagum, C. A., Mahajnah, M., Sharkia, R., et al. (2014). The tumour suppressor gene WWOX is mutated in autosomal recessive cerebellar ataxia with epilepsy and mental retardation. *Brain* 137, 411–419. doi: 10.1093/brain/awt338

Muller-Rover, S., Handjiski, B., van der Veen, C., Eichmuller, S., Foitzik, K., McKay, I. A., et al. (2001). A comprehensive guide for the accurate classification of murine hair follicles in distinct hair cycle stages. *J. Invest. Dermatol.* 117, 3–15. doi: 10.1046/j.0022-202x.2001.01377.x

Nakayama, S., Semba, S., Maeda, N., Aqeilan, R. I., Huebner, K., and Yokozaki, H. (2008). Role of the WWOX gene, encompassing fragile region FRA16D, in suppression of pancreatic carcinoma cells. *Cancer Sci.* 99, 1370–1376. doi: 10.1111/j.1349-7006.2008.00841.x

Nelson, W. J., and Nusse, R. (2004). Convergence of Wnt, beta-catenin, and cadherin pathways. *Science* 303, 1483–1487. doi: 10.1126/science.1094291

Niessen, M. T., Scott, J., Zielinski, J. G., Vorhagen, S., Sotiropoulou, P. A., Blanpain, C., et al. (2013). aPKCλ controls epidermal homeostasis and stem cell fate through regulation of division orientation. *J. Cell Biol.* 202, 887–900. doi: 10.1083/jcb.201307001

Nowak, J. A., Polak, L., Pasolli, H. A., and Fuchs, E. (2008). Hair follicle stem cells are specified and function in early skin morphogenesis. *Cell Stem Cell* 3, 33–43. doi: 10.1016/j.stem.2008.05.009

Nowakowska, M., Pospiech, K., Lewandowska, U., Piastowska-Ciesielska, A. W., and Bednarek, A. K. (2014). Diverse effect of WWOX overexpression in HT29 and SW480 colon cancer cell lines. *Tumour Biol.* 35, 9291–9301. doi: 10.1007/s13277-014-2196-2

Nunez, M. I., Ludes-Meyers, J., and Aldaz, C. M. (2006). WWOX protein expression in normal human tissues. *J. Mol. Histol.* 37, 115–125. doi: 10.1007/s10735-006-9046-5

Poumay, Y., and Pittelkow, M. R. (1995). Cell density and culture factors regulate keratinocyte commitment to differentiation and expression of suprabasal K1/K10 keratins. *J. Invest. Dermatol.* 104, 271–276. doi: 10.1111/1523-1747.ep12612810

Qu, J., Lu, W., Li, B., Lu, C., and Wan, X. (2013). WWOX induces apoptosis and inhibits proliferation in cervical cancer and cell lines. *Int. J. Mol. Med.* 31, 1139–1147. doi: 10.3892/ijmm.2013.1314

Ray, M. A., Johnston, N. A., Verhulst, S., Trammell, R. A., and Toth, L. A. (2010). Identification of markers for imminent death in mice used in longevity and aging research. *J. Am. Assoc. Lab. Anim. Sci.* 49, 282–288.

Rognoni, E., and Watt, F. M. (2018). Skin cell heterogeneity in development, wound healing, and cancer. *Trends Cell Biol.* 28, 709–722. doi: 10.1016/j.tcb.2018.05.002

Saigo, C., Kito, Y., and Takeuchi, T. (2018). Cancerous protein network that inhibits the tumor suppressor function of WW domain-containing oxidoreductase (WWOX) by aberrantly expressed molecules. *Front. Oncol.* 8:350. doi: 10.3389/fonc.2018.00350

Salah, Z., Bar-mag, T., Kohn, Y., Pichiorri, F., Palumbo, T., Melino, G., et al. (2013). Tumor suppressor WWOX binds to ΔNp63α and sensitizes cancer cells to chemotherapy. *Cell Death Dis.* 4:e480. doi: 10.1038/cddis.2013.6

Schrock, M. S., and Huebner, K. (2015). WWOX: a fragile tumor suppressor. *Exp. Biol. Med.* 240, 296–304. doi: 10.1177/1535370214561590

Senoo, M. (2013). Epidermal stem cells in homeostasis and wound repair of the skin. *Adv. Wound Care* 2, 273–282. doi: 10.1089/wound.2012.0372

Tabarki, B., AlHashem, A., AlShahwan, S., Alkuraya, F. S., Gedela, S., and Zuccoli, G. (2015). Severe CNS involvement in WWOX mutations: description of five new cases. *Am. J. Med. Genet. A* 167A, 3209–3213. doi: 10.1002/ajmg.a.37363

Tsai, C. W., Lai, F. J., Sheu, H. M., Lin, Y. S., Chang, T. H., Jan, M. S., et al. (2013). WWOX suppresses autophagy for inducing apoptosis in methotrexate-treated human squamous cell carcinoma. *Cell Death Dis.* 4:e792. doi: 10.1038/cddis.2013.308

Valduga, M., Philippe, C., Lambert, L., Bach-Segura, P., Schmitt, E., Masutti, J. P., et al. (2015). WWOX and severe autosomal recessive epileptic encephalopathy: first case in the prenatal period. *J. Hum. Genet.* 60, 267–271. doi: 10.1038/jhg.2015.17

Varghese, F., Bukhari, A. B., Malhotra, R., and De, A. (2014). IHC Profiler: an open source plugin for the quantitative evaluation and automated scoring of immunohistochemistry images of human tissue samples. *PLoS One* 9:e96801. doi: 10.1371/journal.pone.0096801

Voronkov, A., and Krauss, S. (2013). Wnt/beta-catenin signaling and small molecule inhibitors. *Curr. Pharm. Des.* 19, 634–664. doi: 10.2174/1381612811306040634

Wang, D., Zhang, Z., O'Loughlin, E., Wang, L., Fan, X., Lai, E. C., et al. (2013). MicroRNA-205 controls neonatal expansion of skin stem cells by modulating the PI(3)K pathway. *Nat. Cell Biol.* 15, 1153–1163. doi: 10.1038/ncb2827

Wang, X., Dong, B., Zhang, K., Ji, Z., Cheng, C., Zhao, H., et al. (2018). E-cadherin bridges cell polarity and spindle orientation to ensure prostate epithelial integrity and prevent carcinogenesis in vivo. *PLoS Genet.* 14:e1007609. doi: 10.1371/journal.pgen.1007609

Wu, N., Rollin, J., Masse, I., Lamartine, J., and Gidrol, X. (2012). p63 regulates human keratinocyte proliferation via MYC-regulated gene network and differentiation commitment through cell adhesion-related gene network. *J. Biol. Chem.* 287, 5627–5638. doi: 10.1074/jbc.M111.328120

Yi, R., and Fuchs, E. (2010). MicroRNA-mediated control in the skin. *Cell Death Differ.* 17, 229–235. doi: 10.1038/cdd.2009.92

Conflict of Interest: The authors declare that the research was conducted in the absence of any commercial or financial relationships that could be construed as a potential conflict of interest.

frontiers in Cell and Developmental Biology

MINI REVIEW
published: 30 November 2020
doi: 10.3389/fcell.2020.605996

Aging and Senescence of Dental Pulp and Hard Tissues of the Tooth

Hidefumi Maeda[1,2]*

[1] Department of Endodontology and Operative Dentistry, Kyushu University, Fukuoka, Japan, [2] Department of Endodontology, Kyushu University Hospital, Fukuoka, Japan

The ability to consume a meal using one's own teeth influences an individual's quality of life. In today's global aging society, studying the biological changes in aging teeth is important to address this issue. A tooth includes three hard tissues (enamel, dentin, and cementum) and a soft tissue (dental pulp). With advancing age, these tissues become senescent; each tissue exhibits a unique senescent pattern. This review discusses the structural alterations of hard tissues, as well as the molecular and physiological changes in dental pulp cells and dental pulp stem cells during human aging. The significance of senescence in these cells remains unclear. Thus, there is a need to define the regulatory mechanisms of aging and senescence in these cells to aid in preservation of dental health.

Keywords: aging, dental pulp cells, dental hard tissue, senescence, tooth

OPEN ACCESS

Edited by:
Wolfgang Knabe, Westfälische Wilhelms-Universität Münster, Germany

Reviewed by:
Ralf Johannes Radlanski, Charité – Universitätsmedizin Berlin, Germany
Werner Götz, University of Bonn, Germany

***Correspondence:**
Hidefumi Maeda
hide@dent.kyushu-u.ac.jp

Specialty section:
This article was submitted to Cell Death and Survival, a section of the journal Frontiers in Cell and Developmental Biology

Received: *14 September 2020*
Accepted: *04 November 2020*
Published: *30 November 2020*

Citation:
Maeda H (2020) Aging and Senescence of Dental Pulp and Hard Tissues of the Tooth. Front. Cell Dev. Biol. 8:605996. doi: 10.3389/fcell.2020.605996

INTRODUCTION

Oral health in older individuals is closely related to their general well-being (Gil-Montoya et al., 2015). In particular, tooth loss causes reduced dietary intake, presumably leading to systemic health problems (Iwasaki et al., 2016). Thus, there is an urgent need for individuals to conserve their teeth in the modern aging society. Tooth fracture is an important cause of tooth loss, which affects 32% of individuals with tooth loss in Japan and 62% of such individuals in Sweden (Axelsson et al., 2004; Yoshino et al., 2015). Other causes include dental caries and periodontal diseases. Because of life extension and increasing focus on oral health care, older individuals possess greater numbers of teeth, as well as a greater risk of tooth fracture, than do younger individuals (Yoshino et al., 2015; Tavares et al., 2018). This may be due to aging-related changes in teeth, including hard and soft tissues. A severely fractured tooth must be extracted. Hence, there is a need to understand alterations of tissues in aged teeth to explore the mechanisms underlying their age-related molecular changes; this will aid in elucidating methods that can prevent tooth loss and support a healthy lifestyle. In this review, I summarize the findings (mainly in the past two decades) concerning aging-related structural alterations of hard tissues, as well as the aging-related molecular and physiological changes in dental pulp cells and dental pulp stem cells (DPSCs). I also discuss methods to counteract tooth senescence for health preservation among older individuals.

SENESCENCE OF ENAMEL

Enamel that covers the tooth surface is the hardest tissue in the body (**Figure 1A**) because it comprises >96% minerals (mainly hydroxyapatite crystals). The roles of enamel are to protect

internal tissues (e.g., dentin and dental pulp) from caries-causing bacteria, chemo-mechanical attacks, and thermal attacks; it also mediates chewing force.

In the developing tooth, enamel is formed by epithelial cells (ameloblasts) that originate from ectoderm (**Figure 1A**). These cells interact with mesenchyme-derived dental papilla cells and produce enamel matrix proteins. Initially, the matrix proteins are partially calcified; during enamel maturation, the enamel matrix becomes mineralized, and mature ameloblasts remove both degraded matrix proteins and water to complete the mineralization process (Simmer et al., 2010). At the final stage of differentiation before eruption, ameloblasts exhibit reduced size and no longer contribute to enamel maturation or matrix secretion.

Freshly erupted tooth enamel is more permeable than aged tooth enamel (Bertacci et al., 2007). However, the inorganic components of this tissue can be affected by changes in saliva properties and lifestyle habits during the aging process; in particular, isomorphic and isoionic exchanges lead to increased mineral density (Kunin et al., 2015). During the aging process, enamel is subjected to tooth wear (Bartlett and O'Toole, 2019); it also shows post-eruptive maturation through a reduction in permeability, which leads to greater mineral contents over time, particularly on the outer enamel surface (Park et al., 2008). This results in diminished fracture toughness, partly caused by the reduction of organic matrix (Zheng et al., 2013); it also decreases caries susceptibility (Kotsanos and Darling, 1991). In older individuals, cracks are often observed during clinical examination of the enamel surface, alongside enamel crystals (Yahyazadehfar et al., 2016). However, it is not yet possible to prevent the enhancement of enamel brittleness with age.

SENESCENCE OF DENTIN

Dentin is a hard tissue with a unique structure (**Figure 1A**), which protects and encloses dental pulp tissue in the pulp chamber. It is formed by odontoblasts that differentiate from neural crest-derived ectomesenchymal cells (**Figure 1A**) and comprises approximately 70% minerals, 18% organic materials, and 12% water. In dentinogenesis, dentinal tubules in dentin are formed by the cell processes of odontoblasts localized at the dental pulp periphery (**Figure 1A**). Odontoblasts contribute to the sensing of some external stimuli (e.g., caries and tooth cutting) and enhance dentinal resistance against occlusal force.

During the aging process, dentinal sclerosis (i.e., occlusion of dentinal tubules by mineral deposition) progresses (Azaz et al., 1977). The dentin of older individuals shows a higher elastic modulus (Xu et al., 2014) and lower complex modulus, as compared with that of young individuals (Ryou et al., 2015). These structural alterations in older individuals lead to reduced root dentin fracture resistance (Yan et al., 2017).

Odontoblasts are critical cells that form and maintain dentin. They remain alive throughout life but experience aging (Couve, 1986) and undergo deposition of secondary dentin, which increases the hardness of dentin and constriction of the pulp chamber space (**Figure 1B**; Xu et al., 2014; Carvalho and Lussi, 2017). However, with advancing age, odontoblast densities in human teeth decrease (Daud et al., 2016); moreover, the cell shape of odontoblasts changes from columnar in young individuals to cuboidal in older individuals (**Figure 1A**; Burke and Samarawickrama, 1995). Aged odontoblasts exhibit greater accumulation of lipofuscin, which is a waste product in lysosomes of older individuals that reduces the thickness of the odontoblastic layer (**Figure 1B**) and impedes autophagic and dentinogenic activities (Couve and Schmachtenberg, 2011; Couve et al., 2013). Therefore, regulation of odontoblast senescence may allow maintenance of dentin construction in a manner similar to that of young dentin.

SENESCENCE OF CEMENTUM

Cementum is a calcified tissue that comprises approximately 65% minerals, 23% organic materials, and 12% water, which surrounds root dentin and plays a pivotal role in connecting a tooth to its corresponding bone socket via penetration of periodontal fibers (**Figure 1A**). Thus, cementum is located subgingivally. Cementum is formed by cementoblasts, which differentiate from ectomesenchymal cells; its properties are similar to those of bone (Lehnen et al., 2012). This tissue includes two types: acellular and cellular. The acellular type is present in the coronal and middle portions of the root, while the cellular type is present around the apical portion and encloses cementocytes, such as osteocytes in bone matrix (Ayasaka et al., 1992). However, the features of these cells have not yet been fully elucidated (Zhao et al., 2016).

The characteristic of aging cementum is a continuous increase in thickness, primarily around the root apex (Zander and Hurzeler, 1958; **Figure 1B**). Additionally, in older individuals, gingival recession significantly increases, as compared with that of young individuals (Hartmann and Muller, 2004); moreover, cementum exposure is evident in older individuals (Barker, 1975). Because the exposed cementum is compromised and has a low resistance to an acidic environment (Shellis, 2010), root caries incidence increases with age (Griffin et al., 2004). Thus, the prevention of gingival recession is essential for tooth maintenance. Thus far, no reports have examined the molecular mechanisms of aging cementum; thus, there is no known mechanism to regulate the thickening of cementum with age.

SENESCENCE OF DENTAL PULP

Dental pulp is the soft connective tissue that includes odontoblasts, fibroblasts, mesenchymal stem cells, nerve fibers, and vessels. This tissue is derived from dental papilla, an ectomesenchymal cell condensation in the developing tooth (**Figure 1A**). The dental papilla cells underlying the enamel epithelium can differentiate into odontoblasts; this process is controlled by epithelial–mesenchymal interactions (Thesleff et al., 2001). Under such epithelial–mesenchymal interactions and the effects of various growth factors (e.g., bone morphogenetic proteins, fibroblast growth factors, and WNT), tooth development proceeds with this tissue (Thesleff, 2003).

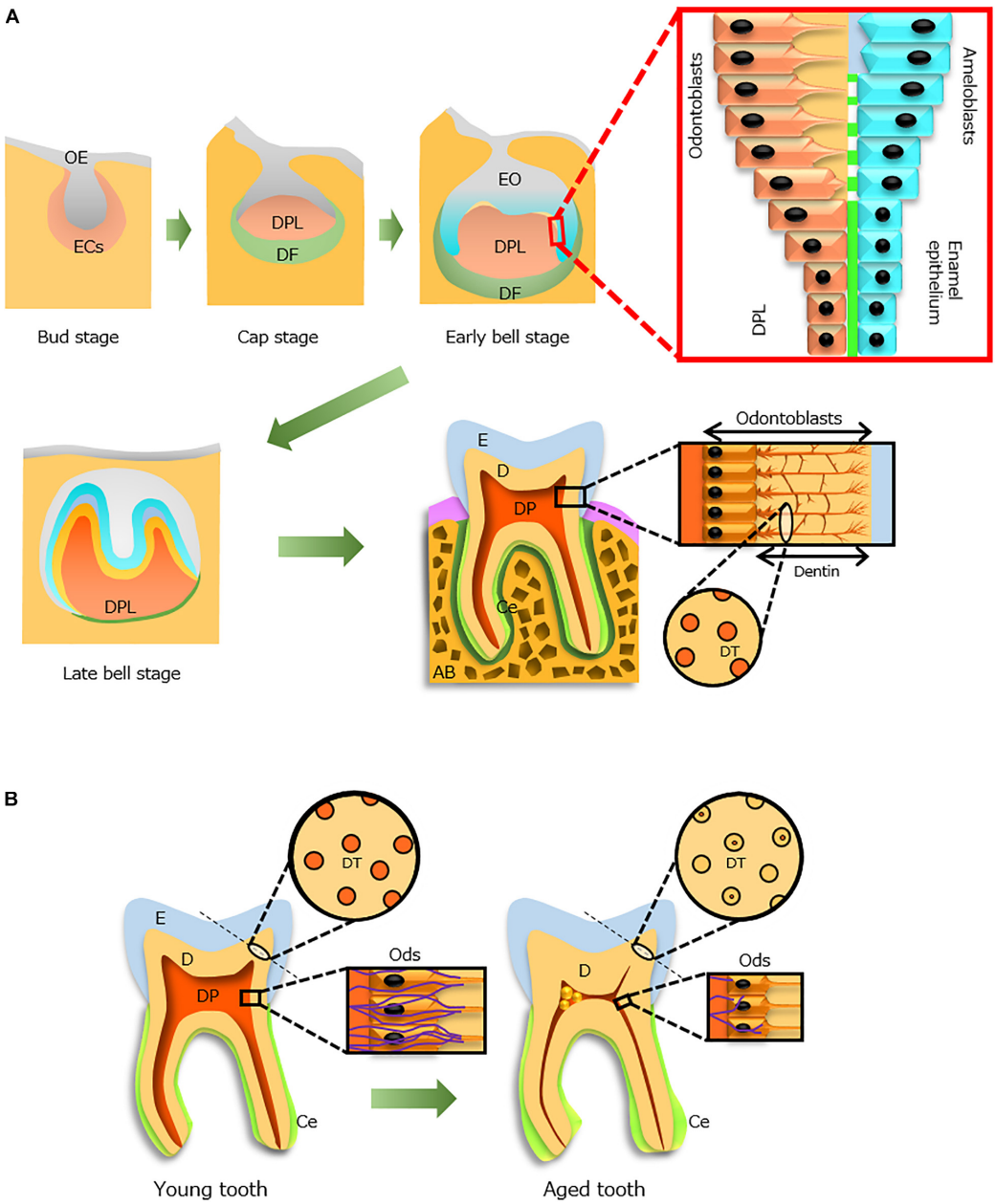

FIGURE 1 | Tooth development during the aging process. **(A)** Tooth development from the bud stage to eruption. Odontoblasts (Ods, orange) and ameloblasts (blue) form dentin (D) and enamel (E), respectively, through epithelial–mesenchymal interactions. An erupted tooth consists of three hard tissues [E, D, and cementum (Ce)] and a soft tissue [dental pulp (DP)]. The processes of Ods extend into the D where dentinal tubules (DTs, circle) are formed. **(B)** Aging alterations of the tooth structure. Constriction of the DP cavity (red), occlusion of DTs in increased D, thickening of the Ce (light green), size reduction of Ods (rectangle), and decreased distribution of nerve fibers (violet, rectangle) with advancing age. AB, alveolar bone; DF, dental follicle; DPL, dental papilla; ECs, ectomesenchymal cells; EO, enamel organ; OE, oral epithelium. Light and dark green indicate Ce and periodontal ligament, respectively.

The structural relationship between dentin and dental pulp is known as the "dentin–pulp complex." As mentioned above, the pulp volume decreases with age because of secondary dentin deposition throughout life (Murray et al., 2002). This continuous deposition of dentin and dystrophic calcification in pulpal arteries interrupts blood circulation in the dental pulp of older individuals (Bernick, 1967a). When comparing the cell density of pulp in 70-year-old individuals with that in 20-year-old individuals, the cell number in older individuals was nearly half that of the younger individuals (Nanci, 2018), indicating a reduction in pulp restoration activity (Murray et al., 2002). Additionally, Hillmann and Geurtsen (1997) reported that the collagen fiber bundle aggregation and calcification in dental pulp increased with advancing age. Dystrophic calcification in the

central pulp of the coronal region and root canal is evident in older individuals, which might be due to their reduced pulpal blood flow (Ersahan and Sabuncuoglu, 2018; Iezzi et al., 2019). Notably, Li et al. (2011) reported that human dental pulp cells (HDPCs) cultured under hypoxic conditions exhibited increased mineralization. Furthermore, a previous study examined the morphological alteration of the dentinal pulp wall during the aging process (Tsurumachi et al., 2008); the shape and modality of calcospherites on the pulp wall became diverse during aging. Such deposition may contribute to the growth of secondary dentin.

Tertiary dentin also deposits on secondary dentin under pathological stimuli such as dentin caries, tooth cutting, and trauma. This dentin includes two types, reactionary and reparative, which differ depending on the degree of stimuli (Smith et al., 1995). These dentinogenic activities are also reduced in older individuals (Murray et al., 2002).

With age, difficulties in endodontic treatment occur due to the constriction of pulp chamber space by hyperplasia of secondary and tertiary dentin, as well as pulp stones (i.e., ectopic calcified particles in the coronal region) and diffuse calcification in radicular pulp (Krasner and Rankow, 2004). A recent study reported the efficiency of cone-beam computed tomography in endodontic diagnosis and treatment planning (Sue et al., 2018), demonstrating its usefulness in current treatment. Additionally, guided endodontic access using cone-beam computed tomography in patients with calcified root canals has been described (Lara-Mendes et al., 2018).

Nerve fibers are widely distributed in dental pulp. In the growing dental papilla of human fetal teeth, expression of nerve growth factor and its low and high affinity receptors (p75NTR and TrkA, respectively) precede the initiation of tooth innervation (Mitsiadis and Pagella, 2016). In particular, p75NTR is thought to condense mesenchymal cells from neural crest cells during the construction of dental papilla. Therefore, these molecules are presumably involved in both tooth development and nerve growth in dental pulp. However, the distribution of nerve fibers in dental pulp decreases, probably because of degeneration with increasing age (Bernick, 1967b; **Figure 1B**). Notably, Couve and Schmachtenberg (2018) characterized two types of Schwann cells that reside in dental pulp: non-myelinating and myelinating. They also found a reduction in the network of these cells at the dentin–pulp interface, along with decreased innervation in old dental pulp; these findings suggested the progression of less symptomatic caries in older individuals because of a reduced response to environmental injuries and pathogens (Couve et al., 2018). Thus, during aging, the pulp cavity constricts and dental pulp cells subsequently reduce their functions and activities (**Figure 1B**).

SENESCENCE OF DENTAL PULP CELLS AND DENTAL PULP STEM CELLS

Cellular senescence, characterized by irreversible arrest of cell proliferation, is evoked by various intrinsic and extrinsic stressors such as DNA damage, oxidative stress, telomere damage, oncogene activation and/or inactivation, and spindle stress (Herbig et al., 2006; van Deursen, 2014). Currently, senescence is viewed as a multistep process comprising biological activity and evolution. The roles of senescent cells in aging have been discussed widely. Briefly, there are two categories of senescence: acute and chronic (van Deursen, 2014). Acute senescence is induced by acute and specific stress, targets specific cells, and is a scheduled process; this type of senescence is involved in normal biological processes (e.g., tissue repair, development, and wound healing). Chronic senescence is promoted by gradual increases in stress and damage, which have detrimental effects on nearby cells; moreover, it does not target specific cells and is an unscheduled process (Dodig et al., 2019). This pathway is considerably different from acute senescence due to the heterogeneity of senescence-associated secretory phenotype (SASP) factors that include cytokines, chemokines, proteases, growth factors, and matrix metalloproteases (Byun et al., 2015).

During the senescence process, senescent cells secrete SASP factors (Coppe et al., 2008) that affect adjacent cells in autocrine or paracrine manners (Acosta et al., 2013; Borodkina et al., 2018). SASP factors play pivotal roles in the above two senescent modalities; these factors have beneficial or detrimental effects on cellular senescence, such as regeneration, degeneration, immune clearance, or growth stimulation (Watanabe et al., 2017). Acute senescent cells are removed by immune cells following stimulation by activated SASP factors; various SASP factors induce chronic inflammation (Dodig et al., 2019), which results in age-associated disorders and tumorigenesis. Although the main roles of SASP factors are to preclude senescent cells by immune clearance, the effectiveness of this process is influenced by age-associated changes that hinder the immune system (Denkinger et al., 2015).

In this context, to prevent cellular senescence, two possible therapies of anti-senescence have been proposed: suppression of SASP factors or selective elimination of senescent cells (Watanabe et al., 2017; de Magalhaes and Passos, 2018). Although these are regarded as promising strategies, there is a need to carefully consider whether targeting SASP factors is a suitable method because these factors have both favorable and unfavorable characteristics.

Senescence of Dental Pulp Stem Cells

Dental pulp stem cells (Gronthos et al., 2000) have attracted considerable attention as promising cells for regenerative endodontics (Murray et al., 2007) and systemic regenerative medicine (Anitua et al., 2018; Yoshida et al., 2020). This attention has arisen because DPSCs exhibit characteristics of mesenchymal stem cells that can differentiate into various cell types such as odontoblastic cells, dental pulp cells, neuronal cells, vascular endothelial cells, retinal cells, islet cells, hepatocytes, smooth muscle cells, osteoblastic cells, adipocytes, and chondrocytes (Anitua et al., 2018; Yoshida et al., 2020). Additionally, during acquisition of DPSCs from patients, invasive stress is very low

relative to stem cell isolation from other organs and tissues. Thus, cell banking has been implemented for on-demand transplantation because human DPSCs (HDPSCs) reside in dental pulp of young individuals at proportions of 0.67–1.02% (Honda et al., 2007). A recent study found the expression of CD24a in multipotent stem cells derived from human dental papilla in a developing tooth germ, which developed into dental pulp and then differentiated into odontoblasts in the mature tooth (Chen et al., 2020). The number of CD24a(+) cells in dental pulp remains unclear, but this discovery might enable efficient isolation and expansion of a pure stem cell population.

These stem cells also undergo aging. The proliferation and differentiation capacities of HDPSCs are impaired in older individuals (Yi et al., 2017). However, HDPSCs show reduced cellular senescence, as well as enhanced osteogenesis and proliferation activities, compared with bone marrow mesenchymal stem cells, periodontal ligament stem cells, and adipose-derived stem cells (Ma et al., 2019).

Various studies have examined the mechanisms of changes in HDPSCs during aging (**Figure 2A**). One study reported that senescent HDPSCs have decreased BMI-1 expression but increased $p16^{INK4A}$ expression; overexpression of BMI-1 in senescent HDPSCs rescued senescence-impaired odontogenic differentiation (Mehrazarin et al., 2011). Feng et al. (2014) reported that the activation of $p16^{INK4A}$ signaling stimulated onset of senescence in HDPSCs. Another report demonstrated that $p16^{INK4A}$ and BMI-1 are involved in the senescence of HDPSCs induced by oxidative stress (Mas-Bargues et al., 2017). However, Gu et al. (2016) showed that Sirtuin 7 is downregulated in senescent HDPSCs through identification of Sirtuin 7 as a target of miR-152, an inducer of senescence in HDPSCs. Another recent notable study showed that HDPSCs from older individuals have decreased expression of the family with sequence similarity 96 member B homeobox (FAM96B) gene; overexpression of FAM96B improved their proliferation and differentiation abilities, whereas it downregulated senescence markers such as senescence-associated-β-galactosidase (SA-β-gal), p16, and p53 (Liang et al., 2020).

Human DPSCs undergoing replicative senescence exhibit increased numbers of autophagic vacuoles (Li et al., 2012; **Figure 2A**). This suggests reduced lysosomal activity due to the accumulation of autophagic vacuoles (Rezzani et al., 2012), which indicates lipofuscin accumulation in lysosomes (Couve et al., 2013). When lysosomal activity decreases in senescent cells, the proton concentration decreases (Colacurcio and Nixon, 2016). Therefore, the optimal pH of lysosomal β-galactosidase is 4, whereas that of SA-β-gal in lysosomes (a biomarker of cell senescence) is 6 (Dimri et al., 1995). Hence, a pH probe is under investigation as a candidate anti-senescence therapy for mesenchymal stem cells (Wang et al., 2018). In this context, Morsczeck (2019) has attempted to clarify the mechanism involved in regulating DPSC senescence, which is important for optimizing related therapeutic applications in regenerative medicine.

Although the above findings may provide methods to prevent tooth aging and promote pulp regeneration, further analyses are needed to integrate these data.

Senescence of Dental Pulp Cells

All cells in dental pulp are generically regarded as dental pulp cells, but they mainly comprise fibroblastic cells. Biological and molecular alterations of HDPCs with age have been reported (**Figure 2B**). With advancing age, HDPCs show reductions in proliferation and alkaline phosphatase activity, thereby indicating impaired restoration of injured pulp tissue (Shiba et al., 2003). Sclerostin produced by osteocytes suppresses osteogenesis (Moester et al., 2010), but its inhibition induces bone formation (Zhang et al., 2020). Sclerostin also inhibits odontoblastic features of HDPCs (Liao et al., 2019), whereas deficiency of sclerostin facilitates reparative dentin formation *in vivo* (**Figure 2B**; Collignon et al., 2017). Notably, Ou et al. (2018) reported that HDPCs from older individuals have increased sclerostin production, while overexpression of sclerostin in young HDPCs induces senescent features (**Figure 2B**).

Additionally, it was recently elucidated that visfatin, a type of adipokine, increases in senescent HDPCs; exogenous visfatin induces HDPC aging along with upregulation of SASP factors, whereas the chemical inhibitor of visfatin, FK866, reduces senescent features in HDPCs (**Figure 2B**; Ok et al., 2020). Another group reported that miR-433, which is increased in aged HDPCs, is a senescence-associated miRNA of HDPCs that targets GRB2 (**Figure 2B**; Wang et al., 2015). Importantly, GRB2 undergoes tyrosine phosphorylation during T-cell aging (Ghosh and Miller, 1995; Chang et al., 2019).

Yi et al. (2017) examined the involvement of peroxisome proliferator-activated receptor gamma (PPARγ) and its downstream effector heme oxygenase 1 in aging HDPCs (**Figure 2B**; Lee et al., 2013b). PPARγ functions in the survival and differentiation of HDPCs and protects against oxidative stress through heme oxygenase 1 (Lee et al., 2013a). Lee et al. (2015) reported that senescent HDPCs showed reductions in these molecules, while increased SA-β-gal activity and decreased PPARγ influenced autophagic activity and cellular homeostasis in senescent HDPCs. The regulation of these two molecules might be important in tooth conservation in older individuals.

In this context, we focused on tumor necrosis factor-alpha (TNF-α), a known SASP factor (**Figure 2C**). In our recent study, we compared odontoblastic differentiation of HDPCs at low replicative senescence [population doubling (PD) 6] with HDPCs at high replicative senescence (PD28); HDPCs at PD28 expressed senescence makers such as p16, p21, p53, and SA-β-gal (Nozu et al., 2018). Similar to other reports, senescent HDPCs showed reduced differentiation activity. However, treatment of senescent HDPCs with TNF-α resulted in higher odontoblastic differentiation activities and mineralization per cell, compared with HDPCs at PD6. These results were related to higher expression levels of TNF receptor 1 (TNFR1) in senescent HDPCs, compared with those levels in younger HDPCs (Nozu et al., 2018). Importantly, senescent HDPCs treated with TNF-α and calcium demonstrated increased odontoblastic features, whereas young HDPCs showed reduction of such features (**Figure 2C**; Nozu et al., 2018). This was consistent with a recent study in which HDPCs exhibited enhancement of mineralization potential with increasing passage (Bakopoulou et al., 2017). In older individuals, ectopic calcification is often observed in dental

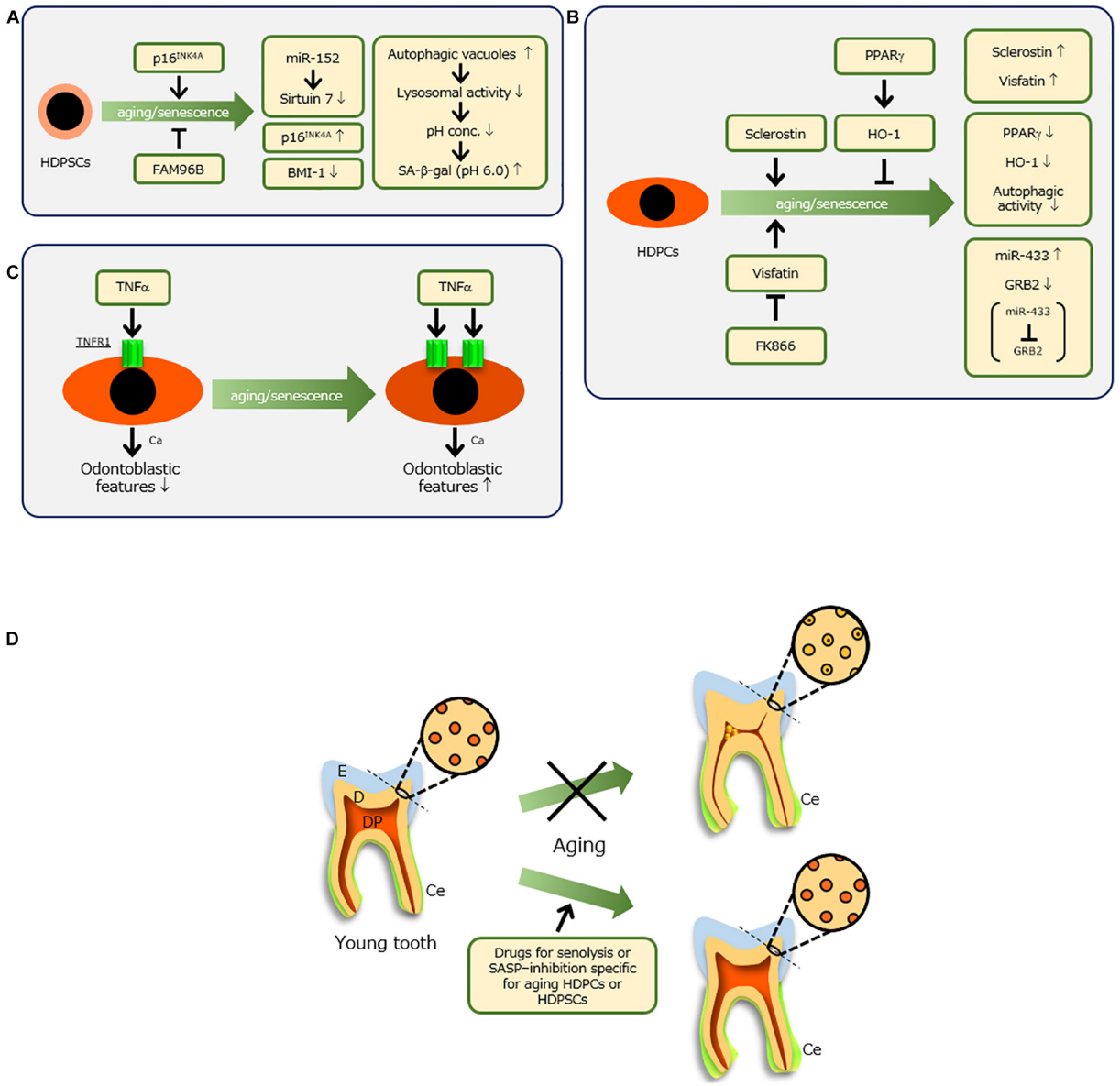

FIGURE 2 | Molecules involved in senescence of human dental pulp stem cells (HDPSCs) **(A)** and human dental pulp cells (HDPCs) **(B)** and their molecular features. **(C)** When senescent HDPCs with increased expression of TNF receptor 1 (TNFR1) were treated with tumor necrosis factor-alpha (TNF-α) and calcium (Ca), their odontoblastic features were enhanced, whereas young HDPCs showed reductions of these features. **(D)** Ideal therapy to preserve a tooth with advancing age. When dental pulp (DP) and dentin (D) are maintained [e.g., by drug-related induction of a non-constrictive DP space and non-occluded dentinal tubules for senolysis or senescence-associated secretory phenotype (SASP) inhibition, specifically targeting aging HDPCs or HDPSCs], healthy teeth might be maintained throughout life. Because no report has examined the molecular mechanism of aging cementum (Ce), it is difficult to prevent thickening of Ce, which does not affect tooth fracture. E, enamel.

pulp, characterized by pulp stones that narrow the pulp chamber space, as well as diffuse calcification in radicular pulp (Bernick, 1967a; Nitzan et al., 1986; Iezzi et al., 2019). As teeth are exposed to long-term stress (e.g., mastication, occlusion, or bruxism), these weak and chronic inflammatory conditions might lead to induction of SASP factors in HDPCs, thereby causing age-related alterations. Overall, because HDPCs and HDPSCs regulate dental pulp senescence, local control of senescence progression might conserve teeth.

CONCLUSION

This review provided an overview of the findings over the past two decades regarding the senescence of hard and soft tissues in teeth. However, this issue has a short history in dentistry. In the modern aging society, it is important to explore methods to counteract the senescence of teeth, particularly HDPCs and HDPSCs, to aid in tooth conservation. As mentioned above, the development and application of drugs for

senolysis or SASP inhibition, specifically targeting aging HDPCs or HDPSCs, are an extremely attractive approach. For success with this method, the method by which senescent cells are targeted is a crucial factor. This issue must be resolved to overcome the health problems affecting the modern aging society. Consequently, maintenance of dental pulp and dentin in a manner similar to that of young teeth will protect against tooth loss by averting tooth fracture, thereby preserving dental health (**Figure 2D**).

AUTHOR CONTRIBUTIONS

The author confirms being the sole contributor of this work and has approved it for publication.

FUNDING

This review was financially supported by a Grant-in-Aid for Scientific Research (Project No. JP17H01598) from the Japan Society for the Promotion of Science.

ACKNOWLEDGMENTS

The author thanks Dr. Itoyama for considerable support during the preparation of this review. The author also thanks Mitchell Arico and Ryan Chastain-Gross, Ph.D., from Edanz Group (https://en-author-services.edanzgroup.com/ac) for editing the English text of a draft of this manuscript.

REFERENCES

Acosta, J. C., Banito, A., Wuestefeld, T., Georgilis, A., Janich, P., Morton, J. P., et al. (2013). A complex secretory program orchestrated by the inflammasome controls paracrine senescence. *Nat. Cell Biol.* 15, 978–990. doi: 10.1038/ncb2784

Anitua, E., Troya, M., and Zalduendo, M. (2018). Progress in the use of dental pulp stem cells in regenerative medicine. *Cytotherapy* 20, 479–498. doi: 10.1016/j.jcyt.2017.12.011

Axelsson, P., Nystrom, B., and Lindhe, J. (2004). The long-term effect of a plaque control program on tooth mortality, caries and periodontal disease in adults. results after 30 years of maintenance. *J. Clin. Periodontol.* 31, 749–757. doi: 10.1111/j.1600-051X.2004.00563.x

Ayasaka, N., Kondo, T., Goto, T., Kido, M. A., Nagata, E., and Tanaka, T. (1992). Differences in the transport systems between cementocytes and osteocytes in rats using microperoxidase as a tracer. *Arch. Oral. Biol.* 37, 363–369. doi: 10.1016/0003-9969(92)90019-5

Azaz, B., Michaeli, Y., and Nitzan, D. (1977). Aging of tissues of the roots of nonfunctional human teeth (impacted canines). *Oral. Surg. Oral. Med. Oral. Pathol.* 43, 572–578. doi: 10.1016/0030-4220(77)90110-4

Bakopoulou, A., Apatzidou, D., Aggelidou, E., Gousopoulou, E., Leyhausen, G., Volk, J., et al. (2017). Isolation and prolonged expansion of oral mesenchymal stem cells under clinical-grade, GMP-compliant conditions differentially affects "stemness" properties. *Stem Cell Res. Ther.* 8:247. doi: 10.1186/s13287-017-0705-0

Barker, B. C. (1975). Relation of the alveolus to the cemento-enamel junction following attritional wear in aboriginal skulls. an enquiry into normality of cementum exposure with aging. *J. Periodontol.* 46, 357–363. doi: 10.1902/jop.1975.46.6.357

Bartlett, D., and O'Toole, S. (2019). Tooth wear and aging. *Aust. Dent. J.* 64(Suppl. 1), S59–S62. doi: 10.1111/adj.12681

Bernick, S. (1967a). Age changes in the blood supply to human teeth. *J. Dent. Res.* 46, 544–550. doi: 10.1177/00220345670460031501

Bernick, S. (1967b). Effect of aging on the nerve supply to human teeth. *J. Dent. Res.* 46, 694–699. doi: 10.1177/00220345670460041101

Bertacci, A., Chersoni, S., Davidson, C. L., and Prati, C. (2007). In vivo enamel fluid movement. *Eur. J. Oral. Sci.* 115, 169–173. doi: 10.1111/j.1600-0722.2007.00445.x

Borodkina, A. V., Deryabin, P. I., Giukova, A. A., and Nikolsky, N. N. (2018). "Social Life" of senescent cells: what is sasp and why study it? *Acta Nat.* 10, 4–14.

Burke, F. M., and Samarawickrama, D. Y. (1995). Progressive changes in the pulpo-dentinal complex and their clinical consequences. *Gerodontology* 12, 57–66. doi: 10.1111/j.1741-2358.1995.tb00132.x

Byun, H. O., Lee, Y. K., Kim, J. M., and Yoon, G. (2015). From cell senescence to age-related diseases: differential mechanisms of action of senescence-associated secretory phenotypes. *BMB Rep.* 48, 549–558. doi: 10.5483/bmbrep.2015.48.10.122

Carvalho, T. S., and Lussi, A. (2017). Age-related morphological, histological and functional changes in teeth. *J. Oral. Rehabil.* 44, 291–298. doi: 10.1111/joor.12474

Chang, P. M., Li, K. L., and Lin, Y. C. (2019). Fucoidan(-)Fucoxanthin ameliorated cardiac function via IRS1/GRB2/ SOS1, GSK3beta/CREB pathways and metabolic pathways in senescent mice. *Mar. Drugs* 17:69. doi: 10.3390/md17010069

Chen, H., Fu, H., Wu, X., Duan, Y., Zhang, S., Hu, H., et al. (2020). Regeneration of pulpo-dentinal-like complex by a group of unique multipotent CD24a(+) stem cells. *Sci. Adv.* 6:eaay1514. doi: 10.1126/sciadv.aay1514

Colacurcio, D. J., and Nixon, R. A. (2016). Disorders of lysosomal acidification-the emerging role of v-ATPase in aging and neurodegenerative disease. *Age. Res. Rev.* 32, 75–88. doi: 10.1016/j.arr.2016.05.004

Collignon, A. M., Amri, N., Lesieur, J., Sadoine, J., Ribes, S., Menashi, S., et al. (2017). Sclerostin deficiency promotes reparative dentinogenesis. *J. Dent. Res.* 96, 815–821. doi: 10.1177/0022034517698104

Coppe, J. P., Patil, C. K., Rodier, F., Sun, Y., Munoz, D. P., Goldstein, J., et al. (2008). Senescence-associated secretory phenotypes reveal cell-nonautonomous functions of oncogenic RAS and the p53 tumor suppressor. *PLoS Biol.* 6:2853–2868. doi: 10.1371/journal.pbio.0060301

Couve, E. (1986). Ultrastructural changes during the life cycle of human odontoblasts. *Arch. Oral. Biol.* 31, 643–651. doi: 10.1016/0003-9969(86)90093-2

Couve, E., Lovera, M., Suzuki, K., and Schmachtenberg, O. (2018). Schwann cell phenotype changes in aging human dental pulp. *J. Dent. Res.* 97, 347–355. doi: 10.1177/0022034517733967

Couve, E., Osorio, R., and Schmachtenberg, O. (2013). The amazing odontoblast: activity, autophagy, and aging. *J. Dent. Res.* 92, 765–772. doi: 10.1177/0022034513495874

Couve, E., and Schmachtenberg, O. (2011). Autophagic activity and aging in human odontoblasts. *J. Dent. Res.* 90, 523–528. doi: 10.1177/0022034510393347

Couve, E., and Schmachtenberg, O. (2018). Schwann cell responses and plasticity in different dental pulp scenarios. *Front. Cell Neurosci.* 12:299. doi: 10.3389/fncel.2018.00299

Daud, S., Nambiar, P., Hossain, M. Z., Rahman, M. R., and Bakri, M. M. (2016). Changes in cell density and morphology of selected cells of the ageing human dental pulp. *Gerodontology* 33, 315–321. doi: 10.1111/ger.12154

de Magalhaes, J. P., and Passos, J. F. (2018). Stress, cell senescence and organismal ageing. *Mech. Ageing Dev.* 170, 2–9. doi: 10.1016/j.mad.2017.07.001

Denkinger, M. D., Leins, H., Schirmbeck, R., Florian, M. C., and Geiger, H. (2015). HSC aging and senescent immune remodeling. *Trends Immunol.* 36, 815–824. doi: 10.1016/j.it.2015.10.008

Dimri, G. P., Lee, X., Basile, G., Acosta, M., Scott, G., Roskelley, C., et al. (1995). A biomarker that identifies senescent human cells in culture and in aging skin in vivo. *Proc. Natl. Acad. Sci. U S A.* 92, 9363–9367. doi: 10.1073/pnas.92.20.9363

Dodig, S., Cepelak, I., and Pavic, I. (2019). Hallmarks of senescence and aging. *Biochem. Med. (Zagreb)* 29:030501. doi: 10.11613/BM.2019.030501

Ersahan, S., and Sabuncuoglu, F. A. (2018). Effect of age on pulpal blood flow in human teeth during orthodontic movement. *J. Oral. Sci.* 60, 446–452. doi: 10.2334/josnusd.17-0316

Feng, X., Xing, J., Feng, G., Huang, D., Lu, X., Liu, S., et al. (2014). p16(INK4A) mediates age-related changes in mesenchymal stem cells derived from human dental pulp through the DNA damage and stress response. *Mech. Ageing Dev.* 14, 46–55. doi: 10.1016/j.mad.2014.09.004

Ghosh, J., and Miller, R. A. (1995). Rapid tyrosine phosphorylation of Grb2 and Shc in T cells exposed to anti-CD3, anti-CD4, and anti-CD45 stimuli: differential effects of aging. *Mech. Ageing Dev.* 80, 171–187. doi: 10.1016/0047-6374(94)01568-7

Gil-Montoya, J. A., de Mello, A. L., Barrios, R., Gonzalez-Moles, M. A., and Bravo, M. (2015). Oral health in the elderly patient and its impact on general well-being: a nonsystematic review. *Clin. Interv. Aging* 10, 461–467. doi: 10.2147/CIA.S54630

Griffin, S. O., Griffin, P. M., Swann, J. L., and Zlobin, N. (2004). Estimating rates of new root caries in older adults. *J. Dent. Res.* 83, 634–638. doi: 10.1177/154405910408300810

Gronthos, S., Mankani, M., Brahim, J., Robey, P. G., and Shi, S. (2000). Postnatal human dental pulp stem cells (DPSCs) in vitro and in vivo. *Proc. Natl. Acad. Sci. U S A.* 97, 13625–13630. doi: 10.1073/pnas.240309797

Gu, S., Ran, S., Liu, B., and Liang, J. (2016). miR-152 induces human dental pulp stem cell senescence by inhibiting SIRT7 expression. *FEBS Lett.* 590, 1123–1131. doi: 10.1002/1873-3468.12138

Hartmann, R., and Muller, F. (2004). Clinical studies on the appearance of natural anterior teeth in young and old adults. *Gerodontology* 21, 10–16. doi: 10.1111/j.1741-2358.2004.00009.x

Herbig, U., Ferreira, M., Condel, L., Carey, D., and Sedivy, J. M. (2006). Cellular senescence in aging primates. *Science* 311:1257. doi: 10.1126/science.1122446

Hillmann, G., and Geurtsen, W. (1997). Light-microscopical investigation of the distribution of extracellular matrix molecules and calcifications in human dental pulps of various ages. *Cell Tissue Res.* 289, 145–154. doi: 10.1007/s004410050860

Honda, M. J., Nakashima, F., Satomura, K., Shinohara, Y., Tsuchiya, S., Watanabe, N., et al. (2007). Side population cells expressing ABCG2 in human adult dental pulp tissue. *Int. Endod. J.* 40, 949–958. doi: 10.1111/j.1365-2591.2007.01301.x

Iezzi, I., Pagella, P., Mattioli-Belmonte, M., and Mitsiadis, T. A. (2019). The effects of ageing on dental pulp stem cells, the tooth longevity elixir. *Eur. Cell Mater.* 37, 175–185. doi: 10.22203/eCM.v037a11

Iwasaki, M., Yoshihara, A., Ogawa, H., Sato, M., Muramatsu, K., Watanabe, R., et al. (2016). Longitudinal association of dentition status with dietary intake in Japanese adults aged 75 to 80 years. *J. Oral. Rehabil.* 43, 737–744. doi: 10.1111/joor.12427

Kotsanos, N., and Darling, A. I. (1991). Influence of posteruptive age of enamel on its susceptibility to artificial caries. *Caries Res.* 25, 241–250. doi: 10.1159/000261371

Krasner, P., and Rankow, H. J. (2004). Anatomy of the pulp-chamber floor. *J. Endod.* 30, 5–16. doi: 10.1097/00004770-200401000-00002

Kunin, A. A., Evdokimova, A. Y., and Moiseeva, N. S. (2015). Age-related differences of tooth enamel morphochemistry in health and dental caries. *EPMA J.* 6:3. doi: 10.1186/s13167-014-0025-8

Lara-Mendes, S. T. O., Barbosa, C. F. M., Santa-Rosa, C. C., and Machado, V. C. (2018). Guided endodontic access in maxillary molars using cone-beam computed tomography and computer-aided design/computer-aided manufacturing system: a case report. *J. Endod.* 44, 875–879. doi: 10.1016/j.joen.2018.02.009

Lee, Y. H., Kang, Y. M., Heo, M. J., Kim, G. E., Bhattarai, G., Lee, N. H., et al. (2013a). The survival role of peroxisome proliferator-activated receptor gamma induces odontoblast differentiation against oxidative stress in human dental pulp cells. *J. Endod.* 39, 236–241. doi: 10.1016/j.joen.2012.11.006

Lee, Y. H., Kim, G. E., Cho, H. J., Yu, M. K., Bhattarai, G., Lee, N. H., et al. (2013b). Aging of in vitro pulp illustrates change of inflammation and dentinogenesis. *J. Endod.* 39, 340–345. doi: 10.1016/j.joen.2012.10.031

Lee, Y. H., Lee, H. Y., Kim, T. G., Lee, N. H., Yu, M. K., and Yi, H. K. (2015). PPARgamma maintains homeostasis through autophagy regulation in dental pulp. *J. Dent. Res.* 94, 729–737. doi: 10.1177/0022034515573833

Lehnen, S. D., Gotz, W., Baxmann, M., and Jager, A. (2012). Immunohistochemical evidence for sclerostin during cementogenesis in mice. *Ann. Anat.* 194, 415–421. doi: 10.1016/j.aanat.2012.02.014

Li, L., Zhu, Y. Q., Jiang, L., and Peng, W. (2012). Increased autophagic activity in senescent human dental pulp cells. *Int. Endod. J.* 45, 1074–1079. doi: 10.1111/j.1365-2591.2012.02064.x

Li, L., Zhu, Y. Q., Jiang, L., Peng, W., and Ritchie, H. H. (2011). Hypoxia promotes mineralization of human dental pulp cells. *J. Endod.* 37, 799–802. doi: 10.1016/j.joen.2011.02.028

Liang, H., Li, W., Yang, H., Cao, Y., Ge, L., Shi, R., et al. (2020). FAM96B inhibits the senescence of dental pulp stem cells. *Cell Biol. Int.* 44, 1193–1203. doi: 10.1002/cbin.11319

Liao, C., Ou, Y., Wu, Y., Zhou, Y., Liang, S., and Wang, Y. (2019). Sclerostin inhibits odontogenic differentiation of human pulp-derived odontoblast-like cells under mechanical stress. *J. Cell Physiol.* 234, 20779–20789. doi: 10.1002/jcp.28684

Ma, L., Hu, J., Cao, Y., Xie, Y., Wang, H., Fan, Z., et al. (2019). Maintained properties of aged dental pulp stem cells for superior periodontal tissue regeneration. *Aging Dis.* 10, 793–806. doi: 10.14336/AD.2018.0729

Mas-Bargues, C., Vina-Almunia, J., Ingles, M., Sanz-Ros, J., Gambini, J., Ibanez-Cabellos, J. S., et al. (2017). Role of p16(INK4a) and BMI-1 in oxidative stress-induced premature senescence in human dental pulp stem cells. *Redox Biol.* 12, 690–698. doi: 10.1016/j.redox.2017.04.002

Mehrazarin, S., Oh, J. E., Chung, C. L., Chen, W., Kim, R. H., Shi, S., et al. (2011). Impaired odontogenic differentiation of senescent dental mesenchymal stem cells is associated with loss of Bmi-1 expression. *J. Endod.* 37, 662–666. doi: 10.1016/j.joen.2011.02.009

Mitsiadis, T. A., and Pagella, P. (2016). Expression of Nerve Growth Factor (NGF), TrkA, and p75(NTR) in developing human fetal teeth. *Front. Physiol.* 7:338. doi: 10.3389/fphys.2016.00338

Moester, M. J., Papapoulos, S. E., Lowik, C. W., and van Bezooijen, R. L. (2010). Sclerostin: current knowledge and future perspectives. *Calcif. Tissue Int.* 87, 99–107. doi: 10.1007/s00223-010-9372-1

Morsczeck, C. (2019). Cellular senescence in dental pulp stem cells. *Arch. Oral. Biol.* 99, 150–155. doi: 10.1016/j.archoralbio.2019.01.012

Murray, P. E., Garcia-Godoy, F., and Hargreaves, K. M. (2007). Regenerative endodontics: a review of current status and a call for action. *J. Endod.* 33, 377–390. doi: 10.1016/j.joen.2006.09.013

Murray, P. E., Stanley, H. R., Matthews, J. B., Sloan, A. J., and Smith, A. J. (2002). Age-related odontometric changes of human teeth. *Oral. Surg. Oral. Med. Oral. Pathol. Oral. Radiol. Endod.* 93, 474–482. doi: 10.1067/moe.2002.120974

Nanci, A. (2018). *Ten Cate's Oral Histology*, 9th Edn. St. Louis, MO: Elsevier.

Nitzan, D. W., Michaeli, Y., Weinreb, M., and Azaz, B. (1986). The effect of aging on tooth morphology: a study on impacted teeth. *Oral. Surg. Oral. Med. Oral. Pathol.* 61, 54–60. doi: 10.1016/0030-4220(86)90203-3

Nozu, A., Hamano, S., Tomokiyo, A., Hasegawa, D., Sugii, H., Yoshida, S., et al. (2018). Senescence and odontoblastic differentiation of dental pulp cells. *J. Cell Physiol.* 234, 849–859. doi: 10.1002/jcp.26905

Ok, C. Y., Park, S., Jang, H. O., Takata, T., Bae, M. K., Kim, Y. D., et al. (2020). Visfatin induces senescence of human dental pulp cells. *Cells* 9:193. doi: 10.3390/cells9010193

Ou, Y., Zhou, Y., Liang, S., and Wang, Y. (2018). Sclerostin promotes human dental pulp cells senescence. *PeerJ* 6:e5808. doi: 10.7717/peerj.5808

Park, S., Wang, D. H., Zhang, D., Romberg, E., and Arola, D. (2008). Mechanical properties of human enamel as a function of age and location in the tooth. *J. Mater. Sci. Mater. Med.* 19, 2317–2324. doi: 10.1007/s10856-007-3340-y

Rezzani, R., Stacchiotti, A., and Rodella, L. F. (2012). Morphological and biochemical studies on aging and autophagy. *Ageing Res. Rev.* 11, 10–31. doi: 10.1016/j.arr.2011.09.001

Ryou, H., Romberg, E., Pashley, D. H., Tay, F. R., and Arola, D. (2015). Importance of age on the dynamic mechanical behavior of intertubular and peritubular dentin. *J. Mech. Behav. Biomed. Mater.* 42, 229–242. doi: 10.1016/j.jmbbm.2014.11.021

Shellis, R. P. (2010). Formation of caries-like lesions in vitro on the root surfaces of human teeth in solutions simulating plaque fluid. *Caries Res.* 44, 380–389. doi: 10.1159/000318224

Shiba, H., Nakanishi, K., Rashid, F., Mizuno, N., Hino, T., Ogawa, T., et al. (2003). Proliferative ability and alkaline phosphatase activity with in vivo cellular aging

in human pulp cells. *J. Endod.* 29, 9–11. doi: 10.1097/00004770-200301000-00003

Simmer, J. P., Papagerakis, P., Smith, C. E., Fisher, D. C., Rountrey, A. N., Zheng, L., et al. (2010). Regulation of dental enamel shape and hardness. *J. Dent. Res.* 89, 1024–1038. doi: 10.1177/0022034510375829

Smith, A. J., Cassidy, N., Perry, H., Begue-Kirn, C., Ruch, J. V., and Lesot, H. (1995). Reactionary dentinogenesis. *Int. J. Dev. Biol.* 39, 273–280.

Sue, M., Oda, T., Sasaki, Y., and Ogura, I. (2018). Age-related changes in the pulp chamber of maxillary and mandibular molars on cone-beam computed tomography images. *Oral. Radiol.* 34, 219–223. doi: 10.1007/s11282-017-0300-1

Tavares, L. H. S., Ferreira, D. C., Cortes, A. Q., Machado, A. G., Abad, E. D. C., Lourenco, E. J. V., et al. (2018). Factors associated with dental fractures in Brazilian individuals. *J. Investig. Clin. Dent.* 9:e12348. doi: 10.1111/jicd.12348

Thesleff, I. (2003). Epithelial-mesenchymal signalling regulating tooth morphogenesis. *J. Cell Sci.* 116(Pt 9), 1647–1648. doi: 10.1242/jcs.00410

Thesleff, I., Keranen, S., and Jernvall, J. (2001). Enamel knots as signaling centers linking tooth morphogenesis and odontoblast differentiation. *Adv. Dent. Res.* 15, 14–18. doi: 10.1177/08959374010150010401

Tsurumachi, T., Huang, T. J., Zhan, W., Hayashi, M., and Ogiso, B. (2008). Scanning electron microscopic study of dentinal pulpal walls in relation to age and tooth area. *J. Oral. Sci.* 50, 199–203. doi: 10.2334/josnusd.50.199

van Deursen, J. M. (2014). The role of senescent cells in ageing. *Nature* 509, 439–446. doi: 10.1038/nature13193

Wang, K., Li, L., Wu, J., Qiu, Q., Zhou, F., and Wu, H. (2015). The different expression profiles of microRNAs in elderly and young human dental pulp and the role of miR-433 in human dental pulp cells. *Mech. Ageing Dev.* 146–148, 1–11. doi: 10.1016/j.mad.2015.03.001

Wang, L., Han, X., Qu, G., Su, L., Zhao, B., and Miao, J. (2018). A pH probe inhibits senescence in mesenchymal stem cells. *Stem Cell Res. Ther.* 9:343. doi: 10.1186/s13287-018-1081-0

Watanabe, S., Kawamoto, S., Ohtani, N., and Hara, E. (2017). Impact of senescence-associated secretory phenotype and its potential as a therapeutic target for senescence-associated diseases. *Cancer Sci.* 108, 563–569. doi: 10.1111/cas.13184

Xu, H., Zheng, Q., Shao, Y., Song, F., Zhang, L., Wang, Q., et al. (2014). The effects of ageing on the biomechanical properties of root dentine and fracture. *J. Dent.* 42, 305–311. doi: 10.1016/j.jdent.2013.11.025

Yahyazadehfar, M., Zhang, D., and Arola, D. (2016). On the importance of aging to the crack growth resistance of human enamel. *Acta Biomater.* 32, 264–274. doi: 10.1016/j.actbio.2015.12.038

Yan, W., Montoya, C., Oilo, M., Ossa, A., Paranjpe, A., Zhang, H., et al. (2017). Reduction in fracture resistance of the root with aging. *J. Endod.* 43, 1494–1498. doi: 10.1016/j.joen.2017.04.020

Yi, Q., Liu, O., Yan, F., Lin, X., Diao, S., Wang, L., et al. (2017). Analysis of senescence-related differentiation potentials and gene expression profiles in human dental pulp stem cells. *Cells Tissues Organ.* 203, 1–11. doi: 10.1159/000448026

Yoshida, S., Tomokiyo, A., Hasegawa, D., Hamano, S., Sugii, H., and Maeda, H. (2020). Insight into the role of dental pulp stem cells in regenerative therapy. *Biology (Basel)* 9:160. doi: 10.3390/biology9070160

Yoshino, K., Ito, K., Kuroda, M., and Sugihara, N. (2015). Prevalence of vertical root fracture as the reason for tooth extraction in dental clinics. *Clin. Oral. Investig.* 19, 1405–1409. doi: 10.1007/s00784-014-1357-4

Zander, H. A., and Hurzeler, B. (1958). Continuous cementum apposition. *J. Dent. Res.* 37, 1035–1044. doi: 10.1177/00220345580370060301

Zhang, Z. H., Jia, X. Y., Fang, J. Y., Chai, H., Huang, Q., She, C., et al. (2020). Reduction of SOST gene promotes bone formation through the Wnt/beta-catenin signalling pathway and compensates particle-induced osteolysis. *J. Cell Mol. Med.* 24, 4233–4244. doi: 10.1111/jcmm.15084

Zhao, N., Foster, B. L., and Bonewald, L. F. (2016). The cementocyte-an osteocyte relative? *J. Dent. Res.* 95, 734–741. doi: 10.1177/0022034516641898

Zheng, Q., Xu, H., Song, F., Zhang, L., Zhou, X., Shao, Y., et al. (2013). Spatial distribution of the human enamel fracture toughness with aging. *J. Mech. Behav. Biomed. Mater.* 26, 148–154. doi: 10.1016/j.jmbbm.2013.04.025

Conflict of Interest: The author declares that the research was conducted in the absence of any commercial or financial relationships that could be construed as a potential conflict of interest.

frontiers in Cell and Developmental Biology

REVIEW
published: 18 December 2020
doi: 10.3389/fcell.2020.619902

Senescence and Apoptosis During *in vitro* Embryo Development in a Bovine Model

*Priscila Ramos-Ibeas[1], Isabel Gimeno[2], Karina Cañón-Beltrán[1], Alfonso Gutiérrez-Adán[1], Dimitrios Rizos[1] and Enrique Gómez[2]**

[1] Department of Animal Reproduction, National Institute for Agriculture and Food Research and Technology (INIA), Madrid, Spain, [2] Servicio Regional de Investigación y Desarrollo Agroalimentario (SERIDA), Gijón, Spain

According to the World Health Organization, infertility affects up to 14% of couples under reproductive age, leading to an exponential rise in the use of assisted reproduction as a route for conceiving a baby. In the same way, thousands of embryos are produced in cattle and other farm animals annually, leading to increased numbers of individuals born. All reproductive manipulations entail deviations of natural phenotypes and genotypes, with *in vitro* embryo technologies perhaps showing the biggest effects, although these alterations are still emerging. Most of these indications have been provided by animal models, in particular the bovine species, due to its similarities to human early embryo development. Oocytes and embryos are highly sensitive to environmental stress *in vivo* and *in vitro*. Thus, during *in vitro* culture, a number of stressful conditions affect embryonic quality and viability, inducing subfertility and/or long-term consequences that may reach the offspring. A high proportion of the embryos produced *in vitro* are arrested at a species-specific stage of development during the first cell divisions. These arrested embryos do not show signs of programmed cell death during early cleavage stages. Instead, defective *in vitro* produced embryos would enter a permanent cell cycle arrest compatible with cellular senescence, in which they show active metabolism and high reactive oxygen species levels. Later in development, mainly during the morula and blastocyst stages, apoptosis would mediate the elimination of certain cells, accomplishing both a physiological role in to balancing cell proliferation and death, and a pathological role preventing the transmission of damaged cells with an altered genome. The latter would acquire relevant importance in *in vitro* produced embryos that are submitted to stressful environmental stimuli. In this article, we review the mechanisms mediating apoptosis and senescence during early embryo development, with a focus on *in vitro* produced bovine embryos. Additionally, we shed light on the protective role of senescence and apoptosis to ensure that unhealthy cells and early embryos do not progress in development, avoiding long-term detrimental effects.

Keywords: assisted reproductive technologies, programmed cell death, cell cycle arrest, DNA fragmentation, TUNEL, caspase

OPEN ACCESS

Edited by:
Wolfgang Knabe, Universität Münster, Germany

Reviewed by:
Wilfried A. Kues, Institute of Farm Animal Genetics, Friedrich Loeffler Institute (FLI), Germany
Heiner Niemann, Hannover Medical School, Germany

****Correspondence:***
Enrique Gómez
egomez@serida.org

Specialty section:
This article was submitted to Cell Death and Survival, a section of the journal Frontiers in Cell and Developmental Biology

Received: *21 October 2020*
Accepted: *01 December 2020*
Published: *18 December 2020*

Citation:
Ramos-Ibeas P, Gimeno I, Cañón-Beltrán K, Gutiérrez-Adán A, Rizos D and Gómez E (2020) Senescence and Apoptosis During in vitro Embryo Development in a Bovine Model. Front. Cell Dev. Biol. 8:619902. doi: 10.3389/fcell.2020.619902

INTRODUCTION

Human *in vitro* embryo production has been one of the most remarkable medical achievements of the past century, enabling infertile couples, persons with heritable genetic diseases, or oncology patients to conceive a baby. Since then, more than 8 million babies have been born from assisted reproductive technologies (ARTs) around the world, and it is estimated that around 2.4 million ART cycles are performed every year, leading to 500,000 babies born (Eshre, 2018). The first human baby produced by *in vitro* fertilization (IVF) was born 42 years ago (Steptoe and Edwards, 1978), and since then ARTs have been optimized in various mammalian species. Soon after, IVF was introduced as a very complex experimental procedure in cattle (Brackett et al., 1982), the species other than human with better-developed ARTs. Over the years, the procedures have been simplified and improved due to the development of *in vitro* maturation (IVM) of oocytes recovered from slaughterhouse ovaries or a living animal (transvaginal ovum pickup: OPU), followed by IVF and *in vitro* culture (IVC). Nowadays, *in vitro* embryo production in cattle is not only used to overcome infertility (due to anovulation, fertilization failure (Looney et al., 1994; Block et al., 2010; Gomez et al., 2020), or productive and heat stress (Ealy et al., 1993; Block et al., 2010; Stewart et al., 2011), but as a faster means to obtain embryos of high genetic value. Worldwide, while the number of *in vivo* collected embryos that are transferred seems to have stabilized, the transfer of *in vitro*-produced (IVP) embryos continues to grow (742,908 embryos in 2018) (Viana, 2019). Although there are important differences between cattle and humans that need to be considered, such as the techniques employed, with intracytoplasmic sperm injection (ICSI) being used only in humans, and the age and fertility status of the animals/patients, cattle are frequently used as a model to study preimplantation embryo development, as well as infertility issues in humans, since most technologies used share many similarities. In fact, much of the initial human-based ARTs were based on work completed in cattle (Sirard, 2018). *In vitro* studies in cattle with early IVP and *in vivo* developed (IVD) embryos are normally focused on the period into which the blastocyst remains enclosed in the zona pellucida (Rizos et al., 2017). These blastocysts, which are 7–8 days old, bear the best pregnancy and birth rates for embryo transfer (ET) to recipients (Ledgard et al., 2012; Randi et al., 2016). Subsequent processes (i.e., trophectoderm –TE- elongation in concurrence with gastrulation) are maternally driven in ruminants, with no *in vitro* studies being up to now supportive of a functionally representative elongation.

However, despite all efforts performed to optimize ARTs, gametes and embryos are still submitted to stressful conditions *in vitro*. IVF and intracytoplasmic sperm injection (ICSI) bypass natural selection barriers and involve IVC of gametes and embryos, where nutrients are limited and toxic substrates and end-products of metabolism can be present (Calle et al., 2012; Ramos-Ibeas et al., 2019). Embryos show outstanding plasticity during preimplantation development and can often grow under suboptimal conditions. However, severe alterations can also lead to a state of developmental arrest similar to cellular senescence or trigger apoptotic cell death (Betts and King, 2001). In this review, we shed some light on the debated aspects of embryonic senescence and apoptosis as mechanisms to impede damaged cells and compromised embryos to progress in development. Such important restrictions at peri-conception stages would avoid long-term deleterious effects on the offspring (Barker, 2007).

IMPACT OF ASSISTED REPRODUCTION ON EMBRYO DEVELOPMENT: DIFFERENCES BETWEEN *IN VIVO* AND *IN VITRO* PRODUCED EMBRYOS

Despite many improvements made in the field of assisted reproduction, *in vitro* embryo production systems are still not as efficient as *in vivo* development (Rizos et al., 2017). Notwithstanding, it should be emphasized that gametes and embryos are exposed to spatial and temporal unnatural conditions during ART, whose consequences are not completely known (Van Eetvelde et al., 2017). In cattle, approximately 90% of oocytes cultured *in vitro* undergo nuclear and cytoplasmic maturation, from which 80% are fertilized and cleave at least once (Lonergan et al., 2003). Contrary to *in vivo* development, whereby one or less frequently two oocytes are ovulated in the cow, *in vitro* procedures permit maturation of virtually all oocytes in the absence of the inhibitory effects of the dominant follicle (Labrecque et al., 2016; Nagano, 2019). Nonetheless, only between 30 and 40% of such oocytes reach the blastocyst stage (Rizos et al., 2017). While at first appearance this may appear inefficient, it is important to remember that the oocytes used for IVM come from small (2–8 mm) follicles, which would never ovulate *in vivo* and whose fate would be atresia. Moreover, it has been demonstrated that pregnancy rate following transfer of IVP blastocysts in heifers is approximately 40–50% compared to 60–70% for IVD embryos (Hasler et al., 1995; Hoshi, 2003; see review by Hansen, 2020). Therefore, the challenge today is to improve current IVM conditions to obtain more blastocysts and to improve IVC conditions to produce better-quality blastocysts, capable of continuing development and implantation after transfer to recipient and resulting in births of viable and healthy individuals.

Oocyte developmental competence, often defined as the ability of the oocyte to mature, be fertilized, and develop to the blastocyst stage, has been associated with the size of the antral follicle from which it is recovered, the stage of the follicular wave, and the site of maturation—*in vivo* or *in vitro* (Pavlok et al., 1992, see review by Lonergan and Fair, 2016). Oocytes matured *in vivo* are of better quality than those matured *in vitro*, and this is reflected in the rates of embryos produced subsequently. Indeed, irrespective of whether embryo development occurred *in vivo* or *in vitro*, when bovine oocytes were matured *in vivo* from superovulated cows, the resultant blastocyst rate was almost 80%, while when oocytes were matured *in vitro*, it was limited to about 35% (Rizos et al., 2002).

In mammals, the cumulus-oocyte complex (COC) provides metabolites and nutrients, like pyruvate, oxaloacetic acid, and amino acids to the oocytes during their growth, besides stimulating them to resume meiosis and progress to metaphase II (Chen et al., 1990). Several studies demonstrated that gene functions and signaling pathways interact between the oocyte and CCs (Regassa et al., 2011). Thus, gene expression patterns in CCs are currently used as indicators of oocyte quality (Tesfaye et al., 2009; Bunel et al., 2015). Besides, IVM and *in vivo* maturation differ in the amounts of mRNA transcripts stored in the ooplasm (Lonergan et al., 2003), with more than 100 differentially expressed genes between *in vitro*- and *in vivo*-matured bovine oocytes being responsible for depleting their developmental competence (Katz-Jaffe et al., 2009; Adona et al., 2016).

In humans, IVM can be an alternative for patients with ovarian pathologies affecting oocyte quality (Ata et al., 2010; Shalom-Paz et al., 2010) and can also reduce the risks of ovarian hyperstimulation syndrome (Sauerbrun-Cutler et al., 2015). However, despite its potential benefits, IVM is still marginally used in human ART, with applications mainly in fertility preservation (Kasum et al., 2015; Shirasawa and Terada, 2017). Therefore, a better understanding of the mechanisms involved in oocyte competence during IVM is crucial in the optimization of this technology.

The fate of an embryo is determined at fertilization. Delays in fertilization or fertilization by a damaged spermatozoon could conceivably lead to oocyte aging or to the formation of a defective embryo, respectively (Tarín et al., 2000). However, in the bovine species, IVC seems to be one of the major factors determining embryo quality. As mentioned before, IVC embryos show poorer morphology, cryotolerance, distinct transcript expression profiles, and pregnancy rates after transfer than IVD embryos (see review by Lonergan, 2007). Alternating *in vitro* and *in vivo* embryo culture demonstrated the importance of developing *in vitro* systems mimicking the *in vivo* situation. Thus, the culture of IVP bovine zygotes *in vivo* in the oviduct of sheep (Rizos et al., 2002), cow (Tesfaye et al., 2007), or mouse (Rizos et al., 2007), increased the quality of the resulting blastocysts. Conversely, IVC of *in vivo* produced bovine zygotes resulted in blastocysts of low quality (Rizos et al., 2002). However, IVC before and during embryonic genome activation (EGA) did not affect embryo development rates, irrespective of where culture took place, although IVC did affect the transcriptome of such blastocysts (Gad et al., 2012).

Negative factors within IVC include media supplementation with fetal calf serum (FCS), which reduces embryo cryotolerance, induces alterations in gene expression and leads to large offspring syndrome in cattle, a disorder caused by epigenetic alterations in the embryo that is phenotypically similar to Beckwith-Wiedemann syndrome in humans (Young et al., 1998; Lazzari et al., 2002; Rizos et al., 2003; Wrenzycki et al., 2005). Compared to *in vivo* derived embryos, IVP blastocysts produced with FCS had 5 times more differentially expressed genes than serum-free IVP blastocysts (1,109 vs. 207) (Heras et al., 2016). Serum derivatives added to culture can also trigger long term detrimental effects, as shown by improved survival to cryopreservation and reduced miscarriage rates observed when bovine serum albumin (BSA) was removed from the culture at the time of blastocyst formation (Murillo-Rios et al., 2017; Gomez et al., 2020). The embryonic genome is epigenetically reprogrammed after fertilization. This process involves activating or silencing specific genes by laying on appropriate methylation patterns (Reik et al., 2001). During this critical period, the embryo is especially vulnerable to epigenetic defects, which can be induced by IVC (El Hajj and Haaf, 2013). Indeed, animal studies have revealed links between different ARTs and imprinting disorders, via altered DNA methylation patterns and histone codes (Urrego et al., 2014). Such disorders are more prevalent in gametes and embryos after ARTs than in their *in vivo*-derived counterparts (Urrego et al., 2014). Thus, IVP embryos show culture-induced, stage-specific, and non-stage-specific, aberrant DNA methylation patterns in paternally or maternally imprinted genes and in several genomic clusters (Salilew-Wondim et al., 2015, 2018). The post-fertilization culture environment is therefore crucial for the quality of the resulting blastocysts (see review by Rizos et al., 2017; Wrenzycki, 2018). To overcome the limitations of conventional IVC and mimic *in vivo* conditions, different embryo culture systems have been developed such as co-culture with bovine oviduct epithelial cells (BOECs) (Schmaltz-Panneau et al., 2014) or supplementation of culture media with oviductal and uterine fluid in sequential culture, as well as the use of extracellular vesicles (EVs) (Rodriguez-Alonso et al., 2020). All these systems entail improvements in IVC for blastocyst development and their quality in terms of cryotolerance, cell counts, cell apoptosis and gene expression (Alminana et al., 2017; Lopera-Vasquez et al., 2017; Almiñana and Bauersachs, 2019). In particular, EVs secreted by donor oviductal cells increased birth rates after embryo transfer in mice due to decreased apoptosis and improved cellular differentiation in embryos (Qu et al., 2019). Furthermore, supplementation of IVC medium with uterine exosomes improved the developmental capacity of embryos generated by somatic cell nuclear transfer (SCNT) (Qiao et al., 2018). Taking together the above findings, it could be suggested that the effect of EVs on early embryonic development may be fundamental, and IVC systems containing EVs can provide new insights to improve gamete maturation, fertilization, and embryo development during ARTs.

In parallel, other research lines based on chemical modifications of simple medium, polarized and three-dimensional (3D) cell co-cultures, lead to improved embryo development and quality. These systems could allow cultured gametes and embryos to experience some of the same mechanical forces, mimicking interactions with the substratum of the oviduct and endometrium, and dynamic changes that occur in the microenvironment of the reproductive tract. The BOEC polarized system consists of growing the cells on inserts to allow media access from basolateral and apical sides, and to maintain the polarized asymmetrical structure of the oviductal epithelial cells. Epithelial cells derived from human, porcine or bovine oviduct maintained polarity and *in vivo*–like morphology when they were cultured for long term in a polarized air-liquid interface system (Levanon et al., 2010; Chen et al., 2013, 2017). It was evidenced that air-liquid system supports embryo development *in vitro* without culture medium supply in porcine, mouse and

bovine species; however, the obtained blastocyst rates could not yet match the outcome of optimized standard IVP procedures, suggesting that further improvement of the model is required (Chen et al., 2017). In cattle, using the 3D printing technology in combination with microfluidics resulted in the creation of "oviduct-on-a-chip" with a U-shaped porous membrane allowing BOEC polarization that could be maintained during long-term mimicking tissue- and organ-specific micro-architecture (Ferraz et al., 2017b). It was demonstrated that culturing BOEC in 3D system improved embryo production by allowing proper sperm and oocyte interactions, fertilization, and completely abolishing polyspermic and parthenogenic activation of oocytes in the absence of added sperm activating factors (Ferraz et al., 2017a). Although technical issues contributed to lower cleavage and developmental rates than in a conventional embryo production system, the DNA methylation intensity and transcript abundance in zygotes produced in the microfluidics device were more similar to embryos produced *in vivo* than to embryos produced in a conventional IVP system (Ferraz et al., 2018).

SENESCENCE DURING EARLY EMBRYO DEVELOPMENT

Cellular senescence is a state of irreversible cell cycle arrest that can be induced through different mechanisms, such as genomic and telomeric damage, epigenetic perturbations, reactive oxygen species (ROS), or activation of oncogenes, and mitogenic signals (Lopez-Otin et al., 2013). This event was first noticed in primary human fibroblasts that had undergone replicative exhaustion after a finite number of passages ("Hayflick's limit") (Hayflick and Moorhead, 1961). Nowadays, this state is known as replicative senescence and is associated with telomeres shortening. However, stress-induced premature senescence can be also induced as a defense mechanism in damaged cells that are not able to undergo apoptosis, and programmed senescence has been reported during development (Lozono-Torres et al., 2019).

Senescent cells show specific morphological and biochemical features, often presenting a large flattened morphology with increased cytoplasmic and nuclear volume in culture (Rhinn et al., 2019). These cells remain metabolically active, resist to apoptosis-inducing stimuli (Baar et al., 2017) and show high ROS levels and β-galactosidase activity (Wang and Dreesen, 2018). At the molecular level, the senescent response is mediated by two main components: the intrinsic arm and the extrinsic arm (Rhinn et al., 2019). The intrinsic arm is mediated by proteins that inhibit cell cycle progression, including tumor protein P53 (p53), p21 (encoded by Cyclin Dependent Kinase Inhibitor 1A; *Cdkn1a*), $p16^{INKA}$ and $p19^{ARF}$ (both encoded by Cyclin Dependent Kinase Inhibitor 2A *Cdkn2a*) (Kuilman et al., 2010; Martinez-Zamudio et al., 2017), and by microRNA-mediated gene silencing (Benhamed et al., 2012). The extrinsic arm comprises the "senescence-associated secretory phenotype" (SASP), mediated by cytokines, chemokines, growth factors, extracellular matrix (ECM), and ECM-remodeling proteins (Freund et al., 2010; Acosta et al., 2013) that are transcriptionally regulated by nuclear factor kappa-light-chain-enhancer of activated B cells (Nfkb), CCAAT/enhancer-binding protein beta (Cebpβ), p38, p53, and GATA binding protein 4 (Gata4) transcription factors (Acosta et al., 2008; Kuilman et al., 2008; Kang et al., 2015). The SASP allows senescent cells to secrete signaling molecules, generating a microenvironment, and activating the immune system to remove damaged or stressed cells (Kang et al., 2011; Sagiv et al., 2016).

Although cellular senescence has been mainly associated with tumor suppression, tissue repair or aging (Baker et al., 2011; Campisi, 2013; Ritschka et al., 2017), features of senescence have been also reported in cells from different mammalian species during embryonic development (Rhinn et al., 2019). In the mouse, senescent cells have been identified by expression of β-galactosidase, p21 and SASP factors in many tissues during specific time windows of fetal development (mesonephros, neural tube, gut endoderm, heart, and the developing limbs, etc.) (Munoz-Espin et al., 2013; Storer et al., 2013; Lorda-Diez et al., 2019). These cells emerge and are removed by macrophages in a tightly controlled manner, resulting in tissue remodeling and patterning. Interestingly, senescent cells in the developing fetus are negative to certain senescence markers described in adult tissues, such as p53, $p16^{INKA}$, $p19^{ARF}$, and DNA damage. Instead, developmental senescence is strictly dependent on p21 and is regulated by the TGFβ/SMAD and PI3K/FOXO pathways (Munoz-Espin et al., 2013; Storer et al., 2013; **Table 1**). This senescence model seems to be conserved in vertebrate development, as similar patterns have been observed in chick (Storer et al., 2013) and human embryos (Munoz-Espin et al., 2013), and could have emerged initially as a basic developmental mechanism that subsequently evolved to a protective role to face aging and tumor suppression in adult tissues.

Going one more step back in development up to the preimplantational embryo, the existence of senescence was first hypothesized almost 20 years ago (Betts and King, 2001). A high

TABLE 1 | Senescence and apoptosis markers detected through development.

Senescence	Adult	Fetus	Early embryo
p53	Yes	No	No
p21	Yes	Yes	Yes
$p16^{INK4A}$	Yes	No	No
$p19^{ARF}$	Yes	No	?
SASP markers	Yes	Yes	?
P66Shc	Yes	?	Yes
Phosphorylated γH2AX	Yes	No	Yes
β-galactosidase	Yes	Yes	Yes
APOPTOSIS			
p53/phospo-p53	Yes	No	No
p21	Yes	Yes	Yes
BAX	Yes	Yes	Yes
Bcl-2	Yes	Yes	?
DNA fragmentation	Yes	Yes	Yes
Apo-1/Fas, FasL	Yes	Yes	No
Activated caspases	Yes	Yes	No
PS externalization	Yes	?	Yes

SASP, Senescence-associated secretory phenotype.

proportion of the embryos produced *in vitro* are arrested at a species-specific stage of development during the first cell divisions, before EGA. These arrested embryos do not show signs of apoptosis or necrosis, since features of programmed cell death are not detected during the early cleavage stages (Byrne et al., 1999; Hardy, 1999; Matwee et al., 2000). Interestingly, when the apoptotic pathway is partially activated by exposing embryos at early cleavage stages to protein kinase inhibitors or mitochondria depolarizing agents, limited caspase activation, and DNA fragmentation can be observed (Matwee et al., 2000; Gjorret et al., 2007). This might suggest that components of the apoptosis machinery are available before EGA, but cannot be physiologically activated due to the absence of mature mitochondria (Plante and King, 1994; Van Blerkom, 2004) or to certain inhibition of the apoptotic pathway (Brad et al., 2007). Instead, defective IVP embryos would enter a state of permanent cell cycle arrest before EGA compatible with cellular senescence, in which they show active metabolism and high ROS levels (Betts and Madan, 2008; **Figure 1**).

Assisted reproductive technologies induce oxidative stress in the embryos (Ramos-Ibeas et al., 2019), which might also generate DNA and telomeric damage before EGA (Betts and Madan, 2008). At these stages of development, many transcripts are scarce, including telomerase, the enzyme responsible for telomere elongation (Betts and King, 1999). Alternatively spliced telomerase variants associated with a lack of telomerase activity have been detected in some human oocytes and poorly developing embryos (Brenner et al., 1999). Moreover, telomere length in human oocytes predicts embryo fragmentation at day 3 of development, supporting the theory of reproductive senescence in women (Keefe et al., 2005). Thus, stress-mediated telomeric damage due to sub-optimal culture conditions, shortened telomeres derived from aged oocytes, or absence of proper telomerase activity in low-quality oocytes or embryos could trigger embryo senescence before EGA (Betts and King, 2001; **Figure 2**).

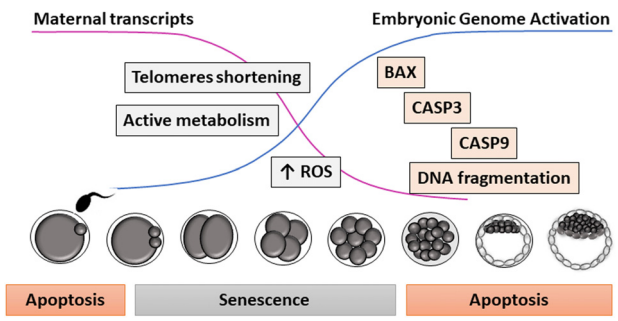

FIGURE 1 | Proposed model for apoptosis and senescence during early embryo development. Due to the low amount of specific embryonic transcripts before embryonic genome activation (i.e., telomerase), embryos are very sensitive to environmental stressors during early cleavage stages, entering into a state of cell arrest resembling senescence. Later in development, embryos (and oocytes before fertilization) can show DNA fragmentation and other morphological signs of apoptosis.

In contrast to senescent adult cells and in the same way as in fetal cells, p53 is not involved in embryo senescence during early cleavage stages (Favetta et al., 2004; Favetta et al., 2007a; Velez-Pardo et al., 2007; Meuter et al., 2014). Furthermore, $p16^{INKA}$, which is involved in the senescence response in adult tissues, has not been detected in embryos (Egashira et al., 2011; Meuter et al., 2014). However, IVP bovine embryos arrested at the 2-cell stage were positive for phosphorylated γH2AX, a senescence marker that was not detected in proliferating 2-cell embryos (Betts and Madan, 2008). Besides, a direct correlation between the oxidative stress adaptor protein p66Shc levels and the duration of the embryonic arrest was found in these relatively transcriptionally silent embryos, so p66Shc might play a key role in the senescence response induced by ROS in early embryos (Favetta et al., 2004, 2007b). Additional markers of senescence in IVP embryos are β-galactosidase and p21 expression (Meuter et al., 2014; Ock et al., 2020; **Table 1**). Upregulation of p21 has been reported in mouse preimplantation embryos in response to heat stress or X-ray radiation that led to developmental delay or blockage in damaged embryos (Ock et al., 2020). In the absence of p21, damaged embryos can progress to the blastocyst stage, although exhibiting increased apoptosis and chromosome instability (Adiga et al., 2007). Thus, p21 plays a protective role in the embryo, mediating a senescent phenotype in response to exogenous stressors.

Therefore, senescence seems to play a protective role during preimplantational development, acting as a checkpoint mechanism to ensure that unhealthy embryos enter into a permanently arrested state and do not progress in development, avoiding long-term effects on health and reproduction. This mechanism would become even more important in IVP embryos, which are exposed to multiple stressors (Ramos-Ibeas et al., 2019). It would be interesting to investigate whether senescent embryos secrete signaling factors that could exert a detrimental effect on the rest of the embryos in culture.

APOPTOSIS DURING EARLY EMBRYO DEVELOPMENT

Cell death exerts an essential role in governing early mammalian embryo development (Hardy, 1997; Betts and King, 2001; Leidenfrost et al., 2011; Vandaele and Van Soom, 2011). Early embryos progress in development faster than tumor cells because of the lower embryonic demand for membranes construction and lack of new biomass synthesis (Krisher and Prather, 2012). A delicate balance between cell proliferation and death is therefore required for successful development to term. This view of cell death, as a regulatory process, alternates with its pathological role (Betts and King, 2001; Leidenfrost et al., 2011). Regulated cell death (RCD) exists mainly in multicellular organisms as a form of genetically programmed elimination of cells that are perceived as dispensable, noxious, or with irreversible damage. Physiological forms of RCD do not require intracellular or extracellular alterations (Conradt, 2009; Fuchs and Steller, 2011). On the contrary, prolonged and/or intense stimulation, insofar as they produce stress and disturb cellular homeostasis, induce pathological RCD (Galluzzi et al., 2016).

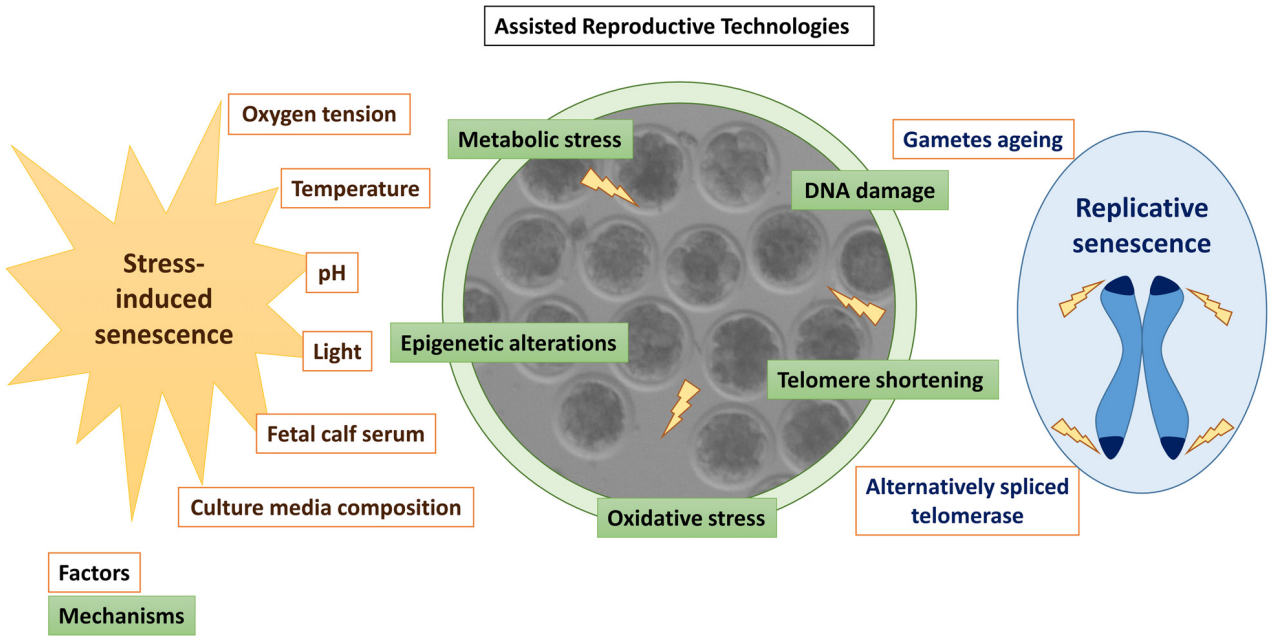

FIGURE 2 | Summary of factors (orange) and mechanisms (green) inducing senescence in *in vitro* produced embryos. Stressors associated with *in vitro* embryo culture are written in brown letters, while factors associated with replicative senescence are written in blue.

Apoptosis is a form of RCD existing in multiple tissues during embryonic and fetal development in mammals. The apoptotic cell is rounded and shrunk, showing condensed, marginalized, and later fragmented chromatin, intact nuclear envelope, shrunk organelles and contained cytoplasm (Voss and Strasser, 2020). A recent hypothesis postulated that apoptosis and cell proliferation are independent processes that work together better than alone in regulating growth (Voss and Strasser, 2020). The role of apoptosis in mammalian development is not only to control cell proliferation, including the deletion of cells and portions of tissues, but also to regulate morphogenesis, including the formation of cavities, and vesicles in compact structures and modeling tissue shape (reviewed by Diamantis et al., 2008). Since the framework of early morphogenetic events is not yet started in early embryo development, the apoptosis mechanisms seem to be limited to eliminate abnormal cells, as there is no information about apoptosis regulating other essential hallmarks until the blastocyst stage. A recent study in a mouse model of chromosome mosaicism supports this hypothesis, where abnormal aneuploid cells are eliminated by autophagy and apoptosis at the peri- and post-implantation stages of development (Singla et al., 2020). In human ART, apoptosis has been postulated as a candidate mechanism to explain elevated monozygotic twining (MZT), which would be facilitated by more labile junctions between the ICM cells in IVP embryos (Hviid et al., 2018). Thus, high glucose in culture increases MZT rates, explained as increased ROS production and subsequent apoptosis that would disrupt the ICM, with the possible help of overpressure during hatching (Ménézo and Sakkas, 2002). Frequent blastocyst collapse could relocate some ICM cells on the trophectoderm wall, thereby forming a second, ectopic ICM, and subsequent MZT (Payne et al., 2007). Embryo biopsy and cryopreservation, together with specific donor conditions have also been cited as factors underlying increased MZT, always with apoptosis as a triggering factor (reviewed by Tauwinklova et al., 2010). In the cow, increased MZT has been not documented within IVP embryos.

Thus, the interest in apoptosis within *in vivo* and *in vitro* produced embryos lies in its strong consistency with a variety of stresses and poor development conditions, and this makes the apoptosis signs timely markers of an abnormal environment and likely responsible of increased MZT in humans. Hence, one of the hallmarks of IVP is an apoptosis rate generally higher than embryos naturally developing in the genital tract (Pomar et al., 2005), indicating that *in vitro* conditions are poorer for the embryo.

Apoptotic Pathways Within Early Embryos

Apoptosis is regulated through two convergent pathways, depending on whether the signals initiating cell death originate within or outside the cell: (1) the extrinsic or death receptor pathway, mainly activated by members of the tumor necrosis factor (TNF) family that bind to their family of cognate receptors (TNFR), and (2) the intrinsic, mitochondrial, or B-cell lymphoma 2 (BCL-2) regulated pathway. Both apoptotic pathways are active –but not completely- in early embryos under stage-specific conditions (Leidenfrost et al., 2011).

Intrinsic Apoptosis

Intrinsic apoptosis pathway proceeds at least by well-defined environmental perturbations (Galluzzi et al., 2018). The bovine

embryo has been identified as responsive to some of such alterations: (1) Endoplasmic reticulum (ER) stress, which simultaneously increases expression of ER stress (Glucose-Regulated Protein, 78 kDa (*GRP78*), Activating Transcription Factor 4 (*ATF4*), Activating Transcription Factor 6 (*ATF6*), Regulator Of G Protein Signaling 1 (*RGS1*) and X-Box Binding Protein 1 (*XBP1*)] and pro-apoptotic [C/EBP Homologous Protein (*CHOP*) and BCL2 Associated X, Apoptosis Regulator (BAX)] genes, at the same time that development rates, cryotolerance, cell survival and apoptotic cell rates improve (Yoon et al., 2014; Khatun et al., 2020); (2) ROS overload can also trigger apoptosis and developmental affectance (Huang and Chan, 2017; Luo et al., 2020); (3) Irregular DNA structures, out of which only a subset can be identified by TUNEL (Gjorret et al., 2003; Leidenfrost et al., 2011); abnormal segregation of chromosomes in mitosis is a possible origin of such structures (Gjorret et al., 2003); (4) Mitotic effects, where apoptosis was observed in response to multinucleate cells (Paula and Hansen, 2008) and cytokinesis becomes blocked leading to a "mitotic catastrophe" by checkpoint activation (Huang et al., 2005); (5) Specific miRNAs that trigger apoptosis, since slow-cleaving bovine embryos in culture release miRNA-30c, which targets cyclin-dependent kinase 12 (CDK12) and lead to apoptosis (Juan et al., 2016; Lin et al., 2019), although it is unknown whether dead cells or live cells with a commitment release miR-30c; 6) Growth factors removal as shown by specific growth factors identified in the genital tract that reduce apoptosis when added to IVC (Trigal et al., 2011; Gomez et al., 2014). In pigs, vascular endothelial growth factor (VEGF) decreased in parallel to an increase in embryo development, concomitant with a reduction in mRNA abundance of caspase 3 (*CASP3*) and increased BCL2 Apoptosis Regulator (*BCL2*) and Nuclear Factor, Erythroid 2 Like 2 *NRF*-2 (Biswas et al., 2018).

Synergies between the above inducers may exert a more tuned regulation of apoptosis and proliferation, as shown in cancer cells, where more than 300 miRNAs respond to retinoic acid (RA) to inhibit cell invasiveness and deregulate growth (Lima et al., 2019). Interestingly, RA is a main activated pathway in the bovine uterus (Bauersachs et al., 2005). *In vitro*, RA regulates apoptosis in the bovine blastocyst through both retinoid receptors RXR and RAR (Rodriguez et al., 2006, 2007; Gomez et al., 2008).

Extrinsic Apoptosis

Extracellular perturbations can trigger apoptosis through the extrinsic pathway, activated by receptor-ligand interaction between extrinsic molecules and mainly two types of receptors in the plasma membrane: (1) Death receptors, activated by cognate ligands; (2) Dependence receptors, activated by falling of ligand concentrations below specific thresholds (Galluzzi et al., 2018). Death receptors include Fas cell surface receptor (FAS, also termed as APO-1 or CD95), and TNF receptor superfamily member 1A (TNFR1), 10a (DR4 or TRAILR1), and 10b (DR5 or TRAIL2) (Wajant, 2002; Aggarwal et al., 2012; Von Karstedt et al., 2017). The extrinsic apoptosis pathway could be partly inactive in bovine embryos because of the lack of convergence with the intrinsic pathway to activate the effector caspases, since caspase-8 would be absent or inactive. Together with caspase-8, FAS/FASL transcripts are at very low abundance or absent in embryos (Leidenfrost et al., 2011). Furthermore, the FAS signaling pathway is inactive in bovine, human and mouse oocytes (Sato, 1998; De Los Santos et al., 2000; Pomar et al., 2004). The alternative pathway of necroptosis, a regulated common morphology of necrotic and apoptotic cells, which in turn should become active by caspase-8 inhibition, has not been studied in bovine embryos to our knowledge. However, morphological evidence associated with this RCD type has been described (Gjorret et al., 2003; Rodriguez et al., 2006). A third signaling pathway through death receptor is represented by Nuclear factor-Kappa-B (NF-ƙh) activation, which usually leads to a wide inflammatory response linked to cell survival (Nguyen-Chi et al., 2017; Von Karstedt et al., 2017). The bovine blastocyst is equipped with NF-ƙB inducers, such as TNF (Correia-Alvarez et al., 2015b) and Interleukin 1 Beta (IL1b) (Correia-Alvarez et al., 2015a). In the uterus, Day 6/Day 8 embryos need to depress a natural pro-inflammatory status to progress in development; evidence of such depression, including reduced NF-ƙin the uterine fluid, has been provided (Munoz et al., 2012). Interestingly, the sex of the embryo determines the extent of such a response in the uterus, with female blastocysts showing higher apoptotic rates in their ICM (Gomez et al., 2013).

Apoptosis Chronology During Early Development Stages

The timing at which the IVP embryo responds to external stimuli through apoptosis -as an endogenous mechanism of removing cells- has been defined in stage-specific studies with embryos. However, perturbations of the oocyte and spermatozoa environments can also result in an apoptotic response in the generated embryo (El Hajj and Haaf, 2013; Wang et al., 2017; Bittner et al., 2018), although this topic is out of the scope of the present review.

Apoptosis and kinetic patterns of development are related, since the incidence of embryos with dying/dead cells increases through development by stage and day. However, the most advanced embryonic stages within a day show lower apoptosis rates. Pioneering studies (Byrne et al., 1999; Matwee et al., 2000; Gjorret et al., 2003) defined the chronology of apoptosis within IVD and IVP cattle embryos. Embryos were examined by morphological apoptotic traits (M) and analysis of DNA fragmentation using terminal deoxynucleotidyl transferase-mediated dUTP nick end labeling (TUNEL) (T) (Gjorret et al., 2003). Only nuclei showing T + M were regarded as completely apoptotic. Apoptotic M was rarely detectable before the 9–16 cell stage. In contrast, significant proportions of mature and immature oocytes showed T staining (Matwee et al., 2000), indicating that apoptotic processes became repressed after fertilization, since no IVD embryos and very few IVP embryos (< 3%) showed complete apoptotic T + M up to the morula stage. The first sign of T + M was observed at the 8-cell stage (Byrne et al., 1999; Matwee et al., 2000; Paula-Lopes and Hansen, 2002; Gjorret et al., 2003), while close to 50% Day-3 IVP embryos (i.e., at different development stages) contained at least one cell showing any sign of M (Leidenfrost et al., 2011). Thus, at the

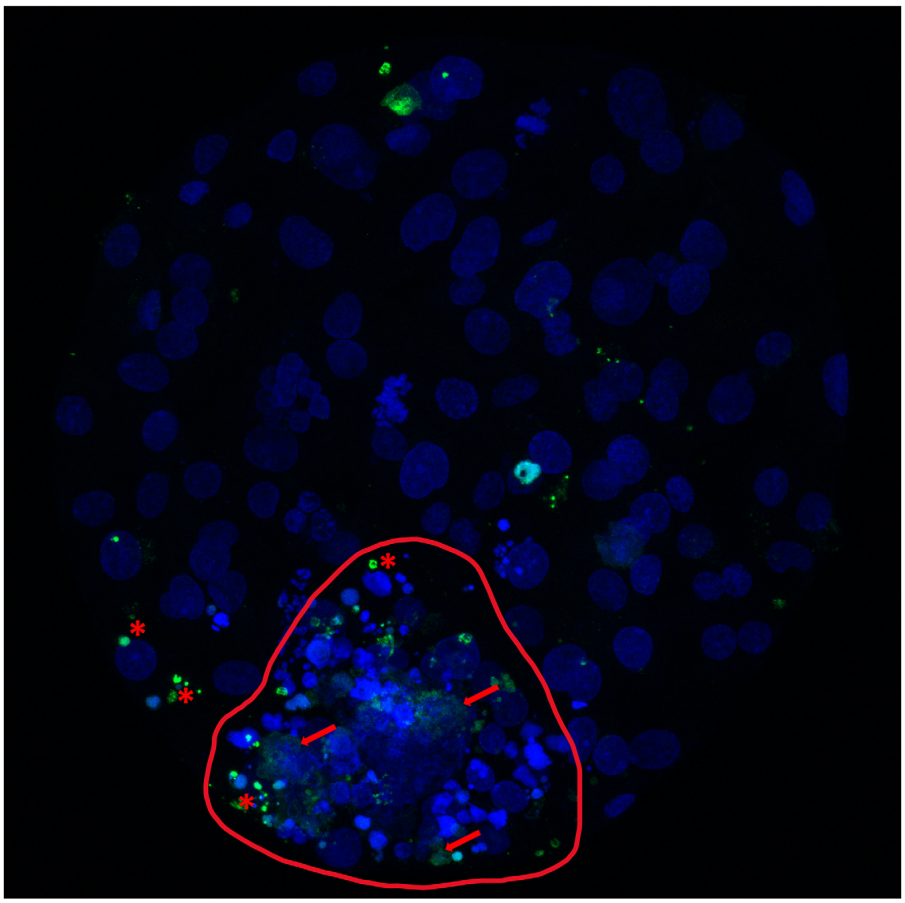

FIGURE 3 | Cell death analysis in a bovine expanded blastocyst produced *in vitro*. Bovine expanded blastocyst produced *in vitro* and stained with bisbenzimide (blue) to visualize all nuclei and TdT-mediated dUTP nick-end labeling (TUNEL; green). Red asterisks mark TUNEL-positive nuclei undergoing the apoptotic pathway (condensed, TUNEL-positive structures that can appear scattered as smaller apoptotic bodies and correspond to chromatin and cytoplasmic condensation, with intact nuclear membrane). Red arrows mark nuclei undergoing necrosis (TUNEL-positive structures, with unclear, swollen and frayed edges; red arrows). The inner cell mass (circled, red line) shows the highest incidence of identified and non-recognizable forms of cell death, in contrast with a lower incidence in the more abundant trophectoderm cells.

blastocyst stage rarely an embryo was found without dying/dead cells, with steadily higher apoptotic rates in the ICM (usually 25–40% total cells in blastocysts) than in the trophectoderm (Gjorret et al., 2003; Rodriguez et al., 2006; Gomez et al., 2008, 2014, 2020; Leidenfrost et al., 2011; Munoz et al., 2014; Murillo et al., 2017), suggesting a more stringent regulation in the developmentally important and yet undifferentiated ICM. Such differences are not apparent in human embryos, although appropriate studies are limited and with low sample numbers (Sjöblom et al., 2002; Hardy et al., 2003).

Signaling pathways and genes involved in the apoptotic response have been analyzed during early embryo development in the bovine species. In an elegant study, Leidenfrost and co-workers analyzed genes involved in both extrinsic and intrinsic apoptosis initiation (**Figure 3**; Leidenfrost et al., 2011). Within IVP embryos, the copy numbers of *CASP3*, X-linked Inhibitor of Apoptosis (*XIAP*), *BAX*, BCL2 Like 1 (*BCL2L1*), Caspase 9 (*CASP9*), and Signal Transducer and Activator of Transcription 3 (*STAT3*) declined from the oocyte until day 3/4, to gradually increase thereafter. Interestingly, transcripts for the extrinsic initiator caspase-8 were undetectable from the oocyte up to the hatching blastocyst stage (Leidenfrost et al., 2011). Contrary to the caspase-9 protein from the intrinsic apoptotic pathway, caspase-8 was not induced in 2-cell embryos by the apoptotic promoter ceramide, which increases the numbers of multinucleated cells (Paula and Hansen, 2008), an effect by which cytokinesis becomes blocked leading to a "mitotic catastrophe" by checkpoint activation (Huang et al., 2005).

Immunocytochemical staining of the effector protein CASP3, revealed also increasing apoptotic rates from cleavage through the blastocyst stages, but CASP3 positive embryos appeared before the 8-cell stage (Oliveira et al., 2016) at higher rates than those with T + M (see the above-cited works). Such differences may represent incomplete repression of apoptotic mechanisms, or activation of specific subsections, as suggested (Gjorret et al., 2003). The EGA, at the 8–16 cell stage in cattle, entails a complete re-organization of the apoptotic machinery in the embryo, which in this way would reach complete capacity to reorganize cell

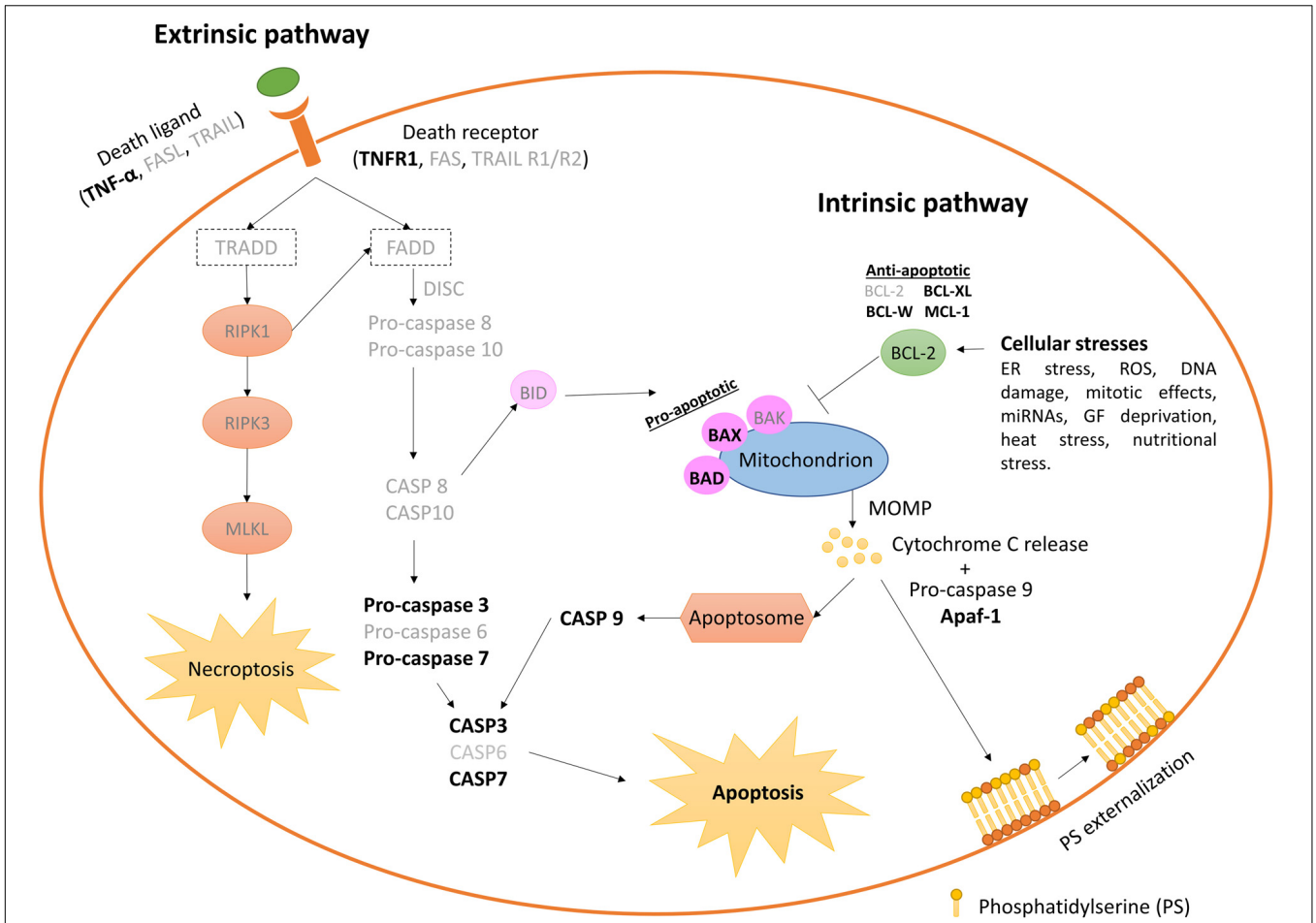

FIGURE 4 | Extrinsic and intrinsic pathways leading apoptosis on the *in vitro* produced bovine embryos. Elements not yet identified in early bovine embryos are shown in lighter types. Only stress sources to which the bovine embryo responds triggering apoptosis cascade are cited. Anti-apoptotic *BCL2* and *BCL-W* gene expression decreases between the oocyte and > 16 cell-stage embryos, while pro-apoptotic *BAX* increases. *BAX* and *BCL2* are absent in > 20 cells embryos (Melka et al., 2010; Fear and Hansen, 2011), although other authors have reported absence of BCL2 during early embryo development (Leidenfrost et al., 2011). CASP3 and CASP9 are found at very low abundance, and CASP8 is undetectable neither in oocytes nor in embryos at any analyzed stage (Leidenfrost et al., 2011). DISC, death-inducing signaling complex; MOMP, mitochondrial outer membrane permeabilization.

growth and differentiation. Altered EGA within IVP embryos would be involved in the distinct occurrence of apoptosis features between IVP embryos and their *in vivo* counterparts.

Embryo Apoptotic Responses to *in vitro* and *in vivo* Stress Sources

Early embryos can respond to a variety of stressors through apoptosis activation *in vivo* and *in vitro* (**Figure 4**). Heat-shock-induced apoptosis can occur in cattle embryos exposed to high environmental temperatures, being more acute in high-producing dairy cows due to their higher metabolic heat; 8–16 cell embryos are the first stage able to respond to heat stress (De Barros and Paula-Lopes, 2018). Nutritional stress is also harmful for embryo development and pregnancy. In a diabetic pregnancy, hyperglycemia has been related with congenital malformations in humans and animals (Eriksson and Wentzel, 2016; Shub and Lappas, 2020). Mimicking maternal diabetes with very high concentrations of glucose in culture reduces blastocyst development rates and trophectoderm cells, while increases apoptotic cell rates in bovine and mouse (Bermejo-Alvarez et al., 2012; Uhde et al., 2018). The metabolomic profile of bovine embryos produced in high-glucose medium showed an increase in glycolysis and hexosamine pathways, and a reduction in the components of the tricarboxylic acid cycle, resulting in a deficient energy production from pyruvate, and in an increase in the polyol pathway as an alternative to produce energy (Uhde et al., 2018). Also, high glucose increased the expression of pro-apoptotic genes *Bax* and *Casp3* and decreased the mitochondrial content and expression of glucose transporters in mouse blastocysts (Shen et al., 2009). All these alterations may induce oxidative stress and the activation of the apoptosis pathway in the embryo (Jimenez et al., 2003). Moreover, negative energy balance (NEB) in cows and obesity in humans are associated with upregulated lipolysis, which increases non-esterified fatty acids (FA) concentrations in blood. Bovine blastocyst obtained from COCs matured with a

high concentration of FA had an increased apoptotic incidence and lower cell numbers (Van Hoeck et al., 2011; Marei et al., 2017), caused by lipid accumulation and increased mitochondrial ROS (Prastowo et al., 2016).

Incidence of apoptosis within *in vivo* embryos is generally lower than in IVP embryos (Gjorret et al., 2003; Pomar et al., 2005; Warzych et al., 2007), although this appreciation is not unanimous (Leidenfrost et al., 2011). Thus, embryonic quality is normally associated with lower apoptotic rates. IVP blastocysts show higher transcript levels for *XIAP*, *BAX*, *BCL2L1*, *CASP3,* and *CASP9* than *in vivo* embryos. However, neither *in vivo* nor IVP embryos show transcripts for *BCL2*, Caspase 8 (*CASP8)*, and Fas Ligand (*FASLG)*; and Fas Cell Surface Death Receptor (*FAS)* transcripts were detected only in the *in vivo* group at very low abundance (Leidenfrost et al., 2011).

Supplementation of *in vitro* culture media with serum increases embryonic Bax expression (Rizos et al., 2003), while improved formulations that increase the stability of glutamine (e.g., as glutamyl-glycine), avoids ammonia production by glutamine degradation (Zuo et al., 2020). Embryo cryopreservation, in particular vitrification and warming, enhances the expression of apoptotic genes like Forkhead Box O3A (*FOXO3A)*, Patatin Like Phospholipase Domain Containing 2 (*PNPLA2*), *BCL2L1*, and *BAX*, although apoptotic phenotypes do not necessarily appear modified (Madrid Gaviria et al., 2019).

Interestingly, Day-6 IVP female embryos can show higher apoptotic rates than males (Oliveira et al., 2016). Such differences, nevertheless, can be due to culture conditions potentially inappropriate for female embryos, as there is sufficient evidence of metabolic differences between males and females (Sturmey et al., 2010; Munoz et al., 2020) and no sex-specific culture media have been presently developed. Finally, the individual bull sperm used for IVF can interact with sex factors to alter the incidence of apoptosis during embryonic development (Oliveira et al., 2016).

ASSESSMENT OF EMBRYO QUALITY THROUGH SENESCENCE AND APOPTOSIS MARKERS

Until now, the most widely used method to select IVP embryos for transfer is a morphological evaluation by standard microscopy. However, even when performed by experienced embryologists, it does not completely reflect embryo competence. Cytoplasmic fragmentation and cytokinesis failure, often observed in IVP embryos (Mateusen et al., 2005), can be estimated by morphological evaluation to assess the viability of the embryo, although the outcome can be imprecise and subjective, depending on the evaluator's criteria. Therefore, the use of alternative markers could improve the selection of more competent embryos. Fragmentation has been associated with apoptosis induction and can lead to a reduction of embryo viability if present to a high degree (Jurisicova et al., 1996). However, although apoptosis evaluation has been suggested as an additional technique to assess embryo quality and viability (Pomar et al., 2005), activation of apoptosis might happen in the embryo as a physiological mechanism to maintain the equilibrium between cell proliferation and death, regardless of external damage or initial oocyte quality (Bakri et al., 2016). In the authors' opinion, current systems to evaluate apoptosis are relative and invasive. Therefore, due to the large variety of embryo production systems available, measuring a critical level of apoptosis able to trigger developmental arrest is not possible yet, although it would be a highly desirable test to analyze embryonic quality. Comparison between embryo culture systems and *in vivo* models is the reference used in practice. Moreover, the early mammalian embryo is able to cope with a number of adverse environmental situations (Laguna-Barraza et al., 2012; Eckert et al., 2015; Fleming et al., 2015; Hansen et al., 2016) without a clear measurable evidence of the embryo resilience. Thus, appropriate analysis of the efficiency of embryonic "repair mechanisms" (i.e., confident evaluation of embryonic quality) would request pregnancy establishment and progression until birth, which makes such experiments highly expensive or, in most cases, directly unapproachable.

Nowadays, apoptosis can be analyzed by different techniques, differentiating those based on biochemical analyses, being the most used the comet and TUNEL reaction assays and annexin V staining, and those based on the analysis of genes and proteins involved in apoptosis pathways. The comet assay is a sensitive technique to detect DNA damage used in numerous eukaryotic cell types and commonly applied in genetic toxicity studies. It is based on electrophoresis migration of denatured DNA fragments and visualization by fluorescence of the comet-like shape that produces the fragmented DNA (Kucharova et al., 2019). Comet is used to detect presence of apoptosis through the visualization of the comet containing broken DNA fragments, but apoptosis level is difficult to quantify. Although in the reproduction field, this technique is mainly used to assess sperm quality and sometimes in oocytes (Chang et al., 2019; Haddock et al., 2020), it has also been adapted to study early embryos, even though the number of studies are very limited and comprise different species. One of its applications is the evaluation of the persistence of induced damage from maternal germ cells in early embryos (Rolland et al., 2017). However, an important limitation of this technique is that it cannot distinguish between DNA fragmentation coming from polar body disintegration (Tatemoto et al., 2000) and DNA fragmentation induced through apoptosis in embryonic cells (Fabian et al., 2003). Moreover, the conventional comet assay cannot distinguish between apoptosis and necrosis, requiring additional techniques to discriminate between them (Morley et al., 2006).

TUNEL assay recognizes fragmented DNA, an event that occurs at the later stage of the apoptotic process. This technique is widely used in studies for quality assessment of embryos and has revealed differences in the onset of apoptosis between *in vitro*- and *in vivo*-produced bovine embryos (Gjorret et al., 2003). Sudano et al. (2014) reported a correlation in apoptosis levels quantified by TUNEL between fresh bovine embryos and post-vitrification survival, which is also used as predictor of embryo quality. In this context, apoptosis incidence has also been analyzed to compare culture medium formulations and IVC conditions, providing information about embryo status. Thus, high oxygen tension and FCS in culture increase apoptosis rates

in embryos (He et al., 2020). The effect of FCS is dose-dependent, and very low doses of serum (0.1% FCS) are not pro-apoptotic, although the embryonic quality and competence are reduced (Murillo et al., 2017; Gomez et al., 2020).

Suboptimal conditions during ARTs subject the embryos to chemical and physical stress, triggering apoptosis, and compromising the integrity of the embryo or leading to long-term deleterious effects (Ramos-Ibeas et al., 2019). IVP equine, porcine, ovine, caprine, and bovine embryos show higher incidence of TUNEL quantified apoptosis than their *in vivo* counterparts (Pomar et al., 2005). However, although TUNEL is a frequently used method for apoptosis detection, its specificity is low since the assay labels all free 3′hydroxyl termini in the DNA, which are also detected during necrosis, DNA repair, mechanical damage, and even active gene transcription. Thus, TUNEL staining would detect any type of DNA damage and should be used in combination with other apoptosis-specific assays (Loo, 2011) or analyzing the morphological features of apoptosis and necrosis observed in the target cells (Rodriguez et al., 2006).

Another technique commonly used for apoptosis assessment within IVP is annexin V staining, which allows the detection of phosphatidylserine (PS) in the membrane lipid bilayer surface. The externalization of PS is one of the earliest events in the apoptosis pathway. Annexin V staining has been observed in all human embryos arrested from the 2-cell stage to uncompacted morula, while only 30% of these embryos were TUNEL-positive (Levy et al., 1998), as well as in 1-cell to 9-cell fragmented embryos (Liu et al., 2000). The presence of PS on the outer leaflet of the membrane lipid bilayer of a cell is the earliest event of the apoptosis process. In healthy cells, PS is found exclusively on the inner layer of the membrane cell (Hanshaw et al., 2005). The externalization of PS had been observed by Levy et al. (1998) and Mateusen et al. (2005) in all stages of the apoptotic preimplantation embryo (2-cell stage embryo until blastocyst stage). There are three possible explanations to these results: (1) Annexin V allows the detection of apoptotic cells in arrested embryos earlier than using TUNEL; (2) Annexin V could be also labeling late-stage senescent cells in arrested embryos, which show mitochondrial depolarization by ROS, an event that may precede apoptosis (Wang et al., 2016); and (3) Necrotic cells can exhibit annexin V (Crowley et al., 2016). Therefore, as recommended for TUNEL, detection of annexin V should be combined with other apoptosis-specific assays or apoptotic morphology studies.

Increased expression of pro-apoptotic genes *BAX* and *CASPASE-3* is associated to IVP 2–4 cell bovine embryos bearing poor morphology (Melka et al., 2010). In the same way, the anti-apoptotic gene *BCL2* increases in bovine embryos with good morphological quality (Yang and Rajamahendran, 2002), and in non-fragmented mouse blastocysts (Exley et al., 1999). Therefore, the ratio between pro-apoptotic BAX and anti-apoptotic BCL2 is used to determine embryo quality and marker of differences between IVP and *in vivo* collected embryos. This occurs in bovine (Gutierrez-Adan et al., 2004) and humans (Metcalfe et al., 2004).

MicroRNAs (miRNAs) are key regulators of gene expression through post-transcriptional and post-translational modifications of mRNA. Mammalian blastocysts release miRNA via exosomes and apoptotic bodies in the spent embryo culture medium. Recently, a new approach to study apoptosis through miRNAs in the spent culture medium of individually cultured blastocysts has been proposed. In this study, miR-294 levels in the spent culture medium were directly correlated with apoptosis in mouse embryos. Although the biological role of miR-294 remains unknown, two hypotheses could explain these results. One is that high levels of miR-294 are involved in the suppression of the apoptosis inhibitor *BCL2*, which in the last term acts promoting apoptosis; although no *BCL2* expression could be detected in this study, so this hypothesis could not be confirmed. The other possibility is that apoptosis triggers miR-294 release; which was confirmed by exposing the embryos to ultraviolet radiation (Makri et al., 2020). In bovine embryos, high levels of miR-30c have been associated with increased apoptosis and reduced development rates (Lin et al., 2019). miR-30c, as miR-30 family member, regulates p53 expression and cell apoptosis (Li et al., 2010), and downregulates Cyclin Dependent Kinase 12 (*CDK12)* and DNA damage response (DDR) genes, which may impact on cell cycle progression. miR-30c is highly conserved between species, and in humans, miR-30c levels increase in the spent culture medium of those embryos that will successfully implant (Capalbo et al., 2016). Thus, miRNAs secreted to the culture medium are potential biomarkers of embryo apoptosis and viability, although their biological functions remain unknown or poorly studied. The analysis of compounds secreted to or taken up from the culture media by embryos, such as metabolites and non-coding RNAs, is advantageous, and non-invasive. In contrast, gene expression analysis, TUNEL assay and annexin V staining are invasive techniques that require biopsy or embryo destruction. Biopsy can be detrimental for the embryo and can also lead to false negatives, discarding embryos with actual pregnancy potential.

Controversies between the association of apoptosis and embryo viability still exist (Haouzi and Hamamah, 2009), as shown by similar apoptotic indexes found by TUNEL between developmentally arrested *in vivo* bovine embryos, fragmented morulae and non-fragmented morulae (Ikeda et al., 2006). Similar results have been reported in the human species by TUNEL and Annexin V (Antczak and Van Blerkom, 1999). These results suggest that an alternative process might be going on in poor-quality embryos at these stages, which causes developmental arrest and cannot be detected with the TUNEL assay, such as cellular senescence.

Embryo senescence might underlie the high frequency of early developmental failure associated with sub-optimal culture conditions (Betts and King, 2001). Senescence markers β-galactosidase, phosphorylated H2A.X and p21 (*Cdkn1a*) mRNA are more abundant in mouse IVP than *in vivo* blastocysts. However, their expression was reduced when embryos were cultured in low oxygen tension (5%), pointing to a stress-induced senescence associated with *in vitro* conditions (Meuter et al., 2014). Another marker of embryo senescence could be telomere length in the oocyte, which is negatively correlated with Day-3 human embryos fragmentation (Keefe et al., 2005). However, the use of such senescence markers entails embryo biopsy or destruction to perform Fluorescent *In Situ* Hybridization (FISH),

gene expression analysis or embryo staining. Therefore, novel markers and non-invasive methods to predict embryo senescence are still needed.

CONCLUSION AND FUTURE DIRECTIONS

Early embryo development represents a very delicate developmental window in which aberrant environmental conditions can easily lead to developmental failure or to long-term negative consequences in health. Due to the increasing use of reproductive technologies in cattle and to the similarities between bovine and human pre-implantation embryos, the bovine species has allowed us to explore many mechanisms involved in developmental failure during this period. However, despite the significant progress made in the field of assisted reproduction during the last decades, still more than 50% of IVP embryos do not reach the blastocyst stage. A high proportion of these embryos enter a state of permanent cell cycle arrest compatible with cellular senescence during the first cell divisions, not showing signs of apoptosis. This protective mechanism might prevent further development of abnormal embryos showing chromosomal anomalies (Almeida and Bolton, 1998) or failure to activate the embryonic genome (Artley et al., 1992), avoiding long-term effects on health and reproduction.

Later in development, after EGA, and mainly at the morula and blastocyst stages, apoptosis would mediate a controlled elimination of certain cells. Apoptosis would then fulfill two different roles: a physiological role maintaining an equilibrium between cell proliferation and death, and a prophylactic role preventing the transmission of damaged cells with an altered genome. This last role would acquire relevant importance in IVP embryos that are submitted to environmental stress, in which apoptosis incidence increases in comparison to IVD embryos. Thus, although later in development, an individual cell might be faced with apoptosis and senescence as alternative fates (Childs et al., 2014), senescence and apoptosis during pre-implantation development would be available during restricted time windows, acting as complementary processes to ensure that damaged cells/embryos do not progress in development.

Currently, common methods to assess apoptosis and senescence in the early embryo, such as immunocytochemistry, gene expression analyses or TUNEL and annexin V staining, are not adequate to evaluate the viability of the embryo before transfer due to their invasive nature. The identification of novel non-invasive markers for apoptosis or senescence remains a crucial goal, such as the analysis of compounds secreted to or taken up from the culture media by embryos, or the possibility of using cumulus cells to analyze the quality of the future embryo, since apoptotic signaling might be already triggered in the oocyte. In parallel, there are other RCD types, such as necroptosis, ferroptosis or cell death induced by the panoptosome, which remain to be explored in early embryos. We hypothesize that such RCD types can be susceptible to alteration in the context of specific traits of early embryonic cells and/or embryo cryopreservation.

Necroptosis is a type of RCD that can be activated through the death receptor pathway via FAS receptor and TNFR1 when caspase-8 lacks or becomes inactive (Shan et al., 2018). In this situation, receptor-interacting serine/threonine-protein kinase-1 (RIPK1) and -3 (RIPK3) activate a mixed lineage kinase domain-like pseudokinase (MLKL). At least in specific circumstances, RIPK1 could also behave as an inhibitor for RIPK3-dependent necroptosis and/or CASP8-dependent extrinsic apoptosis (Orozco et al., 2014). Elucidating these roles in bovine embryo development is challenging. Although necroptosis has not been specifically studied in the early embryo, studies performed by TUNEL alone could have identified a regulated common morphology of necrotic and apoptotic cells. Combining TUNEL staining with a caspase staining may allow such distinction.

Ferroptosis is also a form of RCD driven by iron-dependent lipid peroxidation. Peroxidation of phospholipids, which are integrated into cell membranes, triggers ferroptotic death (Stockwell et al., 2017). The oocyte could be an appropriate objective for ferroptosis damage because of its largest size among the body cells and the high mitochondrial endowment (100,000–300,000 mitochondria in the human gamete (Barritt et al., 2002; Cummins, 2004), which entails a considerable amount and extent of membranes containing the ferroptosis-target phospholipid able to be peroxidized. The mitochondrial numbers decrease with cleavage stages, but they remain higher than normal cells and restart replication in the human expanded blastocyst to reach the maximal counts (Hashimoto et al., 2017) comparable to adult somatic cells (between 80 and 2000 mitochondria per cell) (Cole, 2016). The expanded IVP blastocyst is a preferential stage for cryopreservation, and a ferroptosis target because of the high amount of mitochondrial membranes that can be damaged during cryopreservation.

Panoptosis has been recently described as a multifaceted cell-death signaling platform that integrates multiple cell death types as apoptosis, pyroptosis, and necroptosis which form the collective cell death pathway or PANoptosis (Samir et al., 2020). The PANoptosome drives an inflammatory form of cell death for immune-mediated protection. Modulation of inflammation and immune responses has been described as a strong need in the bovine uterus for embryos to progress in pregnancy (Munoz et al., 2012; Gomez et al., 2013), by which PANoptosis should be considered in future studies that lead to pregnancy establishment in cattle ET.

AUTHOR CONTRIBUTIONS

PR-I, IG, KC-B, AG-A, DR, and EG conducted literature review and wrote the manuscript. All authors contributed to the article and approved the submitted version.

FUNDING

This work was supported by the Spanish Ministry of Science and Innovation (AG-A: RTI2018-093548-B-I00; DR and KC-B:

PID2019-111641RB-I00). PR-I was funded by a Ramón y Cajal contract from MINECO (RYC2018-025666-I). IG was supported by MINECO BES-2017-082200. EG and IG were supported by the Spanish Ministry of Economy and Competitiveness (MINECO) projects AGL2016-78597R and AGL2016-81890-REDT and Fondo Europeo de Desarrollo Regional (FEDER).

REFERENCES

Acosta, J. C., Banito, A., Wuestefeld, T., Georgilis, A., Janich, P., Morton, J. P., et al. (2013). A complex secretory program orchestrated by the inflammasome controls paracrine senescence. *Nat. Cell Biol.* 15, 978-990.

Acosta, J. C., O'loghlen, A., Banito, A., Guijarro, M. V., Augert, A., Raguz, S., et al. (2008). Chemokine signaling via the CXCR2 receptor reinforces senescence. *Cell* 133, 1006–1018. doi: 10.1016/j.cell.2008.03.038

Adiga, S. K., Toyoshima, M., Shiraishi, K., Shimura, T., Takeda, J., Taga, M., et al. (2007). p21 provides stage specific DNA damage control to preimplantation embryos. *Oncogene* 26, 6141–6149. doi: 10.1038/sj.onc.1210444

Adona, P.R., Leal, C.L., Biase, F.H., De Bem, T.H., Mesquita, L.G., Meirelles, F.V., et al. (2016). In vitro maturation alters gene expression in bovine oocytes. *Zygote* 24, 624-633.

Aggarwal, B. B., Gupta, S. C., and Kim, J. H. (2012). Historical perspectives on tumor necrosis factor and its superfamily: 25 years later, a golden journey. *Blood* 119, 651–665. doi: 10.1182/blood-2011-04-325225

Almeida, P. A., and Bolton, V. N. (1998). Cytogenetic analysis of human preimplantation embryos following developmental arrest in vitro. *Reprod. Fertil. Dev.* 10, 505–513. doi: 10.1071/rd98040

Almiñana, C., and Bauersachs, S. (2019). Extracellular Vesicles in the Oviduct: Progress, Challenges and Implications for the Reproductive Success. *Bioengineering* 6:32. doi: 10.3390/bioengineering6020032

Alminana, C., Corbin, E., Tsikis, G., Alcantara-Neto, A. S., Labas, V., Reynaud, K., et al. (2017). Oviduct extracellular vesicles protein content and their role during oviduct-embryo cross-talk. *Reproduction* 154, 253–268. doi: 10.1530/rep-17-0054

Antczak, M., and Van Blerkom, J. (1999). Temporal and spatial aspects of fragmentation in early human embryos: possible effects on developmental competence and association with the differential elimination of regulatory proteins from polarized domains. *Hum. Reprod.* 14, 429–447. doi: 10.1093/humrep/14.2.429

Artley, J. K., Braude, P. R., and Johnson, M. H. (1992). Gene activity and cleavage arrest in human pre-embryos. *Hum. Reprod.* 7, 1014–1021. doi: 10.1093/oxfordjournals.humrep.a137761

Ata, B., Shalom-Paz, E., Chian, R.C., and Tan, S.L. (2010). In vitro maturation of oocytes as a strategy for fertility preservation. *Clin. Obstet Gynecol.* 53, 775-786.

Baar, M. P., Brandt, R. M. C., Putavet, D. A., Klein, J. D. D., Derks, K. W. J., Bourgeois, B. R. M., et al. (2017). Targeted apoptosis of senescent cells restores tissue homeostasis in response to chemotoxicity and aging. *Cell* 169:132. doi: 10.1016/j.cell.2017.02.031

Baker, D. J., Wijshake, T., Tchkonia, T., Lebrasseur, N. K., Childs, B. G., Van De Sluis, B., et al. (2011). Clearance of p16(Ink4a)-positive senescent cells delays ageing-associated disorders. *Nature* 479, 232-236.

Bakri, N. M., Ibrahim, S. F., Osman, N. A., Hasan, N., Jaffar, F. H., Rahman, Z. A., et al. (2016). Embryo apoptosis identification: Oocyte grade or cleavage stage? *Saudi J. Biol. Sci.* 23, S50-S55.

Barker, D. J. (2007). The origins of the developmental origins theory. *J. Intern. Med.* 261, 412–417. doi: 10.1111/j.1365-2796.2007.01809.x

Barritt, J. A., Kokot, M., Cohen, J., Steuerwald, N., and Brenner, C. A. (2002). Quantification of human ooplasmic mitochondria. *Reprod. Biomed. Online* 4, 243–247. doi: 10.1016/s1472-6483(10)61813-5

Bauersachs, S., Ulbrich, S. E., Gross, K., Schmidt, S. E. M., Meyer, H. H. D., Einspanier, R., et al. (2005). Gene expression profiling of bovine endometrium during the oestrous cycle: detection of molecular pathways involved in functional changes. *J. Mol. Endocrinol.* 34, 889–908. doi: 10.1677/jme.1.01799

Benhamed, M., Herbig, U., Ye, T., Dejean, A., and Bischof, O. (2012). Senescence is an endogenous trigger for microRNA-directed transcriptional gene silencing in human cells. *Nat. Cell Biol.* 14:266. doi: 10.1038/ncb2443

Bermejo-Alvarez, P., Roberts, R. M., and Rosenfeld, C. S. (2012). Effect of glucose concentration during in vitro culture of mouse embryos on development to blastocyst, success of embryo transfer, and litter sex ratio. *Mol. Reprod. Dev.* 79, 329–336. doi: 10.1002/mrd.22028

Betts, D. H., and King, W. A. (1999). Telomerase activity and telomere detection during early bovine development. *Dev. Genet.* 25, 397–403. doi: 10.1002/(sici)1520-6408(1999)25:4<397::aid-dvg13>3.0.co;2-j

Betts, D. H., and King, W. A. (2001). Genetic regulation of embryo death and senescence. *Theriogenology* 55, 171–191. doi: 10.1016/s0093-691x(00)00453-2

Betts, D. H., and Madan, P. (2008). Permanent embryo arrest: molecular and cellular concepts. *Mol. Hum. Reprod.* 14, 445–453. doi: 10.1093/molehr/gan035

Biswas, D., So, K. H., Hwang, S. U., Yoon, J. D., Kim, M., Kim, D. Y., et al. (2018). Embryotropic effects of vascular endothelial growth factor on porcine embryos produced by in vitro fertilization. *Theriogenology* 120, 147–156. doi: 10.1016/j.theriogenology.2018.07.024

Bittner, L., Wyck, S., Herrera, C., Siuda, M., Wrenzycki, C., Van Loon, B., et al. (2018). Negative effects of oxidative stress in bovine spermatozoa on in vitro development and DNA integrity of embryos. *Reprod. Fertil. Dev.* 30, 1359–1368. doi: 10.1071/rd17533

Block, J., Bonilla, L., and Hansen, P. J. (2010). Efficacy of in vitro embryo transfer in lactating dairy cows using fresh or vitrified embryos produced in a novel embryo culture medium. *J. Dairy Sci.* 93, 5234–5242. doi: 10.3168/jds.2010-3443

Brackett, B. G., Bousquet, D., Boice, M. L., Donawick, W. J., Evans, J. F., and Dressel, M. A. (1982). Normal development following in vitro fertilization in the cow. *Biol. Reprod.* 27, 147–158. doi: 10.1095/biolreprod27.1.147

Brad, A. M., Hendricks, K. E. M., and Hansen, P. J. (2007). The block to apoptosis in bovine two-cell embryos involves inhibition of caspase-9 activation and caspase-mediated DNA damage. *Reproduction* 134, 789–797. doi: 10.1530/rep-07-0146

Brenner, C. A., Wolny, Y. M., Adler, R. R., and Cohen, J. (1999). Alternative splicing of the telomerase catalytic subunit in human oocytes and embryos. *Mol. Hum. Reprod.* 5, 845–850. doi: 10.1093/molehr/5.9.845

Bunel, A., Jorssen, E. P., Merckx, E., Leroy, J. L., Bols, P. E., and Sirard, M. A. (2015). Individual bovine in vitro embryo production and cumulus cell transcriptomic analysis to distinguish cumulus-oocyte complexes with high or low developmental potential. *Theriogenology* 83, 228–237. doi: 10.1016/j.theriogenology.2014.09.019

Byrne, A. T., Southgate, J., Brison, D. R., and Leese, H. J. (1999). Analysis of apoptosis in the preimplantation bovine embryo using TUNEL. *J. Reprod. Fertil.* 117, 97–105. doi: 10.1530/jrf.0.1170097

Calle, A., Fernandez-Gonzalez, R., Ramos-Ibeas, P., Laguna-Barraza, R., Perez-Cerezales, S., Bermejo-Alvarez, P., et al. (2012). Long-term and transgenerational effects of in vitro culture on mouse embryos. *Theriogenology* 77, 785–793. doi: 10.1016/j.theriogenology.2011.07.016

Campisi, J. (2013). Aging, Cellular Senescence, and Cancer. *Annu. Rev. Physiol.* 75, 685–705.

Capalbo, A., Ubaldi, F. M., Cimadomo, D., Noli, L., Khalaf, Y., Farcomeni, A., et al. (2016). MicroRNAs in spent blastocyst culture medium are derived from trophectoderm cells and can be explored for human embryo reproductive competence assessment. *Fertil. Steril.* 105:225. doi: 10.1016/j.fertnstert.2015.09.014

Chang, H. Y., Chen, H. H., Zhang, L., Wang, Y. L., Xie, X. G., Zhang, Y., et al. (2019). Effect of oocyte vitrification on DNA damage in metaphase II oocytes and the resulting preimplantation embryos. *Mol. Reprod. Dev.* 86, 1603–1614. doi: 10.1002/mrd.23247

Chen, L., Wert, S. E., Hendrix, E. M., Russell, P. T., Cannon, M., and Larsen, W. J. (1990). Hyaluronic acid synthesis and gap junction endocytosis are necessary for normal expansion of the cumulus mass. *Mol. Reprod. Dev.* 26, 236–247. doi: 10.1002/mrd.1080260307

Chen, S., Einspanier, R., and Schoen, J. (2013). In vitro mimicking of estrous cycle stages in porcine oviduct epithelium cells: estradiol and progesterone regulate differentiation, gene expression, and cellular function. *Biol. Reprod.* 89:54.

Chen, S., Palma-Vera, S. E., Langhammer, M., Galuska, S. P., Braun, B. C., Krause, E., et al. (2017). An air-liquid interphase approach for modeling the early embryo-maternal contact zone. *Sci. Rep.* 7:42298.

Childs, B. G., Baker, D. J., Kirkland, J. L., Campisi, J., and Van Deursen, J. M. (2014). Senescence and apoptosis: dueling or complementary cell fates? *EMBO Rep.* 15, 1139–1153. doi: 10.15252/embr.201439245

Cole, L. W. (2016). The evolution of per-cell organelle number. *Front. Cell Dev. Biol.* 4:85. doi: 10.3389/fcell.2016.00085

Conradt, B. (2009). Genetic control of programmed cell death during animal development. *Annu. Rev. Genet.* 43, 493–523. doi: 10.1146/annurev.genet.42.110807.091533

Correia-Alvarez, E., Gomez, E., Martin, D., Carrocera, S., Perez, S., Otero, J., et al. (2015a). Expression and localization of interleukin 1 beta and interleukin 1 receptor (type I) in the bovine endometrium and embryo. *J. Reprod. Immunol.* 110, 1–13. doi: 10.1016/j.jri.2015.03.006

Correia-Alvarez, E., Gomez, E., Martin, D., Carrocera, S., Perez, S., Peynot, N., et al. (2015b). Early embryonic and endometrial regulation of tumor necrosis factor and tumor necrosis factor receptor 2 in the cattle uterus. *Theriogenology* 83, 1028–1037. doi: 10.1016/j.theriogenology.2014.12.007

Crowley, L. C., Marfell, B. J., Scott, A. P., and Waterhouse, N. J. (2016). Quantitation of Apoptosis and Necrosis by Annexin V Binding, Propidium Iodide Uptake, and Flow Cytometry. *Cold Spring Harb Protoc*. 11, 953–957.

Cummins, J. M. (2004). The role of mitochondria in the establishment of oocyte functional competence. *Eur. J. Obstet. Gynecol. Reprod. Biol.* 115(Suppl 1), S23-S29.

De Barros, F. R. O., and Paula-Lopes, F. F. (2018). Cellular and epigenetic changes induced by heat stress in bovine preimplantation embryos. *Mol. Reprod. Dev.* 85, 810–820. doi: 10.1002/mrd.23040

De Los Santos, M. J., Anderson, D. J., Racowsky, C., and Hill, J. A. (2000). Presence of Fas-Fas ligand system and bcl-2 gene products in cells and fluids from gonadotropin-stimulated human ovaries. *Biol. Reprod.* 63, 1811–1816. doi: 10.1095/biolreprod63.6.1811

Diamantis, A., Magiorkinis, E., Sakorafas, G. H., and Androutsos, G. (2008). A brief history of apoptosis: from ancient to modern times. *Onkologie* 31, 702–706. doi: 10.1159/000165071

Ealy, A. D., Drost, M., and Hansen, P. J. (1993). Developmental changes in embryonic resistance to adverse effects of maternal heat stress in cows. *J. Dairy Sci.* 76, 2899–2905. doi: 10.3168/jds.s0022-0302(93)77629-8

Eckert, J. J., Velazquez, M. A., and Fleming, T. P. (2015). Cell signalling during blastocyst morphogenesis. *Adv. Exp. Med. Biol.* 843, 1–21. doi: 10.1007/978-1-4939-2480-6_1

Egashira, A., Kano, K., and Naito, K. (2011). Preimplantation-embryo-specific cell-cycle regulation is attributable to a low expression of retinoblastoma protein rather than its phosphorylation. *J. Reprod. Dev.* 57, 492–499. doi: 10.1262/jrd.10-170o

El Hajj, N., and Haaf, T. (2013). Epigenetic disturbances in in vitro cultured gametes and embryos: implications for human assisted reproduction. *Fertil. Sterility* 99, 632–641. doi: 10.1016/j.fertnstert.2012.12.044

Eriksson, U. J., and Wentzel, P. (2016). The status of diabetic embryopathy. *Upsala J. Med. Sci.* 121, 96–112.

Eshre (2018). "ART Fact Sheet". Available online at: https://www.eshre.eu/Press-Room/Resources.aspx (accessed October 7, 2020).

Exley, G. E., Tang, C. Y., Mcelhinny, A. S., and Warner, C. M. (1999). Expression of caspase and BCL-2 apoptotic family members in mouse preimplantation embryos. *Biol. Reprod.* 61, 231–239. doi: 10.1095/biolreprod61.1.231

Fabian, D., Rehak, P., Czikkova, S., Il'kova, G., Baran, V., and Koppel, J. (2003). Induced cell death of preimplantation mouse embryos cultured in vitro evaluated by comet assay. *Theriogenology* 60, 691–706. doi: 10.1016/s0093-691x(03)00087-6

Favetta, L. A., Madan, P., Mastromonaco, G. F., St John, E. J., King, A., and Betts, D. H. C. (2007a). The oxidative stress adaptor p66Shc is required for permanent embryo arrest in vitro. *BMC Developmental Biology* 7:132. doi: 10.1186/1471-213X-7-132

Favetta, L. A., Robert, C., St John, E. J., Betts, D. H., and King, W. A. (2004). p66(shc), but not p53, is involved in early arrest of in vitro-produced bovine embryos. *Mol. Hum. Reprod.* 10, 383–392. doi: 10.1093/molehr/gah057

Favetta, L. A., St John, E. J., King, W. A., and Betts, D. H. (2007b). High levels of p66(shc) and intracellular ROS in permanently arrested early embryos. *Free Radic. Biol. Med.* 42, 1201–1210. doi: 10.1016/j.freeradbiomed.2007.01.018

Fear, J. M., and Hansen, P. J. (2011). Developmental changes in expression of genes involved in regulation of apoptosis in the bovine preimplantation embryo. *Biol. Reprod.* 84, 43–51. doi: 10.1095/biolreprod.110.086249

Ferraz, M., Henning, H. H. W., Costa, P. F., Malda, J., Melchels, F. P., Wubbolts, R., et al. (2017a). Improved bovine embryo production in an oviduct-on-a-chip system: prevention of poly-spermic fertilization and parthenogenic activation. *Lab. Chip* 17, 905–916. doi: 10.1039/c6lc01566b

Ferraz, M., Henning, H. H. W., Stout, T. A. E., Vos, P., and Gadella, B. M. (2017b). Designing 3-dimensional in vitro oviduct culture systems to study mammalian fertilization and embryo production. *Ann. Biomed. Eng* 45, 1731-1744.

Ferraz, M., Rho, H. S., Hemerich, D., Henning, H. H. W., Van Tol, H. T. A., Holker, M., et al. (2018). An oviduct-on-a-chip provides an enhanced in vitro environment for zygote genome reprogramming. *Nat. Commun.* 9:4934.

Fleming, T. P., Watkins, A. J., Sun, C., Velazquez, M. A., Smyth, N. R., and Eckert, J. J. (2015). Do little embryos make big decisions? How maternal dietary protein restriction can permanently change an embryo's potential, affecting adult health. *Reprod. Fertil. Dev.* 27, 684–692. doi: 10.1071/rd14455

Freund, A., Orjalo, A. V., Desprez, P. -Y., and Campisi, J. (2010). Inflammatory networks during cellular senescence: causes and consequences. *Trends Mol. Med.* 16, 238–246. doi: 10.1016/j.molmed.2010.03.003

Fuchs, Y., and Steller, H. (2011). Programmed cell death in animal development and disease. *Cell* 147, 742–758. doi: 10.1016/j.cell.2011.10.033

Gad, A., Hoelker, M., Besenfelder, U., Havlicek, V., Cinar, U., Rings, F., (2012). Molecular mechanisms and pathways involved in bovine embryonic genome activation and their regulation by alternative in vivo and in vitro culture conditions. *Biol. Reprod.* 87, 1–13. doi: 10.1095/biolreprod.112.099697

Galluzzi, L., Manuel Bravo-San Pedro, J., Kepp, O., and Kroemer, G. (2016). Regulated cell death and adaptive stress responses. *Cell. Mol. Life Sci.* 73, 2405–2410. doi: 10.1007/s00018-016-2209-y

Galluzzi, L., Vitale, I., Aaronson, S. A., Abrams, J. M., Adam, D., Agostinis, P., et al. (2018). Molecular mechanisms of cell death: recommendations of the nomenclature committee on cell death 2018. *Cell Death Differ.* 25, 486–541.

Gjorret, J. O., Fabian, D., Avery, B., and Maddox-Hyttel, P. (2007). Active caspase-3 and ultrastructural evidence of apoptosis in spontaneous and induced cell death in bovine in vitro produced pre-implantation embryos. *Mol. Reprod. Dev.* 74, 961–971. doi: 10.1002/mrd.20714

Gjorret, J. O., Knijn, H. M., Dieleman, S. J., Avery, B., Larsson, L. I., and Maddox-Hyttel, P. (2003). Chronology of apoptosis in bovine embryos produced in vivo and in vitro. *Biol. Reprod.* 69, 1193–1200. doi: 10.1095/biolreprod.102.013243

Gomez, E., Caamano, J. N., Corrales, F. J., Diez, C., Correia-Alvarez, E., Martin, D., et al. (2013). Embryonic sex induces differential expression of proteins in bovine uterine fluid. *J. Prot. Res.* 12, 1199–1210. doi: 10.1021/pr300845e

Gomez, E., Carrocera, S., Martin, D., Jose Perez-Janez, J., Prendes, J., Manuel Prendes, J., et al. (2020). Efficient one-step direct transfer to recipients of thawed bovine embryos cultured in vitro and frozen in chemically defined medium. *Theriogenology* 146, 39–47. doi: 10.1016/j.theriogenology.2020.01.056

Gomez, E., Correia-Alvarez, E., Caamano, J. N., Diez, C., Carrocera, S., Peynot, N., et al. (2014). Hepatoma-derived growth factor: from the bovine uterus to the in vitro embryo culture. *Reproduction* 148, 353–365. doi: 10.1530/rep-14-0304

Gomez, E., Rodriguez, A., Munoz, M., Nestor Caamano, J., Carrocera, S., Martin, D., et al. (2008). Development and quality of bovine morulae cultured in serum-free medium with specific retinoid receptor agonists. *Reprod. Fertil. Dev.* 20, 884–891. doi: 10.1071/rd08103

Gutierrez-Adan, A., Rizos, D., Fair, T., Moreira, P. N., Pintado, B., De La Fuente, J., et al. (2004). Effect of speed of development on mRNA expression pattern in early bovine embryos cultured in vivo or in vitro. *Mol. Reprod. Dev.* 68, 441–448. doi: 10.1002/mrd.20113

Haddock, L., Gordon, S., Lewis, S. E. M., Larsen, P., Shehata, A., and Shehata, H. (2020). Sperm DNA fragmentation is a novel biomarker for early pregnancy loss. *Reprod. Biomed. Online*.

Hansen, P. J. (2020). The incompletely fulfilled promise of embryo transfer in cattle-why aren't pregnancy rates greater and what can we do about it? *J. Anim. Sci.* 98:skaa288.

Hansen, P. J., Dobbs, K. B., Denicol, A. C., and Siqueira, L. G. B. (2016). Sex and the preimplantation embryo: implications of sexual dimorphism in the

preimplantation period for maternal programming of embryonic development. *Cell Tissue Res.* 363, 237–247. doi: 10.1007/s00441-015-2287-4

Hanshaw, R. G., Lakshmi, C., Lambert, T. N., Johnson, J. R., and Smith, B. D. (2005). Fluorescent detection of apoptotic cells by using zinc coordination complexes with a selective affinity for membrane surfaces enriched with phosphatidylserine. *Chembiochem* 6, 2214–2220. doi: 10.1002/cbic.200500149

Haouzi, D., and Hamamah, S. (2009). Pertinence of apoptosis markers for the improvement of in vitro fertilization (IVF). *Curr. Med. Chem.* 16, 1905-1916.

Hardy, K. (1997). Cell death in the mammalian blastocyst. *Mol. Hum. Reprod.* 3, 919–925. doi: 10.1093/molehr/3.10.919

Hardy, K. (1999). Apoptosis in the human embryo. *Rev. Reprod.* 4, 125–134. doi: 10.1530/revreprod/4.3.125

Hardy, K., Stark, J., and Winston, R. M. L. (2003). Maintenance of the inner cell mass in human blastocysts from fragmented embryos. *Biol. Reprod.* 68, 1165–1169. doi: 10.1095/biolreprod.102.010090

Hashimoto, S., Morimoto, N., Yamanaka, M., Matsumoto, H., Yamochi, T., Goto, H., et al. (2017). Quantitative and qualitative changes of mitochondria in human preimplantation embryos. *J. Assist. Reprod. Genet.* 34, 573–580. doi: 10.1007/s10815-017-0886-6

Hasler, J. F., Henderson, W. B., Hurtgen, P. J., Jin, Z. Q., Mccauley, A. D., Mower, S. A., et al. (1995). Production, freezing and transfer of bovine ivf embryos and subsequent calving results. *Theriogenology* 43, 141–152. doi: 10.1016/0093-691x(94)00020-u

Hayflick, L., and Moorhead, P. S. (1961). The serial cultivation of human diploid cell strains. *Exp. Cell Res.* 25, 585–621. doi: 10.1016/0014-4827(61)90192-6

He, H., Zhang, H., Li, Q., Fan, J., Pan, Y., Zhang, T., et al. (2020). Low oxygen concentrations improve yak oocyte maturation and enhance the developmental competence of preimplantation embryos. *Theriogenology* 156, 46–58. doi: 10.1016/j.theriogenology.2020.06.022

Heras, S., De Coninck, D. I., Van Poucke, M., Goossens, K., Bogado Pascottini, O., Van Nieuwerburgh, F., et al. (2016). Suboptimal culture conditions induce more deviations in gene expression in male than female bovine blastocysts. *BMC Genomics* 17:72. doi: 10.1186/s12864-016-2393-z

Hoshi, H. (2003). In vitro production of bovine embryos and their application for embryo transfer. *Theriogenology* 59, 675-685.

Huang, C. -H., and Chan, W. -H. (2017). Rhein induces oxidative stress and apoptosis in mouse blastocysts and has immunotoxic effects during embryonic development. *Int. J. Mol. Sci.* 18:2018. doi: 10.3390/ijms18092018

Huang, X. X., Tran, T., Zhang, L. N., Hatcher, R., and Zhang, P. M. (2005). DNA damage-induced mitotic catastrophe is mediated by the Chk1-dependent mitotic exit DNA damage checkpoint. *Proc. Natl. Acad. Sci. U.S.A.* 102, 1065–1070. doi: 10.1073/pnas.0409130102

Hviid, K. V. R., Malchau, S. S., Pinborg, A., and Nielsen, H. S. (2018). Determinants of monozygotic twinning in ART: a systematic review and a meta-analysis. *Hum. Reprod. Update* 24, 468–483. doi: 10.1093/humupd/dmy006

Ikeda, S., Prendes, J. M., Alonso-Montes, C., Rodriguez, A., Diez, C., Kitagawa, M., et al. (2006). Apoptosis-independent poor morphology of bovine embryos produced by multiple ovulation. *Reprod. Domestic Anim.* 41, 383–385. doi: 10.1111/j.1439-0531.2006.00672.x

Jimenez, A., Madrid-Bury, N., Fernandez, R., Perez-Garnelo, S., Moreira, P., Pintado, B., et al. (2003). Hyperglycemia-induced apoptosis affects sex ratio of bovine and murine preimplantation embryos. *Mol. Reprod. Dev.* 65, 180–187. doi: 10.1002/mrd.10286

Juan, H. C., Lin, Y., Chen, H. R., and Fann, M. J. (2016). Cdk12 is essential for embryonic development and the maintenance of genomic stability. *Cell Death Differ.* 23, 1038–1048. doi: 10.1038/cdd.2015.157

Jurisicova, A., Varmuza, S., and Casper, R. F. (1996). Programmed cell death and human embryo fragmentation. *Mol. Hum. Reprod.* 2, 93–98. doi: 10.1093/molehr/2.2.93

Kang, C., Xu, Q., Martin, T. D., Li, M. Z., Demaria, M., Aron, L., et al. (2015). The DNA damage response induces inflammation and senescence by inhibiting autophagy of GATA4. *Science* 349:aaa5612. doi: 10.1126/science.aaa5612

Kang, T. W., Yevsa, T., Woller, N., Hoenicke, L., Wuestefeld, T., Dauch, D., et al. (2011). Senescence surveillance of pre-malignant hepatocytes limits liver cancer development. *Nature* 479, 547–551. doi: 10.1038/nature10599

Kasum, M., Von Wolff, M., Franulić, D., Čehić, E., Klepac-Pulanić, T., Orešković, S., et al. (2015). Fertility preservation options in breast cancer patients. *Gynecol. Endocrinol.* 31, 846–851.

Katz-Jaffe, M. G., Mccallie, B. R., Preis, K. A., Filipovits, J., and Gardner, D. K. (2009). Transcriptome analysis of in vivo and in vitro matured bovine MII oocytes. *Theriogenology* 71, 939–946. doi: 10.1016/j.theriogenology.2008.10.024

Keefe, D. L., Franco, S., Liu, L., Trimarchi, J., Cao, B., Weitzen, S., et al. (2005). Telomere length predicts embryo fragmentation after in vitro fertilization in women - Toward a telomere theory of reproductive aging in women. *Am. J. Obstetr. Gynecol.* 192, 1256–1260. doi: 10.1016/j.ajog.2005.01.036

Khatun, H., Ihara, Y., Takakura, K., Egashira, J., Wada, Y., Konno, T., et al. (2020). Role of endoplasmic reticulum stress on developmental competency and cryo-tolerance in bovine embryos. *Theriogenology* 142, 131–137. doi: 10.1016/j.theriogenology.2019.09.042

Krisher, R. L., and Prather, R. S. (2012). A role for the Warburg effect in preimplantation embryo development: metabolic modification to support rapid cell proliferation. *Mol. Reprod. Dev.* 79, 311–320. doi: 10.1002/mrd.22037

Kucharova, M., Hronek, M., Rybakova, K., Zadak, Z., Stetina, R., Joskova, V., et al. (2019). Comet assay and its use for evaluating oxidative DNA damage in some pathological states. *Physiol. Res.* 68, 1–15. doi: 10.33549/physiolres.933901

Kuilman, T., Michaloglou, C., Mooi, W. J., and Peeper, D. S. (2010). The essence of senescence. *Genes Dev.* 24, 2463–2479. doi: 10.1101/gad.1971610

Kuilman, T., Michaloglou, C., Vredeveld, L. C. W., Douma, S., Van Doom, R., Desmet, C. J., et al. (2008). Oncogene-induced senescence relayed by an interleukin-dependent inflammatory network. *Cell* 133, 1019–1031. doi: 10.1016/j.cell.2008.03.039

Labrecque, R., Fournier, E., and Sirard, M. A. (2016). Transcriptome Analysis of Bovine Oocytes From Distinct Follicle Sizes: Insights From Correlation Network Analysis. *Mol. Reprod. Dev.* 83, 558–569. doi: 10.1002/mrd.22651

Laguna-Barraza, R., Bermejo-Alvarez, P., Ramos-Ibeas, P., De Frutos, C., Lopez-Cardona, A. P., Calle, A., et al. (2012). Sex-specific embryonic origin of postnatal phenotypic variability. *Reprod. Fertil. Dev.* 25, 38–47. doi: 10.1071/rd12262

Lazzari, G., Wrenzycki, C., Herrmann, D., Duchi, R., Kruip, T., Niemann, H., et al. (2002). Cellular and molecular deviations in bovine in vitro-produced embryos are related to the large offspring syndrome. *Biol. Reprod.* 67, 767–775. doi: 10.1095/biolreprod.102.004481

Ledgard, A. M., Berg, M. C., Mcmillan, W. H., Smolenski, G., and Peterson, A. J. (2012). Effect of asynchronous transfer on bovine embryonic development and relationship with early cycle uterine proteome profiles. *Reprod. Fertil. Dev.* 24, 962–972.

Leidenfrost, S., Boelhauve, M., Reichenbach, M., Guengoer, T., Reichenbach, H. -D., Sinowatz, F., et al. (2011). Cell arrest and cell death in mammalian preimplantation development: lessons from the bovine model. *PLoS One* 6:e22121. doi: 10.1371/journal.pone.0022121

Levanon, K., Ng, V., Piao, H. Y., Zhang, Y., Chang, M. C., Roh, M. H., et al. (2010). Primary ex vivo cultures of human fallopian tube epithelium as a model for serous ovarian carcinogenesis. *Oncogene* 29, 1103–1113. doi: 10.1038/onc.2009.402

Levy, R., Benchaib, M., Cordonier, H., Souchier, C., and Guerin, J. F. (1998). Annexin V labelling and terminal transferase-mediated DNA end labelling (TUNEL) assay in human arrested embryos. *Mol. Hum. Reprod.* 4, 775–783. doi: 10.1093/molehr/4.8.775

Li, J. C., Donath, S., Li, Y. R., Qin, D., Prabhakar, B. S., and Li, P. F. (2010). miR-30 Regulates mitochondrial fission through targeting p53 and the dynamin-related protein-1 pathway. *PLoS Genet.* 6:e1000795. doi: 10.1371/journal.pgen.1000795.

Lima, L., Tavares De Melo, T. C., Marques, D., Goes De Araujo, J. N., Fernandes Leite, I. S., Alves, C. X., et al. (2019). Modulation of all-trans retinoic acid-induced MiRNA expression in neoplastic cell lines: a systematic review. *BMC Cancer* 19:866. doi: 10.1186/s12885-019-6081-7.

Lin, X. Y., Beckers, E., Mc Cafferty, S., Gansemans, Y., Szymanska, K. J., Pavani, K. C., et al. (2019). Bovine embryo-secreted microRNA-30c is a potential non-invasive biomarker for hampered preimplantation developmental competence. *Front. Genet.* 10:315. doi: 10.3389/fgene.2019.00315

Liu, H. C., He, Z. Y., Mele, C. A., Veeck, L. L., Davis, O., and Rosenwaks, Z. C. P. (2000). Expression of apoptosis-related genes in human oocytes and embryos. *J. Assist. Reprod. Genet.* 17, 521–533.

Lonergan, P. (2007). State-of-the-art embryo technologies in cattle. *Soc. Reprod. Fertil. Suppl.* 64, 315–325. doi: 10.5661/rdr-vi-315

Lonergan, P., and Fair, T. (2016). Maturation of Oocytes in Vitro. *Annu. Rev. Anim. Biosci.* 4, 255–268.

Lonergan, P., Rizos, D., Gutiérrez-Adán, A., Fair, T., and Boland, M. P. (2003). Effect of culture environment on embryo quality and gene expression - experience from animal studies. *Reprod. Biomed. Online* 7, 657–663. doi: 10.1016/s1472-6483(10)62088-3

Loo, D.T. (2011). In situ detection of apoptosis by the TUNEL assay: an overview of techniques. *Methods Prot.* 682, 3-13.

Looney, C. R., Lindsey, B. R., Gonseth, C. L., and Johnson, D. L. (1994). Commercial aspects of oocyte retrieval and in-vitro fertilization (ivf) for embryo production in problem cows. *Theriogenology* 41, 67–72. doi: 10.1016/s0093-691x(05)80050-0

Lopera-Vasquez, R., Hamdi, M., Maillo, V., Lloreda, V., Coy, P., Gutierrez-Adan, A., et al. (2017). Effect of bovine oviductal fluid on development and quality of bovine embryos produced in vitro. *Reprod. Fertil. Dev.* 29, 621–629. doi: 10.1071/rd15238

Lopez-Otin, C., Blasco, M. A., Partridge, L., Serrano, M., and Kroemer, G. (2013). The hallmarks of aging. *Cell* 153, 1194–1217.

Lorda-Diez, C. I., Solis-Mancilla, M. E., Sanchez-Fernandez, C., Garcia-Porrero, J. A., Hurle, J. M., and Montero, J. A. (2019). Cell senescence, apoptosis and DNA damage cooperate in the remodeling processes accounting for heart morphogenesis. *J.Anat.* 234, 815–829. doi: 10.1111/joa.12972

Lozono-Torres, B., Estepa-Fernandez, A., Rovira, M., Orzaez, M., Serrano, M., Martinez-Manez, R., et al. (2019). The chemistry of senescence. *Nat. Rev. Chem.* 3, 426–441.

Luo, D., Zhang, J. -B., Liu, W., Yao, X. -R., Guo, H., Jin, Z. L., et al. (2020). Leonurine improves invitro porcine embryo development competence by reducing reactive oxygen species production and protecting mitochondrial function. *Theriogenology* 156, 116–123. doi: 10.1016/j.theriogenology.2020.06.038

Madrid Gaviria, S., Lopez Herrera, A., Urrego, R., Restrepo Betancur, G., and Echeverri Zuluaga, J. J. (2019). Effect of resveratrol on vitrified in vitro produced bovine embryos: recovering the initial quality. *Cryobiology* 89, 42–50. doi: 10.1016/j.cryobiol.2019.05.008

Makri, D., Efstathiou, P., Michailidou, E., and Maalouf, W. E. (2020). Apoptosis triggers the release of microRNA miR-294 in spent culture media of blastocysts. *J. Assist. Reprod. Genet.* 37, 1685–1694. doi: 10.1007/s10815-020-01796-5

Marei, W. F. A., Alvarez, M. A., Van Hoeck, V., Gutierrez-Adan, A., Bols, P. E. J., and Leroy, J. L. M. R. (2017). Effect of nutritionally induced hyperlipidaemia on in vitro bovine embryo quality depends on the type of major fatty acid in the diet. *Reprod. Fertil. Dev.* 29, 1856–1867. doi: 10.1071/rd16297

Martinez-Zamudio, R. I., Robinson, L., Roux, P. -F., and Bischof, O. (2017). SnapShot: cellular senescence pathways. *Cell* 170:816.e811.

Mateusen, B., Van Soom, A., Maes, D. G. D., Donnay, I., Duchateau, L., and Lequarre, A. S. (2005). Porcine embryo development and fragmentation and their relation to apoptotic markers: a cinematographic and confocal laser scanning microscopic study. *Reproduction* 129, 443–452. doi: 10.1530/rep.1.00533

Matwee, C., Betts, D. H., and King, W. A. (2000). Apoptosis in the early bovine embryo. *Zygote* 8, 57–68. doi: 10.1017/s0967199400000836

Melka, M.G., Rings, F., Hoelker, M., Tholen, E., Havlicek, V., Besenfelder, U., et al. (2010). Expression of apoptosis regulatory genes and incidence of apoptosis in different morphological quality groups of in vitro-produced bovine pre-implantation embryos. *Reprod. Domestic Anim.* 45, 915-921.

Ménézo, Y. J., and Sakkas, D. (2002). Monozygotic twinning: is it related to apoptosis in the embryo? *Hum. Reprod.* 17, 247–248. doi: 10.1093/humrep/17.1.247

Metcalfe, A. D., Hunter, H. R., Bloor, D. J., Lieberman, B. A., Picton, H. M., Leese, H. J., et al. (2004). Expression of 11 members of the BCL-2 family of apoptosis regulatory molecules during human preimplantation embryo development and fragmentation. *Mol. Reprod. Dev.* 68, 35–50. doi: 10.1002/mrd.20055

Meuter, A., Rogmann, L. M., Winterhoff, B. J., Tchkonia, T., Kirkland, J. L., and Morbeck, D. E. (2014). Markers of cellular senescence are elevated in murine blastocysts cultured in vitro: molecular consequences of culture in atmospheric oxygen. *J. Assist. Reprod. Genet.* 31, 1259–1267. doi: 10.1007/s10815-014-0299-8

Morley, N., Rapp, A., Dittmar, H., Salter, L., Gould, D., Greulich, K. O., et al. (2006). UVA-induced apoptosis studied by the new apo/necro-Comet-assay which distinguishes viable, apoptotic and necrotic cells. *Mutagenesis* 21, 105–114. doi: 10.1093/mutage/gel004

Munoz, M., Corrales, F. J., Caamano, J. N., Diez, C., Trigal, B., Mora, M. I., et al. (2012). Proteome of the Early Embryo-Maternal Dialogue in the Cattle Uterus. *J. Prot. Res.* 11, 751–766. doi: 10.1021/pr200969a

Munoz, M., Gatien, J., Salvetti, P., Martin-Gonzalez, D., Carrocera, S., and Gomez, E. (2020). Nuclear magnetic resonance analysis of female and male pre-hatching embryo metabolites at the embryo-maternal interface. *Metabolomics* 16:47

Munoz, M., Uyar, A., Correia, E., Ponsart, C., Guyader-Joly, C., Martinez-Bello, D., et al. (2014). Metabolomic Prediction of Pregnancy Viability in Superovulated Cattle Embryos and Recipients with Fourier Transform Infrared Spectroscopy. *Biomed. Res. Int.* 2014:608579

Munoz-Espin, D., Canamero, M., Maraver, A., Gomez-Lopez, G., Contreras, J., Murillo-Cuesta, S., et al. (2013). Programmed cell senescence during mammalian embryonic development. *Cell* 155, 1104–1118. doi: 10.1016/j.cell.2013.10.019

Murillo, A., Muñoz, M., Martín-González, D., Carrocera, S., Martínez-Nistal, A., and Gómez, E. (2017). Low serum concentration in bovine embryo culture enhances early blastocyst rates on Day-6 with quality traits in the expanded blastocyst stage similar to BSA-cultured embryos. *Reprod. Biol.* 17, 162–171. doi: 10.1016/j.repbio.2017.04.002

Murillo-Rios, A., Maillo, V., Munoz, M., Gutierrez-Adan, A., Carrocera, S., Martin-Gonzalez, D., et al. (2017). Short- and long-term outcomes of the absence of protein during bovine blastocyst formation in vitro. *Reprod. Fertil. Dev.* 29, 1064–1073. doi: 10.1071/rd15485

Nagano, M. (2019). Acquisition of developmental competence and in vitro growth culture of bovine oocytes. *J. Reprod. Dev.* 65, 195–201. doi: 10.1262/jrd.2019-022

Nguyen-Chi, M., Laplace-Builhe, B., Travnickova, J., Luz-Crawford, P., Tejedor, G., Lutfalla, G., et al. (2017). TNF signaling and macrophages govern fin regeneration in zebrafish larvae. *Cell Death Dis.* 8:e2979. doi: 10.1038/cddis.2017.374

Ock, S. A., Knott, J. G., and Choi, I. (2020). Involvement of CDKN1A (p21) in cellular senescence in response to heat and irradiation stress during preimplantation development. *Cell Stress Chaperones* 25, 503–508. doi: 10.1007/s12192-020-01090-4

Oliveira, C. S., Saraiva, N. Z., De Lima, M. R., Oliveira, L. Z., Serapiao, R. V., Garcia, J. M., et al. (2016). Cell death is involved in sexual dimorphism during preimplantation development. *Mech. Dev.* 139, 42–50. doi: 10.1016/j.mod.2015.12.001

Orozco, S., Yatim, N., Werner, M. R., Tran, H., Gunja, S. Y., Tait, S. W., et al. (2014). RIPK1 both positively and negatively regulates RIPK3 oligomerization and necroptosis. *Cell Death Differ.* 21, 1511–1521. doi: 10.1038/cdd.2014.76

Paula, L. A. D. C. E., and Hansen, P. J. (2008). Ceramide inhibits development and cytokinesis and induces apoptosis in preimplantation bovine embryos. *Mol. Reprod. Dev.* 75, 1063–1070. doi: 10.1002/mrd.20841

Paula-Lopes, F. F., and Hansen, P. J. (2002). Heat shock-induced apoptosis in preimplantation bovine embryos is a developmentally regulated phenomenon. *Biol. Reprod.* 66, 1169–1177. doi: 10.1093/biolreprod/66.4.1169

Pavlok, A., Lucas-Hahn, A., and Niemann, H. (1992). Fertilization and developmental competence of bovine oocytes derived from different categories of antral follicles. *Mol. Reprod. Dev.* 31, 63–67. doi: 10.1002/mrd.1080310111

Payne, D., Okuda, A., Wakatsuki, Y., Takeshita, C., Iwata, K., Shimura, T., et al. (2007). Time-lapse recording identifies human blastocysts at risk of producing monzygotic twins. *Hum. Reprod.* 22, I9-I10.

Plante, L., and King, W. A. (1994). Light and electron-microscopic analysis of bovine embryos derived by in-vitro and in-vivo fertilization. *J. Assist. Reprod. Genet.* 11, 515–529. doi: 10.1007/bf02216032

Pomar, F. J. R., Roelen, B. A. J., Slot, K. A., Van Tol, H. T. A., Colenbrander, B., and Teerds, K. J. (2004). Role of Fas-mediated apoptosis and follicle-stimulating hormone on the developmental capacity of bovine cumulus oocyte complexes in vitro. *Biol. Reprod.* 71, 790–796. doi: 10.1095/biolreprod.104.028613

Pomar, F. J. R., Teerds, K. J., Kidson, A., Colenbrander, B., Tharasanit, T., Aguilar, B., et al. (2005). Differences in the incidence of apoptosis between in vivo and in vitro produced blastocysts of farm animal species: a comparative

study. *Theriogenology* 63, 2254–2268. doi: 10.1016/j.theriogenology.2004.10.015

Prastowo, S., Amin, A., Rings, F., Held, E., Wondim, D. S., Gad, A., et al. (2016). Fateful triad of reactive oxygen species, mitochondrial dysfunction and lipid accumulation is associated with expression outline of the AMP-activated protein kinase pathway in bovine blastocysts. *Reprod. Fertil. Dev*. doi: 10.1071/RD15319 [Epub ahead of Print].

Qiao, F., Ge, H., Ma, X. N., Zhang, Y., Zuo, Z. Z., Wang, M. Y., et al. (2018). Bovine uterus-derived exosomes improve developmental competence of somatic cell nuclear transfer embryos. *Theriogenology* 114, 199–205. doi: 10.1016/j.theriogenology.2018.03.027

Qu, P. X., Zhao, Y. L., Wang, R., Zhang, Y. L., Li, L., Fan, J. L., et al. (2019). Extracellular vesicles derived from donor oviduct fluid improved birth rates after embryo transfer in mice. *Reprod. Fertil. Dev*. 31, 324–332. doi: 10.1071/rd18203

Ramos-Ibeas, P., Heras, S., Gómez-Redondo, I., Planells, B., Fernández-González, R., Pericuesta, E., et al. (2019). Embryo responses to stress induced by assisted reproductive technologies. *Mol. Reprod. Dev*. 86, 1292–1306.

Randi, F., Fernandez-Fuertes, B., Mcdonald, M., Forde, N., Kelly, A. K., Amorin, H. B., et al. (2016). Asynchronous embryo transfer as a tool to understand embryo-uterine interaction in cattle: is a large conceptus a good thing? *Reprod. Fertil. Dev*. 28, 1999–2006. doi: 10.1071/rd15195

Regassa, A., Rings, F., Hoelker, M., Cinar, U., Tholen, E., Looft, C., et al. (2011). Transcriptome dynamics and molecular cross-talk between bovine oocyte and its companion cumulus cells. *BMC Genomics* 12:57. doi: 10.1186/1471-2164-12-57

Reik, W., Dean, W., and Walter, J. (2001). Epigenetic reprogramming in mammalian development. *Science* 293, 1089–1093. doi: 10.1126/science.1063443

Rhinn, M., Ritschka, B., and Keyes, W. M. (2019). Cellular senescence in development, regeneration and disease. *Development* 146:dev151837. doi: 10.1242/dev.151837

Ritschka, B., Storer, M., Mas, A., Heinzmann, F., Ortells, M. C., Morton, J. P., et al. (2017). The senescence-associated secretory phenotype induces cellular plasticity and tissue regeneration. *Genes Dev.* 31, 172–183. doi: 10.1101/gad.290635.116

Rizos, D., Gutierrez-Adan, A., Perez-Garnelo, S., De La Fuente, J., Boland, M. P., and Lonergan, P. (2003). Bovine embryo culture in the presence or absence of serum: Implications for blastocyst development, cryotolerance, and messenger RNA expression. *Biol. Reprod.* 68, 236–243. doi: 10.1095/biolreprod.102.007799

Rizos, D., Maillo, V., Sanchez-Calabuig, M. J., and Lonergan, P. (2017). The Consequences of Maternal-Embryonic Cross Talk During the Periconception Period on Subsequent Embryonic Development. *Adv. Exp. Med. Biol.* 1014, 69–86. doi: 10.1007/978-3-319-62414-3_4

Rizos, D., Pintado, B., De La Fuente, J., Lonergan, P., and Gutiérrez-Adán, A. (2007). Development and pattern of mRNA relative abundance of bovine embryos cultured in the isolated mouse oviduct in organ culture. *Mol. Reprod. Dev.* 74, 716–723. doi: 10.1002/mrd.20652

Rizos, D., Ward, F., Duffy, P., Boland, M. P., and Lonergan, P. (2002). Consequences of bovine oocyte maturation, fertilization or early embryo development in vitro versus in vivo: implications for blastocyst yield and blastocyst quality. *Mol. Reprod. Dev.* 61, 234–248. doi: 10.1002/mrd.1153

Rodriguez, A., Diez, C., Caamano, J. N., De Frutos, C., Royo, L. J., Munoz, M., et al. (2007). Retinoid receptor-specific agonists regulate bovine in vitro early embryonic development, differentiation and expression of genes related to cell cycle arrest and apoptosis. *Theriogenology* 68, 1118–1127. doi: 10.1016/j.theriogenology.2007.08.007

Rodriguez, A., Diez, C., Ikeda, S., Royo, L. J., Caamano, J. N., Alonso-Montes, C., et al. (2006). Retinoids during the in vitro transition from bovine morula to blastocyst. *Hum. Reprod.* 21, 2149–2157. doi: 10.1093/humrep/del099

Rodriguez-Alonso, B., Sanchez, J. M., Gonzalez, E., Lonergan, P., and Rizos, D. (2020). Challenges in studying preimplantation embryo-maternal interaction in cattle. *Theriogenology* 150, 139–149. doi: 10.1016/j.theriogenology.2020.01.019

Rolland, L., Courbiere, B., Tassistro, V., Sansoni, A., Orsiere, T., Liu, W., et al. (2017). Comet assay on thawed embryos: an optimized technique to evaluate DNA damage in mouse embryos. *Toxicol. Vitro* 44, 266–272. doi: 10.1016/j.tiv.2017.07.010

Sagiv, A., Burton, D. G. A., Moshayev, Z., Vadai, E., Wensveen, F., Ben-Dor, S., et al. (2016). NKG2D ligands mediate immunosurveillance of senescent cells. *Aging Us* 8, 328–344. doi: 10.18632/aging.100897

Salilew-Wondim, D., Fournier, E., Hoelker, M., Saeed-Zidane, M., Tholen, E., Looft, C., et al. (2015). Genome-wide DNA methylation patterns of bovine blastocysts developed in vivo from embryos completed different stages of development in vitro. *PLoS One* 10:e0140467. doi: 10.1371/journal.pone.0140467

Salilew-Wondim, D., Saeed-Zidane, M., Hoelker, M., Gebremedhn, S., Poirier, M., Pandey, H. O., et al. (2018). Genome-wide DNA methylation patterns of bovine blastocysts derived from in vivo embryos subjected to in vitro culture before, during or after embryonic genome activation. *BMC Genomics* 19:424. doi: 10.1186/s12864-018-4826-3

Samir, P., Malireddi, R. K. S., and Kanneganti, T. D. (2020). The PANoptosome: A Deadly Protein Complex Driving Pyroptosis, Apoptosis, and Necroptosis (PANoptosis). *Front. Cell Infect. Microbiol.* 10:238. doi: 10.3389/fcimb.2020.00238

Sato, E. (1998). Morphological dynamics of cumulus-oocyte complex during oocyte maturation. *New Trends Microanat. Reprod.* 6, 103–118.

Sauerbrun-Cutler, M.T., Vega, M., Keltz, M., and Mcgovern, P.G. (2015). In vitro maturation and its role in clinical assisted reproductive technology. *Obstet. Gynecol. Surv.* 70, 45-57.

Schmaltz-Panneau, B., Cordova, A., Dhorne-Pollet, S., Hennequet-Antier, C., Uzbekova, S., Martinot, E., et al. (2014). Early bovine embryos regulate oviduct epithelial cell gene expression during in vitro co-culture. *Anim,. Reprod. Sci.* 149, 103–116. doi: 10.1016/j.anireprosci.2014.06.022

Shalom-Paz, E., Almog, B., Shehata, F., Huang, J., Holzer, H., Chian, R. C., et al. (2010). Fertility preservation for breast-cancer patients using IVM followed by oocyte or embryo vitrification. *Reprod. Biomed. Online* 21, 566–571. doi: 10.1016/j.rbmo.2010.05.003

Shan, B., Pan, H., Najafov, A., and Yuan, J. (2018). Necroptosis in development and diseases. *Genes Dev.* 32, 327–340. doi: 10.1101/gad.312561.118

Shen, X.H., Han, Y.J., Yang, B.C., Cui, X.S., and Kim, N.H. (2009). Hyperglycemia reduces mitochondrial content and glucose transporter expression in mouse embryos developing in vitro. *J. Reprod. Dev.* 55, 534-541.

Shirasawa, H., and Terada, Y. (2017). In vitro maturation of human immature oocytes for fertility preservation and research material. *Reprod. Med. Biol.* 16, 258-267.

Shub, A., and Lappas, M. (2020). Pregestational diabetes in pregnancy: Complications, management, surveillance, and mechanisms of disease-A review. *Prenatal Diag.* 40, 1092–1098. doi: 10.1002/pd.5718

Singla, S., Iwamoto-Stohl, L. K., Zhu, M., and Zernicka-Goetz, M. (2020). Autophagy-mediated apoptosis eliminates aneuploid cells in a mouse model of chromosome mosaicism. *Nat. Commun.* 11:2958.

Sirard, M. A. (2018). 40 years of bovine IVF in the new genomic selection context. *Reproduction* 156, R1-R7.

Sjöblom, C., Wikland, M., and Robertson, S. A. (2002). Granulocyte-macrophage colony-stimulating factor (GM-CSF) acts independently of the beta common subunit of the GM-CSF receptor to prevent inner cell mass apoptosis in human embryos. *Biol. Reprod.* 67, 1817–1823. doi: 10.1095/biolreprod.101.001503

Steptoe, P. C., and Edwards, R. G. (1978). Birth after the reimplantation of a human embryo. *Lancet* 2:366. doi: 10.1016/s0140-6736(78)92957-4

Stewart, B. M., Block, J., Morelli, P., Navarette, A. E., Amstalden, M., Bonilla, L., et al. (2011). Efficacy of embryo transfer in lactating dairy cows during summer using fresh or vitrified embryos produced in vitro with sex-sorted semen. *J. Dairy Sci.* 94, 3437–3445. doi: 10.3168/jds.2010-4008

Stockwell, B. R., Friedmann Angeli, J. P., Bayir, H., Bush, A. I., Conrad, M., Dixon, S. J., et al. (2017). Ferroptosis: a regulated cell death nexus linking metabolism, redox biology, and disease. *Cell* 171, 273–285. doi: 10.1016/j.cell.2017.09.021

Storer, M., Mas, A., Robert-Moreno, A., Pecoraro, M., Ortells, M. C., Di Giacomo, V., et al. (2013). Senescence is a developmental mechanism that contributes to embryonic growth and patterning. *Cell* 155, 1119–1130. doi: 10.1016/j.cell.2013.10.041

Sturmey, R. G., Bermejo-Alvarez, P., Gutierrez-Adan, A., Rizos, D., Leese, H. J., and Lonergan, P. (2010). Amino acid metabolism of bovine blastocysts: a biomarker of sex and viability. *Mol. Reprod. Dev.* 77, 285–296. doi: 10.1002/mrd.21145

Sudano, M. J., Paschoal, D. M., Rascado, T. D., Crocomo, L. F., Magalhaes, L. C. O., Martins, A., et al. (2014). Crucial surviving aspects for vitrified in vitro-produced bovine embryos. *Zygote* 22, 124–131. doi: 10.1017/s0967199412000196

Tarín, J. J., Pérez-Albalá, S., and Cano, A. (2000). Consequences on offspring of abnormal function in ageing gametes. *Hum. Reprod. Update* 6, 532–549. doi: 10.1093/humupd/6.6.532

Tatemoto, H., Sakurai, N., and Muto, N. (2000). Protection of porcine oocytes against apoptotic cell death caused by oxidative stress during in vitro maturation: Role of cumulus cells. *Biol. Reprod.* 63, 805–810. doi: 10.1095/biolreprod63.3.805

Tauwinklova, G., Gaillyova, R., Travnik, P., Oracova, E., Vesela, K., Hromadova, L., et al. (2010). Monozygotic twins with discordant karyotypes following preimplantation genetic screening and single embryo transfer: case report. *J. Assist. Reprod. Genet.* 27, 649–655. doi: 10.1007/s10815-010-9462-z

Tesfaye, D., Ghanem, N., Carter, F., Fair, T., Sirard, M. A., Hoelker, M., et al. (2009). Gene expression profile of cumulus cells derived from cumulus-oocyte complexes matured either in vivo or in vitro. *Reprod. Fertil. Dev.* 21, 451–461. doi: 10.1071/rd08190

Tesfaye, D., Lonergan, P., Hoelker, M., Rings, F., Nganvongpanit, K., Havlicek, V., et al. (2007). Suppression of connexin 43 and E-cadherin transcripts in in vitro derived bovine embryos following culture in vitro or in vivo in the homologous bovine oviduct. *Mol. Reprod. Dev.* 74, 978–988. doi: 10.1002/mrd.20678

Trigal, B., Gomez, E., Diez, C., Caamano, J.N., Martin, D., Carrocera, S., et al. (2011). In vitro development of bovine embryos cultured with activin A. *Theriogenology* 75, 584-588.

Uhde, K., Van Tol, H. T. A., Stout, T. A. E., and Roelen, B. A. J. (2018). Exposure to elevated glucose concentrations alters the metabolomic profile of bovine blastocysts. *PLos One* 13:e0199310. doi: 10.1371/journal.pone.0199310

Urrego, R., Rodriguez-Osorio, N., and Niemann, H. (2014). Epigenetic disorders and altered gene expression after use of Assisted Reproductive Technologies in domestic cattle. *Epigenetics* 9, 803–815. doi: 10.4161/epi.28711

Van Blerkom, J. (2004). Mitochondria in human oogenesis and preimplantation embryogenesis: engines of metabolism, ionic regulation and developmental competence. *Reproduction* 128, 269–280. doi: 10.1530/rep.1.00240

Van Eetvelde, M., Heras, S., Leroy, J. L. M. R., Van Soom, A., and Opsomer, G. (2017). The Importance of the Periconception Period: Immediate Effects in Cattle Breeding and in Assisted Reproduction Such as Artificial Insemination and Embryo Transfer. *Adv. Exp. Med. Biol.* 1014, 41–68. doi: 10.1007/978-3-319-62414-3_3

Van Hoeck, V., Sturmey, R. G., Bermejo-Alvarez, P., Rizos, D., Gutierrez-Adan, A., Leese, H. J., et al. (2011). Elevated non-esterified fatty acid concentrations during bovine oocyte maturation compromise early embryo physiology. *PLoS One* 6:e23183. doi: 10.1371/journal.pone.0023183

Vandaele, L., and Van Soom, A. (2011). Intrinsic factors affecting apoptosis in bovine in vitro produced embryos. *Verhandelingen - Koninklijke Academie voor Geneeskunde van Belgie* 73, 79–104.

Velez-Pardo, C., Morales, A. T., Del Rio, M. J., and Olivera-Angel, M. (2007). Endogenously generated hydrogen peroxide induces apoptosis via mitochondrial damage independent of NF-kappa B and p53 activation in bovine embryos. *Theriogenology* 67, 1285–1296. doi: 10.1016/j.theriogenology.2007.01.018

Viana, J. (2019). "Embryo Technology Newsletter". *Int. Trans. Soc.* 37, 7–25.

Von Karstedt, S., Montinaro, A., and Walczak, H. (2017). Exploring the TRAILs less travelled: TRAIL in cancer biology and therapy. *Nat. Rev. Cancer* 17, 352–366. doi: 10.1038/nrc.2017.28

Voss, A. K., and Strasser, A. (2020). The essentials of developmental apoptosis. *F1000Research* 9, 1–12.

Wajant, H. (2002). The Fas signaling pathway: more than a paradigm. *Science* 296, 1635–1636. doi: 10.1126/science.1071553

Wang, A. S., and Dreesen, O. (2018). Biomarkers of cellular senescence and skin aging. *Front. Genet.* 9:247. doi: 10.3389/fgene.2018.00247

Wang, D., Liu, Y., Zhang, R., Zhang, F., Sui, W., Chen, L., et al. (2016). Apoptotic transition of senescent cells accompanied with mitochondrial hyper-function. *Oncotarget* 7, 28286–28300.

Wang, M., Gao, Y., Qu, P., Qing, S., Qiao, F., Zhang, Y., et al. (2017). Sperm-borne miR-449b influences cleavage, epigenetic reprogramming and apoptosis of SCNT embryos in bovine. *Sci. Rep.* 7:13403.

Warzych, E., Peippo, J., Szydlowski, M., and Lechniak, D. (2007). Supplements to in vitro maturation media affect the production of bovine blastocysts and their apoptotic index but not the proportions of matured and apoptotic oocytes. *Anim. Reprod. Sci.* 97, 334–343. doi: 10.1016/j.anireprosci.2006.01.011

Wrenzycki, C. (2018). Gene expression analysis and in vitro production procedures for bovine preimplantation embryos: Past highlights, present concepts and future prospects. *Reprod. Domestic Anim.* 53, 14–19. doi: 10.1111/rda.13260

Wrenzycki, C., Herrmann, D., Lucas-Hahn, A., Korsawe, K., Lemme, E., and Niemann, H. (2005). Addition to methods used already, such asMessenger RNA expression patterns in bovine embryos derived from in vitro procedures and their implications for development. *Reprod. Fertil. Dev.* 17, 23–35. doi: 10.1071/rd04109

Yang, M. Y., and Rajamahendran, R. C. P. S. (2002). Expression of Bcl-2 and Bax proteins in relation to quality of bovine oocytes and embryos produced in vitro. *Anim. Reprod. Sci.* 70, 159–169. doi: 10.1016/s0378-4320(01)00186-5

Yoon, S. B., Choi, S. A., Sim, B. W., Kim, J. S., Mun, S. E., Jeong, P. S., et al. (2014). Developmental Competence of Bovine Early Embryos Depends on the Coupled Response Between Oxidative and Endoplasmic Reticulum Stress. *Biol. Reprod.* 90:104.

Young, L. E., Sinclair, K. D., and Wilmut, I. (1998). Large offspring syndrome in cattle and sheep. *Rev. Reprod.* 3, 155–163. doi: 10.1530/revreprod/3.3.155

Zuo, Z., Niu, Z., Liu, Z., Ma, J., Qu, P., Qiao, F., et al. (2020). The effects of glycine-glutamine dipeptide replaced L-glutamine on bovine parthenogenetic and IVF embryo development. *Theriogenology* 141, 82–90. doi: 10.1016/j.theriogenology.2019.09.005

Conflict of Interest: The authors declare that the research was conducted in the absence of any commercial or financial relationships that could be construed as a potential conflict of interest.

frontiers in Cell and Developmental Biology

ORIGINAL RESEARCH
published: 05 January 2021
doi: 10.3389/fcell.2020.616801

Cellular Fragments in the Perivitelline Space Are Not a Predictor of Expanded Blastocyst Quality

Bo Yu[1], *Helena T. A. van Tol*[1], *Tom A. E. Stout*[2] *and Bernard A. J. Roelen*[3]*

[1] *Farm Animal Health, Department of Population Health Sciences, Faculty of Veterinary Medicine, Utrecht University, Utrecht, Netherlands,* [2] *Equine Sciences, Department Clinical Sciences, Faculty of Veterinary Medicine, Utrecht University, Utrecht, Netherlands,* [3] *Embryology, Anatomy and Physiology, Department Clinical Sciences, Faculty of Veterinary Medicine, Utrecht University, Utrecht, Netherlands*

The presence of cellular fragments in the perivitelline space is a commonly used parameter to determine quality before transfer of *in vitro* produced (IVP) embryos. However, this parameter is difficult to assess after blastocyst expansion. In this study, we used mechanical hatching to confirm the presence of cellular fragments in the perivitelline space of bovine IVP blastocysts. We further looked for associations between possible apoptosis within extruded cells/ cellular fragments and the quality of bovine blastocysts using quantitative RT-PCR and immunofluorescence. Surprisingly, more than 42% of expanded blastocysts had cellular fragments in the perivitelline space; however, more than 37% of extruded cells were TUNEL negative. We observed no significant difference in embryo quality between expanded blastocysts with and without cellular fragments in the perivitelline space. Overall, our data suggest that embryos extrude abnormal cells to maintain their developmental potential. The presence of fragmented cells is not an indicator of embryo quality.

Keywords: bovine, zona pellucida, cellular fragments, apoptosis, embryo quality, blastocyst

OPEN ACCESS

Edited by:
Wolfgang Knabe,
Universität Münster, Germany

Reviewed by:
Wilfried A. Kues,
Institute of Farm Animal Genetics, Friedrich Loeffler Institute (FLI), Germany
Isabelle Donnay,
Université catholique de Louvain, Belgium

***Correspondence:**
Bernard A. J. Roelen
b.a.j.roelen@uu.nl

Specialty section:
This article was submitted to Cell Death and Survival, a section of the journal Frontiers in Cell and Developmental Biology

Received: *13 October 2020*
Accepted: *09 December 2020*
Published: *05 January 2021*

Citation:
Yu B, van Tol HTA, Stout TAE and Roelen BAJ (2021) Cellular Fragments in the Perivitelline Space Are Not a Predictor of Expanded Blastocyst Quality. Front. Cell Dev. Biol. 8:616801. doi: 10.3389/fcell.2020.616801

INTRODUCTION

In the past 40 years, millions of human babies and bovine calves have been born with the help of *in vitro* fertilization (IVF) (Niederberger et al., 2018; Sirard, 2018). Despite these numbers, the clinical pregnancy rate after embryo transfer is relatively low, at around 30–40%. It has however been established that transfer of embryos with good gross morphology results in higher pregnancy rates (Lindner and Wright, 1983; Desai et al., 2000). Determination of embryo quality is challenging, however, because assessment of morphology is subjective and embryo grading results may vary between clinicians (Lindner and Wright, 1983; Farin et al., 1995; Baxter Bendus et al., 2006). In human IVF, it is common practice to transfer 4- to 8-cell stage embryos to the patient's uterus to shorten the *in vitro* embryo culture time. Currently, there is an increasing tendency to transfer at the blastocyst stage because this might improve implantation and clinical pregnancy rates (Papanikolaou et al., 2005; Gorodeckaja et al., 2019; Sciorio et al., 2019). Indeed, in cattle and most domestic animals, only transfer of morulae-blastocysts reliably leads to pregnancy (Van Soom et al., 2001). Therefore, a means to objectively assess the quality of blastocysts is of great importance for clinicians to aid selection of the best embryo to transfer.

There are two major approaches to evaluating blastocyst quality: invasive and non-invasive. Invasive evaluation of blastocyst quality mostly involves lysis of the embryo for gene expression

analysis, fixation for imaging or preimplantation genetic testing (PGT). The total cell number and the ratio of inner cell mass (ICM) to trophectoderm cells are directly correlated with blastocyst quality (Leppens et al., 1996; Matsuura et al., 2010) but because the ICM is highly compacted, it is difficult to accurately determine either total or ICM cell number using regular microscopy. Thus, staining of the nuclei together with a marker for the ICM and/or trophectoderm lineage after fixation can be a more accurate way to obtain information on blastocyst quality in an experimental setting. Another valuable indicator of blastocyst health is the percentage of cells undergoing apoptosis, which is often assessed using the terminal deoxynucleotidyl transferase (TdT) mediated dUTP nick-end labeling (TUNEL) assay (Neuber et al., 2002). The disadvantage of these invasive evaluations of blastocyst quality is obvious, as these invasive procedures are not compatible with embryo survival. Therefore, in a clinical situation, embryo biopsy to remove a small number of cells for PGT is a more practical method to detect chromosomal or genetic abnormalities prior to embryo transfer, without the need to destroy the whole embryo. In commercial cattle breeding, analysis of cells to analyze for sex and assess genomic characteristics of the embryo is relatively common practice. However, due to extra costs, risks of biopsy and of misdiagnosis because of the difficulty of extrapolating data from a small number of cells to the whole embryo (e.g., in the case of chromosomal mosaics), or because of the limited number of genes that can be analyzed on PGT samples (Kalfoglou et al., 2005; Sermon et al., 2016; Cornelisse et al., 2020), non-invasive techniques based on gross morphological evaluation of embryos are still widely used in practice, particularly in human IVF (Lindner and Wright, 1983; Farin et al., 1995; Bormann et al., 2020).

An important parameter of non-invasive evaluation is the developmental stage in relation to time after fertilization. It has been shown that fast-cleaving embryos are of higher quality than slower-cleaving counterparts and expansion is considered to be an indicator of a "good" blastocyst (van Soom et al., 1997; Balaban et al., 2006). Another emerging non-invasive embryo selection technique is time-lapse embryo imaging, which allows continuous observation of embryo morphology without taking the embryo from optimal culturing conditions (Kovacs, 2014). However, this technique is not ready for routine clinical application, as clinically meaningful outcome parameters of time-lapse embryo imaging have not been fully determined yet (Armstrong et al., 2019).

One of the most commonly used parameters for assessing quality of blastocysts is the presence of extruded blastomeres and the extent of cellular fragmentation in the perivitelline space. Embryos with extensive cellular fragmentation are considered as "fair" or "poor" embryos likely to result in a low likelihood of implantation (Van Soom et al., 2003; Racowsky et al., 2010).

Once a blastocyst expands, the perivitelline space becomes very small, which makes it difficult to identify cellular fragments. Thus, there is a lack of information about cellular fragments in the perivitelline space at the blastocyst stage and its relationship to embryo quality.

To investigate the correlation of the presence of cell fragments in the perivitelline space with blastocyst quality, we mechanically hatched the embryo from the zona pellucida of expanded blastocysts. Surprisingly, there was no significant difference in the quality of blastocysts with or without cells or cellular fragments in the perivitelline space of day 8 blastocysts. Our data confirmed that embryos can tolerate a certain level of cell death and still reach the blastocyst stage. It is suggested that apoptosis and fragmentation are methods to remove abnormal cells from the embryo, and thereby protect the developmental competence of the embryo.

MATERIALS AND METHODS

In vitro Embryo Production

All chemicals were purchased from Sigma Aldrich (St. Louis, MO, USA), unless otherwise stated. Cattle ovaries were obtained from a local slaughterhouse within 2 h after slaughter. Cumulus-oocyte complexes (COCs) were aspirated from 2-8 mm follicles using a winged infusion set (18G) connected to a vacuum aspiration system. COCs were isolated from the aspirated follicular fluid using a stereomicroscope. Groups of 40–60 oocytes were matured and fertilized *in vitro* as described previously (Brinkhof et al., 2015). In short, the oocytes were cultured in maturation medium: M199 (Life Technologies, Bleiswijk, The Netherlands) supplemented with 0.05 IU/mL recombinant hFSH (Organon, Oss, The Netherlands) and with 1% (v/v) penicillin-streptomycin (Life Technologies). Culture was for 23 h at 38.5°C, in an atmosphere of 5% CO_2-in-air after which oocytes were fertilized by co-incubation with $1*10^6$/mL motile frozen/thawed sperm cells. The day on which COCs were co-incubated with sperm was considered as day 0 of embryo development. After incubation with sperm for 20–22 h, zygotes were denuded of their cumulus cells by vortexing for 3 min and then transferred to synthetic oviductal fluid (SOF) [107.63 mmol/L NaCl, 25 mmol/L $NaHCO_3$, 7.16 mmol/L KCl, 1.19 mmol/L KH_2PO_4, 1.78 mmol/L $CaCl_2{\cdot}2H_2O$, 3.20 mmol/L Sodium DL-lactate (60% syrup), 0.74 mmol/L $MgSO_4{\cdot}7H_2O$ (Merck Millipore, Billerica, MA, USA), 0.33 mmol/L Sodium pyruvate, 2.05 mmol/L L-Glutamine, 4 mg/mL BSA (Merck Millipore), 10 U/mL penicillin-streptomycin (Life Technologies), 1% MEM NEAA, 2% BME Amino Acids and 0.5 μL/mL Phenol Red 0.5% in LAL water (Lonza, Basel, Switzerland)] for further development at 38.5°C, in a humidified atmosphere containing 5% CO_2 and 7% O_2. On day 5, embryos were transferred to fresh SOF and cultured until day 9 (Brinkhof et al., 2017).

Mechanical Separation

Day 7–9 expanded blastocysts were collected and placed in a washing medium composed of 6.66 mg/mL NaCl (Merck, Schiphol-Rijk, The Netherlands), 0.24 mg/mL KCl (Merck), 0.17 mg/mL $NaHCO_3$, 0.05 mg/mLNaH_2PO_4 (Merck), 0.22% (v/v) of a 60% sodium lactate solution, 2.38 mg/mL HEPES, 0.20% (v/v) phenol red, 0.39 mg/mL $CaCl_2{\cdot}2H_2O$, 0.10 mg/ mL $MgCl_2{\cdot}6H_2O$ (Merck), 0.11 mg/mL sodium pyruvate, 100 U/mL penicillin-Streptomycin (Gibco, Paisley, UK) and 6.00 mg/mL

bovine serum albumin fraction V (BSA) (MP Biomedicals, Santa Ana, CA, USA), set at an osmolality of 280 ± 2 osmol/kg and pH 7.3 ± 0.05. Embryos were mechanically separated from their zonae pellucida using tungsten needles in washing medium under a stereomicroscope. Isolated embryos and zonae pellucidae were rinsed in PBS before collection for quantitative reverse transcription PCR and immunofluorescence.

RNA Isolation and cDNA Generation

Groups of 47–55 zonae pellucidae containing obvious cell clumps or cellular fragments, and groups of 21–32 embryos were collected and stored in 100 μL RLT buffer (Qiagen, Venlo, The Netherlands) at −80°C until RNA isolation. Total RNA extraction and genomic DNA digestion was performed using the RNeasy Micro Kit (Qiagen) according to the manufacturer's instructions. Complementary DNA (cDNA) was synthesized directly after RNA extraction. The mixture used for reverse transcription (RT) was made up of 10 μL of the RNA sample and 4 μL of 5 × RT buffer (Invitrogen, Breda, The Netherlands) in a total volume of 20 μL containing 10 mM DTT (Invitrogen), 0.5 mM dNTP (Promega, Leiden, the Netherlands), 8 units RNAse inhibitor (Promega) and 150 units Superscript III reverse transcriptase (Invitrogen). Minus-RT controls were prepared from 5 μL RNA sample using the same reagents as above, without the reverse transcriptase. After incubation at 70°C for 5 min, the mixtures were cooled down on ice for 5 min, followed by 1 h at 50°C, and 5 min at 80°C. cDNA samples were stored at −20°C.

Quantitative Reverse Transcription-PCR

Primer pairs (Eurogentec, Maastricht, the Netherlands) were designed on Primer-Blast (http://www.ncbi.nlm.nih.gov/tools/primer-blast) according to *Bos taurus* mRNA (Genbank; http://www.ncbi.nlm.nih.gov/nucleotide). The quantitative reverse transcription PCR (qRT-PCR) mixture contained 10 μL iQ SYBR Green supermix (Bio-Rad, CA, USA), 9 μL RNAse-free and DNAse-free water (Invitrogen) and 1 μL cDNA with a final primer concentration of 500 nM. The specificity and annealing temperature of primers (**Supplementary Table 1**) were first established using a temperature gradient from 55 to 68°C, and cDNA from 100 blastocysts as template. Reactions were performed on the CFX detection system (Bio-Rad) based on the manufacturer's protocol. Mixtures were kept at 95°C for 3 min, followed by 40 cycles of denaturation at 95°C for 20 s, the primer specific annealing temperature for 20 s and extension at 72°C for 20 s. To verify the purity of the amplified products, melting curves were generated after amplification with temperature increments of 0.5°C from 65 to 95°C for 5 s each step. To calculate amplification efficiency, standard curves of primers were generated by 4-fold dilutions of cDNA from 100 blastocysts in each reaction. All the reactions were performed on three independent biological cDNA samples in duplicate. Expression of *RPL15*, *SDHA,* and *YWHAZ* was used for normalization (Brinkhof et al., 2015).

Immunofluorescence

Blastocysts and zonae pellucidae with cellular fragments were collected and fixed in 4% paraformaldehyde (PFA) for 15 min and then stored in 1% PFA at 4°C until further use. After washing twice in PBST (1x PBS, 0.01% Triton X-100), samples were blocked in PBS with 5% goat serum and 0.3% Triton X-100 for 60 min. Following three washes in PBST, samples were incubated with mouse monoclonal antibody against CDX2 (Biogenex, CA, USA; CDX2-88; 1:200) and Alexa Fluor™ 568 Phalloidin (Invitrogen; A12380; 1:100) in dilution buffer (1x PBS, 1% BSA, 0.3% Triton X-100) overnight. After three washes in PBST, secondary antibody incubation was performed with goat anti mouse Alexa488 (Invitrogen) for at least 1 h in the dark. Subsequently, nuclei were stained with DAPI (Sigma Aldrich) for 20 min in the dark. After three washes in PBST, samples were mounted with Vectashield (Brunschwig Chemie, Amsterdam, The Netherlands) on slides and stored at 4°C in the dark before imaging. Fluorescent images were obtained using a confocal laser scanning microscope (SPE-II-DMI4000; Leica, Son, The Netherlands) with a Z-stack projection and were further analyzed using IMARIS software (Bitplane, Zürich, Switzerland).

Combined TUNEL and Immunofluorescence

Apoptotic cells were identified by terminal deoxynucleotidyl transferase dUTP nick end labeling (TUNEL) based on the Click-iT Plus TUNEL assay (Thermo Fisher Scientific, Carlsbad, CA, USA) with a few modifications. After fixation, samples were washed twice in PBST and incubated with 100 μL of TdT reaction buffer at 37°C for 10 min, followed by incubation with TdT reaction mixture for 60 min at 37°C. After two washes in Milli Q water, samples were incubated with 3% BSA and 0.1% Triton X-100 in PBS for 5 min at room temperature. Following two washes in PBST, samples were incubated with 100 μL of the Click-iT Plus TUNEL reaction cocktail for 30 min at 37°C in the dark.

After three washes in PBST, immunofluorescence and imaging were performed as described above.

Statistical Analysis

Statistical analysis was performed using Excel and GraphPad Prism 8 (https://www.graphpad.com/scientific-software/prism/). Pools of embryos or zonae with cellular fragments from three biological replicates were analyzed for gene expression. Individual embryos or zonae with cellular fragments from three biological replicates were analyzed after immunostaining. Differences between two groups were analyzed by two-tailed unpaired Student's *t*-tests, and differences between multiple groups were examined by one-way ANOVA, followed by a *post-hoc* Tukey test. A linear mixed model [SPSS (IBM, Amsterdam, Netherlands)] was used to investigate differences in the total cell number, CDX2 positive cell number and TUNEL positive cell number per blastocyst and cellular fragment comparison. The "individual embryo" was set as "subject," different parameters as "fixed effect" and "run of IVF" as "random effect" because of the variability between batches of ovaries. Statistical significance was set at $P < 0.05$.

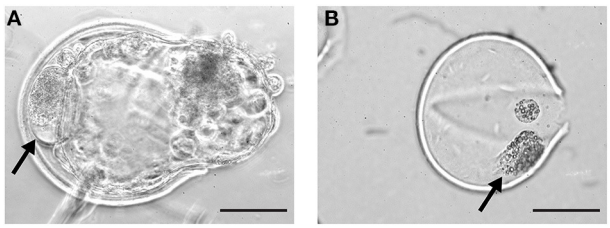

FIGURE 1 | Cellular fragments in day 9 bovine blastocysts. Fragmented cells (arrows) in the perivitelline space of a day 9 hatching blastocyst **(A)** and within the zona pellucida of a hatched blastocyst **(B)**. Scale bar = 50 μm.

RESULTS

The Presence of Cellular Fragments in the Perivitelline Space of Expanded Blastocysts

As cellular fragments can be detected in the perivitelline space of day 9 hatching and hatched blastocysts (**Figure 1**), we presumed that fragmented cells would also be present in the zonae of expanded blastocysts but would not be visible due to the pressure of the expanding blastocyst against the zona pellucida. To preserve the integrity of blastocysts and zonae pellucidae, we examined the presence of cellular fragments following manual removal of the zona pellucida of day 7 (n = 140), 8 (n = 155) and 9 (n = 148) blastocysts (**Supplementary Table 2**). As expected, fragmented cells were also detected between the embryo and the zona pellucida of expanded blastocysts (**Figures 2A,B**). Note that the occurrence of fragmented cells in the perivitelline space is difficult to establish before mechanical separation (**Figures 2A–D**). To our surprise, more than 42% of expanded blastocysts demonstrated cells or cell fragments in the perivitelline space with no significant difference between days 7, 8, and 9 blastocysts (**Figure 2E**, **Supplementary Table 2**).

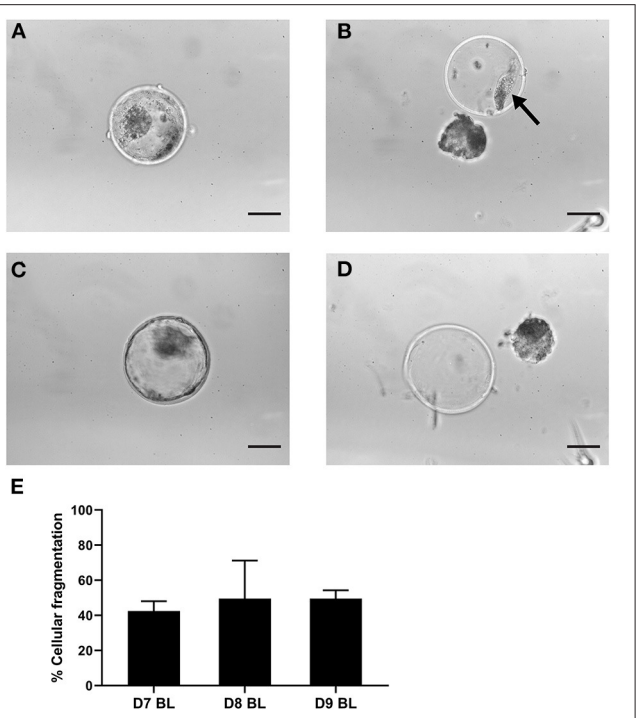

FIGURE 2 | Cellular fragments in the zona pellucida of expanded blastocysts. Representative expanded blastocyst with cellular fragmentation before **(A)** and after **(B)** mechanically induced hatching. Representative expanded blastocyst without cellular fragments before **(C)** and after **(D)** mechanically induced hatching. Arrow indicates cell fragments. **(E)** Graph indicating percentages of blastocysts with cellular fragments in the zona pellucida after 7 (n = 140), 8 (n = 155), 9 (n = 148) days of *in vitro* culture. Error bars indicate standard deviation of three biological replicates. Scale bar = 50 μm.
D, day; BL, blastocyst.

The Level of Apoptosis in Cellular Fragments

It has been suggested that cellular fragmentation in embryos is the result of elimination of abnormal cells (e.g., with chromosomal errors), and is closely related to apoptotic processes (Haouzi and Hamamah, 2009; Daughtry et al., 2019). We first used DAPI to examine nuclear DNA in fragmented cells in the zona pellucida of day 9 blastocysts, with 16/25 (64%) containing DAPI positive fragments. We then evaluated the level of possible apoptosis-related changes in the cells and cellular fragments in 11 zonae of day 9 blastocysts by means of the TUNEL assay. TUNEL positive cells were detected in the majority of cell clumps. Interestingly, we noticed that a mean of 37.4% of the extruded cells were TUNEL negative and contained morphologically normal nuclei as observed after DAPI staining (**Figure 3A**, **Supplementary Table 3**), indicating that a significant number of cells were extruded before cell death was initiated.

Since the cytoskeletal architecture plays a role as sensor and mediator of apoptosis (Desouza et al., 2012), we reasoned the actin cytoskeleton presents in cellular fragments. We therefore analyzed the occurrence of actin cytoskeletal elements using phalloidin staining. We observed large phalloidin positive areas in 10 fragmented cells of day 9 blastocysts (**Figure 3A**, **Supplementary Table 3**), which further suggested that fragmented cells were undergoing apoptotic processes. To examine whether the fragmented cells originated from the trophectoderm, cells were immunostained for CDX2 expression together with phalloidin. No CDX2 expression was detected in fragmented cells, including fragmented cells with an intact nucleus (**Figure 3B**). Together, these data suggest that either the cells were extruded by embryos before the differentiation of trophectoderm, or that trophectoderm cells rapidly lost CDX2 expression after exclusion from the embryo.

To evaluate the difference in apoptosis-related pathways between day 9 blastocysts (n = 87) and extruded cells (n = 151), we next performed qRT-PCR to determine expression of genes in the caspase and Bcl-2 families (Brentnall et al., 2013). Expression of *RPL15*, *SDHA,* and *YWHAZ* was used as a reference for quantification, and expression of these genes followed similar patterns in samples of day 9 blastocysts and extruded cells (data not shown). In contrast to expectations, the

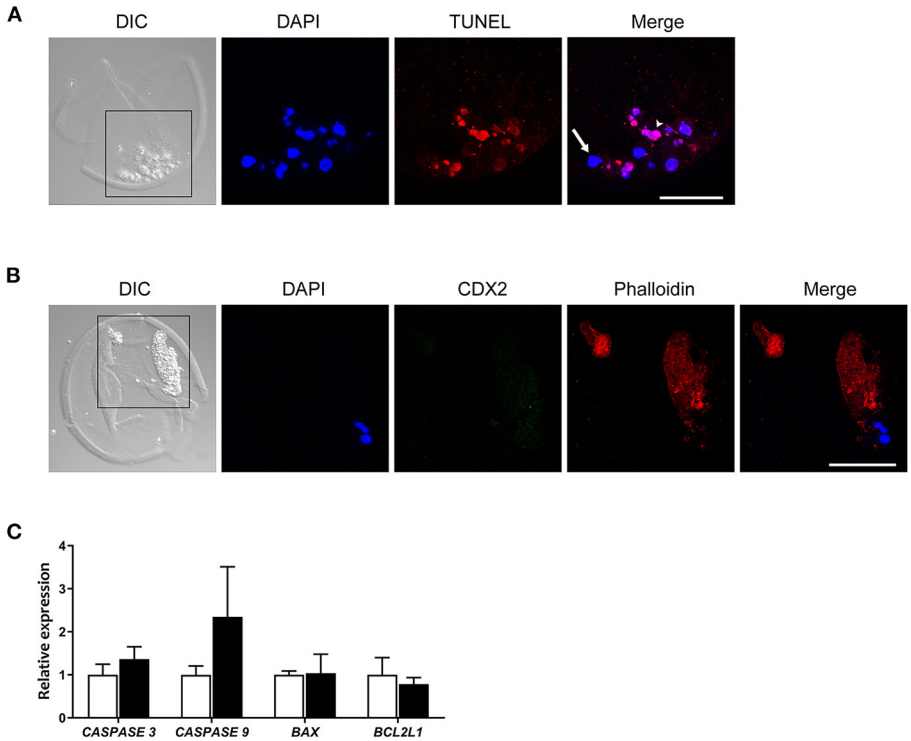

FIGURE 3 | CDX2 and Phalloidin immunofluorescent staining, and apoptosis related gene expression in cellular fragments in the perivitelline space of a day 9 bovine blastocyst. **(A)** TUNEL positive (red, arrowhead) and negative cells (arrow) are indicated in a day 9 blastocyst. Blue represents DAPI staining. **(B)** CDX2 and Phalloidin staining of cellular fragments in a day 9 blastocyst. Black boxes in **(A,B)** indicate the areas presented in the right at higher magnification. Scale bar = 50 μm. **(C)** Relative expression of apoptosis-related genes -in day 9 blastocysts (white bars, $n = 87$) vs. fragmented cells (black bars, $n = 151$) as determined by qRT-PCR. Error bars indicate standard deviation of three biological replicates. DIC, differential interference contrast.

expression of caspase family genes was not statistically different between extruded cells and blastocysts ($P > 0.17$ for *CASPASE 3* expression and $P > 0.11$ for *CASPASE 9* expression). In addition, the expression levels of *BAX* (pro-apoptotic regulator) and *BCL2L1* (anti-apoptotic regulator) were similar in blastocysts and extruded cells (**Figure 3C**).

Blastocyst Quality Comparison

In order to determine whether the presence of cells in the perivitelline space is an indicator of reduced blastocyst quality, we compared the quality of day 8 blastocysts with and without cellular fragmentation using invasive methods.

To simultaneously investigate cell death and the ratio of ICM to trophectoderm cells at the single blastocyst level ($n = 25$), we performed TUNEL staining combined with immunofluorescence staining for CDX2 (trophectoderm biomarker) and DAPI staining to label all nuclei (**Figure 4A**). The percentages of trophectoderm cells were similar between blastocysts with and without cells/cellular fragments in the perivitelline space, 64.6 and 67.0% CDX2 positive cells, respectively (**Figures 4B–D**). A small but similar proportion of TUNEL positive cells was detected in blastocysts with (6.5%) and without (4.5%) fragmented cells (**Figures 4E,F**). TUNEL positive cells were also detected in presumptive ICM cells (CDX2 negative; **Supplementary Tables 4, 5**). Nevertheless, a similar and low percentage of TUNEL positive cells was found in presumptive ICM cells in blastocysts with (4.6%) and without (5.5%) cellular fragmentation (**Figures 4G,H**).

We further examined the expression of *CDX2* and *SOX2* (ICM biomarker) and apoptosis regulator genes in day 8 blastocysts. In agreement with the TUNEL/combined immunofluorescence results, there were no significant differences in the levels of *CDX2*, *SOX2*, *CASPASE 3*, *CASPASE 9*, *BAX*, and *BCL2L1* expression between blastocysts with ($n = 64$) and without ($n = 66$) cellular fragmentation (**Figure 4I**).

DISCUSSION

Despite being used in clinical practice for decades, embryo evaluation prior to transfer is a challenging and subjective procedure. The presence of cellular fragments in the perivitelline space can be identified by clinicians, and is an important empirical criterion of embryo quality (Van Soom et al., 2003). However, our data indicate that the presence of extruded or fragmented cells is common in expanded blastocysts and is not a reliable indicator of blastocyst quality.

Although cellular fragments can be often observed in the perivitelline space of cleavage stage embryos, their presence in

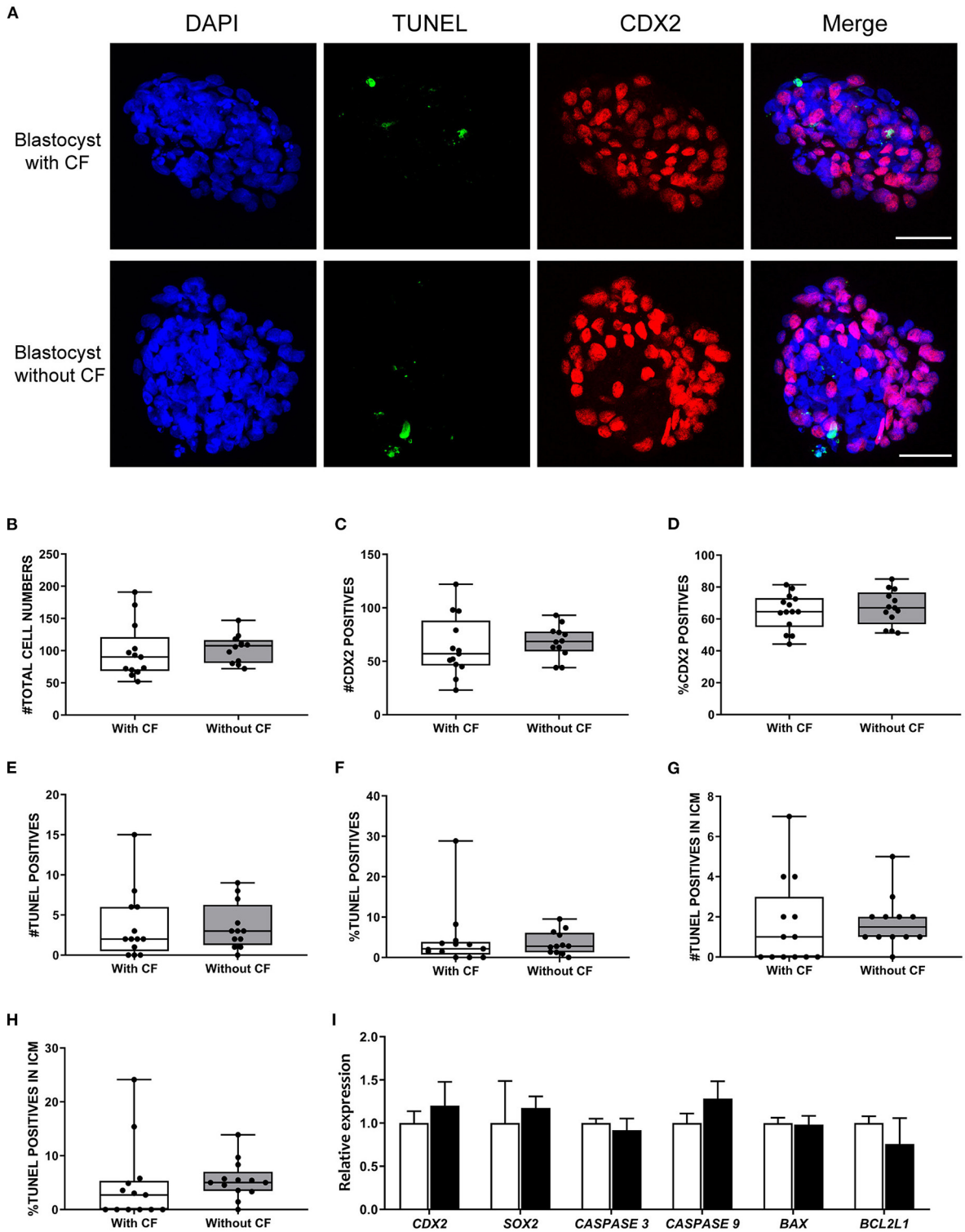

FIGURE 4 | Frequency of apoptosis and ICM to trophectoderm ratio comparison between expanded bovine blastocysts with and without cellular fragments. **(A)** TUNEL (green) and CDX2 (red) immunofluorescence of day 8 blastocysts with and without cellular fragments. Scale bar = 50 μm. Box-whisker plots of total cell number **(B)**, CDX2 positive cells **(C)**, percentage of CDX2 positive cells **(D)**, total TUNEL positive cell number **(E)**, percentage of TUNEL positive cells **(F)**, TUNEL positive cell number in inner cell mass (ICM) **(G)**, percentage of TUNEL positive cell number in ICM **(H)** in blastocysts with cellular fragments (white, $n = 64$) or in blastocyst without (gray, $n = 66$) fragmented cells in the perivitelline space. **(I)** Relative expression of genes in day 8 blastocysts with (white bars) or without (black bars) fragmented cells, as determined by qRT-PCR. Error bars indicate standard deviation of three biological replicates. BL, blastocyst; CF, cellular fragmentation.

the same location around expanded blastocysts is less easy to confirm by regular stereomicroscopy. To identify their presence in expanded blastocysts, we mechanically separated zonae pellucidae and embryos, which allowed examination of the cells detached from the embryo and attached to the zona pellucida. Using electron microscopy, several groups have previously identified fragmented cells or "debris" in the perivitelline space (Vajta et al., 1997; Fair et al., 2001; Rizos et al., 2002), but further examination of the cells was not possible.

Recently, it has been reported that cell fragments contain chromosomal material, possibly resulting from encapsulated micronuclei (Daughtry et al., 2019). Indeed, we detected that more than half of cell fragments were DAPI positive and most of these DAPI positive cells were positive for TUNEL in day 9 blastocysts; nevertheless, we still found more than one third of cell fragments to be TUNEL negative.

In bovine embryos, cellular fragmentation has only been observed after the 8-cell stage, typically from the morula stage onwards (Gjorret et al., 2003; Van Soom et al., 2003). Similarly, apoptosis is also first observed after the 8-cell stage in bovine embryos (Byrne et al., 1999; Gjorret et al., 2003), coinciding with activation of the embryonic genome. Indeed, we found no CDX2 expression in the cellular fragments and there was no difference in the percentages of blastocysts with cellular fragments within the zona pellucida between days 7, 8, and 9 blastocysts, indicating that the cells were excluded from the embryo before the blastocyst stage. Possibly, embryos assess the genomic integrity of cells at around the time of embryonic genome activation and extrusion and fragmentation of cells with chromosomal errors is initiated at this time. Alternatively, the cellular fragments observed at the blastocyst stage result from the progressive degeneration of cells excluded prior to blastocyst formation. This may explain why the majority of cellular fragments were TUNEL positive, i.e., (programmed) cell death may have started after cell exclusion. Removal of cells by programmed cell death within the developing embryos would mainly affect the cell that later form the fetus, i.e., the ICM (Leidenfrost et al., 2011).

Interestingly, the detected mRNA levels in the cell fragments indicate that mRNA was not rapidly degraded. Indeed, the appearance of nuclear material within the fragments, as visualized using DAPI staining, suggested many nuclei were intact. In addition, the levels of caspase gene expression were not increased above those observed in the embryos themselves. These results indicate that not every extruded cell or cell fragment had undergone apoptosis, or that a portion of cellular fragments were at an early stage of apoptosis.

The technique of qRT-PCR does not allow determination of caspase protein activity, is partly dependent on post-translational modification (Parrish et al., 2013). Caspase mRNA can however be used as supplementary evidence of apoptosis (Krishnan et al., 2005; Zhang et al., 2019). Moreover, consistent with caspase gene expression, we did not find any significant differences in *BAX* (pro-apoptotic) and *BCL2L1* (anti-apoptotic) expression between day 9 blastocysts and day 9 zonae pellucidae with cellular fragments, or day 8 blastocysts with and without cellular fragments.

Generally, the presence of cellular fragments in the perivitelline space is considered as an indicator of poor embryo quality (Jurisicova et al., 1998; Chi et al., 2011; Maurer et al., 2015), although it has also been proposed that low levels of fragmentation have no negative impact on implantation and pregnancy rates (Alikani et al., 1999). In our study, there was no significant difference in embryo quality between day 8 blastocysts with cellular fragments and blastocysts without. Since in bovine IVF an average of only 30–40% of the embryos reach the blastocyst stage, it is possible that the embryos with high percentages of chromosomally abnormal cells were already arrested during early embryonic development, and the blastocysts we collected were of relatively high quality. Indeed, few TUNEL positive cell were detected in the blastocysts we collected.

To conclude, the presence of cellular fragments in the perivitelline space is common in expanded blastocysts. A limitation of this study is that even blastocysts with good morphology will not necessarily implant and give rise to healthy offspring. Blastocyst morphology is however a criterion used in practice to select or prioritize embryos for transfer. Although the most convincing demonstration of bovine blastocyst quality, i.e., birth of a healthy calf, has not been examined, we conclude that there is no correlation between the presence of cellular fragments in the perivitelline space and blastocyst quality.

DATA AVAILABILITY STATEMENT

The original contributions presented in the study are included in the article/**Supplementary Material**, further inquiries can be directed to the corresponding author/s.

AUTHOR CONTRIBUTIONS

BY, HT, TS, and BR conceived and designed the experiments. BY, HT, and BR performed the experiments and collected the data. BY analyzed the data. BR contributed the reagents, materials, and analysis tools. BY, TS, and BR wrote the manuscript. All authors read and approved the manuscript.

FUNDING

BY was supported by a Ph.D., scholarship from the Chinese Scholarship Council (CSC): CSC201606300033.

ACKNOWLEDGMENTS

We thank Arend Rijneveld and Christine Oei for assistance with oocyte recovery.

SUPPLEMENTARY MATERIAL

The Supplementary Material for this article can be found online at: https://www.frontiersin.org/articles/10.3389/fcell.2020.616801/full#supplementary-material

REFERENCES

Alikani, M., Cohen, J., Tomkin, G., Garrisi, G. J., Mack, C., and Scott, R. T. (1999). Human embryo fragmentation *in vitro* and its implications for pregnancy and implantation. *Fertil. Steril.* 71, 836–842. doi: 10.1016/S0015-0282(99)00092-8

Armstrong, S., Bhide, P., Jordan, V., Pacey, A., Marjoribanks, J., and Farquhar, C. (2019). Time-lapse systems for embryo incubation and assessment in assisted reproduction. *Cochrane Database Syst. Rev.* 5:Cd011320. doi: 10.1002/14651858.CD011320.pub4

Balaban, B., Yakin, K., and Urman, B. (2006). Randomized comparison of two different blastocyst grading systems. *Fertil. Steril.* 85, 559–563. doi: 10.1016/j.fertnstert.2005.11.013

Baxter Bendus, A. E., Mayer, J. F., Shipley, S. K., and Catherino, W. H. (2006). Interobserver and intraobserver variation in day 3 embryo grading. *Fertil. Steril.* 86, 1608–1615. doi: 10.1016/j.fertnstert.2006.05.037

Bormann, C. L., Kanakasabapathy, M. K., Thirumalaraju, P., Gupta, R., Pooniwala, R., Kandula, H., et al. (2020). Performance of a deep learning based neural network in the selection of human blastocysts for implantation. *Elife* 9:e55302. doi: 10.7554/eLife.55301.sa2

Brentnall, M., Rodriguez-Menocal, L., De Guevara, R. L., Cepero, E., and Boise, L. H. (2013). Caspase-9, caspase-3 and caspase-7 have distinct roles during intrinsic apoptosis. *BMC Cell Biol.* 14:32. doi: 10.1186/1471-2121-14-32

Brinkhof, B., van Tol, H. T., Groot Koerkamp, M. J., Riemers, F. M., Ijzer, S. G., Mashayekhi, K., et al. (2015). A mRNA landscape of bovine embryos after standard and MAPK-inhibited culture conditions: a comparative analysis. *BMC Genomics* 16:277. doi: 10.1186/s12864-015-1448-x

Brinkhof, B., van Tol, H. T., Groot Koerkamp, M. J., Wubbolts, R. W., Haagsman, H. P., and Roelen, B. A. (2017). Characterization of bovine embryos cultured under conditions appropriate for sustaining human naïve pluripotency. *PLoS ONE* 12:e0172920. doi: 10.1371/journal.pone.0172920

Byrne, A. T., Southgate, J., Brison, D. R., and Leese, H. J. (1999). Analysis of apoptosis in the preimplantation bovine embryo using TUNEL. *J. Reprod. Fertil.* 117, 97–105. doi: 10.1530/jrf.0.1170097

Chi, H. J., Koo, J. J., Choi, S. Y., Jeong, H. J., and Roh, S. I. (2011). Fragmentation of embryos is associated with both necrosis and apoptosis. *Fertil. Steril.* 96, 187–192. doi: 10.1016/j.fertnstert.2011.04.020

Cornelisse, S., Zagers, M., Kostova, E., Fleischer, K., van Wely, M., and Mastenbroek, S. (2020). Preimplantation genetic testing for aneuploidies (abnormal number of chromosomes) in *in vitro* fertilisation. *Cochrane Database Syst. Rev.* 9:Cd005291. doi: 10.1002/14651858.CD005291.pub3

Daughtry, B. L., Rosenkrantz, J. L., Lazar, N. H., Fei, S. S., Redmayne, N., Torkenczy, K. A., et al. (2019). Single-cell sequencing of primate preimplantation embryos reveals chromosome elimination via cellular fragmentation and blastomere exclusion. *Genome Res.* 29, 367–382. doi: 10.1101/gr.239830.118

Desai, N. N., Goldstein, J., Rowland, D. Y., and Goldfarb, J. M. (2000). Morphological evaluation of human embryos and derivation of an embryo quality scoring system specific for day 3 embryos: a preliminary study. *Hum. Reprod.* 15, 2190–2196. doi: 10.1093/humrep/15.10.2190

Desouza, M., Gunning, P. W., and Stehn, J. R. (2012). The actin cytoskeleton as a sensor and mediator of apoptosis. *Bioarchitecture* 2, 75–87. doi: 10.4161/bioa.20975

Fair, T., Lonergan, P., Dinnyes, A., Cottell, D. C., Hyttel, P., Ward, F. A., et al. (2001). Ultrastructure of bovine blastocysts following cryopreservation: effect of method of blastocyst production. *Mol. Reprod. Dev.* 58, 186–195. doi: 10.1002/1098-2795(200102)58:2<186::AID-MRD8>3.0.CO;2-N

Farin, P. W., Britt, J. H., Shaw, D. W., and Slenning, B. D. (1995). Agreement among evaluators of bovine embryos produced *in vivo* or *in vitro*. *Theriogenology* 44, 339–349. doi: 10.1016/0093-691X(95)00189-F

Gjorret, J. O., Knijn, H. M., Dieleman, S. J., Avery, B., Larsson, L. I., and Maddox-Hyttel, P. (2003). Chronology of apoptosis in bovine embryos produced *in vivo* and *in vitro*. *Biol. Reprod.* 69, 1193–1200. doi: 10.1095/biolreprod.102.013243

Gorodeckaja, J., Neumann, S., McCollin, A., Ottolini, C. S., Wang, J., Ahuja, K., et al. (2019). High implantation and clinical pregnancy rates with single vitrified-warmed blastocyst transfer and optional aneuploidy testing for all patients. *Hum. Fertil.* 23, 256–267. doi: 10.1080/14647273.2018.1551628

Haouzi, D., and Hamamah, S. (2009). Pertinence of apoptosis markers for the improvement of *in vitro* fertilization (IVF). *Curr. Med. Chem.* 16, 1905–1916. doi: 10.2174/092986709788186075

Jurisicova, A., Latham, K. E., Casper, R. F., Casper, R. F., and Varmuza, S. L. (1998). Expression and regulation of genes associated with cell death during murine preimplantation embryo development. *Mol. Reprod. Dev.* 51, 243–253. doi: 10.1002/(SICI)1098-2795(199811)51:3<243::AID-MRD3>3.0.CO;2-P

Kalfoglou, A. L., Scott, J., and Hudson, K. (2005). PGD patients' and providers' attitudes to the use and regulation of preimplantation genetic diagnosis. *Reprod. Biomed. Online* 11, 486–496. doi: 10.1016/S1472-6483(10)61145-5

Kovacs, P. (2014). Embryo selection: the role of time-lapse monitoring. *Reprod. Biol. Endocrinol.* 12:124. doi: 10.1186/1477-7827-12-124

Krishnan, S., Kiang, J. G., Fisher, C. U., Nambiar, M. P., Nguyen, H. T., Kyttaris, V. C., et al. (2005). Increased caspase-3 expression and activity contribute to reduced CD3zeta expression in systemic lupus erythematosus T cells. *J. Immunol.* 175, 3417–3423. doi: 10.4049/jimmunol.175.5.3417

Leidenfrost, S., Boelhauve, M., Reichenbach, M., Güngör, T., Reichenbach, H. D., Sinowatz, F., et al. (2011). Cell arrest and cell death in mammalian preimplantation development: lessons from the bovine model. *PLoS ONE* 6:e22121. doi: 10.1371/journal.pone.0022121

Leppens, G., Gardner, D. K., and Sakkas, D. (1996). Co-culture of 1-cell outbred mouse embryos on bovine kidney epithelial cells: effect on development, glycolytic activity, inner cell mass:trophectoderm ratios and viability. *Hum. Reprod.* 11, 598–603. doi: 10.1093/HUMREP/11.3.598

Lindner, G. M., and Wright, R. W. Jr. (1983). Bovine embryo morphology and evaluation. *Theriogenology* 20, 407–416. doi: 10.1016/0093-691X(83)90201-7

Matsuura, K., Hayashi, N., Takiue, C., Hirata, R., Habara, T., and Naruse, K. (2010). Blastocyst quality scoring based on morphologic grading correlates with cell number. *Fertil. Steril.* 94, 1135–1137. doi: 10.1016/j.fertnstert.2009.11.003

Maurer, M., Ebner, T., Puchner, M., Mayer, R. B., Shebl, O., Oppelt, P., et al. (2015). Chromosomal aneuploidies and early embryonic developmental arrest. *Int. J. Fertil. Steril.* 9, 346–353. doi: 10.22074/ijfs.2015.4550

Neuber, E., Luetjens, C. M., Chan, A. W., and Schatten, G. P. (2002). Analysis of DNA fragmentation of *in vitro* cultured bovine blastocysts using TUNEL. *Theriogenology* 57, 2193–2202. doi: 10.1016/S0093-691X(02)00901-9

Niederberger, C., Pellicer, A., Cohen, J., Gardner, D. K., Palermo, G. D., O'Neill, C. L., et al. (2018). Forty years of IVF. *Fertil. Steril.* 110, 185–324.e185. doi: 10.1016/j.fertnstert.2018.06.005

Papanikolaou, E. G., D'Haeseleer, E., Verheyen, G., Van de Velde, H., Camus, M., Van Steirteghem, A., et al. (2005). Live birth rate is significantly higher after blastocyst transfer than after cleavage-stage embryo transfer when at least four embryos are available on day 3 of embryo culture. A randomized prospective study. *Hum. Reprod.* 20, 3198–3203. doi: 10.1093/humrep/dei217

Parrish, A. B., Freel, C. D., and Kornbluth, S. (2013). Cellular mechanisms controlling caspase activation and function. *Cold Spring Harb. Perspect. Biol.* 5:a008672. doi: 10.1101/cshperspect.a008672

Racowsky, C., Vernon, M., Mayer, J., Ball, G. D., Behr, B., Pomeroy, K. O., et al. (2010). Standardization of grading embryo morphology. *J. Assist. Reprod. Genet.* 27, 437–439. doi: 10.1007/s10815-010-9443-2

Rizos, D., Fair, T., Papadopoulos, S., Boland, M. P., and Lonergan, P. (2002). Developmental, qualitative, and ultrastructural differences between ovine and bovine embryos produced *in vivo* or *in vitro*. *Mol. Reprod. Dev.* 62, 320–327. doi: 10.1002/mrd.10138

Sciorio, R., Thong, K. J., and Pickering, S. J. (2019). Increased pregnancy outcome after day 5 versus day 6 transfers of human vitrified-warmed blastocysts. *Zygote* 27, 279–284. doi: 10.1017/S0967199419000273

Sermon, K., Capalbo, A., Cohen, J., Coonen, E., De Rycke, M., De Vos, A., et al. (2016). The why, the how and the when of PGS 2.0: current practices and expert opinions of fertility specialists, molecular biologists, and embryologists. *Mol. Hum. Reprod.* 22, 845–857. doi: 10.1093/molehr/gaw034

Sirard, M. A. (2018). 40 years of bovine IVF in the new genomic selection context. *Reproduction* 156, R1–R7. doi: 10.1530/REP-18-0008

Vajta, G., Hyttel, P., and Callesen, H. (1997). Morphological changes of *in-vitro*-produced bovine blastocysts after vitrification, in-straw direct rehydration, and culture. *Mol. Reprod. Dev.* 48, 9–17. doi: 10.1002/(SICI)1098-2795(199709)48:1<9::AID-MRD2>3.0.CO;2-N

Van Soom, A., Mateusen, B., Leroy, J., and De Kruif, A. (2003). Assessment of mammalian embryo quality: what can we learn from embryo morphology? *Reprod. Biomed. Online* 7, 664–670. doi: 10.1016/S1472-6483(10)62089-5

Van Soom, A., Vanroose, G., and de Kruif, A. (2001). Blastocyst evaluation by means of differential staining: a practical approach. *Reprod. Domest. Anim.* 36, 29–35. doi: 10.1046/j.1439-0531.2001.00265.x

van Soom, A., Ysebaert, M. T., and de Kruif, A. (1997). Relationship between timing of development, morula morphology, and cell allocation to inner cell mass and trophectoderm in *in vitro*-produced bovine embryos. *Mol. Reprod. Dev.* 47, 47–56. doi: 10.1002/(SICI)1098-2795(199705)47:1<47::AID-MRD7>3.0.CO;2-Q

Zhang, X., Qin, Y., Pan, Z., Li, M., Liu, X., Chen, X., et al. (2019). Cannabidiol Induces Cell Cycle Arrest and Cell Apoptosis in Human Gastric Cancer SGC-7901 Cells. *Biomolecules* 9:302. doi: 10.3390/biom9080302

Conflict of Interest: The authors declare that the research was conducted in the absence of any commercial or financial relationships that could be construed as a potential conflict of interest.

frontiers in Cell and Developmental Biology

REVIEW
published: 18 January 2021
doi: 10.3389/fcell.2020.620089

Senescence and Apoptosis: Architects of Mammalian Development

*Emma Wanner[1], Harikrishnan Thoppil[2] and Karl Riabowol[2,3]**

[1] Department of Biology, Faculty of Science, University of Calgary, Calgary, AB, Canada, [2] Department of Biochemistry and Molecular Biology, Cumming School of Medicine, University of Calgary, Calgary, AB, Canada, [3] Department of Oncology, Cumming School of Medicine, University of Calgary, Calgary, AB, Canada

Mammalian development involves an exquisite choreography of cell division, differentiation, locomotion, programmed cell death, and senescence that directs the transformation of a single cell zygote to a mature organism containing on the order of 40 trillion cells in humans. How a single totipotent zygote undergoes the rapid stages of embryonic development to form over 200 different cell types is complex in the extreme and remains the focus of active research. Processes such as programmed cell death or apoptosis has long been known to occur during development to help sculpt organs and tissue systems. Other processes such as cellular senescence, long thought to only occur in pathologic states such as aging and tumorigenesis have been recently reported to play a vital role in development. In this review, we focus on apoptosis and senescence; the former as an integral mechanism that plays a critical role not only in mature organisms, but that is also essential in shaping mammalian development. The latter as a well-defined feature of aging for which some reports indicate a function in development. We will dissect the dual roles of major gene families, pathways such as Hox, Rb, p53, and epigenetic regulators such as the ING proteins in both early and the late stages and how they play antagonistic roles by increasing fitness and decreasing mortality early in life but contribute to deleterious effects and pathologies later in life.

Keywords: apoptosis, development, Hox proteins, retinoblastoma, ING proteins, epigenetics, cancer, senescence

OPEN ACCESS

Edited by:
Stefan Washausen, Universität Münster, Germany

Reviewed by:
Ippei Shimizu, Niigata University, Japan
Miguel Godinho Ferreira, Université Côte d'Azur, France

***Correspondence:**
Karl Riabowol
karl@ucalgary.ca

Specialty section:
This article was submitted to Cell Death and Survival, a section of the journal Frontiers in Cell and Developmental Biology

Received: *21 October 2020*
Accepted: *30 December 2020*
Published: *18 January 2021*

Citation:
Wanner E, Thoppil H and Riabowol K (2021) Senescence and Apoptosis: Architects of Mammalian Development. Front. Cell Dev. Biol. 8:620089. doi: 10.3389/fcell.2020.620089

MAMMALIAN DEVELOPMENT

Mammalian development begins with the fertilization of the female gamete, the ovum, by a sperm cell, the male gamete, forming a single celled zygote. Following fertilization, the zygote undergoes rapid cleavage to form a solid ball of cells without cytoplasmic growth (Aiken et al., 2004). The next stage of development, blastulation, shows a series of morphological changes that result in the formation of a blastocyst consisting of an inner cell mass (ICM), outer trophectoderm cell layer, and a fluid filled blastocoelic cavity (Biggers et al., 1988). Gastrulation then ensues, which shapes the three germ cell layers; the endoderm, mesoderm and ectoderm, which during organogenesis develop into the tissues and organs of the developing organism (Solnica-Krezel and Sepich, 2012). The inner germ layer, the endoderm, gives rise to organs of the respiratory and digestive systems

and to the epithelial cells that line the insides of these organs (Zorn and Wells, 2009). The middle mesoderm layer is responsible for the formation of connective tissues, blood and bone, the vascular system, muscles, the heart, the kidneys, and the reproductive organs (Kimelman, 2006). The outer ectoderm germ layer gives rise to the central and peripheral nervous systems, hair, skin, nails, the mouth, the nasal cavity, the lens of the eye and various exocrine glands (Sasai and Robertis, 1997). Neurulation, the formation of the neural tube from the folding in and fusion of the neural plate then occurs, which is essential for brain and spinal cord development (Copp et al., 2003).

Normal development occurs until sexual maturity at which point the slow process of biological aging occurs at varying rates in all cell, tissue and organ types. Aging has been described as a progressive deterioration of physiological functions resulting in increased risk of impairments, disease and mortality (Strehler, 1977). Genomic instability, Telomere attrition, epigenetic alterations, loss of proteostasis, deregulated nutrient sensing, mitochondrial dysfunction, cellular senescence, stem cell exhaustion, and altered intercellular communication have been described as "hallmarks of aging" and likely all contribute to the aging phenotype (López-Otín et al., 2013). Apoptosis has long been known to be essential for the formation and preservation of tissue patterning (Meier et al., 2000). Somewhat unexpectedly, senescence has been proposed to also play roles in development of the placenta (Rajagopalan and Long, 2012; Chuprin et al., 2013) and embryo (Davaapil et al., 2017), functioning mainly in tissue remodeling (Nacher et al., 2006; Muñoz-Espín et al., 2013; Storer et al., 2013; Zhao et al., 2018; Gibaja et al., 2019) and beginning early in evolution (Villiard et al., 2017), but how this occurs is not yet fully understood.

Stem Cells in Development

Stem cells are defined by their ability of unlimited self-renewal and the capacity to divide into differentiated cells of developed tissues (Reya et al., 2001). Following fertilization, the zygote is composed of "totipotent stem cells," meaning its cells can divide and differentiate into all cell types of the organism and extraembryonic tissues (Seydoux and Braun, 2006). Next, after blastulation occurs, the ICM develops the naïve epiblast which gives rise to "pluripotent embryonic stems cells" (ESCs) (Wu et al., 2016). Pluripotency is a property of cells that allows them to give rise to cells of all three germ layers of the developing embryo, but not the extraembryonic structures (Wu et al., 2016). Cells that give rise to particular germ layers are "multipotent stem cells" (Alison et al., 2002). Multipotent stem cells include hematopoietic stem cells (HSC), mesenchymal stem cells (MSC), and neural stem cells (Caplan, 1991; Bhatia et al., 1997; Gage, 2000). They can produce a limited set of differentiated cells of a specific tissue type or organ. "Unipotent stems cells" are only capable of dividing into a single stem cell type. For this reason, they are often called committed progenitor cells (Alison et al., 2002). Adult stem cells exist in different tissues throughout the mature mammal and remain undifferentiated, allowing them to help in tissue regeneration and replenishment (Wagers and Weissman, 2004). In mammals, a molecular mark of the totipotent cells that arise following fertilization is widespread DNA demethylation (Guo et al., 2014; Baker and Pera, 2018). Maintenance of pluripotent ESCs is governed and marked by the expression patterns of key transcription factors including OCT3/4, SOX2, NANOG, Klf4, and c-Myc (Nichols et al., 1998; Avilion et al., 2003; Chambers et al., 2003; Takahashi et al., 2007; Angeles et al., 2015).

The Hox Gene Family Is Central to Mammalian Development

Hox gene family members are crucial to mammalian development. They code for transcription factors that determine the anteroposterior (AP) patterning of bilateral organisms during development (Garcia-Fernàndez, 2004). Vertebrates have 39 Hox genes, that due to gene duplications, are organized into four gene clusters, HoxA, HoxB, HoxC, and HoxD, on separate chromosomes (Lappin et al., 2006; Mallo et al., 2010). Hox genes are activated in a 3′ to 5′ direction, resulting in early developing structures having an anterior identity controlled by 3′ Hox genes, and later formed structures having a posterior identity developed mainly under the control of 5′ Hox genes (Forlani et al., 2003). During embryogenesis in mammals, Hox genes are expressed in all three germ layers, the endoderm, mesoderm and ectoderm (Krumlauf, 1994). The expression of Hox genes directs axial positioning of these developing embryonic tissues (Mallo et al., 2010).

The activation of Hox gene expression domains is controlled by processes that take place at the same time as the formation of the primitive streak during embryogenesis. Initiation of Hox gene transcription is controlled by signaling molecules including Wnt3, Wnt3a, FGF3, FGF8, and Retinoic acid (Bel-Vialar et al., 2002; Manzanares et al., 2002; Walshe et al., 2002; Weisinger et al., 2010; Schulte and Frank, 2013). Wnt signals regulate the formation and functioning of the primitive streak, and thus have been suggested to play a role in the forward anterior spreading of Hox gene expression (Forlani et al., 2003). Wnt signaling is required for expression of Hox genes involved in the developing nervous system of vertebrates. Specifically, Wnt3a signaling is important in hindbrain and spinal cord development through its role in Meis and Hox gene activation (Schulte and Frank, 2013). Similarly, FGF3 and -8 signaling molecule expression is present in the developing nervous system of all vertebrates, and PG2-3 Hox gene expression is dependent on FGF ligands (Walshe et al., 2002; Schulte and Frank, 2013). Retinoic acid (RA) is involved in regulating expression of PG1-4 Hox genes (Bel-Vialar et al., 2002). To function in embryonic development, Hox genes often rely on interactions with the Hox cofactors, TALE homeodomain proteins (Moens and Selleri, 2006). The vertebrate genome codes for the Meis/Prep and PCB TALE homeodomain protein families which are comprised of Meis1-3, Prep1-2, Tgif1-2, and Pbx1-4 proteins, respectively (Schulte and Frank, 2013).

Hox genes encode homeodomain transcription factors, that activate or repress target genes involved in vertebrate development by binding Hox-response enhancers (Pearson et al., 2005). Several Hox genes are involved in establishment of the distinct vertebral column segments from the mesodermal tissue along the neural tube (Deschamps and van Nes, 2005).

Interestingly, *in vitro* in melanocytes, Hox10A has been shown to act with cofactors, Meis1 and PBX1 TALE homeobox transcription factors to activate Cdkn1a which encodes p21, leading to growth arrest, potentially connecting Hox proteins to apoptosis and/or senescence (Bromleigh and Freedman, 2000).

EPIGENETICS IN MAMMALIAN DEVELOPMENT

Epigenetics can be broadly described as the changes made to an organism's hereditary material which result in alterations of gene expression without changes to the DNA sequence (Goldberg et al., 2007). There are several types of epigenetic regulation that affect gene expression, using covalent modifications of DNA or core histones to produce inactive heterochromatin or active euchromatin in mammals (Li, 2002). DNA methylation, the addition of a methyl group to a cytosine nucleotide by a DNA methyltransferase (DNMT) enzyme, usually results in gene silencing, due to transcriptional repression at the promoter region (Das and Singal, 2004). There are many inhibitors of DNMTs that effect the cell cycle. The drug Atorvastatin, inhibits cell proliferation and induces apoptosis rat vascular smooth muscle cells (VMCs) (Zhu et al., 2017). Atorvastatin inhibits DNMT1, reducing methylation in the p16 promoter, increasing the activity of this tumor suppressor (Zhu et al., 2017). The HMG box-containing protein 1 (HBP1) transcription factor, is a repressor of DNMT1 that results in cellular senescence (Pan et al., 2013). HBP1 has a dual transcriptional role in activating senescence, through binding and repressing DNMT1 promoter and binding to the activation element of p16 (Pan et al., 2013). The repression of DNMT1 and decreased methylation of p16 promoter also increases expression of p16, inducing senescence (Pan et al., 2013). The DNA methyltransferase inhibitors (DNMTis), 5-azacytidine and 5-aza-2′-deoxycytidine, have differing cellular responses in tumor cells (Venturelli et al., 2013). 5-azacytidine induces p53-dependent cell senescence indicated by an increase in senescence-associated marker β-galactosidase (SA-β-gal) senescence associated heterochromatin foci (SAHF), and induction of senescence-associated secretory phenotype (SASP) which are markers of senescent cells (Venturelli et al., 2013). However, 5-aza-2′-deoxycytidine induces apoptosis, through the activation of executioner caspases 3 and 7 and downregulation of p53 (Venturelli et al., 2013). Another form of epigenetic regulation is histone-post translational modification (PTM). The tails of histones that localize to the outside edges of nucleosomes can undergo various modifications such as acetylation, methylation, phosphorylation, ubiquitylation and sumoylation, among others (Bannister and Kouzarides, 2011). PTM's help regulate chromatin structure, recruit other chromatin remodeling enzymes, and influence transcription, DNA repair, and replication. Substitution of the four core histones, H2A, H2B, H3, and H4, with histone variants changes the composition of chromatin and is an important epigenetic mechanism (Henikoff and Smith, 2015). Histone variants include CENP-A, H3.3, H2A.X, H2A.Z, macroH2A, and H2A.B. ATP-dependent nucleosome remodeling is another form of epigenetic regulation, in which ATP-dependent protein complexes use energy from ATP hydrolysis to change the interactions of histones with the DNA by relocating nucleosomes, thus altering gene expression (Vignali et al., 2000). The four families of SWI-like ATP-dependent chromatin remodeing complexes, SWI/SNF, ISWI, CHD, and INO80, reposition nucleosomes, making DNA more or less accessible for transcription (Ho and Crabtree, 2010). Short and long non-coding RNAs impose another form of epigenetic regulation that usually results in gene silencing (Peschansky and Wahlestedt, 2013). For example, *Xist* RNA, a long non-coding RNA is essential in X chromosome inactivation in females during mammalian development (Wei et al., 2016) and many different microRNAs affect the levels of numerous mRNAs. Epigenetic modifications have frequently been implicated in both apoptosis and senescence (Moskalev et al., 2014).

The Epigenetic Clock of Aging and Effects on Development

The epigenetic clock of aging refers to findings that specific sites of DNA methylation generally negatively correlate with biological aging (Hannum et al., 2013; Horvath, 2013). Additionally, as organisms age, "epigenetic drift" occurs where methylation patterns are not stably maintained following repeated rounds of DNA repair and replication (Veitia et al., 2017). In mammals, DNA methylation patterns established by *de novo* and maintenance DNA methyl transferases (DNMT's) are essential for embryogenesis (Goll and Bestor, 2005). Between zygote formation and blastocyst formation, both sets of chromosomes undergo demethylation, except imprinted genes whose methylation marks are preserved (Kafri et al., 1992). Following implantation, DNA methylation levels increase in the primitive ectoderm, which forms the whole embryo, but methylation patterns are not established in cells that form the extraembryonic tissues, the primitive endoderm and trophoblast (Chapman et al., 1984). The study done by Okano et al. (1999) demonstrated the importance of DMNT's in embryogenesis as mice null for Dnmt3b, died between embryonic day 14.5 and 18.5 and showed multiple developmental defects. Although the closely related Dnmt3a was not found to be essential for early embryonic development, Dnmt3a null mice died in early development at around 4 weeks (Okano et al., 1999), highlighting the importance of such epigenetic mechanisms for development.

Histone Post Translational Modifications (PTMs) in Development

Early stages of mammalian embryonic development entail development of the totipotent zygote into a nearly hundred cell blastocyst. The pluripotent inner layers of the blastocyst known as the trophoblast eventually give rise to all cell lineages of the fully matured mammal and have unlimited self-renewal (Wu et al., 2016). Following blastula formation, the naïve epiblast develops from the ICM, which gives rise to all pluripotent ESCs. The chromatin of pluripotent stems cells is mainly in an open euchromatin state resulting in transcriptional hyperactivity (Efroni et al., 2008; Gaspar-Maia et al., 2010). Pluripotency of stem cells during embryonic

development is controlled by various epigenetic regulators. Histone PTM's, DNA methylation patterns established by DNMTs, Histone methylation patterns established by histome methyl transferases (HMTs) and histone demethylases (HDMs), histone acetylation patterns through histone acetyltransferase (HAT) and histone deacetylase (HDAC) activity, and chromatin remodeling by ATP-dependent chromatin remodeling complexes all influence ESCs (Gaspar-Maia et al., 2010). Pluripotent ESCs have many epigenetic marks characteristic of active chromatin such as H3K4me and acetylation of H3 and H4, compared to differentiated cells (Gaspar-Maia et al., 2010). HDMs maintain the low level of H3K9me3 and H3K27me seen in undifferentiated ESCs (Gaspar-Maia et al., 2010). DNMTs establish methylation of CpG islands at promoter regions of repressed genes needed for differentiation of ESCs, making up around 30% of genes in these cells (Fouse et al., 2008). The ATP-dependent chromatin-remodeling enzymes CHD1 and esBAF and the TIP60-p400 complex maintain the open euchromatin state of ESCs and repress genes required for their differentiation and loss of pluripotency, respectively (Ho and Crabtree, 2010).

SENESCENCE

Senescence is defined as a phenomenon in which cells enter a state of permanent cell cycle arrest. The first observation of cell senescence was reported by Hayflick and Moorhead while trying to culture primary cells for an extended period of time for the purpose of making viral vaccines. They observed that primary human fibroblasts stop dividing after a certain number of passages that was variable, dependent on the particular donor (Hayflick and Moorhead, 1961) and described it as replicative senescence. Replicative senescence was later attributed to a decline in telomere length that occurred during both *in vitro* culturing and *in vivo* aging (Levy et al., 1992). Senescence was also found to be induced prematurely by activation of the ras oncogene in primary human cells which was negated by the activation of the p53/Rb/p16 pathways (Serrano et al., 1997). This type of senescence, termed oncogene-induced senescence (OIS) demonstrated the potential role of senescence as an anti-cancer mechanism designed to suppress proliferation of cells with oncogenic mutations. Senescence can also be induced by many additional stresses that affect numerous biological processes including oxidative stress, replication stress and notably DNA damage- induced stress shown in **Figure 1**.

Initially senescence was thought of only as a mechanism that contributed to various forms of morbidity associated with aging including immuno-senescence, impaired wound healing, impaired gastrointestinal function, and bone loss and frailty, *inter alia* (Strehler, 1977). While this remains widely accepted, a solely beneficial mechanism was later proposed in which senescence served as a first line of defense against cancers by limiting their growth (Campisi, 2003). However, very recent studies have also begun to link senescence with the emergence of cancer due to the effects of senescent cells on local tissue microenvironments through the secretion of a complex mixture of proinflammatory factors termed the senescence-associated secretory phenotype (SASP). The SASP consists of inflammatory cytokines, growth factors, chemokines, and proteases. While the SASP helps promote recognition and clearance of senescent cells by phagocytosis in the short term, long term secretion has a variety of age-related deleterious effects (Xue et al., 2007). In a landmark study, SASP from senescent cells co-cultured with tumor cells was shown to promote tumor progression (Coppe et al., 2008). Moreover, a cascade effect involving prolonged exposure to SASP inducing senescence in nearby fibroblasts via an ROS/DNA damage mechanism has also been reported (Nelson et al., 2012). Soluble signaling factors are major components of the SASP, the most prominent of which is interleukin-6 (IL-6). Recent evidence suggests a role of the GMP-AMP synthase (cGAS)-stimulator of interferon genes (STING) in SASP regulation. This is initiated by recognition of senescence induced cytosolic DNA by cGAS which in turn activates the STING pathway resulting in production of SASP (Glück et al., 2017). Dysregulation and continuous secretion of IL-6 leads to autoimmune disorders and chronic inflammation. Chronic inflammation has been implicated in numerous morbidities with one of the relatively common ones being Arthritis. Links between IL-6 and arthritis are clear and as a consequence Tocilizumab, a humanized anti-IL-6 receptor antibody was FDA approved to treat inflammation-induced arthritis (Grupp et al., 2013).

Since the first studies that reported deleterious effects of senescent cells *in vivo*, efforts have been made to ameliorate senescence-associated pathologies. The first study of this kind used a drug activated FKBP–Caspase-8 fusion protein to induce apoptosis and was driven by a p16 promoter, which is strongly upregulated in senescent cells (Alcorta et al., 1996; Wong and Riabowol, 1996). This removal of senescent cells was shown to increase health span and delay age-related disorders in a progeroid model of accelerated mouse aging (Baker et al., 2011). This led to the later discovery of the first "senolytic" compounds that can selectively target and eliminate senescent cells: Quercetin and Dasatinib (Zhu et al., 2015). Another study found that the antiapoptotic protein BCL2 that is upregulated in senescent cells to block apoptotic cell death can be targeted by inhibitors such as Navitoclax to deprotect and eliminate senescent cells (Zhu et al., 2016). A Dasatinib- Quercetin combination is now in Phase 2 trials after Phase 1 results showed the potential to decrease the senescent cell burden in human patients with diabetic kidney disease (Hickson et al., 2019). At present there are over a dozen candidate senolytics undergoing clinical trials in varying phases, and the development of increasingly sensitive methods to identify senescent cells (González-Gualda et al., 2020) should allow accurate determination of the efficacy of promising senolytics. A, recent 2020 study used constitutively expressed knock-in system that targets $p16^{High}$ cells to show that removal of particular population of senescent cells could be detrimental. The cell population identified in this study was the $p16^{High}$ vascular endothelial cells in liver sinusoids (LSECs).With age, this particular population of cells are increasingly relied on for detoxification and are not replaced upon removal (Grosse et al., 2020). However, the study also showed that while administration of senolytic cocktail Dasatinib + Quercetin removed $p16^{High}$ macrophages, it did not affect the $p16^{High}$ LSECs. Hence

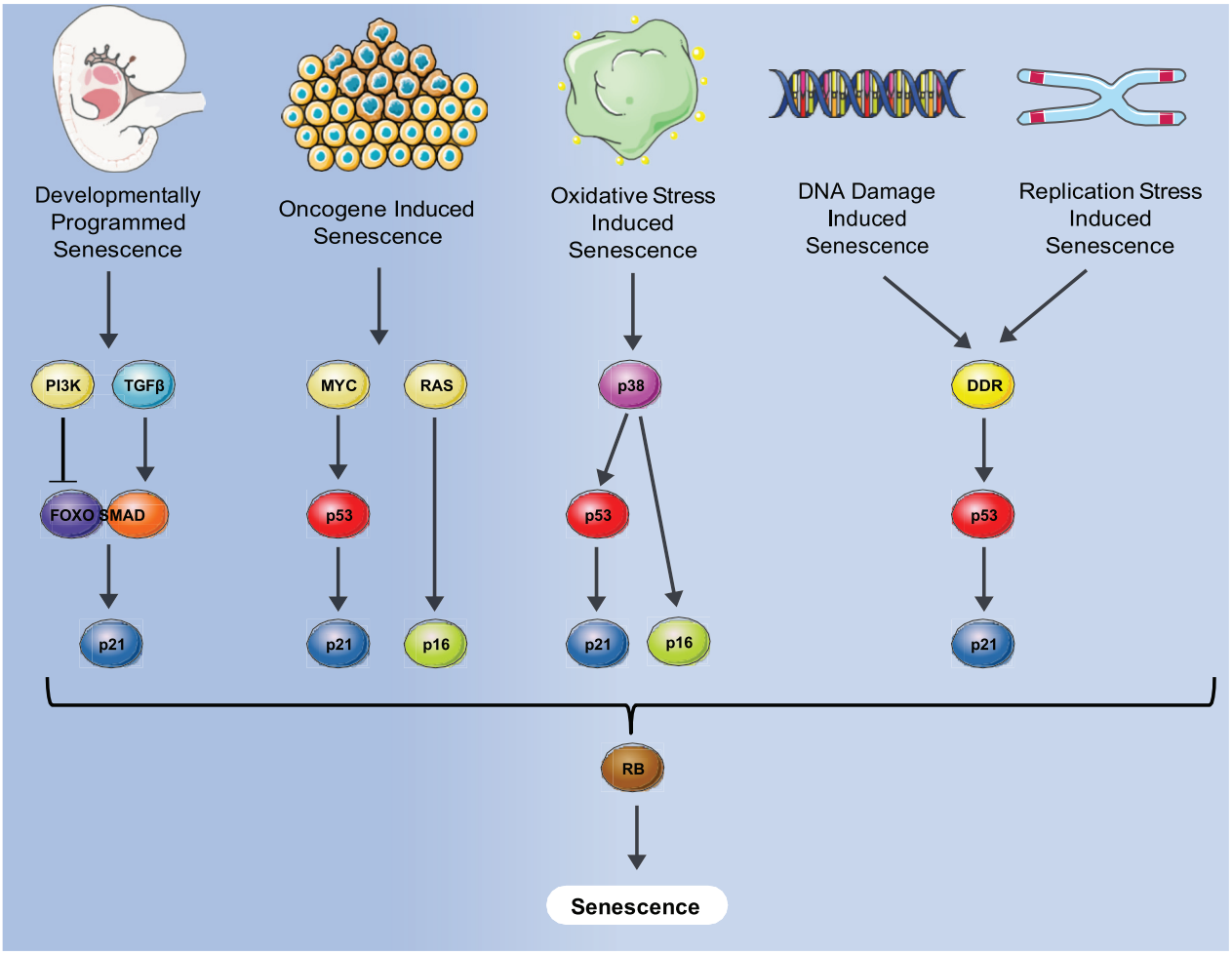

FIGURE 1 | Different senescence induction methods and molecular pathways involved. A variety of stresses such as oncogene, oxidative damage, DNA damage, normal replication and development can induce senescence via either p53-induced expression of p21, p16 expression or both, converging to block Rb inactivation, and leading to senescence where an irreversible cell cycle arrest is imposed.

going forward, much more work needs to be done regarding understanding the deleterious/beneficial functions of crucial sub-populations of senescent cells, especially with novel senolytics already in clinical trials.

Senescence in Development: Contributions of p53

p53, popularly known as guardian of the genome (Lane, 1992) is an essential tumor suppressor that responds to a variety of stresses by activating numerous pathways that lead to cell cycle arrest, senescence, and apoptosis. The essential nature of p53 is clear by the fact that it is mutated in more than half of the human cancers. p53 induced cell cycle arrest was initially discovered in rat embryo fibroblasts using a temperature sensitive mutant (Martinez et al., 1991). P53 induced cell cycle arrest was found to be mediated by p21 which inhibits CDK 2/4 and results in a G1 cell cycle arrest state (Harper et al., 1993). This prevents phosphorylation of Rb, which binds to E2F1 transcription factor and promotes silencing of E2F1 targets necessary for cell cycle progression. p53 induced cell cycle arrest is critical for senescence and knocking out p21 has been shown to prevent this senescence induction (Brown et al., 1997).

Senescence is now appreciated to promote organismal aging and cancer development through effects of the p53 tumor suppressor. This idea was solidified by knockout studies of p53 in mice that showed a lack of developmental defects with the main cause of mortality arising from spontaneous tumor formation (Donehower et al., 1992). However, other studies at the time such as knockout of MDM2 that functions to tag p53 for degradation had shown early embryonic lethality due to unchecked p53 activation (Jones et al., 1995). Further studies with mutated forms of p53 in mice which results in CHARGE syndrome, a complex mixture of eye, heart, nasal cavity, growth, genital, and hearing abnormalities, have suggested that precise spatio/temporal regulation of Tp53 is essential for normal development (Nostrand et al., 2014). The nearly normal development of Tp53-null mice could be due to compensatory

roles by other p53 family proteins such as p63 and p73. This is consistent with studies in *Xenopus laevis* which lacks the p63 and p73 homologs, where p53 knockout results in severe gastrulation defects and early lethality (Wallingford et al., 1997). While p53 knockout alone does not result in embryonic lethality in mice, p53-deficient female mice embryos show an 8-23% occurrence of exencephaly due to failed neural tube closure (Armstrong et al., 1995; Sah et al., 1995). Developmental defects of the eye, upper incisor tooth formation, and polydactyly of the hind legs were also seen at high occurrence in p53 null mice. Lower fertility is also observed in p53 knockout mice, due to abnormalities in spermatogenesis or embryonic implantation difficulties (Beumer et al., 1998; Hu et al., 2007). p53 is also essential for proper differentiation and development of specific tissues (Molchadsky et al., 2010). p53 fulfills this role though regulating genes required for differentiation programs of neuronal cells, osteoblasts, myocytes, adipocytes and B cells, ensuring proper timing and function of differentiation and development (Molchadsky et al., 2010). p53 clearly plays a functional role in development, however, the described phenotypic abnormalities are less crucial to sustaining life than expected by p53's essential role as a tumor suppressor (Jain and Barton, 2018).

Senescence in Development: Contributions of p21

p21 is a cyclin-dependent kinase inhibitor and one of the major effectors of p53. However, p21 can also be activate independently of p53 especially in developmental senescence. p21 binds to PCNA resulting in G1/G2 cell cycle arrest (Luo et al., 1995; Cayrol et al., 1998). While earlier studies suggested p21acts solely as a tumor suppresser, recent studies also suggest that p21 can promote oncogenicity under certain conditions (Roninson, 2002). The CDK inhibitory domain and PCNA binding domains of p21 are responsible for its main growth inhibition characteristics (Chen et al., 1995; Luo et al., 1995). CDK2 inhibition by p21 results in prevention of RB phosphorylation which is necessary for E2F activation and leads to cell cycle arrest (Harper et al., 1993). A variety of structures such as apical ectodermal ridge (AER), neural roof plate, mesonephros, and inner ear endolymphatic sac show certain hallmarks of senescence during the course of normal mammalian embryonic development (Muñoz-Espín et al., 2013; Storer et al., 2013). This developmentally programmed senescence is p21 dependent and unlike other types of senescence such as DNA-damage induced senescence, it is not mediated by p53, but rather regulated by the TGF-β/SMAD and PI3K/FOXO pathways. Developmentally programmed senescence is mainly involved with tissue remodeling, which is executed by macrophages that infiltrate and clear senescent cells. In addition to playing a role in inducing cell cycle arrest and senescence, another major role of p21 in development is the prevention of apoptosis. This is partly due to upregulated anti-apoptotic BCL-2 protein family members in senescent cells (Chang et al., 2016; Zhu et al., 2016). In the mesonephric tubules of p21 null mice embryos, developmentally programmed senescence halts, however, induction of apoptosis takes place the following day which also results in macrophage infiltration followed by clearance of these cells (Muñoz-Espín et al., 2013; Storer et al., 2013). This has led some to suggest that apoptosis and senescence are mutually compensatory mechanisms in mammalian embryonic development, despite being temporally distinct. However, apoptosis does not appear to fully compensate for the absence of developmental senescence. p21 induced senescence plays an important role in the regression of the dorsoventral vaginal septum in female mice. In p21 null female mice, an impaired development of Wolffian duct leads to increased incidence of vaginal septa and decreased fertility (Muñoz-Espín et al., 2013; Storer et al., 2013), suggesting an indirect effect of decreased senescence during development. It will be interesting to see whether future studies confirm the role of p21 induced senescence in other aspects of mammalian development.

Senescence in Development: Contributions of Rb

Retinoblastoma is a tumor suppressor which plays a which plays a pivotal role in cell cycle regulation and tumor progression. The retinoblastoma gene was the first tumor suppressor to be cloned and was a pivotal moment in the field of cancer genetics (Lee et al., 1987). Rb was identified as the protein mutated in the childhood cancer retinoblastoma, and subsequently found to act in a recessive manner, requiring both copies of the *Rb* gene to be mutated to promote aberrant cell growth (Knudson, 1971). Rb's role in cell proliferation was first established by its discovery as a primary target of DNA tumor virus oncoproteins (Whyte et al., 1988). Another important discovery was that overexpression of Rb caused a G1 cell cycle arrest (Goodrich et al., 1991). This was later shown to be a result of Rb's interaction with the E2F family of transcription factors (Dyson, 1998). Rb/E2F pathway functions by recruiting chromatin remodeling factors such as histone deacetylases (HDACs) to repress gene expression (Luo et al., 1998). This was shown to be negatively regulated by CDK mediated phosphorylation of Rb which prevents its binding with E2Fs and HDACs (Harbour and Dean, 2000). Rb tumor suppressor is the primary effector of senescence. Once Rb is fully activated during senescence, it has been speculated that cell cycle arrest becomes permanent and can no longer be reversed by inactivation of Rb or p53. Rb was found to be activated in senescent cells and its enforced expression was found to induce senescence (Lee et al., 2000; Ferbeyre et al., 2002). Moreover, senescence induction by ras oncogene and DNA damaging agents is prevented by adenovirus E1A which targets Rb (Lowe and Ruley, 1993; Serrano et al., 1997). Cells lacking Rb also fail to achieve senescence *in vitro* (Dannenberg et al., 2000; Sage et al., 2000). Knockout or homozygous mutation of the *Rb* gene is embryonically lethal, blocking development between days 13.5 and 15.5 in mice (Jacks et al., 1992). Defects prior to death of the mice include an increase in the number of immature nucleated erythrocytes, inhibition of hepatic erythropoiesis, ectopic proliferation, and apoptosis especially in the hindbrain and death of spinal ganglia (Clarke et al., 1992; Jacks et al., 1992; Lee et al., 1992). The lethal developmental defects of Rb ablation in neurogenesis and hematopoiesis are reversed by insertion

of an *Rb* mini transgene into Rb mutant mice. In embryonic development, loss of Rb has also been shown to cause extensive proliferation of trophoblast cells, damage to the normal labyrinth architect of the placenta, and a decline in vascularization and functional placental transport (Wu et al., 2003).

Retinoblastoma not only plays a role in mammalian development but is also crucial in preventing cancer throughout the lifecycle. Inactivation of Rb can occur through phosphorylation, mutation or viral oncoprotein binding leading to malignant phenotypes (Giacinti and Giordano, 2006). Tumors such as osteosarcomas, small cell-lung carcinomas, breast carcinomas, bladder carcinomas, and glioblastomas have been identified to lack functional Rb, indicating homozygous gene mutations or gene absence contributes to the development of these cancers (Yokota et al., 1988; Horowitz et al., 1990; Venter et al., 1991; Borg et al., 1992; Nielsen et al., 1997). The antagonistic pleiotropy theory of aging described initially by Williams (1957) states that early in life, genes are selected for that increase the organism's fitness, however, they have deleterious effects later in life, contributing to the decline in function described as aging. Apoptosis and senescence have both been thought to display antagonistic pleiotropy through their ability to suppress tumor growth and cancer, but consequently promote an aging phenotype (Campisi, 2003).

APOPTOSIS

Although the process of programmed cell death was first described by Carl Vogt in 1842 while studying tadpole development, the term apoptosis was first used by Kerr et al. (1972) to describe controlled, programmed cell death, and with cells exhibiting distinct changes in morphology.

Apoptosis plays a crucial role in clearing redundant, irregular or dangerous cells, while regulating growth, development and the immune response. Cells undergoing apoptosis form apoptotic bodies, through condensation of their cytoplasm and nucleus, DNA fragmentation, loss of cell-cell adhesion, and blebbing of the cell membrane (Kerr, 1971). Apoptotic bodies are quickly phagocytosed by macrophages or neighboring cells, resulting in relatively low levels of inflammation, in contrast to necrosis (Reed, 2000). Once Apoptosis is initiated, it is carried out through the activation of a caspase-cascade, a series of cystine-aspartic proteases (D'Arcy, 2019). The caspases selectively cleave target proteins, either activating or inactivating them to promote cell death (Hengartner, 2000) in response to cell damage and during development.

Apoptotic Pathways

There are two major pathways used to activate the caspase cascade, the death receptor-mediated (extrinsic) pathway, and the mitochondria-mediated (intrinsic) pathway shown in **Figure 2**. In non- apoptotic cells, caspases exist in an inactive zymogen or procaspase form (Budihardjo et al., 1999). The extrinsic pathway activates the caspase cascade, through binding of death ligands to the tumor necrosis factor superfamily (TNF) of cell surface death receptors. Fas, TNF receptor 1 (TNFR1), Death receptor 3 (DR3), DR4/TNF-related apoptosis-inducing ligand receptor 1 (TRAIL-R1), and Dr5/TRAIL-R2 are mammalian death receptors involved in inducing extrinsic apoptosis (Ashkenazi and Dixit, 1998). Each death receptor is able to bind a specific death ligand; Fas binds FasL, TNFR1 binds TNF, DR3 binds Apo3L, and DR4 and DR5 both bind Apol2. The Fas and TNFR1 death receptors both contain a death domain (DD) that they use to recruit adaptor molecules upon ligand binding. Fas-associated protein with death domain (FADD) and TNF- receptor associated death domain (TRADD) bind with their complementary death domain (DD) to Fas and TNFR1, respectively. The cytoplasmic side of the death receptor and it's corresponding adaptor protein make up the death-inducing signal complex (DISC) (D'Arcy, 2019). The adaptor proteins also contain a death effector domain (DED) that is responsible for recruiting procaspase- 8 and procaspase-10 through their own DED's to the DISC for activation by proteolytic cleavage. Two separate pathways are regulated by active initiator caspases-8 and -10. The initiator caspases cleave the downstream executioner caspases, caspase-3, caspase-6, and caspase-7, activating and allowing them to transform the cell into an apoptotic body (Singh et al., 2019). Caspase-8 can also activate the intrinsic pathway involving mitochondria, through cleavage of BID, which initiates apoptosome formation, activating caspase-9, thus activating the executioner caspases.

The intrinsic apoptosis pathway is activated by stimuli such as irradiation, chemotherapy, deprivation of cytokines, and growth factors or DNA damage (Igney and Krammer, 2002). These stimuli cause the increased transcription and/or posttranslational modification of BH3-only proteins (BIM, PUMA, BID, BMF, BAD, BIK, NOXA, and HRK) that suppress the activity of cell survival BCL-2 proteins (Aubrey et al., 2017). Inhibition of the pro-survival proteins allows the release of BCL-2 family member proteins BAX and BAK that function to produce mitochondrial outer membrane permeabilization (MOMP), allowing the release of cytochrome C, and SMAC/DIABLO into the cytosol. Cytochrome C binds to apoptotic protease activating factor 1 (APAF1) forming the apoptosome, where caspase-9 is activated (Igney and Krammer, 2002). Active caspase-9 cleaves and activates the executioner caspases (caspases-3,6,7) that induce the hallmark characteristics of apoptotic cells. The SMAC/DIABLO protein functions to inhibit the inhibitors of apoptosis proteins (IAPs), allowing apoptosis to occur through both pathways (Igney and Krammer, 2002). Additionally, unresolved Endoplasmic Reticulum (ER) stress can lead to the induction of apoptosis. ER stress is caused by increased rates of misfolded proteins above the load capable of being handled by chaperones including heat shock proteins (Tabas and Ron, 2011). In mammals, misfolded proteins activate the ER-specific unfolded protein response (UPR), which contains three branches that are transduced by upstream signaling molecules, IRE1, PERK, and AFT6 that sense ER stress (Tabas and Ron, 2011). If the UPR fails to restore proper ER function it will switch to a pro-apoptotic function (Szegezdi et al., 2006). IRE1, PERK, and AFT6 all induce the transcription of CHOP (Szegezdi et al., 2006). IRE1 also recruits apoptosis signal-regulating kinase 1 (ASK1), which signals JNK, a protein kinase (Szegezdi et al., 2006). JNK and CHOP suppress the

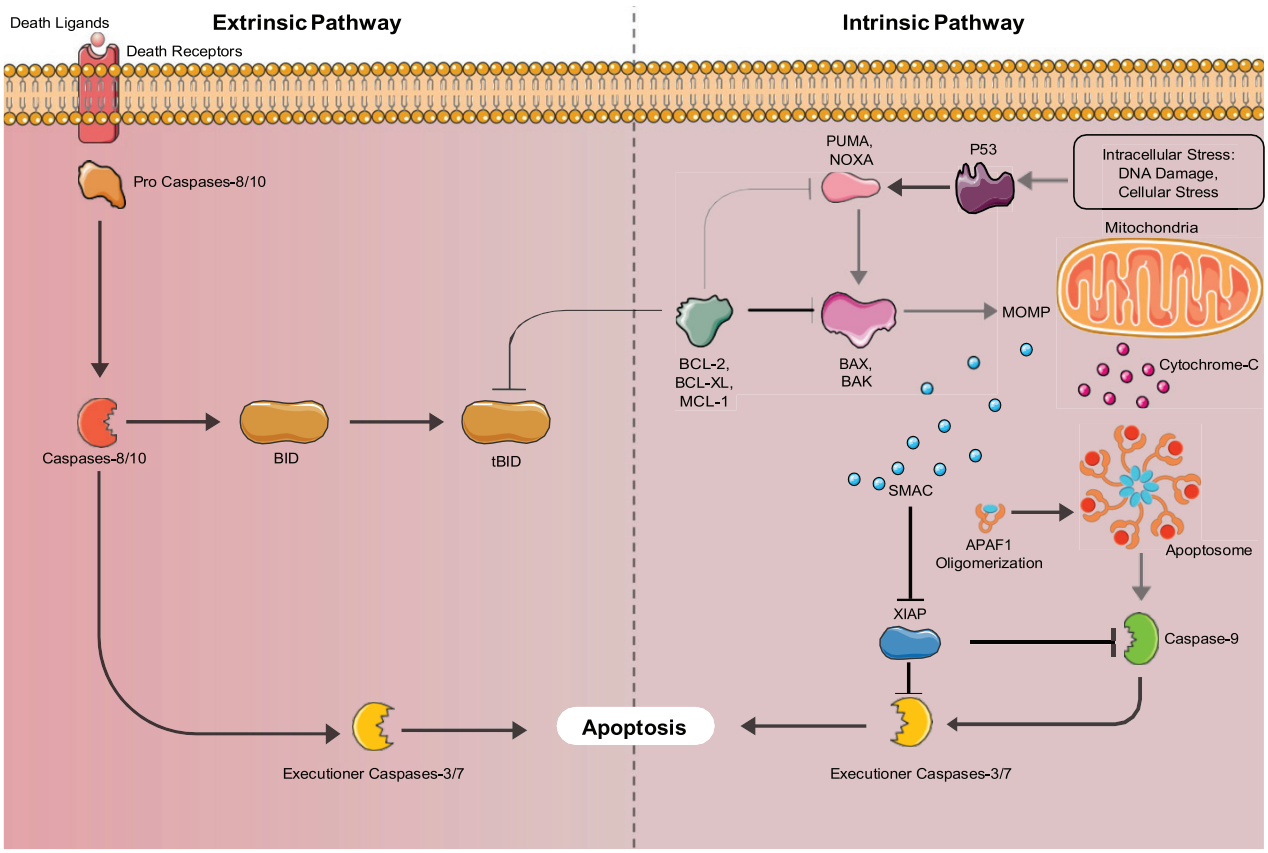

FIGURE 2 | Intrinsic and Extrinsic Apoptosis pathways: Apoptosis can be mediated by either the intrinsic (mitochondria-mediated) pathway or extrinsic (death-receptor mediated) pathways. Both pathways converge upon executioner caspases (Caspase-3 and 7) that induce apoptosis.

anti-apoptotic properties of BCL-2 proteins (Szegezdi et al., 2006). Bax and Bak are then expressed and subsequently activate the caspases that directly initiate apoptosis (Szegezdi et al., 2006). ER stress also induces senescence through the AFT6 branch of the UPR (Druelle et al., 2016). ATF6 was shown by Druelle et al. (2016) in normal human dermal fibroblasts to be important for controlling the increase in SA-β-Gal activity, the cell morphological changes associated with senescence and the ER expansion associated with the senescent phenotype (Druelle et al., 2016). AFT6 upregulates the COX2/PGE_2 intracrine pathway, which contributes to the induction and maintenance of the senescent phenotype (Cormenier et al., 2018).

Another form of cell self-destruction is autophagy. In mammals, autophagy is the mechanism where cytosolic components of a cell are delivered to the lysosome for degradation and the products can be recycled and used as building blocks for biosynthetic reactions or for energy production (Mizushima and Komatsu, 2011). Interestingly, autophagy not only plays a role in cell destruction, but also functions in maintaining stemness. García-Prat et al. (2016) demonstrated that as mice age their muscle stem cells lose their autophagy ability, causing the accumulation of damaged cellular components, with cells senescing and losing their properties of stemness (García-Prat et al., 2016; Tabas and Ron, 2011; Szegezdi et al., 2006; Druelle et al., 2016; Cormenier et al., 2018; Mizushima and Komatsu, 2011).

Apoptosis in Development

In mammals and other vertebrates, apoptosis is crucial for the formation and maintenance of tissue patterning (Meier et al., 2000; Zakeri et al., 2015) and is important for the development of the central nervous system (Naruse and Keino, 1995; Washausen et al., 2018) in a segmental manner (Lumsden et al., 1991; Knabe et al., 2004) including the optic system (Knabe and Kuhn, 1998; Knabe et al., 2000) as noted in **Figure 3**. The formation of the neural tube from the neural plate is thought to be the first critical developmental stage in the CNS aided by apoptosis. Caspase 3 and 9 knockout mice display defective brain development due to excess neuroepithelial cells, while a knockout of caspase 8 affects cardiac muscle development and erythropoiesis (Kuida et al., 1996, 1998; Hakem et al., 1998; Varfolomeev et al., 1998). Caspase 3 mutant mice are born at a lower fequencey than expected by mendelian genetics and most die shortly after birth, due to caspase 3's required role in brain development (Woo et al., 1998). Similarly, caspase 9 deficient mice die prenatally due to their inability to activate the caspase 3 executioner caspase, resulting in perturbations of brain morphology. Caspase

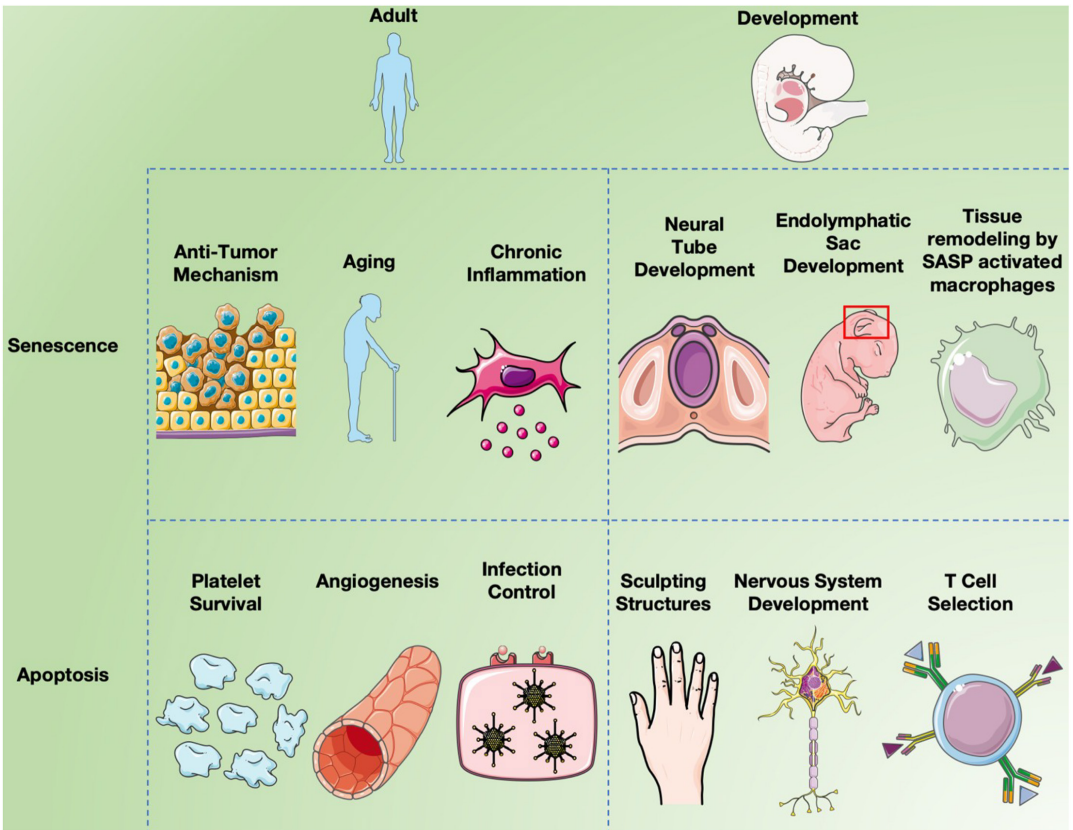

FIGURE 3 | Senescence and apoptosis in development and aging. Cell senescence is clearly a major factor in inducing chronic inflammation by fragmented DNA activating the innate immune response via cGAS- STING, resulting in senescent cells secreting a combination of factors collectively called the SASP (Hopfner and Hornung, 2020). Inflammation induces many aspects of aging, but cell senescence is also believed to serve as a "first line of defense" against cancer since it limits cell replication (Campisi, 2003). While apoptosis long been known to affect different aspects of both development and aging, recent studies have implicated programmed cell senescence in tissue remodeling of different types (Muñoz-Espín et al., 2013; Storer et al., 2013; Zhao et al., 2018).

8 knockout mice are also embryonic lethal as caspase 8 absence obstructs apoptosis induction by TNF death receptors resulting in abnormal phenotypes. Additionally Caspase-8C362S/C362S mice are also embryonic lethal (Fritsch et al., 2019). Mice lacking Apaf-1, a key component of the apoptosome, showed reduced apoptosis in the developing brain, causing hyperproliferation of neurons and craniofacial irregularities (Yoshida et al., 1998). Apaf-1 deficient mice also had persistence of interdigital webs, abnormalities of the lens and retina, and an inability to activate caspase 3, leading to death at embryonic day 16.5 (Cecconi et al., 1998). Less than 10% of mice deficient in Bak and Bax survived and had birth defects such as imperforate vaginal canals, interdigital webbing and excess brain cells (Lindsten et al., 2000). As well, only 2% of Bok, Bax and Bak knockout mice survived to weaning with non-lethal abnormalities (Ke et al., 2018). These observations confirm the importance of apoptosis for normal development.

Apoptosis plays a role in sculpting structures in vertebrates, through the deletion of cells between developing digits as well as deletion of cells to form hollow structures (Jacobson et al., 1997). Structures are formed during development that later do not serve a purpose and are thus removed by apoptosis such as removal of the rudimentary lateral line system of aquatic vertebrates, from mice (Washausen and Knabe, 2018). These structures also include ones needed by only one sex, vestigial structures, and structures only needed for certain developmental stages. Apoptosis eliminates pronephric tubules in mammals, but not in amphibians or fish where they form functional kidneys. The Wolffian and Mullerian ducts are only required in male and female reproductive systems, respectively, and are eliminated by apoptosis in the opposite sex (Meier et al., 2000). Cells may be over produced during embryonic development, and apoptosis helps to control this. During mammalian development, apoptosis also aids in quality control, through removal of irregular, non-functional or dangerous cells, and preventing birth defects and cancer (Jacobson et al., 1997).

Different apoptosis regulatory proteins are expressed variably throughout mammalian development. In early embryonic development of mice, BCL-2 is extensively expressed in all germ layers, but its expression declines during maturation. Norvak and Korsmeyer found that in endodermal epithelial cells of the lung bud, Bcl-2 is expressed in a proximal to distal gradient at E12.5 and increases by day E18.5. In mesodermal tissues, the uterine bud and metanephric cap of the kidney, Bcl-2 is expressed at

E 12.5 (Novack and Korsmeyer, 1994). Retinal neuroepithelial cells derived from the ectoderm show uniform expression of Bcl-2 up until differentiation, then a topographic distribution is established that persists throughout maturation. As predicted, Bcl-2 is only present in regions of cell survival such as the digital zones of the developing limb, and its expression is absent in the interdigital zones where cells die before the end of fetal development. Bcl-2 expression decreases in the central nervous system following neural tube formation but remains highly expressed in the peripheral nervous system (Merry et al., 1994). Caspase 3 has been shown to be highly expressed in the brain during embryonic and early post-natal development, but this declines at 4 weeks postnatal and its absence remains throughout aging (Shimohama et al., 1999). These changes in expression correlate well with the removal and maintenance of various structures during development. **Table 1** details a summary of developmental phenotypes of transgenic mice associated with apoptosis/senescence related genes.

DUAL FUNCTIONS OF p53, Rb, AND ING1 IN SENESCENCE AND APOPTOSIS

The p53 protein can induce senescence followed by apoptosis in cells with unrepairable damage (Amundson et al., 1998). p53's ability to activate apoptosis was clear when thymocytes in p53 knockout mice were shown to be resistant to apoptosis induced by radiation or other stimuli that cause DNA damage (Clarke et al., 1993; Lowe et al., 1993). Cells undergoing p53-dependent apoptosis normally proceed through the intrinsic pathway. The BH3-only proteins PUMA and NOXA are direct targets of p53 for upregulated transcription and expression leading to the induction of apoptosis (Oda et al., 2000; Nakano and Vousden, 2001). BAX and BID are also direct targets of p53, and their expression is upregulated during p53-dependent apoptosis (Toshiyuki and Reed, 1995; Sax et al., 2002). In addition to its function as a transcription factor, p53 acts also acts in the cytoplasm, binding to anti-apoptotic, pro-cell survival BCL-2 proteins (BCL-2 and BCL-x), which releases the pro-apoptotic proteins, BAX and BAK to carry out MOMP, and subsequently the rest of apoptosis (Schuler and Green, 2005). APAF-1, the protein required for apoptosome formation is also a transcriptional target of p53 during apoptosis (Moroni et al., 2001). In cells undergoing apoptosis induced by hypoxia, p53 has been found to target and upregulate the death receptor Fas (Liu et al., 2006). The p53 apoptosis pathway is also activated by the loss of Rb function, to remove cells lacking this protective anti-tumor mechanism (Morgenbesser et al., 1994). p53 mediated apoptosis might also act to prevents birth defects (Norimura et al., 1996). When pregnant mice with $p53^{-/-}$ embryos were exposed to ionizing radiation, there was a high rate of birth defects (70%) and low rate of embryonic lethality (7%) compared to wildtype $p53^{+/+}$ embryos that had 60% embryonic death, and only 20% of offspring with birth defects. p53 is thought to prevent birth defects through eliminating abnormal cells, however, if too many cells are removed through apoptosis the embryo dies.

Depending upon the stage of the cell cycle, Rb can have an anti-apoptotic or pro-apoptotic function (Ianari et al., 2009). Rb plays an anti-apoptotic role in cells present in G0/G1 (non-proliferating), by suppressing EF2 transcription factors, which typically contribute to apoptosis progression by transcriptionally activating p73 and caspase-7 (Iaquinta and Lees, 2007). In contrast, in proliferating cells, Rb acts as a pro-apoptotic regulator in the presence of stressors that cause DNA-damage. Under these conditions Rb is phosphorylated resulting in the formation of the pRB-E2F1- P/CAF complex which is active at pro-apoptotic gene promoters (Ianari et al., 2009). **Figure 3** shows an overview of both post and pre developmental roles senescence and apoptosis plays in mammalian systems.

TABLE 1 | Summary of transgenic mice developmental phenotypes with knockout or knock-in of key genes involved in apoptosis and senescence.

KO mice type	Pathway effected	Developmental phenotype	References
$p21^{-/-}$	Senescence	Impaired development of Wolffian duct, apical ectodermal ridge, and decreased fertility in female mice	Muñoz-Espín et al., 2013; Storer et al., 2013
$p53^{-/-}$	Senescence	Tumour formation 8–23% of female mice develop exencephaly. Defects in eye, upper incisor tooth, and polydactyl of hind legs. Low fertility	Donehower et al., 1992; Armstrong et al., 1995; Sah et al., 1995; Beumer et al., 1998; Hu et al., 2007
$Rb^{-/-}$	Senescence	Embryonic lethal	Jacks et al., 1992
$Ing1^{-/-}$	Apoptosis	Reduced size, increased Bax expression, and DNA damage induced apoptosis	Kichina et al., 2006; Coles et al., 2007
$Bax^{-/-}$ and $Bak^{-/-}$	Apoptosis	Less than 10% survive to weaning, and have birth defects including imperforate vaginal canal, interdigital webbing, and excess brain cells	Lindsten et al., 2000
$Bok^{-/-}$, $Bak^{-/-}$, and $Bax^{-/-}$	Apoptosis	2% survived to weaning with non-lethal abnormalities	Ke et al., 2018
Caspase-$3^{-/-}$	Apoptosis	Excess neuroepithelial cells, death shortly after birth	Kuida et al., 1996; Hakem et al., 1998; Woo et al., 1998
Caspase $9^{-/-}$	Apoptosis	Defective brain development, death shortly after birth	Kuida et al., 1998
Caspase-$8^{-/-}$	Apoptosis	Embryonic lethal	Varfolomeev et al., 1998
Caspase-$8^{C3626/C3626}$	Apoptosis	Embryonic lethal	Fritsch et al., 2019
Apaf-$1^{-/-}$	Apoptosis	Embryonic lethal	Cecconi et al., 1998; Yoshida et al., 1998

Apoptosis and senescence are clearly crucial processes involved in development, as these knockouts show birth defects or premature death.

The ING ("INhibitor of Growth") tumor suppressors are also capable of inducing both senescence and apoptosis, largely by their effects on the p53 and Rb pathways. The first report of ING1 affecting apoptosis came from study of P19 teratocarcinoma cells where serum starvation caused increased expression of ING1 and consequent induction of apoptosis that appeared to occur in collaboration with c-Myc (Helbing et al., 1997). The ability of ING1 to induce apoptosis in response to UV-induced DNA damage was dependent upon the PCNA-interacting Protein (PIP) motif of ING1 (Scott et al., 2001) while the ability of both ING1and ING2 to efficiently induce apoptosis via p53 depends largely on their polybasic regions that bind the bioactive stress-induced phospholipid phosphatidyl inositol 5′-monophosphate (Gozani et al., 2003). Both ING1 and ING2 are stoichiometric members of the Sin3a histone deacetylase complex (Doyon et al., 2006) and directly affect p53 acetylation at lysine residues 373 and/or 382 (Kataoka et al., 2003), activating it as a growth inhibitor and inducer of apoptosis. ING1 was also shown to be required for the full ability of p53 to block cell growth (Garkavtsev et al., 1998) and this was later determined to be a consequence of ING1 stabilizing p53 by multi/mono-ubiquitination, preventing the polyubiquitination and subsequent proteosome- dependent degradation of p53 (Thalappilly et al., 2011). ING1 also promoted p53 accumulation in response to oncogenic stress (Abad et al., 2007). Like p53, ING1 can promote apoptosis through effects at the mitochondria of fibroblasts by interacting with Bax (Bose et al., 2013) and in melanoma cells in response to UV induced DNA damage, ING1 promoted p53-induced Bax expression to alter mitochondrial membrane potential and induce apoptosis (Cheung and Li, 2002). Links between ING proteins and cell senescence were also apparent since knockdown of either ING1 (Garkavtsev and Riabowol, 1997) or ING2 (Pedeux et al., 2005) that are both components of the Sin3a HDAC complex extends cell replicative lifespan, delaying senescence. In contrast, the ING1a splicing variant of ING1 that increases ∼10-fold during cell senescence (Soliman et al., 2008) induces senescence much more rapidly than other stresses (Rajarajacholan and Riabowol, 2015) via disrupting endocytosis that activates the Rb/p16/p57 pathway. ING1a expression imposes most of the hallmarks of cell senescence including growth arrest, senescence-associated b-Galactosidase expression, increased p16 and Rb, senescence-associated heterochromatic foci and phenotypic changes resembling replicative senescence (Rajarajacholan et al., 2013). Knockout of Ing1 results in mice with reduced overall size and body weight, increased turnover of thymocytes, behavioral abnormalities and increased sensitivity to ionizing radiation, and consequently a shortened lifespan. While there were no other obvious developmental abnormalities, an earlier and higher incidence of lymphomas was also reported (Kichina et al., 2006). While Ing1 deficient mouse embryonic fibroblasts (MEF) have an increased growth rate, this was also sustained in p53 deficient MEFs suggesting a p53 independent role in cell proliferation. Ing1 knockout also induces Bax expression and promotes DNA damage-induced apoptosis independent of p53 (Coles et al., 2007).

SUMMARY

The p53, Rb, and ING tumor suppressors all affect cell growth, apoptosis and senescence, and in doing so at different stages of cell lifespan, exhibit a degree of antagonistic pleiotropy. ING1 potentiates the activity of both p53 and Rb as inhibitors of growth and the p53 and Rb pathways show crosstalk through the CDK inhibitors p16 and p21. While p53, Rb, and ING1 play central roles in maintaining normal cell cycle progression and guard against unregulated cell growth to inhibit oncogenesis, these proteins later take on a significantly stronger role in growth inhibition, ultimately blocking cell growth fully in the state of replicative senescence.

AUTHOR CONTRIBUTIONS

EW and HT wrote the first draft. HT produced the figures. KR edited the manuscript and obtained funding. All authors contributed to the article and approved the submitted version.

REFERENCES

Abad, M., Menéndez, C., Füchtbauer, A., Serrano, M., Füchtbauer, E. M., and Palmero, I. (2007). Ing1 mediates p53 accumulation and chromatin modification in response to oncogenic stress. *J. Biol. Chem.* 282, 31060–31067. doi: 10.1074/jbc.m701639200

Aiken, C. E. M., Swoboda, P. P. L., Skepper, J. N., and Johnson, M. H. (2004). The direct measurement of embryogenic volume and nucleo-cytoplasmic ratio during mouse pre- implantation development. *Reproduction* 128, 527–535. doi: 10.1530/rep.1.00281

Alcorta, D. A., Xiong, Y., Phelps, D., Hannon, G., Beach, D., and Barrett, J. C. (1996). Involvement of the cyclin-dependent kinase inhibitor p16 (INK4a) in replicative senescence of normal human fibroblasts. *Proc. Natl. Acad. Sci. U.S.A.* 93, 13742–13747. doi: 10.1073/pnas.93.24.13742

Alison, M. R., Poulsom, R., Forbes, S., and Wright, N. A. (2002). An introduction to stem cells. *J. Pathol.* 197, 419–423.

Amundson, S. A., Myers, T. G., and Fornace, A. J. (1998). Roles for p53 in growth arrest and apoptosis: putting on the brakes after genotoxic stress. *Oncogene* 17, 3287–3299. doi: 10.1038/sj.onc.1202576

Angeles, A. D. L., Ferrari, F., Xi, R., Fujiwara, Y., Benvenisty, N., Deng, H., et al. (2015). Hallmarks of pluripotency. *Nature* 525, 469–478.

Armstrong, J. F., Kaufman, M. H., Harrison, D. J., and Clarke, A. R. (1995). High-frequency developmental abnormalities in p53-deficient mice. *Curr. Biol.* 5, 931–936. doi: 10.1016/s0960-9822(95)00183-7

Ashkenazi, A., and Dixit, V. M. (1998). Death receptors: signaling and modulation. *Science* 281, 1305–1308. doi: 10.1126/science.281.5381.1305

Aubrey, B. J., Kelly, G. L., Janic, A., Herold, M. J., and Strasser, A. (2017). How does p53 induce apoptosis and how does this relate to p53-mediated tumour suppression? *Cell Death Differ.* 25, 104–113. doi: 10.1038/cdd.2017.169

Avilion, A. A., Nicolis, S. K., Pevny, L. H., Perez, L., Vivian, N., and Lovell-Badge, R. (2003). Multipotent cell lineages in early mouse development depend on SOX2 function. *Gene Dev.* 17, 126–140. doi: 10.1101/gad.224503

Baker, C. L., and Pera, M. F. (2018). Capturing totipotent stem cells. *Cell Stem Cell* 22, 25–34. doi: 10.1016/j.stem.2017.12.011

Baker, D. J., Wijshake, T., Tchkonia, T., Lebrasseur, N. K., Childs, B. G., Sluis, B. V. D., et al. (2011). Clearance of p16 Ink4a-positive senescent cells delays ageing-associated disorders. *Nature* 479, 232–236. doi: 10.1038/nature10600

Bannister, A. J., and Kouzarides, T. (2011). Regulation of chromatin by histone modifications. *Cell Res.* 21, 381–395. doi: 10.1038/cr.2011.22

Bel-Vialar, S., Itasaki, N., and Krumlauf, R. (2002). Initiating Hox gene expression: in the early chick neural tube differential sensitivity to FGF and RA signaling subdivides the HoxB genes in two distinct groups. *Dev. Camb. Engl.* 129, 5103–5115.

Beumer, T. L., Roepers-Gajadien, H. L., Gademan, I. S., van Buul, P. P., Gil-Gomez, G., Rutgers, D. H., et al. (1998). The role of the tumor suppressor p53 in spermatogenesis. *Cell Death Differ.* 5, 669–677.

Bhatia, M., Wang, J. C. Y., Kapp, U., Bonnet, D., and Dick, J. E. (1997). Purification of primitive human hematopoietic cells capable of repopulatingimmune-deficientmice. *Proc. Natl. Acad. Sci. U.S.A.* 94, 5320–5325. doi: 10.1073/pnas.94.10.5320

Biggers, J. D., Bell, J. E., and Benos, D. J. (1988). Mammalian blastocyst: transport functions in a developing epithelium. *Am. J. Cell. Physiol.* 255, C419–C432.

Borg, A., Zhang, Q. X., Alm, P., Olsson, H., and Sellberg, G. (1992). The retinoblastoma gene in breast cancer: allele loss is not correlated with loss of gene protein expression. *Cancer Res.* 5, 2991–2994.

Bose, P., Thakur, S., Thalappilly, S., et al. (2013). ING1 induces apoptosis through direct effects at the mitochondria. *Cell Death Dis.* 4:e788. doi: 10.1038/cddis.2013.321

Bromleigh, V. C., and Freedman, L. P. (2000). p21 is a transcriptional target of HOXA10 in differentiating myelomonocytic cells. *Gene Dev.* 14, 2581–2586. doi: 10.1101/gad.817100

Brown, J. P., Wei, W., and Sedivy, J. M. (1997). Bypass of senescence after disruption of p21CIP1/WAF1 gene in normal diploid human fibroblasts. *Science* 277, 831–834. doi: 10.1126/science.277.5327.831

Budihardjo, I., Oliver, H., Lutter, M., Luo, X., and Wang, X. (1999). Biochemical pathways of caspase activation during apoptosis. *Annu. Rev. Cell Dev. Biol.* 15, 269–290. doi: 10.1146/annurev.cellbio.15.1.269

Campisi, J. (2003). Cancer and ageing: rival demons? *Nat. Rev. Cancer* 3, 339–349. doi: 10.1038/nrc1073

Caplan, A. I. (1991). Mesenchymal stem cells. *J. Orthopaed. Res.* 9, 641–650.

Cayrol, C., Knibiehler, M., and Ducommun, B. (1998). p21 binding to PCNA causes G1 and G2 cell cycle arrest in p53-deficient cells. *Oncogene* 16, 311–320. doi: 10.1038/sj.onc.1201543

Cecconi, F., Alvarez-Bolado, G., Meyer, B. I., Roth, K. A., and Gruss, P. (1998). Apaf1 (CED-4 homolog) regulates programmed cell death in mammalian development. *Cell* 94, 727–737. doi: 10.1016/s0092-8674(00)81732-8

Chambers, I., Colby, D., Robertson, M., Nichols, J., Lee, S., Tweedie, S., et al. (2003). Functional expression cloning of nanog, a pluripotency sustaining factor in embryonic stem cells. *Cell* 113, 643–655. doi: 10.1016/s0092-8674(03)00392-1

Chang, J., Wang, Y., Shao, L., Laberge, R.-M., Demaria, M., Campisi, J., et al. (2016). Clearance of senescent cells by ABT263 rejuvenates aged hematopoietic stem cells in mice. *Nat. Med.* 22, 78–83. doi: 10.1038/nm.4010

Chapman, V., Forrester, L., Sanford, J., Hastie, N., and Rossant, J. (1984). Cell lineage-specific undermethylation of mouse repetitive DNA. *Nature* 307, 284–286. doi: 10.1038/307284a0

Chen, J., Jackson, P. K., Kirschner, M. W., and Dutta, A. (1995). Separate domains of p21 involved in the inhibition of Cdk kinase and PCNA. *Nature* 374, 386–388. doi: 10.1038/374386a0

Cheung, K.-J., and Li, G. (2002). p33ING1 enhances UVB-induced apoptosis in melanoma cells. *Exp. Cell Res.* 279, 291–298. doi: 10.1006/excr.2002.5610

Chuprin, A., Gal, H., Biron-Shental, T., Biran, A., Amiel, A., Rozenblatt, S., et al. (2013). Cell fusion induced by ERVWE1 or measles virus causes cellular senescence. *Genes Dev.* 27, 2356–2366. doi: 10.1101/gad.227512.113

Clarke, A. R., Maandag, E. R., Roon, M. V., Lugt, N. M. T. V. D., Valk, M. V. D., Hooper, M. L., et al. (1992). Requirement for a functional Rb-1 gene in murine development. *Nature* 359, 328–330. doi: 10.1038/359328a0

Clarke, A. R., Purdie, C. A., Harrison, D. J., Morris, R. G., Bird, C. C., Hooper, M. L., et al. (1993). Thymocyte apoptosis induced by p53-dependent and independent pathways. *Nature* 362, 849–852. doi: 10.1038/362849a0

Coles, A. H., Liang, H., Zhu, Z., Marfella, C. G. A., Kang, J., Imbalzano, A. N., et al. (2007). Deletion of p37Ing1 in mice reveals a p53-independent role for Ing1 in the suppression of cell proliferation, apoptosis, and tumorigenesis. *Cancer Res.* 67, 2054–2061. doi: 10.1158/0008-5472.can-06-3558

Copp, A. J., Greene, N. D. E., and Murdoch, J. N. (2003). The genetic basis of mammalian neurulation. *Nat. Rev. Genet.* 4, 784–793. doi: 10.1038/nrg1181

Coppe, J. P., Patil, C. K., Rodier, F., Sun, Y., Munoz, D. P., Goldstein, J., et al. (2008). Senescence- associated secretory phenotypes reveal cell-nonautonomous functions of oncogenic RAS and the p53 tumor suppressor. *PLoS Biol.* 6, 2853–2868. doi: 10.1371/journal.pbio.0060301

Cormenier, J., Martin, N., Deslé, J., Salazar-Cardozo, C., Pourtier, A., Abbadie, C., et al. (2018). The ATF6α arm of the Unfolded Protein Response mediates replicative senescence in human fibroblasts through a COX2/prostaglandin E2 intracrine pathway. *Mech. Ageing Dev.* 170, 82–91. doi: 10.1016/j.mad.2017.08.003

Dannenberg, J.-H., van Rossum, A., Schuijff, L., and te Riele, H. (2000). Ablation of the Retinoblastoma gene family deregulates G1 control causing immortalization and increased cell turnover under growth-restricting conditions. *Gene Dev.* 14, 3051–3064. doi: 10.1101/gad.847700

D'Arcy, M. S. (2019). Cell death: a review of the major forms of apoptosis, necrosis and autophagy. *Cell Biol. Int.* 43, 582–592. doi: 10.1002/cbin.11137

Das, P. M., and Singal, R. (2004). DNA methylation and cancer. *J. Clin. Oncol.* 22, 4632–4642.

Davaapil, H., Brockes, J. P., and Yun, M. H. (2017). Conserved and novel functions of programmed cellular senescence during vertebrate development. *Development* 144, 106–114. doi: 10.1242/dev.138222

Deschamps, J., and van Nes, J. (2005). Developmental regulation of the Hox genes during axial morphogenesis in the mouse. *Development* 132, 2931–2942. doi: 10.1242/dev.01897

Donehower, L. A., Harvey, M., Slagle, B. L., McArthur, M. J., Montgomery, C. A., Butel, J. S., et al. (1992). Mice deficient for p53 are developmentally normal but susceptible to spontaneous tumours. *Nature* 356, 215–221. doi: 10.1038/356215a0

Doyon, Y., Cayrou, C., Ullah, M., Landry, A. J., Côté, V., Selleck, W., et al. (2006). ING tumor suppressor proteins are critical regulators of chromatin acetylation required for genome expression and perpetuation. *Mol. Cell.* 21, 51–64. doi: 10.1016/j.molcel.2005.12.007

Druelle, C., Drullion, C., Deslé, J., Martin, N., Saas, L., Cormenier, J., et al. (2016). ATF6α regulates morphological changes associated with senescence in human fibroblasts. *Oncotarget* 7, 67699–67715. doi: 10.18632/oncotarget.11505

Dyson, N. (1998). The regulation of E2F by pRB-family proteins. *Gene Dev.* 12, 2245–2262. doi: 10.1101/gad.12.15.2245

Efroni, S., Duttagupta, R., Cheng, J., Dehghani, H., Hoeppner, D. J., Dash, C., et al. (2008). Global transcription in pluripotent embryonic stem cells. *Cell Stem Cell* 2, 437–447.

Ferbeyre, G., de Stanchina, E., Lin, A. W., Querido, E., McCurrach, M. E., Hannon, G. J., et al. (2002). Oncogenic ras and p53 cooperate to induce cellular senescence. *Mol. Cell. Biol.* 22, 3497–3508. doi: 10.1128/mcb.22.10.3497-3508.2002

Forlani, S., Lawson, K. A., and Deschamps, J. (2003). Acquisition of Hox codes during gastrulation and axial elongation in the mouse embryo. *Development* 130, 3807–3819. doi: 10.1242/dev.00573

Fouse, S. D., Shen, Y., Pellegrini, M., Cole, S., Meissner, A., Neste, L. V., et al. (2008). Promoter CpG methylation contributes to ES cell gene regulation in parallel with Oct4/Nanog, PcG Complex, and Histone H3 K4/K27 Trimethylation. *Cell Stem Cell* 2, 160–169. doi: 10.1016/j.stem.2007.12.011

Fritsch, M., Günther, S. D., Schwarzer, R., Albert, M.-C., Schorn, F., Werthenbach, J. P., et al. (2019). Caspase-8 is the molecular switch for apoptosis, necroptosis and pyroptosis. *Nature* 575, 683–687. doi: 10.1038/s41586-019-1770-6

Gage, F. H. (2000). Mammalian neural stem cells. *Science* 287, 1433–1438. doi: 10.1126/science.287.5457.1433

Garcia-Fernàndez, J. (2004). Hox, ParaHox, ProtoHox: facts and guesses. *Heredity* 94, 145–152. doi: 10.1038/sj.hdy.6800621

García-Prat, L., Martínez-Vicente, M., Perdiguero, E., Ortet, L., Rodríguez-Ubreva, J., Rebollo, E., et al. (2016). Autophagy maintains stemness by preventing senescence. *Nature* 529, 37–42. doi: 10.1038/nature16187

Garkavtsev, I., Grigorian, I. A., Ossovskaya, V. S., Chernov, M. V., Chumakov, P. M., and Gudkov, A. V. (1998). The candidate tumour suppressor p33ING1cooperates with p53 in cell growth control. *Nature* 391, 295–298. doi: 10.1038/34675

Garkavtsev, I., and Riabowol, K. (1997). Extension of the replicative life span of human diploid fibroblasts by inhibition of the p33ING1 candidate tumor suppressor. *Mol. Cell. Biol.* 17, 2014–2019. doi: 10.1128/mcb.17.4.2014

Gaspar-Maia, A., Alajem, A., Meshorer, E., and Ramalho-Santos, M. (2010). Open chromatin in pluripotency and reprogramming. *Nat. Rev. Mol. Cell. Biol.* 12, 36–47. doi: 10.1038/nrm3036

Giacinti, C., and Giordano, A. (2006). RB and cell cycle progression. *Oncogene* 25, 5220–5227. doi: 10.1038/sj.onc.1209615

Gibaja, A., Aburto, M. R., Pulido, S., Collado, M., Hurle, J. M., Varela-Nieto, I., et al. (2019). TGFbeta2-induced senescence during early inner ear development. *Sci. Rep.* 9:5912.

Glück, S., Guey, B., Gulen, M., Wolter, K., Kang, T.-W., Schmacke, N., et al. (2017). Innate immune sensing of cytosolic chromatin fragments through cGAS promotes senescence. *Nat. Cell Biol.* 19, 1061–1070. doi: 10.1038/ncb3586

Goldberg, A. D., Allis, C. D., and Bernstein, E. (2007). Epigenetics: a landscape takes shape. *Cell* 128, 635–638. doi: 10.1016/j.cell.2007.02.006

Goll, M. G., and Bestor, T. H. (2005). Eukaryotic cytosine methyltransferases. *Annu. Rev. Biochem.* 74, 481–514. doi: 10.1146/annurev.biochem.74.010904.153721

González-Gualda, E., Baker, A. G., Fruk, L., and Muñoz-Espín, D. (2020). A guide to assessing cellular senescence in vitro and in vivo. *FEBS J.* 2020:e15570. doi: 10.1111/febs.15570

Goodrich, D. W., Wang, N. P., Qian, Y.-W., Lee, E. Y.-H. P., and Lee, W.-H. (1991). The retinoblastoma gene product regulates progression through the G1 phase of the cell cycle. *Cell* 67, 293–302. doi: 10.1016/0092-8674(91)90181-w

Gozani, O., Karuman, P., Jones, D. R., Ivanov, D., Cha, J., Lugovskoy, A. A., et al. (2003). The PHD finger of the chromatin-associated protein ING2 functions as a nuclear phosphoinositide receptor. *Cell* 114, 99–111. doi: 10.1016/s0092-8674(03)00480-x

Grosse, L., Wagner, N., Emelyanov, A., Molina, C., Lacas-Gervais, S., Wagner, K.-D., et al. (2020). Defined p16 high senescent cell types are indispensable for mouse healthspan. *Cell. Metab.* 32, 87.e6–99.e6.

Grupp, S. A., Kalos, M., Barrett, D., Aplenc, R., Porter, D. L., Rheingold, S. R., et al. (2013). Chimeric antigen receptor-modified T cells for acute lymphoid leukemia. *N. Engl. J. Med.* 368, 1509–1518.

Guo, H., Zhu, P., Yan, L., Li, R., Hu, B., Lian, Y., et al. (2014). The DNA methylation landscape of human early embryos. *Nature* 511, 606–610.

Hakem, R., Hakem, A., Duncan, G. S., Henderson, J. T., Woo, M., Soengas, M. S., et al. (1998). Differential requirement for caspase 9 in apoptotic pathways in vivo. *Cell* 94, 339–352. doi: 10.1016/s0092-8674(00)81477-4

Hannum, G., Guinney, J., Zhao, L., Zhang, L., Hughes, G., Sadda, S., et al. (2013). Genome-wide methylation profiles reveal quantitative views of human aging rates. *Mol. Cell.* 49, 359–367. doi: 10.1016/j.molcel.2012.10.016

Harbour, J. W., and Dean, D. C. (2000). The Rb/E2F pathway: expanding roles and emerging paradigms. *Gene Dev.* 14, 2393–2409. doi: 10.1101/gad.813200

Harper, J. W., Adami, G. R., Wei, N., Keyomarsi, K., and Elledge, S. J. (1993). The p21 Cdk-interacting protein Cip1 is a potent inhibitor of G1 cyclin-dependent kinases. *Cell* 75, 805–816. doi: 10.1016/0092-8674(93)90499-g

Hayflick, L., and Moorhead, P. S. (1961). The serial cultivation of human diploid cell strains. *Exp. Cell Res.* 25, 585–621. doi: 10.1016/0014-4827(61)90192-6

Helbing, C. C., Veillette, C., Riabowol, K., Johnston, R. N., and Garkavtsev, I. (1997). A novel candidate tumor suppressor, ING1, is involved in the regulation of apoptosis. *Cancer Res.* 57, 1255–1258.

Hengartner, M. O. (2000). The biochemistry of apoptosis. *Nature* 407, 770–776.

Henikoff, S., and Smith, M. M. (2015). Histone variants and epigenetics. *CSH Perspect. Biol.* 7:a019364. doi: 10.1101/cshperspect.a019364

Hickson, L. T. J., Prata, L. G. P. L., Bobart, S. A., Evans, T. K., Giorgadze, N., Hashmi, S. K., et al. (2019). Senolytics decrease senescent cells in humans: preliminary report from a clinical trial of Dasatinib plus Quercetin in individuals with diabetic kidney disease. *EBioMedicine* 47, 446–456. doi: 10.1016/j.ebiom.2019.08.069

Ho, L., and Crabtree, G. R. (2010). Chromatin remodelling during development. *Nature* 463, 474–484. doi: 10.1038/nature08911

Hopfner, K. P., and Hornung, V. (2020). Molecular mechanisms and cellular functions of cGAS-STING signalling. *Nat. Rev. Mol. Cell Biol.* 21, 501–521. doi: 10.1038/s41580-020-0244-x

Horowitz, J. M., Park, S. H., Bogenmann, E., Cheng, J. C., Yandell, D. W., Kaye, F. J., et al. (1990). Frequent inactivation of the retinoblastoma anti-oncogene is restricted to a subset of human tumor cells. *Proc. Natl. Acad. Sci. U.S.A.* 87, 2775–2779. doi: 10.1073/pnas.87.7.2775

Horvath, S. (2013). DNA methylation age of human tissues and cell types. *Genome Biol.* 14:R115.

Hu, W., Feng, Z., Teresky, A. K., and Levine, A. J. (2007). p53 regulates maternal reproduction through LIF. *Nature* 450, 721–724. doi: 10.1038/nature05993

Ianari, A., Natale, T., Calo, E., Ferretti, E., Alesse, E., Screpanti, I., et al. (2009). Proapoptotic function of the retinoblastoma tumor suppressor protein. *Cancer Cell* 15, 184–194. doi: 10.1016/j.ccr.2009.01.026

Iaquinta, P. J., and Lees, J. A. (2007). Life and death decisions by the E2F transcription factors. *Curr. Opin. Cell Biol.* 19, 649–657. doi: 10.1016/j.ceb.2007.10.006

Igney, F. H., and Krammer, P. H. (2002). Death and anti-death: tumour resistance to apoptosis. *Nat. Rev. Cancer* 2, 277–288. doi: 10.1038/nrc776

Jacks, T., Fazeli, A., Schmitt, E. M., Bronson, R. T., Goodell, M. A., and Weinberg, R. A. (1992). Effects of an Rb mutation in the mouse. *Nature* 359, 295–300. doi: 10.1038/359295a0

Jacobson, M. D., Weil, M., and Raff, M. C. (1997). Programmed cell death in animal development. *Cell* 88, 347–354. doi: 10.1016/s0092-8674(00)81873-5

Jain, A. K., and Barton, M. C. (2018). p53: emerging roles in stem cells, development and beyond. *Development* 145:dev158360. doi: 10.1242/dev.158360

Jones, S. N., Roe, A. E., Donehower, L. A., and Bradley, A. (1995). Rescue of embryonic lethality in Mdm2-deficient mice by absence of p53. *Nature* 378, 206–208. doi: 10.1038/378206a0

Kafri, T., Ariel, M., Brandeis, M., Shemer, R., Urven, L., McCarrey, J., et al. (1992). Developmental pattern of gene-specific DNA methylation in the mouse embryo and germ line. *Gene Dev.* 6, 705–714. doi: 10.1101/gad.6.5.705

Kataoka, H., Bonnefin, P., Vieyra, D., Feng, X., Hara, Y., Miura, Y., et al. (2003). ING1 represses transcription by direct DNA binding and through effects on p53. *Cancer Res.* 63, 5785–5792.

Ke, F. F. S., Vanyai, H. K., Cowan, A. D., Delbridge, A. R. D., Whitehead, L., Grabow, S., et al. (2018). Embryogenesis and adult life in the absence of intrinsic apoptosis effectors BAX, BAK, and BOK. *Cell* 173, 1217.e17–1230.e17.

Kerr, J. F. R. (1971). Shrinkage necrosis: a distinct mode of cellular death. *J. Pathol.* 105, 13–20. doi: 10.1002/path.1711050103

Kerr, J. F. R., Wyllie, A. H., and Currie, A. R. (1972). Apoptosis: a basic biological phenomenon with wideranging implications in tissue kinetics. *Br. J. Cancer* 26, 239–257. doi: 10.1038/bjc.1972.33

Kichina, J. V., Zeremski, M., Aris, L., Gurova, K. V., Walker, E., Franks, R., et al. (2006). Targeted disruption of the mouse ing1 locus results in reduced body size, hypersensitivity to radiation and elevated incidence of lymphomas. *Oncogene* 25, 857–866. doi: 10.1038/sj.onc.1209118

Kimelman, D. (2006). Mesoderm induction: from caps to chips. *Nat. Rev. Genet.* 7, 360–372. doi: 10.1038/nrg1837

Knabe, W., and Kuhn, H. J. (1998). Pattern of cell death during optic cup formation in the tree shrew *Tupaia belangeri*. *J. Comp. Neurol.* 401, 352–366. doi: 10.1002/(sici)1096-9861(19981123)401:3<352::aid-cne4>3.0.co;2-a

Knabe, W., Süss, M., and Kuhn, H. J. (2000). The patterns of cell death and of macrophages in the developing forebrain of the tree shrew *Tupaia belangeri*. *Anat. Embryol.* 201, 157–168. doi: 10.1007/pl00008237

Knabe, W., Washausen, S., Brunnett, G., and Kuhn, H. J. (2004). Rhombomere-specific patterns of apoptosis in the tree shrew *Tupaia belangeri*. *Cell Tissue Res.* 316, 1–13. doi: 10.1007/s00441-004-0855-0

Knudson, A. G. (1971). Mutation and cancer: statistical study of retinoblastoma. *Proc. Natl. Acad. Sci. U.S.A.* 68, 820–823. doi: 10.1073/pnas.68.4.820

Krumlauf, R. (1994). Hox genes in vertebrate development. *Cell* 78, 191–201. doi: 10.1016/0092-8674(94)90290-9

Kuida, K., Haydar, T. F., Kuan, C.-Y., Gu, Y., Taya, C., Karasuyama, H., et al. (1998). Reduced apoptosis and cytochrome c–mediated caspase activation in mice lacking caspase 9. *Cell* 94, 325–337. doi: 10.1016/s0092-8674(00)81476-2

Kuida, K., Zheng, T. S., Na, S., Kuan, C.-Y., Yang, D., Karasuyama, H., et al. (1996). Decreased apoptosis in the brain and premature lethality in CPP32-deficient mice. *Nature* 384, 368–372. doi: 10.1038/384368a0

Lane, D. P. (1992). p53, guardian of the genome. *Nature* 358, 15–16. doi: 10.1038/358015a0

Lappin, T. R. J., Grier, D. G., Thompson, A., and Halliday, H. L. (2006). HOX genes: seductive science, mysterious mechanisms. *Ulster Medical J.* 75, 23–31.

Lee, E. Y. H. P., Chang, C. Y., Hu, N., Wang, Y. C. J., Lai, C. C., Herrup, K., et al. (1992). Mice deficient for Rb are nonviable and show defects in neurogenesis and haematopoiesis. *Nature* 359, 288–294. doi: 10.1038/359288a0

Lee, S. W., Fang, L., Igarashi, M., Ouchi, T., Lu, K. P., and Aaronson, S. A. (2000). Sustained activation of Ras/Raf/mitogen-activated protein kinase cascade by the tumor suppressor p53. *Proc. Natl. Acad. Sci. U.S.A.* 97, 8302–8305. doi: 10.1073/pnas.150024397

Lee, W., Bookstein, R., Hong, F., Young, L., Shew, J., and Lee, E. (1987). Human retinoblastoma susceptibility gene: cloning, identification, and sequence. *Science* 235, 1394–1399. doi: 10.1126/science.3823889

Levy, M. Z., Allsopp, R. C., Futcher, A. B., Greider, C. W., and Harley, C. B. (1992). Telomere end-replication problem and cell aging. *J. Mol. Biol.* 225, 951–960. doi: 10.1016/0022-2836(92)90096-3

Li, E. (2002). Chromatin modification and epigenetic reprogramming in mammalian development. *Nat. Rev. Genet.* 3, 662–673. doi: 10.1038/nrg887

Lindsten, T., Ross, A. J., King, A., Zong, W.-X., Rathmell, J. C., Shiels, H. A., et al. (2000). The combined functions of proapoptotic Bcl-2 family members bak and bax are essential for normal development of multiple tissues. *Mol. Cell.* 6, 1389–1399. doi: 10.1016/s1097-2765(00)00136-2

Liu, T., Laurell, C., Selivanova, G., Lundeberg, J., Nilsson, P., and Wiman, K. G. (2006). Hypoxia induces p53-dependent transactivation and Fas/CD95-dependent apoptosis. *Cell Death Differ.* 14, 411–421. doi: 10.1038/sj.cdd.4402022

López-Otín, C., Blasco, M. A., Partridge, L., Serrano, M., and Kroemer, G. (2013). The hallmarks of aging. *Cell* 153, 1194–1217.

Lowe, S. W., and Ruley, H. E. (1993). Stabilization of the p53 tumor suppressor is induced by adenovirus 5 E1A and accompanies apoptosis. *Gene Dev.* 7, 535–545. doi: 10.1101/gad.7.4.535

Lowe, S. W., Schmitt, E. M., Smith, S. W., Osborne, B. A., and Jacks, T. (1993). p53 is required for radiation-induced apoptosis in mouse thymocytes. *Nature* 362, 847–849. doi: 10.1038/362847a0

Lumsden, A., Sprawson, N., and Graham, A. (1991). Segmental origin and migration of neural crest cells in the hindbrain region of the chick embryo. *Development* 113, 1281–1291.

Luo, R. X., Postigo, A. A., and Dean, D. C. (1998). Rb interacts with histone deacetylase to repress transcription. *Cell* 92, 463–473. doi: 10.1016/s0092-8674(00)80940-x

Luo, Y., Hurwitz, J., and Massagué, J. (1995). Cell-cycle inhibition by independent CDK and PCNA binding domains in p21Cip1. *Nature* 375, 159–161. doi: 10.1038/375159a0

Mallo, M., Wellik, D. M., and Deschamps, J. (2010). Hox genes and regional patterning of the vertebrate body plan. *Dev. Biol.* 344, 7–15. doi: 10.1016/j.ydbio.2010.04.024

Manzanares, M., Nardelli, J., Gilardi-Hebenstreit, P., Marshall, H., Giudicelli, F., Martínez-Pastor, M. T., et al. (2002). Krox20 and kreisler co-operate in the transcriptional control of segmental expression of Hoxb3 in the developing hindbrain. *EMBO J.* 21, 365–376. doi: 10.1093/emboj/21.3.365

Martinez, J., Georgoff, I., Martinez, J., and Levine, A. J. (1991). Cellular localization and cell cycle regulation by a temperature-sensitive p53 protein. *Gene Dev.* 5, 151–159. doi: 10.1101/gad.5.2.151

Meier, P., Finch, A., and Evan, G. (2000). Apoptosis in development. *Nature* 407, 796–801.

Merry, D. E., Veis, D. J., Hickey, W. F., and Korsmeyer, S. J. (1994). bcl-2 protein expression is widespread in the developing nervous system and retained in the adult PNS. *Dev. Camb. Engl.* 120, 301–311.

Mizushima, N., and Komatsu, M. (2011). Autophagy: renovation of cells and tissues. *Cell* 147, 728–741. doi: 10.1016/j.cell.2011.10.026

Moens, C. B., and Selleri, L. (2006). Hox cofactors in vertebrate development. *Dev. Biol.* 291, 193–206. doi: 10.1016/j.ydbio.2005.10.032

Molchadsky, A., Rivlin, N., Brosh, R., Rotter, V., and Sarig, R. (2010). p53 is balancing development, differentiation and de-differentiation to assure cancer prevention. *Carcinogenesis* 31, 1501–1508. doi: 10.1093/carcin/bgq101

Morgenbesser, S. D., Williams, B. O., Jacks, T., and DePinho, R. A. (1994). p53-dependent apoptosis produced by Rb-deficiency in the developing mouse lens. *Nature* 371, 72–74. doi: 10.1038/371072a0

Moroni, M. C., Hickman, E. S., Denchi, E. L., Caprara, G., Colli, E., Cecconi, F., et al. (2001). Apaf-1 is a transcriptional target for E2F and p53. *Nat. Cell Biol.* 3, 552–558. doi: 10.1038/35078527

Moskalev, A. A., Aliper, A. M., Smit-McBride, Z., Buzdin, A., and Zhavoronkov, A. (2014). Genetics and epigenetics of aging and longevity. *Cell Cycle* 13, 1063–1077.

Muñoz-Espín, D., Canamero, M., Maraver, A., Gomez-Lopez, G., Contreras, J., Murillo-Cuesta, S., et al. (2013). Programmed cell senescence during mammalian embryonic development. *Cell* 155, 1104–1112. doi: 10.1016/j.cell.2013.10.019

Nacher, V., Carretero, A., Navarro, M., Armengol, C., Llombart, C., Rodriguez, A., et al. (2006). The quail mesonephros: a new model for renal senescence? *J. Vasc. Res.* 43, 581–586. doi: 10.1159/000096076

Nakano, K., and Vousden, K. H. (2001). PUMA, a novel proapoptotic gene, is induced by p53. *Mol. Cell.* 7, 683–694. doi: 10.1016/s1097-2765(01)00214-3

Naruse, I., and Keino, H. (1995). Apoptosis in the developing CNS. *Prog. Neurobiol.* 47, 135–155. doi: 10.1016/0301-0082(95)00024-p

Nelson, G., Wordsworth, J., Wang, C., Jurk, D., Lawless, C., Martin-Ruiz, C., et al. (2012). A senescent cell bystander effect: senescence-induced senescence. *Aging Cell* 11, 345–349. doi: 10.1111/j.1474-9726.2012.00795.x

Nichols, J., Zevnik, B., Anastassiadis, K., Niwa, H., Klewe-Nebenius, D., Chambers, I., et al. (1998). Formation of pluripotent stem cells in the mammalian embryo depends on the POU transcription factor Oct4. *Cell* 95, 379–391. doi: 10.1016/s0092-8674(00)81769-9

Nielsen, N. H., Emdin, S. O., Cajander, J., and Landberg, G. (1997). Deregulation of cyclin E and D1 in breast cancer is associated with inactivation of the retinoblastoma protein. *Oncogene* 14, 295–304. doi: 10.1038/sj.onc.1200833

Norimura, T., Nomoto, S., Katsuki, M., Gondo, Y., and Kondo, S. (1996). p53-dependent apoptosis suppresses radiation–induced teratogenesis. *Nat. Med.* 2, 577–580. doi: 10.1038/nm0596-577

Nostrand, J. L. V., Brady, C. A., Jung, H., Fuentes, D. R., Kozak, M. M., Johnson, T. M., et al. (2014). Inappropriate p53 activation during development induces features of CHARGE syndrome. *Nature* 514, 228–232. doi: 10.1038/nature13585

Novack, D. V., and Korsmeyer, S. J. (1994). Bcl-2 protein expression during murine development. *Am. J. Pathol.* 145, 61–73.

Oda, E., Ohki, R., Murasawa, H., Nemoto, J., Shibue, T., Yamashita, T., et al. (2000). Noxa, a BH3-only member of the Bcl-2 family and candidate mediator of p53-induced *Apoptosis*. *Science* 288, 1053–1058. doi: 10.1126/science.288.5468.1053

Okano, M., Bell, D. W., Haber, D. A., and Li, E. (1999). DNA methyltransferases Dnmt3a and Dnmt3b are essential for de novo methylation and mammalian development. *Cell* 99, 247–257. doi: 10.1016/j.rpto.2016.06.003

Pan, K., Chen, Y., Roth, M., Wang, W., Wang, S., Yee, A. S., et al. (2013). HBP1-mediated transcriptional regulation of DNA methyltransferase 1 and its impact on cell senescence. *Mol. Cell. Biol.* 33, 887–903. doi: 10.1128/mcb.00637-12

Pearson, J. C., Lemons, D., and McGinnis, W. (2005). Modulating Hox gene functions during animal body patterning. *Nat. Rev. Genet.* 6, 893–904. doi: 10.1038/nrg1726

Pedeux, R., Sengupta, S., Shen, J. C., Demidov, O. N., Saito, S., Onogi, H., et al. (2005). ING2 regulates the onset of replicative senescence by induction of p300-dependent p53 acetylation. *Mol. Cell. Biol.* 25, 6639–6648. doi: 10.1128/mcb.25.15.6639-6648.2005

Peschansky, V. J., and Wahlestedt, C. (2013). Non-coding RNAs as direct and indirect modulators of epigenetic regulation. *Epigenetics* 9, 3–12.

Rajagopalan, S., and Long, E. O. (2012). Cellular senescence induced by CD158d reprograms natural killer cells to promote vascular remodeling. *Proc. Natl. Acad. Sci. U.S.A.* 109, 20596–20601. doi: 10.1073/pnas.1208248109

Rajarajacholan, U. K., and Riabowol, K. (2015). Aging with ING: a comparative study of different forms of stress induced premature senescence. *Oncotarget* 6, 34118–34127. doi: 10.18632/oncotarget.5947

Rajarajacholan, U. K., Thalappilly, S., and Riabowol, K. (2013). The ING1a tumor suppressor regulates endocytosis to induce cellular senescence via the Rb-E2F pathway. *PLoS Biol.* 11:e1001502. doi: 10.1371/journal.pbio.1001502

Reed, J. C. (2000). Mechanisms of apoptosis. *Am. J. Pathol.* 157, 1415–1430.

Reya, T., Morrison, S. J., Clarke, M. F., and Weissman, I. L. (2001). Stem cells, cancer, and cancer stem cells. *Nature* 414, 105–111.

Roninson, I. B. (2002). Oncogenic functions of tumour suppressor p21Waf1/Cip1/Sdi1: association with cell senescence and tumour-promoting activities of stromal fibroblasts. *Cancer Lett.* 179, 1–14. doi: 10.1016/s0304-3835(01)00847-3

Sage, J., Mulligan, G. J., Attardi, L. D., Miller, A., Chen, S., Williams, B., et al. (2000). Targeted disruption of the three Rb-related genes leads to loss of G1 control and immortalization. *Gene Dev.* 14, 3037–3050. doi: 10.1101/gad.843200

Sah, V. P., Attardi, L. D., Mulligan, G. J., Williams, B. O., Bronson, R. T., and Jacks, T. (1995). A subset of p53-deficient embryos exhibit exencephaly. *Nat. Genet.* 10, 175–180. doi: 10.1038/ng0695-175

Sasai, Y., and Robertis, E. M. D. (1997). Ectodermal patterning in vertebrate embryos. *Dev. Biol.* 182, 5–20. doi: 10.1006/dbio.1996.8445

Sax, J. K., Fei, P., Murphy, M. E., Bernhard, E., Korsmeyer, S. J., and El-Deiry, W. S. (2002). BID regulation by p53 contributes to chemosensitivity. *Nat. Cell Biol.* 4, 842–849. doi: 10.1038/ncb866

Schuler, M., and Green, D. (2005). Transcription, apoptosis and p53: catch-22. *Trends Genet.* 21, 182–187. doi: 10.1016/j.tig.2005.01.001

Schulte, D., and Frank, D. (2013). TALE transcription factors during early development of the vertebrate brain and eye: tale proteins in brain and eye development. *Dev. Dynam.* 243, 99–116. doi: 10.1002/dvdy.24030

Scott, M., Bonnefin, P., Vieyra, D., Boisvert, F. M., Young, D., Bazett-Jones, D. P., et al. (2001). UV-induced binding of ING1 to PCNA regulates the induction of apoptosis. *J. Cell Sci.* 114, 3455–3462.

Serrano, M., Lin, A. W., McCurrach, M. E., Beach, D., and Lowe, S. W. (1997). Oncogenic ras provokes premature cell senescence associated with accumulation of p53 and p16INK4a. *Cell* 88, 593–602. doi: 10.1016/s0092-8674(00)81902-9

Seydoux, G., and Braun, R. E. (2006). Pathway to totipotency: lessons from germ cells. *Cell* 127, 891–904. doi: 10.1016/j.cell.2006.11.016

Shimohama, S., Tanino, H., and Fujimoto, S. (1999). Changes in caspase expression in Alzheimer's disease: comparison with development and aging. *Biochem. Biophys. Res. Co* 256, 381–384. doi: 10.1006/bbrc.1999.0344

Singh, R., Letai, A., and Sarosiek, K. (2019). Regulation of apoptosis in health and disease: the balancing act of BCL-2 family proteins. *Nat. Rev. Mol. Cell. Biol.* 20, 175–193. doi: 10.1038/s41580-018-0089-8

Soliman, M. A., Berardi, P., Pastyryeva, S., Bonnefin, P., Feng, X., Colina, A., et al. (2008). ING1a expression increases during replicative senescence and induces a senescent phenotype. *Aging Cell* 7, 783–794. doi: 10.1111/j.1474-9726.2008.00427.x

Solnica-Krezel, L., and Sepich, D. S. (2012). Gastrulation: making and shaping germ layers. *Annu. Rev. Cell Dev. Biol.* 28, 687–717. doi: 10.1146/annurev-cellbio-092910-154043

Storer, M., Mas, A., Robert-Moreno, A., Pecoraro, M., Ortells, M. C., Giacomo, V. D., et al. (2013). Senescence is a developmental mechanism that contributes to embryonic growth and patterning. *Cell* 155, 1119–1130. doi: 10.1016/j.cell.2013.10.041

Strehler, B. L. (1977). Times, cells, and aging. *Yale J. Biol. Med.* 35:443. doi: 10.1016/b978-0-12-673260-3.50013-2

Szegezdi, E., Logue, S. E., Gorman, A. M., and Samali, A. (2006). Mediators of endoplasmic reticulum stress-induced apoptosis. *EMBO Rep.* 7, 880–885. doi: 10.1038/sj.embor.7400779

Tabas, I., and Ron, D. (2011). Integrating the mechanisms of apoptosis induced by endoplasmic reticulum stress. *Nat. Cell Biol.* 13, 184–190. doi: 10.1038/ncb0311-184

Takahashi, K., Tanabe, K., Ohnuki, M., Narita, M., Ichisaka, T., Tomoda, K., et al. (2007). Induction of pluripotent stem cells from adult human fibroblasts by defined factors. *Cell* 131, 861–872. doi: 10.1016/j.cell.2007.11.019

Thalappilly, S., Feng, X., Pastyryeva, S., Suzuki, K., Muruve, D., Larocque, D., et al. (2011). The p53 tumor suppressor is stabilized by inhibitor of growth 1 (ING1) by blocking polyubiquitination. *PLoS One* 6:e21065. doi: 10.1371/journal.pone.0021065

Toshiyuki, M., and Reed, J. C. (1995). Tumor suppressor p53 is a direct transcriptional activator of the human bax gene. *Cell* 80, 293–299. doi: 10.1016/0092-8674(95)90412-3

Varfolomeev, E. E., Schuchmann, M., Luria, V., Chiannilkulchai, N., Beckmann, J. S., Mett, I. L., et al. (1998). Targeted disruption of the mouse caspase 8 gene ablates cell death induction by the TNF receptors, Fas/Apo1, and DR3 and is lethal prenatally. *Immunity* 9, 267–276. doi: 10.1016/s1074-7613(00)80609-3

Veitia, R. A., Govindaraju, D. R., Bottani, S., and Birchler, J. A. (2017). Aging: somatic mutations, epigenetic drift and gene dosage imbalance. *Trends Cell Biol.* 27, 299–310. doi: 10.1016/j.tcb.2016.11.006

Venter, D. J., Bevan, K. L., Ludwig, R. L., Riley, T. E., Jat, P. S., Thomas, D. G., et al. (1991). Retinoblastoma gene deletions in human glioblastomas. *Oncogene* 6, 445–448.

Venturelli, S., Berger, A., Weiland, T., Essmann, F., Waibel, M., Nuebling, T., et al. (2013). Differential induction of apoptosis and senescence by the DNA methyltransferase inhibitors 5-Azacytidine and 5-Aza-2'-deoxycytidine in solid tumor cells. *Mol. Cancer Ther.* 12, 2226–2236. doi: 10.1158/1535-7163.mct-13-0137

Vignali, M., Hassan, A. H., Neely, K. E., and Workman, J. L. (2000). ATP-dependent chromatin- remodeling complexes. *Mol. Cell. Biol.* 20, 1899–1910.

Villiard, É, Denis, J. F., Hashemi, F. S., Igelmann, S., Ferbeyre, G., and Roy, S. (2017). Senescence gives insights into the morphogenetic evolution of anamniotes. *Biol. Open* 6, 891–896. doi: 10.1242/bio.025809

Wagers, A. J., and Weissman, I. L. (2004). Plasticity of adult stem cells. *Cell* 116, 639–648.

Wallingford, J. B., Seufert, D. W., Virta, V. C., and Vize, P. D. (1997). P53 activity is essential for normal development in *Xenopus*. *Curr. Biol.* 7, 747–757. doi: 10.1016/s0960-9822(06)00333-2

Walshe, J., Maroon, H., McGonnell, I. M., Dickson, C., and Mason, I. (2002). Establishment of hindbrain segmental identity requires signaling by FGF3 and FGF8. *Curr. Biol.* 12, 1117–1123. doi: 10.1016/s0960-9822(02)00899-0

Washausen, S., and Knabe, W. (2018). Lateral line placodes of aquatic vertebrates are evolutionarily conserved in mammals. *Biol. Open* 7:bio031815. doi: 10.1242/bio.031815

Washausen, S., Scheffel, T., Brunnett, G., and Knabe, W. (2018). Possibilities and limitations of three-dimensional reconstruction and simulation techniques to identify patterns, rhythms and functions of apoptosis in the early developing neural tube. *Hist. Philos. Life Sci.* 40:55.

Wei, J.-W., Huang, K., Yang, C., and Kang, C.-S. (2016). Non-coding RNAs as regulators in epigenetics. *Oncol. Rep.* 37, 3–9.

Weisinger, K., Kayam, G., Missulawin-Drillman, T., and Sela-Donenfeld, D. (2010). Analysis of expression and function of FGF-MAPK signaling components in the hindbrain reveals a central role for FGF3 in the regulation of Krox20, mediated by Pea3. *Dev. Biol.* 344, 881–895. doi: 10.1016/j.ydbio.2010.06.001

Whyte, P., Buchkovich, K. J., Horowitz, J. M., Friend, S. H., Raybuck, M., Weinberg, R. A., et al. (1988). Association between an oncogene and an anti-oncogene: the adenovirus E1A proteins bind to the retinoblastoma gene product. *Nature* 334, 124–129. doi: 10.1038/334124a0

Williams, G. C. (1957). Pleiotropy, natural selection, and the evolution of senescence. *Evolution* 11, 398–411. doi: 10.2307/2406060

Wong, H., and Riabowol, K. (1996). Differential CDK-inhibitor gene expression in aging human diploid fibroblasts. *Exp. Gerontol.* 31, 311–325. doi: 10.1016/0531-5565(95)00025-9

Woo, M., Hakem, R., Soengas, M. S., Duncan, G. S., Shahinian, A., Kagi, D., et al. (1998). Essential contribution of caspase 3/CPP32 to apoptosis and its associated nuclear changes. *Gene Dev.* 12, 806–819. doi: 10.1101/gad.12.6.806

Wu, J., Yamauchi, T., and Belmonte, J. C. I. (2016). An overview of mammalian pluripotency. *Development* 143, 1644–1648. doi: 10.1242/dev.132928

Wu, L., Bruin, A. D., Saavedra, H. I., Starovic, M., Trimboli, A., Yang, Y., et al. (2003). Extra- embryonic function of Rb is essential for embryonic development and viability. *Nature* 421, 942–947. doi: 10.1038/nature01417

Xue, W., Zender, L., Miething, C., Dickins, R. A., Hernando, E., Krizhanovsky, V., et al. (2007). Senescence and tumour clearance is triggered by p53 restoration in murine liver carcinomas. *Nature* 445, 656–661. doi: 10.1038/nature05529

Yokota, J., Akiyama, T., Fung, Y. K., Benedict, W. F., Namba, Y., Hanaoka, M., et al. (1988). Altered expression of the retinoblastoma (RB) gene in small-cell carcinoma of the lung. *Oncogene* 3, 471–475.

Yoshida, H., Kong, Y.-Y., Yoshida, R., Elia, A. J., Hakem, A., Hakem, R., et al. (1998). Apaf1 is required for mitochondrial pathways of apoptosis and brain development. *Cell* 94, 739–750. doi: 10.1016/s0092-8674(00)81733-x

Zakeri, Z., Penaloza, C. G., Smith, K., Ye, Y., and Lockshin, R. A. (2015). What cell death does in development. *Int. J. Dev. Biol.* 59, 11–22. doi: 10.1387/ijdb.150220zz

Zhao, Y., Tyshkovskiy, A., Munþoz-Espɪn, D., Tian, X., Serrano, M., de Magalhaes, J. P., et al. (2018). Naked mole rats can undergo developmental, oncogene-induced and DNA damage-induced cellular senescence. *Proc. Natl. Acad. Sci. U.S.A.* 115, 1801–1806. doi: 10.1073/pnas.1721160115

Zhu, B., Gong, Y., Yan, G., Wang, D., Wang, Q., Qiao, Y., et al. (2017). Atorvastatin treatment modulates p16 promoter methylation to regulate p16 expression. *FEBS J.* 284, 1868–1881. doi: 10.1111/febs.14087

Zhu, Y., Tchkonia, T., Fuhrmann-Stroissnigg, H., Dai, H. M., Ling, Y. Y., Stout, M. B., et al. (2016). Identification of a novel senolytic agent, navitoclax, targeting the Bcl-2 family of anti- apoptotic factors. *Aging Cell* 15, 428–435.

Zhu, Y., Tchkonia, T., Pirtskhalava, T., Gower, A. C., Ding, H., Giorgadze, N., et al. (2015). The Achilles' heel of senescent cells: from transcriptome to senolytic drugs. *Aging Cell* 14, 644–658.

Zorn, A. M., and Wells, J. M. (2009). Vertebrate endoderm development and organ formation. *Annu. Rev. Cell Dev. Biol.* 25, 221–251.

Conflict of Interest: The authors declare that the research was conducted in the absence of any commercial or financial relationships that could be construed as a potential conflict of interest.

frontiers in Cell and Developmental Biology

ORIGINAL RESEARCH
published: 26 January 2021
doi: 10.3389/fcell.2021.587096

Programmed Cell Senescence in the Mouse Developing Spinal Cord and Notochord

*Jorge Antolio Domínguez-Bautista, Pilar Sarah Acevo-Rodríguez and Susana Castro-Obregón**

División de Neurociencias, Instituto de Fisiología Celular, UNAM, Mexico City, Mexico

Programmed cell senescence is a cellular process that seems to contribute to embryo development, in addition to cell proliferation, migration, differentiation and programmed cell death, and has been observed in evolutionary distant organisms such as mammals, amphibians, birds and fish. Programmed cell senescence is a phenotype similar to stress-induced cellular senescence, characterized by the expression of the cell cycle inhibitors $p21^{CIP1/WAF}$ and $p16^{INK4A}$, increased activity of a lysosomal enzyme with beta-galactosidase activity (coined senescence-associated beta-galactosidase) and secretion of growth factors, interleukins, chemokines, metalloproteases, etc., collectively known as a senescent-associated secretory phenotype that instructs surrounding tissue. How wide is the distribution of programmed cell senescence during mouse development and its specific mechanisms to shape the embryo are still poorly understood. Here, we investigated whether markers of programmed cell senescence are found in the developing mouse spinal cord and notochord. We found discrete areas and developmental windows with high senescence-associated beta galactosidase in both spinal cord and notochord, which was reduced in mice embryos developed *ex-utero* in the presence of the senolytic ABT-263. Expression of $p21^{CIP1/WAF}$ was documented in epithelial cells of the spinal cord and the notochord, while $p16^{INK4A}$ was observed in motoneurons. Treatment with the senolytic ABT-263 decreased the number of motoneurons, supporting their senescent phenotype. Our data suggest that a subpopulation of motoneurons in the developing spinal cord, as well as some notochord cells undergo programmed cell senescence.

Keywords: Cdkn1a/$p21^{CIP1/WAF}$, Cdkn2a/$p16^{INK4A}$, spinal cord, notochord, endothelial cells, motoneurons, mouse development

OPEN ACCESS

Edited by:
Wolfgang Knabe, Universität Münster, Germany

Reviewed by:
Christoph Viebahn, University of Göttingen, Germany
Andrew J. Copp, University College London, United Kingdom

****Correspondence:***
Susana Castro-Obregón
scastro@ifc.unam.mx

Specialty section:
This article was submitted to Cell Death and Survival, a section of the journal Frontiers in Cell and Developmental Biology

Received: *24 July 2020*
Accepted: *05 January 2021*
Published: *26 January 2021*

Citation:
Domínguez-Bautista JA, Acevo-Rodríguez PS and Castro-Obregón S (2021) Programmed Cell Senescence in the Mouse Developing Spinal Cord and Notochord. Front. Cell Dev. Biol. 9:587096. doi: 10.3389/fcell.2021.587096

INTRODUCTION

Embryonic development is achieved by strongly coordinated mechanisms of cell migration, proliferation, differentiation and programmed cell death. Recently, programmed cell senescence was identified as an additional process that controls mouse development (Munoz-Espin et al., 2013; Storer et al., 2013). The presence of programmed cell senescence has also been reported during specific structures and windows of amphibian, chick and fish development, suggesting that programmed cell senescence contributes to vertebrate organogenesis and may have arisen in evolution as a developmental mechanism (Storer et al., 2013; Davaapil et al., 2017; Da Silva-Alvarez et al., 2020).

The development of the spinal cord and the differentiation of motoneurons are intensively studied due to its importance in organismal physiology and as in search for therapeutic targets for diseases such as amyotrophic lateral sclerosis. During the development of the spinal cord, the roof plate and the floor plate, located in the dorsal and ventral regions of the neural tube, regulate the dorsoventral patterning of different neuron populations by expressing WNT and BMP proteins dorsally, and SHH ventrally (Chizhikov and Millen, 2004; Placzek and Briscoe, 2005). Interestingly, discrete populations of floor plate cells have been identified along the anteroposterior axis, suggesting a variable mode of floor plate induction (Placzek and Briscoe, 2005). Adjacent to the ventral neural tube is located the notochord, a rod-like mesodermal structure that runs the anterior-posterior length, which becomes the rostrocaudal axis. The notochord is a source of developmental signals, such as the Hedgehog proteins, that play key roles in the patterning and proliferation of several organs (Corallo et al., 2015). As a result of signaling gradient of molecules secreted from the notochord and the floor plate, different progenitor cells located in the dorso-ventral axis of the neural tube give rise to V0-3 interneurons and motoneurons (Davis-Dusenbery et al., 2014).

In the developing spinal cord, blood vessels sprout from the perineural vascular plexus and invade the spinal cord at the ventral side. The motoneurons play an active role during blood vessel formation in the spinal cord by expressing vascular endothelial growth factor (VEGF) to allow blood vessel growth, but at the same time express a soluble VEGF receptor to titrate the availability of the growth factor in order to pattern the vasculature and block premature ingression of vessels by an attraction-repulsion mechanism (Himmels et al., 2017).

During the development of the spinal cord, motoneurons are produced in excess and compete for supply of trophic factors produced by synaptic targets. Approximately half of the initially produced motoneurons undergo programmed cell death due to lack of trophic support (Oppenheim, 1989). Programmed cell death occurs mainly by apoptosis in the developing embryo; however, while the lack of caspase-3 or caspase-9 results in obvious and severe forebrain malformations, the organization and morphology of the spinal cord appears normal at embryonic and postnatal stages (Oppenheim et al., 2001). Such lack of an obvious phenotype in caspase-3 or caspase-9 knockout mice may be due to a compensation mechanism of remaining caspases (Buss and Oppenheim, 2004), although it is also possible that genetic elimination of apoptosis is masked by alterative mechanisms to eliminate cells such as autophagic cell death and programmed senescence. In fact, dying neurons in caspase-3 and caspase-9 deficient embryos exhibit a different morphology with cell shrinkage, increased cytoplasmic and nuclear density, and very little chromatin condensation(Oppenheim et al., 2001). A former work showed that reactive oxidative species signal to induce motoneuronal cell elimination by a caspase-independent mechanism, as the number of motoneurons was higher in developing spinal cords explants cultured in the presence of a superoxidase dismutase-catalase mimetic than with caspase inhibitors (Sanchez-Carbente et al., 2005).

While autophagy is primarily a survival mechanism frequently activated to eliminate damaged proteins and organelles, evidence shows that autophagy contributes to programmed cell death for example during the *Drosophila* larval salivary glands regression (Tracy and Baehrecke, 2013), and the elimination of the interdigital web during limb development (Arakawa et al., 2017). Since the number of motoneurons increased in spinal cord explants cultured in the presence of the PI3K inhibitor LY294002, it was suggested that autophagy contributes to eliminate supernumerary motoneurons during spinal cord development, in a mechanism that occurs without DNA fragmentation (i.e., TUNEL negative) (Sanchez-Carbente et al., 2005). Therefore, alternative mechanisms occur simultaneously to adjust the number of motoneurons during spinal cord development, and programmed cell senescence could be one of them.

Cellular senescence is characterized by a durable exit from the cell cycle and acquisition of a flattened morphology; expression of the cell cycle inhibitors $p16^{INK4A}$ (coded by *Cdkn2a* gen), $p21^{CIP1/WAF}$ (coded by *Cdkn1a* gen), and/or p53; expansion of mitochondrial and lysosomal networks; and a high level of senescence-associated-β-galactosidase activity (SA-β-gal). Senescent cells are metabolically active and influence the tissue microenvironment through their secretory phenotype (chemokines, cytokines, growth factors, metalloproteases, etc.) (Czarkwiani and Yun, 2018). During development, programmed cell senescence contributes to tissue remodeling in structures such as the mesonephros, endolymphatic sac and apical ectodermal ridge in mice, but it still has to be understood how they help to shape the embryo. Programmed cell senescence could cooperate with programmed cell death to eliminate transient structures and adjust the final number of cells, and could also secrete developmental signals. Mechanistically, programmed cell senescence depends on the $p21^{CIP1/WAF}$ cell cycle inhibitor and is regulated by the TGF-β/SMAD, PI3K/FOXO and ERK1/2 pathways (Munoz-Espin et al., 2013; Storer et al., 2013). In amphibians also TGF-β triggers programmed cell senescence, although it is independent of ERK1/2 pathways (Davaapil et al., 2017). In contrast to other non-proliferating states as senescence or terminal differentiation, quiescence is a reversible cell cycle exit that takes place in cells that require a strict proliferation regime, such as stem cells. Molecularly, the transcriptional repressor HES1 safeguards against irreversible cell cycle exit during cellular quiescence, and prevents senescence (Sang et al., 2008; Sueda et al., 2019).

Senescent cells activate several prosurvival pathways and become resistant to extrinsic and intrinsic proapoptotic stimuli

Abbreviations: ANOVA, Analysis of Variance; $BCL\text{-}X_L$, B-cell lymphoma-extra large; $p21^{CIP1/WAF}$, Cyclin-dependent kinase inhibitor 1A; CDKN1B/p27, Cyclin-dependent kinase inhibitor 1B; $p16^{INK4A}$, Cyclin-dependent kinase inhibitor 2A; CDKN2B/p15, Cyclin-dependent kinase inhibitor 2B; CQ, Chloroquine; CTRL, Control; DMEM, Dulbecco's Modified Eagle Medium; DMEM/F12, Dulbecco's Modified Eagle Medium/Nutrient Mixture F-12; DMSO, Dimethyl Sulfoxide; ERK1/2, Extracellular signal–Regulated Kinases 1 and 2; FP, Floor plate; IN, Interneurons; LC3, Microtubule-associated protein 1A/1B-light chain 3; MEFs, Mouse Embryonic Fibroblasts; MN, Motoneurons; PBS, Phosphate-Buffered Saline; PECAM, Platelet Endothelial Cell Adhesion Molecule; PI3K/FOXO, Phosphoinositide-3-Kinase/Forkhead box O; RP, Roof plate; SA-β-gal, Senescence-associated beta-galactosidase; SDS, Sodium Dodecyl Sulfate; SEM, Standard Error of the Mean; TGF-β, Transforming Growth Factor beta.

(Kang, 2019). Members of the BCL-2 family, specifically antiapoptotic BCL-X_L and BCL-W, are essential for the survival of senescent cells (Hernandez-Segura et al., 2018). Thus, an approach to eliminate senescent cells for therapeutic or experimental purposes involves compounds, referred to as senolytics, that can specifically induce senescent cells to die. Compounds discovered so far include ABT-263 (Navitoclax), which inhibits different members of the BCL-2 family of antiapoptotic proteins (Chang et al., 2016; Yosef et al., 2016; Hernandez-Segura et al., 2018). This senolitic has been used to demonstrate the presence of programmed cell senescence in zebrafish (Da Silva-Alvarez et al., 2020).

Here we investigated whether there are cells undergoing programmed senescence during mammal spinal cord and notochord development. We found in the roof plate, floor plate, motoneuron zone, and notochord, cells with high SA-β-gal activity. Several cells in the notochord and endothelial cells in the spinal cord also expressed the tumor suppressor $p21^{CIP1/WAF}$; we did not find motoneurons expressing $p21^{CIP1/WAF}$, but we did observe that a subpopulation of motoneurons express $p16^{INK4A}$ and not the quiescent marker HES1. Supporting their senescent nature, a subpopulation of motoneurons was eliminated by the senolytic drug ABT-263. It is tempting to speculate that programmed cell senescence cooperate with programmed cell death to regulate the motoneuronal population during spinal cord development.

MATERIALS AND METHODS

Timed Mating and Open-Book Preparations of Spinal Cords

Mice used in the present study were handled and cared according to the animal care and ethics legislation. All procedures were approved by the Internal Committee of Care and Use of Laboratory Animals of the Institute of Cell Physiology- UNAM (IFC-SCO51-18). Mice had *ad libitum* access to water and food. Estrous cycle of female CD1 mice was monitored by vaginal lavage examination. Females in proestrus or estrus were placed in cages with fertile males overnight. The following morning (9:00 a.m.) was considered as embryonic day 0.5 (E0.5) if a vaginal plug was found. On days E10.5 to E14.5, dams were killed by cervical dislocation, and the uterus was washed in PBS. Embryos were dissected under a stereoscopic microscope. For open-book preparations, spinal cords were dissected from E12.5 to E14.5 embryos, opened dorsally and freed from meninges.

SA-β-Gal Assay

SA-β-gal assay was performed as described elsewhere (Debacq-Chainiaux et al., 2009). Whole embryos from stages E10.5 and E11.5, or open book preparations from spinal cords from E12.5 to E14.5 were washed twice in PBS and fixed 5 min with 2% formaldehyde plus 0.2% glutaraldehyde in PBS at room temperature. Reaction was performed by incubating embryos at 37°C overnight in reaction solution containing 1 mg/ml X-gal, 40 mM citric acid/sodium phosphate buffer pH 6.0, 5 mM potassium ferrocyanide, 5 mM potassium ferricyanide, 150 mM sodium chloride, and 2 mM Magnesium chloride. After SA-β-gal assay, spinal cords were fixed with 4% paraformaldehyde for 20 min. Some samples were used to perform immunofluorescence after fixation with 4% paraformaldehyde.

Immunofluorescence

Whole embryos or dissected spinal cords were fixed in PBS containing 4% paraformaldehyde for 30 min at room temperature, washed twice with PBS, and cryoprotected overnight with 30% sucrose in PBS. Embryos were cryosectioned by embedding in Tissue-Tek® O.C.T., histological sections of 40 μm were obtained using a Leica Cryostat and mounted on Superfrost plus slides. Sections on slides were washed three times with PBS for 5 min each time followed by permeabilization with 0.5% Triton™ X-100 in PBS for 30 min at room temperature. Afterwards, tissue sections were blocked with 2% Bovine Serum Albumin in PBS for 1 h and then incubated overnight at 4°C with the following antibodies: ISLET-1 (1:200, abcam, ab109517), HES1 (1:200, Santa Cruz, sc-25392), F4/80 (1:200, abcam, ab6640), BCL-X_L (1:50, Santa Cruz, sc-1690), PECAM (1:50, BD Pharmingen, 550274), ISLET-1 (1:25, DSHB, 40.2D6), Ki67 (1:500, abcam, ab15580), and $p21^{CIP1/WAF}$ (1:100, abcam, ab109199). Next day, secondary antibodies Alexa Fluor® 488 anti-rat (Invitrogen, A21208), Alexa Fluor® 488 anti-mouse (Invitrogen, A11029), Alexa Fluor® 488 anti-rabbit (Invitrogen, A11034), Alexa Fluor® 594 anti-rabbit (Invitrogen, A11037 Alexa Fluor® 647 anti-rabbit (Jackson Immuno Research, 711-606-152) or Alexa Fluor® 546 anti-rat (Invitrogen, A11081) were incubated at a dilution of 1:500 in 2% BSA for 1 h at room temperature. For $p16^{INK4A}$ (1:150, Santa Cruz, sc-1661) antigen retrieval with citrates buffer was performed before permeabilization/blocking step with 0.5%Tween/5%BSA and 0.1% H_2O_2. Slides were mounted with Fluoromount-G™ (Electron Microscopy Sciences, 1798425), and images were collected in a LSM800 (Zeiss) confocal microscope. All images were collected with 1 Airy Unit aperture of pinhole. The acquisition of SA-β-gal images by confocal microscopy was performed as described elsewhere (Levitsky et al., 2013). The primary and secondary antibodies were incubated in presence of detergents, 0.1% Tween/0.25%Tritón and 0.1%Tween, respectively. For quantification of motoneurons, embryos were cultured *ex-utero* as described below and processed for immunofluorescence using the motoneuron marker ISLET-1. Confocal microscopy images of cervical cross-sections were collected using the EC Plan-Neofluar 20x/0.50 M27 or Plan-Apochromat 40x/1.3 Oil DIC (UV) VIS-IR M27 objectives. CZI files were opened in the Fiji software, and ISLET-1^+-cells in the motoneuron zone were manually counted using the Multi-point tool. A single confocal plane per embryo was used for ISLET-1^+-cell quantification. Data was quantified was analyzed as indicated in the statistical analysis section.

DNA-Damage Induced Senescence in Mouse Embryonic Fibroblasts and Live Dead Assay

Mouse embryonic fibroblasts (MEFs) from passages between 3 and 5 were plated at a density of 6,750 cells/cm^2 in DMEM supplemented with 10% fetal bovine serum plus antibiotic/antimycotic (Life Technologies, 15240062). Next day,

aqueous solution of etoposide was added to a final concentration of 120 μM for 2 h. Then, the medium was replaced with etoposide-free DMEM plus fetal bovine serum. Cells were cultured for 5 d at 37°C and 5% CO_2 without changing the medium. Then, cells were treated for 20 h with 10 μM ABT-263 or equivalent concentrations of DMSO (0.2%) as vehicle-control. After ABT-263 treatment cell viability was quantified using the LIVE/DEAD™ Viability/Cytotoxicity Kit (ThermoFischer, L3224). Briefly medium was replaced with serum-free medium containing 1 μM calcein and 1 μM ethidium homodimer for 25 min. Then, epifluorescent images were collected in live cells using 50% glycerol in PBS as mounting medium. Live or dead cells were quantified manually using the multi-point tool from Fiji software.

Embryo Culture

Mouse embryos of E12 stage were cultured in a roller bottle system using reported protocols (Takahashi and Osumi, 2010; Kalaskar and Lauderdale, 2014). Uterus from pregnant mice were dissected, washed twice in sterile PBS at 37°C, and transferred to DMEM/F12 under a sterility hood. Embryos surrounded by the intact yolk sac were detached from the placenta and then freed from the yolk sac without separating it from the embryo. Dissected embryos were transferred to culture medium at 37°C consisting of KnockOut DMEM (Life Technologies, 10829018) containing 10% KnockOut Serum Replacement (Life Technologies, 10828028), N-2 supplement (Life Technologies, 17502048), 2% bovine serum albumin suitable for cell culture (RMBIO BSA-BAF-25G), and antibiotic/antimycotic (Life Technologies, 15240062). Embryos were pre-cultured in rolling bottles in an incubator at 37°C with continuous flow of 95% O_2/5% CO_2. Then, good heart rate and blood circulation was verified under a stereoscopic microscope for culturing the embryos for additional 15 h in the presence of the autophagy inhibitor spautin-1 (SIGMA, SML0440) or the senolytic ABT-263 (Chemgood, C-1009). Equivalent concentrations of DMSO were included as control conditions to exclude vehicle effect.

Western Blot

As LC3-II is not detectable in lysates of embryonic spinal cord by Western blot, it was enriched by preventing its degradation with chloroquine, added to culture medium to a final concentration of 100 μM during the last hour of embryo culture. The spinal cords were dissected with meninges and total lysates were obtained using a buffer consisting of 68.5 mM Tris HCl at pH 6.8, 2% SDS, and protease inhibitors cOmplete™ULTRA tablets (Sigma 5892791001). Lysate was cleared using a pestle sonicator for 10 s at 30% cycle, and centrifuging at 10,000 g for 10 min at room temperature. Protein was quantified using the DC™-protein assay kit (Bio-Rad, 5000112) using bovine serum albumin as standard. Protein was subjected to electrophoresis, transferred to a PVDF-FL membrane and analyzed using the LC3 antibody (MBL, PD014 at 1:2000 dilution overnight at 4°C) or anti-β-actin (Santa Cruz, sc-47778 at 1:10,000 for 1 h at room temperature). Secondary antibodies (IRDye® 800CW Goat anti-Rabbit (LI-COR, 92632211)and IRDye® 680RD Goat anti-Mouse IgG (LI-COR, 92568070) were diluted 1:10,000 and incubated for 1 h at room temperature. Bands were visualized in an Odyssey® CLx Imager, and quantified with the Image Studio Lite Version 5.2 software.

Statistical Analysis

Data are plotted as mean ± standard error of the mean. One-way ANOVA followed by Bonferroni's multiple comparisons test was performed using GraphPad Prism version 6.01 for Windows, GraphPad Software. $^{*}P \leq 0.05$, $^{**}P \leq 0.01$, $^{***}P \leq 0.001$.

RESULTS

SA-β-gal Activity Is Observed in Motoneurons and Phagocytic Cells of the Developing Spinal Cord

To search for the presence of programmed cell senescence in the mouse developing spinal cord, colorimetric detection of SA-β-gal was performed. Cross-sections of E10.5 and E11.5 embryos showed a dynamic SA-β-gal activity. While at E10.5 no signal was detectable in the neural tube, and only a faint signal was detected in the notochord, at E11.5 a strong signal was observed in the notochord; accordingly, SA-β-gal activity has also been observed in the chicken notochord (Lorda-Diez et al., 2015). We also observed SA-β-gal activity in the floor plate and the ventral area of the neural tube, where the motoneurons are located (**Figure 1A**). We then analyzed the pattern of SA-β-gal activity in open-book preparations of spinal cords from E12.5 to E14.5 embryos. Interestingly, the enzymatic activity observed in the floor plate and motoneuron zone gradually decreased from the rostral region toward the caudal region as development advanced (**Figure 1B**). Note that in the medulla oblongata there is a cluster of cells positive for SA-β-gal activity (arrowheads, **Figure 1B**).

To demonstrate that the staining of SA-β-gal overlaps with the motoneuron zone, the motoneuron marker ISLET-1 was immunodetected in cross-sections of E11.5 embryos previously stained for SA-β-gal and analyzed by confocal microscopy. As expected, the SA-β-gal activity overlaps with the motoneuron columns, but not with the interneurons, which also express ISLET-1. Importantly, SA-β-gal activity was confirmed in the floor plate (**Figure 1C**). Interestingly, in open-book preparations of E13.5 spinal cords we observed that the SA-β-gal in the medulla oblongata also overlaps with motoneurons located there (**Figure 1D**, upper row), as well as in the spinal cord (**Figure 1D**, lower row). Since macrophages have high lysosomal activity (Hall et al., 2017), it could be possible that all the SA-β-gal activity we observed could be produced by phagocytic cells, given the occurrence of phagocytosis during development to clear apoptotic cells generated by programmed cell death, and possibly to clear also senescent cells. To estimate the abundance of macrophages, we investigated whether the cells displaying SA-β-gal activity also express the activated macrophage/microglia marker F4/80. As shown in **Figure 1D**, very few macrophages were found in the medulla oblongata, and while in the spinal cord macrophages clearly showed strong SA-β-gal activity, we detected SA-β-gal activity around cells expressing ISLET1 but not

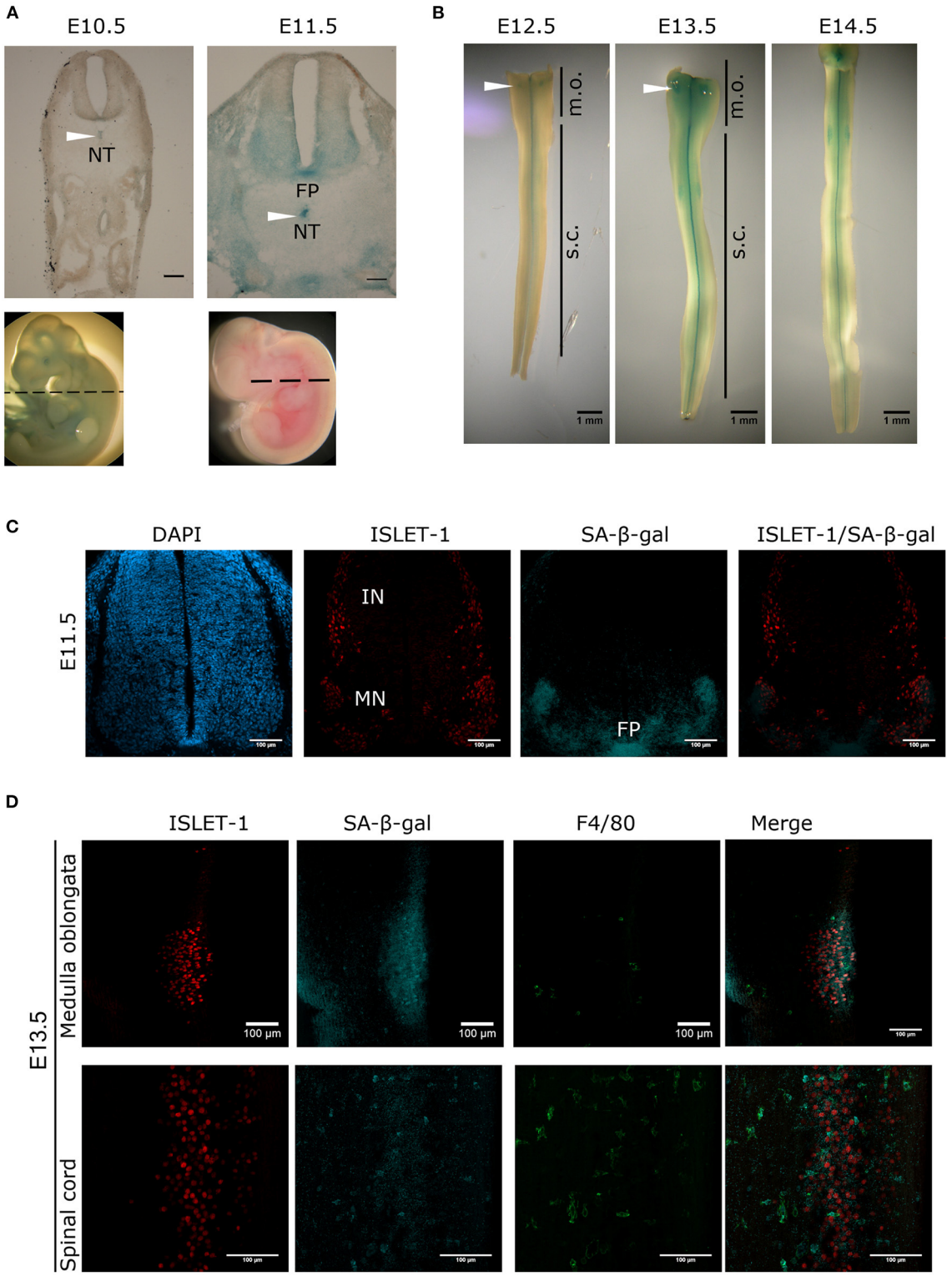

FIGURE 1 | Transient and region-specific SA-β-gal activity in the mouse embryonic spinal cord and notochord. **(A)** Whole embryos from E10.5 and E11.5 were stained for SA-β-gal activity and cross-sectioned at the position indicated with dotted line in embryos shown in the lower row. Notice that the notochord (NT, arrowheads), the floor plate (FP) and the ventral neural tube where motoneurons develop have high SA-β-gal activity at E11.5. Scale bars represent 100 μm. **(B)**

(Continued)

FIGURE 1 | Open-book preparations of spinal cords from E12.5 to E14.5 were subjected to SA-β-gal activity assay. SA-β-gal activity is strongly detected in the floor plate and at lower extent in the region corresponding to motoneurons of the spinal cord (s.c.). Arrowheads indicate SA-β-gal positive cells in the medulla oblongata (m.o.). **(C)** Whole E11.5 embryos were stained for SA-β-gal activity, thoracic sections were obtained and processed for immunodetection of ISLET-1. Confocal analysis shows that SA-β-gal activity overlaps with the motoneuron (MN) zone and the floor (FP) plate, while interneuron (IN) cells that also express ISLET-1, do not display SA-β-gal activity. Maximal projections are shown. Scale bars represent 100 μm. **(D)** Open-book spinal cord of stage E13.5 were stained for SA-β-gal activity and then subjected to whole-mount immunofluorescence against ISLET-1 and F4/80. Cells positive for ISLET-1 in the medulla oblongata (upper row) correspond to cells indicated with white arrowhead in **(B)**. Detection of SA-β-gal activity by confocal microscopy combined with immunodetection of motoneurons (ISLET-1) and activated macrophages (F4/80) shows that these two cell types display SA-β-gal activity both in the medulla oblongata (upper row) and spinal cord (lower row). Maximal projections are shown. Scale bars represent 100 μm. Representative images are shown from at least three embryos or dissected spinal cords analyzed per immunofluorescence.

F4/80, indicating that both macrophages and motoneurons have SA-β-gal activity in the developing spinal cord.

The Cell Cycle Inhibitor p21$^{CIP1/WAF}$ Is Expressed in Endothelial Cells of the Developing Spinal Cord and Some Cells in the Notochord, and p16^{INK4A} Is Expressed in Motoneurons

To corroborate the senescent phenotype in cells in the embryonic spinal cord and notochord, we analyzed whether the senescence marker p21$^{CIP1/WAF}$ was also expressed. First, we confirmed the specificity of our antibody by analyzing the apical ectodermal ridge, a structure known to express p21$^{CIP1/WAF}$ as part of the developmentally programmed cell senescence (Storer et al., 2013). Accordingly, cells in this structure indeed showed immunoreactivity against this antibody (**Supplementary Figure 1A**). Then, cross-sections from E10.5 and E11.5 embryos were analyzed for the expression of p21$^{CIP1/WAF}$. Notably, p21$^{CIP1/WAF}$ was expressed in several parts of the embryo, including the spinal cord (**Figure 2A**) and the notochord, where it was located mainly in the cytoplasm (**Figure 2B**). We could not find motoneurons with a clear expression of p21$^{CIP1/WAF}$ in the spinal cord (**Figure 2C**), which was surprising since some of them had high SA-β-gal activity (**Figures 1C,D**). We identified as endothelial cells (expressing PECAM) the subpopulation of cells in the spinal cord that expressed p21$^{CIP1/WAF}$ (**Figure 2C**). Endothelial cells in the medulla oblongata and in areas of the forelimb and thorax also expressed p21$^{CIP1/WAF}$ (**Supplementary Figures 1B,C**). As cellular senescence is characterized by exit from the cell cycle and lack of cell division, we analyzed the expression of the proliferation marker Ki67. We found that only few cells along the central canal of the spinal cord express Ki67, none in the motoneuron zone (**Figure 2D**).

Even though it was reported the lack of expression of p16^{INK4A} during mammalian programmed cell senescence (Munoz-Espin et al., 2013; Storer et al., 2013), senescent cells in the placenta express p16^{INK4A} (Gal et al., 2019), and in the developing zebrafish programmed cell senescence is accompanied by *Cdkn2a* expression (Da Silva-Alvarez et al., 2020). Therefore, we investigated whether motoneurons undergoing programmed cell senescence might express p16^{INK4A} instead of p21$^{CIP1/WAF}$. As shown in **Figure 3A**, we found abundant cells expressing p16^{INK4A} in the motoneuron zone, and indeed a subpopulation of motoneurons also expressed p16^{INK4A}. We verified that the antibody used to detect p16^{INK4A} provide a signal restricted to programmed cell senescence, by immunostaining the limbs at E12.5 (**Figure 3B**). We observed that only the apical ectodermal ridge immunolabeled positive for p16^{INK4A}.

To distinguish quiescent cells from senescent cells, we analyzed the expression of the transcriptional repressor HES1, which prevents senescence establishment and irreversible cell cycle exit in quiescent cells (Sang et al., 2008; Sueda et al., 2019). **Figure 4** shows that motoneurons identified by ISLET-1 expression did not expressed HES1. Interestingly, we found precisely defined domains of HES1 expression in the floor plate of spinal cords at E10.5 (**Figure 4**, upper panel) and in the roof plate at E12.5 (and **Figure 4**, lower panel), which lack p21$^{CIP1/WAF}$ expression (**Figure 2B**, E10.5). The finding that the roof plate expressed HES1 at E12.5, a zone reported to undergo programmed cell senescence (Storer et al., 2013), suggests that in those areas there are both senescent cells and quiescent cells.

A Subpopulation of Embryonic Motoneurons Are Sensitive to the Senolytic Drug ABT-263

To confirm whether the subpopulation of motoneurons with detectable SA-β-gal activity, and expressing p16^{INK4A} but not HES1 in the developing spinal cord were indeed senescent, we tested their sensitivity to the senolytic ABT-263. To validate our tools, we compared the toxicity of ABT-263 in proliferative *vs.* senescent mouse embryonic fibroblasts. By quantifying the number of live or dead cells, we confirmed that ABT-263 preferentially kills senescent cells (**Supplementary Figure 2**). We then collected embryos at stage E12 and cultured them for 15 h to develop them *ex-utero*, either in the presence of ABT-263 or vehicle only. Using serum-free medium, embryos developed similarly to *in vivo,* as shown in **Figure 5A** and **Supplementary Figure 3A**. We found that embryos cultured with ABT-263 resulted in decreased activity of SA-β-gal in the spinal cord (**Figure 5B**), confirming that programmed senescent cells are also susceptible to ABT-263. Since this senolytic acts by inhibiting antiapoptotic BCL-2 family of proteins, we verified the expression of BCL-X_L in the motoneuron zone in the developing spinal cord (**Figure 5C**). To specifically analyze whether ABT-263 promotes motoneuron senescent cells death, the number of ISLET-1 positive cells was quantified in embryos cultured with ABT-263 compared with control or vehicle only conditions. As shown in **Figure 5C**, exposure to ABT-263 eliminated a subgroup of motoneurons. To verify that the reduction in motoneuron

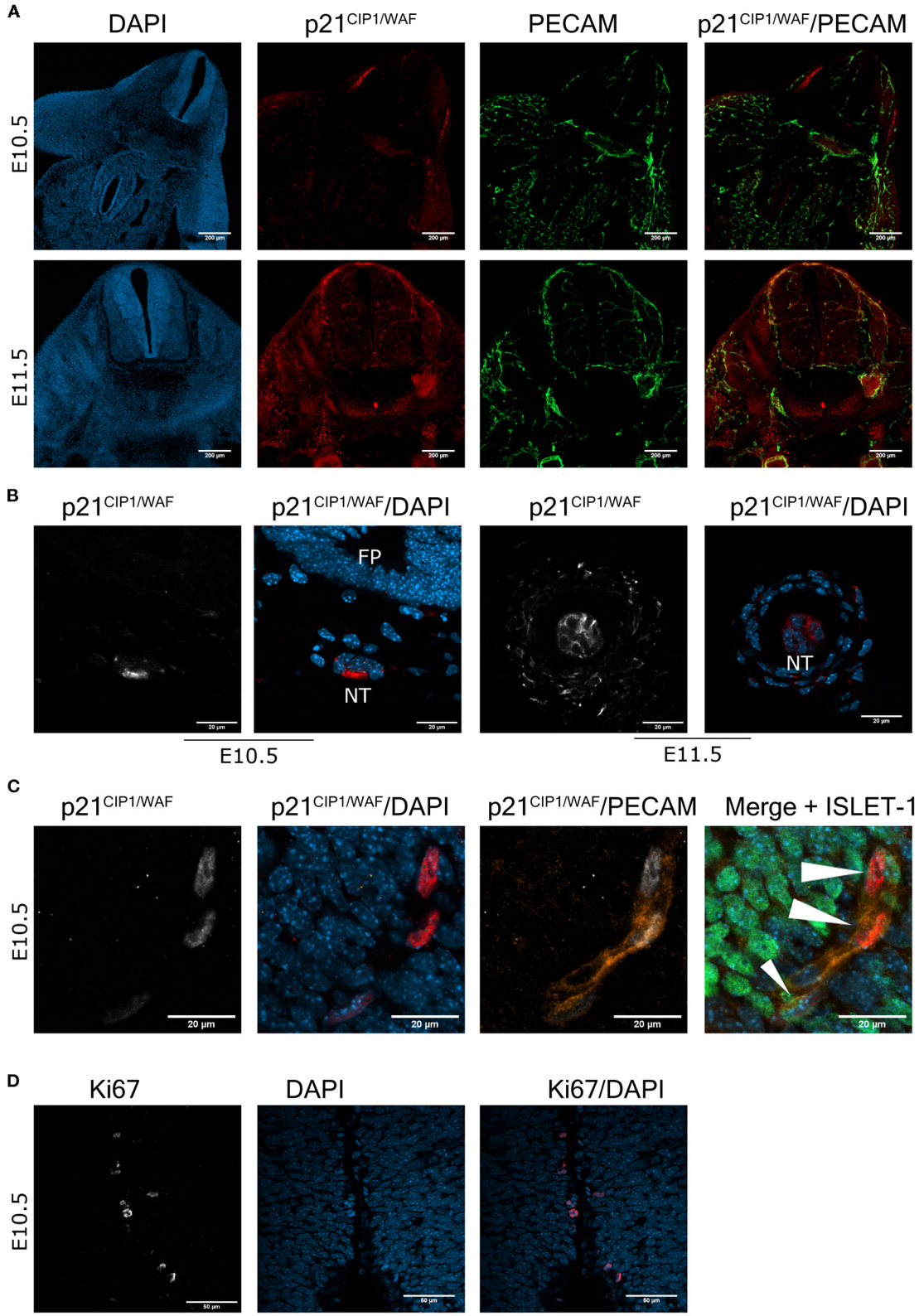

FIGURE 2 | The cell cycle inhibitor p21$^{CIP1/WAF}$ is expressed in the mouse embryonic spinal cord and notochord. **(A)** Endothelial cells express p21$^{CIP1/WAF}$. Brachial or cervical sections from E10.5 and E11.5 embryos, respectively, were processed for immunodetection of p21$^{CIP1/WAF}$ and PECAM. Embryos of the two stages show

(Continued)

FIGURE 2 | expression of p21$^{CIP1/WAF}$ in several organs, including the spinal cord. In the spinal cord, p21$^{CIP1/WAF}$ is expressed in endothelial cells labeled with PECAM. Single confocal planes are shown. Scale bars represent 200 μm. **(B)** p21$^{CIP1/WAF}$ is expressed in some notochord cells. Sections of embryos from stages E10.5 and E11.5 were processed as in **(A)**. Notice that p21$^{CIP1/WAF}$ is located in the cytoplasm of notochord (NT) cells, while it is absent in the floor plate (FP) from the E10.5 embryo. Single confocal planes are shown. Scale bars 20 μm. **(C)** p21$^{CIP1/WAF}$ is expressed in PECAM-positive endothelial cells localized in the vessels that surround the motoneuron column, but not in motoneurons themselves in the spinal cord of E10.5 embryos. White arrowheads indicate p21$^{CIP1/WAF}$ -positive nuclei. Single confocal planes are shown. Scale bars 20 μm. **(D)** Only few cells along the central canal of the spinal cord of E10.5 embryos are proliferating, none in the motoneuron zone. Embryos from E10.5 stage were processed for immunofluorescence against Ki67 in cervical sections. Single confocal plane is shown. Scale bars represent 50 μm. Representative images are shown from at least 3 embryos analyzed per immunofluorescence.

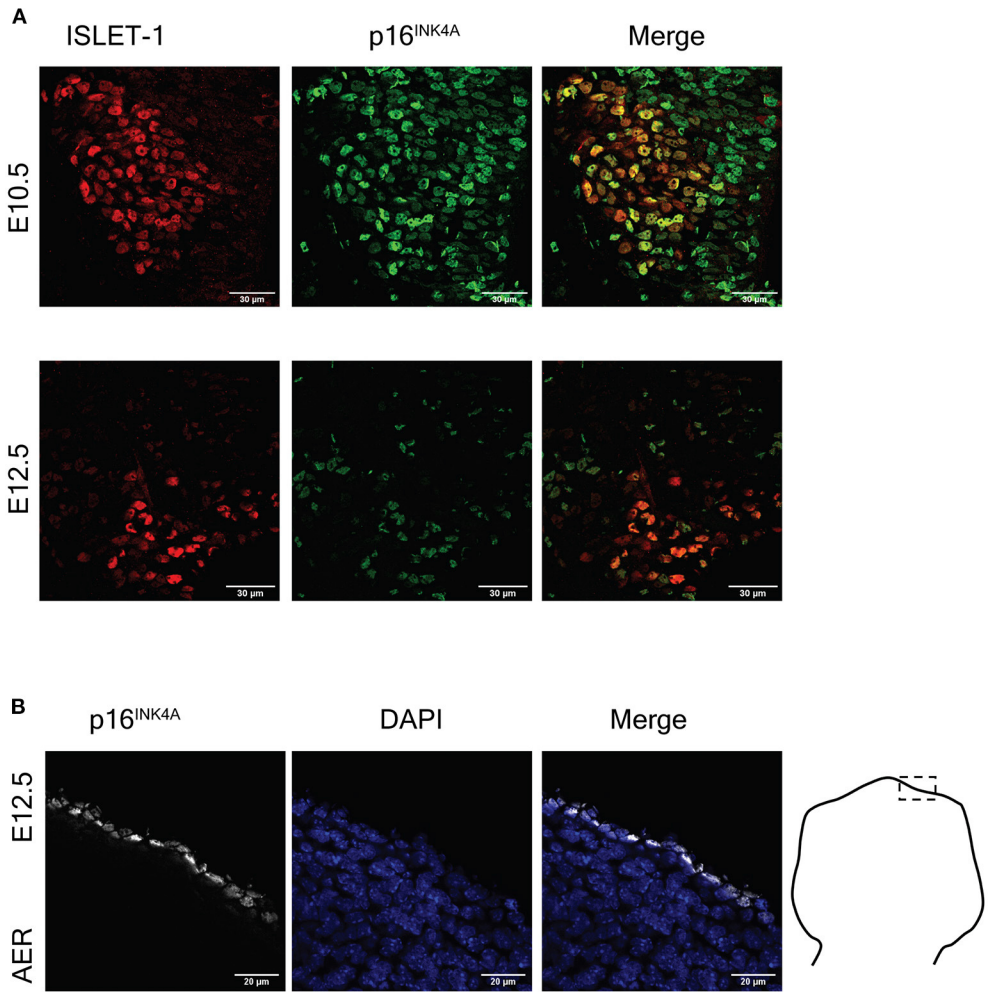

FIGURE 3 | The cell cycle inhibitor p16^{INK4A} is expressed in the mouse embryonic spinal cord and the apical ectodermal ridge. **(A)** Embryonic motoneurons express p16^{INK4A}. Representative images of immunofluorescence analysis to detect ISLET-1 and p16^{INK4A} in cervical sections of embryos from stages E10.5 and E12.5 are shown. The number of motoneurons decreases from E10.5 to E12.5 due to programmed cell death. Note that p16^{INK4A} is expressed in abundant cells in this area, several of them also express ISLET-1. At both stages p16^{INK4A} is expressed in several motoneurons. Scale bars 30 μm. **(B)** Cells of the apical ectodermal ridge (AER) express p16^{INK4A}. Forelimbs of stage E12.5 were sectioned as indicated in the diagram and processed for immunodetection of p16^{INK4A}. Single confocal planes are shown. Scale bars represent 20 μm. Representative images are shown from at least three embryos analyzed per immunofluorescence.

number due to the ABT-263 treatment correlates with increased cell death, pyknotic nuclei were quantified in the motoneuron zone of the spinal cord and notochord. Indeed, ABT-263-treated embryos showed a higher amount of pyknotic nuclei in the motoneuron zone (**Figure 6A**, upper row and **Figure 6B**, left). The number of pyknotic nuclei in the notochord also showed a trend to increase (**Figure 6A**, lower row and **Figure 6B**, right). All together, the data shown suggest that a subpopulation of motoneurons undergo programmed cell senescence, perhaps contributing to eliminate supernumerary motoneurons.

Previous observations have shown that in addition to apoptosis other cellular processes might contribute to the

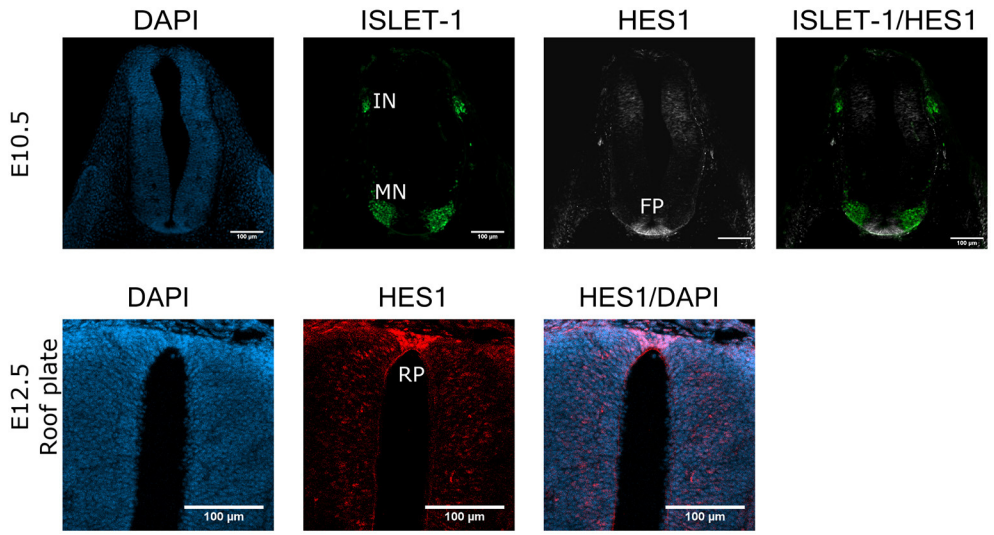

FIGURE 4 | HES1 is expressed in some cells in the floor plate and roof plate in the developing spinal cord. Cross sections of E10.5 or E12.5 embryos (cervical or thoracic, respectively) were analyzed for the expression of HES1 in the spinal cord. The floor plate (FP) of the E10.5 spinal cord contains cells with strong HES1 expression, but none was found in the motoneuron (MN) columns in E10.5 embryos. The roof plate (RP) of the E12.5 embryo also shows clear HES1 expression. Maximal projections of four confocal planes are shown. Scale bars 100 µm. Representative images are shown from at least three embryos anlalyzed.

programmed cell death of motoneurons, and cell death by autophagy was proposed (Sanchez-Carbente et al., 2005). To investigate whether autophagy signaling contributes to motoneurons cell death, embryos collected at stage E12 were cultured 15 h in the presence of the autophagy inhibitor spautin-1 (Liu et al., 2011) or vehicle only. Again, embryos cultured in serum-free medium reproduced *in vivo* development (**Supplementary Figure 3A**); autophagy inhibition was corroborated by Western blot detection of decreased LC3-II levels (**Supplementary Figure 3B**). As occurs during normal development, the number of motoneurons decreased during the course of the culture, reproducing the *in vivo* developmental window of motoneurons programmed cell death. We found that pharmacological inhibition of autophagy did not prevent motoneurons programmed cell death (**Supplementary Figure 3C**). This result suggests that autophagic cell death does not contribute to establish the final number of motoneurons during spinal cord development. In summary, we observed that embryonic motoneurons are insensitive to autophagy inhibition, but sensitive to the senolytic ABT-263, suggesting that programmed cell senescence contributes to the adjustment of motoneurons number. It would be necessary to prevent motoneuron senescence establishment to test this idea.

DISCUSSION

The identification of programmed cell senescence as a developmental process in amphibians, salamanders, fish, birds and mammals, supports the notion that the senescent program emerged during the evolution of vertebrates, and its mechanism is conserved. It is fundamental to uncover the role of programmed cell senescence during development, as well as to decipher the molecular basis for cellular senescence induction under developmental cues. As summarized in **Figure 7**, in this work we found that several cell types acquired senescent features in the spinal cord and notochord of embryos at developmental stages E10.5 - E12.5.

It is important to consider that the finding of endothelial cells of blood vessels with SA-β-gal activity and $p21^{CIP1/WAF}$ expression needs cautious interpretation. Unlike the programmed cell senescence that occurs in transient structures that are eliminated during development, endothelial cells remain in the blood vessels, where they become fundamental components. Consistent with our data, previous studies have shown that during endothelial cell differentiation two markers of senescence are observed: $p21^{CIP1/WAF}$, that mediates the cell cycle arrest necessary for endothelial cell differentiation (Zeng et al., 2006; Marcelo et al., 2013), and SA-β-gal activity, that occurs during differentiation of human prostate epithelial cells (Untergasser et al., 2003). A report that elegantly linked the concepts of senescence and differentiation was published recently (Li et al., 2018). By using genetic lineage tracing, Li and colleagues showed that in the apical ectodermal ridge at mid-stage (E10.5–E13.5) there is a population of $p21^{CIP1/WAF}$ -positive and SA-β-gal-positive cells (i.e., senescent cells). Interestingly, by late-stage (E15.5–E16.5) or after birth, a subset of the previously senescent cells re-entered the cell cycle, proliferated, exhibited epithelial fate and contributed to tissues (Li et al., 2018). Thus, endothelial cells that express $p21^{CIP1/WAF}$ in the developing spinal cord may engage in a senescent program and nevertheless form the blood vessels later in development.

We found some cells in the notochord with SA-beta-gal activity, expression of $p21^{CIP1/WAF}$, and possibly susceptible

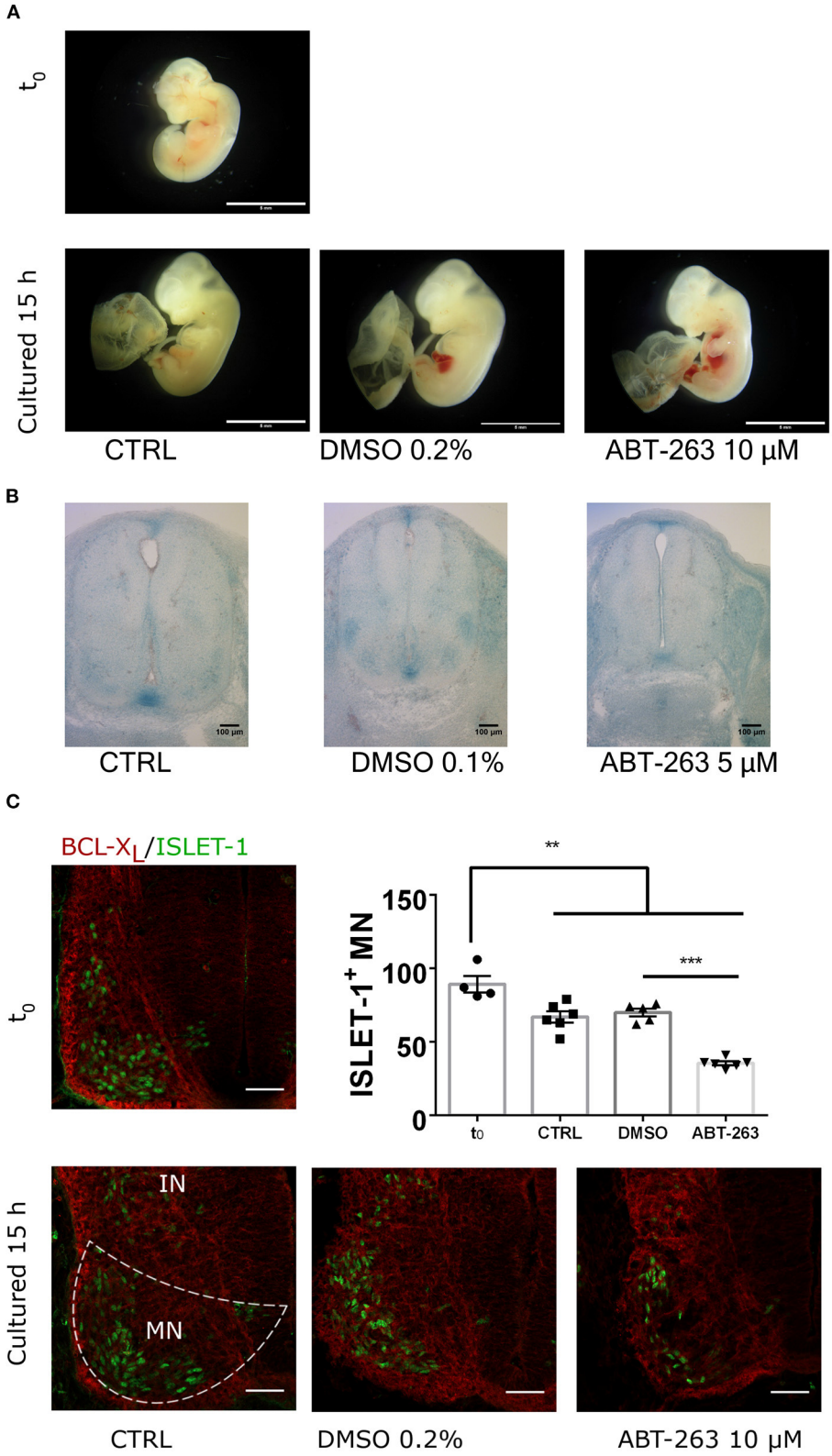

FIGURE 5 | The senolytic ABT-263 reduced SA-β-gal activity in the spinal cord and promotes motoneurons cell death during development. **(A)** Morphology of embryos dissected at E12 (t_0) and cultured for 15 h, in control medium, supplemented with vehicle only or with 10 µM ABT-263. All culture conditions developed

(Continued)

FIGURE 5 | similar growth compared to *in utero* development. Scale bar 5 mm. **(B)** Embryos of the E12 stage were cultured as in **(A)**, stained for SA-β-gal, and cross-sectioned. The treatment with ABT-263 resulted in a decrease of SA-β-gal activity in the motoneuron zone and floor plate. **(C)** Cervical cross-sections of embryos at the beginning (t_0) or after 15 h cultured as in **(A)** were processed for immunofluorescence to detect BCL-X_L and ISLET-1 expression. Single confocal planes are shown. Scale bars 50 μm. Graph plots the quantification of motoneurons (ISLET-1 expressing cells). Each data point represents the number of cells counted in the hemisection of a single embryo. Number of embryos per group: $T_0 = 4$, CTRL $n = 6$, DMSO $n = 5$, ABT-263 $n = 6$. Data are plotted as mean ± SEM; significant differences were obtained by one-way ANOVA analysis followed by Bonferroni's multiple comparisons test; $^{**}p \leq 0.01$; $^{***}p \leq 0.001$.

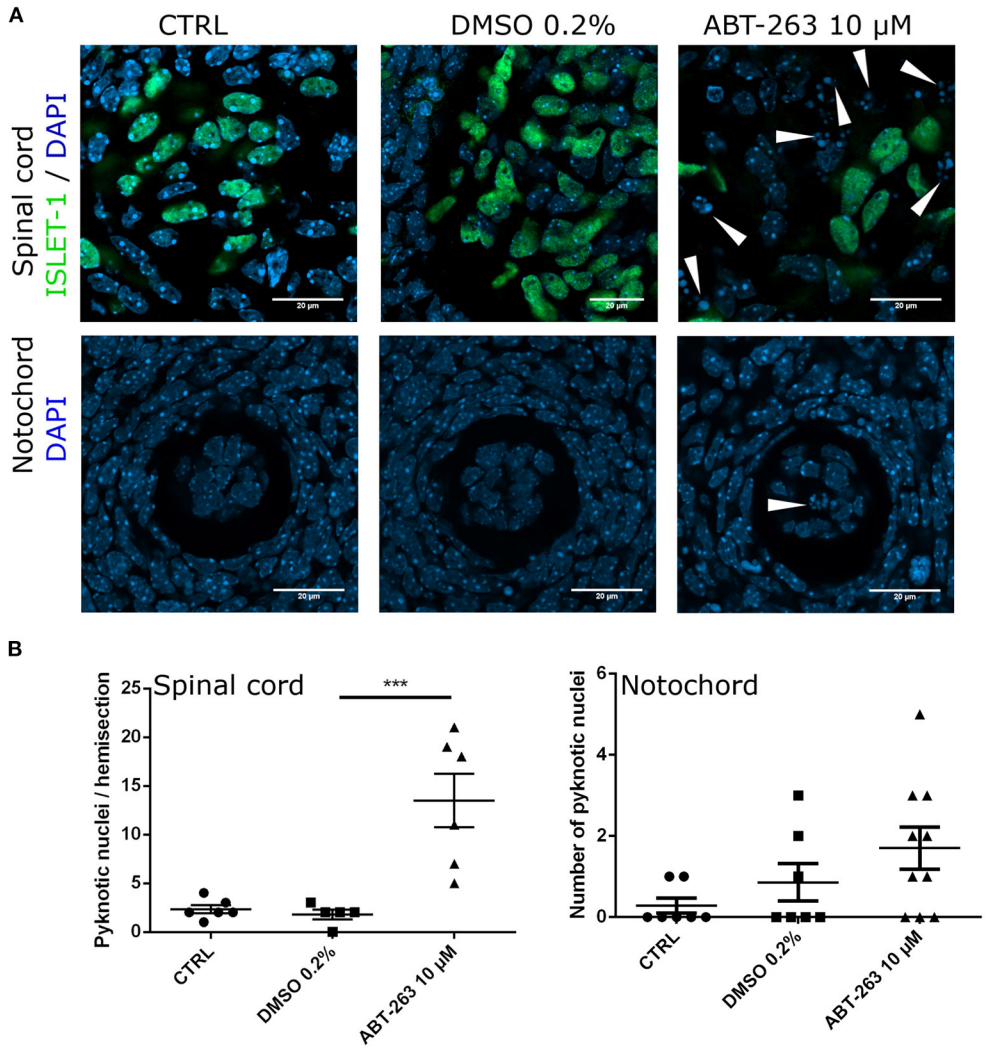

FIGURE 6 | Embryos exposure to the senolytic ABT-263 increased pyknotic nuclei. **(A)** Confocal images of the spinal cord showing the motoneurons and nuclei (upper row), or the notochord (lower row) from embryos cultured with 10 μM ABT-263, vehicle (DMSO 0.2%) or control conditions. **(B)** Left: quantification of pyknotic nuclei in the spinal cord. Each data point represents the number of pyknotic nuclei in the motoneuron zone of a single embryo. At least five embryos were analyzed. Right: quantification of pyknotic nuclei in the notochord. Each data point represents the number of pyknotic nuclei in notochord. Number of embryos per group: CTRL $n = 7$, DMSO $n = 7$, ABT-263 $n = 10$. Data are plotted as mean ± SEM significant differences were obtained from one-way ANOVA followed by Bonferroni's multiple comparisons test. $^{***}p \leq 0.001$.

to the senolitic ABT-263 (**Figure 6**), supporting the senescent nature of those few notochord cells. Given that the notochord is a signaling center for the differentiation of neuron populations of the spinal cord, perhaps the few senescent cells we observed contribute to the secretion of developmental factors. We noticed that $p21^{CIP1/WAF}$ was found in the cytoplasm of notochord cells. While $p21^{CIP1/WAF}$ inhibits cell cycle when it is located in the nucleus, in the cytoplasm it has an anti-apoptotic function due to its ability to bind and inhibit the activity of proapoptotic proteins (Karimian et al., 2016).

A contrasting observation was to find in the floor plate and roof plate both SA-β -gal activity and HES1 (a quiescence

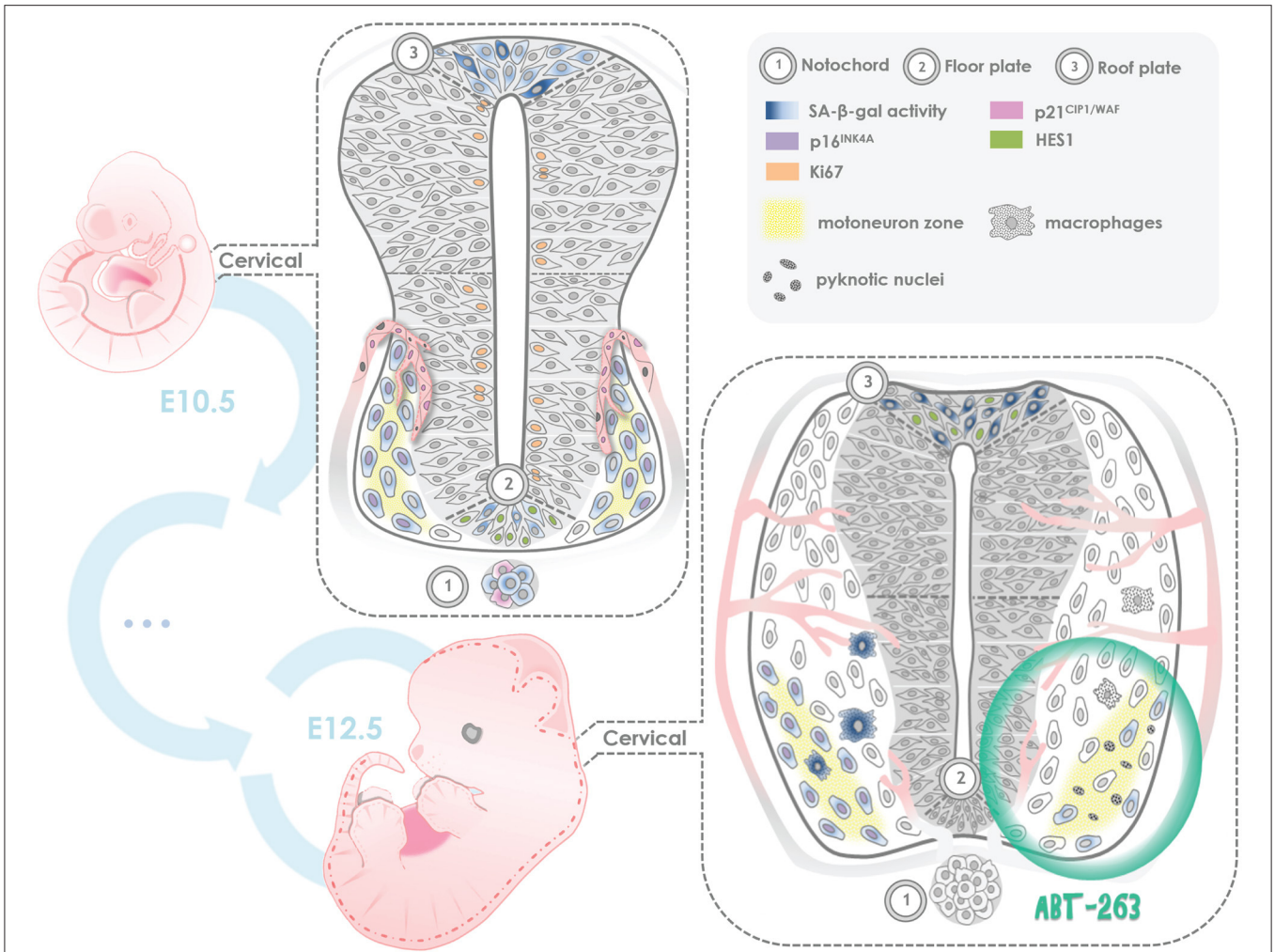

FIGURE 7 | Summary of programmed cell senescence markers found in the mouse embryonic spinal cord and notochord. SA-beta-gal activity and expression of $p21^{CIP1/WAF}$ were detected since stage E10.5 and through stage E12.5 in endothelial cells of blood vessels; $p16^{INK4A}$ expression was found in motoneurons, with lack of expression of Ki67, a proliferation marker, and lack of HES1 expression, a quiescence maintenance factor. Notably, in the floor plate and roof plate both SA-β-gal activity and HES1 expression were observed. We propose that in those regions there are both senescent cells and quiescent cells. In some notochord cells, SA-β-gal activity and cytosolic expression of $p21^{CIP1/WAF}$ were found. Given that the notochord is a signaling center, perhaps the few senescent cells we observed contribute to the secretion of development factors. In *ex-utero* development of E12 embryos, a subpopulation of motoneurons resulted sensitive to the senolytic ABT-263. We propose that programmed cellular senescence cooperates with apoptosis to adjust the number of motoneurons during spinal cord development, and the transient presence of senescent cells contributes to instruct the differentiation of neuronal populations and endothelial cells.

maintenance factor) expression. One possibility is that in those regions there are both senescent cells and quiescent cells. Nevertheless, SA-β-gal activity could also occur in quiescent cells expressing HES1 (Baek et al., 2006). To determine whether indeed the same cell expressing HES1 had high SA-β-gal, we attempted to detect both HES1 and SA-β-gal in the same preparations, but it resulted in strong background and nonspecific binding of the HES1 antibody, probably caused by the fixation protocol for SA-β-gal. Other reports also show that SA-β-gal is detectable in non-senescent cells such as the yolk sac, visceral endoderm, and macrophages (Cristofalo, 2005; Yang and Hu, 2005; Huang and Rivera-Perez, 2014; Hall et al., 2017). The activation of SA-β-gal is also caused by cellular differentiation induced by TGF-β (Untergasser et al., 2003). Nevertheless, previous articles showed SA-β-gal in the neural tube, and concluded that programmed senescence occurs in the roof plate of the spinal cord (Munoz-Espin et al., 2013; Storer et al., 2013; Czarkwiani and Yun, 2018). Indeed, $p21^{CIP1/WAF}$ -positive cells were detected in the closing neural tube (Storer et al., 2013), but expression of $p21^{CIP1/WAF}$ or other cell cycle inhibitor was not shown in the roof plate. Thus, we consider open the possibility that in addition to senescence, quiescence can be accompanied by SA-β-gal in the roof plate.

Given the transient nature of programmed cell senescence, as they are eliminated by macrophages (Storer et al., 2013), cellular

senescence could contribute to eliminate unwanted cells in concert with programmed cell death. This presumed function is supported by finding senescent cells during organ regression (i.e., the mesonephros), and in regions and developmental windows where cell population is balanced (i.e., the endolymphatic sac of the inner ear) (Da Silva-Álvarez et al., 2019). In this work, we observed that a subpopulation of motoneurons undergo programmed cell senescence, revealed by SA-β-gal activity, $p16^{INK4A}$ expression, lack of Ki67 and HES1 expression, and susceptibility to the senolytic ABT-263. Interestingly, senescent motoneurons appear at a developmental window in which supernumerary motoneurons are being eliminated. We propose that programmed cell senescence cooperates with apoptosis to adjust the number of motoneurons during spinal cord development, either by secreting differentiation factors or signals to be cleared by macrophages. In a similar way that senescent cells in the apical ectodermal ridge reintegrated into the tissue (Li et al., 2018), it could also occur that a subpopulation of senescent motoneurons continues to fully differentiate into postmitotic neurons and remain integrated in the tissue.

To confirm a developmental role of senescent motoneurons, we should be able to prevent the acquisition of the senescent phenotype and observe a disruption of the developmental pattern of the neural tube, or an increase in the total number of motoneurons. Currently this experiment is not possible, since TGF-β is the only signaling pathway described to induce programmed cell senescence (Munoz-Espin et al., 2013) but it has also a crucial role in neural tube development. So, if we inhibit TGF-β pathway we won't be able to distinguish the developmental role of TGF-β from the role of senescent cells *per se*. The fact that we detected $p16^{INK4A}$ expression (but not $p21^{CIP1/WAF}$) in some motoneurons, opens the possibility to analyze whether in the absence of $p16^{INK4A}$ motoneurons senescence could be prevented. Cellular senescence mediated by $p16^{INK4A}$ has also been observed during placenta development (Gal et al., 2019), and *Cdkn2a* mRNA was detected in programmed cell senescence in zebrafish (Da Silva-Alvarez et al., 2020); it is possible, then, that different cell types undergoing programmed cell senescence vary in the tumor suppressor gene they expressed.

In summary, our findings allow us to speculate that (1) SA-β-gal activation may occur during the quiescent phenotype of the floor and roof plates, (2) endothelial cells are probably engaged in a phenomenon of reversible senescence, (3) a subpopulation of notochord cells become senescent and could secrete morphogens, and (4) motoneuron programmed senescence could contribute to the elimination of motoneurons during spinal cord development. Further experiments will be needed to test these hypotheses.

DATA AVAILABILITY STATEMENT

The original contributions presented in the study are included in the article/**Supplementary Material**, further inquiries can be directed to the corresponding author/s.

ETHICS STATEMENT

The animal study was reviewed and approved by Internal Committee of Care and Use of Laboratory Animals of the Institute of Cell Physiology- UNAM (IFC-SCO51-18).

AUTHOR CONTRIBUTIONS

JD-B and SC-O contributed to conception and designed of the study. JD-B performed most of the experiments and wrote the first draft of the manuscript. PA-R performed experiments, acquired data and prepared **Figures 3**, **7**. All authors contributed to manuscripts revision, read and approved the submitted version of the manuscript, and are accountable for the content of the work.

FUNDING

Funding was obtained from PAPIIT/UNAM IN206518, CONACyT CB2013-220515, and Fundación Miguel Alemán, A.C. to SC-O. PA-R was recipient of a graduate scholarship from CONACyT (446145), and JD-B was recipient of the postdoctoral DGAPA-UNAM and CONACyT postdoctoral fellowships.

ACKNOWLEDGMENTS

We thank the following persons for their support during the course of this project: Dr. Beatriz Aguilar-Maldonado (technical assistance), Dr. Claudia Rivera-Cerecedo (Animal Facility), Dr. Ruth Rincón-Heredia and Dr. Abraham Rosas-Arellano (Microscopy facility), Eng. Aurey Galván Lobato and Eng. Manuel Ortínez Benavides (Equipment Maintenance Workshop). Data in this work is part of PA-R doctoral dissertation in the Posgrado en Ciencias Bioquímicas de la Universidad Nacional Autónoma de México.

SUPPLEMENTARY MATERIAL

The Supplementary Material for this article can be found online at: https://www.frontiersin.org/articles/10.3389/fcell.2021.587096/full#supplementary-material

Supplementary Figure 1 | The cell cycle inhibitor $p21^{CIP1/WAF}$ is expressed in endothelial cells of the medulla oblongata and forelimb. **(A)** The specificity of the $p21^{CIP1/WAF}$ antibody was validated by analyzing the expression of $p21^{CIP1/WAF}$ in the apical ectodermal ridge of a E12.5 embryo. The section area is indicated on the diagram on the right. Single confocal planes are shown. Scale bars represent 20 μm. **(B)** Cross-section analysis of the medulla oblongata from a representative E12 embryo as indicated on the right. Confocal microscopy shows that $p21^{CIP1/WAF}$ is expressed in endothelial (PECAM-positive) cells. In the upper panel it is shown a low magnification, in the lower panel a higher magnification is shown. Single confocal planes are shown. Scale bars represent 100 or 20 μm. **(C)** Expression of $p21^{CIP1/WAF}$ in endothelial cells of the forelimb and thorax of a representative E13.5 embryo. Single confocal planes are shown. Scale bars 100 μm.

Supplementary Figure 2 | *In vitro* validation of the senolytic effect of ABT-263. Proliferative (non-senescent) and senescent MEFs were treated for 20 h with ABT-263 at the indicated concentrations and the cytotoxic effect was determined quantifying live and dead cells. Since 5 μM ABT-263 induced senescent

fibroblasts death concomitant with a reduction of cells alive. We noticed a decrease in the number of live non-senescent MEFs with 10 μM ABT-263, although the number of dead cells was not affected. Each group was cultured in triplicate wells, and five random fields in each well were used to count the number of live or dead cells. Data are plotted as mean ± SEM significant differences were obtained from one-way ANOVA followed by Bonferroni's multiple comparisons test; $^{*}p \leq 0.05$, $^{**}p \leq 0.01$.

Supplementary Figure 3 | Pharmacological inhibition of autophagy does not alter the amount of motoneurons. **(A)** Morphology of embryos dissected at E12 (t_0) and cultured for 15 h, in control medium, supplemented with vehicle only or with 10 μM spautin-1. All culture conditions developed similar growth compared to *in utero* development. Scale bar 5 mm. Graph shows the weight gain of the embryos after culture. Each dot represents an embryo **(B)** Treatment with spautin-1 inhibits autophagy, as it results in a decrease of LC3-II levels compared to control (CTRL) or vehicle (DMSO). Western blot to detect indicated proteins from total lysates obtained from embryonic spinal cords of E12 embryos cultured with spautin-1, vehicle or control for 15 h. As a reference to distinguish LC3-II, a lysate from mouse embryonic fibroblasts (MEFs) cultured with chloroquine (CQ) was also loaded. Graph shows densitometric LC3-II levels normalized with β-actin as loading control. Data are plotted as mean ± SEM, significant differences were obtained from one-way ANOVA followed by Bonferroni's multiple comparisons test; $^{*}p \leq 0.05$. $n = 4$. **(C)** ISLET-1 positive motoneurons were quantified in cervical cross-sections from embryos dissected at E12 and developed *ex-utero* for 15 h with indicated treatments. The results of four independent embryo cultures are shown, with at least two embryos per condition per culture. Each data point represents the number of cells quantified in the hemisection of a single embryo. The number of motoneurons significantly decreased in all conditions after culture, as occurs during this stage of embryo development, but pharmacologic inhibition of autophagy with spautin-1 did not affect the amount of surviving motoneurons. Data are plotted as mean ± SEM, significant differences were obtained from one-way ANOVA followed by Bonferroni's multiple comparisons test; $^{*}p \leq 0.05$.

REFERENCES

Arakawa, S., Tsujioka, M., Yoshida, T., Tajima-Sakurai, H., Nishida, Y., Matsuoka, Y., et al. (2017). Role of Atg5-dependent cell death in the embryonic development of Bax/Bak double-knockout mice. *Cell Death Differ.* 24, 1598–1608. doi: 10.1038/cdd.2017.84

Baek, J. H., Hatakeyama, J., Sakamoto, S., Ohtsuka, T., and Kageyama, R. (2006). Persistent and high levels of Hes1 expression regulate boundary formation in the developing central nervous system. *Development* 133, 2467–2476. doi: 10.1242/dev.02403

Buss, R. R., and Oppenheim, R. W. (2004). Role of programmed cell death in normal neuronal development and function. *Anat. Sci. Int.* 79, 191–197. doi: 10.1111/j.1447-073x.2004.00088.x

Chang, J., Wang, Y., Shao, L., Laberge, R. M., Demaria, M., Campisi, J., et al. (2016). Clearance of senescent cells by ABT263 rejuvenates aged hematopoietic stem cells in mice. *Nat. Med* 22, 78–83. doi: 10.1038/nm.4010

Chizhikov, V. V., and Millen, K. J. (2004). Mechanisms of roof plate formation in the vertebrate CNS. *Nat. Rev. Neurosci.* 5, 808–812. doi: 10.1038/nrn1520

Corallo, D., Trapani, V., and Bonaldo, P. (2015). The notochord: structure and functions. *Cell. Mol. Life Sci.* 72, 2989–3008. doi: 10.1007/s00018-015-1897-z

Cristofalo, V. J. (2005). SA beta Gal staining: biomarker or delusion. *Exp. Gerontol.* 40, 836–838. doi: 10.1016/j.exger.2005.08.005

Czarkwiani, A., and Yun, M. H. (2018). Out with the old, in with the new: senescence in development. *Curr. Opin. Cell Biol.* 55, 74–80. doi: 10.1016/j.ceb.2018.05.014

Da Silva-Alvarez, S., Guerra-Varela, J., Sobrido-Camean, D., Quelle, A., Barreiro-Iglesias, A., Sanchez, L., et al. (2020). Developmentally-programmed cellular senescence is conserved and widespread in zebrafish. *Aging* 12, 17895–17901. doi: 10.18632/aging.103968

Da Silva-Álvarez, S., Picallos-Rabina, P., Antelo-Iglesias, L., Triana-Martínez, F., Barreiro-Iglesias, A., Sánchez, L., et al. (2019). The development of cell senescence. *Exp. Gerontol.* 128:110742. doi: 10.1016/j.exger.2019.110742

Davaapil, H., Brockes, J. P., and Yun, M. H. (2017). Conserved and novel functions of programmed cellular senescence during vertebrate development. *Development* 144, 106–114. doi: 10.1242/dev.138222

Davis-Dusenbery, B. N., Williams, L. A., Klim, J. R., and Eggan, K. (2014). How to make spinal motor neurons. *Development* 141, 491–501. doi: 10.1242/dev.097410

Debacq-Chainiaux, F., Erusalimsky, J. D., Campisi, J., and Toussaint, O. (2009). Protocols to detect senescence-associated beta-galactosidase (SA-betagal) activity, a biomarker of senescent cells in culture and *in vivo*. *Nat. Protoc.* 4, 1798–1806. doi: 10.1038/nprot.2009.191

Gal, H., Lysenko, M., Stroganov, S., Vadai, E., Youssef, S. A., Tzadikevitch-Geffen, K., et al. (2019). Molecular pathways of senescence regulate placental structure and function. *EMBO J.* 38:e100849. doi: 10.15252/embj.2018100849

Hall, B. M., Balan, V., Gleiberman, A. S., Strom, E., Krasnov, P., Virtuoso, L. P., et al. (2017). p16(Ink4a) and senescence-associated beta-galactosidase can be induced in macrophages as part of a reversible response to physiological stimuli. *Aging* 9, 1867–1884. doi: 10.18632/aging.101268

Hernandez-Segura, A., Nehme, J., and Demaria, M. (2018). Hallmarks of cellular senescence. *Trends Cell Biol.* 28, 436–453. doi: 10.1016/j.tcb.2018.02.001

Himmels, P., Paredes, I., Adler, H., Karakatsani, A., Luck, R., Marti, H. H., et al. (2017). Motor neurons control blood vessel patterning in the developing spinal cord. *Nat. Commun.* 8:14583. doi: 10.1038/ncomms14583

Huang, T., and Rivera-Perez, J. A. (2014). Senescence-associated beta-galactosidase activity marks the visceral endoderm of mouse embryos but is not indicative of senescence. *Genesis* 52, 300–308. doi: 10.1002/dvg.22761

Kalaskar, V. K., and Lauderdale, J. D. (2014). Mouse embryonic development in a serum-free whole embryo culture system. *J. Vis. Exp.* 85:50803. doi: 10.3791/50803

Kang, C. (2019). Senolytics and senostatics: a two-pronged approach to target cellular senescence for delaying aging and age-related diseases. *Mol. Cells* 42, 821–827. doi: 10.14348/molcells.2019.0298

Karimian, A., Ahmadi, Y., and Yousefi, B. (2016). Multiple functions of p21 in cell cycle, apoptosis and transcriptional regulation after DNA damage. *DNA Repair* 42, 63–71. doi: 10.1016/j.dnarep.2016.04.008

Levitsky, K. L., Toledo-Aral, J. J., Lopez-Barneo, J., and Villadiego, J. (2013). Direct confocal acquisition of fluorescence from X-gal staining on thick tissue sections. *Sci. Rep.* 3:2937. doi: 10.1038/srep02937

Li, Y., Zhao, H., Huang, X., Tang, J., Zhang, S., Liu, X., et al. (2018). Embryonic senescent cells re-enter cell cycle and contribute to tissues after birth. *Cell Res.* 28, 775–778. doi: 10.1038/s41422-018-0050-6

Liu, J., Xia, H., Kim, M., Xu, L., Li, Y., Zhang, L., et al. (2011). Beclin1 controls the levels of p53 by regulating the deubiquitination activity of USP10 and USP13. *Cell* 147, 223–234. doi: 10.1016/j.cell.2011.08.037

Lorda-Diez, C. I., Garcia-Riart, B., Montero, J. A., Rodriguez-Leon, J., Garcia-Porrero, J. A., and Hurle, J. M. (2015). Apoptosis during embryonic tissue remodeling is accompanied by cell senescence. *Aging* 7, 974–985. doi: 10.18632/aging.100844

Marcelo, K. L., Goldie, L. C., and Hirschi, K. K. (2013). Regulation of endothelial cell differentiation and specification. *Circ. Res.* 112, 1272–1287. doi: 10.1161/CIRCRESAHA.113.300506

Munoz-Espin, D., Canamero, M., Maraver, A., Gomez-Lopez, G., Contreras, J., Murillo-Cuesta, S., et al. (2013). Programmed cell senescence during mammalian embryonic development. *Cell* 155, 1104–1118. doi: 10.1016/j.cell.2013.10.019

Oppenheim, R. W. (1989). The neurotrophic theory and naturally occurring motoneuron death. *Trends Neurosci.* 12, 252–255. doi: 10.1016/0166-2236(89)90021-0

Oppenheim, R. W., Flavell, R. A., Vinsant, S., Prevette, D., Kuan, C. Y., and Rakic, P. (2001). Programmed cell death of developing mammalian neurons after genetic deletion of caspases. *J. Neurosci.* 21, 4752–4760. doi: 10.1523/JNEUROSCI.21-13-04752.2001

Placzek, M., and Briscoe, J. (2005). The floor plate: multiple cells, multiple signals. *Nat. Rev. Neurosci.* 6, 230–240. doi: 10.1038/nrn1628

Sanchez-Carbente, M. R., Castro-Obregon, S., Covarrubias, L., and Narvaez, V. (2005). Motoneuronal death during spinal cord development is mediated by oxidative stress. *Cell Death Differ.* 12, 279–291. doi: 10.1038/sj.cdd.4401560

Sang, L., Coller, H. A., and Roberts, J. M. (2008). Control of the reversibility of cellular quiescence by the transcriptional repressor HES1. *Science* 321, 1095–1100. doi: 10.1126/science.1155998

Storer, M., Mas, A., Robert-Moreno, A., Pecoraro, M., Ortells, M. C., Di Giacomo, V., et al. (2013). Senescence is a developmental mechanism that contributes to embryonic growth and patterning. *Cell* 155, 1119–1130. doi: 10.1016/j.cell.2013.10.041

Sueda, R., Imayoshi, I., Harima, Y., and Kageyama, R. (2019). High Hes1 expression and resultant Ascl1 suppression regulate quiescent vs. active neural stem cells in the adult mouse brain. *Genes Dev.* 33, 511–523. doi: 10.1101/gad.323196.118

Takahashi, M., and Osumi, N. (2010). The method of rodent whole embryo culture using the rotator-type bottle culture system. *J. Vis. Exp.* 42:2170. doi: 10.3791/2170

Tracy, K., and Baehrecke, E. H. (2013). The role of autophagy in Drosophila metamorphosis. *Curr. Top. Dev. Biol.* 103, 101–125. doi: 10.1016/B978-0-12-385979-2.00004-6

Untergasser, G., Gander, R., Rumpold, H., Heinrich, E., Plas, E., and Berger, P. (2003). TGF-beta cytokines increase senescence-associated beta-galactosidase activity in human prostate basal cells by supporting differentiation processes, but not cellular senescence. *Exp. Gerontol.* 38, 1179–1188. doi: 10.1016/j.exger.2003.08.008

Yang, N. C., and Hu, M. L. (2005). The limitations and validities of senescence associated-beta-galactosidase activity as an aging marker for human foreskin fibroblast Hs68 cells. *Exp. Gerontol.* 40, 813–819. doi: 10.1016/j.exger.2005.07.011

Yosef, R., Pilpel, N., Tokarsky-Amiel, R., Biran, A., Ovadya, Y., Cohen, S., et al. (2016). Directed elimination of senescent cells by inhibition of BCL-W and BCL-XL. *Nat. Commun.* 7:11190. doi: 10.1038/ncomms11190

Zeng, L., Xiao, Q., Margariti, A., Zhang, Z., Zampetaki, A., Patel, S., et al. (2006). HDAC3 is crucial in shear- and VEGF-induced stem cell differentiation toward endothelial cells. *J. Cell. Biol.* 174, 1059–1069. doi: 10.1083/jcb.200605113

Conflict of Interest: The authors declare that the research was conducted in the absence of any commercial or financial relationships that could be construed as a potential conflict of interest.

frontiers in Cell and Developmental Biology

REVIEW
published: 28 January 2021
doi: 10.3389/fcell.2021.623175

Is Senescence-Associated β-Galactosidase a Reliable *in vivo* Marker of Cellular Senescence During Embryonic Development?

José Antonio de Mera-Rodríguez[1], Guadalupe Álvarez-Hernán[1], Yolanda Gañán[2], Gervasio Martín-Partido[1], Joaquín Rodríguez-León[2] and Javier Francisco-Morcillo[1]**

[1] Área de Biología Celular, Departamento de Anatomía, Biología Celular y Zoología, Facultad de Ciencias, Universidad de Extremadura, Badajoz, Spain, [2] Área de Anatomía y Embriología Humana, Departamento de Anatomía, Biología Celular y Zoología, Facultad de Medicina, Universidad de Extremadura, Badajoz, Spain

OPEN ACCESS

Edited by:
Wolfgang Knabe, Universität Münster, Germany

Reviewed by:
Luis Covarrubias, National Autonomous University of Mexico, Mexico
Valery Krizhanovsky, Weizmann Institute of Science, Israel
Vassilis G. Gorgoulis, National and Kapodistrian University of Athens, Greece

***Correspondence:**
Joaquín Rodríguez-León
jrleon@unex.es
Javier Francisco-Morcillo
morcillo@unex.es

Specialty section:
This article was submitted to Cell Death and Survival, a section of the journal Frontiers in Cell and Developmental Biology

Received: *29 October 2020*
Accepted: *05 January 2021*
Published: *28 January 2021*

Citation:
de Mera-Rodríguez JA, Álvarez-Hernán G, Gañán Y, Martín-Partido G, Rodríguez-León J and Francisco-Morcillo J (2021) Is Senescence-Associated β-Galactosidase a Reliable in vivo Marker of Cellular Senescence During Embryonic Development? Front. Cell Dev. Biol. 9:623175. doi: 10.3389/fcell.2021.623175

During vertebrate embryonic development, cellular senescence occurs at multiple locations. To date, it has been accepted that when there has been induction of senescence in an embryonic tissue, β-galactosidase activity is detectable at a pH as high as 6.0, and this has been extensively used as a marker of cellular senescence *in vivo* in both whole-mount and cryosections. Such senescence-associated β-galactosidase (SA-β-GAL) labeling appears enhanced in degenerating regions of the vertebrate embryo that are also affected by programmed cell death. In this sense, there is a strong SA-β-GAL signal which overlaps with the pattern of cell death in the interdigital tissue of the developing limbs, and indeed, many of the labeled cells detected go on to subsequently undergo apoptosis. However, it has been reported that β-GAL activity at pH 6.0 is also enhanced in healthy neurons, and some retinal neurons are strongly labeled with this histochemical technique when they begin to differentiate during early embryonic development. These labeled early post-mitotic neurons also express other senescence markers such as p21. Therefore, the reliability of this histochemical technique in studying senescence in cells such as neurons that undergo prolonged and irreversible cell-cycle arrest is questionable because it is also expressed in healthy post-mitotic cells. The identification of new biomarkers of cellular senescence would, in combination with established markers, increase the specificity and efficiency of detecting cellular senescence in embryonic and healthy mature tissues.

Keywords: cell death, cell senescence, retina, development, histochemistry, limb

CELLULAR SENESCENCE

The study of cellular senescence was initiated by Hayflick and Moorhead (1961). Those authors reported that human fibroblasts isolated from embryonic tissues cease to proliferate after a limited number of cell divisions. We now know that the loss of proliferative activity is the consequence of progressive shortening of telomeres in each replicative round (for a review, see

Bernadotte et al., 2016). Currently, we have learnt a lot about the stimuli that trigger cellular senescence and about the intracellular effector pathways that execute this process. Cellular senescence is characterized by a prolonged and irreversible cell-cycle arrest with secretory features, macromolecular damage, and altered metabolism (Campisi et al., 2011; Rodier and Campisi, 2011; Childs et al., 2015; Hernandez-Segura et al., 2018; Gorgoulis et al., 2019). The cells that exhibit these features of senescence normally accumulate in aging tissues, further linking this cellular state with the aging process in general (Dimri et al., 1995). Cellular senescence is now also considered to be a suppressive mechanism against oncogenesis (Lee and Lee, 2019), acting to block proliferation in cells with oncogenic mutations (Campisi et al., 2011). Recent studies also describe beneficial effects of cellular senescence during embryonic development, tissue repair and regeneration, and cellular reprogramming (Czarkwiani and Yun, 2018; Rhinn et al., 2019). Senescence during embryonic development is involved in tissue remodeling and is usually linked to areas of cell death that arise in degenerating structures (Muñoz-Espín and Serrano, 2014). Therefore, senescent cells can be detected from embryogenesis (when they contribute to tissue development) to adulthood (when they prevent the propagation of damaged cells and contribute to tissue repair and tumor suppression).

Senescent cells are metabolically active and possess some features *in vitro* and *in vivo* which are known biomarkers of cellular senescence (Bernadotte et al., 2016; Matjusaitis et al., 2016; Hernandez-Segura et al., 2018; Wang and Dreesen, 2018). One of the most used methods to assess cellular senescence is the detection of β-galactosidase (β-GAL) activity at pH 6.0, a histochemical assay that is called "senescence associated β-GAL" (SA-β-GAL), because it labels senescent cells, both *in vivo* and *in vitro* (Dimri et al., 1995). However, intense β-GAL labelling at pH 6.0 could also reflect an alteration in lysosomal number or activity in non-proliferating cells (Yegorov et al., 1998) or in terminally differentiated cells such as neurons (Piechota et al., 2016, inter alia). It has been demonstrated that the so-called SA-β-GAL increases with aging in subsets of neurons in different brain areas, but this enzymatic activity is also present in specific populations of neurons in very young mice (for a review, see Walton and Andersen, 2019). In this sense, it is known that neurons become post-mitotic very early in development, and a recent study performed in our laboratory clearly demonstrated that β-GAL activity at pH 6.0 is intense in recently differentiated ganglion cells in the developing avian retina (de Mera-Rodríguez et al., 2019).

In the present communication, we discuss the reliability of SA-β-GAL activity in identifying cellular senescence *in vitro* and *in vivo*. We first focus on the description of the cell-type-specific labeling of SA-β-GAL in embryonic structures of different vertebrates. Then, we consider the possible relationship between areas of intense SA-β-GAL-staining and areas affected by massive cell death in different embryonic structures. Finally, we compare the staining pattern of SA-β-GAL activity with the distribution of other markers of cell senescence, cell death, and cell differentiation in the developing visual system of vertebrates.

SA-β-GAL HISTOCHEMISTRY

Lysosomal β-GAL cleaves β-D-galactose residues in β-D-galactosides. Detectable β-GAL activity is the most extensively used marker for senescent or aging cells whether in culture or in mammalian tissues (Dimri et al., 1995; Debacq-Chainiaux et al., 2009). Specifically, at pH 6.0, the β-GAL enzyme hydrolyses 5-bromo-4-chloro-3-indoyl-β-d-galactopyranoside (X-gal), a colorless, soluble compound consisting of galactose linked to an indole. This reaction releases a deep blue, insoluble product on the cell culture or in the tissue. This histochemical technique is distinct from the acidic β-GAL activity, present in lysosomes of all non-senescent cells and detectable at pH 4.0 (Kuilman et al., 2010). However, it has been demonstrated (Lee et al., 2006) that lysosomal β-GAL is the origin of SA-β-GAL activity, with the increased SA-β-GAL activity detected in senescent cells clearly being a result of the increased expression of *GLB1*, the gene encoding the lysosomal enzyme. Furthermore, increased lysosomal biogenesis has been described in senescent cells (Kurz et al., 2000; Severino et al., 2000; Hernandez-Segura et al., 2018).

Nonetheless, some researchers have clearly shown that in some cases β-GAL activity is not indicative of senescence. For instance, it has been described that β-GAL activity at pH 6.0 might reflect the activity of autophagy due to the intense biogenesis of lysosomes that occurs during this process (Young et al., 2009). Intense β-GAL histochemical signals have also been reported in the visceral endoderm at early stages of mouse embryo development (Huang and Rivera-Pérez, 2014) and in the luminal cells of the duodenum (Going et al., 2002). Furthermore, endogenous β-GAL activity at pH 6.0 is detected cytochemically in immortalized cultured cells and macrophage-like cells (Yegorov et al., 1998), in macrophages and osteoclasts in mature tissues (Bursuker et al., 1982; Kopp et al., 2007; Hall et al., 2017), and in confluent non-transformed fibroblast cultures (Severino et al., 2000). A recent study has shown that Purkinje, choroid plexus, heart muscle, intestinal, and pancreatic cells in mammalian tissues are strongly positive for SA-β-GAL activity (Raffaele et al., 2020). Also, serum starvation and confluent culture increase SA-β-GAL activity (Yang and Hu, 2005). In the case of the nervous system, it has been proposed that β-GAL activity at pH 6.0 might be detected in differentiated neurons (Piechota et al., 2016, see below), and even at early stages of development (de Mera-Rodríguez et al., 2019, see below). All these findings indicate that the reliability of the "so-called" SA-β-GAL assays is questionable because, since the enzyme is not always specific for cell-aging, this histochemical technique is insufficient to characterize cellular senescence.

Senescent cells also show additional signature features that could be used in combination with SA-β-GAL to identify the state of senescence. Morphologically, cultured senescent cells become flat, large, multi-nucleated, and vacuolated (Denoyelle et al., 2006). Recently, it has been shown that senescent cells in tissues of aged mice are larger than non-senescent cells (Biran et al., 2017) and that senescent alveolar progenitors show abnormal elongated morphology (Kobayashi et al., 2020). In contrast, in embryonic living tissues, senescent cells usually have a normal morphology (Muñoz-Espín and Serrano, 2014).

Senescence-associated heterochromatic foci (SAHF) contain trimethylation at Lys9 of histone 3 (H3K9me3), heterochromatin protein 1 homologue-γ (HP1 γ), and macroH2A (Sharpless and Sherr, 2015; Bernadotte et al., 2016; Wang and Dreesen, 2018; Rhinn et al., 2019). Senescent cells undergo long-term exit from the cell cycle, lacking markers of cell proliferation such as Ki67 or PCNA (Rhinn et al., 2019). They also activate tumor suppressor networks, including $p16^{INK4A}$ and $p19^{ARF}$ which function by activating the Rb protein and the p53 transcription factor, respectively (Lowe and Sherr, 2003).

These are among the most commonly used markers of cell senescence in cultured cells and in aged or pathological tissues. However, the analysis of senescence signatures in some populations of cells in the developing embryo shows enhanced expression of the cell cycle inhibitor p21, but not that of typical markers of senescence in aging including p53, p16, or p19 (Muñoz-Espín et al., 2013; Storer et al., 2013).

SA-β-GAL STAINING IN THE DEVELOPING EMBRYO

SA-β-GAL Staining in Whole Mount Embryos

Programmed cellular senescence is an essential process during vertebrate embryonic development (for reviews, see Muñoz-Espín and Serrano, 2014; Czarkwiani and Yun, 2018; Rhinn et al., 2019; Da Silva-Álvarez et al., 2019; Sacco et al., 2021). SA-β-GAL labeled cells are found stereotypically in well-defined time windows during embryonic development (Muñoz-Espín et al., 2013; Storer et al., 2013). SA-β-GAL staining in whole-mount mammalian embryos clearly shows that abundant labeled cells accumulates in the developing limbs, nails, focal areas of the skin, the tip of the tail, heart, eye tissues, inner ear, olfactory epithelium, and the closing neural tube (Muñoz-Espín et al., 2013; Storer et al., 2013; Zhao et al., 2018), with a staining pattern similar to that observed in whole-mount chicken embryos (**Figures 1A–C**) (cf. Storer et al., 2013; Lorda-Díez et al., 2015, 2019; Gibaja et al., 2019). More recently (Da Silva-Álvarez et al., 2020), putative senescent cells during zebrafish development have been characterized in detail by using SA-β-GAL staining in whole mounts, with the strong activity being detected in the yolk, cloaca, central nervous system (CNS), intestine, liver, pronephric ducts, and lens.

SA-β-GAL Staining in Degenerating Embryo Areas: The Case of the Developing Limb

The distribution of SA-β-GAL positive areas in the whole embryo strongly correlates with the distribution of apoptotic cells. Thus, intense SA-β-GAL staining is detected in degenerating structures such as the pronephros of fish (Villiard et al., 2017) and amphibians (Davaapil et al., 2017; Villiard et al., 2017), and in the mesonephros of birds (Nacher et al., 2006) and mammals (Muñoz-Espín et al., 2013; Da Silva-Álvarez et al., 2018). The pattern of cell death in the developing avian heart also strongly correlates with SA-β-GAL staining (Lorda-Díez et al., 2019), as do areas of cell death in the somites, tail bud, and CNS (Muñoz-Espín et al., 2013; Storer et al., 2013). In the case of the developing otic vesicle in the chicken, SA-β-GAL labeled cells are associated with areas of increased apoptosis (**Figures 1A–C**) (Gibaja et al., 2019; Magariños et al., 2020). In mice, it has been found that senescence in the endolymphatic sac has a morphogenetic role analogous to that of apoptosis (Muñoz-Espín et al., 2013).

The chronotopographical coincidence of cell senescence and apoptosis in the embryo is even more evident in the developing limb. Since the scope of this article is discussion of the reliability of β-galactosidase staining as an *in vivo* marker for senescence detection, we would encourage the reader to refer to the detailed review of limb apoptosis and senescence in another article included in this issue authored by Montero et al. (2020). At early stages of limb development, limb outgrowth is controlled by an epithelial thickening at the distal tip of the structure – the apical ectodermal ridge (AER) (**Figures 1D,H,L**). The cells of this signaling center proliferate together with the other tissues in the limb bud but undergo apoptosis from soon after the bud's formation until its disappearance when all the phalanxes have been formed (Rodríguez-León et al., 2013). Concomitant with the apoptotic process (**Figures 1H,L**), AER cells also exhibit SA-β-GAL activity (**Figure 1D**) and express different markers of cellular senescence such as p21 (Storer et al., 2013; Muñoz-Espín et al., 2013; Lorda-Díez et al., 2015; Li et al., 2018). In mice, a lack of p21 activity results in senescence defects and AER structural deficiencies, thereby impairing normal limb development (Storer et al., 2013). Indeed, during limb development in the mouse, strong SA-β-GAL activity is detected in the AER at early stages but almost disappears at more advanced stages (Li et al., 2018). These last authors suggest that some senescent cells in this region of the developing mouse limb undergo apoptosis and are removed by phagocytosis. However, a sub-population of these embryonic cells positive for ß-GAL activity and p21 expression remains in the limb tissues after birth, and re-enter the cell cycle, proliferating *in situ* (Li et al., 2018). These results could suggest that some cells in the population are non-senescent cells or a degree of plasticity in the process of cellular senescence during development. Future works are needed to clarify if cellular senescence during development is a process that have some unique features that distinguish it from the adult cellular senescence.

But this is not the only structure that undergoes apoptosis during limb development. The anterior and posterior margins of the limb bud, as well as the interdigital areas, enter the apoptosis program to sculpt the final shape of the organ (reviewed by Montero et al., 2020). Moreover, the interdigital regression during digit formation has been regarded as an excellent model for the study of how cellular senescence and programmed cell death are related (Lorda-Díez et al., 2015; Sanchez-Fernandez et al., 2019). Apoptotic interdigital areas can be observed for approximately 48 h in the developing chicken limb – from 6.5 to 8.5 days of incubation (Montero and Hurlé, 2010; Lorda-Díez et al., 2015). The classical way to detect the interdigital apoptotic pattern is to use vital dyes such as Neutral Red (**Figures 1H–K**). Staining with this dye allows visualization of tissue removal

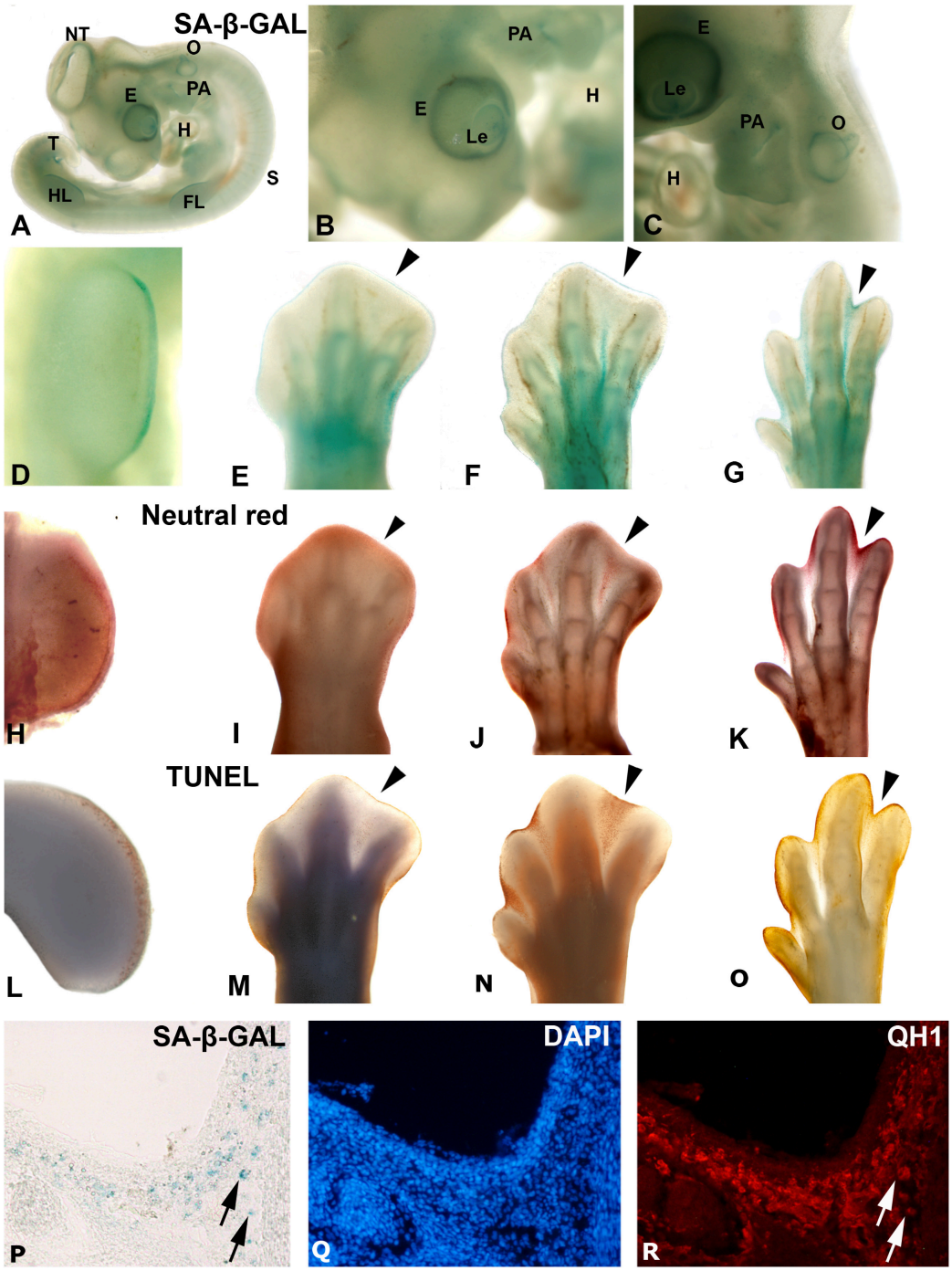

FIGURE 1 | Areas segmenting SA-β-GAL activity and apoptosis during avian embryonic development. Detection of SA-β-GAL activity in embryonic day 3.5 **(A,B)** and E4 **(C)** chicken embryos, and E3.5 **(D)**, E6 **(E)**, E7 **(F)**, and E8 **(G)** hindlimbs. Neutral red staining for cell death detection in E3.5 **(H)**, E6 **(I)**, E7 **(J)**, and E8 **(K)** hindlimbs. TUNEL assay for apoptosis detection in E4 **(L)**, E6 **(M)**, E7 **(N)**, and E8 **(O)** hindlimbs. Labeling of AER can be noted in **(D**,**H**, and **L)**. Arrowheads in **(E–G)**, **(I–K)**, and **(M–O)** point to the third interdigital space during the establishment of cell senescence and the progression of interdigital programmed cell death. SA-β-GAL histochemistry **(P)** and QH1 immunostaining **(R)** label macrophages in the interdigital mesenchyme of quail at stage 36. DAPI staining **(Q)** shows the structure of the interdigital space. E, eye; Fl, forelimb; H, heart, HL, hindlimb, Le, lens; NT, neural tube, O, otic vesicle; PA, pharyngeal arches; T, tail bud.

in the AER (**Figure 1H**) and the progression of interdigital cell death (**Figures 1K,L**). But it cannot distinguish apoptosis (the active and programmed process of death in the cells of a developing tissue) from necrosis (the passive death of cells due, for instance, to toxicity or cellular damage). For this reason, since the decade of the 1990s, the TUNEL assay has been used to

ensure the detection of apoptotic areas during limb development (**Figures 1L–O**). The population of apoptotic cells detected by the two techniques in the interdigital areas coincides with the pattern of SA-β-GAL labeling in these regions (**Figures 1E–G**), evidence for the correlation of the two processes during limb development. Indeed, different studies have shown that cellular senescence and apoptosis coincide during limb development and are essential for proper interdigital regression (Muñoz-Espín et al., 2013; Lorda-Díez et al., 2015; Montero et al., 2016).

Besides the activation of SA-β-GAL activity, another essential feature of cell senescence is cell cycle arrest. In the case of limb interdigital regression, this is connected to up-regulation of genes such as p21, p63, and p73 which block cell cycle progression (Lorda-Díez et al., 2015; Sanchez-Fernandez et al., 2020). Also, various members of the Btg/Tob tumor suppressor gene family are expressed in the interdigital space during the progression of programmed cell death, and overexpression of Btg2 in the early limb mesenchyme results in an anti-proliferative and pro-apoptotic effect on the tissue, leading to the formation of shortened limbs (Lorda-Díez et al., 2015). Interestingly, the expression of these tumor suppressor genes in chicken and mouse embryos, species with free digits, is up-regulated during the course of programmed cell death in the interdigital spaces, but is down-regulated, or maintained at stable levels, in the interdigital areas of the duck which maintains webbed digits in adulthood (Lorda-Díez et al., 2015).

Another important feature of cell senescence is the up-regulation of different components of the senescence-associated secretory phenotype (SASP), namely, different matrix metalloproteinases, IgfBP5, TNF signaling pathway members, and interleukin 8 (Rhinn et al., 2019). Several of these SASP members are up-regulated in the interdigital areas (Lorda-Díez et al., 2015) and in the AER (Storer et al., 2013) when cells are dying by apoptosis.

All this evidence, namely detection of SA-ß-GAL activity and upregulation of cell cycle inhibitors as well as SASP components, supports that SA-β-GAL staining is detected in senescent cells during development in apoptotic areas like those detected in the tetrapod limb. Nevertheless, other populations of non-senescent cells with a high lysosomal mass and/or increased β-GAL lysosomal activity, such as QH1-immunoreactive macrophages in the quail interdigital area, also show strong SA-β-GAL labeling (**Figures 1P–R**), coinciding with previous studies in mice (Hall et al., 2017).

SA-β-GAL Staining in the Nervous System: The Case of the Developing and Mature Retina

The analysis of the SA-β-GAL labeling in the developing and mature CNS is a topic of controversy in the field of neuronal senescence. SA-β-GAL activity has been used to detect putative senescent cells in the aging brain of mice (Ori et al., 2015), in cultures of primary cortical neurons (Chernova et al., 2006), and in cerebellar granule neurons (Bhanu et al., 2010). SA-β-GAL is detected cytochemically in neurons of the hippocampus, and its activity increases in old animals (Geng et al., 2010; Piechota et al., 2016) and in prolonged-cultured hippocampal neurons (Dong et al., 2011; Xu et al., 2019). Furthermore, this enzymatic activity is greater in hippocampal neurons after an injury (Tominaga et al., 2019) and in the Purkinje cells of adult mice (Jurk et al., 2012). Neurodegenerative diseases also cause increased SA-β-GAL staining in astrocytes, oligodendrocytes, and microglial cells (Kritsilis et al., 2018). In sum therefore, SA-β-GAL activity increases in mammalian neurons and glial cells during the aging process and under pathological conditions.

Intense SA-β-GAL activity has also been detected in several types of neurons in very young mice (1–3 months old) *in vivo* and *in vitro* (Jurk et al., 2012; Piechota et al., 2016; Bussian et al., 2018; Musi et al., 2018; Raffaele et al., 2020). In this sense, intense SA-β-GAL staining is detected in several populations of neurons in horizontal cryosections of the head of a 3-day-old mouse. Strong SA-β-GAL signal is detected in the intermediate layer of the olfactory epithelium, the region where the olfactory sensory neurons are located (**Figures 2A,B**), but also in neurons of the trigeminal ganglion (**Figure 2C**) and in the cerebellar Purkinje cells (**Figures 2D,E**). Therefore, the detection of this enzymatic activity in the CNS at relatively early stages of the postnatal life suggests that it cannot be attributed solely to cell senescence either *in vivo* or *in vitro*. Given this scenario, it is quite possible that β-GAL activity at pH 6.0 could be detected in neurons even in embryonic tissues.

The vertebrate retina contains six well-known types of neurons – ganglion, amacrine, horizontal, bipolar, cone, and rod cells. Much is known about the intrinsic programs (mainly coded by transcription factors, but also by extrinsic factors such as growth factors) which are involved in retinogenesis and in the maintenance of neuronal phenotypes (Álvarez-Hernán et al., 2013, 2018, 2019, 2020; Xiang, 2013; Bejarano-Escobar et al., 2014, 2015). Furthermore, several phases of cell death have been reported to occur during development of the vertebrate retina (Cook et al., 1998; Knabe et al., 2000; Péquignot et al., 2003; Francisco-Morcillo et al., 2004, 2014; Rodríguez-Gallardo et al., 2005; Chavarría et al., 2007, 2013; Valenciano et al., 2009; Bejarano-Escobar et al., 2011, 2013). Therefore, the embryonic retina constitutes an excellent model with which to study whether SA-β-GAL activity is linked with neuronal differentiation processes and/or with cell death areas.

Previous studies have shown that SA-β-GAL histochemistry assay shows staining of the retinal pigment epithelium in the developing avian retina (de Mera-Rodríguez et al., 2019) and in the mature retina of rats (Lamoke et al., 2015) and primates (Mishima et al., 1999), including humans (Hjelmeland et al., 1999; Matsunaga et al., 1999). In this sense, some retinal pathologies are linked to cellular senescence that occurs in the retinal pigment epithelium (Kozlowski, 2012). Specific SA-β-GAL enzymatic activity is observed in human retinal blood vessels, mainly in the endothelial and smooth muscle cells (López-Luppo et al., 2017), and intense SA-β-GAL activity is observed in the microvasculature of diabetic rats (Lamoke et al., 2015). With regard to SA-β-GAL activity in neural retinal tissue, in the mouse at early postnatal stages, SA-β-GAL staining is enhanced in retinal ganglion cells and subpopulations of neurons dispersed throughout the inner nuclear layer (INL) (Oubaha et al., 2016).

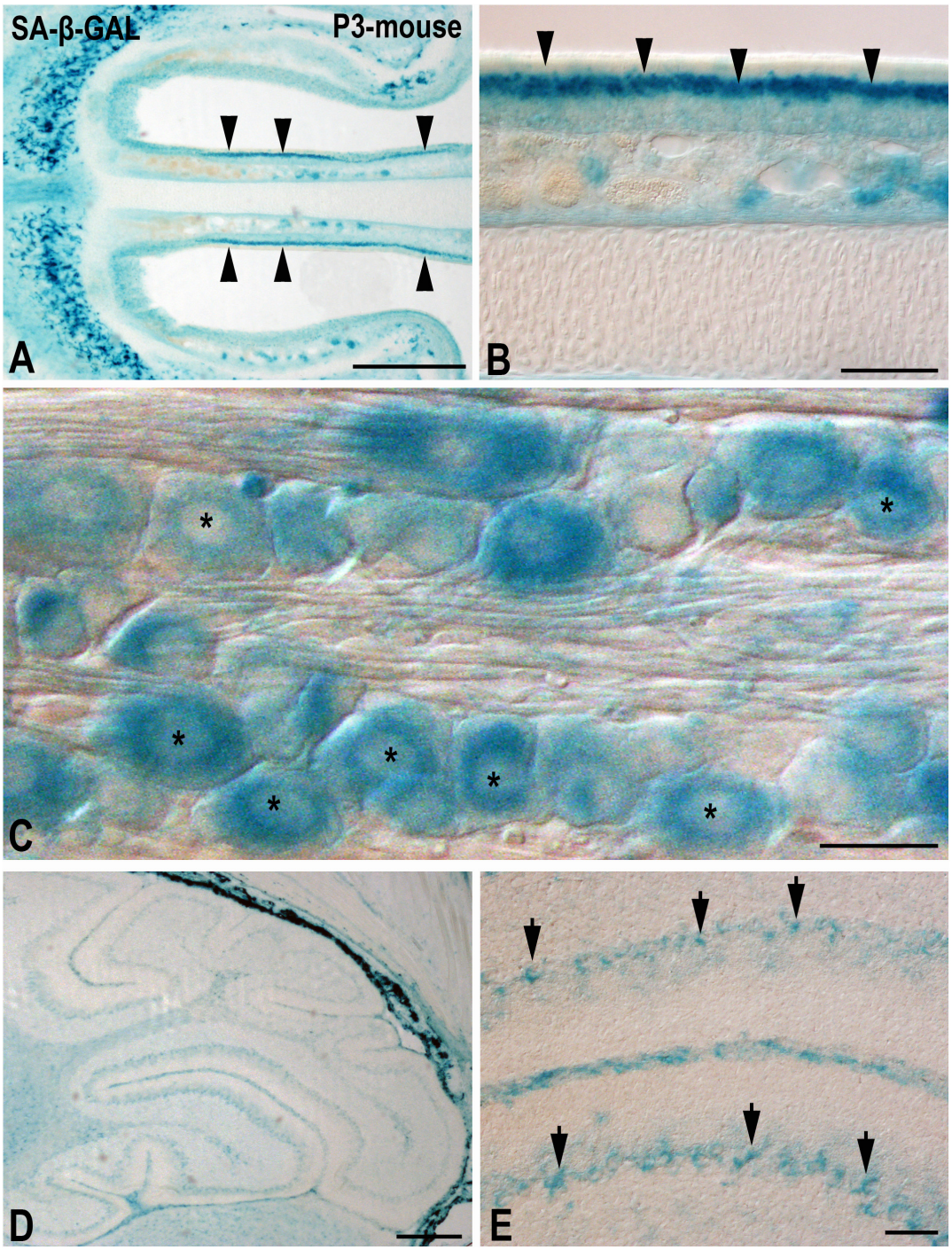

FIGURE 2 | The presence of SA-β-GAL activity in the postnatal day P3 mouse head tissue. Horizontal **(A,B)** and sagittal **(C–E)** cryosections were treated with SA-β-GAL histochemistry. **(A,B)** Intense SA-β-GAL signal is found in the intermediate layer of the olfactory epithelium (arrowheads). **(C)** Strong SA-β-GAL staining is detected in sensory neurons in the trigeminal ganglion (asterisks). **(D,E)** SA-β-GAL activity is detected in the cerebellum, mainly in the Purkinje cell layer (arrows). Scale bars: 200 μm **(A,D)**, 50 μm **(B,E)**, and 20 μm **(C)**.

It has also been reported that, in the adult mouse, SA-β-GAL activity in retinal ganglion cells might be increased by acute intraocular pressure induced ischæmic injury (Li et al., 2017). Other diseases, such as retinopathy of prematurity and proliferative diabetic retinopathy, also lead to cell senescence of several types of retinal neurons (Sapieha and Mallette, 2018).

A recent study performed in our laboratory (de Mera-Rodríguez et al., 2019) has shown that, in the laminated

avian retina, even at embryonic stages, SA-β-GAL labeling is intense in subpopulations of neurons located in the ganglion cell layer (GCL) and in subpopulations of interneurons mainly located in the amacrine cell layer and the horizontal cell layer (**Figures 3A,B**). Therefore, SA-β-GAL activity is intense in recently differentiated and mature retinal neurons. We also found that SA-β-GAL labeling strongly correlates with p21 immunoreactivity in both the laminated (**Figures 3B–D**) and the undifferentiated (**Figures 4A–E**) retina, even in the lens tissue (**Figures 4A,B**) (de Mera-Rodríguez et al., 2019). SA-β-GAL

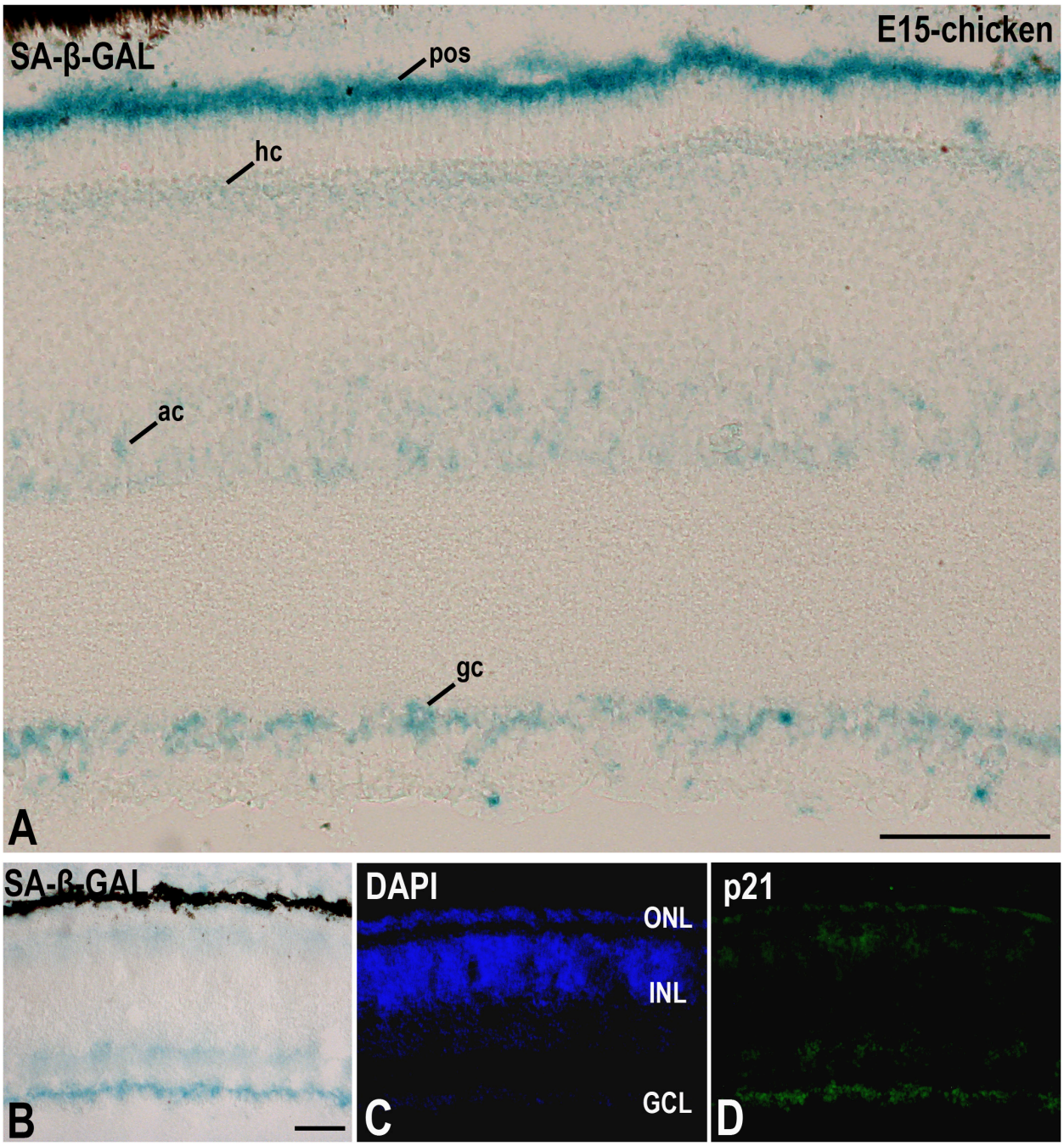

FIGURE 3 | The presence of SA-β-GAL activity in the embryonic day E15 chicken retina. Cryosections of retinas were treated with SA-β-GAL histochemistry **(A,B)** and antibodies against p21 **(B–D)**. DAPI staining shows the laminated structure of the retina **(C)**. SA-β-GAL staining is found in the photoreceptor outer segments and in subpopulations of amacrine and ganglion cells **(A,B)**. The horizontal cell layer appears faintly labeled **(A,B)**. p21 immunostaining strongly correlates with the SA-β-GAL labeling pattern. ac, amacrine cells; gc, ganglion cells; GCL, ganglion cell layer; hc, horizontal cells; INL, inner nuclear layer; ONL, outer nuclear layer; pos, photoreceptor outer segments. Scale bars: 50 μm (**A** and **B–D**).

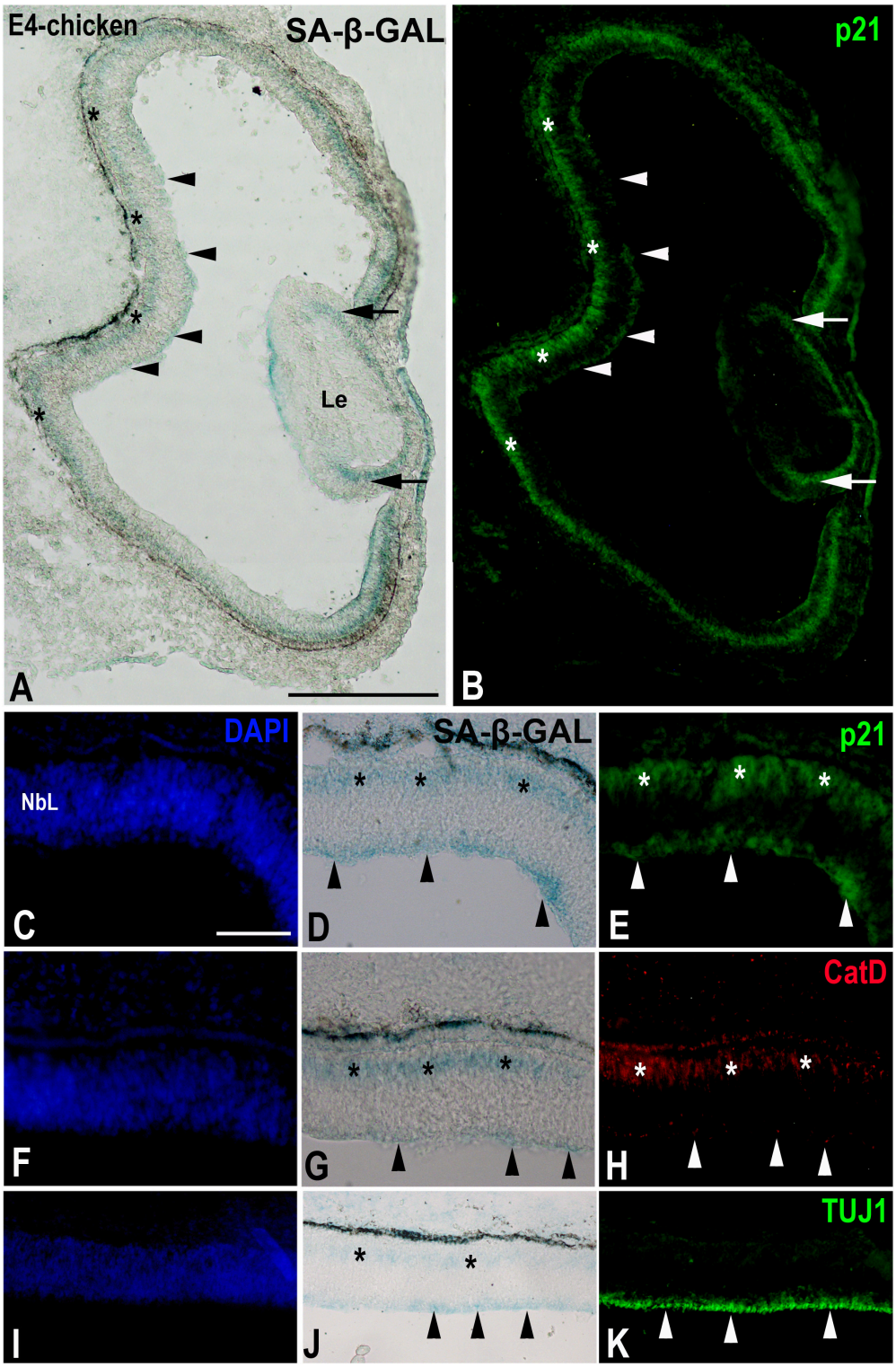

FIGURE 4 | The presence of SA-β-GAL activity in the embryonic day E4 chicken retina. Cryosections of retinas were treated with SA-β-GAL histochemistry and antibodies against p21 **(A–E)**, CatD **(F–H)**, and TUJ1 **(I–K)**. DAPI staining shows that the neural retina consists of a NbL **(C,F,I)**. SA-β-GAL staining is detected in the scleral (asterisks in **A**,**D**,**G**,**J**) and vitreal (arrowheads in **A**,**D**,**G**,**J**) regions of the retina. p21 immunostaining correlates with the SA-β-GAL staining pattern in the undifferentiated retina (arrowheads and asterisks in **B**,**E**) and lens (arrows in **B**). CatD immunoreactivity (arrowheads and asterisks in **H**) is strongly coincident with the SA-β-GAL histochemistry signal (arrowheads and asterisks in **G**). TUJ1 immunoreactivity is intense in the vitreal surface of the NbL (arrowheads in **K**), coinciding with the vitreal SA-β-GAL histochemistry signal detected in the same region (arrowheads in **J**). Le, lens; NbL, neuroblastic layer. Scale bars: 150 μm **(A,B)**, 50 μm **(C–K)**.

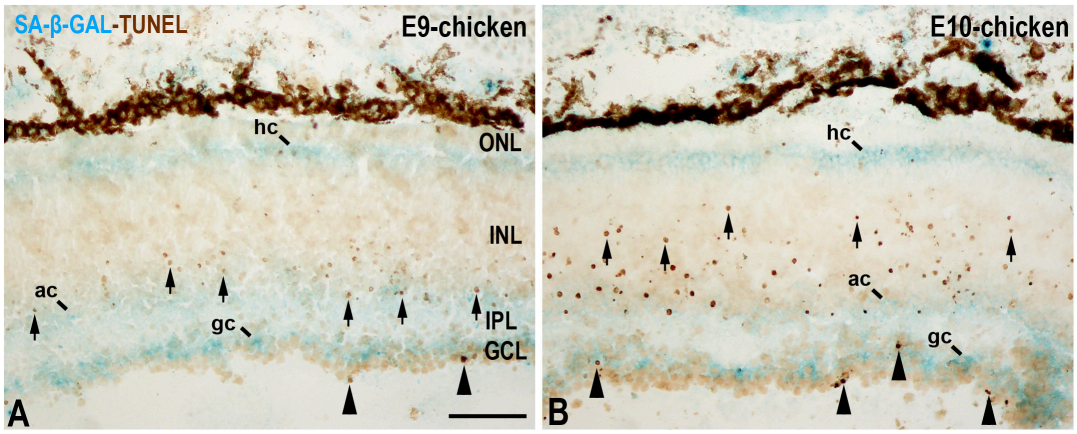

FIGURE 5 | SA-β-GAL activity and cell death in the embryonic day E9 **(A)** and E10 **(B)** chicken retina. Cryosections were doubly stained with SA-β-GAL histochemistry and TUNEL technique. TUNEL-positive nuclei are mainly detected in the GCL (arrowheads) and in the middle region of the INL (arrows). SA-β-GAL activity is observed in the GCL, amacrine cell layer, and horizontal cell layer. ac, amacrine cells; gc, ganglion cells; GCL, ganglion cell layer; hc, horizontal cells; INL, inner nuclear layer; IPL, inner plexiform layer; ONL, outer nuclear layer; pos, photoreceptor outer segments. Scale bar: 50 μm.

staining in the non-laminated retina is mainly restricted to the vitreal and scleral surfaces of the neuroblastic layer (NbL) (**Figures 4A,D,G,J**), strongly correlating with cathepsin D immunoreactivity (**Figures 4F–H**) (de Mera-Rodríguez et al., 2019), a marker for increased lysosome number or activity (Kurz et al., 2000; Wassélius et al., 2003; Ahuja et al., 2008; Bejarano-Escobar et al., 2011; Lorda-Díez et al., 2019). The SA-β-GAL activity located in the vitreal surface of the retina is detected in TUJ1-positive newborn ganglion cell neuroblasts (**Figures 4I–K**). Therefore, SA-β-GAL labeling in the developing visual system correlates strongly with the location of the lysosomal mass, but also with other senescence markers, and seems to be linked to neuronal differentiation.

But is SA-β-GAL activity also linked to apoptotic cells in the developing retina? In the undifferentiated vertebrate retina, apoptotic cells are either dispersed throughout the NbL or concentrated in areas that surround the optic nerve head (Mayordomo et al., 2003; Francisco-Morcillo et al., 2004; Rodríguez-Gallardo et al., 2005; Valenciano et al., 2009; Bejarano-Escobar et al., 2011, 2013). However, SA-β-GAL activity is mainly concentrated in the vitreal and scleral surfaces of the avian NbL (de Mera-Rodríguez et al., 2019). Later, in the laminated retina, apoptosis follows spatiotemporal patterns that are analogs of the cell differentiation pattern (**Figure 5**) (Cook et al., 1998; Marín-Teva et al., 1999). In the E9 chicken retina, cell death is mainly concentrated in the GCL and in the amacrine cell layer (**Figure 5A**) (Cook et al., 1998), and, at E10, TUNEL-positive bodies spread vitreally to the bipolar cell layer (**Figure 5B**). By these stages, SA-β-GAL staining is detected homogeneously in the GCL, amacrine cell layer, and horizontal cell layer (**Figure 5**) (de Mera-Rodríguez et al., 2019). There is therefore no correlation between SA-β-GAL activity and the chronotopographical distribution of dying cells in the developing avian retina. In this case, β-GAL activity at pH 6.0 seems to be related to terminal cell differentiation rather than to cellular senescence.

CONCLUSION

SA-β-GAL activity increases with aging in neurons of the mammalian brain (for a review, see Walton and Andersen, 2019). In the developing limb, this SA-β-GAL activity correlates well with cellular senescence in the areas of programmed cell death that occur physiologically during the development process. Consequently, a proper balance between senescence and apoptosis is needed for accurate formation of the limbs (Lorda-Díez et al., 2015). However, intense SA-β-GAL is also detected in cells that have intrinsically high lysosomal β-GAL activity, such as macrophages, but also in a wide range of post-mitotic cells, including neurons, even at early stages of embryonic development. Other senescence-associated markers, such as p21, are also activated in parallel with SA-β-GAL activity in recently differentiated retinal neurons (de Mera-Rodríguez et al., 2019). It is likely that there are several common mechanisms involved in both the acquisition of the senescent phenotype and the maintenance of long-term non-dividing cells' non-proliferating status. Therefore, it is important to discriminate between senescent cells and post-mitotic cells in studies about aging of the CNS because some accepted markers of senescence (SA-β-GAL, p21 expression) are less specific than originally was expected. The identification of new candidate biomarkers of cellular senescence would, in combination with established markers, increase the specificity and efficiency of detecting senescence *in vivo* and *in vitro*. A future requirement will be to have markers for senescence-like phenotypes in long-term non-proliferating cells, such as neurons.

AUTHOR CONTRIBUTIONS

GÁ-H, JM-R, YG, GM-P, JR-L, and JF-M wrote and critically reviewed the manuscript. All authors approved the final manuscript.

FUNDING

GÁ-H was a recipient of a Fellowship from the *Universidad de Extremadura*. This work was supported by grants from the Spanish *Ministerio de Ciencia y Tecnología* (BFU2007-67540), *Ministerio de Economía y Competitividad* (CGL2015-64650P), *Dirección General de Investigación del Ministerio de Educación y Ciencia* (BFU2017-85547-P), and *Junta de Extremadura, Fondo Europeo de Desarrollo Regional, "Una manera de hacer Europa"* (GR15158, GR18114, and IB18113).

REFERENCES

Ahuja, S., Ahuja-Jensen, P., Johnson, L. E., Caffé, A. R., Abrahamson, M., Ekström, P. A. R., et al. (2008). Rd1 mouse retina shows an imbalance in the activity of cysteine protease cathepsins and their endogenous inhibitor cystatin. *Investig. Ophthalmol. Vis. Sci.* 49, 1089–1096. doi: 10.1167/iovs.07-0549

Álvarez-Hernán, G., Andrade, J. P., Escarabajal-Blázquez, L., Blasco, M., Solana-Fajardo, J., Martín-Partido, G., et al. (2019). Retinal differentiation in syngnathids: comparison in the developmental rate and acquisition of retinal structures in altricial and precocial fish species. *Zoomorphology* 138, 371–385. doi: 10.1007/s00435-019-00447-3

Álvarez-Hernán, G., Bejarano-Escobar, R., Morona, R., González, A., Martín-Partido, G., and Francisco-Morcillo, J. (2013). Islet-1 immunoreactivity in the developing retina of *Xenopus laevis*. *Sci. World J.* 2013:740420.

Álvarez-Hernán, G., Hernández-Núñez, I., Rico-Leo, E. M., Marzal, A., de Mera-Rodríguez, J. A., Rodríguez-León, J., et al. (2020). Retinal differentiation in an altricial bird species, *Taeniopygia guttata*: an immunohistochemical study. *Exp. Eye Res.* 190:107869. doi: 10.1016/j.exer.2019.107869

Álvarez-Hernán, G., Sánchez-Resino, E., Hernández-Núñez, I., Marzal, A., Rodríguez-León, J., Martín-Partido, G., et al. (2018). Retinal histogenesis in an Altricial Avian Species, the Zebra Finch (*Taeniopygia guttata*. Vieillot 1817). *J. Anat.* 233, 106–120. doi: 10.1111/joa.12809

Bejarano-Escobar, R., Álvarez-Hernán, G., Morona, R., González, A., Martín-Partido, G., and Francisco-Morcillo, J. (2015). Expression and function of the LIM-Homeodomain transcription factor Islet-1 in the developing and mature vertebrate retina. *Exp. Eye Res.* 138, 22–31. doi: 10.1016/j.exer.2015.06.021

Bejarano-Escobar, R., Blasco, M., Durán, A. C., Martín-Partido, G., and Francisco-Morcillo, J. (2013). Chronotopographical distribution patterns of cell death and of lectin-positive Macrophages/Microglial cells during the visual system ontogeny of the small-spotted catshark *Scyliorhinus canicula*. *J. Anat.* 223, 171–184. doi: 10.1111/joa.12071

Bejarano-Escobar, R., Blasco, M., Martín-Partido, G., and Francisco-Morcillo, J. (2014). Molecular characterization of cell types in the developing, mature, and regenerating fish retina. *Rev. Fish Biol. Fish.* 24, 127–158. doi: 10.1007/s11160-013-9320-z

Bejarano-Escobar, R., Holguín-Arévalo, M. S., Montero, J. A., Francisco-Morcillo, J., and Martín-Partido, G. (2011). Macrophage and microglia ontogeny in the mouse visual system can be traced by the expression of Cathepsins B and D. *Dev. Dyn.* 240, 1841–1855. doi: 10.1002/dvdy.22673

Bernadotte, A., Mikhelson, V. M., and Spivak, I. M. (2016). Markers of cellular senescence telomere shortening as a marker of cellular senescence. *Aging* 8, 3–11. doi: 10.18632/aging.100871

Bhanu, U. M., Mandraju, R. K., Bhaskar, C., and Kondapi, A. K. (2010). Cultured cerebellar granule neurons as an in vitro aging model: topoisomerase IIβ as an additional biomarker in DNA repair and aging. *Toxicol. Vitr.* 24, 1935–1945. doi: 10.1016/j.tiv.2010.08.003

Biran, A., Zada, L., Karan, P. A., Vadai, E., Roitman, L., Ovadya, Y., et al. (2017). Quantitative identification of senescent cells in aging and disease. *Aging Cell* 16, 661–671. doi: 10.1111/acel.12592

Bursuker, I., Rhodes, J. M., and Goldman, R. (1982). B-Galactosidase—an indicator of the maturational stage of mouse and human mononuclear phagocytes. *J. Cell Physiol.* 112, 385–390. doi: 10.1002/jcp.1041120312

Bussian, T. J., Aziz, A., Meyer, C. F., Swenson, B. L., van Deursen, J. M., and Baker, D. J. (2018). Clearance of senescent glial cells prevents tau-dependent pathology and cognitive decline. *Nature* 562, 578–582. doi: 10.1038/s41586-018-0543-y

Campisi, J., Andersen, J. K., Kapahi, P., and Melov, S. (2011). Cellular senescence: a link between cancer and age-related degenerative disease? *Semin. Cancer Biol.* 21, 354–359.

Chavarría, T., Baleriola, J., Mayordomo, R., De Pablo, F., and De La Rosa, E. J. (2013). Early neural cell death is an extensive, dynamic process in the embryonic chick and mouse retina. *Sci. World J.* 2013:627240.

Chavarría, T., Valenciano, A. I., Mayordomo, R., Egea, J., Comella, J. X., Hallböök, F., et al. (2007). Differential, age-dependent MEK-ERK and PI3K-Akt activation by insulin acting as a survival factor during embryonic retinal development. *Dev. Neurobiol.* 67, 1777–1788. doi: 10.1002/dneu.20554

Chernova, T., Nicotera, P., and Smith, A. G. (2006). Heme deficiency is associated with senescence and causes suppression of N-Methyl-D-Aspartate receptor subunits expression in primary cortical neurons. *Mol. Pharmacol.* 69, 697–705. doi: 10.1124/mol.105.016675

Childs, B. G., Durik, M., Baker, D. J., and Van Deursen, J. M. (2015). Cellular senescence in aging and age-related disease: from mechanisms to therapy. *Nat. Med.* 21, 1424–1435. doi: 10.1038/nm.4000

Cook, B., Portera-Cailliau, C., and Adler, R. (1998). Developmental neuronal death is not a universal phenomenon among cell types in the chick embryo retina. *J. Comp. Neurol.* 396, 12–19. doi: 10.1002/(sici)1096-9861(19980622)396:1<12::aid-cne2>3.0.co;2-l

Czarkwiani, A., and Yun, M. H. (2018). Out with the Old. In with the new: senescence in development. *Curr. Opin. Cell Biol.* 55, 74–80. doi: 10.1016/j.ceb.2018.05.014

Da Silva-Álvarez, S., Guerra-Varela, J., Sobrido-Cameán, D., Quelle, A., Barreiro-Iglesias, A., Sánchez, L., et al. (2020). Developmentally-programmed cellular senescence is conserved and widespread in zebrafish. *Aging* 12, 17895–17901. doi: 10.18632/aging.103968

Da Silva-Álvarez, S., Lamas-González, O., Ferreirós, A., González, P., Gómez, M., García-Caballero, T., et al. (2018). Pkd2 deletion during embryo development does not alter mesonephric programmed cell senescence. *Int. J. Dev. Biol.* 62, 637–640. doi: 10.1387/ijdb.180078mc

Da Silva-Álvarez, S., Picallos-Rabina, P., Antelo-Iglesias, L., Triana-Martínez, F., Barreiro-Iglesias, A., Sánchez, L., et al. (2019). The development of cell senescence. *Exp. Gerontol.* 128:110742.

Davaapil, H., Brockes, J. P., and Yun, M. H. (2017). Conserved and novel functions of programmed cellular senescence during vertebrate development. *Development* 144, 106–114. doi: 10.1242/dev.138222

de Mera-Rodríguez, J. A., Álvarez-Hernán, G., Gañán, Y., Martín-Partido, G., Rodríguez-León, J., and Francisco-Morcillo, J. (2019). Senescence-Associated β-Galactosidase activity in the developing avian retina. *Dev. Dyn.* 248, 850–865. doi: 10.1002/dvdy.74

Debacq-Chainiaux, F., Erusalimsky, J. D., Campisi, J., and Toussaint, O. (2009). Protocols to detect senescence-associated beta-galactosidase (SA-Bgal) activity, a biomarker of senescent cells in culture and in vivo. *Nat. Protoc.* 4, 1798–1806. doi: 10.1038/nprot.2009.191

Denoyelle, C., Abou-Rjaily, G., Bezrookove, V., Verhaegen, M., Johnson, T. M., Fullen, D. R., et al. (2006). Anti-oncogenic role of the endoplasmic reticulum differentially activated by mutations in the MAPK pathway. *Nat. Cell Biol.* 8, 1053–1063. doi: 10.1038/ncb1471

Dimri, G. P., Lee, X., Basile, G., Acosta, M., Scott, G., Roskelley, C., et al. (1995). A biomarker that identifies senescent human cells in culture and in aging skin in vivo. *Proc. Natl. Acad. Sci. U.S.A.* 92, 9363–9367. doi: 10.1073/pnas.92.20.9363

Dong, W., Cheng, S., Huang, F., Fan, W., Chen, Y., Shi, H., et al. (2011). Mitochondrial dysfunction in long-term neuronal cultures mimics changes with aging. *Med. Sci. Monit.* 17, 91–96.

Francisco-Morcillo, J., Bejarano-Escobar, R., Rodríguez-León, J., Navascués, J., and Martín-Partido, G. (2014). Ontogenetic cell death and phagocytosis in the visual system of vertebrates. *Dev. Dyn.* 243, 1203–1225. doi: 10.1002/dvdy.24174

Francisco-Morcillo, J., Hidalgo-Sánchez, M., and Martín-Partido, G. (2004). Spatial and temporal patterns of apoptosis during differentiation of the retina in the turtle. *Anat. Embryol.* 208, 289–299.

Geng, Y. Q., Guan, J. T., Xu, X. H., and Fu, Y. C. (2010). Senescence-associated beta-galactosidase activity expression in aging hippocampal neurons. *Biochem. Biophys. Res. Commun.* 396, 866–869. doi: 10.1016/j.bbrc.2010.05.011

Gibaja, A., Aburto, M. R., Pulido, S., Collado, M., Hurle, J. M., Varela-Nieto, I., et al. (2019). TGFβ2-induced senescence during early inner ear development. *Sci. Rep.* 9, 1–13. doi: 10.1016/b978-0-12-408088-1.00001-4

Going, J. J., Stuart, R. C., Downie, M., Fletcher-Monaghan, A. J., and Nicol Keith, W. (2002). "Senescence-Associated" β-Galactosidase activity in the upper gastrointestinal tract. *J. Pathol.* 196, 394–400. doi: 10.1002/path.1059

Gorgoulis, V., Adams, P. D., Alimonti, A., Bennett, D. C., Bischof, O., Bishop, C., et al. (2019). Cellular senescence: defining a path forward. *Cell* 179, 813–827. doi: 10.1016/j.cell.2019.10.005

Hall, B. M., Balan, V., Gleiberman, A. S., Strom, E., Krasnov, P., Virtuoso, L. P., et al. (2017). P16(Ink4a) and senescence-associated β-Galactosidase can be induced in macrophages as part of a reversible response to physiological stimuli. *Aging* 9, 1867–1884. doi: 10.18632/aging.101268

Hayflick, L., and Moorhead, P. S. (1961). The serial cultivation of human diploid cell strains. *Exp. Cell Res.* 25, 585–621. doi: 10.1016/0014-4827(61)90192-6

Hernandez-Segura, A., Nehme, J., and Demaria, M. (2018). Hallmarks of cellular senescence. *Trends Cell Biol.* 28, 436–453. doi: 10.1016/j.tcb.2018.02.001

Hjelmeland, L. M., Cristofalo, V. J., Funk, W., Rakoczy, E., and Katz, M. L. (1999). Senescence of the retinal pigment epithelium. *Mol. Vis.* 5, 33.

Huang, T., and Rivera-Pérez, J. A. (2014). Senescence-associated β-Galactosidase activity marks the visceral endoderm of mouse embryos but is not indicative of senescence. *Genesis* 52, 300–308. doi: 10.1002/dvg.22761

Jurk, D., Wang, C., Miwa, S., Maddick, M., Korolchuk, V., Tsolou, A., et al. (2012). Postmitotic neurons develop a P21-Dependent senescence-like phenotype driven by a DNA damage response. *Aging Cell* 11, 996–1004. doi: 10.1111/j.1474-9726.2012.00870.x

Knabe, W., Süss, M., and Kuhn, H. J. (2000). The patterns of cell death and of macrophages in the developing forebrain of the tree shrew tupaia belangeri. *Anat. Embryol.* 201, 157–168. doi: 10.1007/pl00008237

Kobayashi, Y., Tata, A., Konkimalla, A., Katsura, H., Lee, R. F., Ou, J., et al. (2020). Persistence of a regeneration-associated, transitional alveolar epithelial cell state in pulmonary fibrosis. *Nat. Cell Biol.* 22, 934–946. doi: 10.1038/s41556-020-0542-8

Kopp, H. G., Hooper, A. T., Shmelkov, S. V., and Rafii, S. (2007). β-Galactosidase staining on bone marrow. The osteoclast pitfall. *Histol. Histopathol.* 22, 971–976.

Kozlowski, M. R. (2012). RPE cell senescence: a key contributor to age-related macular degeneration. *Med. Hypotheses* 78, 505–510. doi: 10.1016/j.mehy.2012.01.018

Kritsilis, M., Rizou, S. V., Koutsoudaki, P. N., Evangelou, K., Gorgoulis, V. G., and Papadopoulos, D. (2018). Ageing, cellular senescence and neurodegenerative disease. *Int. J. Mol. Sci.* 19:2937. doi: 10.3390/ijms19102937

Kuilman, T., Michaloglou, C., Mooi, W. J., and Peepers, D. S. (2010). The essence of senescence. *Genes Dev.* 24, 2463–2479. doi: 10.1101/gad.1971610

Kurz, D. J., Decary, S., Hong, Y., and Erusalimsky, J. D. (2000). Senescence-Associated β-galactosidase reflects an increase in lysosomal mass during replicative ageing of human endothelial cells. *J. Cell Sci.* 113, 3613–3622.

Lamoke, F., Shaw, S., Yuan, J., Ananth, S., Duncan, M., Martin, P., et al. (2015). Increased oxidative and nitrative stress accelerates aging of the retinal vasculature in the diabetic retina. *PLoS One* 10:e0139664. doi: 10.1371/journal.pone.0139664

Lee, B. Y., Han, J. A., Im, J. S., Morrone, A., Johung, K., Goodwin, E. C., et al. (2006). Senescence-Associated β-Galactosidase is lysosomal β-Galactosidase. *Aging Cell* 5, 187–195.

Lee, S., and Lee, J. S. (2019). Cellular senescence: a promising strategy for cancer therapy. *BMB Rep.* 52, 35–41. doi: 10.5483/bmbrep.2019.52.1.294

Li, L. U., Zhao, Y., and Zhang, H. (2017). P16INK4a upregulation mediated by TBK1 induces retinal ganglion cell senescence in ischemic injury. *Cell Death Dis.* 8, 1–12.

Li, Y., Zhao, H., Huang, X., Tang, J., Zhang, S., Li Yan, et al. (2018). Embryonic senescent cells re-enter cell cycle and contribute to tissues after birth. *Cell Res.* 28, 775–778. doi: 10.1038/s41422-018-0050-6

López-Luppo, M., Catita, J., Ramos, D., Navarro, M., Carretero, A., Mendes-Jorge, L., et al. (2017). Cellular senescence is associated with human retinal microaneurysm formation during aging. *Investig. Ophthalmol. Vis. Sci.* 58, 2832–2842. doi: 10.1167/iovs.16-20312

Lorda-Díez, C. I., García-Riart, B., Montero, J. A., Rodríguez-León, J., García-Porrero, J. A., and Hurlé, J. M. (2015). Apoptosis during embryonic tissue remodeling is accompanied by cell senescence. *Aging* 7, 974–985. doi: 10.18632/aging.100844

Lorda-Díez, C. I., Solis-Mancilla, M. E., Sanchez-Fernandez, C., Garcia-Porrero, J. A., Hurle, J. M., and Montero, J. A. (2019). Cell senescence, apoptosis and DNA damage cooperate in the remodeling processes accounting for heart morphogenesis. *J. Anat.* 234, 815–829. doi: 10.1111/joa.12972

Lowe, S. W., and Sherr, C. J. (2003). Tumor suppression by Ink4a-Arf: progress and puzzles. *Curr. Opin. Genet. Dev.* 13, 77–83. doi: 10.1016/s0959-437x(02)00013-8

Magariños, M., Barajas-Azpeleta, R., Varela-Nieto, I., and Aburto, M. R. (2020). Otic neurogenesis is regulated by TGFβ in a senescence-independent manner. *Front. Cell. Neurosci.* 14:217. doi: 10.3389/fncel.2020.00217

Marín-Teva, J. L., Almendros, A., Calvente, R., Cuadros, M. A., and Navascués, J. (1999). Proliferation of actively migrating ameboid microglia in the developing quail retina. *Anat. Embryol.* 200, 289–300. doi: 10.1007/s004290050280

Matjusaitis, M., Chin, G., Sarnoski, E. A., and Stolzing, A. (2016). Biomarkers to identify and isolate senescent cells. *Ageing Res. Rev.* 29, 1–12. doi: 10.1016/j.arr.2016.05.003

Matsunaga, H., Handa, J. T., Aotaki-Keen, A., Sherwood, S. W., West, M. D., and Hjelmeland, L. M. (1999). β-Galactosidase histochemistry and telomere loss in senescent retinal pigment epithelial cells. *Investig. Ophthalmol. Vis. Sci.* 40, 197–202.

Mayordomo, R., Valenciano, A. I., De La Rosa, E. J., and Hallböök, F. (2003). Generation of retinal ganglion cells is modulated by caspase-dependent programmed cell death. *Eur. J. Neurosci.* 18, 1744–1750. doi: 10.1046/j.1460-9568.2003.02891.x

Mishima, K., Handa, J. T., Aotaki-Keen, A., Lutty, G. A., Morse, L. S., and Hjelmeland, L. M. (1999). Senescence-Associated β-Galactosidase histochemistry for the primate eye. *Investig. Ophthalmol. Vis. Sci.* 40, 1590–1593.

Montero, J. A., and Hurlé, J. M. (2010). Sculpturing digit shape by cell death. *Apoptosis* 15, 365–375. doi: 10.1007/s10495-009-0444-5

Montero, J. A., Lorda-Diez, C. I., and Hurle, J. M. (2020). Confluence of cellular degradation pathways during interdigital tissue remodeling in embryonic tetrapods. *Front. Cell Dev. Biol.* 8:593761. doi: 10.3389/fcell.2020.593761

Montero, J. A., Sanchez-Fernandez, C., Lorda-Diez, C. I., Garcia-Porrero, J. A., and Hurle, J. M. (2016). DNA damage precedes apoptosis during the regression of the interdigital tissue in vertebrate embryos. *Sci. Rep.* 6, 1–12.

Muñoz-Espín, D., Cañamero, M., Maraver, A., Gómez-López, G., Contreras, J., Murillo-Cuesta, S., et al. (2013). Programmed cell senescence during mammalian embryonic development. *Cell* 155, 1104–1118. doi: 10.1016/j.cell.2013.10.019

Muñoz-Espín, D., and Serrano, M. (2014). Cellular senescence: from physiology to pathology. *Nat. Rev. Mol. Cell Biol.* 15, 482–496. doi: 10.1038/nrm3823

Musi, N., Valentine, J. M., Sickora, K. R., Baeuerle, E., Thompson, C. S., Shen, Q., et al. (2018). Tau protein aggregation is associated with cellular senescence in the brain. *Aging Cell* 17:e12840. doi: 10.1111/acel.12840

Nacher, V., Carretero, A., Navarro, M., Armengol, C., Llombart, C., Rodríguez, A., et al. (2006). The quail mesonephros: a new model for renal senescence? *J. Vasc. Res.* 43, 581–586. doi: 10.1159/000096076

Ori, A., Toyama, B. H., Harris, M. S., Bock, T., Iskar, M., Bork, P., et al. (2015). Integrated transcriptome and proteome analyses reveal organ-specific proteome deterioration in old rats. *Cell Syst.* 1, 224–237. doi: 10.1016/j.cels.2015.08.012

Oubaha, M., Miloudi, K., Dejda, A., Guber, V., Mawambo, G., Germain, M. A., et al. (2016). Senescence-associated secretory phenotype contributes to pathological angiogenesis in retinopathy. *Sci. Transl. Med.* 8:362ra144. doi: 10.1126/scitranslmed.aaf9440

Péquignot, M. O., Provost, A. C., Sallé, S., Taupin, P., Sainton, K. M., Marchant, D., et al. (2003). Major Role of BAX in apoptosis during retinal development and in establishment of a functional postnatal retina. *Dev. Dyn.* 228, 231–238. doi: 10.1002/dvdy.10376

Piechota, M., Sunderland, P., Wysocka, A., Nalberczak, M., Sliwinska, M. A., Radwanska, K., et al. (2016). Is Senescence-Associated β-Galactosidase a marker of neuronal senescence? *Oncotarget* 7, 81099–81109. doi: 10.18632/oncotarget.12752

Raffaele, M., Kovacovicova, K., Bonomini, F., Rezzani, R., Frohlich, J., and Vinciguerra, M. (2020). Senescence-like phenotype in post-mitotic cells of mice entering middle age. *Aging* 12, 13979–13990. doi: 10.18632/aging.103637

Rodríguez-León, J., Tomas, A. R., Johnson, A., and Kawakami, Y. (2013). Recent advances in the study of limb development: the emergence and function of the apical ectodermal ridge. *J. Stem Cells* 8, 79–98.

Rhinn, M., Ritschka, B., and Keyes, W. M. (2019). Cellular senescence in development, regeneration and disease. *Development* 146:dev151837. doi: 10.1242/dev.151837

Rodier, F., and Campisi, J. (2011). Four faces of cellular senescence. *J. Cell Biol.* 192, 547–556. doi: 10.1083/jcb.201009094

Rodríguez-Gallardo, L., Lineros-Domínguez, M. D. C., Francisco-Morcillo, J., and Martín-Partido, G. (2005). Macrophages during retina and optic nerve development in the mouse embryo: relationship to cell death and optic fibres. *Anat. Embryol.* 210, 303–316. doi: 10.1007/s00429-005-0051-3

Sacco, A., Belloni, L., and Latella, L. (2021). From development to aging: the path to cellular senescence. *Antioxid Redox Signal.* doi: 10.1089/ars.2020.8071 [Epub ahead of print].

Sanchez-Fernandez, C., Lorda-Díez, C. I., García-Porrero, J. A., Montero, J. A., and Hurlé, J. M. (2019). UHRF genes regulate programmed interdigital tissue regression and chondrogenesis in the embryonic limb. *Cell Death Dis.* 10:347. doi: 10.1038/s41419-019-1575-4

Sanchez-Fernandez, C., Lorda-Diez, C. I., Hurlé, J. M., and Montero, J. A. (2020). The methylation status of the embryonic limb skeletal progenitors determines their cell fate in chicken. *Commun. Biol.* 3, 1–12.

Sapieha, P., and Mallette, F. A. (2018). Cellular senescence in postmitotic cells: beyond growth arrest. *Trends Cell Biol.* 28, 595–607. doi: 10.1016/j.tcb.2018.03.003

Severino, J., Allen, R. G., Balin, S., Balin, A., and Cristofalo, V. J. (2000). Is β-Galactosidase staining a marker of senescence in vitro and in vivo? *Exp. Cell Res.* 257, 162–171. doi: 10.1006/excr.2000.4875

Sharpless, N. E., and Sherr, C. J. (2015). Forging a signature of in vivo senescence. *Nat. Rev. Cancer* 15, 397–408. doi: 10.1038/nrc3960

Storer, M., Mas, A., Robert-Moreno, A., Pecoraro, M., Ortells, M. C., Di Giacomo, V., et al. (2013). Senescence is a developmental mechanism that contributes to embryonic growth and patterning. *Cell* 155, 1119–1130. doi: 10.1016/j.cell.2013.10.041

Tominaga, T., Shimada, R., Okada, Y., Kawamata, T., and Kibayashi, K. (2019). Senescence-Associated-β-Galactosidase staining following traumatic brain injury in the mouse cerebrum. *PLoS One* 14:e0213673. doi: 10.1371/journal.pone.0213673

Valenciano, A. I., Boya, P., and De La Rosa, E. J. (2009). Early neural cell death: numbers and cues from the developing neuroretina. *Int. J. Dev. Biol.* 53, 1515–1528. doi: 10.1387/ijdb.072446av

Villiard, É, Denis, J.-F., Hashemi, F. S., Igelmann, S., Ferbeyre, G., and Roy, S. (2017). Senescence gives insights into the morphogenetic evolution of anamniotes. *Biol. Open* 6, 891–896. doi: 10.1242/bio.025809

Walton, C. C., and Andersen, J. K. (2019). Unknown fates of (Brain) oxidation or UFO: close encounters with neuronal senescence. *Free Radic. Biol. Med.* 134, 695–701. doi: 10.1016/j.freeradbiomed.2019.01.012

Wang, A. S., and Dreesen, O. (2018). Biomarkers of cellular senescence and skin aging. *Front. Genet.* 9:247. doi: 10.3389/fgene.2018.00247

Wassélius, J., Wallin, H., Abrahamson, M., and Ehinger, B. (2003). Cathepsin B in the rat eye. *Graefe's Arch. Clin. Exp. Ophthalmol.* 241, 934–942. doi: 10.1007/s00417-003-0782-x

Xiang, M. (2013). Intrinsic control of mammalian retinogenesis. *Cell Mol. Life Sci.* 70, 2519–2532. doi: 10.1007/s00018-012-1183-2

Xu, T., Sun, L., Shen, X., Chen, Y., Yin, Y., Zhang, J., et al. (2019). NADPH Oxidase 2-Mediated NLRP1 inflammasome activation involves in neuronal senescence in hippocampal neurons in vitro. *Int. Immunopharmacol.* 69, 60–70. doi: 10.1016/j.intimp.2019.01.025

Yang, N. C., and Hu, M. L. (2005). The limitations and validities of senescence associated-β-galactosidase activity as an aging marker for human foreskin fibroblast Hs68 cells. *Exp. Gerontol.* 40, 813–819. doi: 10.1016/j.exger.2005.07.011

Yegorov, Y. E., Akimov, S. S., Hass, R., Zelenin, A. V., and Prudovsky, I. A. (1998). Endogenous β-Galactosidase activity in continuously nonproliferating cells. *Exp. Cell Res.* 243, 207–211. doi: 10.1006/excr.1998.4169

Young, A. R. J., Narita, M., Ferreira, M., Kirschner, K., Sadaie, M., Darot, J. F. J., et al. (2009). Autophagy mediates the mitotic senescence transition. *Genes Dev.* 23, 798–803. doi: 10.1101/gad.519709

Zhao, Y., Tyshkovskiy, A., Muñoz-Espín, D., Tian, X., Serrano, M., De Magalhaes, J. P., et al. (2018). Naked mole rats can undergo developmental, oncogene-induced and dna damage-induced cellular senescence. *Proc. Natl. Acad. Sci. U.S.A.* 115, 1801–1806. doi: 10.1073/pnas.1721160115

Conflict of Interest: The authors declare that the research was conducted in the absence of any commercial or financial relationships that could be construed as a potential conflict of interest.

frontiers in Cell and Developmental Biology

ORIGINAL RESEARCH
published: 09 February 2021
doi: 10.3389/fcell.2021.622152

Sulforaphane Protects Against Ethanol-Induced Apoptosis in Human Neural Crest Cells Through Diminishing Ethanol-Induced Hypermethylation at the Promoters of the Genes Encoding the Inhibitor of Apoptosis Proteins

Yihong Li[1,2†], Huadong Fan[1,2†], Fuqiang Yuan[1,2], Lanhai Lu[1,2], Jie Liu[1,2], Wenke Feng[1,2,3], Huang-Ge Zhang[4,5] and Shao-Yu Chen[1,2]*

[1] Department of Pharmacology and Toxicology, University of Louisville Health Science Center, Louisville, KY, United States, [2] University of Louisville Alcohol Research Center, Louisville, KY, United States, [3] Department of Medicine, University of Louisville, Louisville, KY, United States, [4] Department of Microbiology and Immunology, James Graham Brown Cancer Center, University of Louisville, Louisville, KY, United States, [5] Robley Rex Veterans Affairs Medical Center, Louisville, KY, United States

The neural crest cell (NCC) is a multipotent progenitor cell population that is sensitive to ethanol and is implicated in the Fetal Alcohol Spectrum Disorders (FASD). Studies have shown that sulforaphane (SFN) can prevent ethanol-induced apoptosis in NCCs. This study aims to investigate whether ethanol exposure can induce apoptosis in human NCCs (hNCCs) through epigenetically suppressing the expression of anti-apoptotic genes and whether SFN can restore the expression of anti-apoptotic genes and prevent apoptosis in ethanol-exposed hNCCs. We found that ethanol exposure resulted in a significant increase in the expression of DNMT3a and the activity of DNMTs. SFN treatment diminished the ethanol-induced upregulation of DNMT3a and dramatically reduced the activity of DNMTs in ethanol-exposed hNCCs. We also found that ethanol exposure induced hypermethylation at the promoter regions of two inhibitor of apoptosis proteins (IAP), NAIP and XIAP, in hNCCs, which were prevented by co-treatment with SFN. SFN treatment also significantly diminished ethanol-induced downregulation of NAIP and XIAP in hNCCs. The knockdown of DNMT3a significantly enhanced the effects of SFN on preventing the ethanol-induced repression of NAIP and XIAP and apoptosis in hNCCs. These results demonstrate that SFN can prevent ethanol-induced apoptosis in hNCCs by preventing ethanol-induced hypermethylation at the promoter regions of the genes encoding the IAP proteins and diminishing ethanol-induced repression of NAIP and XIAP through modulating DNMT3a expression and DNMT activity.

Keywords: sulforaphane, ethanol, apoptosis, DNA methylation, IAP proteins, neural crest cells

OPEN ACCESS

Edited by:
Marta Magarinos, Autonomous University of Madrid, Spain

Reviewed by:
Laura Maria Frago, Autonomous University of Madrid, Spain
Juan Antonio Montero, University of Cantabria, Spain

***Correspondence:**
Shao-Yu Chen
shaoyu.chen@louisville.edu

† These authors have contributed equally to this work

Specialty section:
This article was submitted to Cell Death and Survival, a section of the journal Frontiers in Cell and Developmental Biology

Received: *27 October 2020*
Accepted: *20 January 2021*
Published: *09 February 2021*

Citation:
Li Y, Fan H, Yuan F, Lu L, Liu J, Feng W, Zhang H-G and Chen S-Y (2021) Sulforaphane Protects Against Ethanol-Induced Apoptosis in Human Neural Crest Cells Through Diminishing Ethanol-Induced Hypermethylation at the Promoters of the Genes Encoding the Inhibitor of Apoptosis Proteins. Front. Cell Dev. Biol. 9:622152. doi: 10.3389/fcell.2021.622152

INTRODUCTION

Prenatal alcohol exposure can cause a spectrum of physical abnormalities and mental dysfunctions in children, which are defined as Fetal Alcohol Spectrum Disorders (FASD) (Koren et al., 2003; Sokol et al., 2003). Previous studies by Kotch and Sulik, as well as Dunty et al., have revealed that ethanol exposure during the early stages of development resulted in excessive cell death in neural crest cells (NCCs), which contributes heavily to ethanol-induced malformations (Kotch and Sulik, 1992; Dunty et al., 2001). Using a chick-specific antibody to NCCs, Cartwright and Smith confirmed that the prenatal ethanol exposure resulted in the loss of cranial NCCs in chicken embryos (Cartwright and Smith, 1995). Studies from our laboratory have also shown that ethanol exposure significantly increased apoptosis in NCCs *in vitro* (Chen et al., 2015; Li et al., 2019b).

Multiple signaling pathways have been shown to be involved in the ethanol-induced apoptosis in NCCs, including the Bcl2 family (Chen et al., 2015; Yuan et al., 2018), Seven *in absentia* homolog1 (Siah1) (Sun et al., 2014; Yuan et al., 2017), p53 and MAPK signaling (Yuan et al., 2017, 2020) and Nrf2 signaling (Chen et al., 2013). However, the potential role of the inhibitor of apoptosis proteins (IAP) in ethanol-induced apoptosis in NCCs remains to be defined. IAP family is composed of eight members presenting one to three BIR domains from the baculovirus (Birnbaum et al., 1994). They are frequently overexpressed in cancer cells that are resistant to apoptosis (Silke and Meier, 2013). DNA hypomethylation at the promoters of IAP genes and the overexpression of the IAPs have been found in different cancers, including ovarian, hepatocellular carcinoma (HCC), and glioma (Hervouet et al., 2013). Studies have also shown that the loss of methylation induced by DNA methyltransferase (DNMT) inhibitor at the promoters of the IAP genes is associated with apoptosis resistance (Hervouet et al., 2013).

It is well-known that DNA hypermethylation in the promoter regions of genes is associated with gene repression (Jones and Baylin, 2002) and plays an important role in the repression of many genes involved in various cellular functions, including DNA repair, cell adhesion, and apoptosis (Teodoridis et al., 2004; Gopisetty et al., 2006). DNA methylation has been shown to be associated with the repression of the apoptotic genes in cancer cells (Murphy et al., 2008; Malekzadeh et al., 2009; Hervouet et al., 2013). Hypermethylation at the *Casp 8* promoter was correlated with a low Casp 8 expression in cancer cells and contributed to apoptosis resistance in different cancer cell lines, such as pediatric cancer (Harada et al., 2002), lung carcinomas (Shivapurkar et al., 2002), and breast cancer (Wu et al., 2010). Studies have shown that ethanol exposure can alter DNA methylation (Haycock and Ramsay, 2009; Ouko et al., 2009; Zhou et al., 2011) and histone modification (Zhong et al., 2010; Bekdash et al., 2013; Subbanna et al., 2013, 2014). An earlier study by Garro has also shown that fetal DNA was hypermethylated after ethanol exposure during embryonic development (Garro et al., 1991).

DNA methylation occurs on the cytosine residue of CpG dinucleotides through the transfer of 5-methylcytosine from the methyl donor S-adenosylmethionine (SAM) to the CpG. The reaction is catalyzed by a family of enzymes called DNA methyltransferases (DNMTs), including DNMT1, DNMT3a, and DNMT3b (Singal and Ginder, 1999). DNMT1 is responsible for the maintenance of established patterns of DNA methylation, while DNMT3a and DNMT3b mediate the establishment of new or *de novo* DNA methylation patterns (Chen et al., 2003; Jones and Liang, 2009b). Alteration of DNA methylation by DNMTs may trigger hypermethylation or hypomethylation of gene promoters and consequently result in activating or inhibiting gene expression (Hervouet et al., 2010, 2013).

Sulforaphane (SFN) is a vegetable-derived isothiocyanate that is abundant in cruciferous vegetables such as broccoli. Our previous studies have shown that SFN prevented ethanol-induced apoptosis through upregulating the antioxidant gene Nrf2 in NCCs (Chen et al., 2013). In addition to acting as an Nrf2 inducer, SFN has been found to regulate gene expression by inhibiting the activity of DNMTs (Meeran et al., 2012). It has also been reported that SFN can inhibit LPS-induced DNMT3a gene expression and confer resistance to LPS-induced apoptosis in porcine monocyte-derived dendritic cells (Qu et al., 2015).

In the present study, we determined whether SFN can prevent ethanol-induced apoptosis in hNCCs through epigenetic modulation of anti-apoptotic genes. We found that ethanol exposure resulted in a significant increase in the expression of DNMT3a and the activity of DNMTs. SFN treatment diminished the ethanol-induced upregulation of DNMT3a and dramatically reduced the activity of DNMTs in ethanol-exposed hNCCs. Ethanol exposure also induced hypermethylation at the promoter regions of two IAP proteins, NAIP and XIAP, in hNCCs, which were prevented by co-treatment with SFN. SFN treatment also significantly diminished ethanol-induced downregulation of NAIP and XIAP in hNCCs. The knockdown of DNMT3a significantly enhanced the effects of SFN on preventing the ethanol-induced repression of NAIP and XIAP and apoptosis in hNCCs. These results demonstrate that SFN can prevent ethanol-induced apoptosis in hNCCs by diminishing the ethanol-induced hypermethylation at the promoter regions of the genes encoding the IAP proteins.

MATERIALS AND METHODS

Human Neural Crest Cell Differentiation, Culture and Treatment

hNCCs were differentiated from human embryonic stem cell (hESC) line H9 (WA09)), which was purchased from WiCell® (Madison, WI, United States). hESCs were maintained in mTeSR™1 (StemCell Technologies, Inc., Vancouver, Canada) on hESCs-qualified Matrigel™ (BD Biosciences, San Jose, CA) coated plates, following the WiCell's protocols. The differentiation of hNCCs from hESCs was performed as previously reported (Menendez et al., 2013; Avery and Dalton, 2016) with modification. Briefly, the hESCs® were first adapted to Accutase solution (Stem Cell Technologies, Vancouver, BC,

Abbreviations: DNMT, DNA methyltransferase; FASD, Fetal Alcohol Spectrum Disorders; hNCCs, Human neural crest cells; IAP, Inhibitor of apoptosis protein; MSP, Methylation-specific PCR; SFN, Sulforaphane.

Canada) and dissociated into single cells and cultured in the hESCs maintenance medium. When hESCs reached 75–85% confluence, the hESCs maintenance medium was removed, and the hESCs were detached by adding the Accutase® solution. The collected hESCs were resuspended and cultured in the hNCCs differentiation medium (DMEM/F-12 Medium, 14.3 M L-Glutamine + β-mercaptoethanol, MEM Non-Essential Amino Acid, 10 μg/mL Fgf2, 10 μg/mL Heregulin β-1, 200 μg/mL Long R3-IGF1, 10 mM CHIR 99021, 10 mM SB421542 and Penicillin and streptomycin). When cells reached 75–85% confluence, the differentiating cells were passed using Accutase® and then maintained in hNCCs differentiation medium. After culture in hNCCs-differentiation medium for around 10 days, hNCCs were collected, and NCC identity was analyzed by examining the NCC markers p75, HNK1, and AP2 using immunocytochemistry, flow cytometry and/or RT-PCR. For treatments, hNCCs were first pretreated with 1 μM SFN (LST Laboratories, St. Paul, MN) for 24 h, and then the cells were concurrently exposed to 1 μM SFN and 50 mM ethanol for an additional 24 h. To maintain the stable ethanol levels, the cell culture dishes were placed in a plastic desiccator containing ethanol in distilled water, as described previously (Yan et al., 2010).

Quantitative Real-Time PCR

Quantitative real-time PCR was performed as previously described (Fan et al., 2019). Briefly, total RNA was isolated from control and treated hNCCs using a QIAGEN RNeasy mini kit (QIAGEN, Valencia, CA) according to the manufacturer's instruction. The cDNAs were synthesized using QuantiTect Reverse Transcription Kit (QIAGEN, Valencia, CA) following the manufacturer's protocol. Quantitative RT-PCR was performed using FastStart SYBR Green Master (Roche Applied, Indianapolis, IN, United States) on a Rotor-Gene 600 Real-time PCR system (Corbett LifeScience, Mannheim, Germany). The following primer pairs were used for this analysis: NAIP (Homo sapiens) forward: 5′-GCCTAGATGCAGTTCAGTTGG-3′, reverse: 3′-GGCACCAAAGAGGATTAGGCT-3′; XIAP (Homo sapiens) forward: 5′-GGTGAAGGAGATACCGTGCG-3′, reverse: 3′-GCATGTGTCTCAGATGGCCT-5′; β-Actin (Homo sapiens) forward: 5′-AGAAGGATTCCTATGTGGGCG-3′, reverse: 3′-GGATAGCACAGCCTGGATAGCA-5′. The primers were synthesized by Integrated DNA Technologies, Inc. (IDT, Coralville, IA, United States). All assays were carried out in triplicate. Relative quantitative analysis was performed by comparing the threshold cycle number for target genes and a reference β-Actin mRNA.

Western Blotting

Western blotting was performed by the standard protocol as previously described (Yuan et al., 2017). Briefly, hNCCs from control and experimental groups were washed with PBS and then lysed in cold RIPA lysis buffer with 1 mM PMSF and protease cocktail inhibitors. Whole-cell lysis was centrifuged at 12,000 × *g* for 10 min at 4°C, and the supernatants were used for Western blot. Protein concentrations were measured by using BSA Protein Assay Reagent Kit (Pierce, Thermo Scientific, Waltham, MA). Proteins were probed with the following antibodies: anti-cleaved caspase-3 rabbit mAb (Cell Signaling, Beverly, MA, United States), anti-DNMT3a rabbit mAb (Cell Signaling, Beverly, MA, United States), anti-NAIP sheep pAb (R&D system, Minneapolis, MN, United States), anti-XIAP rabbit mAb (Cell Signaling, Beverly, MA, United States), and anti-β–Actin mouse mAb (Santa Cruz, Santa Cruz, CA). The densitometry of the blots was analyzed using ImageJ software (National Institute of Health, United States). All Western blot analyses were performed in triplicate.

Analysis of DNMT Activity

hNCCs from the control and treated groups were harvested, and nuclear extracts were isolated by using the EpiQuik Nuclear Extraction Kit (Epigentek, Farmingdale, NY) according to the manufacturer's protocol. The protein concentrations of nuclear extraction were measured using the BCA protein assay kit (Thermo Scientific, Irvine, CA). DNMT activity was determined with an EpiQuik DNA Methyltransferase Activity Assay kit (Epigentek, Farmingdale, NY), following the manufacturer's instruction.

Methylated Specific PCR (MSP)

The methylation status of CpG island on the promoters of NAIP and XAIP was determined by MSP. Genomic DNA was extracted from control and treated hNCCs using DNeasy Blood & Tissue Kit (QIAGEN, Valencia, CA) according to the manufacturer's instruction. Bisulfite conversion of the genomic DNA was performed using the EpiTect Bisulfite Kit (QIAGEN, Valencia, CA). Bisulfite-modified DNA was amplified using two primer sets specific for the detection of the methylated (M) and unmethylated (U) sequences. The following primer pairs were used for MSP analysis. NAIP (M) forward: 5′-AGGTTGGAGTATCGTGGC-3′, reverse: 3′-GAACGTAATAACGAACGCCT-5′, NAIP (U) forward: 5′-TTTAGGTTGGAGTATTGTGGT-3′, reverse: 3′-ACCAAACATAATAACAAACACCT-5′; XIAP (M) forward: 5′-GGCGGAGGTTGTAGTGAGTC-3′, reverse: 3′-ATAAACATAAACCACCGCGC-5′, XIAP (U) forward: 5′-GGAGGTGGAGGTTGTAGTGAGTT-3′, reverse: 3′-TATAAACATAAACCACCACACCC-5′. Real-time qMSP assays were performed on a Rotor-Gene 600 Real-time PCR system (Corbett LifeScience, Mannheim, Germany), and the PCR products were separated on 2% agarose gel. The intensity of DNA bands was measured by using NIH ImageJ software (National Institute of Health, United States). Methylation levels were calculated as the intensity of the methylated DNA band relative to the combined intensity of the methylated and unmethylated DNA bands.

siRNA Transfection

hNCCs were transfected with DNMT3a siRNA (SMART pool: On-TARGET plus human DNMT3a) (GE Healthcare Dharmacon, Lafayette, CO) or scramble control siRNA (IDT, Coralville, IA) in a final concentration of 25 nM by using Lipofectamine™2000 (Thermo Fisher, Waltham, MA),

according to the manufacturer's instruction. The cells were harvested 24 h after transfection for experiments.

Analysis of Cell Viability and Apoptosis

Cell viability was measured using an MTS (3-(4,5-dimethylthiazol-2-yl)-5-(3- arboxymethoxyphenyl)-2-(4-sulfophenyl)-2*H*-tetrazolium salt) assay kit (Promega, Madison, WI), as described previously (Chen et al., 2013). Apoptosis was determined by the analysis of caspase-3 cleavage by Western blot and by flow cytometry using a FITC Annexin V apoptosis detection kit (BD Bioscience, Franklin Lakes, NJ, United States) as described previously (Li et al., 2019b).

Statistical Analysis

Statistical analyses were performed using GraphPad Prism software (GraphPad Software, San Diego, CA, United States). All data were expressed as mean ± SEM of at least three independent experiments. Comparisons between groups were analyzed by one-way ANOVA. Multiple comparison post-tests were conducted using Bonferroni's test. Differences between groups were considered significant at $p < 0.05$.

RESULTS

SFN Treatment Significantly Diminished Ethanol-Induced Apoptosis in hNCCs

For this study, hNCCs were differentiated from human embryonic stem cells and validated by examining the expression of NCC marker HNK1 using immunocytochemistry (**Figure 1A**). To determine whether SFN treatment can diminish the ethanol-induced reduction in cell viability in hNCCs, the cells were treated with ethanol alone or pretreated with SFN at different concentrations for 24 h, followed by concurrent exposure to SFN and ethanol for an additional 24 h. As shown in **Figure 1B**, SFN at 1 μM significantly diminished the reduction of cell viability in hNCCs exposed to 50 mM ethanol. Treatment with SFN also significantly reduced caspase-3 activation in hNCCs exposed to 50 mM ethanol for 24 h (**Figure 1C**).

SFN Diminished Ethanol-Induced Increase in DNMT Activity and Up-Regulation of DNMT3a in hNCCs

To determine the effects of ethanol and SFN on the activity and expression of DNMT, hNCCs were pretreated with 1 μM

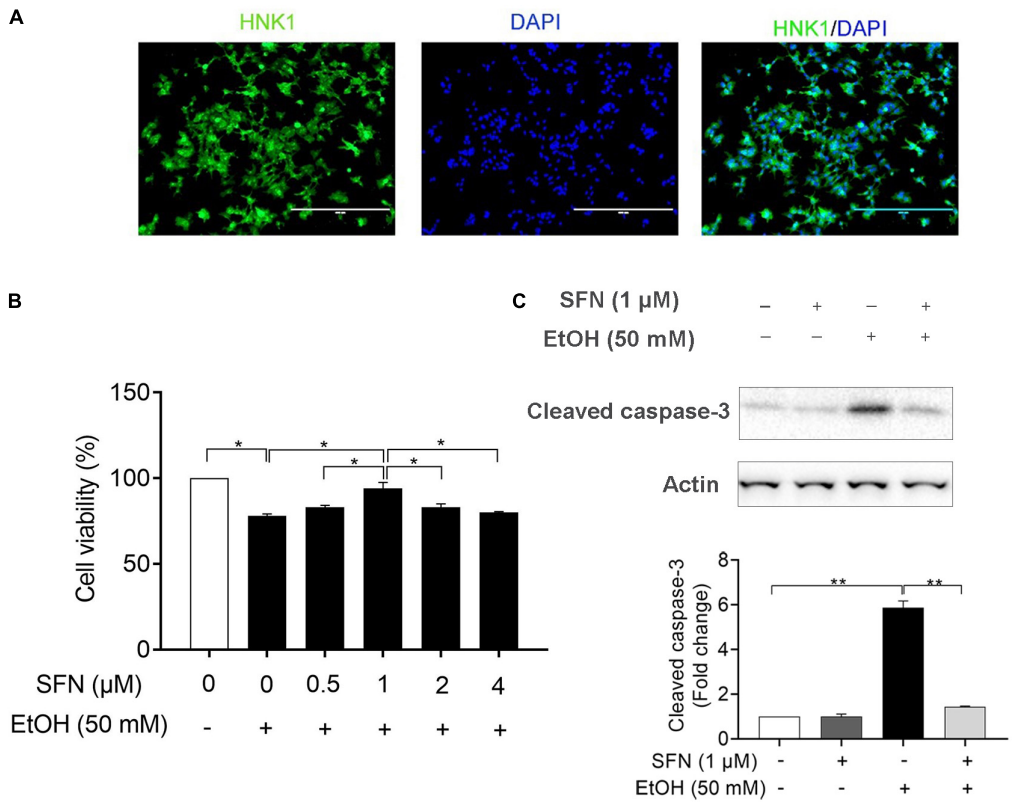

FIGURE 1 | SFN significantly diminished the ethanol-induced apoptosis in hNCCs. **(A)** Immunocytochemistry of NCC marker, HNK1, in hNCCs differentiated from hESCs. **(B)** hNCCs were treated with 50 mM ethanol alone or pretreated with SFN at different concentrations for 24 h, followed by concurrent exposure to SFN and ethanol for an additional 24 h. Cell viability was determined by MTS assay. **(C)** hNCCs were treated with 1 μM SFN for 24 h, followed by concurrent exposure to 1 μM SFN and 50 mM ethanol for an additional 24 h. Apoptosis was determined by the analysis of caspase-3 cleavage using Western blotting. Data are expressed as a percentage of control **(B)** or fold change over control **(C)** and represent the mean ± SEM of three separated experiments. *$p < 0.05$, **$p < 0.01$.

SFN for 24 h, followed by 24 h of concurrent exposure to 1 μM SFN and 50 mM ethanol. As shown in **Figure 2A**, ethanol exposure significantly increased the DNMT activity in hNCCs. Treatment with SFN dramatically reduced the ethanol-induced increase in the activity of DNMT in hNCCs. To determine whether ethanol and SFN also affect the expression of DNMT, the protein expression of DNMT3a, one of the three DNMTs, which is involved in DNA methylation in eukaryotic cells (Leonhardt and Bestor, 1993; Jones and Liang, 2009a), was analyzed by Western blotting. We found that exposure to 50 mM ethanol resulted in a significant increase in the protein expression of DNMT3a in hNCCs. Co-treatment with SFN and ethanol significantly reduced ethanol-induced increase in DNMT3a protein expression (**Figure 2B**).

SFN Diminished the Ethanol-Induced Hypermethylation at the Promoters of NAIP and XIAP in hNCCs

To determine whether ethanol-induced up-regulation of DNMT3a and increase in DNMT activity can result in hypermethylation at the promoters of the IAP genes and whether SFN can diminish ethanol-induced hypermethylation at the promoters of these genes, the methylation status of the CpG islands at the promoters of XIAP and NIAP in hNCCs was analyzed by using methylation-specific PCR (MSP). As shown in **Figure 3**, exposure of hNCCs to ethanol for 24 h resulted in a significant increase in the methylation levels at the promoters of XIAP and NIAP. Co-treatment with SFN significantly diminished ethanol-induced hypermethylation at the promoters of these anti-apoptotic genes in hNCCs. These results demonstrate that ethanol exposure can induce hypermethylation at the promoters of NAIP and XIAP in hNCCs, which can be prevented by co-treatment with SFN.

SFN Diminished Ethanol-Induced Down-Regulation of IAP Genes in hNCCs

To determine whether ethanol-induced hypermethylation at the promoters of NAIP and XIAP can repress the expression of NAIP and XIAP and whether SFN can prevent ethanol-induced down-regulation of NAIP and XIAP by diminishing ethanol-induced hypermethylation at the promoters of these genes in hNCCs, the mRNA expression of NAIP and XIAP was analyzed in hNCCs. As shown in **Figure 4**, exposure to 50 mM ethanol for 24 h resulted in a dramatic reduction in mRNA expression of NAIP and XIAP in hNCCs. Treatment with SFN significantly diminished ethanol-induced down-regulation of NAIP and XIAP in hNCCs, indicating that SFN can diminish ethanol-induced repression of NAIP and XIAP in hNCCs by preventing ethanol-induced hypermethylation at the promoters of NAIP and XIAP.

Knockdown of DNMT3a Significantly Diminished Ethanol-Induced Down-Regulation of NAIP and XIAP and Enhanced the Effects of SFN Against Ethanol-Induced Down-Regulation of NIAP and XIAP in hNCCs

To determine whether the upregulation of DNMT3a contributes to the ethanol-induced down-regulation of NAIP and XIAP, DNMT3a was knocked down by siRNA in hNCCs before

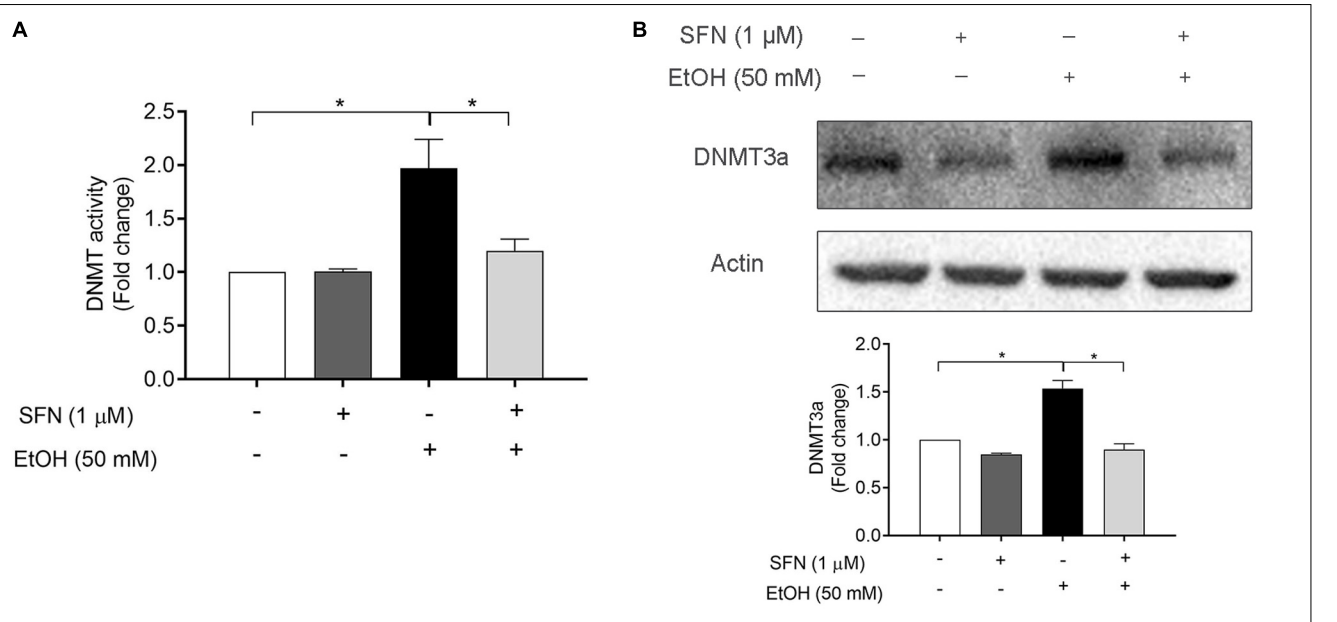

FIGURE 2 | SFN diminished ethanol-induced increase in DNMT activity and the up-regulation of DNMT3a in hNCCs. hNCCs were treated with 1 μM SFN for 24 h, followed by concurrent exposure to 1 μM SFN and 50 mM ethanol for an additional 24 h. **(A)** The DNMT activity was determined by using an EpiQuik DNA Methyltransferase Activity Assay kit. **(B)** The protein expression of DNMT3a was determined by Western blotting. Data are expressed as fold change over control and represent the mean ± SEM of three separated experiments. *$p < 0.05$.

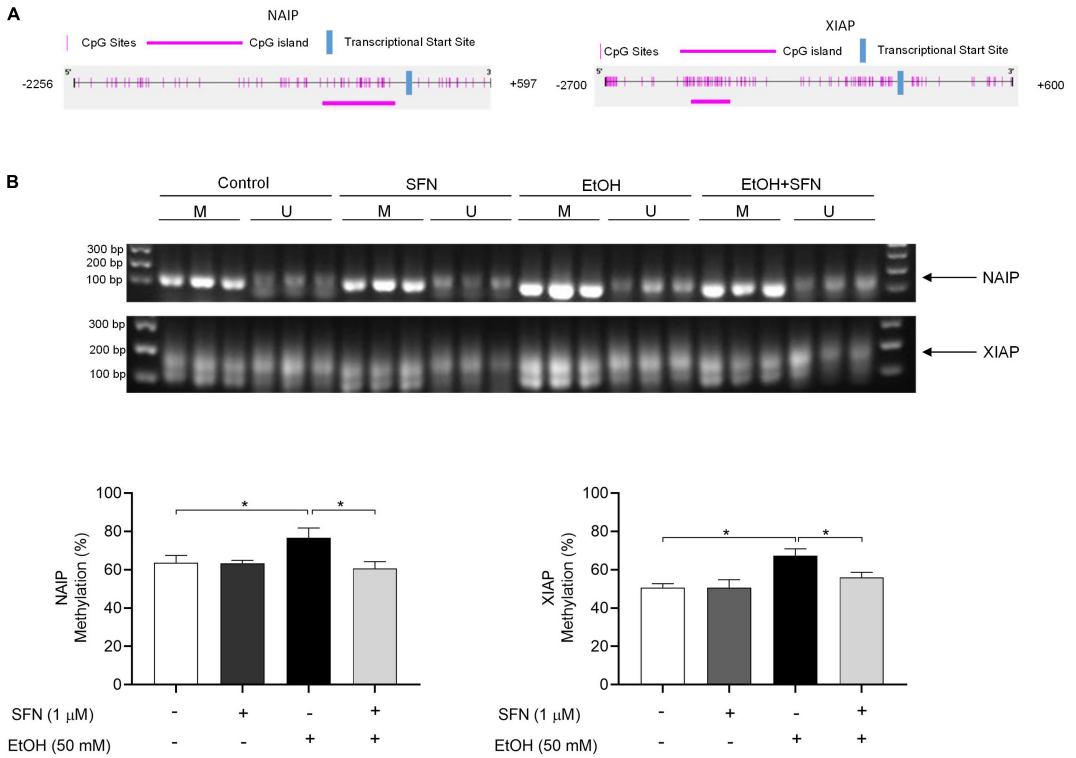

FIGURE 3 | SFN significantly diminished the ethanol-induced hypermethylation at the promoters of XIAP and NAIP in hNCCs. hNCCs were treated with 1 μM SFN for 24 h, followed by concurrent exposure to 1 μM SFN and 50 mM ethanol for an additional 24 h. **(A)** Schematic illustration of the CpG sites and CpG island in the promoters of NAIP and XIAP. The selected CpG island in the NAIP gene promoter is in the region from –634 to –64 bp in the promoter of NAIP. The selected CpG island in the XIAP gene promoter is in the region from –2156 to –1734 bp in the promoter of XIAP. **(B)** DNA methylation status at the CpG island of the promoters of NAIP and XIAP was determined by using MSP. Data are expressed as the percentage of methylation and represent the mean ± SEM of three separated experiments. *$p < 0.05$. M, methylated DNA, U, unmethylated DNA.

treatment with ethanol or/and SFN. We found that the knockdown of DNMT3a significantly diminished ethanol-induced decreases in the mRNA expression of NAIP and XIAP.

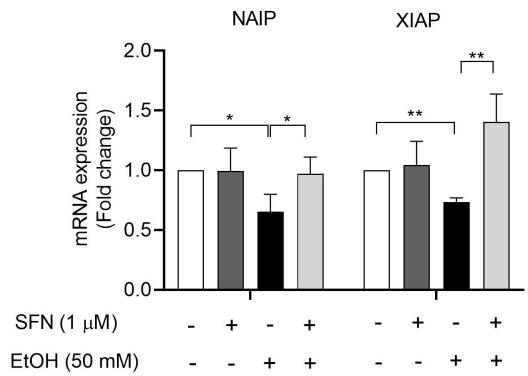

FIGURE 4 | SFN diminished ethanol-induced down-regulation of IAP genes in hNCCs. hNCCs were treated with 1 μM SFN for 24 h, followed by concurrent exposure to 1 μM SFN and 50 mM ethanol for an additional 24 h. The mRNA expression of the NAIP and XIAP was determined by using qRT-PCR. The data were expressed as fold change over control and represent the mean ± SEM of three separated experiments. *$p < 0.05$, **$P < 0.01$.

Down-regulation of DNMT3a by siRNA also enhanced the effects of SFN against ethanol-induced down-regulation of NIAP and XIAP in hNCCs. In addition, knockdown of DNMT3a significantly diminished ethanol-induced decreases in the protein expression of NAIP and XIAPI and significantly enhanced the effects of SFN against ethanol-induced reductions in the protein expression of NAIP and XIAP (**Figure 5**). These results indicate that the down-regulation of DNMT3a and the inhibition of DNMT activity by SFN can diminish ethanol-induced repression of anti-apoptotic genes in hNCCs.

Knockdown of DNMT3a Diminished Ethanol-Induced Apoptosis and Enhanced the Protective Effects of SFN Against Ethanol-Induced Apoptosis in hNCCs

To determine whether ethanol-induced upregulation of DNMT3a and subsequent repression of anti-apoptotic genes, NAIP and XIAP, contributes to ethanol-induced apoptosis and whether SFN can prevent ethanol-induced apoptosis by diminishing ethanol-induced upregulation of DNMT3a, DNMT3a was knocked down by siRNA in hNCCs. Apoptosis was determined by the analysis of caspase-3 activation using

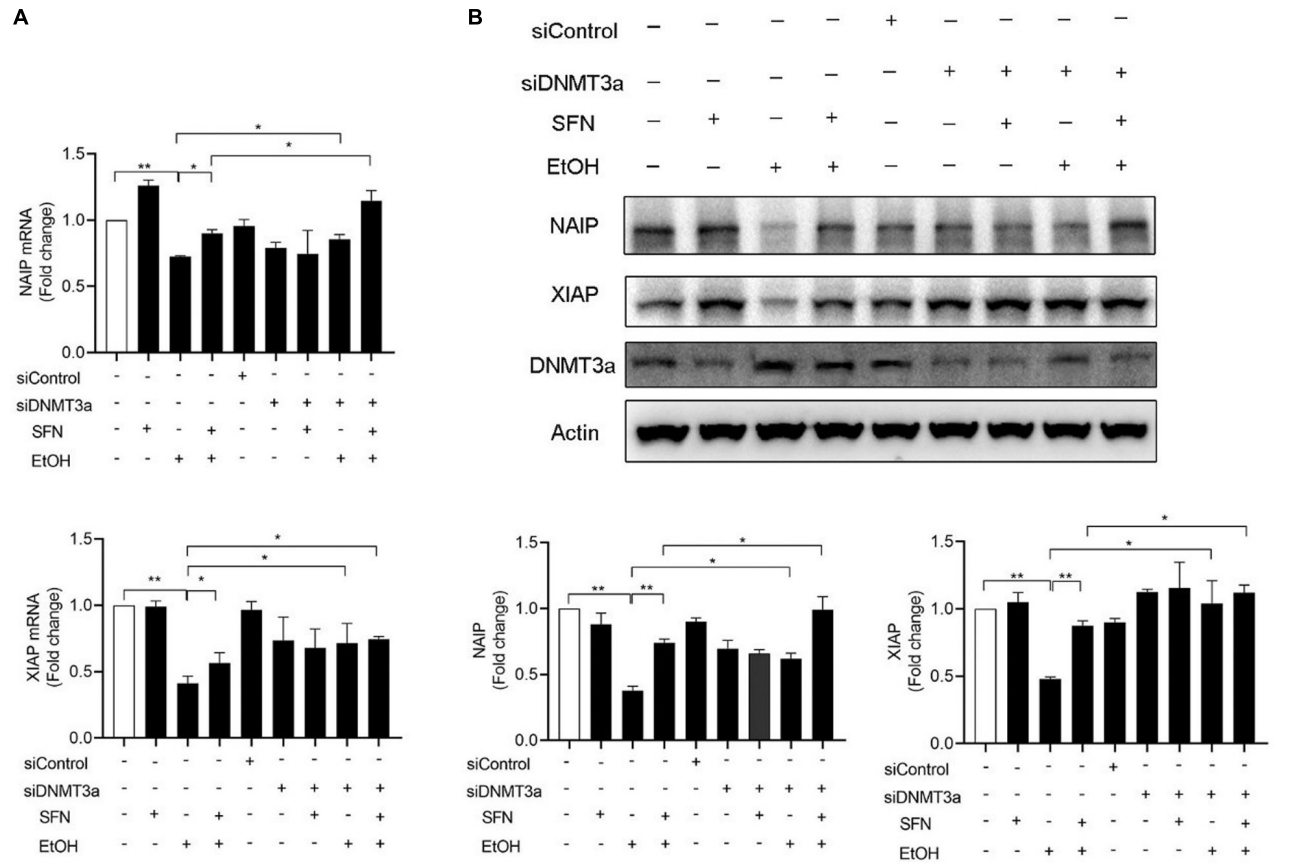

FIGURE 5 | The knockdown of DNMT3a diminished ethanol-induced down-regulation of NAIP and XIAP and enhanced the effects of SFN against ethanol-induced down-regulation of NAIP and XIAP in hNCCs. hNCCs transfected with control-siRNA or DNMT3a-siRNA were treated with 1 μM SFN for 24 h, followed by concurrent exposure to 1 μM SFN and 50 mM ethanol for an additional 24 h. **(A)** The mRNA expression of NAIP and XIAP was determined by qRT-PCR. **(B)** The protein expression of NAIP and XIAP was determined by Western blotting. Data are expressed as fold change over control and represent the mean ± SEM of three separated experiments. $^{*}p < 0.05$, $^{**}p < 0.01$.

Western blot. As shown in **Figure 6A**, the knockdown of DNMT3a by siRNA significantly reduced ethanol-induced caspase-3 activation, indicating that the knockdown of DNMT3a can diminish ethanol-induced apoptosis in hNCCs. These results were further confirmed by the results from the flow cytometric analysis of Annexin V staining, which have clearly shown that knockdown of DNMT3a can significantly reduce the number of early apoptotic cells in ethanol-exposed hNCCs (**Figure 6B**). The knockdown of DNMT3a also significantly enhanced the protective effects of SFN against ethanol-induced apoptosis. These results demonstrate that ethanol-induced upregulation of DNMT3a contributes to ethanol-induced apoptosis and that SFN can prevent ethanol-induced apoptosis in hNCCs by diminishing ethanol-induced upregulation of DNMT3a and reducing the activity of DNMTs.

DISCUSSION

Ethanol-induced apoptosis in NCCs is one of the major mechanisms underlying the pathogenesis of FASD. Previous studies have demonstrated that ethanol exposure during the early stages of development resulted in excessive cell death in NCCs in mouse embryos (Kotch and Sulik, 1992; Dunty et al., 2001). Using an *in vitro* model of mouse NCCs, JoMa1.3, our laboratory has also shown that ethanol exposure significantly increased apoptosis in NCCs (Chen et al., 2015; Li et al., 2019b). In this study, we have shown that exposure to ethanol resulted in a significant increase in apoptosis in hNCCs. This is the first study that demonstrates that ethanol can induce apoptosis in human NCCs.

Apoptosis can be induced and regulated by multiple signaling pathways, including the inhibitor of apoptosis proteins (IAP), a group of negative regulators of apoptosis. IAPs contribute to cell survival by controlling the formation of cell-death-activating platforms, including the apoptosome in Drosophila and the Ripoptosome in mammals, and mediating activation of NF-kB and subsequent induction of pro-survival gene transcription through their ability to functions as E3 ligases (Silke and Meier, 2013). IAPs have been implicated in the pathology of human cancers by inhibiting apoptosis, and the overexpression of IAPs has been found in various cancers (Wright and Duckett, 2005).

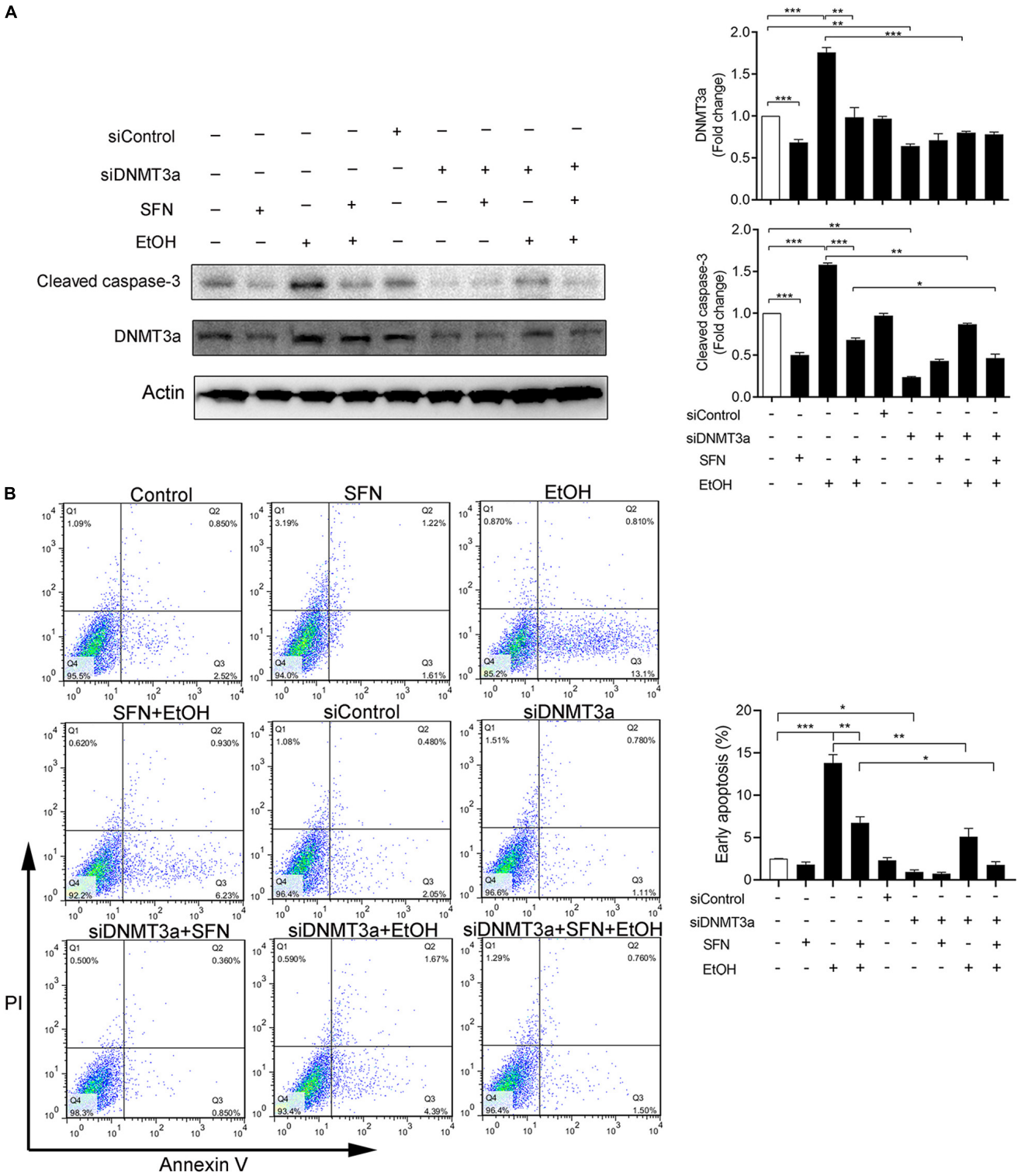

FIGURE 6 | The knockdown of DNMT3a diminished ethanol-induced apoptosis and enhanced the protective effects of SFN in hNCCs. hNCCs transfected with control-siRNA or DNMT3a-siRNA were treated with 1 μM SFN for 24 h, followed by concurrent exposure to 1 μM SFN and 50 mM ethanol for an additional 24 h. The protein expression of DNMT3a was determined by Western blotting **(A)**. Apoptosis was determined by the analysis of caspase-3 cleavage by Western blotting **(A)** or flow cytometry with Annexin V-FITC apoptosis detection kit **(B)**. Data are expressed as fold change over control **(A)** or percentage **(B)** and represent the mean ± SEM of three separated experiments. $^{*}p < 0.05$, $^{**}p < 0.01$, $^{***}p < 0.001$.

Studies have also revealed the importance of IAPs in the adaptive response to cell damages (Marivin et al., 2012). It was reported that XIAP and NIAP are involved in the adaptive response of neuronal cells to hypoxic-ischemia-induced injury (Holcik et al., 2000; Russell et al., 2008; West et al., 2009). The down-regulation of XIAP has also been linked to neurodegenerative disorders, including Wilson's and Huntington's diseases (Goffredo et al., 2005; Weiss et al., 2010). In addition, IAPs were found to be critical for embryonic development. The knockdown of birc5a resulted in multiple defects in the nervous system, the cardiovascular system, and the hematopoietic system (Delvaeye et al., 2009). In this study, we have shown that ethanol exposure can significantly decrease the expression of NAIP and XIAP and induce apoptosis in hNCCs and that SFN treatment that can diminish ethanol-induced down-regulation of NAIP and XIAP can also decrease the ethanol-induced apoptosis in hNCCs, demonstrating that down-regulation of NAIP and XIAP contributes to ethanol-induced apoptosis in hNCCs.

Epigenetic modifications, including DNA methylation and histone modifications, are well-known mechanisms for the regulation of gene expression and are involved in the regulation of many genes associated with various cellular functions, including apoptosis (Boyanapalli and Kong, 2015; Sui et al., 2015; Kang et al., 2019). Studies have shown that epigenetic modifications contribute to the detrimental consequences of alcohol abuse during pregnancy in the developing fetus (Basavarajappa and Subbanna, 2016). Recent studies in our laboratory have demonstrated that ethanol exposure significantly increased apoptosis through decreasing histone acetylation at the promoters of the anti-apoptotic gene, Bcl2 (Yuan et al., 2018). We have also shown that ethanol-induced reduction in the enrichment of trimethylation of histone H3 Lysine 4 (H3K4me3) at the promoters of Snail1 contributes to ethanol-induced apoptosis in NCCs (Li et al., 2019b). In this study, we have shown that ethanol exposure resulted in a significant increase in the methylation levels at the promoters of XIAP and NIAP and decreased the expression of these anti-apoptotic genes in hNCCs. These results indicate that, in addition to histone modification, DNA methylation also contributes to the regulation of the anti-apoptotic genes in ethanol-exposed NCCs.

DNMTs are key enzymes that catalyze the DNA methylation process by transferring a methyl group to DNA (Robertson et al., 1999; Uysal et al., 2015). DNMT3a is the main enzyme involved in DNA methylation in mammals (Singal and Ginder, 1999). It is well-known that DNMT3a plays a critical role in the establishment of methylation patterns during development (Zahnow et al., 2016). In addition, the defect of DNMT3a was reported to result in non-progressive neurodevelopmental conditions (Weissman et al., 2014). Environmental stimuli in pregnant rat have been found to increase DNMT3a expression and alter DNA methylation levels in their offspring (Jensen Pena et al., 2012). A study has also demonstrated that ethanol exposure increased the expression of DNMT3a in rats (Sakharkar et al., 2014). In addition, it has been reported that DNMT3a can regulate the expression of apoptosis-related genes in cancer cells through changing the methylation levels at the promoter regions of the apoptosis-related genes, such as *Bad, Bax and Bcl2* (Jing et al., 2019; Li et al., 2019a; Wei et al., 2019). Consistent with these findings, we found that ethanol exposure significantly increased the expression of DNMT3a in hNCCs. Ethanol exposure also resulted in a significant increase in the activity of DNMT. In addition, knockdown of DNMT3a dramatically diminished ethanol-induced down-regulation of NAIP and XIAP, demonstrating that the ethanol-induced upregulation of DNMT3a contributes to the hypermethylation at the promoters of NAIP and XIAP and the down-regulation of these anti-apoptotic genes in hNCCs exposed to ethanol.

It has been reported that SFN can act as an inhibitor of histone deacetylase (HDAC) and DNMTs to modulate epigenetic modification of genes in varied types of cells (Ali Khan et al., 2015; Su et al., 2018; Yuan et al., 2018). Studies have demonstrated that SFN can suppress the LPS-induced apoptosis in monocyte-derived dendritic cells through down-regulating DNMT3a and the suppression of TGF-β signaling (Qu et al., 2015). Recent studies from our laboratory have also demonstrated that SFN can reduce ethanol-induced apoptosis in NCCs by diminishing ethanol-induced reduction of histone acetylation at the promoter of Bcl2 and preventing the down-regulation of Bcl2 in ethanol-exposed NCCs (Yuan et al., 2018). In the present study, we found that SFN treatment diminished ethanol-induced upregulation of DNMT3a and dramatically reduce the activity of DNMTs in ethanol-exposed hNCCs. Treatment with SFN also diminished the ethanol-induced hypermethylation at the promoters of NAIP and XIAP and the down-regulation of NAIP and XIAP and subsequently reduced ethanol-induced apoptosis in hNCCs. These results demonstrate that SFN can prevent ethanol-induced apoptosis in hNCCs by epigenetically modulating the DNA methylation at the promoters of anti-apoptotic genes.

In conclusion, the present study has demonstrated that SFN treatment diminished the ethanol-induced upregulation of DNMT3a and dramatically reduced the activity of DNMTs in ethanol-exposed hNCCs. We also found that ethanol exposure induced hypermethylation at the promoter regions of NAIP and XIAP, which were prevented by co-treatment with SFN. SFN also diminished ethanol-induced down-regulation of NAIP and XIAP and apoptosis in hNCCs. The knockdown of DNMT3a significantly enhanced the effects of SFN on preventing the ethanol induced repression of NAIP and XIAP and apoptosis in hNCCs. These results demonstrate that ethanol-induced upregulation of DNMT3a and the hypermethylation at the promoters of NAIP and XIAP and subsequent down-regulation of NAIP and XIAP contribute to ethanol-induced apoptosis in hNCCs and that SFN can prevent ethanol-induced apoptosis in hNCCs by preventing ethanol-induced hypermethylation at the promoters of the genes encoding the IAP proteins. These findings suggest that SFN may represent a promising and effective agent for the prevention of ethanol-induced apoptosis and FASD.

DATA AVAILABILITY STATEMENT

All datasets generated in this study are included in the article.

AUTHOR CONTRIBUTIONS

YL and S-YC conceptualized and designed the experiments and participated in data interpretation and manuscript preparation. YL, HF, and JL performed the experiments and participated in data analysis. FY, LL, WF, and H-GZ participated in data interpretation and discussion. All authors reviewed the manuscript.

FUNDING

This work was supported by the National Institutes of Health Grants AA028435, AA021434, AA024337 (S-YC), and AA023190 (WF) from the National Institute on Alcohol Abuse and Alcoholism. H-GZ was supported by a Research Career Scientist (RCS) award.

REFERENCES

Ali Khan, M., Kedhari Sundaram, M., Hamza, A., Quraishi, U., Gunasekera, D., Ramesh, L., et al. (2015). Sulforaphane reverses the expression of various tumor suppressor genes by targeting DNMT3B and HDAC1 in human cervical cancer cells. *Evid. Based Complement. Alternat. Med.* 2015:412149. doi: 10.1155/2015/412149

Avery, J., and Dalton, S. (2016). Methods for derivation of multipotent neural crest cells derived from human pluripotent stem cells. *Methods Mol. Biol.* 1341, 197–208. doi: 10.1007/7651_2015_234

Basavarajappa, B. S., and Subbanna, S. (2016). Epigenetic mechanisms in developmental alcohol-induced neurobehavioral deficits. *Brain Sci.* 6:12. doi: 10.3390/brainsci6020012

Bekdash, R. A., Zhang, C., and Sarkar, D. K. (2013). Gestational choline supplementation normalized fetal alcohol-induced alterations in histone modifications, DNA methylation, and proopiomelanocortin (POMC) gene expression in beta-endorphin-producing POMC neurons of the hypothalamus. *Alcohol Clin. Exp. Res.* 37, 1133–1142. doi: 10.1111/acer.12082

Birnbaum, M. J., Clem, R. J., and Miller, L. K. (1994). An apoptosis-inhibiting gene from a nuclear polyhedrosis virus encoding a polypeptide with Cys/His sequence motifs. *J. Virol.* 68, 2521–2528. doi: 10.1128/jvi.68.4.2521-2528.1994

Boyanapalli, S. S., and Kong, A. T. (2015). "Curcumin, the King of Spices": epigenetic regulatory mechanisms in the prevention of cancer, neurological, and inflammatory diseases. *Curr. Pharmacol. Rep.* 1, 129–139. doi: 10.1007/s40495-015-0018-x

Cartwright, M. M., and Smith, S. M. (1995). Increased cell death and reduced neural crest cell numbers in ethanol-exposed embryos: partial basis for the fetal alcohol syndrome phenotype. *Alcohol Clin. Exp. Res.* 19, 378–386. doi: 10.1111/j.1530-0277.1995.tb01519.x

Chen, T., Ueda, Y., Dodge, J. E., Wang, Z., and Li, E. (2003). Establishment and maintenance of genomic methylation patterns in mouse embryonic stem cells by Dnmt3a and Dnmt3b. *Mol. Cell. Biol.* 23, 5594–5605. doi: 10.1128/mcb.23.16.5594-5605.2003

Chen, X., Liu, J., and Chen, S. Y. (2013). Sulforaphane protects against ethanol-induced oxidative stress and apoptosis in neural crest cells by the induction of Nrf2-mediated antioxidant response. *Br. J. Pharmacol.* 169, 437–448. doi: 10.1111/bph.12133

Chen, X., Liu, J., Feng, W. K., Wu, X., and Chen, S. Y. (2015). MiR-125b protects against ethanol-induced apoptosis in neural crest cells and mouse embryos by targeting Bak 1 and PUMA. *Exp. Neurol.* 271, 104–111. doi: 10.1016/j.expneurol.2015.04.026

Delvaeye, M., De Vriese, A., Zwerts, F., Betz, I., Moons, M., Autiero, M., et al. (2009). Role of the 2 zebrafish survivin genes in vasculo-angiogenesis, neurogenesis, cardiogenesis and hematopoiesis. *BMC Dev. Biol.* 9:25. doi: 10.1186/1471-213X-9-25

Dunty, W. C. Jr., Chen, S. Y., Zucker, R. M., Dehart, D. B., and Sulik, K. K. (2001). Selective vulnerability of embryonic cell populations to ethanol-induced apoptosis: implications for alcohol-related birth defects and neurodevelopmental disorder. *Alcohol Clin. Exp. Res.* 25, 1523–1535. doi: 10.1111/j.1530-0277.2001.tb02156.x

Fan, H., Yuan, F., Yun, Y., Wu, T., Lu, L., Liu, J., et al. (2019). MicroRNA-34a mediates ethanol-induced impairment of neural differentiation of neural crest cells by targeting autophagy-related gene 9a. *Exp. Neurol.* 320:112981. doi: 10.1016/j.expneurol.2019.112981

Garro, A. J., McBeth, D. L., Lima, V., and Lieber, C. S. (1991). Ethanol consumption inhibits fetal DNA methylation in mice: implications for the fetal alcohol syndrome. *Alcohol Clin. Exp. Res.* 15, 395–398. doi: 10.1111/j.1530-0277.1991.tb00536.x

Goffredo, D., Rigamonti, D., Zuccato, C., Tartari, M., Valenza, M., and Cattaneo, E. (2005). Prevention of cytosolic IAPs degradation: a potential pharmacological target in Huntington's Disease. *Pharmacol. Res.* 52, 140–150. doi: 10.1016/j.phrs.2005.01.006

Gopisetty, G., Ramachandran, K., and Singal, R. (2006). DNA methylation and apoptosis. *Mol. Immunol.* 43, 1729–1740. doi: 10.1016/j.molimm.2005.11.010

Harada, K., Toyooka, S., Shivapurkar, N., Maitra, A., Reddy, J. L., Matta, H., et al. (2002). Deregulation of caspase 8 and 10 expression in pediatric tumors and cell lines. *Cancer Res.* 62, 5897–5901.

Haycock, P. C., and Ramsay, M. (2009). Exposure of mouse embryos to ethanol during preimplantation development: effect on DNA methylation in the h19 imprinting control region. *Biol. Reprod.* 81, 618–627. doi: 10.1095/biolreprod.108.074682

Hervouet, E., Cheray, M., Vallette, F. M., and Cartron, P. F. (2013). DNA methylation and apoptosis resistance in cancer cells. *Cells* 2, 545–573. doi: 10.3390/cells2030545

Hervouet, E., Vallette, F. M., and Cartron, P. F. (2010). Impact of the DNA methyltransferases expression on the methylation status of apoptosis-associated genes in glioblastoma multiforme. *Cell Death Dis.* 1:e8. doi: 10.1038/cddis.2009.7

Holcik, M., Thompson, C. S., Yaraghi, Z., Lefebvre, C. A., MacKenzie, A. E., and Korneluk, R. G. (2000). The hippocampal neurons of neuronal apoptosis inhibitory protein 1 (NAIP1)-deleted mice display increased vulnerability to kainic acid-induced injury. *Proc. Natl. Acad. Sci. U.S.A.* 97, 2286–2290. doi: 10.1073/pnas.040469797

Jensen Pena, C., Monk, C., and Champagne, F. A. (2012). Epigenetic effects of prenatal stress on 11beta-hydroxysteroid dehydrogenase-2 in the placenta and fetal brain. *PLoS One* 7:e39791. doi: 10.1371/journal.pone.0039791

Jing, W., Song, N., Liu, Y. P., Qu, X. J., Qi, Y. F., Li, C., et al. (2019). DNMT3a promotes proliferation by activating the STAT3 signaling pathway and depressing apoptosis in pancreatic cancer. *Cancer Manag. Res.* 11, 6379–6396. doi: 10.2147/CMAR.S201610

Jones, P. A., and Baylin, S. B. (2002). The fundamental role of epigenetic events in cancer. *Nat. Rev. Genet.* 3, 415–428. doi: 10.1038/nrg816

Jones, P. A., and Liang, G. (2009a). Rethinking how DNA methylation patterns are maintained. *Nat. Rev. Genet.* 10, 805–811.

Jones, P. A., and Liang, G. N. (2009b). OPINION Rethinking how DNA methylation patterns are maintained. *Nat. Rev. Genet.* 10, 805–811. doi: 10.1038/nrg2651

Kang, K. A., Piao, M. J., Hyun, Y. J., Zhen, A. X., Cho, S. J., Ahn, M. J., et al. (2019). Luteolin promotes apoptotic cell death via upregulation of Nrf2 expression by DNA demethylase and the interaction of Nrf2 with p53 in human colon cancer cells. *Exp. Mol. Med.* 51, 1–14. doi: 10.1038/s12276-019-0238-y

Koren, G., Nulman, I., Chudley, A. E., and Loocke, C. (2003). Fetal alcohol spectrum disorder. *CMAJ* 169, 1181–1185.

Kotch, L. E., and Sulik, K. K. (1992). Patterns of ethanol-induced cell death in the developing nervous system of mice; neural fold states through the time of

anterior neural tube closure. *Int. J. Dev. Neurosci.* 10, 273–279. doi: 10.1016/0736-5748(92)90016-s

Leonhardt, H., and Bestor, T. H. (1993). Structure, function and regulation of mammalian DNA methyltransferase. *EXS* 64, 109–119. doi: 10.1007/978-3-0348-9118-9_5

Li, J., Su, X., Dai, L., Chen, N., Fang, C., Dong, Z., et al. (2019a). Temporal DNA methylation pattern and targeted therapy in colitis-associated cancer. *Carcinogenesis* 41, 235–244. doi: 10.1093/carcin/bgz199

Li, Y., Yuan, F., Wu, T., Lu, L., Liu, J., Feng, W., et al. (2019b). Sulforaphane protects against ethanol-induced apoptosis in neural crest cells through restoring epithelial-mesenchymal transition by epigenetically modulating the expression of Snail1. *Biochim. Biophys. Acta Mol. Basis Dis.* 1865, 2586–2594. doi: 10.1016/j.bbadis.2019.07.002

Malekzadeh, K., Sobti, R. C., Nikbakht, M., Shekari, M., Hosseini, S. A., Tamandani, D. K., et al. (2009). Methylation patterns of Rb1 and Casp-8 promoters and their impact on their expression in bladder cancer. *Cancer Invest.* 27, 70–80. doi: 10.1080/07357900802172085

Marivin, A., Berthelet, J., Plenchette, S., and Dubrez, L. (2012). The inhibitor of apoptosis (IAPs) in adaptive response to cellular stress. *Cells* 1, 711–737. doi: 10.3390/cells1040711

Meeran, S. M., Patel, S. N., Li, Y., Shukla, S., and Tollefsbol, T. O. (2012). Bioactive dietary supplements reactivate ER expression in ER-negative breast cancer cells by active chromatin modifications. *PLoS One* 7:e37748. doi: 10.1371/journal.pone.0037748

Menendez, L., Kulik, M. J., Page, A. T., Park, S. S., Lauderdale, J. D., Cunningham, M. L., et al. (2013). Directed differentiation of human pluripotent cells to neural crest stem cells. *Nat. Protoc.* 8, 203–212. doi: 10.1038/nprot.2012.156

Murphy, T. M., Perry, A. S., and Lawler, M. (2008). The emergence of DNA methylation as a key modulator of aberrant cell death in prostate cancer. *Endocr. Relat. Cancer* 15, 11–25. doi: 10.1677/Erc-07-0208

Ouko, L. A., Shantikumar, K., Knezovich, J., Haycock, P., Schnugh, D. J., and Ramsay, M. (2009). Effect of alcohol consumption on CpG methylation in the differentially methylated regions of H19 and IG-DMR in male gametes: implications for fetal alcohol spectrum disorders. *Alcohol Clin. Exp. Res.* 33, 1615–1627. doi: 10.1111/j.1530-0277.2009.00993.x

Qu, X. Q., Proll, M., Neuhoff, C., Zhang, R., Cinar, M. U., Hossain, M. M., et al. (2015). Sulforaphane epigenetically regulates innate immune responses of porcine monocyte-derived dendritic cells induced with lipopolysaccharide. *PLoS One* 10:e0121574. doi: 10.1371/journal.pone.0121574

Robertson, K. D., Uzvolgyi, E., Liang, G., Talmadge, C., Sumegi, J., Gonzales, F. A., et al. (1999). The human DNA methyltransferases (DNMTs) 1, 3a and 3b: coordinate mRNA expression in normal tissues and overexpression in tumors. *Nucleic Acids Res.* 27, 2291–2298. doi: 10.1093/nar/27.11.2291

Russell, J. C., Whiting, H., Szuflita, N., and Hossain, M. A. (2008). Nuclear translocation of X-linked inhibitor of apoptosis (XIAP) determines cell fate after hypoxia ischemia in neonatal brain. *J. Neurochem.* 106, 1357–1370. doi: 10.1111/j.1471-4159.2008.05482.x

Sakharkar, A. J., Tang, L., Zhang, H., Chen, Y., Grayson, D. R., and Pandey, S. C. (2014). Effects of acute ethanol exposure on anxiety measures and epigenetic modifiers in the extended amygdala of adolescent rats. *Int. J. Neuropsychopharmacol.* 17, 2057–2067. doi: 10.1017/S1461145714001047

Shivapurkar, N., Toyooka, S., Eby, M. T., Huang, C. X., Sathyanarayana, U. G., Cunningham, H. T., et al. (2002). Differential inactivation of caspase-8 in lung cancers. *Cancer Biol. Ther.* 1, 65–69. doi: 10.4161/cbt.1.1.45

Silke, J., and Meier, P. (2013). Inhibitor of apoptosis (IAP) proteins-modulators of cell death and inflammation. *Cold Spring Harb. Perspect. Biol.* 5:a008730. doi: 10.1101/cshperspect.a008730

Singal, R., and Ginder, G. D. (1999). DNA methylation. *Blood* 93, 4059–4070.

Sokol, R. J., Delaney-Black, V., and Nordstrom, B. (2003). Fetal alcohol spectrum disorder. *JAMA* 290, 2996–2999. doi: 10.1001/jama.290.22.2996

Su, X., Jiang, X., Meng, L., Dong, X., Shen, Y., and Xin, Y. (2018). Anticancer activity of sulforaphane: the epigenetic mechanisms and the Nrf2 signaling pathway. *Oxid. Med. Cell. Longev.* 2018:5438179. doi: 10.1155/2018/5438179

Subbanna, S., Nagre, N. N., Umapathy, N. S., Pace, B. S., and Basavarajappa, B. S. (2014). Ethanol exposure induces neonatal neurodegeneration by enhancing CB1R Exon1 histone H4K8 acetylation and up-regulating CB1R function causing neurobehavioral abnormalities in adult mice. *Int. J. Neuropsychopharmacol.* 18:yu028. doi: 10.1093/ijnp/pyu028

Subbanna, S., Shivakumar, M., Umapathy, N. S., Saito, M., Mohan, P. S., Kumar, A., et al. (2013). G9a-mediated histone methylation regulates ethanol-induced neurodegeneration in the neonatal mouse brain. *Neurobiol. Dis.* 54, 475–485. doi: 10.1016/j.nbd.2013.01.022

Sui, X., Zhu, J., Zhou, J., Wang, X., Li, D., Han, W., et al. (2015). Epigenetic modifications as regulatory elements of autophagy in cancer. *Cancer Lett.* 360, 106–113. doi: 10.1016/j.canlet.2015.02.009

Sun, H., Chen, X., Yuan, F., Liu, J., Zhao, Y., and Chen, S. Y. (2014). Involvement of seven in absentia homolog-1 in ethanol-induced apoptosis in neural crest cells. *Neurotoxicol. Teratol.* 46, 26–31. doi: 10.1016/j.ntt.2014.08.006

Teodoridis, J. M., Strathdee, G., and Brown, R. (2004). Epigenetic silencing mediated by CpG island methylation: potential as a therapeutic target and as a biomarker. *Drug Resist. Updat.* 7, 267–278. doi: 10.1016/j.drup.2004.06.005

Uysal, F., Akkoyunlu, G., and Ozturk, S. (2015). Dynamic expression of DNA methyltransferases (DNMTs) in oocytes and early embryos. *Biochimie* 116, 103–113. doi: 10.1016/j.biochi.2015.06.019

Wei, D., Yu, G., and Zhao, Y. (2019). MicroRNA-30a-3p inhibits the progression of lung cancer via the PI3K/AKT by targeting DNA methyltransferase 3a. *Onco. Targets Ther.* 12, 7015–7024. doi: 10.2147/OTT.S213583

Weiss, K. H., Runz, H., Noe, B., Gotthardt, D. N., Merle, U., Ferenci, P., et al. (2010). Genetic analysis of BIRC4/XIAP as a putative modifier gene of Wilson disease. *J. Inherit. Metab. Dis.* 33(Suppl. 3), S233–S240. doi: 10.1007/s10545-010-9123-5

Weissman, J., Naidu, S., and Bjornsson, H. T. (2014). Abnormalities of the DNA methylation mark and its machinery: an emerging cause of neurologic dysfunction. *Semin. Neurol.* 34, 249–257. doi: 10.1055/s-0034-1386763

West, T., Stump, M., Lodygensky, G., Neil, J. J., Deshmukh, M., and Holtzman, D. M. (2009). Lack of X-linked inhibitor of apoptosis protein leads to increased apoptosis and tissue loss following neonatal brain injury. *ASN Neuro.* 1:e00004. doi: 10.1042/AN20090005

Wright, C. W., and Duckett, C. S. (2005). Reawakening the cellular death program in neoplasia through the therapeutic blockade of IAP function. *J. Clin. Invest.* 115, 2673–2678. doi: 10.1172/JCI26251

Wu, Y., Alvarez, M., Slamon, D. J., Koeffler, P., and Vadgama, J. V. (2010). Caspase 8 and maspin are downregulated in breast cancer cells due to CpG site promoter methylation. *BMC Cancer* 10:32. doi: 10.1186/1471-2407-10-32

Yan, D., Dong, J., Sulik, K. K., and Chen, S. Y. (2010). Induction of the Nrf2-driven antioxidant response by tert-butylhydroquinone prevents ethanol-induced apoptosis in cranial neural crest cells. *Biochem. Pharmacol.* 80, 144–149. doi: 10.1016/j.bcp.2010.03.004

Yuan, F., Chen, X., Liu, J., Feng, W., Cai, L., Wu, X., et al. (2018). Sulforaphane restores acetyl-histone H3 binding to Bcl-2 promoter and prevents apoptosis in ethanol-exposed neural crest cells and mouse embryos. *Exp. Neurol.* 300, 60–66. doi: 10.1016/j.expneurol.2017.10.020

Yuan, F., Chen, X., Liu, J., Feng, W., Wu, X., and Chen, S. Y. (2017). Up-regulation of Siah1 by ethanol triggers apoptosis in neural crest cells through p38 MAPK-mediated activation of p53 signaling pathway. *Arch. Toxicol.* 91, 775–784. doi: 10.1007/s00204-016-1746-3

Yuan, F., Yun, Y., Fan, H., Li, Y., Lu, L., Liu, J., et al. (2020). MicroRNA-135a protects against ethanol-induced apoptosis in neural crest cells and craniofacial defects in zebrafish by modulating the siah1/p38/p53 pathway. *Front. Cell Dev. Biol.* 8:1058.

Zahnow, C. A., Topper, M., Stone, M., Murray-Stewart, T., Li, H., Baylin, S. B., et al. (2016). Inhibitors of DNA methylation, histone deacetylation, and histone

demethylation: a perfect combination for cancer therapy. *Adv. Cancer Res.* 130, 55–111. doi: 10.1016/bs.acr.2016.01.007

Zhong, L., Zhu, J., Lv, T., Chen, G., Sun, H., Yang, X., et al. (2010). Ethanol and its metabolites induce histone lysine 9 acetylation and an alteration of the expression of heart development-related genes in cardiac progenitor cells. *Cardiovasc. Toxicol.* 10, 268–274. doi: 10.1007/s12012-010-9081-z

Zhou, F. C., Balaraman, Y., Teng, M., Liu, Y., Singh, R. P., and Nephew, K. P. (2011). Alcohol alters DNA methylation patterns and inhibits neural stem cell differentiation. *Alcohol Clin. Exp. Res.* 35, 735–746. doi: 10.1111/j.1530-0277.2010.01391.x

Conflict of Interest: The authors declare that the research was conducted in the absence of any commercial or financial relationships that could be construed as a potential conflict of interest.

frontiers in Cell and Developmental Biology

ORIGINAL RESEARCH
published: 15 February 2021
doi: 10.3389/fcell.2021.626224

Hypoxia-Responsive Oxygen Nanobubbles for Tissues-Targeted Delivery in Developing Tooth Germs

Eun-Jung Kim[1†], Ji-Eun Lee[1†], Semi Yoon[2], Dong-Joon Lee[1], Han Ngoc Mai[1], Hiroko Ida-Yonemochi[3], Jonghoon Choi[2] and Han-Sung Jung[1*]*

[1] Division in Anatomy and Developmental Biology, Department of Oral Biology, Taste Research Center, Oral Science Research Center, BK21 FOUR Project, Yonsei University College of Dentistry, Seoul, South Korea, [2] School of Integrative Engineering, Chung-Ang University, Seoul, South Korea, [3] Division of Anatomy and Cell Biology of the Hard Tissue, Department of Tissue Regeneration and Reconstruction, Niigata University Graduate School of Medical and Dental Sciences, Niigata, Japan

OPEN ACCESS

Edited by:
Wolfgang Knabe, Universität Münster, Germany

Reviewed by:
Sanjiv Neupane, Stony Brook University, United States
Paul Sharpe, King's College London, United Kingdom

***Correspondence:**
Han-Sung Jung
hsj8076@gmail.com
Jonghoon Choi
nanomed@cau.ac.kr

[†] *These authors have contributed equally to this work*

Specialty section:
This article was submitted to Cell Death and Survival, a section of the journal Frontiers in Cell and Developmental Biology

Received: *05 November 2020*
Accepted: *12 January 2021*
Published: *15 February 2021*

Citation:
Kim E-J, Lee J-E, Yoon S, Lee D-J, Mai HN, Ida-Yonemochi H, Choi J and Jung H-S (2021) Hypoxia-Responsive Oxygen Nanobubbles for Tissues-Targeted Delivery in Developing Tooth Germs. Front. Cell Dev. Biol. 9:626224. doi: 10.3389/fcell.2021.626224

Hypoxia is a state of inadequate supply of oxygen. Increasing evidence indicates that a hypoxic environment is strongly associated with abnormal organ development. Oxygen nanobubbles (ONBs) are newly developed nanomaterials that can deliver oxygen to developing tissues, including hypoxic cells. However, the mechanisms through which nanobubbles recover hypoxic tissues, such as developing tooth germs remain to be identified. In this study, tooth germs were cultured in various conditions: CO_2 chamber, hypoxic chamber, and with 20% ONBs for 3 h. The target stages were at the cap stage (all soft tissue) and bell stage (hard tissue starts to form). Hypoxic tooth germs were recovered with 20% ONBs in the media, similar to the tooth germs incubated in a CO_2 chamber (normoxic condition). The tooth germs under hypoxic conditions underwent apoptosis both at the cap and bell stages, and ONBs rescued the damaged tooth germs in both the cap and bell stages. Using kidney transplantation for hard tissue formation *in vivo*, amelogenesis and dentinogenesis imperfecta in hypoxic conditions at the bell stage were rescued with ONBs. Furthermore, glucose uptake by tooth germs was highly upregulated under hypoxic conditions, and was restored with ONBs to normoxia levels. Our findings indicate that the strategies to make use of ONBs for efficient oxygen targeted delivery can restore cellular processes, such as cell proliferation and apoptosis, glucose uptake, and hypomineralization in hypoxic environments.

Keywords: tooth, hypomineralization, hypoxia, oxygen nanobubble, apoptosis, proliferation, metabolism

INTRODUCTION

Tooth development is a complex process mediated through a series of signals between two adjacent tissues, the epithelium, and the underlying mesenchyme (Kim et al., 2008). Mammalian teeth form via morphogenesis of individual tooth germs, which begin as dental placodes in the embryonic oral ectoderm and sequentially pass through the bud, cap, and bell stages (Kwon et al., 2015). During morphogenesis, the epithelium is called enamel organ, which consists of the inner enamel epithelium and differentiating to enamel producing ameloblasts, the outer enamel epithelium and the stellate reticulum and stratum intermedium cells (Jussila and Thesleff, 2012). The growth and folding of the inner enamel epithelium during the bell stage determine the size and shape of the tooth crown (Yu and Klein, 2020). The shape is fixed when the organic matrix of dentin and enamel

mineralize because dentin or enamel does not remodels later (Lesot and Brook, 2009).

Signals from the dental epithelium first induce the differentiation of underlying mesenchymal cells into odontoblasts (Jussila and Thesleff, 2012). The odontoblasts deposit dentin matrix and signal back to the epithelium, inducing differentiation of epithelial cells into functional ameloblasts (Karcher-Djuricic et al., 1985). Odontoblasts are responsible for the formation of dentin and pre-dentin, which is an immature mineralized tissue (Smith and Nanci, 1995). Enamel development and mineralization is a complex process that tightly regulates ameloblasts.

Enamel or dentin formation are affected by several factors, and the changes induced during enamel or dentin formation impact the enamel or dentin (Heijs et al., 2007; Padavala and Sukumaran, 2018). Developmental defects of the enamel and dentin occur in rare genetic disorders, and are termed amelogenesis imperfecta (AI) or dentinogenesis imperfecta (DGI) (Barron et al., 2008). AI describes a group of genetic conditions that result in defects in the formation of the tooth enamel. Mutations in many genes including amelogenin (AmelX for female and AMELY for males), enamelin (ENAM), and ameloblastin (Ambn), are known to cause AI, and affect the proteins secreted by enamel secreting cells, ameloblasts (Smith and Nanci, 1995; Smith et al., 2017). AI has been broadly classified into hypoplastic and hypomineralized types (Gadhia et al., 2012). Dentine encloses the dental pulp and is surrounded by the enamel. DGI and dentine dysplasia (DD) include a group of autosomal dominant genetic conditions characterized by abnormal dentine structures (Barron et al., 2008). DGI type I is inherited by osteogenesis imperfecta and recent genetic studies suggest that involvement of mutations in the genes encoding collagen type 1, COL1A1, and COL1A2. All other forms of DGI, appear to result from mutations in the gene encoding dentine sialophosphoprotein (DSPP), suggesting that these conditions are allelic. Demarcated enamel opacities that affect one or more permanent first molars, and frequently also incisors, can occur in teeth. This condition is referred to molar-incisor hypomineralization (MIH) (Alaluusua, 2010; Garg et al., 2012; Sidaly et al., 2015; Lee et al., 2020). Hypoxia has been suggested as a possible etiological factor of MIH. Although the occurrence of MIH in humans does not impact survival, it can have aesthetic effects, and cause dental defects. However, the etiology of hypomineralization during enamel or dentin formation is not fully understood.

Oxygen is the most critical molecule for survival of most organisms (Sitkovsky et al., 2004). Hypoxia is a condition of insufficient supply of oxygen to cells and tissues. Hypoxia inducible factor 1 (HIF-1α), a key regulator of hypoxia response, has complex roles. HIF-1α can induce apoptosis, prevent cell proliferation, or even stimulate cell proliferation. The severity of hypoxia determines whether cells become apoptotic or adapt to hypoxia and survive (Greijer and van der Wall, 2004; Guo, 2017).

HIF-1α initiates apoptosis by inducing high concentrations of pro-apoptotic proteins, and causes stabilization of p53 (Greijer and van der Wall, 2004). p53 plays a critical role in inducing cell cycle arrest or apoptosis (Nakamizo et al., 2008). Under normal conditions, p53 remains inactive due to its rapid degradation by the ubiquitin ligase, Mdm2 (Marine and Lozano, 2010). However, upon cellular stress, such as in hypoxic conditions, p53 becomes phosphorylated resulting in inhibition of Mdm2-mediated degradation and accumulation of transcriptionally active p53, which activates several targets including cell cycle inhibitors and pro-apoptotic proteins resulting in apoptosis or proliferation arrest (Yan et al., 2009; Sadagopan et al., 2012). Furthermore, caspases play an essential role in apoptosis (Guo, 2017). p53 and other signaling pathways lead to caspase activation, including caspase-3, that cleaves essential cellular proteins and causes apoptosis (Speidel, 2010). On the other hand, regulation by HIF-1α is closely related to energy metabolism (Rastogi et al., 2007). In response to hypoxia, cells increase glucose uptake by upregulating membranous expression of glucose transporter-1 (GLUT-1) (Malhotra and Brosius, 1999). Facilitating GLUT-1 can reduce hypoxia-induced apoptosis due to the protective role of glycolysis of glucose. During tooth development, glucose uptake mediated in GLUT-1 is essential for early tooth morphogenesis and size determination of murine molars (Ida-Yonemochi et al., 2012). However, the mechanisms through which HIF-1α, induced by hypoxic conditions, regulates tooth development and mineralization by cellular events, such as proliferation, cell apoptosis and metabolism has not been studied.

Oxygen nanobubble (ONB) is a newly developed material, which can deliver acceptable oxygen to developing tissues, including hypoxic cells (Bhandari et al., 2017; Khan et al., 2018). ONBs consist of a phospholipid hydrophilic shell with oxygen gas inside (Bhandari et al., 2017; Khan et al., 2018). ONBs release oxygen via a diffusion mechanism, as phospholipids are permeable to gas (Bhandari et al., 2017; Khan et al., 2018). ONBs released ∼500 μg/mL more oxygen (Bhandari et al., 2017; Khan et al., 2018). It has been demonstrated that ONBs reverse hypoxia and suppress HIF-1α activity in tumor cells (Khan et al., 2018). This study aimed to investigate whether oxygen delivery into developing tooth germs via ONBs improves the hypoxic condition, and understand how the mineralization of enamel and dentin can be regulated using ONBs. A new hypoxia-based strategy for regenerative approaches in the dental field is presented.

MATERIALS AND METHODS

All experiments were performed according to the guidelines of the Yonsei University College of Dentistry, Intramural Animal Use and Care Committee (2019-0306).

Animals

Adult ICR mice (purchased from Koatech Co, Pyeongtaek, Korea) were housed in a temperature-controlled room (22°C) under artificial lighting (lights on from 05:00 to 17:00) and 55% relative humidity with access to food and water *ad libitum*. Embryos were obtained from time-mated pregnant mice. E0 was designated as the day on which the presence of a vaginal plug was confirmed. Embryos from each developmental stage (E13 for cap stage, and E16 for bell stage) were used in this study.

Preparation of Oxygen Nanobubbles (ONBs)

The ONBs were prepared by following the method reported previously (Khan et al., 2018, 2019, 2020). The mixture of DSPC and DSPE-PEG-Amine was added to a 3-neck-flask that the molar ratio of the solution was to become DSPC: DSPE-PEG-Amine = 85:15. The solution of DSPC and DSPE-PEG-Amine was then introduced to an oven set at 70°C for 2 h to remove a chloroform in the solution. Next, the 10 mL of DPBS was added to the completely dried mixture to resuspend the solute. The redissolved solution was sonicated for 10 min at 60°C that was above the transition temperature (i.e., 55°C) of DSPC and DSPE-PEG-Amine. At the same time, the solution was bubbled with an oxygen gas for 3 min. While supplying an oxygen gas to the mixture, a tip sonication was carried out to decrease the size of bubbles (on/off for 2 s each, for 5 min total, at 25°C). After the sample was filtered through a 1 μm PTFE syringe filter, it was stored in a refrigerator at 4°C before the experiments. ONB samples of other compositions were also produced in the same way as described above.

In vitro Organ Culture

The lower molar tooth germs were carefully dissected from the mandibles of mouse embryos at E13 and E16. These dissected tooth germs were placed in the Trowell-type organ culture for 3 h. The hypoxic experiment and ONBs treatment experiment followed the procedure of Khan et al. (2018). Briefly, 35 mm organ-culture dishes were placed inside the hypoxic chamber during the hypoxia experiment. Argon gas was purged through the chamber for 20 min to replace the air inside the chamber. For the reversal of hypoxic condition, 20% ONB was treated on tooth germs *in vitro* culture media (10% FBS in DMEM) for 1 h after cultured in hypoxic condition.

Luciferase Assay

Mouse HIF-1α CDS was cloned into pCMV-Myc vector (Addgene, MA, USA), promoter regions of mouse GLUT1 and GLUT2 were cloned into the pGL3 basic vector (Promega, WI, USA). Human Embryonic kidney (HEK293T) cells were grown in 60 mm cell dishes to 80% confluence before transfection with total of 3 μg each of the reporter plasmids and Myc tagged HIF-1α plasmid. The total amount of plasmid concentration used for transfection was normalized using the pCMV empty vector. The Renilla pRL-SV40 plasmid was used as a control for the transfection efficiency. FugeneFD (Promega) was used as transfection reagent. Forty-eight hours after transfection, cells were harvested, and luciferase activity in the cells was analyzed by a Dual- Luciferase Reporter Assay System (Promega).

Immunofluorescence

The specimens were embedded in wax using conventional methods. Sections (4 μm thickness) of the specimens were boiled in 10 mM citrate buffer (pH 6.0) for 20 min and cooled at room temperature for 20 min. The specimens were incubated with primary antibodies against HIF-1α (Abcam, CAM, UK; dilution 1:200), phosphorylated p53 (Cell signaling; dilution 1:100), cleaved Caspase-3 (Cell signaling, MA, USA; dilution 1:100), PCNA (Abcam; dilution 1:200), Glut-1(Abcam; dilution 1:200), Glut-2 (Novus biologicals, CR, USA; dilution 1:200), MMP20 (Abcam; dilution 1:200), Amelx (Santa Cruz Biotechnology, TX, USA; dilution 1:200), Dmp1 (LSBio, WA, USA; dilution 1:200), Dspp (Santa Cruz Biotechnology; dilution 1:200) at 4°C overnight. The specimens were incubated with goat anti-rabbit Alexa Fluor 488 (Thermo Fisher Scientific, MA, USA; dilution 1:200), goat anti-mouse Alexa Fluor 555 (Thermo Fisher Scientific; dilution 1:200) antibodies. The sections were counterstained with DAPI (Molecular Probes, OR, USA, dilution 1:1,000) and examined using a confocal laser microscope (DMi8; Leica, Wetzlar, Germany).

Scanning Electron Microscope

Calcified tooth, after fracture, were analyzed by SEM. Calcified teeth from kidney transplant were fixed in 4% paraformaldehyde, post-fixed with osmium, dehydrated in a series of graded ethanols, with a final immersion in 100% hexaethyldisilazane. Samples were then mounted on carbon stubs, coated with gold/palladium with a Balzar Med 10 evaporator and examined with a FE-SEM (Merlin, Zeiss) scanning electron microscope coupled with an energy-dispersion spectrometer (EDS) system.

Statistical Analysis

GraphPad Prism software was used for statistical analysis and graphical representations of the data (GraphPad, La Jolla, CA). ANOVA were performed on the data and significance was checked. Non-significant values have been shown as ns in the results section, while *, **, ***, and **** describe p-values of < 0.05, 0.01, 0.001, and 0.0001, respectively.

Kidney Transplantation

The kidney was taken from the incision of dorsal side of 6-week-old ICR male mouse. The small hole at the renal capsule covering the kidney were made carefully with tungsten needle. Tooth germs cultured with each condition were inserted into the hole. The kidney were then placed back inside the abdominal cavity, and the incision was sutured. One week after the surgery, the mice were sacrificed in a CO_2 chamber and the kidneys were taken out, and fixed in 4% paraformaldehyde and scanned using a microCT scanner. Images were reconstructed using microview software. After scanning, samples were decalcified with 10% EDTA and performed histological analyses.

Real Time-Quantitive Polymerase Chain Reaction (RT-qPCR)

For quantification of the levels of RNA, the tooth germs under each condition were microdissected at E16 and RNA was extracted with TRIzol reagent. After DNase I treatment, the RNA was purified with an RNeasy Kit (Qiagen, Hilden, Germany). RT-qPCR was performed with a Thermal Cycler Dice™ Real Time System and SYBR Premix EX Taq™ (Takara, Kyoto, Japan) according to the manufacturer's instructions.

The primers used for amplification were as follows:

Bmp2

Forward 5′-TCAGCATGTTTGGCCTGAAGCA-3′

Reverse 5′-GCCGTTTTCCCACTCATCCTCGGAA-3′
Bmp4
Forward 5′-GACTTCGAGGCGACACTTCT-3′
Reverse 5′-ACTGGTCCCTGGGATGTTCT-3′
Bmp7
Forward 5′-ACTCCTACATGAACGCCACCAACCA-3′
Reverse 5′-TCGAAGATTTGGAAAGGTGTGGCCC-3′
Fgf2
Forward 5′-GAATTCCGGCTCTACTGCAAGAAC-3′
Reverse 5′-GAATTCTTATACTGCCCAGTTCGT-3′
Fgf10
Forward 5′-CATGTGCGGAGCTACAATCA-3′
Reverse 5′-CCCCTTCTTGTTCATGGCTA-3′
Shh
Forward 5′-GCTCTACCACATTGGCACCT-3′
Reverse 5′-TGCGCTTTCCCATCAGTT-3′

RESULTS

Induction of HIF-1α and Change in Proliferation and Apoptosis in Tooth Germs at E13 Under Hypoxic Conditions

To identify the role of oxygen in enamel and dentin mineralization, tooth germs at the cap (consisting of soft tissue only) and bell (in which hard tissue begins to form) stages were cultured *in vitro* for 3 h under normoxic and hypoxic conditions (**Figure 1A**). Hypoxic tooth germs were incubated for 1 h in culture media containing 20% ONB to reverse the hypoxic condition. The average size of the ONB particles used in this study is 117.1 nm (±0.798 nm) (**Figure 1B**), and the concentration of the particles is 2.62E+08 particles/mL (±3.24E+10 particles/mL) (**Figure 1C**).

To investigate the induction of hypoxic response, immunofluorescence was performed. At the cap stage (E13), no HIF-1α was found in the tooth germs under normoxic conditions (**Figure 2A**). However, HIF-1α was induced in the oral epithelium, dental epithelium, and dental mesenchyme under hypoxic conditions (**Figure 2B**). Interestingly, HIF-1α expression disappeared in the ONB group (**Figures 2C,D**).

To evaluate the changes in cell proliferation and apoptosis under hypoxic conditions, the expression of proliferating cell nuclear antigen (PCNA), phosphorylated p53, and cleaved Caspase-3 were analyzed by immunofluorescence. Many proliferative cells were observed in E13 tooth germs under normoxic conditions (**Figure 2E**). However, no PCNA positive cells were observed in E13 tooth germs under hypoxic conditions (**Figure 2F**). Inhibition of cell proliferation caused by hypoxia was restored by treatment with ONBs (**Figures 2G,H**). Moreover, tooth germs in normoxia underwent apoptosis in the small part of dental epithelium, including enamel knot, as evidenced by expression of phosphorylated p53 and cleaved Capsase-3 (**Figures 2I,M**). However, many phosphorylated p53-apoptotic cells were found in the dental epithelium and mesenchyme in tooth germs under hypoxic conditions (**Figure 2J**). Further, cleaved Caspase-3 was detected, especially in the dental epithelium, and in a few cells in the dental mesenchyme (**Figure 2N**). Interestingly, phosphorylated p53 and cleaved Caspase-3 positive cells were rarely found in tooth germs treated with ONBs (**Figures 2K,L,O,P**). However, p53 expression was not shown in each condition (data not shown). To investigate the effect of oxygen on the mineralization of tooth, E13 tooth germs were cultured *in vitro* in normoxia, hypoxia for 3 h, and with ONBs for another 1 h, followed by transplantation of these culture tooth germs into kidney capsule for 4 weeks for calcification (**Figure 3**). Compared to the mineralization of teeth under normoxic conditions (**Figures 3A,D**), the mineralization of E13 tooth germs cultured under hypoxic conditions (**Figures 3B,E**) or treated with nanobubbles were not significantly different (**Figures 3C,F,G**).

Induction of HIF-1α and Change in Proliferation and Apoptosis in Tooth Germs at E16 Under Hypoxic Conditions

Furthermore, immunofluorescence was performed to evaluate the changes in cell proliferation and apoptosis under hypoxic conditions at the bell stage. At the bell stage (E16), few HIF-1α positive cells were found in the dental epithelium and mesenchyme in normoxia (**Figure 4A**). However, hypoxia-induced HIF-1α were found in the dental epithelium and mesenchyme (**Figure 4B**). In ONBs, no HIF-1α positive cells were observed in the tooth germs (**Figures 4C,D**). Thus, ONBs reversed the hypoxic response in the tooth germs not only at the cap stage but also at the bell stage. PCNA was expressed in the dental epithelium and mesenchyme under normoxic conditions (**Figure 4E**), whereas its expression decreased significantly in the tooth germs under hypoxic conditions (**Figure 4F**). The reduced cell proliferation was restored by ONBs (**Figures 4G,H**). Hypoxia-induced apoptosis in E16 was very similar to that observed in E13 (**Figure 2**). Phosphorylated p53 and cleaved Caspase-3, markers of cell apoptosis, were expressed in very few cells in the tooth epithelium including enamel knot and mesenchyme at E16 under normoxic conditions (**Figures 4I,M**). However, in tooth germs under hypoxic conditions, the number of phosphorylated p53 and cleaved Caspase-3 positive cells in the tooth epithelium and mesenchyme at E16 were greatly increased (**Figures 4J,N**), and the numbers were restored following ONBs treatment (**Figures 4K,L,O,P**). These results suggest that ONB reverses the hypoxic response of tooth germs at the cap and bell stages. Furthermore, cell proliferation and apoptosis induced by hypoxic conditions were restored by ONBs in the developing tooth germs. The mineralization of E16 tooth germs was different from that of E13 as evident from the micro-CT images (**Figure 5**). Micro-CT revealed that tooth size was smaller under hypoxic conditions (**Figures 5B,E**) than that under normoxic conditions (**Figures 5A,D**). Further, only 1 or 2 teeth were observed in hypoxic condition (**Figures 5B,E**), whereas three teeth, including M1, M2, and M3 were found in normoxic condition. Furthermore, the cusp morphology of the tooth was flattened in hypoxic conditions. Following ONBs treatment, three teeth were observed, and the teeth sizes were similar to that of the normoxic tooth (**Figures 5C,F**). The mineralization density of teeth was decreased by hypoxic condition than by normoxia condition, but this decreased mineralization was reversed with ONBs (**Figure 5G**).

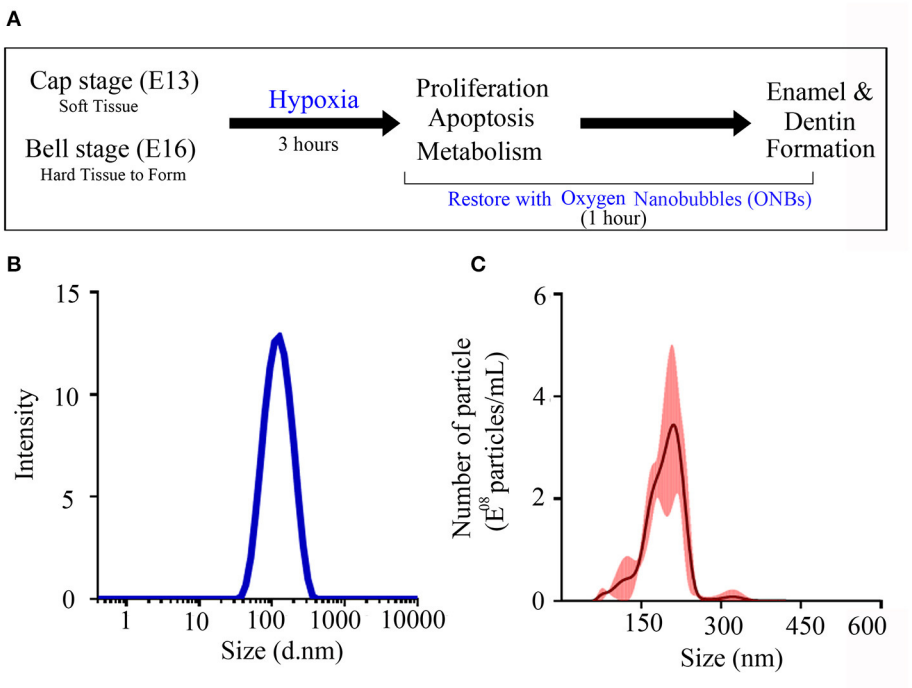

FIGURE 1 | Characterization of oxygen nanobubbles. **(A)** The experiment schematic diagram. Cap stage (E13) and bell stage (E16) tooth germs were cultured in normoxia condition and hypoxia condition. These damaged tooth germs with hypoxic condition were tried to recover with oxygen nanobubbles (ONBs) for 1 h. After 3 h, *in vitro* cultured tooth germs under normoxia, hypoxia condition, and rescued by ONBs were collected, and confirmed the changes of cell proliferation, apoptosis, and metabolism. Furthermore, hard tissue including enamel and dentin were produced under the kidney capsule for 1 week and for 4 weeks. **(B,C)** The size characterization of ONBs using analytical methods. **(B)** The average particle size of ONBs obtained by a dynamic light scattering (DLS) measurement. Average diameter: 117.1 nm (±0.798 nm). **(C)** The average particle size and the enumeration of ONBs measured by a nanoparticle tracking analysis (NTA) method. Total particle concentration: 2.62E+08 particles/mL (±3.24E+10 particles/mL).

To verify that tooth germs under hypoxia recovered with ONBs, the tooth germs were cultured under hypoxic conditions for 3, 6, 9, and 18 h, respectively. However, tooth germs treated with hypoxia for longer than 3 h failed to recover even with ONBs. Therefore, in this study, hypoxia treatment for 3 h was carried out in the experimental group (data not shown).

Effects of Reduced Oxygen Level on Energy Metabolism in Tooth Germs at E13 and E16

To determine the effect of hypoxia on metabolism, we examined Glut-1 and Glut-2 expression under hypoxic conditions, given that Glut-1 and Glut-2 are expressed during tooth development (Ida-Yonemochi et al., 2012). Glut-1 expression was especially shown in the dental epithelium under normoxic conditions at E13 (**Figure 6A**). Under hypoxic conditions, Glut-1 expression increased in both the dental epithelium and dental mesenchyme (**Figure 6B**). Interestingly, hypoxia-induced Glut-1 expression was not much increased in tooth germs following ONBs treatment (**Figures 6C,D**). Glut-2 was expressed mainly in the dental epithelium under normoxic conditions but expression was weaker than that of Glut-1 (**Figure 6E**). Under hypoxic conditions, Glut-2 expression was not significantly induced in the dental mesenchyme as well as in the dental epithelium (**Figure 6F**). Furthermore, ONBs treatment did not change Glut-2 expression (**Figures 6G,H**). At E16, Glut-1 was expressed in the dental epithelium and slightly expressed in the dental mesenchyme under normoxic conditions (**Figure 6I**). Under hypoxic conditions, Glut-1 expression increased (**Figure 6J**), and the expression increased further in the dental epithelium and dental mesenchyme with ONBs treatment (**Figures 6K,L**). Glut-2 was expressed in the dental epithelium, and was slightly expressed in the dental mesenchyme under normoxic conditions (**Figure 6M**). Glut-2 expression increased in the dental epithelium under hypoxic conditions (**Figure 6N**). With ONBs, Glut-2 expression was slightly decreased than under hypoxic condition, but increased than under normoxic condition (**Figures 6O,P**). HIF-1α modulates GLUT-1 and GLUT-2 promoter activity. As shown in **Figure 6Q**, GLUT-1 and GLUT-2 promoter activity was significantly increased following transient expression of HIF-1α. These results suggested that HIF-1α by hypoxic conditions during tooth development induced glucose metabolism by positively regulating Glut-1 and Glut-2. Moreover, glucose metabolism, including Glut-1 and Glut-2

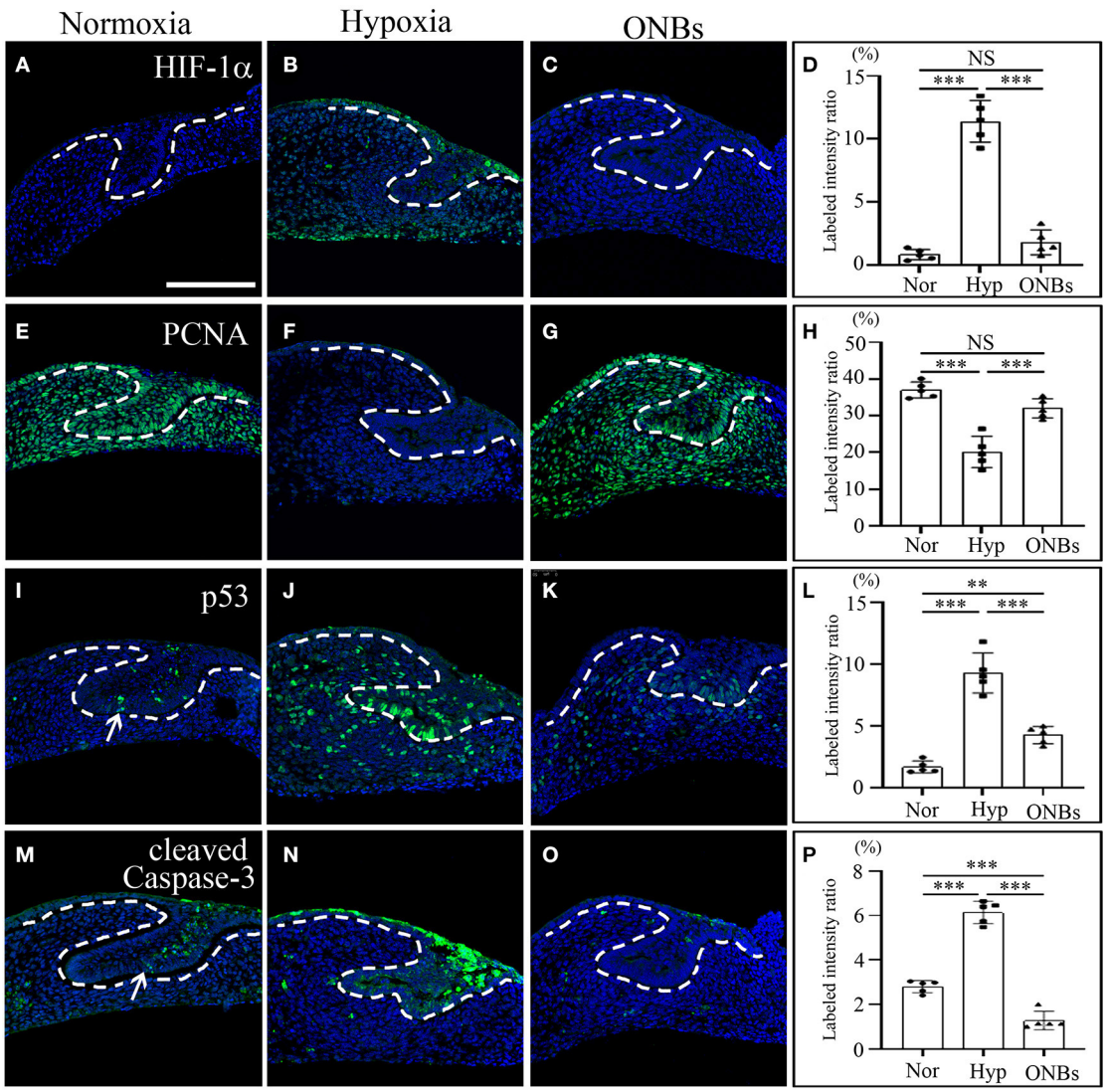

FIGURE 2 | Change of cell proliferation and apoptosis at E13 tooth germs in normoxia, hypoxia, and ONB treatment. At E13, immunofluorescence was performed to show the expression change of **(A–D)** HIF-1α, **(E–H)** PCNA, **(I–L)** phosphorylated p53, **(M–P)** cleaved Caspase-3 in the frontal sections of tooth germs. HIF-1α expression is not expressed **(A)** in normoxia, increased **(B)** in hypoxia, but decreased **(C)** in ONBs. PCNA is highly expressed **(E)** in normoxia, decreased **(F)** in hypoxia, and recovered **(G)** in ONBs. **(I)** Phosphorylated p53 and **(M)** cleaved Caspase-3 are expressed in dental epithelium, including enamel knot, shown in increase **(J,N)** in hypoxia, but in decrease **(K,O)** in ONBs. **(D,H,L,P)** Quantification of labeled intensity of HIF-1α, PCNA, p53, cleaved Caspase-3 in normoxia, hypoxia, ONBs ($N = 5$) (Scale bar = 100 μm. Nor, normoxia; Hyp, Hypoxia; ONBs, Oxygen Nanobubbles; $^{**}p$-values <0.01, $^{***}p$-values <0.001. Arrow; positive in enamel knot).

expression, is necessary for the repair of tooth mineralization at E16 by oxygen.

Decreased Bmps and Shh Expression Under Hypoxic Tooth Germs

In present study, we performed qRT-PCR to identify signaling pathways associated with the hypoxic conditioned tooth germs. Tooth morphogenesis are regulated by epithelial-mesenchymal interactions, which are mediated by signaling pathways including Hedgehog (Hh), Fibroblast growth factor (FGF), and Bone morphogenic protein (Bmp) (Jussila and Thesleff, 2012; Graf et al., 2016). The expression levels of *Bmp2*, *Bmp4*, and *Bmp7*, which are related Bmp genes with tooth development (Graf et al., 2016), were checked. The expression level of *Bmp2* were not changed under hypoxic condition but increased with ONBs (**Figure 7A**). On the other hand, the expression level of *Bmp4* (**Figure 7B**) and *Bmp7* (**Figure 7C**), which have been known to be expressed in enamel knot and dental mesenchyme (Graf et al., 2016), was decreased under hypoxic condition, and the expression was significantly increased with ONB-restored tooth germs. *Fgf2*, which plays a role for amelogenesis,

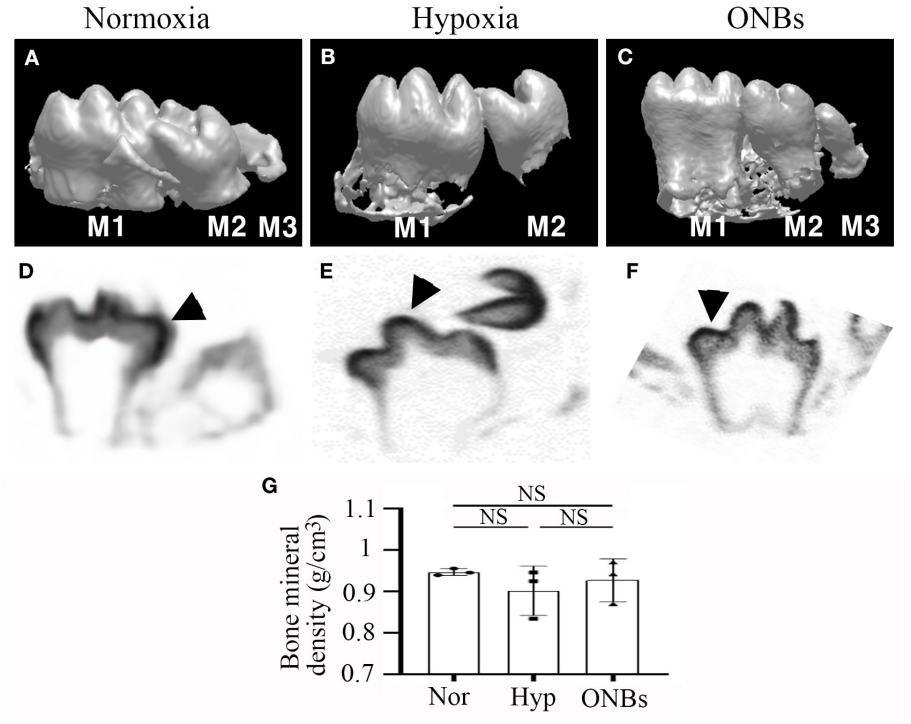

FIGURE 3 | microCT images of Calcified tooth in hypoxia at E13. microCT images of calcified E13 tooth germs in **(A,D)** normoxia, **(B,E)** hypoxia, and **(C,F)** ONBs ($N = 5$). **(A–C)** 3D reconstruction images. **(G)** Quantification of bone mineral density ($N = 3$). **(D–F)** Sagittal view (M, Molar; Arrowheads, mineralization region; NS, non-significant).

expression was not regulated with hypoxia (Du et al., 2018). Furthermore, the expression was not changed with ONBs, neither (**Figure 7D**). During tooth development, *Fgf10* is expressed in dental mesenchyme during the early stage, and in the differentiating odontoblasts at later stage (Du et al., 2018). The expression level of *Fgf10* was downregulated with hypoxic condition, and the expression level was increased with ONBs (**Figure 7E**). *Shh* is involved in tooth development, and expressed in enamel knot and in dental epithelium (Cho et al., 2011). Hypoxic tooth germs downregulated Shh expression, while ONBs restored the expression level of *Shh* (**Figure 7F**). These results suggested that oxygen level regulates tooth-related signaling pathway, and mineralization of tooth development.

Characteristic Defects in Enamel and Dentin in Hypoxic Tooth Germs Are Rescued With ONBs

To analyse the hypomineralization defects in enamels of hypoxic tooth germs, we examined the enamel structure of calcified teeth under hypoxic conditions and ONBs treatment using scanning electron microscopy (SEM) (**Figure 8**). The enamel of teeth in normoxia showed a solid structure as enamel rods (**Figures 8A,A'**), whereas the enamel rods of teeth under hypoxic conditions were disorganized, and many pores were observed (**Figures 8B,B'**). The teeth treated with ONBs had enamel structures similar to those of normoxic teeth (**Figures 8C,C'**). The surface characteristics of the teeth under normoxic conditions indicated a compact and mineralized dentin (**Figures 8D,D'**). Compared to the teeth under normoxic conditions, dentinal tubules were not clearly seen in the porous and unclear dentin surface of the teeth under hypoxic conditions (**Figures 8E,E'**). Crystallization was very low under hypoxic conditions compared to that under normoxic conditions. The unmineralized dentin observed under hypoxic conditions was totally rescued by ONBs (**Figures 8F,F'**).

Quantitative analysis of the enamel and dentin using energy dispersive spectroscopy (EDS) revealed that both the enamel and dentin were mainly composed of Ca, P, O, and C under normoxic conditions (**Figure 8G**). The EDS patterns of teeth under hypoxic conditions were different from those of teeth under normoxic conditions (**Supplementary Figure 1**). Ca and P levels were decreased in the enamel of teeth under hypoxic conditions, whereas the elements O and C were similar to the elements in the tooth under normoxic conditions. Levels of Ca, P, O, and C were increased in the dentin of teeth under hypoxic conditions, compared to the elements in the teeth in normoxic conditions. After ONB treatment, Ca and P were restored in the enamel, but O and C levels were decreased compared to that in normoxia and hypoxia. After ONBs treatment, Ca, P, and O were increased in the dentin more than that of the dentin in normoxic and hypoxic conditions, whereas the level of C decreased to the

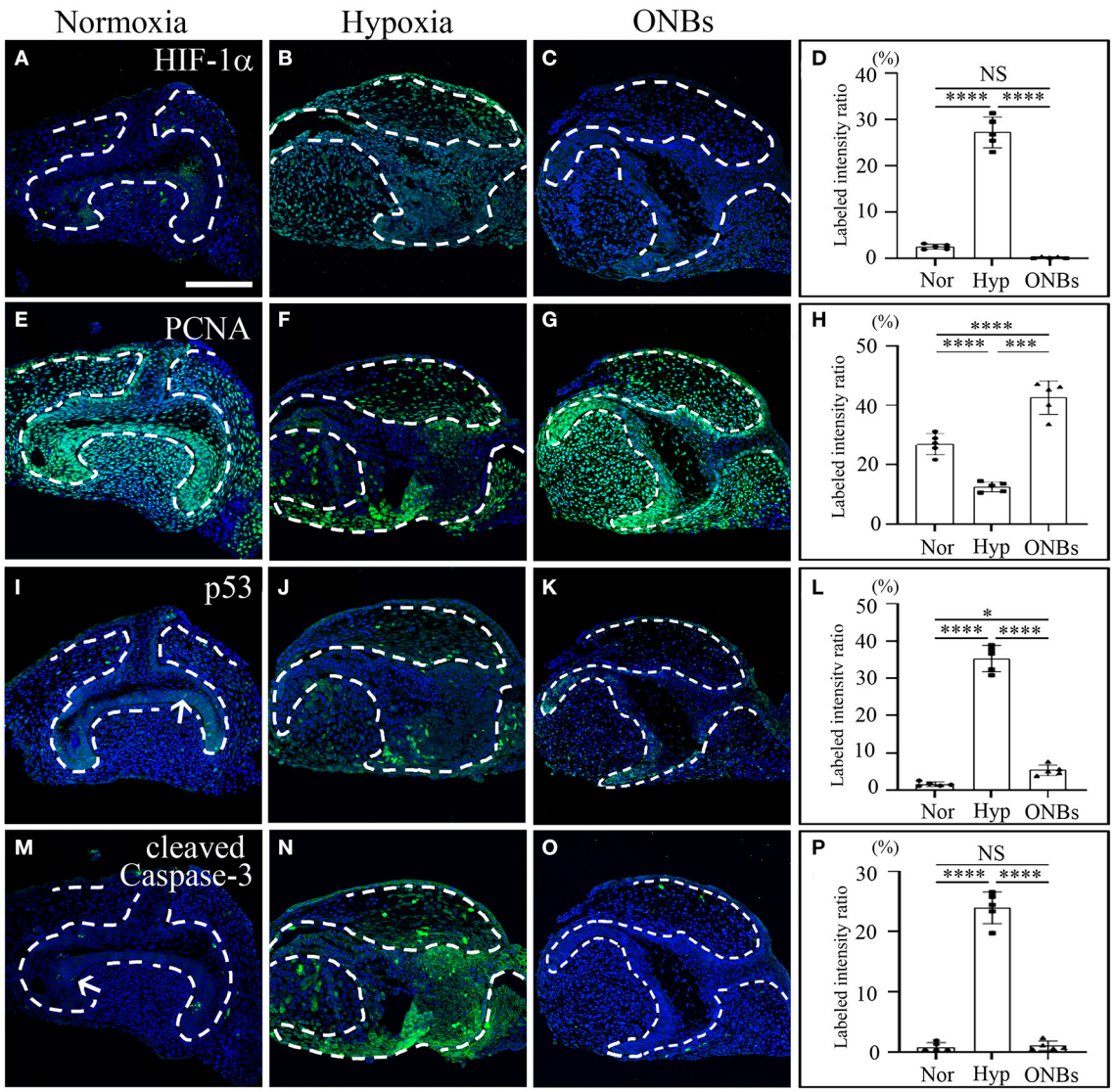

FIGURE 4 | Change of cell proliferation and apoptosis at E16 tooth germs in normoxia, hypoxia, and ONB treatment. Bell stage tooth germs (E16) cultured in normoxia, hypoxia, ONBs were compared. Immunofluorescence was performed to show the expression change of **(A–C)** HIF-1α, **(E–G)** PCNA, **(I–K)** phosphorylated p53, **(M–O)** cleaved Caspase-3 in the frontal sections of tooth germs. HIF-1α expression is not expressed **(A)** in normoxia, increased **(B)** in hypoxia, but decreased **(C)** in ONBs. PCNA is highly expressed **(E)** in normoxia, decreased **(F)** in hypoxia, and recovered **(G)** in ONBs. Phosphorylated p53 and cleaved Caspase-3 are expressed little at enamel knot **(I,M)** in normoxia, shown in increase **(J,N)** in hypoxia, but in decrease **(K,O)** in ONBs. **(D,H,L,P)** Quantification of labeled intensity of HIF-1α, PCNA, phosphorylated p53, cleaved Caspase-3 in normoxia, hypoxia, ONBs ($N = 5$) (Scale bar = 100 μm. Nor, normoxia; Hyp, Hypoxia; ONBs, Oxygen Nanobubbles; **p*-values <0.05, ****p*-values <0.001, *****p*-values <0.0001, Arrow; positive cells in enamel knot).

normoxia levels. These results suggested that hypomineralization of the enamel and dentin occurred under hypoxic conditions, and treatment with ONBs can rescue the hypomineralization.

Effect on Tooth Mineralization Under Hypoxic Condition at E16

To identify the hypomineralization of enamel and dentin under hypoxic conditions, tooth germs were cultured with normoxia, hypoxia, and ONBs condition, incubated for 1 week under the kidney capsule for the calcification, and histological analysis was performed with enamel and dentin proteins (**Figure 9**). Under normoxic condition, enamel space by enamel decalcification, shrink ameloblasts, dentin, odontoblasts, and pulp were found (**Figure 9A**). AmelX (**Figure 9A**) and MMP20 (**Figure 9D**) was strongly detected in the enamel matrix in the secretory ameloblasts only, but disappeared at the tip of molar cusp which were undergoing enamel mineralization. The enamel layer showed more matrix protein and ameloblasts were obviously longer compared with that in normoxia (**Figures 9B,E**). Interestingly with ONBs, matured

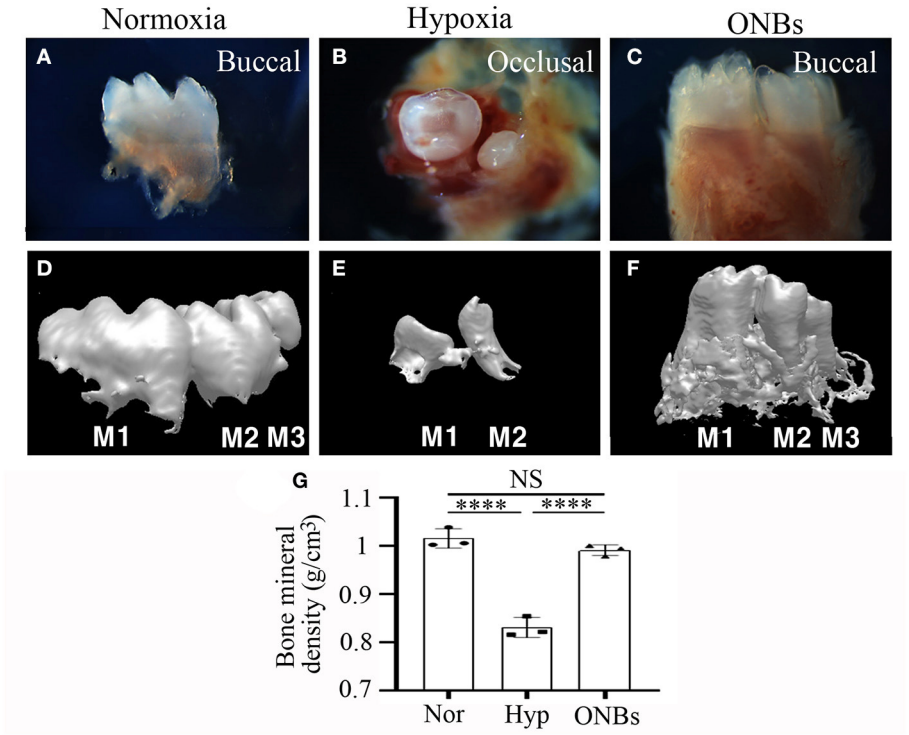

FIGURE 5 | Images of Calcified tooth in hypoxia at E16. **(A–C)** Images and **(D–F)** 3D reconstruction images of micro-CT of calcified E16 tooth germs in **(A,D)** normoxia, **(B,E)** hypoxia, and **(C,F)** ONBs ($N = 5$). **(G)** Quantification of bone mineral density ($N = 3$) (**A,C,D–F** are buccal view. **B** is occlusal view). ****p-values <0.0001.

ameloblasts where were processing enamel mineralization, were shorten, similar to normoxia tooth (**Figures 9C,F**). AmelX and MMP20 expression were found in the enamel matrix in the secretory ameloblasts only (**Figures 9C,F**). These abnormal expression results demonstrated that in hypoxic condition tooth, enamel crystallization were aberrant, and occurred an imperfecta in amelogenesis.

Furthermore, we confirmed dentinogenesis (Dmp1 and DSPP) using immunofluorescence. Dmp1 and DSPP were expressed in odontoblasts, dentin, and pulp (**Figures 9G,J**) of the normoxic teeth. However, the expression of Dmp1 and DSPP decreased in the odontoblast layer and dentin in hypoxic teeth (**Figures 9H,K**). Interestingly, DMP1 and DSPP were expressed very strongly not only in the odontoblast layer but also in the dentin tubules with ONBs (**Figures 9I,L**). These results revealed that decrease in oxygen level at E16, when mineralization begins, alters the tooth size and cuspal morphology, and results in defects in amelogenesis and dentinogenesis. Furthermore, ONB-mediated increase in oxygen level restores the morphology and ameliorates the defects induced by the hypoxia.

DISCUSSION

Supply of sufficient oxygen is essential for the survival of tissues, otherwise, cells and tissues undergo necrosis and programmed cell death (Suvarnapathaki et al., 2019). Our findings reveal that it is possible to reverse hypoxic tooth germs with oxygen nanobubbles. The present study identified the effects of change in oxygen level on tooth mineralization during tooth development. Hypoxic condition promote angiogenesis, glucose transport, anaerobic metabolism, invasion, resistance, and survival, particularly by modulating the apoptotic process (Al Tameemi et al., 2019). Numerous reports have shown that HIF-1α is closely linked to positive and negative regulation of the apoptotic process via the p53 or Caspase pathway (Bruick, 2000; Erler et al., 2004; Cosse et al., 2009). Hypoxia has a significant effect on neuronal cell apoptosis, via Caspase-3 activation (Deng et al., 2019). Hypoxia ischemia leads to significant increase in Caspase-3 expression and neuronal apoptosis in the brain of neonatal mice (Deng et al., 2019). In most cases, increase in p53 level induces apoptosis in cells exposed to hypoxia, although an increase in p53 protein level without subsequent apoptosis has been observed (Kilic et al., 2007; Sermeus and Michiels, 2011). The presence of both HIF-1α and p53 seems to be essential for hypoxia-induced cell death (Sermeus and Michiels, 2011). In the present study, exposure of tooth germs at E13 and E16 to hypoxia for 3 h increased cell apoptosis and decreased cell proliferation, as evidenced by that the expression of phosphorylated p53 and cleaved Caspase3 were increased and the expression of PCNA was decreased. The hypoxia-induced effects in E13 and E16 tooth germs were reversed with ONBs. ONBs reverse hypoxia and suppress HIF-1α activity in tumor cells (Khan et al., 2018). Thus, ONB treatment can

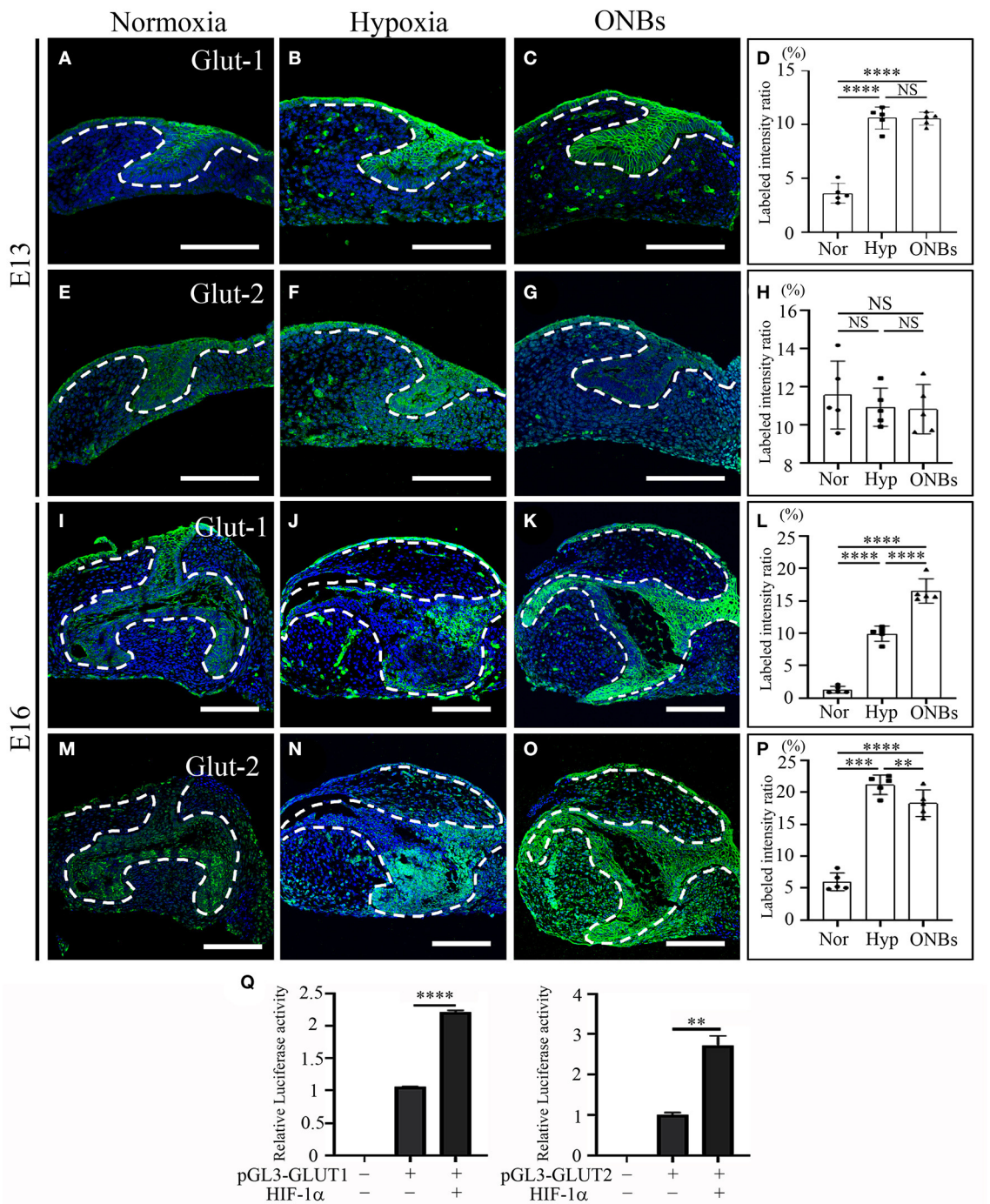

FIGURE 6 | Change of Glucose transporters such Glut-1, and Glut-2 at E13 and E16 in normoxia, hypoxia, and ONB treatment. Cap stage tooth germs (E13) and bell stage tooth germs (E16) cultured in normoxia, hypoxia, ONBs were compared. The expression of Glut-1 at E13 **(A)** in normoxia, **(B)** in hypoxia, and **(C)** in ONBs. **(D)** Glut-1 expression in hypoxia shows in increase than that in normoxia, and similar as ONBs. Glut-2 expression are similar among **(E)** in normoxia, **(F)** hypoxia, and **(G)** ONBs. The expression of Glut-1 at E16 **(I)** in normoxia, **(J)** in hypoxia, and **(K)** in ONBs. At E16, Glut-1 expression **(J)** in hypoxia shows in increase than that **(I)** in normoxia, and lower than **(K)** in ONBs. Glut-2 expression **(N)** in hypoxia is stronger than **(M)** in normoxia. **(O)** When ONBs treatment, the expression of Glut-2 is slightly reduced compare to hypoxia. These results were quantified in **(D,H,L,P)** ($N = 5$). **(Q)** Compared to the pGL3-basic, treatment with 3 μg of HIF-1α expression vector leads to a significant increase of GLUT-1 and GLUT-2 containing HIF-1α binding site ($N = 3$) (Scale bar = 100 μm. Nor, normoxia; Hyp, Hypoxia; ONBs, Oxygen Nanobubbles; ***p*-values <0.01, ****p*-values <0.001, *****p*-values <0.0001).

overcome hypoxic stress caused by cellular processes, including cell proliferation and apoptosis, not only in cancer cells, but also in normal tissues.

A previous study demonstrated that the expression pattern of GLUTs, including Glut-1 and Glut2 during tooth development (Ida-Yonemochi et al., 2012). Glut-1 was expressed in the

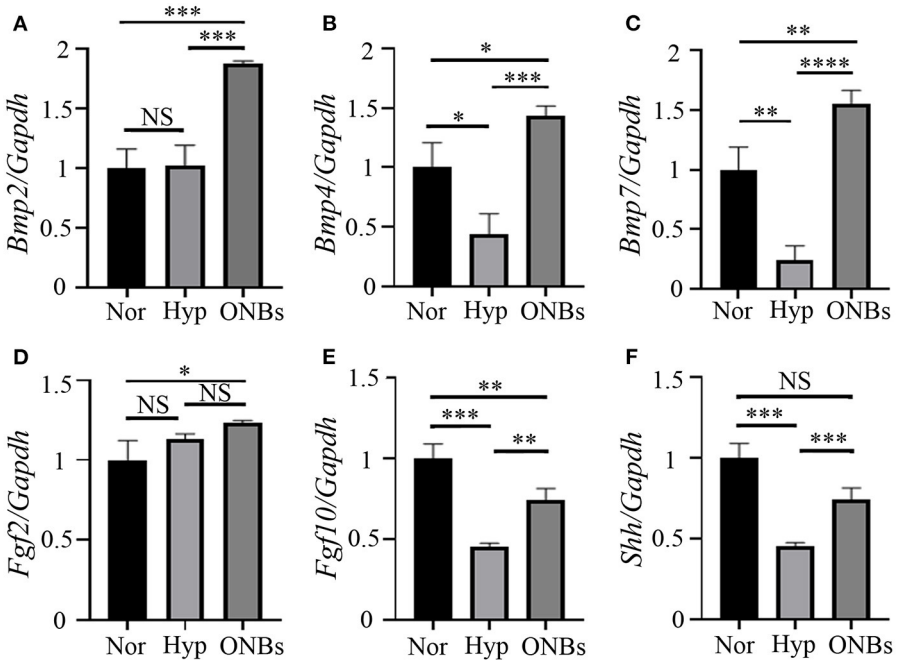

FIGURE 7 | Signaling pathways related with hypoxic condition Expression analysis of Bmp signaling, Fgf signaling, and Shh signaling with tooth germs under normoxia, hypoxia, and ONBs condition. **(A)** *Bmp2* expression levels in tooth germs under normoxia is not changed with hypoxia condition, but upregulated with ONBs. The expression level of **(B)** *Bmp4* and **(C)** *Bmp7* was downregulated in tooth germs under hypoxic condition, but restored with ONB treatment. **(D)** *Fgf2* expression is not changed with hypoxic condition, and ONBs. However, **(E)** *Fgf10* expression level is decreased in tooth germs under hypoxic condition, and shows in increase of tooth germs with ONB treatment. **(F)** *Shh* expression is downregulated under hypoxic condition, and this down regulated expression is recovered with ONBs (Expression level is normalized with *Galdh*. **p*-values <0.1, ***p*-values <0.01, ****p*-values <0.001, *****p*-values <0.0001).

epithelium of bud to cap stage molar tooth germs, but was decreased in the bell stage. Glut-2 expression appeared at E16 (bell stage). Furthermore, inhibition of Glut-1/2 resulted in a change in tooth morphology. HIF-1α regulates the activity of GLUT-1 and GLUT-3 (Chen et al., 2001; Hayashi et al., 2004; Liu et al., 2009). Furthermore, genetic deletion of Glut-1, either before or after the onset of chondrogenesis in the limb, severely impairs chondrocyte proliferation and hypertrophy, resulting in dramatic shortening and hypomineralization of the limbs (Lee et al., 2018). In this study, using luciferase assay, we demonstrated that HIF-1α positively regulates both Glut-1 and Glut-2. Glut-1 expression was found to increase in the tooth germs under hypoxic conditions at E13 and E16, and was similar or increased further with ONBs. Glut-2 expression was increased in hypoxic condition only at E16, when mineralization begins. When the oxygen level is low at the initial stage of tooth development (soft tissue stage), tooth repair is performed by including glucose metabolism through Glut-1 rather than Glut-2. However, if the oxygen level drops at the beginning of the mineralization during the tooth development process, tooth repair is performed by inducing glucose metabolism through both Glut-1 and Glut-2.

Tooth morphogenesis is regulated by the dental epithelium, which differentiates to enamel producing ameloblasts and the growth and folding of inner dental epithelium determines the size and morphology of tooth crown (Jussila and Thesleff, 2012). Furthermore, the epithelial signaling centers expressing multiple signaling molecules, such as primary enamel knot, and secondary enamel knots plays a pivotal role for the tooth morphogenesis regulated with the mesenchyme (Sadier et al., 2019) and initiate differentiation of odontoblasts (Thesleff et al., 2001). After the odontoblasts differentiation, they signal back to the dental epithelium, which is involved in the ameloblast induction include *Bmp2*, and *Bmp4* (Wang et al., 2004). Furthermore, Shh from the dental epithelial cells is required to ameloblast differentiation and maturation (Dassule et al., 2000). Fgf signaling is known to be important in the differentiation of ameloblasts. *Fgf2* and *Fgf10* regulates enamel and dentine formation in mouse tooth germ (Harada et al., 2002; Tsuboi et al., 2003). In addition, many studies reported that Bmp signaling, Fgf signaling, Shh signaling is regulated by hypoxia (Conte et al., 2008; Wang et al., 2010; Wu and Paulson, 2010; Zhang et al., 2018). When tooth germs undergo the hypoxic condition during the mineralization, tooth morphology and mineralization have defects through cell proliferation, apoptosis and glucose metabolism changes. It was confirmed that the expression of *Bmp4* and *Bmp7*, *Fgf10*, and *Shh were* decreased in the low oxygen condition. When ONB was treated, the expression of *Fgf10* and *Shh* was reversed. Furthermore, the expression level of *Bmp4* and *Bmp7* was reversed, which was much higher than that in the normoxia condition. Therefore, cellular events due to oxygen changes

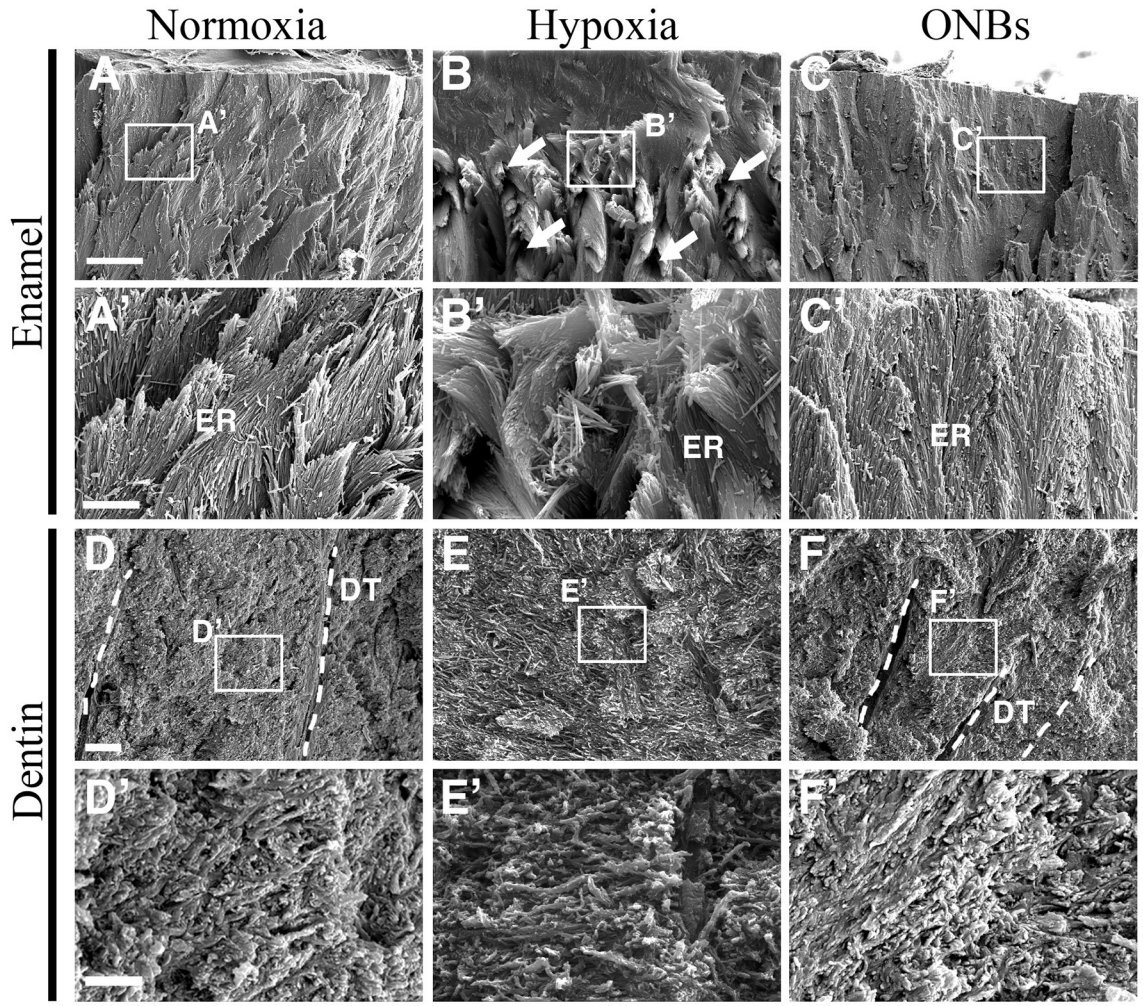

G

(%)	Ca	P	O	C	Ca/C ratio	Ca/P ratio
Enamel						
Normoxia	50.40	20.02	21.31	4.66	10.82	2.52
Hypoxia	35.54	12.26	26.17	4.09	8.69	2.90
ONBs	48.35	17.20	15.93	2.97	16.28	2.81
Dentin						
Normoxia	32.13	12.11	19.31	9.27	3.47	2.65
Hypoxia	35.18	13.74	33.56	12.43	2.83	2.56
ONBs	37.80	15.44	35.30	10.07	3.75	2.45

FIGURE 8 | SEM images of calcified teeth with Hypoxic condition SEM images of **(A–C)** enamel and **(D–F)** dentin of cut surface from the cuspal parts of calcified teeth in normoxia, hypoxia, and ONBs. **(A,A')** In normoxia teeth, enamel rods are well-organized. **(B,B')** Very disorganized enamel rods in teeth in hypoxia. **(C,C')** Enamel rods are recovered to well-organized. **(E,E')** Dentin in teeth in hypoxia condition has no significant change in structure compared to **(D,D')** dentin in teeth in normoxia teeth, but is very sparse and has many pores. **(F,F')** The dentin of the teeth with ONBs treatment recovered to be denser and more compact than that of normoxia. **(G)** EDS analysis of calcified teeth under hypoxia ($N = 3$) [Scale bar = 10 μm **(A–C)**, 2 μm **(A'–C',D–F)**, 600 nm **(D'–F')**, **(A'–F')** are higher magnification in **(A–F)**, dotted line = dentinal tubules (DT); ER, enamel rods].

interact with Bmp, Shh, and Fgf signaling pathway to regulate the size and morphology of tooth, as well as amelogenesis and dentinogenesis.

Enamel development consists of secretory and maturation stage (Lagerstrom-Fermer and Landegren, 1995). During secretory stage, columnar ameloblasts secrete enamel proteins, such as amelogenin (AmelX), ameloblastin, and enamelin, into the enamel matrix (Lagerstrom-Fermer and Landegren, 1995). MMP20 expressed in ameloblasts at the secretory stage have the enamel proteins (Bartlett et al., 2006). During maturation stage, ameloblasts shrink in size and reduce the expression of enamel proteins, which undergo enzymatic degradation

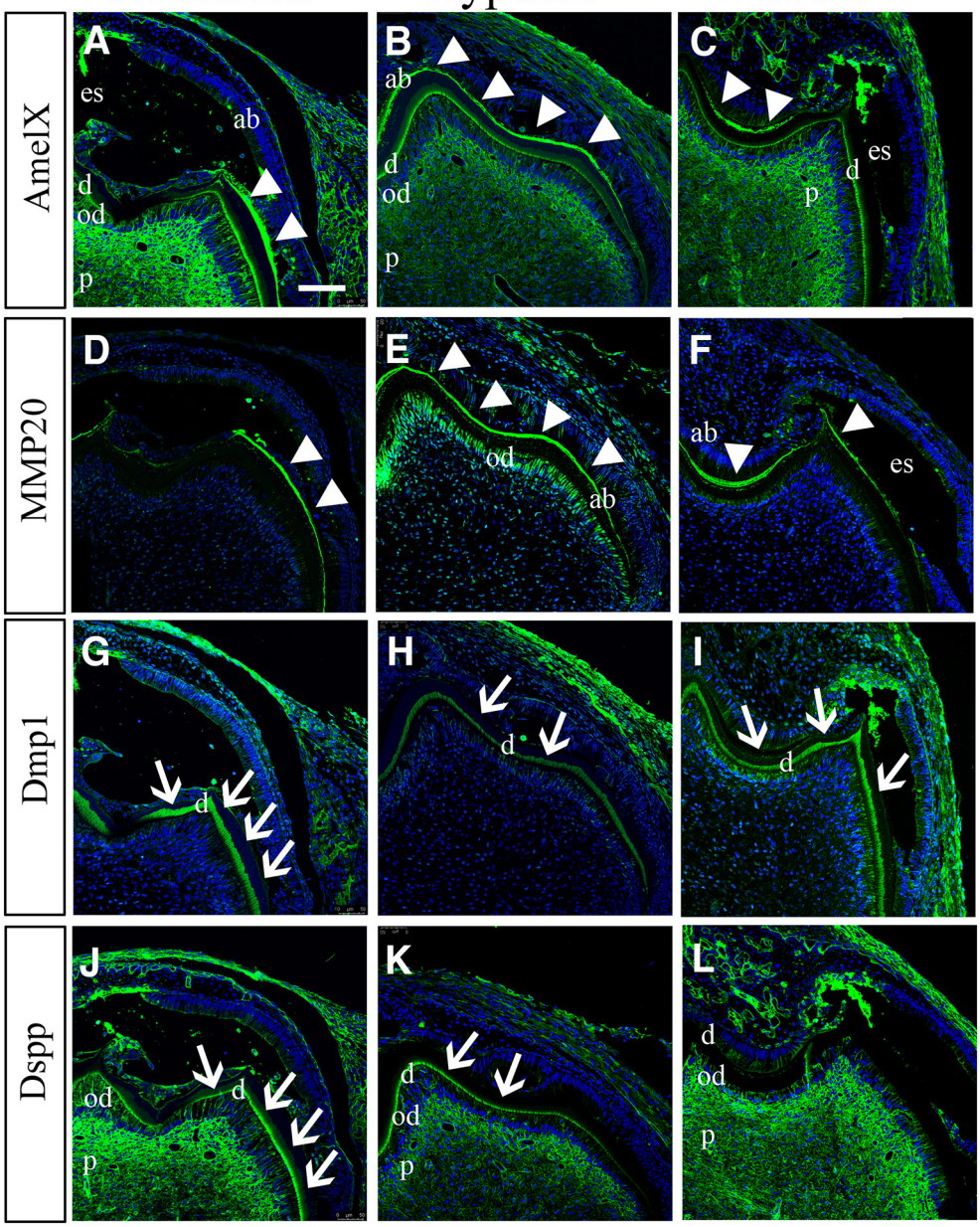

FIGURE 9 | Effect on tooth calcification under hypoxic condition at E16. E16 tooth germs were transplanted into kidney capsule for the calcification. **(A,D)** Under normoxic conditions, enamel space by enamel decalcification, shrink ameloblasts, dentin, odontoblasts, and pulp are found. **(A)** AmelX and **(D)** MMP20 is strongly detected in the enamel matrix (arrowheads) in the secretory ameloblasts. **(B,D)** In hypoxia condition, ameloblasts are obviously longer compared with normoxia tooth. **(B)** AmelX and **(E)** MMP20 expression are shown in the all area of the tooth enamel organ. **(C,F)** With ONBs, ameloblasts are shorten, similar to normoxia tooth. **(C)** AmelX and **(D)** MMP20 is expressed in the enamel matrix in the secretory ameloblasts. Under normoxia condition, **(G)** Dmp1 is expressed in dentin (arrow), and **(J)** DSPP are expressed in odontoblasts, and in dentin (arrow). In hypoxia, **(H)** Dmp1 is expressed very weakly in dentin, and **(K)** DSPP expression is shown weak in dentin and odontoblasts. With ONBs, **(I)** Dmp1 and **(L)** DSP are very strongly expressed in dentin, and in odontoblasts ($N = 3$) (Scale bar = 100 μm. ab, ameloblast; es, enamel space; d, dentin; ob, odontoblast; d, dentin; white arrowhead, enamel matrix; arrow, dentin).

by Kallikrein-related peptidase-1 (KLK-4) to facilitate enamel mineralization (Smith et al., 2017). When hypoxic teeth were incubated for 1 week in kidney capsules, amelogenesis appeared to be delayed due to the remaining high expression of enamel matrix, long ameloblasts, and enamel protein. Eventually, after 4 weeks, the mineral density decreased by nearly 20%. In addition, dentin mineralization is controlled by several molecular events, such as DSPP, DMP1, however, several mutations in the Dspp

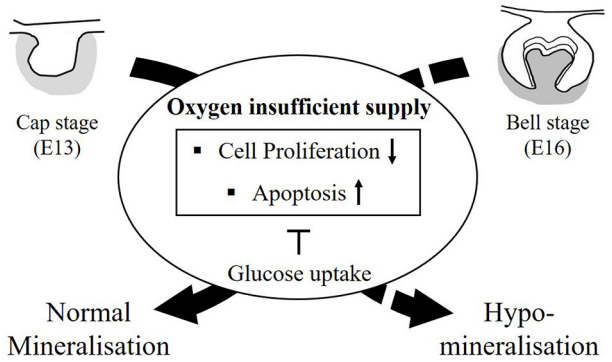

FIGURE 10 | The summary diagram. The tooth germs at the cap stage (E13, all soft tissue) and at the bell stage (E16, start to form hard tissue) were cultured with oxygen insufficient supply, such as hypoxia condition. After 3 h, cell cycle arrest by p53 and apoptosis by Caspase-3 were increased in damaged tooth germ by induced HIF-1α in hypoxic condition. Cell proliferation in damaged tooth germs were decreased. Furthermore, glucose uptake, such as Glut-1, Glut-2 in hypoxic condition was increased for block the cell cycle arrest and apoptosis. The hard tissue, including enamel and dentin is formed in kidney capsule for 4 weeks. Enamel mineralization from tooth germs at E13 (all soft tissue) with hypoxic condition are normally formed. However, the damaged tooth germs with hypoxic condition at E16 (mineralization period) did not produce the normal mineralized teeth, but hypomineralized teeth. The newly developed oxygen nanobubbles can reverse the tooth that has suffered hypoxic damage, and furthermore, this treated tooth with oxygen nanobubbles restore the mineralization.

gene results in widened predentin zoes, decreased dentin width, and high incidence of pulp exposures similar to that in DGI (Sreenath et al., 2003). With hypoxic condition when mineralization starts, Dspp and Dmp1 expression is decreased than that in normoxia after 1-week calcification. After 4 weeks of calcification, AmelX-positive cells in matured ameloblasts were rarely found in hypoxic calcified teeth, and MMP20-positive ameloblasts in the secretory stage had expression along the DEJ (**Supplementary Figures 2B,E**). However, ONB treatment showed an increase in AmelX-expressing matured ameloblast and a decrease in MMP20 expression in secretory stage, restoring ameloblast maturation and mineralization in enamel formation (**Supplementary Figures 2C,F**). Furthermore, DMP1 and DSPP expression was decreased in dentin and odontoblast in hypoxic condition (**Supplementary Figures 2H,K**) compared to normoxia condition (**Supplementary Figures 2G,J**). With ONBs, hypomineralization of dentin by hypoxia is restored (**Supplementary Figures 2I,L**). In addition, Dmp1 and DSPP expression was shown strongly an increase more than that in normoxia. Further study is needed to identify how oversupply of oxygen affects the mineralization of enamel and dentin.

MIH occurs when problems arise during the mineralization period of the permanent first molar and incisors (Lee et al., 2020). In humans, the mineralization of these teeth begins at the end of the gestation period (Tourino et al., 2016). It has been suggested that MIH occurs in children due to lack of oxygen, and, hypoxic conditions, due to asthma and/or bronchitis during the mineralization period, which may be closely related to amelogenesis. In hypomineralized enamel, the enamel mineral content is reduced, and it exhibits lower hardness values. In the ultrastructure of hypomineralized enamel, the crystals appear to be more loosely and irregularly packed than in the normal enamel (Bozal et al., 2015). Furthermore, the elements of O, Ca, and the Ca/P ratio are not different from those in normal teeth (Martinovic et al., 2015). However, C was significantly increased in hypomineralized enamel compared to that in normal enamel, while the P and Ca/C ratios were significantly lower in hypomineralized enamel than in normal enamel. MIH affects all hard dental tissues, such as enamel and dentin (Padavala and Sukumaran, 2018). In SEM analyses, no structural differences could be discerned between the dentin below normal enamel and the dentin below hypomineralized enamel (Heijs et al., 2007). The level of C was highest in dentin below hypomineralized enamel and lowest in dentin below normal enamel. The Ca/P ratios for dentin below hypomineralized enamel were in principle identical to those of normal enamel. When the Ca/C ratio was analyzed, dentin below hypomineralized enamel had the lowest value, whereas dentin below normal enamel had the highest. In this study, EDS analysis of the enamel revealed that tooth component, such as Ca, P, and Ca/C ratio showed lower under hypoxic condition, but O and Ca/P ratios were very similar. The Ca/C ratio was much lower than that of normoxia tooth. Furthermore, EDS analysis of dentin showed that while the Ca/P ratio was the same as that of normoxia enamel, but the Ca/C ratio was lower than that of dentin under normoxic conditions. The changes of composition of dentin and enamel under hypoxic conditions are similar to those of observed in hypomineralized teeth in MIH. These findings suggest prenatal oxygen deficiency at E16, or bell stage, when the hard tissues, such as enamel and dentin, start to form, as an etiology for hypomineralized teeth through cellular events with glucose metabolism (**Figure 10**). It was identified that the mineralization defect was restored through ONBs treatment when hypoxia-induced defects occurred for 3 h. However, this study involves restoring embryonic tissue under short exposure to low oxygen conditions. In the future, further studies on efficient oxygen delivery to treat tissues exposed to long-term hypoxia will be needed. In conclusion, we suggest that ONB can be used to successfully restore hypomineralized enamel and dentin caused by hypoxia by supplying oxygen and help researchers develop regenerative medicine treatment to improve clinical care.

DATA AVAILABILITY STATEMENT

The original contributions presented in the study are included in the article/**Supplementary Material**, further inquiries can be directed to the corresponding author/s.

ETHICS STATEMENT

The animal study was reviewed and approved by the Yonsei University College of Dentistry, Intramural Animal Use and Care Committee (2019-0306).

AUTHOR CONTRIBUTIONS

H-SJ and E-JK designed study. E-JK, J-EL, SY, D-JL, and HM performed the research. E-JK, J-EL, SY, D-JL, HM, HI-Y, JC, and H-SJ discussed the data. E-JK, J-EL, HI-Y, and H-SJ analyzed the data. E-JK, J-EL, and H-SJ wrote the paper. All authors contributed to the article and approved the submitted version.

FUNDING

This research was supported by the Bio & Medical Technology Development Program of the National Research Foundation (NRF) and funded by the Korean government (MSIP&MOHW) (No. 2017M3A9E4048172). This research was financially supported by grants from the National Research Foundation of Korea (NRF) Grant funded by the Korean Government (MSIP) (NRF-2016R1A5A2008630 and NRF-2019R1A2C3005294).

SUPPLEMENTARY MATERIAL

The Supplementary Material for this article can be found online at: https://www.frontiersin.org/articles/10.3389/fcell.2021.626224/full#supplementary-material

Supplementary Figure 1 | The EDS patterns of enamel and dentin. The peak patterns of EDS analysis of **(A,C,E)** enamel and **(B,D,F)** dentin on mineralized tooth with normoxia, hypoxia condition.

Supplementary Figure 2 | Effect on tooth calcification under hypoxic condition at E16. E16 tooth germs were transplanted into kidney capsule for 4 weeks for the calcification. Immunofluorescence was performed to show **(A–C)** AmelX, **(D–F)** MMP20, **(G–I)** Dmp1, and **(J–L)** Dspp expressions. **(A)** AmelX is expressed in mature ameloblasts in normoxia, but **(B)** the expression is found very little in hypoxia. **(C)** With ONBs, AmelX expression is mature ameloblasts are recovered. **(D)** MMP20 in secretory ameloblasts is expressed very little; however, **(E)** MMP20-positive secretory stage cells are increased in hypoxic condition. **(F)** MMP20 expression in ONBs are as similar as that in normoxia. **(G)** Dmp1 and **(J)** DSPP are expressed in odontoblasts, and in dentin in normoxia. In hypoxia, very little **(H)** Dmp1 and **(K)** DSPP positive cells are found in odontoblasts. and in dentin, **(I)** DMP1 and **(L)** DSPP are very strongly expressed in dentin, and in odontoblasts ($N = 3$) (Scale bar = 100 μm. ab, ameloblast; es, enamel space; d, dentin; ob, odontoblast; p, predentin; d, dentin; dotted line, dentioenamel junction; arrowheads; ameloblast, arrow: odontoblast).

REFERENCES

Al Tameemi, W., Dale, T. P., Al-Jumaily, R. M. K., and Forsyth, N. R. (2019). Hypoxia-modified cancer cell metabolism. *Front. Cell Dev. Biol.* 7:4. doi: 10.3389/fcell.2019.00004

Alaluusua, S. (2010). Aetiology of molar-incisor hypomineralisation: a systematic review. *Eur. Arch. Paediatr. Dent.* 11, 53–58. doi: 10.1007/bf03262713

Barron, M. J., McDonnell, S. T., Mackie, I., and Dixon, M. J. (2008). Hereditary dentine disorders: dentinogenesis imperfecta and dentine dysplasia. *Orphanet. J. Rare Dis.* 3:31. doi: 10.1186/1750-1172-3-31

Bartlett, J. D., Skobe, Z., Lee, D. H., Wright, J. T., Li, Y., Kulkarni, A. B., et al. (2006). A developmental comparison of matrix metalloproteinase-20 and amelogenin null mouse enamel. *Eur. J. Oral Sci.* 114, 18–23; discussion 39–41, 379. doi: 10.1111/j.1600-0722.2006.00292.x

Bhandari, P. N., Cui, Y., Elzey, B. D., Goergen, C. J., Long, C. M., and Irudayaraj, J. (2017). Oxygen nanobubbles revert hypoxia by methylation programming. *Sci. Rep.* 7:9268. doi: 10.1038/s41598-017-08988-7

Bozal, C. B., Kaplan, A., Ortolani, A., Cortese, S. G., and Biondi, A. M. (2015). Ultrastructure of the surface of dental enamel with molar incisor hypomineralization (MIH) with and without acid etching. *Acta odontol. Latinoam.* 28, 192–198. doi: 10.1590/s1852-48342015000200016

Bruick, R. K. (2000). Expression of the gene encoding the proapoptotic Nip3 protein is induced by hypoxia. *Proc. Natl. Acad. Sci. U.S.A.* 97, 9082–9087. doi: 10.1073/pnas.97.16.9082

Chen, C., Pore, N., Behrooz, A., Ismail-Beigi, F., and Maity, A. (2001). Regulation of glut1 mRNA by hypoxia-inducible factor-1. Interaction between H-ras and hypoxia. *J. Biol. Chem.* 276, 9519–9525. doi: 10.1074/jbc.M010144200

Cho, S. W., Kwak, S., Woolley, T. E., Lee, M. J., Kim, E. J., Baker, R. E., et al. (2011). Interactions between Shh, Sostdc1 and Wnt signaling and a new feedback loop for spatial patterning of the teeth. *Development* 138, 1807–1816. doi: 10.1242/dev.056051

Conte, C., Riant, E., Toutain, C., Pujol, F., Arnal, J. F., Lenfant, F., et al. (2008). FGF2 translationally induced by hypoxia is involved in negative and positive feedback loops with HIF-1alpha. *PLoS ONE* 3:e3078. doi: 10.1371/journal.pone.0003078

Cosse, J. P., Ronvaux, M., Ninane, N., Raes, M. J., and Michiels, C. (2009). Hypoxia-induced decrease in p53 protein level and increase in c-jun DNA binding activity results in cancer cell resistance to etoposide. *Neoplasia* 11, 976–986. doi: 10.1593/neo.09632

Dassule, H. R., Lewis, P., Bei, M., Maas, R., and McMahon, A. P. (2000). Sonic hedgehog regulates growth and morphogenesis of the tooth. *Development* 127, 4775–4785.

Deng, C., Li, J., Li, L., Sun, F., and Xie, J. (2019). Effects of hypoxia ischemia on caspase-3 expression and neuronal apoptosis in the brain of neonatal mice. *Exp. Ther. Med.* 17, 4517–4521. doi: 10.3892/etm.2019.7487

Du, W., Du, W., and Yu, H. (2018). The role of fibroblast growth factors in tooth development and incisor renewal. *Stem Cells Int.* 2018:7549160. doi: 10.1155/2018/7549160

Erler, J. T., Cawthorne, C. J., Williams, K. J., Koritzinsky, M., Wouters, B. G., Wilson, C., et al. (2004). Hypoxia-mediated down-regulation of Bid and Bax in tumors occurs via hypoxia-inducible factor 1-dependent and -independent mechanisms and contributes to drug resistance. *Mol. Cell Biol.* 24, 2875–2889. doi: 10.1128/mcb.24.7.2875-2889.2004

Gadhia, K., McDonald, S., Arkutu, N., and Malik, K. (2012). Amelogenesis imperfecta: an introduction. *Br. Dent. J.* 212, 377–379. doi: 10.1038/sj.bdj.2012.314

Garg, N., Jain, A. K., Saha, S., and Singh, J. (2012). Essentiality of early diagnosis of molar incisor hypomineralization in children and review of its clinical presentation, etiology and management. *Int. J. Clin. Pediatr. Dent.* 5, 190–196. doi: 10.5005/jp-journals-10005-1164

Graf, D., Malik, Z., Hayano, S., and Mishina, Y. (2016). Common mechanisms in development and disease: BMP signaling in craniofacial development. *Cytokine Growth Factor Rev.* 27, 129–139. doi: 10.1016/j.cytogfr.2015.11.004

Greijer, A. E., and van der Wall, E. (2004). The role of hypoxia inducible factor 1 (HIF-1) in hypoxia induced apoptosis. *J. Clin. Pathol.* 57, 1009–1014. doi: 10.1136/jcp.2003.015032

Guo, Y. (2017). Role of HIF-1a in regulating autophagic cell survival during cerebral ischemia reperfusion in rats. *Oncotarget* 8, 98482–98494. doi: 10.18632/oncotarget.21445

Harada, H., Toyono, T., Toyoshima, K., Yamasaki, M., Itoh, N., Kato, S., et al. (2002). FGF10 maintains stem cell compartment in developing mouse incisors. *Development* 129, 1533–1541.

Hayashi, M., Sakata, M., Takeda, T., Yamamoto, T., Okamoto, Y., Sawada, K., et al. (2004). Induction of glucose transporter 1 expression through hypoxia-inducible factor 1alpha under hypoxic conditions in trophoblast-derived cells. *J. Endocrinol.* 183, 145–154. doi: 10.1677/joe.1.05599

Heijs, S. C., Dietz, W., Norén, J. G., Blanksma, N. G., and Jälevik, B. (2007). Morphology and chemical composition of dentin in permanent first molars with the diagnose MIH. *Swed. Dent. J.* 31, 155–164.

Ida-Yonemochi, H., Nakatomi, M., Harada, H., Takata, H., Baba, O., and Ohshima, H. (2012). Glucose uptake mediated by glucose transporter 1 is essential for early tooth morphogenesis and size determination of murine molars. *Dev. Biol.* 363, 52–61. doi: 10.1016/j.ydbio.2011.12.020

Jussila, M., and Thesleff, I. (2012). Signaling networks regulating tooth organogenesis and regeneration, and the specification of dental mesenchymal and epithelial cell lineages. *Cold Spring Harb. Perspect. Biol.* 4:a008425. doi: 10.1101/cshperspect.a008425

Karcher-Djuricic, V., Staubli, A., Meyer, J. M., and Ruch, J. V. (1985). Acellular dental matrices promote functional differentiation of ameloblasts. *Differentiation* 29, 169–175. doi: 10.1111/j.1432-0436.1985.tb00311.x

Khan, M. S., Hwang, J., Lee, K., Choi, Y., Seo, Y., Jeon, H., et al. (2019). Anti-tumor drug-loaded oxygen nanobubbles for the degradation of HIF-1α and the upregulation of reactive oxygen species in tumor cells. *Cancers (Basel)* 11:1464. doi: 10.3390/cancers11101464

Khan, M. S., Hwang, J., Seo, Y., Shin, K., Lee, K., Park, C., et al. (2018). Engineering oxygen nanobubbles for the effective reversal of hypoxia. *Artif. Cell Nanomed. B* 46, S318–S327. doi: 10.1080/21691401.2018.1492420

Khan, M. S., Kim, J. S., Hwang, J., Choi, Y., Lee, K., Kwon, Y., et al. (2020). Effective delivery of mycophenolic acid by oxygen nanobubbles for modulating immunosuppression. *Theranostics* 10, 3892–3904. doi: 10.7150/thno.41850

Kilic, M., Kasperczyk, H., Fulda, S., and Debatin, K. M. (2007). Role of hypoxia inducible factor-1 alpha in modulation of apoptosis resistance. *Oncogene* 26, 2027–2038. doi: 10.1038/sj.onc.1210008

Kim, Y. J., Kim, J. Y., Cho, J. W., Cha, D. S., Lee, M. J., Osamu, T., et al. (2008). Implications for tooth development on ENU-induced ectodermal dysplasia mice. *Birth Defects Res. B Dev. Reprod. Toxicol.* 83, 97–103. doi: 10.1002/bdrb.20146

Kwon, H. J. E., Li, L., and Jung, H. S. (2015). Hippo pathway/Yap regulates primary enamel knot and dental cusp patterning in tooth morphogenesis. *Cell Tissue Res.* 362, 447–451. doi: 10.1007/s00441-015-2267-8

Lagerstrom-Fermer, M., and Landegren, U. (1995). Understanding enamel formation from mutations causing X-linked amelogenesis imperfecta. *Connect. Tissue Res.* 32, 241–246. doi: 10.3109/03008209509013729

Lee, D. W., Kim, Y. J., Oh Kim, S., Choi, S. C., Kim, J., Lee, J. H., et al. (2020). Factors associated with molar-incisor hypomineralization: a population-based case-control study. *Pediatr. Dentistry* 42, 134–140.

Lee, S. Y., Abel, E. D., and Long, F. (2018). Glucose metabolism induced by Bmp signaling is essential for murine skeletal development. *Nat. Commun.* 9:4831. doi: 10.1038/s41467-018-07316-5

Lesot, H., and Brook, A. H. (2009). Epithelial histogenesis during tooth development. *Arch. Oral Biol.* 54, S25–S33. doi: 10.1016/j.archoralbio.2008.05.019

Liu, Y., Li, Y., Tian, R., Liu, W., Fei, Z., Long, Q., et al. (2009). The expression and significance of HIF-1α and GLUT-3 in glioma. *Brain Res.* 1304, 149–154. doi: 10.1016/j.brainres.2009.09.083

Malhotra, R., and Brosius, F. C. III. (1999). Glucose uptake and glycolysis reduce hypoxia-induced apoptosis in cultured neonatal rat cardiac myocytes. *J. Biol. Chem.* 274, 12567–12575. doi: 10.1074/jbc.274.18.12567

Marine, J. C., and Lozano, G. (2010). Mdm2-mediated ubiquitylation: p53 and beyond. *Cell Death Differ.* 17, 93–102. doi: 10.1038/cdd.2009.68

Martinovic, B., Ivanovic, M., Milojkovic, Z., and Mladenović, R. (2015). Analysis of the mineral composition of hypomineralized first permanent molars. *Vojnosanit. Pregl.* 72:71. doi: 10.2298/VSP140310071M

Nakamizo, A., Amano, T., Zhang, W., Zhang, X. Q., Ramdas, L., Liu, T. J., et al. (2008). Phosphorylation of Thr18 and Ser20 of p53 in Ad-p53-induced apoptosis. *Neurooncology* 10, 275–291. doi: 10.1215/15228517-2008-015

Padavala, S., and Sukumaran, G. (2018). Molar incisor hypomineralization and its prevalence. *Contemp. Clin. Dent.* 9, S246–S250. doi: 10.4103/ccd.ccd_161_18

Rastogi, S., Banerjee, S., Chellappan, S., and Simon, G. R. (2007). Glut-1 antibodies induce growth arrest and apoptosis in human cancer cell lines. *Cancer Lett.* 257, 244–251. doi: 10.1016/j.canlet.2007.07.021

Sadagopan, S., Veettil, M. V., Chakraborty, S., Sharma-Walia, N., Paudel, N., Bottero, V., et al. (2012). Angiogenin functionally interacts with p53 and regulates p53-mediated apoptosis and cell survival. *Oncogene* 31, 4835–4847. doi: 10.1038/onc.2011.648

Sadier, A., Twarogowska, M., Steklikova, K., Hayden, L., Lambert, A., Schneider, P., et al. (2019). Modeling Edar expression reveals the hidden dynamics of tooth signaling center patterning. *PLoS Biol* 17:e3000064. doi: 10.1371/journal.pbio.3000064

Sermeus, A., and Michiels, C. (2011). Reciprocal influence of the p53 and the hypoxic pathways. *Cell Death Dis.* 2:e164. doi: 10.1038/cddis.2011.48

Sidaly, R., Risnes, S., Khan, Q. E., Stiris, T., and Sehic, A. (2015). The effect of hypoxia on the formation of mouse incisor enamel. *Arch. Oral Biol.* 60, 1601–1612. doi: 10.1016/j.archoralbio.2015.08.009

Sitkovsky, M. V., Lukashev, D., Apasov, S., Kojima, H., Koshiba, M., Caldwell, C., et al. (2004). Physiological control of immune response and inflammatory tissue damage by hypoxia-inducible factors and adenosine A2A receptors. *Annu. Rev. Immunol.* 22, 657–682. doi: 10.1146/annurev.immunol.22.012703.104731

Smith, C. E., and Nanci, A. (1995). Overview of morphological changes in enamel organ cells associated with major events in amelogenesis. *Int. J. Dev. Biol.* 39, 153–161.

Smith, C. E. L., Kirkham, J., Day, P. F., Soldani, F., McDerra, E. J., Poulter, J. A., et al. (2017). A fourth KLK4 mutation is associated with enamel hypomineralisation and structural abnormalities. *Front. Physiol.* 8:333. doi: 10.3389/fphys.2017.00333

Speidel, D. (2010). Transcription-independent p53 apoptosis: an alternative route to death. *Trends Cell Biol.* 20, 14–24. doi: 10.1016/j.tcb.2009.10.002

Sreenath, T., Thyagarajan, T., Hall, B., Longenecker, G., D'Souza, R., Hong, S., et al. (2003). Dentin sialophosphoprotein knockout mouse teeth display widened predentin zone and develop defective dentin mineralization similar to human dentinogenesis imperfecta type III. *J. Biol. Chem.* 278, 24874–24880. doi: 10.1074/jbc.M303908200

Suvarnapathaki, S., Wu, X. C., Lantigua, D., Nguyen, M. A., and Camci-Unal, G. (2019). Breathing life into engineered tissues using oxygen-releasing biomaterials. *NPG Asia Mater.* 11:65. doi: 10.1038/s41427-019-0166-2

Thesleff, I., K. S., and Jernvall, J. (2001). Enamel knots as signaling centers linking tooth morphogenesis and odontoblast differentiation. *Adv. Dent. Res.* 15:5. doi: 10.1177/08959374010150010401

Tourino, L. F. P. G., Corrêa-Faria, P., Ferreira, R. C., Bendo, C. B., Zarzar, P. M., and Vale, M. P. (2016). Association between molar incisor hypomineralization in schoolchildren and both prenatal and postnatal factors: a population-based study. *PLoS ONE* 11:e0156332. doi: 10.1371/journal.pone.0156332

Tsuboi, T., Mizutani, S., Nakano, M., Hirukawa, K., and Togari, A. (2003). Fgf-2 regulates enamel and dentine formation in mouse tooth germ. *Calcif Tissue Int.* 73, 496–501. doi: 10.1007/s00223-002-4070-2

Wang, G., Zhang, Z., Xu, Z., Yin, H., Bai, L., Ma, Z., et al. (2010). Activation of the sonic hedgehog signaling controls human pulmonary arterial smooth muscle cell proliferation in response to hypoxia. *Biochim. Biophys. Acta* 1803, 1359–1367. doi: 10.1016/j.bbamcr.2010.09.002

Wang, X. P., Suomalainen, M., Jorgez, C. J., Matzuk, M. M., Werner, S., and Thesleff, I. (2004). Follistatin regulates enamel patterning in mouse incisors by asymmetrically inhibiting BMP signaling and ameloblast differentiation. *Dev. Cell* 7, 719–730. doi: 10.1016/j.devcel.2004.09.012

Wu, D. C., and Paulson, R. F. (2010). Hypoxia regulates BMP4 expression in the murine spleen during the recovery from acute anemia. *PLoS ONE* 5:e11303. doi: 10.1371/journal.pone.0011303

Yan, H., Xue, G., Mei, Q., Wang, Y., Ding, F., Liu, M. F., et al. (2009). Repression of the miR-17-92 cluster by p53 has an important function in hypoxia-induced apoptosis. *EMBO J.* 28, 2719–2732. doi: 10.1038/emboj.2009.214

Yu, T., and Klein, O. D. (2020). Molecular and cellular mechanisms of tooth development, homeostasis and repair. *Development* 147:dev184754. doi: 10.1242/dev.184754

Zhang, H., Liu, Y., Yan, L., Du, W., Zhang, X., Zhang, M., et al. (2018). Bone morphogenetic protein-7 inhibits

endothelial-mesenchymal transition in pulmonary artery endothelial cell under hypoxia. *J. Cell Physiol.* 233, 4077–4090. doi: 10.1002/jcp.26195

Conflict of Interest: The authors declare that the research was conducted in the absence of any commercial or financial relationships that could be construed as a potential conflict of interest.

frontiers in Cell and Developmental Biology

ORIGINAL RESEARCH
published: 09 March 2021
doi: 10.3389/fcell.2021.586767

Retinoic Acid Signaling Plays a Crucial Role in Excessive Caffeine Intake-Disturbed Apoptosis and Differentiation of Myogenic Progenitors

Nian Wu[1,2†], Yingshi Li[1†], Xiangyue He[1,3†], Jiayi Lin[1†], Denglu Long[1], Xin Cheng[1], Beate Brand-Saberi[4], Guang Wang[1,2] and Xuesong Yang[1,2*]*

[1] Division of Histology and Embryology, International Joint Laboratory for Embryonic Development and Prenatal Medicine, Medical College, Jinan University, Guangzhou, China, [2] Key Laboratory for Regenerative Medicine of the Ministry of Education, Jinan University, Guangzhou, China, [3] Department of Pathology, Medical School, Jinan University, Guangzhou, China, [4] Department of Anatomy and Molecular Embryology, Institute of Anatomy, Ruhr-University Bochum, Bochum, Germany

OPEN ACCESS

Edited by:
Wolfgang Knabe,
Universität Münster, Germany

Reviewed by:
Francoise Helmbacher,
UMR7288 Institut de Biologie du Développement de Marseille (IBDM), France
Erika Jorge,
Federal University of Minas Gerais, Brazil

***Correspondence:**
Xuesong Yang
yang_xuesong@126.com
Guang Wang
wangguang7453@126.com;
t_wangguang@jnu.edu.cn

† These authors have contributed equally to this work

Specialty section:
This article was submitted to Cell Death and Survival, a section of the journal Frontiers in Cell and Developmental Biology

Received: 24 July 2020
Accepted: 04 February 2021
Published: 09 March 2021

Citation:
Wu N, Li Y, He X, Lin J, Long D, Cheng X, Brand-Saberi B, Wang G and Yang X (2021) Retinoic Acid Signaling Plays a Crucial Role in Excessive Caffeine Intake-Disturbed Apoptosis and Differentiation of Myogenic Progenitors. Front. Cell Dev. Biol. 9:586767. doi: 10.3389/fcell.2021.586767

Whether or not the process of somitogenesis and myogenesis is affected by excessive caffeine intake still remains ambiguous. In this study, we first showed that caffeine treatment results in chest wall deformities and simultaneously reduced mRNA expressions of genes involved in myogenesis in the developing chicken embryos. We then used embryo cultures to assess in further detail how caffeine exposure affects the earliest steps of myogenesis, and we demonstrated that the caffeine treatment suppressed somitogenesis of chicken embryos by interfering with the expressions of crucial genes modulating apoptosis, proliferation, and differentiation of myogenic progenitors in differentiating somites. These phenotypes were abrogated by a retinoic acid (RA) antagonist in embryo cultures, even at low caffeine doses in C2C12 cells, implying that excess RA levels are responsible for these phenotypes in cells and possibly *in vivo*. These findings highlight that excessive caffeine exposure is negatively involved in regulating the development of myogenic progenitors through interfering with RA signaling. The RA somitogenesis/myogenesis pathway might be directly impacted by caffeine signaling rather than reflecting an indirect effect of the toxicity of excess caffeine dosage.

Keywords: caffeine, myogenesis, somitogenesis, apoptosis, chicken emrbyo, retinoic acid signaling

INTRODUCTION

Caffeine intake during pregnancy has been reported to be potentially teratogenic. On the one hand, both the metabolic rate and the half-life of caffeine significantly increase in maternity (Yu et al., 2016), but on the other hand, the lipophilic characteristic of caffeine allows it to transfer freely across all biological membranes, including the placental barrier (Grosso and Bracken, 2005). Therefore, maternal caffeine intake during pregnancy increases the risk of poor birth outcomes. For example, current studies in humans have shown that the birth defects induced by maternal caffeine

intake include low birth weight, childhood overweight, and cognitive impairment (Qian et al., 2019). The caffeine exposure has been also reported to disrupt chondrogenesis and osteogenesis (Wink et al., 1996; Reis et al., 2013). As far as we know, muscle and cartilage cells are derived from the somites during the early stage of embryonic development (Christ and Ordahl, 1995; Jang and Baik, 2013). However, it still remains elusive whether or not the differentiation of somitic precursor populations of muscle cells as well as the myogenesis can be affected by caffeine exposure.

Mouse, rat, and chicken embryos have been extensively used as the models for studying congenital birth defects in different organ systems that have been induced by teratogen exposure (Dangata and Kaufman, 1997; Bupp Becker and Shibley, 1998; Illanes et al., 1999; Cavieres and Smith, 2000; Debelak and Smith, 2000; Roda-Moreno et al., 2000; Miller et al., 2001; Sawada et al., 2002). The chicken embryo is actually a leading model in somitogenesis studies and many of the landmark experiments, which greatly contribute to our current understanding of the process of vertebrate segmentation (Pourquié, 2004). During the early stages of chicken embryo development, somites develop from the paraxial mesoderm and constitute the segmental pattern of the body (Christ and Ordahl, 1995). They are formed in pairs by epithelialization and located on both sides of the neural tube. Somite formation results from a tight spatiotemporal control of expressions of "oscillating genes," including the Notch signaling pathway, Wnt/beta-catenin signaling pathway, fibroblast growth factors (FGFs), Hox genes, and retinoic acid (RA) (Borycki et al., 2000; Dubrulle et al., 2001; Carapuco et al., 2005; Hamade et al., 2006). The subsequent compartmentalization of the somites is accomplished by signals emerging from neighboring tissues (Brand-Saberi et al., 1996). Diffusible factors positively or negatively control apoptosis during development. Wnts, Bone morphogenetic proteins (BMPs), and N-cadherin are implicated in dermomyotome differentiation (Capdevila et al., 1998; Linask et al., 1998), while Sonic hedgehog (Shh) is the main notochord-derived factor responsible for sclerotome differentiation (Münsterberg et al., 1995). Shh positively controls the survival of mesoderm-derived somite cells and is also capable of inducing myotomal markers in combination with the Wnts (Münsterberg et al., 1995; Marcelle et al., 1997; Cotrina et al., 2000). Apart from requirement for somite differentiation, inhibition of BMP4 signaling was reported to be important in myotomal development as well (Reshef et al., 1998). Noggin, a BMP4 antagonist, can be activated by Shh and Wnt signaling pathways (Hirsinger et al., 1997).

The earliest muscle-specific markers expressed in the somites are members of the myogenic regulatory gene family (MRF) encoding basic helix–loop–helix transcription factors, which comprise MyoD (Myod1), Myf5, MRF4, and myogenin. Myoblasts are committed to the skeletal muscle lineage by MyoD and Myf5 expression, while MRF4 and myogenin are involved in the initiation of differentiation of myogenic progenitors into myoblasts (Bober et al., 1994; Jang and Baik, 2013). The Pax gene family plays key roles in the formation of living tissues and organs during embryogenesis, of which Pax3 and Pax7 mark myogenic progenitor cells (Relaix et al., 2005; Buckingham and Relaix, 2007). Pax7 is also uniquely indispensable for satellite cells, which arise from a population of muscle progenitor cells that originate in the central domain of the dermomyotome (McKinnell et al., 2008). Myf5 has been reported to be directly regulated by Pax7 in the differentiation of satellite cell-derived myoblasts (McKinnell et al., 2008).

Using chicken embryos, our previous studies have revealed the effects of caffeine exposure on the development of the fetal nervous system, eye, and angiogenesis (Ma et al., 2012, 2014, 2016; Wang et al., 2019). Since there were no reports about caffeine influence on the process of myogenesis and somitogenesis, we set out to explore the effects and underlying biological mechanisms of caffeine on the critical time period of myogenesis during the early embryo development using the chicken embryo as a model system.

MATERIALS AND METHODS

Experimental Chicken Embryos

Fertilized Leghorn eggs were obtained from the Avian Farm of the South China Agriculture University (Guangzhou, China) and incubated until reaching the required developmental stage (Hambuger and Hamilton) in a humidified incubator (Hamburger and Hamilton, 1951). For the caffeine-treated early stage embryos, the HH4 chicken embryos (about 12-h incubation) in early chick (EC) culture were treated with 300 μM of caffeine (Nacalai, Japan), 300 μM of caffeine + 10^{-5} M of AGN (AGN, an active RA receptor antagonist AGN193109), or same the amount of phosphate-buffered saline (PBS) until the experimentally required developmental stage. Moreover, the antibiotics penicillin/streptomycin were added to the EC culture (Chapman et al., 2001). For the elder stage embryos, HH10 (about 1.5-day incubation) pre-incubated chicken embryos were exposed to 5, 10, 15, 30 μmol/egg caffeine, or same the amount of avian saline through injection into windowed eggs *in vivo* (Ma et al., 2012, 2014, 2016; Wang et al., 2019). The surviving embryos were harvested for further analyses.

Explant Culture

The somites and presomitic mesoderm (PSM) absence of the neural tube were separated from HH10 chicken embryos as previously reported (Wang et al., 2015). The explant were incubated in DMEM–F12 culture medium (Gibco, Grand Island, NY) or 300 μM of caffeine DMEM–F12 inside an incubator (Galaxy S; RS Biotech, Scotland, UK) at 37°C and 5% CO2 for 24 h.

Cell Culture and Scratch Wound Migration Assay

C2C12 cells were purchased from Guangzhou Jennio Biotech Co., Ltd, China, and cultured in culture medium (DMEM–F12 GIBCO). A "scratch wound" was created by scraping a monolayer culture of C2C12 cells using a sterile 10-μl pipette tip; the images were taken using an inverted microscope (Nikon Eclipse TiU, Japan). The length of the wound gap was measured using Image pro-Plus software. The assays were performed three times using triplicate culture well.

Histology

E6 (HH28) and E9 (HH35) chicken embryos were fixed in 4% paraformaldehyde at 4°C for 24 h. The specimens were then dehydrated, cleared in xylene, and embedded in paraffin wax before being serially sectioned at 5 μm using a rotary microtome (Leica RM2126RT, Germany). The sections were stained with hematoxylin and eosin (H&E) (Sigma-Aldrich, USA), Safranin O (Sigma-Aldrich, USA), and Masson (Sigma-Aldrich, USA) following standardized protocols. The frozen sections were prepared by sectioning at thickness of 15–20 μm on a cryotome (Leica CM1900, Bensheim, Germany).

Immunofluorescence Staining

The harvested HH10 and E2.5 (HH17) chicken embryos were fixed in 4% paraformaldehyde overnight at 4°C. Whole-mount embryo immunostaining was performed using the following antibodies: c-Caspase3 (cleaved Caspase3, 1:200, Cell Signaling Technology, Danvers, MA), Pax7 (1:200, DSHB, Iowa City, IA), phospho-Histone H3 (PH3, 1:200, Cell Signaling Technology, USA), and MF-20 (1:200, DSHB, Iowa City, IA). Briefly, the fixed embryos were incubated with primary antibody overnight at 4°C on a shaker. After extensive washing, the embryos were incubated with either anti-mouse IgG conjugated to Alexa Fluor 555 or anti-rabbit IgG conjugated to Alexa Fluor 488 (1:1,000; Invitrogen, Waltham, MA, USA) overnight at 4°C on a shaker. All the embryos were later counterstained with DAPI (1:1,000; Invitrogen, Waltham, MA, USA) at room temperature for 1 h.

In situ Hybridization

Whole-mount *in situ* hybridization of chicken embryos was performed according to a standard *in situ* hybridization protocol (Henrique et al., 1995). Briefly, digoxigenin-labeled probes were synthesized again BMP4 (Chapman et al., 2004), Wnt3a (Chapman et al., 2004), Shh (Chapman et al., 2004), Myf5, and RALDH2. RNA antisense Myf5 and RALDH2 probes used were obtained by reverse transcription polymerase chain reaction (RT-PCR) technique as described by Bales et al. (1993). Specific primers are described in **Supplementary Table 1**. Total RNAs were isolated from HH10 chicken embryos.

RNA Isolation and Quantitative PCR

Total RNA was extracted using a TRIzol kit (Invitrogen, Waltham, MA, USA), from the whole HH10 chicken embryos, somites and PSM explants, C2C12 cells, or the E6 and E9 embryos after removing the head, viscera, and cartilage. First-strand cDNA was synthesized to a final volume of 20 μl using a SuperScript RIII first-strand kit (Invitrogen, USA). Following RT, PCR amplification of the cDNA was performed using chicken specific primers. Specific primers are described in **Supplementary Table 1**. The PCRs were performed in a Bio-Rad S1000™ Thermal cycler (Bio-Rad, Hercules, CA, USA) as the manufacturer described. The final reaction volume of 50 μl is composed of 1 μl of first-strand cDNA, 25 μM of forward primer, 25 μM of reverse primer, 10 μl of PrimeSTAR™ Buffer (Mg^{2+} plus), 4 μl of dNTPs Mixture (Takara, Tokyo, Japan), and 0.5 μl of PrimeSTAR™ HS DNA Polymerase (2.5 U/μl; Takara, Japan) in RNase-free water. The cDNAs were amplified for 30 cycles. One round of amplification was performed at 94°C for 30 s, at 58°C for 30 s, and at 72°C for 30 s. The PCR products (20 μl) were resolved in 1% agarose gels (Biowest, Hong Kong, China) in 1× TAE buffer (0.04 M of triacetate and 0.001 M of EDTA), and 10,000× GeneGreen Nucleic Acid Dye (Tiangen, Beijing, China) solution. The resolved products were visualized in a transilluminator (Syngene, Cambridge, UK), and photographs were captured using a computer-assisted gel documentation system (Syngene). The expression of genes was normalized to GAPDH. At least 15 HH10 embryos or explants were mixed for one sample; at least three E6 or E9 embryos were mixed for one sample. The quantitative PCR results shown are representative of three independent experiments.

Western Blot

Chest wall tissues (removed cartilage) were collected from E9 control of 300 μM caffeine-treated chicken embryos**.** Western blot analysis was performed in accordance with the standard procedure using the c-Caspase3 (cleaved Caspase3, 1:500, Cell Signaling Technology, Danvers, MA). The protein was isolated using a radioimmunoprecipitation assay (Sigma-Aldrich) buffer supplemented with protease inhibitor. Protein concentrations were quantified with the bicinchoninic acid assay. The loading control was a β-actin antibody (1:3,000; Proteintech, Rosemont, IL). Quantity One (Bio-Rad) was used to capture the chemiluminescent signals and analyze the data. All samples were performed in triplicate.

Enzyme-Linked Immunosorbent Assay

ELISA kits (Meibiao Biol Tech, Jiangsu, China) were used to measure RA from HH10 chicken embryos according to the manufacturer's instructions. The results were calculated using interpolation from a standard curve created by a series of RA concentrations.

Protein–Protein Interaction Network Analysis

STRING (Search Tool for the Retrieval of Interacting Genes/Proteins, https://string-db.org) was used for the protein–protein interaction (PPI) network analysis.

Photography

Following immunofluorescence staining or *in situ* hybridization, whole-mount embryos were photographed using a stereo-fluorescent microscope (Olympus MVX10) and associated Olympus software package Image-Pro Plus 7.0. The embryos were sectioned into 14-μm-thick slices using a cryostat microtome (Leica CM1900), and sections were photographed using an epifluorescence microscope (Olympus LX51, Leica DM 4000B) with the CN4000 FISH Olympus software package.

Data Analysis

Data analyses and construction of statistical charts were performed using the GraphPad software (La Jolla, CA, USA). All data were expressed as the mean value (mean ± SEM). Statistical evaluation was performed using ANOVA with Tukey's pairwise comparisons or independent samples *t*-test. Statistical

significance was defined as $P < 0.05$. The data are indicated with * for $P < 0.05$, ** for $P < 0.01$, and *** for $P < 0.001$. All the details on statistics are summarized in the **Supplementary Material**.

RESULTS

Excess Caffeine Exposure Causes Chest Wall Deformities in Chicken Embryos

In our previous study on the effects of caffeine on the monoamine neurotransmitter system, we have investigated the effect of low doses of caffeine (i.e., 2.5, 5, and 10 μmol/egg) on the development of chicken embryos (Li et al., 2012). To obtain the adequate numbers of alive embryos with significant phenotype, we exposed HH10 (E1.5) chicken embryos with 5, 10, 15, and 30 μmol/egg caffeine every 48 h, and the embryos were harvested on the 9th day (**Supplementary Figure 1A**). The results manifested that caffeine exposure increased embryo mortality in a dose-dependent manner (**Supplementary Figure 1B**). The death rate of embryos increased to around 50% when the caffeine concentration reached 15 μmol/egg. The harvested chicken embryos were treated with 15 μmol/egg caffeine and PBS (control) for further investigations.

We first checked the weight of the 9-day-old embryos. The embryo weight of chicken embryos in the caffeine-treated group was about 20% lower than that in the control group (**Supplementary Figure 1C**). Actually, the embryo weight decreased from Day 6 (**Supplementary Figure 3A**). The morphological phenotypes of the embryos harvested on Day 9 were examined; and more than 75% of the embryos in the caffeine-treated group showed varying degrees of chest wall deformities (**Supplementary Figures 1D,E**). H&E, Safranin O, and Masson staining were performed on the transverse serial sections of both control and caffeine-treated embryos with mild chest wall deformities. Cartilage territorial matrix (keratan sulfate and chondroitin sulfate) is much basophilic on H&E staining. Safranin O is a basic dye that stains cartilage (proteoglycans, chondrocytes, and type II collagen) in varying shades of red. Cartilage and collagenous fiber are colored in blue, while muscle tissue is colored in red on Masson staining. The results demonstrated a significant suppression of cartilage fusion (red arrows in **Supplementary Figures 2J1,N,P**) and muscle tissue anomaly (Masson staining, blue arrow in **Supplementary Figure 2P**), indicating that chest wall development is affected by directly exposing the developing chicken embryos to high doses of caffeine.

Among the tissues affected by the deformity, muscles were particularly reduced in size. We therefore chose to examine the expression of the key genes involved in the myogenesis. Quantitative PCR data indicated that the mRNA expressions of MYH7B (a myosin heavy chain essential for the thick filaments of striated muscle), MEF2A [a myocyte enhancer factor (MEF) significant in muscle differentiation], myogenin (controlling the terminal differentiation of myoblasts into myocytes), Myod1 (muscle regulatory factor), and Pax7 (marking myogenic progenitor cells and regulating their entry into the program of skeletal muscle differentiation) were reduced in the presence of caffeine (**Supplementary Figure 2Q**). We further examined the expression of these genes in E6 chicken embryos, and we found a similar decreasing trend (**Supplementary Figure 3B**). These results are consistent with the reduction in muscle size observed by histology.

Caffeine Treatment Suppressed the Somitogenesis of Chicken Embryos During Embryogenesis

Since the majority of the musculoskeletal system derives originally from the somites, we then investigated the effect of caffeine on somitogenesis. The HH4 chicken embryos (normally pre-incubated for about 12 h) were incubated in EC culture with or without 300 μM of caffeine (300 μM *in vitro* corresponds to 15 μmol/egg as one egg is equal to 50 g) and then harvested until stage HH10 (**Figure 1A**). The embryo mortality (up to around 40%) was increased with time in response to caffeine exposure (**Figures 1B,C**). The length of the caffeine-treated embryos was generally shorter compared with the corresponding control group after 18- and 34-h incubation (**Figures 1B,D**). Most of the control embryos reached HH10 (10 pairs of somite stage) after 34 h of incubation, whereas the caffeine-treated embryos did not. Moreover, at 34 h, caffeine-treated embryos exhibited a reduced number of somite pairs as compared with the control group (**Figure 1E**).

Embryos of the caffeine-treated group were further incubated until stage HH10 and then compared with the HH10 embryos in the control group. Immunofluorescence staining of Pax7 indicated the abnormal somite formation induced by caffeine treatment (**Figures 1F–K,G1,H1,J1,K1**; $n = 6$ embryos in the control group and n = 12/18 embryos in the caffeine-treated group). The mRNA levels of Pax7 were clearly decreased in the somites in the presence of caffeine compared with controls (**Figure 1L**). These results indicated that caffeine treatment had an early effect by interfering with somitogenesis of chicken embryos.

Caffeine Treatment Interfered With the Expressions of Crucial Genes Modulating Apoptosis, Proliferation, and Cell Differentiation in Somites

To investigate whether caffeine treatment affects the apoptosis, we used immunofluorescence c-Caspase3 staining to determine the presence of apoptotic cells in the whole embryo following caffeine treatment. The apoptosis was generalized, and the numbers of c-Caspase3-positive cells were significantly increased in the somites of the caffeine-treated group compared with the control (**Figures 2A–E,B1,D1**). These data indicated that caffeine treatment promoted cell apoptosis in somites. To further prove that the increased apoptosis is linked to the chest wall defect, we determined the c-Caspase3 expression using western blot in the sample from the chest wall without cartilage in E9 chicken embryos. The results indicated that c-Caspase3 expression in the chest wall from caffeine-treated embryos was much higher than the one from the control (**Figure 2F**). The similar results were also obtained in the

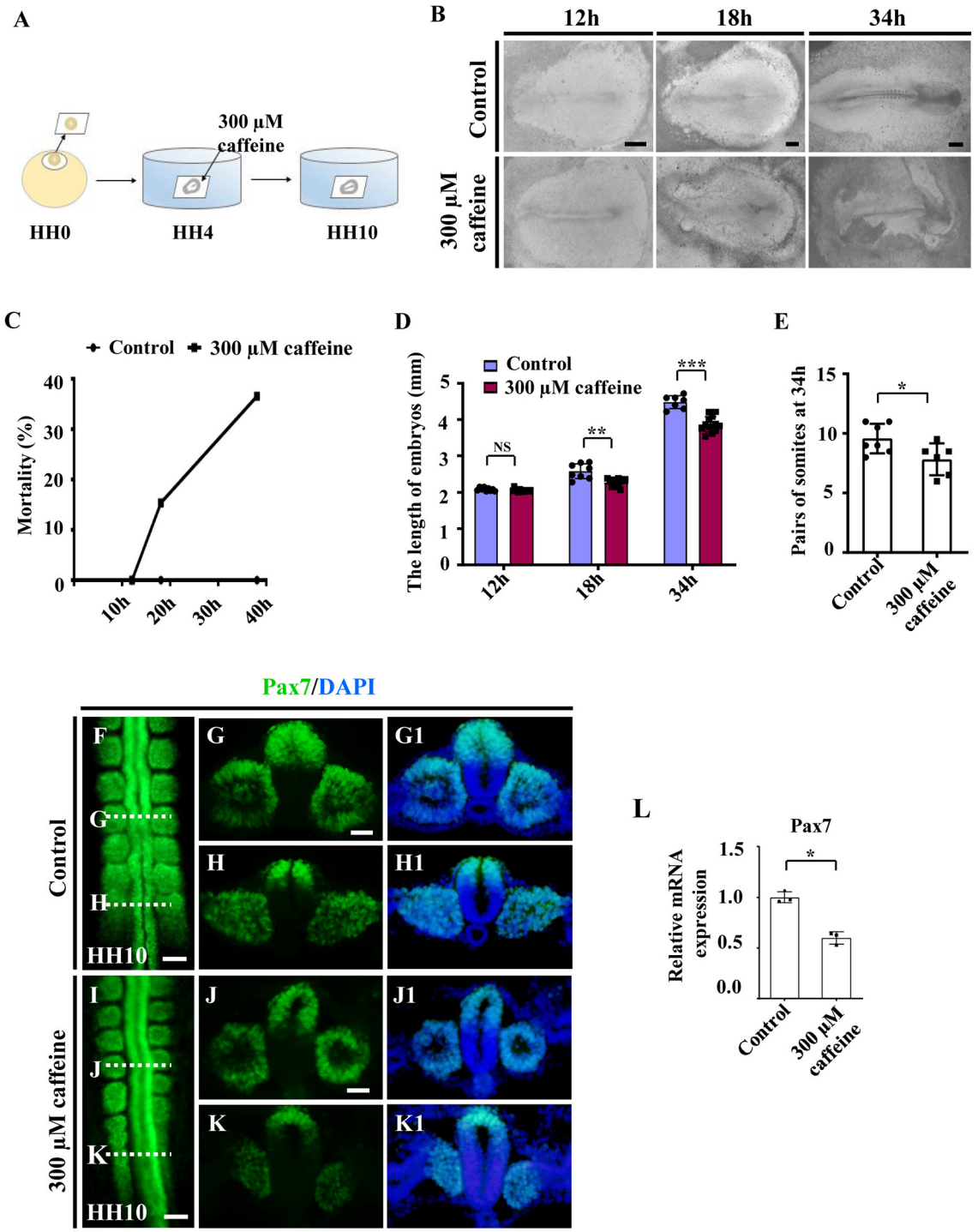

FIGURE 1 | Assessment of chicken somitogenesis following caffeine treatment. **(A)** The sketch illustrates the development of chicken embryos in early chick (EC) culture with or without caffeine. Caffeine was applied to the embryos at HH4 (12-h incubation). **(B)** Representative images of whole chicken embryos from the control and caffeine-treated groups, taken after 12, 18, and 34 h of incubation. **(C)** The curve chart showing the comparisons of mortality of chicken embryos from the control and caffeine-treated groups. **(D,E)** The bar charts showing the comparisons of length and somite pairs of chicken embryos between the control and caffeine-treated groups. **(F–K, G1–K1)** Immunofluorescence staining of Pax7 in the chicken embryos from the control **(F)** and caffeine-treated **(I)** groups, and the corresponding transverse sections for Pax7 and merge with DAPI staining **(G,H,J,K,G1,H1,J1,K1)**. Panels **(G/J)** and **(H/K)** are from the seventh somites and presomitic mesoderm (PSM) of somites, respectively. **(L)** Quantitative RT-PCR data showing the mRNA expression of Pax7 from the control and caffeine-treated groups. Scale bars = 500 μm in panel **(B)**; 100 μm in panels **(F, I)**; 50 μm in panels **(G,H,J,K,G1,H1,J1,K1)**. $^{*}P < 0.05$, $^{**}P < 0.01$, $^{***}P < 0.001$.

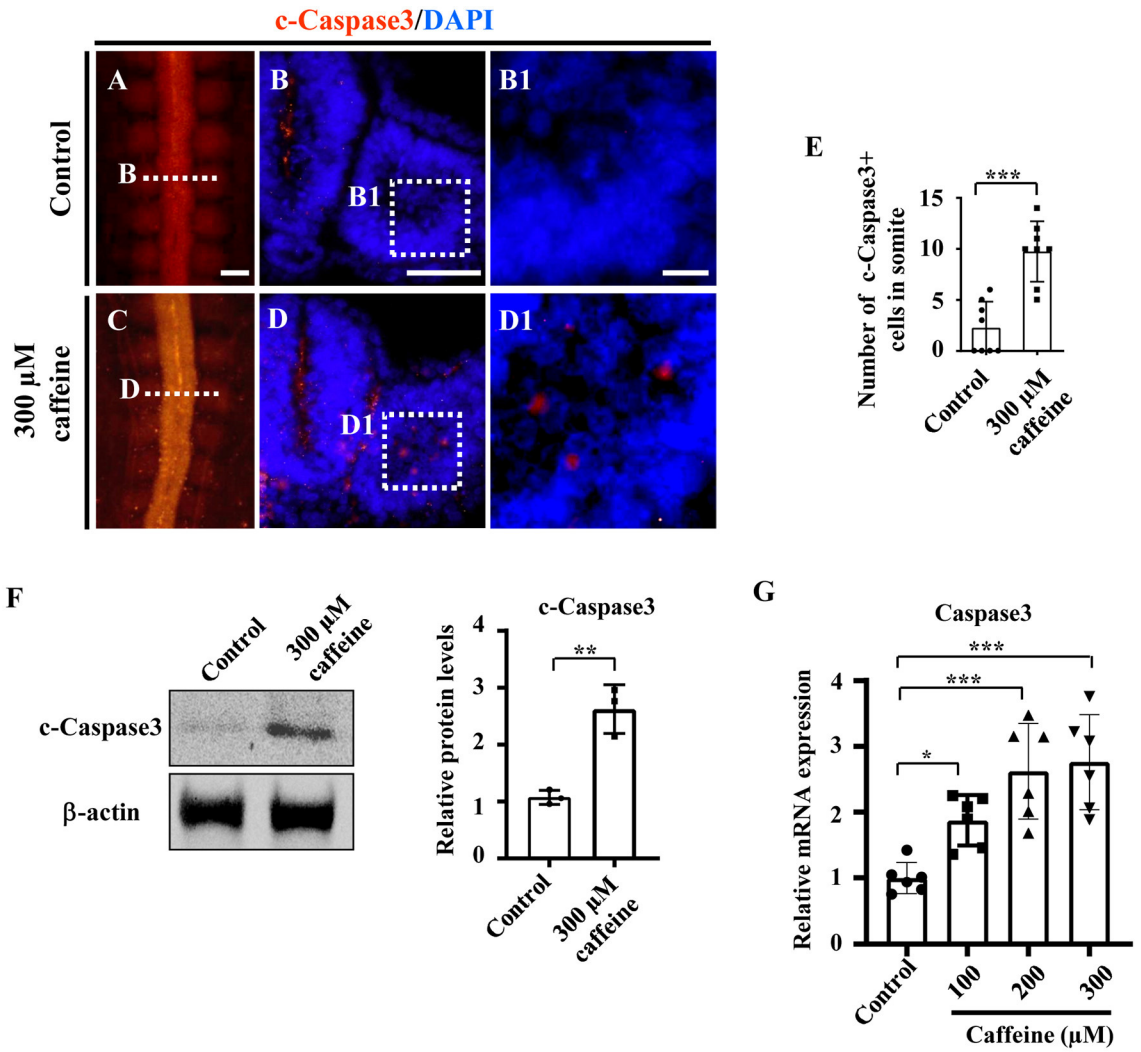

FIGURE 2 | Determination of cell apoptosis in the developing somites of HH10 embryos and C2C12 cells following caffeine treatment. **(A–D)** Immunofluorescence staining of c-Caspase3 in the chicken embryos from control **(A)** and caffeine-treated **(C)** groups, and the corresponding transverse sections for c-Caspase3 and merge with DAPI staining **(B,D)**. Panels **(B/D)** is from the fifth pair of somites. **(B1,D1)** High-magnification images from the sites indicated by **(B,D)**, respectively. **(E)** The bar chart showing the proportion of c-Caspase3-positive cell numbers in somite from the control and caffeine-treated groups. c-Caspase3, cleaved Caspase3. **(F)** Western blotting showing c-Caspase3 expressions in chicken embryos without the head, viscera, and cartilage from the control and caffeine-treated groups. **(G)** Quantitative RT-PCR data showing the mRNA expression of c-Caspase3 in C2C12 cells after caffeine treatment. Scale bars = 100 μm in panels **(A,C)**; 50 μm in panels **(B,D)**; 10 μm in panels **(B1,D1)**. $^{*}P < 0.05$, $^{**}P < 0.01$, $^{***}P < 0.001$.

mouse C2C12 cells treated with 300 μM of caffeine and lower doges of 100 and 200 μM (**Figure 2G**). Quantitative PCR data indicated that the Caspase3 mRNA was increased in a dose-dependent manner (**Figure 2G**). To investigate whether or not caffeine could directly cause the cell apoptosis of somites, we determined c-Caspase3 expression in the cultured explants composed of somite and PSM *in vitro*. The quantitative PCR data indicated that the Caspase3 mRNA levels were increased following 300 μM caffeine treatment (**Supplementary Figures 4A,B**). These results suggest that caffeine treatment can directly lead to cell apoptosis in somite.

In order to explore what caused the reduction of tissue size, cell proliferation was also detected on the HH10 embryos and C2C12 cells, as well as somite and PSM explants. Interestingly, the number of PH3-positive cells was significantly increased in the somites of the caffeine-treated group compared with the control (note: the red arrows indicate the PH3-positive cells in the somites) (**Supplementary Figures 5A–E**). Quantitative PCR data demonstrated that the Cyclin D1 mRNA levels were also increased in somite and PSM explants (**Supplementary Figure 4C**). The increase was observed in a dose-dependent manner in C2C12 cells (**Supplementary Figure 5F**). These results show that the

reduced size does not result from a reduced proliferation rate, as it is unexpectedly associated with an increase in proliferation in somites.

We then determined the expression of Myf5 in the somite, which is a myogenic precursor marker. The whole-mount *in situ* hybridization (**Figures 3A,C**), and the corresponding sections (**Figures 3B,D**) showed that caffeine treatment dramatically inhibited the expression of Myf5 during somite differentiation of chicken embryos. Quantitative PCR data indicated that the mRNA expression of Myf5 was also reduced in the presence of caffeine (**Figure 3E** and **Supplementary Figures 4C, 5D**).

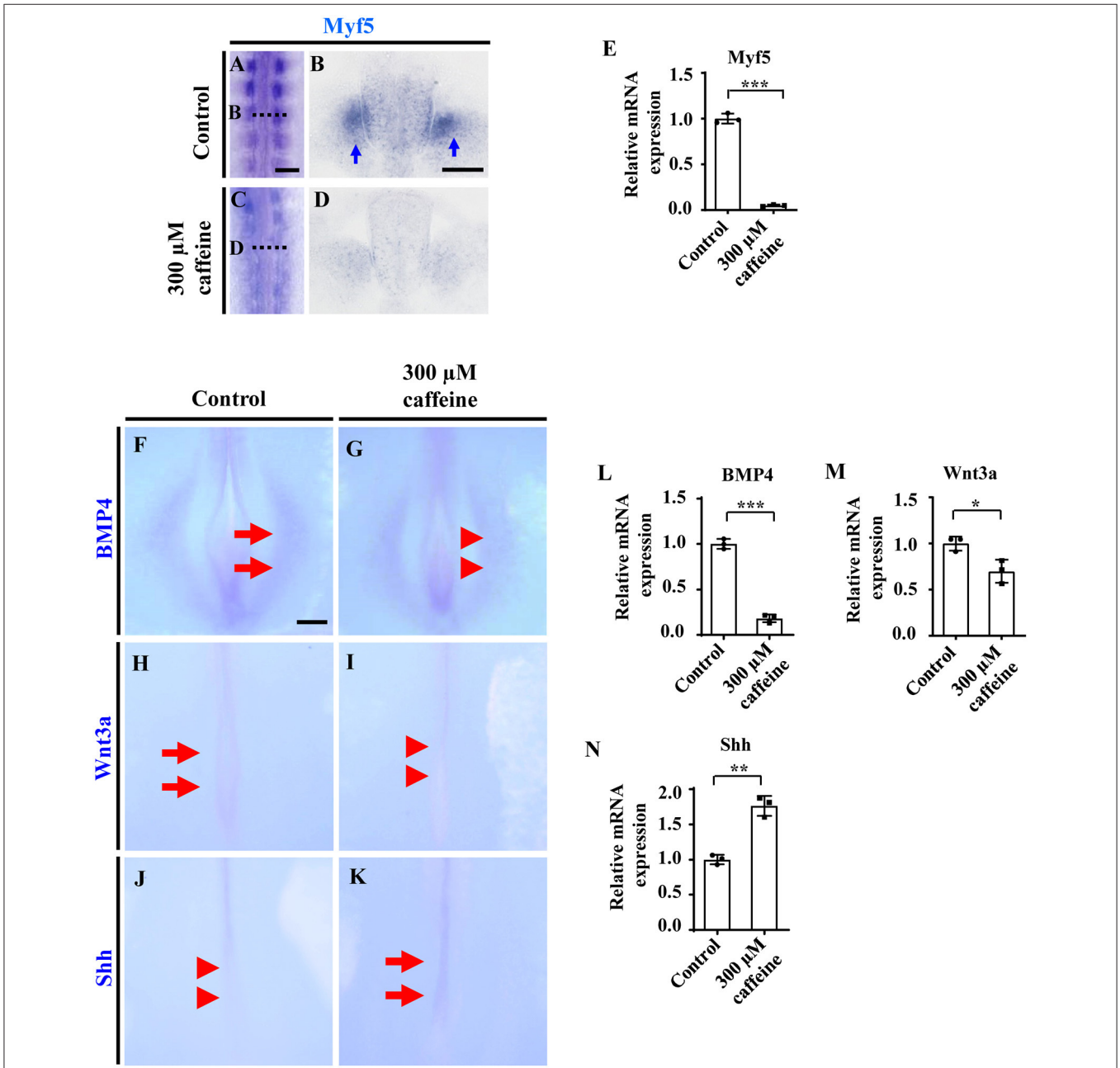

FIGURE 3 | Determination of cell differentiation in the developing somites following caffeine treatment. **(A–D)** Whole-mount *in situ* hybridization for Myf5 in the chicken embryos from control **(A)** and caffeine-treated **(C)** groups, and the corresponding transverse sections **(B,D)**. Panels **(B/D)** is from the fifth pair of somites. **(E)** Quantitative RT-PCR data showing the mRNA expression of Myf5 from the control and caffeine-treated groups. **(F–K)** Whole-mount *in situ* hybridization for BMP4, Wnt3a, and Shh in the chicken embryos from control **(F,H,J)** and caffeine-treated **(G,I,K)** groups. **(L–N)** Quantitative RT-PCR data showing the mRNA expression of BMP4, Wnt3a, and Shh from the control and caffeine-treated groups. Scale bars = 100 μm in panels **(A,C)**; 50 μm in panels **(B,D)**; 200 μm in panels **(F–K)**. $^{*}P < 0.05$, $^{**}P < 0.01$, $^{***}P < 0.001$.

In situ hybridization and quantitative PCR were carried out to determine the expression change of diffusible factors that are involved in regulating cell survival positively or negatively during development. Whole-mount *in situ* hybridization of BMP4, Wnt3a, and Shh showed that caffeine treatment significantly inhibited the expression of BMP4 ($n = 6$ embryos in the control group and $n = 5/6$ embryos in the caffeine-treated group) and Wnt3a ($n = 6$ embryos in the control group and $n = 5/6$ embryos in the caffeine-treated group) but increased the expression of Shh ($n = 6$ embryos in the control group and $n = 4/6$ embryos in the caffeine-treated group) at the posterior level in HH10 chicken embryos (red arrowheads in **Figures 3G,I,J** indicated the lower expression compared with the arrows in **Figures 3F,H,K**, indicating expressions). Quantitative PCR results verified the alteration on these gene (**Figures 3L–N**).

Caffeine Treatment Leads to Dramatic Alteration of Retinoic Acid Signaling During Somite Differentiation

The asymmetries of somite pairs in caffeine-treated chicken embryos (**Figures 1J,K**) are reminiscent of the published research findings, which demonstrated that RALDH2 was required to ensure the symmetric production of somite pairs during somitogenesis (Kawakami et al., 2005; Vermot et al., 2005; Sirbu and Duester, 2006). Moreover, RALDH2 could influence somitogenesis and myogenesis by means of acting on Shh and BMP4 (Power et al., 1999; Mic and Duester, 2003; Pourquié, 2018). Therefore, it is reasonable to infer that caffeine treatment-suppressed somite development was achieved by interfering with RA pathway.

Consistently with the link highlighted above (somite/RALDH2), these abnormalities in somite development are associated with an increase in RALDH2 levels. These findings are further corroborated by the observation by ELISA. The ELISA data showed that the RA concentration (RA synthesis being ensured by RALDH2) was increased in caffeine-treated HH10 chicken embryos (**Figure 4A**). Accordingly, the mRNA levels of RALDH2 in chicken embryos, C2C12 cells, as well as somite and PSM explants, were significantly enhanced (**Figures 4B,B1** and **Supplementary Figures 4D, 5F**). The caffeine-induced increase of RALDH2 expression in chicken embryos was verified by RALDH2 whole-mount *in situ* hybridization and corresponding transverse sections (**Figures 4C,D,C1–D3**). RALDH2 expression was significantly increased on somites at C1/D1 and C2/D2 levels in the caffeine-treated group compared with the control group ($n = 5$ embryos in the control group and $n = 5/7$ embryos in the caffeine-treated group). However, the RALDH2 expression at C3/D3 level seemed to get weaker in some of the embryos in the caffeine-treated group ($n = 5$ embryos in the control group and $n = 3/7$ embryos in the caffeine-treated group). These results revealed that the total mRNA level of RALDH2 in chicken embryos was promoted in the presence of caffeine, especially obvious after the somite formation.

Moreover, we used immunohistochemistry to determine the expression levels of the myosin marker MF-20 in the control, caffeine-treated, and RA-treated E2.5 chicken embryos. The results showed that MF-20 expression was significantly decreased in both groups compared with the control (**Figures 4E–H,E1–G1,E2–G2**). All the data indicate that RA signaling could be involved in caffeine-induced inhibition of somitogenesis and subsequent compartment formation/differentiation of somite during the early chicken embryo development. These matched the finding from the bioinformatics approach through exploring the relationships in the context of pharmacological target proteins of caffeine [adenosine A2A receptor gene (ADORA2A) and acetylcholinesterase (AChE)], apoptosis, and somitogenesis/myogenesis proteins (**Figure 4I**).

To further confirm that the RA signaling plays an important role in caffeine disturbed somitogenesis and myogenesis, we detected whether or not the caffeine-induced abnormalities of somite development could be rescued by AGN (a potent RA receptor antagonist) (Bayha et al., 2009). We exposed the chicken embryos to caffeine and/or the AGN, and we found that blocking the RA signaling with AGN could significantly rescue the caffeine-induced reductions of embryo length and somite pairs (**Figures 5A,B**). The data from immunofluorescence staining and *in situ* hybridization manifested that the reduction of Pax7 and Myf5 expression caused by caffeine could be reversed by adding AGN (Pax7: $n = 5$ embryos in the control group, $n = 4/5$ embryos in the caffeine-treated group, and $n = 5/6$ embryos in the caffeine+AGN group; Myf5: $n = 5$ embryos in the control group, $n = 5/5$ embryos in the caffeine-treated group, and $n = 6/6$ embryos in the caffeine+AGN group), whereas the increased expression of c-Caspase3 caused by caffeine could be reversed by adding AGN ($n = 5$ embryos in the control group, $n = 5/5$ embryos in the caffeine-treated group, and $n = 6/6$ embryos in the caffeine+AGN group) (**Figures 5C–H,C1–H1,I–K**). Similar results were obtained on C2C12 cells after adding AGN (**Supplementary Figures 4A–C,E**). Taken together, these results indicated that RA signaling played an indispensable role in the negative effects of caffeine on somitogenesis and myogenesis (Grant et al., 2018).

In order to investigate whether the phenotypes and the mechanism involving RA signaling can be uncoupled from the lethality caused by toxic levels of caffeine, we determined the effect of caffeine at low doses on C2C12 cells after adding AGN. At 25 and 50 μM (which are equal to 1.25 and 2.5 μmol/egg, respectively), the increased RNA levels of Caspase3 and Cyclin D1 as well as the decreased levels of Myf5 and BMP4 can be reverted with the RA antagonist AGN (**Figures 6A–D**). The RALDH2 RNA levels were also increased after lower dosages of caffeine treatment (**Figure 6E**). These results suggest that the elevated RA levels have a probability of occurring as a cellular signaling response to caffeine exposure. These observed regulatory changes may not be directly caused by the caffeine toxicity.

DISCUSSION

Caffeine is a widely consumed psychostimulant all around the world, and its intake by adults mainly comes from coffee,

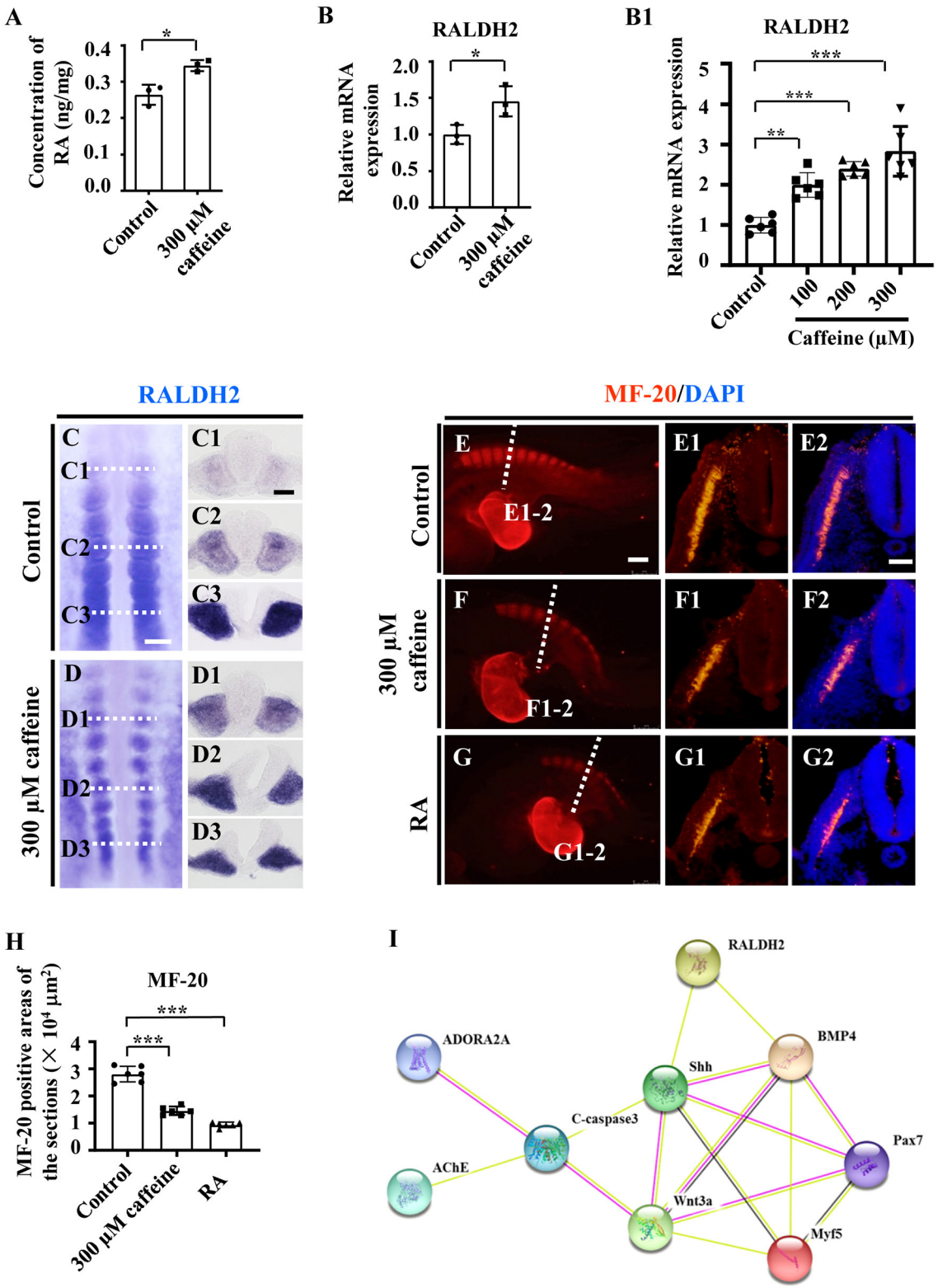

FIGURE 4 | Assessment of the somitogenesis-related gene expressions following caffeine treatment. **(A)** ELISA data showing the concentration of retinoic acid (RA) in the control and caffeine-treated groups of HH10 chicken embryos. **(B,B1)** Quantitative RT-PCR data showing the mRNA expression of RALDH2 from the control and

(Continued)

FIGURE 4 | caffeine-treated groups of HH10 chicken embryos **(B)** and C2C12 cells **(B1)**. **(C,D,C1–C3,D1–D3)** Whole-mount *in situ* hybridization for RALDH2 in the chicken embryos from the control **(C)** and caffeine-treated **(D)** groups, and the corresponding transverse sections. Panels **(C1/D1,C2/D2,C3/D3)** are from the third, sixth, and ninth pairs of somites, respectively. **(E–G,E1–G1,E2–G2)** Immunofluorescence staining of MF-20 in the E2.5 chicken embryos from the control **(E)**, caffeine-treated **(F)**, and RA-treated **(G)** groups, and the corresponding transverse sections (fifth pair of somites) for MF-20 and merge with DAPI staining **(E1–G1,E2–G2)**. **(H)** Quantitative data showing the areas of MF-20 immunofluorescence staining in E1, F1, and G1. **(I)** The protein–protein interactions from the STRING database showing the network of ADORA2A, AChE, c-Caspase3, RALDH2, Shh, BMP4, Pax7, Wnt3a, and Myf5. Scale bars = 100 μm in panels **(C,D)**; 50 μm in panels **(C1–C3,D1–D3)**; 200 μm in panels **(E–G)**; 50 μm in panels **(E1–G1,E2–G2)**. $^{*}P < 0.05$, $^{**}P < 0.01$, $^{***}P < 0.001$.

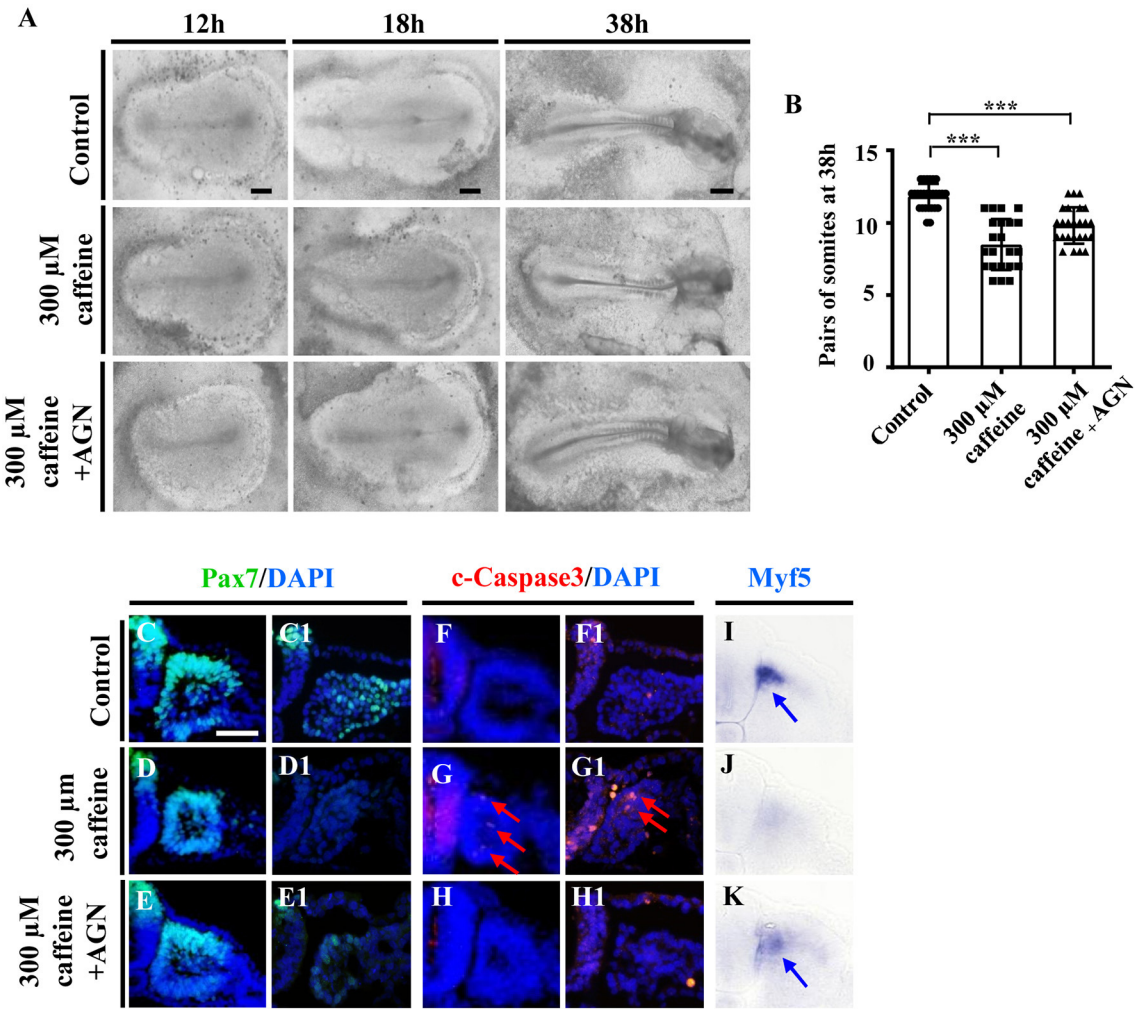

FIGURE 5 | Determination of the expression of cell apoptosis and differentiation in the developing somites following caffeine treatment and blockage of retinoic acid (RA) signaling. **(A)** Representative images of the 12th-, 18th-, and 38th-h whole chicken embryos from the control, caffeine-treated, and caffeine+AGN-treated groups. **(B)** The bar charts showing the comparisons of somite pairs chicken embryo between the control, caffeine-treated, and caffeine+AGN-treated groups at 38 h. **(C–H)** Immunofluorescence staining of Pax7 or c-Caspase3 in the transverse sections from the control **(C,C1,F,F1)**, caffeine-treated **(D,D1,G,G1)**, and caffeine+AGN-treated **(E,E1,H,H1)** groups, and merge with DAPI staining. **(I–K)** The transverse sections of whole-mount *in situ* hybridization for Myf5 in the chicken embryos from the control **(I)**, caffeine-treated **(J)**, and caffeine+AGN-treated **(K)** groups. Panels **(C/D/E,F/G/H,I/J/K)** are from the seventh pairs of somites; (**C1/D1/E1,F1/G1/H1)** are from the presomitic mesoderm (PSM) of somites. Scale bars = 500 μm in panel **(A)**; 50 μm in panels **(C–K)**. $^{***}P < 0.001$.

cola drinks, and tea (Nehlig, 2018). Growing data have shown that the daily consumed product implies negative affect on both central nervous system and cardiovascular system (Nehlig et al., 1992; Zulli et al., 2016; Grant et al., 2018). It has also been reported that caffeine can easily penetrate the mammalian placenta and can increase the risk of causes of teratogenesis in young fetuses (Santos and Lima, 2016; Yadegari et al., 2016). Caffeine consumption (>300 mg/day) during pregnancy was associated with an increased risk of fetal growth restriction, and this association continued throughout pregnancy. Interestingly, the assessment of the more physiologically relevant doses of caffeine on embryonic development and uterine receptivity in

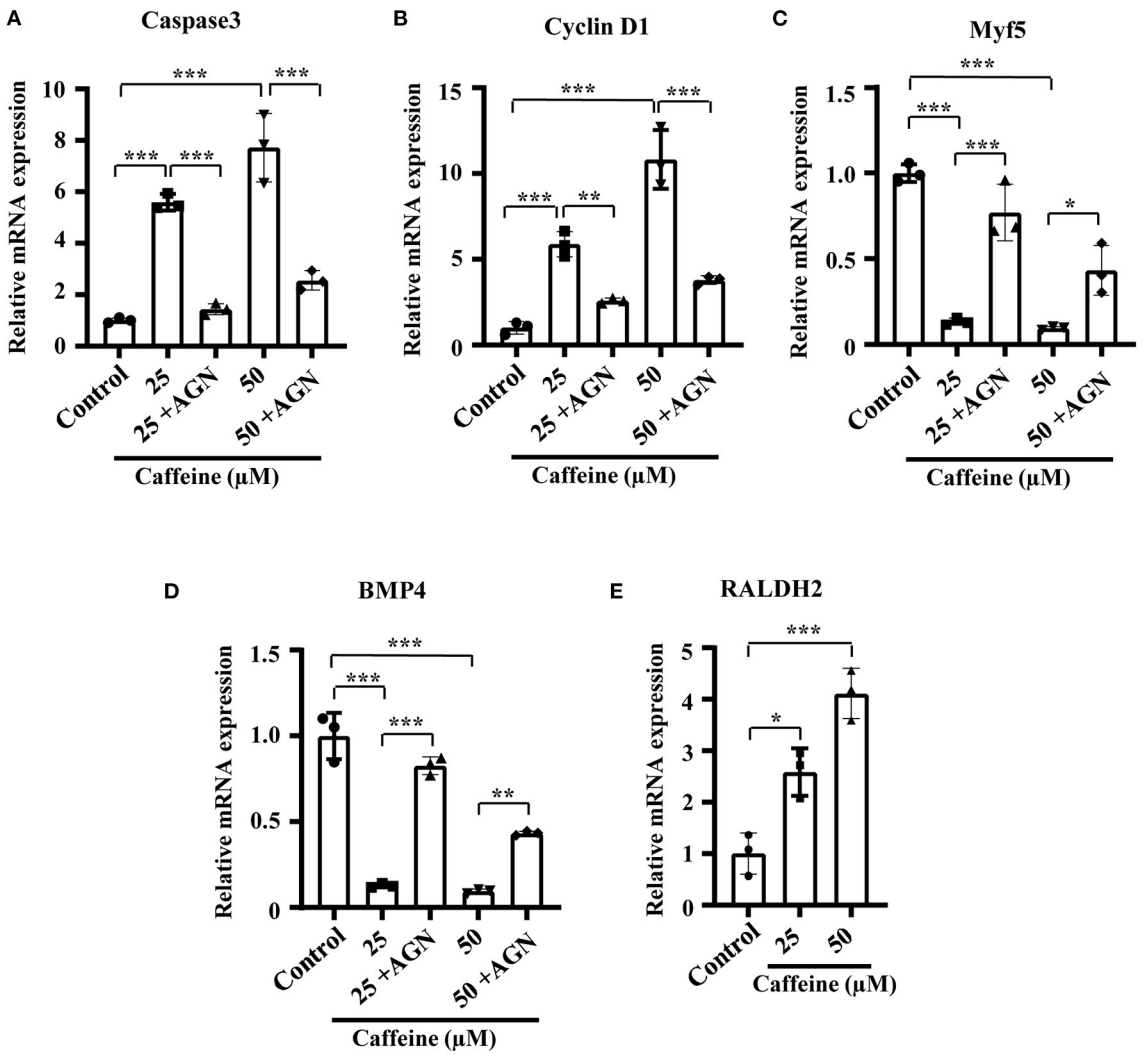

FIGURE 6 | Quantitative RT-PCR data of Caspase3 **(A)**, Cyclin D1 **(B)**, Myf5 **(C)**, RALDH2 **(D)**, and BMP4 **(E)** in C2C12 cells after caffeine treatment and blockage of retinoic acid (RA) signaling. $^{*}P < 0.05$, $^{**}P < 0.01$, $^{***}P < 0.001$.

mice indicated that there was no effect at low doses (2 mg/g), but effects started at 5 mg/g (Qian et al., 2018). In rats, maternal coffee consumption could cause the higher accumulation of caffeine in fetal brain than in serum (Wilkinson and Pollard, 1993). Since 100–600 μM of caffeine could affect neurogenesis in the mouse model (Narod et al., 1991; Marret et al., 1997), we applied 15 μmol/egg of caffeine (each egg contains about 50 ml of albumen and yolk) or EC culture mixed with 300 μM of caffeine based on our previous study (Ma et al., 2012, 2014, 2016; Wang et al., 2019). We do not deny that the concentration of caffeine is hardly representative of the conditions of high caffeine exposure during pregnancy. But we speculate that the caffeine doses are within the acceptable range in acute toxicity studies (note: the chicken embryo develops and hatches in 20–21 days only).

In this study, by using the chicken embryo model, we found that caffeine exposure reduced the weight of developing chicken embryos and also induced a delay in somite formation and chest wall malformations (**Supplementary Figures 1C–E** and **Figures 1D,E**). In fact, the chest wall comprises fat, skin, muscles, and the thoracic skeleton (Clemens et al., 2011). Congenital chest wall deformities are considered to be anomalies in chest wall growth and can be seen with various anomalies of the musculoskeletal system and collagen fibers (Mak et al., 2016). Abnormal cartilage fusion and muscle tissue formation were very obvious in the caffeine-treated group with mild unclosed chest wall (**Supplementary Figures 2J1,N,P**).

Moreover, there was a significant reduction in mRNA expressions of myogenesis-related genes including MYH7B, MEF2A, Myod1, myogenin, and Pax7 (**Supplementary Figure 2Q**). MYH7B has been found to be expressed in a range of muscle tissues in *Xenopus*, chicken, and mouse embryos (Warkman et al., 2012). MEF2 genes (MEF2A, B, C, and D), which lack myogenic activity alone, interact with MRFs (Myf5, MRF4, Myod1, and myogenin) to synergistically

activate muscle-specific genes and the myogenic differentiation program, and the two families directly regulate the expression of an extensive array of muscle structural genes (Molkentin and Olson, 1996; Blais et al., 2005). Pax7 marks myogenic progenitor cells and regulates their behavior and their the entrance program of skeletal muscle differentiation through networking with MRFs (Relaix et al., 2005; Buckingham and Relaix, 2007). All these results indicated that caffeine exposure impaired myogenesis of the early-stage embryos. It seems to correspond with the previous research on zebrafish that the caffeine exposure led to myofibril misalignment (da Costa and de Lemos Menezes, 2018).

Somites have been considered to be the precursors of the axial skeleton and skeletal muscles, and the majority of the musculoskeletal system derives originally from the somites. We then determined the effect of caffeine on somitogenesis. The HH4 embryos treated with caffeine to 18th and 34th hour (HH10) exhibited significant reduction in both length of embryos and pairs of somites (**Figures 1D,E**). The somite defects could also be easily observed by Pax7 immunofluorescence staining (**Figures 1J,K**). We had employed Pax7 to study the effects of caffeine exposure on neural crest cell migration, as Pax7 is also the one of the earliest markers of avian neural crest cells and expressed at the dorsal side of the neural tube and migratory neural crest cells (Ma et al., 2012). The diversity of Pax7 expression might be due to the different kinds of cells and/or the different stages of embryos. Moreover, we found some abnormalities caused by caffeine treatment on the regions of the head (**Figure 5A**). The somite and PSM explants, as well as the *in vitro* experiments of myoblast cells, suggest that caffeine could affect the somite development directly (**Supplementary Figure 4**). Also, the chicken embryos required longer time to reach HH10 stage (36 h) compared with the control (34 h). These results suggest that excessive caffeine exposure can cause the disturbance on somitogenesis in chicken embryonic development.

The next aim was to study the pathological mechanism of embryonic myogenesis disturbance by caffeine. First, caffeine exposure could promote cell apoptosis in the somites (**Figures 2A–E,B1,D1**), which might be partially responsible for caffeine-induced defects in somitogenesis and myogenesis. These might be generally similar to the finding that caffeine induces apoptosis through p53, Bax, and Caspase3 pathways (He et al., 2003). Accordingly, myogenic regulatory factor Myf5 in the developing chicken embryos in the presence of caffeine was observed to be down-regulated (**Figures 3A–E**).

In order to explore the underlying mechanism about the reduction of tissue size induced by caffeine treatment, we then determined the potential effect of caffeine on cell proliferation. Interestingly, the result implied that the caffeine exposure played a positive role in the cell proliferation of somites (**Figure 6B** and **Supplementary Figures 4C, 5**). This finding is similar to the previous reports that caffeine promoted the proliferation of rat neuronal cells, human lung adenocarcinoma cells, and small airway epithelial cells (Al-Wadei et al., 2006; Sahu et al., 2013). Physiological cell death in the somites has been reported to be the result of the interaction of nerve growth factor with its receptor, whereas Shh induces a decrease of nerve growth factor mRNA leading to trophic support for the survival of somite cells (Teillet et al., 1998; Borycki et al., 1999; Cotrina et al., 2000; Kruger et al., 2001). Shh works together with the RA pathway to ensure the robustness of somite formation (Resende et al., 2010). Our data indicate that caffeine treatment led to the increased expressions of Shh and RA (**Figures 3N**, **4A**). It may explain the observation that the expressions of PH3 and Cyclin D1 at mRNA levels increased following caffeine treatment (**Figure 6B** and **Supplementary Figures 4C, 5**). Apart from Shh, members of the Wnt family are implicated in muscle development (Münsterberg et al., 1995). A previous finding has shown that the expression of BMP4 is increased with progression of myogenesis and that down-regulation of BMP signal components inhibits myotube differentiation and maturation (Umemoto et al., 2011). In this study, Wnt3a and BMP expressions were evidently suppressed following caffeine exposure (**Figures 3L,M**). It suggests that aberrant somitic differentiation induced by caffeine might partially derive from the abnormal expressions of these crucial genes and proteins involved in regulating somite differentiation. Conclusively, caffeine exposure could lead to increased Shh expression in the neural tube and notochord and then in turn activate the ectopic expression of Noggin, subsequently resulting in the blocking of BMP4 specification of the lateral somites. The blocking of BMP4 would negatively result in a reduction of Wnt3a expression.

We then determined the expression of RALDH2, which was identified as a major RA generating enzyme in the early embryo. Both RALDH2 and RA were increased significantly in the caffeine-treated group (**Figures 4A–D,B1,C1–C3,D1–D3**). Similar results were obtained on C2C12 cells and the isolated somites and PSM (**Figure 6E** and **Supplementary Figure 4F**). These findings correspond with the research that RA treatment induces extensive apoptosis and down-regulation of Wnt3a (Shum et al., 1999). BMP4 expression is proximally inhibited by RA signaling, and BMP signaling may be responsible for regulating the pattern of myogenic cell migration in Raldh2–/– forelimb buds (Mic and Duester, 2003). It may address the observation that the migration ability of C2C12 cells was inhibited following caffeine treatment in the scratch wound migration assay (**Supplementary Figure 6**).

Furthermore, the expression of myosin marker, MF-20, was observed to be reduced in caffeine and RA separately treated groups (**Figures 4F–H,F1,F2,G1,G2**). Caffeine and RA either separately or in combination impaired the skeleton development of mouse embryos (Lashein et al., 2016). All of these indicate that excessive RA may negatively mediate the somitogenesis and somite differentiation in the caffeine-treated group. To verify our hypothesis, a potent RA receptor antagonist, AGN, was added together with caffeine to the chicken embryos, which rescued the reduced embryo length and pairs of somites in the corresponding caffeine-treated group (**Figures 5A,B**). Moreover, the expressions of Pax7 and Myf5 increased and c-Caspase3 expression decreased (**Figures 5C–K,C1–E1,F1–H1**), which further confirmed the crucial role of RA signaling in the process. Similar results on mRNA levels of Caspase3, Cyclin D1, Myf5, and BMP4 were obtained on C2C12 cells following low doses of caffeine and AGN treatment (**Figures 6A–D**).

We have previously reported that caffeine exposure induced its cytotoxic effects by generating excess reactive oxygen species

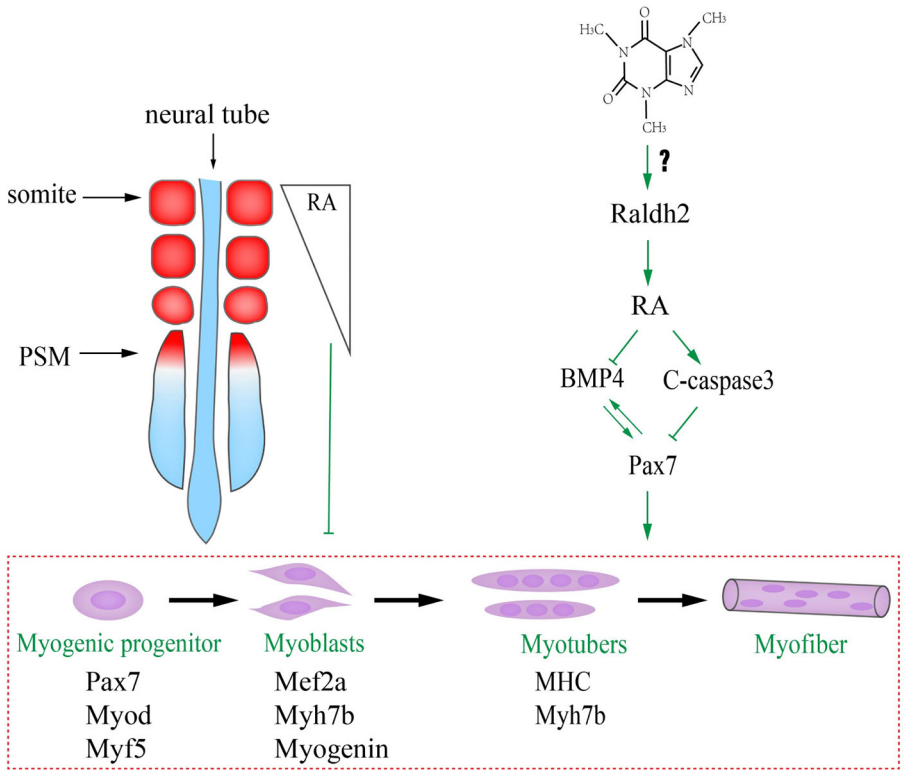

FIGURE 7 | Proposed mechanism about excessive caffeine intake-disturbed differentiation of myogenic progenitors through retinoic acid (RA) signaling pathway.

(ROS) that could adversely affect chicken embryo development including the suppression of neurogenesis (Ma et al., 2014), and the excess ROS generation interfered with the RA production during embryogenesis (Song et al., 2020). The underlying mechanism in this study might be that caffeine disturbed the RA production during embryogenesis by increasing the RALDH2 expression (**Figure 7**). Consequently, the turbulence of RA metabolism, which acts as the crucial signaling to modulate the biological clock on somitogenesis and somite differentiation via influencing BMP signaling, occurred when somites form and differentiate into dermomyotome (later will convert to myotome and dermatome) and sclerotome. On the other hand, the elevated RA promotes c-Caspase3 but suppressed Pax7 expressions. Furthermore, excess caffeine exposure could lead to generalized systemic toxicity. Whether or not there is a direct link between caffeine and RA pathway needs further investigation.

DATA AVAILABILITY STATEMENT

The original contributions presented in the study are included in the article/**Supplementary Material**, further inquiries can be directed to the corresponding author/s.

ETHICS STATEMENT

The animal study was reviewed and approved by Laboratory Animal Ethics Committee of Jinan University.

AUTHOR CONTRIBUTIONS

GW and XY designed the research project. YL, XH, JL, NW, and DL carried out the experiments and interpreted data. NW wrote the manuscript with input from GW and XY. XC, and BB-S commented on the manuscript. All authors contributed to the article and approved the submitted version.

FUNDING

This study was supported by NSFC grant (31971108 and 31771331), Science and Technology Planning Project of Guangdong Province (2017A020214015 and 2017A050506029), Science and Technology Program of Guangzhou (201710010054). Fundamental Research Funds for the Central Universities (11620323), and Guangdong Natural Science Foundation (2020A1515110784).

ACKNOWLEDGMENTS

We would like to thank Ms. Pei-Ling Zhang, Yu Zhang, and Zheng-lai Ma for technical help.

SUPPLEMENTARY MATERIAL

The Supplementary Material for this article can be found online at: https://www.frontiersin.org/articles/10.3389/fcell.2021.586767/full#supplementary-material

REFERENCES

Al-Wadei, H. A., Takahashi, T., and Schuller, H. M. (2006). Caffeine stimulates the proliferation of human lung adenocarcinoma cells and small airway epithelial cells via activation of PKA, CREB and ERK1/2. *Oncol. Rep.* 15, 431–435. doi: 10.3892/or.15.2.431

Bales, K., Hannon, K., Smith, I. I., C., and Santerre, R. (1993). Single-stranded RNA probes generated from PCR-derived DNA templates. *Mol. Cell. Probes* 7, 269–275. doi: 10.1006/mcpr.1993.1040

Bayha, E., Jørgensen, M. C., Serup, P., and Grapin-Botton, A. (2009). Retinoic acid signaling organizes endodermal organ specification along the entire antero-posterior axis. *PLoS One* 4:e5845. doi: 10.1371/journal.pone.0005845

Blais, A., Tsikitis, M., Acosta-Alvear, D., Sharan, R., Kluger, Y., and Dynlacht, B. D. (2005). An initial blueprint for myogenic differentiation. *Genes Dev.* 19, 553–569. doi: 10.1101/gad.1281105

Bober, E., Brand-Saberi, B., Ebensperger, C., Wilting, J., Balling, R., Paterson, B. M., et al. (1994). Initial steps of myogenesis in somites are independent of influence from axial structures. *Development* 120, 3073–3082.

Borycki, A., Brown, A. M., and Emerson, C. P. Jr. (2000). Shh and Wnt signaling pathways converge to control Gli gene activation in avian somites. *Development* 127, 2075–2087. Available online at: https://dev.biologists.org/content/develop/127/10/2075.full.pdf

Borycki, A.-G., Brunk, B., Tajbakhsh, S., Buckingham, M., Chiang, C., and Emerson, C. (1999). Sonic hedgehog controls epaxial muscle determination through Myf5 activation. *Development* 126, 4053–4063.

Brand-Saberi, B., Wilting, J., Ebensperger, C., and Christ, B. (1996). The formation of somite compartments in the avian embryo. *Int. J. Dev. Biol.* 40, 411–420.

Buckingham, M., and Relaix, F. (2007). The role of Pax genes in the development of tissues and organs: Pax3 and Pax7 regulate muscle progenitor cell functions. *Annu. Rev. Cell Dev. Biol.* 23, 645–673. doi: 10.1146/annurev.cellbio.23.090506.123438

Bupp Becker, S. R., and Shibley, I. A. Jr. (1998). Teratogenicity of ethanol in different chicken strains. *Alcohol Alcohol.* 33, 457–464. doi: 10.1093/alcalc/33.5.457

Capdevila, J., Tabin, C., and Johnson, R. L. (1998). Control of dorsoventral somite patterning by Wnt-1 and β-catenin. *Dev. Biol.* 193, 182–194. doi: 10.1006/dbio.1997.8806

Carapuco, M., Novoa, A., Bobola, N., and Mallo, M. (2005). Hox genes specify vertebral types in the presomitic mesoderm. *Genes Dev.* 19, 2116–2121. doi: 10.1101/gad.338705

Cavieres, M. F., and Smith, S. M. (2000). Genetic and developmental modulation of cardiac deficits in prenatal alcohol exposure. *Alcohol. Clin. Exp. Res.* 24, 102–109. doi: 10.1111/j.1530-0277.2000.tb04559.x

Chapman, S. C., Brown, R., Lees, L., Schoenwolf, G. C., and Lumsden, A. (2004). Expression analysis of chick Wnt and frizzled genes and selected inhibitors in early chick patterning. *Dev. Dyn.* 229, 668–676. doi: 10.1002/dvdy.10491

Chapman, S. C., Collignon, J., Schoenwolf, G. C., and Lumsden, A. (2001). Improved method for chick whole-embryo culture using a filter paper carrier. *Dev. Dyn.* 220, 284–289. doi: 10.1002/1097-0177(20010301)220:3<284::AID-DVDY1102>3.0.CO;2-5

Christ, B., and Ordahl, C. P. (1995). Early stages of chick somite development. *Anatomy Embryol.* 191, 381–396. doi: 10.1007/BF00304424

Clemens, M. W., Evans, K. K., Mardini, S., and Arnold, P. G. (2011). Introduction to chest wall reconstruction: anatomy and physiology of the chest and indications for chest wall reconstruction. *Semin. Plast. Surg.* 25, 5–015. doi: 10.1055/s-0031-1275166

Cotrina, M. L., González-Hoyuela, M., Barbas, J. A., and Rodríguez-Tébar, A. (2000). Programmed cell death in the developing somites is promoted by nerve growth factor via its p75NTR receptor. *Dev. Biol.* 228, 326–336. doi: 10.1006/dbio.2000.9948

da Costa, K. V. T., and de Lemos Menezes, P. (2018). Effect of caffeine on vestibular evoked myogenic potential: a systematic review with meta-analysis. *Braz. J. Otorhinolaryngol.* 84, 381–388. doi: 10.1016/j.bjorl.2017.11.003

Dangata, Y. Y., and Kaufman, M. H. (1997). Morphometric analysis of the postnatal mouse optic nerve following prenatal exposure to alcohol. *J. Anatomy* 191 (Pt 1), 49–56. doi: 10.1046/j.1469-7580.1997.19110049.x

Debelak, K. A., and Smith, S. M. (2000). Avian genetic background modulates the neural crest apoptosis induced by ethanol exposure. *Alcohol. Clin. Exp. Res.* 24, 307–314. doi: 10.1111/j.1530-0277.2000.tb04612.x

Dubrulle, J., McGrew, M. J., and Pourquie, O. (2001). FGF signaling controls somite boundary position and regulates segmentation clock control of spatiotemporal Hox gene activation. *Cell* 106, 219–232. doi: 10.1016/S0092-8674(01)00437-8

Grant, S. S., Magruder, K. P., and Friedman, B. H. (2018). Controlling for caffeine in cardiovascular research: a critical review. *Int. J. Psychophysiol.* 133, 193–201. doi: 10.1016/j.ijpsycho.2018.07.001

Grosso, L. M., and Bracken, M. B. (2005). Caffeine metabolism, genetics, and perinatal outcomes: a review of exposure assessment considerations during pregnancy. *Ann. Epidemiol.* 15, 460–466. doi: 10.1016/j.annepidem.2004.12.011

Hamade, A., Deries, M., Begemann, G., Bally-Cuif, L., Genet, C., Sabatier, F., et al. (2006). Retinoic acid activates myogenesis *in vivo* through Fgf8 signalling. *Dev. Biol.* 289, 127–140. doi: 10.1016/j.ydbio.2005.10.019

Hamburger, V., and Hamilton, H. L. (1951). A series of normal stages in the development of the chick embryo. *J. Morphol.* 88, 49–92. doi: 10.1002/jmor.1050880104

He, Z., Ma, W.-Y., Hashimoto, T., Bode, A. M., Yang, C. S., and Dong, Z. (2003). Induction of apoptosis by caffeine is mediated by the p53, Bax, and caspase 3 pathways. *Cancer Res.* 63, 4396–4401. Available online at: https://cancerres.aacrjournals.org/content/63/15/4396.long

Henrique, D., Adam, J., Myat, A., Chitnis, A., Lewis, J., and Ish-Horowicz, D. (1995). Expression of a Delta homologue in prospective neurons in the chick. *Nature* 375, 787–790. doi: 10.1038/375787a0

Hirsinger, E., Duprez, D., Jouve, C., Malapert, P., Cooke, J., and Pourquié, O. (1997). Noggin acts downstream of Wnt and Sonic Hedgehog to antagonize BMP4 in avian somite patterning. *Development* 124, 4605–4614.

Illanes, J., Fuenzalida, M., Romero, S., González, P., and Lemus, D. (1999). Ethanol effect on the chick embryo ossification: a macroscopic and microscopic study. *Biol. Res.* 32, 77–84.

Jang, Y.-N., and Baik, E. J. (2013). JAK-STAT pathway and myogenic differentiation. *Jak-Stat* 2, e23282. doi: 10.4161/jkst.23282

Kawakami, Y., Raya, A., Raya, R. M., Rodriguez-Esteban, C., and Izpisua Belmonte, J. C. (2005). Retinoic acid signalling links left-right asymmetric patterning and bilaterally symmetric somitogenesis in the zebrafish embryo. *Nature* 435, 165–171. doi: 10.1038/nature03512

Kruger, M., Mennerich, D., Fees, S., Schafer, R., Mundlos, S., and Braun, T. (2001). Sonic hedgehog is a survival factor for hypaxial muscles during mouse development. *Development* 128, 743–752. Available online at: https://dev.biologists.org/content/develop/128/5/743.full.pdf

Lashein, F. E.-D. M., Seleem, A. A., and Ahmed, A. A. (2016). Effect of caffeine and retinoic acid on skeleton of mice embryos. *J. Basic Appl. Zool.* 75, 36–45. doi: 10.1016/j.jobaz.2016.06.003

Li, X., He, R., Qin, Y., Tsoi, B., Li, Y., Ma, Z., et al. (2012). Caffeine interferes embryonic development through over-stimulating serotonergic system in chicken embryo. *Food Chem. Toxicol.* 50, 1848–1853. doi: 10.1016/j.fct.2012.03.037

Linask, K. K., Ludwig, C., Han, M.-D., Liu, X., Radice, G. L., and Knudsen, K. A. (1998). N-cadherin/catenin-mediated morphoregulation of somite formation. *Dev. Biol.* 202, 85–102. doi: 10.1006/dbio.1998.9025

Ma, Z., Wang, G., Cheng, X., Chuai, M., Kurihara, H., Lee, K. K. H., et al. (2014). Excess caffeine exposure impairs eye development during chick embryogenesis. *J. Cell. Mol. Med.* 18, 1134–1143. doi: 10.1111/jcmm.12260

Ma, Z. L., Qin, Y., Wang, G., Li, X. D., He, R. R., Chuai, M. L., et al. (2012). Exploring the caffeine-induced teratogenicity on neurodevelopment using early chick embryo. *PLoS One* 7:e34278. doi: 10.1371/journal.pone.0034278

Ma, Z. L., Wang, G., Lu, W. H., Cheng, X., Chuai, M. L., Lee, K. K. H., et al. (2016). Investigating the effect of excess caffeine exposure on placental angiogenesis using chicken 'functional' placental blood vessel network. *J. Appl. Toxicol.* 36, 285–295. doi: 10.1002/jat.3181

Mak, S. M., Bhaludin, B. N., Naaseri, S., Di Chiara, F., Jordan, S., and Padley, S. (2016). Imaging of congenital chest wall deformities. *Br. J. Radiol.* 89, 20150595. doi: 10.1259/bjr.20150595

Marcelle, C., Stark, M. R., and Bronner-Fraser, M. (1997). Coordinate actions of BMPs, Wnts, Shh and noggin mediate patterning of the dorsal somite. *Development* 124, 3955–3963.

Marret, S., Gressens, P., Van-Maele-Fabry, G., Picard, J., and Evrard, P. (1997). Caffeine-induced disturbances of early neurogenesis in whole mouse embryo cultures. *Brain Res.* 773, 213–216. doi: 10.1016/S0006-8993(97)00938-4

McKinnell, I. W., Ishibashi, J., Le Grand, F., Punch, V. G., Addicks, G. C., Greenblatt, J. F., et al. (2008). Pax7 activates myogenic genes by recruitment of a histone methyltransferase complex. *Nat. Cell Biol.* 10, 77–84. doi: 10.1038/ncb1671

Mic, F. A., and Duester, G. (2003). Patterning of forelimb bud myogenic precursor cells requires retinoic acid signaling initiated by Raldh2. *Dev. Biol.* 264, 191–201. doi: 10.1016/S0012-1606(03)00403-2

Miller Jr, R. R., Heckel, C. D., Koss, W. J., Montague, S. L., and Greenman, A. L. (2001). Ethanol-and nicotine-induced membrane changes in embryonic and neonatal chick brains. *Comp. Biochem. Physiol. C Toxicol. Pharmacol.* 130, 163–178. doi: 10.1016/S1532-0456(01)00227-7

Molkentin, J. D., and Olson, E. N. (1996). Combinatorial control of muscle development by basic helix-loop-helix and MADS-box transcription factors. *Proc. Natl. Acad. Sci. U. S. A.* 93, 9366–9373. doi: 10.1073/pnas.93.18.9366

Münsterberg, A., Kitajewski, J., Bumcrot, D. A., McMahon, A. P., and Lassar, A. B. (1995). Combinatorial signaling by Sonic hedgehog and Wnt family members induces myogenic bHLH gene expression in the somite. *Genes Dev.* 9, 2911–2922. doi: 10.1101/gad.9.23.2911

Narod, S. A., de Sanjosé, S., and Victora, C. (1991). Coffee during pregnancy: a reproductive hazard? *Am. J. Obstet. Gynecol.* 164, 1109–1114. doi: 10.1016/0002-9378(91)90597-K

Nehlig, A. (2018). Interindividual differences in caffeine metabolism and factors driving caffeine consumption. *Pharmacol. Rev.* 70, 384–411. doi: 10.1124/pr.117.014407

Nehlig, A., Daval, J. L., and Debry, G. (1992). Caffeine and the central nervous system: mechanisms of action, biochemical, metabolic and psychostimulant effects. *Brain Res.* 17, 139–170. doi: 10.1016/0165-0173(92)90012-B

Pourquié, O. (2004). The chick embryo: a leading model in somitogenesis studies. *Mech. Dev.* 121, 1069–1079. doi: 10.1016/j.mod.2004.05.002

Pourquié, O. (2018). Somite formation in the chicken embryo. *Int. J. Dev. Biol.* 62, 57–62. doi: 10.1387/ijdb.180036op

Power, S. C., Lancman, J., and Smith, S. M. (1999). Retinoic acid is essential for Shh/Hoxd signaling during rat limb outgrowth but not for limb initiation. *Dev. Dyn.* 216, 469–480. doi: 10.1002/(SICI)1097-0177(199912)216:4/5<469::AID-DVDY15>3.0.CO;2-3

Qian, J., Chen, Q., Ward, S. M., Duan, E., and Zhang, Y. (2019). Impacts of caffeine during pregnancy. *Trends Endocrinol. Metab.* 31, 218–227. doi: 10.1016/j.tem.2019.11.004

Qian, J., Zhang, Y., Qu, Y., Zhang, L., Shi, J., Zhang, X., et al. (2018). Caffeine consumption during early pregnancy impairs oviductal embryo transport, embryonic development and uterine receptivity in mice. *Biol. Reprod.* 99, 1266–1275. doi: 10.1093/biolre/ioy155

Reis, A. M. S., Raad, R. V., de Melo Ocarino, N., and Serakides, R. (2013). *In vitro* effects of caffeine in growth cartilage of rats. *Acta Ortoped. Bras.* 21, 307. doi: 10.1590/S1413-78522013000600001

Relaix, F., Rocancourt, D., Mansouri, A., and Buckingham, M. (2005). A Pax3/Pax7-dependent population of skeletal muscle progenitor cells. *Nature* 435, 948–953. doi: 10.1038/nature03594

Resende, T. P., Ferreira, M., Teillet, M.-A., Tavares, A. T., Andrade, R. P., and Palmeirim, I. (2010). Sonic hedgehog in temporal control of somite formation. *Proc. Natl. Acad. Sci. U. S. A.* 107, 12907–12912. doi: 10.1073/pnas.1000979107

Reshef, R., Maroto, M., and Lassar, A. B. (1998). Regulation of dorsal somitic cell fates: BMPs and Noggin control the timing and pattern of myogenic regulator expression. *Genes Dev.* 12, 290–303. doi: 10.1101/gad.12.3.290

Roda-Moreno, J., Pascual-Morenilla, M., Roda-Murillo, O., Lopez-Soler, M., and Arrebola-Nacle, F. (2000). Action of ethanol on different skull and brain parameters in the chick embryo. *J. Craniofac. Genet. Dev. Biol.* 20, 44–48.

Sahu, S., Kauser, H., Ray, K., Kishore, K., Kumar, S., and Panjwani, U. (2013). Caffeine and modafinil promote adult neuronal cell proliferation during 48 h of total sleep deprivation in rat dentate gyrus. *Exp. Neurol.* 248, 470–481. doi: 10.1016/j.expneurol.2013.07.021

Santos, R. M. M., and Lima, D. R. A. (2016). "Coffee health effects from early fetal development through childhood and adolescence," in *Translational Toxicology*, eds. C. Hughes, M. Waters (Cham: Humana Press; Springer), 321–337.

Sawada, K., Sakata-Haga, H., Komatsu, S., Ohta, K., Jeong, Y. G., and Fukui, Y. (2002). A selective loss of small-diameter myelinated optic nerve axons in rats prenatally exposed to ethanol. *Congen. Anom.* 42, 125–129. doi: 10.1111/j.1741-4520.2002.tb00861.x

Shum, A. S., Poon, L. L., Tang, W. W., Koide, T., Chan, B. W., Leung, Y.-C. G., et al. (1999). Retinoic acid induces down-regulation of Wnt-3a, apoptosis and diversion of tail bud cells to a neural fate in the mouse embryo. *Mech. Dev.* 84, 17–30. doi: 10.1016/S0925-4773(99)00059-3

Sirbu, I. O., and Duester, G. (2006). Retinoic-acid signalling in node ectoderm and posterior neural plate directs left-right patterning of somitic mesoderm. *Nat. Cell Biol.* 8, 271–277. doi: 10.1038/ncb1374

Song, J., Wang, C., Long, D., Li, Z., You, L., Brand-Saberi, B., et al. (2020). Dysbacteriosis-induced LPS elevation disturbs the development of muscle progenitor cells by interfering with retinoic acid signaling. *FASEB J.* 34, 6837–6853. doi: 10.1096/fj.201902965R

Teillet, M., Watanabe, Y., Jeffs, P., Duprez, D., Lapointe, F., and Le Douarin, N. (1998). Sonic hedgehog is required for survival of both myogenic and chondrogenic somitic lineages. *Development* 125, 2019–2030.

Umemoto, T., Furutani, Y., Murakami, M., Matsui, T., and Funaba, M. (2011). Endogenous Bmp4 in myoblasts is required for myotube formation in C2C12 cells. *Biochim. Biophys. Acta* 1810, 1127–1135. doi: 10.1016/j.bbagen.2011.09.008

Vermot, J., Gallego Llamas, J., Fraulob, V., Niederreither, K., Chambon, P., and Dolle, P. (2005). Retinoic acid controls the bilateral symmetry of somite formation in the mouse embryo. *Science* 308, 563–566. doi: 10.1126/science.1108363

Wang, G., Jiang, L. M., Tan, B. Y., Li, P. Z., Zhang, P. L., Zhang, Y., et al. (2019). Cell survival controlled by lens-derived Sema3A-Nrp1 is vital on caffeine-suppressed corneal innervation during chick organogenesis. *J. Cell. Physiol.* 234, 9826–9838. doi: 10.1002/jcp.27671

Wang, G., Li, Y., Wang, X. Y., Chuai, M., Yeuk-Hon Chan, J., Lei, J., et al. (2015). Misexpression of BRE gene in the developing chick neural tube affects neurulation and somitogenesis. *Mol Biol Cell* 26, 978–992. doi: 10.1091/mbc.E14-06-1144

Warkman, A. S., Whitman, S. A., Miller, M. K., Garriock, R. J., Schwach, C. M., Gregorio, C. C., et al. (2012). Developmental expression and cardiac transcriptional regulation of Myh7b, a third myosin heavy chain in the vertebrate heart. *Cytoskeleton* 69, 324–335. doi: 10.1002/cm.21029

Wilkinson, J. M., and Pollard, I. (1993). Accumulation of theophylline, theobromine and paraxanthine in the fetal rat brain following a single oral dose of caffeine. *Dev. Brain Res.* 75, 193–199. doi: 10.1016/0165-3806(93)90023-4

Wink, C., Rossowska, M., and Nakamoto, T. (1996). Effects of caffeine on bone cells and bone development in fast-growing rats. *Anat. Rec.* 246, 30–38. doi: 10.1002/(SICI)1097-0185(199609)246:1<30::AID-AR4>3.0.CO;2-J

Yadegari, M., Khazaei, M., Anvari, M., and Eskandari, M. (2016). Prenatal caffeine exposure impairs pregnancy in rats. *Int. J. Fertil. Steril.* 9, 558–562. doi: 10.22074/ijfs.2015.4616

Yu, T., Campbell, S. C., Stockmann, C., Tak, C., Schoen, K., Clark, E. A., et al. (2016). Pregnancy-induced changes in the pharmacokinetics of caffeine and its metabolites. *J. Clin. Pharmacol.* 56, 590–596. doi: 10.1002/jcph.632

Zulli, A., Smith, R. M., Kubatka, P., Novak, J., Uehara, Y., Loftus, H., et al. (2016). Caffeine and cardiovascular diseases: critical review of current research. *Eur. J. Nutr.* 55, 1331–1343. doi: 10.1007/s00394-016-1179-z

Conflict of Interest: The authors declare that the research was conducted in the absence of any commercial or financial relationships that could be construed as a potential conflict of interest.

frontiers in Cell and Developmental Biology

MINI REVIEW
published: 18 March 2021
doi: 10.3389/fcell.2021.655048

From Cell Death to Regeneration: Rebuilding After Injury

*Dylan J. Guerin, Cindy X. Kha and Kelly Ai-Sun Tseng**

School of Life Sciences, University of Nevada, Las Vegas, Las Vegas, NV, United States

The ability to regrow lost or damaged tissues is widespread, but highly variable among animals. Understanding this variation remains a challenge in regeneration biology. Numerous studies from *Hydra* to mouse have shown that apoptosis acts as a potent and necessary mechanism in regeneration. Much is known about the involvement of apoptosis during normal development in regulating the number and type of cells in the body. In the context of regeneration, apoptosis also regulates cell number and proliferation in tissue remodeling. Apoptosis acts both early in the process to stimulate regeneration and later to regulate regenerative patterning. Multiple studies indicate that apoptosis acts as a signal to stimulate proliferation within the regenerative tissues, producing the cells needed for full regeneration. The conservation of apoptosis as a regenerative mechanism demonstrated across species highlights its importance and motivates the continued investigation of this important facet of programmed cell death. This review summarizes what is known about the roles of apoptosis during regeneration, and compares regenerative apoptosis with the mechanisms and function of apoptosis in development. Defining the complexity of regenerative apoptosis will contribute to new knowledge and perspectives for understanding mechanisms of apoptosis induction and regulation.

Keywords: regeneration, apoptosis, tissue repair, caspase, cell death, Wnt, BMP, liver

OPEN ACCESS

Edited by:
Wolfgang Knabe,
Universität Münster, Germany

Reviewed by:
James Monaghan,
Northeastern University, United States
Christopher Gregory,
University of Edinburgh,
United Kingdom

***Correspondence:**
Kelly Ai-Sun Tseng
kelly.tseng@unlv.edu

Specialty section:
This article was submitted to Cell Death and Survival, a section of the journal Frontiers in Cell and Developmental Biology

Received: *18 January 2021*
Accepted: *22 February 2021*
Published: *18 March 2021*

Citation:
Guerin DJ, Kha CX and Tseng KA (2021) From Cell Death to Regeneration: Rebuilding After Injury. Front. Cell Dev. Biol. 9:655048. doi: 10.3389/fcell.2021.655048

INTRODUCTION

The ability to regenerate lost or damaged tissues is an impressive ability that is not common to all animals. How this feat is achieved by those that can is an ongoing question. Helpfully, a number of species with regenerative capacity are available as model organisms. Some invertebrates, such as the cnidarian *Hydra* and the planarian flatworm, display remarkable regenerative capacity. Both animals regenerate whole organisms from small body fragments (Trembley, 1744; Pallas, 1766). Hydra can even regenerate its entire body plan from reaggregated cells (Noda, 1971; Gierer et al., 1972). This regenerative capacity depends on reserves of active adult stem cells: pluripotent stem cells (neoblasts) in planaria and multipotent interstitial stem cells in *Hydra* (Wagner et al., 2011; Hobmayer et al., 2012; Scimone et al., 2014). Successful regeneration depends on these stem cells to respond to injury by proliferating and their progeny differentiating to return the organism to full structural and functional integrity (Baguñà, 1976; Saló and Baguñà, 1984; Reddien and Sanchez Alvarado, 2004).

Although vertebrates cannot regenerate an entire animal from small body fragments, some are remarkable for their ability to regrow substantial and complex body parts. One well-studied model is the zebrafish, *Danio rerio*, which regenerates several structures including the epidermis,

retina, heart, and appendages (Marques et al., 2019). Another model with high regenerative capacity is the axolotl *Ambystoma mexicanum*, which can regenerate severed limbs and damaged hearts (Joven et al., 2019). Furthermore, some amphibians, such as the clawed frog *Xenopus laevis*, display age-dependent regeneration of larval tails, limbs, and embryonic eyes (Dent, 1962; Morgan and Davis, 1902; Beck et al., 2003; Kha and Tseng, 2018; Kha et al., 2018). This age-dependent feature of *Xenopus* facilitates an examination of the mechanisms that regulate endogenous changes in regenerative capacity and to test strategies for stimulating regeneration in non-regenerative states. Even though mammalian regenerative capacity is more restricted than in these other models, mammals can regenerate some tissues, including the liver and digit tips in mice and humans (Higgins and Anderson, 1931; Illingworth, 1974; Han et al., 2008), and the entire epidermis in the African spiny mouse (Seifert et al., 2012).

Across species and tissues, the broad steps of regeneration after injury are as follows: a successful wound healing response, the initiation of regeneration, followed by cell proliferation and cellular differentiation to rebuild lost tissues (reviewed in Gurtner et al., 2008; Pfefferli and Jaźwińska, 2015; Kakebeen and Wills, 2019). The source of the contributing cell population varies between systems. Unlike invertebrates, vertebrate regeneration appears to often be achieved through the use of lineage-restricted progenitor cells, such as for limb regeneration in zebrafish (Poss et al., 2000; Stewart and Stankunas, 2012), axolotl (Kragl et al., 2009; Makanae et al., 2014), and *Xenopus* (Gargioli and Slack, 2004). Other mechanisms such as transdifferentiation to regenerate amphibian lens are also used (Eguchi, 1963; Freeman, 1963). The proliferation and differentiation of these cells to regenerate the lost organ requires the action of complex mechanisms, only some of which have been characterized.

One important mechanism in regeneration is apoptosis. Apoptosis, a type of programmed cell death, is a fundamental and evolutionarily conserved process (Metzstein et al., 1998). Apoptosis is required for organogenesis, tissue remodeling, homeostasis, wound healing, and regeneration (Elmore, 2007; Li et al., 2010; D'Arcy, 2019). Dysregulation of apoptosis can have severe consequences including cancer and autoimmune disorders (Goldar et al., 2015). Apoptosis is initiated by the cleavage of inactive initiator caspase proteins to expose their catalytic domains, which allow them to activate executioner caspases through subsequent cleavage events (Cohen, 1997). The executioner caspases then initiate a cascade of events resulting in the breakup of the cell into smaller apoptotic bodies. These are engulfed by macrophages, completing the process (Budai et al., 2019).

Apoptosis has been widely studied in many contexts and in diverse organisms (reviewed in Brill et al., 1999; Pérez-Garijo and Steller, 2015; Tuzlak et al., 2016). Apoptotic cells have been shown to exert diverse non-autonomous effects on neighboring cells through the release of mitogenic factors, inducing cell proliferation (Morata et al., 2011). The role of apoptosis as a regenerative mechanism was more recently identified. Prior work determined that apoptosis is required for regeneration across multiple organisms and tissues (Tseng et al., 2007; Chera et al., 2009; Li et al., 2010; Sîrbulescu and Zupanc, 2010; Gauron et al., 2013; Kha et al., 2018; Brock et al., 2019). How apoptosis promotes successful regeneration is beginning to be understood. In this review, we discuss the requirement of apoptosis in different regenerative contexts, the initiators and downstream effects of apoptosis during regeneration, and gaps in the field. We focus on recent advances that highlight the importance of apoptosis as a specific response to stimulate and regulate regeneration and not merely as a consequence of tissue damage.

INITIATION AND REGULATION OF REGENERATIVE APOPTOSIS

Apoptosis is commonly observed starting early in the regeneration process. Programmed cell death has long been known to contribute to wound healing after injury (Greenhalgh, 1998). However, apoptosis has additional and separable functions specific to regeneration after the initial wound healing phase. Pathways regulating these apoptotic events have been identified in some models.

Apoptosis occurs during the early phases of regeneration in two peaks in some regenerative systems. In *Hydra* and planaria, the first peak of apoptosis occurs from 1 to 4 h after bisection (Chera et al., 2009; Beane et al., 2013). At 3 days, there is a second peak of apoptosis (Pellettieri et al., 2010). A similar pair of apoptotic peaks is seen during adult zebrafish fin regeneration from 1 to 12 h post amputation (hpa) and 15 to 72 hpa. The second peak of apoptosis is specific to regeneration, as simple wounding of the fin that healed quickly failed to induce this second peak (Gauron et al., 2013). In *Xenopus laevis* tadpole tail regeneration, there is only one sustained increased in apoptosis at the injury site. Apoptosis is absent during the wound healing phase and is first activated during formation of the regeneration bud at 12 hpa and remains active during the entire initial proliferative phase from 12 to 48 hpa (Tseng et al., 2007).

An important regulator of apoptosis in regeneration is BMP signaling (Guimond et al., 2010). BMP signaling regulates anterior-posterior patterning, proliferation, differentiation, and apoptosis in the developing vertebrate limb (Pignatti et al., 2014). Here, BMP activates apoptosis in the apical ectodermal ridge and the limb mesenchyme (Gañan et al., 1998; Guha et al., 2002). BMP signaling is also required for regeneration of axolotl limbs (Guimond et al., 2010; Vincent et al., 2020). In this system, the regulation of apoptosis by BMP2 appears to function the same for both the developing and regenerating limb (Guimond et al., 2010). The overexpression of BMP2 increased apoptosis in the regenerating limb, while overexpression of the BMP inhibitor Noggin caused a decrease in apoptosis relative to controls (Guimond et al., 2010). A similar mechanism is also seen in mouse digit formation, where inhibition of BMP via Noggin caused a reduction in apoptosis in the inter-digit region, resulting in a flipper like appendage instead of a hand (Wang et al., 2004).

Another well-known signaling pathway active in apoptosis induction during regeneration is the Jun-N terminal Kinase (JNK) signaling pathway (Santabárbara-Ruiz et al., 2015; Diaz-Garcia et al., 2016; Camilleri-Robles et al., 2019). JNK regulates

apoptosis in the developing brain. A knockout of *Jnk1* and *Jnk2* caused both reduced apoptosis in the hindbrain and increased apoptosis in the forebrain (Kuan et al., 1999). JNK signaling is required for both apoptosis and regeneration following bisection in planaria (Almuedo-Castillo et al., 2014). In *Drosophila* wing imaginal disc regeneration, JNK signaling is required to induce apoptosis (Diaz-Garcia et al., 2016). Together, the studies suggest that JNK plays a regulatory role for apoptosis in development that may act similarly in regenerative apoptosis.

There is an interesting link between apoptosis and reactive oxygen species (ROS). ROS are detected early in regeneration and are necessary for regeneration in multiple species (Love et al., 2013; Ferreira et al., 2018; Novianti et al., 2019). Perhaps not coincidentally, ROS are important for apoptosis-dependent regeneration. In zebrafish fin regeneration, ROS levels increased at the injury site immediately following amputation and continued rising for 16 h before returning to baseline. The high levels of ROS around 15 hpa correlated closely with the beginning of the second round of apoptosis. Additionally, ROS levels peaked at 2 h after wounding injuries to the fin that did not require tissue regeneration, suggesting a specific importance of ROS for apoptosis-dependent regeneration (Gauron et al., 2013). ROS are also required for regeneration of the *Drosophila* imaginal disc, where they regulate JNK signaling (Santabárbara-Ruiz et al., 2015). The intersection of ROS, JNK signaling, and apoptosis is an exciting direction for further investigation.

REGULATION OF REGENERATIVE MECHANISMS BY APOPTOSIS

Apoptosis can promote proliferation during development, notably in the developing *Drosophila* imaginal discs where apoptotic cells promote compensatory proliferation in neighboring cells (reviewed in Diwanji and Bergmann, 2018). Although the specific roles of apoptosis in regeneration are still being explored, it is known that apoptosis can drive proliferation during regeneration in *Hydra*, planaria, *Xenopus*, and zebrafish. As proliferation is a critical aspect of regeneration (Gargioli and Slack, 2004; Jopling et al., 2010; Kha et al., 2018; Stocum, 2019), apoptosis is therefore an important regulator of regeneration.

Apoptotic cells can act as initiators of cell signaling in development (Morata et al., 2011). This is also true in regenerative contexts, for example the importance of apoptotic cells as a source of Wnt3 during *Hydra* head regeneration (Chera et al., 2009). Wnt/β-catenin signaling is also stimulated by apoptosis in zebrafish epithelium regeneration (Brock et al., 2019). In both systems, the Wnt ligand is found in apoptotic bodies and engulfed by neighboring stem cells to induce proliferation. This Wnt-induced proliferation is required for regeneration, as inhibition of Wnt signaling abolished regeneration (Chera et al., 2009; Brock et al., 2019). The observation of apoptosis-induced Wnt-dependent proliferation in both an invertebrate and a vertebrate is exciting, suggesting a potential conserved regenerative mechanism that could be tested as a strategy to induce mammalian regeneration.

Apoptotic cells secrete additional mitogenic signals in a number of models (Ryoo and Bergmann, 2012). Apoptotic cells in *Drosophila* secrete Hedgehog (the ortholog of vertebrate Sonic hedgehog) to induce proliferation during eye development (Fan and Bergmann, 2008). Prostaglandin signaling downstream of Caspase activity induces proliferation in mouse cells (Li et al., 2010), with a similar role proposed in zebrafish hematopoiesis (North et al., 2007). Whether apoptosis induces proliferation through these pathways during regeneration remains unclear.

Apoptosis as a patterning mechanism has been extensively studied in development (reviewed in Pérez-Garijo and Steller, 2015; Lin and Xu, 2019). However, much less is known about the patterning role of apoptosis in a regenerative context. An excellent example of an apoptosis requirement for pattering in regeneration is its asymmetric distribution and differential function following bisection in planaria and *Hydra*. Organismal bisection generates both anterior and posterior segments. Although each fragment undergoes apoptosis after bisection, the number of apoptotic cells is significantly higher in the head-regenerating posterior fragment than the tail-regenerating anterior fragment (Chera et al., 2009; Pellettieri et al., 2010). In *Hydra*, inhibition of apoptosis in the head-regenerating fragment blocked head regeneration. However, apoptotic inhibition of the foot-regenerating fragment did not block foot regeneration. Ectopic induction of apoptosis in the foot-regenerating fragment resulted in animals with heads in the presumptive foot region (Chera et al., 2009). These findings showed that a higher level of apoptosis is needed for head restoration, whereas a lower level is sufficient for induction of proliferation. In planarian regeneration, the second apoptotic peak is regulated by bioelectrical signaling and required for proper head patterning but not cell proliferation. Inhibition of the ion transporter H^+, K^+-ATPase caused a reduction of apoptosis and resulted in a shrunken head due to the lack of adjustment in organ size and placement (Beane et al., 2013). These studies indicate that apoptosis plays an instructive role in regenerative patterning of complex tissues.

THE GOLDILOCKS PRINCIPLE IN REGENERATIVE APOPTOSIS

Apoptosis is a potent mechanism that needs to be tightly controlled in regeneration. As in the tale of Goldilocks, the level of apoptosis needs to be "just the right amount" for successful regeneration. During regeneration, unchecked apoptosis could deplete the tissue of the cellular materials necessary to regenerate if it outpaces proliferation. Although one functional consequence of apoptosis is to promote proliferation, apoptosis itself is not always a marker of regeneration, even in normally regenerative tissues. For example, apoptosis is necessary for regeneration of the *Xenopus* tadpole tail. However, if the tail is amputated during the refractory period when the tadpole temporarily loses its tail regeneration ability, there is increased activated Caspase-3 activity relative to the regenerative tail (Tseng et al., 2007), suggesting that there is likely a limiting mechanism where a specific level of apoptosis is required for regeneration. Similarly,

if the salamander limb is denervated during regeneration, the normally regenerative tissues will morphologically regress due to increased apoptosis (Mescher et al., 2000). During mouse liver regeneration, Nitric oxide synthase-deficient animals exhibit both increased apoptosis and decreased regeneration relative to controls (Rai et al., 1998).

IAPs (Inhibitors of apoptosis proteins) are known regulators of apoptosis in development and disease yet their role in regeneration is unclear. Bcl-2 orthologs are expressed during axolotl limb regeneration (Bucan et al., 2018). However, the expression patterns of IAPs in other models have not been defined. Overexpression of p35 (a baculoviral caspase inhibitor) showed only a minor effect on *Drosophila* wing disc regeneration (Diaz-Garcia et al., 2016). Similarly, Bcl-2 overexpression did not enhance axonal regeneration of retinal ganglion cells in mice (Inoue et al., 2002). Further molecular and functional studies are needed to assess the potential roles of IAPs in regulating regenerative apoptosis.

MAMMALIAN REGENERATION: APOPTOSIS IN THE REGENERATING LIVER

Mammals, including humans, have limited regenerative ability but are able to regrow lost liver tissues following partial hepatectomy—resection of up to two thirds of the liver (Higgins and Anderson, 1931). Apoptosis in this context also differs somewhat from its conserved role in the models discussed in the earlier sections. An additional complexity in studying the role of apoptosis in liver regeneration is that different regenerative mechanisms can be activated depending on the method of injury (reviewed in Fausto et al., 2006; Mao et al., 2014). Following partial hepatectomy or acute chemical damage to the mammalian liver, TNF is released, stimulating ROS and NF-κB to induce apoptosis. Apoptosis induced neighboring progenitors to proliferate (Czaja et al., 1989; FitzGerald et al., 1995). Consistent with this finding, mice deficient in both Caspase-3 and Caspase-7 showed decreased liver progenitor proliferation, and impaired wound healing and regeneration following partial hepatectomy (Li et al., 2010). The liver is a distinct case from the earlier examples because mammalian liver regeneration results in the regrown liver achieving its former size but not its former shape. These may constitute distinct regenerative responses, which in turn may involve different roles for apoptosis.

DISCUSSION AND FUTURE DIRECTIONS

Apoptosis is a key mechanism of regeneration. Although apoptosis is demonstrably required for regeneration across diverse organisms and tissues, some important aspects of early stages of regeneration during which apoptosis is active are unknown. The roles of JNK, BMP and Wnt signaling pathways as inducers of apoptosis provide exciting leads but open questions remain (**Figure 1**). It is known that ROS are produced by macrophages following wounding (Bae et al., 2009). Moreover,

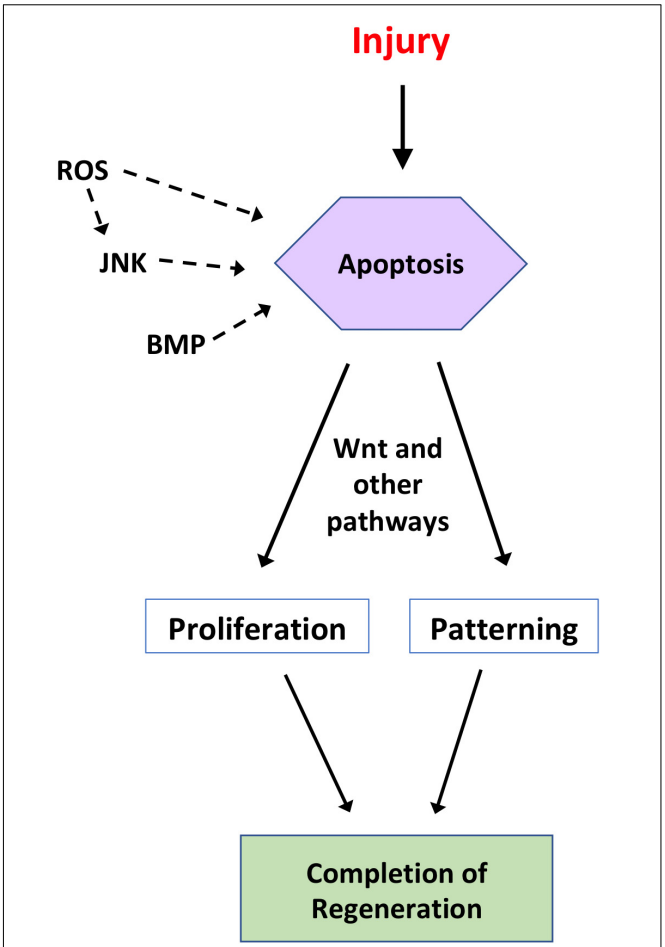

FIGURE 1 | Summary of the regulation and roles of apoptosis during regeneration. Following injury to a tissue, apoptosis can act as a regenerative mechanism, depending on the organism and tissue in question. In some regenerative systems, apoptosis is regulated by ROS, JNK, and/or BMP signaling. In turn, apoptosis regulates proliferative and/or patterning signals, such as Wnt signaling, to drive initiation and completion of regeneration. This figure is not intended to be comprehensive and represents an amalgamation of studies from several model systems discussed in the text.

the immune system is implicated in regulating endogenous regenerative ability (Fukazawa et al., 2009; reviewed in Mescher, 2017). A key aspect of the immune response is efferocytosis, the phagocytic clearance of apoptotic cells. In mice, reduced efferocytosis of apoptotic cardiomyocytes induced by myocardial infarction led to enlarged infarct size (Wan et al., 2013). In *Hydra* head regeneration, an immediate and large wave of efferocytosis by endodermal epithelial cells (immune-like cells) was seen beneath the injury plane (Chera et al., 2009) but whether this process plays an active role in regeneration is unknown. Regardless, these studies suggest that understanding the role of efferocytosis in regenerative apoptosis could be a promising area for investigation.

Another important question is which cell types are targeted for apoptosis and where they are located, which has been answered in only a few systems. Even among more fully characterized systems,

such as *Hydra* head regeneration, only a portion of the interstitial stem cells undergo apoptosis, which leads to the question of whether there is a specific induction program or if it is a stochastic process. Additionally, in most systems, regenerative events must coordinate the outgrowth of multiple tissue types (Mochii et al., 2007; Lehoczky et al., 2011). Does each lineage undergo a separate round of apoptosis or is there one global apoptotic event that affects all lineages? One tool for addressing this question is the use of fluorescent reporters for caspase activation, allowing real time imaging of caspase activity (Bardet et al., 2008). Another powerful tool for answering this question is single-cell RNA sequencing, which allows for the analysis of individual cells during regeneration.

It is unknown whether regenerative apoptosis functions in the same manner across the multiple organisms and tissues in which it is found. WNT ligands found in apoptotic bodies during zebrafish epithelium and *Hydra* head regeneration act to promote proliferation (Chera et al., 2009; Brock et al., 2019). That this mechanism is conserved between an invertebrate and a vertebrate suggests that this potentially can be used to stimulate regeneration in non-capable tissues. Additionally, optogenetic tools can be used for spatiotemporal specificity in inducing apoptosis in the tissues of interest after injury (Jewhurst et al., 2014).

The mechanisms linking apoptosis to regeneration remain largely elusive. An intriguing finding is that apoptosis but not JNK signaling induced expression of a pluripotency marker during zebrafish fin regeneration, suggesting that regenerative apoptosis may influence cellular reprogramming (Gauron et al., 2013). Investigators may also turn to the regulation and functions of apoptosis in development for clues since developmental mechanisms are often used in regeneration (Beck et al., 2003; Lin and Slack, 2008; Taniguchi et al., 2014). However, the developmental role of apoptosis is not always recapitulated in regeneration. In zebrafish fin regeneration, JNK signaling induced proliferation but apoptosis induction is JNK independent (Gauron et al., 2013). In *Xenopus*, tail formation does not involve apoptosis, but apoptosis is required for tail regeneration (Johnston et al., 2005; Tseng et al., 2007). In this context, understanding how regenerative apoptosis is induced may provide strategies for stimulating regeneration in tissues where apoptosis does not normally play a developmental role.

The role of apoptosis in regeneration is an important one that merits a detailed investigation. Apoptosis can control the microenvironment in which tumors arise, making the study of apoptosis important for cancer treatment (Gregory et al., 2016). Similar to cancer, regeneration induces excessive cell proliferation—in this case, to restore a lost structure. In contrast to cancer, regenerative proliferation is tightly controlled such that the process terminates once the missing structure is restored. Comparative studies of apoptosis in cancer and regeneration may help to delineate the differences in controlled vs. dysregulated proliferation. Further investigations into this topic may provide new perspectives in understanding the functions of apoptosis in diseased tissues.

AUTHOR CONTRIBUTIONS

DG, CK, and KT contributed to the planning, drafting, and writing of the manuscript. All authors contributed to the article and approved the submitted version.

FUNDING

This work was supported by funds from the University of Nevada, Las Vegas. Article publication costs were supported by the UNLV University Libraries Open Article Fund.

ACKNOWLEDGMENTS

We regret any omission due to space constraints. We thank members of the Tseng lab for helpful discussions and comments.

REFERENCES

Almuedo-Castillo, M., Crespo, X., Seebeck, F., Barscherer, K., Salo, E., and Adell, T. (2014). JNK controls the onset of mitosis in planarian stem cells and triggers apoptotic cell death required for regeneration and remodeling. *PLoS Genet.* 10:e08152.

Bae, Y. S., Lee, J. H., Choi, S. H., Kim, S., Almazan, F., Witztum, J. L., et al. (2009). Macrophages generate reactive oxygen species in response to minimally oxidized low-density lipoprotein: toll-like receptor 4- and spleen tyrosine kinase-dependent activation of NADPH oxidase 2. *Circ. Res.* 104, 210–218.

Baguñà, J. (1976). Mitosis in the intact and regenerating planarian Dugesia mediterranea n. sp. I. Mitotic studies during growth, feeding and starvation. *J, Exp. Zool.* 195, 65–80. doi: 10.1002/jez.1401950106

Bardet, P. L., Kolahgar, G., Mynett, A., Miguel-Aliaga, I., Briscoe, J., Meier, P., et al. (2008). A fluorescent reporter of caspase activity for live imaging. *Proc. Natl. Acad. Sci. U.S.A.* 105, 13901–13905. doi: 10.1073/pnas.0806983105

Beane, W. S., Morokuma, J., Lemire, J. M., and Levin, M. (2013). Bioelectric signaling regulates head and organ size during planarian regeneration. *Development* 140, 313–322. doi: 10.1242/dev.086900

Beck, C. W., Christen, B., and Slack, J. M. W. (2003). Molecular pathways needed for regeneration of spinal cord and muscle in a vertebrate. *Dev. Cell* 5, 429–439. doi: 10.1016/S1534-5807(03)00233-8

Brill, A., Torchinsky, A., Carp, H., and Toder, V. (1999). The role of apoptosis in normal and abnormal embryonic development. *J. Assist. Reprod. Genet.* 16, 512–519. doi: 10.1023/a:1020541019347

Brock, C. K., Wallin, S. T., Ruiz, O. E., Samms, K. M., Mandal, A., Sumner, E. A., et al. (2019). Stem cell proliferation is induced by apoptotic bodies from dying cells during epithelial tissue maintenance. *Nat. Commun.* 10:1044. doi: 10.1038/s41467-019-09010-6

Bucan, V., Peck, C. T., Nasser, I., Liebsch, C., Vogt, P. M., and Strauß, S. (2018). Identification of axolotl BH3-only proteins and expression in axolotl organs and apoptotic limb regeneration tissue. *Biol. Open* 7:bio036293. doi: 10.1242/bio.036293

Budai, Z., Ujlaky-Nagy, L., Kis, G. N., Antal, M., Bankó, C., Bacsó, Z., et al. (2019). Macrophages engulf apoptotic and primary necrotic thymocytes through

similar phosphatidylserine-dependent mechanisms. *FEBS Open Bio* 9, 446–456. doi: 10.1002/2211-5463.12584

Camilleri-Robles, C., Serras, F., and Corominas, M. (2019). Role of *D-GADD45* in JNK-dependent apoptosis and regeneration in *Drosophila*. *Genes* 10:378. doi: 10.3390/genes10050378

Chera, S., Ghila, L., Dobretz, K., Wenger, Y., Bauer, C., Buzgariu, W., et al. (2009). Apoptotic cells provide an unexpected source of Wnt3 signaling to drive hydra head regeneration. *Dev. Cell* 17, 279–289. doi: 10.1016/j.devcel.2009.07.014

Cohen, G. M. (1997). Caspases: the executioners of apoptosis. *Biochem. J.* 326(Pt 1), 1–16. doi: 10.1042/bj3260001

Czaja, M. J., Flanders, K. C., Biempica, L., Klein, C., Zern, M. A., and Weiner, F. R. (1989). Expression of tumor necrosis factor-alpha and transforming growth factor-beta 1 in acute liver injury. *Growth Factors* 1, 219–226. doi: 10.3109/08977198908997998

D'Arcy, M. S. (2019). Cell death: a review of the major forms of apoptosis, necrosis and autophagy. *Cell Biol. Int.* 43, 582–592. doi: 10.1002/cbin.11137

Dent, J. N. (1962). Limb regeneration in larvae and metamorphosing individuals of the South African clawed toad. *J. Morphol.* 110, 61–77. doi: 10.1002/jmor.1051100105

Diaz-Garcia, S., Ahmed, S., and Baonza, A. (2016). Analysis of the function of apoptosis during imaginal wing disc regeneration in *Drosophila melanogaster*. *PLoS One* 11:e08152. doi: 10.1371/journal.pone.0165554

Diwanji, N., and Bergmann, A. (2018). An unexpected friend - ROS in apoptosis-induced compensatory proliferation: implications for regeneration and cancer. *Semin. Cell Dev. Biol.* 80, 74–82. doi: 10.1016/j.semcdb.2017.07.004

Eguchi, G. (1963). Electron microscopic studies on lens regeneration. I. Mechanism of depigmentation of the iris. *Embryologia* 8, 45–62.

Elmore, S. (2007). Apoptosis: a review of programmed cell death. *Toxicol. Pathol.* 35, 495–516. doi: 10.1080/01926230701320337

Fan, Y., and Bergmann, A. (2008). Distinct mechanisms of apoptosis-induced compensatory proliferation in proliferating and differentiating tissues in the *Drosophila* eye. *Dev. Cell* 14, 399–410. doi: 10.1016/j.devcel.2008.01.003

Fausto, N., Campbell, J. S., and Riehle, K. J. (2006). Liver regeneration. *Hepatology* 43(2 Suppl. 1), S45–S53. doi: 10.1002/hep.20969

Ferreira, F., Raghunathan, V., Luxardi, G., Zhu, K., and Zhao, M. (2018). Early redox activities modulate *Xenopus* tail regeneration. *Nat. Commun.* 9, 1–15. doi: 10.1038/s41467-018-06614-2

FitzGerald, M. J., Webber, E. M., Donovan, J. R., and Fausto, N. (1995). Rapid DNA binding by nuclear factor kappa B in hepatocytes at the start of liver regeneration. *Cell Growth Differ. Mol. Biol. J. Am. Assoc. Cancer Res.* 6, 417–427.

Freeman, G. (1963). Lens regeneration from the cornea of *Xenopus laevis*. *J. Exp. Zool.* 154, 39–65. doi: 10.1002/jez.1401540105

Fukazawa, T., Naora, Y., Kunieda, T., and Kubo, T. (2009). Suppression of the immune response potentiates tadpole tail regeneration during the refractory period. *Development* 136, 2323–2327. doi: 10.1242/dev.033985

Gañan, Y., Macias, D., Basco, R. D., Merino, R., and Hurle, J. M. (1998). Morphological diversity of the avian foot is related with the pattern of Msx gene expression in the developing autopod. *Dev. Biol.* 196, 33–41. doi: 10.1006/dbio.1997.8843

Gargioli, C., and Slack, J. M. W. (2004). Cell lineage tracing during *Xenopus* tail regeneration. *Development* 131, 2669–2679. doi: 10.1242/dev.01155

Gauron, C., Rampon, C., Bouzaffour, M., Ipendey, E., Teillon, J., Volovitch, M., et al. (2013). Sustained production of ROS triggers compensatory proliferation and is required for regeneration to proceed. *Sci. Rep.* 3:2084. doi: 10.1038/srep02084

Gierer, A., Berking, S., Bode, H., David, C. N., Flick, K., Hansmann, G., et al. (1972). Regeneration of hydra from reaggregated cells. *Nat. New Biol.* 239, 98–101. doi: 10.1038/newbio239098a0

Goldar, S., Khaniani, M. S., Derakhshan, S. M., and Baradaran, B. (2015). Molecular mechanisms of apoptosis and roles in cancer development and treatment. *Asian Pac. J. Cancer Prev.* 16, 2129–2144. doi: 10.7314/APJCP.2015.16.6.2129

Greenhalgh, D. G. (1998). The role of apoptosis in wound healing. *Int. J. Biochem. Cell Biol.* 30, 1019–1030. doi: 10.1016/s1357-2725(98)00058-2

Gregory, C. D., Ford, C. A., and Voss, J. J. (2016). Microenvironmental effects of cell death in malignant disease. *Adv. Exp. Med. Biol.* 930, 51–88. doi: 10.1007/978-3-319-39406-0_3

Guha, U., Gomes, W. A., Kobayashi, T., Pestell, R. G., and Kessler, J. A. (2002). In vivo evidence that BMP signaling is necessary for apoptosis in the mouse limb. *Dev. Biol.* 249, 108–120. doi: 10.1006/dbio.2002.0752

Guimond, J. C., Lévesque, M., Michaud, P. L., Berdugo, J., Finnson, K., Philip, A., et al. (2010). BMP-2 functions independently of SHH signaling and triggers cell condensation and apoptosis in regenerating axolotl limbs. *BMC Dev. Biol.* 10:15. doi: 10.1186/1471-213X-10-15

Gurtner, G. C., Werner, S., Barrandon, Y., and Longaker, M. T. (2008). Wound repair and regeneration. *Nature* 453, 314–321. doi: 10.1038/nature07039

Han, M., Yang, X., Lee, J., Allan, C. H., and Muneoka, K. (2008). Development and regeneration of the neonatal digit tip in mice. *Dev. Biol.* 315, 125–135. doi: 10.1016/j.ydbio.2007.12.025

Higgins, G. M., and Anderson, R. M. (1931). Experimental pathology of the liver. I. Restoration of the liver of the white rat following partial surgical removal. *Arch. Pathol.* 12:186.

Hobmayer, B., Jenewein, M., Eder, D., Eder, M. K., Glasauer, S., Gufler, S., et al. (2012). Stemness in Hydra - a current perspective. *Int. J. Dev. Biol.* 56, 509–517. doi: 10.1387/ijdb.113426bh

Illingworth, C. M. (1974). Trapped fingers and amputated finger tips in children. *J. Pediatr. Surg.* 9, 853–858. doi: 10.1016/s0022-3468(74)80220-4

Inoue, T., Hosokawa, M., Morigiwa, K., Ohashi, Y., and Fukuda, Y. (2002). Bcl-2 overexpression does not enhance in vivo axonal regeneration of retinal ganglion cells after peripheral nerve transplantation in adult mice. *J. Neurosci.* 22, 4468–4477. doi: 10.1523/JNEUROSCI.22-11-04468.2002

Jewhurst, K., Levin, M., and McLaughlin, K. A. (2014). Optogenetic control of apoptosis in targeted tissues of *Xenopus laevis* Embryos. *J. Cell Death* 7, 25–31. doi: 10.4137/JCD.S18368

Johnston, J., Chan, R., Calderon-Segura, M., McFarlane, S., and Browder, L. W. (2005). The roles of Bcl-xL in modulating apoptosis during development of *Xenopus laevis*. *BMC Dev. Biol.* 5:20. doi: 10.1186/1471-213X-5-20

Jopling, C., Sleep, E., Raya, M., Martí, M., Raya, A., and Izpisúa Belmonte, J. C. (2010). Zebrafish heart regeneration occurs by cardiomyocyte dedifferentiation and proliferation. *Nature* 464, 606–609. doi: 10.1038/nature08899

Joven, A., Elewa, A., and Simon, A. (2019). Model systems for regeneration: salamanders. *Development* 146:dev167700. doi: 10.1242/dev.167700

Kakebeen, A. D., and Wills, A. E. (2019). More than just a bandage: closing the gap between injury and appendage regeneration. *Front. Physiol.* 10:81. doi: 10.3389/fphys.2019.00081

Kha, C. X., Son, P. H., Lauper, J., and Tseng, K. A. (2018). A model for investigating developmental eye repair in *Xenopus laevis*. *Exp Eye Res.* 169, 38–47. doi: 10.1016/j.exer.2018.01.007

Kha, C. X., and Tseng, K. A. (2018). Developmental dependence for functional eye regrowth in *Xenopus laevis*. *Neural Regen. Res.* 13, 1735–1737. doi: 10.4103/1673-5374.238611

Kragl, M., Knapp, D., Nacu, E., Khattak, S., Maden, M., Epperlein, H. H., et al. (2009). Cells keep a memory of their tissue origin during axolotl limb regeneration. *Nature* 460, 60–65. doi: 10.1038/nature08152

Kuan, C. Y., Yang, D. D., Samanta Roy, D. R., Davis, R. J., Rakic, P., and Flavell, R. A. (1999). The Jnk1 and Jnk2 protein kinases are required for regional specific apoptosis during early brain development. *Neuron* 22, 667–676. doi: 10.1016/s0896-6273(00)80727-8

Lehoczky, J. A., Robert, B., and Tabin, C. J. (2011). Mouse digit tip regeneration is mediated by fate-restricted progenitor cells. *Proc. Natl. Acad. Sci. U.S.A.* 108, 20609–20614. doi: 10.1073/pnas.1118017108

Li, F., Huang, Q., Chen, J., Peng, T., Roop, D. R., Bedford, J. S., et al. (2010). Apoptotic cells activate the "phoenix rising" pathway to promote wound healing and tissue regeneration. *Sci. Signal.* 3:ra13. doi: 10.1126/scisignal.2000634

Lin, G., and Slack, J. M. (2008). Requirement for Wnt and FGF signaling in *Xenopus* tadpole tail regeneration. *Dev. Biol.* 316, 323–335. doi: 10.1016/j.ydbio.2008.01.032

Lin, W., and Xu, G. (2019). Autophagy: a role in the apoptosis, survival, inflammation, and development of the retina. *Ophthalmic Res.* 61, 65–72. doi: 10.1159/000487486

Love, N. R., Chen, Y., Ishibashi, S., Kritsiligkou, P., Lea, R., Koh, Y., et al. (2013). Amputation-induced reactive oxygen species are required for successful *Xenopus* tadpole tail regeneration. *Nat. Cell Biol.* 15, 222–228. doi: 10.1038/ncb2659

Makanae, A., Mitogawa, K., and Satoh, A. (2014). Implication of two different regeneration systems in limb regeneration. *Regeneration* 1, 1–9. doi: 10.1002/reg2.16

Mao, S. A., Glorioso, J. M., and Nyberg, S. L. (2014). Liver regeneration. *Transl. Res.* 163, 352–362. doi: 10.1016/j.trsl.2014.01.005

Marques, I. J., Lupi, E., and Mercader, N. (2019). Model systems for regeneration: zebrafish. *Development* 146:dev167692. doi: 10.1242/dev.167692

Mescher, A. L. (2017). Macrophages and fibroblasts during inflammation and tissue repair in models of organ regeneration. *Regeneration* 4, 39–53. doi: 10.1002/reg2.77

Mescher, A. L., White, G. W., and Brokaw, J. J. (2000). Apoptosis in regenerating and denervated, nonregenerating urodele forelimbs. *Wound Repair. Regen.* 8, 110–116. doi: 10.1046/j.1524-475x.2000.00110.x

Metzstein, M. M., Stanfield, G. M., and Horvitz, H. R. (1998). Genetics of programmed cell death in *C. elegans*: past, present and future. *Trends Genet.* 14, 410–416. doi: 10.1016/s0168-9525(98)01573-x

Mochii, M., Taniguchi, Y., and Shikata, I. (2007). Tail regeneration in the *Xenopus* tadpole. *Dev. Growth Differ.* 49, 155–161. doi: 10.1111/j.1440-169X.2007.00912.x

Morata, G., Shlevkov, E., and Pérez-Garijo, A. (2011). Mitogenic signaling from apoptotic cells in *Drosophila*. *Dev. Growth Differ.* 53, 168–176. doi: 10.1111/j.1440-169X.2010.01225.x

Morgan, T. H., and Davis, S. E. (1902). The internal factors in the regeneration of the tadpole tail. *Arch. Entw. Mech. Org.* 15, 314–318.

Noda, K. (1971). Reconstruction of dissociated cells of hydra. *Zool. Mag.* 80, 27–31.

North, T. E., Goessling, W., Walkley, C. R., Lengerke, C., Kopani, K. R., Lord, A. M., et al. (2007). Prostaglandin E2 regulates vertebrate haematopoietic stem cell homeostasis. *Nature* 447, 1007–1011. doi: 10.1038/nature05883

Novianti, T., Juniantito, V., Jusuf, A. A., Arida, E. A., Jusman, S. W. A., and Sadikin, M. (2019). Expression and role of HIF-1α and HIF-2α in tissue regeneration: a study of hypoxia in house gecko tail regeneration. *Organogenesis* 15, 69–84. doi: 10.1080/15476278.2019.1644889

Pallas, P. S. (1766). *Miscellanea Zoologica: Quibus Novae Imprimis Atqueobscurae Animalium Species Describuntur et Observationibus Iconibusqueillustrantur*. Hagae Comitum: Apud Pterum van Cleef.

Pellettieri, J., Fitzgerald, P., Watanabe, S., Mancuso, J., Green, D. R., and Sánchez Alvarado, A. (2010). Cell death and tissue remodeling in planarian regeneration. *Dev. Biol.* 338, 76–85. doi: 10.1016/j.ydbio.2009.09.015

Pérez-Garijo, A., and Steller, H. (2015). Spreading the word: non-autonomous effects of apoptosis during development, regeneration and disease. *Development* 142, 3253–3262. doi: 10.1242/dev.127878

Pfefferli, C., and Jaźwińska, A. (2015). The art of fin regeneration in zebrafish. *Regeneration* 2, 72–83. doi: 10.1002/reg2.33

Pignatti, E., Zeller, R., and Zuniga, A. (2014). To BMP or not to BMP during vertebrate limb bud development. *Semin. Cell Dev. Biol.* 2014, 119–127. doi: 10.1016/j.semcdb.2014.04.004

Poss, K. D., Shen, J., Nechiporuk, A., McMahon, G., Thisse, B., Thisse, C., et al. (2000). Roles for Fgf signaling during zebrafish fin regeneration. *Dev. Biol.* 222, 347–358. doi: 10.1006/dbio.2000.9722

Rai, R. M., Lee, F. Y., Rosen, A., Yang, S. Q., Lin, H. Z., Koteish, A., et al. (1998). Impaired liver regeneration in inducible nitric oxide synthasedeficient mice. *Proc. Natl. Acad. Sci. U.S.A.* 95, 13829–13834. doi: 10.1073/pnas.95.23.13829

Reddien, P. W., and Sanchez Alvarado, A. (2004). Fundamentals of planarian regeneration. *Annu. Rev. Cell Dev. Biol.* 20, 725–757. doi: 10.1146/annurev.cellbio.20.010403.09511

Ryoo, H. D., and Bergmann, A. (2012). The role of apoptosis-induced proliferation for regeneration and cancer. *Cold Spring Harb. Perspect. Biol.* 4:a008797. doi: 10.1101/cshperspect.a008797

Saló, E., and Baguñà, J. (1984). Regeneration and pattern formation in planarians I. The pattern of mitosis in anterior and posterior regeneration in Dugesia (G) tigrina, and a new proposal for blastema formation. *J. Embryol. Exp. Morphol.* 83, 63–80.

Santabárbara-Ruiz, P., López-Santillán, M., Martínez-Rodríguez, I., Binagui-Casas, A., Pérez, L., Milán, M., et al. (2015). ROS-Induced JNK and p38 signaling is required for unpaired cytokine activation during *Drosophila* regeneration. *PLoS Genet.* 11:e1005595. doi: 10.1371/journal.pgen.1005595

Scimone, M. L., Kravarik, K. M., Lapan, S. W., and Reddien, P. W. (2014). Neoblast specialization in regeneration of the planarian *Schmidtea mediterranea*. *Stem Cell Rep.* 3, 339–352. doi: 10.1016/j.stemcr.2014.06.001

Seifert, A. W., Kiama, S. G., Seifert, M. G., Goheen, J. R., Palmer, T. M., and Maden, M. (2012). Skin shedding and tissue regeneration in African spiny mice (Acomys). *Nature* 489, 561–565. doi: 10.1038/nature11499

Sîrbulescu, R. F., and Zupanc, G. K. (2010). Inhibition of caspase-3-mediated apoptosis improves spinal cord repair in a regeneration-competent vertebrate system. *Neuroscience* 171, 599–612. doi: 10.1016/j.neuroscience.2010.09.002

Stewart, S., and Stankunas, K. (2012). Limited dedifferentiation provides replacement tissue during zebrafish fin regeneration. *Dev. Biol.* 365, 339–349. doi: 10.1016/j.ydbio.2012.02.031

Stocum, D. L. (2019). Nerves and proliferation of progenitor cells in limb regeneration. *Dev. Neurobiol.* 79, 468–478. doi: 10.1002/dneu.22643

Taniguchi, Y., Watanabe, K., and Mochii, M. (2014). Notochord-derived hedgehog is essential for tail regeneration in *Xenopus* tadpole. *BMC Dev. Biol.* 14:27. doi: 10.1186/1471-213X-14-27

Trembley, A. (1744). *Mémoires Pour Servir à l'histoire d'un Genre de Polypes d'eau Douce, à Bras en Forme de Cornes*. Paris: Chez Durand.

Tseng, A. S., Adams, D. S., Qiu, D., Koustubhan, P., and Levin, M. (2007). Apoptosis is required during early stages of tail regeneration in *Xenopus laevis*. *Dev. Biol.* 301, 62–69. doi: 10.1016/j.ydbio.2006.10.048

Tuzlak, S., Kaufmann, T., and Villunger, A. (2016). Interrogating the relevance of mitochondrial apoptosis for vertebrate development and postnatal tissue homeostasis. *Genes Dev.* 30, 2133–2151. doi: 10.1101/gad.289298.116

Vincent, E., Villiard, E., Sader, F., Dhakal, S., Kwok, B. H., and Roy, S. (2020). BMP signaling is essential for sustaining proximo-distal progression in regenerating axolotl limbs. *Development* 147:dev170829. doi: 10.1242/dev.170829

Wagner, D. E., Wang, I. E., and Reddien, P. W. (2011). Clonogenic neoblasts are pluripotent adult stem cells that underlie planarian regeneration. *Science* 332, 811–816. doi: 10.1126/science.1203983

Wan, E., Yeap, X. Y., Dehn, S., Terry, R., Novak, M., Zhang, S., et al. (2013). Enhanced efferocytosis of apoptotic cardiomyocytes through myeloid-epithelial-reproductive tyrosine kinase links acute inflammation resolution to cardiac repair after infarction. *Circ. Res.* 113, 1004–1012. doi: 10.1161/CIRCRESAHA.113.301198

Wang, C. K., Omi, M., Ferrari, D., Cheng, H. C., Lizarraga, G., Chin, H. J., et al. (2004). Function of BMPs in the apical ectoderm of the developing mouse limb. *Dev. Biol.* 269, 109–122. doi: 10.1016/j.ydbio.2004.01.016

Conflict of Interest: The authors declare that the research was conducted in the absence of any commercial or financial relationships that could be construed as a potential conflict of interest.

frontiers in Cell and Developmental Biology

ORIGINAL RESEARCH
published: 18 March 2021
doi: 10.3389/fcell.2021.630947

Embryo Buoyancy and Cell Death Gene Expression During Embryogenesis of Yellow-Tail Kingfish *Seriola lalandi*

Jaime Palomino[1,2], Camila Gómez[2], María Teresa Otarola[1,2], Phillip Dettleff[3,4], Daniel Patiño-García[1,5], Renan Orellana[1,5] and Ricardo D. Moreno[1]**

[1] Departamento de Ciencias Fisiológicas, Facultad de Ciencias Biológicas, Pontificia Universidad Católica de Chile, Santiago, Chile, [2] Laboratorio de Reproducción Animal, Facultad de Ciencias Veterinarias y Pecuarias, Universidad de Chile, Santiago, Chile, [3] Laboratorio FAVET-INBIOGEN, Facultad de Ciencias Veterinarias y Pecuarias, Universidad de Chile, Santiago, Chile, [4] Facultad de Medicina Veterinaria y Agronomía, Universidad de Las Américas, Sede La Florida, Santiago, Chile, [5] Departamento de Ciencias Quiímicas y Biológicas, Facultad de Salud, Universidad Bernardo O'Higgins, Santiago, Chile

OPEN ACCESS

Edited by:
Stefan Washausen,
Universität Münster, Germany

Reviewed by:
Alaa El-Din Hamid Sayed,
Assiut University, Egypt
Paulo Gavaia,
University of Algarve, Portugal

***Correspondence:**
Jaime Palomino
japalominom@yahoo.com;
jpalomin@veterinaria.uchile.cl
Ricardo D. Moreno
rmoreno@bio.puc.cl

Specialty section:
This article was submitted to Cell Death and Survival, a section of the journal Frontiers in Cell and Developmental Biology

Received: 18 November 2020
Accepted: 09 February 2021
Published: 18 March 2021

Citation:
Palomino J, Gómez C, Otarola MT, Dettleff P, Patiño-García D, Orellana R and Moreno RD (2021) Embryo Buoyancy and Cell Death Gene Expression During Embryogenesis of Yellow-Tail Kingfish Seriola lalandi. Front. Cell Dev. Biol. 9:630947. doi: 10.3389/fcell.2021.630947

In pelagic fish, embryo buoyancy is a noteworthy aspect of the reproductive strategy, and is associated with overall quality, survival, and further developmental success. In captivity, the loss of buoyancy of early embryos correlates with high mortality that might be related to massive cell death. Therefore, the aim of this study was to evaluate under captivity conditions the expression of genes related to the apoptosis process during the early embryonic development of the pelagic fish *Seriola lalandi,* and its relationship to the buoyancy of embryos. The relative expression of *bcl2*, *bax-like*, *casp9*, *casp8*, and *casp3* was evaluated by RT-qPCR and FasL/Fas protein levels by western blot in five development stages of embryos sorted as floating or low-floating. All genes examined were expressed in both floating and low-floating embryos up to 24 h of development. Expression of the pro-apoptotic factors *bax, casp9, casp8,* and *casp3* was higher in low-floating as compared with floating embryos in a developmental stage-specific manner. In contrast, there was no difference in expression of *bcl2* between floating and low-floating embryos. Fas protein was detected as a single band in floating embryos without changes in expression throughout development; however, in low-floating embryos, three higher intensity reactive bands were detected in the 24-h embryos. Interestingly, FasL was only detected at 24-h in floating embryos, whereas in low-floating samples this ligand was present at all stages, with a sharp increase as development progressed. Cell death, as evaluated by the terminal deoxynucleotidyl transferase-mediated dUTP nick-end labeling assay, was highly increased in low-floating embryos as compared to floating embryos throughout all developmental stages, with the highest levels observed during the gastrula stage and at 24 h. The results of this study suggest that an increase in cell death, probably associated with the intrinsic and extrinsic apoptosis pathways, is present in low-floating embryos that might explain their lower developmental potential under captivity conditions.

Keywords: *Seriola*, yellow-tail kingfish, apoptosis, buoyancy, pelagic

INTRODUCTION

Seriola lalandi is a globally distributed marine pelagic fish with growing importance worldwide for the aquaculture industry (Stuart and Drawbridge, 2013; Orellana et al., 2014; Sanchís-Benlloch et al., 2017). However, there are major knowledge gaps regarding its reproductive physiology and early embryo development that hamper scaling of production (Moran et al., 2007; Yang et al., 2016). A major distinctive reproductive strategy of pelagic fishes is the floatability (buoyancy) of eggs and embryos during the early stages of development. During captivity, the loss of buoyancy (i.e., sinking down to the bottom of the tank) of eggs and early embryos has been proposed as a major cause of developmental failure (Carnevali et al., 2001a; Sawaguchi et al., 2006; Sundby and Kristiansen, 2015). Buoyancy in pelagic fish embryos is a consequence of hydration that occurs mainly in the final stages of oocyte maturation in the ovary. This process involves passive water uptake by the oocyte, stimulated by an osmotic gradient created by accumulation of free amino acids derived from proteolysis of yolk proteins (Carnevali et al., 2001b; Fabra et al., 2005; Sawaguchi et al., 2006). There is evidence that the efficiency of the hydration process is highly relevant to the attainment of high buoyancy, allowing eggs and embryos to survive, and complete development (Ådlandsvik et al., 2001; Seoka et al., 2003; Jung et al., 2012, 2014). In addition, low embryo survival has been mentioned as one of the main drawbacks of pelagic fish farming, which is partly due to the production of low buoyancy eggs and embryos (Carnevali et al., 2001a, 2003; Thomé et al., 2012). Mechanisms associated with the cell death process, which would be determined during the formation of the oocyte in the ovary, have previously been associated with the loss of buoyancy in pelagic fish embryos (Carnevali et al., 2003; Thomé et al., 2012).

Regulated cell death involves a growing number of mechanisms that relay the cellular context and various stimuli (external or internal) to eliminate damaged cells or tissue remodeling during morphogenesis (Cole and Ross, 2001). Apoptosis is a particular and conserved, highly regulated type of cell death that is protein-directed, and necessary for the elimination of unwanted or altered cells, particularly during embryo development (Huang et al., 2000; Tittel and Steller, 2000; Bedoui et al., 2020). One of the main characteristics of apoptosis is the activation of a series of cysteine-aspartic intracellular proteases known as caspases (D'Arcy, 2019). The common strategy is to first assemble a multiprotein complex containing apical or initiator procaspases, which in turn activate executioner caspases (Shi, 2002, 2006). Apical caspase activation can be induced by the intrinsic (also known as the mitochondrial) pathway or the extrinsic (cell death receptor) pathway (Moreno et al., 2011; Kiraz et al., 2016; Bedoui et al., 2020). The extrinsic pathway begins with the activation of death receptors, such as tumor necrosis factor receptor (TNFR) or Fas (CD95/Apo-1) (Dewson and Kluck, 2009; Moreno et al., 2011), by binding with their cognate ligands (TNF-alpha and Fas ligand (FasL), respectively) (Kiraz et al., 2016). Activation of cell death receptors requires their trimerization and the formation of a multiprotein complex at the intracellular domain composed of inactive (pro-) apical initiator caspases (8 or 10), along with adaptor proteins such as FADD (Kiraz et al., 2016). Oligomerization of initiator caspases 8 or 10 induces activation, which is further stabilized by processing the prodomain, and proteolytic activation of executioner caspases 3 or 7 (Cullen and Martin, 2009; D'Amelio et al., 2010). In contrast, the intrinsic apoptotic pathway is initiated in response to a variety of stimuli that act on multiple targets within the cell (e.g., oxidative stress or DNA damage.). The main characteristic of this pathway is the complex interplay of pro-and antiapoptotic proteins of the BCL2 family that mainly regulate mitochondrial outer membrane permeability. In this way, BAK and BAX proapoptotic proteins play a major role in forming a pore at the mitochondrial outer membrane that allows the release of apoptogenic factors, including cytochrome *c* and DIABLO (also known as SMAC). This event allows the assembly of a multiprotein complex named the apoptosome, which is composed of apoptosis protease-activating factor-1 (APAF-1), cytochrome c, dATP, and the apical procaspase 9 (Willis and Adams, 2005; Youle and Strasser, 2008). Upon assembly into this complex, procaspase 9 becomes activated and then proteolytically activates the executioner caspases 3 and 7 (D'Amelio et al., 2010; Bedoui et al., 2020). Therefore, both pathways meet at the final caspase activation step (caspase3), which proteolyzes different cellular components, such as the inhibitor of calcium activated DNAase (ICAD), allowing release of CAD, an enzyme that degrades DNA internucleosomally (Luthi and Martin, 2007; Dix et al., 2008; Kiraz et al., 2016; Bedoui et al., 2020).

In fish, cell death as evaluated by DNA fragmentation or the presence of active caspase-3 has been shown to occur in the ovary as an important factor in progression of follicular atresia (Takle and Andersen, 2007; Thomé et al., 2012; Morais et al., 2016). In the tropical fish *Prochilodus argenteus*, high activity of caspase 3 and a greater number of apoptotic cells as revealed by means of the terminal deoxynucleotide transferase-mediated dUTP nick-end labeling (TUNEL) technique was observed in the ovarian cells of fish exposed to low oxygen concentrations. These observations coincided with the arrest and failure in the folliculogenesis process (Thomé et al., 2012). In this same species, BAX protein displayed an intense expression in follicles 2–3 days after spawning. In contrast, BCL2 showed higher expression immediately after spawning, and decreased on day 2 and 3 after spawning (Morais et al., 2016). Studies regarding the importance of apoptosis during fish embryonic development have been addressed mainly in zebrafish (Eimon and Ashkenazi, 2010) as a model to study teleost fishes; however, it is important to note that several steps in the reproductive strategy of marine pelagic species differ. In zebrafish, the spatial and temporal patterns of apoptosis during development, as evaluated by TUNEL labeling, shows an upregulation of cell death during the period 12–96 h post-fertilization (Cole and Ross, 2001). In transgenic zebrafish embryos overexpressing caspase 3, high levels of apoptosis and morphological abnormalities in specific tissues were detected. These embryos were also more sensitive to ultraviolet radiation compared to wild type (Yamashita et al., 2008). Similar findings were reported when mRNA encoding caspase 3 was injected into zebrafish early embryos (Valencia et al., 2007). Regarding participation of components of the

extrinsic pathway of apoptosis during zebrafish embryogenesis, it was observed that overexpression of caspase 8 induced embryonic mortality (Eimon et al., 2006). Overall, these findings suggest that eggs and embryos of teleost fishes have the machinery to elicit cell death during normal development or after environmental injuries (AnvariFar et al., 2017).

To our knowledge, there is only one report addressing the relationship between apoptosis and the buoyancy levels of eggs in a pelagic teleost fish (Carnevali et al., 2003). In the gilthead seabream *Sparus aurata*, it was shown that non-floating eggs had a lower capacity for protein and RNA synthesis, which led to them being less active than floating eggs. Furthermore, non-floating eggs displayed apoptotic characteristics such as cellular contraction, DNA fragmentation and an increased volume of mitochondria (Carnevali et al., 2003). Additionally, participation of the Fas/FasL system was proposed, since both proteins were detected in non-floating eggs, but only Fas was present in floating ones (Carnevali et al., 2003). Therefore, the aim of this study was to determine whether the loss of buoyancy of *S. lalandi* embryos during early development is related to increased cell death and expression of a particular apoptosis pathway.

MATERIALS AND METHODS

Ethical Approval

All procedures were reviewed and approved by the Ethic and Animal Care Committees of the Faculty of Biological Sciences of Pontifical Catholic University of Chile, Faculty of Veterinary Sciences, University of Chile and Research Ethics Committee of the Chilean National Foundation for Scientific and Technological Research.

Animal Management and Sampling Procedures

Broodstock was comprised of 90 adult individuals conditioned in three indoor tanks 2.5 m deep and with a capacity of 20,000 L in the hatchery center of Acuinor SA Company, Caldera, Atacama Region, Chile. Animals were kept at a male to female ratio of 2:1 with artificial thermo-photoperiod management, where spawning events occurred spontaneously with temperatures above 19°C and 14 h of light. Feeding consisted of commercial pellets (Vitalis®, Skretting, Puerto Montt, Chile) and fresh food (fisheries fish, squid, and cuttlefish) that were provided according to the protocols of the company. Samples for this study were collected during three spawning periods (one season per tank between January 2017 and March 2018). Two independent batches from each tank (six biological replicates or six batches) were monitored from spawning, and embryos were collected at different developmental stages as described by Palomino et al. (2014, 2017). Briefly, fertilized eggs were channeled from a skimmer on the surface of each tank into a separate egg collector tank, where the embryo development progressed (22–23°C). The development stages collected in this work were 2/4C (considered first and second cleavage), morula, blastula, gastrula, and 24 h post fertilization embryos, which are identified as 2/4C, M, B, G, and 24H, respectively (**Figures 1A–E**). **Figure 1** represents the separation procedure of embryos according to their buoyancy level (left side) and representative morphological characteristics of these embryos (right side). Embryos were transferred from the embryo collector tank to a conical 4 L inverted flask, where they were kept for 10 min. After this time, floating samples (approximately 50 individuals) were collected from the surface using a 500 μm mesh. Sinking embryos located at the bottom of the flask, which were dead and displayed structural damages as described in *S. aurata* by Carnevali et al. (2003), were discarded by removing 200 mL of water by means of a faucet. Embryos displaying a reduced buoyancy level (classified as low-floating) were obtained by extraction of 3 L of water where approximately 20 individuals could be collected. Samples were stored in RNAlater solution (Ambion®, Thermo Fisher Scientific, Waltham, MA, United States) for assessment of mRNA expression through real-time polymerase chain reaction (RT-qPCR) or frozen at −20°C for western blot analysis. For TUNEL assays, floating and low-floating embryos from M to 24H stages were processed for cell separation as described below. Ovary samples obtained by cannulation of the gonophore of three anesthetized adult females were used to standardize qPCR assay conditions.

Batches and Sample Characterization

The hatching rate of each spawning batch used in this study was quantified after 70 h of incubation of embryos in the egg collector tank (22–23°C) using the morphological criteria described by Moran et al. (2007). Thus, the fraction of newly hatched larvae approximately 4.8 mm in length was registered in a 50 mL sub-sample. Buoyancy, evaluated as the floating rate (FR) at different developmental stages, was assayed in a 30 mL sub-sample obtained from the egg collector tank, which was deposited during 10 min in a 50 mL beaker. Then, floating samples were isolated and their fraction recorded (%FR) by counting both floating and low-floating embryos. Additionally, in order to ensure that data obtained in this work corresponded to the developmental stage proposed, a sample of 20 embryos was fixed in 4% formaldehyde for evaluation under phase contrast microscopy with a Leica DME microscope (Leica Microsystems, Wetzlar, Germany). Batches used met criteria for morphological homogeneity (Moran et al., 2007; Yang et al., 2016), where at least 70% of the individuals corresponded to the same stage of development ($n = 14$). Sample characterization also included the assessment of the diameters of individuals and their oil globules in floating and low-floating embryos at each developmental stage. An eyepiece graticule ocular lens was used for these determinations, which were performed at 100 × magnification with a Leica DME phase contrast microscope.

RNA Isolation and Real-Time Polymerase Chain Reaction

One single total RNA extraction was done from each spawning event (six biological replicates). For this, Gene JET RNA Purification Kit (Thermo Scientific, Eugene, OR, United States) was used according to the manufacturer's instructions. The concentration of total RNA was determined in a Qubit®

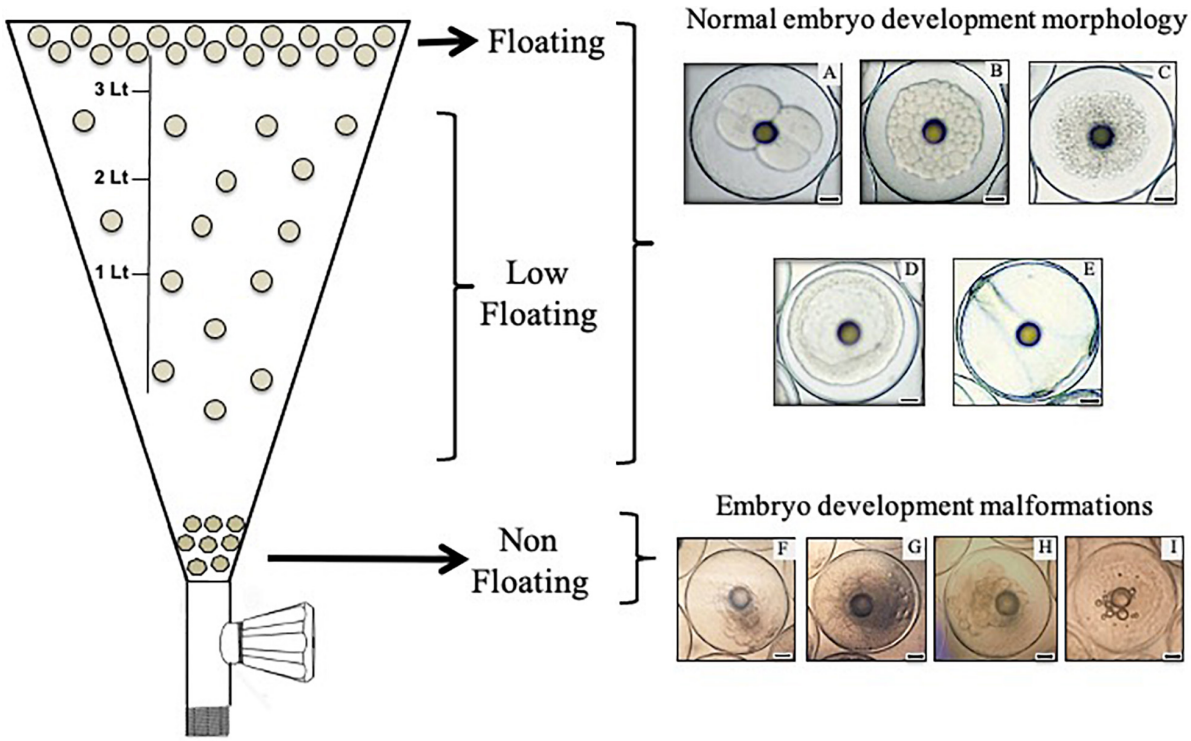

FIGURE 1 | Scheme representing the process of separation and collection of embryos according to their buoyancy level in a 4 L inverted flask (left side). In this work, only floating and low-floating embryos were collected and assessed. Floating samples were collected from the surface of the flask. Using of a faucet located at the bottom of the flask, non-floating embryos were discarded and embryos displaying a reduced buoyancy level (classified here as low-floating) were obtained by extraction of 3 L of water. The right side shows images of representative embryos of the development stages collected in this work. **(A)** Considered first and second cleavage, **(B)** morula, **(C)** blastula, **(D)** gastrula and **(E)** 24 h post-fertilization embryos (2/4C, M, B, G, and 24H, respectively). Normal morphology was observed in both floating and low-floating embryos. **(F–I)** Embryo development malformations, which are representative of non-floating embryos. Bars = 0.2 mm.

fluorometer using the Qubit® RNA Assay Kit, (Molecular Probes Invitrogen, Eugene, OR, United States). DNA contamination was removed by DNase I treatment, and reverse transcription (RT) was performed using the SuperScript™ First-Strand Synthesis System (Invitrogen). Then, complementary DNA (cDNA) concentration was determined using the ssDNA Qubit® Assay Kit (Molecular Probes®, Invitrogen). The primers used in this study are shown in **Table 1**. Primers for target genes *bcl2, bax, casp9, casp3*, and *casp8* were designed using Primer3[1] for amplicons between 80 and 213 base pairs (see **Table 1**). Gene amplifications were in performed in triplicate using an Illumina® Eco Real-Time PCR System Model EC-100-1001 and Maxima SYBR Green/Fluorescein qPCR Master Mix (Thermo Fisher Scientific, Waltham, MA, United States) following the manufacturers' conditions. Control samples without reverse transcriptase, cDNA template, and primers were included in each plate. Relative expression analysis for each target gene was performed in floating and low-floating embryos during different embryo development stages using the $2^{-\Delta\Delta Ct}$ method (Vandesompele et al., 2002). The constitutive genes *actb* and *map1b* were used as reference genes for normalization of expression (Palomino et al., 2017).

[1]www-genome.wi.mit.edu/cgi-bin/primer/primer3.cgi

Western Blot Analysis

Expression levels of FasL/Fas protein were determined using western blot analysis of floating or low-floating embryos at different developmental stages. Three protein extraction procedures were performed based on three pools, with each one constituted of embryos obtained from two independent spawning events (a total of six spawning events). Embryos were put into 1 mL of RIPA buffer (50 mM Tris–HCl, pH 8.0, 250 mM NaCl, 2 4 mM EDTA, and 1% NP-40) plus protease inhibitor cocktail (Pierce, Thermo Fisher Scientific). Samples were then sonicated for 30 s with 50% pulse in a Branson 5,450D Digital Sonifier, (Branson Ultrasonics, Danbury, CT, United States) and centrifuged at 14,000 × *g* for 15 min at 21°C to remove cellular debris. Protein concentrations were quantified using a Qubit 2.0 fluorometer (Invitrogen, Budapest, Hungary) and the Qubit Protein Assay Kit (Molecular Probes®, Invitrogen). Then, 50 μg of protein extract from each sample was resolved in a 12% SDS-polyacrylamide gel at 120 V in 1% running solution (TRIS 25 mM, glycine 250 mM, 0.1% SDS in distilled water). Electrophoretically separated peptides were transferred to a polyvinylidene-fluoride membrane (Immobilon-P membrane, Millipore Corp., Bedford, MA, United States) using the Mini-Vertical Slab Gel/Blotting Electrophoresis System (DCX-700, C.B.S. Scientific Company,

TABLE 1 | Sequence of qPCR primers.

Gene	Entrez gene ID	Forward sequence (5′-3′)	Reverse sequence (5′-3′)	Size (pb)
casp3	111663309	CTTGTGGTTCACTCGTGTCA	ATACTATGACCGGGTCCTGG	104
casp8	111666542	CTGACACGAGGAGGAAGAGG	ATTGGGCAGAAGACAAATCG	213
casp9	111651602	TCCCTTTCAGGTGATGGACT	CTCTCCCAGTTTCCTCTCCA	106
bax	111669314	GGTGGAACAACTGCTCAAGA	TGCATGAAGATGTCCTGAGC	105
bcl2	111670485	CAAGGAGGAGATGACATCGC	TCCAGCTGTTAAGAGGTCCA	80
actb	111225231	AGGGAAATCGTGCGTGACAT	GCTGAAGTTGTTGGGCGTTT	563
map1b	111647584	TCATCAAGATTATCAGGAGGCG	GGAAGCATACACCATGTAGAGG	158

Inc., Del Mar, CA, United States). The membranes were immersed in blocking solution (100 mM Tris–HCl, pH 8.0; 5% (w/v) skim milk; 35 mM NaCl and 0.1% (v/v) Tween 20 (Sigma-Aldrich, St Louis, MO, United States) for 30 min and incubated overnight at 4°C with an antibody previously tested in fish by Carnevali et al., 2003 (rabbit anti-mouse Fas polyclonal antibody diluted 1:200, Santa Cruz Biotechnology Cat# sc-1023, RRID:AB_2100247). Its specificity was ascertained using a blocking peptide (Santa Cruz Biotechnology Cat# sc-716, RRID:AB_2100358). To detect Fas ligand/TNFSF6, we used a mouse anti-rat monoclonal antibody diluted 1:100 (R and D Systems Cat# MAB1858, RRID:AB_2100788), which results in a band ≈44 kDa consistent with membrane-Fas ligand/TNFSF6 as revealed by Carnevali et al. (2003) using a Santa Cruz Biotechnology antibody. After washing with 0.1% phosphate buffered saline (PBS)-Tween 20, membranes were incubated for 1 h at 20–23°C with 1:500 of goat anti-rabbit antibody (Abcam Cat# ab6722, RRID:AB_954595) or goat anti-mouse IgG antibody (Abcam Cat# ab6790, RRID:AB_954670) conjugated to alkaline phosphatase. Charge controls were performed by incubating the membranes with 1:500 of anti-β-actin antibody (Sigma-Aldrich Cat# A1978, RRID:AB_476692), and incubation with the second antibody was performed as a negative control. Protein bands were visualized with 5-bromo-4-chloro-3-indolyl phosphate (BCIP)/nitro blue tetrazolium (NBT) substrate (SC-24981, Santa Cruz Biotechnology Inc.) in 0.1 M Tris, pH 9.5. Band intensity was evaluated by densitometry using the Gel Documentation System Biosens SC-645 (Biotop, Shanghai Bio-Tech Co., Shanghai, China) and expressed as arbitrary units of target protein/β-actin ratio.

Cells Preparation for TUNEL Assay and Flow Cytometry Assessment

In order to identify the fragmented DNA that is a hallmark of apoptotic cells in floating and low-floating *S. lalandi* embryos, the TUNEL method was applied through flow cytometry in cell suspensions obtained from morula to 24H embryos. Cell suspensions were prepared according to the embryo dissociation method described by Bresciani et al. (2018). Briefly, approximately 30 embryos were mechanically dissociated by harsh pipetting in 500 μL of a dissociation mix solution of 460 μL of 0.25% trypsin-EDTA (Gibco Life Technologies, Carlsbad, CA, United States) plus 40 μL of 100 mg/mL of collagenase (Sigma-Aldrich). This procedure was performed in a 1.5 mL Eppendorf tube over a heat block set at 30°C until the sample was fully homogenized. The dissociation procedure was stopped by adding 800 μL of Dulbecco's modified Eagle's medium (Merck KGaA, Darmstadt, Germany) supplemented with 10% fetal bovine serum (Merck KGaA). This mixture was centrifuged for 5 min at 700 × *g* and the supernatant discarded. Pelleted cells were washed twice by resuspension in 500 μL of 1 × PBS and fixed in 2% paraformaldehyde in PBS. Then, pelleted cells were washed twice in 1 × PBS by centrifugation and permeabilized by incubation in 100 μL of 0.1% Triton X-100 prepared in 0.1% sodium citrate for 2 min on ice. After washing twice in 1 × PBS, cells were treated with the *In Situ* Cell Death Detection Kit, Fluorescein (Roche Diagnostics Gmbh, Mannheim, Germany) according to the company's protocol for cell suspensions. Before analysis in the flow cytometer, cells were stained with 1 mg/mL propidium iodide (PI) to discriminate cells from debris. The TUNEL reaction was assessed though flow cytometric analyses on a Gallius Cytometer (Beckman Coulter, Brea, CA, United States) with standard settings, including compensation protocols for proper fluorophore discrimination. Events with very low forward scatter, representing debris, were excluded from analysis by forward and side-scatter gating. The proportion of labeled cells with PI and positive for TUNEL reaction were detected on a logarithmic scale in the FL3 and FL1 fluorescence detectors, respectively.

Statistical Analysis

Six replicates, which are representative of different batches of separate spawning events, were used for morphometric evaluations (buoyancy rate, embryo and oil drop diameters), analysis of gene expression, and flow cytometry assessments. For western blots and band intensity analysis, three replicates were made. Data were analyzed by ANOVA using the InfoStat Professional Program, National University of Córdoba, Argentina. Each model included the main effects of the developmental stages, the buoyancy conditions and their interaction. Significant differences among means were evaluated using Tukey's test. All values were considered significantly different for $P < 0.05$ (Sokal, 1995).

RESULTS

Characterization of Batches and Samples

The six batches assessed in this work displayed an average hatching rate of 85.5 ± 7.5% [mean ± standard deviation (SD)] after 70 h of incubation. As stated in the introduction,

as part of *S. lalandi* reproductive strategy, the developmental competence of eggs and embryos is related to the buoyancy level at the different early developmental stages. The embryo stages collected in this work were first and second cleavage (2/4C), morula (M), blastula (B), gastrula (G), and 24 h post fertilization embryos (24H) (**Figures 1A–E**). Embryos were divided into three different categories according to buoyancy level: (1) floating samples were embryos that remained at the top of the water column and showed translucid and clear blastomeres (**Figures 1A–E**); (2) low-floating samples were embryos that had a lower buoyancy and remained in a middle range between the surface and the bottom of the tank; they showed a similar aspect to the floating sample; and (3) non-floating embryos were samples that sank to the bottom of the tank. They usually showed fragmented and opaque blastomeres (**Figures 1F–I**). These embryos did not reach further developmental stages. Given that non-floating embryos showed morphological characteristics of cell death and have been previously characterized in pelagic eggs (Carnevali et al., 2003), we compared the floating versus the low-floating populations.

In the present study, most of the embryos retained a high buoyancy (>80%) at all developmental stages; however, embryos beyond gastrula stages showed a significant reduction in floatability (**Figure 2A**). When analyzed separately, embryo diameter was similar between floating and low-floating samples, regardless of developmental stage (**Figure 2B**). Another morphological parameter frequently used in fish embryo/egg analysis is the diameter of cytoplasmic oil drops, which is regarded as an important element to confer buoyancy during the first stages of development. Results showed that oil droplet diameter did not change throughout development or when compared between floating and low-floating samples, suggesting that other mechanisms influence the loss of buoyancy (**Figure 2C**).

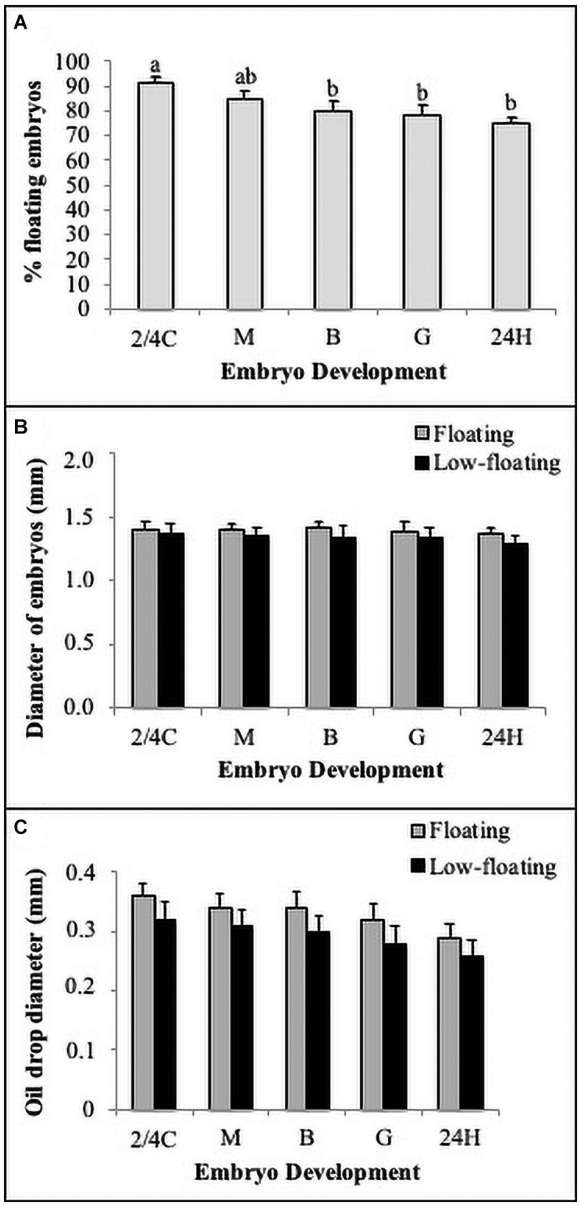

FIGURE 2 | Morpho-biometric parameters of embryos. **(A)** Buoyancy level (% floatability) of batches observed in each developmental stage. **(B)** Total embryo and **(C)** oil drop diameters quantified in floating (gray bars) and non-floating (black bars) embryos. Bars represent mean ± SD of six replicates and the different letters above the bars indicate significant differences ($P < 0.05$). $N = 120$.

Detection of Apoptosis Elements in *Seriola lalandi* Embryos

Levels of *bax* mRNA encoding the proapoptotic BAX protein remained similar throughout all developmental stages in floating embryos (**Figure 3A**). In low-floating embryos, there was a constant increase in levels of *bax* mRNA from 2/4C to G stage, and expression was sharply higher than in floating samples (Figure3A, asterisk). Interestingly, *bax* mRNA levels were similar between floating and non-floating embryos at the 24H stage (**Figure 3A**). In contrast, *bcl2* mRNA levels were similar between floating and non-floating embryos at all developmental stages, and showed a sharp increase from 2/4C to M in both groups and remained similar up to 24H only in low-floating embryos (**Figure 3B**). The levels of *bcl2* mRNA decreased at G and 24H only in floating embryos (**Figure 3B**).

Since upregulation of *bax* and downregulation of *bcl2* is related to activation of the intrinsic apoptotic pathway, we examined the mRNA levels of *casp9*, which encodes the initiator caspase in this pathway. Our results showed that *casp9* mRNA levels significantly increased in low-floating embryos when they reached the B stage and then decreased at G (**Figure 3C**). Only B stage low-floating embryos had a higher level of *casp9* mRNA expression than floating samples. Interestingly, in floating samples, levels of *casp9* were higher at 24H than G. Executioner *casp3* mRNA levels were similar between floating and low-floating samples at 2/4C, M, and 24H stages but were significantly higher in low-floating embryos at B and G stages (**Figure 3D**). These results suggest that the intrinsic pathway is active in low-floating embryos.

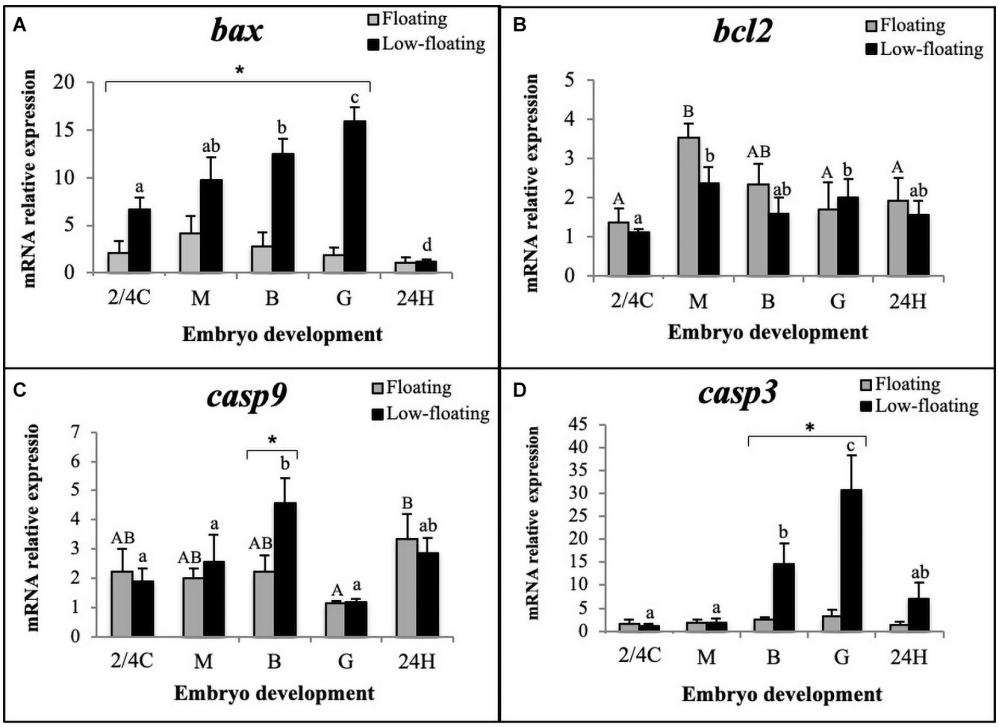

FIGURE 3 | Relative expression assessment of **(A)** *bax*, **(B)** *bcl2*, **(C)** *casp9*, and **(D)** *casp3* mRNAs throughout *S. lalandi* embryo development in floating (gray bars) and low-floating (black bars) samples. Different uppercase letters above bars indicate statistical differences within floating embryos. Similarly, different lowercase letters above bars indicate statistical differences within low-floating embryos. Differences between floating and low-floating embryos are identified with an asterisk over a bracket. Bars represent mean ± SD of six replicates. Results were considered statistically significant when $P < 0.05$.

Concerning the extrinsic apoptotic pathway, the mRNA levels of *casp8* in low-floating embryos were higher than in floating samples regardless of developmental stage, and reached their highest levels at the G stage in low-floating embryos and then at 24H in floating and low-floating samples (**Figure 4A**). We next sought to determine at the protein level if *S. lalandi* embryos express Fas and FasL, the initiator of the extrinsic pathway. In floating samples, Fas was detected as a single band of 50 kDa, with similar expression levels throughout all the studied stages of development (**Figure 4B**). In low-floating embryos, the antibody against Fas detected a strong band of 50 kDa and two other fainter bands of 65 and 40 kDa. The 50 kDa band detected here with the antibody against Fas is similar to that reported in mammals. The three bands (65, 50, and 40 kDa) detected in low-floating embryos were not observed when the antibody against Fas was pre-incubated with a blocking peptide, suggesting that the label was specific (**Figures 4B,C**). Interestingly, in floating eggs, the ligand of Fas (FasL) was detected as a single weak band of 44 kDa only in 24H embryos (**Figure 4B**). In contrast, in low floating eggs, the antibody against FasL gave a single faint band of 44 kDa in 2/4C embryos, then increased at M stage. It remained steady until G stage and then increased again in 24H embryos (**Figure 4C**). These results suggest the presence of the extrinsic pathway components in *S. lalandi* during early development.

Finally, in order to determine the extent of cell death, blastomeres of embryos at different developmental stages were disaggregated, and DNA fragmentation was evaluated using TUNEL. A representative result from low-floating G embryos shows the evaluation of TUNEL (+) cells (**Figure 5A**) and propidium iodide uptake as a measure for cellular debris (**Figure 5B**). Dot plot analysis showed the Q1 and Q2 populations that were used in the analysis (**Figure 5C**). Results indicated that M, B, G, and 24H low-floating embryos showed a higher level of TUNEL (+) cells than floating embryos, regardless of the developmental stage (**Figure 5D**). Cell death was similar in between M and B, regardless of their buoyancy state, and sharply increased at G stage only in low-floating samples. Floating 24H stage embryos showed a sharp increase in TUNEL labeling as compared with the other stages (**Figure 5D**).

DISCUSSION

Under captive conditions, it has been observed that the developmental potential of *S. lalandi* embryos rests largely on their buoyancy (Moran et al., 2007; Yang et al., 2016). Buoyancy is a characteristic of many pelagic marine fishes and is associated with embryo survival and development. In this work, we have identified a differential expression of apoptosis markers in embryos with low buoyancy as compared to those with positive

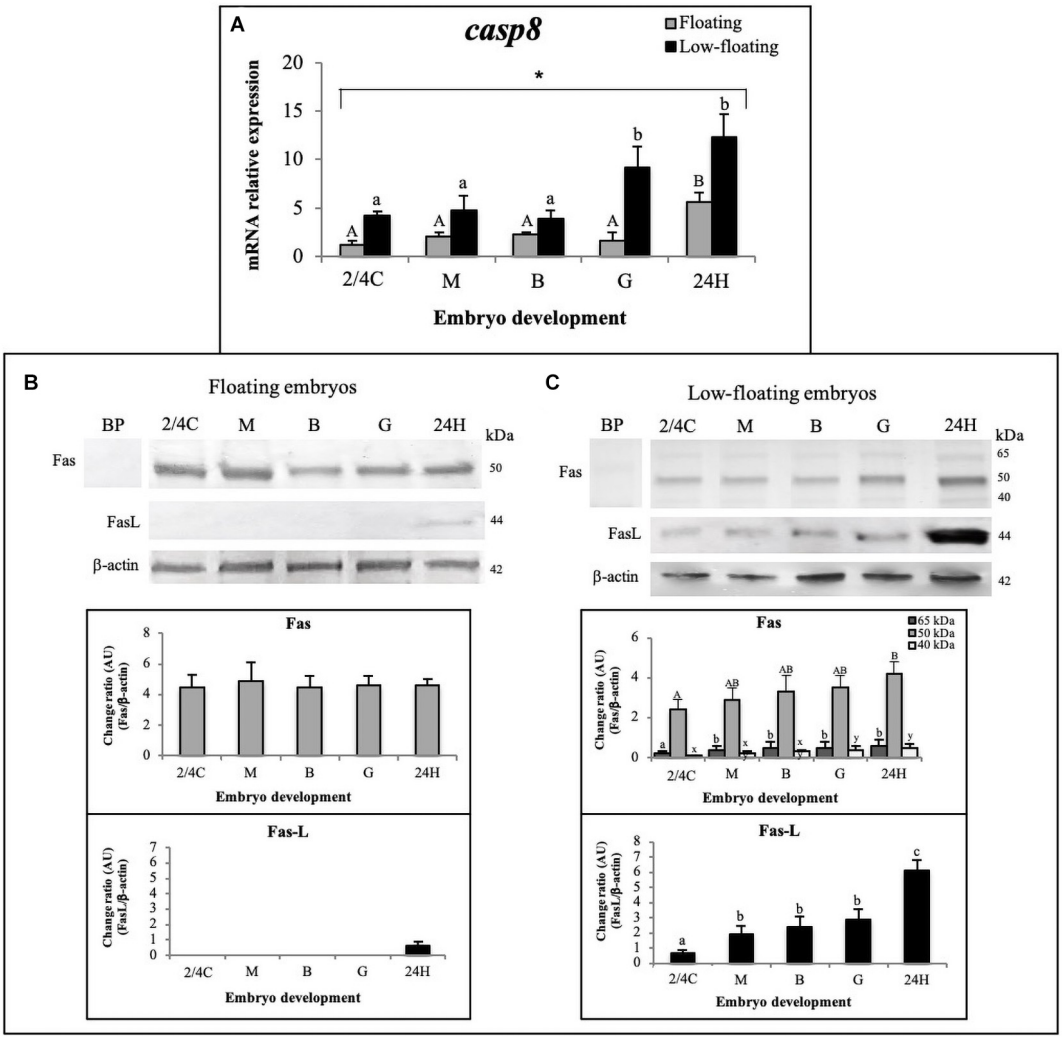

FIGURE 4 | Detection of the apoptosis extrinsic pathway throughout *S. lalandi* development in floating and low-floating embryos. **(A)** Relative expression assessment of *casp8* mRNA, in floating (gray bars) and low-floating (black bars) samples representing mean ± SD of six replicates for floating and low-floating embryos, respectively. Different uppercase or lowercase letters above bars indicate statistical differences ($P < 0.05$) within floating or low-floating embryos, respectively. Differences between floating and low-floating embryos are identified with an asterisk over a bracket. **(B,C)** Western blot analysis of Fas and FasL proteins during *S. lalandi* embryo development in floating **(B)** and low-floating **(C)** embryos. In floating embryos **(B)**, both Fas and FasL were detected as single bands of 50 and 44 kDa, respectively. However, in low-floating embryos **(C)**, western blot analysis of Fas revealed three bands of 65 (dark gray bars), 50 (gray bars) and 44 (white bars) kDa. In these samples, FasL was detected as a single band of 44 kDa. Bands were analyzed by densitometry. BP: Antibody anti-Fas preincubated with a blocking peptide. Bars represent the mean ± SD intensity of each band. Different uppercase letters above the bars indicate statistical differences within floating embryos. Similarly, different lowercase letters above bars indicate statistical differences within low-floating embryos ($P < 0.05$).

buoyancy, suggesting a close association between cell death and loss of buoyancy during early development.

In marine pelagic species, the loss of buoyancy in eggs and embryos has been shown to be associated with a decrease or failure in development. Various morphological abnormalities and characteristics related to cell death have been observed in non-floating spawned eggs/embryos (i.e., those that sink to the bottom of the culture tank) of *S. aurata* under captive conditions (Carnevali et al., 2001a, 2003). In the current study, we observed that non-floating embryos showed several morphological malformations in the blastomeres and cytoplasmic oil droplets. These malformations clearly preclude further development, so we devoted our study to comparing the expression of molecules associated with apoptosis in embryos that remain on the surface (considered viable and good quality) to those that although remaining floating, did do so to a lesser degree. No differences between floating and low-floating embryos were found in the diameter of the embryo or in the oil drop at any of the observed stages. In addition, morphologic differences were not evident between these samples. Considering that only embryos with high buoyancy are completely viable for complete development, these results indicate that using embryo

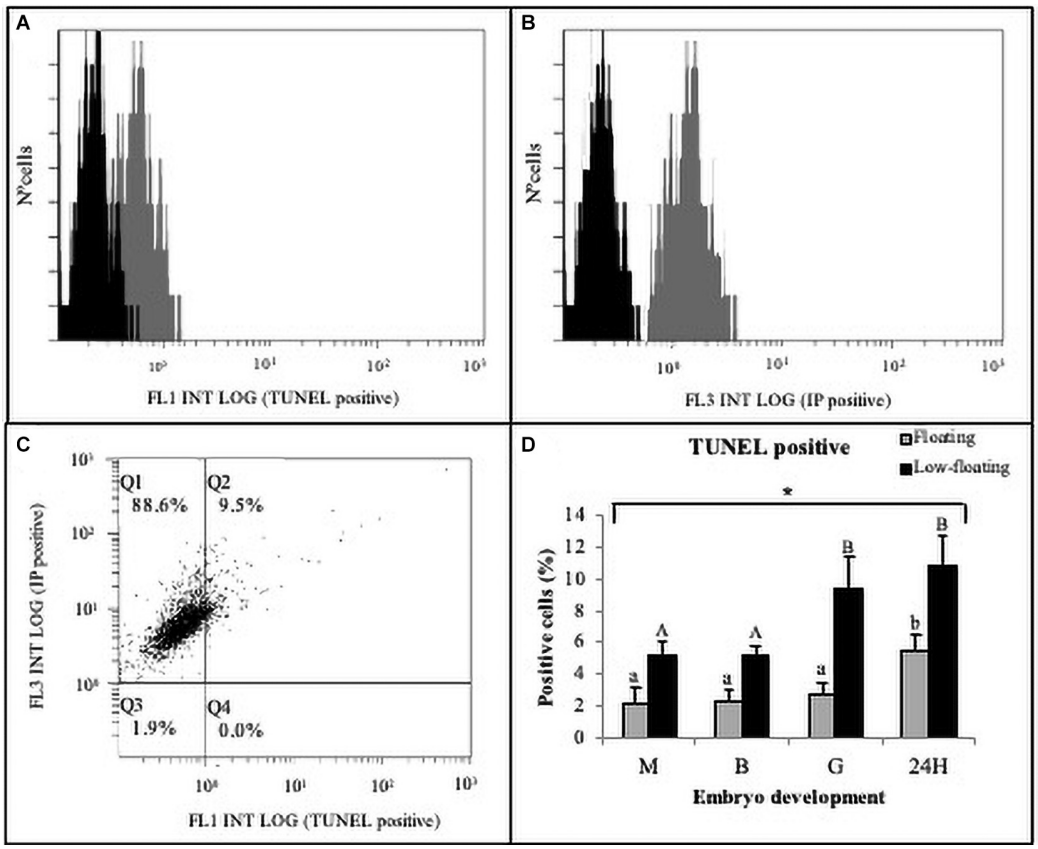

FIGURE 5 | Cell death detection in *S. lalandi* early development. Floating and low-floating embryos cells were disaggregated at each developmental stage as described in the materials and methods. Cell death was assayed by terminal deoxynucleotide transferase-mediated dUTP nick-end labeling (TUNEL) in cell suspensions using flow cytometry. **(A,B)** Representative histograms resulting from flow cytometry analysis to TUNEL **(A)** and propidium iodide (PI) uptake **(B)**, which were detected by FL1 and FL3 detectors, respectively. The horizontal axis of the histograms represents the signal intensity (log scale) and the vertical axis represents the number of cells. Each histogram displays the populations of both negative control cells (black curve) and cells stained by TUNEL and PI (dark gray curves). No signal was detected with a negative control of autofluorescence, and cells were detected within the first decade of logarithmic scale for both stains. **(C)** Representative fluorescence dot plot analysis of embryo cells positive to TUNEL staining (FL1) versus PI (FL3). Quadrants Q1 and Q2 represent PI positive cells, and debris were discarded in quadrants Q3 and Q4. TUNEL positive cells were detected in quadrant Q2. Cells used for flow cytometer representations **(A–C)** correspond to low-floating gastrulae embryos. **(D)** Bar graph summarizing the analysis by flow cytometry of TUNEL staining in cells obtained from different embryonic stages in floating (gray bars) and low-floating (black bars) samples. Bars represent the mean ± SD of six experimental replicates and 2,000–4,000 cells were evaluated in each experiment. Different uppercase letters above the bars indicate statistical differences within floating embryos. Conversely, different lowercase letters above bars indicate statistical differences within low-floating embryos. In all stages assessed, there were statistical differences between floating and low-floating embryos, which are identified with an asterisk over a bracket. Differences were considered statistically significant when $P < 0.05$.

morphology alone as a quality marker is not a good parameter for assessing viability and development potential.

Embryos with low buoyancy are frequently observed in the culture of pelagic species, even in spawning lots that present high survival parameters. Among these parameters, the hatching rate obtained in this work (85%), was higher than that seen in other pelagic fish, such as the common dentex (*Dentex dentex*), where a hatching rate of 61.6% was observed (Samaee et al., 2010) and the medregal *Seriola dumerili*, with a hatching rate of 65% (Jerez et al., 2006). However, a decrease in the proportion of floating embryos was observed as development progressed. This decrease in buoyancy throughout development has been documented in others marine pelagic species, such as the Atlantic cod *Gadus morhua* (Jung et al., 2012, 2014), the European anchovy *Engraulis encrancicolus* (Ospina-Álvarez et al., 2012) and the blue whiting *Micromesistius poutassou* (Ådlandsvik et al., 2001). In these species, the loss of buoyancy throughout development was associated with a slight increase in the specific gravity of the embryo, which has been attributed mainly to the passive loss of water to the hyperosmotic environment until the formation of osmoregulation mechanisms, which occurs after gastrulation in teleost fish (Riis-Vestergaard, 1987; Pérez-Robles et al., 2015). Therefore, in this work we attempted to determine whether the physiological processes of buoyancy are related to programmed cell death.

Here, we show in both floating and low-floating eggs the presence of a major band with a size of 50 kDa that was detected with an anti-Fas antibody. Interestingly, in low-floating eggs alone we detect two other higher and lower molecular weight bands. In mammals, it has been reported that Fas

consists of 335 aa and a size of 35 kDa (Takahashi et al., 1994; Peter et al., 2003). Since this protein is *N*-glycosylated at two sites in the extracellular domains, in addition to undergoing other post-translational modifications such as phosphorylation, palmitoylation, nitrosylation and glutathionylation, the mature form ranges between 48–54 kDa, which is close to the size of 50 kDa reported in the present work (Peter et al., 2003; Seyrek and Lavrik, 2019). The lower and higher molecular weight bands may represent different forms of post-translational modifications. This hypothesis is reinforced by the finding that when using the blocking peptide, all three bands detected by the antibody were no longer observed.

The FasL antibody detected only one band of 44 kDa in floating and low-floating samples. Interestingly, the genome of *Seriola dumerili* (greater amberjack), a close related species, shows three FasL-like genes with a predicted range of 238–267 aa (REF), which is very close to the 278 aa mouse protein (Suda et al., 1993). The predicted size of FasL is 32 kDa, but since it has several glycosylation sites, the mature form ranges between 38–42 kDa, which is close to the 44 kDa protein detected in the present study (Suda et al., 1993; Peter et al., 2003).

We observed that embryos with low buoyancy had higher levels of various apoptosis markers compared to high buoyancy embryos. Furthermore, we did not observe significant variations in cell death markers in floating embryos in the stages studied, except for an increase in *Casp9*, *Casp8*, and FasL in the 24H embryos. These results suggest that there is no significant morphological remodeling due to apoptosis during early development in *S. lalandi* until the 24H stage. However, further studies using higher resolution techniques are needed to determine whether local increases of cell death that were not resolved in this study are important during early development. Taking into account that the floating embryos represent normality in our model, the results of this work agree with evidence that relates apoptosis with normal development of the notochord in vertebrates. In zebrafish, it has been shown that the notochord begins to form during gastrulation, and that the extrinsic apoptotic pathway mediated by the Fas/FasL system is involved in the regression of notochord cells for their correct formation (Ferrari et al., 2014). Considering the developmental stages evaluated in this work, the formation of the notochord in the development of *S. lalandi* would occur between the gastrula stages and 24-h embryos, so the increase in the expression of apoptotic markers of the extrinsic pathway is consistent in these embryos. The results suggest that components of both the intrinsic and extrinsic pathways of apoptosis are expressed in the early development of *S. lalandi*.

Previous studies in *S. aurata* (Carnevali et al., 2001a, 2003) showed expression of both Fas and FasL in non-floating unfertilized eggs, whereas only Fas was expressed in floating eggs. These results agree with the expression profile of these proteins observed in the present study at early stages of development (from 2/4C to gastrula) in low-floating embryos, suggesting that upregulation of FasL might promote or be involved in cell death. FasL-induced Fas activation in low-floating embryos may be either autocrine or paracrine (**Figure 6**), leading to induction of the extrinsic pathway as suggested by our results showing a high expression level of *casp8* mRNA at all developmental stages, and *casp3* mRNA in B and G stages.

The intrinsic pathway is initiated by mitochondrial damage, which has been reported in non-floating eggs of *S. aurata* eggs (Carnevali et al., 2003). Furthermore, a greater amount of protein was detected in floating compared with non-floating eggs in *S. aurata*. It was hypothesized that the higher protein availability in floating eggs could generate a higher amount of free amino acids resulting from their proteolytic processing, which would increase the internal osmotic strength, stimulating egg hydration (passive water uptake) and increasing the buoyancy of eggs and embryos (Carnevali et al., 2001a; Fabra et al., 2005). In addition, the authors observed lower levels of cathepsin D and L activity in sinking eggs as compared to floating ones. Cathepsins are the main enzymes involved in yolk proteolysis, resulting in free amino acids (Carnevali et al., 2006; Sawaguchi et al., 2006; Palomino et al., 2017). The floating eggs of *S. aurata* presented high activity of both cathepsins, but in the non-floating eggs, very high levels of cathepsin D and very low levels of cathepsin L were present (Carnevali et al., 2001a). There is evidence that cathepsin D induces apoptosis both *in vitro* and *in vivo* and promotes the release of cytochrome C from the mitochondria (Chwieralski et al., 2006; Minarowska et al., 2007). Therefore, one of the possible physiological upstream signals of apoptosis induction in eggs of pelagic fish could be the loss of buoyancy followed by activation of cathepsin D (**Figure 6**). In previous studies in *S. lalandi*, a similar pattern of enzymatic activity in floating eggs to that described in *S. aurata* was observed (Palomino et al., 2017); therefore, it is possible that given the similarities in the reproductive strategy of both species, the molecular characteristics related to apoptosis seen in this work in embryos of low buoyancy are also related to the participation of cathepsin D in the induction of apoptosis (**Figure 6**).

In addition, one of the interesting results was that embryos with low floatability showed a higher rate of cell death than the floating ones, even though the morphology between both groups was not different. In this work, cell death was evaluated using the TUNEL technique, which is a tool that allows the extent of DNA fragmentation to be determined. In the case of apoptosis, fragmentation is performed by calcium activated DNAse (CAD), which cleaves the DNA between nucleosomes to generate a ladder pattern when evaluated in agarose gels (**Figure 6**; Bedoui et al., 2020). This enzyme is activated upon degradation of its inhibitor (ICAD) by caspase-3 (**Figure 6**). However, it is important to consider that other types of cell death, such as necrosis, also induce DNA fragmentation, although not in a periodic pattern like apoptosis. It is important to keep in mind that the TUNEL technique by itself cannot distinguish whether the fragmentation is in a periodic manner or the result of multiple fragments (i.e., apoptosis vs. necrosis). Therefore, it is highly recommended that several techniques are used to elucidate the correct manner of cell death (Kroemer et al., 2009; Banfalvi, 2017).

One important question is whether the loss in buoyancy promotes cell death or whether given some damage (e.g., oxidative stress, loss of DNA integrity) in the embryos, cell

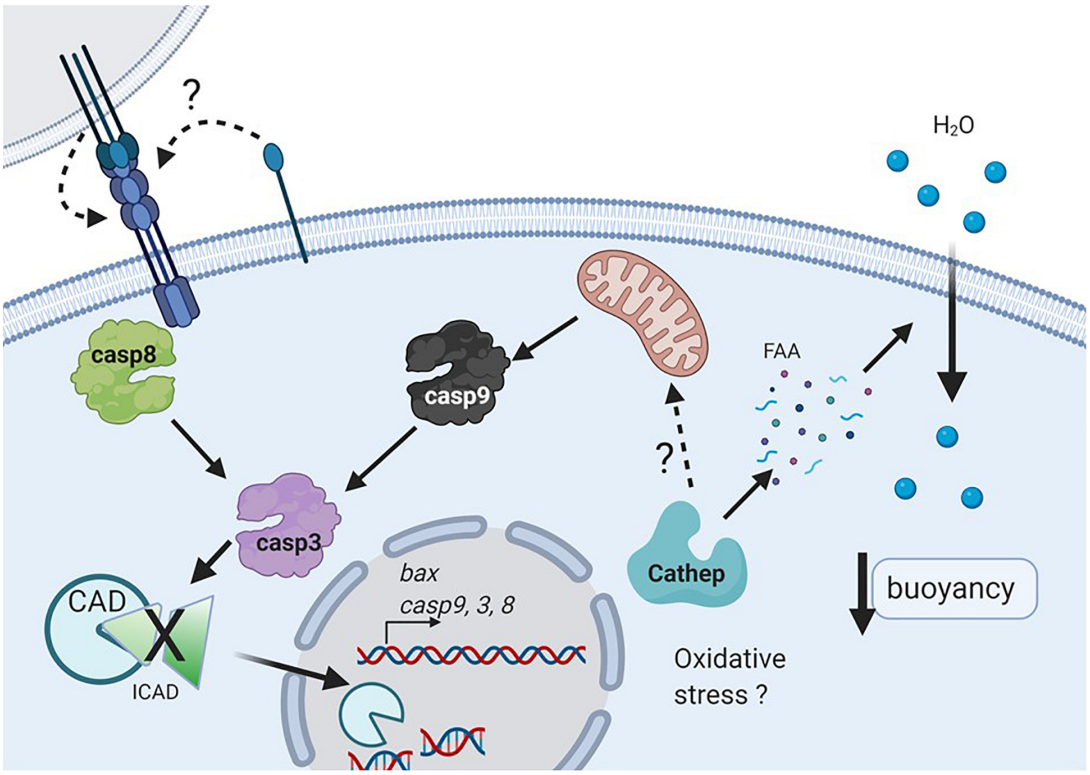

FIGURE 6 | Working model of cell death during early development in pelagic fish. Oxidative stress or nutrient deprivation (e.g., autophagy) may activate cathepsins (probably cathepsin D), that could degrade intracellular yolk proteins and then increase free amino acids (FAA), and promote water uptake which determines egg and embryo buoyancy. Cathepsin D may activate the intrinsic pathway (e.g., caspase 9), which along with caspase 8 will activate the executioner caspase 3 (**Figure 6**). In addition, the extrinsic pathway may be triggered by activation of Fas upon autocrine or juxtacrine binding of FasL. Active caspase 3 will degrade different substrates such as ICAD, allowing the activation and translocation of CAD to the nucleus, where it can degrade DNA (Created with BioRender.com).

death is induced and results in a loss of buoyancy (**Figure 6**). The data in this study suggest that from embryos in the 2/4 cell state, there is a higher proportion that will go into cell death in embryos with low buoyancy. In other species, it has been observed that the beginning of physiological apoptosis coincides with the activation of the embryonic genome, which occurs in the blastula stage (Kane and Kimmel, 1993; O'Boyle et al., 2007; Fernández et al., 2013). Therefore, it is possible that the apoptosis markers observed from the blastula in both floating and low-buoyancy embryos correspond to molecules involved in physiological apoptosis. In the case of the 2/4 cell and morula stages, where a consistent increase in the expression of caspases and other markers of cell death was not observed, it is possible that cell death is due to a different mechanism that involves environmental damage or is due to a maternal effect where optimal conditions for the development and ovulation of good quality oocytes did not exist (Morais et al., 2012; Thomé et al., 2012). Therefore, embryos derived from these oocytes would present increased expression of markers of cell death and match those with low buoyancy.

In conclusion, we have presented for the first-time suggestive evidence that the loss of buoyancy in early embryos in the pelagic fish *S. lalandi* is related to an increase in apoptosis. However, we cannot rule out the participation of other mechanisms of cell death. To date, most of the information on early fish development comes from benthic embryo models (e.g., killifish, zebrafish), where the egg/embryo buoyancy is not an important characteristic in determining developmental potential. Further studies are required to determine the mechanisms at the molecular level that connect buoyancy with the activation of cell death.

DATA AVAILABILITY STATEMENT

The raw data supporting the conclusions of this article will be made available by the authors, without undue reservation.

ETHICS STATEMENT

The animal study was reviewed and approved by Ethics and Animal Care Committees of Faculty of Biological Sciences of Pontifical Catholic University of Chile, Faculty of Veterinary Sciences, University of Chile. Written informed consent was obtained from the owners for the participation of their animals in this study.

AUTHOR CONTRIBUTIONS

MO and CG: performing experiments and collecting data. PD: collecting data and primer design. DP-G: manuscript writing and data analysis. RO: manuscript writing. RM: data analysis and manuscript writing. JP: experimental design planning, data analysis, and final manuscript approval. All authors contributed to the article and approved the submitted version.

FUNDING

We gratefully acknowledge the financial support of FONDECYT grant 1201343 to JP. We are also grateful to Broodstock Program of CORFO-15PTEC-45861 and FONDEQUIP grant (number EQM120156).

ACKNOWLEDGMENTS

We would like to thank Acuinor SA Company for their generous collaboration in providing us the samples for this study. We also would like to thank Juan Enrique Gaete and Arzomina Jiménez for their assistance during sampling procedures and for embryo photographs. Finally, we would like to thank Mónica De los Reyes for their generous collaboration in providing us access to the flow cytometer. We would also like to thank Editage (www.editage.com) for English language editing.

REFERENCES

Ådlandsvik, B., Coombs, S., Sundby, S., and Temple, G. (2001). Buoyancy and vertical distribution of eggs and larvae of blue whiting (*Micromesistius poutassou*): observations and modelling. *Fish. Res.* 50, 59–72. doi: 10.1016/S0165-7836(00)00242-3

AnvariFar, H., Amirkolaie, A. K., Miandare, H. K., Ouraji, H., Jalali, M. A., Üçüncü, S. İ. (2017). Apoptosis in fish: environmental factors and programmed cell death. *Cell. Tissue. Res.* 368 425–439. doi: 10.1007/s00441-016-2548-x

Banfalvi, G. (2017). Methods to detect apoptotic cell death. *Apoptosis* 22, 306–323. doi: 10.1007/s10495-016-1333-3

Bedoui, S., Herold, M. J., and Strasser, A. (2020). Emerging connectivity of programmed cell death pathways and its physiological implications. *Nat. Rev. Mol. Cell Biol.* 21, 678–695. doi: 10.1038/s41580-020-0270-8

Bresciani, E., Broadbridge, E., and Liu, P. P. (2018). An efficient dissociation protocol for generation of single cell suspension from zebrafish embryos and larvae. *MethodsX* 5, 1287–1290. doi: 10.1016/j.mex.2018.10.009

Carnevali, O., Cionna, C., Tosti, L., Lubzens, E., and Maradonna, F. (2006). Role of cathepsins in ovarian follicle growth and maturation. *Gen. Comp. Endocrinol.* 146, 195–203. doi: 10.1016/j.ygcen.2005.12.007

Carnevali, O., Mosconi, G., Cambi, A., Ridolfi, S., Zanuy, S., and Polzonetti-Magni, A. M. (2001b). Changes of lysosomal enzyme activities in sea bass (*Dicentrarchus labrax*) eggs and developing embryos. *Aquaculture* 202, 249–256. doi: 10.1016/S0044-8486(01)00775-X

Carnevali, O., Mosconi, G., Cardinali, M., Meiri, I., and Polzoneti-Magni, A. M. (2001a). Molecular components related to egg viability in the gilthead sea bream, *Sparus aurata*. *Mol. Reprod. Dev.* 58, 330–335. doi: 10.1002/1098-2795(200103)58:3<330::AID-MRD11<3.0.CO;2-7

Carnevali, O., Polzonetti, V., Cardinali, M., Pugnaloni, A., Natalini, P., Zmora, N., et al. (2003). Apoptosis in sea bream *Sparus aurata* eggs. *Mol. Reprod. Dev.* 66, 291–296. doi: 10.1002/mrd.10356

Chwieralski, C. E., Welte, T., and Bühling, F. (2006). Cathepsin-regulated apoptosis. *Apoptosis* 11, 143–149. doi: 10.1007/s10495-006-3486-y

Cole, L. K., and Ross, L. S. (2001). Apoptosis in the developing zebrafish embryo. *Dev. Biol.* 240, 123–142. doi: 10.1006/dbio.2001.0432

Cullen, S., and Martin, S. (2009). Caspase activation pathways: some recent progress. *Cell. Death. Differ.* 16, 935–938. doi: 10.1038/cdd.2009.59

D'Amelio, M., Cavallucci, V., and Cecconi, F. (2010). Neuronal caspase-3 signaling: not only cell death. *Cell. Death. Differ.* 17 1104–1114. doi: 10.1038/cdd.2009.180

D'Arcy, M. S. (2019). Cell death: a review of the major forms of apoptosis, necrosis and autophagy. *Cell Biol. Int.* 43, 582–592. doi: 10.1002/cbin.11137

Dewson, G., and Kluck, R. M. (2009). Mechanisms by which Bak and Bax permeabilise mitochondria during apoptosis. *J. Cell Sci.* 122(Pt 16), 2801–2808.

Dix, M. M., Simon, G. M., and Cravatt, B. F. (2008). Global mapping of the topography and magnitude of proteolytic events in apoptosis. *Cell* 134, 679–691. doi: 10.1016/j.cell.2008.06.038

Eimon, P. M., Kratz, E., Varfolomeev, E., Hymowitz, S. G., Stern, H., Zha, J., et al. (2006). Delineation of the cell-extrinsic apoptosis pathway in the zebrafish. *Cell Death Differ.* 13, 1619–1630. doi: 10.1038/sj.cdd.4402015

Eimon, P., and Ashkenazi, A. (2010). The zebrafish as a model organism for the study of apoptosis. *Apoptosis* 15, 331–349. doi: 10.1007/s10495-009-0432-9

Fabra, M., Raldúa, D. A., Power, P. M. T., Deen, J., and Cerdà, J. (2005). Marine fish egg hydration is aquaporin mediated. *Science* 307:545. doi: 10.1126/science.1106305

Fernández, C. G., Roufidou, C., Antonopoulou, E., and Sarropoulou, E. (2013). Expression of developmental-stage-specific genes in the gilthead sea bream *Sparus aurata* L. *Mar. Biotechnol.* 15, 313–320. doi: 10.1007/s10126-012-9486-8

Ferrari, L., Pistocchi, A., Libera, L., Boari, N., Mortini, P., Bellipanni, G., et al. (2014). FAS/FASL are dysregulated in chordoma and their loss-of-function impairs zebrafish notochord formation. *Oncotarget* 5, 5712–5724. doi: 10.18632/oncotarget.2145

Huang, Q., Deveraux, Q. L., Maeda, S., Salvesen, G. S., Stennicke, H. R., Hammock, B. D., et al. (2000). Evolutionary conservation of apoptosis mechanisms: lepidopteran and baculoviral inhibitor of apoptosis proteins are inhibitors of mammalian caspase-9. *Proc. Natl. Acad. Sci. U.S.A.* 97, 1427–1432. doi: 10.1073/pnas.97.4.1427

Jerez, S., Samper, M., Santamaría, F. J., Villamandos, J. E., Cejas, J. R., and Felipe, B. C. (2006). Natural spawning of greater amberjack (*Seriola dumerili*) kept in captivity in the Canary Islands. *Aquaculture* 252, 199–207. doi: 10.1016/j.aquaculture.2005.06.031

Jung, K. M., Folkvord, A., Kjesbu, O., Agnalt, A. L., Thorsen, A., and Sundby, S. (2012). Egg buoyancy variability in local populations of Atlantic cod (*Gadus morhua*). *Mar. Biol.* 159, 1959–1980. doi: 10.1007/s00227-012-1984-8

Jung, K. M., Folkvord, A., Kjesbu, O. S., and Sundby, S. (2014). Experimental parameterization of principal physics in buoyancy variations of marine teleost eggs. *PLoS One* 9:e104089. doi: 10.1371/journal.pone.0104089

Kane, D. A., and Kimmel, C. B. (1993). The zebrafish midblastula transition. *Development*. 119, 447–456.

Kiraz, Y., Adan, A., Kartal Yandim, M., and Baran, Y. (2016). Major apoptotic mechanisms and genes involved in apoptosis. *Tumour. Biol.* 37, 8471–8486. doi: 10.1007/s13277-016-5035-9

Kroemer, G., Galluzzi, L., Vandenabeele, P., Abrams, J., Alnemri, E. S., Baehrecke, E. H., et al. (2009). Classification of cell death: recommendations of the Nomenclature Committee on Cell Death 2009. *Cell Death Differ.* 16, 3–11. doi: 10.1038/cdd.2008.150

Luthi, A. U., and Martin, S. J. (2007). The CASBAH: a searchable database of caspase substrates. *Cell Death Differ.* 14, 641–650. doi: 10.1038/sj.cdd.4402103

Minarowska, A., Minarowski, L., Karwowska, A., and Gacko, M. (2007). Regulatory role of cathepsin D in apoptosis. *Folia Histochem. Cytobiol.* 45, 159–163.

Morais, R., Thomé, R., Santos, H., Bazzoli, N., and Rizzo, E. (2016). Relationship between bcl-2, bax, beclin-1, and cathepsin-D proteins during postovulatory follicular regression in fish ovary. *Theriogenology* 85, 1118–1131. doi: 10.1016/j.theriogenology.2015.11.024

Morais, R. D., Thomé, R. G., Lemos, F. S., Bazzoli, N., and Rizzo, E. (2012). Autophagy and apoptosis interplay during follicular atresia in fish ovary: a morphological and immunocytochemical study. *Cell. Tissue. Res.* 347, 467–478. doi: 10.1007/s00441-012-1327-6

Moran, D., Smith, C., Gara, B., and Poortenaar, C. (2007). Reproductive behavior and early development in yellowtail kingfish (*Seriola lalandi* Valenciennes 1833). *Aquaculture* 262, 95–104. doi: 10.1016/j.aquaculture.2006.10.005

Moreno, R. D., Urriola-Munoz, P., and Lagos-Cabre, R. (2011). The emerging role of matrix metalloproteases of the ADAM family in male germ cell apoptosis. *Spermatogenesis* 1, 195–208. doi: 10.4161/spmg.1.3.17894

O'Boyle, S., Bree, R. T., McLoughlin, S., Grealy, M., and Byrnes, L. (2007). Identification of zygotic genes expressed at the midblastula transition in zebrafish. *Biochem. Biophys. Res. Commun.* 358, 462–468. doi: 10.1016/j.bbrc.2007.04.116

Orellana J., Waller, B., and Wecker, B. (2014). Culture of yellowtail kingfish (*Seriola lalandi*) in a marine recirculating aquaculture system (RAS) with artificial seawater. *Aquacult. Eng.* 58, 20–28. doi: 10.1016/j.aquaeng.2013.09.004

Ospina-Álvarez, A., Palomera, I., and Parada, C. (2012). Changes in egg buoyancy during development and its effects on the vertical distribution of anchovy eggs. *Fish. Res.* 117–118, 86–95. doi: 10.1016/j.fishres.2011.01.030

Palomino, J., Herrera, G., Dettleff, P., and Martínez, V. (2014). Growth differentiation factor 9 and bone morphogenetic protein 15 expression in previtellogenic oocytes and during early embryonic development of yellow-tail kingfish *Seriola lalandi*. *Biol. Res.* 47:60. doi: 10.1186/0717-6287-47-60

Palomino, J., Herrera, G., Dettleff, P., Patel, A., Torres-Fuentes, J. L., and Martínez, V. (2017). Assessment of cathepsin mRNA expression and enzymatic activity during early embryonic development in the yellowtail kingfish *Seriola lalandi*. *Anim. Reprod. Sci.* 80, 23–29. doi: 10.1016/j.anireprosci.2017.02.009

Pérez-Robles, J., Diaz, F., Re, A. D., Giffard-Mena, I., Abdo-de la Parra, M. I., and Ibarra-Castro, L. (2015). Osmoregulation, growth, and survival during the larval development of bullseye puffer fish *Sphoeroides annulatus* (Jenyns, 1842, Pisces: Tetraodontidae). *Mar. Freshw. Behav. Phy.* 48, 397–415. doi: 10.1080/10236244.2015.1085692

Peter, M. E., Barnhart, B. C., and Algeciras-Schimnich, A. (2003). "CD95L/FasL and its receptor CD95 (APO- 1 /Fas)," in *The Cytokine Handbook*, 4th Edn, eds A. W. Thomson and M. T. Lotze (London: Elsevier Science Ltd).

Riis-Vestergaard, J. (1987). Physiology of teleost embryos related to environmental challenges. *Sarsia* 72, 351–358. doi: 10.1080/00364827.1987.10419735

Samaee, S. M., Mente, E., Estevez, A., Gimenez, G., and Lahnsteiner, F. (2010). Embryo and larva development in common dentex (*Dentex dentex*), a pelagophil teleost: the quantitative composition of egg-free amino acids and their interrelations. *Theriogenology* 73, 909–919. doi: 10.1016/j.theriogenology.2009.11.017

Sanchís-Benlloch, P. J., Nocillado, J., and Ladisa, C. (2017). *In-vitro* and *in vivo* biological activity of recombinant yellowtail kingfish (*Seriola lalandi*) follicle stimulating hormone. *Gen. Comp. Endocrinol.* 241, 41–49. doi: 10.1016/j.ygcen.2016.03.001

Sawaguchi, S., Kagawa, H., Ohkubo, N., Hiramatsu, N., Sullivan, C. V., and Matsubara, T. (2006). Molecular characterization of three forms of vitellogenin and their yolk protein products during oocyte growth and maturation in red seabream (*Pagrus major*), a marine teleost spawning pelagic eggs. *Mol. Reprod. Dev.* 73, 719–736. doi: 10.1002/mrd.20446

Seoka, M., Yamada, S., Iwata, Y., Yanagisawa, T., Nakagawa, T., and Kumai, H. (2003). Differences in the biochemical content of buoyant and non-buoyant eggs of the Japanese eel, Anguilla japonica. *Aquaculture* 216, 355–362. doi: 10.1016/S0044-8486(02)00459-3

Seyrek, K., and Lavrik, I. N. (2019). Modulation of CD95-mediated signaling by post-translational modifications: towards understanding CD95 signaling networks. *Apoptosis* 24, 385–394. doi: 10.1007/s10495-019-01540-0

Shi, Y. (2002). Apoptosome: the cellular engine for the activation of caspase-9. *Structure* 10, 285–288. doi: 10.1016/S0969-2126(02)00732-3

Shi, Y. (2006). Mechanical aspects of apoptosome assembly. *Curr. Opin. Cell Biol.* 18, 677–684. doi: 10.1016/j.ceb.2006.09.006

Sokal, R. R. (1995). *Biometry: The Principles and Practice of Statistics in Biological Research*. New York, NY: W. H. Freeman, 887.

Stuart, K. R., and Drawbridge, M. A. (2013). Captive spawning and larval rearing of California yellowtail (*Seriola lalandi*). *Aquac. Res.* 44, 728–737. doi: 10.1111/j.1365-2109.2011.03077.x

Suda, T., Takahashi, T., Golstein, P., and Nagata, S. (1993). Molecular cloning and expression of the fas ligand, a novel member of the tumor necrosis factor family. *Cell* 75, 1169–1176. doi: 10.1016/0092-8674(93)90326-l

Sundby, S., and Kristiansen, T. (2015). The principles of buoyancy in marine fish eggs and their vertical distributions across the world oceans. *PLoS One* 10:e0138821. doi: 10.1371/journal.pone.0138821

Takahashi, T., Tanaka, M., Inazawa, J., Abe, T., Suda, T., and Nagata, S. (1994). Human fas ligand: gene structure, chromosomal location and species specificity. *Int. Immunol.* 6, 1567–1574. doi: 10.1093/intimm/6.10.1567

Takle, H., and Andersen, O. (2007). Caspases and apoptosis in fish. *J. Fish. Biol.* 71, 326–349.

Thomé, R., Domingos, F., Santos, H., Martinelli, P., Sato, Y., Rizzo, E., et al. (2012). Apoptosis, cell proliferation and vitellogenesis during the folliculogenesis and follicular growth in teleost fish. *Tissue Cell* 44, 54–62. doi: 10.1016/j.tice.2011.11.002

Tittel, J. N., and Steller, H. (2000). A comparison of programmed cell death between species. *Genome Biol.* 1:REVIEWS0003. doi: 10.1186/gb-2000-1-3-reviews0003

Valencia, C. A., Bailey, C., and Liu, R. (2007). Novel zebrafish caspase-3 substrates. *Biochem. Biophys. Res. Commun.* 361, 311–316. doi: 10.1016/j.bbrc.2007.06.173

Vandesompele, J., De Preter, K., Pattyn, F., Poppe, B., Van Roy, N., De Paepe, A., et al. (2002). Accurate normalization of real-time quantitative RT-PCR data by geometric averaging of multiple internal control genes. *Genome Biol.* 3:research0034.1. doi: 10.1186/gb-2002-3-7-research0034

Willis, S. N., and Adams, J. M. (2005). Life in the balance: how BH3-only proteins induce apoptosis. *Curr. Opin. Cell. Biol.* 17, 617–625. doi: 10.1016/j.ceb.2005.10.001

Yamashita, M., Mizusawa, N., Hojo, M., and Yabu, T. (2008). Extensive apoptosis and abnormal morphogenesis in pro-caspase-3 transgenic zebrafish during development. *J. Exp. Biol.* 211, 1874–1881. doi: 10.1242/jeb.012690

Yang, S. G., Hur, S. W., and Ji, S. C. (2016). Morphological development of embryo, larvae and juvenile in yellowtail kingfish, *Seriola lalandi*. *Dev. Reprod.* 20, 131–140. doi: 10.12717/DR.2016.20.2.131

Youle, R. J., and Strasser, A. (2008). The BCL-2 protein family: opposing activities that mediate cell death. *Nat. Rev. Mol. Cell Biol.* 9, 47–59. doi: 10.1038/nrm2308

Conflict of Interest: The authors declare that the research was conducted in the absence of any commercial or financial relationships that could be construed as a potential conflict of interest.

frontiers in Cell and Developmental Biology

ORIGINAL RESEARCH
published: 20 April 2021
doi: 10.3389/fcell.2021.659531

The Role of Mcl-1 in Embryonic Neural Precursor Cell Apoptosis

*Robert T. Flemmer[1], Sarah P. Connolly[1], Brittany A. Geizer[1], Joseph T. Opferman[2] and Jacqueline L. Vanderluit[1]**

[1] Division of BioMedical Sciences, Memorial University, St. John's, NL, Canada, [2] Department of Cellular and Molecular Biology, St. Jude Children's Research Hospital, Memphis, TN, United States

Myeloid cell leukemia-1 (Mcl-1), an anti-apoptotic Bcl-2 protein, regulates neural precursor cell (NPC) survival in both the developing and adult mammalian nervous system. It is unclear when during the neurogenic period Mcl-1 becomes necessary for NPC survival and whether Bax is the sole pro-apoptotic target of Mcl-1. To address these questions, we used the nervous system-specific Nestin-Cre Mcl-1 conditional knockout mouse line (Mcl-1 CKO) to assess the anti-apoptotic role of Mcl-1 in developmental neurogenesis. Loss of Mcl-1 resulted in a wave of apoptosis beginning in the brainstem and cervical spinal cord at embryonic day 9.5 (E9.5) and in the forebrain at E10.5. Apoptosis was first observed ventrally in each region and spread dorsally over time. Within the spinal cord, apoptosis also spread in a rostral to caudal direction following the path of differentiation. Breeding the Mcl-1 CKO mouse with the Bax null mouse rescued the majority of NPC from apoptosis except in the dorsomedial brainstem and ventral thoracic spinal cord where only 50% were rescued. This demonstrates that Mcl-1 promotes NPC survival primarily by inhibiting the activation of Bax, but that Bax is not the sole pro-apoptotic target of Mcl-1 during embryonic neurogenesis. Interestingly, although co-deletion of Bax rescued the majority of NPC apoptosis, it resulted in embryonic lethality at E13, whereas conditional deletion of both Mcl-1 and Bax rescued embryonic lethality. In summary, this study demonstrates the widespread dependency on Mcl-1 during nervous system development.

Keywords: Bcl-2, neurogenesis, nervous system, development, cell death, Bax

OPEN ACCESS

Edited by:
Stefan Washausen, Universität Münster, Germany

Reviewed by:
Germain Gillet, Université Claude Bernard Lyon 1, France
Zhiyong Zhao, University of Maryland, Baltimore, United States
Brona M. Murphy, Royal College of Surgeons in Ireland, Ireland

****Correspondence:***
Jacqueline L. Vanderluit
j.vanderluit@mun.ca

Specialty section:
This article was submitted to Cell Death and Survival, a section of the journal Frontiers in Cell and Developmental Biology

Received: *27 January 2021*
Accepted: *29 March 2021*
Published: *20 April 2021*

Citation:
Flemmer RT, Connolly SP, Geizer BA, Opferman JT and Vanderluit JL (2021) The Role of Mcl-1 in Embryonic Neural Precursor Cell Apoptosis. Front. Cell Dev. Biol. 9:659531. doi: 10.3389/fcell.2021.659531

INTRODUCTION

Nervous system development follows a highly coordinated process. As formation of the neural tube completes, neurogenesis begins. Neural stem cells switch from dividing symmetrically to expand the neural stem cell pool to dividing asymmetrically and initiating neurogenesis by a stem cell and a committed neural progenitor cell. The number of neural precursor cells (NPC) and ultimately the number of neurons in the mature nervous system is regulated by a balance between survival- versus death- promoting proteins. The B cell lymphoma 2 (Bcl-2) family of pro- and anti-apoptotic proteins regulate this balance. Two anti-apoptotic Bcl-2 proteins, Myeloid cell leukemia-1 (Mcl-1) and Bcl-2 related gene long isoform (Bcl-xL) are required for cell survival during the process of neurogenesis. Mcl-1 is required for neural progenitor survival during

the initial stages of neurogenesis, whereas Bcl-xL is required for the survival of newly generated neurons (Motoyama et al., 1995; Arbour et al., 2008; Fogarty et al., 2019). Nervous system-specific conditional deletion of both Mcl-1 and Bcl-xL results in apoptotic death of the entire CNS and lethality at embryonic day 12 (E12) indicating a requirement for both proteins throughout the developing nervous system (Fogarty et al., 2019). Conditional deletion of Bcl-xL alone, however, affects the survival of only select neuron populations including upper layer cortical neurons, cholinergic neurons, spinal cord interneurons, and motor neurons (Savitt et al., 2005; Fogarty et al., 2016; Nakamura et al., 2016). Less is known about whether Mcl-1 is required ubiquitously in NPC throughout the developing nervous system.

Mcl-1 is unique from the anti-apoptotic Bcl-2 proteins. Mcl-1 expression is tightly regulated, and Mcl-1 protein has a short half-life of only a few hours (Warr et al., 2005; Zhong et al., 2005; Adams and Cooper, 2007). Mcl-1 was initially linked to a potential role in cell differentiation as early studies showed that Mcl-1 expression increases as lymphoid cells differentiate (Kozopas et al., 1993). Germline Mcl-1 knockout mice are lethal at E3.5 due to a failure in trophoblast differentiation (Rinkenberger et al., 2000). Mcl-1 expression fluctuates during the cell cycle with expression peaking in M-phase as cells exit to differentiate and then decreasing thereafter (Harley et al., 2010). Furthermore, overexpression of Mcl-1 in embryonic NPC induces premature cell cycle exit (Hasan et al., 2013). Taken together, these studies suggest a potential role for Mcl-1 in cell cycle exit or differentiation.

In the developing nervous system, Mcl-1 is required for cell survival through the period of neurogenesis as neural stem cells differentiate into immature neurons (Fogarty et al., 2019). In nervous-system specific Mcl-1 conditional knockout mice, apoptosis is observed in proliferating Nestin+ neural precursor cells, as well as doublecortin + neuroblasts and βIII tubulin + immature neurons (Arbour et al., 2008). Although Mcl-1 conditional knockout mice are embryonic lethal at E15.5, it's unclear when Mcl-1 becomes necessary for NPC survival. Mcl-1 expression begins early in nervous system development, with *mcl-1* mRNA detected at E10 (Fogarty et al., 2019). In the Mcl-1 CKO, apoptosis is observed as early as E10 in the developing spinal cord and by E11 in the forebrain demonstrating that Mcl-1 is required early in neurogenesis (Fogarty et al., 2019). As earlier time points have not been examined, it is unclear whether Mcl-1 is required prior to the onset of neurogenesis in the Nestin-positive neural precursor pool.

Here we used the nervous system specific Mcl-1 conditional knockout mouse to investigate the role of endogenous Mcl-1 in early nervous system development.

MATERIALS AND METHODS

Mice

All mouse lines were maintained on a C57Bl/6J background. Mcl-1 conditional knockout (Mcl-1 CKO) mice were generated as previously described by breeding our Nestin:Cre mouse line (Berube et al., 2005) with the Mcl-1 floxed mouse line (Opferman et al., 2003; Arbour et al., 2008; Hasan et al., 2013; Fogarty et al., 2019). The Mcl-1 CKO/BaxNull embryos were generated by crossing the Mcl-1 CKO mouse line with the BaxNull mouse line (cat# 002994, Jackson Laboratories, MN, United States) (Knudson et al., 1995). The Mcl-1 CKO/BaxNull/BaxFloxed embryos were generated by breeding the Mcl-1 CKO/BaxNull line with the BaxFloxed mouse line (cat# 006329, Jackson Laboratories, MN, United States) (Takeuchi et al., 2005). Tissue samples were collected from each embryo during dissection for genotyping. DNA extraction was performed with the REDExtract-N-Amp^{TM} Tissue PCR Kit according to manufacturer's instructions (Sigma-Aldrich Co., LLC, XNAT-100RXN, MO, United States). PCRs were performed with previously published primers for *cre*, *mcl-1* (Arbour et al., 2008; Malone et al., 2012), the null *bax* allele (Knudson et al., 1995) and the floxed *bax* allele (Takeuchi et al., 2005). Mice were housed on a 12-h light/dark cycle with access to food and water *ad libitum*. For timed pregnancies, mice were bred for 3 days and checked twice daily for vaginal plugs. The presence of a vaginal plug was taken as embryonic day 0.5. All experiments were approved by Memorial University of Newfoundland's Institutional Animal Care Committee according to the Guidelines of the Canadian Council on Animal Care.

Tissue Processing, Immunohistochemistry, and Western Blot

Pregnant dams were euthanized with an intraperitoneal injection of 300 μl of sodium pentobarbital (Euthanyl, 240 mg/ml, CDMV, QC, and CA) followed by cervical dislocation. Post-euthanasia, embryos were removed and fixed in 4% paraformaldehyde in phosphate buffered saline (1 × PBS), pH 7.4 overnight at 4°C. Embryonic tissues were cryoprotected in a 30% w/v sucrose solution in 1 × PBS then embedded in Tissue-Tek® O.C.T. Compound (Sakura Finetek, 4583, CA, United States) and frozen in dry ice-cooled isopentane. The forebrains and brainstems were sectioned in the coronal plane and spinal cords were sectioned in the horizontal plane at 14 μm thick and collected on Superfrost Plus Microscope Slides (Fisher Scientific, 12-550-15, PA, United States).

Slides were washed in 1XPBS pH 7.4 and incubated with primary antibody, rabbit anti-active Caspase-3 (cCasp-3)(1:400, BD Biosciences, cat.# 559565, RRID:397274). The next day, slides were incubated for 1 h at room temperature with a donkey anti-rabbit IgG tagged with Alexa Fluor 488 (Thermo Fisher Scientific, cat# A21206, RRID:AB_2535792). Prior to coverslipping, nuclei were stained with bisbenzimide (Hoechst 33258; Sigma-Aldrich Inc., B1155, MO, United States).

For Western Blot analysis, tissue samples were lysed in immunoprecipitation buffer (25 mM Tris, pH 7.4, 150 mM NaCl, 1 mM CaCl, 1% Triton X-100) (Sigma, 93426, MO, United States), containing the following protease inhibitors: 200 μg/ml phenylmethylsulfonyl fluoride (Sigma, P7626, MO, United States), 1 μg/ml aprotinin (Sigma, A-6103, MO, United States) 1 μg/ml leupeptin (Sigma, L-2882, MO, United States), 1 mM dithiothreitol (DTT; Sigma, 43816, MO,

United States). Protein concentration was determined with the BioRad Protein Assay reagent (500-0006, CA, United States) following manufacturer's instructions. Proteins were run on a 10% SDS-PAGE gel with Bio-Rad Precision Plus Protein^{TM} Standards Kaleidoscope^{TM} (#161-0375 Rev B, CA, United States) molecular weight ladder. Protein were transferred to a 0.2 μm nitrocellulose membrane (Bio-Rad, 1620112, CA, United States). Immunoblotting was performed overnight with antibodies to Mcl-1 [(1:1,000); Rockland, 600-401-394, RRID:AB_2266446], anti-β-Actin [(1:2,500), Sigma, A5316, RRID:AB_476743] or anti-glyceraldehyde-3-phosphate dehydrogenase (GAPDH) (1:2,500, Cell Signaling Technology, 5714, RRID:AB_10622025) followed by the appropriate HRP-conjugated secondary antibody either Goat anti-Rabbit IgG HRP conjugate (1:2,000, BioRad, cat# 1706515, RRID:AB_11125142) or Goat anti-mouse IgG HRP conjugate (1:2,000, BioRad, cat# 1706516, RRID:AB_11125547). Blots were developed with the Western Lightning Plus-ECL Enhanced Chemiluminescence Kit (Perkin Elmer Labs Inc., 02118) according to manufacturer's instructions.

Microscopy, Cell Counting and Statistical Analysis

Immunostained tissues were imaged using a Zeiss AxioImager Z.1 microscope (Carl Zeiss Microscopy, Jenna, Germany) with a Colibri LED light source (Carl Zeiss Microscopy, Jenna, Germany). Images were acquired with a Zeiss AxioCam MRm camera (Carl Zeiss Microscopy, Jenna, Germany) using Zeiss AxioVision v4.8 software (Carl Zeiss Microscopy, Jenna, Germany).

Cell counts were completed using ImageJ software[1]. For counts of cCasp-3+ cells in forebrain or ventral spinal cord sections, a 125 μm × 125 μm box was placed within the lateral ganglionic eminence and the ventral-medial lumbar spinal cord, respectively. Cells were counted as cCasp-3 positive (cCasp-3 +) if they had positive immunostaining for cCasp-3 and a completely condensed nucleus, as visualized with Hoechst stain. For both brain and spinal cord counts, three representative sections were counted per embryo.

One-way ANOVA was used to compare the percent of apoptotic cells and the total number of Hoechst nuclei across the genotypes with significance assessed at $\alpha < 0.05$. Tukey's *post hoc* analysis was performed when main effects were detected with significance assessed at $p < 0.05$. All statistical analysis was completed using GraphPad PrismV (GraphPad Software, Inc., CA, United States).

RESULTS

To determine the anti-apoptotic role of Mcl-1 in mammalian developmental neurogenesis, we first examined the onset of Mcl-1 expression. Western blot analysis of Mcl-1 protein revealed that Mcl-1 is expressed in the head (Hd) and body (Bd) of the developing embryo as early as embryonic day 8 (E8) (**Figure 1A**). Mcl-1 protein is detected in neuronal tissue of the forebrain (Fb) and spinal cords (Sp) of E10 and E12 embryos. In the Mcl-1 CKO mice, a 50% reduction in Mcl-1 protein expression is observed within the nervous system by E10 (**Figures 1B,C**). By E12, Mcl-1 protein expression in the MKO nervous system is further reduced to ∼10% of wild type littermates (Fogarty et al., 2019).

Mcl-1 is required for neural precursor cell survival (Arbour et al., 2008; Malone et al., 2012); however, it is not clear at what point in nervous system development Mcl-1 becomes necessary for survival. To address this question, we determined the onset of apoptosis in Mcl-1 CKO embryos. We looked for the onset of apoptosis at each level of the developing nervous system: the forebrain, brainstem and spinal cord from E9 to E11. In the developing forebrain, NPC are dividing rapidly to expand their numbers at E9 just prior to the start of neurogenesis at E10, and by E11 neurogenesis is in progress (Takahashi et al., 1996). In the spinal cord, neurogenesis begins earlier as there is less of an expansion of NPC numbers. Apoptotic cells were identified by two criteria: immunopositivity for active Caspase-3 (cCasp-3) and nuclear condensation with Hoechst staining.

Apoptosis was examined in coronal sections through the forebrain of Mcl-1 CKO and littermate controls at each time point (**Figure 2**). At E9, the developing forebrain in both control and Mcl-1 CKO embryos appeared healthy with no evidence of apoptotic cells (**Figures 2B–C′**). By E10, numerous apoptotic cells were observed in forebrains of Mcl-1 CKO embryos with the highest concentrations of apoptotic cells along the ventral telencephalon (**Figures 2C,C′**). Apoptotic cells were spread across both medial and lateral ganglionic eminences and in the dorsal cortex, small clusters were observed by E11 (**Figures 2C,C′**). In contrast, few to no apoptotic cells were observed in the developing forebrains of control littermates from E9 to E11 (**Figures 2B,B′**). This shows that in the Mcl-1 CKO, apoptosis begins at E10 in the developing forebrain starting in the ventral telencephalon and spreads laterally and dorsally.

Previous studies have focused primarily on the role of Mcl-1 in NPC within the developing brain while less is known of Mcl-1's role in the brainstem and spinal cord. Here we examined whether apoptosis followed the same chronological pattern in the brainstem and spinal cord as in the forebrain of Mcl-1 CKO embryos. In contrast to the forebrain, small clusters of apoptotic cells first appeared in the ventral brainstem at E9 (arrowheads in **Figure 3B**). By E10, apoptosis had spread across the ventral to dorsal aspect of the brainstem. Apoptosis was extensive throughout the brainstem at E11, with the exception of the more lateral regions of the brainstem and a thin region lining the ventricular surface that appeared to be spared (arrows in **Figure 3B**). Similar to the brainstem, apoptotic cells were first observed in the ventral portion of the upper spinal cord at E9 (arrowheads in **Figure 3C**). By E10, apoptosis had expanded from a few cells to covering the ventral third of the cord excluding the ventral lateral horns (arrows in **Figure 3D**). By E11, apoptosis had spread from the ventral to all but the most dorsal region of the upper spinal cord. In contrast to the brainstem and upper spinal cord, apoptosis was initiated 1 day later at E10 in the lumbar spinal cord; however, the first few apoptotic cells were also observed in the ventral spinal cord (**Figure 3C**). By E11, apoptosis had spread into the dorsal spinal cord. Taken together, these

[1]http://imagej.nih.gov/ij/

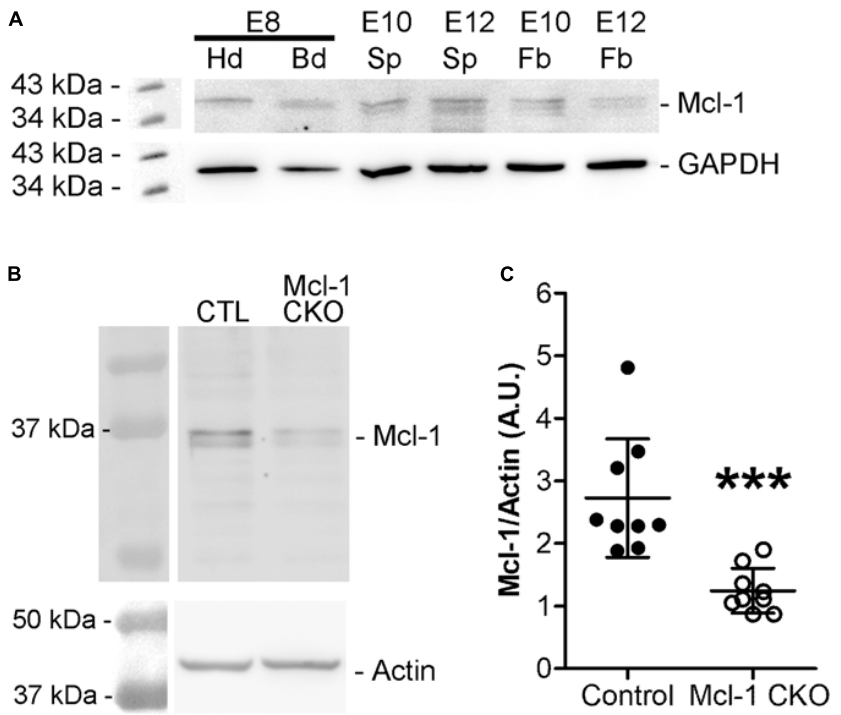

FIGURE 1 | Mcl-1 protein expression is observed at E8. **(A)** Western blots for Mcl-1 in C57BL/6J wild-type E8 embryonic heads compared to E10 and E12 forebrain expression (n = 2 blots). Each E8 head sample contained one pooled litter. Each E10 sample contained three pooled nervous system samples and each E12 sample contained two pooled nervous system samples. GAPDH was used as a loading control. Hd, head, Bd, body, Sp, spinal cord, and Fb, forebrain **(B)** Western analysis of Mcl-1 protein expression in developing nervous system of E10 Mcl-1 CKO and littermate controls. **(C)** Densitometry analysis of Mcl-1 protein levels. Mcl-1 protein levels (A.U.) were normalized to actin (n = 9 samples/genotype) $^{***}p < 0.001$, error bars represent ± SD.

results show that in the Mcl-1 CKO embryo, apoptosis spreads in two directions. Apoptosis begins rostrally in the brainstem and spreads caudally down the spinal cord from E9 to E11, and within each level, apoptosis begins in the ventral portion and spreads into the dorsal region.

To understand the anti-apoptotic role of Mcl-1 in the developing nervous system, we sought to identify the mechanism by which Mcl-1 promotes NPC survival. Mcl-1 binds and inhibits pro-apoptotic Bcl-2 effector proteins, Bax and Bak with different affinities (Chen et al., 2005). Although Mcl-1 has a stronger affinity for Bak, the role of Bak in the developing nervous system is minimal and only observed when co-deleted with Bax (Lindsten et al., 2000). In contrast to Bak, Bax has a prominent role in nervous system development including regulating the size of the neuronal population (Knudson et al., 1995; Deckwerth et al., 1996). We therefore questioned whether Bax also has a pro-apoptotic role in the proliferating NPC population. If true, Mcl-1 may promote NPC survival by inhibiting Bax activation. To address this question, we crossed the Mcl-1 CKO mice with the Bax null mouse line (Knudson et al., 1995) and examined whether the loss of Bax rescued NPC from apoptosis in the Mcl-1 CKO/Bax null embryos.

Apoptosis was examined in coronal sections throughout the rostral to caudal extent of the developing forebrain at E11 (**Figure 4A**). Numerous apoptotic cells were observed in the ventral forebrains of Mcl-1 CKO embryos with the majority of cells located in the medial and lateral ganglionic eminences (**Figures 4B–D**). In the Mcl-1 CKO/BaxNull forebrain, only a scattered few apoptotic cells were observed throughout the forebrain (arrows in **Figures 4B,C**). To determine the extent at which co-deletion of Bax rescues apoptotic NPC in the Mcl-1 CKO, we compared the number of apoptotic cells within a 125 μm × 125 μm boxed area in the lateral ganglionic eminences of Ctl (n = 5), Mcl-1 Het (n = 4), Mcl-1 CKO (n = 5) and Mcl-1 CKO/BaxNull embryos (n = 4) (**Figures 5A,D,E**). In both control littermates and Mcl-1 Het embryos there were few to no apoptotic cells observed (**Figures 5B,D,E**). In the Mcl-1 CKO embryos ∼31.7 ± 10.4% of cells were apoptotic whereas, in the Mcl-1 CKO/BaxNull embryos, only 2.4 ± 1.7% of cells were apoptotic. A one-way ANOVA revealed a main effect of genotype on the percent of apoptotic cells [$F(3,17) = 36.45$, $p < 0.0001$] (**Figure 5B**). Tukey's multiple comparison *post hoc* test showed that Mcl-1 CKO had significantly more apoptotic cells than all other genotypes ($p < 0.001$) and that there was no significant difference in the percent of apoptotic cells in the Mcl-1 CKO/BaxNull compared to control and Mcl-1 Het. To test whether the density of cells within our counting area was comparable across genotypes, a one-way ANOVA was performed on the mean number of nuclei per boxed area. No significant differences were found across the different genotypes [$F(3,17) = 1.498$, $p = 0.2584$] (**Figure 5C**).

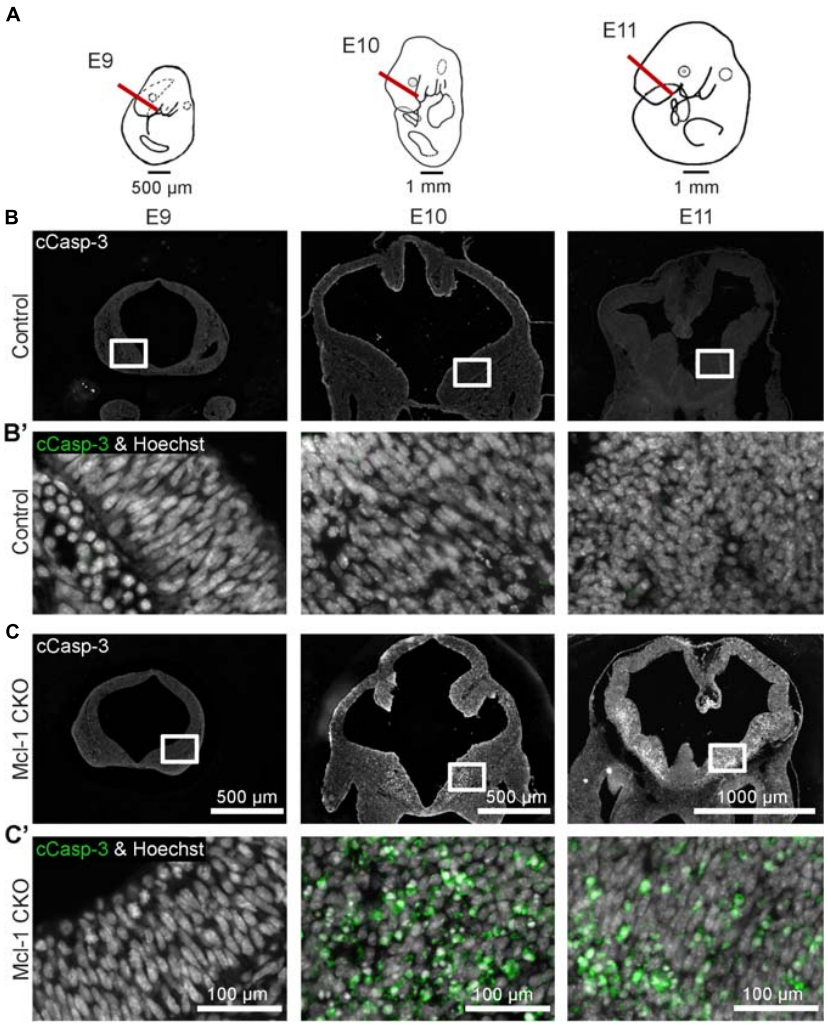

FIGURE 2 | Conditional deletion of Mcl-1 results in apoptosis beginning at E10 in the forebrain. **(A)** Line drawings of E9-E11 embryos demonstrating where coronal sections from developing forebrain were collected. **(B)** Representative images of coronal sections through the forebrains of CTL embryos at E9 (n = 3), E10 (n = 2) and E11 (n = 4) immunostained for cCasp-3 (white). **(B')** Higher magnification images of boxed areas in B double-labeled for cCasp-3 (green) and Hoechst (white). **(C)** Representative images of coronal sections through the forebrains of Mcl-1 CKO embryos at E9 (n = 3), E10 (n = 2) and E11 (n = 4) immunostained for cCasp-3 (white). **(C')** Higher magnification images of boxed areas in C double-labeled for cCasp-3 (green) and Hoechst (white). Arrows indicate apoptotic cells.

To determine whether Bax also rescues apoptotic NPC throughout the entire nervous system in the Mcl-1 CKO, we examined the brainstem and cervical, thoracic and lumbar levels of the spinal cords (**Figure 6A**). In E11 control littermates, only a few apoptotic cells were observed in the ventral brainstem (**Figure 6B**). In the Mcl-1 CKO embryo, apoptosis was widespread throughout the brainstem, and extended across the ventral to dorsal spinal cord at each level (**Figures 6B–E**). In contrast to the results in the forebrain, NPC in the Mcl-1 CKO did not appear to be completely rescued in the brainstem and spinal cord with co-deletion of Bax. Clusters of apoptotic cells were observed in the dorsomedial region of the brainstem and in the ventral thoracic spinal cord of the Mcl-1 CKO/BaxNull embryo (arrows in **Figures 6B,D**). NPC were rescued at the cervical and lumbar levels of the spinal cord.

To determine the extent at which co-deletion of Bax rescues apoptotic cells in the Mcl-1 CKO spinal cord, we compared the number of apoptotic cells within a 125 µm × 125 µm boxed area in the ventral thoracic spinal cords of Ctl (n = 5), Mcl-1 Het (n = 5), Mcl-1 CKO (n = 5) and Mcl-1 CKO/BaxNull embryos (n = 4) (**Figures 7A,D,E**). Similar to the apoptosis counts in the forebrain, there is little to no apoptosis in the spinal cords of littermate control or Mcl-1 HET embryos (**Figures 7B,D,E**). In the Mcl-1 CKO embryos 30.5 ± 4.1% of cells were apoptotic whereas, 16.7 ± 11.7% of cells were apoptotic in the Mcl-1 CKO/BaxNull embryos, demonstrating a 50% rescue with Bax co-deletion. A one-way ANOVA revealed a main effect of genotype on the percent of apoptotic cells [$F(3,18) = 33.64$, $p < 0.001$] (**Figure 7B**). Tukey's multiple comparison *post hoc* test showed that the Mcl-1 CKO ($p < 0.0001$) and Mcl-1

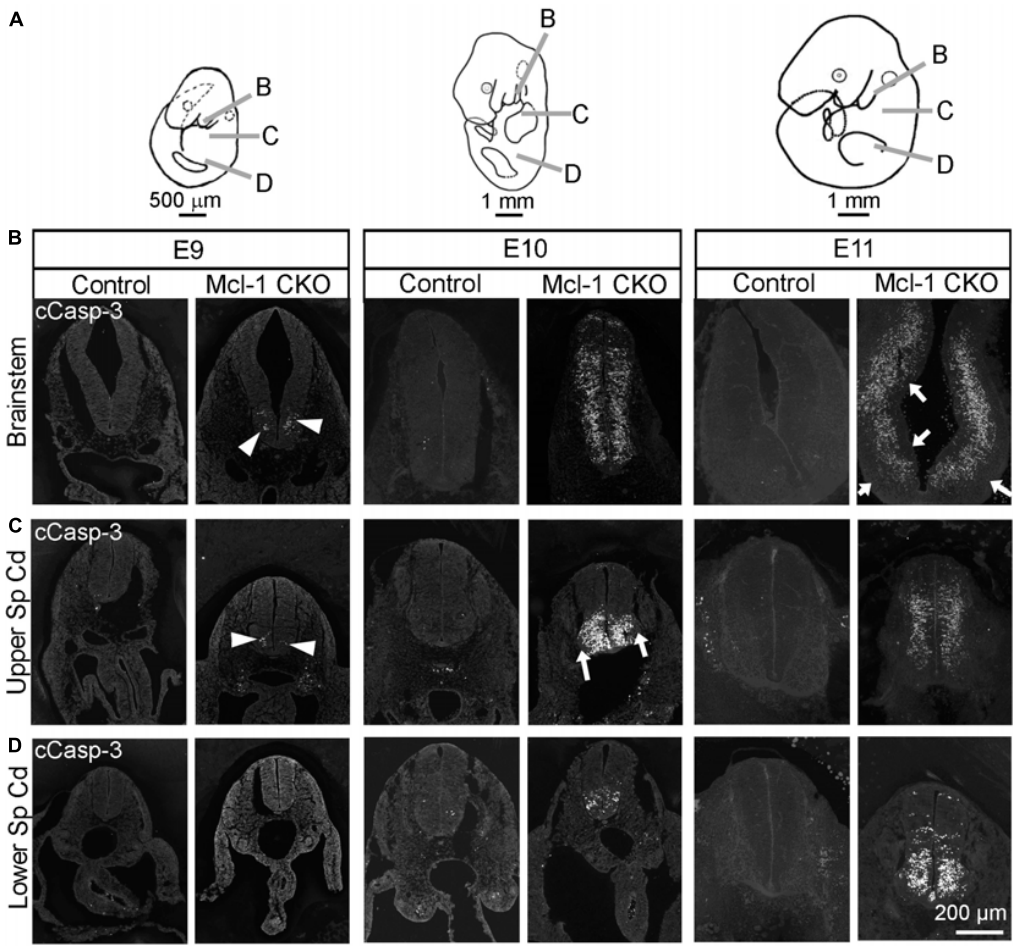

FIGURE 3 | Apoptosis spreads across to axes in the brainstem and spinal cord of Mcl-1 CKO embryos. **(A)** Line drawings of embryos demonstrating the location of sections collected from the brainstem and spinal cord. Immunohistochemistry for cCasp-3 on sections from the **(B)** brainstem, **(C)** upper spinal cord, and **(D)** lower spinal cord of wild type (Control) and Mcl-1 CKO embryos from E9 to E11 (E9, $n = 3$; E10, $n = 2$; E11, $n = 4$). Arrowheads point to clusters of apoptotic cells. Arrows indicate lateral and medial regions not immuno-positive for cCasp-3.

CKO/BaxNull ($p < 0.01$) spinal cords had significantly more apoptotic cells than control and Mcl-1 Het. Furthermore, Mcl-1 CKO/BaxNull had significantly fewer apoptotic cells than Mcl-1 CKO ($p < 0.05$). To test whether the density of cells within our counting area was comparable across genotypes, a one-way ANOVA was performed on the mean number of nuclei per boxed area. A main effect of genotype was detected [$F(3,18) = 5.29$, $p < 0.05$]. The follow-up Tukey's multiple comparison *post hoc* revealed that there were significantly more nuclei within the Mcl-1 CKO counting area than in the littermate controls (**Figure 7C**). As the total nuclei counts include both healthy and apoptotic nuclei, difficulties arise with apoptotic nuclei fragmenting which may slightly skew the overall nuclei counts. These results show that Bax co-deletion rescued 50% of cells from apoptosis in spinal cord of the Mcl-1 CKO in contrast to the almost complete rescue in the forebrain.

Co-deletion of Bax and Mcl-1 rescued most NPC from apoptotic cell death throughout the developing nervous system. Despite this rescue, Mcl-1 CKO/BaxNull embryos did not survive beyond E12.5 (**Table 1**). In surprising contrast, Mcl-1 CKO embryos are lethal at E15.5 and Bax Null mice are viable and healthy (Knudson et al., 1995; Arbour et al., 2008). We questioned whether the conditional deletion of Bax only in the nervous system would rescue the embryonic lethality. Transgenic mice carrying floxed Bax alleles were crossed with Mcl-1 CKO/BaxNull mouse line and viable offspring were born and survived up to postnatal day 16 (**Table 2**). This demonstrates that co-deletion of Bax rescues both cell death within the CNS as well as the embryonic lethality.

DISCUSSION

This study investigated the anti-apoptotic role of Mcl-1 in mammalian neurogenesis. There are two main findings: first, Nestin:Cre mediated deletion of Mcl-1 results in apoptosis throughout the spinal cord, brainstem, and forebrain and

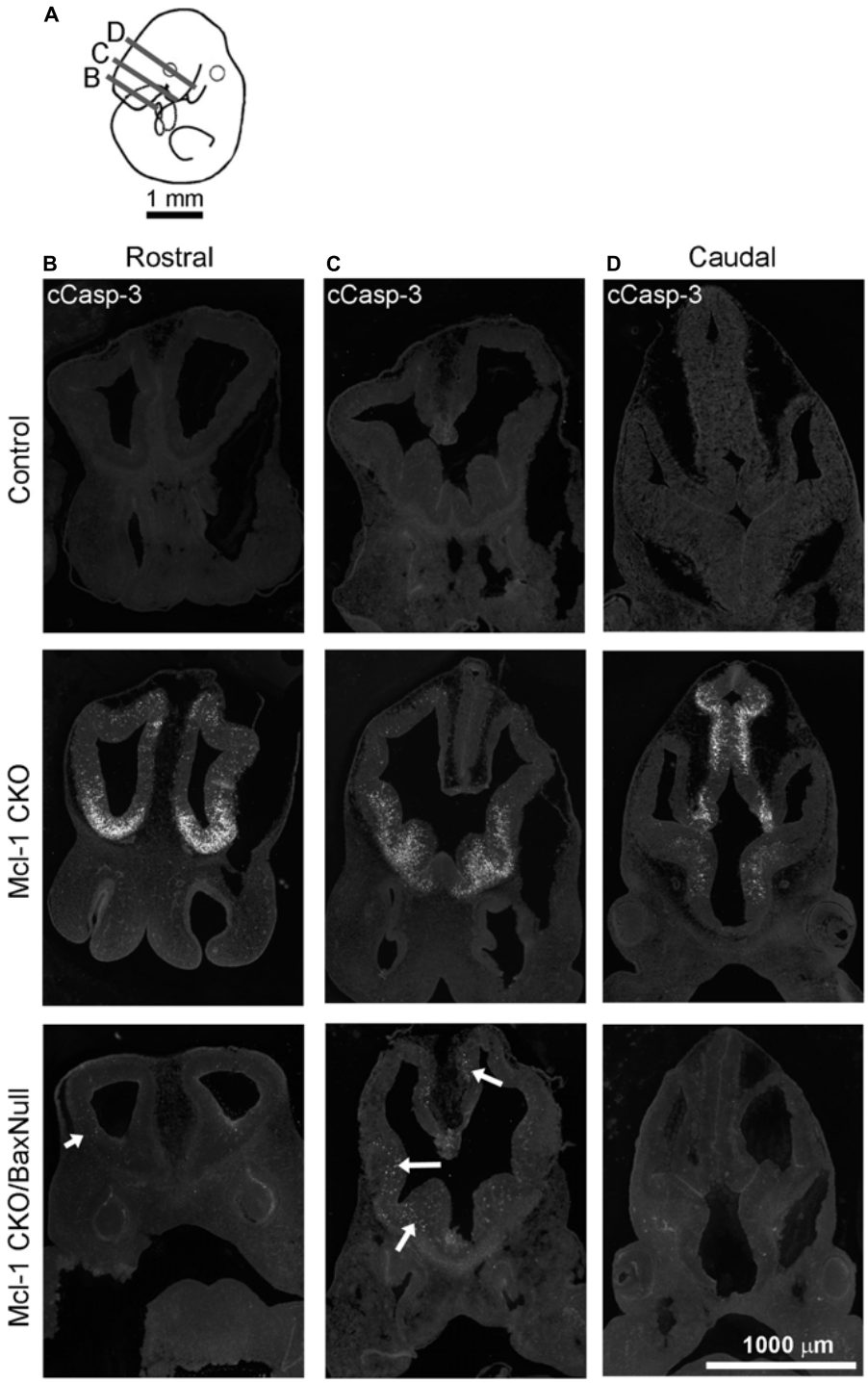

FIGURE 4 | NPC are rescued from apoptotic cell death throughout the developing forebrain of E11 Mcl-1 CKO embryos when Bax is co-deleted. **(A)** Line drawing of E11 embryo indicating location of coronal sections collected through the rostral to caudal extent of the forebrain. Representative coronal sections immunostained for cCasp-3 taken from the **(B)** rostral, **(C)** middle, and **(D)** caudal portion of forebrains from wild type (Control) (n = 4), Mcl-1 CKO (n = 4) and Mcl-1 CKO/BaxNull (n = 4) embryos. Arrows indicate regions where there are occasional apoptotic cells in the forebrains of Mcl-1 CKO/Bax null embryos.

coincides with the initiation of neurogenesis. Second, Mcl-1's anti-apoptotic function in the developing nervous system is to inhibit Bax activation. Although co-deletion of Mcl-1 and Bax rescued the majority of cells from apoptosis throughout the nervous system, the rescue was incomplete in the brainstem and ventral thoracic spinal cord, demonstrating

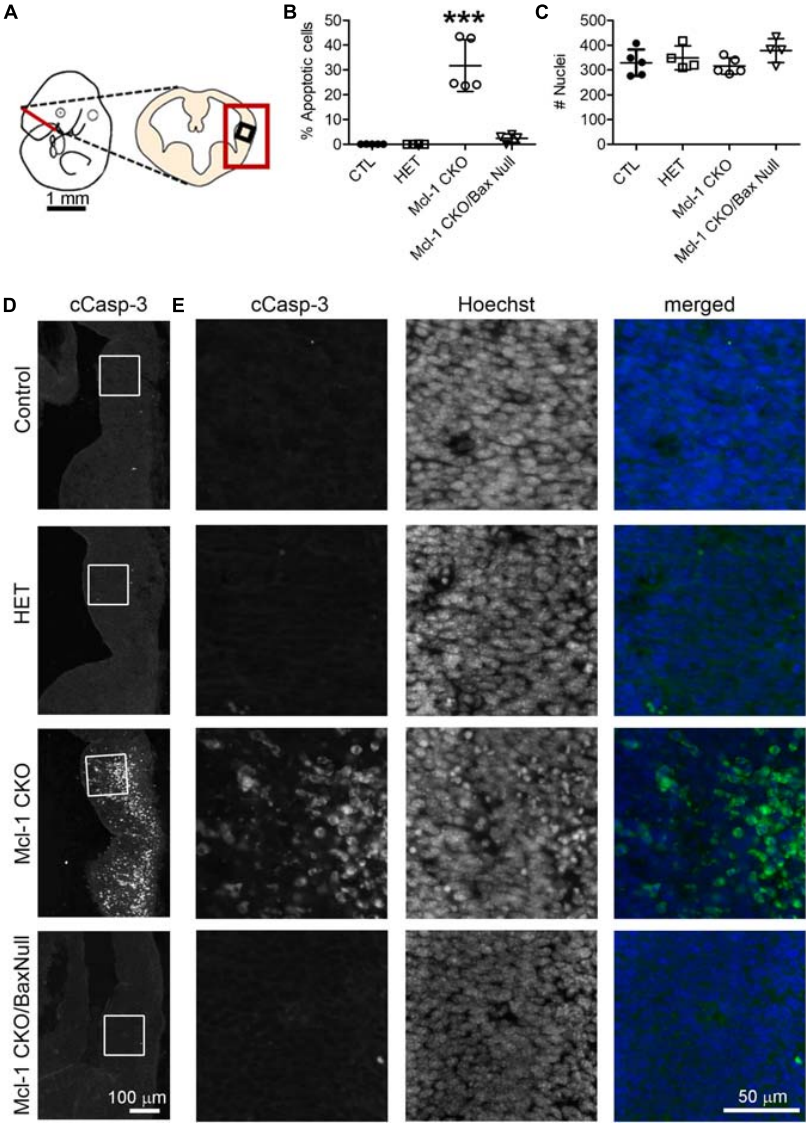

FIGURE 5 | Co-deletion of anti-apoptotic Mcl-1 and pro-apoptotic Bax rescued NPC from apoptosis at E11 in the ventral forebrain. **(A)** Line diagram of an E11 embryo showing a coronal section through the forebrain at the level of the lateral ganglionic eminence. Large red box depicts where representative images were taken in D and small black box identifies the area where counts were performed in E. **(B)** The number of cCasp-3 + cells were quantified within a 125 μm × 125 μm area (boxed area in D, E) and represented as a percentage of the total number of Hoechst + nuclei. There were significantly more apoptotic cells in the Mcl-1 CKO forebrains and this was largely rescued in the Mcl-1 CKO/Bax null forebrain. **(C)** A comparison of the total number of Hoechst + nuclei revealed no significant differences across the genotypes. A one-way ANOVA was performed on the means followed by Tukey's multiple comparison test. CTL (n = 5), Mcl-1 CKO (n = 5), Mcl-1 CKO/BaxNull (n = 4). **(D)** Representative sections through the ventral forebrain of E11 control, Mcl-1 CKO and Mcl-1 CKO/BaxNull embryos. **(E)** Higher magnification of boxed areas in D showing individual panels for cCasp-3 immunostaining, Hoechst and merged (cCasp-3 = green, Hoechst = blue). ***$p < 0.001$, error bars represent ± SD.

that Bax is not the sole pro-apoptotic target of Mcl-1 in the developing nervous system.

Mcl-1 Is Required for Developmental Neurogenesis

Mcl-1 has a role in early embryonic development as germline deletion of *mcl-1* is embryonic lethal at E3.5 (Rinkenberger et al., 2000). Mcl-1 is expressed in the early murine embryo, with expression peaking at E5 and then decreasing slightly by E6.5 (Rinkenberger et al., 2000). In the developing nervous system, *mcl-1* mRNA was detected at E10 in the spinal cord and at E11 in the forebrain; however, earlier time points were not assessed (Arbour et al., 2008; Fogarty et al., 2019). As formation of the murine neural tube from the neural plate begins at E8, we investigated this time point to determine whether Mcl-1 was expressed during patterning of the nervous system (Copp et al., 2003). Mcl-1 protein is expressed in the murine embryonic head

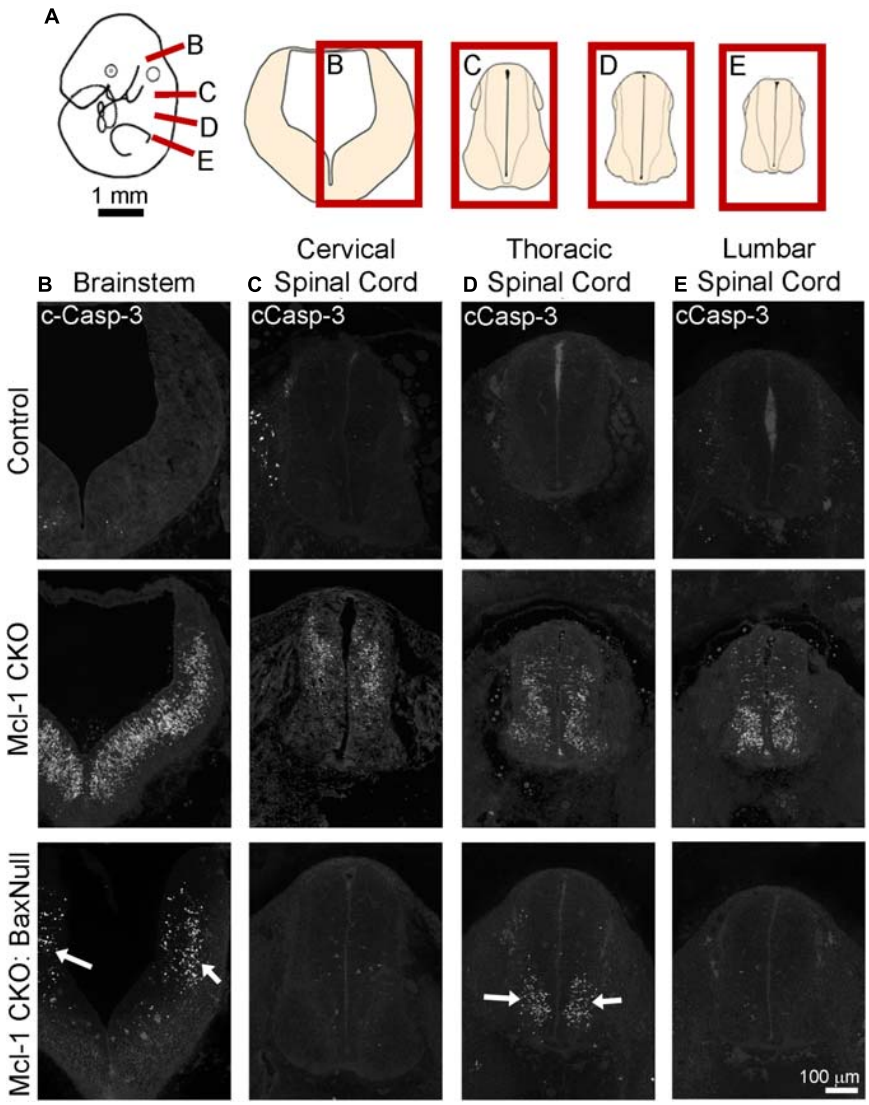

FIGURE 6 | Co-deletion of Mcl-1 and Bax does not rescue all NPC from apoptotic cell death in the developing nervous system at E11. **(A)** Diagram of an E11 embryo showing the levels of brainstem and spinal cord. Representative sections of cCasp-3 immunohistochemistry (white) at the level of the **(B)** brainstem, **(C)** cervical spinal cord, **(D)** thoracic spinal cord, and **(E)** lumbar spinal cord of CTL (n = 4), Mcl-1 CKO (n = 4) and Mcl-1 CKO/BaxNull (n = 3). Arrows point to apoptotic cells in Mcl-1 CKO/BaxNull embryos.

at E8 as demonstrated by western blot. The small size of the E8 mouse embryo hindered a clean dissection of neural tissue from non-neural tissue although the majority of the tissue sample was neural tissue. Mcl-1 therefore is expressed early in nervous system development.

Mcl-1 is not required for patterning of the nervous system. We have previously shown that the early stages of nervous system development including neural tube formation are not affected in either the Mcl-1 CKO or the double Mcl-1 and Bclx CKO embryo (Fogarty et al., 2019). Here, we show that this is because apoptosis only begins at E9 in the spinal cord and E10 in the forebrain after early patterning of the nervous system is completed and coincides with the onset of neurogenesis. Our findings are consistent with knockout mouse studies of the pro-apoptotic Bcl-2 family members where deletion of two or all three of the multi BH3 domain pro-apoptotic proteins, $Bax^{-/-}$:$Bak^{-/-}$ or $Bax^{-/-}$:$Bak^{-/-}$:$Bok^{-/-}$ revealed that apoptosis is not required for morphogenesis of the developing nervous system, but rather for regulating the size of neuronal populations (Lindsten et al., 2000, 2003; Ke et al., 2018).

Mcl-1's anti-apoptotic role is linked to NPC differentiation. Mcl-1 was initially identified in a screen for genes that are upregulated during myeloid cell differentiation (Kozopas et al., 1993). Germline deletion of *mcl-1* is peri-implantation lethal due to a failure of trophectoderm differentiation (Rinkenberger et al., 2000). We have previously shown that apoptotic cells in the Mcl-1 CKO double label with antibodies to Nestin, a neural precursor marker, or doublecortin, a neuroblast

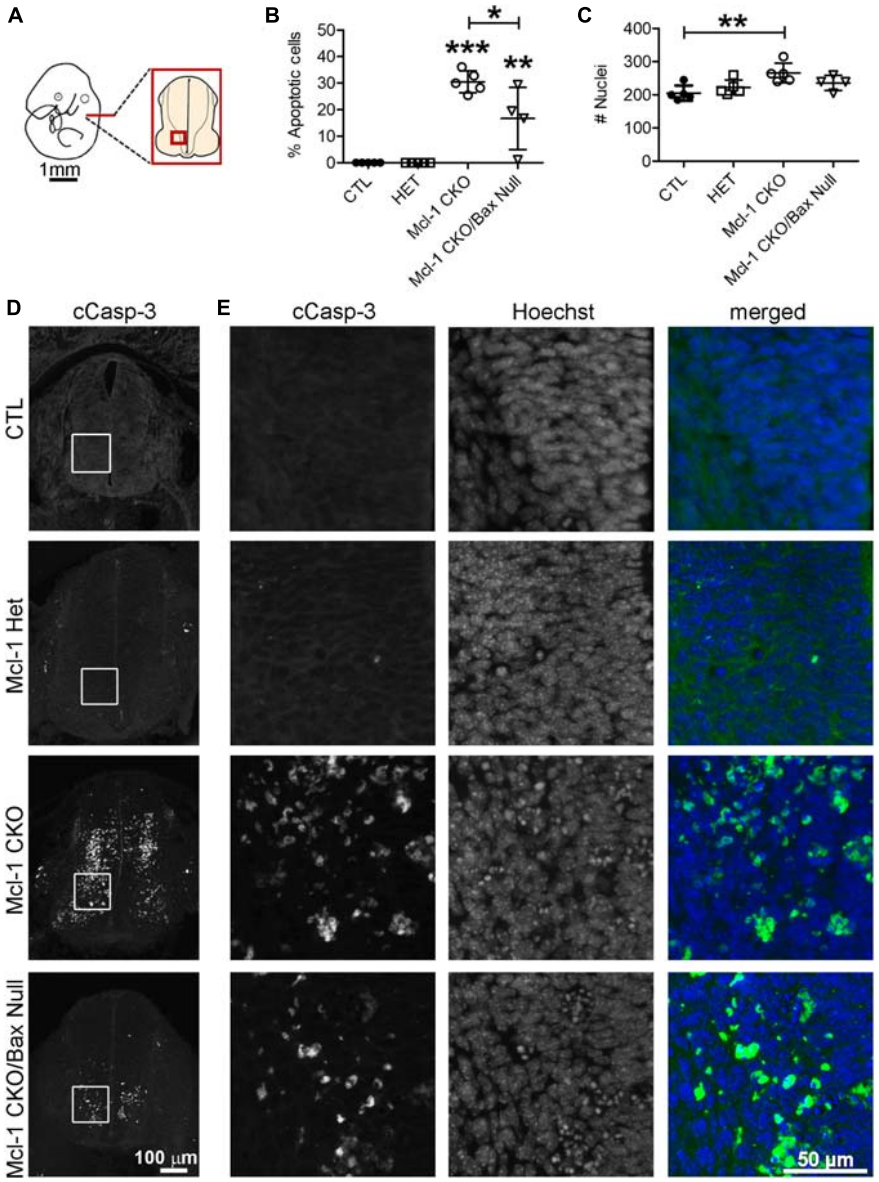

FIGURE 7 | Incomplete rescue of NPC cell death in the developing spinal cord of Mcl-1 CKO/BaxNull embryos. **(A)** Line diagram of an E11 embryo depicting the location of spinal cord sections. **(B)** The number of cCasp-3 + cells were quantified within a 125 µm × 125 µm area (boxed area in D, E) and represented as a percentage of the total number of Hoechst + nuclei. Co-deletion of Bax in the Mcl-1 CKO/BaxNull embryo rescued 50% of NPC from apoptosis in the ventral spinal cord. **(C)** A comparison of the total number of Hoechst + nuclei revealed more cells in the Mcl-1 CKO, which may be due to quantification of apoptotic bodies versus healthy nuclei. A one-way ANOVA was performed on the means followed by Tukey's multiple comparison test. **(D)** Representative sections through the ventral spinal cords of E11 controls Mcl-1 Het, Mcl-1 CKO and Mcl-1 CKO/BaxNull embryos. **(E)** Higher magnification of boxed counting areas in D showing individual panels for cCasp-3 immunostaining, Hoechst and merged (cCasp-3 = green, Hoechst = blue). $*p < 0.05$, $**p < 0.01$, $***p < 0.001$, and error bars represent ± SD.

marker or with βIII tubulin-1, an immature neuron marker (Arbour et al., 2008). This demonstrates that NPC die during the process of differentiation from proliferating cell to immature neuron. In this study, we show that apoptosis in the Mcl-1 CKO begins earlier in the developing brainstem and rostral spinal cord than in the ventral forebrain and then spreads across the nervous system. This differential timing of apoptosis corresponds with timing and spread of neurogenesis in each region. Neurogenesis begins at E9.5 in the spinal cord (Alaynick et al., 2011). In the forebrain, expansion of the NPC pool occurs from E9–E10 preceding the onset of neurogenesis at E11 (Angevine and Sidman, 1961; Takahashi et al., 1995). In each region of the nervous system, apoptosis started in the ventral cell populations and over time spread across two axes, from ventral to dorsal as well as from rostral to caudal. This progression closely mirrors the pattern of differentiation in the developing nervous system. Differentiation in the spinal

cord also begins ventrally and progresses dorsally (McConnell, 1981). Furthermore, rostral signaling by retinoic acid released from the somatic mesoderm causes cells of the developing neural tube to differentiate, whereas caudal Wnt and Fgf signaling prevents differentiation. This results in a progression of differentiation that begins rostrally and progresses caudally over time (Gouti et al., 2015). The similarity between the progression of apoptosis in the Mcl-1 CKO and the progression of differentiation in the developing nervous system suggests that NPC are dependent on Mcl-1 for cell survival during developmental neurogenesis.

Mcl-1 Exerts Its Pro-survival Function Through Inhibition of Bax Activation in NPC

Mcl-1 blocks the initiation of apoptosis by binding and inhibiting the activity of BH3-only proteins and the multi BH-domain pro-apoptotic proteins, Bax and Bak (Czabotar et al., 2014). As Mcl-1 has multiple pro-apoptotic targets, we focused on Bax, as it is the dominant pro-apoptotic protein expressed in the developing nervous system (Krajewski et al., 1994). Germline deletion of Bax rescues neurons from developmental death resulting in a 24–35% increase in neuronal populations (Deckwerth et al., 1996; White et al., 1998). In contrast, Bak null mice do not appear to have a CNS phenotype (Lindsten et al., 2000). Germline deletion of both Bax and Bak worsens the severity of the Bax null phenotype and expands the populations of NPC, immature neurons and glial cells, indicating they both have a role in regulating the NPC population (Lindsten et al., 2000). Our data and previous data show that co-deletion of Mcl-1 and Bax rescues the majority of apoptotic cells in the nervous system of Mcl-1 CKO embryos (Fogarty et al., 2019). However, a thorough rostral to caudal assessment of the entire nervous system at E11 revealed only a partial reduction in apoptosis. Clusters of apoptotic cells remained in the dorsal brainstem and ventral thoracic spinal cord of Mcl-1 CKO:Bax Null embryos demonstrating that Bax deletion alone is insufficient to prevent apoptosis entirely in the Mcl-1 CKO embryos. These findings demonstrate that Mcl-1 promotes cell survival primarily by blocking the pro-apoptotic activity of Bax during early developmental neurogenesis. The incomplete rescue indicates that Bax is not the sole pro-apoptotic target of Mcl-1 in the developing nervous system. Further investigations are necessary to identify additional pro-apoptotic targets of Mcl-1. Interestingly, although germline deletion of Bax rescued the majority of cells from apoptosis, it resulted in earlier embryonic lethality at E12 versus E15.5 in the Mcl-1 CKO embryo. In contrast, conditional deletion of Bax did rescue NPC apoptosis and embryonic lethality.

TABLE 1 | Survival of Mcl-1 CKO/BaxNull embryos.

Mcl-1 CKO/BaxNull	Embryonic time point		
	E11	E12	E13
Number of litters	17	3	16
Number of embryos	173	22	136
Number of knock-outs (%)	13 (7.51%)	1 (4.55%)	1 (0.74%)
Predicted number with Mendelian ratio (%)	11 (6.25%)	1 (6.25%)	7 (5.31%)

TABLE 2 | Survival of Mcl-1 CKO/BaxNull/BaxFloxed embryos.

Mcl-1 CKO/BaxNull: BaxFloxed	Embryonic and postnatal time points					
	E11	E13	E15	E18	P2	P16
Number of litters	9	1	7	1	3	1
Number of embryos	86	9	66	7	27	9
Number of knock-outs (%)	9 (10.47%)	1 (11.11%)	16 (24.24%)	1 (14.29%)	3 (11.11%)	2 (22.22%)
Predicted number with Mendelian ratio (%)	8 (9.08%)	2 (25%)	12 (18.94%)	2 (25%)	5 (17.13%)	2 (25%)

The Changing Role of Mcl-1 During Nervous System Development

The role of Mcl-1 in nervous system development has been examined with a variety of conditional knockout mice, each demonstrating unique roles for Mcl-1 in different cell populations. Foxg1-Cre and Nestin-Cre mediated deletion of Mcl-1 results in loss of Mcl-1 in the NPC population early in development of the forebrain and central nervous system, respectively (Akagi et al., 2001; Berube et al., 2005; Arbour et al., 2008). Both conditional knockouts resulted in Caspase-3 activation and widespread NPC apoptosis (Arbour et al., 2008). Similarly, electroporation or transfection of the Nestin-Cre plasmid into adult NPC carrying floxed Mcl-1 alleles (Mcl-$1^{flox/flox}$) resulted in a 50% loss of NPC by apoptosis (Malone et al., 2012). This demonstrates that Mcl-1 is required for the survival of NPC from the onset of neurogenesis in the developing nervous system and into the adult brain. Further studies including the current showed that Mcl-1 maintains NPC survival during the stages of neurogenesis as cells exit the cell cycle to differentiate into neurons (Arbour et al., 2008; Fogarty et al., 2019). Nestin-Cre mediated deletion of both Mcl-1 and Bcl-xL revealed that Mcl-1 is the main anti-apoptotic regulator of NPC survival with Bcl-xL having a partially supportive role. Once NPC exit the cell cycle and become post-mitotic immature neurons, the roles change with Bcl-xL being the main anti-apoptotic regulator while Mcl-1's role is greatly diminished (Fogarty et al., 2019). In contrast to NPC in the embryonic CNS, committed neural progenitors and cerebellar ganglion neurons (CGN) in the postnatal cerebellum are not dependent on Mcl-1 for survival (Crowther et al., 2013; Veleta et al., 2020). Math1-Cre mediated deletion of Mcl-1 does not result in apoptosis of cerebellar neural progenitors and CGN, rather conditional deletion of Bcl-xL does (Crowther et al., 2013). Math1-Cre mediated co-deletion of Mcl-1 and Bcl-xL reveals that Mcl-1 functions in

a subsidiary role to Bcl-xL by exacerbating the loss of Bcl-xL (Veleta et al., 2020). As post mitotic neurons differentiate and mature they become more resistant to apoptosis and the role of Mcl-1 also changes (Kole et al., 2013; Annis et al., 2016). CamKII-Cre mediated deletion of Mcl-1 in cortical neurons results in autophagic cell death demonstrating that Mcl-1 functions in an anti-autophagic role in post mitotic neurons (Germain et al., 2011). Taken together, these studies demonstrate the roles of Mcl-1 are dynamic, changing through development and with different cell populations.

In summary, we show that Nestin-Cre mediated deletion of Mcl-1 results in apoptotic NPC cell death in the embryonic spinal cord, brainstem and forebrain demonstrating that NPC throughout the developing nervous system are dependent on Mcl-1 for survival. Apoptosis coincides with the onset of neurogenesis in each region of the developing nervous system indicating that Mcl-1 is required during cell differentiation but not prior. Co-deletion of Mcl-1 and Bax rescued the vast majority of cells from apoptosis demonstrating that Mcl-1 functions primarily to inhibit pro-apoptotic Bax during developmental neurogenesis. However in the ventral thoracic spinal cord and in the dorsal brainstem, there were still a significant number of apoptotic cells, demonstrating the presence of other pro-apoptotic targets of Mcl-1. In conclusion, these findings focus the anti-apoptotic role of Mcl-1 in the embryonic nervous system to the neurogenic period.

DATA AVAILABILITY STATEMENT

The raw data supporting the conclusions of this article will be made available by the authors, without undue reservation.

ETHICS STATEMENT

The animal study was reviewed and approved by Memorial University Animal Care Committee.

AUTHOR CONTRIBUTIONS

RF and JV designed the experiments. RF, SC, BG performed the experiments and gathered the data. RF and JV wrote the manuscript. JO provided the Mcl1 floxed mice, provided input on the design of the project and the final manuscript. All authors contributed to the article and approved the submitted version.

FUNDING

Financial support for this project was provided by a Discovery grant #RGPIN-2016-4895 from the Natural Sciences and Engineering Research Council of Canada to JV.

REFERENCES

Adams, K. W., and Cooper, G. M. (2007). Rapid turnover of mcl-1 couples translation to cell survival and apoptosis. *J. Biol. Chem.* 282, 6192–6200.

Akagi, K., Kanai, M., Saya, H., Kozu, T., and Berns, A. (2001). A novel tetracycline-dependent transactivator with E2F4 transcriptional activation domain. *Nucleic Acids Res.* 29:E23.

Alaynick, W. A., Jessell, T. M., and Pfaff, S. L. (2011). SnapShot: spinal cord development. *Cell* 146, 178–178.e1.

Angevine, J. B. Jr., and Sidman, R. L. (1961). Autoradiographic study of cell migration during histogenesis of cerebral cortex in the mouse. *Nature* 192, 766–768.

Annis, R. P., Swahari, V., Nakamura, A., Xie, A. X., Hammond, S. M., and Deshmukh, M. (2016). Mature neurons dynamically restrict apoptosis via redundant premitochondrial brakes. *FEBS J.* 283, 4569–4582.

Arbour, N., Vanderluit, J. L., Le Grand, J. N., Jahani-Asl, A., Ruzhynsky, V. A., Cheung, E. C., et al. (2008). Mcl-1 is a key regulator of apoptosis during CNS development and after DNA damage. *J. Neurosci.* 28, 6068–6078.

Berube, N. G., Mangelsdorf, M., Jagla, M., Vanderluit, J., Garrick, D., Gibbons, R. J., et al. (2005). The chromatin-remodeling protein ATRX is critical for neuronal survival during corticogenesis. *J. Clin. Invest.* 115, 258–267.

Chen, L., Willis, S. N., Wei, A., Smith, B. J., Fletcher, J. I., Hinds, M. G., et al. (2005). Differential targeting of prosurvival Bcl-2 proteins by their BH3-only ligands allows complementary apoptotic function. *Mol. Cell* 17, 393–403.

Copp, A. J., Greene, N. D., and Murdoch, J. N. (2003). The genetic basis of mammalian neurulation. *Nat. Rev. Genet.* 4, 784–793.

Crowther, A. J., Gama, V., Bevilacqua, A., Chang, S. X., Yuan, H., Deshmukh, M., et al. (2013). Tonic activation of Bax primes neural progenitors for rapid apoptosis through a mechanism preserved in medulloblastoma. *J. Neurosci.* 33, 18098–18108.

Czabotar, P. E., Lessene, G., Strasser, A., and Adams, J. M. (2014). Control of apoptosis by the BCL-2 protein family: implications for physiology and therapy. *Nat. Rev. Mol. Cell Biol.* 15, 49–63.

Deckwerth, T. L., Elliott, J. L., Knudson, C. M., Johnson, E. M. Jr., Snider, W. D., and Korsmeyer, S. J. (1996). BAX is required for neuronal death after trophic factor deprivation and during development. *Neuron* 17, 401–411.

Fogarty, L. C., Flemmer, R. T., Geizer, B. A., Licursi, M., Karunanithy, A., Opferman, J. T., et al. (2019). Mcl-1 and Bcl-xL are essential for survival of the developing nervous system. *Cell Death Differ.* 26, 1501–1515.

Fogarty, L. C., Song, B., Suppiah, Y., Hasan, S. M., Martin, H. C., Hogan, S. E., et al. (2016). Bcl-xL dependency coincides with the onset of neurogenesis in the developing mammalian spinal cord. *Mol. Cell. Neurosci.* 77, 34–46.

Germain, M., Nguyen, A. P., Le Grand, J. N., Arbour, N., Vanderluit, J. L., Park, D. S., et al. (2011). MCL-1 is a stress sensor that regulates autophagy in a developmentally regulated manner. *EMBO J.* 30, 395–407.

Gouti, M., Metzis, V., and Briscoe, J. (2015). The route to spinal cord cell types: a tale of signals and switches. *Trends Genet.* 31, 282–289.

Harley, M. E., Allan, L. A., Sanderson, H. S., and Clarke, P. R. (2010). Phosphorylation of Mcl-1 by CDK1-cyclin B1 initiates its Cdc20-dependent destruction during mitotic arrest. *EMBO J.* 29, 2407–2420.

Hasan, S. M., Sheen, A. D., Power, A. M., Langevin, L. M., Xiong, J., Furlong, M., et al. (2013). Mcl1 regulates the terminal mitosis of neural precursor cells in the mammalian brain through p27Kip1. *Development* 140, 3118–3127.

Ke, F. F. S., Vanyai, H. K., Cowan, A. D., Delbridge, A. R. D., Whitehead, L., Grabow, S., et al. (2018). Embryogenesis and adult life in the absence of intrinsic apoptosis effectors BAX, BAK, and BOK. *Cell* 173, 1217–1230.e17.

Knudson, C. M., Tung, K. S., Tourtellotte, W. G., Brown, G. A., and Korsmeyer, S. J. (1995). Bax-deficient mice with lymphoid hyperplasia and male germ cell death. *Science* 270, 96–99.

Kole, A. J., Annis, R. P., and Deshmukh, M. (2013). Mature neurons: equipped for survival. *Cell Death Dis.* 4:e689.

Kozopas, K. M., Yang, T., Buchan, H. L., Zhou, P., and Craig, R. W. (1993). MCL1, a gene expressed in programmed myeloid cell differentiation, has sequence similarity to BCL2. *Proc. Natl. Acad. Sci. U.S.A.* 90, 3516–3520.

Krajewski, S., Krajewska, M., Shabaik, A., Miyashita, T., Wang, H. G., and Reed, J. C. (1994). Immunohistochemical determination of in vivo distribution of Bax, a dominant inhibitor of Bcl-2. *Am. J. Pathol.* 145, 1323–1336.

Lindsten, T., Golden, J. A., Zong, W. X., Minarcik, J., Harris, M. H., and Thompson, C. B. (2003). The proapoptotic activities of Bax and Bak limit the size of the neural stem cell pool. *J. Neurosci.* 23, 11112–11119.

Lindsten, T., Ross, A. J., King, A., Zong, W. X., Rathmell, J. C., Shiels, H. A., et al. (2000). The combined functions of proapoptotic Bcl-2 family members bak and bax are essential for normal development of multiple tissues. *Mol. Cell* 6, 1389–1399.

Malone, C. D., Hasan, S. M., Roome, R. B., Xiong, J., Furlong, M., Opferman, J. T., et al. (2012). Mcl-1 regulates the survival of adult neural precursor cells. *Mol. Cell. Neurosci.* 49, 439–447.

McConnell, J. A. (1981). Identification of early neurons in the brainstem and spinal cord. II. An autoradiographic study in the mouse. *J. Comp. Neurol.* 200, 273–288.

Motoyama, N., Wang, F., Roth, K. A., Sawa, H., Nakayama, K., Negishi, I., et al. (1995). Massive cell death of immature hematopoietic cells and neurons in Bcl-x-deficient mice. *Science* 267, 1506–1510.

Nakamura, A., Swahari, V., Plestant, C., Smith, I., Mccoy, E., Smith, S., et al. (2016). Bcl-xL is essential for the survival and function of differentiated neurons in the cortex that control complex behaviors. *J. Neurosci.* 36, 5448–5461.

Opferman, J. T., Letai, A., Beard, C., Sorcinelli, M. D., Ong, C. C., and Korsmeyer, S. J. (2003). Development and maintenance of B and T lymphocytes requires antiapoptotic MCL-1. *Nature* 426, 671–676.

Rinkenberger, J. L., Horning, S., Klocke, B., Roth, K., and Korsmeyer, S. J. (2000). Mcl-1 deficiency results in peri-implantation embryonic lethality. *Genes Dev.* 14, 23–27.

Savitt, J. M., Jang, S. S., Mu, W., Dawson, V. L., and Dawson, T. M. (2005). Bcl-x is required for proper development of the mouse substantia nigra. *J. Neurosci.* 25, 6721–6728.

Takahashi, T., Nowakowski, R. S., and Caviness, V. S. Jr. (1995). The cell cycle of the pseudostratified ventricular epithelium of the embryonic murine cerebral wall. *J. Neurosci.* 15, 6046–6057.

Takahashi, T., Nowakowski, R. S., and Caviness, V. S. Jr. (1996). The leaving or Q fraction of the murine cerebral proliferative epithelium: a general model of neocortical neuronogenesis. *J. Neurosci.* 16, 6183–6196.

Takeuchi, O., Fisher, J., Suh, H., Harada, H., Malynn, B. A., and Korsmeyer, S. J. (2005). Essential role of BAX,BAK in B cell homeostasis and prevention of autoimmune disease. *Proc. Natl. Acad. Sci. U.S.A.* 102, 11272–11277.

Veleta, K. A., Cleveland, A. H., Babcock, B. R., He, Y. W., Hwang, D., Sokolsky-Papkov, M., et al. (2020). Antiapoptotic Bcl-2 family proteins BCL-xL and MCL-1 integrate neural progenitor survival and proliferation during postnatal cerebellar neurogenesis. *Cell Death Differ.* [Online ahead of print].

Warr, M. R., Acoca, S., Liu, Z., Germain, M., Watson, M., Blanchette, M., et al. (2005). BH3-ligand regulates access of MCL-1 to its E3 ligase. *FEBS Lett.* 579, 5603–5608.

White, F. A., Keller-Peck, C. R., Knudson, C. M., Korsmeyer, S. J., and Snider, W. D. (1998). Widespread elimination of naturally occurring neuronal death in Bax-deficient mice. *J. Neurosci.* 18, 1428–1439.

Zhong, Q., Gao, W., Du, F., and Wang, X. (2005). Mule/ARF-BP1, a BH3-only E3 ubiquitin ligase, catalyzes the polyubiquitination of Mcl-1 and regulates apoptosis. *Cell* 121, 1085–1095.

Conflict of Interest: The authors declare that the research was conducted in the absence of any commercial or financial relationships that could be construed as a potential conflict of interest.

frontiers in Cell and Developmental Biology

ORIGINAL RESEARCH
published: 14 June 2021
doi: 10.3389/fcell.2021.660494

The E3 Ligase PIAS1 Regulates p53 Sumoylation to Control Stress-Induced Apoptosis of Lens Epithelial Cells Through the Proapoptotic Regulator Bax

Qian Nie†, Huimin Chen†, Ming Zou†, Ling Wang†, Min Hou†, Jia-Wen Xiang, Zhongwen Luo, Xiao-Dong Gong, Jia-Ling Fu, Yan Wang, Shu-Yu Zheng, Yuan Xiao, Yu-Wen Gan, Qian Gao, Yue-Yue Bai, Jing-Miao Wang, Lan Zhang, Xiang-Cheng Tang, Xuebin Hu, Lili Gong, Yizhi Liu and David Wan-Cheng Li*‡*

State Key Laboratory of Ophthalmology, Zhongshan Ophthalmic Center, Sun Yat-sen University, Guangzhou, China

Protein sumoylation is one of the most important post-translational modifications regulating many biological processes (Flotho A & Melchior F. 2013. *Ann Rev. Biochem*. 82:357–85). Our previous studies have shown that sumoylation plays a fundamental role in regulating lens differentiation (Yan et al., 2010. *PNAS*, 107(49):21034-9.; Gong et al., 2014. *PNAS*. 111(15):5574–9). Whether sumoylation is implicated in lens pathogenesis remains elusive. Here, we present evidence to show that the protein inhibitor of activated STAT-1 (PIAS1), a E3 ligase for sumoylation, is implicated in regulating stress-induced lens pathogenesis. During oxidative stress-induced cataractogenesis, expression of PIAS1 is significantly altered at both mRNA and protein levels. Upregulation and overexpression of exogenous PIAS1 significantly enhances stress-induced apoptosis. In contrast, silence of PIAS1 with CRISPR/Cas9 technology attenuates stress-induced apoptosis. Mechanistically, different from other cells, PIAS1 has little effect to activate JNK but upregulates Bax, a major proapoptotic regulator. Moreover, Bax upregulation is derived from the enhanced transcription activity of the upstream transcription factor, p53. As revealed previously in other cells by different laboratories, our data also demonstrate that PIAS1 promotes SUMO1 conjugation of p53 at K386 residue in lens epithelial cells and thus enhances p53 transcription activity to promote Bax upregulation. Silence of Bax expression largely abrogates PIAS1-mediated enhancement of stress-induced apoptosis. Thus, our results demonstrated that PIAS1 promotes oxidative stress-induced apoptosis through positive control of p53, which specifically upregulates expression of the downstream proapoptotic regulator Bax. As a result, PIAS1-promoted apoptosis induced by oxidative stress is implicated in lens pathogenesis.

Keywords: sumoylation, apoptosis, PIAS1, p53, Bax, lens, cataract, oxidative stress

OPEN ACCESS

Edited by:
Wolfgang Knabe,
Universität Münster, Germany

Reviewed by:
Guillaume Bossis,
Centre National de la Recherche Scientifique (CNRS), France
Stefan Müller,
Goethe University Frankfurt, Germany
Leena Latonen,
University of Eastern Finland, Finland

****Correspondence:***
David Wan-Cheng Li
liwancheng@gzzoc.com
Yizhi Liu
liuyizhi@gzzoc.com

† These authors have contributed equally to this work

‡ORCID:
David Wan-Cheng Li
orcid.org/0000-0002-7398-7630

Specialty section:
This article was submitted to Cell Death and Survival, a section of the journal Frontiers in Cell and Developmental Biology

Received: *29 January 2021*
Accepted: *20 April 2021*
Published: *14 June 2021*

Citation:
Nie Q, Chen H, Zou M, Wang L, Hou M, Xiang J-W, Luo Z, Gong X-D, Fu J-L, Wang Y, Zheng S-Y, Xiao Y, Gan Y-W, Gao Q, Bai Y-Y, Wang J-M, Zhang L, Tang X-C, Hu X, Gong L, Liu Y and Li DW (2021) The E3 Ligase PIAS1 Regulates p53 Sumoylation to Control Stress-Induced Apoptosis of Lens Epithelial Cells Through the Proapoptotic Regulator Bax. Front. Cell Dev. Biol. 9:660494. doi: 10.3389/fcell.2021.660494

INTRODUCTION

Sumoylation is a unique class of protein post-translational modification, discovered in the past century (Boddy et al., 1996; Matunis et al., 1996; Okura et al., 1996; Shen et al., 1996). The small ubiquitin-like modifier (SUMO) proteins can interact with over 6,000 proteins, regulating their activity, interactions, localization, or stability through a reversible covalent modification (Geiss-Friedlander and Melchior, 2007; Flotho and Melchior, 2013; Sheng et al., 2019). Three major SUMO isoforms have been identified in vertebrates, which are known as SUMO1, SUMO2, and SUMO3 (Hay, 2005).

Sumoylation is an enzymatic reaction catalyzed by the E1 activating enzyme, the E2 conjugating enzyme, and several E3 ligases in the presence of ATP as energy supply, and reversed by several SUMO isopeptidases known as SENPs (Johnson, 2004; Hickey et al., 2012). Previous studies have shown that protein sumoylation plays an important role in regulating different biological processes including cell division, autophagy, transformation, aging, and apoptosis (Johnson, 2004; Hendriks and Vertegaal, 2016). Moreover, sumoylation is also implicated in various human diseases caused by gene mutation and stress response (Flotho and Melchior, 2013; Seeler and Dejean, 2017; Yang et al., 2017; Sheng et al., 2019; Princz and Tavernarakis, 2020).

During sumoylation reaction, E3 ligases have been reported to stabilize the binding between the SUMO target proteins and the E2 conjugating enzyme, controlling the transfer of SUMO from E2 to substrate proteins (Hay, 2005; Hickey et al., 2012; Flotho and Melchior, 2013). Since the E1 activating enzyme (consisting of SAE1-UBA2 heterodimer) and the E2 conjugating enzyme (UBC9) are the unique enzymes, the E3 ligases play a key role in the selection of SUMO isoforms and target proteins (Hay, 2005; Geiss-Friedlander and Melchior, 2007; Hendriks and Vertegaal, 2016; Pichler et al., 2017). In mammals, the protein inhibitor of activated STAT (PIAS) family of E3 ligases contain five subtypes, namely, PIAS1, PIAS2a, PIAS2b, PIAS3, and PIAS4, among which PIAS1 is known to promote cell apoptosis depending on its SUMO E3 ligase activity (Shuai and Liu, 2005; Palvimo, 2007; Rytinki et al., 2009; Sudharsan and Azuma, 2012; Yang et al., 2013; Rabellino et al., 2017; Li et al., 2020). PIAS1 can regulate apoptosis by mediating sumoylation of both transcription factors and kinases (Liu and Shuai, 2001; Megidish et al., 2002; Shishido et al., 2008; Alm-Kristiansen et al., 2011; Leitao et al., 2011; Sudharsan and Azuma, 2012; Li et al., 2013; Yang et al., 2013; Chiou et al., 2014; Wang et al., 2018) and thus becomes involved in various human diseases including cardiovascular diseases, neuronal disorder, and cancer development (Fatkin et al., 1999; Sternsdorf et al., 1999; Li et al., 2003; Steffan et al., 2004; Kim et al., 2006, 2007; Ballatore et al., 2007; Evdokimov et al., 2008; Subramaniam et al., 2009; Flotho and Melchior, 2013; Yang et al., 2017). One of the targets modified by PIAS1 is the tumor suppressor p53. Several laboratories have shown that p53 can be conjugated by SUMO1 through the action of PIAS1 (Gostissa et al., 1999; Rodriguez et al., 1999; Muller et al., 2000; Kahyo et al., 2001; Kwek et al., 2001; Schmidt and Muller, 2002; Okubo et al., 2004). Whether PIAS1 is implicated in ocular diseases, especially lens cataractogenesis, remains elusive.

Cataract is an aging disease that, in most cases, is derived from aging process or stress induction such as oxidative stress (Spector, 1995 and references therein). Mechanistically, we have previously demonstrated that stress-induced apoptosis is a common cellular basis for non-congenital cataractogenesis (Li et al., 1995a,b; Li and Spector, 1996). In lens epithelial cells (LECs), apoptosis is mainly mediated by endogenous and exogenous apoptotic pathways (Li, 1997; Li et al., 2001; Mao et al., 2001, 2004; Yao et al., 2003; Kim and Koh, 2011). Bcl-2 family proteins play a crucial role in mediating endogenous apoptotic pathway, and among which Bax is one of the most important pro-apoptotic proteins (Mao et al., 2004; Czabotar et al., 2014; Singh et al., 2019; Walensky, 2019; Moldoveanu and Czabotar, 2020).

In this study, we present evidence to show that during oxidative stress-induced apoptosis, PIAS1 expression is significantly changed at the mRNA and protein levels. The change in PIAS1 expression is closely related with apoptosis. PIAS1 knockout *via* CRISPR/Cas9 technology attenuates oxidative stress-induced apoptosis. In contrast, expression of exogenous PIAS1 enhances oxidative stress-induced apoptosis of LECs. To define the underlying mechanism, we analyzed the apoptosis-related factors in PIAS1 overexpression and knockout cells. Our results reveal that PIAS1 affects the expression level of the pro-apoptotic protein Bax. Furthermore, we demonstrate that PIAS1 regulation of Bax occurs through regulation of p53 sumoylation at the K386 residue in LECs. The sumoylation-deficient p53 K386R mutant can protect cells against the stress-induced apoptosis. Finally, in Bax knockout cells, we found that absence of Bax significantly abrogates PIAS1-mediated apoptosis under oxidative stress induction. Taken together, our results demonstrate that PIAS1 is implicated in lens cataractogenesis. Mechanistically, PIAS1 sumoylates p53 at K386 to upregulate Bax and thus promotes oxidative stress-induced apoptosis through p53-Bax pathway.

RESULTS

Oxidative Stress Induces PIAS1 Alteration in Lens Epithelial Cells

It is well established that oxidative stress plays a causing role in cataractogenesis (Giblin et al., 1995; Li et al., 1995a,b; Spector, 1995; Li and Spector, 1996; Reddy et al., 2001; Raghavan et al., 2016; Rakete and Nagaraj, 2016; Barnes and Quinlan, 2017; Fan et al., 2017; Wang et al., 2017). In our glucose oxidase (GO) treatment-induced cataract model (**Supplementary Figure 1**), we found that GO also regulates PIAS1 expression. As shown in **Figure 1A**, 40 mU GO induced time-dependent upregulation of PIAS1 mRNA in the first 2 h. As treatment time was extended, PIAS1 mRNA level became downregulated. Similar pattern of PIAS1 protein expression was observed (**Figures 1B,C**). As GO concentration was increased, PIAS1 expression was downregulated (**Supplementary Figure 2A**). Consistent with our previous studies (Sun et al., 2020; Wang et al., 2020), GO treatment generated hydrogen peroxide (**Figure 1D** and

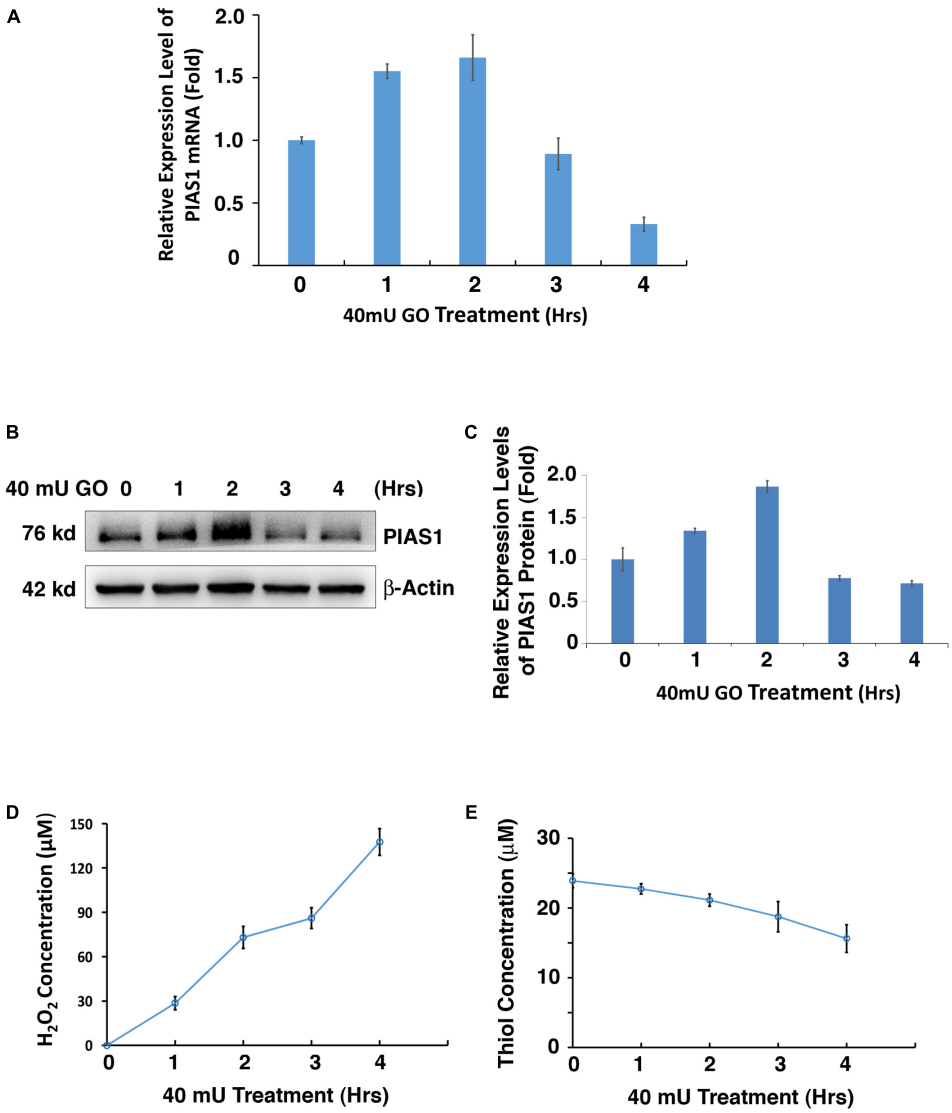

FIGURE 1 | Oxidative stress regulates PIAS1 expression in lens epithelial cells. **(A)** The expression of mRNA levels of PIAS1 under 40 mU GO treatment from 0 to 4 h was determined by real-time PCR. Ct values of each sample were normalized with the Ct value of β-actin. **(B)** Western blot analysis of PIAS1 protein level under 40 mU GO treatment from 0 to 4 h. The β-actin was used as a loading control. **(C)** Quantification of the Western blot results in panel **(A)**. **(D)** Dynamic H_2O_2 concentration generated from 40 mU GO in αTN4-1 cells from 0 to 4 h. **(E)** Dynamic changes of free thiol content upon 40 mU GO treatment in αTN4-1 cells from 0 to 4 h. All experiments were repeated three times. Error bar represents standard deviation, $N = 3$.

Supplementary Figure 2C) and caused a significant drop of the free thiol level (**Figure 1E** and **Supplementary Figure 2D**). These results indicate that PIAS1 is regulated by oxidative stress. Whether the change of PIAS1 level is linked to lens pathology remains to be further studied.

PIAS1 Promotes Oxidative Stress-Induced Apoptosis of Lens Epithelial Cells

Next, we test if GO-regulated changes in PIAS1 expression are linked to lens pathogenesis. Using CRISPR/Cas9 technology, we generated a PIAS1-knockout (KO) cell line with mouse lens epithelial cells, αTN4-1. The PIAS1 knockout strategy, as shown in **Figure 2A**, is conducted with the deletion of nucleotides in exon 3. The knockout result was confirmed by direct DNA sequencing and the absence of PIAS1 protein expression as verified by Western blot analysis (**Figure 2B**). Treatment of mock KO αTN4-1 cells (MOCK-KO) and PIAS1 KO cells with 20–200 mU GO for 3 h revealed differential apoptosis in the two types of cells. As shown in **Figure 2C**, cells with PIAS1 knockout displayed enhanced viability as measured by ATP loss. Next, we overexpressed PIAS1 by establishing pEGFP-C3-PIAS1 stable cell line with the vector pEGFP-C3 as control in αTN4-1 cells. The expression of EGFP or EGFP-PIAS1 fusion protein was verified by Western blot analysis using antibodies

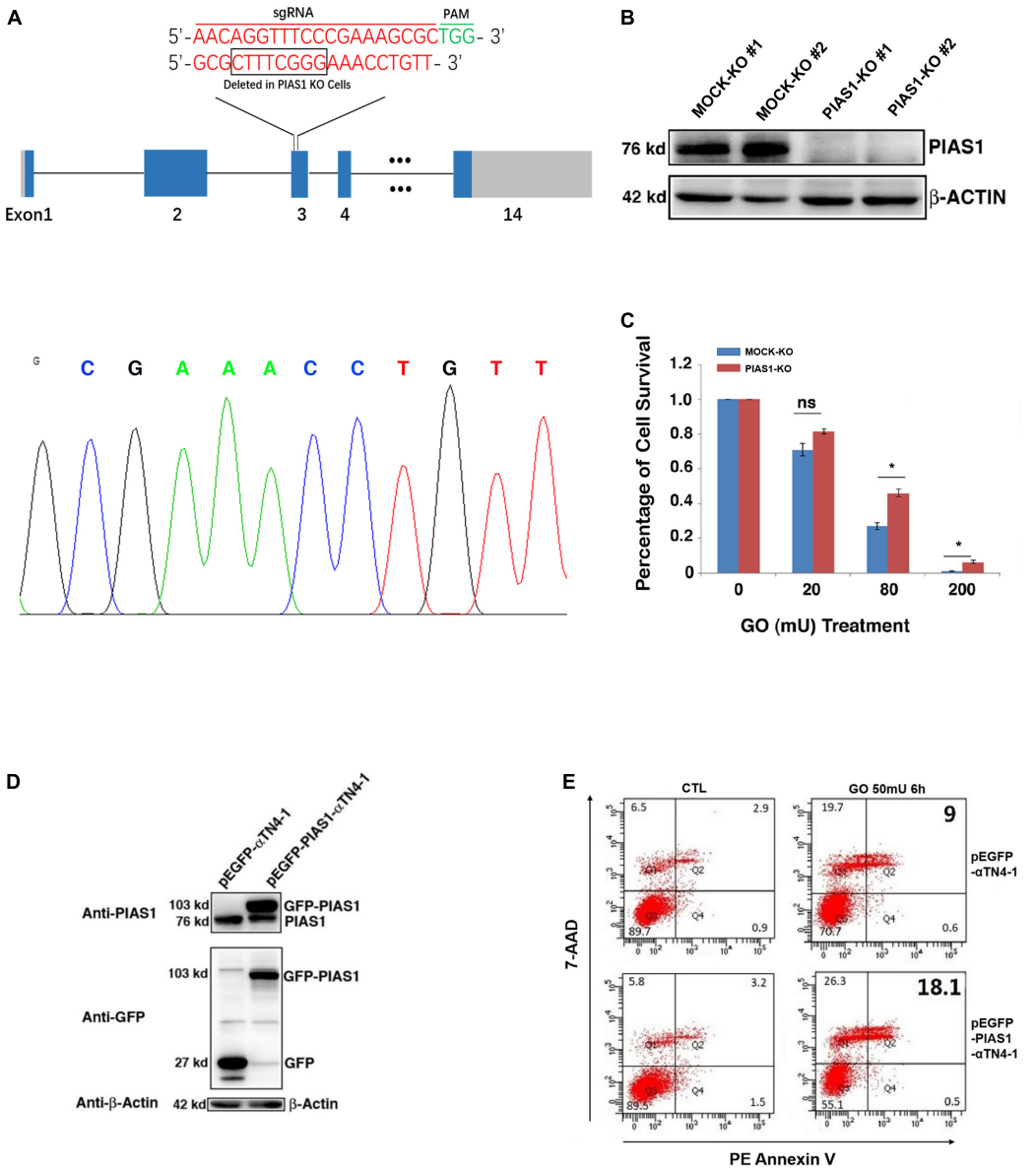

FIGURE 2 | PIAS1 promotes oxidative stress-induced apoptosis of lens epithelial cells. **(A)** Schematic diagram of the strategy for generating the PIAS1 knockout cells by CRISPR/Cas9 gene editing technology. Two sets of sgRNAs were used to generate the knockout cell line (top). Eight nucleotides were deleted in exon 3 and the deletion was verified by DNA sequencing (bottom). The mapping sequence of the genomic DNA with deletion in PIAS1 knockout cells was shown. PAM, protospacer adjacent motif. **(B)** Western blot analysis of the expression levels of PIAS1 in αTN4-1 negative-control vector (MOCK-KO) and PIAS1 knockout (PIAS1-KO) cells. Note that expression of PIAS1 was not detectable in PIAS1 knockout cells. The β-actin was used as a loading control. **(C)** Apoptosis rate in MOCK-KO ad PIAS1-KO cells under treatment of 20, 80, and 200 mU GO for 3 h as measured with CellTiter-Glo® Luminescent Cell Viability Assay analysis. **(D)** Western blot analysis of endogenous and exogenous expression of PIAS1 in pEGFP-αTN4-1 and pEGFP-PIAS1-αTN4-1 cells detected with anti-GFP and anti-PIAS1 antibodies. The β-actin was used as a loading control. **(E)** Apoptosis rate in pEGFP-αTN4-1 and pEGFP-PIAS1-αTN4-1 cells under treatment of 50 mU GO for 6 h measured by flow cytometry. Cells with the indicated treatment were stained with phycoerythrin annexin V (PE) and 7-amino-actinomycin (7-ADD) before flow cytometry analysis. Numbers indicate percentage of apoptotic and non-apoptotic cells in each gate. All experiments were repeated three times. Error bar represents standard deviation, $N = 3$. $^*p < 0.05$; ns, statistically not significant.

against PIAS1 and GFP (**Figure 2D**). We then performed flow cytometry analysis to detect possible differential apoptosis by staining with phycoerythrin annexin V (PE) and 7-amino-actinomycin (7-AAD) in EGFP expression and EGFP-PIAS1 fusion protein overexpression αTN4-1 cells. Compared with EGFP expression cells, overexpression of EGFP-PIAS1 displayed prominent sensitivity to oxidative stress by twofold under GO treatment (**Figure 2E**). Taken together, these results demonstrate that PIAS1 promotes oxidative stress-induced apoptosis of lens epithelial cells.

PIAS1 Mediates p53 Sumoylation in Lens Epithelial Cells at the K386 Residue

To address the underlying mechanism through which PIAS1 promotes oxidative stress-induced apoptosis, we first examined if PIAS1 can activate JNK kinases since previous studies have shown that PIAS1 can activate JNK to trigger apoptosis in different human cell lines (Liu and Shuai, 2001; Leitao et al., 2011). As shown in **Supplementary Figure 3**, PIAS1 overexpression or knockout did not change JNK1/2 total protein levels or activity levels (as reflected by JNK1/2 phosphorylation). Next, we examined if PIAS1 can act as a sumoylation E3 ligase to promote apoptosis. In this regard, since the tumor suppressor p53 is a master regulator of apoptosis (Kruiswijk et al., 2015) and early studies from numerous laboratories have shown that PIAS1 promotes SUMO1-conjugated sumoylation of p53 at K386 residue (Gostissa et al., 1999; Rodriguez et al., 1999; Muller et al., 2000; Kahyo et al., 2001; Kwek et al., 2001; Schmidt and Muller, 2002; Okubo et al., 2004), we explored if PIAS1 can also mediate p53 sumoylation in mouse lens epithelial cells, αTN4-1. First, immunoprecipitation (Co-IP) linked Western blot analysis with both anti-p53 and anti-SUMO1 antibodies revealed the presence of a band above the p53, which can be detected by both anti-p53 and anti-SUMO1 antibodies (**Supplementary Figure 4**). To confirm that PIAS1 indeed mediates p53 sumoylation in lens epithelial cells, we generated a K386R mutant p53 to disrupt its sumoylation. Both wild-type and K386R mutant p53 as well as the vector Flag were transfected into αTN4-1 cells without or with PIAS1 knockout. Co-IP analysis of the total proteins extracted from these different cell lines revealed the interaction between PIAS1 and the wild-type p53 but not the K386R-p53 (**Figure 3B**), and the presence of sumoylated p53 in Flag-p53-WT transfected cells but not in Flag-p53-K386R-transfected cells (**Figure 3D**). Moreover, sumoylated p53 was only detectable when wild-type PIAS1 was present (**Figure 3F**). When PIAS1 was mutated into Flag-PIAS1-C351S, the sumoylated p53 was no longer detectable (lane 2 of **Figure 3F**). Together, these results demonstrated that in lens epithelial cells, PIAS1 can mediate p53 sumoylation at K386 residue as previously detected in other cells (Gostissa et al., 1999; Rodriguez et al., 1999; Muller et al., 2000; Kahyo et al., 2001; Kwek et al., 2001; Schmidt and Muller, 2002; Okubo et al., 2004).

PIAS1 Regulates Expression of the Pro-apoptotic Protein Bax in Lens Epithelial Cells

To further understand how PIAS1 promotes apoptosis of lens epithelial cells, we next examined the possible regulation of the Bcl-2 family members by PIAS1. As shown in **Figure 4**, the expression levels of the mRNA and protein for the proapoptotic regulator Bax were significantly downregulated in PIAS1 knockout cells. In contrast, the expression level of the protein for another proapoptotic regulator, Bak, remain almost unchanged (**Supplementary Figure 5**). Next, we examined whether overexpression of PIAS1 could regulate the expression level of Bax. As shown in **Figure 4**, Bax was significantly upregulated in PIAS1 overexpression cells. Thus, in lens epithelial cells, PIAS1 promotes apoptosis through regulation of Bax, a component of the intrinsic apoptotic pathway.

Desumoylation of p53 Protects Lens Epithelial Cells From Oxidative Stress-Induced Apoptosis

The positive regulation of PIAS1 on p53 sumoylation promotes us to further analyze the association between p53 sumoylation and oxidative stress-induced apoptosis in LECs. To do so, we first generated the p53 knockout cell line using CRISPR/Cas9 technology (**Supplementary Figure 6**). Then, we transfected the p53(-/-) αTN4-1 cells with Flag, Flag-p53-WT, and Flag-p53-K386R, respectively. Forty-eight hours post-transfection, the cells were treated with 40 mU GO and the apoptosis rate was examined using two methods: live/dead viability/cytotoxicity assay and ATP loss analysis. As shown in **Figures 5A,B**, Flag-p53-K386R-transfected cells were much more resistant against 40 mU GO-induced apoptosis than the Flag-p53-WT-transfected cells did. ATP loss analysis further confirmed that de-sumoylated p53 conferred much stronger resistance to oxidative stress-induced apoptosis than p53-WT did (**Figure 5C**). Interestingly, cells transfected with the Flag vector without p53 were also more sensitive to oxidative stress-induced apoptosis than the p53-K386R-transfected cells. Together, these results confirmed that PIAS1-mediated p53 sumoylation is implicated in oxidative stress-induced apoptosis of lens epithelial cells.

PIAS1-Mediated p53 Sumoylation at K386 Enhances Expression of the Downstream Proapoptotic Regulator Bax

Since PIAS1 mediates p53 sumoylation, we next tested whether the sumoylated p53 would confer enhanced transcription activity on its downstream target genes. To do so, we transfected αTN4-1 cells with Flag vector, Flag-p53-WT, and Flag-p53-K386R plasmids separately. The endogenous p53 was knocked out in these cells (**Supplementary Figure 6**). As shown in **Figures 6A,B**, both p53-WT and p53-K386R displayed similar protein levels. Next, we examined the expression level of Bax in three different types of cells. As shown in **Figure 6C**, qRT-PCR revealed that overexpression of exogenous wild-type p53 enhanced 50% upregulation of Bax mRNA. Such upregulation was also detected at the protein level (**Figures 6D,E**). In contrast, expression of exogenous p53-K386R suppressed about 10% of Bax expression as compared with the vector Flag-transfected αTN4-1 cells with the endogenous p53 knocked out.

To further confirm the differential control of Bax promoter by wild-type and K386R mutant p53, we performed luciferase and ChIP assays. As shown in **Figures 7A,B**, the dose-dependent expression levels of WT-p53 and K386R mutant p53 with three different doses of plasmids transfected were confirmed with Western blot analysis. In the same transfected cells, significant dose-dependent upregulation of luciferase activity driven by Bax promoter was observed under overexpression of wild-type p53. Under overexpression of K386R mutant p53, however, luciferase activity from the same Bax promoter was significantly decreased with transfection of the same amount of p53 plasmids

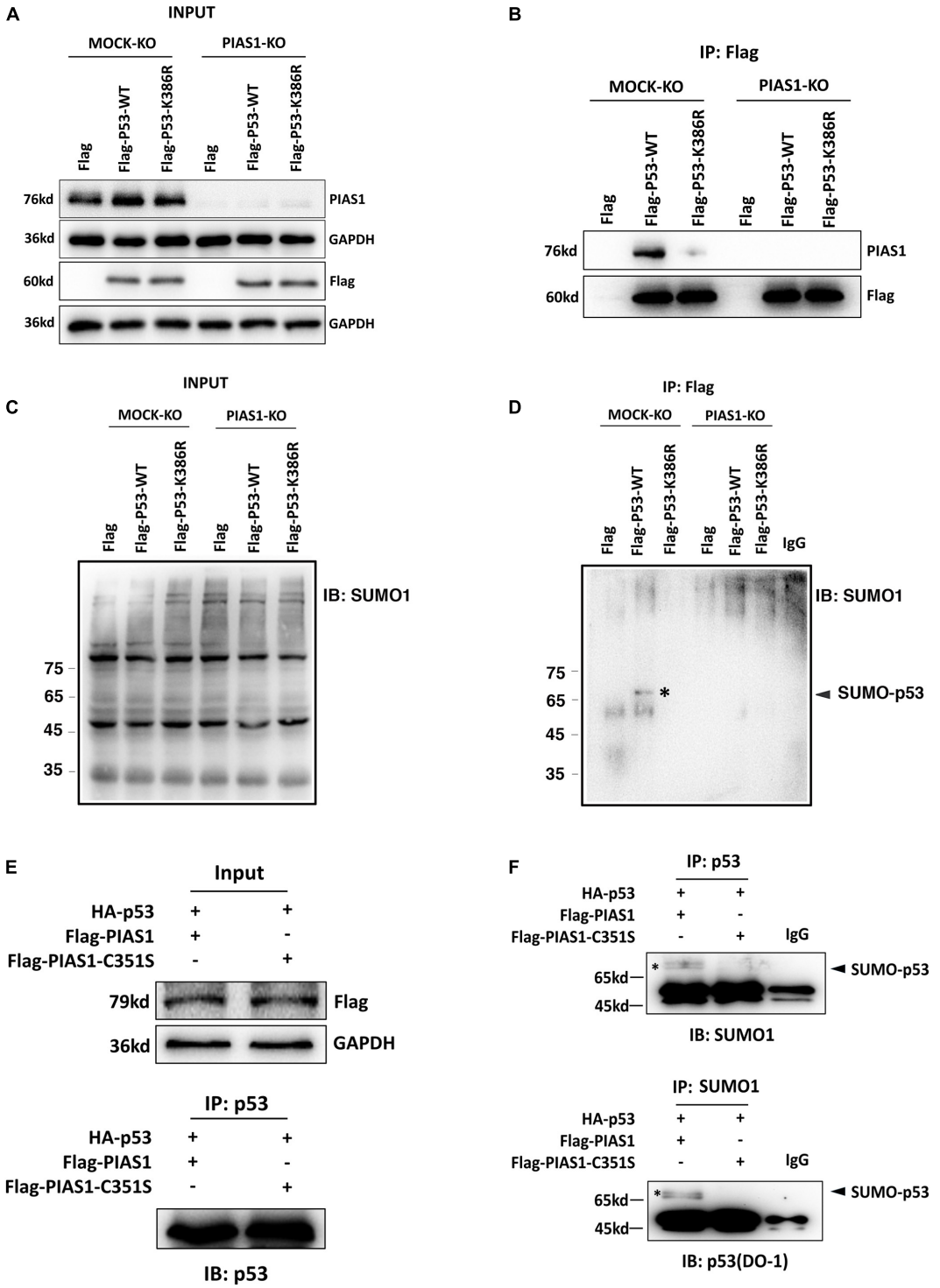

FIGURE 3 | PIAS1 mediates p53 sumoylation in lens epithelial cells at the K386 residue. **(A–D)** MOCK-KO and PIAS1-KO cells were transfected with Flag, Flag-p53-WT, or Flag-p53-K386R as indicated. Forty-eight hours after transfection, whole-cell lysates were blotted (IB) with anti-PIAS1, anti-Flag antibodies **(A)**, and anti-SUMO1 antibody **(C)**. The cell lysates were immunoprecipitated (IP) with anti-Flag antibody, followed by blotting (IB) with anti-PIAS1, anti-Flag antibodies **(B)**, and anti-SUMO1 antibody **(D)**. The SUMO1-p53 conjugated band was detected (labeled with *). **(E,F)** MOCK-KO and PIAS1-KO cells were co-transfected with HA-p53 and Flag-PIAS1 or Flag-PIAS1-C351S plasmids as indicated. Forty-eight hours after transfection, whole-cell lysates were blotted (IB) with anti-Flag antibody **(E**, top**)**. The cell lysates were immunoprecipitated (IP) with anti-p53 antibody, followed by blotting (IB) with anti-p53 (DO-1) antibody **(E**, bottom**)** and anti-SUMO1 antibody **(F**, top**)**. In turn, the cell lysates were immunoprecipitated (IP) with anti-SUMO1 antibody, followed by blotting (IB) with anti-p53 (DO-1) antibody **(F**, bottom**)**. The sumoylated p53 was detected (labeled with*). The IP experiments were conducted in the presence of a desumoylation inhibitor, 20 mM NEM.

(**Figure 7C**). Following transfection with Flag, Flag-p53-WT, or Flag-p53-K386R in p53-KO cells, cross-linked DNA fragments were immunoprecipitated using specific anti-p53 antibody or IgG as control for ChIP assay. The resulting PCR products were quantified to determine level of p53 bound to the Bax promoter by fluorescence real-time quantitative PCR. We found that p53 level was relatively high within the Bax promoter region in wild-type p53-transfected cells but much lower when cells were transfected with p53-K386R mutant (**Figure 7D**). Since K386R mutant p53 was still bound to the Bax promoter with a lower affinity, we reasoned that p53 desumoylation targets the Bax promoter region to restrain Bax transcription, thus inhibiting Bax expression. Taken together, p53 sumoylation enhances expression of Bax through its direct binding to the Bax promoter region.

Knockout of Endogenous Bax Partially Inhibited the Stress-Induced Apoptosis in Lens Epithelial Cells Expressing Exogenous PIAS1

To further confirm that PIAS1-induced upregulation of Bax was indeed the main reason for the enhanced apoptosis of the PIAS1 overexpression cells under GO treatment, we next analyzed the effect of PIAS1 overexpression on oxidative stress-induced apoptosis in MOCK-KO and Bax-KO cells. First, we established a Bax knockout (Bax-KO) cell line using CRISPR/Cas9 technology (**Figure 8A**). The complete lack of Bax protein expression was verified by Western blot analysis (**Figure 8B**). Furthermore, the Flag vector or the Flag-PIAS1 plasmid was transfected into MOCK-KO and Bax-KO cells, and their expression in MOCK-KO and Bax-KO cells were verified (**Figures 8C,D**). When these cells were treated with 40 mU GO for 0, 2 and 4 h, cellTiter-Glo® luminescent cell viability assays revealed that lack of Bax led to much increased levels of survival in Bax-KO cells than those in MOCK-KO cells (**Figure 8E**). Taken together, PIAS1 regulates stress-induced apoptosis in LECs through control of p53-sumoylation and upregulation of its target, Bax.

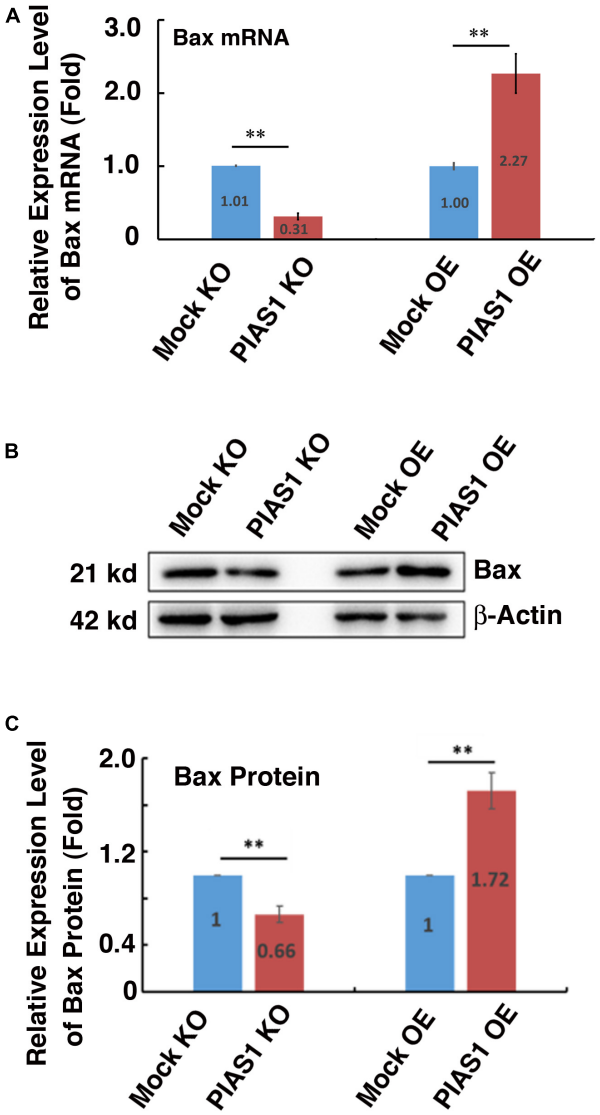

FIGURE 4 | PIAS1 regulates expression of the pro-apoptotic protein Bax in lens epithelial cells. **(A)** qRT-PCR analysis of the mRNA expression level of Bax in MOCK-KO, PIAS1-KO, MOCK OE (pEGFP-αTN4-1), and PIAS1-OE (pEGFP-PIAS1-αTN4-1) cells. Cp values of each sample were normalized with the Cp value of β-actin. **(B)** Western blot analysis of the protein expression level of Bax in MOCK-KO and PIAS1-KO, MOCK OE (pEGFP-αTN4-1), and PIAS1-OE (pEGFP-PIAS1-αTN4-1) cells. The β-actin was used as a loading control. **(C)** Quantification of the Western blot results in panel **(B)**. All experiments were repeated three times. Error bar represents standard deviation, $N = 3$. $^{**}p < 0.01$.

DISCUSSION

In the present study, we have demonstrated the following: (1) oxidative stress induces dose-dependent changes of both mRNA and protein of the sumoylation E3 ligase PIAS1 during oxidative stress-induced apoptosis and pathogenesis; (2) knockout of PIAS1 promotes survival during oxidative stress-induced apoptosis; in contrast, overexpression of the exogenous PIAS1 enhances stress-induced apoptosis; (3) PIAS1 overexpression upregulates expression level of the proapoptotic regulator Bax; on the other hand, PIAS1 knockout attenuates expression of Bax but shows no effect on Bak; (4) Co-IP linked Western blot analysis reveals that PIAS1 also mediates p53 sumoylation at K386 in lens epithelial cells; (5) while wild-type p53 promotes Bax expression to enhance apoptosis of lens epithelial cells, p53 K386R mutant downregulates Bax expression and thus attenuates oxidative stress-induced apoptosis; and (6) knockout of Bax significantly attenuates PIAS1 promotion of apoptosis under treatment by oxidative stress. Together, our results demonstrate that PIAS1 promotes stress-induced apoptosis, leading to the observed stress-induced cataractogenesis (**Supplementary Figure 1**), which is consistent with our previous studies (Li et al., 1995a,b; Li and Spector, 1996). Mechanistically, PIAS1 mediates p53 sumoylation to upregulate expression of the proapoptotic regulator Bax. Thus, our study

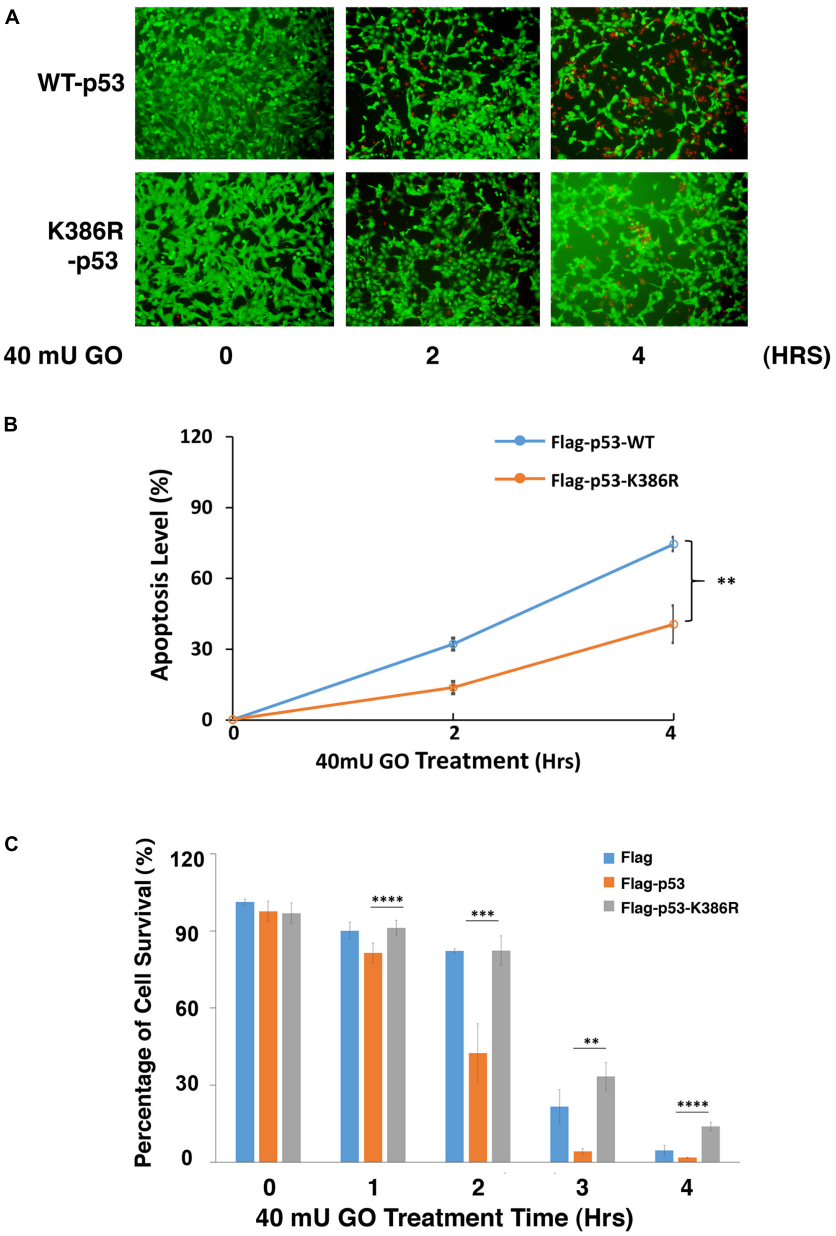

FIGURE 5 | Desumoylation of p53 protects lens epithelial cells from oxidative stress-induced apoptosis. p53-KO αTN4-1 cells were transfected with Flag, Flag-p53-WT, or Flag-p53-K386R as indicated. **(A)** Forty-eight hours after transfection, Live/Dead Viability/Cytotoxicity assay was conducted to analyze cell apoptosis under 40 mU GO treatment for 0 to 4 h. **(B)** The live/dead cells in panel **(A)** were quantified from three different experiments. **(C)** The cellTiter-Glo® luminescent cell viability assay was conducted to analyze cell apoptosis under 40 mU GO treatment for 0 to 4 h. All experiments were repeated three times. Error bar represents standard deviation, $N = 3$. $^{**}p < 0.01$, $^{***}p < 0.005$, $^{****}p < 0.0001$.

provides novel evidence to show that sumoylation is linked to lens cataractogenesis (**Figure 8F**).

Protein Sumoylation Regulates Both Ocular Development and Pathogenesis

During ocular development, previous studies from different laboratories including ours have demonstrated that sumoylation plays critical roles in retina differentiation (Onishi et al., 2010; Roger et al., 2010) and lens formation (Yan et al., 2010; Gong et al., 2014). Sumoylation determines the differentiation direction of cone and rod cells in the retina (Onishi et al., 2010; Roger et al., 2010). SUMO1-conjugated sumoylation is necessary to activate the function of the p32 Pax6 (Yan et al., 2010), which plays a fundamental role in establishing the lens placode and vesicle (Cvekl and Ashery-Padan, 2014). Moreover, we demonstrated that different SUMOs can act on the same transcription factor to display contrast functions in regulating lens differentiation

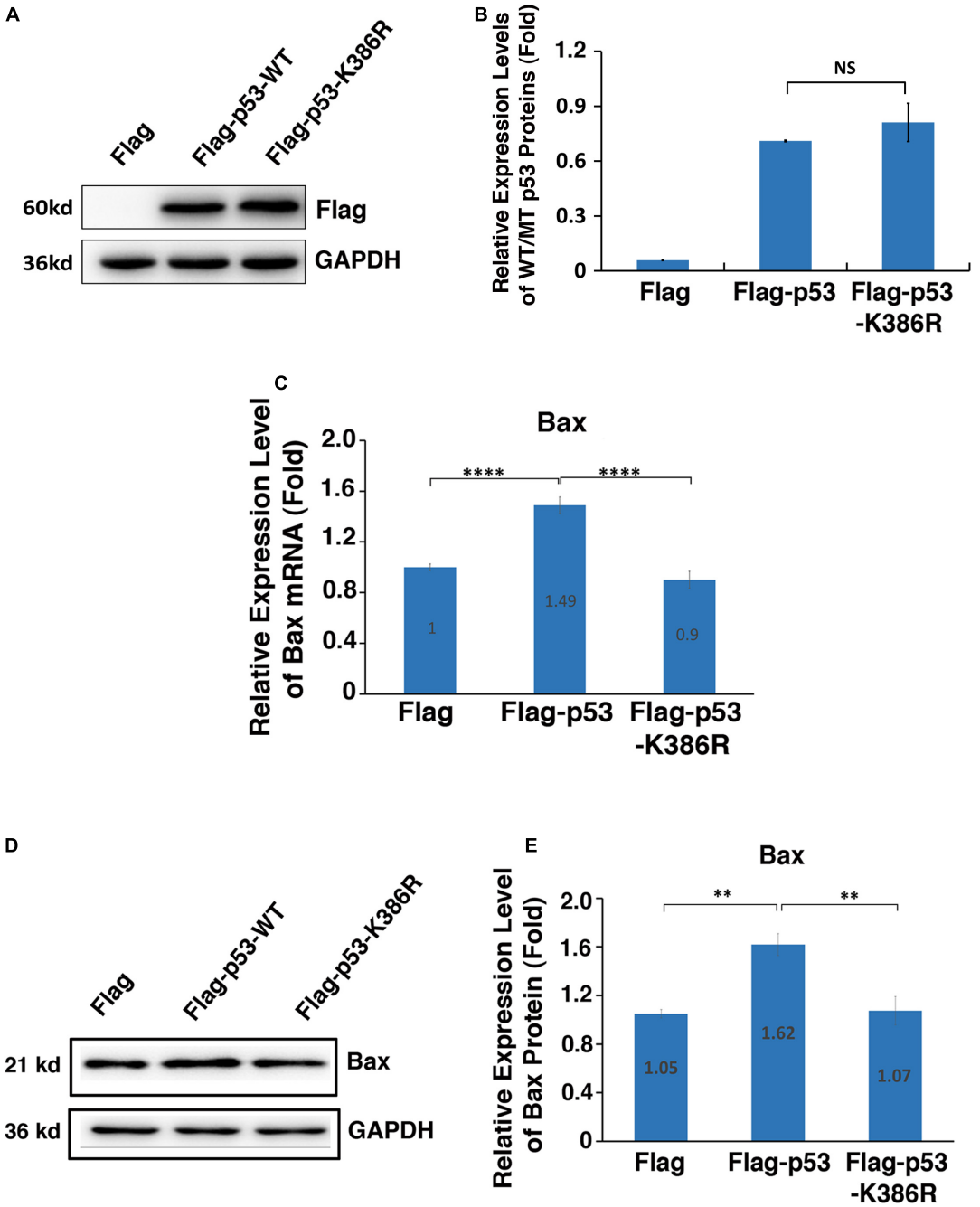

FIGURE 6 | PIAS1-mediated p53 sumoylation at K386 enhances expression of the downstream proapoptotic regulator Bax. p53-KO αTN4-1 cells were transfected with Flag, Flag-p53-WT, or Flag-p53-K386R as indicated. Forty-eight hours after transfection, the mRNA or protein expression levels of exogenous p53 and Bax were analyzed. **(A)** The protein expression of exogenous p53 in three samples were analyzed by Western blot as indicated. The GAPDH was used as a loading control. **(B)** Quantification of the Western blot results in panel **(A)**. **(C)** The mRNA expression level of Bax in three samples was analyzed by qRT-PCR. Cp values of each sample were normalized with the Cp value of β-actin. **(D)** The protein expression level of Bax in three samples was analyzed by Western blot as indicated. The GAPDH was used as a loading control. **(E)** Quantification of the Western blot results in panel **(D)**. All experiments were repeated three times. Error bar represents standard deviation, $N = 3$. NS, not significant, $^{**}p < 0.01$, $^{****}p < 0.0001$.

(Gong et al., 2014). Since sumoylation provides an indispensable function in ocular development, we speculate that sumoylation may also be implicated in ocular pathogenesis, especially during stress-induced cataract formation.

Cataract is defined as the opacity in the ocular lens, which is derived from genetic mutations (Shiels and Hejtmancik, 2019), environmental stresses, and aging (Spector, 1995; Li, 1997). At the cellular level, our previous studies have shown that

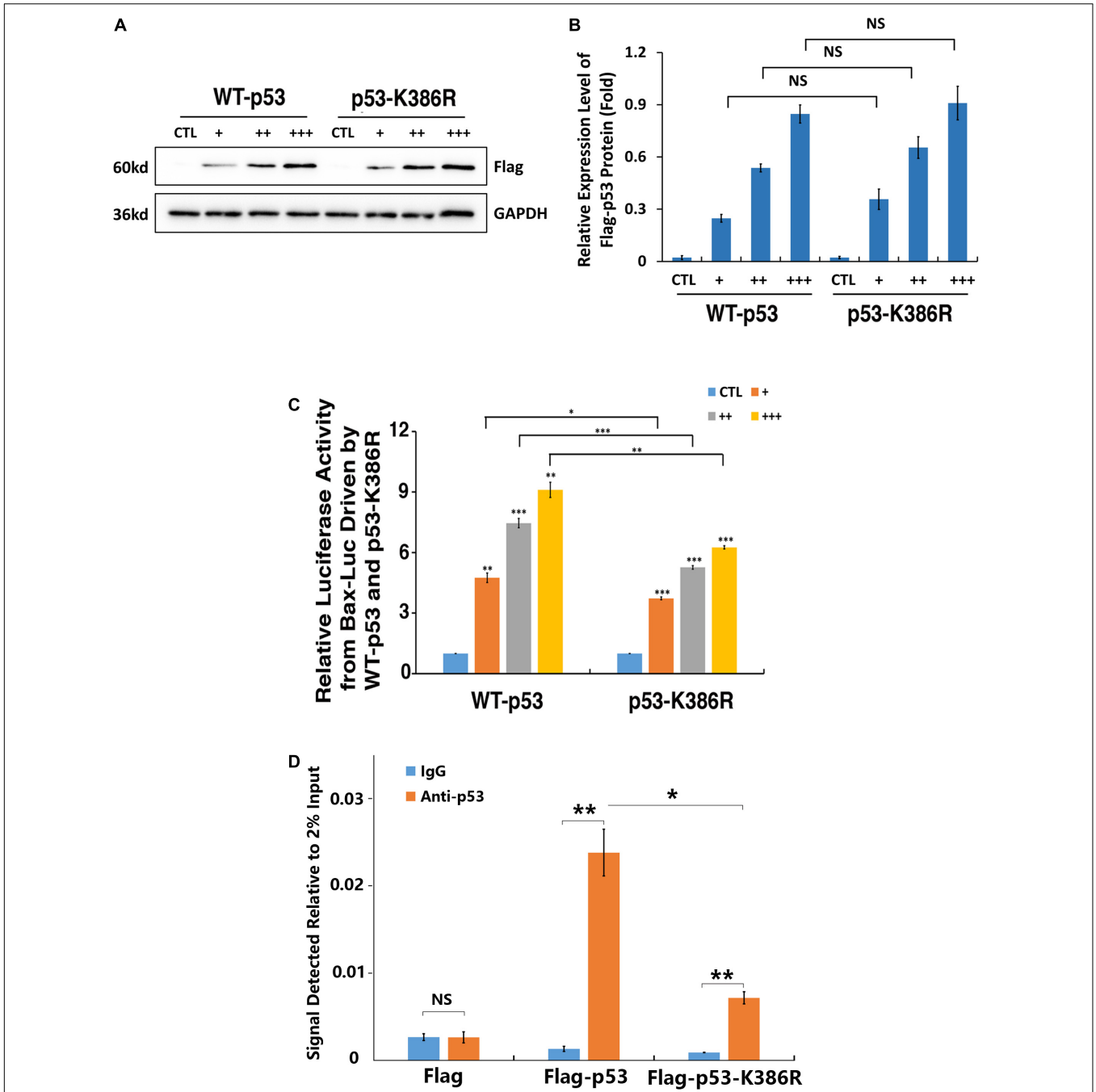

FIGURE 7 | p53 sumoylation at K386 enhances the binding with Bax promoter. **(A–C)** p53-KO αTN4-1 cells were co-transfected with 1 μg of pGL3-Bax, 50 ng of pRL-TK, and empty vector (CTL), Flag-p53-WT, or Flag-p53-K386R at three different doses, 50 ng/well (+), 100 ng/well (++), and 200 ng/well (+++). **(A)** The Western blot analysis was conducted to detect exogenous p53 expression levels. The GAPDH was used as a loading control. **(B)** Quantification of the Western blot results in panel **(A)**. **(C)** Dual-luciferase activity was measured 36 h after transfection. **(D)** p53 sumoylation deficiency decreased the occupancy of p53 on the Bax promoter as measured by ChIP assay. ChIP was performed using an anti-p53 antibody and IgG as a negative control in p53-KO cells transfected with Flag, Flag-p53-WT, or Flag-p53-K386R. The occupancy was normalized to 2% DNA input and calculated in comparison with IgG control. All experiments were repeated three times. Error bar represents standard deviation, $N = 3$. NS, not significant, $^{*}p < 0.05$, $^{**}p < 0.01$, $^{***}p < 0.005$.

various stress conditions such as oxidative stress (Li et al., 1995a), UV irradiation (Li and Spector, 1996), and abnormal calcium (Li et al., 1995b) can all induce apoptosis of lens epithelial cells followed by cataractogenesis. At the molecular level, our recent study of the sumoylation patterns in different age groups of cataract patients revealed that sumoylation of total proteins in the capsular epithelial cells of cataractous lenses are significantly enhanced from 50 to 70 s (Liu et al., 2020), indicating

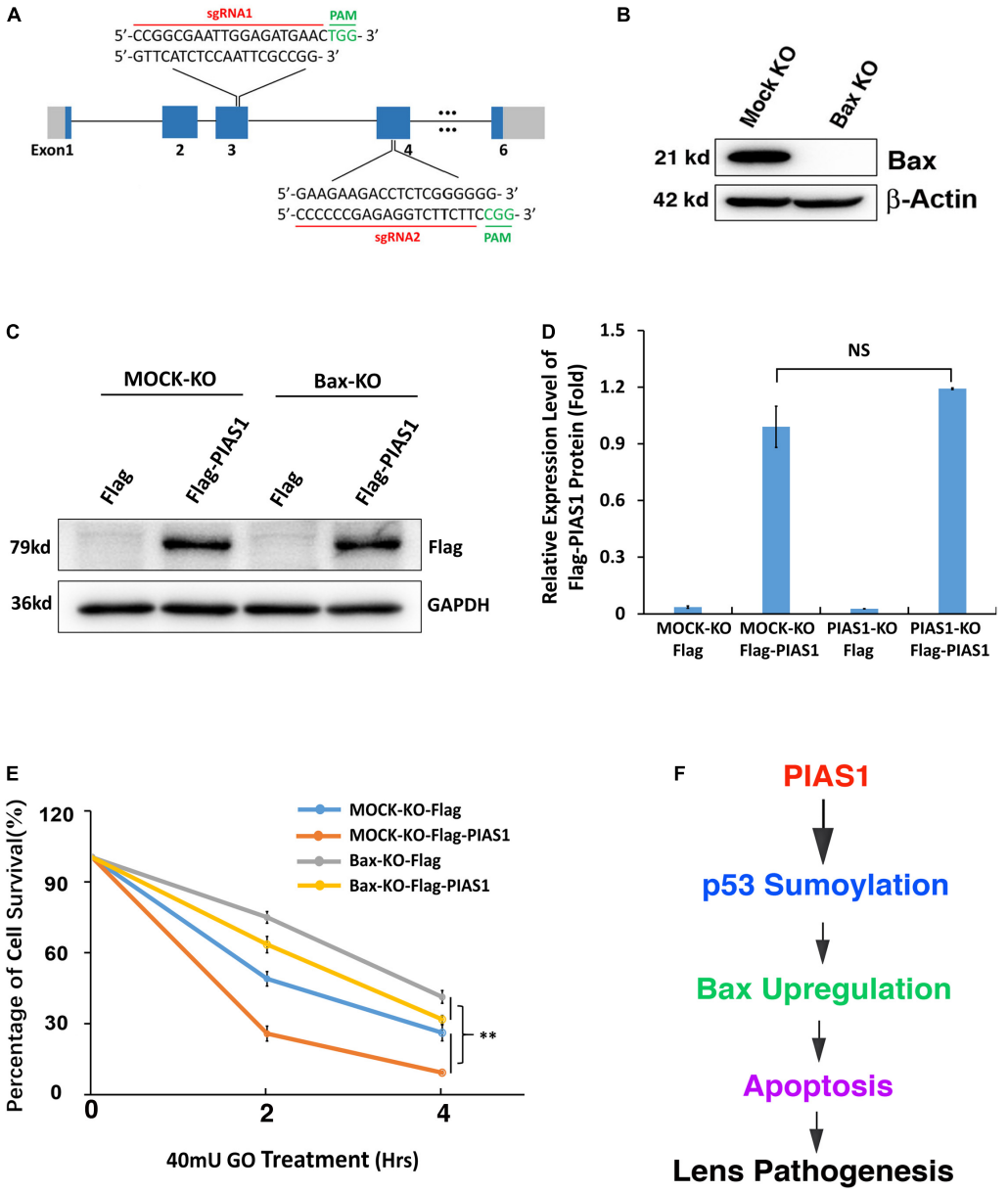

FIGURE 8 | Knockout of endogenous Bax partially inhibited the stress-induced apoptosis in lens epithelial cells expressing exogenous PIAS1. **(A)** Schematic diagram of the strategy for generating the Bax knockout cells by CRISPR/Cas9 gene editing technology. **(B)** Western blot analysis of the expression levels of Bax in αTN4-1 MOCK-KO and Bax knockout (Bax-KO) cells. Note that Bax was not detectable in Bax-KO cells. The β-actin was used as a loading control. **(C)** MOCK-KO and Bax-KO cells were transfected with Flag or Flag-PIAS1 as indicated. Forty-eight hours after transfection, Western blot analysis of the expression levels of exogenous PIAS1 was conducted in MOCK-KO and Bax-KO cells. **(D)** Quantification of the Western blot results in panel **(C)**. **(E)** The transfected cells were then induced to apoptosis under 40 mU GO for 2 or 4 h and cell viability was measured by CellTiter-Glo® Luminescent Cell Viability Assay. **(F)** Diagram shows how PIAS1 regulates oxidative stress-induced apoptosis of lens epithelial cells, leading to cataractogenesis. All experiments were repeated three times. Error bar represents standard deviation, $N = 3$. NS, not significant, $^{**}p < 0.01$.

that sumoylation is linked to cataractogenesis. In the present study, we demonstrated that during oxidative stress-induced cataractogenesis, the sumoylation E3 ligase PIAS1 is upregulated in the first 120 min (**Figure 1**). The upregulated PIAS1 is capable to promote p53 sumoylation at K386 residue (**Figure 3** and **Supplementary Figure 4**). As a result, expression of the p53 downstream target Bax becomes upregulated, which triggers stress-induced apoptosis (**Figures 5–8**), leading to observed cataractogenesis (**Supplementary Figure 1** and **Figure 8F**). Thus, our results further confirm that sumoylation promotes cataractogenesis.

In retina, we have recently revealed that during oxidative stress-induced age-related macular degeneration (AMD), de-sumoylation of p53 is essential to mediate heterochromatin

protection of retinal pigmental epithelial cells under the oxidative stress insult (Gong et al., 2018). Taken together, sumoylation regulates both ocular development and pathogenesis.

PIAS1 Regulates Different Targets to Promote or Attenuate Apoptosis

The proapoptotic function of PIAS1 was initially demonstrated in human 293T cells and human osteosarcoma U2OS cells. It was found that ectopic expression of PIAS1 in U2OS cells activated JNK1 and triggered apoptosis (Liu and Shuai, 2001). Subsequently, in H1299 cells, it was found that PIAS1 can activate p53-mediated gene expression such as p21 independent of its ligase activity (Megidish et al., 2002). More recently, Yang et al. (2013) found that exposure to zinc induced apoptosis of prostate cancer cells and resulted in transactivation of p21 (WAF1/Cip1) in a Smad-dependent and p53-independent manner. During this process, it was found that PIAS1-modulated Smad2/4 complex activation plays an important role (Yang et al., 2013).

In the present study, we did not observe PIAS1 activation of JNK under PIAS1 overexpression or knockout (**Supplementary Figure 3**). Therefore, we sought after other mechanisms mediating PIAS1 promotion of apoptosis. Since the tumor suppressor p53 is a master regulator of apoptosis (Kruiswijk et al., 2015), we next considered if PIAS1 regulates p53.

Previous studies have shown that p53 is SUMO-1 conjugated at K386 residue (Gostissa et al., 1999; Rodriguez et al., 1999; Muller et al., 2000; Kahyo et al., 2001; Kwek et al., 2001; Schmidt and Muller, 2002; Okubo et al., 2004). Moreover, regarding the ligase mediating p53 sumoylation, Kahyo et al. (2001) revealed that PIAS1 can interact with p53 and catalyze its sumoylation in U2OS cells (Kahyo et al., 2001). In the present study, we confirmed the results of these earlier studies in mouse lens epithelial cells. *In vitro* mutagenesis and Co-IP linked Western blot analysis revealed that PIAS1 mediates p53 sumoylation at K386 residue (**Figure 3** and **Supplementary Figure 4**). Furthermore, we demonstrated that sumoylated p53 promotes expression of its downstream proapoptotic regulator, Bax (**Figures 6**, **7**). Bax upregulation plays a crucial role in mediating PIAS1 induction of apoptosis of lens epithelial cells under stress condition since Bax knockout through CRISPR/Cas9 technology significantly attenuates PIAS1-mediated apoptosis (**Figure 8**). Together, here we demonstrate that Bax but not Bak is a novel key target to mediate PIAS1-promoted apoptosis in mouse lens epithelial cells.

Besides its role to promote apoptosis, PIAS1 can modulate different targets to promote survival. AKT is an important kinase to promote survival (Xiao et al., 2010). PIAS1-mediated AKT sumoylation at K276 by SUMO1 is crucial for its activation. Both K276R and E278A mutations reduce AKT sumoylation, completely abolish AKT kinase activity, but do not affect its ubiquitination (Li et al., 2013). More recently, Xie et al. (2018) demonstrated that PIAS1 can protect against myocardial ischemia–reperfusion injury by stimulating PPARγ sumoylation (Xie et al., 2018). Thus, PIAS1 can promote both apoptosis and survival depending on environmental conditions, tissue specificity, and the targets modified.

In summary, our present study confirms that sumoylation plays an important role in lens pathogenesis. Specifically, we demonstrate that PIAS1, an important E3 ligase for sumoylation, is subjected to regulation by oxidative stress. Oxidative stress-induced PIAS1 expression promotes p53 sumoylation and, therefore, upregulates expression of the proapoptotic regulator Bax. Together, we have shown that Bax is a novel target to mediate PIAS1 induction of apoptosis. PIAS1 promotes oxidative stress-induced apoptosis through the p53-Bax pathway, leading to cataractogenesis.

MATERIALS AND METHODS

Materials

Various molecular biology reagents were purchased from MP Biomedicals Ltd., CA, and Invitrogen Life Technologies, Gaithersburg, MD. All the oligos were purchased from Sangon Biotech (Shanghai) Co., Ltd. Protein size markers were purchased from GenStar (Beijing) Co., Ltd. Various antibodies were obtained from Cell Signaling Technology, Boston, MA; abCam Inc., Cambridge, MA; Santa Cruz Biotechnology, Inc., Dallas, TX; Sigma-Aldrich, St. Louis, MO; Proteintech (Wuhan) Co., Ltd; and Ray Biotech (Beijing) Co., Ltd.

Animals

Four-week-old C57BL/6J mice were used to induce an *in vitro* cataract model (**Supplementary Figure 1**). Mice were housed in standard cages in a specific pathogen-free facility of Sun Yat-sen University. The room was maintained on a 12-h light–dark cycle at a constant temperature of 25°C and 50% humidity and the animals were fed with commercial laboratory food and sterilized water. In all the cases, animal protocols to use mice were approved by the IACUC of Zhongshan Ophthalmic Center of Sun Yat-sen University.

Cell Culture, Plasmid Construction, and Establishment of Gene Overexpression or Knockout Stable Cell Lines

Mouse lens epithelial cell line αTN4-1 was cultured in Dulbecco's modified Eagle's medium (DMEM) supplemented with 10% fetal bovine serum (FBS; Atlanta Biologicals) and 1% penicillin/streptomycin in 5% CO_2 at 37°C.

The CRISPR/Cas9-based gene KO vector pSp Cas9(BB)-2A-Puro (PX459) is a gift from Dr. Mengqing Xiang in Zhongshan Ophthalmic Center of Sun Yat-sen University. The sgRNA sequences used for PIAS1, p53, and Bax gene KO are shown in **Supplementary Table 1**. These sgRNAs were inserted into PX459 using the *Bbs*I restriction sites. For expression vector, the construction of full-length cDNA of PIAS1 or p53 was cloned by PCR. The PIAS1 cDNA was first subcloned into an enhanced green fluorescence protein expression vector, pEGFP-C3, at the *Eco*RI and *Bam*HI sites, and subsequently was subcloned into a Flag expression vector, p3 × FLAG-CMV-10, at the *Hin*dIII and *Kpn*I sites. The p53 cDNA was subcloned into a Flag expression vector, p3 × FLAG-CMV-10, at the *Eco*RI and *Xba*I

sites. The point mutation of p53 (K386R) and PIAS1(C351S) primers were designed according to the QuikChange Site-Directed Mutagenesis. The primers used for gene overexpression and point mutation are listed in **Supplementary Table 1**.

For establishment of stable cell lines, αTN4-1 cells were transfected with the above plasmids using Lipofectamine 3000 (Life Technologies) according to the manufacturer's instructions. Forty-eight hours after transfection, cells stably expressing the plasmids were selected by 1.0 μg/ml puromycin for PX459 and 500 μg/ml G418 for pEGFP-C3 and p3 × FLAG-CMV-10. After about 4 weeks, individual clones for the stable cell lines were established and confirmed by Western blot analysis and DNA sequencing.

Protein Extraction and Western Blot

Total proteins were extracted by RIPA buffer (1% NP-40, 1% sodium deoxycholate, 0.1% SDS, 50 mM Tris-HCl, pH 8.0, and 150 mM NaCl) supplemented with the Protease Inhibitor Cocktail and then cell lysates were sonicated and centrifuged at 13,000 rpm for 10 min at 4°C. The supernatants were transferred to new tubes. Fifty micrograms of total proteins in each sample were separated by 10 or 12% SDS-polyacrylamide gel and transferred to PVDF membranes. The protein blots were blocked with 5% non-fat milk in TBST (10 mM Tris-HCl, pH 8.0, 150 mM NaCl, and 0.05% Tween-20) and further incubated with primary antibodies overnight at 4°C. Primary antibodies used in Western blot are shown in **Supplementary Table 2**. The horseradish peroxidase-conjugated secondary antibodies (CST; #7077 and #7074) were then applied for 1 h at room temperature. Immunoreactivity was detected with a chemiluminescence detection kit (ECL Ultra; New cell & Molecular Biotech Co., Ltd.), and the blots were visualized using a Tanon chemiluminescence system (China).

Free Thiol Content Assay

The Free Thiol Content Assay was performed as previously described (Sun et al., 2020; Wang et al., 2020) and using the fluorometric thiol quantitation kit (Sigma-Aldrich, #MAK151). Briefly, αTN4-1 cells were treated with GO and then washed with PBS three times, lysed in 150 μl of the assay buffer, and 20 μl of the cell lysates were used for each assay reaction. The reaction was allowed for 10–60 min at room temperature in the dark (with foil to wrap the plate). The fluorescence intensity was measured by Synergy H4 Hybrid Microplate Reader (BioTek, Winooski, VT, United States) at 490 nm (ex) and 535 nm (em).

Apoptosis Assays

Cell apoptosis was determined by cellTiter-Glo® luminescent cell viability assay, flow cytometry, and Live/Dead Viability/Cytotoxicity. The cellTiter-Glo® luminescent cell viability assay was conducted as previously described (Wang et al., 2020). The flow cytometry was performed with the PE Annexin V Apoptosis Detection Kit I (559763; BD Pharmingen). Cells were seeded into six-well plates about 70% confluence and then treated with 40 mU GO for different times as indicated in the figures to induce cell apoptosis. After stimulation, cells were collected and washed with cold PBS, finally suspended in binding buffer, and 5 μl each of annexin V (PE) and 7-amino-actinomycin (7-AAD) were added into suspended cells and incubated at room temperature for 20 min. The stained cells were analyzed with a BD LSRFortessa Cell analyzer (649225; BD). The Live/Dead Viability/Cytotoxicity Kit (L3224; Thermo Fisher Scientific) was used to distinguish live and dead cells. Live cells are characterized by the presence of ubiquitous intracellular esterase activity and revealed by calcein AM. The polyanionic dye calcein is well retained within live cells, producing an intense uniform green fluorescence in live cells. EthD-1 enters cells with damaged membranes and displays red fluorescence upon binding to nucleic acids, thereby producing a bright red color in dead cells and EthD-1 is excluded by the membrane of live cells. The images were captured with a Zeiss microscope.

Immunoprecipitation

Whole-cell extracts were prepared with lysis buffer (25 mM Tris-HCl, pH 7.4, 150 mM NaCl, 5% glycerol, 1% Non-idetP-40, and 1 mM EDTA) and precleared with Protein A/G PLUS-agarose beads (sc-2003; Santa Cruz Biotechnology). Pre-cleared lysates were then incubated with anti-p53 antibody (sc-126; Santa Cruz Biotechnology and #2524, CST) or anti-FLAG antibody (F1804; Sigma-Aldrich) overnight, followed by incubation with Protein A/G PLUS-agarose beads for 2 h at 4°C. The eluted proteins were analyzed by Western blots. For detection of sumoylated p53, freshly prepared 20 mM SENP inhibitor, NEM, was added during cell lysis and washing steps.

RNA Extraction and qRT-PCR

Total RNAs from αTN4-1 cells were isolated using TRIzol Reagent (Invitrogen). One microgram of total RNA was transcribed (RT) into 20 μl of cDNA using the HiScript II Q RT SuperMix for qPCR kit (R223-01; Vazyme) in which the genomic DNA was removed by DNase I digestion. Fluorescence real-time quantitative PCR was performed on the LightCycler 480 qPCR system (Roche) with ChamQ SYBR Color qPCR Master Mix (Q411-02; Vazyme) according to the manufacturer's procedures. The assays were performed in triplicate, and the Ct values were normalized to β-actin. The primers used are listed in **Supplementary Table 1**.

Luciferase Assay

The DNA fragment containing mouse Bax promoter region was amplified by PCR using the primers listed in **Supplementary Table 1**. Next, the fragment was cloned into the pGL3 promoter vector containing a luciferase reporter gene at the *Kpn*I and *Hin*dIII sites. Renilla luciferase pRL-TK (Promega) vector was used to normalize the background in these experiments. For our luciferase assays, approximately 80% confluent p53-KO αTN4-1 cells were co-transfected with 1 μg of pGL3-Bax, 50 ng of pRL-TK, and varied amounts (50, 100, or 200 ng/well) of empty vector (CTL) or Flag-p53, Flag-p53-K386R, and then incubated for 36 h.

The Dual-Luciferase Reporter Assay System (#RG027, Beyotime) was used to quantify luminescence from transfected cells, and the Firefly and Renilla luciferase signals were measured by the Synergy H4 Hybrid Microplate Reader (BioTek, Winooski, United States). Relative luciferase activity (Luc) was calculated by the ratio of Firefly and Renilla luciferase signals.

ChIP Assay

The ChIP assay was performed using the ChIP chromatin immunoprecipitation kit (CST, 9003) according to the manufacturer's instruction. P53 KO cells were transfected with Flag, Flag-p53-WT, or Flag-p53-K386R. Forty-eight hours later, the transfected cells were fixed in 20 ml of DMEM with 1% formaldehyde at room temperature for 10 min. The cells were washed with PBS, and the harvested cells were sonicated 45 times for 2 s each at power 60% to produce chromatin DNA fragments between 150 and 900 bp in size. Supernatants were collected for IP with 5 μg of p53 antibody (CST; #2524) or 5 μg of normal IgG through overnight incubation at 4°C. Next, 30 μl of magnetic protein A/G beads was added into the mixtures and allowed incubation for 2 h at 4°C. Protein–DNA complexes were washed with low salt buffer three times and high salt buffer one time, and eluted from magnetic protein A/G beads with elution buffer at 65°C for 30 min. Crosslinks were reversed by adding 6 μl of 5 M NaCl and 2 μl of proteinase K into the mixture, and the reaction mixture was incubated for an additional 2 h at 65°C. Finally, DNA fragments were purified on Spin columns and subsequently used for qPCR. The primers used for ChIP-qPCR are listed in **Supplementary Table 1**.

Statistics

All results shown are reported as the mean ± standard deviation (SD). Significance was calculated using the unpaired two-tailed *t*-test. Differences were considered statistically significant at $p < 0.05$.

DATA AVAILABILITY STATEMENT

The raw data supporting the conclusions of this article will be made available by the authors, without undue reservation.

ETHICS STATEMENT

The animal study was reviewed and approved by The IACUC of Zhongshan Ophthalmic Center of Sun Yat-sen University.

AUTHOR CONTRIBUTIONS

QN and DWL designed the research and wrote the manuscript. QN, HC, MZ, LW, MH, J-WX, ZL, X-DG, J-LF, YW, S-YZ, YX, Y-WG, QG, Y-YB, and J-MW performed the experiments. QN, LZ, X-CT, XH, LG, YL, and DWL analyzed the data. All authors contributed to the article and approved the submitted version.

FUNDING

This study was supported in part by grants from the National Natural Science Foundation of China (Nos. 81970787, 82000876, 81770910, 81970784, and 81900842), the joint key project grant from the Natural Science Foundation of Guangdong province–Guangzhou City (2019B1515120014), and the Fundamental Research Funds of the State Key Laboratory of Ophthalmology, Zhongshan Ophthalmic Center, Sun Yat-sen University (3030901010111 and 3030901010110).

ACKNOWLEDGMENTS

We thank Dr. Mengqing Xiang for the CRISPR/Cas9-based gene KO vector pSp Cas9(BB)-2A-Puro (PX459). We also thank Dr. Paul Russel for the αTN4-1 mouse lens epithelial cell line. We also thank all members of David Li's Laboratory in the State Key Laboratory of Ophthalmology in Zhongshan Ophthalmic Center of Sun Yat-sen University.

SUPPLEMENTARY MATERIAL

The Supplementary Material for this article can be found online at: https://www.frontiersin.org/articles/10.3389/fcell.2021.660494/full#supplementary-material

REFERENCES

Alm-Kristiansen, A. H., Lorenzo, P. I., Molvaersmyr, A. K., Matre, V., Ledsaak, M., Saether, T., et al. (2011). PIAS1 interacts with FLASH and enhances its co-activation of c-Myb. *Mol. Cancer* 10:21. doi: 10.1186/1476-4598-10-21

Ballatore, C., Lee, V. M., and Trojanowski, J. Q. (2007). Tau-mediated neurodegeneration in Alzheimer's disease and related disorders. *Nat. Rev. Neurosci.* 8, 663–672. doi: 10.1038/nrn2194

Barnes, S., and Quinlan, R. A. (2017). Small molecules, both dietary and endogenous, influence the onset of lens cataracts. *Exp. Eye Res.* 156, 87–94. doi: 10.1016/j.exer.2016.03.024

Boddy, M. N., Howe, K., Etkin, L. D., Solomon, E., and Freemont, P. S. (1996). PIC 1, a novel ubiquitin-like protein which interacts with the PML component of a multiprotein complex that is disrupted in acute promyelocytic leukaemia. *Oncogene* 13, 971–982.

Chiou, H. Y., Liu, S. Y., Lin, C. H., and Lee, E. H. (2014). Hes-1 SUMOylation by protein inhibitor of activated STAT1 enhances the suppressing effect of Hes-1 on GADD45alpha expression to increase cell survival. *J. Biomed. Sci.* 21:53. doi: 10.1186/1423-0127-21-53

Cvekl, A., and Ashery-Padan, R. (2014). The cellular and molecular mechanisms of vertebrate lens development. *Development* 141, 4432–4447. doi: 10.1242/dev.107953

Czabotar, P. E., Lessene, G., Strasser, A., and Adams, J. M. (2014). Control of apoptosis by the BCL-2 protein family: implications for physiology and therapy. *Nat. Rev. Mol. Cell Biol.* 15, 49–63. doi: 10.1038/nrm3722

Evdokimov, E., Sharma, P., Lockett, S. J., Lualdi, M., and Kuehn, M. R. (2008). Loss of SUMO1 in mice affects RanGAP1 localization and formation of PML nuclear bodies, but is not lethal as it can be compensated by SUMO2 or SUMO3. *J. Cell Sci.* 121, 4106–4113. doi: 10.1242/jcs.038570

Fan, X., Monnier, V. M., and Whitson, J. (2017). Lens glutathione homeostasis: discrepancies and gaps in knowledge standing in the way of novel therapeutic approaches. *Exp. Eye Res.* 156, 103–111. doi: 10.1016/j.exer.2016.06.018

Fatkin, D., MacRae, C., Sasaki, T., Wolff, M. R., Porcu, M., Frenneaux, M., et al. (1999). Missense mutations in the rod domain of the lamin A/C gene as causes of dilated cardiomyopathy and conduction-system disease. *N. Engl. J. Med.* 341, 1715–1724. doi: 10.1056/NEJM199912023412302

Flotho, A., and Melchior, F. (2013). Sumoylation: a regulatory protein modification in health and disease. *Annu. Rev. Biochem.* 82, 357–385. doi: 10.1146/annurev-biochem-061909-093311

Geiss-Friedlander, R., and Melchior, F. (2007). Concepts in sumoylation: a decade on. *Nat. Rev. Mol. Cell Biol.* 8, 947–956. doi: 10.1038/nrm2293

Giblin, F. J., Padgaonkar, V. A., Leverenz, V. R., Lin, L. R., Lou, M. F., Unakar, N. J., et al. (1995). Nuclear light scattering, disulfide formation and membrane damage in lenses of older guinea pigs treated with hyperbaric oxygen. *Exp. Eye Res.* 60, 219–235. doi: 10.1016/s0014-4835(05)80105-8

Gong, L., Ji, W. K., Hu, X. H., Hu, W. F., Tang, X. C., Huang, Z. X., et al. (2014). Sumoylation differentially regulates Sp1 to control cell differentiation. *Proc. Natl. Acad. Sci. U.S.A.* 111, 5574–5579. doi: 10.1073/pnas.1315034111

Gong, L., Liu, F., Xiong, Z., Qi, R., Luo, Z., Gong, X., et al. (2018). Heterochromatin protects retinal pigment epithelium cells from oxidative damage by silencing p53 target genes. *Proc. Natl. Acad. Sci. U.S.A.* 115, E3987–E3995. doi: 10.1073/pnas.1715237115

Gostissa, M., Hengstermann, A., Fogal, V., Sandy, P., Schwarz, S. E., Scheffner, M., et al. (1999). Activation of p53 by conjugation to the ubiquitin-like protein SUMO-1. *EMBO J.* 18, 6462–6471. doi: 10.1093/emboj/18.22.6462

Hay, R. T. (2005). SUMO: a history of modification. *Mol. Cell* 18, 1–12. doi: 10.1016/j.molcel.2005.03.012

Hendriks, I. A., and Vertegaal, A. C. (2016). A comprehensive compilation of SUMO proteomics. *Nat. Rev. Mol. Cell Biol.* 17, 581–595. doi: 10.1038/nrm.2016.81

Hickey, C. M., Wilson, N. R., and Hochstrasser, M. (2012). Function and regulation of SUMO proteases. *Nat. Rev. Mol. Cell Biol.* 13, 755–766. doi: 10.1038/nrm3478

Johnson, E. S. (2004). Protein modification by SUMO. *Annu. Rev. Biochem.* 73, 355–382. doi: 10.1146/annurev.biochem.73.011303.074118

Kahyo, T., Nishida, T., and Yasuda, H. (2001). Involvement of PIAS1 in the sumoylation of tumor suppressor p53. *Mol. Cell* 8, 713–718. doi: 10.1016/s1097-2765(01)00349-5

Kim, J. H., Choi, H. J., Kim, B., Kim, M. H., Lee, J. M., Kim, I. S., et al. (2006). Roles of sumoylation of a reptin chromatin-remodelling complex in cancer metastasis. *Nat. Cell Biol.* 8, 631–639. doi: 10.1038/ncb1415

Kim, J. H., Lee, J. M., Nam, H. J., Choi, H. J., Yang, J. W., Lee, J. S., et al. (2007). SUMOylation of pontin chromatin-remodeling complex reveals a signal integration code in prostate cancer cells. *Proc. Natl. Acad. Sci. U.S.A.* 104, 20793–20798. doi: 10.1073/pnas.0710343105

Kim, S. T., and Koh, J. W. (2011). Mechanisms of apoptosis on human lens epithelium after ultraviolet light exposure. *Korean J. Ophthalmol.* 25, 196–201. doi: 10.3341/kjo.2011.25.3.196

Kruiswijk, F., Labuschagne, C. F., and Vousden, K. H. (2015). p53 in survival, death and metabolic health: a lifeguard with a licence to kill. *Nat. Rev. Mol. Cell Biol.* 16, 393–405. doi: 10.1038/nrm4007

Kwek, S. S., Derry, J., Tyner, A. L., Shen, Z., and Gudkov, A. V. (2001). Functional analysis and intracellular localization of p53 modified by SUMO-1. *Oncogene* 20, 2587–2599. doi: 10.1038/sj.onc.1204362

Leitao, B. B., Jones, M. C., and Brosens, J. J. (2011). The SUMO E3-ligase PIAS1 couples reactive oxygen species-dependent JNK activation to oxidative cell death. *FASEB J.* 25, 3416–3425. doi: 10.1096/fj.11-186346

Li, C., McManus, F. P., Plutoni, C., Pascariu, C. M., Nelson, T., Alberici, D. L., et al. (2020). Quantitative SUMO proteomics identifies PIAS1 substrates involved in cell migration and motility. *Nat. Commun.* 11:834. doi: 10.1038/s41467-020-14581-w

Li, D. W., Xiang, H., Mao, Y. W., Wang, J., Fass, U., Zhang, X. Y., et al. (2001). Caspase-3 is actively involved in okadaic acid-induced lens epithelial cell apoptosis. *Exp. Cell Res.* 266, 279–291. doi: 10.1006/excr.2001.5223

Li, D. W. (1997). "The lens epithelium, apoptosis and cataract formation," in *Eye Lens Epithelium: Damaging Mechanisms and Lens Transparency*, eds G. Glaesser, O. Hockwin, and G. F. J. M. Vrensen (Halle: German Academy of Natural Sciences), 81–108.

Li, R., Wei, J., Jiang, C., Liu, D., Deng, L., Zhang, K., et al. (2013). Akt SUMOylation regulates cell proliferation and tumorigenesis. *Cancer Res.* 73, 5742–5753. doi: 10.1158/0008-5472.CAN-13-0538

Li, W. C., Kuszak, J. R., Dunn, K., Wang, R. R., Ma, W., Wang, G. M., et al. (1995a). Lens epithelial cell apoptosis appears to be a common cellular basis for non-congenital cataract development in humans and animals. *J. Cell Biol.* 130, 169–181. doi: 10.1083/jcb.130.1.169

Li, W. C., Kuszak, J. R., Wang, G. M., Wu, Z. Q., and Spector, A. (1995b). Calcimycin-induced lens epithelial cell apoptosis contributes to cataract formation. *Exp. Eye Res.* 61, 91–98. doi: 10.1016/s0014-4835(95)80062-x

Li, W. C., and Spector, A. (1996). Lens epithelial cell apoptosis is an early event in the development of UVB-induced cataract. *Free Radic. Biol. Med.* 20, 301–311. doi: 10.1016/0891-5849(96)02050-3

Li, Y., Wang, H., Wang, S., Quon, D., Liu, Y. W., and Cordell, B. (2003). Positive and negative regulation of APP amyloidogenesis by sumoylation. *Proc. Natl. Acad. Sci. U.S.A.* 100, 259–264. doi: 10.1073/pnas.0235361100

Liu, B., and Shuai, K. (2001). Induction of apoptosis by protein inhibitor of activated Stat1 through c-Jun NH2-terminal kinase activation. *J. Biol. Chem.* 276, 36624–36631. doi: 10.1074/jbc.M101085200

Liu, F. Y., Fu, J. L., Wang, L., Nie, Q., Luo, Z., Hou, M., et al. (2020). Molecular signature for senile and complicated cataracts derived from analysis of sumoylation enzymes and their substrates in human cataract lenses. *Aging Cell* 19:e13222. doi: 10.1111/acel.13222

Mao, Y. W., Liu, J. P., Xiang, H., and Li, D. W. (2004). Human alphaA- and alphaB-crystallins bind to Bax and Bcl-X(S) to sequester their translocation during staurosporine-induced apoptosis. *Cell Death Differ.* 11, 512–526. doi: 10.1038/sj.cdd.4401384

Mao, Y.-W., Xiang, H., Wang, J., Korsmeyer, S., Reddan, J., and Li, D. W. (2001). Human *bcl*-2 gene attenuates the ability of rabbit lens epithelial cells against H_2O_2-induced apoptosis through down-regulation of the α B-crystallin gene. *J. Biol. Chem.* 276, 43435–43445. doi: 10.1074/jbc.M102195200

Matunis, M. J., Coutavas, E., and Blobel, G. (1996). A novel ubiquitin-like modification modulates the partitioning of the Ran-GTPase-activating protein RanGAP1 between the cytosol and the nuclear pore complex. *J. Cell Biol.* 135, 1457–1470. doi: 10.1083/jcb.135.6.1457

Megidish, T., Xu, J. H., and Xu, C. W. (2002). Activation of p53 by protein inhibitor of activated Stat1 (PIAS1). *J. Biol. Chem.* 277, 8255–8259. doi: 10.1074/jbc.C200001200

Moldoveanu, T., and Czabotar, P. E. (2020). BAX, BAK, and BOK: a coming of age for the BCL-2 family effector proteins. *Cold Spring Harb. Perspect. Biol.* 12:a036319. doi: 10.1101/cshperspect.a036319

Muller, S., Berger, M., Lehembre, F., Seeler, J. S., Haupt, Y., and Dejean, A. (2000). c-Jun and p53 activity is modulated by SUMO-1 modification. *J. Biol. Chem.* 275, 13321–13329. doi: 10.1074/jbc.275.18.13321

Okubo, S., Hara, F., Tsuchida, Y., Shimotakahara, S., Suzuki, S., Hatanaka, H., et al. (2004). NMR structure of the N-terminal domain of SUMO ligase PIAS1 and its interaction with tumor suppressor p53 and A/T-rich DNA oligomers. *J. Biol. Chem.* 279, 31455–31461. doi: 10.1074/jbc.M403561200

Okura, T., Gong, L., Kamitani, T., Wada, T., Okura, I., Wei, C. F., et al. (1996). Protection against Fas/APO-1- and tumor necrosis factor-mediated cell death by a novel protein, sentrin. *J. Immunol.* 157, 4277–4281.

Onishi, A., Peng, G. H., Chen, S., and Blackshaw, S. (2010). Pias3-dependent SUMOylation controls mammalian cone photoreceptor differentiation. *Nat. Neurosci.* 13, 1059–1065. doi: 10.1038/nn.2618

Palvimo, J. J. (2007). PIAS proteins as regulators of small ubiquitin-related modifier (SUMO) modifications and transcription. *Biochem. Soc. Trans.* 35, 1405–1408. doi: 10.1042/BST0351405

Pichler, A., Fatouros, C., Lee, H., and Eisenhardt, N. (2017). SUMO conjugation - a mechanistic view. *Biomol. Concepts* 8, 13–36. doi: 10.1515/bmc-2016-0030

Princz, A., and Tavernarakis, N. (2020). SUMOylation in neurodegenerative diseases. *Gerontology* 66, 122–130. doi: 10.1159/000502142

Rabellino, A., Andreani, C., and Scaglioni, P. P. (2017). The role of PIAS SUMO E3-ligases in cancer. *Cancer Res.* 77, 1542–1547. doi: 10.1158/0008-5472.CAN-16-2958

Raghavan, C. T., Smuda, M., Smith, A. J., Howell, S., Smith, D. G., Singh, A., et al. (2016). AGEs in human lens capsule promote the TGFbeta2-mediated EMT

of lens epithelial cells: implications for age-associated fibrosis. *Aging Cell* 15, 465–476. doi: 10.1111/acel.12450

Rakete, S., and Nagaraj, R. H. (2016). Identification of Kynoxazine, a Novel fluorescent product of the reaction between 3-hydroxykynurenine and Erythrulose in the human lens, and its role in protein modification. *J. Biol. Chem.* 291, 9596–9609. doi: 10.1074/jbc.M116.716621

Reddy, V. N., Giblin, F. J., Lin, L. R., Dang, L., Unakar, N. J., Musch, D. C., et al. (2001). Glutathione peroxidase-1 deficiency leads to increased nuclear light scattering, membrane damage, and cataract formation in gene-knockout mice. *Invest. Ophthalmol. Vis. Sci.* 42, 3247–3255.

Rodriguez, M. S., Desterro, J. M., Lain, S., Midgley, C. A., Lane, D. P., and Hay, R. T. (1999). SUMO-1 modification activates the transcriptional response of p53. *EMBO J.* 18, 6455–6461. doi: 10.1093/emboj/18.22.6455

Roger, J. E., Nellissery, J., Kim, D. S., and Swaroop, A. (2010). Sumoylation of bZIP transcription factor NRL modulates target gene expression during photoreceptor differentiation. *J. Biol. Chem.* 285, 25637–25644. doi: 10.1074/jbc.M110.142810

Rytinki, M. M., Kaikkonen, S., Pehkonen, P., Jaaskelainen, T., and Palvimo, J. J. (2009). PIAS proteins: pleiotropic interactors associated with SUMO. *Cell. Mol. Life Sci.* 66, 3029–3041. doi: 10.1007/s00018-009-0061-z

Schmidt, D., and Muller, S. (2002). Members of the PIAS family act as SUMO ligases for c-Jun and p53 and repress p53 activity. *Proc. Natl. Acad. Sci. U.S.A.* 99, 2872–2877. doi: 10.1073/pnas.052559499

Seeler, J. S., and Dejean, A. (2017). SUMO and the robustness of cancer. *Nat. Rev. Cancer* 17, 184–197. doi: 10.1038/nrc.2016.143

Shen, Z., Pardington-Purtymun, P. E., Comeaux, J. C., Moyzis, R. K., and Chen, D. J. (1996). UBL1, a human ubiquitin-like protein associating with human RAD51/RAD52 proteins. *Genomics* 36, 271–279. doi: 10.1006/geno.1996.0462

Sheng, Z., Wang, X., Ma, Y., Zhang, D., Yang, Y., Zhang, P., et al. (2019). MS-based strategies for identification of protein SUMOylation modification. *Electrophoresis* 40, 2877–2887. doi: 10.1002/elps.201900100

Shiels, A., and Hejtmancik, J. F. (2019). Biology of inherited cataracts and opportunities for treatment. *Annu. Rev. Vis. Sci.* 5, 123–149. doi: 10.1146/annurev-vision-091517-034346

Shishido, T., Woo, C. H., Ding, B., McClain, C., Molina, C. A., Yan, C., et al. (2008). Effects of MEK5/ERK5 association on small ubiquitin-related modification of ERK5: implications for diabetic ventricular dysfunction after myocardial infarction. *Circ. Res.* 102, 1416–1425. doi: 10.1161/CIRCRESAHA.107.168138

Shuai, K., and Liu, B. (2005). Regulation of gene-activation pathways by PIAS proteins in the immune system. *Nat. Rev. Immunol.* 5, 593–605. doi: 10.1038/nri1667

Singh, R., Letai, A., and Sarosiek, K. (2019). Regulation of apoptosis in health and disease: the balancing act of BCL-2 family proteins. *Nat. Rev. Mol. Cell Biol.* 20, 175–193. doi: 10.1038/s41580-018-0089-8

Spector, A. (1995). Oxidative stress-induced cataract: mechanism of action. *FASEB J.* 9, 1173–1182.

Steffan, J. S., Agrawal, N., Pallos, J., Rockabrand, E., Trotman, L. C., Slepko, N., et al. (2004). SUMO modification of Huntingtin and Huntington's disease pathology. *Science* 304, 100–104. doi: 10.1126/science.1092194

Sternsdorf, T., Puccetti, E., Jensen, K., Hoelzer, D., Will, H., Ottmann, O. G., et al. (1999). PIC-1/SUMO-1-modified PML-retinoic acid receptor alpha mediates arsenic trioxide-induced apoptosis in acute promyelocytic leukemia. *Mol. Cell. Biol.* 19, 5170–5178. doi: 10.1128/mcb.19.7.5170

Subramaniam, S., Sixt, K. M., Barrow, R., and Snyder, S. H. (2009). Rhes, a striatal specific protein, mediates mutant-huntingtin cytotoxicity. *Science* 324, 1327–1330. doi: 10.1126/science.1172871

Sudharsan, R., and Azuma, Y. (2012). The SUMO ligase PIAS1 regulates UV-induced apoptosis by recruiting Daxx to SUMOylated foci. *J. Cell Sci.* 125, 5819–5829. doi: 10.1242/jcs.110825

Sun, Q., Gong, L., Qi, R., Qing, W., Zou, M., Ke, Q., et al. (2020). Oxidative stress-induced KLF4 activates inflammatory response through IL17RA and its downstream targets in retinal pigment epithelial cells. *Free Radic. Biol. Med.* 147, 271–281. doi: 10.1016/j.freeradbiomed.2019.12.029

Walensky, L. D. (2019). Targeting BAX to drug death directly. *Nat. Chem. Biol.* 15, 657–665. doi: 10.1038/s41589-019-0306-6

Wang, B., Hom, G., Zhou, S., Guo, M., Li, B., Yang, J., et al. (2017). The oxidized thiol proteome in aging and cataractous mouse and human lens revealed by ICAT labeling. *Aging Cell* 16, 244–261. doi: 10.1111/acel.12548

Wang, J., Nasser, M. I., Adlat, S., Ming, J. M., Jiang, N., and Gao, L. (2018). Atractylenolide II induces apoptosis of prostate cancer cells through regulation of AR and JAK2/STAT3 signaling pathways. *Molecules* 23:3298. doi: 10.3390/molecules23123298

Wang, L., Nie, Q., Gao, M., Yang, L., Xiang, J. W., Xiao, Y., et al. (2020). The transcription factor CREB acts as an important regulator mediating oxidative stress-induced apoptosis by suppressing alphaB-crystallin expression. *Aging* 12, 13594–13617. doi: 10.18632/aging.103474

Xiao, L., Gong, L. L., Yuan, D., Deng, M., Zeng, X. M., Chen, L. L., et al. (2010). Protein phosphatase-1 regulates Akt1 signal transduction pathway to control gene expression, cell survival and differentiation. *Cell Death Differ.* 17, 1448–1462. doi: 10.1038/cdd.2010.16

Xie, B., Liu, X., Yang, J., Cheng, J., Gu, J., and Xue, S. (2018). PIAS1 protects against myocardial ischemia-reperfusion injury by stimulating PPARgamma SUMOylation. *BMC Cell Biol.* 19:24. doi: 10.1186/s12860-018-0176-x

Yan, Q., Gong, L., Deng, M., Zhang, L., Sun, S., Liu, J., et al. (2010). Sumoylation activates the transcriptional activity of Pax-6, an important transcription factor for eye and brain development. *Proc. Natl. Acad. Sci. U.S.A.* 107, 21034–21039. doi: 10.1073/pnas.1007866107

Yang, N., Zhao, B., Rasul, A., Qin, H., Li, J., and Li, X. (2013). PIAS1-modulated Smad2/4 complex activation is involved in zinc-induced cancer cell apoptosis. *Cell Death Dis.* 4:e811. doi: 10.1038/cddis.2013.333

Yang, Y., He, Y., Wang, X., Liang, Z., He, G., Zhang, P., et al. (2017). Protein SUMOylation modification and its associations with disease. *Open Biol.* 7:170167. doi: 10.1098/rsob.170167

Yao, K., Wang, K., Xu, W., Sun, Z., Shentu, X., and Qiu, P. (2003). Caspase-3 and its inhibitor Ac-DEVD-CHO in rat lens epithelial cell apoptosis induced by hydrogen peroxide *in vitro*. *Chin. Med. J.* 116, 1034–1038.

Conflict of Interest: The authors declare that the research was conducted in the absence of any commercial or financial relationships that could be construed as a potential conflict of interest.

frontiers in Cell and Developmental Biology

REVIEW
published: 16 July 2021
doi: 10.3389/fcell.2021.702404

Caspases in the Developing Central Nervous System: Apoptosis and Beyond

Trang Thi Minh Nguyen[1], Germain Gillet[1,2] and Nikolay Popgeorgiev[1]**

[1] Centre de Recherche en Cancérologie de Lyon, U1052 INSERM, UMR CNRS 5286, Centre Léon Bérard, Université Claude Bernard Lyon 1, Lyon, France, [2] Hospices Civils de Lyon, Laboratoire d'Anatomie et Cytologie Pathologiques, Centre Hospitalier Lyon Sud, Pierre Bénite, France

The caspase family of cysteine proteases represents the executioners of programmed cell death (PCD) type I or apoptosis. For years, caspases have been known for their critical roles in shaping embryonic structures, including the development of the central nervous system (CNS). Interestingly, recent findings have suggested that aside from their roles in eliminating unnecessary neural cells, caspases are also implicated in other neurodevelopmental processes such as axon guidance, synapse formation, axon pruning, and synaptic functions. These results raise the question as to how neurons regulate this decision-making, leading either to cell death or to proper development and differentiation. This review highlights current knowledge on apoptotic and non-apoptotic functions of caspases in the developing CNS. We also discuss the molecular factors involved in the regulation of caspase-mediated roles, emphasizing the mitochondrial pathway of cell death.

Keywords: caspases, mitochondria, central nervous system, apoptosis, embryonic development

OPEN ACCESS

Edited by:
Wolfgang Knabe, Universität Münster, Germany

Reviewed by:
Nicolas Unsain, Medical Research Institute Mercedes and Martín Ferreyra (INIMEC), Argentina
Emilie Hollville, University of North Carolina at Chapel Hill, United States

***Correspondence:**
Germain Gillet
germain.gillet@univ-lyon1.fr
Nikolay Popgeorgiev
nikolay.popgeorgiev@univ-lyon1.fr

Specialty section:
This article was submitted to Cell Death and Survival, a section of the journal Frontiers in Cell and Developmental Biology

Received: *29 April 2021*
Accepted: *23 June 2021*
Published: *16 July 2021*

Citation:
Nguyen TTM, Gillet G and Popgeorgiev N (2021) Caspases in the Developing Central Nervous System: Apoptosis and Beyond. Front. Cell Dev. Biol. 9:702404. doi: 10.3389/fcell.2021.702404

INTRODUCTION

Apoptosis is considered to be a programmed cell death (PCD) through which a multicellular organism removes damaged cells without affecting neighboring cells (Wickman et al., 2012). Apoptotic cells exhibit specific characteristics, including cell shrinkage, chromatin condensation and fragmentation, and cell membrane blebbing, followed by apoptotic body formation (Taylor et al., 2008). Shreds of evidence suggest that apoptosis, which is considered to be a self-destructive program, may also take place in healthy cells to ensure the daily functions of tissues and organs (Suzanne and Steller, 2013; Shalini et al., 2015).

The central nervous system (CNS), including the brain and spinal cord, is a complex structure that begins to appear at early stages of embryonic development. The first significant event is the formation of the neural tube from the neural plate during primary and secondary neurulation. During primary neurulation, a portion of dorsal ectoderm specifies into neural plate. Neural plate cells can be distinguished from surrounding non-neural cells by their elongated morphology. Shortly after its establishment, neural plate border thickens and rises up to create a U-shape groove. The two lateral sides of the neural groove continue to bend toward each other until their edges meet and merge to form the neural tube. Secondary neurulation then begins at the caudal end. In this latter process, that takes place in chicken and some mammalian embryos, mesenchymal cells gather to form the medullary cord under the ectoderm layer. In the next step, the medullary cord is reshaped to create a hollow cavity (Smith and Schoenwolf, 1997; Gilbert, 2000).

From a simple straight structure at the beginning, the anterior part of the neural tube expands to form three primary vesicles: prosencephalon (forebrain), mesencephalon (midbrain), and rhombencephalon (hindbrain). These latter vesicles continue to subdivide and ultimately form the different regions of the brain (Smith and Schoenwolf, 1997; Stiles and Jernigan, 2010). Concurrently, neural progenitors, derived from the neuroepithelial cells of the ectoderm, differentiate into neurons and glial cells (Götz and Huttner, 2005; Paridaen and Huttner, 2014). Neurons and glial cells are organized into layers (cortex) or clusters (nuclei). From the luminal germinal neuroepithelium, newborn cells migrate outward to form layers at the marginal zone (Ayala et al., 2007). The most recently born neurons migrate through the previous cell layers to give rise to the more superficial regions.

Apoptosis is known to play essential roles in the development of the CNS. Indeed, cell death events have been largely described in the brain of vertebrate embryos, whereas experimental suppression of apoptosis in the developing embryo mainly results in deleterious malformations in the nervous system (Yamaguchi and Miura, 2015).

Caspases, a family of intracellular proteases considered to be the executioners of apoptosis, have been highlighted for their role in the development of the CNS (Yuan and Yankner, 2000). Indeed, by acting as cell death accelerators, they precisely delineate the size of cell populations in the developing embryo, including in the brain and spinal cord. Intriguingly, recent studies suggest that caspases not only induce apoptosis but also promote neural development processes, including axon branching and synapse formation, independent of their apoptosis-related roles (D'Amelio et al., 2010; Mukherjee and Williams, 2017). However, the mechanisms underlying the choice by neural cells to activate either death-related or differentiation-promoting roles of caspases remain obscure.

In this review, we highlight the current knowledge on the apoptotic and non-apoptotic roles of caspases in the development of the CNS. We depict molecular aspects of caspase regulation, which might be critical for neural cell destiny during embryonic development and further discuss current "controversies" in the field.

OVERVIEW OF THE CASPASE FAMILY OF APOPTOSIS EXECUTIONERS

In metazoans, apoptotic mechanisms are evolutionarily conserved and allow multicellular organisms to preserve tissue homeostasis (Ameisen, 2002). Ced-3 was the first apoptosis executioner discovered in *Caenorhabditis elegans* (Ellis and Horvitz, 1986). Its first mammalian homologs, interleukin-1β-converting enzyme in humans and nedd-2 in mice, were described shortly after (Yuan et al., 1993). Homologs of these proteins were also found in insects, namely Dcp-1 and Drice in Drosophila. These proteins were named caspases, which stands for Cysteine Aspartyl-Specific Proteinases, reflecting their specificity for sites containing aspartic acid peptide bonds, which they cleave through the cysteine present in their active site. So far, about 15 caspase family members have been described in humans and mice (Shalini et al., 2015). Of note, in mammals, certain caspases are implicated also in inflammation. In this respect, it has been found that a given caspase can contribute to either apoptosis or inflammation, but not both (Martinon and Tschopp, 2004; Shalini et al., 2015). This review focuses on apoptotic caspases and their roles in the development of the nervous system.

Classification and Structure

Apoptotic caspases, including those in humans, are classified into two groups: the initiators (caspase-8, -9, and -10) and the executioners (caspase-3, -6, and -7). These proteases are synthesized as proteolytically inactive zymogens. On the one hand, initiator caspases comprise an extended prodomain in the N-terminus moiety, upstream of the conserved region encoding the large and small subunits of the active site (**Figure 1A**). On the other hand, executor caspases have a short or even absent prodomain. During the process of initiator caspase activation, the prodomain and the linker region between both subunits, are removed, giving rise to a homodimer (namely, a tetramer) with two active sites (**Figure 1B**; Li and Yuan, 2008; Shalini et al., 2015). Initiator caspases can self-activate *via* autocatalysis, however, additional interactions with an activating protein platform is usually required. For instance, activation rate is several orders of magnitude higher when caspase-9 is docked in a supramolecular complex referred to as the apoptosome, compared to the free form (Rodriguez and Lazebnik, 1999). In this respect, two well-known activation platforms of initiator caspases are death-inducing signaling complex (DISC) and the apoptosome complex. The former activates caspase-8, and the latter activates caspase-9 (**Figure 2**). Unlike the initiators, executor caspases, lacking a proper prodomain, can dimerize shortly after being synthesized. However, the linker region between the large and small subunits prevents activation. Removal of the linker is performed by initiator caspases, such a caspase-8 and -9, after which activated executioners cleave a broad set of substrates, leading to apoptosis (Kumar, 2007).

Caspase Substrates

Several hundreds of proteins are cleaved by caspases during apoptosis, but only a small proportion is considered to be of biological significance for cell remodeling (Julien and Wells, 2017). Among the most well-known targets of caspases are cytoskeletal proteins, including actin and tubulin (Mashima et al., 1999; Sokolowski et al., 2014), and nuclear envelope proteins, including lamins (Slee et al., 2001; Raz et al., 2006).

In fact, a number of caspase-substrates are involved in non-apoptotic processes, including cell proliferation and differentiation (Kuranaga and Miura, 2007). During such processes, cleavage of caspase targets remains strictly controlled in time and space, avoiding detrimental cell death. For instance, in erythropoiesis, the transcription factor GATA-1 is protected from caspase-mediated proteolysis by the chaperon protein Hsp70 (De Maria et al., 1999; Ribeil et al., 2007).

So far, an exhaustive view of the specific roles of each member of the caspase family is lacking. The precise map of their actual

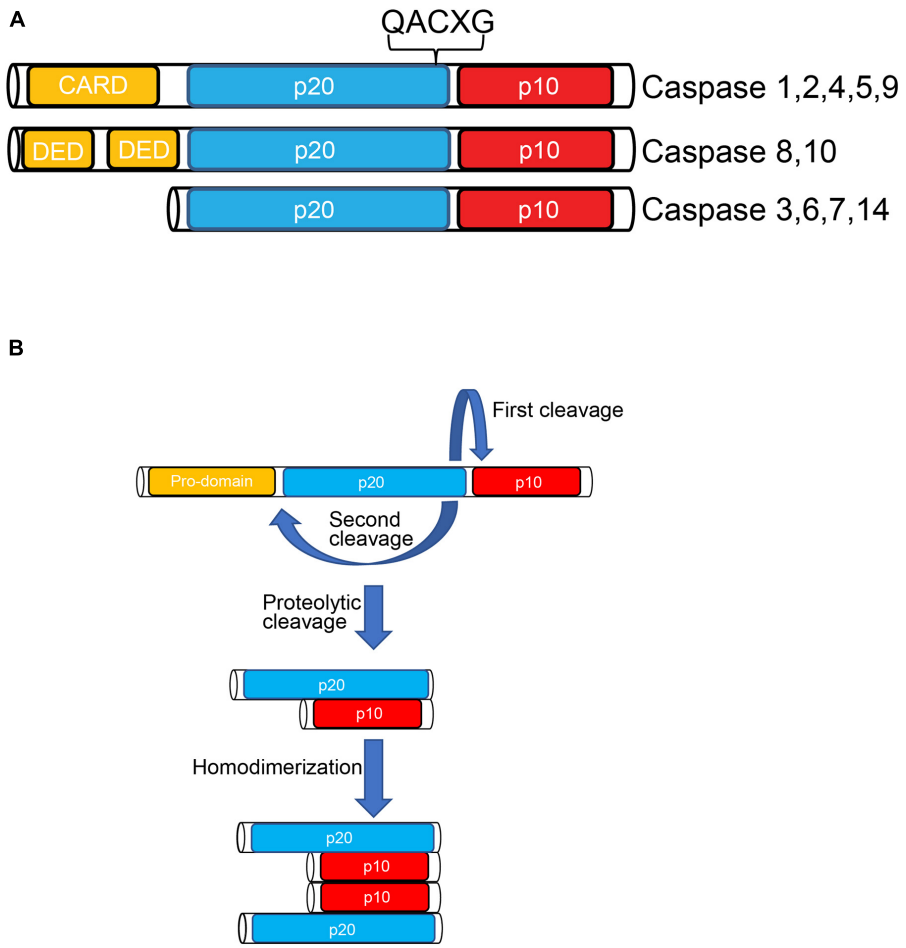

FIGURE 1 | The caspase family of proteases. **(A)** Members of the caspase family, are synthesized as inactive precursors called zymogens composed of a prodomain, a p20 large subunit and a p10 small subunit. The p20 subunit contains the active site of the enzyme harboring a "QACXG" pentapeptide motif. Initiator Caspases are characterized by the presence of a long N-terminal prodomain whereas the N-terminus domain of effector caspases is shorter. **(B)** Caspase activation is achieved by proteolytic cleavage between the large and small subunits and removal of the N-terminus prodomain. This post translational modification leads to new conformational state in which caspase homodimers are fully active.

substrates also remains to be determined, although the preferred cleavage sites of each caspase were identified by proteomic studies. For instance, caspase-3 and -7 both cleave the same DEVD motif. However, caspase-3 was shown to be more efficient than caspase-7 in cleaving well-known substrates such as Bid, XIAP, and caspase-6. Moreover, the amplification of the apoptotic cascade through the caspase-9 feeding loop depends on caspase-3 but not on caspase-7 (Walsh et al., 2008).

MECHANISMS OF CASPASE REGULATION

The caspase activation cascade occurs *via* two broadly recognized pathways, referred to as extrinsic and intrinsic. In the extrinsic pathway stimulation of death receptors such as Fas/Apo1 or TRAIL, leads to the activation of initiator caspase-8 and downstream cleavage of effector caspase-3. The intrinsic pathway involves the mitochondria, and notably the release of cytochrome c from the mitochondrial intermembrane space into the cytosol. Released cytochrome c binds to the Apaf-1 docking protein and facilitates the formation of the apoptosome complex that recruits and activates caspase-9. This caspase-9/Apaf-1/cytochrome c apoptosome complex is the holoenzyme form of caspase-9, which activates the caspase-3 apoptosis executioner by proteolytic cleavage (**Figure 2**; Hengartner, 2000).

Bcl-2 Family Proteins

Mitochondria play a central role in caspases activation through the intrinsic pathway (Singh et al., 2019). Upon various death-inducing stimuli the mitochondrial outer membrane (MOM) is altered, allowing cytochrome c release into cytosol and subsequent activation of the caspase cascade. This phenomenon, referred to as mitochondrial outer membrane permeabilization (MOMP), is strictly regulated by the Bcl-2 protein family (Kale et al., 2018).

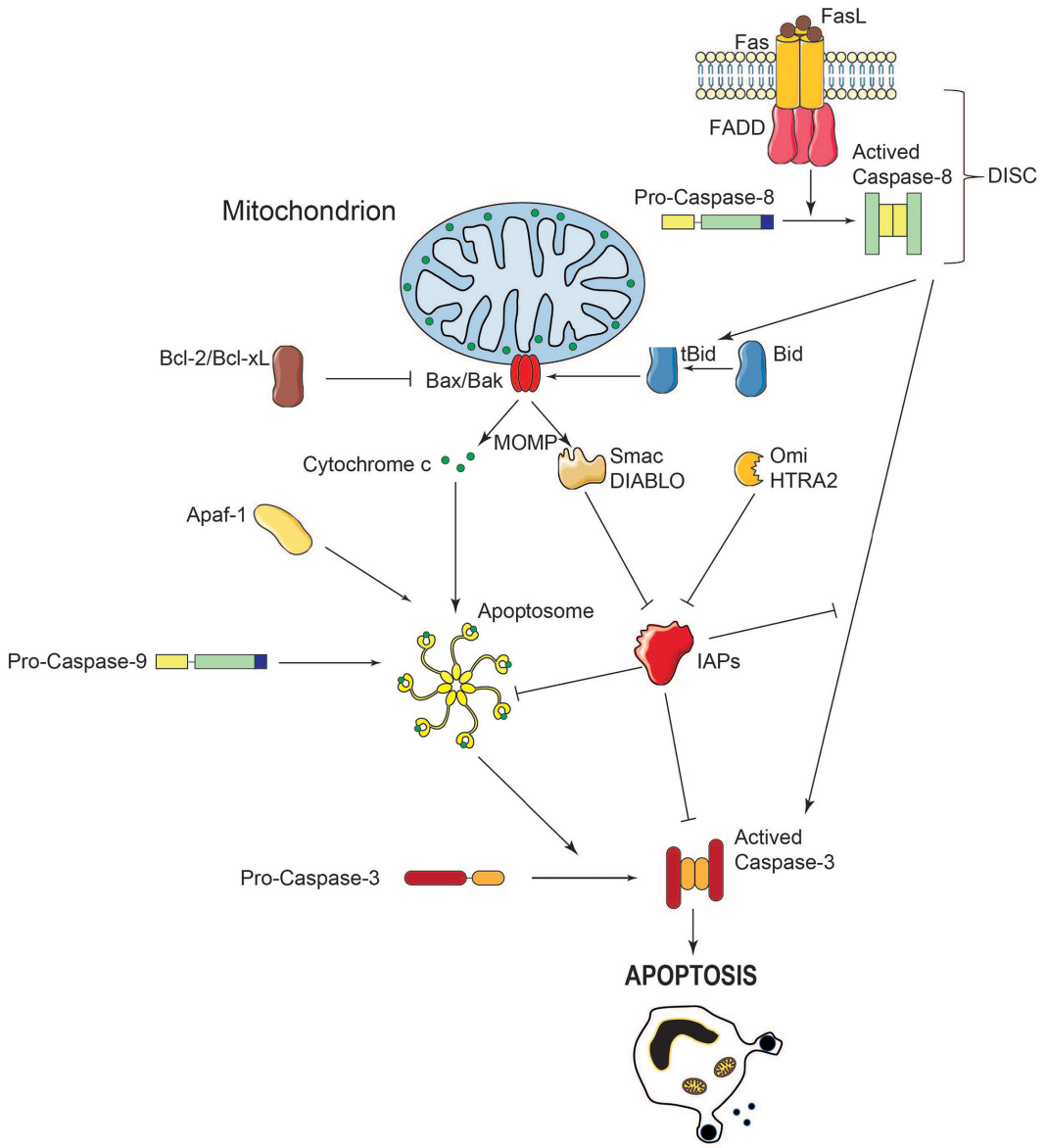

FIGURE 2 | Schematic representation of caspase activation and regulation during MOMP. During apoptosis, the MOM is permeabilized, leading to the release of pro-apoptotic molecules into the cytosol. When released in the cytosol, cytochrome c interacts with the adaptor protein Apaf-1 in presence of ATP. A multiprotein complex called the apoptosome, comprising cytochrome c, Apaf-1 and caspase-9 activates caspase-3, leading to cell death. The IAPs prevent caspase activation and apoptosis whereas Smac/Diablo and HtrA2/Omi exert the opposite effect by reversible direct binding and/or proteolytic cleavage. Crosstalk between extrinsic and intrinsic apoptosis pathways takes place through caspase-8-mediated Bid cleavage which activates Bax and Bak and subsequent MOMP.

Bcl-2 proteins share one or multiple conserved Bcl-2 homology (BH) domains (Youle and Strasser, 2008). Based on structure and function analyses, Bcl-2 proteins have been classified into three groups: BH3-only, pro-apoptotic multidomain, and anti-apoptotic multidomain (Youle and Strasser, 2008; Chipuk et al., 2010). Once activated, pro-apoptotic multidomain proteins, such as Bax and Bak, form homo- and hetero-oligomeric channels on the MOM, inducing the leakage of apoptogenic agents into the cytosol (Bleicken et al., 2013; Zhang et al., 2017). Anti-apoptotic multidomain Bcl-2 homologs, including Bcl-2, Bcl-xL, and Mcl-1, neutralize Bax and Bak through a hydrophobic groove formed by their BH1, BH2 and BH3 domains, therefore protecting the cell from apoptosis (Petros et al., 2004). BH3-only proteins are pro-apoptotic proteins that play the role of "sentinels" capable of integrating diverse cellular stresses and of shifting the balance between pro- and anti-apoptotic toward MOMP by antagonizing anti-apoptotic Bcl-2 family members or activating Bax and Bak (Youle and Strasser, 2008).

Caspase Inhibitors

Caspase activity is also controlled by the inhibitor of apoptosis proteins (IAPs). Such control may occur *via* either direct inhibition or degradation through ubiquitination

and downstream ubiquitin-targeted proteasome machinery (Joazeiro and Weissman, 2000; Zhang et al., 2019). Intriguingly, X-linked IAP (XIAP) was also shown to be a direct caspase inhibitor, independent of ubiquitin. Indeed, XIAP inhibits the enzymatic activity of both initiator and executor caspases (Eckelman et al., 2006). Following MOMP-induction, other apoptogenic molecules aside from cytochrome c, including Smac/DIABLO, HtrA2/Omi, AIF, and endonuclease G are also released into the cytosol. In turn, Smac/DIABLO and HtrA2/Omi neutralize the IAPs, which results in caspase-induced cell remodeling (Du et al., 2000).

Regulation Through Phosphorylation

Both initiator (capase-8 and -9) and executioner caspases (caspase-3 and -7) are directly regulated by phosphorylation (Parrish et al., 2013; Zamaraev et al., 2017). Caspase-3 activity has been reported to be inhibited by p38MAPK though phosphorylation of the highly conserved S150 residue, which is reversed by protein phosphatase 2A (PP2A) (Alvarado-Kristensson et al., 2004; Alvarado-Kristensson and Andersson, 2005). Caspase-9 has the largest subset of reported phosphorylation sites. Most of these sites are located in the large and small subunits but not in the active site (Zamaraev et al., 2017). Tyr153 is the only phosphorylation site reported to promote caspase-9 activation whereas other sites impede auto-processing and block substrate binding (Raina et al., 2005; Allan and Clarke, 2007; Serrano et al., 2017; Serrano and Hardy, 2018). Both inhibitory and activating phosphorylation sites are present in caspase-3, whereas only the former have been described in caspase-7 (Alvarado-Kristensson et al., 2004; Voss et al., 2005; Eron et al., 2017). However, the regulation of caspase activity by phosphorylation remains to be formally demonstrated in nerve cells.

APOPTOTIC ROLE OF CASPASES IN THE DEVELOPING NERVOUS SYSTEM

Control of Neural Tube Closure

Numerous apoptotic events occur during the development of the nervous system in vertebrates and invertebrates. At an early developmental stage, apoptotic cells are found at the boundaries between the non-neural ectoderm and the neuroepithelial layer during and after neural tube closure (NTC) (Geelen and Langman, 1977; Weil et al., 1997). Interestingly, apoptosis takes place throughout the major steps of NTC, including neural fold bending and fusion processes, remodeling of the dorsal neural tube and of the ectoderm, as well as migration of neural crest cells away from the neural tube (Massa et al., 2009; Washausen et al., 2018). Indeed, suppression of apoptosis with caspase inhibitors entirely impedes the NTC in the chick embryo (Weil et al., 1997). Furthermore, there is evidence of a potential link between mutations in apoptosis-related genes (*caspase-3, caspase-9*, and *apaf-1*) and neural tube closure defects in human (Liu et al., 2018; Spellicy et al., 2018; Zhou et al., 2018).

In mice, *caspase-3*- and *apaf-1*-null embryos only show neural tube closure defects in the midbrain and the hindbrain, while neurulation proceeds normally in the forebrain and the spinal cord. Interestingly, pharmacological inhibition of apoptosis using the pan caspase inhibitor z-VAD-FMK or the p53 inhibitor Pifithrin-α does not impact neural tube closure in *ex vivo* cultured embryos (Massa et al., 2009). This observation suggests that the observed neural tube closure defect may not be a direct consequence of the suppression of apoptosis but could be due to the abnormal persistence of certain signal-secreting cell populations that should have been eliminated by apoptosis. Indeed, this may explain why neural tube malformations were not observed in *ex vivo* cultures, where secreted factors are expected to be rapidly diluted in the culture medium.

Control of Cell Population Size

Apoptosis is widely recognized as main regulator of cell number during development. In developing CNS, neurons are generated excessively. Then, this population is trimmed down *via* apoptosis: neurons without proper connection with their target are eliminated. In the context where apoptosis is suppressed or compromised, the nervous system, especially the brain, would be overloaded with neurons, leading to protrusions and ventricular obstruction (Jacobson et al., 1997; Buss et al., 2006).

Several knock out mouse models demonstrated the critical role of caspase-dependent apoptosis in controlling the size of neuron populations during development. *Caspase-3* invalidation in 129 × 1/SvJ mice leads to exencephaly, a defect in which the brain exhibits abnormal protrusions and ventricular absence due to hyperplasia (Kuida et al., 1996). Moreover, *caspase-9*-null embryos showed prenatal malformations in the brain and the spinal cord, similar to those observed in *caspase-3*-null embryos, including protrusion formation and ventricular obstructions. Both *caspase-3*- and *caspase-9*-null mice die rapidly after birth (Kuida et al., 1998). Of note, these mice show an abnormal increase in neuron number, suggesting that MOMP is indeed required for neuronal death during the development of the CNS. Interestingly, invalidation of *apaf-1*, a gene coding for a key component of the apoptosome, results in more severe hyperplasia phenotype than in *caspase-3*- or *caspase-9*-null mice, further supporting the role of the intrinsic apoptosis pathway in brain homeostasis (Cecconi et al., 1998; Yoshida et al., 1998). Finally, mouse embryonic fibroblasts derived from *cytochrome c*-null embryos failed to activate caspase-3 in response to different apoptotic stimuli. Of note, the latter embryos exhibited delayed development, dying at E10.5 (Li et al., 2000). However, it remains unclear if these effects are due to apoptosis failure or mitochondrial electron transport chain deficiency.

Regarding the extrinsic pathway of apoptosis, even though *caspase-8* invalidation, causes heart malformation erythrocyte congestion, and neural tube defects, leading to embryonic death at E13.5, the malformations observed in the nervous system are conceivably not directly linked to *caspase-8* silencing (Varfolomeev et al., 1998; Sakamaki et al., 2002).

It should also be noted that malformations of the neural tube induced by the invalidation of *caspase-3* and *apaf-1* are mouse-strain specific. Indeed, contrary to 129 × 1/SvJ mice, *caspase-3*-null C57BL/6J mice showed no macroscopic anomalies and reached adulthood without any detectable brain pathology

(Leonard et al., 2002). Similar strain-dependent effect was also observed in *apaf-1*-null mice. In effect, C57BL/6J and CD1 mice show significantly delayed lethality compared to 129/Sv mice. These controversial observations might be due to some redundancy between effector caspases. Actually, although neither caspase-6 nor caspase-7 appear to be critical for CNS development, caspase-7 is capable to trigger apoptosis in a caspase-3-independent manner and is potentially responsible for the "rescued" phenotype in C57BL/6J *caspase-3*-null mice (Houde et al., 2004; Lakhani, 2006; Uribe et al., 2012).

Finally, although this issue was not addressed in above studies, compensation by other types of PCD such as autophagy and necroptosis cannot be eliminated.

The notion that, during development, cell number is exclusively controlled by apoptosis has recently been challenged by Nonomura et al. (2013). In this study, apoptosis suppression by *caspase-9* or *apaf-1* invalidation, even in a 129S1 background, did not lead to an increase of nerve cell number, whereas severe brain malformations were still observed. Actually, the size of neuron populations would be controlled by proliferation rate and other types of PCD.

In contrast, apoptosis was shown to be essential to control the FGF-8-producing cell population. Indeed, after the NTC, apoptosis is maintained in the midline of the neural tube, where these cells are localized. During development, activation of apoptosis around day E10 leads to the removal of these FGF-8-producing cells, preventing ectopic diffusion of FGF-8 to the ventral telencephalon (Nonomura et al., 2013). Together, these observations support the notion that the roles of apoptosis in the developing nervous system are actually cell-type specific.

NON-APOPTOTIC ROLES OF CASPASES IN THE DEVELOPING NERVOUS SYSTEM

Axon Branching and Arborization

Recent studies proposed that caspases, particularly caspase-3, play multiple roles aside from apoptosis. Activation of caspase-3 has been observed transiently and locally in the axons, notably at the level of branching points (Campbell and Okamoto, 2013; Katow et al., 2017). Intriguingly, this transient activation of caspase-3 did not always lead to apoptosis of the host neuron. Inhibition of caspase-3 in these models resulted in a decrease in the number of axonal branches. Caspase-3 cleavage was also shown to mediate the growth cone formation (Campbell and Holt, 2003; Verma, 2005).

The role of caspase-3 in axon regeneration was further highlighted in a model of axon disruption in *Caenorhabditis elegans*. In the latter, the homolog of vertebrate caspase-3 is encoded by the *ced-3* gene. Using neurons from a *ced-3*-null *C. elegans* strain, Pinan-Lucarre et al. (2012) showed that axons had lower outgrowth rate, being unable to re-connect after axotomy. Recently, in *C. elegans* Wang et al. (2019) successfully detected increased ced-3 activity following axotomy which was correlated to axon regeneration. Moreover, in neurons derived from rat DRG, caspase-3 inhibitors were found to impact growth cone formation, which is critical for restoring injured axons (Verma, 2005).

The mechanisms by which caspase-3 regulates growth cone formation and axon branching are still elusive. However, the contribution of the cytoskeleton is presumably important. In axons and dendrites, cytoskeleton components comprise actin microfilaments, microtubules, and intermediate filaments. In developing neurons, actin filaments are mainly found in growth cones. In contrast, microtubules are evenly distributed along the axons. However, it should be noted that the rate of microtubule remodeling is much higher in the axon terminus, compared to axon shafts. The growth cone is a guiding structure at the terminus of developing axons, characterized by actin enriched structures referred to as filopodia and lamellipodia (Pacheco and Gallo, 2016). Most interestingly, cytoskeletal actin was reported to be a substrate for caspase-3. Actin cleavage by caspase-3 gives rise to a 15 kD fragment inducing a more condensed and fragmented actin network (Mashima et al., 1999). Moreover, caspase-3 was demonstrated to cleave Rho-associated kinase ROCK I, generating a truncated form with higher intrinsic kinase activity. Such activated ROCK I stabilizes actin microfilaments, phosphorylates myosin light chains, and promotes the coupling between actin and myosin filaments, causing cellular contractions (Coleman et al., 2001). Thus, in the context of neuronal cells, caspase-3 may exert the same function in order to stabilize the cytoskeleton of new axon branches.

Aside from actin microfilaments, intermediate filaments are also potential targets of caspase-3 in axons. Immature neurons mainly express vimentin and nestin as intermediate filaments, which are replaced by neurofilaments in mature neurons. Beside their role as scaffolding structures, vimentin and nestin function as adaptors, contributing to axon growth cues (Adolf et al., 2016; Bott et al., 2019).

In addition to the cytoskeleton, caspases may further contribute to axon guidance through their impact on cell adhesion molecules, such as Neural cell adhesion molecule (NCAM), and extracellular vesicle proteins (Westphal et al., 2010; Weghorst et al., 2020).

Axon Pruning

Axon pruning is a process that eliminates collateral extensions or small terminus arborization with improper connectivity at the axon terminus. This process occurs at embryonic or early postnatal stage to fine-tune neural connectivity and has been well described in the peripheral nervous system (PNS). Axon pruning can be reproduced *in vitro* through the withdrawal of trophic factors such as nerve growth factor (NGF) or brain-derived neurotrophic factor (BDNF) from neuron cultures, including from DRG. In the developing CNS, although still poorly understood, similar mechanisms of network fine-tuning may occur at early postnatal stage (Innocenti and Price, 2005; De León Reyes et al., 2019).

In the sympathetic and DRG models, caspase-6 is widely recognized as an active contributor to axon pruning (Nikolaev et al., 2009; Cusack et al., 2013; Unsain et al., 2013). In contrast, the role of caspase-3 was initially overlooked. In the study of

Nikolaev et al. (2009), activation of caspase-3 was not detected in axons using an immunofluorescent marker or the fluorescent reporter FAM-DEVD-fmk in sympathetic neurons in culture, following NGF withdrawal. Furthermore, inactivation of caspase-3 with pharmacological inhibitors or siRNAs did not prevent caspase-6 cleavage and axon degeneration.

However, recent reports from different laboratories highlighted the implication of caspase-3 in axon pruning, using genetic approaches. These latter studies demonstrated that *caspase-3* KO prevented axon degeneration in NGF-deprived neurons. Interestingly, *in vitro* studies showed that, caspase-6 can be only processed by caspase-3, even at low levels of active caspase-3 (Simon et al., 2012; Cusack et al., 2013; Unsain et al., 2013). The difference between these observations and the ones of Nikolaev might be due to the small amounts of activated caspase-3 in this context, which cannot be detected by immunofluorescence. In fact, small remaining amounts of active caspase-3, having escaped pharmacological inhibitors or siRNA are presumably sufficient to promote the observed caspase-6-dependent pruning.

The roles of caspases in axonal network fine-tuning remains to be further investigated. Recently, regarding *in vivo* studies, caspase-3 has been shown to be activated in the axon and not in the cell body of spinal cord neurons of postnatal mice. Suppression of caspase-3 activation by *bax/bak* double KO led to a less tailored network of neuron branches in the spinal cord at postnatal day 14, which disturbed the reorganization of the corticospinal circuit and consequently impaired the development of skilled movements in adult mice (Gu et al., 2017).

Synapse Maturation and Synaptic Functions

Recent studies have suggested that, aside from refining the developing axonal network, caspases also promote fine-tuning of protein structure at the level of the synapses, which may be critical for their functioning. Synapses are at the key player structures regarding neuron communication. There are two existing types of synapses referred to as electrical and chemical, the latter being the most abundant in the CNS. In electrical synapses, signals are transmitted by an electrical current through gap junctions. In chemical synapses, communication between two neurons is performed by the secretion of a neurotransmitter in the synaptic cleft. Once released into the synaptic cleft, the neurotransmitter binds to receptors at the post-synaptic level and induces electrical signals by acting on ion channel permeability (Purves et al., 2018).

In the PNS, caspase-3 fine-tunes the post-synaptic neurotransmitter receptor network. During development, this process namely occurs at the neuromuscular junction, regarding the nicotinic acetyl choline receptor (AchR). Indeed, at early stages of development, AchRs are abundantly distributed. Later on, AchRs gather into clusters that are stabilized by agrin released from axon terminals. Moreover, motor neurons secrete acetylcholine, which acts as a negative signal, disrupting AChR clusters that do not interact with axon terminals. Of note, this disrupting effect of acetylcholine is mediated by caspase-3 which cleaves Disheveled 1 (Dvl1), a signaling protein of the Wnt pathway. Indeed, prevention of caspase-3 activation or Dvl1 cleavage suppresses acetylcholine-dependent AChR cluster disruption (Wang et al., 2014).

Certain similarities between synaptogenesis processes in the CNS and the PNS have been described, such as clustering of neurotransmitter receptors at the post-synaptic level (Garner et al., 2002; Purves et al., 2018). Regarding the underlying molecular mechanisms, agrin-like molecules and Ephrin-Bs have been reported to contribute to the clustering of *N*-methyl-D-aspartate (NMDA) and α-amino-3-hydroxy-5-methyl-4-isoxazolepropionic acid (AMPA) receptors, respectively (Garner et al., 2002). It remains to be explored if the role of caspase-3 in sculpturing post-synaptic receptor clusters in the PNS is conserved in the CNS.

Caspase-3 is also involved in synaptic plasticity, notably in long-term depression (LTD), a process during which the efficiency of synaptic transmission is lowered in the long-term. This process was thoroughly studied in the context of the glutamatergic synapse. The post-synaptic region of these synapses contains AMPA and NMDA receptors, which both respond to glutamate. Coordination between both receptors is critical for optimal synaptic transmission. In LTD, the AMPA receptor is withdrawn from the post-synaptic membrane by endocytosis, which leads to a decrease in synaptic sensitivity (Purves et al., 2018). Interestingly, caspase-3 activation is essential for AMPA receptor internalization at the synapse in response to NMDA stimulation *in vitro* (Li et al., 2010). Inhibition of the XIAP caspase-3 inhibitor enhances AMPA receptor internalization and increases LTD (Gibon et al., 2016). In addition, caspase-3 mediates synapse loss upon long-term exposure to NMDA (Henson et al., 2017). Furthermore, local activation of caspase-3 induced by Mito-killer Red photo-stimulation results in local spine shrinkage and subsequent elimination of spines without neuronal apoptosis (Erturk et al., 2014). Dendritic spine regulation by BDNF is also mediated by caspase-3 (Guo et al., 2016). *In vivo*, *caspase-3* KO mice display a lack of attention and hyperactive disorder, potentially related to a failure in synaptic plasticity mechanisms, such as AMPA receptor regulation in response to chronic or repeated stimuli (Lo et al., 2015). In contrast, *xiap* KO mice exhibit better learning performance, which could be explained by increased LTD (Gibon et al., 2016).

In addition, caspase-3 regulates synaptic vesicle pool and eliminates dysfunctional dendritic spines (Chen et al., 2020). Collectively, these data highlight the central roles of caspase-3 in synaptic plasticity and functions.

Local and Temporal Activation of Caspases in Non-apoptotic Processes

Activation of caspases in the above described non-apoptotic contexts seem to be both local and transient. Most of the time, ultimate caspase-3 activation is required for axon remodeling and synapse functions. Mitochondria present at axon terminals were reported to be critical for axon branching (Courchet et al.,

2013), suggesting that such caspase-3 activation presumably depends on the mitochondrial pathway. Indeed, the release of cytochrome c into the cytosol appears to occur prior to local caspase-3 activation (Li et al., 2010; Guo et al., 2016). Finally, caspase-9 inhibition was shown to prevent such local caspase-3 activation, further confirming the contribution of mitochondria (Ohsawa et al., 2010; Erturk et al., 2014; Khatri et al., 2018). Intriguingly, even though the role of caspase-9 in local caspase-3 processing appears to be clearly established in this context, the role of the apoptosome remains unclear (Ohsawa et al., 2010; Cusack et al., 2013).

Although most studies acknowledge that the mitochondrial pathway is the key player in caspase-3 activation in non-apoptotic contexts, it remains unclear how neurons can control caspase-3 activity locally and temporally. *A priori*, several scenarios are possible (**Figure 3**).

First, it is likely that a limited number of mitochondria are actually permeabilized and release cytochrome c, to allow such sub-optimal caspase activation. MOMP was widely thought to be a point of no-return from which cells commit suicide. There is evidence that apoptotic signals can be initiated by a limited number of mitochondria and then spread throughout the cell in "apoptotic waves" (Pacher and Hajnóczky, 2001; Cheng and Ferrell, 2018). In axons, mitochondria are more distant compared to the cell body. This topological barrier might result in the permeabilization of a fraction of the mitochondria, leaving most of them intact and healthy.

The mechanisms underlying the propagation of "apoptotic waves" is a matter of debate. Indeed, Ca^{2+} may play a role in this respect. Aside from cytochrome c and cognate apoptogenic agents, depolarized mitochondria initiate Ca^{2+} waves and trigger the depolarization of surrounding mitochondria (Pacher and Hajnóczky, 2001; Ziegler et al., 2021). Actually, the propagation of waves of released cytochrome c have been reported during apoptosis (Lartigue et al., 2008; Cheng and Ferrell, 2018). Such a propagation of waves of cytochrome c into the cytosol seems to independent of pro-apoptotic proteins Bax and Bak. Intriguingly, the presence of cytochrome c in the cytosol failed to trigger cell death in sympathetic neurons (Deshmukh and Johnson, 1998). Overall, these observations suggest that additional mechanisms controlling apoptosis are presumably involved in neuronal cells. Indeed, in post-mitotic neurons, an E3 ligase, referred to as Cullin 9 (CUL9) or Parkin-like cytoplasmic protein (PARC) was reported to mediate cytosolic cytochrome c degradation (Gama et al., 2014), suggesting that, in neurons, the propagation of cytosolic cytochrome c may be blocked by proteasome-mediated degradation.

Of note, partial cytochrome c release has been described in physiological contexts, beyond apoptosis. Basically, under certain conditions, MOMP may occur only in some mitochondria while the others remain intact (Tait et al., 2010). Incomplete MOMP appears to have physiological effects in some instances. For example, microbial infection stimulates MOMP in a fraction of mitochondria of the host cell, allowing sublethal caspase activation to promote cytokine secretion in the context of an innate immune response (Brokatzky et al., 2019). Thus, partial caspase activation might occur through similar mechanisms in developing neurons **(Figure 3)**.

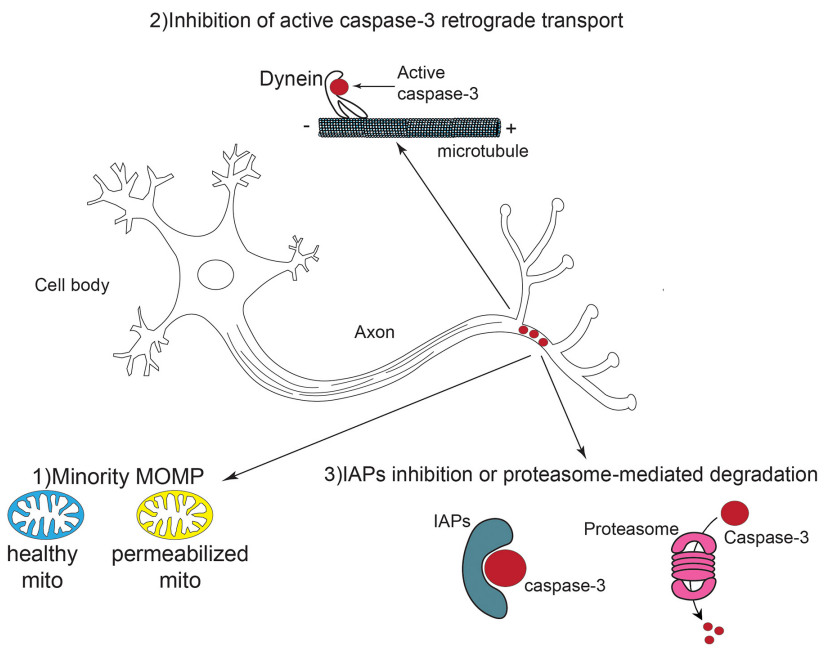

FIGURE 3 | Schematic representation of local caspase activation and potential regulation pathways in neural development. Caspase-3 is activated locally and transiently in the axons of developing and mature neurons. This activation might result from a phenomenon called "minority MOMP" in which only a subpopulation of mitochondria is permeabilized while the others remain healthy. The retrograde transport of active caspases *via* dynein is also inhibited. Finally, IAPs can suppress caspase-3 activity through direct inhibition or proteasome mediated degradation.

Second, in neurons, it can be anticipated that some mechanisms may have been set up to avoid uncontrolled propagation of active caspases. Indeed, there are shreds of evidence of cleaved caspase retrograde transport *via* the microtubule network (Carson et al., 2005; García et al., 2013; Barreiro-Iglesias et al., 2017). Activated caspase-8 was demonstrated to interact with the dynactin/dynein complex, which is responsible for retrograde axonal transport, and to be transferred in this way from axon terminals to the cell body (Carson et al., 2005; Barreiro-Iglesias et al., 2017). Thus, retrograde movement of caspase-8 leads to caspase-3 cleavage along the axons as well as in the cell body. Activated caspase-3 was also found to directly associate with dynein, suggesting that it can be transported back to the soma through a similar mechanism (García et al., 2013). In non-apoptotic contexts, including neuron differentiation, the interaction between activated caspase-3 and the dynactin/dynein complex might thus be inhibited.

Third, active caspases, after having performed their extra-apoptotic mission, must be rapidly neutralized to avoid deleterious alterations of cell components due to uncontrolled proteolysis. The IAP family of caspase inhibitors, including XIAP, may contribute to such neutralization. Indeed, in dorsal root ganglio (DRG) neurons, XIAP is localized in axons and slackens off caspase-3-dependent axonal degeneration (Unsain et al., 2013). Caspases can also be eliminated through IAP-mediated ubiquitinylation and proteasomal degradation. Evidence indicates a dynamic equilibrium of proteasome anterograde and retrograde transport in neurons. Proteasome components are actively transported to distal axons *via* kinesin motors (Otero et al., 2014). Indeed, the presence of the proteasome at the end of axons is essential to maintain protein homeostasis. This is highlighted in certain neurodegenerative pathologies such as Alzheimer's disease, in which proteasomal degradation is aberrant along the axons. On the contrary, in nascent synapses, proteasome components are retrogradely transported *via* dynein motors, which permits the stabilization of synaptic structures (Hsu et al., 2015). Apparently, by controlling anterograde and retrograde transports, the guidance of proteasome components in axons is precisely controlled in accordance with intra- and extra-cellular cues. Thus, it might be assumed that local proteasome recruitment may occur to regulate caspase activation during axonal growth or branching.

Bcl-2 FAMILY: POTENTIAL REGULATORS OF CASPASE ROLES IN THE DEVELOPING CNS

Apoptosis and Mitochondria

As mentioned above, it has long been acknowledged that the Bcl-2 family regulates caspase activation *via* the mitochondrial pathway of apoptosis. Pore formation in the MOM by pro-apoptotic proteins Bax and Bak is a key step of this canonical pathway. These pores permit the release of cytochrome c and other apoptogenic molecules into the cytosol. In addition, Bax and Bak also mediate the release of Ca^{2+} from the endoplasmic reticulum (ER) lumen (Scorrano et al., 2003). Consequently, mitochondria are overloaded with Ca^{2+}, which further induces the mitochondrial permeability transition pore (MPTP) (Giorgi et al., 2012). The nature of MPTP is still ambiguous, however, it seems to act synergistically with the Bax/Bak pores to foster the release of intermembrane-space components into the cytosol (Zhang and Armstrong, 2007). Finally, it is noteworthy that the anti-apoptotic proteins, including Bcl-2, Bcl-xL, Mcl-1, and Bcl-w, antagonize Bax and Bak in both mitochondria- and Ca^{2+}-dependent PCD pathways.

In the developing CNS, Bax, Bak, Bcl-xL, and Mcl-1 are expressed at a high level (Lindsten et al., 2000; Arbour et al., 2008; Nakamura et al., 2016). Bcl-2 is also found to be highly expressed during embryonic development, although *bcl-2* invalidation does not seem to affect the development of the CNS in mice (Michaelidis et al., 1996). Bax and Bak apoptosis accelerators often show overlapping roles. *Bax* invalidation does not entirely eliminate apoptosis in the developing CNS but affects some specific neural populations, including neuroblasts, retinal ganglion cells and Cajal–Retzius neurons (Knudson et al., 1995; Péquignot et al., 2003; Ledonne et al., 2016). *Bak* KO mice develop normally without detectable malformation in the CNS (Lindsten et al., 2000). *Bax/bak* double KO leads to perinatal lethality in about 90% homozygous offspring (Lindsten et al., 2000).

There is evidence that the loss of Bax and Bak, can be partly compensated by the apoptosis accelerator Bok, a multidomain Bcl-2 homolog whose functions remain poorly understood (Ke et al., 2018).

Although ventricular obstruction was observed due to an abnormal increase of neuron number in *bax/bak* double KO, these mice did not exhibit exencephaly, unlike *caspase-3*- or *caspase-9*- null mice. Interestingly, interdigital webs and imperforate vagina were observed in *bax/bak* double KO, but not in *caspase-3*- or *caspase-9*- null mice (Lindsten et al., 2000). These diverging phenotypes presumably underscore the role of Bax and Bak roles in the other types of PCD (Kawai et al., 2009; Karch et al., 2013, 2017).

Conversely, regarding cell death inhibitors, the two anti-apoptotic Bcl-2 homologs Mcl-1, and Bcl-xL, appear to hamper apoptotic cell death in neurons. Indeed, Mcl-1 is critical for the survival of neural progenitors (Arbour et al., 2008), whereas Bcl-xL protects post-mitotic neurons from cell death (Nakamura et al., 2016). Of note, the full KO of *bcl-x* leads to embryonic lethality due to massive apoptosis in the CNS (Motoyama et al., 1995; Fogarty et al., 2016; Nakamura et al., 2016).

Incomplete MOMP and Non-apoptotic Functions

Bcl-2 proteins have also been found to regulate incomplete MOMP in several instances (Singh et al., 2019; Bock and Tait, 2020). A suggested model for incomplete MOMP is based on the heterogeneous distribution of Bcl-2 proteins in the MOM. According to this model, mitochondria harboring high amounts of anti-apoptotic proteins, such as Bcl-2 and Bcl-xL, would be protected from Bax and Bak-induced permeabilization,

whereas mitochondria deprived of apoptosis inhibitors would be privileged prey for Bax and Bak (Tait et al., 2010).

The mechanism allowing such heterogeneity is still unclear. It might involve a signal to recruit Bax/Bak to a specific population of mitochondria and/or a signal to shift anti-apoptotic proteins either to another mitochondrial pool or to the cytosol. In line with this, the retromer is a system conceivably able to mediate the translocation of anti-apoptotic proteins to distinct mitochondrial populations. Indeed, a recent study showed that Bcl-xL forms a complex with VPS35/VPS26 retromer proteins. This complex promotes the mitochondrial localization of Bcl-xL (Farmer et al., 2019). Thus, a signal may be present on mitochondria to recruit this Bcl-xL-retromer complex. Anti-apoptotic proteins might also be eliminated from mitochondria through Mitochondrial-anchored protein ligase (MAPL)-mediated mitochondria-derived vesicles, a structure transferring MOM proteins from the mitochondria to the peroxisome (Neuspiel et al., 2008).

In mature neurons, moderate Bax activation is observed in response to NMDA receptor-dependent LTD. Interestingly, in this instance, translocation of Bax to mitochondria could not be detected, suggesting that only a minor fraction of Bax, already present at the level of the mitochondria, was activated. Alternatively, Bax translocation might be too low to be detected with current methods (Jiao and Li, 2011). Nevertheless, such partial Bax activation may also occur in developing neurons.

Mitochondrial Dynamics

Finally, Bcl-2 proteins were reported to control mitochondrial morphology and motility. Indeed, Bcl-xL increases both the fusion and fission rate of mitochondria (Berman et al., 2009). Furthermore, Bcl-xL interacts with dynamin-related protein (Drp1) and promotes the transport of mitochondria in axons (Li et al., 2008). In hippocampal neurons, this interaction favors mitochondrial fission to form "tiny mitochondria" capable of being distributed to new axon branches. It was also reported that inhibition of Bcl-xL by ABT-737 lowers the number of mitochondria along the axon, decreasing synapse number and synaptic vesical clusters.

CONCLUSION

Caspase-mediated apoptosis has been considered as an essential mechanism regulating CNS development in vertebrates for years. Recent studies propose new insights into how apoptosis shapes the mammalian nervous system. These new observations challenge the conventional model of cell number control. Current data suggest that apoptosis may affect the behavior of neighboring cells or trim down a specific cell population (Nonomura et al., 2013; Yamaguchi and Miura, 2015). Genetically-modified mouse models have highlighted the role of caspase-3 as the main caspase effector in the developing CNS. However, why the effect of *caspase-3* invalidation in mice is strain-specific is still an open question. This is possibly due to the compensation of other effector caspases, such as caspase-7 (Houde et al., 2004). In this respect, compensation mechanisms either from other types of PCD, such as autophagy, or proliferation inhibition by senescence, should also be considered.

Novel techniques allowing to detect slight and transient caspase-3 activation in neurons have been recently documented. It is conceivable that such activation is physiologically relevant in the context of neurogenesis and day-to-day synaptic functions. The existence of two "opposite" effects of caspase-3 activation suggests that nerve cells may be equipped with the adequate regulation pathways to engage in distinct cell fates. The Bcl-2 family protein is a potential candidate to regulate these pathways. As Bcl-2 proteins control caspase-3 activation through MOM permeability, they may also allow incomplete MOMP and subsequent caspase-3 activation at low levels. The upstream mechanisms underlying this Bcl-2 family-dependent incomplete MOMP are currently unknown. They definitely deserve to be further studied in the near future.

AUTHOR CONTRIBUTIONS

TN, GG, and NP wrote the manuscript. All authors contributed to the article and approved the submitted version.

FUNDING

This work was supported by Ligue Nationale Contre le Cancer (Comité du Rhône) (to NP), Fondation ARC (grant no. PGA1 RF20180206799 to GG), and Institut National du Cancer (to GG). TN is a fellow from fondation ARC.

ACKNOWLEDGMENTS

We would like to thank Brigitte Manship for manuscript editing.

REFERENCES

Adolf, A., Leondaritis, G., Rohrbeck, A., Eickholt, B. J., Just, I., Ahnert-Hilger, G., et al. (2016). The intermediate filament protein vimentin is essential for axonotrophic effects of *Clostridium botulinum* C3 exoenzyme. *J. Neurochem.* 139, 234–244. doi: 10.1111/jnc.13739

Allan, L. A., and Clarke, P. R. (2007). Phosphorylation of caspase-9 by CDK1/cyclin B1 protects mitotic cells against apoptosis. *Mol. Cell* 26, 301–310. doi: 10.1016/j.molcel.2007.03.019

Alvarado-Kristensson, M., and Andersson, T. (2005). Protein phosphatase 2A regulates apoptosis in neutrophils by dephosphorylating both p38 MAPK and its substrate caspase 3*. *J. Biol. Chem.* 280, 6238–6244. doi: 10.1074/jbc.M409718200

Alvarado-Kristensson, M., Melander, F., Leandersson, K., Rönnstrand, L., Wernstedt, C., and Andersson, T. (2004). p38-MAPK signals survival by phosphorylation of caspase-8 and caspase-3 in human neutrophils. *J. Exp. Med.* 199, 449–458. doi: 10.1084/jem.20031771

Ameisen, J. C. (2002). On the origin, evolution, and nature of programmed cell death: a timeline of four billion years. *Cell Death Differ.* 9, 367–393. doi: 10.1038/sj.cdd.4400950

Arbour, N., Vanderluit, J. L., Le Grand, J. N., Jahani-Asl, A., Ruzhynsky, V. A., Cheung, E. C. C., et al. (2008). Mcl-1 is a key regulator of apoptosis during

CNS development and after DNA damage. *J. Neurosci.* 28, 6068–6078. doi: 10.1523/JNEUROSCI.4940-07.2008

Ayala, R., Shu, T., and Tsai, L.-H. (2007). Trekking across the brain: the journey of neuronal migration. *Cell* 128, 29–43. doi: 10.1016/j.cell.2006.12.021

Barreiro-Iglesias, A., Sobrido-Cameán, D., and Shifman, M. I. (2017). Retrograde activation of the extrinsic apoptotic pathway in spinal-projecting neurons after a complete spinal cord injury in lampreys. *BioMed. Res. Int.* 2017:5953674. doi: 10.1155/2017/5953674

Berman, S. B., Chen, Y., Qi, B., McCaffery, J. M., Rucker, E. B., Goebbels, S., et al. (2009). Bcl-xL increases mitochondrial fission, fusion, and biomass in neurons. *J. Cell Biol.* 184, 707–719. doi: 10.1083/jcb.200809060

Bleicken, S., Landeta, O., Landajuela, A., Basañez, G., and García-Sáez, A. J. (2013). Proapoptotic bax and bak proteins form stable protein-permeable pores of tunable size. *J. Biol. Chem.* 288, 33241–33252. doi: 10.1074/jbc.M113.512087

Bock, F. J., and Tait, S. W. G. (2020). Mitochondria as multifaceted regulators of cell death. *Nat. Rev. Mol. Cell Biol.* 21, 85–100. doi: 10.1038/s41580-019-0173-8

Bott, C. J., Johnson, C. G., Yap, C. C., Dwyer, N. D., Litwa, K. A., and Winckler, B. (2019). Nestin in immature embryonic neurons affects axon growth cone morphology and semaphorin3a sensitivity. *Mol. Biol. Cell* 30, 1214–1229. doi: 10.1091/mbc.E18-06-0361

Brokatzky, D., Dörflinger, B., Haimovici, A., Weber, A., Kirschnek, S., Vier, J., et al. (2019). A non-death function of the mitochondrial apoptosis apparatus in immunity. *EMBO J.* 38:e100907. doi: 10.15252/embj.2018100907

Buss, R. R., Sun, W., and Oppenheim, R. W. (2006). Adaptive roles of programmed cell death during nervous system development. *Annu. Rev. Neurosci.* 29, 1–35. doi: 10.1146/annurev.neuro.29.051605.112800

Campbell, D. S., and Holt, C. E. (2003). Apoptotic pathway and MAPKs differentially regulate chemotropic responses of retinal growth cones. *Neuron* 37, 939–952. doi: 10.1016/S0896-6273(03)00158-2

Campbell, D. S., and Okamoto, H. (2013). Local caspase activation interacts with Slit-Robo signaling to restrict axonal arborization. *J. Cell Biol.* 203, 657–672. doi: 10.1083/jcb.201303072

Carson, C., Saleh, M., Fung, F. W., Nicholson, D. W., and Roskams, A. J. (2005). Axonal dynactin p150Glued transports caspase-8 to drive retrograde olfactory receptor neuron apoptosis. *J. Neurosci.* 25, 6092–6104. doi: 10.1523/JNEUROSCI.0707-05.2005

Cecconi, F., Alvarez-Bolado, G., Meyer, B. I., Roth, K. A., and Gruss, P. (1998). Apaf1 (CED-4 Homolog) regulates programmed cell death in mammalian development. *Cell* 94, 727–737. doi: 10.1016/S0092-8674(00)81732-8

Chen, H., Tian, J., Guo, L., and Du, H. (2020). Caspase inhibition rescues F1Fo ATP synthase dysfunction-mediated dendritic spine elimination. *Sci. Rep.* 10:17589. doi: 10.1038/s41598-020-74613-9

Cheng, X., and Ferrell, J. E. (2018). Apoptosis propagates through the cytoplasm as trigger waves. *Science* 361, 607–612. doi: 10.1126/science.aah4065

Chipuk, J. E., Moldoveanu, T., Llambi, F., Parsons, M. J., and Green, D. R. (2010). The BCL-2 family reunion. *Mol. Cell* 37, 299–310. doi: 10.1016/j.molcel.2010.01.025

Coleman, M. L., Sahai, E. A., Yeo, M., Bosch, M., Dewar, A., and Olson, M. F. (2001). Membrane blebbing during apoptosis results from caspase-mediated activation of ROCK I. *Nat. Cell Biol.* 3, 339–345. doi: 10.1038/35070009

Courchet, J., Lewis, T. L., Lee, S., Courchet, V., Liou, D.-Y., Aizawa, S., et al. (2013). Terminal axon branching is regulated by the LKB1-NUAK1 kinase pathway via presynaptic mitochondrial capture. *Cell* 153, 1510–1525. doi: 10.1016/j.cell.2013.05.021

Cusack, C. L., Swahari, V., Hampton Henley, W., Michael Ramsey, J., and Deshmukh, M. (2013). Distinct pathways mediate axon degeneration during apoptosis and axon-specific pruning. *Nat. Commun.* 4:1876. doi: 10.1038/ncomms2910

D'Amelio, M., Cavallucci, V., and Cecconi, F. (2010). Neuronal caspase-3 signaling: not only cell death. *Cell Death Differ.* 17, 1104–1114. doi: 10.1038/cdd.2009.180

De León Reyes, N. S., Mederos, S., Varela, I., Weiss, L. A., Perea, G., Galazo, M. J., et al. (2019). Transient callosal projections of L4 neurons are eliminated for the acquisition of local connectivity. *Nat. Commun.* 10:4549. doi: 10.1038/s41467-019-12495-w

De Maria, R., Zeuner, A., Eramo, A., Domenichelli, C., Bonci, D., Grignani, F., et al. (1999). Negative regulation of erythropoiesis by caspase-mediated cleavage of GATA-1. *Nature* 401, 489–493. doi: 10.1038/46809

Deshmukh, M., and Johnson, E. M. (1998). Evidence of a novel event during neuronal death: development of competence-to-die in response to cytoplasmic cytochrome c. *Neuron* 21, 695–705. doi: 10.1016/S0896-6273(00)80587-5

Du, C., Fang, M., Li, Y., Li, L., and Wang, X. (2000). Smac, a mitochondrial protein that promotes cytochrome C–dependent caspase activation by eliminating IAP inhibition. *Cell* 102, 33–42. doi: 10.1016/S0092-8674(00)00008-8

Eckelman, B. P., Salvesen, G. S., and Scott, F. L. (2006). Human inhibitor of apoptosis proteins: why XIAP is the black sheep of the family. *EMBO Rep.* 7, 988–994. doi: 10.1038/sj.embor.7400795

Ellis, H. M., and Horvitz, H. R. (1986). Genetic control of programmed cell death in the nematode C. elegans. *Cell* 44, 817–829. doi: 10.1016/0092-8674(86)90004-8

Eron, S. J., Raghupathi, K., and Hardy, J. A. (2017). Dual site phosphorylation of caspase-7 by PAK2 blocks apoptotic activity by two distinct mechanisms. *Structure* 25, 27–39. doi: 10.1016/j.str.2016.11.001

Erturk, A., Wang, Y., and Sheng, M. (2014). Local pruning of dendrites and spines by caspase-3-dependent and proteasome-limited mechanisms. *J. Neurosci.* 34, 1672–1688. doi: 10.1523/JNEUROSCI.3121-13.2014

Farmer, T., O'Neill, K. L., Naslavsky, N., Luo, X., and Caplan, S. (2019). Retromer facilitates the localization of Bcl-xL to the mitochondrial outer membrane. *Mol. Biol. Cell* 30, 1138–1146. doi: 10.1091/mbc.E19-01-0044

Fogarty, L. C., Song, B., Suppiah, Y., Hasan, S. M. M., Martin, H. C., Hogan, S. E., et al. (2016). Bcl-xL dependency coincides with the onset of neurogenesis in the developing mammalian spinal cord. *Mol. Cell. Neurosci.* 77, 34–46. doi: 10.1016/j.mcn.2016.09.001

Gama, V., Swahari, V., Schafer, J., Kole, A. J., Evans, A., Huang, Y., et al. (2014). The E3 ligase PARC mediates the degradation of cytosolic cytochrome c to promote survival in neurons and cancer cells. *Sci. Signal.* 7:ra67. doi: 10.1126/scisignal.2005309

García, M. L., Fernández, A., and Solas, M. T. (2013). Mitochondria, motor neurons and aging. *J. Neurol. Sci.* 330, 18–26. doi: 10.1016/j.jns.2013.03.019

Garner, C. C., Zhai, R. G., Gundelfinger, E. D., and Ziv, N. E. (2002). Molecular mechanisms of CNS synaptogenesis. *Trends Neurosci.* 25, 243–250. doi: 10.1016/S0166-2236(02)02152-5

Geelen, J. A. G., and Langman, J. (1977). Closure of the neural tube in the cephalic region of the mouse embryo. *Anat. Rec.* 189, 625–639. doi: 10.1002/ar.1091890407

Gibon, J., Unsain, N., Gamache, K., Thomas, R. A., De Leon, A., Johnstone, A., et al. (2016). The X-linked inhibitor of apoptosis regulates long-term depression and learning rate. *FASEB J.* 30, 3083–3090. doi: 10.1096/fj.201600384R

Gilbert, S. F. (2000). *Developmental Biology*, 7th Edn. Sunderland, MA: Sinauer Associates.

Giorgi, C., Baldassari, F., Bononi, A., Bonora, M., De Marchi, E., Marchi, S., et al. (2012). Mitochondrial Ca2+ and apoptosis. *Cell Calcium* 52, 36–43. doi: 10.1016/j.ceca.2012.02.008

Götz, M., and Huttner, W. B. (2005). The cell biology of neurogenesis. *Nat. Rev. Mol. Cell Biol.* 6, 777–788. doi: 10.1038/nrm1739

Gu, Z., Serradj, N., Ueno, M., Liang, M., Li, J., Baccei, M. L., et al. (2017). Skilled movements require non-apoptotic Bax/Bak pathway-mediated corticospinal circuit reorganization. *Neuron* 94, 626–641.e4. doi: 10.1016/j.neuron.2017.04.019

Guo, J., Ji, Y., Ding, Y., Jiang, W., Sun, Y., Lu, B., et al. (2016). BDNF pro-peptide regulates dendritic spines via caspase-3. *Cell Death Dis.* 7:e2264. doi: 10.1038/cddis.2016.166

Hengartner, M. O. (2000). The biochemistry of apoptosis. *Nature* 407, 770–776. doi: 10.1038/35037710

Henson, M. A., Tucker, C. J., Zhao, M., and Dudek, S. M. (2017). Long-term depression-associated signaling is required for an in vitro model of NMDA receptor-dependent synapse pruning. *Neurobiol. Learn. Mem.* 138, 39–53. doi: 10.1016/j.nlm.2016.10.013

Houde, C., Banks, K. G., Coulombe, N., Rasper, D., Grimm, E., Roy, S., et al. (2004). Caspase-7 expanded function and intrinsic expression level underlies strain-specific brain phenotype of caspase-3-null mice. *J. Neurosci.* 24, 9977–9984. doi: 10.1523/JNEUROSCI.3356-04.2004

Hsu, M.-T., Guo, C.-L., Liou, A. Y., Chang, T.-Y., Ng, M.-C., Florea, B. I., et al. (2015). Stage-dependent axon transport of proteasomes contributes to axon development. *Dev. Cell* 35, 418–431. doi: 10.1016/j.devcel.2015.10.018

Innocenti, G. M., and Price, D. J. (2005). Exuberance in the development of cortical networks. *Nat. Rev. Neurosci.* 6, 955–965. doi: 10.1038/nrn1790

Jacobson, M. D., Weil, M., and Raff, M. C. (1997). Programmed cell death in animal development. *Cell* 88, 347–354. doi: 10.1016/S0092-8674(00)81873-5

Jiao, S., and Li, Z. (2011). Nonapoptotic function of BAD and BAX in long-term depression of synaptic transmission. *Neuron* 70, 758–772. doi: 10.1016/j.neuron.2011.04.004

Joazeiro, C. A. P., and Weissman, A. M. (2000). RING finger proteins: mediators of ubiquitin ligase activity. *Cell* 102, 549–552. doi: 10.1016/S0092-8674(00)00077-5

Julien, O., and Wells, J. A. (2017). Caspases and their substrates. *Cell Death Differ.* 24, 1380–1389. doi: 10.1038/cdd.2017.44

Kale, J., Osterlund, E. J., and Andrews, D. W. (2018). BCL-2 family proteins: changing partners in the dance towards death. *Cell Death Differ.* 25, 65–80. doi: 10.1038/cdd.2017.186

Karch, J., Kwong, J. Q., Burr, A. R., Sargent, M. A., Elrod, J. W., Peixoto, P. M., et al. (2013). Bax and Bak function as the outer membrane component of the mitochondrial permeability pore in regulating necrotic cell death in mice. *eLife* 2:e00772. doi: 10.7554/eLife.00772

Karch, J., Schips, T. G., Maliken, B. D., Brody, M. J., Sargent, M. A., Kanisicak, O., et al. (2017). Autophagic cell death is dependent on lysosomal membrane permeability through Bax and Bak. *eLife* 6:e30543. doi: 10.7554/eLife.30543

Katow, H., Kanaya, T., Ogawa, T., Egawa, R., and Yawo, H. (2017). Regulation of axon arborization pattern in the developing chick ciliary ganglion: possible involvement of caspase 3. *Dev. Growth Differ.* 59, 115–128. doi: 10.1111/dgd.12346

Kawai, K., Itoh, T., Itoh, A., Horiuchi, M., Wakayama, K., Bannerman, P., et al. (2009). Maintenance of the relative proportion of oligodendrocytes to axons even in the absence of BAX and BAK. *Eur. J. Neurosci.* 30, 2030–2041. doi: 10.1111/j.1460-9568.2009.06988.x

Ke, F. F. S., Vanyai, H. K., Cowan, A. D., Delbridge, A. R. D., Whitehead, L., Grabow, S., et al. (2018). Embryogenesis and adult life in the absence of intrinsic apoptosis effectors BAX, BAK, and BOK. *Cell* 173, 1217–1230.e17. doi: 10.1016/j.cell.2018.04.036

Khatri, N., Gilbert, J. P., Huo, Y., Sharaflari, R., Nee, M., Qiao, H., et al. (2018). The autism protein Ube3A/E6AP remodels neuronal dendritic arborization via caspase-dependent microtubule destabilization. *J. Neurosci.* 38, 363–378. doi: 10.1523/JNEUROSCI.1511-17.2017

Knudson, C. M., Tung, K. S. K., Tourtellotte, W. G., Brown, G. A. J., and Korsmeyer, S. J. (1995). Bax-Deficient mice with lymphoid hyperplasia and male germ cell death. *Science* 270, 96–99. doi: 10.1126/science.270.5233.96

Kuida, K., Haydar, T. F., Kuan, C.-Y., Gu, Y., Taya, C., Karasuyama, H., et al. (1998). Reduced apoptosis and cytochrome c–mediated caspase activation in mice lacking caspase 9. *Cell* 94, 325–337. doi: 10.1016/S0092-8674(00)81476-2

Kuida, K., Zheng, T. S., Na, S., Kuan, C.-Y., Yang, D., Karasuyama, H., et al. (1996). Decreased apoptosis in the brain and premature lethality in CPP32-deficient mice. *Nature* 384, 368–372. doi: 10.1038/384368a0

Kumar, S. (2007). Caspase function in programmed cell death. *Cell Death Differ.* 14, 32–43. doi: 10.1038/sj.cdd.4402060

Kuranaga, E., and Miura, M. (2007). Nonapoptotic functions of caspases: caspases as regulatory molecules for immunity and cell-fate determination. *Trends Cell Biol.* 17, 135–144. doi: 10.1016/j.tcb.2007.01.001

Lakhani, S. A. (2006). Caspases 3 and 7: key mediators of mitochondrial events of apoptosis. *Science* 311, 847–851. doi: 10.1126/science.1115035

Lartigue, L., Medina, C., Schembri, L., Chabert, P., Zanese, M., Tomasello, F., et al. (2008). An intracellular wave of cytochrome c propagates and precedes Bax redistribution during apoptosis. *J. Cell Sci.* 121, 3515–3523. doi: 10.1242/jcs.029587

Ledonne, F., Orduz, D., Mercier, J., Vigier, L., Grove, E. A., Tissir, F., et al. (2016). Targeted inactivation of Bax reveals a subtype-specific mechanism of cajal-retzius neuron death in the postnatal cerebral cortex. *Cell Rep.* 17, 3133–3141. doi: 10.1016/j.celrep.2016.11.074

Leonard, J. R., Klocke, B. J., D'sa, C., Flavell, R. A., and Roth, K. A. (2002). Strain-Dependent neurodevelopmental abnormalities in caspase-3-deficient mice. *J. Neuropathol. Exp. Neurol.* 61, 673–677. doi: 10.1093/jnen/61.8.673

Li, H., Chen, Y., Jones, A. F., Sanger, R. H., Collis, L. P., Flannery, R., et al. (2008). Bcl-xL induces Drp1-dependent synapse formation in cultured hippocampal neurons. *Proc. Natl. Acad. Sci. U.S.A.* 105, 2169–2174. doi: 10.1073/pnas.0711647105

Li, J., and Yuan, J. (2008). Caspases in apoptosis and beyond. *Oncogene* 27, 6194–6206. doi: 10.1038/onc.2008.297

Li, K., Li, Y., Shelton, J. M., Richardson, J. A., Spencer, E., Chen, Z. J., et al. (2000). Cytochrome c deficiency causes embryonic lethality and attenuates stress-induced apoptosis. *Cell* 101, 389–399. doi: 10.1016/S0092-8674(00)80849-1

Li, Z., Jo, J., Jia, J.-M., Lo, S.-C., Whitcomb, D. J., Jiao, S., et al. (2010). Caspase-3 activation via mitochondria is required for long-term depression and AMPA receptor internalization. *Cell* 141, 859–871. doi: 10.1016/j.cell.2010.03.053

Lindsten, T., Ross, A. J., King, A., Zong, W.-X., Rathmell, J. C., Shiels, H. A., et al. (2000). The combined functions of proapoptotic Bcl-2 family members Bak and Bax are essential for normal development of multiple tissues. *Mol. Cell* 6, 1389–1399. doi: 10.1016/s1097-2765(00)00136-2

Liu, X., Zhang, Q., Jiang, Q., Bai, B., Du, X., Wang, F., et al. (2018). Genetic screening and functional analysis of CASP9 mutations in a Chinese cohort with neural tube defects. *CNS Neurosci. Ther.* 24, 394–403. doi: 10.1111/cns.12797

Lo, S.-C., Wang, Y., Weber, M., Larson, J. L., Scearce-Levie, K., and Sheng, M. (2015). Caspase-3 deficiency results in disrupted synaptic homeostasis and impaired attention control. *J. Neurosci.* 35, 2118–2132. doi: 10.1523/JNEUROSCI.3280-14.2015

Martinon, F., and Tschopp, J. (2004). Inflammatory caspases: linking an intracellular innate immune system to autoinflammatory diseases. *Cell* 117, 561–574. doi: 10.1016/j.cell.2004.05.004

Mashima, T., Naito, M., and Tsuruo, T. (1999). Caspase-mediated cleavage of cytoskeletal actin plays a positive role in the process of morphological apoptosis. *Oncogene* 18, 2423–2430. doi: 10.1038/sj.onc.1202558

Massa, V., Savery, D., Ybot-Gonzalez, P., Ferraro, E., Rongvaux, A., Cecconi, F., et al. (2009). Apoptosis is not required for mammalian neural tube closure. *Proc. Natl. Acad. Sci. U.S.A.* 106, 8233–8238. doi: 10.1073/pnas.0900333106

Michaelidis, T. M., Sendtner, M., Cooper, J. D., Airaksinen, M. S., Holtmann, B., Meyer, M., et al. (1996). Inactivation of bcl-2 results in progressive degeneration of motoneurons, sympathetic and sensory neurons during early postnatal development. *Neuron* 17, 75–89. doi: 10.1016/S0896-6273(00)80282-2

Motoyama, N., Wang, F., Roth, K., Sawa, H., Nakayama, K., Nakayama, K., et al. (1995). Massive cell death of immature hematopoietic cells and neurons in Bcl-x-deficient mice. *Science* 267, 1506–1510. doi: 10.1126/science.7878471

Mukherjee, A., and Williams, D. W. (2017). More alive than dead: non-apoptotic roles for caspases in neuronal development, plasticity and disease. *Cell Death Differ.* 24, 1411–1421. doi: 10.1038/cdd.2017.64

Nakamura, A., Swahari, V., Plestant, C., Smith, I., McCoy, E., Smith, S., et al. (2016). Bcl-xL is essential for the survival and function of differentiated neurons in the cortex that control complex behaviors. *J. Neurosci.* 36, 5448–5461. doi: 10.1523/JNEUROSCI.4247-15.2016

Neuspiel, M., Schauss, A. C., Braschi, E., Zunino, R., Rippstein, P., Rachubinski, R. A., et al. (2008). Cargo-selected transport from the mitochondria to peroxisomes is mediated by vesicular carriers. *Curr. Biol.* 18, 102–108. doi: 10.1016/j.cub.2007.12.038

Nikolaev, A., McLaughlin, T., O'Leary, D. D. M., and Tessier-Lavigne, M. (2009). APP binds DR6 to trigger axon pruning and neuron death via distinct caspases. *Nature* 457, 981–989. doi: 10.1038/nature07767

Nonomura, K., Yamaguchi, Y., Hamachi, M., Koike, M., Uchiyama, Y., Nakazato, K., et al. (2013). Local apoptosis modulates early mammalian brain development through the elimination of morphogen-producing cells. *Dev. Cell* 27, 621–634. doi: 10.1016/j.devcel.2013.11.015

Ohsawa, S., Hamada, S., Kuida, K., Yoshida, H., Igaki, T., and Miura, M. (2010). Maturation of the olfactory sensory neurons by Apaf-1/caspase-9-mediated caspase activity. *Proc. Natl. Acad. Sci. U.S.A.* 107, 13366–13371. doi: 10.1073/pnas.0910488107

Otero, M. G., Alloatti, M., Cromberg, L. E., Almenar-Queralt, A., Encalada, S. E., Devoto, V. M. P., et al. (2014). Fast axonal transport of the proteasome complex depends on membrane interaction and molecular motor function. *J. Cell Sci.* 127, 1537–1549. doi: 10.1242/jcs.140780

Pacheco, A., and Gallo, G. (2016). Actin filament-microtubule interactions in axon initiation and branching. *Brain Res. Bull.* 126, 300–310. doi: 10.1016/j.brainresbull.2016.07.013

Pacher, P., and Hajnóczky, G. (2001). Propagation of the apoptotic signal by mitochondrial waves. *EMBO J.* 20, 4107–4121. doi: 10.1093/emboj/20.15.4107

Paridaen, J. T., and Huttner, W. B. (2014). Neurogenesis during development of the vertebrate central nervous system. *EMBO Rep.* 15, 351–364. doi: 10.1002/embr.201438447

Parrish, A. B., Freel, C. D., and Kornbluth, S. (2013). Cellular mechanisms controlling caspase activation and function. *Cold Spring Harb. Perspect. Biol.* 5:a008672. doi: 10.1101/cshperspect.a008672

Péquignot, M. O., Provost, A. C., Sallé, S., Taupin, P., Sainton, K. M., Marchant, D., et al. (2003). Major role of BAX in apoptosis during retinal development and in establishment of a functional postnatal retina. *Dev. Dyn.* 228, 231–238. doi: 10.1002/dvdy.10376

Petros, A. M., Olejniczak, E. T., and Fesik, S. W. (2004). Structural biology of the Bcl-2 family of proteins. *Biochim. Biophys. Acta* 1644, 83–94. doi: 10.1016/j.bbamcr.2003.08.012

Pinan-Lucarre, B., Gabel, C. V., Reina, C. P., Hulme, S. E., Shevkoplyas, S. S., Slone, R. D., et al. (2012). The core apoptotic executioner proteins CED-3 and CED-4 promote initiation of neuronal regeneration in *Caenorhabditis elegans*. *PLoS Biol.* 10:e1001331. doi: 10.1371/journal.pbio.1001331

Purves, D., Augustine, G. J., Fitzpatrick, D., Hall, W. C., LaMantia, A.-S., Mooney, R. D., et al. (2018). *Neuroscience*. New York, NY: Oxford University Press.

Raina, D., Pandey, P., Ahmad, R., Bharti, A., Ren, J., Kharbanda, S., et al. (2005). c-Abl tyrosine kinase regulates caspase-9 autocleavage in the apoptotic response to DNA damage*. *J. Biol. Chem.* 280, 11147–11151. doi: 10.1074/jbc.M413787200

Raz, V., Carlotti, F., Vermolen, B. J., van der Poel, E., Sloos, W. C. R., Knaän-Shanzer, S., et al. (2006). Changes in lamina structure are followed by spatial reorganization of heterochromatic regions in caspase-8-activated human mesenchymal stem cells. *J. Cell Sci.* 119, 4247–4256. doi: 10.1242/jcs.03180

Ribeil, J.-A., Zermati, Y., Vandekerckhove, J., Cathelin, S., Kersual, J., Dussiot, M., et al. (2007). Hsp70 regulates erythropoiesis by preventing caspase-3-mediated cleavage of GATA-1. *Nature* 445, 102–105. doi: 10.1038/nature05378

Rodriguez, J., and Lazebnik, Y. (1999). Caspase-9 and APAF-1 form an active holoenzyme. *Genes Dev.* 13, 3179–3184. doi: 10.1101/gad.13.24.3179

Sakamaki, K., Inoue, T., Asano, M., Sudo, K., Kazama, H., Sakagami, J., et al. (2002). Ex vivo whole-embryo culture of caspase-8-deficient embryos normalize their aberrant phenotypes in the developing neural tube and heart. *Cell Death Differ.* 9, 1196–1206. doi: 10.1038/sj.cdd.4401090

Scorrano, L., Oakes, S. A., Opferman, J. T., Cheng, E. H., Sorcinelli, M. D., Pozzan, T., et al. (2003). BAX and BAK regulation of endoplasmic reticulum Ca2+: a control point for apoptosis. *Science* 300, 135–139. doi: 10.1126/science.1081208

Serrano, B. P., and Hardy, J. A. (2018). Phosphorylation by protein kinase A disassembles the caspase-9 core. *Cell Death Differ.* 25, 1025–1039. doi: 10.1038/s41418-017-0052-9

Serrano, B. P., Szydlo, H. S., Alfandari, D., and Hardy, J. A. (2017). Active site–adjacent phosphorylation at Tyr-397 by c-Abl kinase inactivates caspase-9. *J. Biol. Chem.* 292, 21352–21365. doi: 10.1074/jbc.M117.811976

Shalini, S., Dorstyn, L., Dawar, S., and Kumar, S. (2015). Old, new and emerging functions of caspases. *Cell Death Differ.* 22, 526–539. doi: 10.1038/cdd.2014.216

Simon, D. J., Weimer, R. M., McLaughlin, T., Kallop, D., Stanger, K., Yang, J., et al. (2012). A caspase cascade regulating developmental axon degeneration. *J. Neurosci.* 32, 17540–17553. doi: 10.1523/JNEUROSCI.3012-12.2012

Singh, R., Letai, A., and Sarosiek, K. (2019). Regulation of apoptosis in health and disease: the balancing act of BCL-2 family proteins. *Nat. Rev. Mol. Cell Biol.* 20, 175–193. doi: 10.1038/s41580-018-0089-8

Slee, E. A., Adrain, C., and Martin, S. J. (2001). Executioner caspase-3, -6, and -7 perform distinct, non-redundant roles during the demolition phase of apoptosis*. *J. Biol. Chem.* 276, 7320–7326. doi: 10.1074/jbc.M008363200

Smith, J. L., and Schoenwolf, G. C. (1997). Neurulation: coming to closure. *Trends Neurosci.* 20, 510–517. doi: 10.1016/S0166-2236(97)01121-1

Sokolowski, J. D., Gamage, K. K., Heffron, D. S., LeBlanc, A. C., Deppmann, C. D., and Mandell, J. W. (2014). Caspase-mediated cleavage of actin and tubulin is a common feature and sensitive marker of axonal degeneration in neural development and injury. *Acta Neuropathol. Commun.* 2:16. doi: 10.1186/2051-5960-2-16

Spellicy, C. J., Norris, J., Bend, R., Bupp, C., Mester, P., Reynolds, T., et al. (2018). Key apoptotic genes APAF1 and CASP9 implicated in recurrent folate-resistant neural tube defects. *Eur. J. Hum. Genet.* 26, 420–427. doi: 10.1038/s41431-017-0025-y

Stiles, J., and Jernigan, T. L. (2010). The basics of brain development. *Neuropsychol. Rev.* 20, 327–348. doi: 10.1007/s11065-010-9148-4

Suzanne, M., and Steller, H. (2013). Shaping organisms with apoptosis. *Cell Death Differ.* 20, 669–675. doi: 10.1038/cdd.2013.11

Tait, S. W. G., Parsons, M. J., Llambi, F., Bouchier-Hayes, L., Connell, S., Muñoz-Pinedo, C., et al. (2010). Resistance to caspase-independent cell death requires persistence of intact mitochondria. *Dev. Cell* 18, 802–813. doi: 10.1016/j.devcel.2010.03.014

Taylor, R. C., Cullen, S. P., and Martin, S. J. (2008). Apoptosis: controlled demolition at the cellular level. *Nat. Rev. Mol. Cell Biol.* 9, 231–241. doi: 10.1038/nrm2312

Unsain, N., Higgins, J. M., Parker, K. N., Johnstone, A. D., and Barker, P. A. (2013). XIAP regulates caspase activity in degenerating axons. *Cell Rep.* 4, 751–763. doi: 10.1016/j.celrep.2013.07.015

Uribe, V., Wong, B. K. Y., Graham, R. K., Cusack, C. L., Skotte, N. H., Pouladi, M. A., et al. (2012). Rescue from excitotoxicity and axonal degeneration accompanied by age-dependent behavioral and neuroanatomical alterations in caspase-6-deficient mice. *Hum. Mol. Genet.* 21, 1954–1967. doi: 10.1093/hmg/dds005

Varfolomeev, E. E., Schuchmann, M., Luria, V., Chiannilkulchai, N., Beckmann, J. S., Mett, I. L., et al. (1998). Targeted disruption of the mouse caspase 8 gene ablates cell death induction by the TNF receptors, Fas/Apo1, and DR3 and is lethal prenatally. *Immunity* 9, 267–276. doi: 10.1016/S1074-7613(00)80609-3

Verma, P. (2005). Axonal protein synthesis and degradation are necessary for efficient growth cone regeneration. *J. Neurosci.* 25, 331–342. doi: 10.1523/JNEUROSCI.3073-04.2005

Voss, O. H., Kim, S., Wewers, M. D., and Doseff, A. I. (2005). Regulation of monocyte apoptosis by the protein kinase cδ-dependent phosphorylation of caspase-3*. *J. Biol. Chem.* 280, 17371–17379. doi: 10.1074/jbc.M412449200

Walsh, J. G., Cullen, S. P., Sheridan, C., Lüthi, A. U., Gerner, C., and Martin, S. J. (2008). Executioner caspase-3 and caspase-7 are functionally distinct proteases. *Proc. Natl. Acad. Sci. U.S.A.* 105, 12815–12819. doi: 10.1073/pnas.0707715105

Wang, G., Sun, L., Reina, C. P., Song, I., Gabel, C. V., and Driscoll, M. (2019). CED-4 CARD domain residues can modulate non-apoptotic neuronal regeneration functions independently from apoptosis. *Sci. Rep.* 9:13315. doi: 10.1038/s41598-019-49633-9

Wang, J.-Y., Chen, F., Fu, X.-Q., Ding, C.-S., Zhou, L., Zhang, X.-H., et al. (2014). Caspase-3 cleavage of dishevelled induces elimination of postsynaptic structures. *Dev. Cell* 28, 670–684. doi: 10.1016/j.devcel.2014.02.009

Washausen, S., Scheffel, T., Brunnett, G., and Knabe, W. (2018). Possibilities and limitations of three-dimensional reconstruction and simulation techniques to identify patterns, rhythms and functions of apoptosis in the early developing neural tube. *Hist. Philos. Life Sci.* 40:55. doi: 10.1007/s40656-018-0222-1

Weghorst, F., Mirzakhanyan, Y., Samimi, K., Dhillon, M., Barzik, M., Cunningham, L. L., et al. (2020). Caspase-3 cleaves extracellular vesicle proteins during auditory brainstem development. *Front. Cell. Neurosci.* 14:573345. doi: 10.3389/fncel.2020.573345

Weil, M., Jacobson, M. D., and Raff, M. C. (1997). Is programmed cell death required for neural tube closure? *Curr. Biol.* 7, 281–284. doi: 10.1016/S0960-9822(06)00125-4

Westphal, D., Sytnyk, V., Schachner, M., and Leshchyns'ka, I. (2010). Clustering of the neural cell adhesion molecule (NCAM) at the neuronal cell surface induces caspase-8- and -3-dependent changes of the spectrin meshwork required for NCAM-mediated neurite outgrowth. *J. Biol. Chem.* 285, 42046–42057. doi: 10.1074/jbc.M110.177147

Wickman, G., Julian, L., and Olson, M. F. (2012). How apoptotic cells aid in the removal of their own cold dead bodies. *Cell Death Differ.* 19, 735–742. doi: 10.1038/cdd.2012.25

Yamaguchi, Y., and Miura, M. (2015). Programmed cell death in neurodevelopment. *Dev. Cell* 32, 478–490. doi: 10.1016/j.devcel.2015.01.019

Yoshida, H., Kong, Y.-Y., Yoshida, R., Elia, A. J., Hakem, A., Hakem, R., et al. (1998). Apaf1 is required for mitochondrial pathways of apoptosis and brain development. *Cell* 94, 739–750. doi: 10.1016/S0092-8674(00)81733-X

Youle, R. J., and Strasser, A. (2008). The BCL-2 protein family: opposing activities that mediate cell death. *Nat. Rev. Mol. Cell Biol.* 9, 47–59. doi: 10.1038/nrm2308

Yuan, J., and Yankner, B. A. (2000). Apoptosis in the nervous system. *Nature* 407, 802–809. doi: 10.1038/35037739

Yuan, J., Shaham, S., Ledoux, S., Ellis, H. M., and Horvitz, H. R. (1993). The C. elegans cell death gene ced-3 encodes a protein similar to mammalian interleukin-1β-converting enzyme. *Cell* 75, 641–652. doi: 10.1016/0092-8674(93)90485-9

Zamaraev, A. V., Kopeina, G. S., Prokhorova, E. A., Zhivotovsky, B., and Lavrik, I. N. (2017). Post-translational modification of caspases: the other side of apoptosis regulation. *Trends Cell Biol.* 27, 322–339. doi: 10.1016/j.tcb.2017.01.003

Zhang, D., and Armstrong, J. S. (2007). Bax and the mitochondrial permeability transition cooperate in the release of cytochrome c during endoplasmic reticulum-stress-induced apoptosis. *Cell Death Differ.* 14, 703–715. doi: 10.1038/sj.cdd.4402072

Zhang, J., Webster, J. D., Dugger, D. L., Goncharov, T., Roose-Girma, M., Hung, J., et al. (2019). Ubiquitin ligases cIAP1 and cIAP2 limit cell death to prevent inflammation. *Cell Rep.* 27, 2679–2689.e3. doi: 10.1016/j.celrep.2019.04.111

Zhang, M., Zheng, J., Nussinov, R., and Ma, B. (2017). Release of cytochrome C from Bax pores at the mitochondrial membrane. *Sci. Rep.* 7:2635. doi: 10.1038/s41598-017-02825-7

Zhou, X., Zeng, W., Li, H., Chen, H., Wei, G., Yang, X., et al. (2018). Rare mutations in apoptosis related genes APAF1, CASP9, and CASP3 contribute to human neural tube defects. *Cell Death Dis.* 9:43. doi: 10.1038/s41419-017-0096-2

Ziegler, D. V., Vindrieux, D., Goehrig, D., Jaber, S., Collin, G., Griveau, A., et al. (2021). Calcium channel ITPR2 and mitochondria–ER contacts promote cellular senescence and aging. *Nat. Commun.* 12:720. doi: 10.1038/s41467-021-20993-z

Conflict of Interest: The authors declare that the research was conducted in the absence of any commercial or financial relationships that could be construed as a potential conflict of interest.

frontiers in Cell and Developmental Biology

ORIGINAL RESEARCH
published: 07 October 2021
doi: 10.3389/fcell.2021.704730

The Ribosome Biogenesis Factor Ltv1 Is Essential for Digestive Organ Development and Definitive Hematopoiesis in Zebrafish

Chong Zhang, Rui Huang, Xirui Ma, Jiehui Chen, Xinlu Han, Li Li, Lingfei Luo, Hua Ruan and Honghui Huang**

Key Laboratory of Freshwater Fish Reproduction and Development, Ministry of Education, State Key Laboratory Breeding Base of Eco-Environments and Bio-Resources of the Three Gorges Reservoir Region, School of Life Sciences, Southwest University, Chongqing, China

Ribosome biogenesis is a fundamental activity in cells. Ribosomal dysfunction underlies a category of diseases called ribosomopathies in humans. The symptomatic characteristics of ribosomopathies often include abnormalities in craniofacial skeletons, digestive organs, and hematopoiesis. Consistently, disruptions of ribosome biogenesis in animals are deleterious to embryonic development with hypoplasia of digestive organs and/or impaired hematopoiesis. In this study, *ltv1*, a gene involved in the small ribosomal subunit assembly, was knocked out in zebrafish by clustered regularly interspaced short palindromic repeats (CRISPRs)/CRISPR associated protein 9 (Cas9) technology. The recessive lethal mutation resulted in disrupted ribosome biogenesis, and $ltv1^{\Delta 14/\Delta 14}$ embryos displayed hypoplastic craniofacial cartilage, digestive organs, and hematopoiesis. In addition, we showed that the impaired cell proliferation, instead of apoptosis, led to the defects in exocrine pancreas and hematopoietic stem and progenitor cells (HSPCs) in $ltv1^{\Delta 14/\Delta 14}$ embryos. It was reported that loss of function of genes associated with ribosome biogenesis often caused phenotypes in a P53-dependent manner. In $ltv1^{\Delta 14/\Delta 14}$ embryos, both P53 protein level and the expression of *p53* target genes, *Δ113p53* and *p21*, were upregulated. However, knockdown of *p53* failed to rescue the phenotypes in $ltv1^{\Delta 14/\Delta 14}$ larvae. Taken together, our data demonstrate that LTV1 ribosome biogenesis factor (Ltv1) plays an essential role in digestive organs and hematopoiesis development in zebrafish in a P53-independent manner.

Keywords: Ltv1, ribosome biogenesis, digestive organs, hematopoiesis, P53

OPEN ACCESS

Edited by:
Wolfgang Knabe,
University of Münster, Germany

Reviewed by:
Nadine Hein,
Australian National University, Australia
Anthony Henras,
Université de Toulouse, France
Seth Corey,
Cleveland Clinic, United States

****Correspondence:***
Hua Ruan
ruanhua23@126.com
Honghui Huang
honghuih@126.com

Specialty section:
This article was submitted to Cell Death and Survival, a section of the journal Frontiers in Cell and Developmental Biology

Received: *03 May 2021*
Accepted: *13 September 2021*
Published: *07 October 2021*

Citation:
Zhang C, Huang R, Ma X, Chen J, Han X, Li L, Luo L, Ruan H and Huang H (2021) The Ribosome Biogenesis Factor Ltv1 Is Essential for Digestive Organ Development and Definitive Hematopoiesis in Zebrafish. Front. Cell Dev. Biol. 9:704730. doi: 10.3389/fcell.2021.704730

INTRODUCTION

The ribosome is a fundamental macromolecular machine, found within all living cells, that synthesizes proteins according to mRNA sequences. Ribosome biogenesis is a very intricate process in cells (Warner, 2001). Eukaryotic ribosome consists of the large 60S and small 40S subunits, which are assembled to form the functional 80S ribosome. In addition to the four ribosomal RNAs (rRNAs) and 82 core ribosomal proteins, which are the components of the 80S ribosome, over 200 non-ribosomal proteins are involved in ribosome biogenesis. This precisely controlled process is inextricably associated with many fundamental cellular activities, such as growth and division (Panse and Johnson, 2010). Disruption of ribosome biogenesis leads to a

class of human genetic diseases, collectively termed as ribosomopathies (Narla and Ebert, 2010). Although these diseases are all related to the ribosome dysfunction, ribosomopathies display different clinical manifestations and mechanisms. The symptomatic features of ribosomopathies often include craniofacial defects, digestive organs dysplasia, hematological abnormalities, and the increased risk of some blood cancers (Narla and Ebert, 2010). Ribosomopathies with defects in digestive organs and/or hematological abnormalities include Shwachman-Diamond syndrome (SDS), 5q-syndrome, Diamond-Blackfan anemia (DBA), X-linked dyskeratosis congenita (DC), Treacher Collins syndrome (TCS), and North American Indian childhood cirrhosis (NAIC) (Armistead and Triggs-Raine, 2014).

Numerous genetic models have been established for the investigation of the mechanisms underlying ribosomopathies. In mice, conditional deletion of the syntenic region, including *Rps14*, absent in 5q-syndrome leads to macrocytic anemia, which is the key clinical feature of the disease (Barlow et al., 2010). In zebrafish, knockdown of *rps19* expression causes hematopoietic and developmental abnormalities that is similar to the symptoms of DBA (Danilova et al., 2008). Besides DBA, zebrafish models of SDS (Provost et al., 2012; Carapito et al., 2017; Oyarbide et al., 2020), 5q-syndrome (Ear et al., 2016), NAIC (Wilkins et al., 2013), and DC (Zhang et al., 2012; Anchelin et al., 2013) were generated and characterized. These models are valuable resources to develop potential therapies of ribosomopathies according to the underlying mechanisms. In addition to causative genes in ribosomopathies, some other genes involved in ribosome biogenesis were either mutated or knocked down in zebrafish, such as *bms1l* (Wang et al., 2012, 2016), *kri1l* (Jia et al., 2015), *nol9* (Bielczyk-Maczynska et al., 2015), *nom1* (Qin et al., 2014), and *pwp2h* (Boglev et al., 2013). Depletion of these genes causes disrupted rRNA processing and leads to defects in digestive organs and/or hematological abnormalities, which suggest common roles for ribosome biogenesis factors in organogenesis.

Evidences from a number of animal models of ribosomopathies suggest that P53 is often activated in ribosome dysfunction (Danilova et al., 2008, 2011; Jones et al., 2008; Fumagalli et al., 2009; Barlow et al., 2010; Pereboom et al., 2011; Taylor et al., 2012; Zhang et al., 2012; Boglev et al., 2013; Wilkins et al., 2013; Qin et al., 2014; Bielczyk-Maczynska et al., 2015; Ear et al., 2016). In some cases, inhibition of *p53* is able to rescue the phenotypes (Danilova et al., 2008, 2011; Jones et al., 2008; Barlow et al., 2010; Pereboom et al., 2011; Taylor et al., 2012; Zhang et al., 2012; Bielczyk-Maczynska et al., 2015; Ear et al., 2016), but not in others (Provost et al., 2012; Boglev et al., 2013; Jia et al., 2015). These studies suggest that targeting the P53 pathway could be a therapeutic strategy. However, it should be noted that being a tumor suppression gene, *p53* inhibition may increase risk of cancer development.

LTV1 ribosome biogenesis factor (Ltv1) is a non-ribosomal factor required for the processing of 40S ribosomal subunit (Ameismeier et al., 2018; Collins et al., 2018). Alterations of LTV1 can cause aberrant processing of 18S rRNA in yeast, fruit fly and human cells (Seiser et al., 2006; Tafforeau et al., 2011; Ghalei et al., 2015; Kressler et al., 2015). In Δ*LTV1* yeast cells, the accumulation of 18S rRNA precursors (20S, 21S, and 23S rRNA) is evident, accounted by the decreased pre-rRNA cleavage at sites A0, A1, and A2 (Seiser et al., 2006). Similarly, in fruit fly and human cells, LTV1 deficiency leads to increased level of 21S rRNA, hence a reduced production of the final 18S rRNA and eventually a higher than expected ratio of 28S/18S rRNA (Tafforeau et al., 2011; Kressler et al., 2015). Cell growth is inhibited in *LTV1* loss-of-function yeast strains (Seiser et al., 2006). The fruit fly *LTV1* mutant larvae exhibit development delay and lethality at the second larvae stage (Kressler et al., 2015). These studies suggest the conserved role of *LTV1* in ribosome biogenesis and cell growth from yeast to multicellular animals. However, the function of *LTV1* in vertebrate development remains poorly understood.

Here, we reported that knockout of *ltv1* in zebrafish embryo disrupted ribosome biogenesis. The zebrafish $ltv1^{\Delta 14/\Delta 14}$ larvae displayed aberrant cartilage structure, defects in digestive organs, characterized by smaller size of liver, intestine and exocrine pancreas, and impaired definitive hematopoiesis. Further characterization of $ltv1^{\Delta 14/\Delta 14}$ larvae showed that the decreased proliferation gave rise to the dysplastic features of exocrine pancreas and hematopoietic stem and progenitor cells (HSPCs). Although P53 and its target genes Δ*113p53* and *p21* were upregulated, knockdown of *p53* failed to rescue the developmental abnormalities in $ltv1^{\Delta 14/\Delta 14}$ mutant.

RESULTS

Craniofacial Cartilage Was Defective in $ltv1^{\Delta 14/\Delta 14}$ Zebrafish Mutant Embryo

Ltv1 is highly conserved by amino acid sequence homology between human and zebrafish, with approximately 60.9% identity and 76.2% similarity (**Supplementary Figure 1**). To determine the function of *ltv1*, zebrafish $ltv1^{-/-}$ mutants were generated using the clustered regularly interspaced short palindromic repeat (CRISPR)/CRISPR associated protein 9 (Cas9)-mediated approach, and a guide RNA (gRNA) was designed to target the exon 7 of *ltv1*. Two F1 mutant alleles were identified with 14 and 7 bp nucleotides deletion, respectively in the coding region (**Figure 1A**). Both mutations were predicted to result in frame shifts and premature stop codons in mutant transcripts, encoding two truncated Ltv1 proteins with 284 and 283 N-terminal and 32 and 31 missense amino acids, respectively (**Figure 1B**). These two mutant alleles could not genetically complement each other, and the $ltv1^{\Delta 14/\Delta 14}$ mutant allele was used for the following experiments. RNA whole mount *in situ* hybridization (WISH) showed that *ltv1* transcripts were almost absent in $ltv1^{\Delta 14/\Delta 14}$ mutant at 3 days post fertilization (dpf), indicating that the knockout of *ltv1* was successful (**Figure 1C**). The mutant mRNA probably underwent a nonsense-mediated decay.

The $ltv1^{\Delta 14/\Delta 14}$ mutant embryos were morphologically indistinguishable from siblings before 2 dpf with normal blood flow and heart beating. However, at 3 dpf, $ltv1^{\Delta 14/\Delta 14}$ mutants displayed pericardial edema and aplasia in the head (**Figure 1D**). At 5 dpf, mutants exhibited underdeveloped intestine, smaller

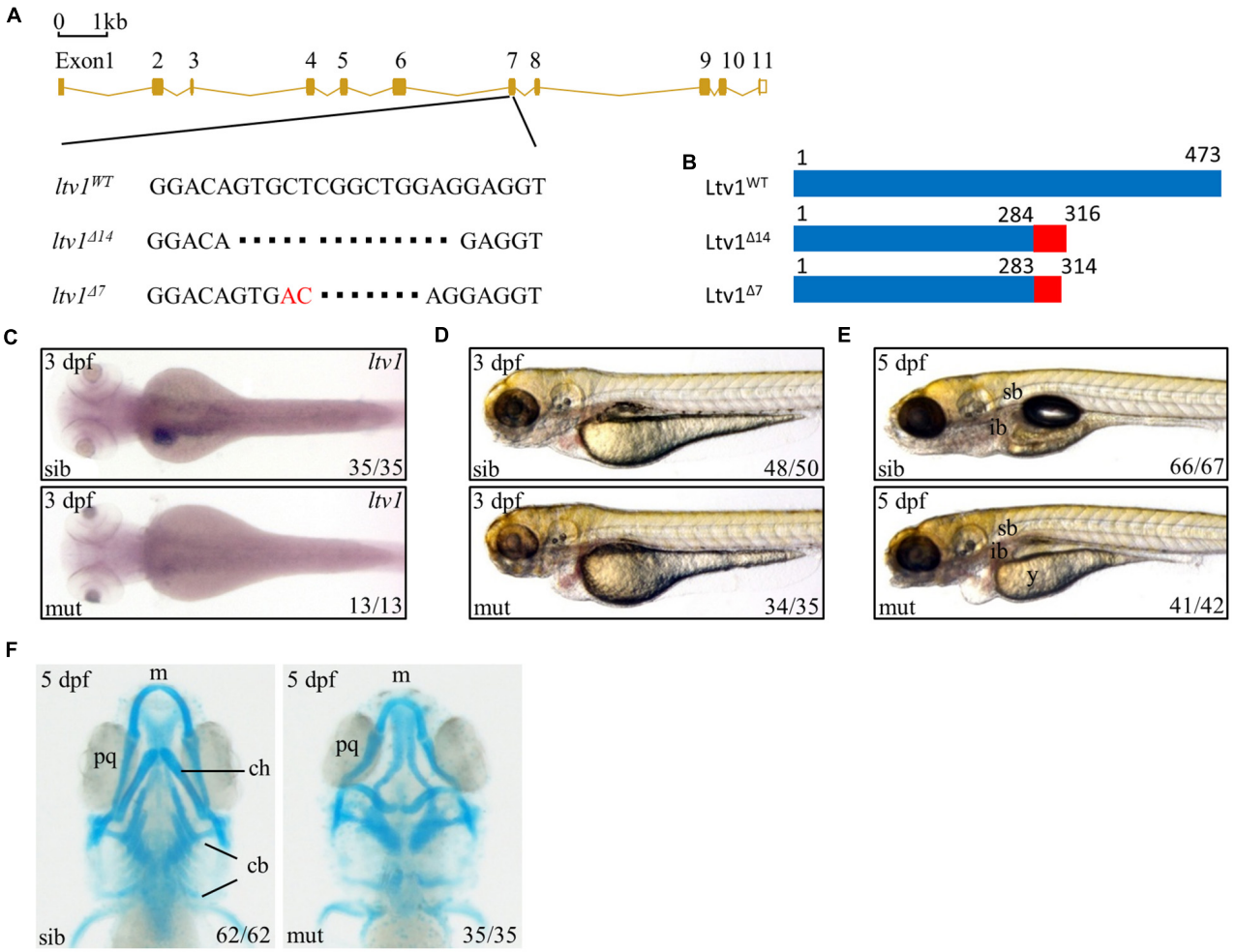

FIGURE 1 | Knockout of *ltv1* and craniofacial defects in *ltv1*$^{\Delta 14/\Delta 14}$ mutant. **(A)** The sequences flanking the deletion site in *ltv1* mutants (*ltv1*$^{\Delta 7,14}$) are shown. The deleted nucleotides are denoted by dashes. In *ltv1*$^{\Delta 7/\Delta 7}$ mutant, 9 bp nucleotides are deleted and 2 bp nucleotides (red font) are inserted. **(B)** Two *ltv1* mutant alleles (*ltv1*$^{\Delta 14}$ and *ltv1*$^{\Delta 7}$) harbor frameshift mutations that are predicted to give rise to truncated Ltv1 proteins as shown. **(C)** WISH using *ltv1* antisense RNA probe at 3 dpf. **(D,E)** Representative images of *ltv1*$^{\Delta 14/\Delta 14}$ mutants and siblings at 3 and 5 dpf. **(F)** Alcian blue-labeled craniofacial cartilage in ventral view at 5 dpf. Abbreviations used: sb, swimming bladder; ib, intestinal bulb; y, yolk; m, Meckel's; pq, palatoquadrate; ch, ceratohyal; cb, ceratobranchial.

liver, uninflated swim bladder, and impaired yolk absorption (**Figure 1E**). These phenotypes were completely penetrant and the mutant larvae died from 8 to 11 dpf.

Disruption of ribosome biogenesis can cause abnormal craniofacial skeletons in zebrafish (Mayer and Fishman, 2003; Provost et al., 2012; Qin et al., 2014). Thus, Alcian blue staining was performed to check the craniofacial cartilage structure of *ltv1*$^{\Delta 14/\Delta 14}$ mutant. At 5 dpf, mutants displayed severe abnormalities in craniofacial cartilage, including smaller Meckel's cartilage, curly palatoquadrate and lack of ceratohyal, and five ceratobranchial cartilage (**Figure 1F**).

Digestive Organs Were Hypoplastic in *ltv1*$^{\Delta 14/\Delta 14}$ Mutant Embryo

To further characterize the digestive organ phenotype observed in bright field, WISH was performed to analyze the specific organ formation. Both the liver (marked by *fabp10*) and exocrine pancreas (marked by *trypsin*) of *ltv1*$^{\Delta 14/\Delta 14}$ displayed a smaller size compared with sibling at 3 dpf (**Figures 2A–C**). However, no visible defect was found in the endocrine pancreas (marked by *insulin*) (**Figure 2D**). In zebrafish, differentiated intestinal cells include three types: enterocytes, goblet cells, and enteroendocrine cells (Chen et al., 2009). In *ltv1*$^{\Delta 14/\Delta 14}$ mutant, enterocytes (marked by *fabp2*) at 3 dpf (**Figure 2E**) and goblet cells (Alcian blue-stained) at 5 dpf (**Figures 2F,H**) were substantially decreased in number. In zebrafish, both the enteroendocrine and goblet cells of the intestine could be labeled by 2F11 monoclonal antibody (Roach et al., 2013). In zebrafish, goblet cells are only distributed in the posterior part (Roach et al., 2013), not in the intestine bulb, so the 2F11 antibody marked cells in the intestine bulb are enteroendocrine cells. The number of enteroendocrine cells in the intestine bulb was reduced significantly in *ltv1*$^{\Delta 14/\Delta 14}$ mutant at 4 dpf (**Figures 2G,H**). To examine the gut morphology,

DCFH-DA, a dye that could label zebrafish gut lumen, was used to visualize the intestine. At 5 dpf, although the overall shape of the mutant intestine resembled that of the sibling, the lumen was narrower than that of the sibling (**Figure 2I**).

Developmental defects of digestive organs could be due to impaired differentiation of endodermal cells. The genes *foxA1*, *foxA3*, and *gata6* are early endodermal markers that can also label digestive organ primordia in zebrafish (Tao and Peng, 2009). These three genes expressed normally in the *ltv1*$^{\Delta 14/\Delta 14}$ mutant endoderm at 1 dpf (data not shown). Both liver and pancreatic buds were found to be smaller in the mutant than that in the sibling, while the intestine seemed normal at 2 dpf (**Figures 2J,K** and **Supplementary Figures 2A,B**). These data suggested that the process from the endoderm to bud initiation was intact whereas bud expansion, taking place at a later stage, was affected in the mutant. To test whether liver specification was impaired in the *ltv1*$^{\Delta 14/\Delta 14}$ mutant, two of the earliest markers of hepatoblasts, *prox1* and *hhex*, were analyzed (Ober et al., 2006). Consistent with *foxA1*, *foxA3*, and *gata6*, the expression of *prox1* and *hhex* revealed a slightly smaller liver bud in the mutant compared with the sibling at 2 dpf (**Supplementary Figures 2C,D**). A noticeable hypoplastic liver phenotype in the *ltv1*$^{\Delta 14/\Delta 14}$ mutants could be observed at 34 hours post fertilization (hpf) by tracing the *prox1* expression at earlier developmental time points (**Supplementary Figures 2E,F**). There are two types of glandular tissue in the zebrafish pancreas: exocrine pancreas and endocrine pancreas (Field et al., 2003). By checking *pdx1* (precursor cell of endocrine pancreas), *gcga* (alpha cell), *insulin* (beta cell), and *sst2* (delta cell) expression at 2 dpf, no obvious defect was observed in *ltv1*$^{\Delta 14/\Delta 14}$ mutants (**Supplementary Figures 2G–J**). These data suggested that cell differentiation of endocrine pancreas was not affected in the mutant. However, the number of *ptf1a*$^{+}$ cells (exocrine pancreas progenitor cells) decreased significantly at 2 dpf in the *ltv1*$^{\Delta 14/\Delta 14}$ mutant on the *ptf1a:gfp* background (**Supplementary Figures 2K,L**). Thus, hypoplasia of digestive organs in *ltv1*$^{\Delta 14/\Delta 14}$ mutant embryos could be a consequence of impaired organ progenitor cell expansion.

The *ltv1*$^{\Delta 14/\Delta 14}$ Mutation Impaired Definitive Hematopoiesis During Embryogenesis

Hematopoietic defects are usually related to the ribosome biogenesis gene deficiency in zebrafish (Oyarbide et al., 2019). Therefore, to figure out the role of *ltv1* in hematopoiesis, different blood cell lineages were examined. HSPCs (marked by *c-myb*, *ikaros*, and *runx1* transgene) in the mutant were pronouncedly reduced in the caudal hematopoietic tissue (CHT), thymus and kidney at 4 dpf (**Figures 3A–D**). In addition, blood cell lineage markers, such as *gata1* (erythrocyte progenitors), α*e1* (erythrocytes), *mfap4* (macrophages), *csf1ra* (macrophages), *lyz* (neutrophils), *rag1* (lymphocytes), and Sudan Black (neutrophils) staining, were all significantly reduced in the *ltv1*$^{\Delta 14/\Delta 14}$ mutant at 4 dpf (**Figures 3E–L**), indicating the impaired development of definitive erythrocytes, myeloid cells, and lymphocytes.

Two waves of hematopoiesis are involved in zebrafish: the primitive wave and the definitive wave (Jagannathan-Bogdan and Zon, 2013). To assess the status of primitive hematopoiesis in the *ltv1*$^{\Delta 14/\Delta 14}$ mutant, two genes regulating the primitive erythroid and myeloid fates, *gata1* and *pu.1*, were examined using WISH at 20 and 22 hpf, respectively, and no visible defect was observed in the mutant (**Supplementary Figures 3A,B**). The results of *c-myb* expression from 2 to 4 dpf showed that a decreased *c-myb* expression was detectable starting from 3 dpf (**Figure 3A** and **Supplementary Figures 4A–C**). Taken together, the primitive hematopoiesis was unaffected while the definitive hematopoiesis was impaired in the *ltv1*$^{\Delta 14/\Delta 14}$ mutant, probably due to the reduced HSPCs.

To confirm whether *ltv1* mutation is indeed responsible for the mutant phenotypes observed, zebrafish wild type and mutant form *ltv1* mRNAs were used for rescue experiments. At 3 dpf, both the smaller liver and reduced HSPC phenotypes in the *ltv1*$^{\Delta 14/\Delta 14}$ mutant were rescued by zebrafish wild-type *ltv1* mRNA efficiently but not by the mutant form (**Supplementary Figures 5A–D**).

Proliferation of Exocrine Pancreas Progenitor Cells and Hematopoietic Stem and Progenitor Cells in *ltv1*$^{\Delta 14/\Delta 14}$ Mutant Embryo Was Significantly Reduced

Disrupted cell proliferation and/or enhanced apoptosis may account for the digestive organs and hematopoiesis defects. The terminal deoxynucleotidyl transferase dUTP nick end labeling (TUNEL) assay revealed no apoptotic cell in the pancreas region in sectioned *ltv1*$^{\Delta 14/\Delta 14}$ mutant and sibling at 3 dpf, indicating that apoptosis is not the reason of the dysplastic exocrine pancreas in the mutant (**Supplementary Figure 6A**). In order to detect the level of cell proliferation, phospho-Histone H3 (pH3) immunostaining and bromodeoxyuridine (BrdU) labeling experiments were performed in mutants and siblings on *ptf1a:gfp* background at 2 dpf. In *ltv1*$^{\Delta 14/\Delta 14}$ mutants, both pH3 and BrdU-labeled *ptf1a*$^{+}$ cells were significantly reduced after normalizing for total pancreatic cells (**Figures 4A,B,A',B'**). Thus, the impaired exocrine pancreas in *ltv1*$^{\Delta 14/\Delta 14}$ mutants would be most likely due to the decreased cell proliferation of the exocrine pancreas progenitor cells.

Consistent with the results observed in the exocrine pancreas, TUNEL assay revealed similar apoptotic level of HSPCs in the CHT between *ltv1*$^{\Delta 14/\Delta 14}$ mutants and siblings at 2.5 dpf (**Supplementary Figures 6B,C**). The proliferation of HSPCs was also reduced in *ltv1*$^{\Delta 14/\Delta 14}$ mutants as indicated by the decreased pH3 and BrdU signals of HSPCs in the CHT at 2.5 dpf (**Figures 4C,D,C',D'**). Thus, defects in the definitive hematopoiesis were most likely attributed to decreased proliferation of HSPCs, instead of cell death.

ltv1 Expression Was Enriched in Digestive Organs During Embryogenesis

To investigate the reason behind tissue specificity of the mutant phenotypes observed, the expression pattern of *ltv1* in zebrafish embryos was examined by WISH using the antisense *ltv1* RNA

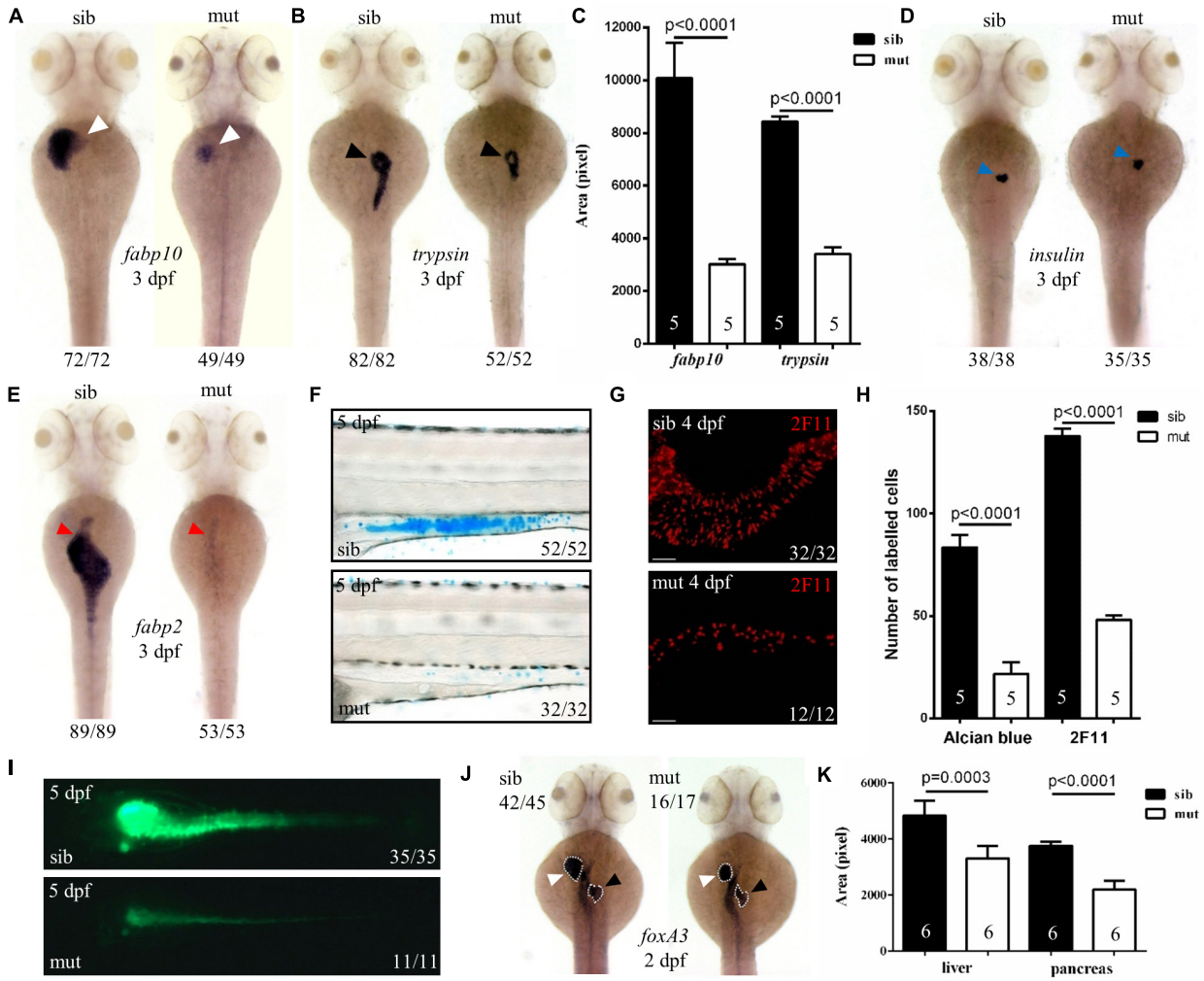

FIGURE 2 | Defects in the development of digestive organs in *ltv1*$^{\Delta 14/\Delta 14}$ mutant. **(A,B,D,E)** WISH using the hepatocyte marker *fabp10*, acinar cell marker *trypsin*, beta cell marker *insulin*, and enterocyte marker *fabp2* at 3 dpf. **(C)** Quantification of *fabp10* (siblings, *N* = 5; mutants, *N* = 5) or *trypsin* (siblings, *N* = 5; mutants, *N* = 5) positive area in panel **(A)** or **(B)**, respectively. Bars represent means with SD. **(F)** Alcian blue-stained goblet cells at 5 dpf. **(G)** Enteroendocrine cells (2F11^{+}) in the intestine bulb at 4 dpf. **(H)** Quantification of Alcian blue-stained (siblings, *N* = 5; mutants, *N* = 5) or 2F11-positive (siblings, *N* = 5; mutants, *N* = 5) cells in panel **(F)** or **(G)**, respectively. Bars represent means with SD. **(I)** Gut lumen labeled by DCFH-DA at 5 dpf. **(J)** WISH using the pan-endodermal marker *foxA3* at 2 dpf. **(K)** Quantification of the liver and pancreas area labeled by *foxA3* (siblings, *N* = 6; mutants, *N* = 6) in panel **(J)**. Bars represent means with SD. White arrowhead: liver; black arrowhead: exocrine pancreas; blue arrowhead: endocrine pancreas; red arrowhead: intestine.

probe. The sense probe was used as a negative control. At one-cell stage, *ltv1* mRNA was easily detected (**Figures 5A,E**), which suggested that *ltv1* was a maternal expression gene. From 50%-epiboly to 13 hpf, *ltv1* transcripts were distributed ubiquitously (**Figures 5B,C**), while no positive staining was detected for sense probe (**Figures 5F,G**). At 24 hpf, *ltv1* transcripts were found in the eyes and pharyngeal primordia (**Figures 5D,H,I**). Between 48 and 72 hpf, *ltv1* transcripts were abundant in the eyes, liver, intestine, and pancreas (**Figures 5J,K**). At 96 and 120 hpf, *ltv1* was highly expressed in the exocrine pancreas (**Figures 5L,M**). The digestive organ and pharyngeal primordia-specific expression pattern of *ltv1* was consistent with the hypoplastic phenotypes of these tissues during embryogenesis in the mutant. HSPCs and differentiated hematopoietic lineages were also affected severely in *ltv1*$^{\Delta 14/\Delta 14}$ mutants; however, no clear *ltv1* mRNA signal was detected in the aorta-gonad-mesonephros (AGM) or CHT by WISH using *ltv1* RNA probe from 24 to 120 hpf.

Ribosome Biogenesis Was Disrupted in *ltv1*$^{\Delta 14/\Delta 14}$ Mutant Embryo

In eukaryotic cells, the 28S, 18S, and 5.8S rRNAs are cleaved by various nucleases from a single primary transcript, known as the pre-rRNA. It was reported that deletion of *ltv1* could lead to aberrant processing of 18S rRNA in yeast, fruit fly, and human cells and accumulation of its precursor 20S (yeast) or 21S rRNA (fruit fly and human cells), implying a conserved role of *ltv1* in 18S rRNA processing. To test if it were the

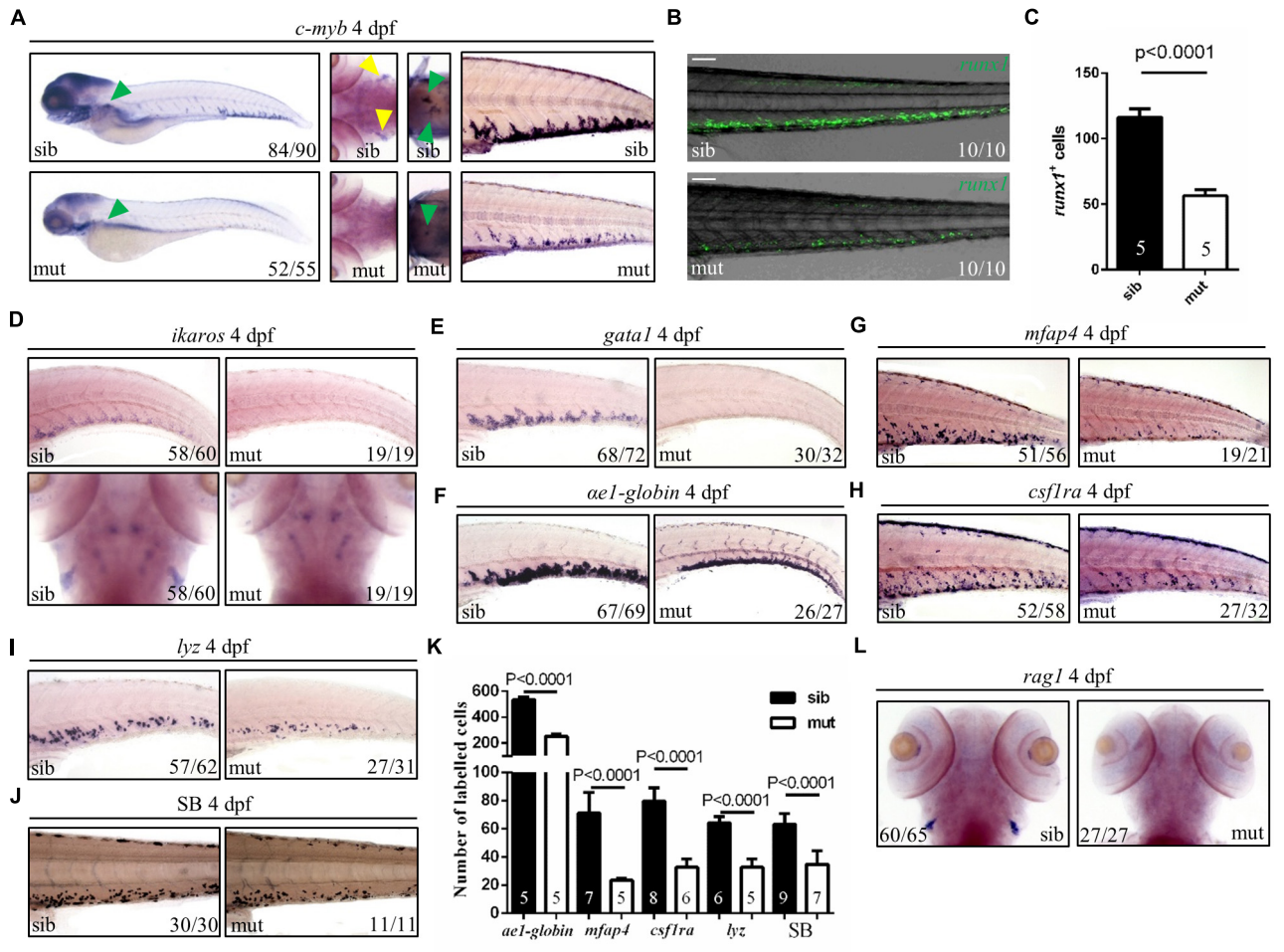

FIGURE 3 | Defects of definitive hematopoiesis in *ltv1*$^{\Delta 14/\Delta 14}$ mutant. **(A)** WISH of HSPC marker *c-myb* in the thymus, kidney and CHT at 4 dpf. **(B)** Representative confocal images of *ltv1*$^{\Delta 14/\Delta 14}$; *runx1:en-gfp* mutants and siblings at 4 dpf. **(C)** Quantification of *runx1*$^{+}$ cells of *ltv1*$^{\Delta 14/\Delta 14}$; *runx1:en-gfp* mutants (*N* = 5) and siblings (*N* = 5) at 4 dpf. Bars represent means with SD. **(D)** WISH of HSPC marker *ikaros* in the CHT and thymus at 4 dpf. **(E–I)** WISH of erythrocyte progenitor marker *gata1* **(E)**, erythrocyte marker *αe1-globin* **(F)**, macrophage markers *mfap4* **(G)** and *csf1ra* **(H)**, and neutrophil marker *lyz* **(I)** in the CHT at 4 dpf. **(J)** Sudan Black-stained neutrophils in the CHT at 4 dpf. **(K)** Quantification of *αe1-globin*, *mfap4*, *csf1ra*, *lyz*, and SB-positive (Sudan Black) cells in panels **(F–J)**, respectively. Numbers of each group are shown in the respective columns. Bars represent means with SD. **(L)** WISH of lymphocyte marker *rag1* at 4 dpf. Yellow arrowhead: thymus; green arrowhead: kidney. Scale bar: 100 μm.

case in zebrafish, Northern blot was used to analyze rRNA processing using the probes that could hybridize the ETS, ITS1, ITS2 (ETS/ITS: external/internal-transcribed spacer region), and 18S rRNA (Azuma et al., 2006). ETS, ITS1, and ITS2 probes could mark the rRNA precursor and the intermediate and some minor products (**Figure 6A**). The ETS and ITS1 probes revealed that the full-length precursor "a" accumulated significantly in *ltv1*$^{\Delta 14/\Delta 14}$ mutants, indicating the disruption of rRNA processing (**Figure 6B**). The "d," which might correspond to the 20S rRNA in yeast or 21S rRNA in human cells, accumulated while the "c" decreased, showing the impaired 18S rRNA processing in the mutants (**Figure 6B**). Consistently, the amount of 18S rRNA was declined slightly in the mutants (**Figure 6C**). Although the "e" increased slightly, the "b" showed no obvious difference in the mutants (**Figure 6B**), suggesting the intact 28S rRNA processing in *ltv1*$^{\Delta 14/\Delta 14}$ mutants. To quantify the amount of 18S and 28S rRNA, E-bioanalyzer analysis was performed and the results showed that the 18S rRNA was reduced obviously in *ltv1*$^{\Delta 14/\Delta 14}$ mutants at 5 dpf, while the amount of 28S rRNA remained comparable (**Figure 6D**). The altered quantity of 18S rRNA therefore caused the imbalance of the 28S/18S ratio in mutants, which is 3.1, compared with 2.0 in siblings (**Figure 6E**). Consistent with rRNA quantification data, the ribosome fractionation results showed that the amount of 40S subunits and 80S monosomes decreased, while that of the 60S subunits increased about twofold (**Figures 6F,G**).

Phenotypes in *ltv1*$^{\Delta 14/\Delta 14}$ Mutant Were Independent of P53

A growing number of studies suggest that P53 may play a vital role in phenotypes relevant to ribosome dysfunction

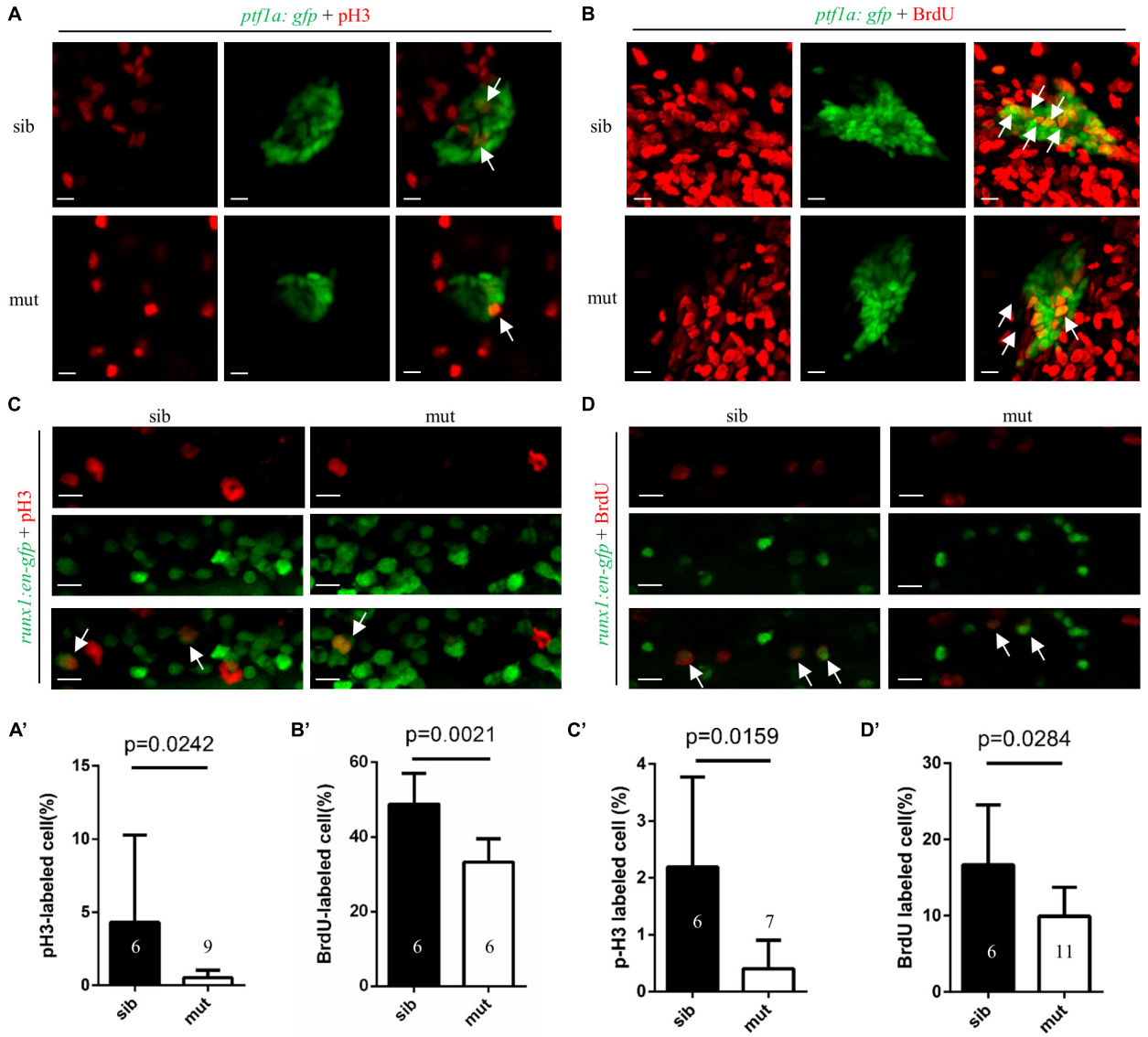

FIGURE 4 | Impaired proliferation of exocrine pancreas progenitors and HSPCs in *ltv1*$^{\Delta 14/\Delta 14}$ mutant. **(A,B)** Representative confocal images of pH3 immunostaining **(A)** or BrdU labeling **(B)** in *ltv1*$^{\Delta 14/\Delta 14}$; *ptf1a:gfp* mutants and siblings at 2 dpf. **(A',B')** The percentage of pH3^{+} **(A')**, siblings, *N* = 6; mutants, *N* = 9) or BrdU^{+} **(B')**, siblings, *N* = 6; mutants, *N* = 6) cells within the *ptf1a*$^{+}$ population in *ltv1*$^{\Delta 14/\Delta 14}$ mutants and siblings at 2 dpf. Bars represent means with SD. **(C,D)** Representative confocal images of pH3 immunostaining **(C)** and BrdU labeling **(D)** in *ltv1*$^{\Delta 14/\Delta 14}$; *runx1:en-gfp* mutants and siblings at 2.5 dpf. **(C',D')** The percentage of pH3^{+} **(C')**, siblings, *N* = 6; mutants, *N* = 7) and BrdU^{+} **(D')**, siblings, *N* = 6; mutants, *N* = 11) cells within the *runx1*$^{+}$ population in *ltv1*$^{\Delta 14/\Delta 14}$ mutants and siblings at 2.5 dpf. Bars represent means with SD. White arrow: merged cell. Scale bar: 10 μm.

(Armistead and Triggs-Raine, 2014). In *ltv1*$^{\Delta 14/\Delta 14}$ mutants, there was a clear increase in the expression level of *p53* at 3 dpf, as indicated by WISH using a *p53* probe which can detect both *p53* and Δ*113p53* (**Figure 7A**). In addition, the P53 protein level was upregulated obviously in mutants (**Figure 7B**). Then mRNA levels of Δ*113p53* and *p21*, downstream genes of *p53*, were evaluated by quantitative polymerase chain reaction (PCR). Consistently, both Δ*113p53* and *p21* mRNA levels were increased significantly in *ltv1*$^{\Delta 14/\Delta 14}$ mutant, which further suggested the activation of *p53* pathway (**Figure 7C**). To determine if the downregulation of *p53* could rescue the mutant phenotypes, knockdown of *p53* was achieved by the *p53*^{ATG} morpholino injection. The increased P53 expression was attenuated in the mutant, which validated the efficacy of *p53* knockdown (**Figure 7B**). However, neither the smaller liver nor the reduced HSPC phenotype in *ltv1*$^{\Delta 14/\Delta 14}$ mutant could be alleviated by *p53* knockdown (data not shown), suggesting that the mutant phenotypes were independent of P53.

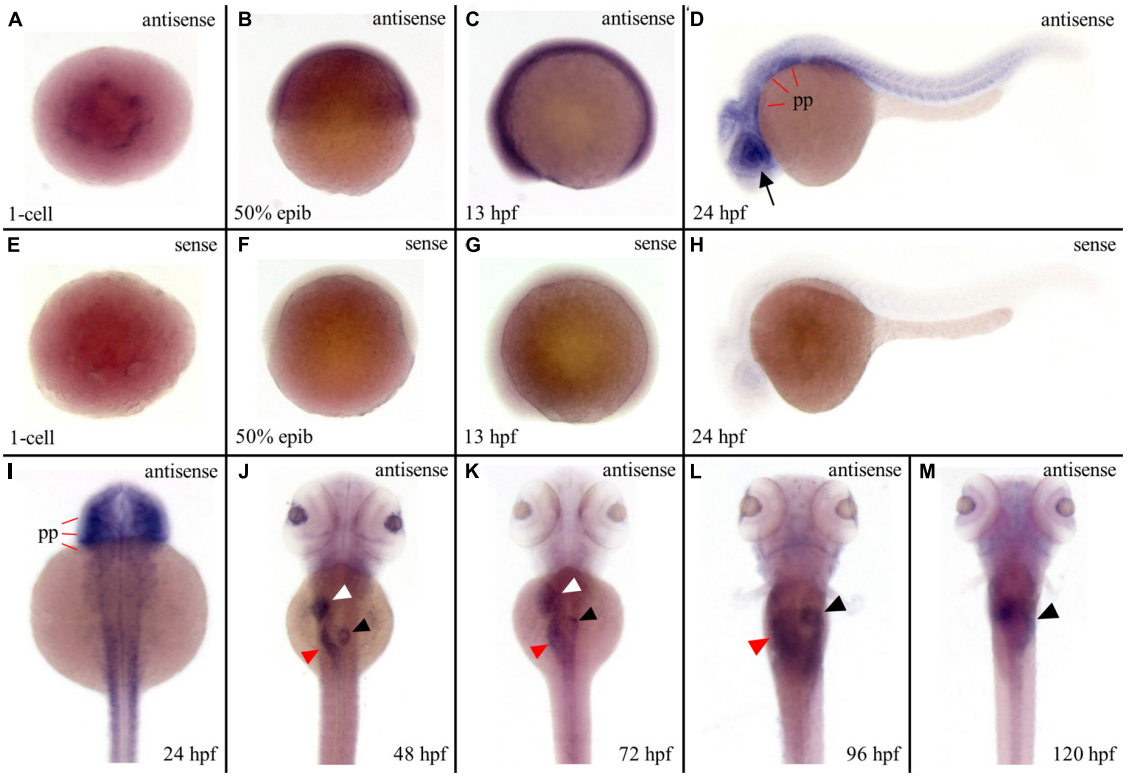

FIGURE 5 | Strong expression of *ltv1* in digestive organs. **(A,I–M)** Dorsal views. **(B–D)** Lateral views, anterior to the left. **(A–D,I–M)** WISH using *ltv1* antisense probe in wild-type embryos at the stages as indicated in each panel. **(E–H)** As a negative control, *ltv1* sense probe is used to perform the WISH. Black arrow: eye. White arrowhead: liver. Red arrowhead: intestine. Black arrowhead: exocrine pancreas. pp: pharyngeal primordia.

DISCUSSION

Ltv1 is a non-ribosomal protein essential for 18S rRNA processing in yeast, fruit fly, and human cells (Seiser et al., 2006; Tafforeau et al., 2011; Ghalei et al., 2015; Kressler et al., 2015). In this report, Ltv1 was demonstrated functionally conserved in zebrafish as illustrated by disrupted 18S rRNA processing in the *ltv1* mutants. Deletion of zebrafish *ltv1* resulted in defective growth of liver, exocrine pancreas, intestine, abnormal craniofacial structures and impaired development of HSPCs, definitive erythrocytes, myeloid cells, and lymphocytes. These phenotypic features resembled some specific ribosomopathy models in zebrafish studies (Provost et al., 2012; Carapito et al., 2017; Oyarbide et al., 2019, 2020).

Ltv1 is an assembly factor that can facilitate the incorporation of Rps3 and Rps10 into the small ribosomal subunit in yeast. Ltv1 deficiency led to mispositioned Rps3 in ribosomes (Collins et al., 2018). In zebrafish, knockdown of *rps3* could result in morphological defects, including reduced head size, pericardial edema, and erythropoiesis failure (Yadav et al., 2014). These phenotypic features are consistent with those in $ltv1^{\Delta 14/\Delta 14}$ zebrafish mutants. Hence, it is interesting to investigate whether *ltv1* functions through *rps3* in digestive system development and hematopoiesis. However, it should be noticed that the morphological defects of *rps3* morphants could be rescued by knockdown of *p53*, while the erythroid failure could not be alleviated (Yadav et al., 2014). In $ltv1^{\Delta 14/\Delta 14}$ mutants, none of the defects in morphology, digestive organogenesis, or hematopoiesis could be rescued by *p53* knockdown. It was reported that Rps3 could directly interact with P53 and MDM2 (Yadavilli et al., 2009). This may be underlying the P53-dependent recovery of morphological deformities of the *rps3* morphants. Further genetic investigation is required to validate the relationship between *ltv1* and *rps3*. Ribosomes from Ltv1-deficient yeast harbored less Rps10 protein (Collins et al., 2018). Rps10 was found to be mutated in 6.4% of patients with DBA (Doherty et al., 2010). To the edge of our knowledge, no zebrafish mutant of *rps10* has been constructed. It will be meaningful to analyze the phenotypes of *rps10* mutants and investigate the genetic interaction among *ltv1*, *rps3*, and *rps10* in zebrafish.

What is the justification for dysfunction in a macromolecule as ubiquitous and essential as the ribosome causing ribosomopathies with defects in selective tissues? Xue and Barna (2012) believed that the tissue specificity of gene expression in ribosomal biogenesis was the cause. Agreed with this point, *ltv1* was found highly expressed in digestive organs during embryogenesis, which may partially explain the phenotypes of *ltv1* mutants in these organs. However, despite of no detectable expression of *ltv1* in the AGM and CHT, HSPCs and differentiated hematopoietic lineages were impaired severely.

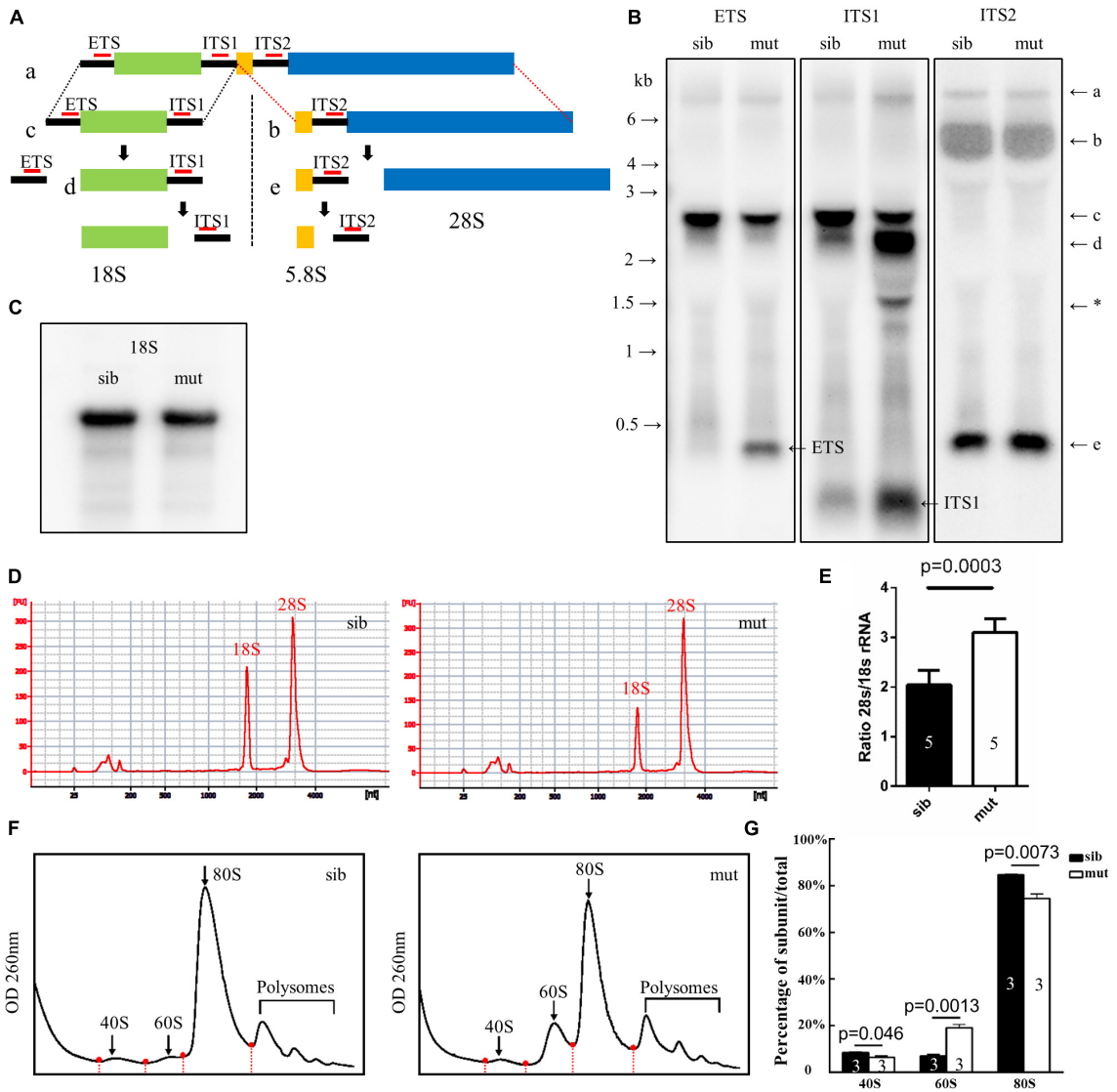

FIGURE 6 | Defects in 18S rRNA processing in *ltv1*$^{\Delta 14/\Delta 14}$ mutant. **(A)** Schematic diagram showing the processing pathway of 28S, 18S, and 5.8S rRNAs. The hybridization sites of each probe are indicated by red bars, respectively. **(B,C)** Northern blot analysis using the corresponding probes as indicated to detect 18S rRNA or the intermediate products of rRNA processing. Asterisk: unidentified rRNA intermediate product. **(D)** Representative analysis result by E-bioanalyzer. **(E)** The ratio of 28S/18S rRNA is increased in *ltv1*$^{\Delta 14/\Delta 14}$ mutants ($N = 5$), as compared with siblings ($N = 5$). Bars represent means with SD. ETS, external transcribed spacer; ITS, internal transcribed spacer. **(F)** Representative ribosome fractionation results of siblings and *ltv1*$^{\Delta 14/\Delta 14}$ mutants at 4 dpf. The peaks of 40S, 60S, and 80S are indicated by arrows. Red dots on the curves represent the lowest points flanking the peaks. The area under respective peaks of 40S, 60S, and 80S, circled by curves, dashed lines, and baselines are measured. **(G)** Percentages of 40S, 60S, and 80S in total lysate in siblings and *ltv1*$^{\Delta 14/\Delta 14}$ mutants at 4 dpf. Bars represent means with SD. Quantifications of three independent experiments are analyzed.

Some zebrafish models of ribosomopathy, such as *sbds* (Provost et al., 2012), *rpl11* (Danilova et al., 2011), *rpl24*, *rpl35a* (Yadav et al., 2014), etc., all displayed hematopoietic defects at different levels. While all the respective genes were highly expressed in digestive organs, no description of gene expression in AGM or CHT was reported (Venkatasubramani and Mayer, 2008; Provost et al., 2013), similar to that observed in *ltv1*. One possible explanation is that these genes deficiencies may lead to impaired hematopoiesis indirectly, probably by impairment of the niche of HSPCs. Like *ltv1*, zebrafish *nol9* encoded a non-ribosomal protein, and *nol9* mutants displayed defects in both digestive organs and hematopoiesis. Transmission electron microscopy (TEM) analysis revealed great changes in the CHT niche in *nol9* mutants, including extracellular matrix (ECM) and endothelial cells (Bielczyk-Maczynska et al., 2015).

It has been demonstrated here that Ltv1 is essential for ribosome biogenesis and organogenesis of digestive system and hematopoiesis. Among the existing zebrafish models with deficient ribosome biogenesis, most of them exhibited hypoplasia of liver, pancreas, and intestine, including *nil per os* (*npo*)

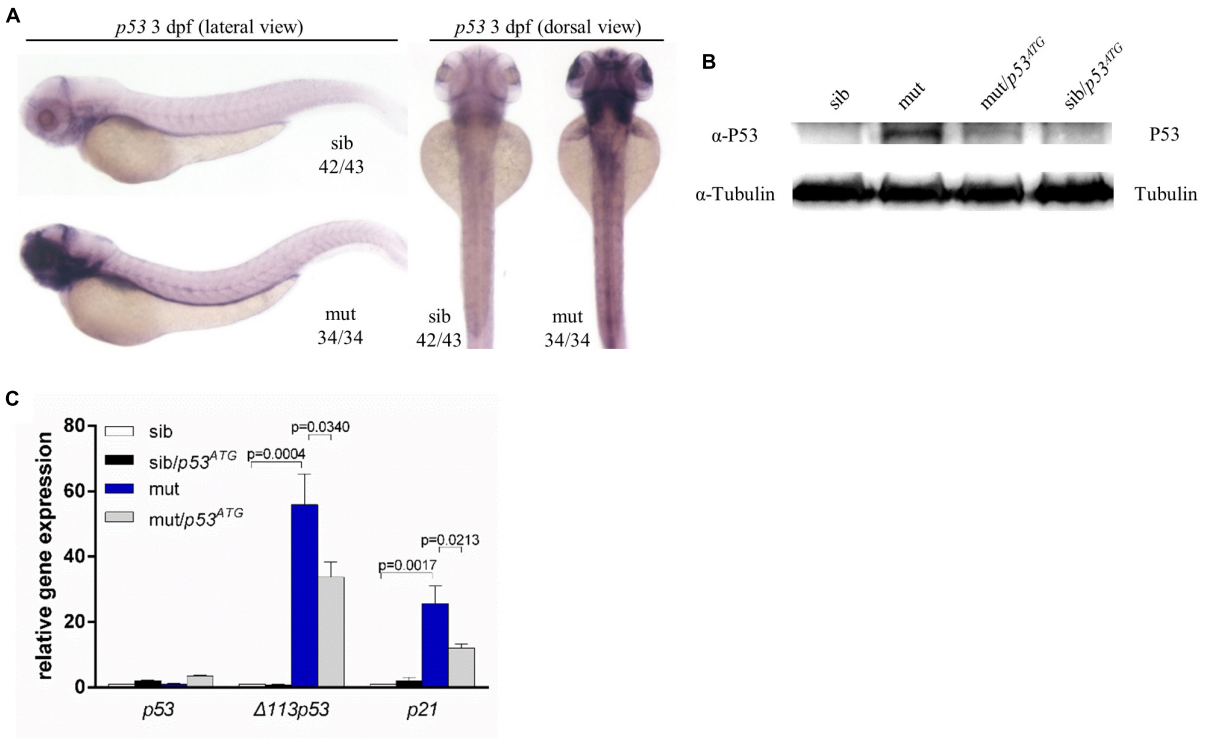

FIGURE 7 | P53 Independence of phenotypes in *ltv1*$^{\Delta 14/\Delta 14}$ mutant. **(A)** WISH of *p53* probe for detecting both *p53* and Δ*113p53* at 3 dpf. **(B)** Western blot results of P53 protein of *p53*^{ATG} MO-treated or MO-untreated mutants and siblings at 3 dpf. **(C)** Evaluation of expression of *p53* and its transcriptional targets Δ*113p53* and *p21* by quantitative PCR.

(Mayer and Fishman, 2003), *titania* (*tti*) (Boglev et al., 2013), *bms1-like* (*bms1l*) (Wang et al., 2012), and *nucleolar protein with MIF4G domain 1* (*nom1*) (Qin et al., 2014), while some displayed defects in definitive hematopoiesis, for example, *kri1l* (Jia et al., 2015). To the best of our knowledge, only one mutant *nol9* (Bielczyk-Maczynska et al., 2015) described both phenotypes. Interestingly, in line with *ltv1*$^{\Delta 14/\Delta 14}$ mutants, *nol9* mutants showed arrested development of exocrine pancreas and HSPCs as a result of reduced proliferative rate. Although *nol9* and *ltv1* are involved in the 28S and 18S rRNA processing, respectively, the similar phenotypes in these two models suggest the conserved function of ribosome biogenesis genes during embryogenesis.

Several studies revealed that excess free ribosomal proteins, while ribosome biogenesis was impaired, could outcompete P53 in binding the E3 ubiquitin ligase MDM2, consequently protecting P53 from degradation (Zhang et al., 2003; Dai and Lu, 2004; Dai et al., 2004). In some ribosome biogenesis-deficient models, phenotypes could be rescued by inhibition of P53 (Zhang et al., 2012; Bielczyk-Maczynska et al., 2015; Ear et al., 2016). However, in some other cases, P53-independent cell apoptosis and cell proliferation arrest have also been described (Provost et al., 2012; Boglev et al., 2013; Qin et al., 2014; Yadav et al., 2014; Jia et al., 2015). Although P53 protein and target genes Δ*113p53* and *p21* were upregulated in *ltv1*$^{\Delta 14/\Delta 14}$ mutants, knockdown of *p53* could not rescue the defects of the liver or HSPCs, suggesting a *p53*-independent mechanism was involved, which agreed with the fact that the abnormal rRNA processing in LTV1-deficient human cells was P53 independent (Tafforeau et al., 2011). In addition to P53, some other pathways were reported to be involved in the ribosome-deficient zebrafish models. In zebrafish *kri1l* mutants, an increased level of autophagy was observed, and blocking autophagy could significantly restore the definitive hematopoiesis (Jia et al., 2015). In contrast, inhibition of autophagy reduced the lifespan of zebrafish mutants of *pwp2h* gene, which encoded a protein promoting the small ribosomal subunit processing. In *pwp2h* mutants, autophagy was considered a survival mechanism triggered by ribosomal efficiency (Boglev et al., 2013). The question that whether autophagy is involved in the *ltv1* function in zebrafish is required further validation. Rpl35a was mutated in 3.3% DBA (Farrar et al., 2008). In zebrafish *rpl35a* knockdown embryos, upregulation of mammalian target of rapamycin (mTOR) could rescue the morphological defects and the erythroid failure (Yadav et al., 2014). This case suggested that mTOR functioned downstream of *rpl35a*. Urb1, a protein promoting the big ribosomal subunit assembly in zebrafish, was demonstrated to play a role downstream of mTOR in digestive organ formation (He et al., 2017). It is also possible that mTOR pathway is involved in *ltv1*-dependent digestive organ development and hematopoiesis.

In *ltv1*$^{\Delta 14/\Delta 14}$ mutants, the proliferation was inhibited and *p53* was activated. It was reported that activation of *p53* could lead to cell cycle arrest *via p21* upregulation (Georgakilas et al., 2017).

However, it is possibly not the case in *ltv1*$^{\Delta 14/\Delta 14}$ mutants because inhibition of *p53* could not restore the growth of the liver and HSPCs. The P53-independent mechanism underlying the cell cycle arrest might be the key way through which *ltv1* functions in zebrafish. Pescadillo was a protein that played an essential role in 28S rRNA processing and the zebrafish *pescadillo*-deficient embryos displayed underdeveloped liver, gut, and craniofacial cartilage (Allende et al., 1996; Lapik et al., 2004; Provost et al., 2012). Cyclin D1 was indispensable for cell proliferation in cells. As a cyclin-dependent kinase inhibitor, P27 could decrease catalytic activity of cyclin D1 through direct interaction, and so that led to cell cycle arrest (Razavipour et al., 2020). It was reported that the cell cycle arrest in *pescadillo*-deficient cells was due to cyclin D1 downregulation and activation of P27, which was independent of P53 (Li et al., 2009). In erythroid cell lines, ribosome synthesis defects could lead to decreased level of PIM1, a kinase implicated in cell proliferation. The reduction of PIM1 induced cell cycle arrest *via* accumulated P27 in a P53-independent way (Iadevaia et al., 2010). It is interesting to investigate that whether the *ltv1*$^{\Delta 14/\Delta 14}$ mutants share the same P27-regulated mechanism, regardless of P53, underlying the cell proliferation inhibition with these two cases.

It should be highlighted that the phenotypes of *ltv1*$^{\Delta 14/\Delta 14}$ and *sbds*-deficient embryos share some similar features such as the affected exocrine pancreas and hematopoiesis (Burroughs et al., 2009). Although the Sbds protein plays a role in 60S ribosomal subunit biogenesis (Menne et al., 2007), Ltv1 is required for the assembly of 40S ribosomal subunit (Ameismeier et al., 2018; Collins et al., 2018). The expression pattern of *sbds* is very similar to that of *ltv1* in zebrafish (Venkatasubramani and Mayer, 2008). In line with *ltv1*$^{\Delta 14/\Delta 14}$ larvae, morpholino knockdown of *sbds* in zebrafish causes defects in exocrine pancreas, of which could not be rescued by *p53* downregulation, while the endocrine pancreas is normal (Provost et al., 2012). Together with other animal models with ribosome biogenesis dysfunction, *ltv1* zebrafish mutant not only provides new candidate genes for the screening of ribosomopathies with unknown genetic deterioration but also serves as a tool to investigate molecular and cellular mechanisms underlying ribosomal genes deficiency phenotypes. As a powerful model for chemical screen, the corresponding zebrafish mutants may be used for the identification of potential compounds for treating specific ribosomopathies.

MATERIALS AND METHODS

Zebrafish Strains and Embryos Collection

Wild-type Tübingen fish line, transgenic line *ptf1a:gfp* (Godinho et al., 2005), and *runx1:en-gfp* (He et al., 2015) were used and maintained under standard conditions.

Genomic DNA Extraction

Embryos or fish scales were lysed in the buffer (10 mM Tris–HCl, 50 mM KCl, 0.3% Tween-20, 0.3% NP40, and 1/10 volume proteinase K, Invitrogen, Waltham, MA, United States) at 55°C for 12 h and then the reaction was inactivated by increasing the temperature to 95°C for 20 min. The crude lysate could be used as the template for PCR directly.

Generation of *ltv1* Mutants by Clustered Regularly Interspaced Short Palindromic Repeat/Cas9 System

The gRNA was designed to target a site in the exon 7 of *ltv1* at the sequence GGACAGTGCTCGGCTGG*AGG* (PAM site in italics). Zebrafish Cas9 mRNA and the *ltv1* gRNA were synthesized as described (Chang et al., 2013; Ear et al., 2016). At one-cell stage, Cas9 mRNA (300 pg) and gRNA (50 pg) were injected into wild-type embryos. At 36 hpf, about 10 embryos were pooled and lysed, and the primers (*ltv1* fw: 5′-TGGTAAGGAGTCTGATTATC-3′ and *ltv1* rv: 5′-CCAATCCATGTGATGCATAC-3′) were used to amplified DNA fragment harboring gRNA targeted site. PCR products were subjected to sequencing to identify potential indels in the region. Upon detecting mutation, the rest of the embryos were raised to adults (F0). Pooled F1 embryos obtained by crossing F0 with wild-type fish were examined for indels in *ltv1* gene using the PCR method described above. The nature of indels could be obtained by sequencing and mutant allele specific primers were then designed according to specific indels.

Genotyping of *ltv1*$^{\Delta 14/\Delta 14}$ Mutants

The common forward primer (*ltv1* fw) was described above. The mutant and wild-type allele-specific reverse primers were listed as follow: wt rv: 5′-CTTTGATGACCTCCTC-3′ and *ltv1*$^{\Delta 14}$ rv: 5′-CTTTGATGACCTCTGT-3′.

RNA Whole Amount *in situ* Hybridization

The following digoxigenin-labeled antisense RNA probes were used: *fabp10*, *trypsin*, *insulin*, *fabp2*, *foxA1*, *foxA3*, *gata6*, *hhex*, *prox1*, *pdx1*, *gcga*, *sst2*, *c-myb*, *ikaros*, *gata1*, α*e1-globin*, *mfap4*, *csf1ra*, *lyz*, *rag1*, *apoe*, and *pu.1*. WISH was performed as described previously (Huang et al., 2008; Li et al., 2011).

Mutant Rescue

Zebrafish wild-type *ltv1* cDNAs were cloned into pCS2 + vector. Mutant form cDNA was obtained by site-directed mutagenesis. The microinjection was performed at one-cell stage, 0.5 ng *in vitro* transcribed either zebrafish wild-type *ltv1* mRNA or *ltv1*$^{\Delta 14}$ mRNA was used to try to rescue the mutant phenotypes. At 3 days post injection (dpi), embryos were fixed for WISH using the liver-specific *fabp10* or *c-myb* probe.

Immunochemistry Staining

Immunohistochemistry staining was performed as described previously (Chen et al., 2005). The primary antibodies were goat anti-GFP (Abcam, Cambridge, MA, United States; 1:400), rabbit anti-pH3 (Santa Cruz Biotechnology, Santa Cruz, CA, United States; 1:200), and mouse 2F11 (Abcam, 1:1,000). GFP antibody was used to enhance the GFP signal in *runx1:en-gfp*.

Bromodeoxyuridine Labeling

For BrdU labeling, BrdU (Roche Diagnostics, Indianapolis, IN, United States; 1 nl, 30 mM) was injected into the pericardium of embryos. Consequently, the embryos were incubated for 1.5–2 h at 28.5°C. After three times of washing with PBST, the embryos were fixed using 4% PFA. After being treated with 2 N HCl for 1 h, the embryos were incubated with mouse anti-BrdU (Roche Diagnostics, United States; 1:50) and goat anti-GFP (Abcam, United States; 1:400) antibodies at 4°C overnight, and finally visualized by Alexa Fluor 555 donkey anti-mouse (Life Technology, Carlsbad, CA, United States; 1:400) and Alexa Fluor 488 donkey anti-goat (Life Technology, United States; 1:400) antibodies.

TUNEL Assay

Whole embryo and cryosectioned samples were prepared for TUNEL assay, and *in situ* cell death detection kit, TMR Red (Roche Diagnostics, United States) was used following the manuals provided.

Dyes Staining

Alcian blue, Neutral red, and Sudan black (Sigma-Aldrich, Burlington, MA, United States) staining was conducted as described previously (Herbomel et al., 2001; Le Guyader et al., 2008; Chen et al., 2009; Li et al., 2011). DCFH-DA (Wako, Japan) was used as described previously (Shi et al., 2014).

Northern Blot

Total RNA was extracted from mutant and sibling embryos at 120 hpf using TriPure Isolation Reagent (Roche Diagnostics, United States). The DIG-labeled DNA probes were PCR-amplified using previously described primers (Azuma et al., 2006). Equal amount of total RNAs were subjected to electrophoresis. The probe hybridization and detection process were carried out as previously described (Chen et al., 2005).

Quantification of 18S and 28S Ribosomal RNA

Total RNA was extracted from *ltv1*$^{\Delta 14/\Delta 14}$ mutants and siblings at 5 dpf. Then, RNA were subjected to E-Bioanalyzer (Agilent 2100) analysis according to the manual.

Ribosome Fractionation

For each group, 300 embryos at 4 dpf were collected and rinsed by pre-chilled PBS (containing 100 μg/ml cycloheximide) for three times. After removing the yolk through 23 G needles, the embryos were resuspended in 500 μl pre-chilled lysis buffer (5 mM Tris–HCl pH 7.5, 2.5 mM $MgCl_2$, 1.5 mM KCl, 100 μg/ml cycloheximide, 2 mM DTT, 0.32 U/μl RNase inhibitor, 0.5% Triton X-100, 0.5% sodium deoxycholate, 1 × EDTA-free Protease Inhibitor Cocktail, Abcam) and sheared on ice through 23, 25, and 27 G needles gradually. Then the lysate was centrifuged at 15,000× *g* for 10 min at 4°C to remove the nuclei and cellular debris pellet. The liquid supernatant was gently loaded on 5–50% gradient sucrose solution (containing 20 mM HEPES pH 7.6, 0.1 M KCl, 5 mM $MgCl_2$, 10 μg/ml cycloheximide, 0.1× EDTA-free Protease Inhibitor Cocktail, 32 U/ml RNase inhibitor), which was made by Gradient Master (Biocomp, Gyeongju, South Korea) and centrifuged at 36,000 rpm for 4 h at 4°C in SW41 Ti rotor. The fractions were collected using the Piston Gradient Fractionator (Biocomp) and scanned continuously by Triax Flow Cells detector (Biocomp) to measure the absorbance at 260 nm.

p53 Knockdown With Morpholinos

To knock down *p53*, *p53*-morpholino (MO)^{ATG} (5′-GCGCCATTGCTTTGCAAGAATTG-3′, Gene Tools, 1 nl, 0.7 mM) was injected to one-cell stage embryos (Chen et al., 2005). The morpholino against human β-*globin* was used as the negative control (Chen et al., 2005).

Quantitative PCR

Total RNA was extracted from whole embryos using TriPure Isolation Reagent (Roche Diagnostics, United States). cDNAs were generated using Oligo (dT) and SuperScript III reverse transcriptase (Life Technologies, United States). For each sample, three parallel repeated tests were performed. The measured expression of *ef1α* was the internal control for each gene. The primers used: *ef1α* fw: 5′-CTTCTCAGGCTGACTGTGC-3′, *ef1α* rv: 5′-CCGCTAGCATTACCCTCC-3′, *p53* fw: 5′-TGGAGAGGAGGTCGGCAAAATCAA-3′, *p53* rv: 5′-GAC TGCGGGAACCTGAGCCTAAAT-3′, Δ*113p53* fw: 5′-ATAT CCTGGCGAACATTTGGAGGG-3′, Δ*113p53* rv: 5′-CCTCCT GGTCTTGTAATGTCAC-3′, *p21* fw: 5′-GAAGCGCAAA CAGACCAACAT-3′ and *p21* rv: 5′-GCAGCTCAATTACGA TAAAGA-3′.

Western Blot

p53^{ATG} MO-injected or *p53*^{ATG} MO-uninjected embryos were de-yolked at 3 dpf. Then the embryos were treated with pre-extraction buffer (1 mM EDTA, 0.1 mM Na_3VO_4, 20 mM NaF, 1 mM DTT, 100 mM PMSF, and a work concentration of Protease Inhibitor Cocktail in PBS) and lysed in SDS lysis buffer. Subsequently, the lysate was used in Western blot. The primary antibodies used were α-P53 antibody (Abcam, 1:1,000) and α-tubulin antibody (Pierce, 1:500).

Statistical Methods

The experimental data were analyzed in GraphPad Prism 6.0. The unpaired Student's *t*-test was used for comparing the means of two groups.

DATA AVAILABILITY STATEMENT

The original contributions presented in the study are included in the article/**Supplementary Material**, further inquiries can be directed to the corresponding author/s.

ETHICS STATEMENT

The animal study was reviewed and approved by Institutional Animal Care and Use Committee in Southwest University, China.

AUTHOR CONTRIBUTIONS

HH and HR designed the project. CZ, RH, XM, JC, and XH performed the experiments. CZ and HH wrote the manuscript. LLi and LLu commented on the manuscript. All authors contributed to the article and approved the submitted version.

FUNDING

This work was supported by National Key R&D Program of China 2018YFA0801000 and 2018YFA0800502, National Natural Science Foundation of China 31471365.

ACKNOWLEDGMENTS

We thank Li Jan Lo (Zhejiang University, China) for suggestion on the manuscript, LLi (Southwest University, China) for blood cell markers, and Bo Zhang and Jingwei Xiong (Peking University, China) for plasmids for CRISPR/Cas9 system.

SUPPLEMENTARY MATERIAL

The Supplementary Material for this article can be found online at: https://www.frontiersin.org/articles/10.3389/fcell.2021.704730/full#supplementary-material

Supplementary Figure 1 | Ltv1 is conserved among human, mouse and zebrafish. Alignment of Ltv1 protein sequence from human, mouse, and zebrafish.

Supplementary Figure 2 | The liver bud growth and exocrine pancreas expansion are affected in *ltv1*$^{\Delta 14/\Delta 14}$ mutant. **(A–J)** Embryos at 2 dpf, 34 hpf, and 30 hpf were subjected to WISH to analyze the liver and pancreas formation. The probes used include: pan-endodermal markers *foxA1*, *gata6*; hepatic markers *hhex*, *prox1*; pancreas marker *pdx1*; endocrine pancreas markers *gcga*, *insulin*, and *sst2*. **(K)** Representative confocal images of *ltv1*$^{\Delta 14/\Delta 14}$*/ptf1a:gfp* mutants and siblings at 2 dpf. **(L)** Quantification of *ptf1a*$^{+}$ cells of *ltv1*$^{\Delta 14/\Delta 14}$*/ptf1a:gfp* mutants and siblings at 2 dpf. Bars represent means with SD. White arrowhead: liver. Blue arrowhead: endocrine pancreas. Scale bar: 10 μm.

Supplementary Figure 3 | The primitive hematopoiesis is normal in *ltv1*$^{\Delta 14/\Delta 14}$ mutant. **(A,B)** WISH of primitive hematopoiesis regulators *gata1* **(A)** and *pu.1* **(B)** at 20 and 22 hpf, respectively.

Supplementary Figure 4 | The defects of HSPC is observable at 3 dpf. **(A)** WISH of *c-myb* in the CHT at 2 dpf. **(B)** Quantification of *c-myb*$^{+}$ HSPCs in the CHT of *ltv1*$^{\Delta 14/\Delta 14}$ mutants and siblings at 2 dpf. **(C)** *ltv1*$^{\Delta 14/\Delta 14}$ mutants displayed significantly decreased *c-myb* expression in the CHT at 3 dpf compared with the siblings.

Supplementary Figure 5 | The mutant phenotypes can be rescued by zebrafish *ltv1* mRNA injection. **(A,C)** Representative images of *fabp10* or *c-myb* expression of unrescued and partially and fully rescued mutants after the injection of zebrafish wild-type *ltv1* mRNA. **(B,D)** The rescue efficiency of the liver or HSPC phenotypes in mutants after the injection of zebrafish wild-type or Δ14 *ltv1* mRNA ($N \geq 30$ in every group). Bars represent means with SD.

Supplementary Figure 6 | Apoptotic level of the exocrine pancreas and HSPCs are not increased in *ltv1*$^{\Delta 14/\Delta 14}$ mutant. **(A)** No apoptotic cells are found in the pancreas region in cryosectioned samples from both *ltv1*$^{\Delta 14/\Delta 14}$ mutants and siblings at 3 dpf. **(B)** Representative confocal images of the *ltv1*$^{\Delta 14/\Delta 14}$*/runx1:en-gfp* mutants and siblings after TUNEL assay at 2.5 dpf. **(C)** Ratio of apoptotic cells in *runx1*$^{+}$ HSPCs in *ltv1*$^{\Delta 14/\Delta 14}$ mutants ($N = 6$) and siblings ($N = 6$) at 2.5 dpf. Bars represent means with SD. White arrow: merged cell. Scale bar: 10 μm.

REFERENCES

Allende, M. L., Amsterdam, A., Becker, T., Kawakami, K., Gaiano, N., and Hopkins, N. (1996). Insertional mutagenesis in zebrafish identifies two novel genes, pescadillo and dead eye, essential for embryonic development. *Genes Dev.* 10, 3141–3155. doi: 10.1101/gad.10.24.3141

Ameismeier, M., Cheng, J., Berninghausen, O., and Beckmann, R. (2018). Visualizing late states of human 40S ribosomal subunit maturation. *J. Cell Biol.* 558, 249–253.

Anchelin, M., Alcaraz-Pérez, F., Martínez, C. M., Bernabé-García, M., Mulero, V., and Cayuela, M. L. (2013). Premature aging in telomerase-deficient zebrafish. *Dis. Model. Mech.* 6, 1101–1112. doi: 10.1242/dmm.011635

Armistead, J., and Triggs-Raine, B. (2014). Diverse diseases from a ubiquitous process: the ribosomopathy paradox. *FEBS Lett.* 588, 1491–1500. doi: 10.1016/j.febslet.2014.03.024

Azuma, M., Toyama, R., Laver, E., and Dawid, I. B. (2006). Perturbation of rRNA synthesis in the bap28 mutation leads to apoptosis mediated by p53 in the zebrafish central nervous system. *J. Biol. Chem.* 281, 13309–13316. doi: 10.1074/jbc.M601892200

Barlow, J. L., Drynan, L. F., Hewett, D. R., Holmes, L. R., Lorenzo-Abalde, S., Lane, A. L., et al. (2010). A p53-dependent mechanism underlies macrocytic anemia in a mouse model of human 5q- syndrome. *Nat. Med.* 16, 59–66. doi: 10.1038/nm.2063

Bielczyk-Maczynska, E., Lam Hung, L., Ferreira, L., Fleischmann, T., Weis, F., Fernandez-Pevida, A., et al. (2015). The ribosome biogenesis protein nol9 is essential for definitive hematopoiesis and pancreas morphogenesis in zebrafish. *PLoS Genet.* 11:e1005677. doi: 10.1371/journal.pgen.1005677

Boglev, Y., Badrock, A. P., Trotter, A. J., Du, Q., Richardson, E. J., Parslow, A. C., et al. (2013). Autophagy induction is a Tor- and Tp53-independent cell survival response in a zebrafish model of disrupted ribosome biogenesis. *PLoS Genet.* 9:e1003279. doi: 10.1371/journal.pgen.1003279

Burroughs, L., Woolfrey, A., and Shimamura, A. (2009). Shwachman-diamond syndrome: a review of the clinical presentation, molecular pathogenesis, diagnosis, and treatment. *Hematol. Oncol. Clin. North Am.* 23, 233–248. doi: 10.1016/j.hoc.2009.01.007

Carapito, R., Konantz, M., Paillard, C., Miao, Z., Pichot, A., Leduc, M. S., et al. (2017). Mutations in signal recognition particle SRP54 cause syndromic neutropenia with Shwachman-diamond-like features. *J. Clin. Invest.* 127, 4090–4103. doi: 10.1172/jci92876

Chang, N., Sun, C., Gao, L., Zhu, D., Xu, X., Zhu, X., et al. (2013). Genome editing with RNA-guided Cas9 nuclease in zebrafish embryos. *Cell Res.* 23, 465–472. doi: 10.1038/cr.2013.45

Chen, J., Ruan, H., Ng, S. M., Gao, C., Soo, H. M., Wu, W., et al. (2005). Loss of function of def selectively up-regulates Delta113p53 expression to arrest expansion growth of digestive organs in zebrafish. *Genes Dev.* 19, 2900–2911. doi: 10.1101/gad.1366405

Chen, Y. H., Lu, Y. F., Ko, T. Y., Tsai, M. Y., Lin, C. Y., Lin, C. C., et al. (2009). Zebrafish cdx1b regulates differentiation of various intestinal cell lineages. *Dev. Dyn.* 238, 1021–1032. doi: 10.1002/dvdy.21908

Collins, J. C., Ghalei, H., Doherty, J. R., Huang, H., and Culver, R. N. (2018). Ribosome biogenesis factor Ltv1 chaperones the assembly of the small subunit head. *J. Cell Biol.* 217, 4141–4154. doi: 10.1083/jcb.201804163

Dai, M. S., and Lu, H. (2004). Inhibition of MDM2-mediated p53 ubiquitination and degradation by ribosomal protein L5. *J. Biol. Chem.* 279, 44475–44482. doi: 10.1074/jbc.M403722200

Dai, M. S., Zeng, S. X., Jin, Y., Sun, X. X., David, L., and Lu, H. (2004). Ribosomal protein L23 activates p53 by inhibiting MDM2 function in response to ribosomal perturbation but not to translation inhibition. *Mol. Cell Biol.* 24, 7654–7668. doi: 10.1128/mcb.24.17.7654-7668.2004

Danilova, N., Sakamoto, K. M., and Lin, S. (2008). Ribosomal protein S19 deficiency in zebrafish leads to developmental abnormalities and defective erythropoiesis through activation of p53 protein family. *Blood* 112, 5228–5237. doi: 10.1182/blood-2008-01-132290

Danilova, N., Sakamoto, K. M., and Lin, S. (2011). Ribosomal protein L11 mutation in zebrafish leads to haematopoietic and metabolic defects. *Br. J. Haematol.* 152, 217–228. doi: 10.1111/j.1365-2141.2010.08396.x

Doherty, L., Sheen, M. R., Vlachos, A., Choesmel, V., O'Donohue, M. F., Clinton, C., et al. (2010). Ribosomal protein genes RPS10 and RPS26 are commonly mutated in Diamond-Blackfan anemia. *Am. J. Hum. Genet.* 86, 222–228. doi: 10.1016/j.ajhg.2009.12.015

Ear, J., Hsueh, J., Nguyen, M., Zhang, Q., Sung, V., Chopra, R., et al. (2016). A zebrafish model of 5q-syndrome using CRISPR/Cas9 targeting RPS14 reveals a p53-independent and p53-dependent mechanism of erythroid failure. *J. Genet. Genomics* 43, 307–318. doi: 10.1016/j.jgg.2016.03.007

Farrar, J. E., Nater, M., Caywood, E., McDevitt, M. A., Kowalski, J., Takemoto, C. M., et al. (2008). Abnormalities of the large ribosomal subunit protein, Rpl35a, in Diamond-Blackfan anemia. *Blood* 112, 1582–1592. doi: 10.1182/blood-2008-02-140012

Field, H. A., Dong, P. D. S., Beis, D., and Stainier, D. Y. R. (2003). Formation of the digestive system in zebrafish. II. Pancreas morphogenesis⋆. *Dev. Biol.* 261, 197–208. doi: 10.1016/s0012-1606(03)00308-7

Fumagalli, S., Di Cara, A., Neb-Gulati, A., Natt, F., Schwemberger, S., Hall, J., et al. (2009). Absence of nucleolar disruption after impairment of 40S ribosome biogenesis reveals an rpL11-translation-dependent mechanism of p53 induction. *Nat. Cell Biol.* 11, 501–508. doi: 10.1038/ncb1858

Georgakilas, A. G., Martin, O. A., and Bonner, W. M. (2017). p21: a two-faced genome guardian. *Trends Mol. Med.* 23, 310–319. doi: 10.1016/j.molmed.2017.02.001

Ghalei, H., Schaub, F. X., Doherty, J. R., Noguchi, Y., Roush, W. R., Cleveland, J. L., et al. (2015). Hrr25/CK1delta-directed release of Ltv1 from pre-40S ribosomes is necessary for ribosome assembly and cell growth. *J. Cell Biol.* 208, 745–759.

Godinho, L., Mumm, J. S., Williams, P. R., Schroeter, E. H., Koerber, A., Park, S. W., et al. (2005). Targeting of amacrine cell neurites to appropriate synaptic laminae in the developing zebrafish retina. *Development* 132, 5069–5079. doi: 10.1242/dev.02075

He, J., Yang, Y., Zhang, J., Chen, J., Wei, X., He, J., et al. (2017). Ribosome biogenesis protein Urb1 acts downstream of mTOR complex 1 to modulate digestive organ development in zebrafish. *J. Genet. Genomics* 44, 567–576. doi: 10.1016/j.jgg.2017.09.013

He, Q., Zhang, C., Wang, L., Zhang, P., Ma, D., Lv, J., et al. (2015). Inflammatory signaling regulates hematopoietic stem and progenitor cell emergence in vertebrates. *Blood* 125, 1098–1106. doi: 10.1182/blood-2014-09-601542

Herbomel, P., Thisse, B., and Thisse, C. (2001). Zebrafish early macrophages colonize cephalic mesenchyme and developing brain, retina, and epidermis through a M-CSF receptor-dependent invasive process. *Dev. Biol.* 238, 274–288. doi: 10.1006/dbio.2001.0393

Huang, H., Ruan, H., Aw, M. Y., Hussain, A., Guo, L., Gao, C., et al. (2008). Mypt1-mediated spatial positioning of Bmp2-producing cells is essential for liver organogenesis. *Development* 135, 3209–3218. doi: 10.1242/dev.024406

Iadevaia, V., Caldarola, S., Biondini, L., Gismondi, A., Karlsson, S., Dianzani, I., et al. (2010). PIM1 kinase is destabilized by ribosomal stress causing inhibition of cell cycle progression. *Oncogene* 29, 5490–5499. doi: 10.1038/onc.2010.279

Jagannathan-Bogdan, M., and Zon, L. I. (2013). Hematopoiesis. *Development* 140, 2463–2467. doi: 10.1242/dev.083147

Jia, X. E., Ma, K., Xu, T., Gao, L., Wu, S., Fu, C., et al. (2015). Mutation of kri1l causes definitive hematopoiesis failure via PERK-dependent excessive autophagy induction. *Cell Res.* 25, 946–962. doi: 10.1038/cr.2015.81

Jones, N. C., Lynn, M. L., Gaudenz, K., Sakai, D., Aoto, K., Rey, J. P., et al. (2008). Prevention of the neurocristopathy Treacher Collins syndrome through inhibition of p53 function. *Nat. Med.* 14, 125–133. doi: 10.1038/nm1725

Kressler, D., Pertschy, B., Kim, W., Kim, H. D., Jung, Y., Kim, J., et al. (2015). Drosophila low temperature viability protein 1 (LTV1) is required for ribosome biogenesis and cell growth downstream of *Drosophila* Myc (dMyc). *J. Biol. Chem.* 290, 13591–13604.

Lapik, Y. R., Fernandes, C. J., Lau, L. F., and Pestov, D. G. (2004). Physical and functional interaction between Pes1 and Bop1 in mammalian ribosome biogenesis. *Mol. Cell* 15, 17–29. doi: 10.1016/j.molcel.2004.05.020

Le Guyader, D., Redd, M. J., Colucci-Guyon, E., Murayama, E., Kissa, K., Briolat, V., et al. (2008). Origins and unconventional behavior of neutrophils in developing zebrafish. *Blood* 111, 132–141. doi: 10.1182/blood-2007-06-095398

Li, J., Yu, L., Zhang, H., Wu, J., Yuan, J., Li, X., et al. (2009). Down-regulation of pescadillo inhibits proliferation and tumorigenicity of breast cancer cells. *Cancer Sci.* 100, 2255–2260. doi: 10.1111/j.1349-7006.2009.01325.x

Li, L., Jin, H., Xu, J., Shi, Y., and Wen, Z. (2011). Irf8 regulates macrophage versus neutrophil fate during zebrafish primitive myelopoiesis. *Blood* 117, 1359–1369. doi: 10.1182/blood-2010-06-290700

Mayer, A. N., and Fishman, M. C. (2003). Nil per os encodes a conserved RNA recognition motif protein required for morphogenesis and cytodifferentiation of digestive organs in zebrafish. *Development* 130, 3917–3928.

Menne, T. F., Goyenechea, B., Sanchez-Puig, N., Wong, C. C., Tonkin, L. M., Ancliff, P. J., et al. (2007). The Shwachman-Bodian-Diamond syndrome protein mediates translational activation of ribosomes in yeast. *Nat. Genet.* 39, 486–495. doi: 10.1038/ng1994

Narla, A., and Ebert, B. L. (2010). Ribosomopathies: human disorders of ribosome dysfunction. *Blood* 115, 3196–3205. doi: 10.1182/blood-2009-10-178129

Ober, E. A., Verkade, H., Field, H. A., and Stainier, D. Y. (2006). Mesodermal Wnt2b signalling positively regulates liver specification. *Nature* 442, 688–691. doi: 10.1038/nature04888

Oyarbide, U., Shah, A. N., Amaya-Mejia, W., Snyderman, M., Kell, M. J., Allende, D. S., et al. (2020). Loss of Sbds in zebrafish leads to neutropenia and pancreas and liver atrophy. *JCI Insight* 5:e134309. doi: 10.1172/jci.insight.134309

Oyarbide, U., Topczewski, J., and Corey, S. J. (2019). Peering through zebrafish to understand inherited bone marrow failure syndromes. *Haematologica* 104, 13–24. doi: 10.3324/haematol.2018.196105

Panse, V. G., and Johnson, A. W. (2010). Maturation of eukaryotic ribosomes: acquisition of functionality. *Trends Biochem. Sci.* 35, 260–266. doi: 10.1016/j.tibs.2010.01.001

Pereboom, T. C., van Weele, L. J., Bondt, A., and MacInnes, A. W. (2011). A zebrafish model of dyskeratosis congenita reveals hematopoietic stem cell formation failure resulting from ribosomal protein-mediated p53 stabilization. *Blood* 118, 5458–5465. doi: 10.1182/blood-2011-04-351460

Provost, E., Wehner, K. A., Zhong, X., Ashar, F., Nguyen, E., Green, R., et al. (2012). Ribosomal biogenesis genes play an essential and p53-independent role in zebrafish pancreas development. *Development* 139, 3232–3241. doi: 10.1242/dev.077107

Provost, E., Weier, C. A., and Leach, S. D. (2013). Multiple ribosomal proteins are expressed at high levels in developing zebrafish endoderm and are required for normal exocrine pancreas development. *Zebrafish* 10, 161–169. doi: 10.1089/zeb.2013.0884

Qin, W., Chen, Z., Zhang, Y., Yan, R., Yan, G., Li, S., et al. (2014). Nom1 mediates pancreas development by regulating ribosome biogenesis in zebrafish. *PLoS One* 9:e100796. doi: 10.1371/journal.pone.0100796

Razavipour, S. F., Harikumar, K. B., and Slingerland, J. M. (2020). p27 as a transcriptional regulator: new roles in development and cancer. *Cancer Res.* 80, 3451–3458. doi: 10.1158/0008-5472.can-19-3663

Roach, G., Heath Wallace, R., Cameron, A., Emrah Ozel, R., Hongay, C. F., Baral, R., et al. (2013). Loss of ascl1a prevents secretory cell differentiation within the zebrafish intestinal epithelium resulting in a loss of distal intestinal motility. *Dev. Biol.* 376, 171–186. doi: 10.1016/j.ydbio.2013.01.013

Seiser, R. M., Sundberg, A. E., Wollam, B. J., Zobel-Thropp, P., Baldwin, K., Spector, M. D., et al. (2006). Ltv1 is required for efficient nuclear export of the ribosomal small subunit in *Saccharomyces cerevisiae*. *Genetics* 174, 679–691. doi: 10.1074/jbc.M109.040774

Shi, Y., Zhang, Y., Zhao, F., Ruan, H., Huang, H., Luo, L., et al. (2014). Acetylcholine serves as a derepressor in loperamide-induced opioid-induced bowel dysfunction (OIBD) in zebrafish. *Sci. Rep.* 4:5602. doi: 10.1038/srep05602

Tafforeau, L., Zorbas, C., Langhendries, J.-L., Mullineux, S.-T., Stamatopoulou, V., Mullier, R., et al. (2011). The complexity of human ribosome biogenesis revealed by systematic nucleolar screening of pre-rRNA processing factors. *Mol. Cell* 51, 539–551. doi: 10.1016/j.molcel.2013.08.011

Tao, T., and Peng, J. (2009). Liver development in zebrafish (*Danio rerio*). *J. Genet. Genomics* 36, 325–334. doi: 10.1016/s1673-8527(08)60121-6

Taylor, A. M., Humphries, J. M., White, R. M., Murphey, R. D., Burns, C. E., and Zon, L. I. (2012). Hematopoietic defects in rps29 mutant zebrafish depend upon p53 activation. *Exp. Hematol.* 40, 228–237e225.

Venkatasubramani, N., and Mayer, A. N. (2008). A zebrafish model for the Shwachman-Diamond syndrome (SDS). *Pediatr. Res.* 63, 348–352. doi: 10.1203/PDR.0b013e3181659736

Wang, Y., Luo, Y., Hong, Y., Peng, J., and Lo, L. (2012). Ribosome biogenesis factor Bms1-like is essential for liver development in zebrafish. *J. Genet. Genomics* 39, 451–462. doi: 10.1016/j.jgg.2012.07.007

Wang, Y., Zhu, Q., Huang, L., Zhu, Y., Chen, J., Peng, J., et al. (2016). Interaction between Bms1 and Rcl1, two ribosome biogenesis factors, is evolutionally conserved in zebrafish and human. *J. Genet. Genomics* 43, 467–469. doi: 10.1016/j.jgg.2016.05.001

Warner, J. R. (2001). Nascent ribosomes. *Cell* 107, 133–136.

Wilkins, B. J., Lorent, K., Matthews, R. P., and Pack, M. (2013). p53-mediated biliary defects caused by knockdown of cirh1a, the zebrafish homolog of the gene responsible for North American Indian Childhood Cirrhosis. *PLoS One* 8:e77670. doi: 10.1371/journal.pone.0077670

Xue, S., and Barna, M. (2012). Specialized ribosomes: a new frontier in gene regulation and organismal biology. *Nat. Rev. Mol. Cell Biol.* 13, 355–369. doi: 10.1038/nrm3359

Yadav, G. V., Chakraborty, A., Uechi, T., and Kenmochi, N. (2014). Ribosomal protein deficiency causes Tp53-independent erythropoiesis failure in zebrafish. *Int. J. Biochem. Cell Biol.* 49, 1–7. doi: 10.1016/j.biocel.2014.01.006

Yadavilli, S., Mayo, L. D., Higgins, M., Lain, S., Hegde, V., and Deutsch, W. A. (2009). Ribosomal protein S3: a multi-functional protein that interacts with both p53 and MDM2 through its KH domain. *DNA Repair* 8, 1215–1224. doi: 10.1016/j.dnarep.2009.07.003

Zhang, Y., Morimoto, K., Danilova, N., Zhang, B., and Lin, S. (2012). Zebrafish models for dyskeratosis congenita reveal critical roles of p53 activation contributing to hematopoietic defects through RNA processing. *PLoS One* 7:e30188. doi: 10.1371/journal.pone.0030188

Zhang, Y., Wolf, G. W., Bhat, K., Jin, A., Allio, T., Burkhart, W. A., et al. (2003). Ribosomal protein L11 negatively regulates oncoprotein MDM2 and mediates a p53-dependent ribosomal-stress checkpoint pathway. *Mol. Cell Biol.* 23, 8902–8912.

Conflict of Interest: The authors declare that the research was conducted in the absence of any commercial or financial relationships that could be construed as a potential conflict of interest.

Publisher's Note: All claims expressed in this article are solely those of the authors and do not necessarily represent those of their affiliated organizations, or those of the publisher, the editors and the reviewers. Any product that may be evaluated in this article, or claim that may be made by its manufacturer, is not guaranteed or endorsed by the publisher.

frontiers in Cell and Developmental Biology

REVIEW
published: 08 October 2021
doi: 10.3389/fcell.2021.717404

Programmed Cell Death Not as Sledgehammer but as Chisel: Apoptosis in Normal and Abnormal Craniofacial Patterning and Development

*Claudia Compagnucci[1,2,3], Kira Martinus[1], John Griffin[3,4] and Michael J. Depew[1,3]**

[1] Institute for Cell and Neurobiology, Center for Anatomy, Charité Universitätsmedizin Berlin, CCO, Berlin, Germany, [2] Genetics and Rare Diseases Research Division, Ospedale Pediatrico Bambino Gesù, Rome, Italy, [3] Department of Craniofacial Development, King's College London, London, United Kingdom, [4] School of Biological Sciences, University of East Anglia, Norwich, United Kingdom

OPEN ACCESS

Edited by:
Stefan Washausen,
Universität Münster, Germany

Reviewed by:
John Abramyan,
University of Michigan–Dearborn, United States
Anthony Graham,
King's College London, United Kingdom

***Correspondence:**
Michael J. Depew
michael.depew@charite.de

Specialty section:
This article was submitted to Cell Death and Survival, a section of the journal Frontiers in Cell and Developmental Biology

Received: 30 May 2021
Accepted: 28 July 2021
Published: 08 October 2021

Citation:
Compagnucci C, Martinus K, Griffin J and Depew MJ (2021) Programmed Cell Death Not as Sledgehammer but as Chisel: Apoptosis in Normal and Abnormal Craniofacial Patterning and Development. Front. Cell Dev. Biol. 9:717404. doi: 10.3389/fcell.2021.717404

Coordination of craniofacial development involves an complex, intricate, genetically controlled and tightly regulated spatiotemporal series of reciprocal inductive and responsive interactions among the embryonic cephalic epithelia (both endodermal and ectodermal) and the cephalic mesenchyme — particularly the cranial neural crest (CNC). The coordinated regulation of these interactions is critical both ontogenetically and evolutionarily, and the clinical importance and mechanistic sensitivity to perturbation of this developmental system is reflected by the fact that one-third of all human congenital malformations affect the head and face. Here, we focus on one element of this elaborate process, apoptotic cell death, and its role in normal and abnormal craniofacial development. We highlight four themes in the temporospatial elaboration of craniofacial apoptosis during development, namely its occurrence at (1) positions of epithelial-epithelial apposition, (2) within intra-epithelial morphogenesis, (3) during epithelial compartmentalization, and (4) with CNC metameric organization. Using the genetic perturbation of *Satb2*, *Pbx1/2*, *Fgf8,* and *Foxg1* as exemplars, we examine the role of apoptosis in the elaboration of jaw modules, the evolution and elaboration of the lambdoidal junction, the developmental integration at the mandibular arch hinge, and the control of upper jaw identity, patterning and development. Lastly, we posit that apoptosis uniquely acts during craniofacial development to control patterning cues emanating from core organizing centres.

Keywords: craniofacial, hinge and caps, *Satb2*, *Fgf8*, *Foxg1*, *Pbx*, branchial arch, apoptosis

INTRODUCTION

Craniogenesis, the development of a patterned and functionally integrated head, is an especially elaborate process, one under intense developmental and evolutionary pressures (Gans and Northcutt, 1983; Depew and Simpson, 2006; Green et al., 2015; Marcucio et al., 2015). This applies to the pattern, development and morphogenesis of both the central nervous and the associated cranial peripheral nervous systems (CNS and PNS, respectively) as well as to the craniofacial tissues

informing and supporting them, (i.e., to both the contents and the container). The developmental system that coordinates and patterns the craniofacial primordia involves a complex, intricate, genetically controlled, and tightly regulated spatiotemporal series of reciprocal inductive and responsive interactions. These include interactions between the embryonic cephalic epithelia (both endodermal and ectodermal) and the cephalic mesenchyme — particularly the cranial neural crest (CNC). The coordinated regulation of these interactions is critical both ontogenetically and evolutionarily, and the clinical importance and mechanistic sensitivity to perturbation of this developmental system is reflected by the fact that one-third of all human congenital malformations affect the head and face (Gorlin et al., 1990). Orofacial clefting alone (including cleft palate (CP) and/or cleft lip (CL)) constitutes, for example, one of the most common human birth defects (from 1 in 500 to 1 in 2,000 births depending on the population; Dixon et al., 2011; Ferretti et al., 2011).

Here, we focus on one element of this elaborate process — apoptotic programmed cell death (PCD) — and its role in normal and abnormal craniofacial development (CFD). Rather than intending an exhaustive catalogue, our aims are rather more modest. Firstly, we aim to provide a sufficient correlative overview of the mechanics and normal topography of apoptosis during CFD to promote the notion of apoptosis as an active biologic tool during the elaboration of CFD and morphogenesis, one acting more as a scalpel than as a sledgehammer. In this context, we present basic primers of both embryonic CFD (specifically highlighting early jaw development as an illustrative focal point) and the mechanics of apoptosis that together provide reference points as we discuss apoptosis in normal and abnormal CFD. These sections are intended to inform those new to the topics and can easily be skipped by those previously well-versed. We then describe features of the normal topography of apoptosis during early CFD, focusing on: (1) positions of embryonic epithelial-epithelial apposition and fusion; (2) intra-epithelial morphogenesis; (3) embryonic epithelial compartmentalization; and (4) early CNC organization. In addressing apoptosis in abnormal CFD we take two approaches. First, we turn to the molecular mechanics of apoptosis to underscore how CFD is (and is not) affected by mutations in the genes encoding components of the apoptosis machinery. In the other, we utilize examples from our own work that we believe exemplify the correlations between targeted mutations of craniofacial patterning genes (including of *Satb2*, *Pbx*, *Fgf8,* and *Foxg1*), aberrant CFD and morphogenesis, and the alteration of apoptotic profiles during CFD. And secondly, we utilize what has been presented from our first aim to posit a potentially unique role for developmentally programmed apoptosis in idiosyncratic aspects of early CDF and patterning.

Craniofacial Patterning, Development, and Morphogenesis: A Brief Primer

Much of our understanding of CDF follows from appreciation of the biology of, and patterning influences on, the CNC (Gans and Northcutt, 1983; Depew and Simpson, 2006; Bronner-Fraser, 2008); this brief primer focuses on this subject. Vertebrate craniogenesis typically begins in earnest with the advent of the recently gastrulated anterior mesendoderm coming to underlie the embryonic ectoderm and the initial partition of this ectoderm into neurectoderm (NE), surface cephalic ectoderm (SCE), and a transitional zone separating them (**Figure 1A**; Rubenstein et al., 1998; Depew and Compagnucci, 2008). While patterned regionalization progresses within the NE, CNC are eventually induced at the neural plate border lateral to the NE (Gans and Northcutt, 1983; Redies and Puelles, 2001; Bronner and LeDouarin, 2012; Green et al., 2015). Once induced and committed, CNC undergo an epithelial-mesenchymal transition (EMT) at the neural folds (NF) and migrate to colonize the regions surrounding the developing anlage of the ear, nose, eye, anterior CNS, and the meristic, metameric branchial (pharyngeal or visceral) arches (BA) (Arey, 1934; Nelsen, 1953; Goodrich, 1958; Wake, 1979; Minoux and Rijli, 2010; Etchevers et al., 2019; **Figure 1B**). The arches are transient embryonic structures of the developing head and neck for which an historic cacophony of naming schemes, depending upon anatomic tradition or phyla being described, exists (**Figure 1C**; Depew et al., 2005). To maintain continuity of naming with much of the literature being cited below we herein refer to the arches numerically from cranial to caudal as BA1 to BA6. The BAs will eventually give rise to many significant craniofacial structures, including most of the jaw skeleton (BA1), the auditory ossicles (BA1 and BA2), the muscles of mastication (BA1) and facial expression (BA2), the hyoid apparatus (BA2/3), the aortic arches, and their derivatives (e.g., portions of the aorta, truncus pulmonalis, and the carotid arteries; BA3/4/6), as well as the pharyngeal pouch (PP) tissues and glands (e.g., palatine tonsils, thymus, parathyroid, ultimobranchial body, and thyroid).

Significantly, cranio-caudal regionalization of the delaminating CNC initially establishes two disparate, functionally pre-patterned populations. One is an anterior equipotent *Hox*-gene negative, mostly *Otx2*-positive, population (aka., the "trigeminal" CNC) that migrates into BA1, surrounds the forebrain and eye, and migrates to colonize the frontonasal region (**Figure 1B**; Creuzet et al., 2002; Minoux and Rijli, 2010). It is this population that will directly yield the skeletal tissues of the jaws and anterior neurocranium. This CNC population is functionally interchangeable and neuro-axial origin does not direct disparate interpretations of subsequent positional patterning information. The second is a posterior *Hox*-gene positive population that fills the remainder of the BAs. Unlike the trigeminal CNC, the neuro-axial level of origin of this population does instruct the subsequent interpretation of positional information.

Being fungible in nature, the *Hox*-negative CNC receive positional patterning information locally from the cephalic epithelia. Thus, understanding the proximate patterning of the SCE and pharyngeal (foregut) endoderm (PE) is crucial to overall understanding of CFD. While the CNC is migrating from the NF, a signaling cascade establishes an iterative, cranio-caudal sequence of invaginations within the nascent PE

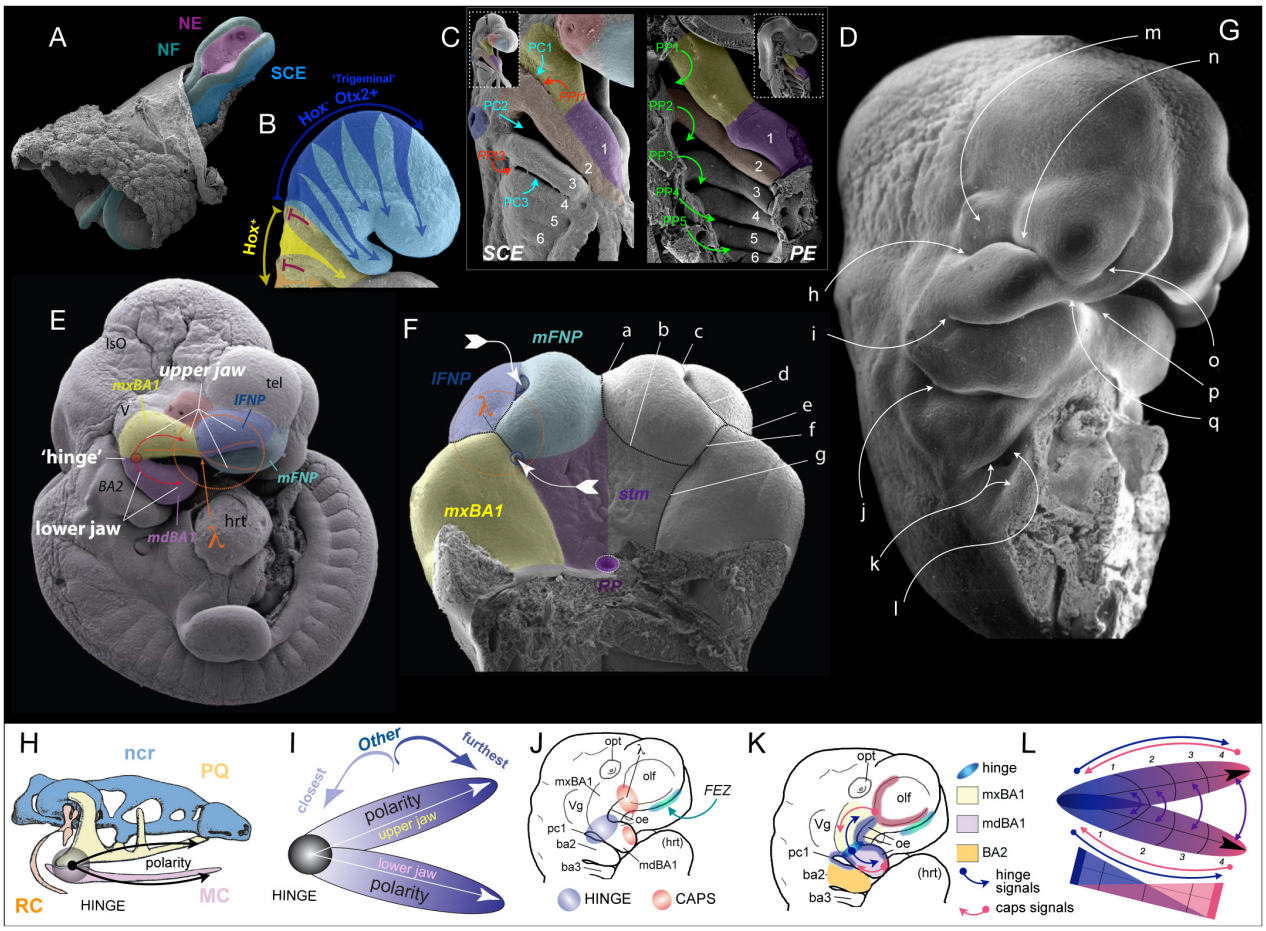

FIGURE 1 | Early craniofacial patterning and development. **(A–G)** Scanning electron micrographs of shark **(A,C,D)** and mouse **(B,E–G)** embryos. **(A)** Nuerulation in a shark. NF, neural fold; NE, neurectoderm; SCE, surface cephalic ectoderm. **(B)** Fungible, trigeminal cranial neural crest (CNC) fills BA1 and the FNP. E9.25 mouse embryo. *Hox*$^{-}$: blue. *Hox*$^{+}$: yellow arrows entering BA2 from R4, orange entering BA3 from R6. Red T-bars indicate the apoptotic culling of R3 and R5 CNC. **(C,D)** SCE and PE in the BA of a hemisected shark embryo. 1–6, BA number. PC1–3, pharyngeal clefts 1–3 (SCE). PP1–5, pharyngeal pouches 1–5 (PE). PPt1/3, pharyngeal plates. lavender, mdBA1; yellow, mxBA1; red, optic primordia; light blue, FNP; dark blue, otic pit; orange, BA2. **(E)** E10.5 mouse embryo showing the topography of the craniofacial primordia, the hinge region and λ (the lambdoidal junction). IsO, isthmic organizer; tel, telencephalon; hrt, heart; lFNP, lateral frontonasal process; mFNP, medial frontonasal process; V, trigeminal ganglion. Colour as above. **(F)** E11.5 mouse embryo (with the lower jaw primordia removed) showing the embryonic primordia of the λ and correlated anatomical boundaries. The converging white arrows indicate the invaginating external nares and internal (primary) choanae whose infoldings must unite and perforate to form a nasal cavity (fossa) that communicates directly with the lower respiratory system via a nasopharynx. ***a***, internasal line (frontal groove); ***b***, naso-stomodeal line; ***c***, dorsal intranasal line; ***d***, ventral intranasal line (nasal fin); ***e***, nasolacrimal line (groove); ***f***, oronasal groove (medial-choanal line); ***g***, stomodeo-palatal line. **(G)** E11.5 mouse embryo highlighting positions of epithelial-epithelial apposition. ***h***, ridge of optical furrow from which the lower eyelid will sprout; ***i***, mxBA1-mdBA1 fusion at the oral commissure; ***j***, first pharyngeal cleft and plate; ***k***, opercular ridge of BA2 and epipericardial ridge with which it fuses; ***l***, cervical sinus; ***m***, recently pinched off lens; ***n***, nasolacrimal groove; ***o***, nasal fin; ***p***, mentum (mdBa1-mdBA1); ***q***, mFNP-mxBA1. **(H)** Schematic of prototypical vertebrate chondrocranium and the inherent polarity of it jaws. ncr, neurocranium; RC, Reichert's cartilage; HINGE, circle at articulation; MC, Meckel's cartilage; PQ, palatoquadrate cartilage. **(I)** Schema of the inherent polarity of appositional jaws. **(J)** Orientation of hinge and caps topography on an E10 mouse embryo. opt, optic primordia; Vg, trigeminal ganglion; FEZ, facial (frontonasal) ectodermal zone which helps integrate the frontonasal midline; oe, oral ectoderm. **(K)** Topography of epithelial signaling from the hinge (blue) and caps (red) signaling centres. **(L)** Modularity due to polarity in jaw development. Apposing gradients of signaling information create modules (here, 1–4) within the developing jaw primordia.

that creates the pharyngeal pouches (PP; Shone and Graham, 2014). These invaginations then segregate the streams of CNC in the BAs by apposing and contacting corresponding pharyngeal (branchial) cleft (PC) invaginations of the SCE covering the BAs (**Figures 1C,D**). This contact transiently creates points of epithelial-epithelial apposition, each referred to as a pharyngeal plate (PPt). The epithelia of these contact points express signaling molecules that contribute to the patterning of the BAs (Depew and Compagnucci, 2008). Though the SCE naturally contains cells fated to be epidermal in nature, it also yields the cranial placodes (Pipsa and Thesleff, 2003; Bhattacharyya et al., 2004; Bailey et al., 2006; Patthey et al., 2014; Streit, 2018) and, notably, the known patterning centres for the anterior cranium and jaws (Depew et al., 2002a,b; Hu et al., 2003; Creuzet et al., 2006; Depew and Compagnucci, 2008; Minoux and Rijli, 2010; Cajal et al., 2014;

Marcucio et al., 2015). To enable greater understanding of our subsequent exemplars of apoptosis in the context of normal and abnormal CFD it is expedient below to provide here some further detail of these patterning centres, BA1, and jaw development.

In part because the trigeminal CNC are, initially at least, equipotent in their response to local patterning cues, among the fundamental tasks in patterning BA1 and the jaws are: (1) establishing upper jaw versus lower jaw positional identity within the CNC, (2) generating and maintaining the point of articulation between the upper and lower jaw arcades, and (3) keeping the arcades in appropriate functional registration during subsequent development and morphogenesis. Actualization of these tasks involves elaboration of a "hinge and caps" system of establishing positional information in the CNC through several regional signaling centres (Depew et al., 2002a; Depew and Compagnucci, 2008; Compagnucci et al., 2013). BA1 is molecularly and developmentally subdivided at its "hinge" region into a distal, lower jaw-generating mandibular branch (mdBA1) and a more proximal, upper jaw generating maxillary branch (mxBA1; **Figure 1E**). Epithelially secreted signals from PPt1 (i.e., from PC1 and PP1, **Figures 1C–E**), coordinated with those from the oral ectoderm (OE; **Figures 1J,K**), generate a craniofacial organizing centre at the hinge that establishes the point of articulation (Rijli et al., 1993; Beverdam et al., 2002; Depew et al., 2002a; Depew and Compagnucci, 2008). Through mechanisms not yet fully understood, but clearly involving the restriction of *Dlx5/6* expression to mdBA1 (in part through *Foxg1* expression in the SCE and the regulation of Endothelin signalling in mxBA1) the hinge organizing centre likewise plays a significant role in instructing the CNC to either adopt a mxBA1-upper jaw identity or a mdBA1-lower jaw identity (Depew and Compagnucci, 2008; Sato et al., 2008; Compagnucci and Depew, submitted).

Crucially, BA1 primordia and the jaws that they give rise to are both fundamentally polarized (**Figures 1H–L**). This characteristic enables the functional registration of the upper and lower jaws from the point of their proximal articulations (at the hinge) to their distal endpoints (aka, their "caps"), and the hinge organizing centre alone is (theoretically) sufficient to generate such polarity. Notably, however, during gnathostome (jawed vertebrate) development, the upper jaws in all but Chondrichthyans incorporate a premaxillary component associated with the olfactory placode and capsule. Olfactory placodogenesis results in the invagination of a nasal pit into the underlying CNC, a morphogenic event that in amniotes distinctly delineates medial (mFNP) and lateral (lFNP) FNP primordia (**Figures 1E,F**). A significant transient embryonic structure of amniotes is the lambdoidal junction (hereafter λ) that develops where mxBA1, the lFNP and the mFNP converge (being fully elaborated around E10.5 in a mouse; Tamarin and Boyde, 1977; Depew et al., 2002a,b; Depew and Simpson, 2006; Depew and Compagnucci, 2008; Ferretti et al., 2011). In a topographically complex manner, the SCE of λ secretes a significant range of signaling molecules such that λ acts as the upper jaw "cap" organizing centre integrating mxBA1 development distal to the hinge region with that of the FNP. This includes the structural integration of the premaxillae, maxillae, and nasal capsules. It also includes the formation of choanae, unified lips, primary palates, and (in gnathostomes that possess them) secondary palates. As we will describe below, apoptosis plays a critical, clinically significant role in CFD associated with λ.

Though much less complex structurally and developmentally, the SCE of the distal-most midline of mdBA1 also secretes many of the same signaling molecules as λ — thereby creating the corresponding lower-jaw "cap" organizing centre. In sum, the CNC are patterned by the integration of the hinge organizing signals with countering epithelially derived patterning signals posteroproximally propagated through mdBA1 from the mandibular organizing "cap" and patterning signals posterodistally emanating through mxBA1 from the maxillary "cap" centred at λ (**Figure 1K**).

Apoptosis: A General Description

Apoptosis, recognized as a specific subcategory of PCD, is a fundamental component of both animal development and adult homeostasis (Fuchs and Steller, 2011; Suzanne and Steller, 2013). Among the developmental mechanisms necessary for normal vertebrate morphogenesis are (1) epithelial invagination and evagination, (2) closure of epithelial tubes and vesicles, (3) separation of tissue components, (4) migration of anlage and rudiments, (5) the conjoining of appositional anlage, (6) the regulation of tissue specific cell-population size, and (7) the removal of only transiently necessary (or vestigial) tissues. As we will discuss below, the ontogenetic topography of such processes often correlates with the temporospatial topography of apoptosis (Glücksmann, 1951; Saunders, 1966; Kerr et al., 1972; Jacobson et al., 1997; Fuchs and Steller, 2011; Ghose and Shaham, 2020; Voss and Strasser, 2020). As an evolutionarily conserved mechanism of organismal cellular auto-culling, apoptosis results in a controlled, distinct, canonical and readily recognizable set of changes in cellular ultrastructure. Such changes include: (1) the rounding and shrinking of cell size (cytoplasmic compaction); (2) nuclear changes accompanied by the condensation and marginalization of chromatin (pyknosis) and eventual internucleosomal DNA fragmentation (karyorrhexis); (3) organelle shrinkage, fragmentation and rearrangement of cytoskeletal elements; (4) the advent of plasma membrane blebbing and the eventual separation of cell fragments into apoptotic bodies; (5) the release of "Apoptotic cell-derived extracellular vesicles" (ApoEVs) and their subsequent specific communications with surrounding tissues; and (6) the eventual phagocytic engulfment and degradation of cellular corpses (Kerr et al., 1972; Voss and Strasser, 2020). While other forms of PCD and senescence have been characterized, as well as have pathological forms of cell death, we are herein primarily concerned with apoptotic PCD and its roles in craniofacial pattern, development, and morphogenesis.

Overview of Historic Thoughts on Apoptosis' Role in Development

Numerous posited rationales for why an organism would benefit from programming intra-organismal cellular death have been put

forth. Appreciation of plausible roles for PCD during embryonic development has historically revolved around differentially perceived developmental and morphologic needs to eliminate *unwanted* cells, in particular during such developmental and morphogenic processes topographically correlated with apoptosis as those briefly enumerated above (e.g., epithelial invagination; Glücksmann, 1951; Saunders, 1966; Kerr et al., 1972; Shuler, 1995; Jacobson et al., 1997; Meier et al., 2000; Fuchs and Steller, 2011; Voss and Strasser, 2020). Briefly amalgamating posited developmental roles here, apoptosis has, for instance, been associated with the elimination of cells that seem to have no function as they are part of the development of a vestigial structure. This is exemplified by the programmed loss of mammalian pronephric tubules (exemplifying "phylogenetic" apoptosis) and the sex-specific reduction of either Müllerian or Wolffian ducts ("histogenic" apoptosis) (Glücksmann, 1951; Saunders, 1966; Jacobson et al., 1997). Apoptosis is likewise a perceived developmental mechanism that eliminates cells that have already functioned during embryonic ontogeny but which are no longer necessary. The elimination of Cajal-Retzius cells, the seminal colonizer neurons of the outer layer of the developing neocortex that are essential for both establishing the initial neocortical layering and functionally interacting with the overlying nascent meninges, exemplifies this type of role (Wong and Marín, 2019). Moreover, tissue specific ontogeny, such as with cerebral cortical development, can often be an intricate dance between progenitor cell division and proliferation on the one hand and regulated cell-type specific differentiation on the other. This dance often includes steps leading to the generation of excess numbers of cells, and apoptotois has been well documented as a significant mechanism for subsequently controlling appropriate neuronal cell numbers during development (Vecino and Acera, 2015; Wong and Marín, 2019). Apoptotic function has also been ascribed to the ontogenetic elimination of cells that are outright abnormal, misplaced, non-functional, or harmful, including limiting T- and B-cell lymphocyte expansion where reactivity to self or failure to form useful, antigen-specific receptors is at play.

These examples of larger scale developmental apoptosis are representative more of a sledgehammer-like rather than of a scalpel-like approach to cellular elimination. A notable scalpel-like corollary here comes when the population of cells under size control is small and contains cells actively secreting morphogen patterning signals. This is seen in the regulative cell death zone associated with controlling the numbers of Shh-expressing cell in the zone of polarizing activity of the limb bud (Sanz-Ezquerro and Tickle, 2000), the anterior neural ridge (Nonomura et al., 2013), and in the enamel knot signalling centres of developing teeth (Vaahtokari et al., 1996; Ahtiainen et al., 2016). Importantly, "morphogenic" apoptosis has also been deemed a principal sculptor of embryonic structures during morphogenesis, organogenesis and remodelling - the holotype sculpture being the apoptotic elimination of cells in the inter-digital webbing of the developing amniote autopod (Glücksmann, 1951; Saunders, 1966; Hinchliffe, 1981).

Molecular Toolbox and Machinery Underlying Apoptois

With this cursory look at the "where" and "why" of apoptosis in development, we briefly consider "how" it occurs. The molecular mechanisms underlying apoptosis have been well reviewed elsewhere (e.g., Jacobson et al., 1997; Meier et al., 2000; Taylor et al., 2008; Fuchs and Steller, 2011; Ravichandran, 2011; Tuzlak et al., 2016; Dorstyn et al., 2018; Voss and Strasser, 2020; Wanner et al., 2021) and are thus only succinctly presented here. Depending on the source of apoptotic instigation, two convergent mechanistic pathways of apoptosis - an intrinsic (or mitochondrial) and an extrinsic (or death receptor) - have typically been recognized. The intrinsic pathway is developmentally initiated by such events as a local change in growth factor or neurotrophic support level, metabolic stress, or extracellular matrix (ECM) detachment and epithelial cell extrusion (i.e., forms of anoikis). Much like many other molecular and cellular equilibrating acts, the intrinsic pathway response to apoptotic stimuli is believed to be regulated by a balanced activity of two classes (i.e., BH3-only and multi-BH domain) of pro-apoptotic members of the BCL-2 gene family with the pro-survival (anti-apoptotic) BCL-2 members (e.g., BCL-2, BCL-W, BCL-XL, A1/BFL-1, and MCL-1) which converge on caspases (cysteine-aspartic proteases) to effectuate apoptotic cell death. In the un-stimulated steady-state, anti-apoptotic BCL-2 proteins keep pro-apoptotic BH3-only effectors, such as BAK, BAX and BOK, in an inactive state. Once presented with apoptotic stimuli, however, BH3 proteins (e.g., BAD, BID, BIK, BIM, HRK, NOXA, and PUMA) inhibit anti-apoptotic BCL-2 proteins, thereby releasing effector BH3-only proteins to oligomerize and perforate the mitochondrial outer membrane (MOM) by pore formation. Once perforated, MOM permeabilization allows the egress of cytochrome c into the cytoplasm, wherein it interacts with APAF-1 (apoptosis activating factor 1) and an *initiator* caspase, such as procaspase-9, to create an "apoptosome" and sequently enzymatically activate the initiator procaspase. Activated Caspase-9, in turn, enzymatically cleaves a second class of inactive procaspases, the *executioner* (or effector) caspases, in particular Caspases-3, -6, and/or -7. This activates executioner caspases to cleave - and so to either activate or inhibit - a multitude of other proteins. Among these newly activated proteins are endonucleases that drive DNA fragmentation and inhibitors of flippases which then unbalance the constituent components of the bi-layered organization of the plasma membrane. Subsequently, these latter events reveal "find me" and "eat me" signals leading to the eventual phagocytic engulfment and degradation of apoptotic debris (Ellis et al., 1991; Taylor et al., 2008; Fuchs and Steller, 2011). Apoptotic stimuli, moreover, may also liberate initiator caspases from their inhibition by various IAP (Inhibitors of Apoptosis, such X-linked inhibitor of apoptosis, or XIAP) gene family encoded proteins.

As suggested by its sobriquet, the extrinsic death receptor pathway is initiated by the cognate receptor binding of tumour necrosis factor (TNF) family ligands, in particular of FAS ligand (FASL) to FAS receptor, which then potentiates

two distinct series of events. When present, procaspase-8 is activated (through a TRADD-RIPK1-FADD pathway) to cleave and thereby activate effector Caspases-3, -6, and/or -7 which can effectuate the proteolytic conversion of inactive BID into activated tBID — which then activates BAK and BAX with predicable consequences. Absent facient Caspase-8, the necroptotic cell death regimen (involving RIPK1, RIPK3 kinase activation, and MLKL phosphorylation and membrane translocation) can be initiated; notably, however, this leads to changes in cellular morphology that are distinct from those encountered with apoptosis and the process is thought to rarely occur during development (Voss and Strasser, 2020).

Axiomatically, expression of the components of the apoptosis machinery are under the disparate regulation by numerous transcription factors, including p53/63/73, AP-1, NF-κB, IRF-1, Myc, Foxo, Hox, and Snail (Dudgeon et al., 2009). Expression of such factors collectively establishes a regulatory balance between pro-apoptotic and anti-apoptotic proteins in the cell and thus ultimately controls cell death decisions at the cellular level.

Apoptosis as Chisel I: The Topography of Apoptosis During Normal CFD

In his compendium 70 years ago on cell death in normal vertebrate ontogeny, Glücksmann (1951) enumerated numerous accounts of cell death associated in some fashion with CFD. As with elsewhere in the vertebrate body, he established that cell death could often be correlated with craniofacial tissues changing shape. Among those topographies that he enumerated were the developing optic lens, vesicle and cup, the otocyst, the oronasal junction, the PPts, and the palatal shelves. To date, however, a comprehensive exposition of the normal, predictable spatiotemporal ontogeny of apoptosis explicitly in the craniofacial tissues of vertebrate embryos has yet to materialize. Sufficient subsequent efforts at detection of apoptotic PCD, typically through TdT-mediated dUTP nick end labeling (TUNEL), electron microscopy, or immunohistochemical assays of activated Caspase-3, permits some further categorization of the predictable time and place of the occurrence of embryonic craniofacial apoptosis. Though not intended to be exhaustive in nature, and noting occasional overlap between categories, we highlight four evolving themes in the temporospatial elaboration of apoptosis during CFD as occurring: (1) at positions of epithelial-epithelial apposition; (2) within intra-epithelial morphogenesis; (3) during epithelial compartmentalization; and (4) with CNC metameric organization. With most of these we suggest that apoptosis acts as a fine tool to sculpt the developing tissues for the needs of subsequent development and morphogenesis.

Apoptosis and Epithelial-Epithelial Apposition and Fusion

Craniofacial apoptosis is predictably and consistently found where cranial epithelia of one source grows to meet, in apposition, other epithelia — especially where the meeting, fusion, and subsequent degeneration is fundamental to further growth and development (**Figures 1F,G**). As we present below, such topographies are exemplified by the appositions of the developing palatal shelves, the meeting of the FNP and mxBA1 at λ, the eyelids, the PPts and precervical sinus, and the buccopharyngeal membrane. Indeed, defects in epithelial fusion in any such local typically result in the development of clinically important congenital malformations (Ray and Niswander, 2012; Molè et al., 2020). This apposition may be apical-apical in nature wherein contact is initiated at the apical surfaces of the two epithelia, a situation especially common where it involves two SCE-derived epithelia (**Figures 1G**, **2**). Such an apposition is typified, for example, by the apposition of the mammalian secondary palatal shelves, where they merge with the primary palate, and where the nasal septum joins the palate (Shuler, 1995; Cuervo and Covarrubias, 2004; Jin and Ding, 2006; Yamamoto et al., 2020). Apoptosis-associated apposition may also be basal-basal in nature wherein initial contact between epithelial sheets occurs along their basal lamina and basement membranes. This is typified by the apposition of the PE and the SCE, such as at the buccopharyngeal membrane and the PPts (Watermann, 1977; Shone and Graham, 2014; Chen et al., 2017).

Typical of apical-apical apoptotic appositions is the growth and convergence of the mammalian secondary palate, a multi-step process that begins with specification of CNC within mxBA1 (Dixon et al., 2011). This is followed first by a vertical mesenchymal growth phase where the shelves initially expand vertically from mxBA1 along the sides of the growing tongue and then, subsequently, by reorienting the direction of proliferation and extending horizontally above the tongue and towards the midline (**Figure 2A**). During these phases an essential, specialized superficial layer of the epithelia, the periderm, covers the developing palate, acting as a barrier to unwanted epithelial-epithelial adhesions (e.g., with the tongue) that would mechanically arrest palatal growth and fusion and result in CP (Richardson et al., 2014). Horizontal growth continues until the contralateral shelf epithelia, here commonly referred to as medial edge epithelium (MEE), make contact and fuse to generate a midline epithelial seam (MES; **Figure 2D**). In order for a continuous palatal shelf to form, and thereby separate the oral and nasal cavities, the cells, basal lamina and basement membranes of the MEE must be removed at the MES. This allows palatal fusion at the midline and failure to achieve this leads to CP. After years of significant contention over the primacy of cellular mechanisms of MES disintegration, genetic fate mapping and manipulation in mice suggests three mechanisms are each involved: (1) apoptosis, (2) EMT, and (3) epithelial cell migration and extrusion either towards the oral or nasal palatal surface (Cuervo and Covarrubias, 2004; Losa et al., 2018).

Notably, apical-apical apoptotic apposition is also seen at λ where the epithelium of the inferolateral mFNP converges (beginning around E10.5 in a mouse) to meet mxBA1 and the inferolateral lFNP at the ventral intranasal line (nasal fin; **Figures 1F,G**, **2**). As with the palatal shelves, apposing epithelial cells first appear to extend fillipodia across the gap separating both halves in order to intercalate and anchor themselves in between cells of the contralateral anlage. This then facilitates the coalescence of the appositional epithelial sheets and generates an epithelial seam at the nasal fin (Cox, 2004; Jiang et al., 2006; Ray and Niswander, 2012). The seam must subsequently disintegrate

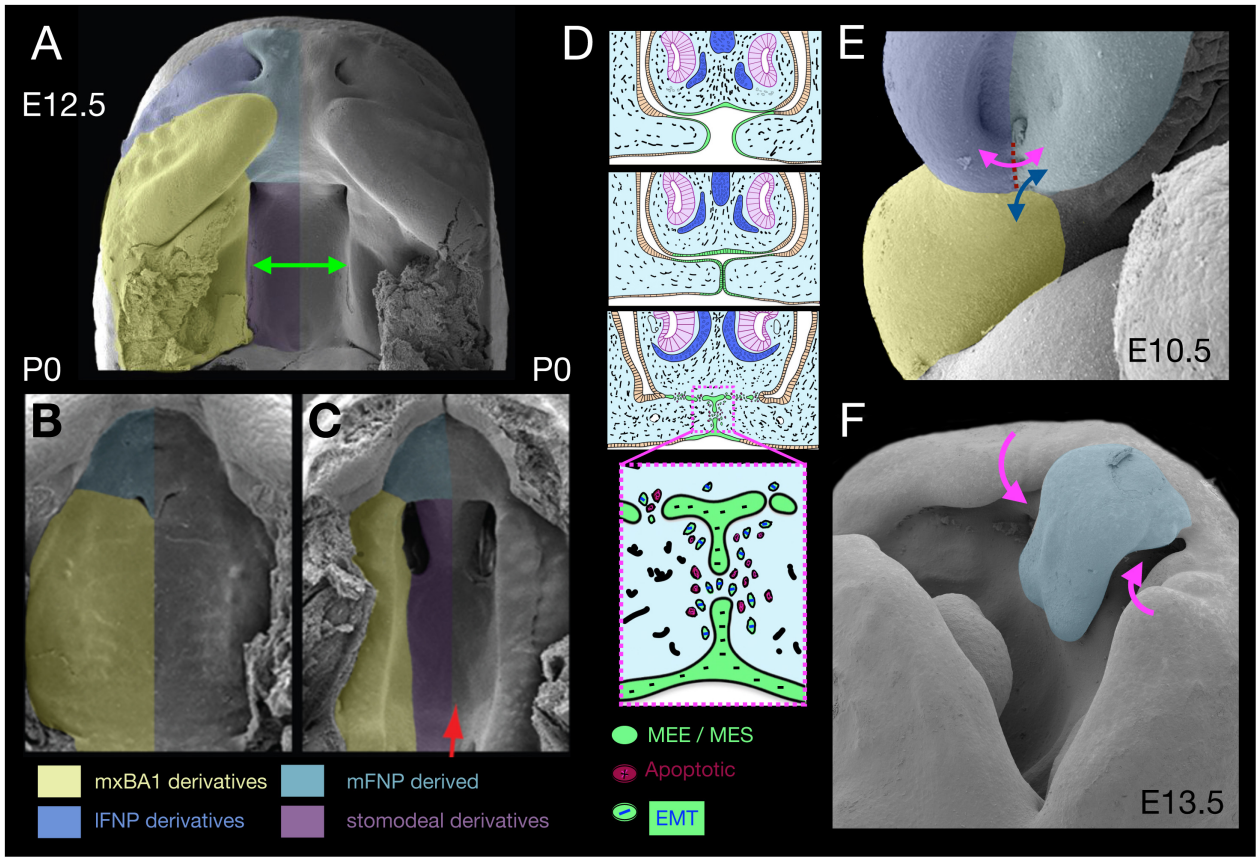

FIGURE 2 | Apical-apical epithelial apposition, orofacial clefting, and apoptosis. **(A–C)** Pseudocoloured scanning electron micrographs of the secondary palate at E12.5 (**A**, green arrow) and P0 **(B)**. The secondary palate in panel **(C)** is cleft due to a *deficiency* of *Gas1*. **(D)** Schema of the apposition of nasal septum and secondary palatal shelves wherein apoptosis acts in conjunction with epithelial-mesenchymal transition (EMT) and migration to remove the MEE/MES. **(E)** λ in an E10.5 mouse embryo. Dotted red line, topography of nasal fin. Double headed arrows indicate significant appositions. magenta, nasal fin; blue, mxBA1-mFNP. **(F)** E13.5 mouse embryo evincing a cleft lip and cleft primary palate (magenta arrows). Blue psuedocolour indicates the mFNP derivative.

in order for the full, normal mergence of the primordia at λ to result in the formation of the primary palate and a continuous, externally even upper lip. Failure of this process leads to CL and primary CP (1CP; **Figure 2F**). Apoptotic culling helps to ensure that adequate cell numbers are removed from the tips of the epithelial seams to facilitate adhesion of the converging midfacial processes and occurs before and during mFNP, mxBA1 and lFNP fusion. Analysis of the levels of apoptotic cells of the disintegrating seam from E10.5 to E11.5 in mice (being highest around E10.75) has suggested that no more than 40% of the SCE-derived epithelial cells at λ undergo apoptosis, a percentage thought to be insufficient to the clearance of all the nasal fin cells (Losa et al., 2018). Thus, full nasal fin epithelial disintegration involves additional mechanisms. As with the palatal shelves, fate mapping and conditional genetic manipulation in mice suggests the same three general mechanisms that are involved in MES disintegration — that is, apoptosis, EMT, and epithelial cell migration — act in concert to bring about normal seam disintegration at λ (Losa et al., 2018). Critical to the overall process, apoptosis here is topographically highly focal and surgical (i.e., is scalpel-like).

Though best studied due to their greater clinical urgency, apical-apical apposition of the palatal shelves and at λ are certainly not the only places such appositions occur during craniofacial development. Apoptotic cells are evident where epithelia of mxBA1 and mdBA1 apically appose at the OE of the hinge (i.e., the embryonic oral commissure) and subsequently fuse to ensure the buccal organ is continuous laterally and the obicularis oris muscle can completely encircle the oral opening (Lotz et al., 2006). Failure of fusion along this part of the orotragal line underlies macrostomia (Kobraei et al., 2016). The mdBA1 midline (mentum) epithelia likewise undergo apoptotsis-positive apposition and their failure to do so is associated with lower median cleft lip (Oostrom et al., 1996; Lotz et al., 2006). Apoptosis is also detected in the epithelium of contralateral mFNP when they appose, and failure to fuse at the midline results in mid facial clefting (Griffin et al., 2013; Lantz et al., 2020). In each of these cases, apoptosis appears to cull relatively small numbers of cells to achieve a significant sequent morphological affect.

Formation, migration, closure and subsequent re-opening of the eyelids provides yet another example of complex craniofacial apical-apical epithelial appositions for which apoptosis appears

as a part of the normal ontogenic progression. The optic and periocular SCE undergoes repeated rounds of coordinated epithelial morphogenesis and migration during development — to first generate a lens placode, and then to invaginate the placode to form a lens vesicle, pinch off completely as a vesicle from the SCE, generate a distinct corneal layer, build and properly position corneal (conjunctival) furrows, and then undergo focal glandular branching morphogenesis and tubulogenesis (to contribute, for example, to the formation of the nasolacrimal duct). Importantly, the SCE-derived epithelium must also establish a migratory wave of cells, encased in an epithelial periderm layer, to build eyelids that will grow as migratory waves across the sclera and then appose one another over the cornea, fuse and eventually split open again — all without becoming physically attached to the corneal or scleral surfaces (Pei and Rhodin, 1970, 1971; Harris and McLeod, 1982; Findlater et al., 1993; Meng et al., 2014). Once the upper and lower eyelid anlage converge, epithelial apposition creates an unique epithelial seam — the eyelid junction epithelium (EJE) — replete with cellular extrusions. However, unlike with the apical-apical fusions of the palate or the nasal fin, which need to disintegrate comparatively rapidly to keep up with palatal growth, the fusion of the eyelids must be maintained for a protracted period of time. This difference results in distinct cellular and extracellular dynamics relative to the palate or nasal fin (Ray and Niswander, 2012; Meng et al., 2014). However, once the proper developmental stage has been reached, and apoptotic signals (likely through Smad1 mediated death-receptor up regulation) are received, the EJE undergoes focal apoptosis (Sharov et al., 2003; Meng et al., 2014). This, combined with stimulated keratinocyte differentiation, is thought to lead to eyelid separation and opening. Significantly, the cephalic end of vertebrate embryos exhibits numerous other examples of apical-apical appositions and fusions apparently involving apoptosis. Many of these, such as neural tube closure (NTC), have been well documented and are amply discussed elsewhere (e.g., Yamaguchi and Miura, 2013; Nikolopoulou et al., 2017; Molè et al., 2020).

As noted above, basal-basal epithelial apoptosis-associated appositions likewise occur during normal craniofacial development, and includes both SCE-SCE and SCE-PE epithelial contacts. In addition to the primary and secondary palates and the upper lip, morphogenesis at λ includes the formation of the primary chonae, the internal oronasal aperture (Tamarin, 1982). Externally, as the amniote nasal pits invaginate between the mFNP and lFNP (to eventually create the nasal duct) each primary choanal pit begins its invagination at the medial end of the oronasal groove (medial-choanal line; **Figure 1F**). After significant intranasal epithelial morphogenesis, coupled with differential proliferation of the underlying CNC, an oronasal membrane composed of two SCE-derived epithelial sheets with apposing basement membranes separates the oral and nasal cavities (Tamarin, 1982). Rupture of this membrane is essential for the tetrapodal ability to breath with the mouth closed, proceeds without cell intercalation, and is accompanied by apoptotic cells at the site of disintegration (Weingaertner et al., 2006; Chen et al., 2017). Here, again, apoptosis appears to play a more surgical role than an obliterative one.

SCE-PE basal-basal epithelial apoptosis-associated appositions also characterize the development and rupture of both the buccopharyngeal membrane and the PPts (Watermann, 1977; Tamarin, 1982; Shone and Graham, 2014). The buccopharyngeal (oral) membrane separates the SCE of the stomodeum from the foregut PE, and its rupture is essential for vertebrate life. Rupture appears to follow stepwise beginning with SCE reorientation, controlled loss of basement membrane integrity, apoptotic culling and cell migration within the SCE, and eventual SCE-PE cellular intercalation followed by rupture. Absence of rupture, though rare, does occur. Of particular comparative evolutionary importance are the SCE-PE appositions. Accumulating evidence suggests that it is the reiterative pattern and proliferation within the forming PE that instigates PP-PC contact (Haworth et al., 2004; Graham et al., 2005). The behaviour of this contact differs cranio-caudally within the PPts (Shone and Graham, 2014). With the first PPt, once contact is initiated the PE epithelia regresses leaving an intact PC epithelia (which is necessary for the continuity of the tympanic membrane). For the caudal PPts, apoptosis is evident — mostly in the SCE-derived PC — allowing the PP epithelia to intercalate and displace the ectoderm whereupon the PPts either rupture or maintain their integrity while allowing the PE epithelia to extrude between the BAs (Shone and Graham, 2014). Subsequently, the caudal (aboral or "opercular") border of BA2 typically undergoes a distinctive proliferation that results in its overlapping of the cervical sinus, a transient depression containing the remaining caudal BA (**Figures 1G,K**; Frazer, 1926). In tetrapods, this opercular border will eventually grow caudad to appose and fuse, along its caudal margin, with the epipericardial ridge. In doing so it must act internally with the now mixed SCE-PE epithelial populations of the lateral surfaces of the BA (Shone and Graham, 2014). Errant development of this process results in fistulae of the ear and neck (Arey, 1934).

Apoptosis and Intra-Epithelial Morphogenesis

Epithelial folding is a fundamental morphogenic event as it acts to transform simpler two-dimensional epithelial sheets into complex three dimensional structures that are often essential for tissue or organ function as well as for organismal life (Davidson, 2012). Indeed, much of vertebrate embryonic craniofacial morphogenesis and organogenesis is the product of forces acting within and on epithelial sheets. With respect to embryonic epithelial folding, this mechanistically includes changing forces initiated by apoptotic cells (Suzanne and Steller, 2013; Monier and Suzanne, 2015; Monier et al., 2015). For instance, some apoptotic epithelial cells have been shown to regulate epithelial folding by utilizing a dynamic pico-basal myosin II cable to exert a transient pulling force on the apical surface of the epithelium in which they are dying (Monier et al., 2015). Among the numerous examples of significant craniofacial tissues for which intra-epithelial morphogenesis involves apoptosis are the optic lens and mammalian teeth. Apoptosis is clearly found during lens pit formation and morphogenesis (see below) where it is believed to be necessary to establish the correct number of cells in the invaginating lens pit

and to physically separate from the surrounding SCE (Findlater et al., 1993; Morgenbesser et al., 1994; Pan and Griep, 1995; Lang, 1997; Meng et al., 2014). The three dimensional cusp pattern of mammalian molars takes shape through the enamel knot signaling centres that are developmental cleared through apoptosis (Vaahtokari et al., 1996; Pipsa and Thesleff, 2003; Ahtiainen et al., 2016).

Apoptosis and Epithelial Compartmentalization

While the NE, PE and SCE each undergo compartmentalization, we selectively highlight here the specification, individuation and subsequent development of the cranial sensory placodes as exemplifying regionalization and compartmentalization that mechanistically involves apoptosis. From the presumptive SCE arises a pre-placodal region (PPR), unique to this surface ectoderm, that has been shown to represent a specialized competence for placodal induction (Jacobson, 1963; Washausen et al., 2005; Bailey and Streit, 2006; Schlosser, 2010; Saint-Jeannet and Moody, 2014; Streit, 2018). Experimental evidence supports the notion that once the PPR has been specified there follow sequent inductive steps to regionalize identity as posterior (otic and epibranchial) and anterior (olfactory, lens, and adenohypophyseal), with the trigeminal being intermediate. It is within the anterior PPR that the SCE will give rise to the epithelia of λ. Within this anterior domain all placodal progenitor cells are initially specified as lens regardless of subsequent fate, and induction of non-lens fate requires both the active induction of unique identity (through distinct sets of inductive cues) and the active repression of lens fate (which is mediated in part by the CNC; Bailey et al., 2006). Within all sensory placodes, moreover, individual neural placodal fates have to be actively acquired and cellular differentiation and delimitation controlled. The trigeminal and epibranchial placodes, for instance, will physically generate ganglionic neuroblasts that must delaminate and intermingle with CNC-derived cells to create (1) the trigeminal ganglia of cranial nerve (CN) V, (2) the geniculate ganglion of CNVII, (3) the petrosal ganglion of CNIX, and (4) the nodose ganglion of CNX. Meanwhile the olfactory and otic placodes will generate, *in situ*, their own specialized neurosensory cells. Strong evidence indicates that topographically regulated apoptosis normally seen within the amniote SCE assists the eventual individuation of the trigeminal and, within the PPR, the physical compartmentalization of the epibranchial and otic placodes (Washausen et al., 2005; Knabe et al., 2009; Washausen and Knabe, 2013). Notably, aquatic vertebrates have unique lateral line placodes derived from within the PPR that generate mechanosensory and electosensory neuroblasts well suited to life in water. It has recently been demonstrated that, in cultured whole murine embryos in which apoptosis is arrested by the pan-caspase inhibitor by Q-VD-Oph, lateral line placodes develop in the PPR topographically within the apoptotic domains that also help discriminate the epibranchial placodes from the otic placode (Washausen and Knabe, 2018). Thus, in an apparent example of Glückmann's phylogenetic apoptosis, PCD within the amniote SCE removes the potential for unnecessary lateral line placodogenesis.

Apoptosis and CNC Organization

Much of the vertebrate embryo is segmental in nature. In post-cranial development, metameric organization (including of the truncal neural crest) follows mesodermal positional cues (Graham et al., 1996). The cranial ends of vertebrate embryos are also metameric, in particular the BAs and the rhombomeres (R) of the hindbrain (Graham et al., 1993; Minoux and Rijli, 2010). Fate mapping studies of the CNC has shown a correspondence of rhombomeric segmentation, neural crest emigration, and BA metamerism (Noden and Trainor, 2005). Anteriorly, the fungible trigeminal CNC emigrates to line BA1, surround the forebrain, and take position below the anterior SCE. This equipotent Hox^{-} population includes cells that delaminate from R1 and R2, the midbrain, and the posterior forebrain. The Hox^{+}, post-trigeminal CNC of BA2 and BA3 mostly emigrates from the even numbered posterior R such that R4 CNC enters BA2 while R6 CNC enters BA3. This coordinated segmentation is key to generating positional information between the BAs. Notably, this mechanism for pattern control is actively maintained by the early apoptosis-induced elimination of CNC at the third and fifth rhombomeres (Graham et al., 1993).

CFD in the Face of Mutations of the Apoptotic Machinery or Regulators of Its Transcription

Understanding of the mechanistic control of a great many developmental processes has enormously benefited from successful reverse genetics approaches in mice. Sometimes, however, such approaches muddy the waters of initial understanding, especially when expectation of phenotype fails to fit phenotypic outcome in loss of function studies. This appears to have been the general case with regard to many of the initial interpretations of the loss of function of components of the apoptotic machinery either as individual or as compound mutations (e.g., Linsten et al., 2000; Tuzlak et al., 2016). For instance, null mutations in *Apaf1* in mice resulted in significant rostral neural tube closure defects, mid-facial clefting, failure of palatal shelf fusion, and jaw dysmorphology (Cecconi et al., 1998; Yoshida et al., 1998; Long et al., 2013). These significant malformations set expectations relatively high that mutations in other components of the apoptotic machinery would yield at least similar defects. When null mutations for other machinery components, such as BAK and BAX (either singly or in compound), were reported to have more underwhelming phenotypic consequences (Linsten et al., 2000) these expectations were revaluated (Tuzlak et al., 2016). A survey of single and compound mutations of the individual components of the apoptosis machinery, however, indicates that abnormal craniogenesis - of both the contents and the container - is as consistent a recognized phenotype as any with the loss of function of the apoptosis machinery (e.g., Voss and Strasser, 2020). With regard to apoptosis during CFD, however, two factors have subsequently manifested. First, the apoptotic machinery appears to have built-in redundancies (as might be expected for a system in need of regulatory balance). This becomes evident, for example, with the compound mutations

of like-type components of the apoptotic machinery such as the pro-apoptotic BH3-only effectors BAK, BAX, and BOK (Ke et al., 2013, 2018). In the absence of BOK alone no readily discernible phenotypic abnormalities are noted (Ke et al., 2013). With BOK homozygosity compounded with losses of either BAK or BAX, phenotypic abnormalities are only slight exacerbations of the small phenotypic changes noted with single null mutations of BAK or BAX (Ke et al., 2013). Compound mutation of all three, however, results in significant craniofacial defects, including exencephaly, midfacial clefting and hypognathism of the lower jaw (Ke et al., 2018). Compound mutations of the anti-apoptotic BCL-2 members MCL-1 and BCL-X likewise result in craniofacial defects including midline truncations of the upper and lower jaws (Grabow et al., 2018). Analysis of the loss of function of key transcriptional regulators of the apoptotic machinery components has also added to the notion of an absolute necessity for apoptosis during CFD. This is apodictic when, for instance, looking at abnormal CFD due to the loss of the p53/63/73 family transcription factors (Pan and Griep, 1995; Thomason et al., 2008, 2010; Van Nostrand et al., 2014, 2017; Richardson et al., 2017; Lin-Shiao et al., 2019). Second, it has become clear that the phenotypic investigative scope typically utilized to assess change has often been set low in magnification. Subtle changes in CFD such as in the size and shape of individual skeletal or dental elements — changes that by definition are not readily discernible — are likely to have been overlooked or undetected in many knock-out studies. However, when higher resolution examinations of specific biological systems are conducted, such as with the olfactory system and the loss of Caspases 3 and 7, detection of the smaller phenotypic alterations in CFD become evident (Cowan and Roskams, 2004).

Apoptosis as Chisel II: Apoptosis in Abnormal Craniofacial Development

Analysis of both naturally occurring and targeted mutations in vertebrates has frequently included correlations between changes in the spatiotemporal topography of apoptosis and the larger phenotypic outcome of the mutation. Assessing the immense breadth of all such analyses lies well beyond our here intended scope; rather, to facilitate the notion of craniofacial apoptosis as chisel rather than sledge-hammer, we highlight four instances for which alteration of apoptosis has been invoked as integral to the phenotypic outcome of a mutation associated with craniofacially expressed genes. To aid the discussion, and to underscore the rationale of the hypotheses at the core of our second aim, we focus our examples around apoptosis and the molecular dynamics of jaw patterning. Specifically, we discuss (1) how the absence of *Satb2* leads to increased apoptosis within the CNC of the coordinated jaw developmental modules in which it is expressed, (2) the role of *Pbx* genes in controlling apoptosis in the nasal fin at λ and the plausible significance of this for CFD and evolution, (3) how attenuation of *Fgf8* expression leads to increased apoptosis in the CNC at the hinge as well as decouples jaw integration, and (4) how loss of *Foxg1* leads to drastically altered apoptotic topography in the SCE and its signaling centres that results in the loss of suppression of lower jaw molecular identity in the upper jaw primordia.

Satb2, Apoptosis, and the Elaboration of Jaw Modules

As described earlier, reflective of the polarity in the developing jaw anlage and driven by the topography of its patterning centres, the jaw primordia are partitioned into distinct developmental modules (**Figures 1L**, **3C**). Such modules are evolutionarily dissociable units consisting of integrated character states that are relatively independent of other nearby character states. Developmental regulation of such modules and their integration, including through control of intra-module cell population size, provides a key mechanism bridging CFD and evolution (Fish et al., 2011). Within the developing craniofacial primordia of late pharyngula stage embryos (and being most conspicuous from E10 onwards in mice), a *Satb2* (Special AT-rich sequence-binding protein 2) positive CNC population defines an integrated set of coordinated modules, topographically peri-sagittal to the midline, between the upper and lower jaws (**Figure 3**; Britanova et al., 2006; Fish et al., 2011). *Satb2* is a highly conserved member of a small, novel gene family that functions as a transcription factor which binds to nuclear matrix-attachment regions where it can simultaneously regulate transcription of multiple genes and augment the potential for enhancers to act over large distances (Britanova et al., 2006; Zarate et al., 2015). Satb2 is also a target for SUMOylation, a reversible modification of the protein that modulates its activity as a transcription factor.

Although originally identified as the human gene at *2q32-q33* associated with CP, it is now recognized as the core of *SATB2*-associated syndrome (SAS), a condition characterized by distinct craniofacial abnormalities, developmental delay, and intellectual disability (Zarate and Fish, 2017). Notably, it remains one of the few identified genes wherein haploinsufficiency in both humans and mice (roughly 25% of heterozygotes in the latter) is significantly associated with isolated CP (Britanova et al., 2006; Zarate and Fish, 2017). *Satb2*-dosage sensitivity in CFD is particularly conspicuous: Loss of both alleles of *Satb2* in mice leads to the morphogenic failure of the entire developmental module in which it is expressed, while leaving structures to either side autonomously developing (**Figures 3G–J**; Britanova et al., 2006). Mirroring the human condition, haploinsufficiency of *Satb2* in mice leads to hypoplasia of structures specifically derived from this module (**Figures 3K–M**). Significantly, in the absence of *Satb2,* high levels of apoptotic cells are found specifically within the mesenchyme of the effected modules (**Figures 3D,E**), providing a mechanistic link between a discrete module and the elaboration of its development and morphogeneis. Arguably, the relatively precise restriction of apoptosis and structural loss to the $Satb2^{+}$ coordinated developmental modules themselves is mechanistically more chisel-like than sledgehammer-like in nature, and provides a framework to approach functional jaw integration and evolution (Fish et al., 2011).

Pbx, Apoptosis, and the Vertebrate Evolution of λ

Pbx genes encode TALE (three amino acid loop extension) homeodomain transcription factors known for their interactions

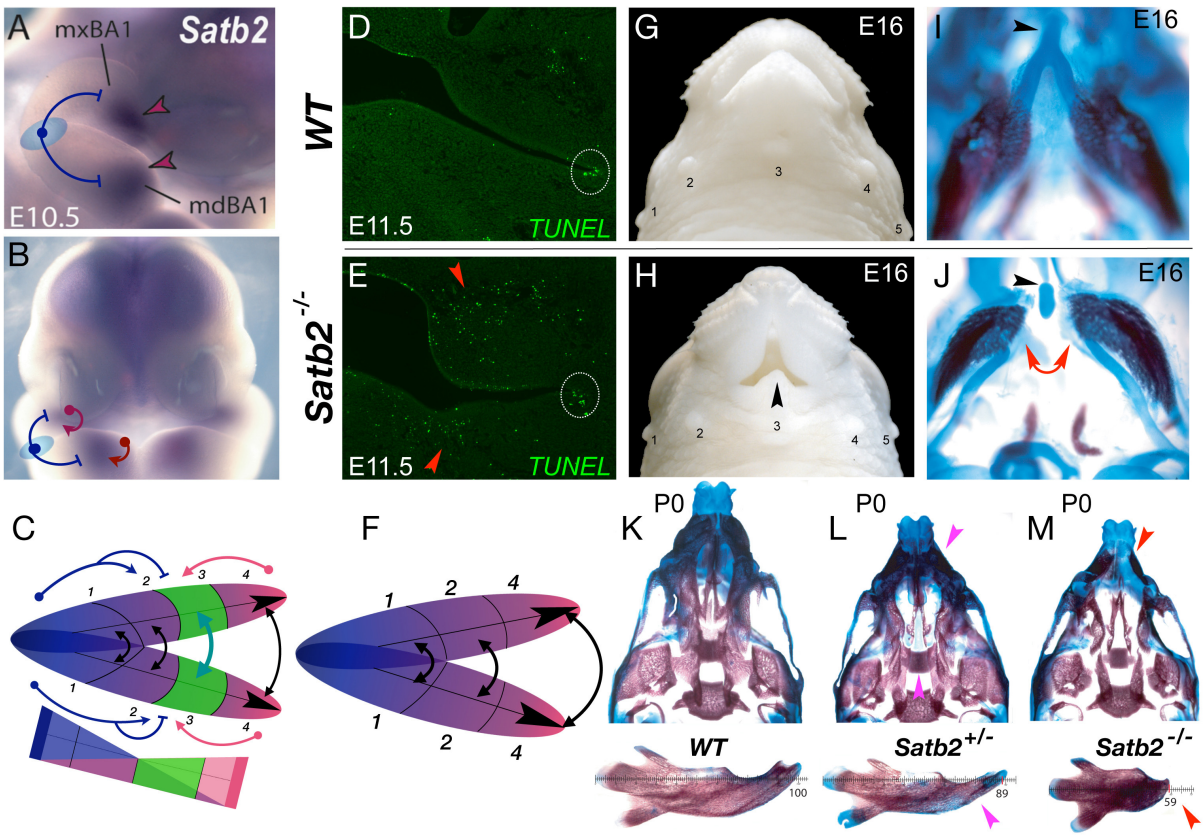

FIGURE 3 | *Satb2*, apoptosis, and the elaboration of jaw modules. **(A,B)** Lateral **(A)** and frontal **(B)** aspects of E10.5 mouse embryos showing *Satb2* expression in BA1 and the FNP. Blue T-bars suggest a plausible hinge-related repression of *Satb2* and a red arrows a caps-related induction. **(C)** Schema depicting the coordinated nature of the *Satb2*-positive module (#3, in green). **(D,E)** Module restricted increase in apoptosis due to the loss of *Satb2*. Frontal section of wild type (WT) and *Satb2* null E11.5 embryos. Dotted white circle indicate the usual apoptosis at the oral commissure. **(F)** Schema of jaw development after the loss of the *Satb2*-positive module. **(G,H)** Gross anatomy of the snout of wild type (WT) and *Satb2* null embryos at E16. Black arrowhead indicates the maintenance of structure at the midline. 1–5, sinus follicles, noted for orientation. **(I,J)** Differential staining of bone (red) and cartilage (blue) of the samples in G and H. Red arrows indicate the drastic perisagittal loss of structure within Meckel's cartilage of the *Satb2* module. Black arrowheads indicate the rostral process of Meckel's cartilage, a structure developed at the midline. **(K–M)** Differential skeletal staining of P0 wild type, *Satb2* heterozygous and *Satb2* homozygous neonatal crania (top) and dissected mandibles (bottom) demonstrating the conspicuous nature of gene dosage on the elaboration of development of the *Satb2* module. Magenta arrowheads highlight deficiencies in *Satb2* heterozygotes, while red arrowheads highlight the greater losses in the same structures in the *Satb2* null skull.

with *Hox* and *Meis* encoded proteins, and they govern disparate developmental processes including apoptosis in the seam of the nasal fin at λ (Selleri et al., 2001; Ferretti et al., 2011; Losa et al., 2018). Notably, *Pbx* genes display distinct expression patterns at λ in both the SCE and the subjacent CNC (**Figures 4A,B**). Compound mutations of *Pbx1* homozygosity and either *Pbx2* or *Pbx3* heterozygosity lead to craniofacial dysmorpholgies, including CL and CP, that are presaged by deficiencies during the development of λ (**Figures 4C–F**; Ferretti et al., 2011). Moreover, conditional inactivation of *Pbx1* specifically in the SCE (using a *Foxg1*^{Cre} driver) on a *Pbx2* or *Pbx3* heterozygous background likewise leads to CL and 1CP (**Figures 4G,H**) while CNC-specific inactivation using a *Wnt1*^{Cre} driver does not (Ferretti et al., 2011). Developmentally preceding CL and 1CP, combinatorial inactivation results in the arrest of the normal apoptosis at the seam of the nasal fin (**Figures 4I,J**).

Intensive investigation of *Pbx* regulatory control of development at λ has revealed an unique *Pbx-Wnt-p63-Irf6* regulatory module that correlates with the gradual increase in complexity at λ of the mxBA1–FNP connections and associated derived structures (e.g., the choanae, upper lips, and secondary palate) through evolutionary transitions among amniotes (Ferretti et al., 2011). Compound deficits of *Pbx* lead to decreased Wnt signaling at λ. Pbx and partner proteins bind to a *Wnt9/Wnt3* responsive element and drive expression at λ; notably, loss of *Wnt9b* also leads to CL and CP. *p63* is known for its transcriptional regulation of apoptotic activity (Yang et al., 1999; Gressner et al., 2005; Rinne et al., 2007; Pietsch et al., 2008; Dudgeon et al., 2009) and its deficiency in either human or mouse results in various craniofacial abnormalities, including CL and CP (Rinne et al., 2007; Thomason et al., 2008). Wnt signalling is mediated by Lef1/Tcf transcriptional binding to target genes, and it has been demonstrated that these Wnt

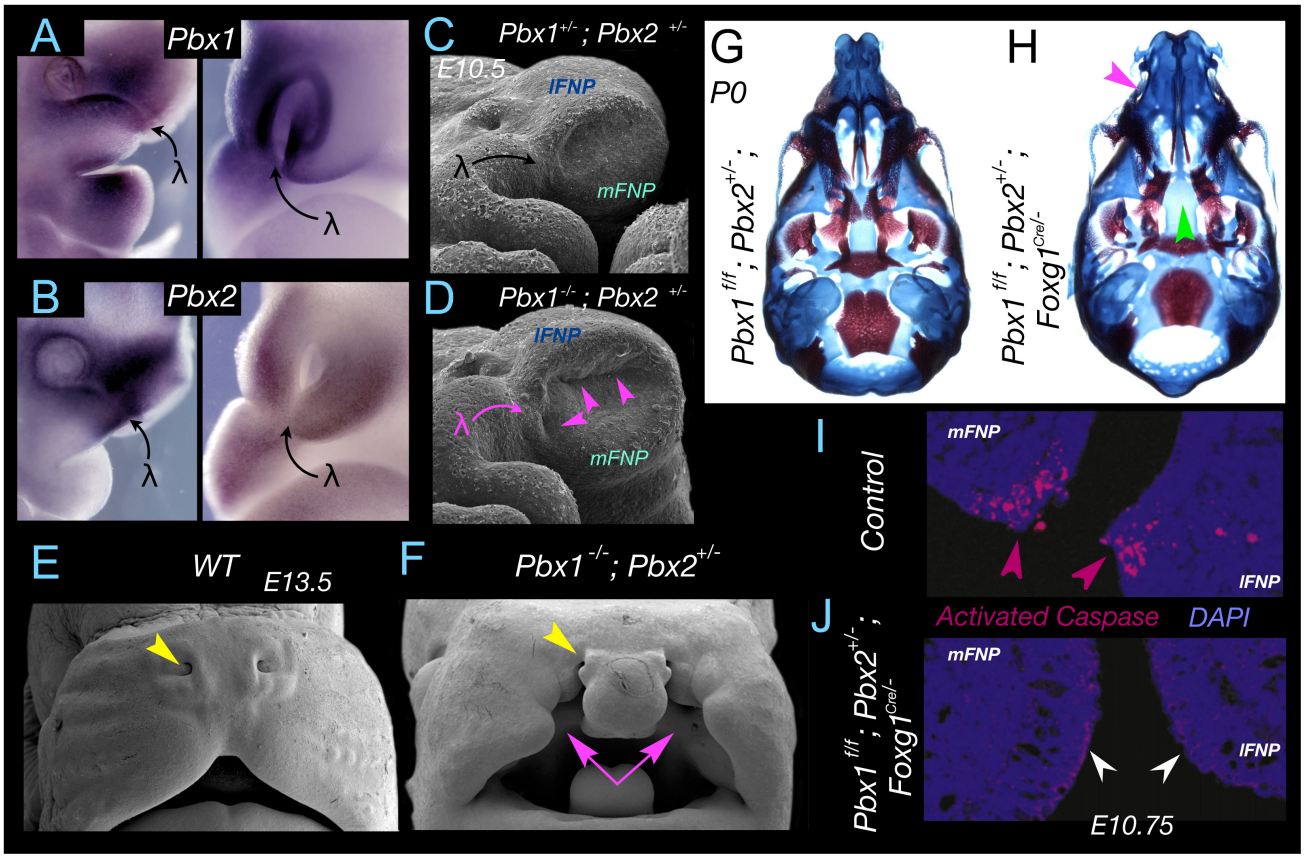

FIGURE 4 | *Pbx*, apoptosis, and apical-apical epithelial apposition at λ. **(A,B)** *Pbx1* **(A)** and *Pbx2* **(B)** expression at λ in E10.75-E11 mouse embryos. Expression is found in both the epithelium and the CNC. **(C,D)** Significant alteration of λ and the topography of the mFNP, IFNP and mxBA1 appositions (magenta arrowheads) in $Pbx1^{-/-}$; $Pbx2^{+/-}$ mouse embryos. **(E,F)** Cleft lip and primary palate (magenta arrows) in a $Pbx1^{-/-}$; $Pbx2^{+/-}$ mouse embryo. Yellow arrowhead indicates the position of the external nares to deficiencies elsewhere (this compound mutant dies pre-term). **(G,H)** Demonstration of the role of *Pbx* in the epithelia of λ. Differential staining of bone (red) and cartilage (blue) of neonates in which Pbx1 has been flowed by a $Foxg1^{Cre}$ driver that is expressed only in the SCE epithelia and not the CNC. **(G)** $Pbx1^{f/f}$; $Pbx2^{+/-}$ and **(H)** $Pbx1^{f/f}$; $Pbx2^{+/-}$; $Foxg1^{Cre/-}$ I. Magenta arrow indicates the clefting of the primary palate. Green arrow indicates the clefting of the secondary palate. **(I,J)** Demonstration, through immunohistochemical detection of activated Caspase 3, of normal apoptosis at the nasal fin in a control embryo **(I)** and loss of apoptosis in the altered mFNP-IFNP apposition in $Pbx1^{f/f}$; $Pbx2^{+/-}$; $Foxg1^{Cre/-}$ embryos **(J)** at E10.75.

signaling effectors transactivate *p63* through a specific regulatory region that is conserved within amniotes. Loss of either *Pbx* or *Wnt9b* leads to diminished p63 expression at λ and therefore loss of its contributions to the pro-apoptotic/anti-apoptotic balance. Furthermore, *Irf6*, the human homologue of which is the gene most commonly mutated in non-syndromic CL and CP (Dixon et al., 2011), is expressed in the MES and nasal fin seam epithelia; p63, in turn, directly binds to a known orofacial enhancer within the *Irf6* locus (Thomason et al., 2010). Unsurprisingly, *Irf6* is also down regulated at λ in both *Pbx* compound and $Wnt9b^{-/-}$ mutant embryos. Although the genomic elements regulating *p63* and *Irf6* within the Pbx-controlled module are conserved in mammals, they do not exist in other amniotes, Xenopus, or fish (Ferretti et al., 2011), a fact important to study of the biology and evolution of the mammalian λ. A mature λ is absent in fish and basal tetrapods and its complexity progressively grows within amniotes and mammals, where in the latter it is most developmentally and functionally complex and critical for the morphogenesis and positioning of, among other things, the choanae, upper lips, and primary and secondary palates (Compagnucci et al., 2011). It is conceivable that the *Pbx*-instigated regulatory module at λ is an evolutionary innovation associated with the appearance in mammals of an elaborated choanae and secondary palate. Investigations of these molecular dynamics in crocodilians, which through a processes of convergent evolution also possess secondary palates, have yet to be conducted but will likely be of note. Overall, the increased complexity of the regulatory module itself correlates with the gradual increase in complexity of λ and associated structures through evolutionary transitions from basal tetrapods to amniotes and then to mammals. Notably, at the heart of the module is the effectuation of apoptosis at λ, a notion further confirmed by the rescue of CL and CP by the reintroduction of apoptosis at the nasal fin in the *Pbx* compound mutants wherein the *Wnt* signaling cascade is conditionally activated in the same

epithelial cells in which *Pbx* has been conditionally inactivated (Ferretti et al., 2011; Losa et al., 2018). It would seem, then, that significant evolutionary advances have followed an increasingly involved genomic blueprint for the precise, scalpel-like apoptotic sculpting of λ.

Fgf8, Apoptosis, and Developmental Integration at the Hinge

Fgf8 encodes a potent vertebrate morphogen that is dynamically expressed during SCE ontogeny and its loss leads to increased apoptosis in the hinge region CNC and changes in the molecular topography of the SCE (Crossley and Martin, 1995; Trumpp et al., 1999; Griffin et al., 2013). Cumulative evidence from many experimental sources and paradigms indicates that the elaborate ontogeny of *Fgf8* expression in the SCE reflects a dynamic and significant signaling environment to be encountered by the CNC responsible for generating rostral cranial skeletal structures (Trumpp et al., 1999; Abu-Issa et al., 2002; Frank et al., 2002; Storm et al., 2006; Depew and Compagnucci, 2008; Compagnucci et al., 2011; Griffin et al., 2013). In addition to being an organizing factor at the anterior neural ridge and the isthmus (midbrain - hindbrain boundary), *Fgf8* is expressed at the hinge in PPt1 epithelia and the hinge-centric OE of mxBA1 and mdBA1 (**Figures 5A,B**). Thus, the hinge as an organizing centre involves the coordinated integration two local sources of Fgf8.

Utilizing a tissue specific, *Nestin*^{Cre}-mediated BA1 conditional knockout of *Fgf8* it has been demonstrate that loss of *Fgf8* in the OE (including BA1) of the mouse is accompanied by the catastrophic loss of the hinge region of both the upper and lower jaws. This included of all the developmental modules within BA1 except those furthest from the hinge and centred at the caps (see *Fgf8*^{flox}*; Fgf8*$^{null;Nes-Cre}$ in **Figures 5C–F**; Trumpp et al., 1999). The presence of some caps signaling is reflected, for instance, by the retention of the midline rostral process of Meckel's cartilage (mdBA1 cap) and the well developed premaxillae (λ cap; **Figures 5E,F**). In these experiments the inactivation of *Fgf8* in the PPt1 notably occurred slightly later and was correlated with the maintenance of a small population of cells in BA1 at the PC1 (**Figure 5D**) that gave rise to the malleus (the mammalian articular element homologue) and portions of the ectotympanic (**Figures 5E,F**). Cell proliferation assays of BrdU incorporation, combined with Nile blue sulfate and TUNEL assays, demonstrated that the patent catastrophic losses in the mutants were due to extensive apoptosis of the BA1 CNC (Trumpp et al., 1999). This established Fgf8 as an essential signaling factor of the vertebrate BA1 hinge and indicated that expression in the OE and PPt is both integral to the normal formation of the jaw skeleton.

Among the approaches subsequently used address the relationship between levels of Fgf8 signaling and the complex craniofacial skeleton has been the employment of genetic attenuation of *Fgf8* dosage in mice through use of combinations of hypomorphic (*Neo*) and null murine *Fgf8* alleles. This allows for a modulation of Fgf8 signaling by reducing functional expression levels to approximately 20% (*Fgf8*$^{null/Neo}$), 40% (*Fgf8*$^{Neo/Neo}$), 50% (*Fgf8*$^{+/null}$), or 70% (*Fgf8*$^{+/Neo}$) of normal (wild-type) levels (Meyers et al., 1998; Abu-Issa et al., 2002; Frank et al., 2002; Storm et al., 2003; Storm et al., 2006; Griffin et al., 2013). These graded challenges to *Fgf8*-regulated cranial morphogenesis demonstrate that *Fgf8* dosage determines murine mid-facial integration and polarity within the nasal and optic capsules (Griffin et al., 2013). The highest levels of attenuation lead to disruption of the normal morphological continuity of jaw and associated skeletal structures (**Figure 5G**). In *Fgf8*$^{null/Neo}$ mutants, syngnathia develops between the distal dentary and the nasal-capsule associated portions of the maxilla. Specifically, this involves loss of the components of both the functional lower jaw articulation (i.e., the proximal dentary structures such as the condylar, coronoid, and angular processes) and the functional upper jaw articulation (e.g., articular portion of the squamosal; **Figure 5G**). Skeletal structures associated with the PPt1 (e.g., malleus, ectotympanic, goniale, incus, and tegmen tympani) are truncated and dysmorphic while BA2 derivatives (e.g., stapes and Reichert's cartilage) are either lacking or highly dysmorphic. Attenuation of Fgf8 signal strength thus challenges integration between the OE and PPt signals, a point further supported by the loss of normal continuity through the oral-aboral axis of BA1 of responsive craniofacial regulatory genes such as *Dlx2* and *Dlx6* (**Figures 5H,I,K,L**). Notably, these changes correlate with a significant alteration in the regional topography of apoptosis (**Figures 5J,M**).

Foxg1, Apoptosis, and Control of Upper Jaw Patterning and Development

Foxg1 is an evolutionarily conserved member of the *Fox/Forkhead* family of winged-helix transcription factors (Xuan et al., 1995). *Foxg1* has principally been investigated for its crucial role in forebrain development; however, its loss has recently been shown to also affect upper jaw patterning and the topographic profiles of apoptosis in the SCE associated the hinge (Xuan et al., 1995; Hanashima et al., 2004; Danesin and Hobart, 2012; Hou et al., 2020; Compagnucci and Depew, submitted). With regard to its role in CNS development, *Foxg1* functions to regulate forebrain induction, regional patterning, and corticogenesis and mice lacking functional *Foxg1* have significant cephalic hypotrophy with substantial morphogenic deficits of telencephalic structures, including dorsally of the neocortex and ventrally of the basal ganglia. Sufficient evidence of neurodevelopmental deficits stemming from *FOXG1* haploinsufficiency or duplication in humans has led to the recognition of "FOXG1-related disorders" as a distinct clinical classification variously involving microcephaly, mental impairment, autism spectrum disorders, and a congenital variant of Rett (RTT) syndrome (Ariani et al., 2008; Florian et al., 2012; Mitter et al., 2018; Hou et al., 2020). Importantly, FOXG1 syndrome in humans is also typified by characteristic craniofacial features, including a prominent metopic suture, large ears, bilateral epicanthic folds, a bulbous nasal tip, depressed nasal bridge, tented or thickened upper lip, prognathism, hypermetropia, and synophyrys (Florian et al., 2012). A significant linkage between the *FOXG1* locus at 14q12 and non-syndromic orofacial clefting has also recently been reported (Mohamad Shah et al., 2018).

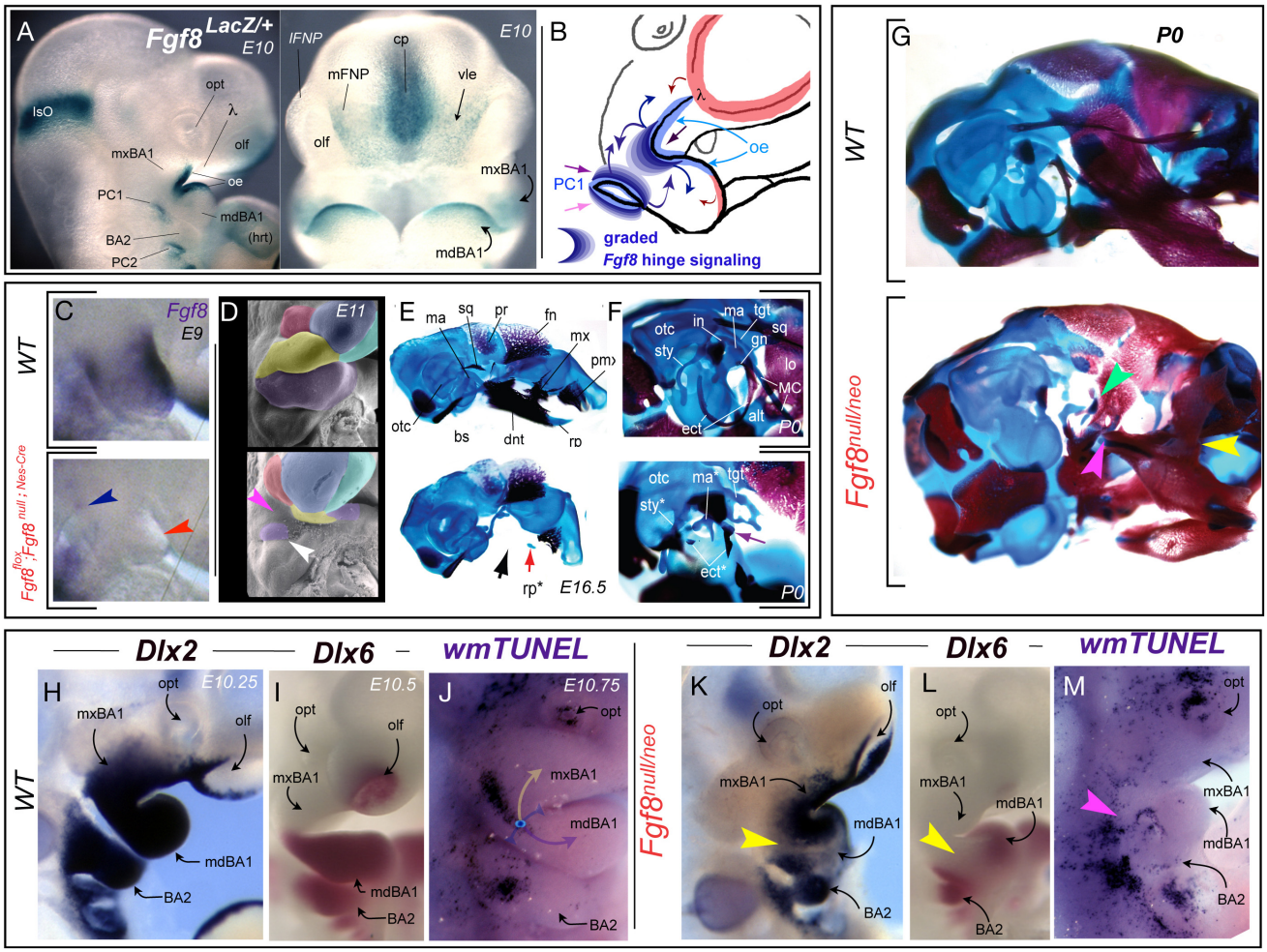

FIGURE 5 | *Fgf8*, apoptosis, and developmental integration at the hinge. **(A)** *Fgf8* expression, notable in the oral ectoderm (oe) and pharyngeal cleft (PC1) as assayed by X-gal staining due to β-galactosidase activity resulting from the insertion of a *LacZ* cassette in the *Fgf8* locus. **(B)** Schema depicting the graded *Fgf8* signaling environment that the BA1 CNC must interpret at the hinge. **(C–F)** Tissue specific inactivation of *Fgf8* in the oral ectoderm and pharyngeal cleft. **(C)** *Fgf8* expression at E9 demonstrating (red arrowhead) that the gene has been inactivated in the oral ectoderm of BA1. Blue arrowhead, slight persistent PC1 expression. **(D)** Psuedocoloured scanning electron micrographs of wild type and $Fgf8^{flox}$; $Fgf8^{null;Nes-Cre}$ E11 embryos. White arrowhead, mdBA1 tissue associated with the developing malleus. Magenta arrowhead, catastrophic loss of most of the BA1 primordia. **(E–G)** Differential staining of bone (red) and cartilage (blue) in E16 (E) and P0 (F) wild type and $Fgf8^{flox}$;$Fgf8^{null;Nes-Cre}$ embryos. Black arrow, devastating loss of hinge-associated structure. Red arrow, remnants of the mdBA1 cap associated rostral process (rp). Purple arrow, the remnants of the ectotympanic (etc) and malleus (ma). **(G)** Genetic attenuation of *Fgf8* demonstrating the disintegration of hinge structures. Yellow arrowhead, dentary-maxillary synganthia. Magenta arrowhead, loss of the lower jaw articulation structures. Green, malleo-ectotympanic tissue. **(H–M)** Topography of altered gene expression and apoptosis in E10.25–10.75 mouse embryos. **(H,K)** *Dlx2* expression. Yellow arrowhead in K, separation in oral and aboral domains due to decreased *Fgf8* levels across the huge region. **(I,L)** *Dlx6* expression. Yellow arrowhead in L, separation in oral and aboral domains due to decreased *Fgf8* levels. **(J,M)** Alterations of apoptotic topography, including loss of normal mxBA1 apoptotic swath (magenta arrowhead).

Notably, *Foxg1* is broadly expressed in the SCE overlying the upper jaw primordia (including λ) and hinge (**Figure 6A**). Loss of function in mice reveals that *Foxg1* is required during CFD for both neurocranial and viscerocranial development, including the sensory capsules, neurocranial base, middle ear, and upper jaws (Compagnucci and Depew, submitted). Notably, *Foxg1* acts to suppress the induction of lower jaw identity in the upper jaw primordia as without *Foxg1* mxBA1 partially acquire deep mdBA1 molecular identities (exemplified by the ectopic expression of lower jaw master-regulatory gene, *Dlx5*; **Figures 6D,E**). Significantly, changes in middle ear and upper jaw development are preceded by drastic alterations of the topography of apoptotic PCD within the SCE, including the BA1 epithelia at the hinge and that between the frontonasal (facial) ectodermal zone and the olfactory placode (**Figures 6B,C,F**). For instance, at E9.25, the $Foxg1^{+/-}$ embryonic SCE exhibits the well characterized foci of apoptotic cells associated with the sculpting of the PPR (see above), as well as associated with the recently closed anterior neuropore (and commissural plate) and the medial olfactory field (i.e., just lateral to the *Fgf8*+ ventrolateral

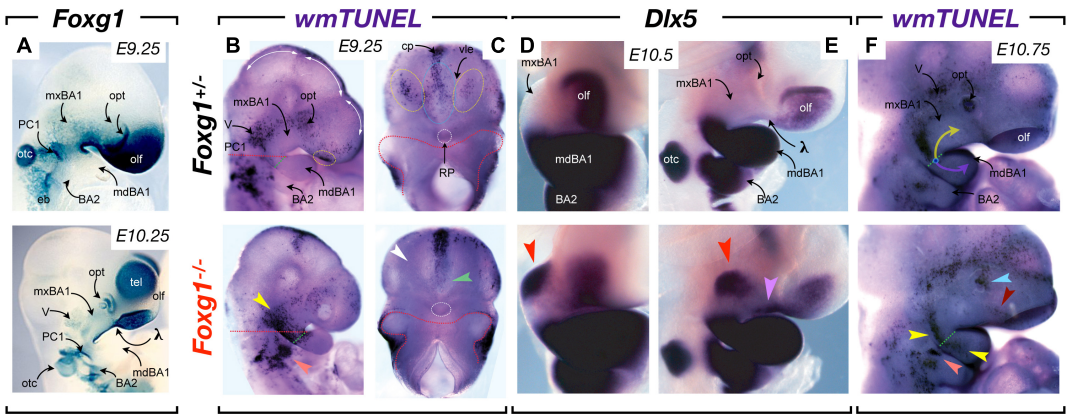

FIGURE 6 | *Foxg1*, apoptosis, and control of upper jaw patterning and development. **(A)** *Foxg1* expression, notable in mxBA1, FNP and hinge SCE, and absence in mdBA1, as assayed by X-gal staining due to β-galactosidase activity resulting from the insertion of a *LacZ* cassette in the *Foxg1* locus. **(B,C)** Whole mount TUNEL assay of E9.25 *Foxg1*$^{+/-}$ and *Foxg1*$^{-/-}$ embryos. **(B)** Lateral view. Dotted red lines indicate planes of separation for **(C)**. Dotted green lines indicate the nascent hinge region. Dotted yellow circles indicate the normal foci of apoptotic cells in the medial olfactory fields of the SCE. Yellow arrowhead, extensive ectopic apoptosis connecting the trigeminal, the aboral border of mxBA1, and the hinge (including the oral ectoderm) evinced in null embryos. White arrowhead, loss of apoptotic foci in the medial olfactory fields of the SCE. Green arrowhead, loss in the ventral SEC below the closed anterior neuropore. **(D,E)** Frontal **(D)** and lateral **(E)** views of E10 *Foxg1*$^{+/-}$ and *Foxg1*$^{-/-}$ embryos highlighting the ectopic induction of *Dlx5* (red arrowhead). A master regulatory gene for mdBA1 identity, expression in the mxBA1 demonstrates that Foxg1 acts to suppress the acquisition of lower jaw identity in the upper jaw developmental field. Lavender arrowhead, ectopic epithelial expression of *Dlx5*. **(F)** Apoptosis in E10.75 *Foxg1*$^{+/-}$ and *Foxg1*$^{-/-}$ embryos. Yellow arrow, mxBA1 hinge signaling. Lavender arrow, mdBA1 hinge signaling. Dotted green line, oral-aboral axis at the hinge. Yellow arrowheads, alterations of mxBA1 apoptosis and expansion into mdBA1. Orange arrowhead, ectopic BA2 apoptotic foci. Light blue arrowhead, alteration of apoptosis in the lens pit. Dark red arrowhead, reorientation of apoptosis normally associated with the nasolacrimal groove.

epithelia). In *Foxg1*$^{-/-}$ littermates these fields are all altered: apoptosis is undetected in the medial olfactory field and it is expanded in the middle SCE of BA2. Most noticeably, extensive ectopic apoptosis is found along the aboral border of BA1 and bridging the OE and PC1 at the hinge (**Figures 6B,C**). A day and a half later in development and the usual topography of apoptotic cells in the SCE retains its predictable nature in *Foxg1*$^{+/-}$ embryos. This includes an elongate swath, essentially restricted to mxBA1, that runs dorsoventrally from the caudal end of the trigeminal ganglion and ends along the OE-PPt1 oral-aboral axis (**Figure 6F**). It also includes a patch centrally located on the SCE of BA2. In mutants, however, the mxBA1 apoptotic foci is restricted oro-aborally and extends from mxBA1 into mdBA1. Thus, with the loss of *Foxg1,* a change of apoptotic topography in the craniofacial primordia presages the eventual disruption of mxBA1 patterning and development. This is particularly notable as these changes occur where the hinge and upper cap signaling centres are being established.

Apoptosis: A Scalpel for Craniofacial Development Patterning and Plausibly Unique Roles in CFD

Using the genetic perturbation of *Satb2*, *Pbx*, *Fgf8,* and *Foxg1* as exemplars, we have examined the correlation of aberrant apoptosis in the elaboration of jaw modules, the evolution and elaboration of λ, the developmental integration at the mandibular arch hinge, and the control of upper jaw identity, patterning and development. With each of these examples we have presented a correlation between a targeted mutation, changes in apoptotic profiles, and abnormal CFD with particular focus on abnormal jaw development. We have also seen that apoptosis is evident at stereotypic and predictable locations during normal CFD. Apoptotic cells, for example, are readily detectable in embryos in locations wherein epithelial-epithelial appositions are occurring (e.g., the palatal shelves, the nasal fin, the oronasal, and buccopharyngeal membranes) as well as within craiofacial epithelia that are undergoing obvious and significant morphogenesis (e.g., the lens pit and developing mammalian molars). Additionally, we have seen that normally observable focal patches of apoptotic cells correlate with the placodal compartmentalization within the SCE.

Apoptotic cells are, however, also notably detectable during CFD in topographies that do not readily lend themselves either to an aspect of the epithelial morphogenesis or apposition or to structural compartmentalization. This is exemplified, for instance, by the patch of apoptotic cells found within mxBA1 ectoderm at E10.5 in mice (see **Figures 5J**, **6F**). Moreover, in our primer on CFD we suggested that among the fundamental tasks in patterning BA1 and the jaws were the following: (1) to establish upper jaw versus lower jaw positional identity; (2) to generate and maintain the point of articulation between the upper and lower jaw arcades; and (3) to keep the jaw arcades in appropriate functional registration during subsequent development and morphogenesis. We posit here that the mxBA1 apoptotic patch facilitates the actualization of these tasks. More specifically, we posit that PCD in this location uniquely facilitates both the patterned integration of the two components of the hinge signal — the PPt1 and the OE — and the patterned

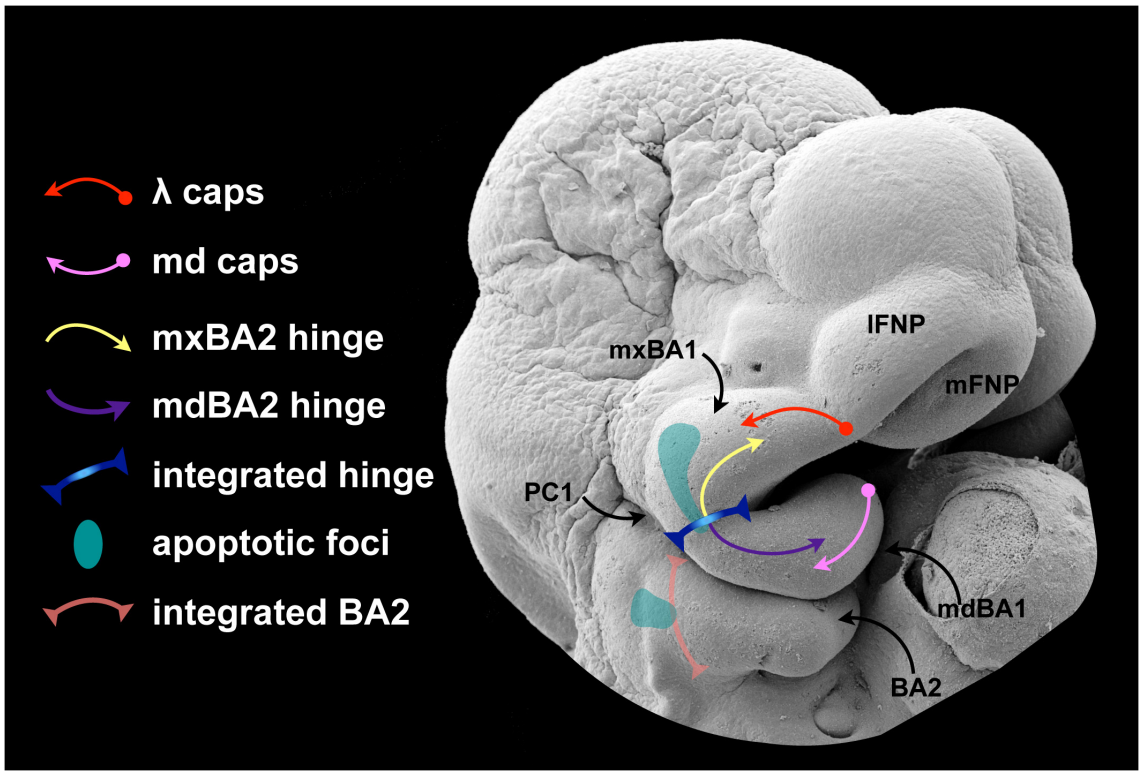

FIGURE 7 | A proposed role for apoptosis in hinge and caps signaling.

suppression of lower jaw molecular identity form upper jaw cellular primordia (**Figure 7**).

It is patent that developmental mechanisms must be employed that properly instruct an equipotent, fungible population of CNC to (1) discriminate instructions for upper jaw pattern and development from those for lower jaw pattern and development and (2) then discriminate and integrate both OE-derived, *Fgf8*-generated developmental cues and aboral, PPt1-derived *Fgf8*-generated developmental cues. We know that *Foxg1,* restricted in its expression to the upper jaw-associated SCE as it is, is part of solution to the first task: in its absence, normal structural development across the hinge is lost and a large domain of mxBA ectopically acquires a mdBA1 molecular identity. Thus *Foxg1* makes the epithelial environment of the upper jaw distinct from that of the lower jaw. Included in this environment is control of the foci of apoptotic cells in the SCE. Though admittedly full understanding of the correlation of morphogen level and morphogenic outcome has yet to be achieved, we also know that thresholds of morphogens such as *Fgf8* are necessary for normal patterning across the hinge. Perturbation of morphogen levels leads to alteration of gene expression, morphology and the topography of apoptosis. These two things — control of epithelial environment and control of morphogen concentration — are likely linked on numerous levels.

Apoptotic control of a morphogen producing cell population is not an undocumented occurrence during development. Cell death has previously been proposed as a mechanism for regulating the effective potency of a secreted morphogen by regulating the numbers of cells producing the factor. Such a mechanism for patterning has been suggested for the PCD associated with Shh-producing cells in the limb bud, *Fgf8*-producing cells of the anterior neural ridge, and the epithelial patterning centres of the enamel knot of developing teeth (Vaahtokari et al., 1996; Sanz-Ezquerro and Tickle, 2000; Nonomura et al., 2013; Ahtiainen et al., 2016). In each of these cases, control of the patterning influence of the signaling molecule is through the apoptotic removal of the morphogen producing cells themselves.

With regard to the SCE, we suggest that another mechanism to regulate the effective elaboration of patterning signals is to program apoptotic foci as a means of micromanaging epithelial environments that inform the CNC. It is possible that the mxBA1 apoptotic foci, for example, acts to restrict the spread of a hinge signal that could otherwise easily be interpreted by regionally subjacent mxBA1 CNC to make them act as though they were mdBA1 CNC. Either physical presentation of factors from the apoptotic cells or the topographic restrictions of the effective spread of a signal through the epithelium could both subtly but effectively micromanage CNC interpretations of local patterning cues either specific to mxBA1-hinge signals or for integrated OE and PPt1 signaling (schmatized in **Figure 7**). In either case, it is conceivable that, rather than having no biological function, the predictable apoptotic foci apparent in mxBA1 acts as a subtle sculptor of patterning cues regulating

important, though not necessarily life enabling, aspects of CFD and morphogenesis.

Similar roles may well be posited for other patches of apoptosis detected during CFD, including those found in the SCE between the anterior neuropore and the olfactory placode. However, while we have some regard for the topography of the normal apoptotic profile during CFD, understanding of the total picture of the spatiotemporal topography of apoptosis during vertebrate CFD — let alone all of its plausible functions — has yet to be fully realized. With regard to roles for apoptosis in normal CFD and patterning, moreover, we would suggest that investigative optics are better set at higher magnification and evidence of a scalpel's touch rather than a sledgehammer's punch be sought as we address the goal of understanding the roles that apoptosis plays during CFD.

AUTHOR CONTRIBUTIONS

MD and CC conceptualized the themes presented and prepared the manuscript. All authors participated in data collection and interpretation, contributed to the article, and approved the submitted version.

FUNDING

This work was supported by the Royal Society (United Kingdom; MD), the Dental Institute of King's College London (MD, CC, and JG), Friends of Guy's Hospital (MD), and the Charite Universitätsmedizin Berlin (MD and KM). CC and JG were funded by Marie Curie Early Training Fellowships (MEST-CT-2004-504025).

ACKNOWLEDGMENTS

We regret the omission of numerous significant contributions to the understanding of apoptosis in craniofacial development due to space constraints. We thank JD for significant support and discussion.

REFERENCES

Abu-Issa, R., Smyth, G., Smoak, I., Yamamura, K., and Meyers, E. N. (2002). Fgf8 is required for pharyngeal arch and cardiovascular development in the mouse. *Development* 129, 4613–4625. doi: 10.1242/dev.129.19.4613

Ahtiainen, L., Uski, I., Thesleff, I., and Mikkola, M. L. (2016). Early epithelial signaling center governs tooth budding morphogenesis. *J. Cell. Biol.* 214, 753–767. doi: 10.1083/jcb.201512074

Arey, L. B. (1934). *Developmental Anatomy: A Textbook and Laboratory manual of embryology*. London: W. B, Saunders Co.

Ariani, F., Hayek, G., Rondinella, D., Artuso, R., Mencarelli, M. A., Spanhol-Rosseto, A., et al. (2008). FOXG1 is responsible for the congenital variant of Rett syndrome. *Am. J. Hum. Genet.* 83, 89–93. doi: 10.1016/j.ajhg.2008.05.015

Bailey, A. P., and Streit, A. (2006). Sensory organs: making and breaking the pre-placodal region. *Curr. Top. Dev. Biol.* 72, 167–204. doi: 10.1016/S0070-2153(05)72003-2

Bailey, A. P., Bhattacharyya, S., Bronner-Fraser, M., and Streit, A. (2006). Lens specification is the ground state of all sensory placodes, from which FGF promotes olfactory identity. *Dev. Cell.* 11, 505–517. doi: 10.1016/j.devcel.2006.08.009

Beverdam, A., Merlo, G. R., Paleari, L., Mantero, S., Genova, F., Barbieri, O., et al. (2002). Jaw transformation with gain of symmetry after Dlx5/Dlx6 inactivation: mirror of the past? *Genesis* 34, 221–227. doi: 10.1002/gene.10156

Bhattacharyya, S., Bailey, A. P., Bronner-Fraser, M., and Streit, A. (2004). Segregation of lens and olfactory precursors from a common territory: cell sorting and reciprocity of Dlx5 and Pax6 expression. *Dev. Biol.* 271, 403–414. doi: 10.1016/j.ydbio.2004.04.010

Britanova, O., Depew, M. J., Schwark, M., Thomas, B. L., Miletich, I., Sharpe, P., et al. (2006). Satb2 haploinsufficiency phenocopies 2q32-q33 deletions, whereas loss suggests a fundamental role in the coordination of jaw development. *Am. J. Hum. Genet.* 79, 668–678. doi: 10.1086/508214

Bronner, M. E., and LeDouarin, N. M. (2012). Development and evolution of the neural crest: an overview. *Dev. Biol.* 366, 2–9. doi: 10.1016/j.ydbio.2011.12.042

Bronner-Fraser, M. (2008). On the trail of the "new head" in les treilles. *Development* 135, 2995–2999. doi: 10.1242/dev.019901

Cajal, M., Creuzet, S. E., Papanayotou, C., Sabéran-Djoneidi, D., Chuva de Sousa Lopes, S. M., Zwijsen, A., et al. (2014). A conserved role for non-neural ectoderm cells in early neural development. *Development* 141, 4127–4138. doi: 10.1242/dev.107425

Cecconi, F., Alvarez-Bolado, G., Meyer, B. I., Roth, K. A., and Gruss, P. (1998). Apaf1 (CED-4 homolog) regulates programmed cell death in mammalian development. *Cell* 94, 727–737. doi: 10.1016/s0092-8674(00)81732-8

Chen, J., Jacox, L. A., Saldanha, F., and Sive, H. (2017). Mouth development. *Wiley Interdiscip Rev. Dev. Biol.* 6:e275. doi: 10.1002/wdev.275

Compagnucci, C., Debiais-Thibaud, M., Coolen, M., Fish, J., Griffin, J. N., Bertocchini, F., et al. (2013). Pattern and polarity in the development and evolution of the gnathostome jaw: both conservation and heterotopy in the branchial arches of the shark, *Scyliorhinus canicula*. *Dev. Biol.* 377, 428–448. doi: 10.1016/j.ydbio.2013.02.022

Compagnucci, C., Fish, J. L., Schwark, M., Tarabykin, V., and Depew, M. J. (2011). Pax6 regulates craniofacial form through its control of an essential cephalic ectodermal patterning center. *Genesis* 49, 307–325. doi: 10.1002/dvg.20724

Cowan, C. M., and Roskams, A. J. (2004). Caspase-3 and caspase-9 mediate developmental apoptosis in the mouse olfactory system. *J. Comput. Neurol.* 474, 136–148. doi: 10.1002/cne.20120

Cox, T. C. (2004). Taking it to the max: the genetic and developmental mechanisms coordinating midfacial morphogenesis and dysmorphology. *Clin. Genet.* 65, 163–176. doi: 10.1111/j.0009-9163.2004.00225.x

Creuzet, S., Couly, G., Vincent, C., and Le Douarin, N. M. (2002). Negative effect of Hox gene expression on the development of the neural crest-derived facial skeleton. *Development* 129, 4301–4313. doi: 10.1242/dev.129.18.4301

Creuzet, S. E., Martinez, S., and Le Douarin, N. M. (2006). The cephalic neural crest exerts a critical effect on forebrain and midbrain development. *Proc. Natl. Acad. Sci. U.S.A.* 103, 14033–14038. doi: 10.1073/pnas.0605899103

Crossley, P. H., and Martin, G. R. (1995). The mouse Fgf8 gene encodes a family of polypeptides and is expressed in regions that direct outgrowth and patterning in the developing embryo. *Development* 121, 439–451. doi: 10.1242/dev.121.2.439

Cuervo, R., and Covarrubias, L. (2004). Death is the major fate of medial edge epithelial cells and the cause of basal lamina degradation during palatogenesis. *Development* 131, 15–24. doi: 10.1242/dev.00907

Danesin, C., and Hobart, C. (2012). A fox stops the Wnt: implications for forebrain development and diseases. *Curr. Opin. Genet. Dev.* 22, 323–330. doi: 10.1016/j.gde.2012.05.001

Davidson, L. A. (2012). Epithelial machines that shape the embryo. *Trends Cell Biol.* 22, 82–87. doi: 10.1016/j.tcb.2011.10.005

Depew, M., Tucker, A. S., and Sharpe, P. (2002a). "Craniofacial development," in *Mouse Development: Patterning, Morphogenesis and Organogenesis*, eds J. Rossant and P. T. Tam (San Diego: Academic Press), 421–498.

Depew, M. J., and Compagnucci, C. (2008). Tweaking the hinge and caps: testing a model of the organization of jaws. *J. Exp. Zool. B Mol. Dev. Evol.* 310, 315–335. doi: 10.1002/jez.b.21205

Depew, M. J., Lufkin, T., and Rubenstein, J. L. R. (2002b). Specification of jaw subdivisions by Dlx genes. *Science* 298, 381–385. doi: 10.1126/science.1075703

Depew, M. J., and Simpson, C. A. (2006). 21st century neontology and the comparative development of the vertebrate skull. *Dev. Dyn.* 235, 1256–1291. doi: 10.1002/dvdy.20796

Depew, M. J., Simpson, C. A., Morasso, M., and Rubenstein, J. L. (2005). Reassessing the Dlx code: the genetic regulation of branchial arch skeletal pattern and development. *J. Anat.* 207, 501–561. doi: 10.1111/j.1469-7580.2005.00487

Dixon, M. J., Marazita, M. L., Beaty, T. H., and Murray, J. C. (2011). Cleft lip and palate: understanding genetic and environmental influences. *Nat. Rev. Genet.* 12, 167–178. doi: 10.1038/nrg2933

Dorstyn, L., Akey, C. W., and Kumar, S. (2018). New insights into apoptosome structure and function. *Cell Death Differ.* 25, 1194–1208. doi: 10.1038/s41418-017-0025-z

Dudgeon, C., Qiu, W., Sun, Q., Zhang, L., and Yu, J. (2009). "Transcriptional regulation of apoptosis," in *Essentials of Apoptosis*, eds Z. Dong and X. M. Yin (Totowa, NJ: Humana Press), doi: 10.1007/978-1-60327-381-7_10

Ellis, R. E., Yuan, J., and Horvitz, H. R. (1991). Mechanisms and functions of cell death. *Annu. Rev. Cell. Biol.* 7, 663–698. doi: 10.1146/annurev.cb.07.110191.003311

Etchevers, H. C., Dupin, E., and Le Douarin, N. M. (2019). The diverse neural crest: from embryology to human pathology. *Development* 146:dev169821. doi: 10.1242/dev.169821

Ferretti, E., Li, B., Zewdu, R., Wells, V., Hebert, J. M., Karner, C., et al. (2011). A conserved Pbx-Wnt-p63-Irf6 regulatory module controls face morphogenesis by promoting epithelial apoptosis. *Dev. Cell.* 21, 627–641. doi: 10.1016/j.devcel.2011.08.005

Findlater, G. S., McDougall, R. D., and Kaufman, M. H. (1993). Eyelid development, fusion and subsequent reopening in the mouse. *J. Anat.* 183(Pt. 1), 121–129.

Fish, J. L., Villmoare, B., Köbernick, K., Compagnucci, C., Britanova, O., Tarabykin, V., et al. (2011). Satb2, modularity, and the evolvability of the vertebrate jaw. *Evol. Dev.* 13, 549–564. doi: 10.1111/j.1525-142X.2011.00511.x

Florian, C., Bahi-Buisson, N., and Bienvenu, T. (2012). FOXG1-related disorders: from clinical description to molecular genetics. *Mol. Syndromol.* 2, 153–163.

Frank, D. U., Fotheringham, L. K., Brewer, J. A., Muglia, L. J., Tristani-Firouzi, M., Capecchi, M. R., et al. (2002). An Fgf8 mouse mutant phenocopies human 22q11 deletion syndrome. *Development* 129, 4591–4603. doi: 10.1242/dev.129.19.4591

Frazer, J. E. (1926). The disappearance of the precervical sinus. *J. Anat.* 61, 132–143.

Fuchs, Y., and Steller, H. (2011). Programmed cell death in animal development and disease. *Cell* 147, 742–758. doi: 10.1016/j.cell.2011.10.033

Gans, C., and Northcutt, R. G. (1983). Neural crest and the origin of vertebrates: a new head. *Science* 220, 268–273. doi: 10.1126/science.220.4594.268

Ghose, P., and Shaham, S. (2020). Cell death in animal development. *Development* 147:dev191882. doi: 10.1242/dev.191882

Glücksmann, A. (1951). Cell deaths in normal vertebrate ontogeny. *Biol. Rev. Camb. Philos Soc.* 26, 59–86. doi: 10.1111/j.1469-185x.1951.tb00774.x

Goodrich, E. S. (1958). *Studies on the Structure and Development of Vertebrates*. New York: Dover Publications.

Gorlin, R. J., Cohen, M. M., and Levin, L. S. (1990). *Syndromes of the Head and Neck*. New York, NY: Oxford University Press.

Grabow, S., Kueh, A. J., Ke, F., Vanyai, H. K., Sheikh, B. N., Dengler, M. A., et al. (2018). Subtle changes in the levels of BCL-2 proteins cause severe craniofacial abnormalities. *Cell. Rep.* 24, 3285–3295.e4. doi: 10.1016/j.celrep.2018.08.048

Graham, A., Heyman, I., and Lumsden, A. (1993). Even-numbered rhombomeres control the apoptotic elimination of neural crest cells from odd-numbered rhombomeres in the chick hindbrain. *Development* 119, 233–245. doi: 10.1242/dev.119.1.233

Graham, A., Koentges, G., and Lumsden, A. (1996). Neural crest apoptosis and the establishment of craniofacial pattern: an honorable death. *Mol. Cell. Neurosci.* 8, 76–83. doi: 10.1006/mcne.1996.0046

Graham, A., Okabe, M., and Quinlan, R. (2005). The role of the endoderm in the development and evolution of the pharyngeal arches. *J. Anat.* 207, 479–487. doi: 10.1111/j.1469-7580.2005.00472.x

Green, S. A., Simoes-Costa, M., and Bronner, M. E. (2015). Evolution of vertebrates as viewed from the crest. *Nature* 520, 474–482. doi: 10.1038/nature14436

Gressner, O., Schilling, T., Lorenz, K., Schulze Schleithoff, E., Koch, A., Schulze-Bergkamen, H., et al. (2005). TAp63alpha induces apoptosis by activating signaling via death receptors and mitochondria. *EMBO J.* 24, 2458–2471. doi: 10.1038/sj.emboj.7600708

Griffin, J. N., Compagnucci, C., Hu, D., Fish, J., Klein, O., Marcucio, R., et al. (2013). Fgf8 dosage determines midfacial integration and polarity within the nasal and optic capsules. *Dev. Biol.* 374, 185–197. doi: 10.1016/j.ydbio.2012.11.014

Hanashima, C., Li, S. C., Shen, L., Lai, E., and Fishell, G. (2004). Foxg1 suppresses early cortical cell fate. *Science* 303, 56–59. doi: 10.1126/science.1090674

Harris, M. J., and McLeod, M. J. (1982). Eyelid growth and fusion in fetal mice. a scanning electron microscope study. *Anat. Embryol. (Berl)* 164, 207–220. doi: 10.1007/BF00318505

Haworth, K. E., Healy, C., Morgan, P., and Sharpe, P. T. (2004). Regionalisation of early head ectoderm is regulated by endoderm and prepatterns the orofacial epithelium. *Development* 131, 4797–4806. doi: 10.1242/dev.01337

Hinchliffe, J. R. (1981). "Cell death in embryogenesis," in *Cell Death in Biology and Pathology*, eds I. D. Bowen and R. A. Lockshin (Chapman and Hall Ltd), 35–78. doi: 10.1007/978-94-011-6921-9_3

Hou, P.-S., hAilín, D. Ó, Vogel, T., and Hanashima, C. (2020). Transcription and beyond: delineating FOXG1 function in cortical development and disorders. *Front. Cell. Neurosci.* 14:35. doi: 10.3389/fncel.2020.00035

Hu, D., Marcucio, R. S., and Helms, J. A. (2003). A zone of frontonasal ectoderm regulates patterning and growth in the face. *Development* 130, 1749–1758. doi: 10.1242/dev.00397

Jacobson, A. G. (1963). The determination and positioning of the nose, lens and ear. I. Interactions within the ectoderm, and between the ectoderm and the underlying tissues. *J. Exp. Zool.* 154, 273–284. doi: 10.1002/jez.1401540303

Jacobson, M. D., Weil, M., and Raff, M. C. (1997). Programmed cell death in animal development. *Cell* 88, 347–354. doi: 10.1016/s0092-8674(00)81873-5

Jiang, R., Bush, J. O., and Lidral, A. C. (2006). Development of the upper lip: morphogenetic and molecular mechanisms. *Dev. Dyn.* 235, 1152–1166. doi: 10.1002/dvdy.20646

Jin, J.-Z., and Ding, J. (2006). Analysis of cell migration, transdifferentiation and apoptosis during mouse secondary palate fusion. *Development* 133, 3341–3347. doi: 10.1242/dev.02520

Ke, F., Bouillet, P., Kaufmann, T., Strasser, A., Kerr, J., and Voss, A. K. (2013). Consequences of the combined loss of BOK and BAK or BOK and BAX. *Cell Death Dis.* 4:e650. doi: 10.1038/cddis.2013.176

Ke, F. F. S., Vanyai, H. K., Cowan, A. D., Delbridge, A. R. D., Whitehead, L., Grabow, S., et al. (2018). Embryogenesis and adult life in the absence of intrinsic apoptosis effectors BAX, BAK, and BOK. *Cell* 173, 1217–1230.e17. doi: 10.1016/j.cell.2018.04.036

Kerr, J. F., Wyllie, A. H., and Currie, A. R. (1972). Apoptosis: a basic biological phenomenon with wide-ranging implications in tissue kinetics. *Br. J. Cancer* 26, 239–257. doi: 10.1038/bjc.1972.33

Knabe, W., Obermayer, B., Kuhn, H.-J., Brunnett, G., and Washausen, S. (2009). Apoptosis and proliferation in the trigeminal placode. *Brain Struct. Funct.* 214, 49–65. doi: 10.1007/s00429-009-0228-2

Kobraei, E. M., Lentz, A. K., Eberlin, K. R., Hachach-Haram, N., and Hamdan, U. S. (2016). Macrostomia: a practical guide for plastic and reconstructive surgeons. *J. Craniofac. Surg.* 27, 118–123. doi: 10.1097/SCS.0000000000002294

Lang, R. A. (1997). Apoptosis in mammalian eye development: lens morphogenesis, vascular regression and immune privilege. *Cell Death Differ.* 4, 12–20. doi: 10.1038/sj.cdd.4400211

Lantz, B., White, C., Liu, X., Wan, Y., Gabriel, G., Lo, C. W. Y., et al. (2020). Finding the unicorn, a new mouse model of midfacial clefting. *Genes (Basel)* 11:E83. doi: 10.3390/genes11010083

Linsten, T., Ross, A. J., King, A., Zong, W. X., Rathmell, J. C., Shiels, H. A., et al. (2000). The combined functions of proapoptotic Bcl-2 family members bak and bax are essential for normal development of multiple tissues. *Mol. Cell.* 6, 1389–1399. doi: 10.1016/s1097-2765(00)00136-2

Lin-Shiao, E., Lan, Y., Welzenbach, J., Alexander, K. A., Zhang, Z., Knapp, M., et al. (2019). p63 establishes epithelial enhancers at critical craniofacial development genes. *Sci Adv* 5:eaaw0946. doi: 10.1126/sciadv.aaw0946

Long, A. B., Kaiser, W. J., Mocarski, E. S., and Caspary, T. (2013). Apaf1 apoptotic function critically limits Sonic hedgehog signaling during craniofacial development. *Cell Death Differ.* 20, 1510–1520. doi: 10.1038/cdd.2013.97

Losa, M., Risolino, M., Li, B., Hart, J., Quintana, L., Grishina, I., et al. (2018). Face morphogenesis is promoted by Pbx-dependent EMT via regulation of Snail1 during frontonasal prominence fusion. *Development* 145:dev157628. doi: 10.1242/dev.157628

Lotz, K., Proff, P., Bienengraeber, V., Fanghaenel, J., Gedrange, T., and Weingaertner, J. (2006). Apoptosis as a creative agent of embryonic development of bucca, mentum and nasolacrimal duct. an in vivo study in rats. *J. Craniomaxillofac. Surg.* 34(Suppl. 2), 8–13. doi: 10.1016/S1010-5182(06)60003-6

Marcucio, R., Hallgrimsson, B., and Young, N. M. (2015). Facial morphogenesis: physical and molecular interactions between the brain and the face. *Curr. Top. Dev. Biol.* 115, 299–320. doi: 10.1016/bs.ctdb.2015.09.001

Meier, P., Finch, A., and Evan, G. (2000). Apoptosis in development. *Nature* 407, 796–801. doi: 10.1038/35037734

Meng, Q., Jin, C., Chen, Y., Chen, J., Medvedovic, M., and Xia, Y. (2014). Expression of signaling components in embryonic eyelid epithelium. *PLoS One* 9:e87038. doi: 10.1371/journal.pone.0087038

Meyers, E. N., Lewandoski, M., and Martin, G. R. (1998). An Fgf8 mutant allelic series generated by Cre- and Flp-mediated recombination. *Nat. Genet.* 18, 136–141. doi: 10.1038/ng0298-136

Minoux, M., and Rijli, F. M. (2010). Molecular mechanisms of cranial neural crest cell migration and patterning in craniofacial development. *Development* 137, 2605–2621. doi: 10.1242/dev.040048

Mitter, D., Pringsheim, M., Kaulisch, M., Plümacher, K. S., Schröder, S., Warthemann, R., et al. (2018). FOXG1 syndrome: genotype-phenotype association in 83 patients with FOXG1 variants. *Genet. Med.* 20, 98–108. doi: 10.1038/gim.2017.75

Mohamad Shah, N. S., Salahshourifar, I., Sulong, S., Wan Sulaiman, W. A., and Halim, A. S. (2018). Discovery of candidate genes for nonsyndromic cleft lip palate through genome-wide linkage analysis of large extended families in the Malay population. *BMC Genet.* 17:39. doi: 10.1186/s12863-016-0345-x

Molè, M. A., Galea, G. L., Rolo, A., Weberling, A., Nychyk, O., De Castro, S. C., et al. (2020). Integrin-mediated focal anchorage drives epithelial zippering during mouse neural tube closure. *Dev. Cell.* 52, 321–334.e6. doi: 10.1016/j.devcel.2020.01.012

Monier, B., Gettings, M., Gay, G., Mangeat, T., Schott, S., Guarner, A., et al. (2015). Apico-basal forces exerted by apoptotic cells drive epithelium folding. *Nature* 518, 245–248. doi: 10.1038/nature14152

Monier, B., and Suzanne, M. (2015). The morphogenetic role of apoptosis. *Curr. Top. Dev. Biol.* 114, 335–362. doi: 10.1016/bs.ctdb.2015.07.027

Morgenbesser, S. D., Williams, B. O., Jacks, T., and DePinho, R. A. (1994). p53-dependent apoptosis produced by Rb-deficiency in the developing mouse lens. *Nature* 371, 72–74. doi: 10.1038/371072a0

Nelsen, O. E. (1953). *Comparative Embryology of the Vertebrates*. New York: The Blakiston Company.

Nikolopoulou, E., Galea, G. L., Rolo, A., Greene, N. D. E., and Copp, A. J. (2017). Neural tube closure: cellular, molecular and biomechanical mechanisms. *Development* 144, 552–566. doi: 10.1242/dev.145904

Noden, D. M., and Trainor, P. A. (2005). Relations and interactions between cranial mesoderm and neural crest populations. *J. Anat.* 207, 575–601. doi: 10.1111/j.1469-7580.2005.00473.x

Nonomura, K., Yamaguchi, Y., Hamachi, M., Koike, M., Uchiyama, Y., Nakazato, K., et al. (2013). Local apoptosis modulates early mammalian brain development through the elimination of morphogen-producing cells. *Dev. Cell* 27, 621–634. doi: 10.1016/j.devcel.2013.11.015

Oostrom, C. A., Vermeij-Keers, C., Gilbert, P. M., and van der Meulen, J. C. (1996). Median cleft of the lower lip and mandible: case reports, a new embryologic hypothesis, and subdivision. *Plast. Reconstr. Surg.* 97, 313–320. doi: 10.1097/00006534-199602000-00006

Pan, H., and Griep, A. E. (1995). Temporally distinct patterns of p53-dependent and p53-independent apoptosis during mouse lens development. *Genes Dev.* 9, 2157–2169. doi: 10.1101/gad.9.17.2157

Patthey, C., Schlosser, G., and Shimeld, S. M. (2014). The evolutionary history of vertebrate cranial placodesI: cell type evolution. *Dev. Biol.* 389, 82–97. doi: 10.1016/j.ydbio.2014.01.017

Pei, Y. F., and Rhodin, J. A. (1970). The prenatal development of the mouse eye. *Anat. Rec.* 168, 105–125. doi: 10.1002/ar.1091680109

Pei, Y. F., and Rhodin, J. A. (1971). Electron microscopic study of the development of the mouse corneal epithelium. *Invest. Ophthalmol.* 10, 811–825.

Pietsch, E. C., Sykes, S. M., McMahon, S. B., and Murphy, M. E. (2008). The p53 family and programmed cell death. *Oncogene* 27, 6507–6521. doi: 10.1038/onc.2008.315

Pipsa, J., and Thesleff, I. (2003). Mechanisms of ectodermal organogenesis. *Dev. Biol.* 262, 195–205. doi: 10.1016/s0012-1606(03)00325-7

Ravichandran, K. S. (2011). Beginnings of a good apoptotic meal: the find-me and eat-me signaling pathways. *Immunity* 35, 445–455. doi: 10.1016/j.immuni.2011.09.004

Ray, H. J., and Niswander, L. (2012). Mechanisms of tissue fusion during development. *Development* 139, 1701–1711. doi: 10.1242/dev.068338

Redies, C., and Puelles, L. (2001). Modularity in vertebrate brain development and evolution. *Bioessays* 23, 1100–1111. doi: 10.1002/bies.10014

Richardson, R., Mitchell, K., Hammond, N. L., Mollo, M. R., Kouwenhoven, E. N., Wyatt, N. D., et al. (2017). p63 exerts spatio-temporal control of palatal epithelial cell fate to prevent cleft palate. *PLoS Genet* 13:e1006828. doi: 10.1371/journal.pgen.1006828

Richardson, R. J., Hammond, N. L., Coulombe, P. A., Saloranta, C., Nousiainen, H. O., Salonen, R., et al. (2014). Periderm prevents pathological epithelial adhesions during embryogenesis. *J. Clin. Invest.* 124, 3891–3900. doi: 10.1172/JCI71946

Rijli, F. M., Mark, M., Lakkaraju, S., Dierich, A., Dollé, P., and Chambon, P. (1993). A homeotic transformation is generated in the rostral branchial region of the head by disruption of Hoxa-2, which acts as a selector gene. *Cell* 75, 1333–1349. doi: 10.1016/0092-8674(93)90620-6

Rinne, T., Brunner, H. G., and van Bokhoven, H. (2007). p63-associated disorders. *Cell Cycle* 6, 262–268. doi: 10.4161/cc.6.3.3796

Rubenstein, J. L., Shimamura, K., Martinez, S., and Puelles, L. (1998). Regionalization of the prosencephalic neural plate. *Annu. Rev. Neurosci.* 21, 445–477. doi: 10.1146/annurev.neuro.21.1.445

Saint-Jeannet, J.-P., and Moody, S. A. (2014). Establishing the pre-placodal region and breaking it into placodes with distinct identities. *Dev. Biol.* 389, 13–27. doi: 10.1016/j.ydbio.2014.02.011

Sanz-Ezquerro, J. J., and Tickle, C. (2000). Autoregulation of Shh expression and Shh induction of cell death suggest a mechanism for modulating polarising activity during chick limb development. *Development* 127, 4811–4823. doi: 10.1242/dev.127.22.4811

Sato, T., Kurihara, Y., Asai, R., Kawamura, Y., Tonami, K., Uchijima, Y., et al. (2008). An endothelin-1 switch specifies maxillomandibular identity. *Proc. Natl. Acad. Sci. U.S.A.* 105, 18806–18811. doi: 10.1073/pnas.0807345105

Saunders, J. W. Jr. (1966). Death in embryonic systems. *Science* 154, 604–612. doi: 10.1126/science.154.3749.604

Schlosser, G. (2010). Making senses development of vertebrate cranial placodes. *Int. Rev. Cell Mol. Biol.* 283, 129–234. doi: 10.1016/S1937-6448(10)83004-7

Selleri, L., Depew, M. J., Jacobs, Y., Chanda, S. K., Tsang, K. Y., Cheah, K. S., et al. (2001). Requirement for Pbx1 in skeletal patterning and programming chondrocyte proliferation and differentiation. *Development* 128, 3543–3557. doi: 10.1242/dev.128.18.3543

Sharov, A. A., Weiner, L., Sharova, T. Y., Siebenhaar, F., Atoyan, R., Reginato, A. M., et al. (2003). Noggin overexpression inhibits eyelid opening by altering epidermal apoptosis and differentiation. *EMBO J.* 22, 2992–3003. doi: 10.1093/emboj/cdg291

Shone, V., and Graham, A. (2014). Endodermal/ectodermal interfaces during pharyngeal segmentation in vertebrates. *J. Anat.* 225, 479–491. doi: 10.1111/joa.12234

Shuler, C. F. (1995). Programmed cell death and cell transformation in craniofacial development. *Crit. Rev. Oral. Biol. Med.* 6, 202–217. doi: 10.1177/10454411950060030301

Storm, E. E., Rubenstein, J. L. R., and Martin, G. R. (2003). Dosage of Fgf8 determines whether cell survival is positively or negatively regulated in the developing forebrain. *Proc. Natl. Acad. Sci. U.S.A.* 100, 1757–1762. doi: 10.1073/pnas.0337736100

Storm, E. E., Garel, S., Borello, U., Hebert, J. M., Martinez, S., McConnell, S. K., et al. (2006). Dose-dependent functions of Fgf8 in regulating telencephalic patterning centers. *Development* 133, 1831–1844. doi: 10.1242/dev.02324

Streit, A. (2018). Specification of sensory placode progenitors: signals and transcription factor networks. *Int. J. Dev. Biol.* 62, 195–205. doi: 10.1387/ijdb.170298as

Suzanne, M., and Steller, H. (2013). Shaping organisms with apoptosis. *Cell Death Differ.* 20, 669–675. doi: 10.1038/cdd.2013.11

Tamarin, A. (1982). The formation of the primitive choanae and the junction of the primary and secondary palates in the mouse. *Am. J. Anat.* 165, 319–337. doi: 10.1002/aja.1001650308

Tamarin, A., and Boyde, A. (1977). Facial and visceral arch development in the mouse embryo: a study by scanning electron microscopy. *J. Anat.* 124, 563–580.

Taylor, R. C., Cullen, S. P., and Martin, S. J. (2008). Apoptosis: controlled demolition at the cellular level. *Nat. Rev. Mol. Cell. Biol.* 9, 231–241. doi: 10.1038/nrm2312

Thomason, H. A., Dixon, M. J., and Dixon, J. (2008). Facial clefting in Tp63 deficient mice results from altered Bmp4, Fgf8 and Shh signaling. *Dev. Biol.* 321, 273–282. doi: 10.1016/j.ydbio.2008.06.030

Thomason, H. A., Zhou, H., Kouwenhoven, E. N., Dotto, G.-P., Restivo, G., Nguyen, B.-C., et al. (2010). Cooperation between the transcription factors p63 and IRF6 is essential to prevent cleft palate in mice. *J. Clin. Invest.* 120, 1561–1569. doi: 10.1172/JCI40266

Trumpp, A., Depew, M. J., Rubenstein, J. L., Bishop, J. M., and Martin, G. R. (1999). Cre-mediated gene inactivation demonstrates that FGF8 is required for cell survival and patterning of the first branchial arch. *Genes Dev.* 13, 3136–3148. doi: 10.1101/gad.13.23.3136

Tuzlak, S., Kaufmann, T., and Villunger, A. (2016). Interrogating the relevance of mitochondrial apoptosis for vertebrate development and postnatal tissue homeostasis. *Genes Dev.* 30, 2133–2151. doi: 10.1101/gad.289298.116

Vaahtokari, A., Aberg, T., and Thesleff, I. (1996). Apoptosis in the developing tooth: association with an embryonic signaling center and suppression by EGF and FGF-4. *Development* 122, 121–129. doi: 10.1242/dev.122.1.121

Van Nostrand, J. L., Bowen, M. E., Vogel, H., Barna, M., and Attardi, L. D. (2017). The p53 family members have distinct roles during mammalian embryonic development. *Cell Death Differ.* 24, 575–579. doi: 10.1038/cdd.2016.128

Van Nostrand, J. L., Brady, C. A., Jung, H., Fuentes, D. R., Kozak, M. M., Johnson, T. M., et al. (2014). Inappropriate p53 activation during development induces features of CHARGE syndrome. *Nature* 514, 228–232. doi: 10.1038/nature13585

Vecino, E., and Acera, A. (2015). Development and programed cell death in the mammalian eye. *Int. J. Dev. Biol.* 59, 63–71. doi: 10.1387/ijdb.150070ev

Voss, A. K., and Strasser, A. (2020). The essentials of developmental apoptosis. *F1000 Res.* 9:148. doi: 10.12688/f1000research.21571.1

Wake, M. H. (1979). *Hyman's Comparative Vertebrate Anatomy*, 3rd Edn. Chicago, IL: The University of Chicago Press.

Wanner, E., Thoppil, H., and Riabowol, K. (2021). Senescence and apoptosis: architects of mammalian development. *Front. Cell Dev. Biol.* 8:620089. doi: 10.3389/fcell.2020.620089

Washausen, S., and Knabe, W. (2013). Apoptosis contributes to placode morphogenesis in the posterior placodal area of mice. *Brain Struct. Funct.* 218, 789–803. doi: 10.1007/s00429-012-0429-y

Washausen, S., and Knabe, W. (2018). Lateral line placodes of aquatic vertebrates are evolutionarily conserved in mammals. *Biol. Open.* 7:bio031815. doi: 10.1242/bio.031815

Washausen, S., Obermayer, B., Brunnett, G., Kuhn, H.-J., and Knabe, W. (2005). Apoptosis and proliferation in developing, mature, and regressing epibranchial placodes. *Dev. Biol.* 278, 86–102. doi: 10.1016/j.ydbio.2004.10.016

Watermann, R. E. (1977). Ultrastructure of oral (buccopharyngeal) membrane formation and rupture in the hamster embryo. *Dev. Biol.* 58, 219–229. doi: 10.1016/0012-1606(77)90088-4

Weingaertner, J., Proff, P., Bienengraeber, V., Gedrange, T., Fanghaenel, J., and Lotz, K. (2006). In vivo study of apoptosis as a creative agent of embryonic development of the primary nasal duct in rats. *J. Craniomaxillofac. Surg.* 34(Suppl. 2), 3–7. doi: 10.1016/S1010-5182(06)60002-4

Wong, F. K., and Marín, O. (2019). Developmental cell death in the cerebral cortex. *Annu. Rev. Cell. Dev. Biol.* 35, 523–542. doi: 10.1146/annurev-cellbio-100818-125204

Xuan, S., Baptista, C. A., Balas, G., Tao, W., Soares, V. C., and Lai, E. (1995). Winged helix transcription factor BF-1 is essential for the development of the cerebral hemispheres. *Neuron* 14, 1141–1152. doi: 10.1016/0896-6273(95)90262-7

Yamaguchi, Y., and Miura, M. (2013). How to form and close the brain: insight into the mechanism of cranial neural tube closure in mammals. *Cell Mol. Life Sci.* 70, 3171–3186. doi: 10.1007/s00018-012-1227-7

Yamamoto, S., Kurosaka, H., Miura, J., Aoyama, G., Sarper, S. E., Oka, A., et al. (2020). Observation of the epithelial cell behavior in the nasal septum during primary palate closure in mice. *Front. Physiol.* 11:538835. doi: 10.3389/fphys.2020.538835

Yang, A., Schweitzer, R., Sun, D., Kaghad, M., Walker, N., Bronson, R. T., et al. (1999). p63 is essential for regenerative proliferation in limb, craniofacial and epithelial development. *Nature* 398, 714–718. doi: 10.1038/19539

Yoshida, H., Kong, Y. Y., Yoshida, R., Elia, A. J., Hakem, A., Hakem, R., et al. (1998). Apaf1 is required for mitochondrial pathways of apoptosis and brain development. *Cell* 94, 739–750. doi: 10.1016/s0092-8674(00)81733-x

Zarate, Y. A., and Fish, J. L. (2017). SATB2-associated syndrome: mechanisms, phenotype, and practical recommendations. *Am. J. Med. Genet. A* 173, 327–337. doi: 10.1002/ajmg.a.38022

Zarate, Y. A., Perry, H., Ben-Omran, T., Sellars, E. A., Stein, Q., Almureikhi, M., et al. (2015). Further supporting evidence for the SATB2-associated syndrome found through whole exome sequencing. *Am. J. Med. Genet. A* 167A, 1026–1032. doi: 10.1002/ajmg.a.36849

Conflict of Interest: The authors declare that the research was conducted in the absence of any commercial or financial relationships that could be construed as a potential conflict of interest.

Publisher's Note: All claims expressed in this article are solely those of the authors and do not necessarily represent those of their affiliated organizations, or those of the publisher, the editors and the reviewers. Any product that may be evaluated in this article, or claim that may be made by its manufacturer, is not guaranteed or endorsed by the publisher.

frontiers in Cell and Developmental Biology

ORIGINAL RESEARCH
published: 08 November 2021
doi: 10.3389/fcell.2021.703836

Activation of the WNT-BMP-FGF Regulatory Network Induces the Onset of Cell Death in Anterior Mesodermal Cells to Establish the ANZ

*Martha Elena Díaz-Hernández†, Claudio Iván Galván-Hernández, Jessica Cristina Marín-Llera, Karen Camargo-Sosa†, Marcia Bustamante, Sabina Wischin and Jesús Chimal-Monroy**

Instituto de Investigaciones Biomédicas, Universidad Nacional Autónoma de México, Ciudad Universitaria, México, Mexico

The spatiotemporal control of programmed cell death (PCD) plays a significant role in sculpting the limb. In the early avian limb bud, the anterior necrotic zone (ANZ) and the posterior necrotic zone are two cell death regions associated with digit number reduction. In this study, we evaluated the first events triggered by the FGF, BMP, and WNT signaling interactions to initiate cell death in the anterior margin of the limb to establish the ANZ. This study demonstrates that in a period of two to 8 h after the inhibition of WNT or FGF signaling or the activation of BMP signaling, cell death was induced in the anterior margin of the limb concomitantly with the regulation of *Dkk*, *Fgf8,* and *Bmp4* expression. Comparing the gene expression profile between the ANZ and the undifferentiated zone at 22HH and 25HH and between the ANZ of 22HH and 25HH stages correlates with functional programs controlled by the regulatory network FGF, BMP, and WNT signaling in the anterior margin of the limb. This work provides novel insights to recognize a negative feedback loop between FGF8, BMP4, and DKK to control the onset of cell death in the anterior margin of the limb to the establishment of the ANZ.

Keywords: limb development, ANZ, Fgf signaling, Wnt signaing, BMP signaling, programmed cell death, morphogenesis, Anterior Necrotic Zone

OPEN ACCESS

Edited by:
Marta Magarinos, Autonomous University of Madrid, Spain

Reviewed by:
Xiao-Jing Zhu, Hangzhou Normal University, China
Irene Delgado, Spanish National Centre for Cardiovascular Research, Spain

****Correspondence:***
Jesús Chimal-Monroy
jchimal@unam.mx

†Present address:
Martha Elena Díaz-Hernández, Department of Orthopaedics, Emory University, Atlanta VA Medical Center, Decatur, GA, United States
Karen Camargo-Sosa, Department of Biology and Biochemistry, University of Bath, Bath, United Kingdom

Specialty section:
This article was submitted to Cell Death and Survival, a section of the journal Frontiers in Cell and Developmental Biology

Received: *30 April 2021*
Accepted: *18 October 2021*
Published: *08 November 2021*

Citation:
Díaz-Hernández ME, Galván-Hernández CI, Marín-Llera JC, Camargo-Sosa K, Bustamante M, Wischin S and Chimal-Monroy J (2021) Activation of the WNT-BMP-FGF Regulatory Network Induces the Onset of Cell Death in Anterior Mesodermal Cells to Establish the ANZ. Front. Cell Dev. Biol. 9:703836. doi: 10.3389/fcell.2021.703836

INTRODUCTION

Programmed cell death (PCD) is essential to regulate the final morphology and sculpting limbs (Pajni-Underwood et al., 2007; Montero et al., 2020). PCD participates in separating digits and zeugopodial elements (Hinchliffe and Thorogood, 1974; Zuzarte-Luis and Hurle, 2005). The anterior and posterior margins of the avian limb are associated with digit reduction (Saunders and Gasseling, 1962; Zuzarte-Luis and Hurle, 2002; 2005). Those regions are called the anterior necrotic zone (ANZ) and posterior necrotic zone (PNZ) (Saunders and Gasseling, 1962). Meanwhile, PCD in the interdigital regions takes part in species with free digits.

The process of cell death is under the control of the apical ectodermal ridge (AER); it is well known that limb truncation and massive cell death occur after the elimination of the AER, demonstrating that cell survival of mesodermal cells depends on the signals from this epithelium. The molecular analysis of AER indicates that Fibroblast Growth Factor (FGF) family

members expressed in the AER govern cell proliferation and cell survival. FGF8 signaling protects the mesodermal cells from cell death (Niswander et al., 1993; Sun et al., 2002; Mariani et al., 2008; Ten Berge et al., 2008; Mariani et al., 2017). Mutant mice for the *Fgf8* gene or the blockade of the function of FGF signaling induces cell death in the mesodermal cells (Montero et al., 2001; Sun et al., 2002; Mariani et al., 2008; Mariani et al., 2017). FGF8 participates promoting a positive feedback loop, inducing the expression of *Fgf10* in the mesoderm whose interaction with the FGF receptor 2b (FGFR2b) in the AER promotes the expression of *Wnt3a* (Xu et al., 1998; Danopoulos et al., 2013; Haro et al., 2014; Jin et al., 2018). WNT3A induces the expression of transcription factors *Sp6* and *Sp8* that induce *Fgf8* expression in the AER (Kawakami et al., 2001; Kawakami et al., 2004). WNT signaling from the AER participates in maintaining the undifferentiated state of mesodermal cells under AER (Ten Berge et al., 2008). The function of WNT-ß catenin signaling may be blocked by DKK, an antagonist of this signaling pathway. Gene deletion of DKK results in cell death inhibition, and *Dkk* expression is observed in cell death regions during limb development (Grotewold et al., 1999; Mukhopadhyay et al., 2001; Grotewold and Ruther, 2002a; b).

During limb development, the bone morphogenetic proteins (BMP) signaling is another pathway controlling cell death. *Bmp2, Bmp4,* and *Bmp7* expression are observed in the interdigital regions and the anterior and posterior margins of the limb (Hogan, 1996; Yokouchi et al., 1996; Macias et al., 1997; Chen and Zhao, 1998; Merino et al., 1999; Salas-Vidal et al., 2001; Zuzarte-Luis et al., 2004). The implantation of BMP-soaked beads promotes cell death in the interdigital tissue, whereas the blockade of BMP signaling with NOGGIN or GREMLIN inhibits it (Ganan et al., 1996; Macias et al., 1997; Zuzarte-Luis et al., 2004). BMP stimulates the SMAD1/5/8 signaling pathway in blood vessels and mesodermal cells, promoting cell death in mesodermal cells, and inhibiting *Fgf8* expression in the AER (Zuzarte-Luis et al., 2004; Monteiro et al., 2008; Abarca-Buis et al., 2011).

High levels of FGF signaling in the interdigital mesoderm downregulate *Bmp* genes, inhibiting cell death (Montero et al., 2001; Hernandez-Martinez et al., 2009). However, FGF2 signaling promoted cell death induced by BMP proteins, suggesting that FGF also works in a feedback loop with BMP signaling (Montero et al., 2001). Mesodermal cells become competent to signaling pathways that control cell fate when WNT and FGF signals are depleted underneath AER (Ten Berge et al., 2008). If cells receive cell death-promoting factors, presumably BMPs, cells enter the cell death program (Montero et al., 2001; Hernandez-Martinez et al., 2009). Otherwise, the cell differentiation program begins if mesodermal cells receive chondrogenic signals (Chimal-Monroy et al., 2003; Montero et al., 2008; Marin-Llera et al., 2019). Thus, FGF and WNT signaling together with BMP signaling establish a well-known regulatory network to control the undifferentiated state, cell proliferation, and cell survival during limb development (Niswander et al., 1993; Montero et al., 2001; Sun et al., 2002; Mariani et al., 2008; Ten Berge et al., 2008; Hernandez-Martinez et al., 2009; Mariani et al., 2017). The participation of this regulatory network is better known during the PCD in the interdigital regions than in the ANZ or PNZ. A previous study demonstrated that a BMP-pulse of 4 h was sufficient to induce cell death in the anterior margin of the limb (Abarca-Buis et al., 2011). Notably, TUNEL-positive cells show no co-localization of nuclear phosphorylated SMAD1/5/8 proteins suggesting that BMP signaling participates in a molecular cascade in the ANZ, culminating in cell death (Abarca-Buis et al., 2011).

Because a short pulse of BMP is sufficient to induce cell death in the anterior margin of the limb, this work aimed to determine how the regulatory network integrated by FGF, BMP, and WNT signaling pathways participate in the establishment of the ANZ. The results presented here demonstrated that inhibition of WNT or FGF signaling or the activation of BMP signaling during a short period is sufficient to induce cell death in the anterior margin of the limb and to regulate *Dkk*, *Fgf8,* and *Bmp4* expression. Thus, the regulatory network of the FGF-BMP-WNT signaling pathway induces cell death in the anterior margin of the limb to establishing the ANZ.

MATERIAL AND METHODS

Ethics

This protocol was reviewed and approved by the Institutional Review Board for the Care and Use of Laboratory Animals of the Instituto de Investigaciones Biomédicas, Universidad Nacional Autónoma de México (UNAM, Mexico City, Mexico).

Eggs and Embryo Manipulations

Fertilized White Leghorn chicken eggs (ALPES, Puebla, Mexico) were incubated at 38°C and staged according to Hamburger and Hamilton (1951). Eggs were windowed to expose the right limb at developing stages from 22 to 25 HH for experimental procedures. Heparin beads (Cat. H6508, Sigma-Aldrich, St. Louis, MO, United States) or in Affigel (Bio-Rad Laboratories, Hercules, CA) were soaked in 1 mg/ml FGF8 (cat. 100-25A), FGF10 (100-26), 1 mg/ml DKK (cat. 120-30) BMP4 (cat. 120-05), BMP7 (cat. 120-30P) or 2 mg/ml NOGGIN (cat. 120-10C) from Peprotech, Mexico City, Mexico. Ag1-X2 ionic exchange beads (Cat. 1401231, Sigma-Aldrich, Mexico) were soaked in 4 mg/ml SU502 and placed in the ANZ of embryonic limbs. Manipulated embryos were incubated for short times according to the experiments and processed for lysotracker staining, *in situ* hybridization, or both.

RNA Probes and in Situ Hybridization

RNA antisense probes were labeled with UTP-digoxigenin (11209256910, Roche Applied Science, Indianapolis, IN, United States) and used for whole-mount *in situ* hybridization (ISH) as described previously (Merino et al., 1998). Samples were treated with 60 µg/ml proteinase K for 25 min at 21°C for *Bmp7*, *Fgfr1*, *Fgfr2*, *Fgfr3*, *Mkp3*, *Msx2*, and *Wif*. *Bambi* required 70 µg/ml proteinase K for 28 min at 25°C; 60 µg/ml was used for 22 min at 21°C for *Bmp4* and *Dkk*. *Fgf8* was treated with 15 µg/ml for 20 min at 21°C. The hybridization temperature was 68°C, and post-hybridization washes were at 70°C for all genes. The signal of ISH was visualized with BM-Purple substrate for alkaline phosphatase (Roche Applied Science). Images were acquired

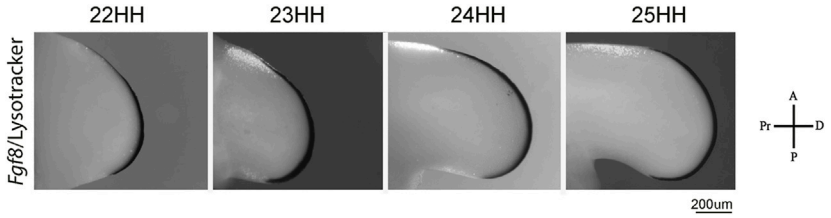

FIGURE 1 | Progressive loss of the apical ectodermal coincides with the apparition of cell death in the anterior margin of the limb. *In situ* hybridization of *Fgf8* gene expression and cell death pattern evidenced by lysotracker stain at limb development stages from 22 to 25 HH. Notice that cell death occurs in regions in which *Fgf8* expression is disappearing.

with the Nikon Stereoscope Fluorescence Microscope SMZ1500 (Nikon Corporation, NY, United States) or in AxioZoom V.16 microscope (Carl Zeiss, Oberkochen, Germany) using Zen lite software (Carl Zeiss, Oberkochen, Germany).

Detection of Cell Death With Lysotracker and Neutral Red Staining

Embryonic limbs were incubated in 1 μM LysoTracker Red DND-99 (Cat. L7528, Molecular Probes) at 37°C for 15 min. Samples were rinsed twice in PBS and fixed in 4% PFA overnight at 4°C. Some samples were also processed for ISH as described previously (Abarca-Buis et al., 2011). After ISH, limb buds were dehydrated in increasing methanol-PBS-Tween series and cleared with 2:1 benzylic alcohol: benzyl benzoate solution for 1 h each (Parish, 1999). For Neutral Red staining, limbs were isolated, washed in PBS, and stained with 2% Neutral Red in PBS time at 37°C. Images were acquired with a Nikon Stereoscope Fluorescence Microscope SMZ1500 (Nikon Corporation, NY, United States) and Fluorescence Microscope Axio Zoom. V16 Carl Zeiss, Göttingen, Germany.

Real-Time RT-PCR

RNA extractions were performed with NucleoSpin RNA (Macherey-Nagel, cat. no. 740955, Düren, Germany), and retrotranscription of total RNA was achieved using the RevertAid RT kit (Thermo Fisher Scientific, cat. no. K1691, Waltham, MA, United States) according to the manufacturer's instructions. Expression levels were analyzed using a real-time PCR system and quantified with SYBR green (Thermo Fisher). The *Rpl13* gene was used as a normalizer. The expression level was evaluated relative to a calibrator according to the $2^{-(\Delta\Delta Ct)}$ equation. Each value represented the mean ± SD of three independent experiments and was analyzed using Student's *t*-test. Statistical significance was set at $p < 0.05$.

RESULTS

Anterior Necrotic Zone Appears by the Progressive Loss of the Apical Ectodermal Ridge

To associate the gene expression pattern of *Fgf8*, a survival signal, and the presence of cell death in the ANZ during limb outgrowth, embryonic limbs from 22HH to 25HH were stained with lysotracker and hybridized for *Fgf8* (**Figure 1**). The results indicated that cell death was observed in the anterior margin of the limb from stage 23 HH to 25 HH (**Figure 1**). Concurrently as the limb outgrowth occurs, the *Fgf8* expression is gradually downregulated in the AER from the proximal to the distal region, near the ANZ. Thus, these results exhibited a boundary between the downregulation of *Fgf8* from the AER and the appearance of the ANZ while progressive cell death in mesodermal cells is observed (**Figure 1**).

FGF-, BMP-, and WNT-Signaling Pathways Are Active in the Anterior Margin of the Limb Bud When the ANZ Is Established

The association of the expression patterns of the genes related to FGF-, BMP-, and WNT-signaling pathways with the boundary observed between *Fgf8,* and the appearance of progressive cell death was studied at the 24 HH stage. At this developing stage, cell death and *Fgf8* expression are precisely located at neighboring positions (**Figure 2**), allowing us to study how FGF-, BMP-, and WNT-signaling pathways regulate the onset of cell death and the appearance of ANZ in the developing limb.

The genes related to FGF signaling, such as *Mkp3, a* target of this signaling pathway, and the three receptors of FGF, *Fgfr1*, *Fgfr2*, and *Fgfr3* (**Figure 2A**) were evaluated. *Mkp3* and *Fgfr1* were expressed in the distal part of the anterior margin and in the anterior half of the distal position. Besides, *Mkp3* was expressed in the central part of the proximal region. *Fgfr2* was mainly expressed in both anterior and posterior margins, whereas *Fgr3* was slightly expressed in an extended way in the mesoderm (**Figure 2A**).

Regarding BMP signaling, the expression of *Bmp4*, *Bmp7*, and *Bambi* was evaluated. *Bmp4* was expressed in both anterior and posterior margins of the limb (**Figure 2B**). In contrast, *Bmp7* expression was mainly localized in the most distal region of the limb riming undifferentiated region underneath AER and the anterior margin of the limb (**Figure 2B**). *Bambi* expression was observed preferentially in the proximal region of the anterior margin and the most distal region of the posterior margin of the limb (**Figure 2B**). In addition, as a marker of undifferentiated cells and regulated by BMP signaling, we evaluated the *Msx2* gene expression pattern.

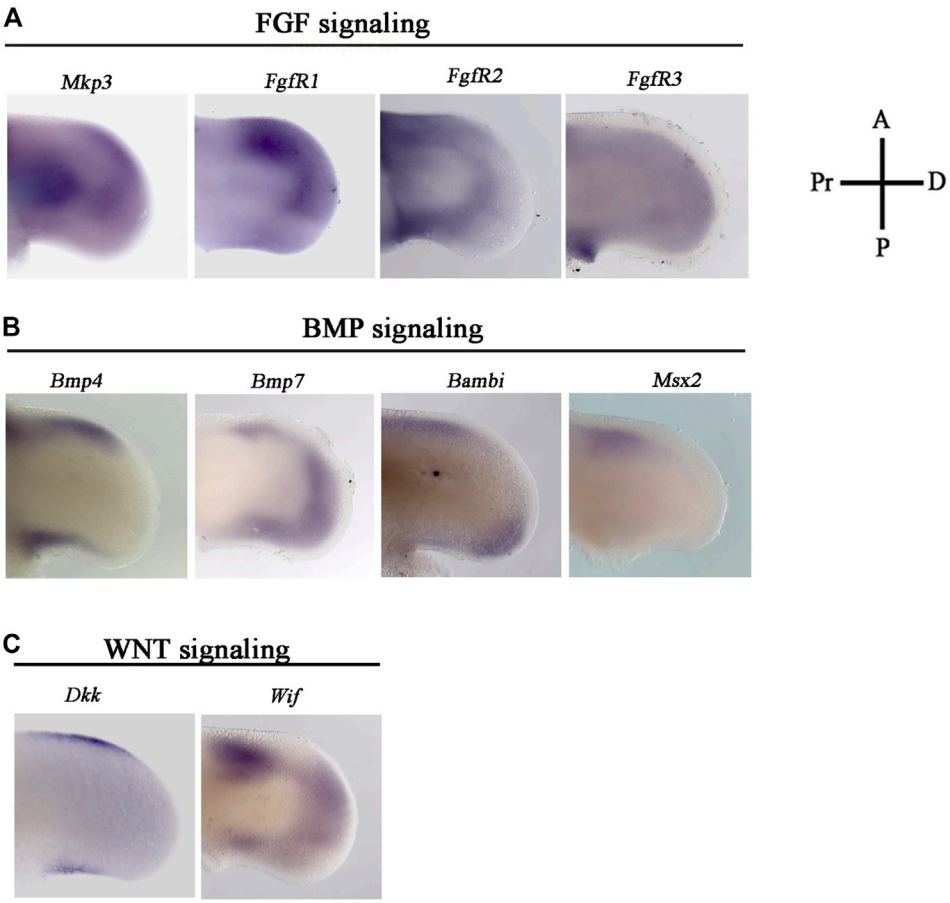

FIGURE 2 | Gene expression pattern of effector genes related with WNT, FGF, BMP signaling in the ANZ and PNZ. Cell death pattern and *in situ* hybridizations of **(A)** *Mkp3, Fgfr1, Fgfr2, Fgfr3, Bmp4, Bmp7, Bambi, Msx2, Dkk, and Wif.* They were evaluated in the anterior margin of the limb at developing stage 24 HH. **(A)** *Mkp3, Fgfr1*, *Fgfr2*, and *Fgfr3* are genes related to FGF signaling. **(B)** *Bmp4*, *Bmp7*, *Bambi,* and *Msx2* related to BMP signaling, whereas **(C)** *Dkk, Wif,* related to WNT signaling. Notice the dynamic expression of all genes in the ANZ.

Results showed that it is expressed in the anterior margin of the limb (**Figure 2B**).

On the other hand, *Dkk* and *Wif* gene expression was analyzed as genes related to Wnt signaling (**Figure 2C**). *Dkk* gene expression was localized in the anterior and posterior margins of the limb (**Figure 2**). *Wif* gene expression was observed in all anterior and posterior margins and the distal region of the limb (**Figure 2C**). These results showed a dynamic gene expression pattern suggesting that all three signaling pathways are active during the process of cell death in the anterior and posterior limb margins.

FGF, WNT, and BMP Signaling Control the Induction and Maintenance of Cell Death in the ANZ

Although the gene expression pattern is quite similar in the anterior and posterior margin of the limb, here was decided to determine the minimum time to promote cell death in the ANZ modulating the function of FGF, WNT, and BMP signaling pathways. As a first approach, FGF8-soaked beads or FGF signaling inhibitor (SU5402)-soaked beads were placed in the anterior margin of the limb at the 24 HH stage (**Figure 3A**). The results showed that FGF8 treatments did not inhibit cell death. In contrast, inhibiting FGF signaling for 6 h was sufficient to increase cell death in this region (**Figure 3A**). On the other hand, the minimal time to induce cell death after inhibiting WNT signaling with DKK-soaked beads in the anterior margin of the limb was 8 h. In contrast, as expected, WNT3A soaked beads did not inhibit cell death (**Figure 3B**).

It is known that a short pulse of BMP induces cell death in the ANZ (Abarca-Buis et al., 2011) and because the expression of the *Bmp4* and *Bmp7* is observed in the anterior margin. Here the cell death promoted by both proteins was evaluated. The results showed that cell death in the ANZ stimulated by BMP4 and BMP7 occurs after 6 h (**Figure 3C**) and is inhibited by NOGGIN after 6 h of treatment (**Figure 3C**). Taking together, these results suggest that the minimum time to trigger cell death in the ANZ is

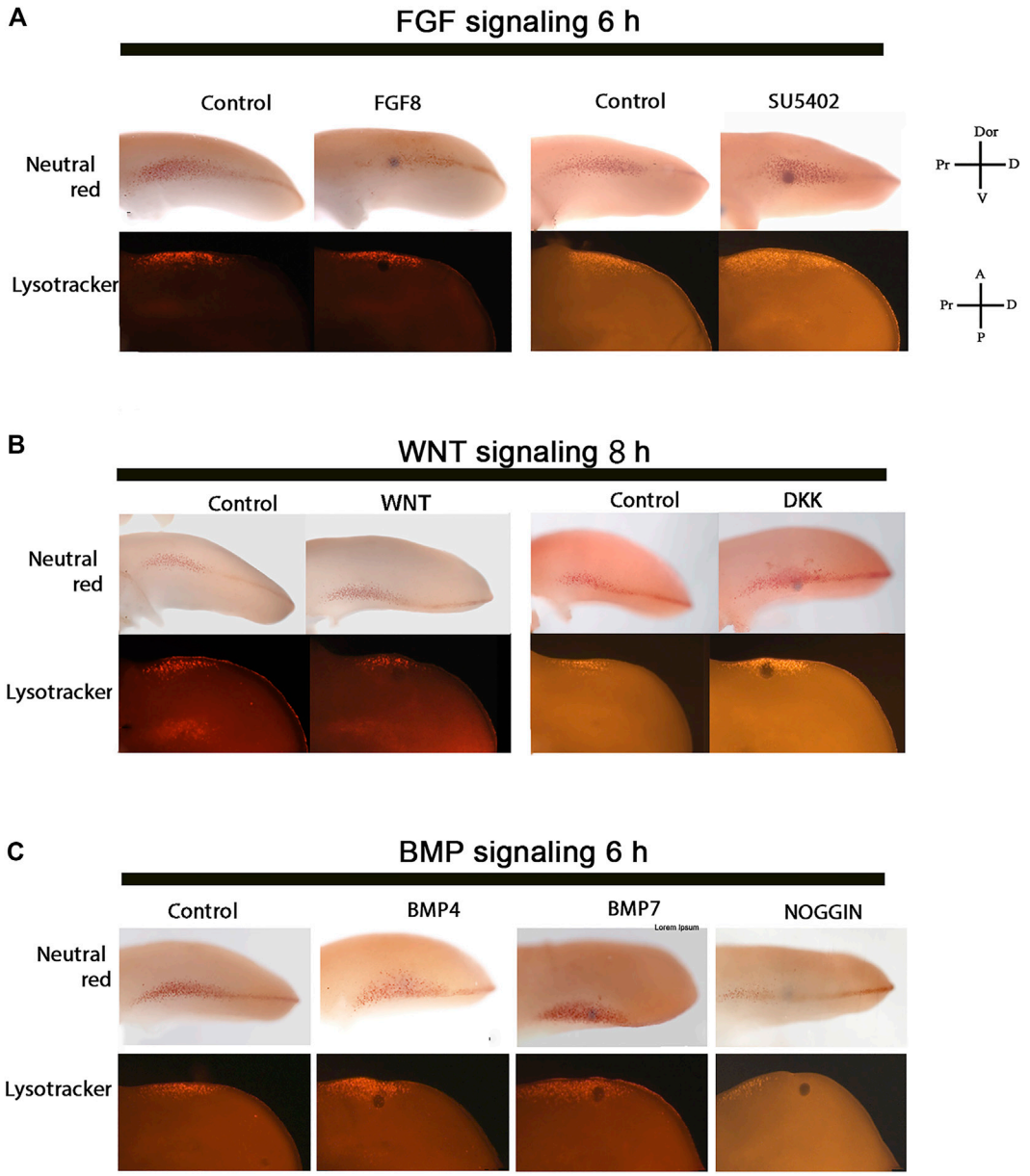

FIGURE 3 | Control of PCD in the ANZ by FGF, WNT, and BMP signaling. The cell death pattern was evaluated in the ANZ at limb developing stage 24 HH after FGF, WNT, and BMP signaling treatments. **(A)** FGF8 treatment for 6 h did not modify the cell death pattern but inhibiting FGF signaling resulted in the promotion of PCD. **(B)** WNT3A treatment for 8 h did not alter the cell death pattern, but DKK-treatment to inhibit Wnt signaling induced cell death after 8 h. **(C)** BMP4- or BMP7- treatment for 6 h promoted cell death, whereas NOGGIN inhibited cell death after 6 h of treatment. Notice that the minimum time to trigger cell death in the ANZ is 6 h after inhibiting FGF or activating BMP signaling, whereas DKK needed 8 h to promote cell death. The images at the top of each line correspond to samples stained with Neutral Red, while the images at the bottom are stained with Lysotracker. The axis showed in A can be used for B and C.

6 h after inhibition of FGF and activation of BMP signaling or 8 h after inhibiting WNT signaling.

FGF- and BMP-Signaling Are Coordinated to Regulate Cell Death in the ANZ

The inhibition of FGF or activation of BMP signaling triggers cell death after 6 h. Thus, to determine the relation between FGF and *Bmp4* and *Dkk* expression during the induction of cell death, the gene expression of *Bmp4* and *Dkk* was evaluated after inhibiting or activating FGF signaling (**Figure 4**). The results demonstrated that *Dkk* expression was inhibited after 2 h of treatment, whereas *Bmp4* inhibition occurred after 4 h (**Figure 4A**). However, after the administration of proteins FGF8 or FGF10 to activate FGF signaling, only FGF10 induced moderately *Bmp4* expression without important changes in the expression of *Dkk* and *Bmp4* by FGF8 (**Figures 4 B, C**). Thus, because the inhibition of FGF signaling for two or 4 h, downregulated *Dkk* and *Bmp4,*

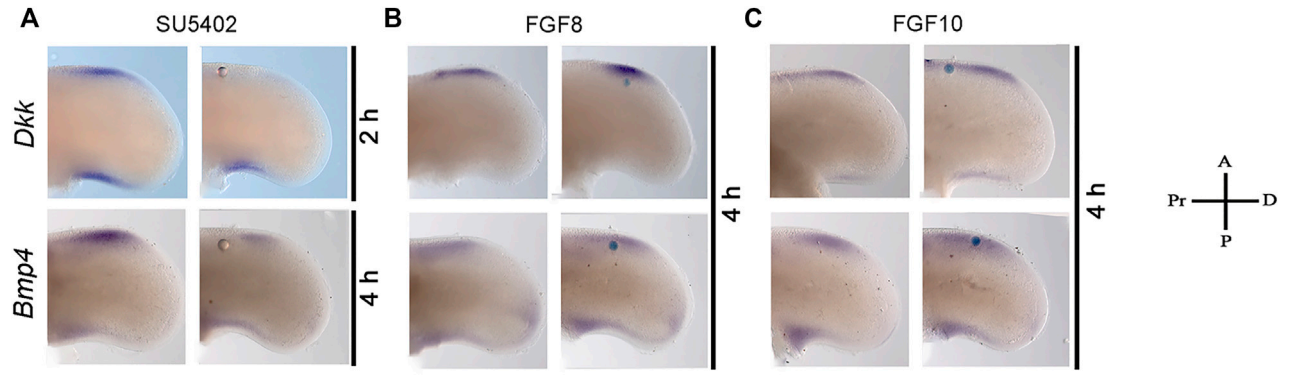

FIGURE 4 | Inhibition of *Dkk* and *Bmp4* gene expression by treatment with an inhibitor on FGF signaling. Gene expression pattern of *Bmp4* and *Dkk* in the anterior margin of the limb at developing stage 24HH. **(A)** *Dkk* expression inhibition was observed after 2 h of treatment with SU5402, while Bmp4 was inhibited after 4 h. The gene expression pattern of *Dkk* and *Bmp4* was not modified at least 4 h after **(B)** FGF8- and **(C)** FGF10-treatment.

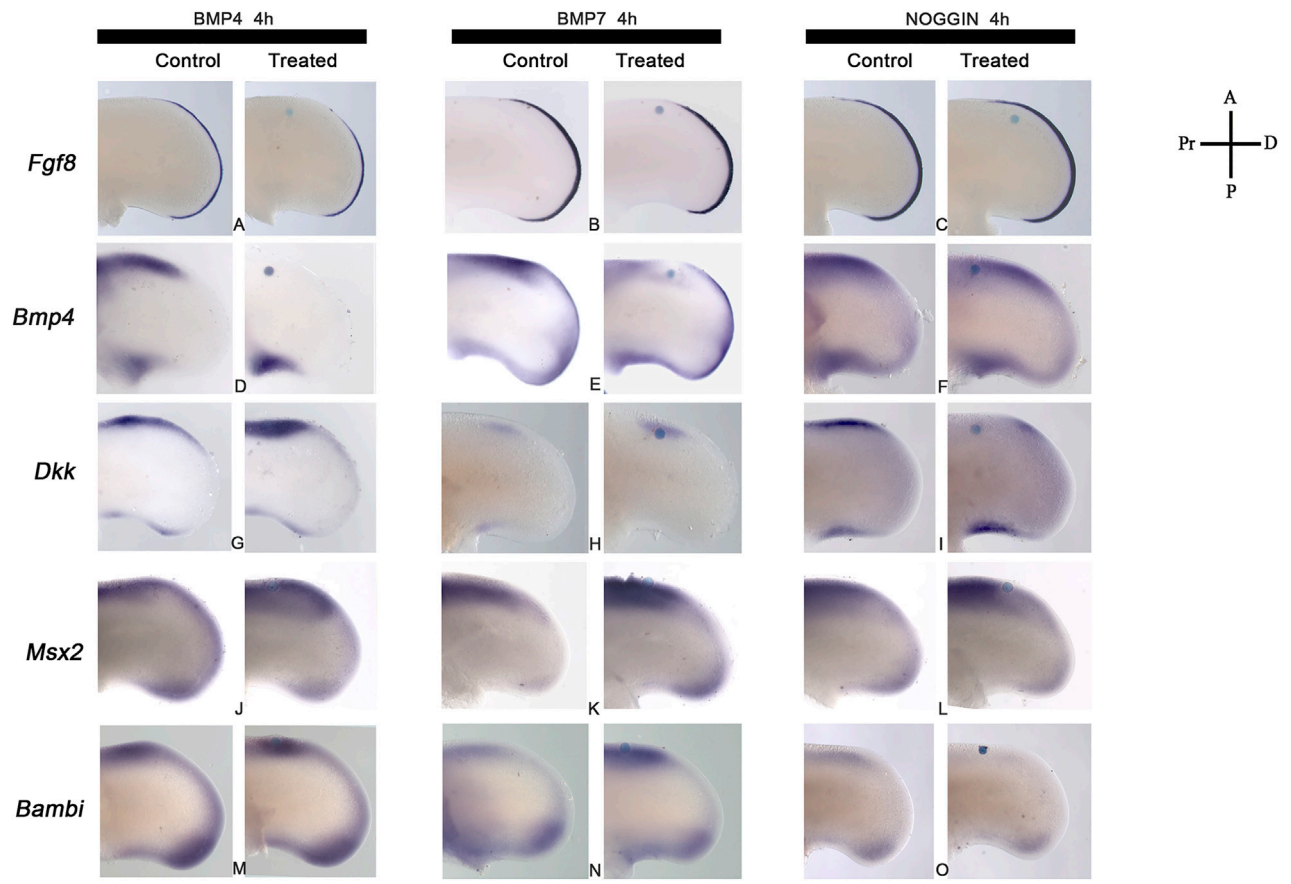

FIGURE 5 | BMP signaling regulates *Fgf8, Bmp4, Dkk, Msx2, and Bambi* gene expression. Regulation of **(A–C)** *Fgf8*, **(D–F)** *Bmp4,* **(G–I)** *Dkk,* **(J–L)** *Msx2,* **(M–O)** *Bambi* gene expression in the anterior limb margin after BMP4, BMP7, or Noggin. *Fgf8* **(B, C)** and Bmp4 **(D, E)** are downregulated after 4 h of BMP4 or BMP7. Notice the stronger effect of BMP4 than BMP7. In contrast, NOGGIN-treatment maintained the expression of both genes after treatments. **(G–I)** Upregulation of Dkk gene expression after 4 h of BMP4- or BMP7-treatment and downregulation of *Dkk* after 4 h of NOGGIN treatment. **(J–L)** *Msx2* and **(M–O)** *Bambi* gene expression were upregulated by BMP4 and BMP7. In contrast, NOGGIN inhibited *Bambi* expression during the first 4 h of treatment but not *Msx2* [Panel **(L, O)**].

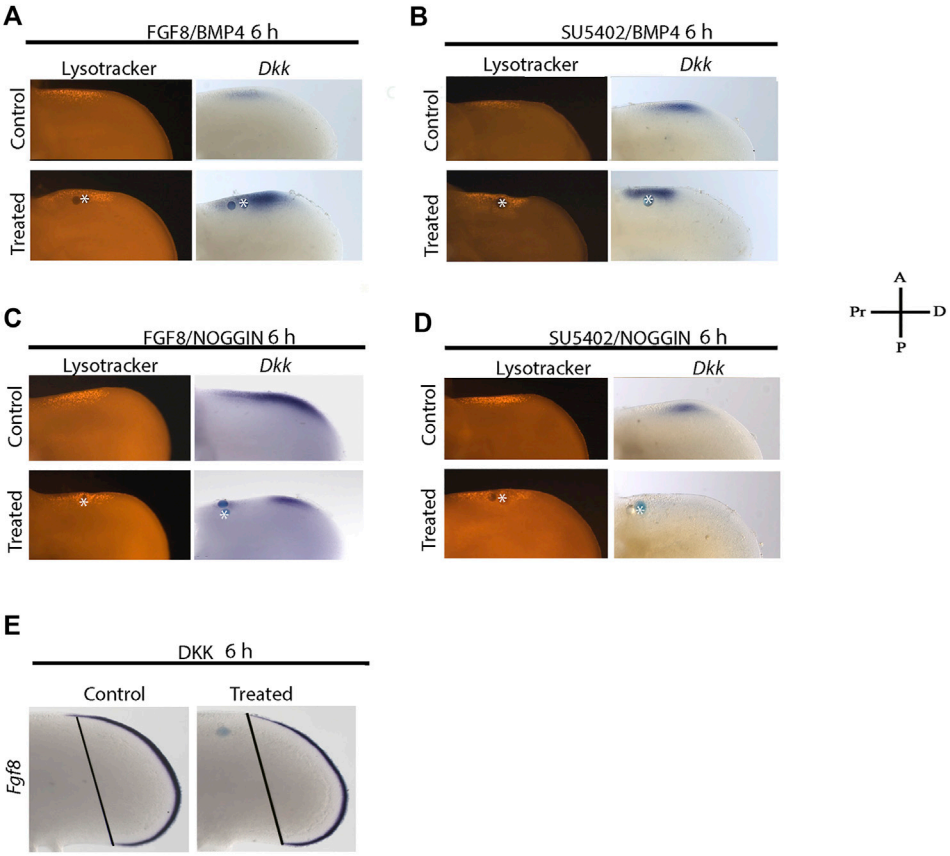

FIGURE 6 | The last step to induce cell death is the inhibition of FGF signaling.Double treatments were done to promote or block FGF and BMP signaling for 6 h. Under these conditions, lysotracker staining and *Dkk* gene expression were evaluated. **(A)** Double FGF8 and BMP4 treatment promoted *Dkk* expression, and cell death was observed closer to the BMP bead. **(B)** Inhibiting FGF signaling in the presence of BMP4, *Dkk* was still expressed. **(C)** Treatment with NOGGIN and in the presence of FGF8 significantly inhibited *Dkk* expression, but it slightly diminished the area of cell death. **(D)** Double treatment inhibiting FGF and BMP signaling inhibited *Dkk* gene expression, but no cell death. **(E)** *Fgf8* gene expression is inhibited in response to DKK protein. Notice that the blue line of the right limb (DKK treatment)—representing the expression of Fgf8 from the limb posterior margin to the anterior limb margin—is shorter than the contralateral limb.

respectively, it is possible to suggest the expression of *Dkk* and *Bmp4* in the anterior margin of the limb depends on FGF signaling.

The next step was to determine the minimum time required for BMP signaling to regulate *Fgf8*, *Bmp4*, and *Dkk* gene expression in the anterior margin of the limb for promoting cell death (**Figures 5A–I**). The results showed that BMP4 or BMP7 proteins had regulated Fgf8, Bmp4, and Dkk gene expression differentially (**Figures 5A,B,D,E,G,H**). BMP4 protein inhibited *Fgf8* in the AER and *Bmp4* in the anterior margin of the limb after 4 h of treatment (**Figures 5A,D**). In contrast, BMP7 slightly affected *Fgf8* gene expression, and it faintly inhibited *Bmp4* gene expression (**Figures 5B,E**). Furthermore, NOGGIN-treatment effects on *Fgf8* expression were minor (**Figure 5C**), while *Bmp4* gene expression was not affected after 4 h (**Figure 5F**). Regarding *Dkk* gene expression, the treatment with BMP4 showed a more significant effect than BMP7 (**Figures 5G,H**). Blocking BMP signaling with NOGGIN demonstrated that *Dkk* gene expression depended on BMP signaling (**Figure 5I**). *Msx2* and *Bambi* are regulated by BMP signaling (**Figures 5J–O**). The results showed that *Msx2* was regulated by BMP or NOGGIN treatment (**Figures 5J–L**). In contrast, NOGGIN treatment inhibited *Bambi* expression entirely, but BMP4 or BMP7 induced it slightly at least 4 h (**Figures 5M–O**). These results showed that BMP signaling self-regulate *Bmp4* and regulates *Fgf8*, *Dkk*, *Msx2*, and *Bambi* gene expression at short times in the ANZ.

Inhibition of FGF Signaling Is the Last Step in the Molecular Cascade of Cell Death

To determine the hierarchy of FGF and BMP signaling to promote cell death and regulate *Dkk* gene expression, we performed double treatments to promote or block FGF and BMP signaling for 6 h. Under these conditions, the dual treatment of FGF8 and BMP4 promoted *Dkk* expression inducing cell death closer to the BMP bead (**Figure 6A**). Nevertheless, if FGF signaling is inhibited in the presence of BMP4, *Dkk* is still expressed (**Figure 6B**). In contrast, if BMP signaling is blocked and FGF8 is present, the expression of Dkk

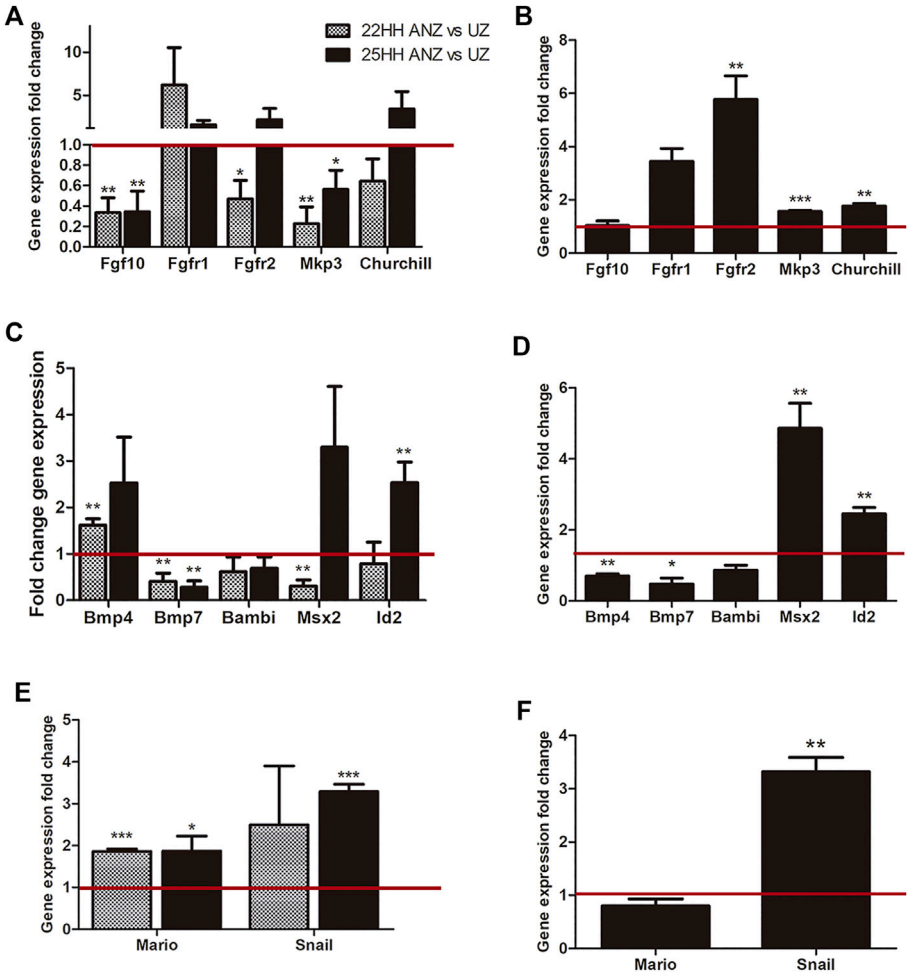

FIGURE 7 | qRT-PCR analysis and comparison dynamics of gene expression in the presumptive ANZ and the ANZ. qRT-PCR of FGF-related genes (Fgf10, Fgfr1, Fgfr2, Mkp3, Churchill) and BMP-related genes (Bmp4, Bmp7, Bambi, Mario, Snail). **(A, C, E)** Comparison of gene expression between the presumptive ANZ in 22 HH vs its undifferentiated zone (UZ) and between the ANZ versus its UZ. **(B, D, F)** Analysis of gene expression in the ANZ at 25 HH stage relative to the presumptive ANZ at 22 HH stage (set to 1.0, red line). Data represent three independent experiments. Statistical significance was set as follows: $^{***}p < 0.0001$, $^{**}p < 0.005$, $^{*}p < 0.05$.

was inhibited, and the area of cell death was slightly diminished (**Figure 6C**). The double blockade of FGF and BMP signaling inhibited *Dkk* gene expression. Under these conditions, cell death is still induced (**Figure 6D**). Finally, we evaluated the expression of *Fgf8* in the AER in the response of DKK protein that inhibited *Fgf8* (**Figure 6E**). These results suggest that FGF signaling must be inhibited in the ANZ and is probably the last step in the molecular cascade to trigger PCD by BMP signaling.

Dynamic of Gene Expression in Presumptive ANZ and ANZ

Once it was established that the onset of cell death requires the negative loop triggered by FGF signaling, a comparison of an expression profile of genes related to the maintenance of the undifferentiated stage and the commitment to cell death was performed (**Figure 7**). The tissue of limb primordia from 22 HH and the ANZ from 25 HH were dissected in two regions: 1) the mesodermal cells of the anterior margin at stage 22 HH (here called presumptive ANZ) or the ANZ at stage 25 HH, and 2) cells from the undifferentiated zone from both developing stages. It allowed us to clearly distinguish the location of genes expressed before establishing ANZ (stage 22 HH) and once established the ANZ (stage 25 HH). In both stages, the profile expression of this zone was compared with its respective undifferentiated zone.

Regarding genes related to the FGF signaling (**Figures 7A,B**), results showed that *Fgf10* expression was lower in the presumptive ANZ and ANZ than in the undifferentiated zone in both stages. *Fgfr1* tends to be upregulated in the presumptive ANZ than in the undifferentiated zone, but this study found no difference at both stages (**Figure 7A**). In the presumptive ANZ, *Fgfr2* expression was lower than in the undifferentiated zone, but at stage 25HH, the expression levels were similar in the ANZ and the undifferentiated zone (**Figure 7A**). However, comparing the levels of *fgf10*, *Fgfr1* and *Fgfr2* expressed between the presumptive ANZ at 22 HH and ANZ at 25 HH, the *Fgf10* expression did not

show significant changes (**Figure 7B**). In contrast, the expression levels of both receptors increased at stage 25HH than a stage 22HH, although only *Fgfr2* increased significatively (**Figure 7A**). Next, the expression of Mkp3 and Churchill was evaluated, two target genes of FGF signaling (Kawakami et al., 2003; Sheng et al., 2003). In the presumptive ANZ and ANZ, the expression levels of *Mkp3* decrease compared to the undifferentiated zone, while *Churchill* has no significant changes (**Figure 7A**). Moreover, comparing the expression levels of both genes, they had a higher level in the ANZ than in the presumptive ANZ (**Figure 7B**). These data showed an interesting dynamic of FGF signaling.

The next group of genes analyzed was *Bmp4, Bmp7*, *Bambi*, and those regulated by BMP signaling (**Figures 7C,D**). At stage 22HH, the *Bmp4* expression is higher in the presumptive ANZ than in the undifferentiated zone. In contrast, the *Bmp7* showed lower expression while *Bambi* did not show significant differences (**Figure 7C**). At stage 25HH, the expression of these genes in the ANZ was like the observed at stage 22HH (**Figure 7D**). We also evaluated the expression of *Msx2* and *Id2*, two genes that are regulated by BMP signaling. In the presumptive ANZ, the expression level of *Msx2* was lower than the undifferentiated zone, whereas *Id2* did not show changes in both regions. In contrast, the expression of *Msx2* was elevated in the ANZ regarding the undifferentiated zone (**Figure 7C**). *Id2* expression levels increased at stage 25HH in the ANZ compared with the undifferentiated zone, but at stage 22HH, no differences were found (**Figure 7C**). Comparing the presumptive ANZ with the ANZ, *Msx2* and *Id2* presented higher expression levels in the ANZ (**Figure 7D**). In contrast, the levels of *Bmp4* and *Bmp7* were lower, while Bambi is similar in both developing stages (**Figure 7D**).

The next group of genes evaluated is either regulated by BMP and FGF signaling or both (**Figures 7E,F**). *Mario* is a gene associated with the formation of digit 2, and it is induced by FGF and inhibited by BMP (Amano and Tamura, 2005). *Snail* is a transcription factor related to areas of undifferentiated mesenchyme and cell death; BMP and FGF signaling induce both genes (Ros et al., 1997; Montero et al., 2001). Results showed that the expression levels of both genes in the presumptive ANZ and ANZ are higher than in the undifferentiated zone (**Figure 7E**). Comparing the expression levels between the presumptive ANZ and ANZ, it was found that *Snail* expression is higher than *Mario* (**Figure 7F**).

DISCUSSION

The AER is a signaling center where FGF, WNT, and BMP signaling pathways play an essential role in controlling cell proliferation, cell survival, and cell differentiation (Fernandez-Teran and Ros, 2008; Ten Berge et al., 2008; Mariani et al., 2017). During sculpturing of the limb, mesodermal cells underneath AER in the anterior margin of the limb undergo cell death giving rise to the ANZ that appears gradually, in coordination with the progressive loss of the AER (Todt and Fallon, 1987; Fernandez-Teran et al., 2006; Fernandez-Teran and Ros, 2008).

The intricate regulatory network between BMP, FGF, and WNT signaling that controls cell death in interdigital tissue is well known (Ganan et al., 1996; Pizette and Niswander, 1999; Danopoulos et al., 2013; Haro et al., 2014; Jin et al., 2018). However, the first events triggered by this regulatory network to initiate cell death in the anterior limb undergoing ANZ formation are not well established. The present study aimed to elucidate the earliest events triggered by the regulatory network of FGF, WNT, and BMP signaling in the control of cell death to induce the ANZ formation in the anterior margin of the limb. Previously, it was reported that a short pulse of BMP is sufficient to trigger cell death in the anterior margin of the limb (Abarca-Buis et al., 2011). An interval of two to 8 h is sufficient to induce cell death after the inhibition of WNT or FGF or the activation of BMP signaling. Besides, cell death induction is coordinated with the regulation of *Dkk*, *Fgf8,* and *Bmp4* expression. Inhibition of FGF signaling inhibited *Dkk* expression after 2 h of treatment, demonstrating that FGF is necessary to induce *Dkk* gene expression. In contrast, DKK treatment-induced cell death after 8 h. Likewise, DKK and BMP4 inhibit *Fgf8* expression; thus, it is possible to postulate that the negative feedback loop between *Bmp4*, *Fgf8*, and *Dkk* controls the onset of cell death in the ANZ.

It has been demonstrated that the expression of *Fgf8* in the anterior AER is not redundant with other *Fgf* genes expressed in posterior AER (Moon and Capecchi, 2000; Moon et al., 2000; Delgado et al., 2008). Massive cell death in the anterior margin results from BMP activation (Yokouchi et al., 1996). The mutant mouse for *Bmpr1a* demonstrates that this receptor mediates BMP signaling in controlling *Fgf8* expression (Pajni-Underwood et al., 2007). Interestingly in the posterior region of the limb deprived of SHH, signaling massive cell death occurs concomitantly with up-regulation of *Bmp4* (Sanz-Ezquerro and Tickle, 2000). The absence of SHH signaling increases the repressor form of GLI3 (GLI3R), which regulates *Bmp* expression as observed in the anterior margin; GLI3R is abundant and correlates with an increase in *Bmp4* expression (Bastida et al., 2004).

In this work, comparing the expression profile of *Fgfr1* and *Fgfr2* between the presumptive ANZ with the undifferentiated region at stage 22 HH showed differential expression. *Fgfr1* expression is higher than *Fgfr2* in the presumptive ANZ. In addition, the lower levels of expression of *Churchill* or *Mkp3* that are FGF signaling targets might suggest that minimal amounts of *Fgfr1* or *Fgfr2* are enough to avoid cell death. Furthermore, FGF signaling may be active at low levels before ANZ formation. However, the levels of *Bmp4* might be the result of a regulation of GLI3R (Bastida et al., 2004), and it is possible that although higher expression of *Id2* and *Msx2* together with the low level of *Mkp3* expression observed in the anterior margin of the limb might be not sufficient to induce cell death. Thus, the balance of FGF and BMP signaling may favor FGF signaling.

As development progress, the ANZ is established. At stage 25HH, the expression levels of *Fgfr1* and *Fgfr2* and *Churchill* increase. However, the *Mkp3* level maintains slightly higher in the well-established ANZ than in the undifferentiated region. Interestingly, levels of *Churchill* are higher, which might indicate that FGF signaling is being inhibited (Kok et al., 2010). Other genes such as *Mario* and *Wif* (data not shown) are higher expressed in ANZ, BMP, whereas FGF signaling induces Mario. It has been involved in the boundary between non-digit digit two in the chick embryo (Amano and

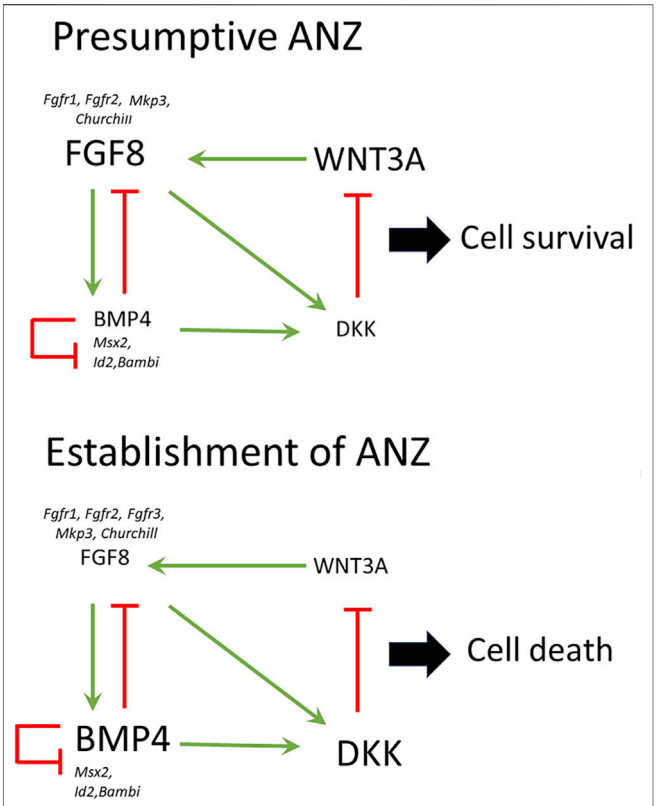

FIGURE 8 | Establishment of the ANZ by the WNT-BMP-FGF regulatory network. In this model, WNT3A and BMP signaling antagonistically regulate *Fgf8* expression and consequently cell death. WNT3A induces the expression of *Fgf8* in the AER. BMP signaling inhibited *Fgf8* expression; meanwhile, DKK inhibits the function of WNT/ß catenin signaling, and consequently, the expression of *Fgf8* is inhibited. In the presumptive ANZ, the high levels of FGF8 from AER are necessary for cell survival, but FGF8 is also required for promoting cell death regulating *Bmp4* and *Dkk* expression. The establishment of ANZ occurs when the levels of FGF signaling are reduced and BMP signaling increases leading to the inhibition of *Fgf8* in the AER inducing cell death. *Fgfr1, Fgfr2, Mkp3, Churchill, Msx2, Id2, and Bambi* are expressed differentially in the presumptive ANZ and the established ANZ.

Tamura, 2005), whereas *Wif* is an inhibitor of WNT/β catenin. *Wif* together with DKK may inhibit WNT signaling and, consequently, FGF signaling, promoting cell death. The levels of expression of *Bmp7* and *Bambi* in both stages are lower than the undifferentiated zone indicating this minor participation in establishing ANZ.

Finally, comparing gene expression levels between the presumptive ANZ at stage 22HH and the ANZ of 25HH demonstrates that FGF and BMP signaling is more active in stage 25HH when the ANZ is well-established. These data suggest that the control of FGF and BMP signaling is necessary to regulate cell death.

Based on data obtained in the present study and from the literature, we propose the following model to explain the onset of cell death in the anterior margin of the limb to give rise to ANZ (**Figure 8**). First, it is known that WNT3A mediated by *Sp6/Sp8* induces the *Fgf8* expression in the AER (Haro et al., 2014). On the other hand, BMP signaling inhibited *Fgf8* expression. Thus, WNT3A and BMP signaling antagonistically regulate *Fgf8* expression and consequently cell death (Hernandez-Martínez et al., 2009). Because *Bmp4* and other genes such as *Churchill* and *Mkp3* depend on FGF signaling (Kawakami et al., 2003), it is possible to suggest that the extent and location of cell death depend on the capacity of FGF signaling to control the levels of *Bmp4* expression. High levels of BMP signaling, presumably BMP4, inhibit *Fgf8* in a higher extension of the AER; consequently, cell death occurs. Also, BMP4 induces *Dkk* expression, and thus it is reasonable to speculate that if the levels of BMP signaling are high, then high levels of DKK are present in the anterior margin of the limb. DKK inhibits the function of WNT/ß catenin signaling resulting in an inhibition of FGF8 signaling. Remarkably as FGF signaling presumably, FGF8 from AER is necessary for cell survival but is also required for promoting cell death because it promotes *Bmp4* and *Dkk* expression. Thus, different levels of FGF activity may control the negative loop to promote AER regression and, consequently, the onset of cell death. As limb development progress, this negative feedback loop occurs progressively. Other genes such as *Msx2* and *Bambi,* although necessary for cell death (Montero et al., 2001), seem not to be regulated during the early establishment of the ANZ.

In conclusion, this work adds new insights to comprehend the establishment of a regulatory network by FGF, WNT, and BMP signaling to induce cell death in anterior mesodermal cells establishing the ANZ.

DATA AVAILABILITY STATEMENT

The original contributions presented in the study are included in the article/Supplementary Material, further inquiries can be directed to the corresponding author.

AUTHOR CONTRIBUTIONS

JC-M, MED-H, and JCM-L conceived and designed the experiments. MED-H, CG-H, KC-S, MB, JCM-L, and SW performed the experiments. All authors analyzed the data. JC-M and JCM-L wrote the final version of the manuscript. The manuscript was revised and approved by all authors.

FUNDING

This work was supported by the Dirección General de Asuntos del Personal Académico (DGAPA)-Universidad Nacional Autónoma de México (grant numbers IN211117 and IN213314) and Consejo Nacional de Ciencia y Tecnología (CONACyT) (grant number 1887 CONACyT-Fronteras de la Ciencia) awarded to JC-M. JC M-L was the recipient of a postdoctoral fellowship from the Consejo Nacional de Ciencia y Tecnología (CONACyT Fronteras de la Ciencia-1887).

ACKNOWLEDGMENTS

Authors thank to Dr. Miguel Tapia Rodriguez from Instituto de Investigaciones Biomédicas, UNAM for his technical assistance.

REFERENCES

Abarca-Buis, R. F., Bustamante, M., Cuervo, R., Aguilar-Fernández-de-Lara, D., and Chimal-Monroy, J. (2011). Smad8 Is Expressed in the Anterior Necrotic Zone: Evidence for a Role of Bone Morphogenetic Proteins/SMAD Signaling in the Activation of a Molecular cascade that Culminates in Cell Death. *Dev. Growth Differ.* 53, 780–792. doi:10.1111/j.1440-169x.2011.01285.x

Amano, T., and Tamura, K. (2005). Region-specific Expression Ofmario Reveals Pivotal Function of the Anterior Nondigit Region on Digit Formation in Chick wing Bud. *Dev. Dyn.* 233, 326–336. doi:10.1002/dvdy.20390

Bastida, M. F. l., Delgado, M. D., Wang, B., Fallon, J. F., Fernandez-Teran, M., and Ros, M. A. (2004). Levels of Gli3 Repressor Correlate withBmp4 Expression and Apoptosis during Limb Development. *Dev. Dyn.* 231, 148–160. doi:10.1002/dvdy.20121

Chen, Y., and Zhao, X. (1998). Shaping Limbs by Apoptosis>. *J. Exp. Zool.* 282, 691–702. doi:10.1002/(sici)1097-010x(19981215)282:6<691:aid-jez5>3.0.co;2-s

Chimal-Monroy, J., Rodriguez-Leon, J., Montero, J. A., Gañan, Y., Macias, D., Merino, R., et al. (2003). Analysis of the Molecular cascade Responsible for Mesodermal Limb Chondrogenesis: Sox Genes and BMP Signaling. *Developmental Biol.* 257, 292–301. doi:10.1016/s0012-1606(03)00066-6

Danopoulos, S., Parsa, S., Al Alam, D., Tabatabai, R., Baptista, S., Tiozzo, C., et al. (2013). Transient Inhibition of FGFR2b-Ligands Signaling Leads to Irreversible Loss of Cellular β-Catenin Organization and Signaling in AER during Mouse Limb Development. *PLoS One* 8, e76248. doi:10.1371/journal.pone.0076248

Delgado, I., Domínguez-Frutos, E., Schimmang, T., and Ros, M. A. (2008). The Incomplete Inactivation ofFgf8 in the Limb Ectoderm Affects the Morphogenesis of the Anterior Autopod through BMP-Mediated Cell Death. *Dev. Dyn.* 237, 649–658. doi:10.1002/dvdy.21452

Fernández-Terán, M. A., Hinchliffe, J. R., and Ros, M. A. (2006). Birth and Death of Cells in Limb Development: a Mapping Study. *Dev. Dyn.* 235, 2521–2537. doi:10.1002/dvdy.20916

Fernandez-Teran, M., and Ros, M. A. (2008). The Apical Ectodermal Ridge: Morphological Aspects and Signaling Pathways. *Int. J. Dev. Biol.* 52, 857–871. doi:10.1387/ijdb.072416mf

Ganan, Y., Macias, D., Duterque-Coquillaud, M., Ros, M. A., and Hurle, J. M. (1996). Role of TGF Beta S and BMPs as Signals Controlling the Position of the Digits and the Areas of Interdigital Cell Death in the Developing Chick Limb Autopod. *Development* 122, 2349–2357. doi:10.1242/dev.122.8.2349

Grotewold, L., and Rüther, U. (2002a). Bmp, Fgf and Wnt Signalling in Programmed Cell Death and Chondrogenesis during Vertebrate Limb Development: the Role of Dickkopf-1. *Int. J. Dev. Biol.* 46, 943–947.

Grotewold, L., and Ruther, U. (2002b). The Wnt Antagonist Dickkopf-1 Is Regulated by Bmp Signaling and C-Jun and Modulates Programmed Cell Death. *EMBO J.* 21, 966–975. doi:10.1093/emboj/21.5.966

Grotewold, L., Theil, T., and Rüther, U. (1999). Expression Pattern of Dkk-1 during Mouse Limb Development. *Mech. Development* 89, 151–153. doi:10.1016/s0925-4773(99)00194-x

Hamburger, V., and Hamilton, H. L. (1951). A Series of normal Stages in the Development of the Chick Embryo. *J. Morphol.* 88, 49–92. doi:10.1002/jmor.1050880104

Haro, E., Delgado, I., Junco, M., Yamada, Y., Mansouri, A., Oberg, K. C., et al. (2014). Sp6 and Sp8 Transcription Factors Control AER Formation and Dorsal-Ventral Patterning in Limb Development. *Plos Genet.* 10, e1004468. doi:10.1371/journal.pgen.1004468

Hernández-Martínez, R., Castro-Obregón, S., and Covarrubias, L. (2009). Progressive Interdigital Cell Death: Regulation by the Antagonistic Interaction between Fibroblast Growth Factor 8 and Retinoic Acid. *Development* 136, 3669–3678. doi:10.1242/dev.041954

Hinchliffe, J. R., and Thorogood, P. V. (1974). Genetic Inhibition of Mesenchymal Cell Death and the Development of Form and Skeletal Pattern in the Limbs of Talpid3 (Ta3) Mutant Chick Embryos. *J. Embryol. Exp. Morphol.* 31, 747–760. doi:10.1242/dev.31.3.747

Hogan, B. L. (1996). Bone Morphogenetic Proteins in Development. *Curr. Opin. Genet. Development* 6, 432–438. doi:10.1016/s0959-437x(96)80064-5

Jin, L., Wu, J., Bellusci, S., and Zhang, J. S. (2018). Fibroblast Growth Factor 10 and Vertebrate Limb Development. *Front. Genet.* 9, 705. doi:10.3389/fgene.2018.00705

Kawakami, Y., Capdevila, J., Büscher, D., Itoh, T., Esteban, C. R., and Belmonte, J. C. I. (2001). WNT Signals Control FGF-dependent Limb Initiation and AER Induction in the Chick Embryo. *Cell* 104, 891–900. doi:10.1016/s0092-8674(01)00285-9

Kawakami, Y., Esteban, C. R., Matsui, T., Rodri´guez-Leo´n, J., Kato, S., and Belmonte, J. C. I. (2004). Sp8 and Sp9, Two Closely Related Buttonhead-like Transcription Factors, Regulate Fgf8expression and Limb Outgrowth in Vertebrate Embryos. *Development* 131, 4763–4774. doi:10.1242/dev.01331

Kawakami, Y., Rodríguez-León, J., Koth, C. M., Büscher, D., Itoh, T., Raya, Á., et al. (2003). MKP3 Mediates the Cellular Response to FGF8 Signalling in the Vertebrate Limb. *Nat. Cel Biol* 5 (6), 513–519. doi:10.1038/ncb989

Kok, F. O., Shepherd, I. T., and Sirotkin, H. I. (2010). Churchill and Sip1a Repress Fibroblast Growth Factor Signaling During Zebrafish Somitogenesis. *Dev. Dyn.* 239, 548–558. doi:10.1002/dvdy.22201

Macias, D., Ganan, Y., Sampath, T. K., Piedra, M. E., Ros, M. A., and Hurle, J. M. (1997). Role of BMP-2 and OP-1 (BMP-7) in Programmed Cell Death and Skeletogenesis during Chick Limb Development. *Development* 124, 1109–1117. doi:10.1242/dev.124.6.1109

Mariani, F. V., Ahn, C. P., and Martin, G. R. (2008). Genetic Evidence that FGFs Have an Instructive Role in Limb Proximal-Distal Patterning. *Nature* 453, 401–405. doi:10.1038/nature06876

Mariani, F. V., Fernandez-Teran, M., and Ros, M. A. (2017). Ectoderm-mesoderm Crosstalk in the Embryonic Limb: The Role of Fibroblast Growth Factor Signaling. *Dev. Dyn.* 246, 208–216. doi:10.1002/dvdy.24480

Marín-Llera, J. C., Garciadiego-Cázares, D., and Chimal-Monroy, J. (2019). Understanding the Cellular and Molecular Mechanisms that Control Early Cell Fate Decisions during Appendicular Skeletogenesis. *Front. Genet.* 10, 977. doi:10.3389/fgene.2019.00977

Merino, R., Gañan, Y., Macias, D., Economides, A. N., Sampath, K. T., and Hurle, J. M. (1998). Morphogenesis of Digits in the Avian Limb Is Controlled by FGFs, TGFβs, and Noggin through BMP Signaling. *Developmental Biol.* 200, 35–45. doi:10.1006/dbio.1998.8946

Merino, R., Gañán, Y., Macias, D., Rodríguez-león, J., and Hurle, J. M. (1999). Bone Morphogenetic Proteins Regulate Interdigital Cell Death in the Avian Embryo. *Ann. New York Acad. Sci.* 887, 120–132. doi:10.1111/j.1749-6632.1999.tb07927.x

Monteiro, R. M., De Sousa Lopes, S. M. C., Bialecka, M., De Boer, S., Zwijsen, A., and Mummery, C. L. (2008). Real Time Monitoring of BMP Smads Transcriptional Activity during Mouse Development. *Genesis* 46, 335–346. doi:10.1002/dvg.20402

Montero, J. A., Gañan, Y., Macias, D., Rodriguez-Leon, J., Sanz-Ezquerro, J. J., Merino, R., et al. (2001). Role of FGFs in the Control of Programmed Cell Death during Limb Development. *Development* 128, 2075–2084. doi:10.1242/dev.128.11.2075

Montero, J. A., Lorda-Diez, C. I., Gañan, Y., Macias, D., and Hurle, J. M. (2008). Activin/Tgfβ and BMP Crosstalk Determines Digit Chondrogenesis. *Developmental Biol.* 321, 343–356. doi:10.1016/j.ydbio.2008.06.022

Montero, J. A., Lorda-Diez, C. I., Sanchez-Fernandez, C., and Hurle, J. M. (2020). Cell Death in the Developing Vertebrate Limb: A Locally Regulated Mechanism Contributing to Musculoskeletal Tissue Morphogenesis and Differentiation. *Dev. Dyn.* 250 (9), 1236–1247. doi:10.1002/dvdy.237

Moon, A. M., Boulet, A. M., and Capecchi, M. R. (2000). Normal Limb Development in Conditional Mutants of Fgf4. *Development* 127, 989–996. doi:10.1242/dev.127.5.989

Moon, A. M., and Capecchi, M. R. (2000). Fgf8 Is Required for Outgrowth and Patterning of the Limbs. *Nat. Genet.* 26, 455–459. doi:10.1038/82601

Mukhopadhyay, M., Shtrom, S., Rodriguez-Esteban, C., Chen, L., Tsukui, T., Gomer, L., et al. (2001). Dickkopf1 Is Required for Embryonic Head Induction and Limb Morphogenesis in the Mouse. *Developmental Cel* 1, 423–434. doi:10.1016/s1534-5807(01)00041-7

Niswander, L., Tickle, C., Vogel, A., Booth, I., and Martin, G. R. (1993). FGF-4 Replaces the Apical Ectodermal ridge and Directs Outgrowth and Patterning of the Limb. *Cell* 75, 579–587. doi:10.1016/0092-8674(93)90391-3

Pajni-Underwood, S., Wilson, C. P., Elder, C., Mishina, Y., and Lewandoski, M. (2007). BMP Signals Control Limb Bud Interdigital Programmed Cell Death by

Regulating FGF Signaling. *Development* 134, 2359–2368. doi:10.1242/dev.001677

Parish, C. R. (1999). Fluorescent Dyes for Lymphocyte Migration and Proliferation Studies. *Immunol. Cel Biol* 77, 499–508. doi:10.1046/j.1440-1711.1999.00877.x

Pizette, S., and Niswander, L. (1999). BMPs Negatively Regulate Structure and Function of the Limb Apical Ectodermal ridge. *Development* 126, 883–894. doi:10.1242/dev.126.5.883

Ros, M. A., Sefton, M., and Nieto, M. A. (1997). Slug, a Zinc finger Gene Previously Implicated in the Early Patterning of the Mesoderm and the Neural Crest, Is Also Involved in Chick Limb Development. *Development* 124, 1821–1829. doi:10.1242/dev.124.9.1821

Salas-Vidal, E., Valencia, C. n., and Covarrubias, L. (2001). Differential Tissue Growth and Patterns of Cell Death in Mouse Limb Autopod Morphogenesis. *Dev. Dyn.* 220, 295–306. doi:10.1002/dvdy.1108

Sanz-Ezquerro, J. J., and Tickle, C. (2000). Autoregulation of Shh Expression and Shh Induction of Cell Death Suggest a Mechanism for Modulating Polarising Activity during Chick Limb Development. *Development* 127, 4811–4823. doi:10.1242/dev.127.22.4811

Saunders, J. W., Jr., Gasseling, M. T., and Saunders, L. C. (1962). Cellular Death in Morphogenesis of the Avian wing. *Developmental Biol.* 5, 147–178. doi:10.1016/0012-1606(62)90008-8

Sheng, G., dos Reis, M., and Stern, C. D. (2003). Churchill, a Zinc finger Transcriptional Activator, Regulates the Transition between Gastrulation and Neurulation. *Cell* 115 (5), 603–613. doi:10.1016/s0092-8674(03)00927-9

Sun, X., Mariani, F. V., and Martin, G. R. (2002). Functions of FGF Signalling from the Apical Ectodermal ridge in Limb Development. *Nature* 418, 501–508. doi:10.1038/nature00902

Ten Berge, D., Brugmann, S. A., Helms, J. A., and Nusse, R. (2008). Wnt and FGF Signals Interact to Coordinate Growth with Cell Fate Specification during Limb Development. *Development* 135, 3247–3257. doi:10.1242/dev.023176

Todt, W. L., and Fallon, J. F. (1987). Posterior Apical Ectodermal ridge Removal in the Chick wing Bud Triggers a Series of Events Resulting in Defective Anterior Pattern Formation. *Development* 101, 501–515. doi:10.1242/dev.101.3.501

Xu, X., Weinstein, M., Li, C., Naski, M., Cohen, R. I., Ornitz, D. M., et al. (1998). Fibroblast Growth Factor Receptor 2 (FGFR2)-Mediated Reciprocal Regulation Loop between FGF8 and FGF10 Is Essential for Limb Induction. *Development* 125, 753–765. doi:10.1242/dev.125.4.753

Yokouchi, Y., Sakiyama, J., Kameda, T., Iba, H., Suzuki, A., Ueno, N., et al. (1996). BMP-2/-4 Mediate Programmed Cell Death in Chicken Limb Buds. *Development* 122, 3725–3734. doi:10.1242/dev.122.12.3725

Zuzarte-Luís, V., and Hurlé, J. M. (2002). Programmed Cell Death in the Developing Limb. *Int. J. Dev. Biol.* 46, 871–876.

Zuzarte-Luís, V., Montero, J. A., Rodriguez-León, J., Merino, R., Rodríguez-Rey, J. C., and Hurlé, J. M. (2004). A New Role for BMP5 during Limb Development Acting through the Synergic Activation of Smad and MAPK Pathways. *Dev. Biol.* 272, 39–52. doi:10.1016/j.ydbio.2004.04.015

Zuzarte-Luis, V., and Hurle, J. M. (2005). Programmed Cell Death in the Embryonic Vertebrate Limb. *Semin. Cel Developmental Biol.* 16, 261–269. doi:10.1016/j.semcdb.2004.12.004

Conflict of Interest: The authors declare that the research was conducted in the absence of any commercial or financial relationships that could be construed as a potential conflict of interest.

Advantages of publishing in Frontiers

OPEN ACCESS
Articles are free to read for greatest visibility and readership

FAST PUBLICATION
Around 90 days from submission to decision

HIGH QUALITY PEER-REVIEW
Rigorous, collaborative, and constructive peer-review

TRANSPARENT PEER-REVIEW
Editors and reviewers acknowledged by name on published articles

Frontiers
Avenue du Tribunal-Fédéral 34
1005 Lausanne | Switzerland

Visit us: www.frontiersin.org
Contact us: frontiersin.org/about/contact

REPRODUCIBILITY OF RESEARCH
Support open data and methods to enhance research reproducibility

DIGITAL PUBLISHING
Articles designed for optimal readership across devices

FOLLOW US
@frontiersin

IMPACT METRICS
Advanced article metrics track visibility across digital media

EXTENSIVE PROMOTION
Marketing and promotion of impactful research

LOOP RESEARCH NETWORK
Our network increases your article's readership